INTERNATIONAL SUMMER SCHOOL ON SUBATOMIC PHYSICS 2011

New Frontiers of Nuclear Physics

School Chair Persons

H. Feldmeier
GSI, Darmstadt, Germany

J. Meng
Peking University, Beijing, China

H. Sakurai
RIKEN, Saitama, Japan

Beijing, China
August 27-31, 2011

Printed in August 2011

第六届 北京亚原子物理国际暑期学校 2011年8月27日— 31日

INTERNATIONAL SUMMER SCHOOL ON SUBATOMIC PHYSICS

6th Course: New Frontiers of Nuclear Physics

Beijing, August 27-31, 2011

Co-organized by:

RIKEN Nishina Center, Wako, Japan
Gesellschaft für Schwerionenforschung GmbH (GSI), Darmstadt, Germany
Grand Accélérateur National d'Ions Lourds (GANIL), Caen, France
Institute of Modern Physics (IMP), Chinese Academy of Sciences, Lanzhou, China
Institute of Theoretical Physics (ITP), Chinese Academy of Sciences, Beijing, China
China Institute of Atomic Energy (CIAE), Beijing, China
China Center of Advanced Science and Technology (CCAST), Beijing , China
Beijing Institute of Modern Physics (BIMP), Beijing, China
Chinese Nuclear Physics Society (CNPS), Beijing, China
Peking University (PKU), Beijing, China

The school will consist of lectures by the following invited lecturers and of short presentations by the participants. Invited lecturers are:

K. Blaum (MPI-K Heidelberg, Germany, *Precision mass measurements of short-lived radionuclides*), **S. Gales** (GANIL, France, *GANIL -SPIRAL2*), **C.J. Lin** (CIAE, China, *Experimental progress in two-proton correlated emission*), **W.P. Liu** (CIAE, China, *Introduction of nuclear astrophysics and related experimental techniques*), **T. Nakatsukasa** (RIKEN, Japan, *Single-particle and collective motions in nuclei*), **M. Ploszajczak** (GANIL, France, *The shell model for open quantum systems*), **P. Ring** (TUM, Germany, *Density functional theory for ground states and excited states in nuclei*), **H. Sakurai** (RIKEN, Japan, *New generation of nuclear physics with RIBF*), **A. Schwenk** (TU Darmstadt, Germany, *Chiral effective field theory and nuclear structure*), **B. Sherrill** (MSU, USA, *Methods and facilities for production of radioactive ion beams, An introduction to nuclear astrophysics*), **I. Tanihata** (Osaka Univ., Japan/BUAA, China, *Neutron halo and tensor forces in nuclei*), **Y.H. Zhang** (IMP, China, *Mass measurements of short-lived nuclides using CSRe in Lanzhou*), **Y.L. Ye** (PKU, China, *Breakup reaction and it's application to the study of nuclear structure*), **S.G. Zhou** (ITP, China, *Properties and synthesis of superheavy elements*)

Advisory committee

J. Äystö (Jyväskylä), R. Casten (Yale), S. Gales (GANIL), Z.Z. Gan (BIMP), P.W. Ji (NSFC), T. Kishimoto (Osaka), W. Nazarewicz (Oak Ridge), T. Otsuka (Tokyo), W.Q. Shen (SINAP), S. Shimoura (Tokyo), I. Tanihata (Osaka /BUAA), H. Toki (Osaka), Y. L. Wu (ITP), G.Q. Xiao (IMP), Y. Yano (RIKEN), M.H. Ye (CCAST), Y.L. Ye (PKU), W.L. Zhan (IMP), H.Q. Zhang (CIAE), Z.Y. Zhang (IHEP), E.G. Zhao (ITP)

Organizing committee

W.Q. Chao (CCAST), H. Feldmeier (GSI, co-chair), W.P .Liu (CIAE), J. Meng (PKU, chair), M. Pu (NSFC), H. Sakurai (RIKEN, co-chair), H.S. Xu (IMP), S.G. Zhou (ITP), S.Y. Zhu (CNPS)

Topics include:

Theoretical and Experimental Nuclear Physics and Nuclear Astrophysics

Goals of the school

The school will be held every two years in summer and it is intended for graduate students and young researchers who are interested in the fields of subatomic physics. It aims: (1) to promote and encourage talented young physicists and students and build an efficient linkage of young researchers with the other international colleagues; (2) to exchange ideas and share information in depth research on typical problems at the forefront of contemporary developments in nuclear physics; (3) to deepen the future research cooperation and strengthen the interaction between theoretical and experimental studies; (4) to present the most recent research results; (5) to stimulate contact between the people and promote the culture exchange and communication of young generation.

Date and Place

The lectures will begin in the morning of August 27, and end in the afternoon of August 31. The school is hosted by Peking University in Beijing.

Tour and Other:

A half-day excursion is planned. We can also help to book tickets for sightseeing to other cities in China after the summer school. Please tell us your requests when you send back the registration form.

Registration Fee and Local Fees

(1) Local expenses are covered and no registration fee is charged for the lecturers; (2) For the participants, fees for registration and local expenses in total are US$500; (3) Supports for local expenses and/or registration fee are available upon application; (4) The accompany person should pay US$200 for the welcome party, meals, banquet, and culture events.

Those who are interested in participation should complete the registration on the website www.jcnp.org

Dr. H.Z. Liang, Dr. L.L. Li, and Dr. L. Liu
isssp@jcnp.org
http://www.jcnp.org/
School of Physics,
Peking University, Beijing 100871, China
Tel.: 86-10-62767013 Fax: 86-10-62765620

Contents

MAX PLANCK INSTITUTE FOR NUCLEAR PHYSICS

Beijing, ISSSP 2011

"Precision Mass Measurements of Short-Lived Radionuclides PART 1 - BASICS"

Klaus Blaum

August 29, 2011

Klaus.blaum@mpi-hd.mpg.de

MAX PLANCK INSTITUTE FOR NUCLEAR PHYSICS

Outline

- **Introduction and methods**
- **Principle of Penning trap and storage ring mass spectrometry (see talk by Prof. Zhang)**
- **Setup and measurement procedure**
- **Precision measurements of nuclear masses and their applications**

MAX PLANCK INSTITUTE FOR NUCLEAR PHYSICS

Introduction and Motivation

MAX PLANCK INSTITUTE FOR NUCLEAR PHYSICS

Storage and cooling techniques

Penning trap

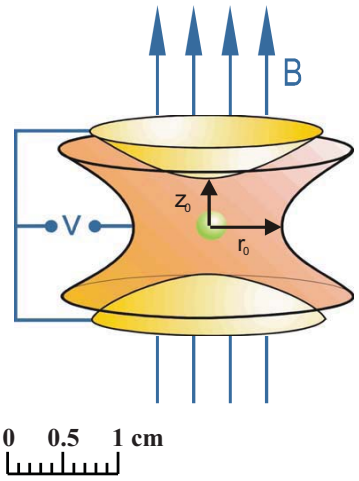

Storage ring

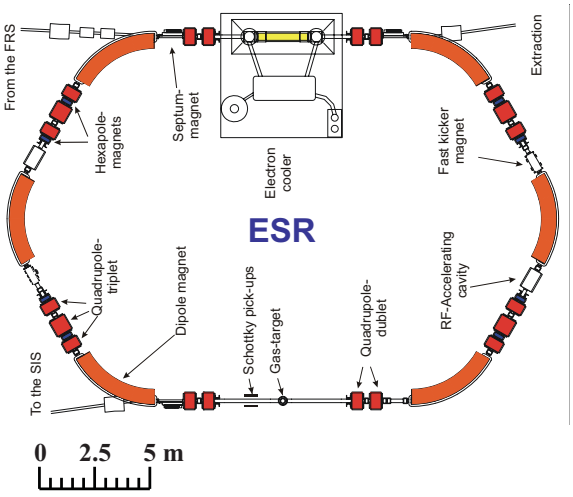

particles at nearly rest in space — **relativistic particles**

* ion cooling * long storage times
* single-ion sensitivity * high accuracy

Why measuring atomic masses?

MAX PLANCK INSTITUTE FOR NUCLEAR PHYSICS

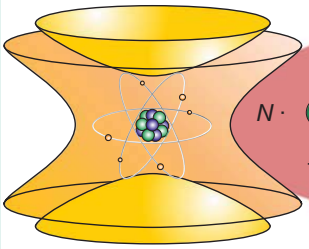

	δm/m
General physics & chemistry	$\leq 10^{-5}$
Nuclear structure physics - separation of isobars	$\leq 10^{-6}$
Astrophysics - separation of isomers	$\leq 10^{-7}$
Weak interaction studies	$\leq 10^{-8}$
Metrology - fundamental constants Neutrino physics	$\leq 10^{-9}$
CPT tests	$\leq 10^{-10}$
QED in highly-charged ions - separation of atomic states	$\leq 10^{-11}$

Why measuring atomic masses?

MAX PLANCK INSTITUTE FOR NUCLEAR PHYSICS

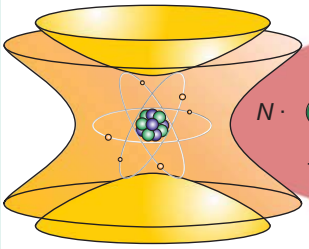

Sources:
Accelerator or reactor based radioactive beam facilities and electron beam ion traps.

CERN **IMP/GSI** **MPIK** **TRIGA**

	Experimental setups
General physics & chem	KATRIN-TRAP
Nuclear structure physics - separat	*CSRe/ESR*
Astrophysics - separati	TRIGA-TRAP
Weak interaction studies	ISOLTRAP
Metrology - fundamenta Neutrino physics	SHIPTRAP
CPT tests	THe-TRAP
QED in highly-charged ior - separation of	PENTA-TRAP

A brief history of mass spectrometry

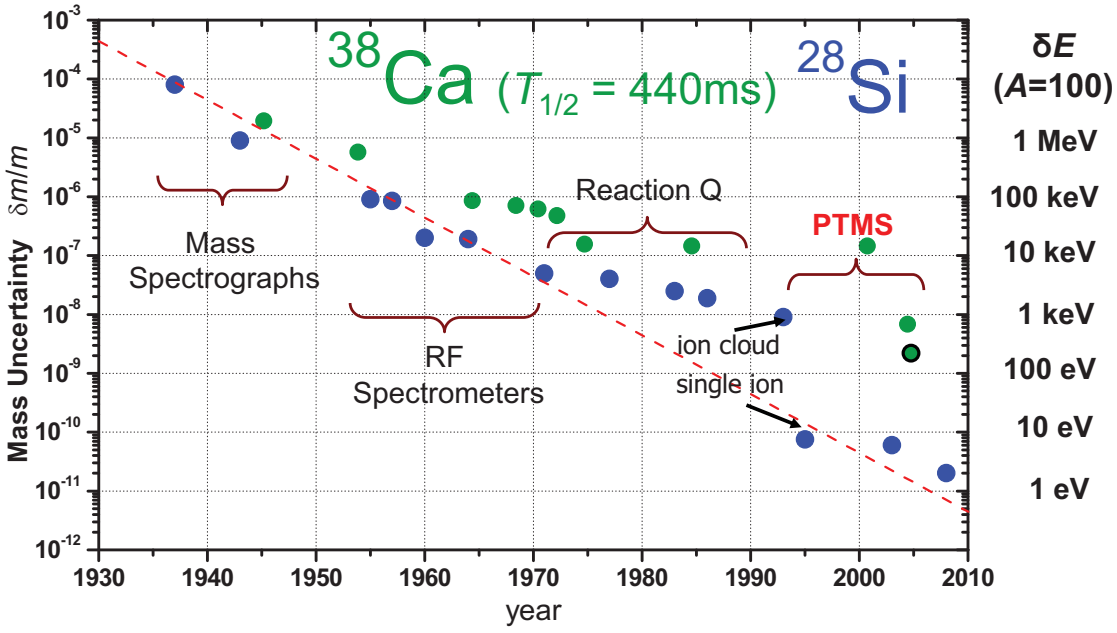

MAX PLANCK INSTITUTE FOR NUCLEAR PHYSICS

Penning trap mass spectrometers worldwide

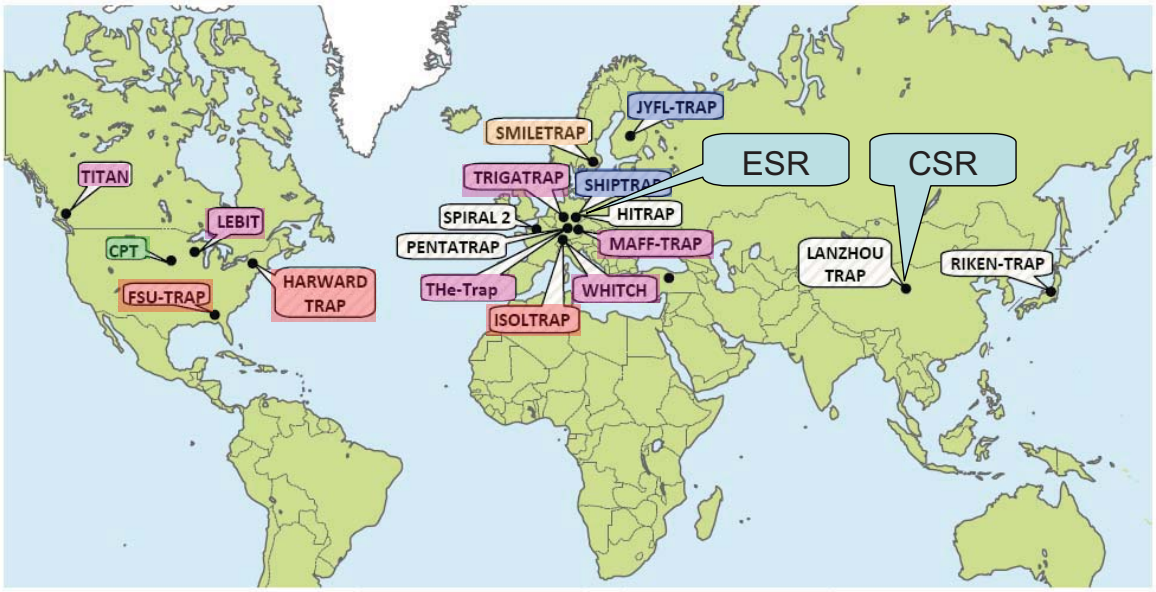

In operation since 1989 1993 1999 2004 2009

(rest under construction)

Storage rings for MS

MAX PLANCK INSTITUTE FOR NUCLEAR PHYSICS

MAX PLANCK INSTITUTE FOR NUCLEAR PHYSICS

Principle of storage ring and Penning trap mass spectrometry

MAX PLANCK INSTITUTE FOR NUCLEAR PHYSICS

Storage ring mass spectrometry

Schottky Mass Spectrometry

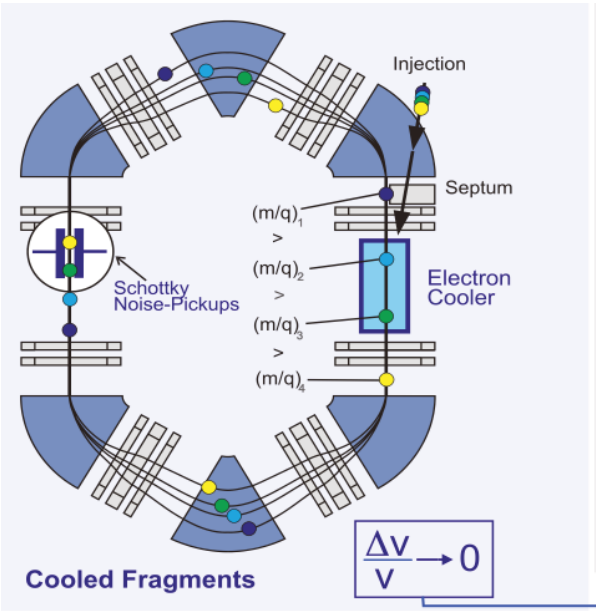

Isochronous Mass Spectrometry

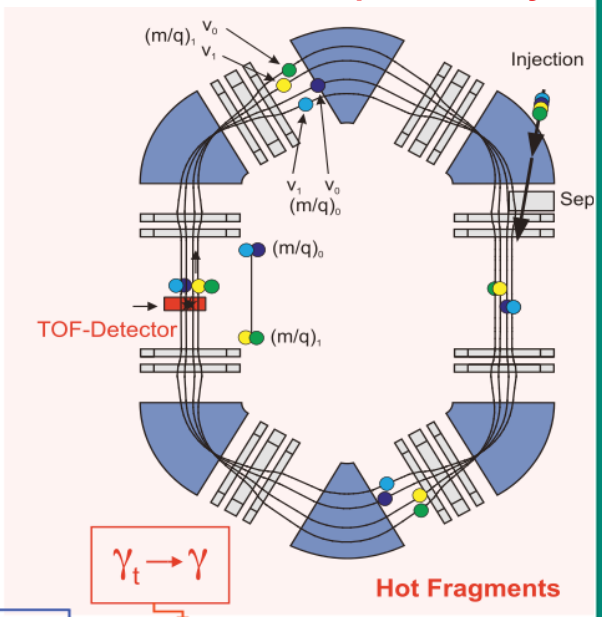

$$\frac{\Delta f}{f} = -\frac{1}{\gamma_t^2}\frac{\Delta(m/q)}{m/q} + \frac{\Delta v}{v}\left(1-\frac{\gamma^2}{\gamma_t^2}\right)$$

B. Franzke, H. Geissel & G. Münzenberg, Mass Spectrometry Reviews 27 (2008) 428

Principle of Penning trap mass spectrometry

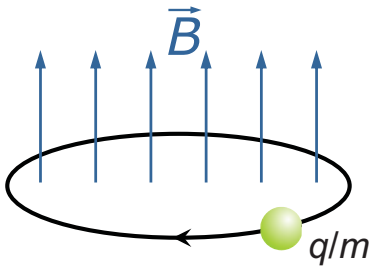

Cyclotron frequency:

$$f_c = \frac{1}{2\pi} \cdot \frac{q}{m} \cdot B$$

PENNING trap

- Strong homogen. magnetic field
- Weak electric 3D quadrupole field

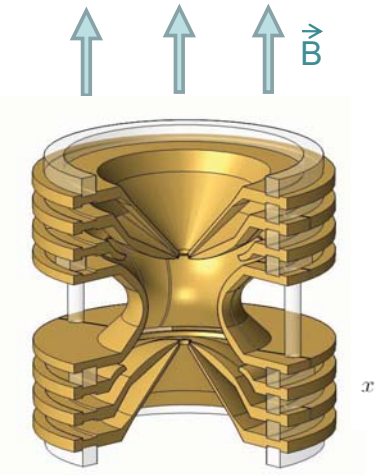

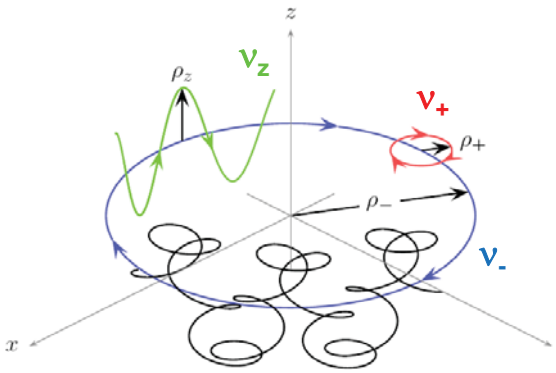

Typical freq.
q = e
m = 100 u
B = 6 T

$\Rightarrow$ f_- ≈ 1kHz
f_+ ≈ 1MHz

MAX PLANCK INSTITUTE FOR NUCLEAR PHYSICS

TOF cyclotron resonance detection

(3) TOF measurement

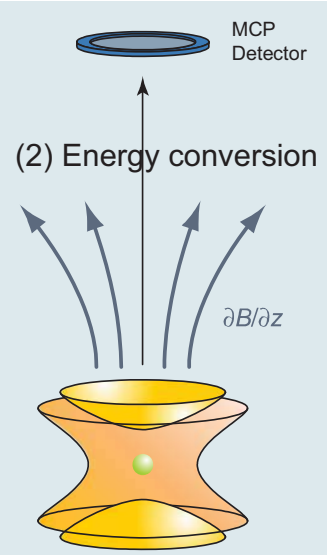

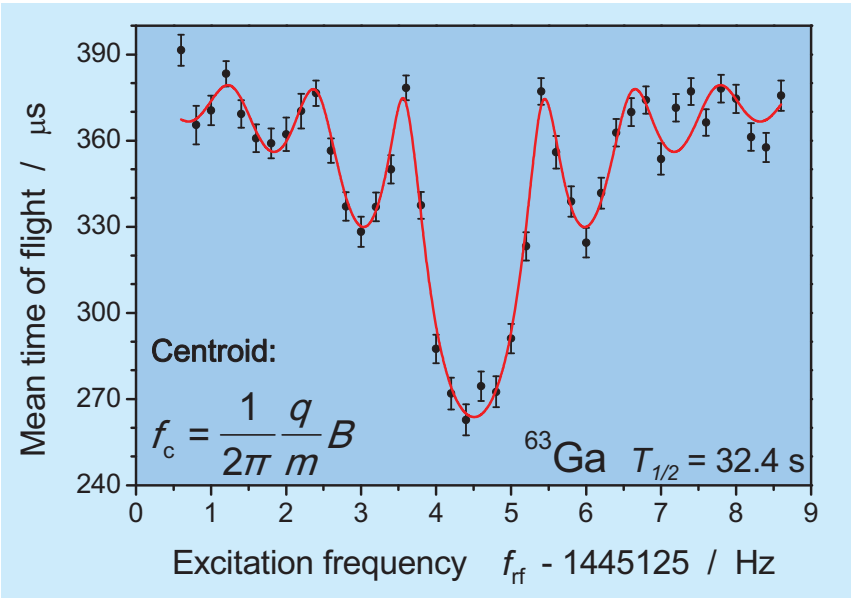

Determine atomic mass from frequency ratio with a well-known "reference mass".

$$\frac{f_{c,ref}}{f_c} = \frac{m - m_e}{m_{ref} - m_e}$$

TRIGA-SPEC: TRIGA-LASER + TRIGA-TRAP

project start @ TRIGA: 01/08
start data taking: 05/09

steady 100 kW,
pulsed 250 MW,
neutron flux 1.8x10^{11} / cm^{2}s

Nucl. Instrum. Meth. A 594, 162 (2008)

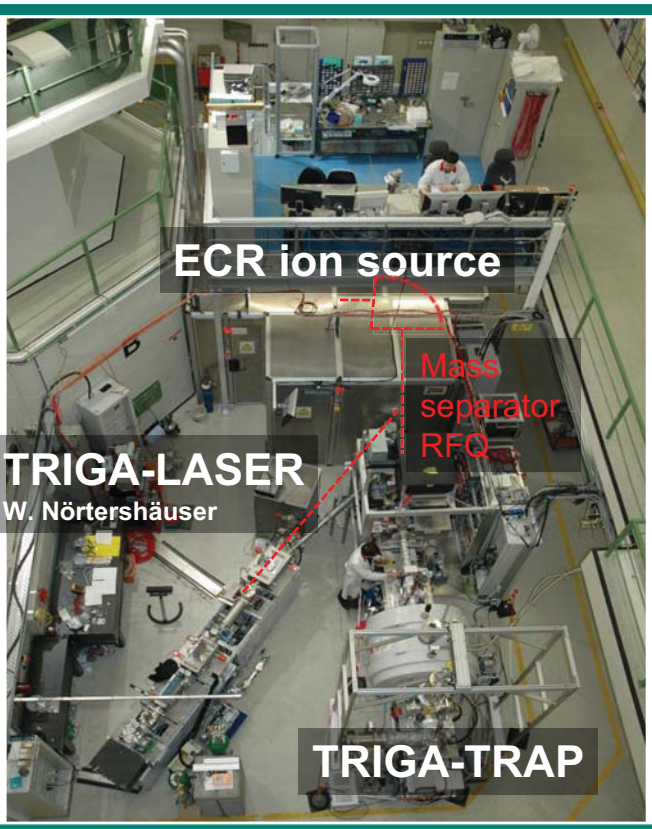

MAX PLANCK INSTITUTE FOR NUCLEAR PHYSICS

The TRIGA-TRAP experiment

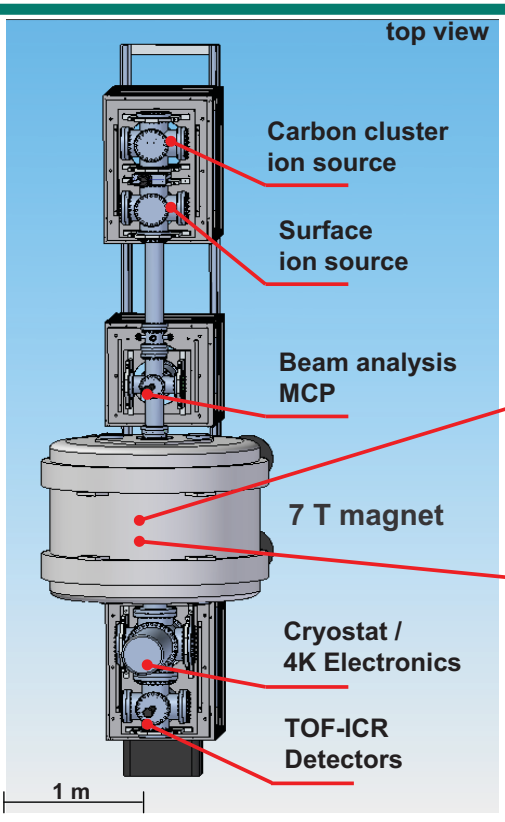

Purification trap:

- Cleaning of unwanted ion species by buffer-gas cooling
- Preparation of a mono-isotopic ion bunch

Precision trap:

- High-precision mass measurements with single ions

MAX PLANCK INSTITUTE FOR NUCLEAR PHYSICS

MAX PLANCK INSTITUTE FOR NUCLEAR PHYSICS

Performance
- Sensitivity
- Resolution
- Precision

Non-destructive ion detection

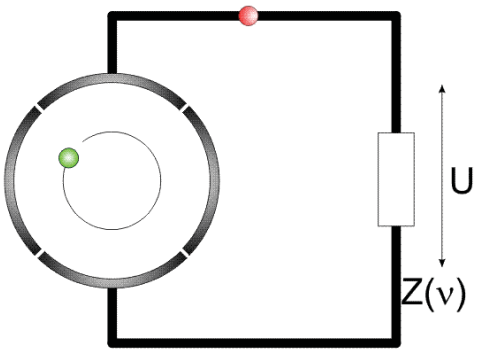

ion signal

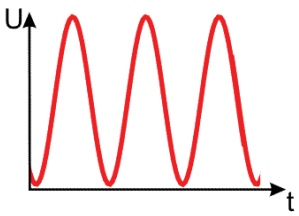

very small signal ~fA

mass/frequency spectrum

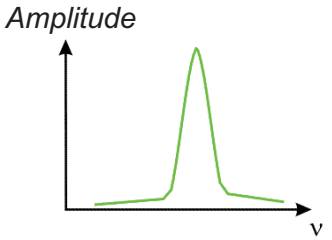

„FT-ICR“
Fourier-**T**ransform-
Ion **C**yclotron **R**esonance

Induced current: $I_{eff} = 1/\sqrt{2} \cdot r_{ion} / D \cdot \omega \cdot q$

(Schottky et al. ...)

Signal / Noise $S/N \sim 1 / T^{1/2}$

Operation of traps and electronics at **cryogenic** (4 K) temperature.

Single ion sensitivity

MAX PLANCK INSTITUTE FOR NUCLEAR PHYSICS

Schottky detection in a storage ring

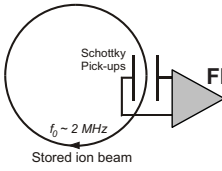

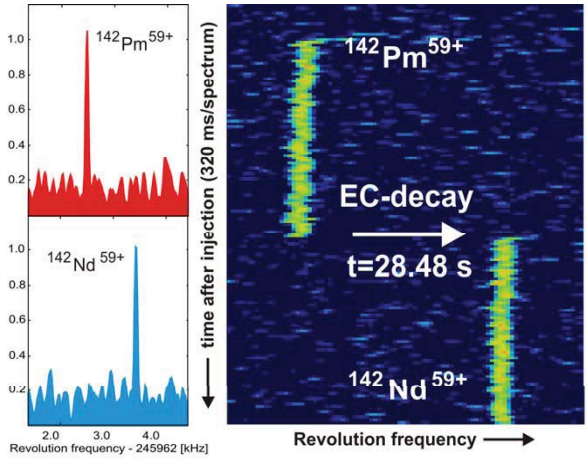

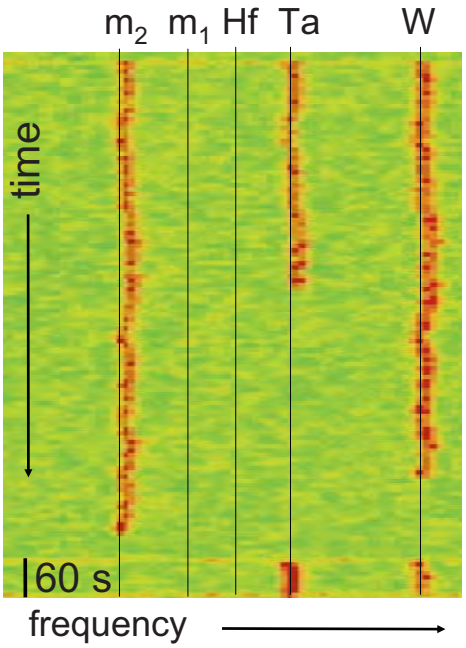

Discovery of new isotopes and isomers.

Hf: Phys. Rev. Lett. 105 (2010) 172501

Single ion sensitivity

MAX PLANCK INSTITUTE FOR NUCLEAR PHYSICS

Schottky detection in a storage ring

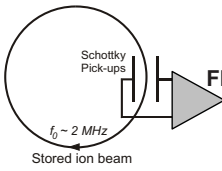

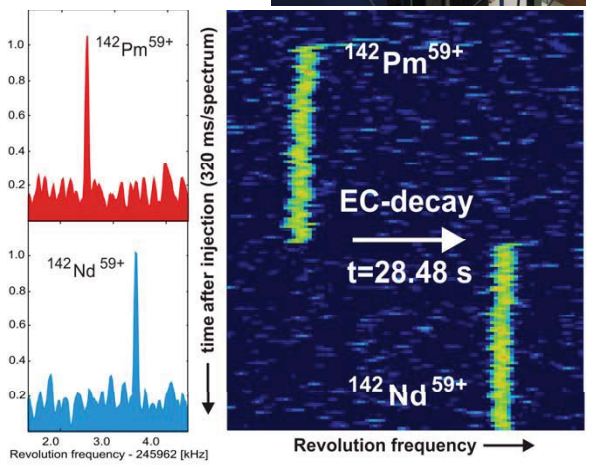

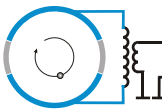

Narrow band FT-ICR in a Penning trap

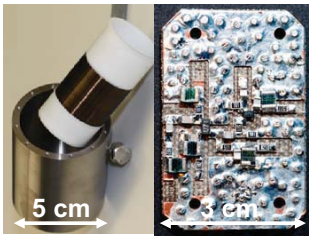

$T = 4$ K
$P = 5.5$ mW
$e_n = 400$ pV/$\sqrt{\text{Hz}}$
$i_n < 2$ fA/$\sqrt{\text{Hz}}$
$\nu_z = 600$ kHz

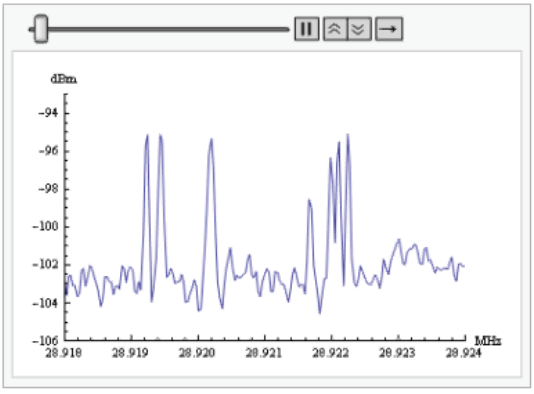

Separation of isomeric states

Isomerism in ^{68}Cu:

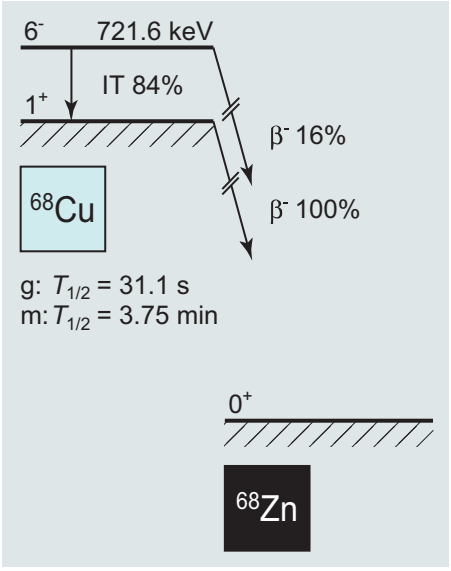

as produced by ISOLDE

isolation of the 1^+ ground state

isolation of the 6^- isomeric state

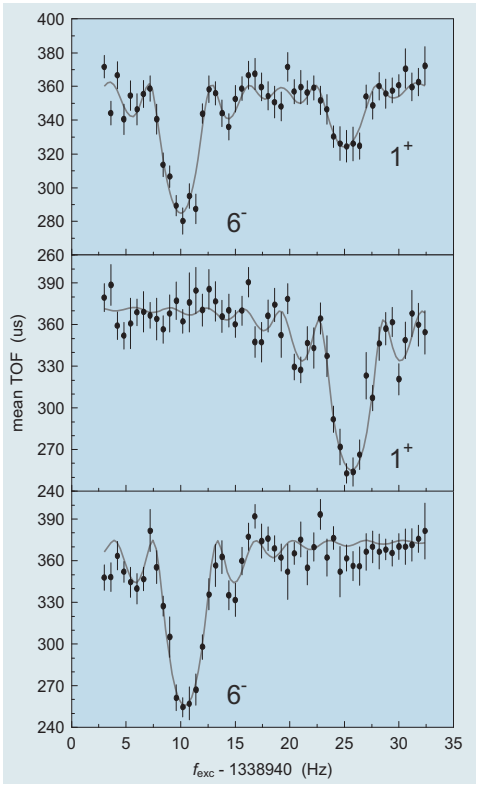

Resolving power of excitation: $R \approx 10^7$

$\Rightarrow$ Population inversion of nuclear states

$\Rightarrow$ Preparation of an isomerically pure beam

K. Blaum *et al.*, Europhys. Lett. 67, 586 (2004)

MAX PLANCK INSTITUTE FOR NUCLEAR PHYSICS

The discovery of a new isomer, ^{65m}Fe

E_{ex} = 402(10) keV

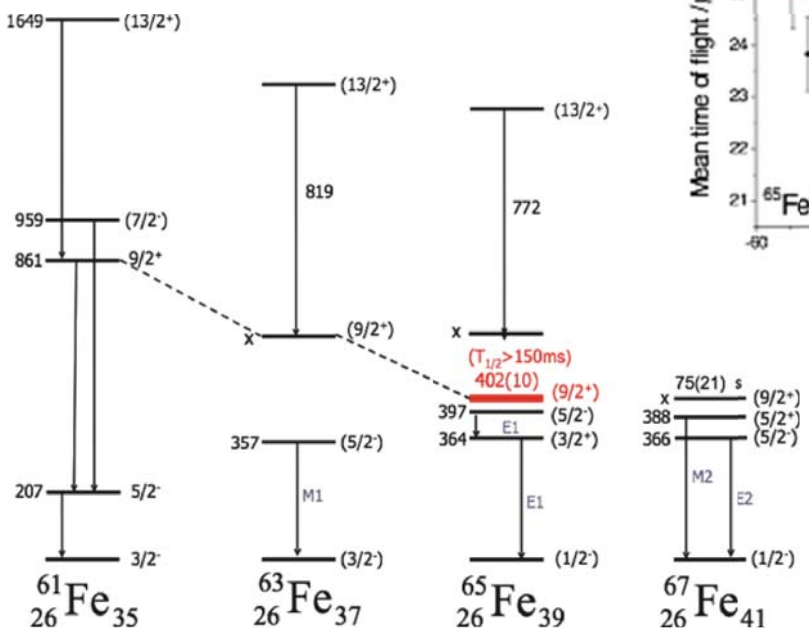

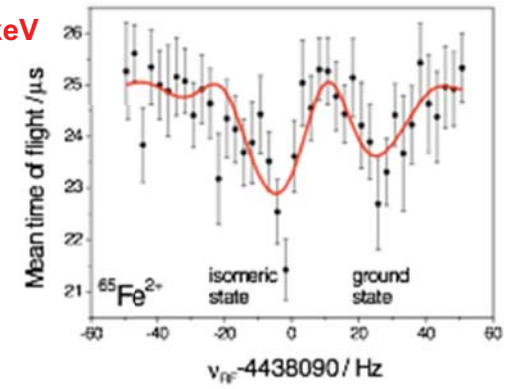

tentative level scheme including new isomeric state in ^{65}Fe[1,2]

LEBIT (MSU)

M. Block *et al.*, Phys. Rev. Lett. 100, 132501 (2008)

MAX PLANCK INSTITUTE FOR NUCLEAR PHYSICS

Applications:

Test of nuclear mass models

MAX PLANCK INSTITUTE FOR NUCLEAR PHYSICS

Mass uncertainty in the latest AME-2011

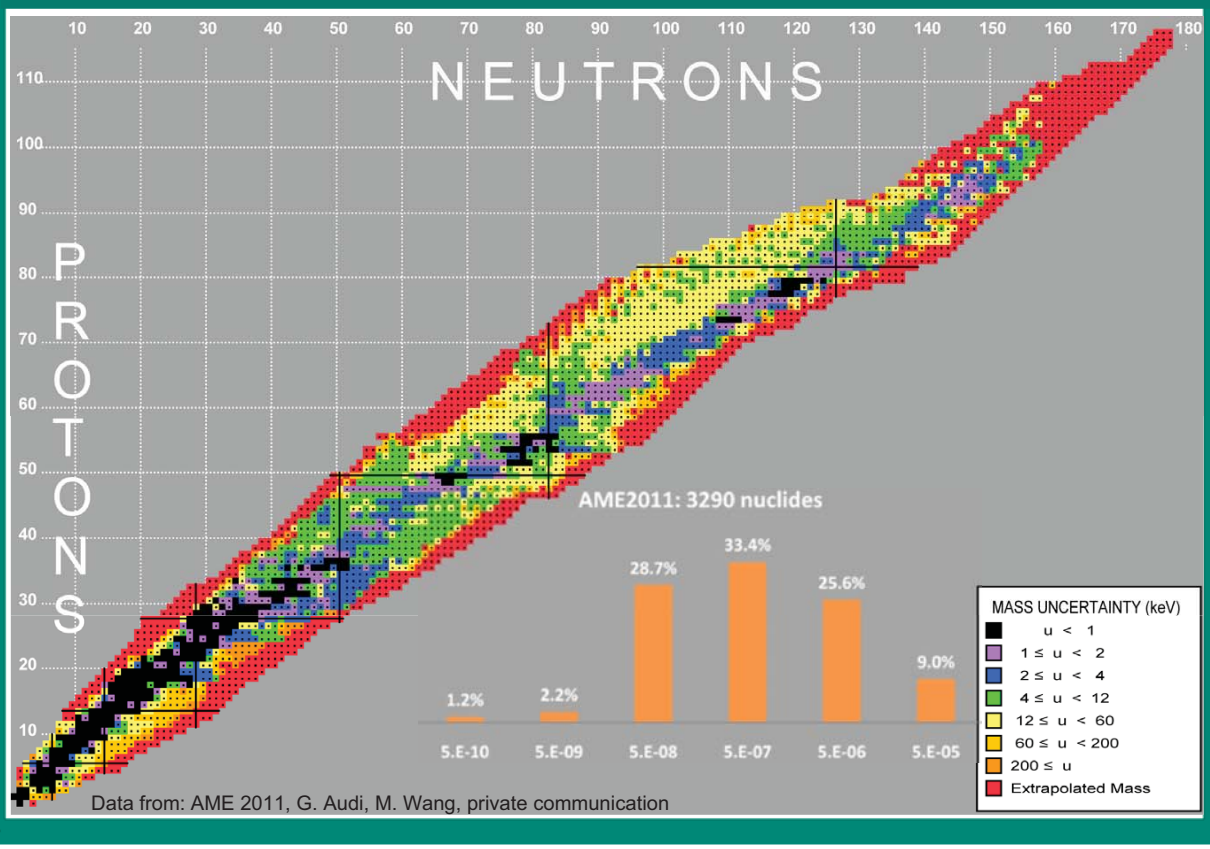

Data from: AME 2011, G. Audi, M. Wang, private communication

On the limits of nuclear existence: n drip-line

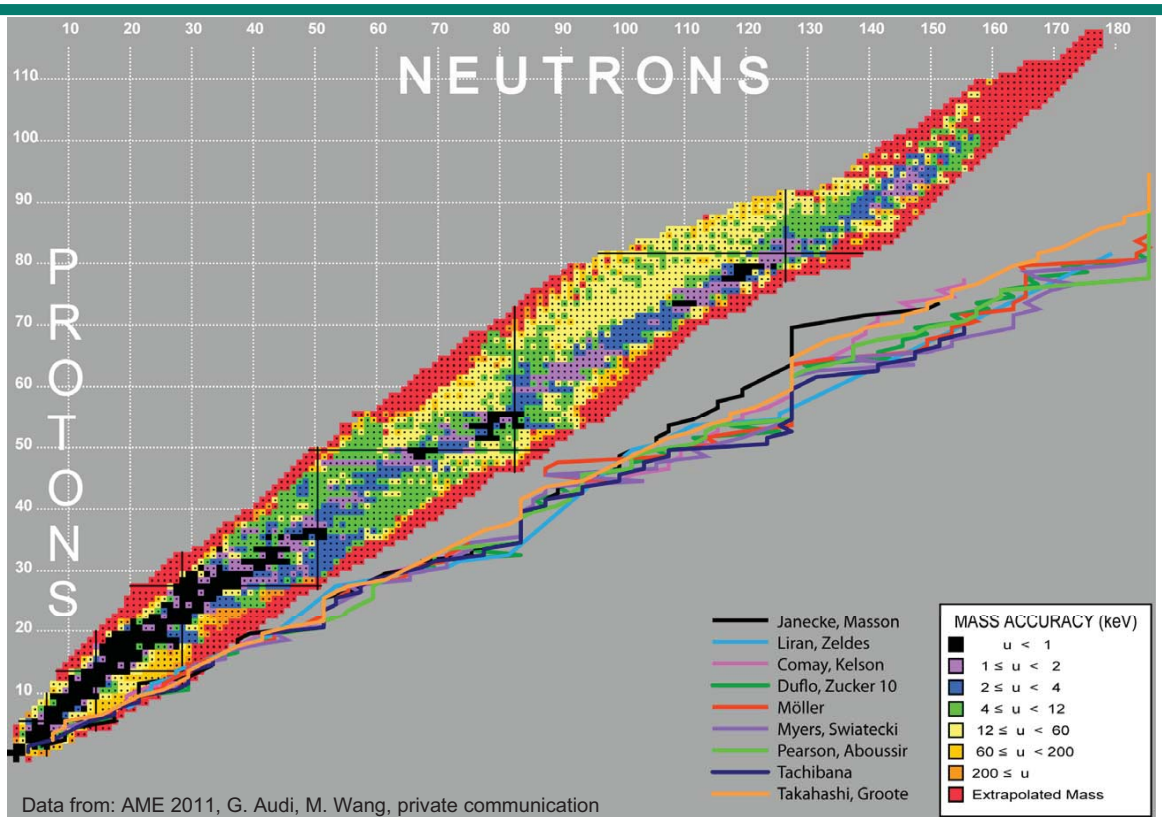

MAX PLANCK INSTITUTE FOR NUCLEAR PHYSICS

Test of nuclear mass models

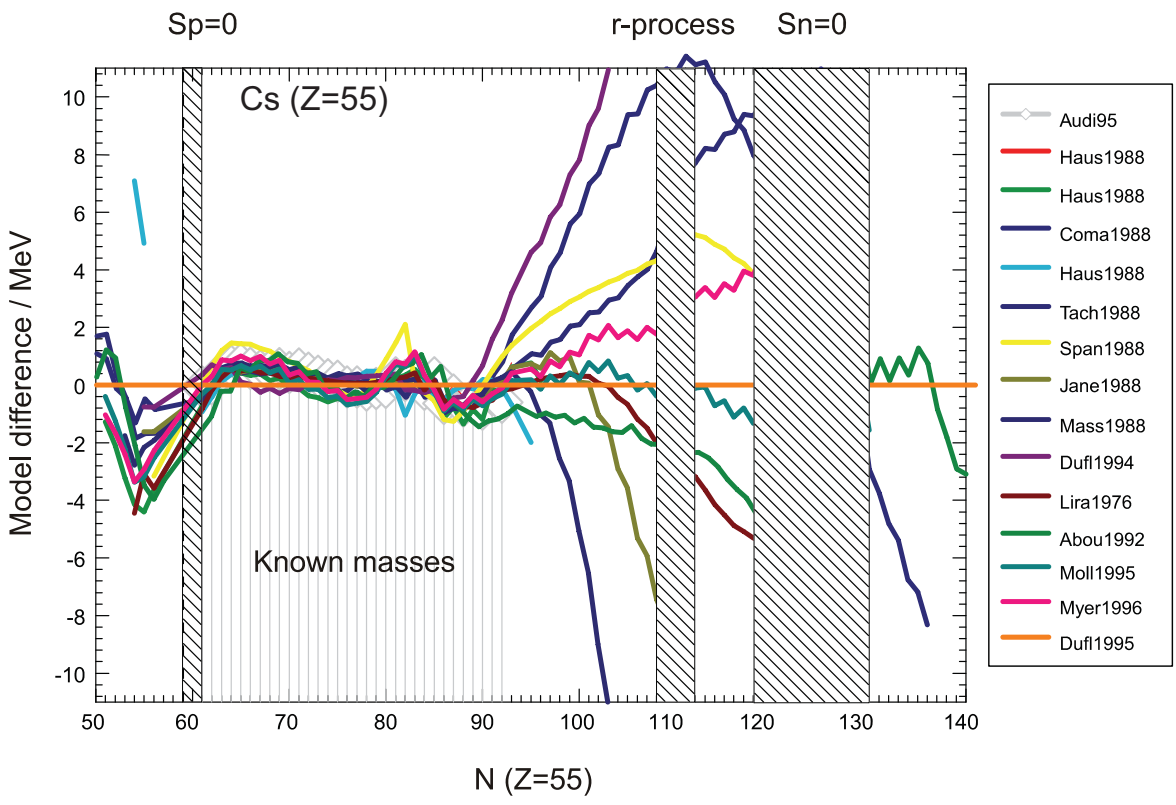

MAX PLANCK INSTITUTE FOR NUCLEAR PHYSICS

Isobaric Multiplet Mass Equation

Mass formula for multiplets of nuclear states with same mass and isospin

$M = a + bT_z + cT_z^2$ $+ dT_z^3$

Commonly used quadratic form

?

A = 33, T = 3/2 quartet:

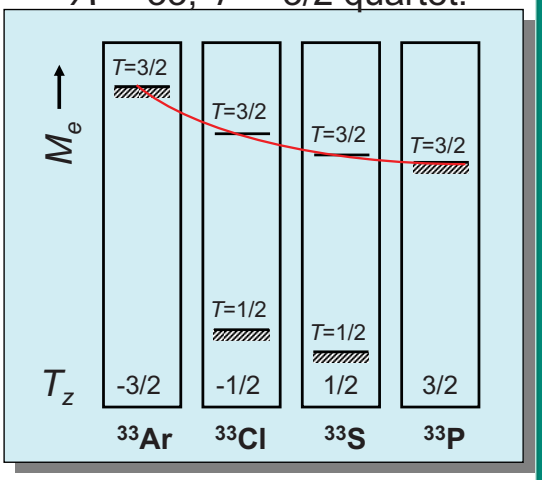

ISOLTRAP (ISOLDE), JYFLTRAP (Jyväskylä)

Most stringent test of IMME

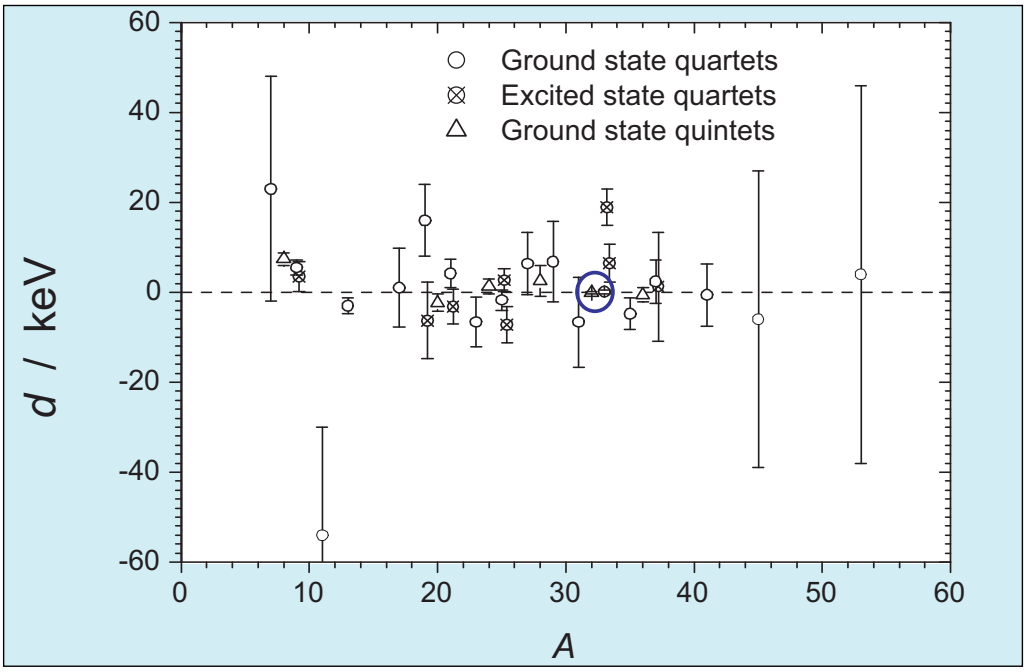

ISOLTRAP measurements 2002:

- ^{33}Ar with $u(m)$ = 0.44 keV
- ^{32}Ar with $u(m)$ = 1.8 keV

New status: K. B. *et al.*, Phys. Rev. Lett. 91, 260801 (2003).

A = 33, T = 3/2 quartet: d = -0.13(45) keV

A = 32, T = 2 quintet: d = -0.11(30) keV

MAX PLANCK INSTITUTE FOR NUCLEAR PHYSICS

End of Lecture I

MAX PLANCK INSTITUTE FOR NUCLEAR PHYSICS

Beijing, ISSSP 2011

"Precision Mass Measurements of Short-Lived Radionuclides PART 2: APPLICATIONS"

Klaus Blaum

August 30, 2011

MAX-PLANCK-INSTITUT FÜR KERNPHYSIK

EMMI

GSI

JOHANNES GUTENBERG UNIVERSITÄT MAINZ

Klaus.blaum@mpi-hd.mpg.de

MAX PLANCK INSTITUTE FOR NUCLEAR PHYSICS

Applications:

Nuclear structure studies

MAX PLANCK INSTITUTE FOR NUCLEAR PHYSICS

Applications of precision masses

High-accuracy mass measurements allow one to determine the atomic and nuclear binding energies reflecting all forces in the atom/nucleus.

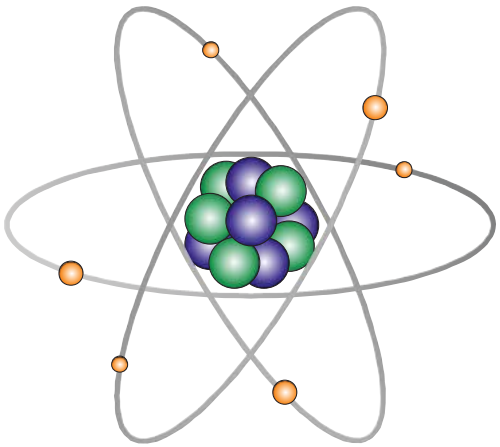

– binding energy

$$M_{Atom} = N \cdot m_{neutron} + Z \cdot m_{proton} + Z \cdot m_{electron} - (B_{atom} + B_{nucleus})/c^2$$

Nuclear structure studies

MAX PLANCK INSTITUTE FOR NUCLEAR PHYSICS

$S_p = B(Z,N) - B(Z\text{-}1,N)$

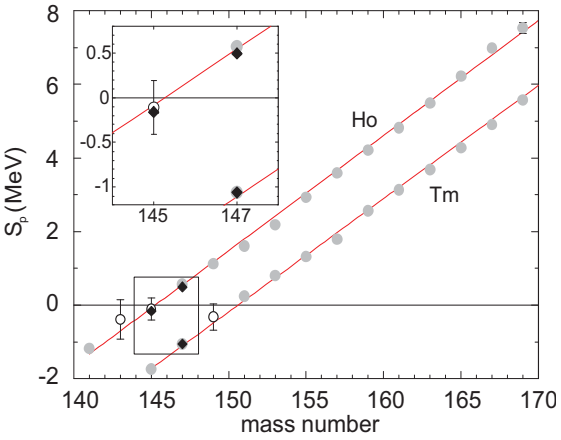

SHIPTRAP: First direct mass measurement beyond the proton dripline.

C. Rauth *et al.*, Phys. Rev. Lett. 100, 012501 (2008)
M. Dworschak *et al.*, Phys. Rev. Lett. 100, 072501 (2008)
W. Geithner *et al.*, Phys. Rev. Lett. 101, 252502 (2008)
J. Hakala *et al.*, Phys. Rev. Lett. 101, 052502 (2008)

$S_{2n} = B(Z,N) - B(Z,N\text{-}2)$

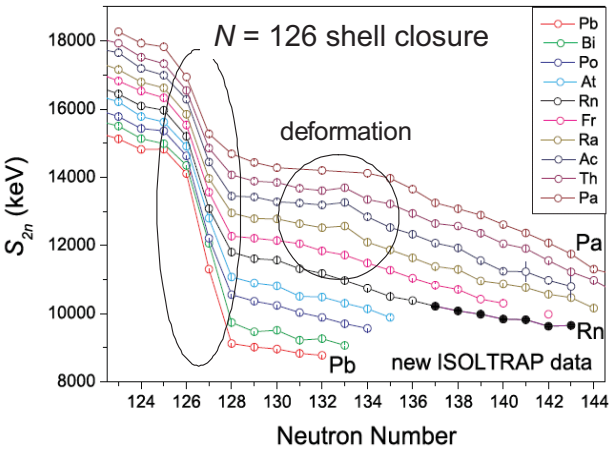

CPT/ISOLTRAP/JYFLTRAP/LEBIT/TITAN: Investigation of shell closures, halos, …

B. Cakirli *et al.*, Phys. Rev. Lett. 102, 082501 (2009)
D. Neidherr *et al.*, Phys. Rev. Lett. 102, 112501 (2009)
J.S.E. Wieslander *et al.*, Phys. Rev. Lett. 103, 122501 (2009)
S. Naimi *et al.*, Phys. Rev. Lett. 105, 032502 (2010)

Quantum phase transition

MAX PLANCK INSTITUTE FOR NUCLEAR PHYSICS

Nuclear mass measurements

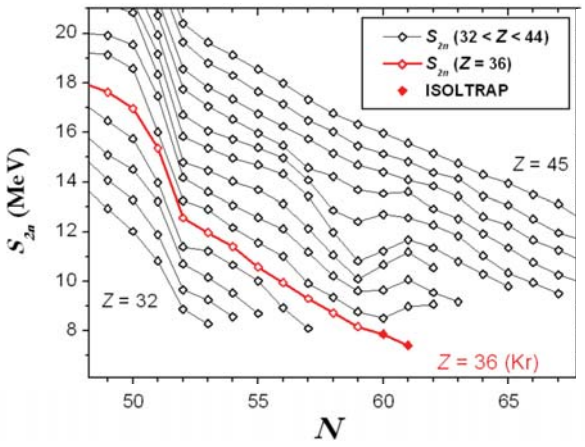

Nuclear charge radii measurements

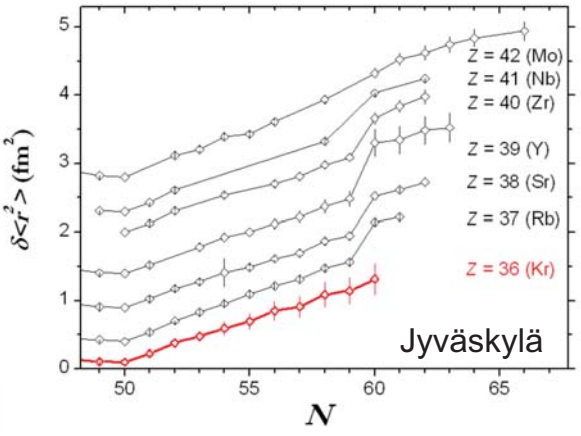

End of phase transition region reached: critical-point boundary

Kr masses: Phys. Rev. Lett. 105, 032502 (2010)
Kr charge radii: Phys. Rev. Lett. 102, 222501 (2009)

ISOLTRAP (ISOLDE)

FURIOS (IGISOL)

Experimental proton-neutron interaction

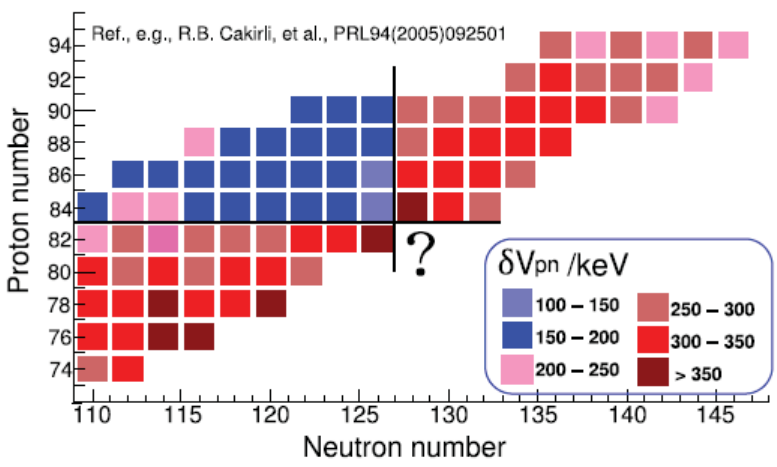

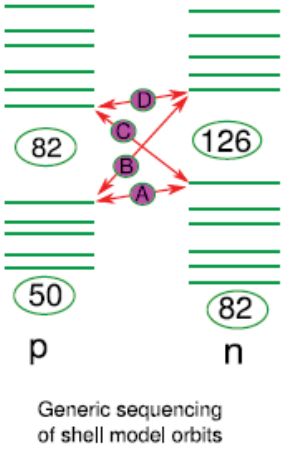

For even-even nuclei

$$\delta V_{pn}(Z,N) = \tfrac{1}{4}[\{B(Z,N) - B(Z,N-2)\} - \{B(Z-2,N) - B(Z-2,N-2)\}]$$

p-n interactions are sensitive to the spatial overlaps of the proton and neutron wave functions

MAX PLANCK INSTITUTE FOR NUCLEAR PHYSICS

Experimental proton-neutron interaction

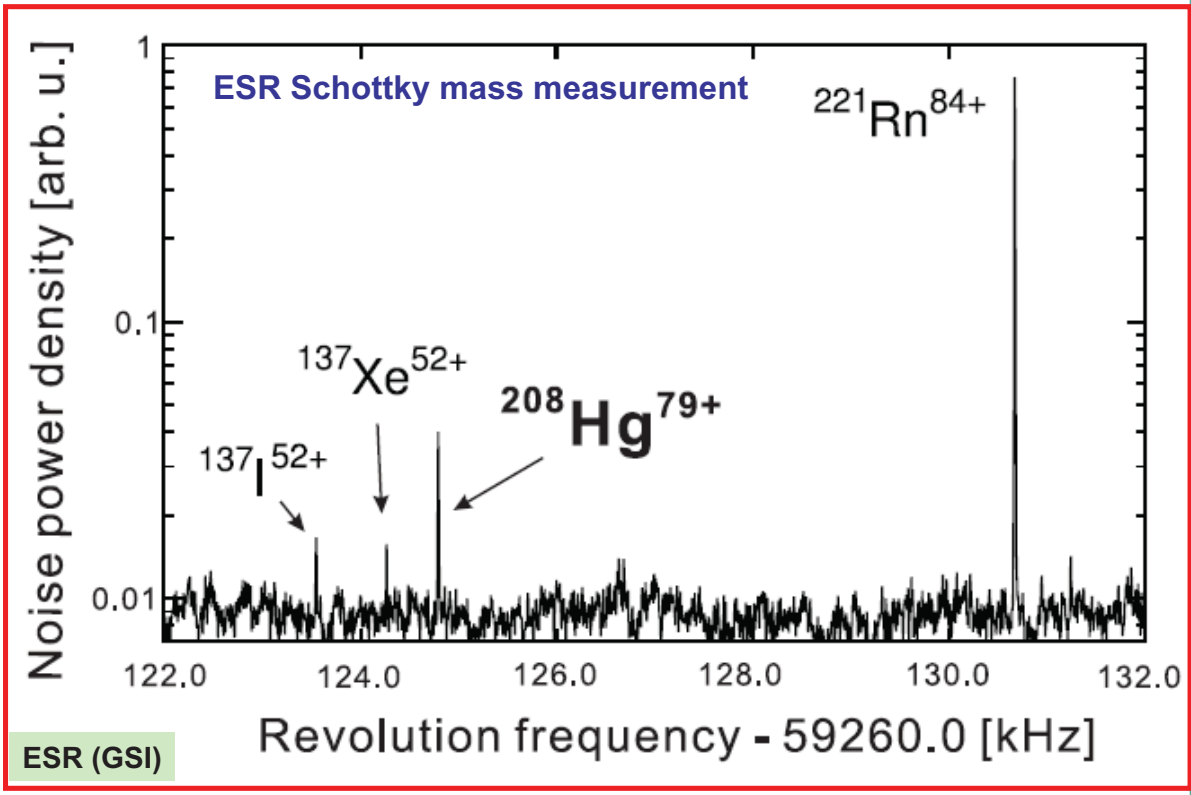

MAX PLANCK INSTITUTE FOR NUCLEAR PHYSICS

Experimental proton-neutron interaction

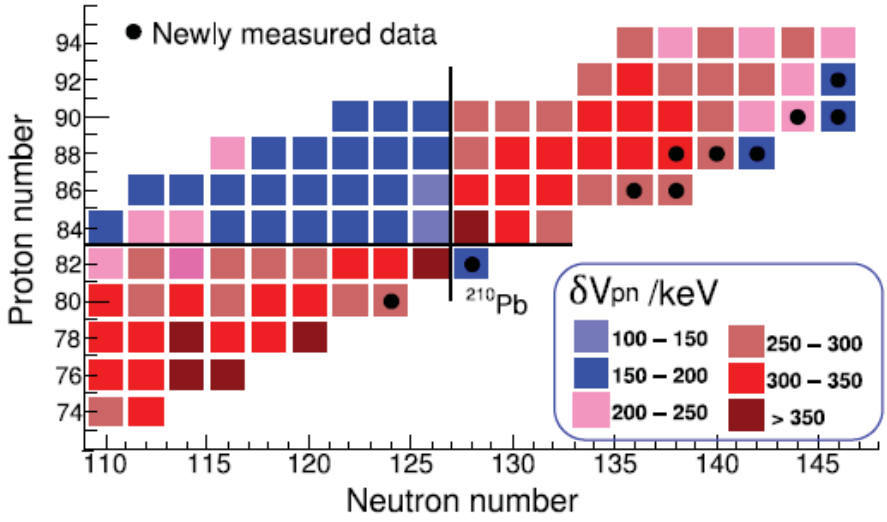

For even-even nuclei

$$\delta V_{pn}(Z,N) = \tfrac{1}{4}[\{B(Z,N)-B(Z,N-2)\}-\{B(Z-2,N)-B(Z-2,N-2)\}]$$

ESR (GSI)

L. Chen *et al.*, Phys. Rev. Lett. 102, 122503 (2009)

MAX PLANCK INSTITUTE FOR NUCLEAR PHYSICS

Experimental proton-neutron interaction

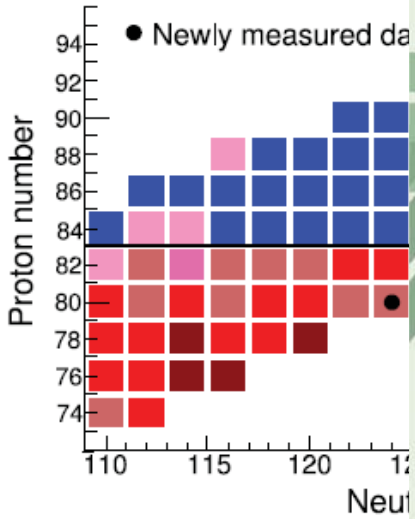

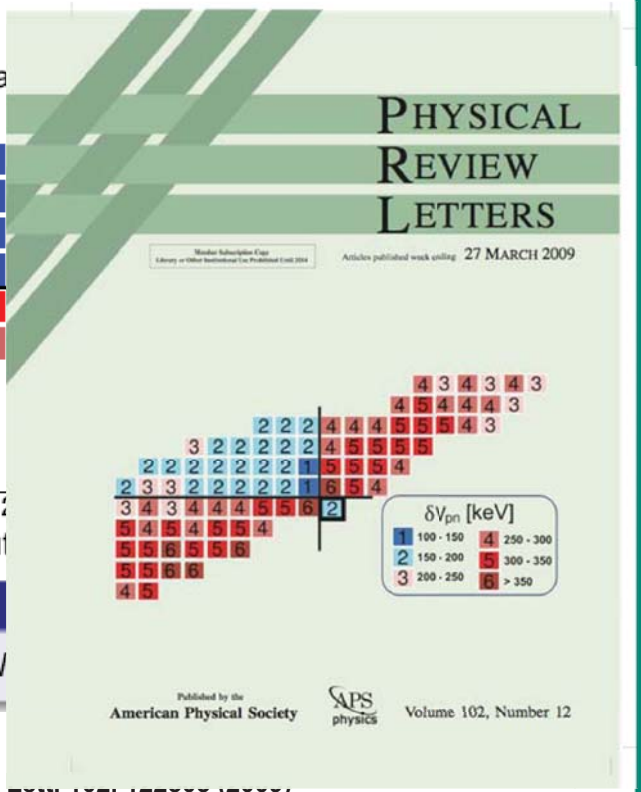

For even-even nuclei

$$\delta V_{pn}(Z,N) = \tfrac{1}{4}[\{B(Z,N)-B(Z,N$$

ESR (GSI)

L. Chen *et al.*, Phys. Rev.

Experiment – Theory (DFT)

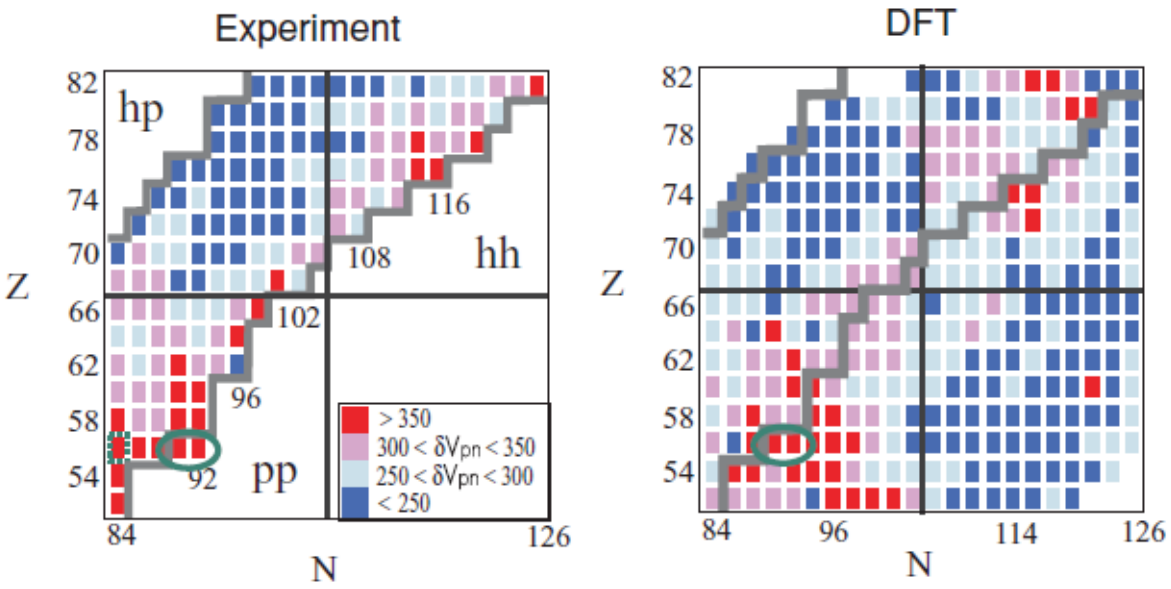

Excellent agreement on a few 10 keV level!

ISOLTRAP (ISOLDE)

D. Neidherr *et al.*, PRC 80, 044323 (2009)
M. Stoitsov *et al.*, PRL 98, 132502 (2007)

MAX PLANCK INSTITUTE FOR NUCLEAR PHYSICS

Direct mass measurements on No and Lr

M. Block et al., Nature 463, 785 (2010)
M. Dworschak et al., PRC 81, 064312 (2010)

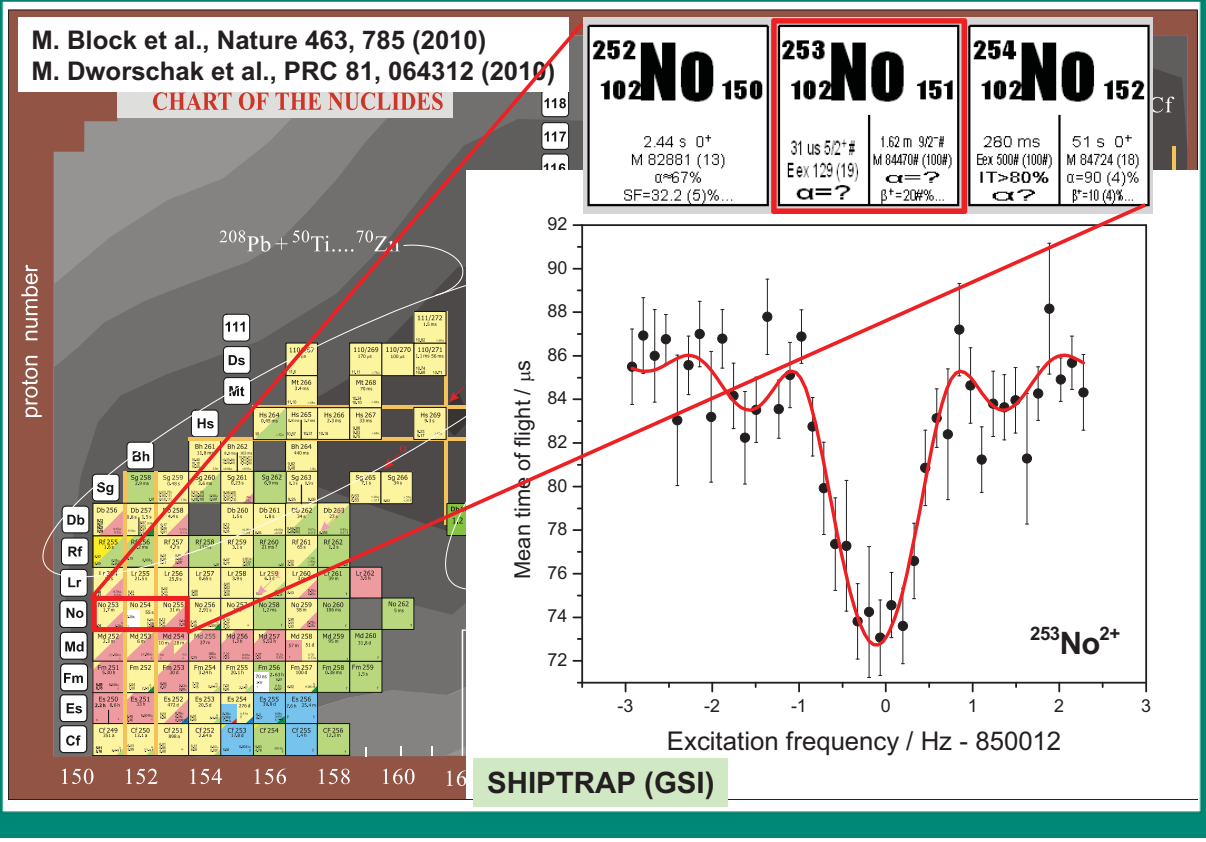

SHIPTRAP (GSI)

Direct mass measurements on No and Lr

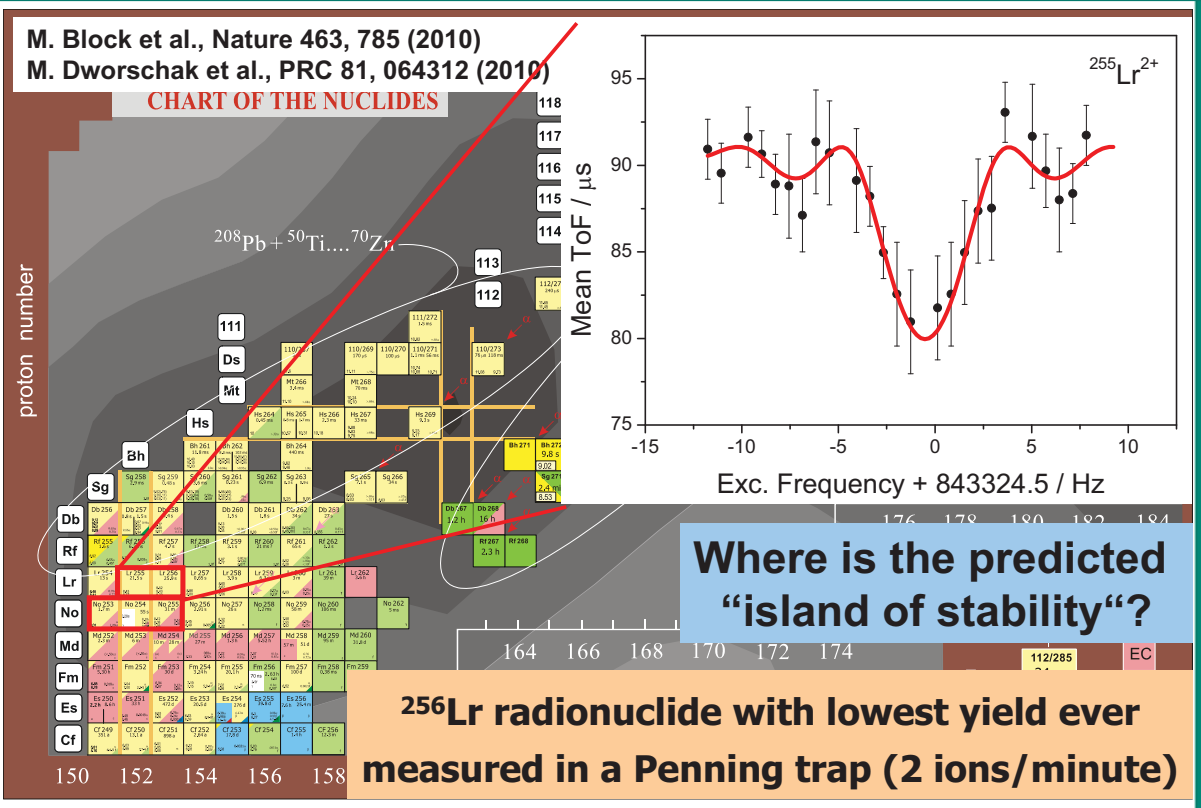

MAX PLANCK INSTITUTE FOR NUCLEAR PHYSICS

Applications:

Investigation of nuclear halos

Investigation of halo nuclides

MAX PLANCK INSTITUTE FOR NUCLEAR PHYSICS

characteristic properties of nuclear halos

large matter radius

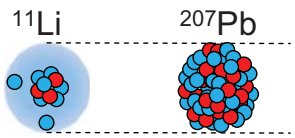

weakly bound

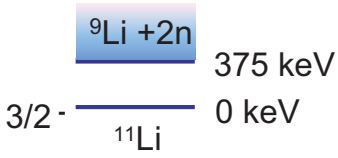

increased charge radius

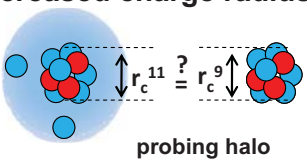

probing halo neutron – nucleus interaction

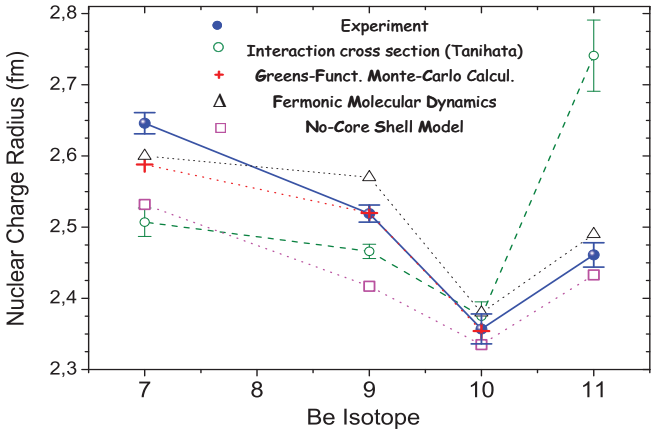

12Be

COLLAPS (ISOLDE)

[11]Be: Phys. Rev. Lett. 102, 062503 (2009)

„Size“ and structure determination of the neutron halos in [11,12]Be

Investigation of nuclear halos

MAX PLANCK INSTITUTE FOR NUCLEAR PHYSICS

… via nuclear mass (binding energy) and charge radii measurements!

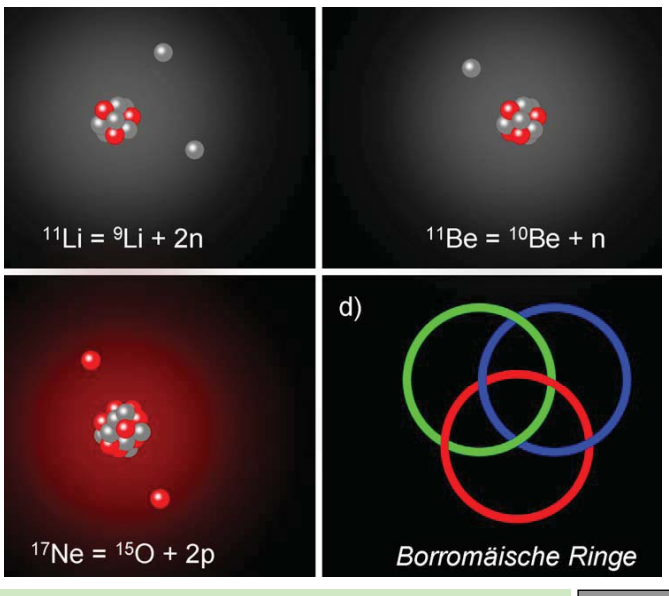

[6,8]He
P. Mueller *et al.*, PRL 99, 252501 (2007)
V.L. Ryjkov *et al.*, PRL 101, 012501 (2008)

[9,11]Li:
R. Neugart *et al.*, PRL 101, 132502 (2008)
M. Smith *et al.*, PRL 101, 202501 (2008)

[11]Be:
W. Nörtershäuser *et al.*, PRL102, 062503 (2009)
R. Ringle *et al.*, PLB 675, 170 (2009)

[17]Ne:
W. Geithner *et al.*, PRL102, 252502 (2008)

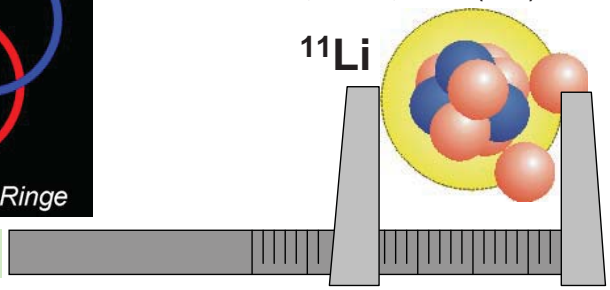

Argonne, GANIL, GSI, ISOLDE, TRIUMF

Investigation of nuclear halos

… via nuclear mass (binding energy) and charge radii measurements!

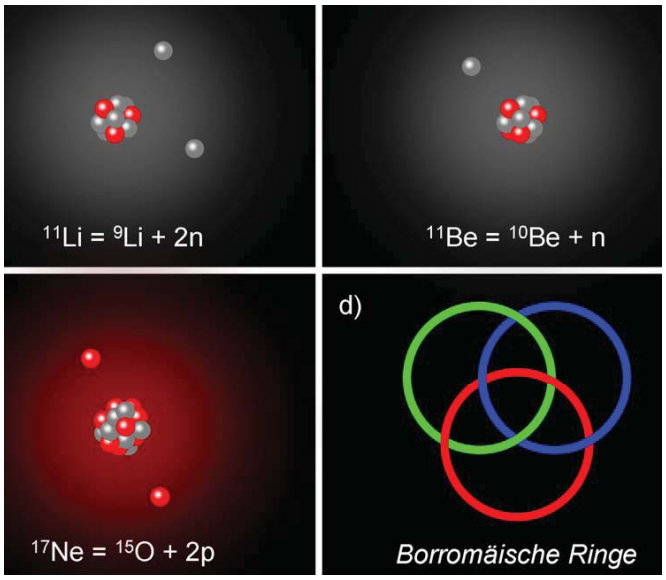

^{6,8}He
P. Mueller *et al.*, PRL 99, 252501 (2007)
V.L. Ryjkov *et al.*, PRL 101, 012501 (2008)

^{9,11}Li:
R. Neugart *et al.*, PRL 101, 132502 (2008)
M. Smith *et al.*, PRL 101, 202501 (2008)

^{11}Be:
W. Nörtershäuser *et al.*, PRL102, 062503 (2009)
R. Ringle *et al.*, PLB 675, 170 (2009)

^{17}Ne:
W. Geithner *et al.*, PRL102, 252502 (2008)

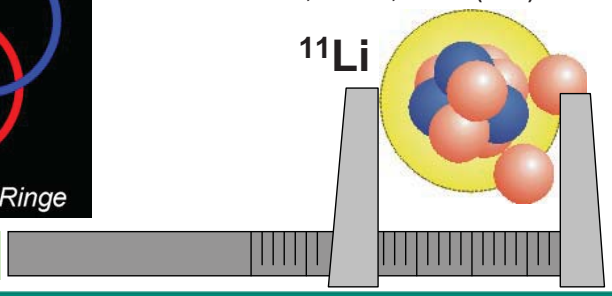

Argonne, GANIL, GSI, ISOLDE, TRIUMF

MAX PLANCK INSTITUTE FOR NUCLEAR PHYSICS

Applications:

Nuclear astrophysics

MAX PLANCK INSTITUTE FOR NUCLEAR PHYSICS

Nuclear astrophysics

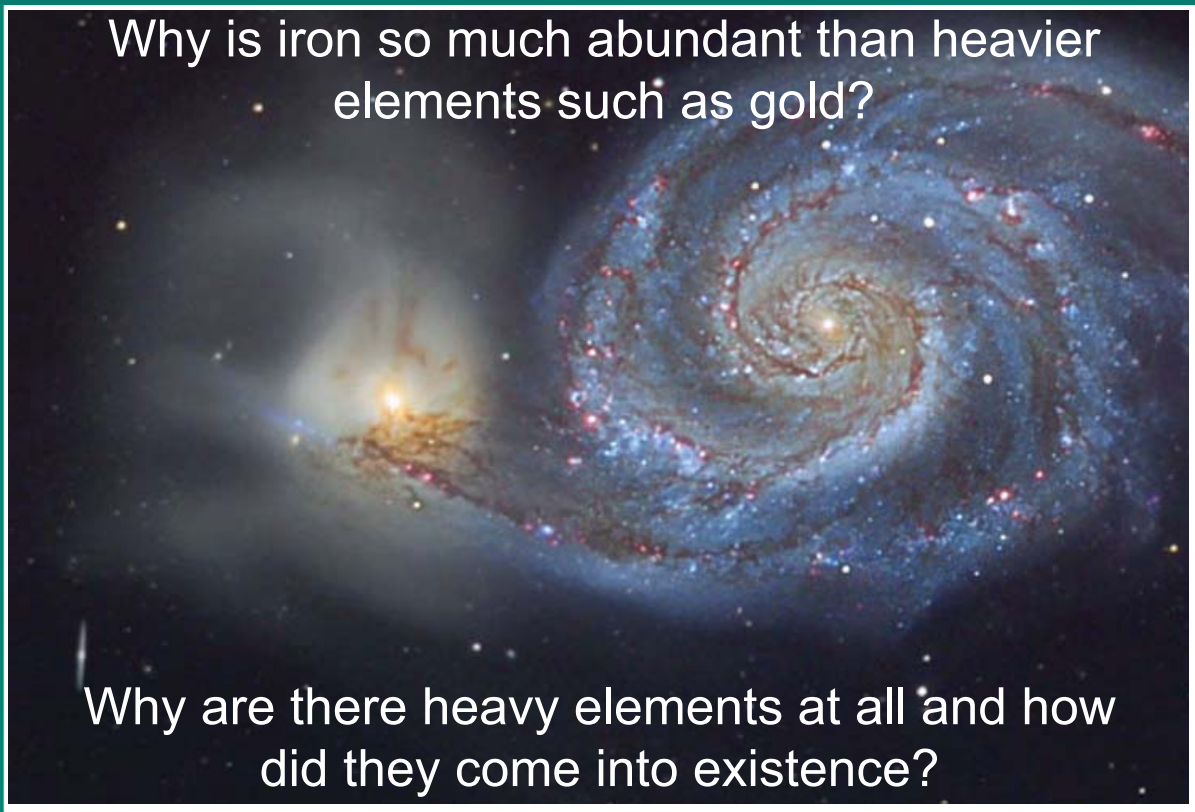

MAX PLANCK INSTITUTE FOR NUCLEAR PHYSICS

Nuclides at the rp-process path

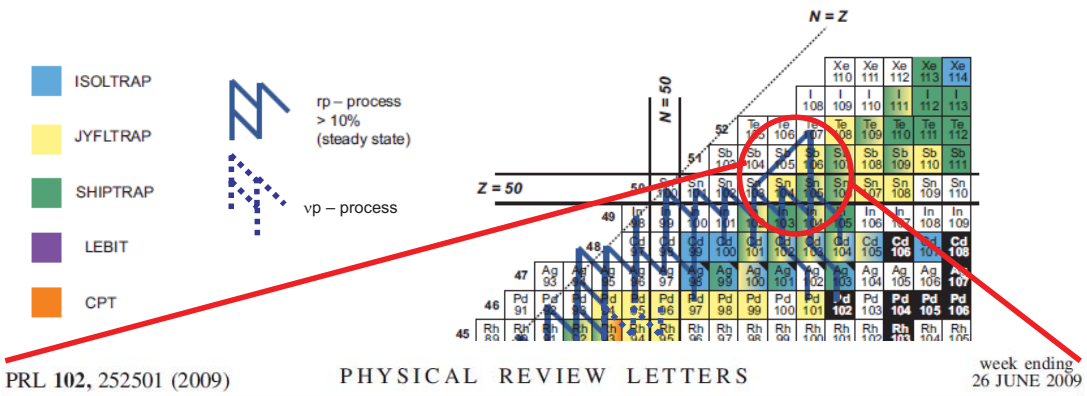

PRL 102, 252501 (2009) PHYSICAL REVIEW LETTERS week ending 26 JUNE 2009

Quenching of the SnSbTe Cycle in the *rp* Process

V.-V. Elomaa,[1,*] G. K. Vorobjev,[2,3] A. Kankainen,[1] L. Batist,[2] S. Eliseev,[2,3,†] T. Eronen,[1] J. Hakala,[1] A. Jokinen,[1] I. D. Moore,[1] Yu. N. Novikov,[2,3] H. Penttilä,[1] A. Popov,[2] S. Rahaman,[1,‡] J. Rissanen,[1] A. Saastamoinen,[1] H. Schatz,[4] D. M. Seliverstov,[2] C. Weber,[1,§] and J. Äystö[1]

[1]*Department of Physics, University of Jyväskylä, Post Office Box 35, FI-40014, Finland*

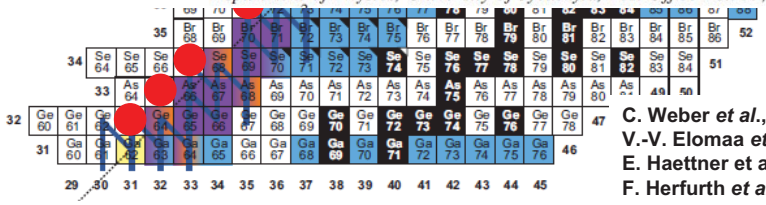

JYFLTRAP (IGISOL)

C. Weber *et al.*, Phys. Rev. C 78, 054310 (2008)
V.-V. Elomaa *et al.*, Phys. Rev. Lett. 102, 252501 (2011)
E. Haettner et al., Phys. Rev. Lett. 106, 122501 (2011)
F. Herfurth *et al.*, Eur. Phys. J. A 47, 75 (2011)

Nuclides at the rp-process


NATURE PHYSICS

NUCLEAR ASTROPHYSICS

Star bursts pinned down

One of the main uncertainties in the burn-up of X-ray bursts from neutron stars has been removed with the weighing of a key nucleus, ^{65}As, at a new ion storage ring.

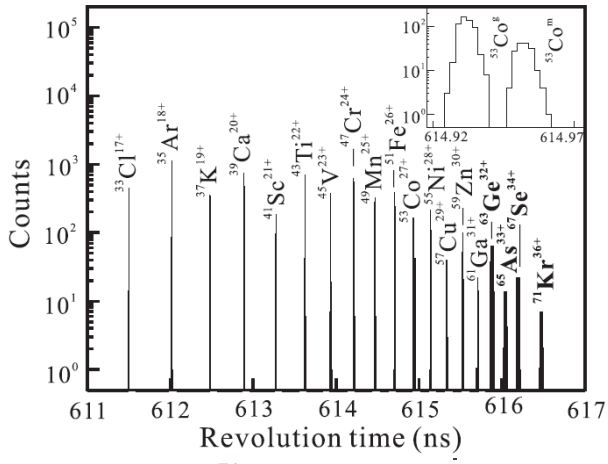

Rate of ^{71}Kr was just 2 ions/day

New masses: ^{63}Ge, ^{65}As, ^{67}Se, and ^{71}Kr

X. Tu *et al.*, Phys. Rev. Lett. 106, 112501 (2011)

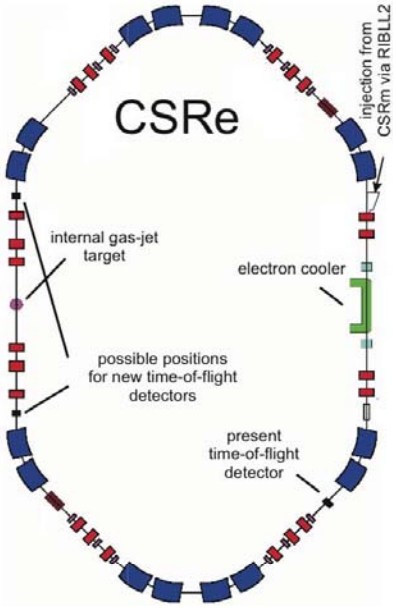

CSRe (IMP, Lanzhou)

r-process: Impact of IMS-ESR results

Isochronus-Mass-Spectrometry

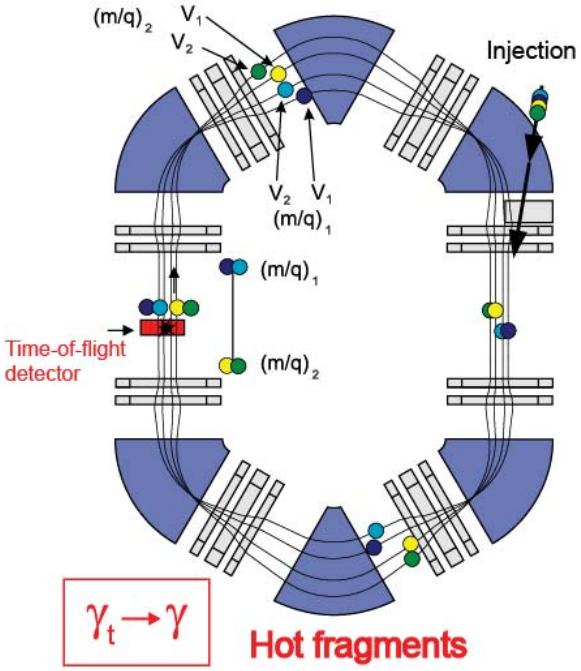

ESR (GSI)

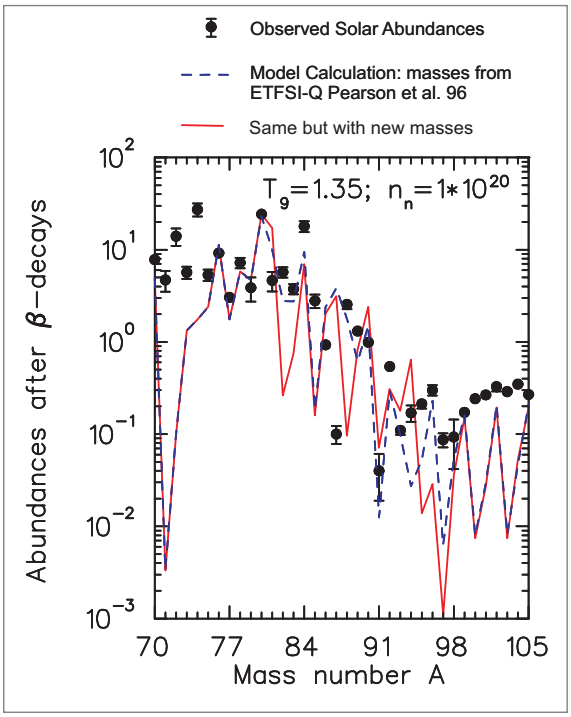

B. Pfeiffer, GSI Report 2006-03

MAX PLANCK INSTITUTE FOR NUCLEAR PHYSICS

Applications:

Neutrino physics

MAX PLANCK INSTITUTE FOR NUCLEAR PHYSICS

Neutrino-less double EC (0ν2*EC*)

Is the neutrino a Majorana or Dirac particle?

2ν2EC ($T_{1/2}$>10^{24}y) *0ν2EC* ($T_{1/2}$>10^{30}y)

$$\frac{1}{T_{1/2}} = C \times m_\nu^2 \times |M|^2 \times |\Psi_{1e}|^2 \times |\Psi_{2e}|^2 \times \frac{\Gamma}{(Q - B_{2h} - E_\gamma)^2 + \frac{1}{4}\Gamma^2}$$

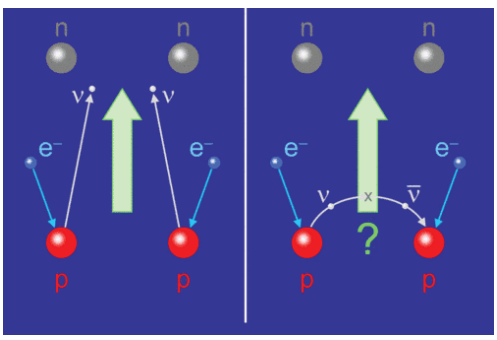

SHIPTRAP (GSI), JYFLTRAP (IGISOL), ISOLTRAP (ISOLDE)

Neutrino-less double EC (0ν2*EC*)

Is the neutrino a Majorana or Dirac particle?

2ν2EC ($T_{1/2}$>10^{24}y) *0ν2EC* ($T_{1/2}$>10^{30}y)

$$\frac{1}{T_{1/2}} = C \times m_\nu^2 \times |M|^2 \times |\Psi_{1e}|^2 \times |\Psi_{2e}|^2 \times \frac{\Gamma}{(Q - B_{2h} - E_\gamma)^2 + \frac{1}{4}\Gamma^2}$$

0ν2EC might be resonantly enhanced ($T_{1/2}$~10^{25}y)

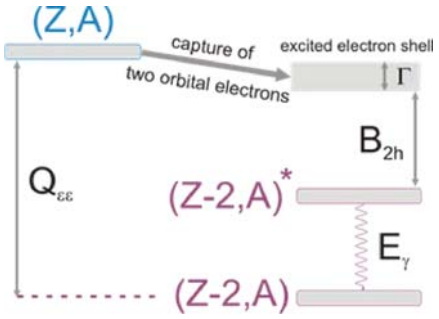

Contribution of Penning traps:

Search for nuclides with $\Delta=(Q_{\varepsilon\varepsilon}-B_{2h}-E_\gamma) < 1$ keV by measurements of $Q_{\varepsilon\varepsilon}$–values at ~100 eV accuracy level

Resonance enhancement factors

2*EC* - transition	Δ (old), keV	Δ (new), keV	$T_{1/2} \cdot m^2$, yr
^{152}Gd → ^{152}Sm	-0.2(3.5)	0.9(0.2)	10^{26}
^{164}Er → ^{164}Dy	5.2(3.9)	6.81(0.12)	10^{30}
^{180}W → ^{180}Hf	13.7(4.5)	12.4(0.2)	10^{27}

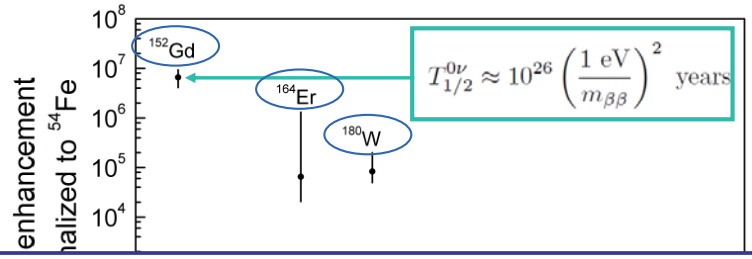

If $m_{\beta\beta}$ = 1 eV ⇒ 30 kg for 1 capture event a year

If $m_{\beta\beta}$ = 0.1 eV ⇒ 3 tons for 1 capture event a year

^{152}Gd can be used for a search for 0ν2EC

THe-TRAP for KATRIN

A high-precision $Q(^3T\text{-}^3He)$-value measurement

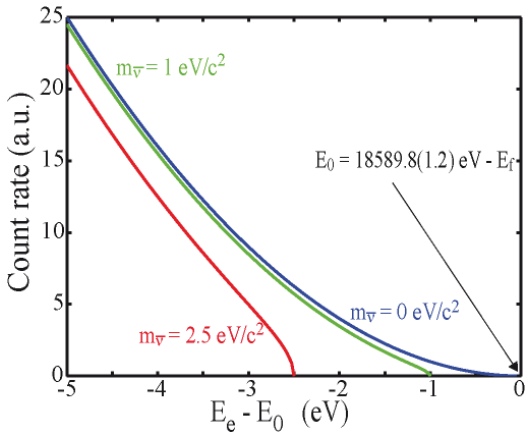

$^3_1H \rightarrow {}^3_2He + e^- + \bar{\nu}$ Q_{lit} =18 589.8 (1.2) eV

We aim for: $\delta Q(^3T \rightarrow {}^3He)$ = 20 meV
$\delta m/m = 7 \cdot 10^{-12}$

ΔT < 0.2 K/d at 24°C
$\Delta B/B$ < 100 ppt / h $\Delta x \leq 0.1$ μm

THe-TRAP (MPIK)

First $^{12}C^{4+}/^{16}O^{6+}$ mass ratio measurement at $\delta m/m_{stat} = 4 \cdot 10^{-11}$ performed.

Summary and Outlook

Nuclear structure studies

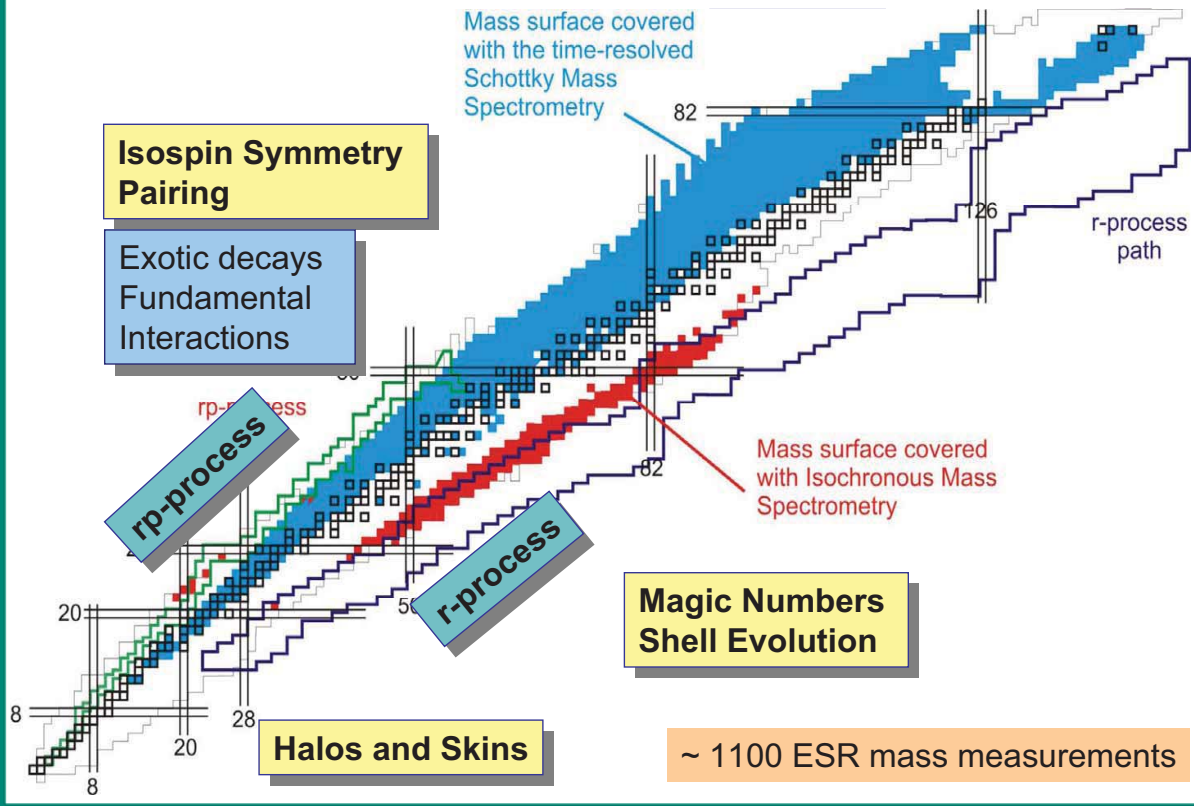

MAX PLANCK INSTITUTE FOR NUCLEAR PHYSICS

Future trap/ring/laser facilities at FAIR

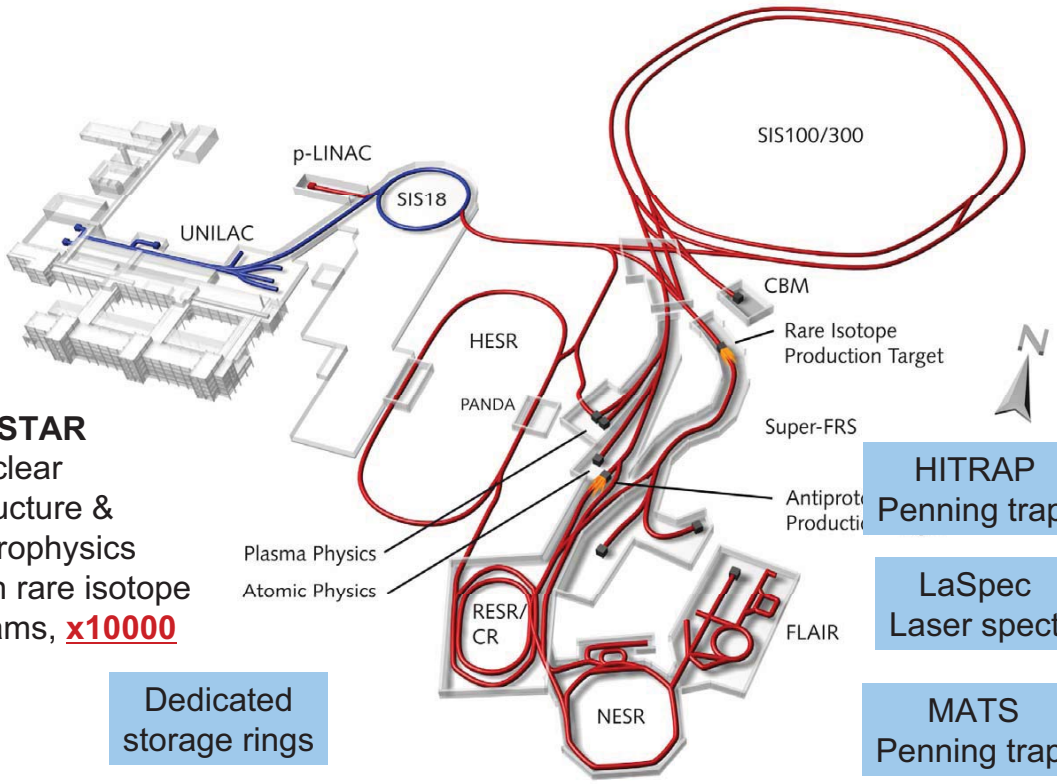

NUSTAR
Nuclear Structure & Astrophysics with rare isotope beams, **x10000**

HITRAP Penning traps

LaSpec Laser spect.

MATS Penning traps

Dedicated storage rings

MAX PLANCK INSTITUTE FOR NUCLEAR PHYSICS

Future trap/ring/laser facilities at FAIR

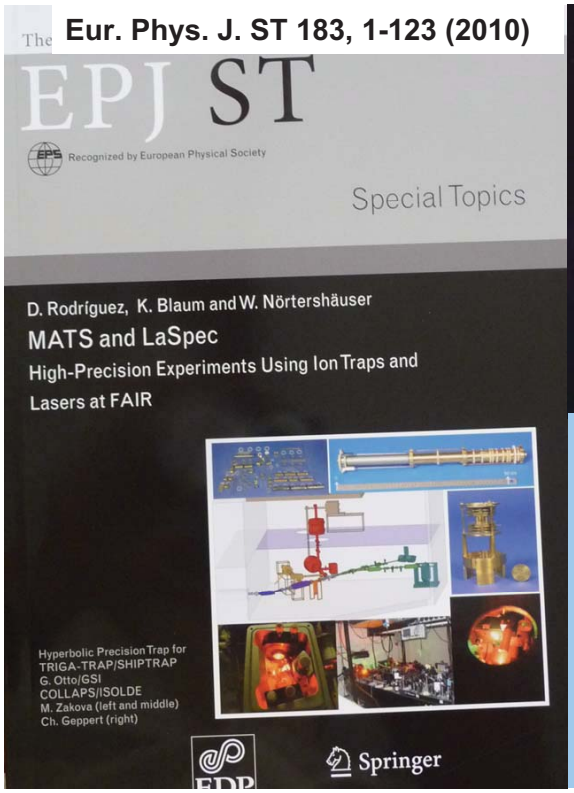

Why is iron so much abundant than heavier elements such as gold?

Why are there heavy elements at all and how did they come into existence?

MAX PLANCK INSTITUTE FOR NUCLEAR PHYSICS

Summary

Breathtaking results in the precise determination of nuclear masses have been achieved!

- Masses reveal new nuclear structure phenomenon (nuclear quantum phase transition)
- Masses are of utmost importance for reliable nucleosynthesis calculations
- First direct mass measurements above uranium bridge the gap to the island of stability
- Discovery of a suitable candidate for 0ν2EC search
- Development of novel and unique storage devices (CSRe, The-Trap, PENTATRAP, MATS)
- … and many more!

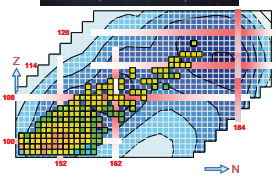

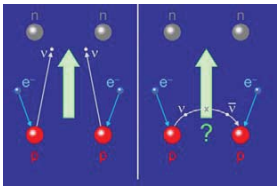

MAX PLANCK INSTITUTE FOR NUCLEAR PHYSICS

Thanks

Edmund Myers (FSU); Georg Bollen / Rian Ringle (LEBIT / Michigan State University); Guy Savard / Jason Clark (CPT / Argonne National Laboratory); Michael Block (SHIPTRAP / GSI Darmstadt); Wilfried Nörtershäuser / Szilard Nagy (TRIGA-SPEC / Mainz, COLLAPS / CERN); Christine Weber (MLLTRAP / LMU Munich); Hans Geissel / Yuri Litvinov / Christoph Scheidenberger (ESR / GSI Darmstadt); Susanne Kreim / Burcu Cakirli (ISOLTRAP / ISOLDE-CERN, MPIK); Jens Dilling (TITAN / TRIUMF Vancouver); Juha Äystö / Tommi Eronen/ Ari Jokinen (JYFLTRAP Jyväskylä); Xinwen Ma / Xu Hushan / Yuhu Zhang / Xiaolin Tu (IMP Lanzhou)

Thanks a lot for the invitation and your attention!

Email: klaus.blaum@mpi-hd.mpg.de

WWW: www.mpi-hd.mpg.de/blaum/

Prof. Dr. Sydney Gales, GANIL, CEA/DSM-CNRS/IN2P3, France

Content of the lectures at the International summer school on subatomic physics
Aug 2011, Beijing (China)

Title: **GANIL-SPIRAL2: A new generation of Radioactive Ion Beam Facility**
Physics Highlights and Technical Challenges

Abstract: GANIL presently offers unique opportunities in nuclear physics and many other fields that arise from not only the provision of low-energy stable beams, fragmentation beams and re-accelerated radioactive species, but also from the availability of a wide range of state-of-the-art spectrometers and instrumentation. Current research topics include ;the key nuclei to our understanding of the origin and structure of matter in the universe, neutron halos, modification of shell structure investigated around closed shells (N=8,20,28,40), the nucleus as a laboratory for study of fundamental interactions and fusion and fission studies with very heavy ion beams (Xe , U) and the Vamos spectrometer. A few examples of recent highlights are discussed in the present paper.

With the construction of SPIRAL2 over the next few years, GANIL is in a good position to retain its world-leading capability. As selected by the ESFRI committee, the next generation of ISOL facility in Europe is represented by the SPIRAL2 project to be built at GANIL (Caen, France). SPIRAL 2 is based on a high power, CW, superconducting LINAC, delivering 5 mA of deuteron beams at 40MeV (200KW) directed on a C converter+ Uranium target and producing therefore more 10^{13} fissions/s. The expected radioactive beams intensities in the mass range from A=60 to A=140, will surpass by two order of magnitude any existing facilities in the world. These unstable atoms will be available at energies between few KeV/n to 15 MeV/n. The same driver will accelerate high intensity (100*A to 1 mA), heavier ions (Ar up to Xe) at maximum energy of 14 MeV/n. Under the 7FP program of European Union called *Preparatory phase*, the SPIRAL2 project has been granted a budget of about 4M€ to build up an international consortium around this new venture. The status of the construction of SPIRAL2 accelerator and associated physics instruments in collaboration with EU and International partners will be presented.

Keywords: physics with secondary radioactive beams, in flight and Isol methods. Superconducting Linac Accelerator and target ion source systems. Nuclear structure and reactions far from stability, detectors and instrumentation.
PACS: 25-60.-t, 29.17. +w, 29.27.Eg, 25.85.-w

Outlines of the lectures

1. ***Introduction: Nuclear Physics : The Science and the International context***
2. ***The keys questions in the emerging field of "exotic nuclei"***
3. ***Physics with secondary radioactive beams***
4. ***GANIL-SPIRAL1 :the facilities***
5. ***Physics Highlights***
6. ***SPIRAL2 Facility***

6.1International Context
6.2 Beams and Detectors

1. ***Physics Opportunities with high-intensity stable-ion and RI beams***
2. ***Status of the Construction of SPIRAL2***
3. ***Conclusions & Long(er) Range Plan***

Main References

Books

1) A.Bohr and B.Mottelson Nuclear,Structure, vol .2,editor Benjamin,New-York 1975
2) G.R.Satchler, Direct Nuclear reactions ,Oxford University press ,New-york (1983)

Major conferences Proceedings

1) First Int conf on Radioactive beams ,Berkeley ,Oct 1989,ed by WD Myers , J.Nitschke, E.B .Norman ,World Scientific ,1990
Second Int conf on Radioactive beams , Louvain la Neuve ,aug 1991 ,ed Th.delbar,Adam
Third Int conf …….MSU(USA) edited by D.Morrissey 1994
2) Nuclei at the limits of stability ,
A.C. Mueller and B. M.Sherill,Ann .Rev.of Nucl and Part .Science 43(1993)529
3) Nuclear Physics to day
S.Gales Nuc.Phys A654(1999)19-33
4) Exotic nuclei :Recent highlights and perspectives
A.C.Mueller Nucl.Phys.A654(1999)235c
5) Reactions with radioactive beams
I.Tanihata ,Nucl.Phys A654(1999) 235c
6) Superheavy elements
S.Hofmann ,Nucl.phys.A654(1999) 252c
7) Theoritical aspects of science with radioactive beams
J.Dobaczewski and W.Nazarewitz,Phil.trans.R.Soc.London A(1998)356,2007
8) Nuclear structure and reactions studies at SPIRAL
A.Navin,F.De Olieveira Santos,P.Roussel-Chomaz and O.Sorlin
J.Phys.G:Nucl.Part.Phys.38(2011)024004
9) www.scholarpedia.org/article/
GANIL-SPIRAL-SPIRAL2: A Heavy ion beam European Large scale facility for the French and International community

8 www.**ganil**-spiral2.eu/

Some Phys Rev.Lett references

9. A. Lemasson et al., Phy. Rev. Lett.**103**(2009) 232701
10. B.Bastin et al., Phys.Rev.Lett.**101**(2008) 092501
11. L. Gaudefroy et al .,Phys. Rev. Lett.**102** (2009) 092501
12. D. Suzuki et al., Phys.Rev.Lett.**103** (2009) 152503
13. D. Jacquet, M. Morjean, Progress in Particle and Nuclear Physics **63** (2009) 155-185
14. M.Morjean et al., Phys.Rev.Lett.**101**(2008) 072701
15 A. Shrivastava et al., Phys. Rev.C**80**(2009) 051305
16.www.ganil.fr/research/developments/spiral2/
14. *www.eurisol.org*
15. *cordis.europa.eu/esfri/publications.html*
16. H. Savajols et al. S3, SPIRAL2 Technical Proposal
www.ganil.fr/research/developments/spiral2/collaborations.html

And give a look to the web site of NUPECC (European coll committee for NP)
At www.nupecc.org and the associated review reports (see publications)

a. Nuclear Physics in Europe :Highlights and Perspectives ed .by S.Gales et al (dec 1997 and new editions 2001,2007, 2010)
b. Radioactive Nuclear beam facilities beams ed by B.Jonson, J.Vervier ,A.C.Mueller (april 2000)

Outlines

1.Introduction: Nuclear Physics : The Science:

The keys questions in the emerging field of “exotic nuclei”

2.Physics with secondary radioactive beams

3.GANIL-SPIRAL1 :the facilities

4. Physics Highligths

5.SPIRAL2 Facility

- *5.1 International Context*
- *5.2 Beams and Detectors*
- *5.3 Physics Opportunities with high-intensity stable-ion and RI beams*

6. Status of the Construction of SPIRAL2

7.Conclusions & Long(er) Range Plan

Probing the structure of matter with heavy ions@ GANIL

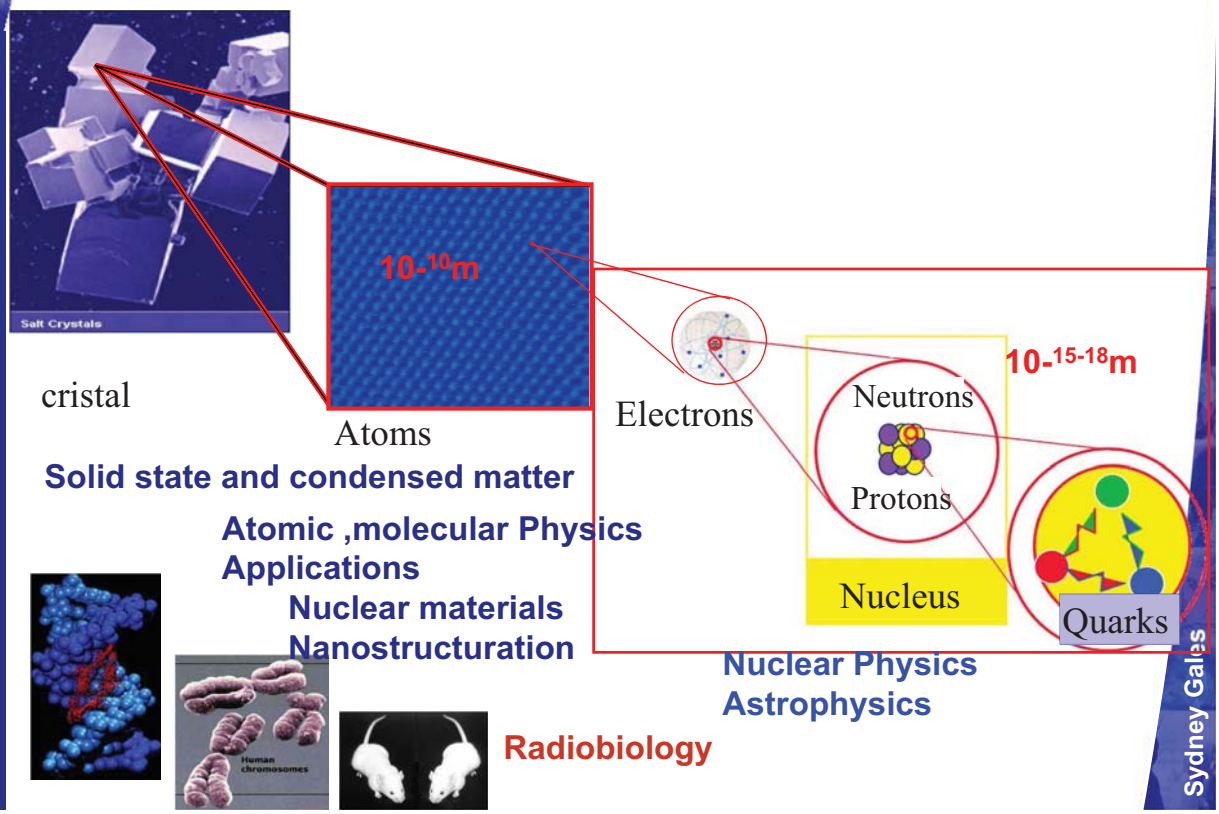

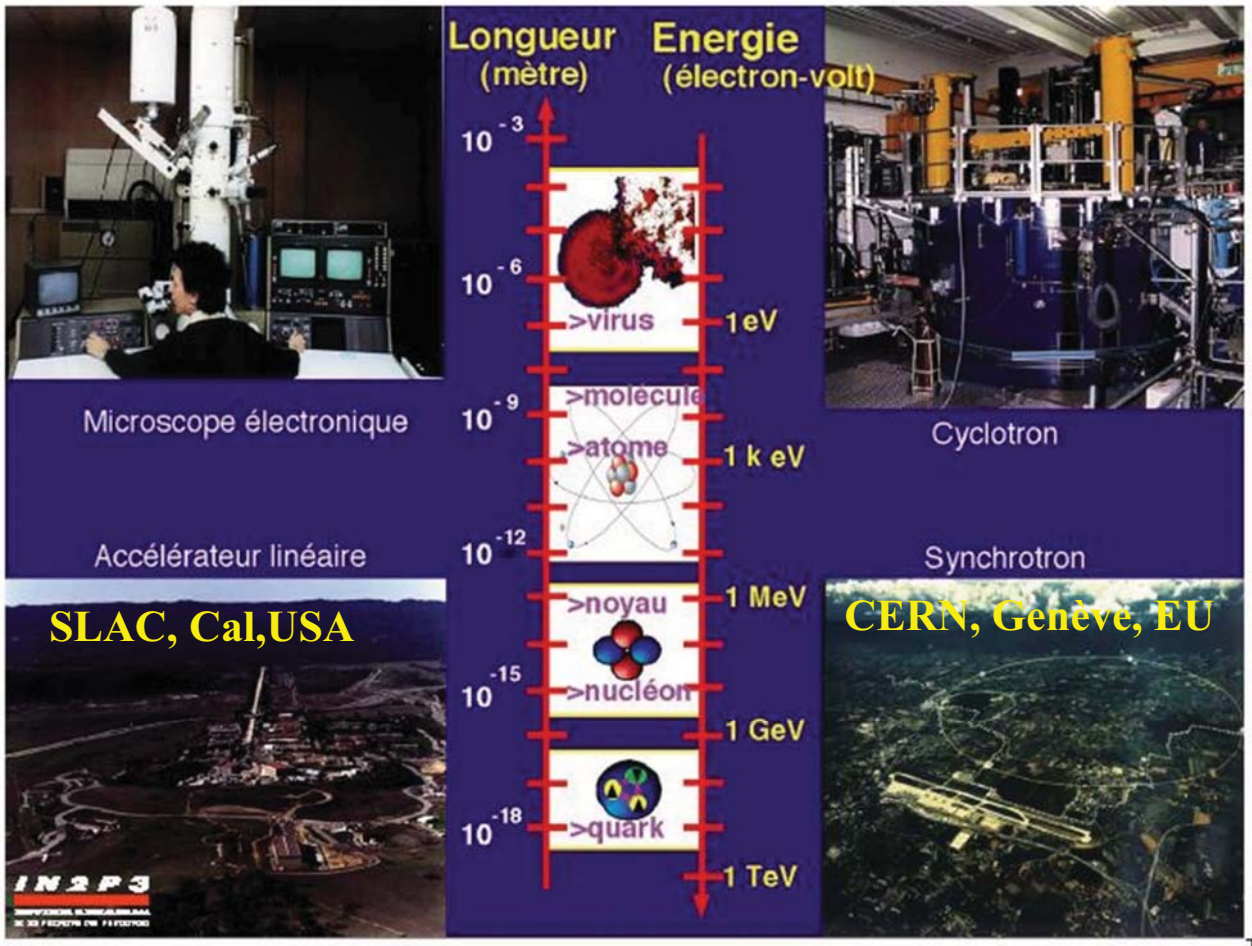

The cathode ray tube: a "complete accelerator at home"

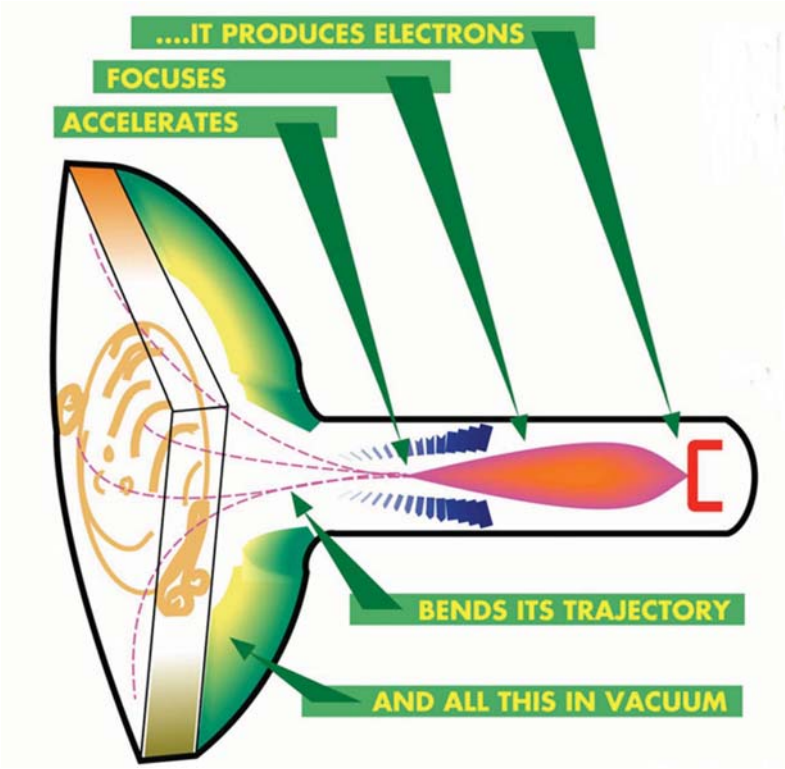

Figure from a CERN Website

GANIL Spiral2
International summer shcool on Subatomic Physics–Beijing Aug 27-31 2011

Science Pillards of GANIL-SPIRAL2

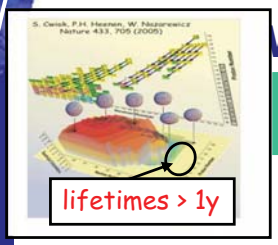

What are the limits of the heaviest elements?

SCIENCE Magazine- Top 125 Questions:
Are there stable high-atomic-number elements?

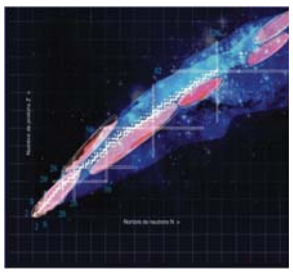

What are the limits of stability, Exploration of terra incognita, neutron rich region,haloes and skin,vanishing shells,new decays, new shapes

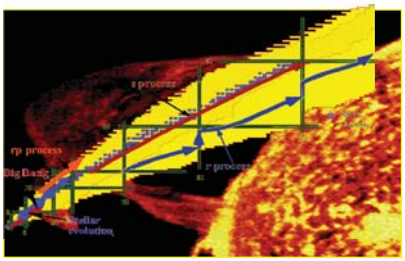

How the elements are made in the Universe Astrophysics

A new landscape Far of Stability
A huge discovery potential

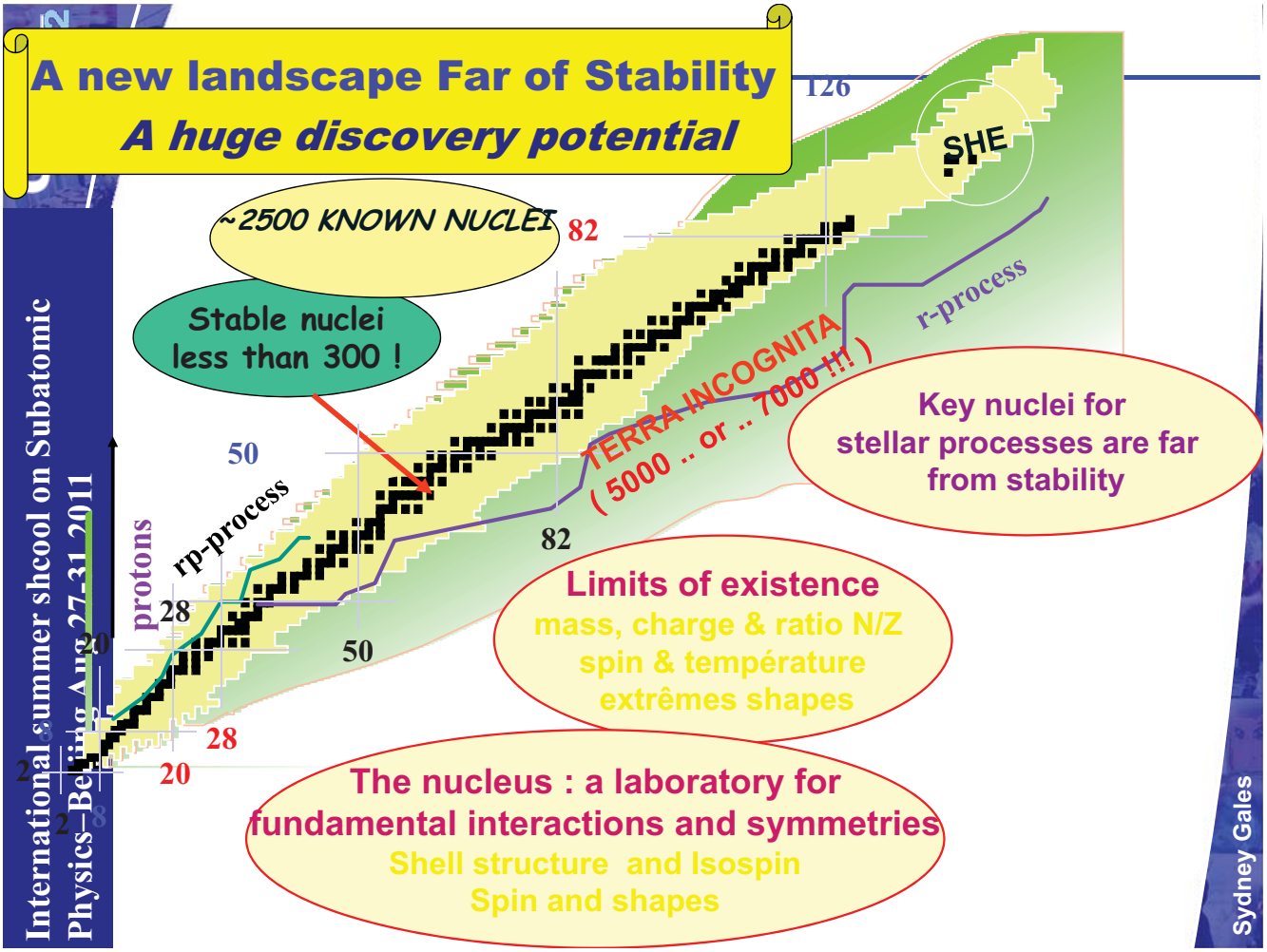

International summer shcool on Subatomic Physics–Beijing Aug 27-31 2011

Sydney Gales

GANIL Spiral2

Isospin Dependence of Mean Field and Residual Interactions

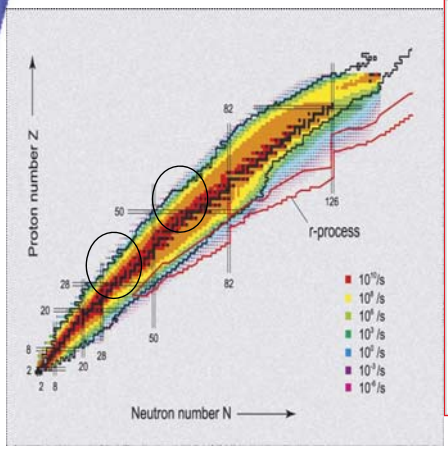

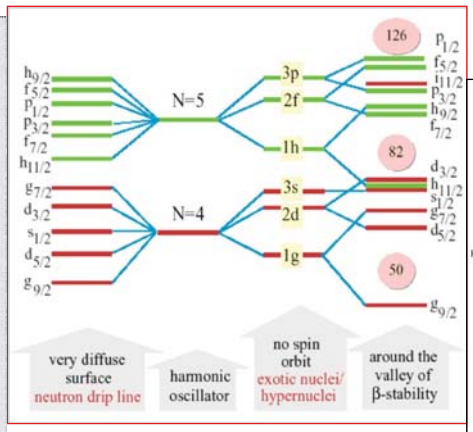

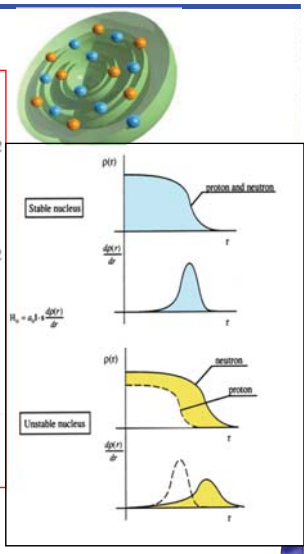

Modifications of mean field and residual interactions by e.g. diffuse surface

Evolution of shell structure towards ^{78}Ni and ^{132}Sn (Skin)

Study using light-ion transfer reactions – (p,d), (d,^{3}He)
- measure properties of bound and unbound states
- E^x, $L^{\square}$, SF

International summer shcool on Subatomic Physics–Beijing Aug 27-31 2011

Sydney Gales

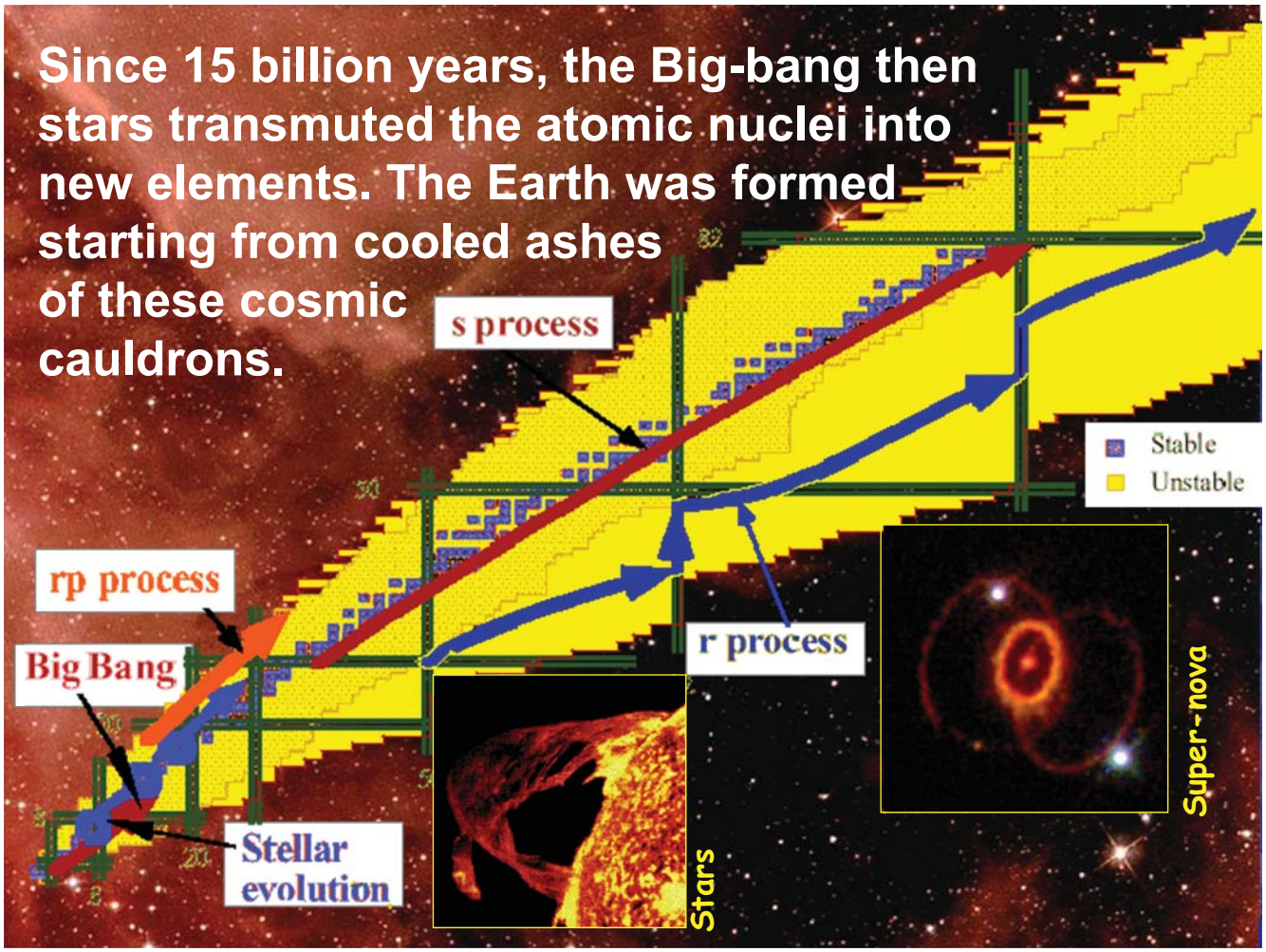

GANIL Spiral2

International summer shcool on Subatomic Physics–Beijing Aug 27-31 2011

Nuclear Reactions and « exotic beams »

Protons,deuterons

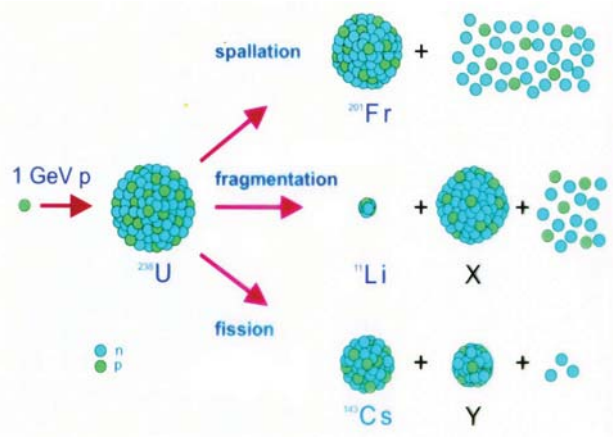

Heavy Ions C,Ca,Xe,U

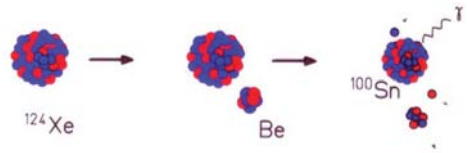

fragmentation

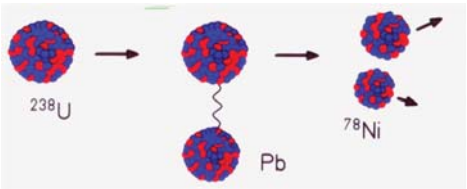

Coulomb dissociation

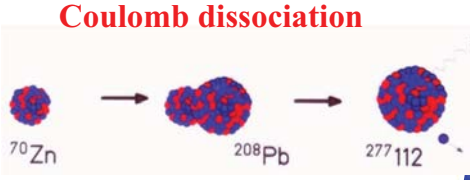

fusion

Sydney Gales

NuPECC WG 2000

"Next generation of RIB facilities should aim at intensities 1000 times higher than in the facilities presently running or at the commissioning stage. Two truly complementary facilities based respectively on the « In flight and Isol » methods are needed to cover the foreseen physics issues, and they should be second to none world-wide"

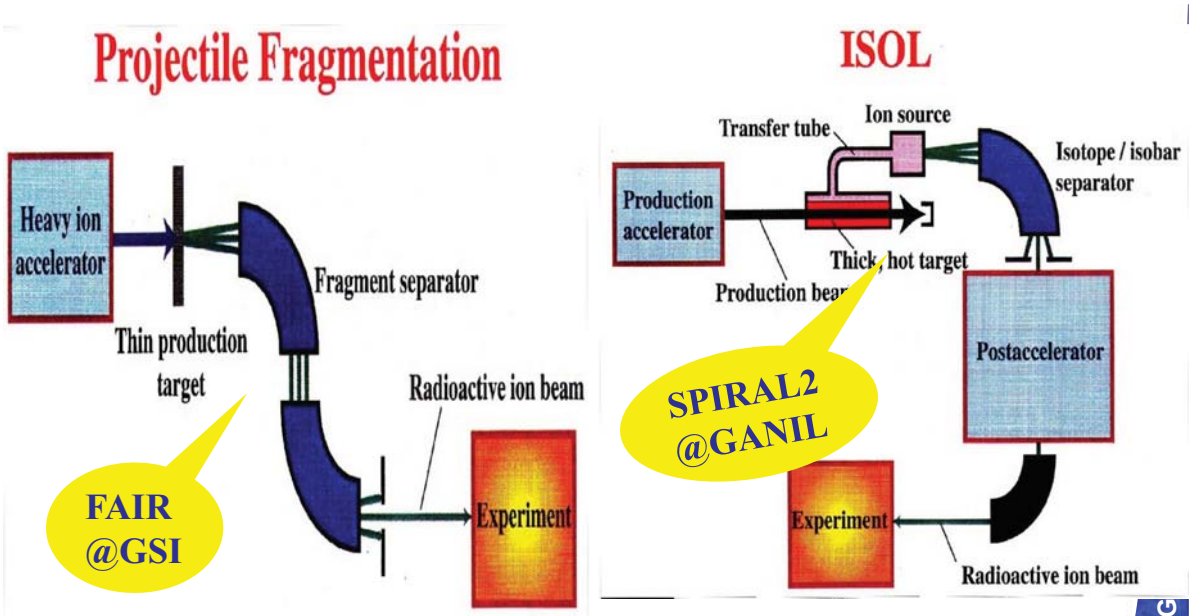

A wide spectrum of nuclear reactions to produce proton rich and neutron rich nuclei

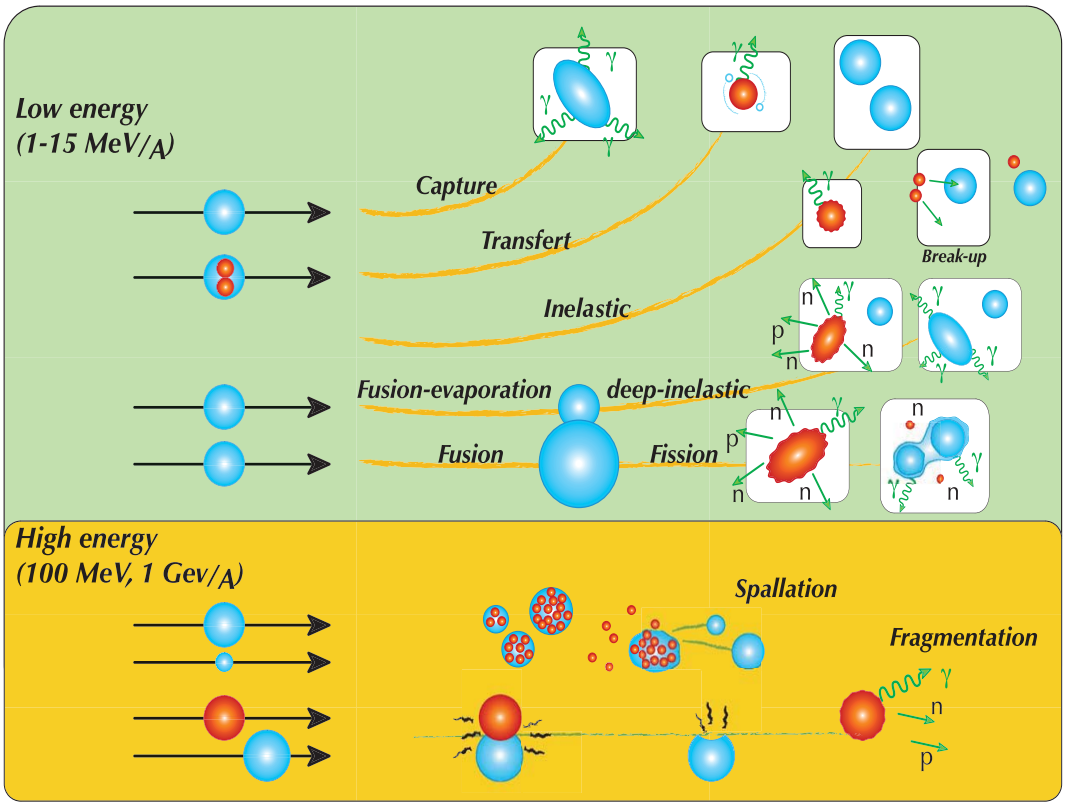

Nuclear reaction cross-sections

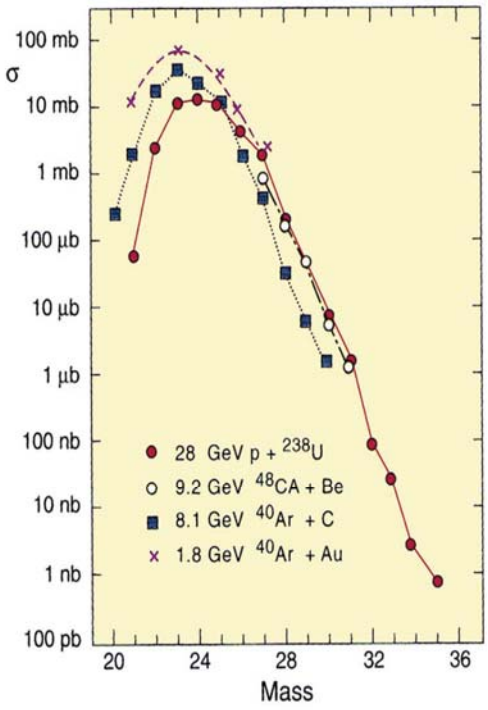

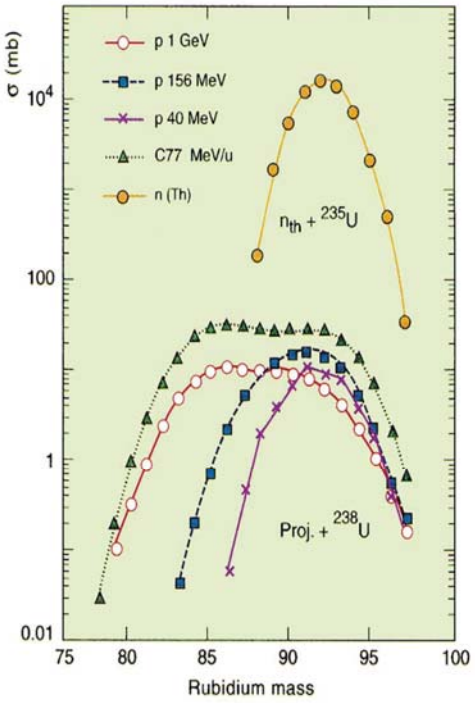

GANIL Spiral2
International summer shcool on Subatomic Physics–Beijing Aug 27-31 2011

Secondary Radioactive Ion Beam (RIB) intensities

$$I = \sigma \times \Phi \times N \times \varepsilon 1 \times \varepsilon 2 \times \varepsilon 3 \times \varepsilon 4 \times \varepsilon 5$$

σ : cross-section, Φ : primary-beam intensity,
N: target thickness,
ε1: product release and transfer efficiency
ε2: ion-source efficiency,
ε3: efficiency due to radioactive decay losses
ε4: the efficiency of the spectrometer
ε5: the post-acceleration efficiency

$$\Phi \times N = \text{Luminosity}$$

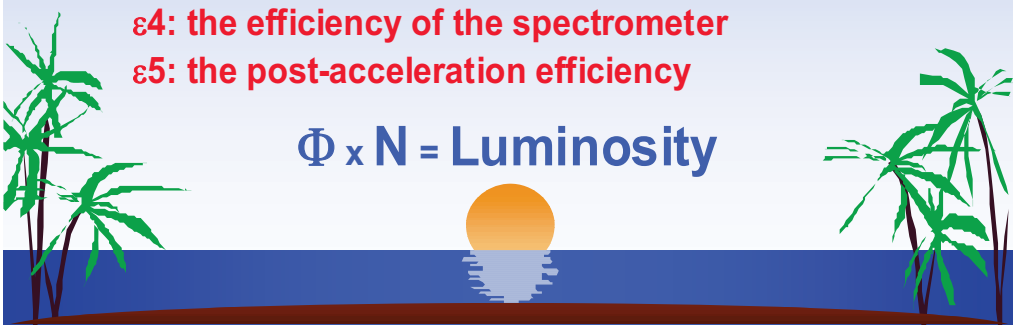

Sydney Gales

Reaction cross-sections ,energy and needed rates for secondary RIB

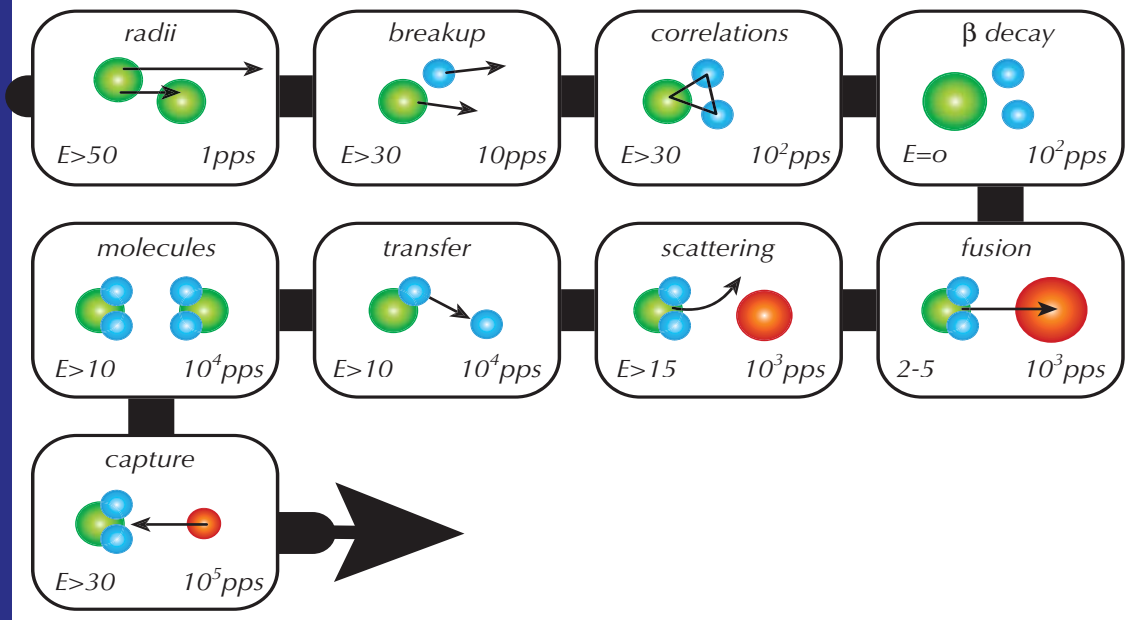

GANIL Spiral2
International summer shcool on Subatomic Physics–Beijing Aug 27-31 2011

Reaction cross-sections and interaction radius

measurement of flux absorption

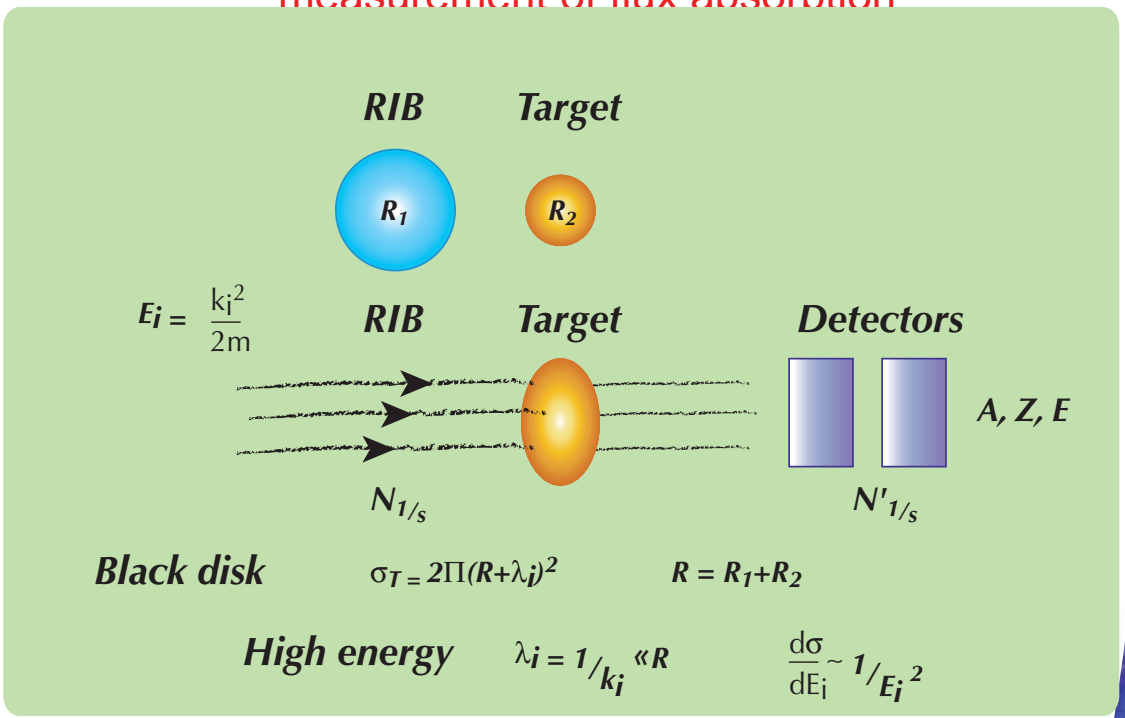

Sydney Gales

Interaction Cross Sections at ~800A MeV

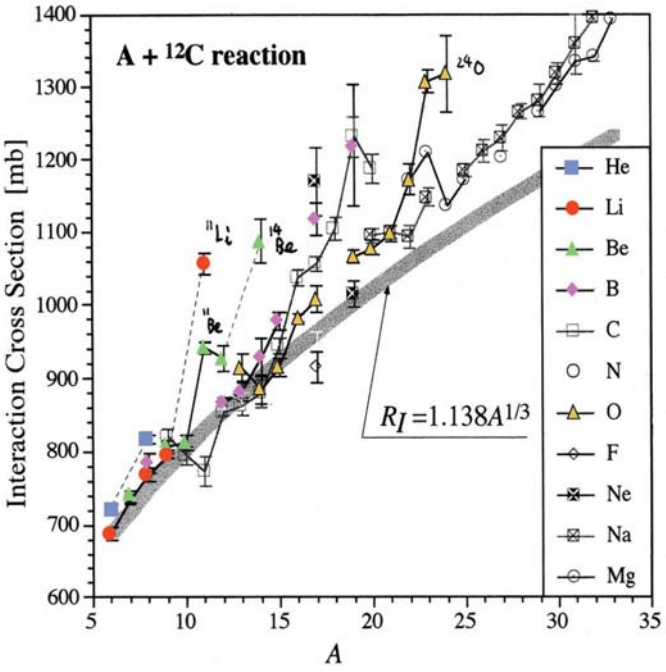

He: I. Tanihata et al. PL 160B (1985) 380.
Li, Be: I. Tanihata et al. PRL 55 (1985) 2676.
B: I. Tanihata et al. PL B 206 (1988) 592.
M. Obuti et al. NP A 609 (1996) 74.
A. Ozawa et al. NP A 608 (1996) 63.
K. Suzuki et al., Submitted for publication.
C, O : A. Ozawa et al. Submitted for publications
Ne and A=17: A. Ozawa et al. PL 334B (1994) 18.
A=20: L. Chulkov et al. NP A 603 (1996) 219-237.
Na: T. Suzuki et al. PRL 75 (1995) 3241.
Mg: T. Suzuki et al. NP A 630 (1998) 661-677.

GANIL Spiral2
International summer shcool on Subatomic Physics–Beijing Aug 27-31 2011

Inverse kinematics: Reactions with secondary beams

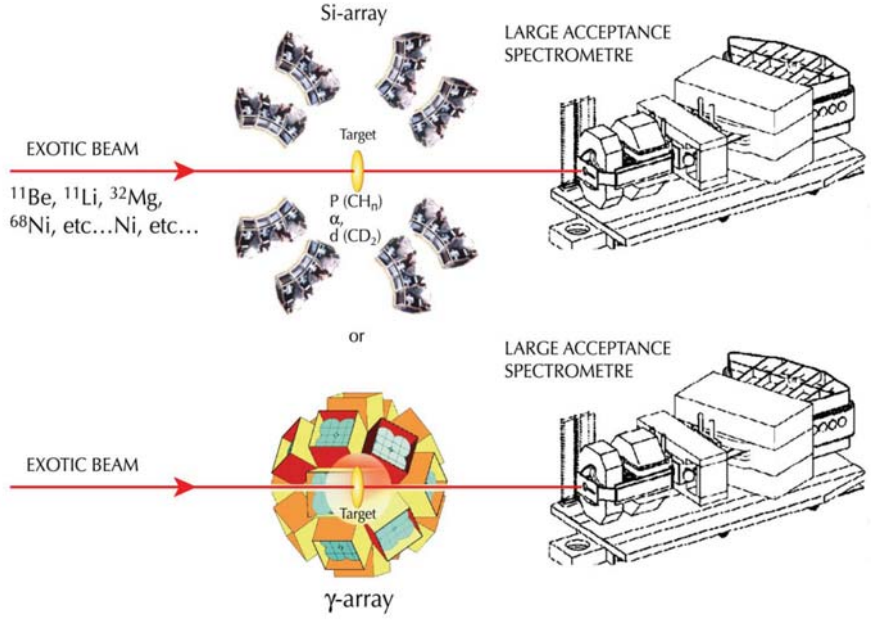

Sydney Gales


GANIL at
Jules Horowitz Campus
London
Caen
Paris
CERN

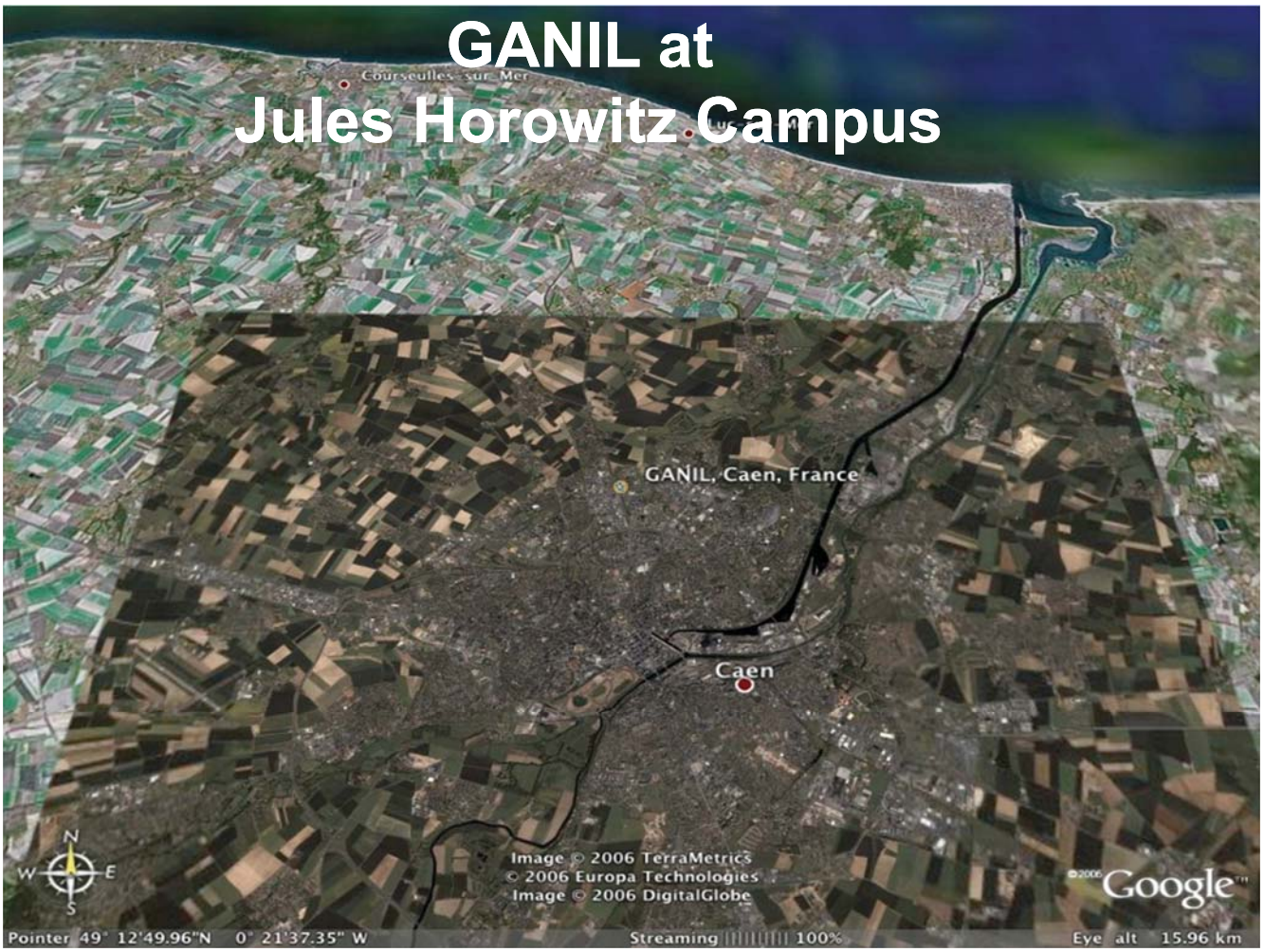
GANIL at
Jules Horowitz Campus
Courseulles-sur-Mer
GANIL, Caen, France
Caen
Image © 2006 TerraMetrics
© 2006 Europa Technologies
Image © 2006 DigitalGlobe
©2006 Google
Pointer 49° 12'49.96"N 0° 21'37.35" W
Streaming 100%
Eye alt 15.96 km

An Interdisciplinary Large Scale Facility for the French ,European and International Communities

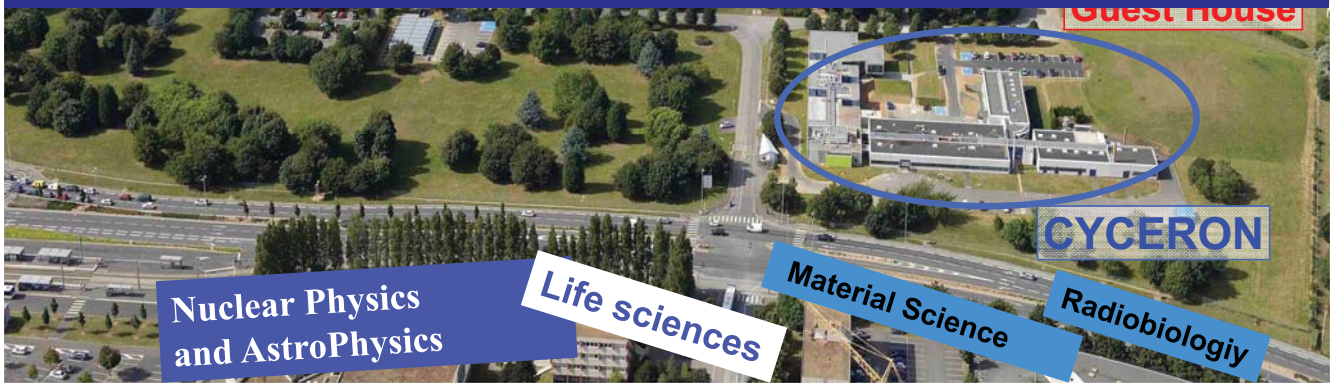

Production of intense Heavy Ion beams : Ion source

Example of the ECR source

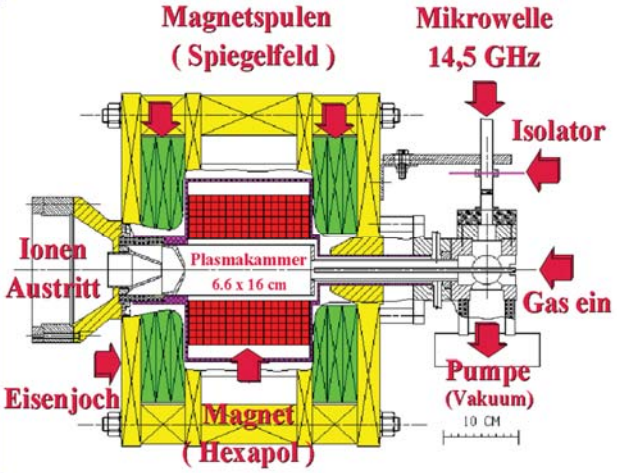

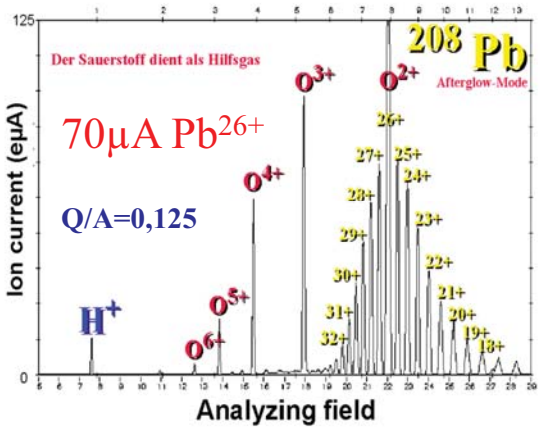

High current sources: e.g. > 10 mA U^{4+}
and also > 100 mA p

'hot plasma'

Transparency from a lecture by
O. Boine-Frankenheim, GSI

Sydney Gales

Properties of Cyclotrons

- The frequency of revolution, the so-called cyclotron frequency has to be constant

$$\nu = 1/T = = qB_m /2\pi m_0$$

showing the link between mass, field and frequency,
note, that this can be used for high-precision nuclear mass measurements

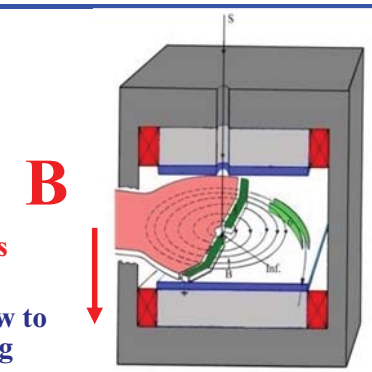

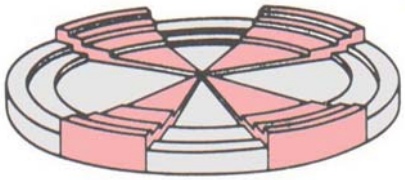

- but the formula, even more importantly, also suggests how to overcome the initial relativistic effects in a cyclotron (starting around 20 MeV for a proton):
the relativistic mass increase with increasing $\beta=v/c$ of $m=\gamma m_0$, $\gamma=(1-\beta^2)^{-1/2}$ can be compensated by correspondingly increasing the magnetic field in order to maintain the frequency ν constant, this can be done by shap the poles (see figure) and adding "trim coils", such an accelerator is called an isochroneous cyclotron,
- a cyclotron typically has 1-4 accelerating cavities, with an energy gain of up to a few hundred keV
- thus the beam typically makes hundreds of turns in the accelerator, and the turn separation is rather small

The factor K is often used to describe a cyclotron's characteristics

$$W_{kin}/A = 48\,(B_m\,\rho)^2\,(Q/A)$$

or

$$W_{kin}/A = K\,(Q/A)^2$$

The PSI & RIBF cyclotrons

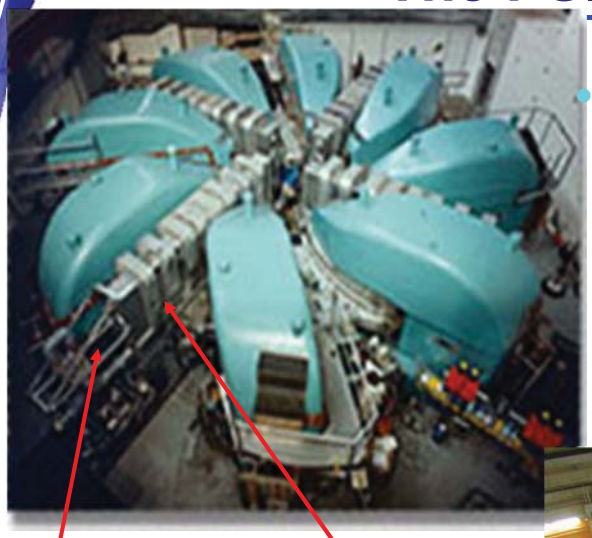

- The K=590 cyclotron of the PSI (Zurich) facility is a 8 separated sector machine with 4 accelerating cavities
The injection energy of 70 MeV is provided by another cyclotron –
Started in 1970
The exceptional experience gained at PSI allows now to approach an intensity of almost 2 mA (> 1MW of beam power world record for a SSC)

SRC World's First and Strongest K2600MeV RIKEN –Started 2007 Superconducting Ring Cyclotron

400 MeV/u Light-ion beam
345 MeV/u Uranium beam

GANIL
GRAND ACCELERATEUR NATIONAL D'IONS LOURDS

First beam in 1983

STABLE BEAMS

- from C to U
- energies up to 95 A.MeV
- intensities up to 2.10^{13} pps (6 kW)

RIB production schemes

- in-flight method : SISSI, LISE
- ISOL method : SPIRAL (SIRA)
- Inverse kinematics: HI+C target

Up to 10000 hours of stable and radioactive beams per year
600 users/year (40% outside of France)
Operation budget (without salaries): 9M€/year
Staff 250 (10% physicists)

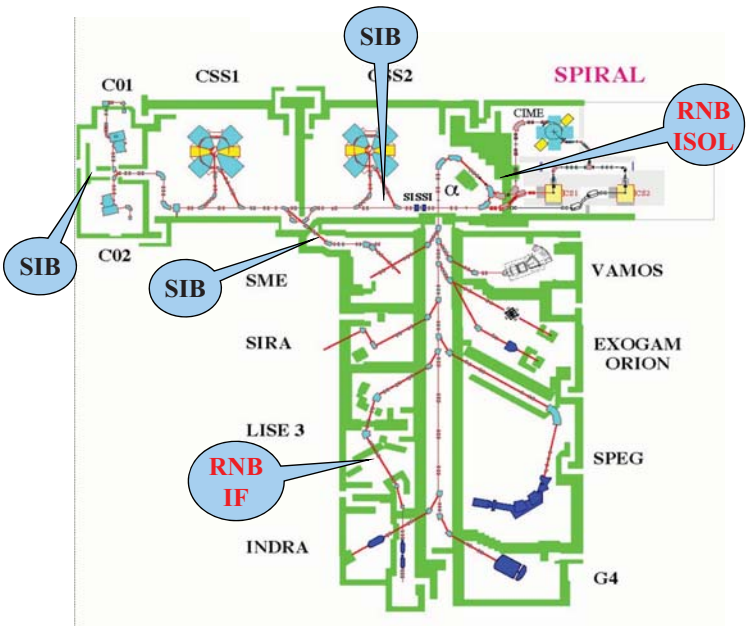

Primary Beams:

Ion:	^{12}C	^{36}Ar	^{86}Kr	^{238}U
Energy(AMeV):	95	95	60	24
Int. (pps) :	10^{13}	$3x10^{12}$	$5x10^{11}$	10^{10}

GANIL Spiral 2

International summer shcool on Subatomic P

Multi-Beam Operating Mode: 4 experiments in parallel

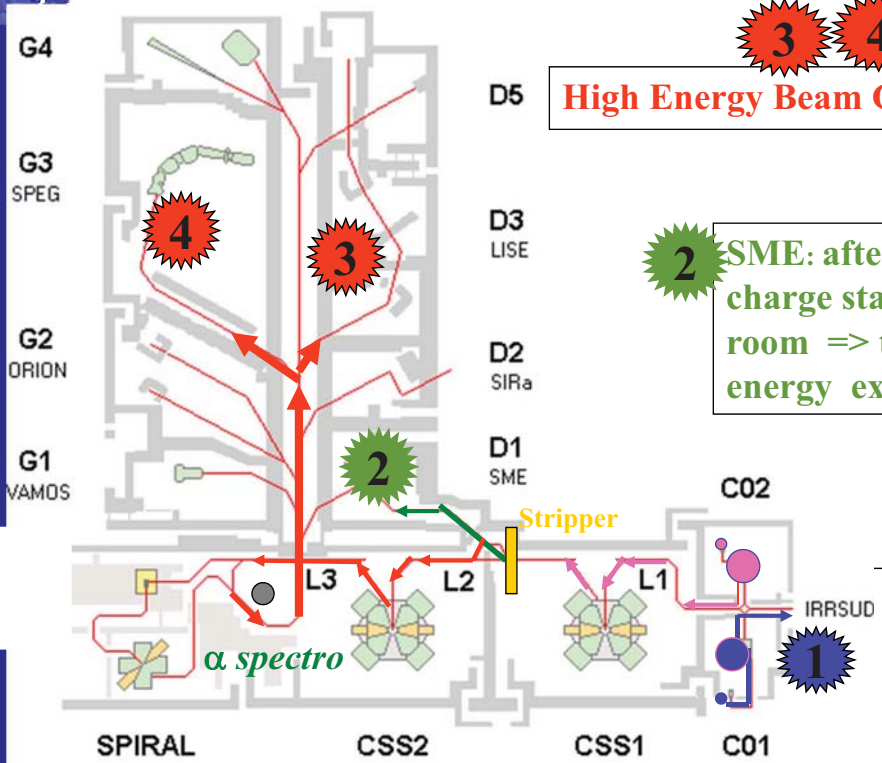

3 4

High Energy Beam GANIL [24, 95] MeV/A

2 **SME: after a stripper, one charge state is sent to the D1 room => the medium energy exit [3.7, 13.7] MeV/A**

IRRSUD: low energy beam irradiation line

[0.3, 1.0] MeV/A 1

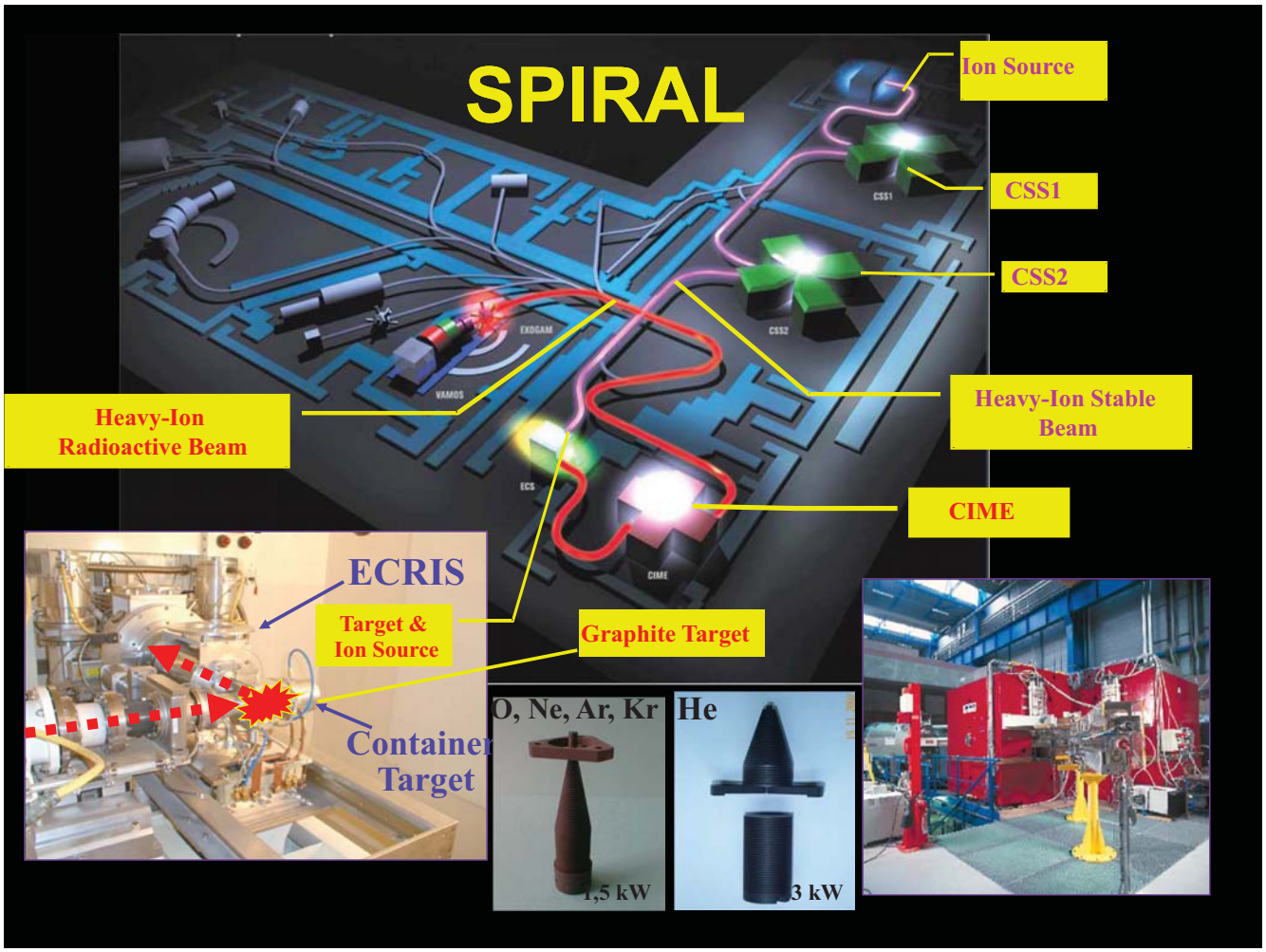

GANIL Spiral2

International summer shcool on Subatomic Physics–Beijing Aug 27-31 2011

SPIRAL operation

(http://www.ganil.fr/operation/available_beams/radioactive_beams.htm)

Table of elements

	I	II											III	IV	V	VI	VII	VIII
1	H																	He
2	Li	Be											B	C	N	O	F	Ne
3	Na	Mg											Al	Si	P	S	Cl	Ar
4	K	Ca	Sc	Ti	V	Cr	Mn	Fe	Co	Ni	Cu	Zn	Ga	Ge	As	Se	Br	Kr
5	Rb	Sr	Y	Zr	Nb	Mo	Tc	Ru	Rh	Pd	Ag	Cd	In	Sn	Sb	Te	I	Xe

7 elements, 40 isotopes

SPIRAL scientific production 2001 – 2008 :
70 physics articles
12 PhD Thesis
53 technical articles
7 PhD thesis

Recent overview article:
Navin Alahari et al.
J. Phys. G: Nucl. Part. Phys. 38 (2011) 024004.

Sydney Gales

SPIRAL1 operating mode:
4 experiments in parallel

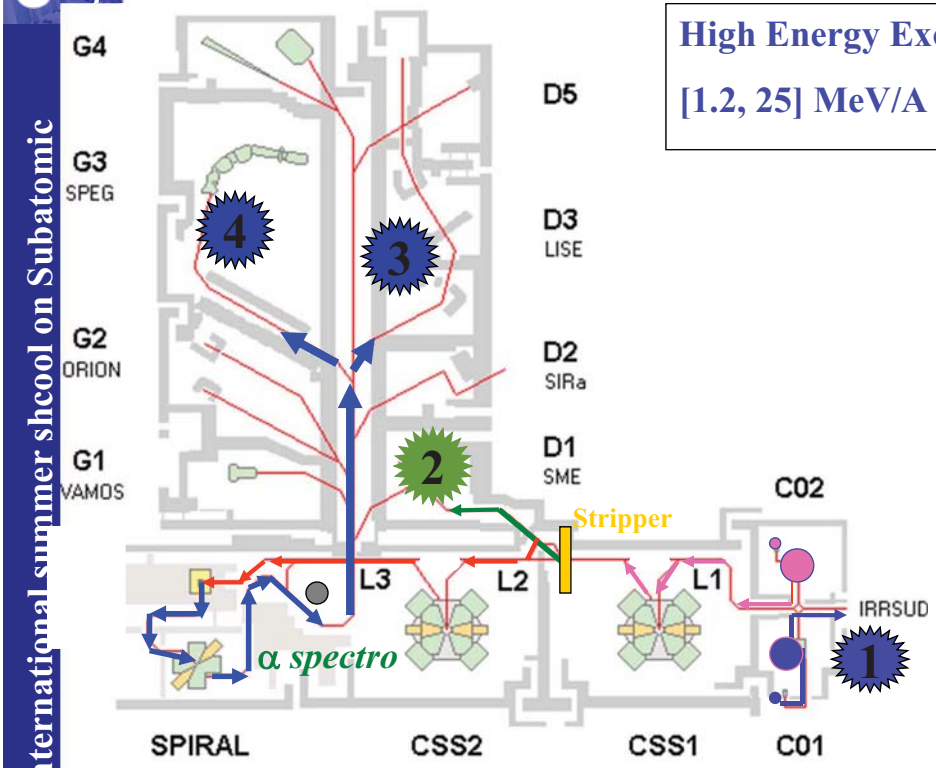

laboratoire commun CEA/DSM Spiral2 CNRS/IN2P3

Heavy ion beams ,among the most intense in the world
From Carbone to Uranium
0 to 95 MeV/n
"Exotic" Beams In Flight and/or SPIRAL 0-25 MeV/n
An ensemble of detectors and spectrometers rather unique In the world !!

« Exotic Nuclei »

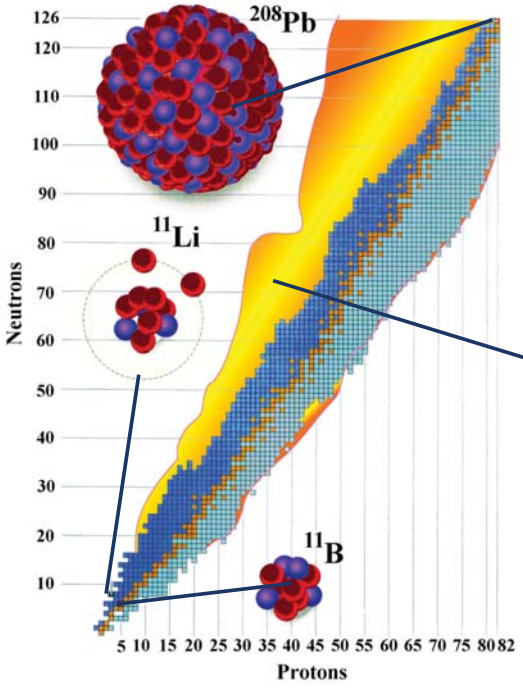

H. Rousseau, *Forêt Vierge ...*

GANIL Spiral2
International summer shcool on Subatomic Physics–Beijing Aug 27-31 2011

A Typical Experiment with RIB (@ Ganil)

MUST: Y. Blumenfeld et al., *NIM* **A366** (1999) 298
CATS: S. Ottini-Hustache et al., *NIM* **A431** (1999) 476

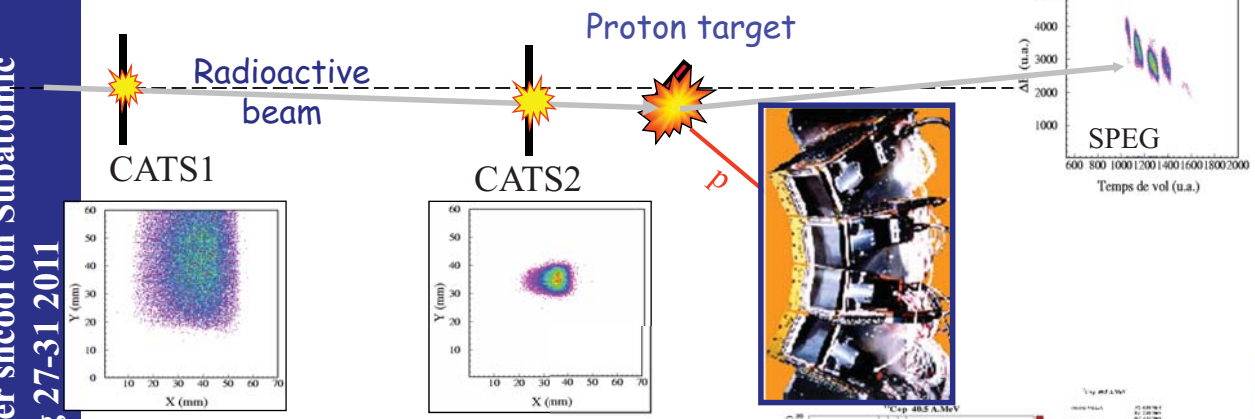

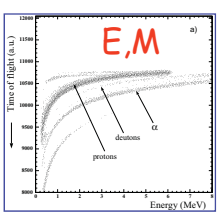

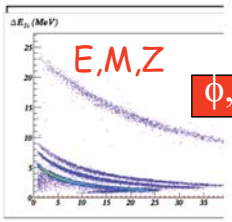

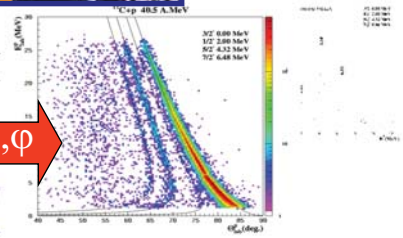

Sydney Gales

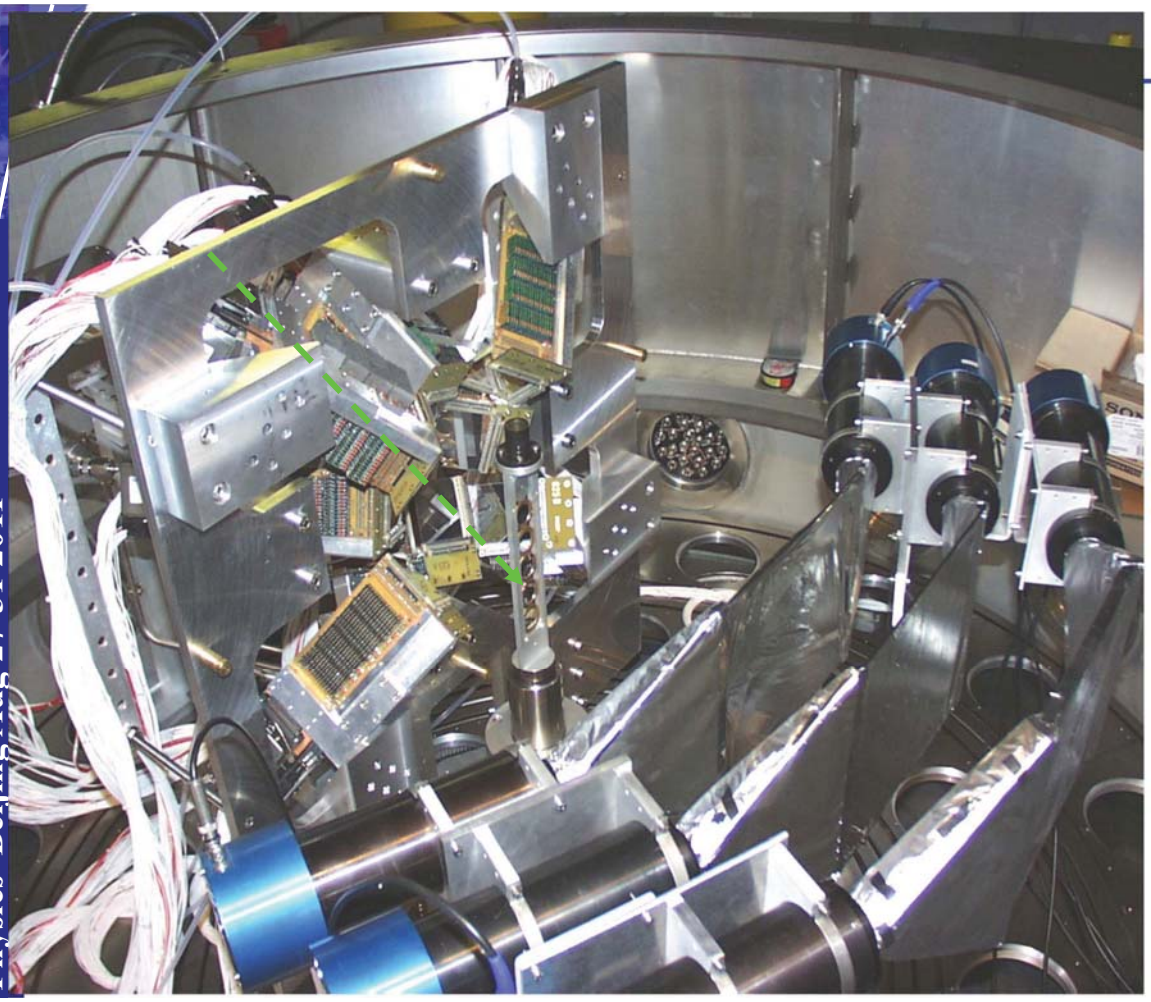

^{6}He (p,p') halo or skin?

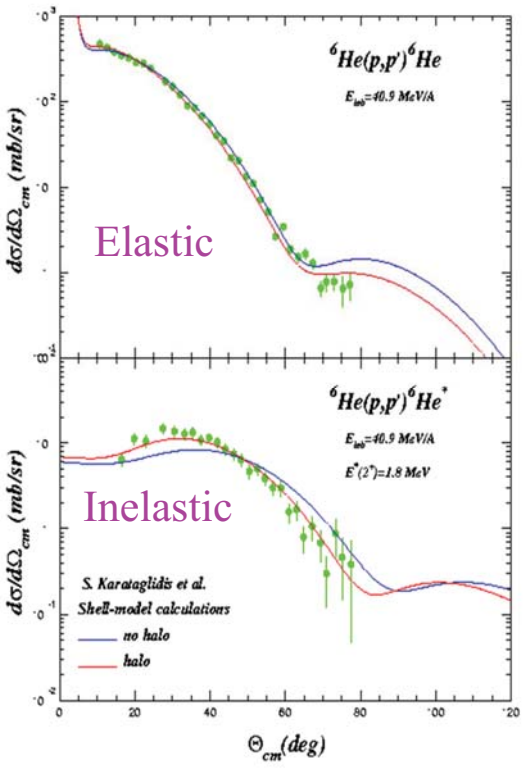

A. Lagoyannis et al PLB 518 (2001) 27

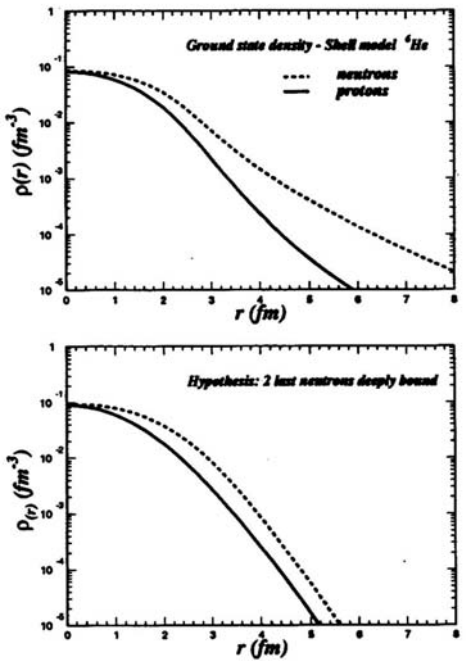

Sydney Gales

➲ Hydrogen 7: the most "exotic" nuclear system ever observed

➲ With the most intense ^{8}He beam from SP1

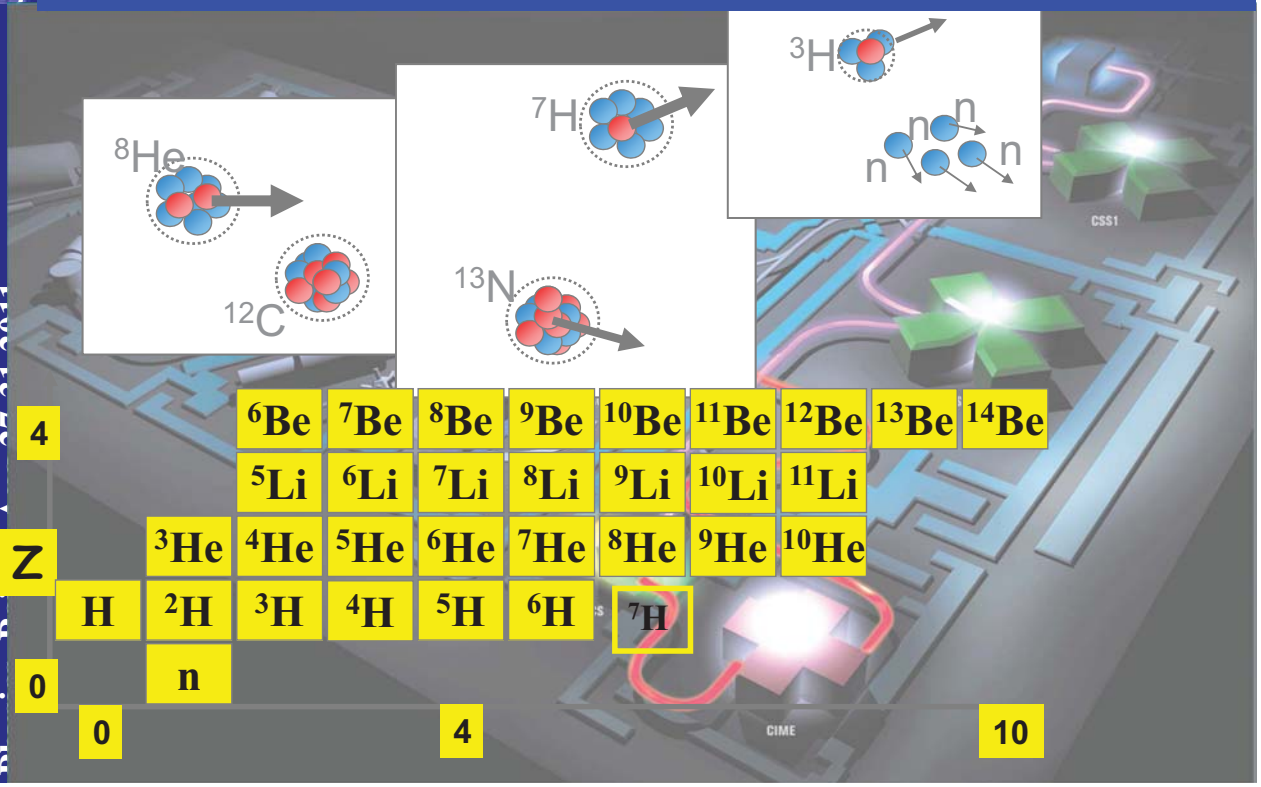

Z									
4	^{6}Be	^{7}Be	^{8}Be	^{9}Be	^{10}Be	^{11}Be	^{12}Be	^{13}Be	^{14}Be
	^{5}Li	^{6}Li	^{7}Li	^{8}Li	^{9}Li	^{10}Li	^{11}Li		
	^{3}He	^{4}He	^{5}He	^{6}He	^{7}He	^{8}He	^{9}He	^{10}He	
	H	^{2}H	^{3}H	^{4}H	^{5}H	^{6}H	^{7}H		
0		n							
	0			4				10	

Active target MAYA

➲ The target is also the detector

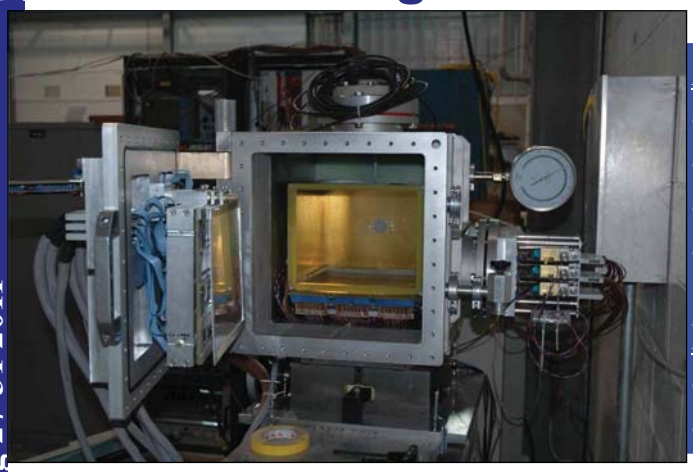

MAYA target-detector

Advantages:
- Thick target
- detection efficiency 100%
- angular coverage 4π
- Very low energy threshold

Principle :
- 3D imaging of the reaction
- Identification of products

From MAYA active target 3D detector

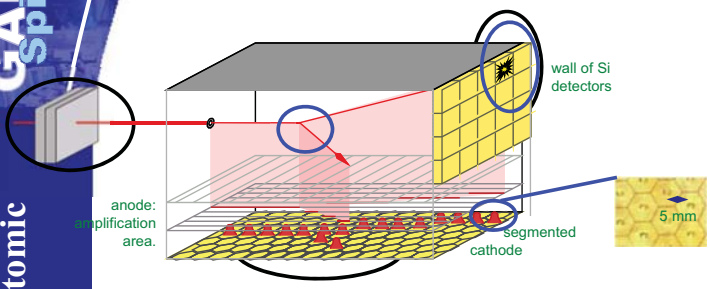

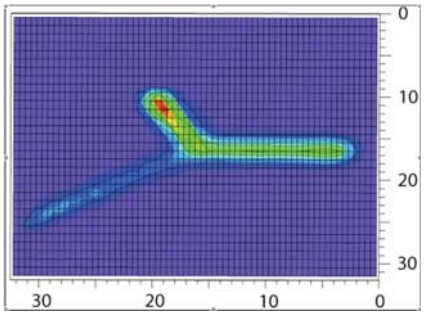

$^{12}C(^{8}He,^{7}H->^{3}H+4n)^{13}N$

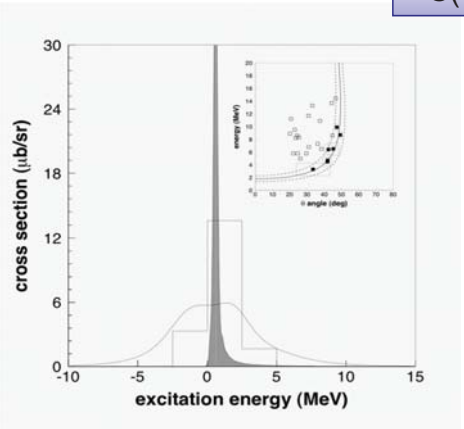

^{7}H observed

M. Caamaño *et al.*, Phys. Rev. Lett. 99, 062502 (2007)

Revisiting two proton radioactivity with TPC

B.Blank et al

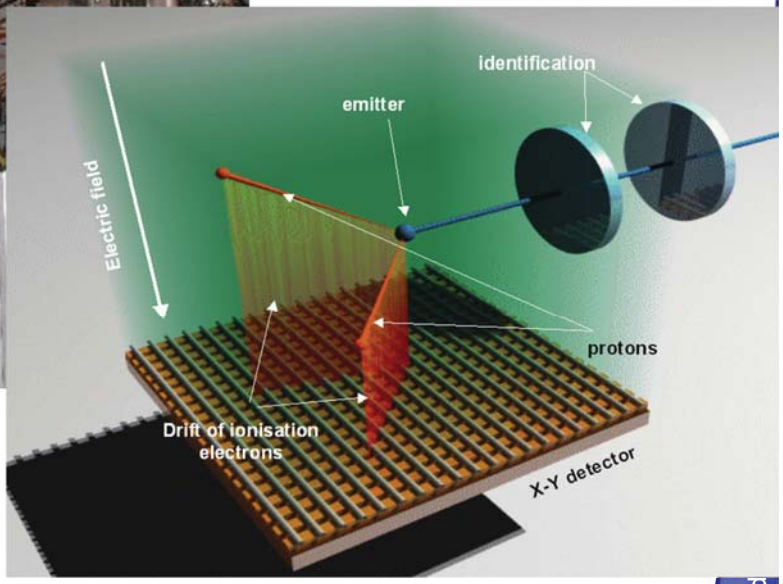

Universal Magic Numbers Mayer and Jensen (1949)

Shells N=28

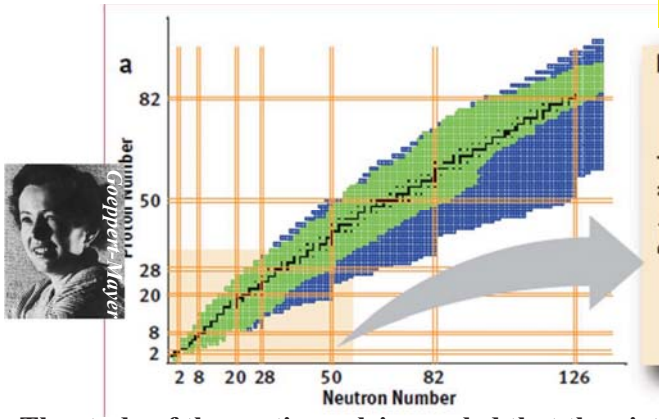

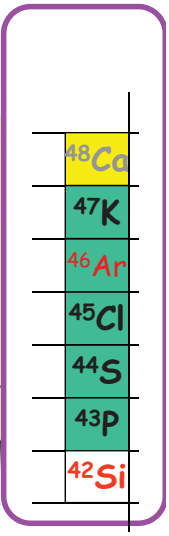

N=28

The study of the exotic nuclei revealed that the picture of "magic number" has to be refined…

At N=28, the ^{48}Ca is "magic" (spherical) but different experimental observations lead to the conclusion that the deformation plays an important role when Z≤20.

- strongly deformed ^{42}Si
- spherical-prolate shape coexistence in ^{44}S

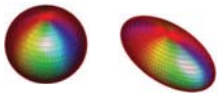

GANIL Spiral2

I) Motivations and goals "Key nucleus" 42Si

nature Vol 435|16 June 2005
LETTERS

To Nature (MSU 2005)

'Magic' nucleus ^{42}Si

J. Fridmann[1], I. Wiedenhöver[1], A. Gade[2], L. T. Baby[1], D. Bazin[2], B. A. Brown[2], C. M. Campbell[2], J. M. Cook[2], P. D. Cottle[1], E. Diffenderfer[1], D.-C. Dinca[2], T. Glasmacher[2], P. G. Hansen[2], K. W. Kemper[1], J. L. Lecouey[2], W. F. Mueller[2], H. Olliver[2], E. Rodriguez-Vieitez[2], J. R. Terry[2], J. A. Tostevin[1] & K. Yoneda[2]

^{48}Ca (>10^{12} pps) → ^{44}S (100-150 pps) → ^{42}Si* (8/day) → ^{42}Si + γ

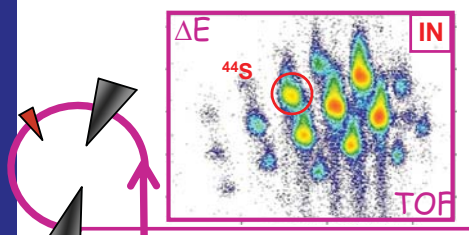

• 2nd Fragmentation

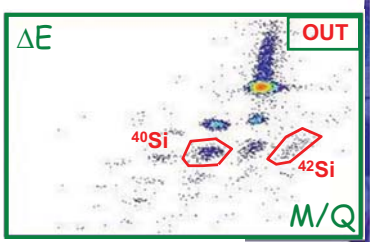

44S → 42Si

Secondary beams

SISSI

48Ca → 44S

Gamma Ball

SPEG (ε~100%)

60 A.MeV
• I(48Ca) ~ 4 μAe -
• First Fragmentation

Collaboration GANIL,IPNO,LPC Caen,SPhN/Dapnia
IFIN Roumanie, Univ Bonn, Univ Paisley, FLNR/JINR
Univ Surrey, IPHC, Univ Madrid

International summer shcool on Subatomic Physics–Beijing Aug 27-31 2011

Sydney Gales

GANIL "in flight" ^{42}Si Results

One example N=28 shell

GANIL+SISSI
« In beam gamma Spectroscopy »

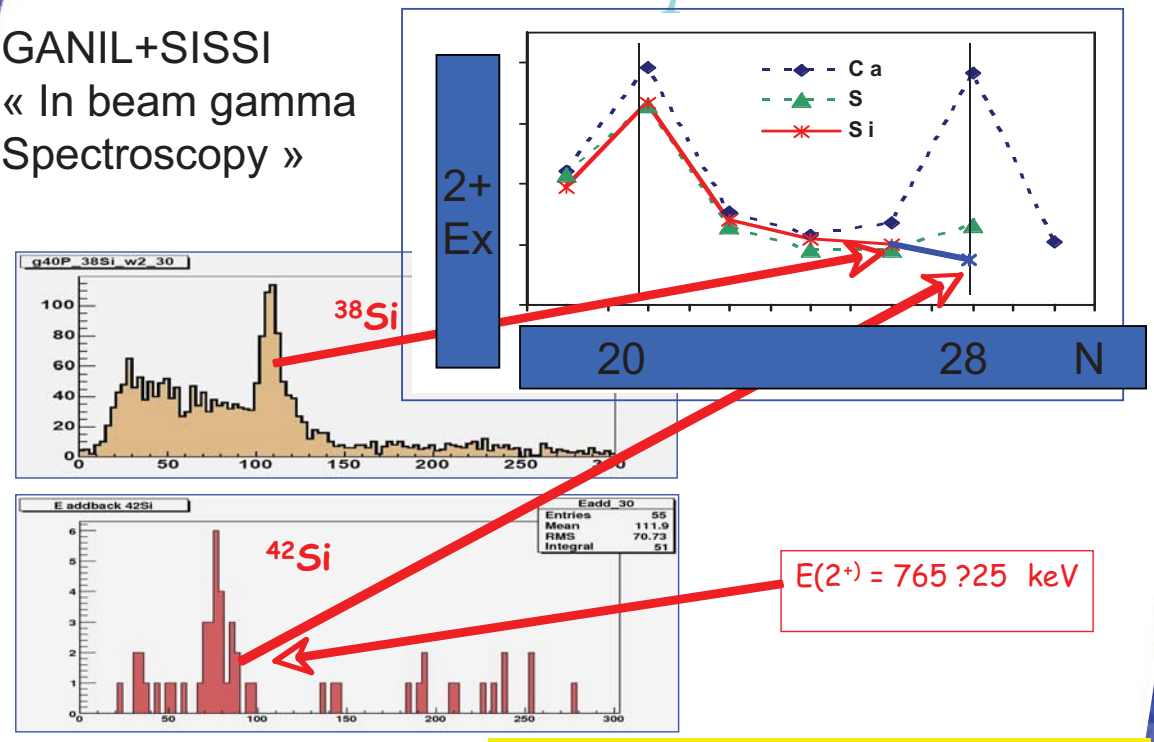

B. Bastin, S. Grévy et al.
PRL99,022503 (2007)

GANIL Spiral2
International summer shcool on Subatomic Physics–Beijing Aug 27-31 2011

New Frontier with ^{238}U intense beams and VAMOS –EXOGAM

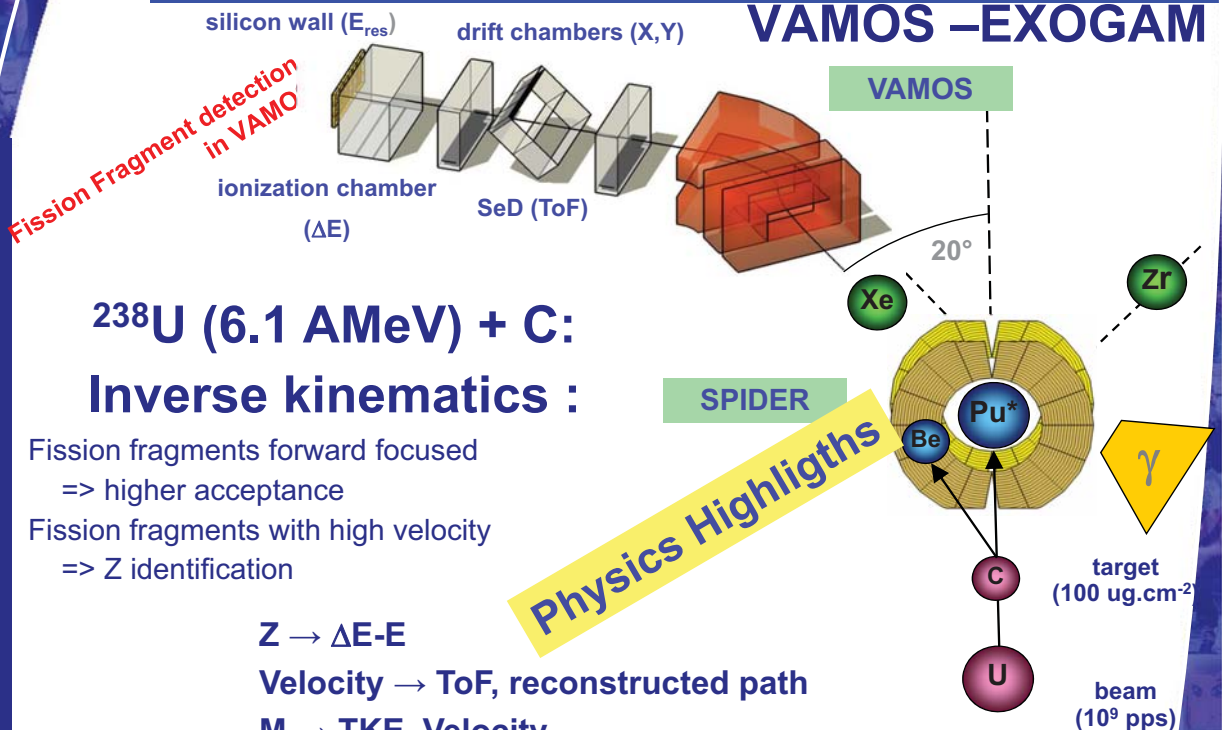

^{238}U (6.1 AMeV) + C:
Inverse kinematics :

Fission fragments forward focused
=> higher acceptance
Fission fragments with high velocity
=> Z identification

Physics Highligths

Z → ΔE-E
Velocity → ToF, reconstructed path
M → TKE, Velocity
M/Q → Bρ, Velocity
30 < Z < 60 **ΔZ/Z ~ 1.5 %**
70 < M < 160 **ΔM/M ~ 0.6 %**

Sydney Gales

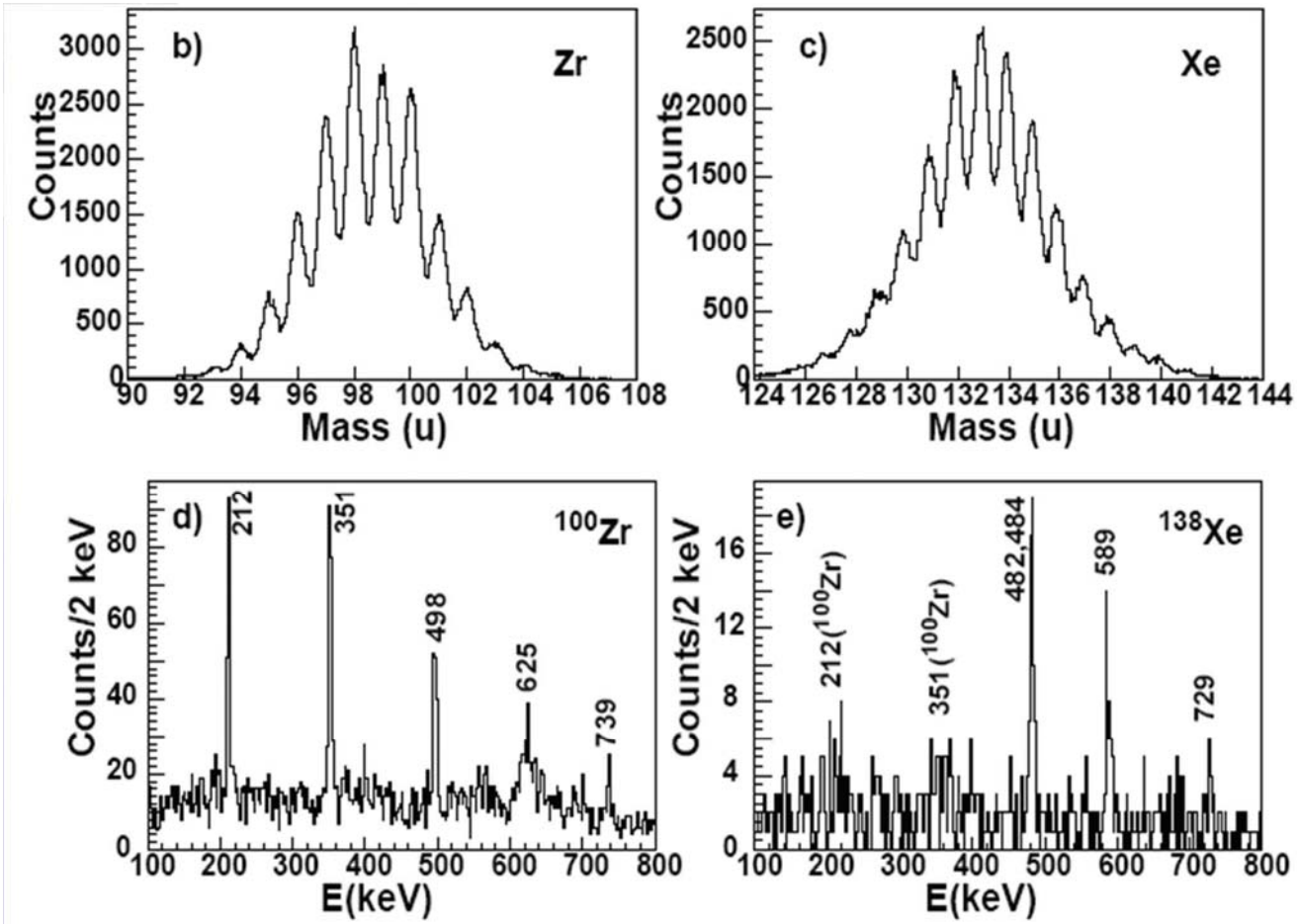

GANIL Spiral2

International summer shcool on Subatomic Physics–Beijing Aug 27-31 2011

END of Part 1

Sydney Gales

Properties of Cyclotrons

- The cyclotron frequency ν formula

$$\nu = qB_m / 2\pi m_0$$

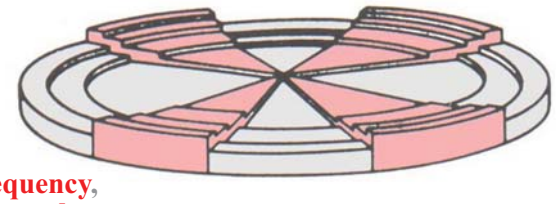

showing the link between mass, field and frequency, note, that this can be used for high-precision nuclear mass measurements

- but the formula, even more importantly, also suggests how to overcome the initial relativistic effects in a cyclotron (starting around 20 MeV for a proton): the relativistic mass increase with increasing $\beta=v/c$ of $m=\gamma \cdot m_0$, $\gamma=(1-\beta^2)^{-1/2}$ can be compensatedby correspondingly increasing the magnetic field in order to maintain the frequency ν constant, this can be done by shaping the poles (see figure) and adding "trim coils", such an accelerator is called an isochroneous cyclotron,

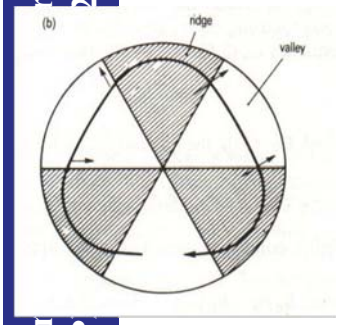

- Unfortunately, a cyclotron can not have any direct focusing elements inside and that for flight paths which exceed kilometers
- The way to overcome partially the absence of vertical focusing, is to use alternate gradient focusing by passing in successively in sectors of strong and weak (or zero fields.) called Sector Separated Cyclotrons

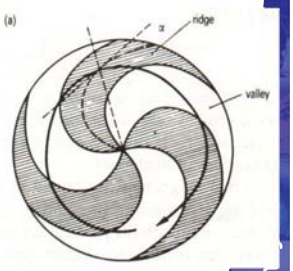

ISOL

at the highest power levels

- One stage :direct use of charged particles, minimize dE/dx (low Z, high E at 1 GeV max. 100 - 200 kW)

- Two stage :use neutral particles in second stage, i.e. neutrons & photons for neutrons 5 MW of proton beam (like spallation source)

Combine also (fragmentation + gas collec- tion scheme) is also in this class

What are the limits of the heaviest elements?

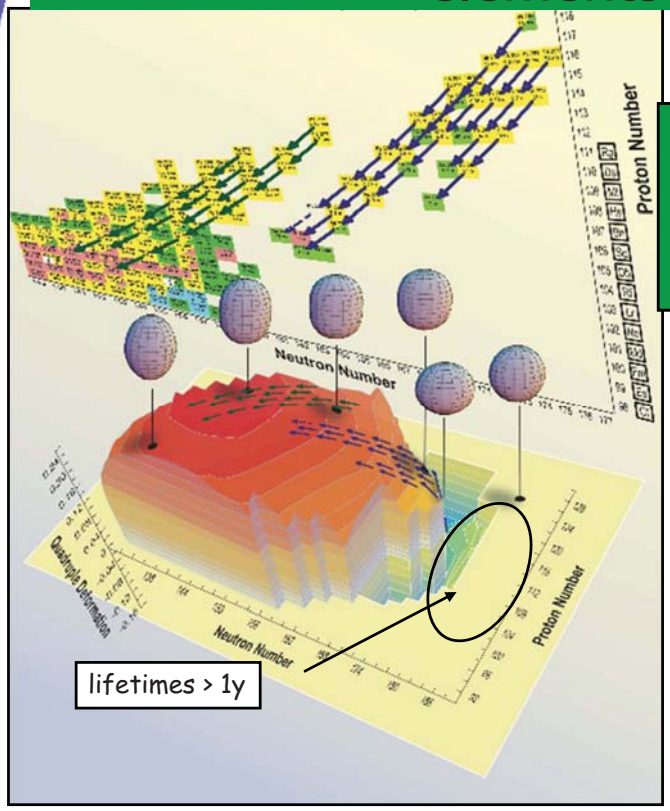

SCIENCE Magazine- July 2005 Top 125 Questions: Are there stable high-atomic-number elements?

Physics Highligths

Search for New Super-Heavy Elements@GANIL

Z=120 via fusion of ***Ni+U*** reaction – Coll **IPNO Orsay-GANIL**

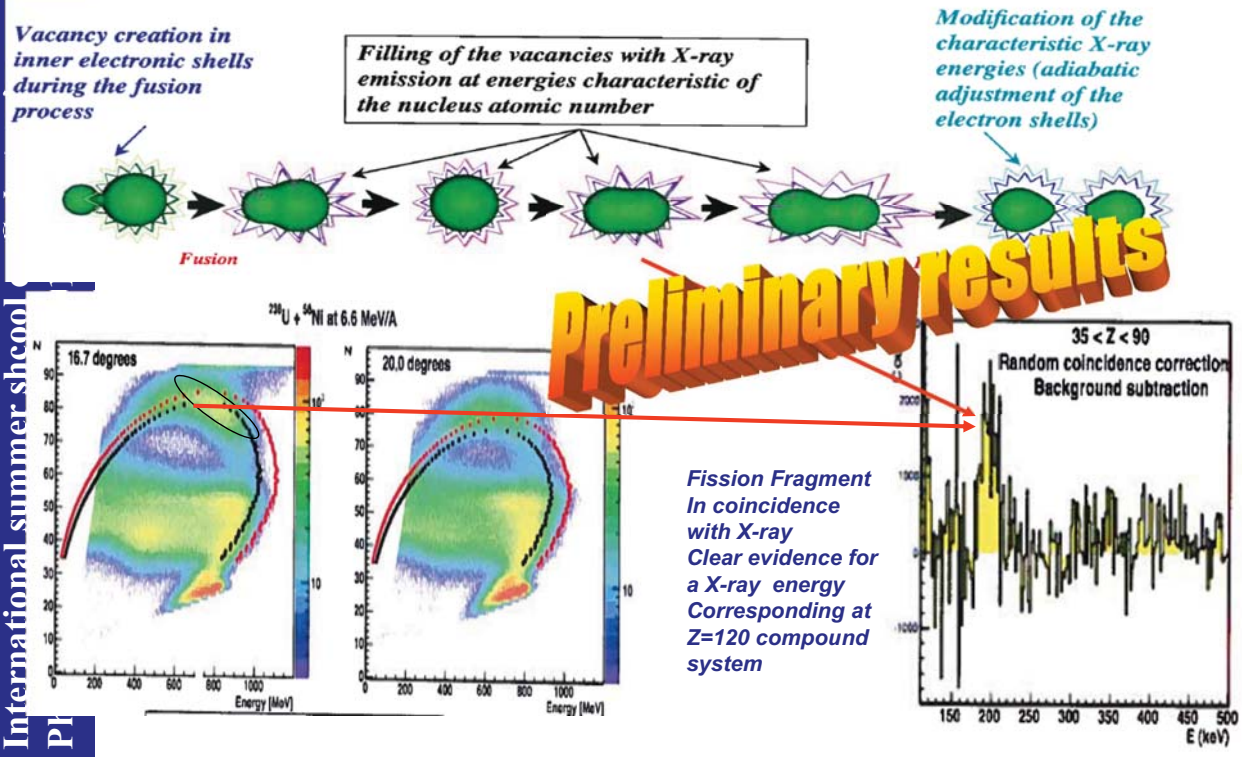

Fission Fragment In coincidence with X-ray Clear evidence for a X-ray energy Corresponding at Z=120 compound system

1961 Goldanski predicts 2 protons radioactivity

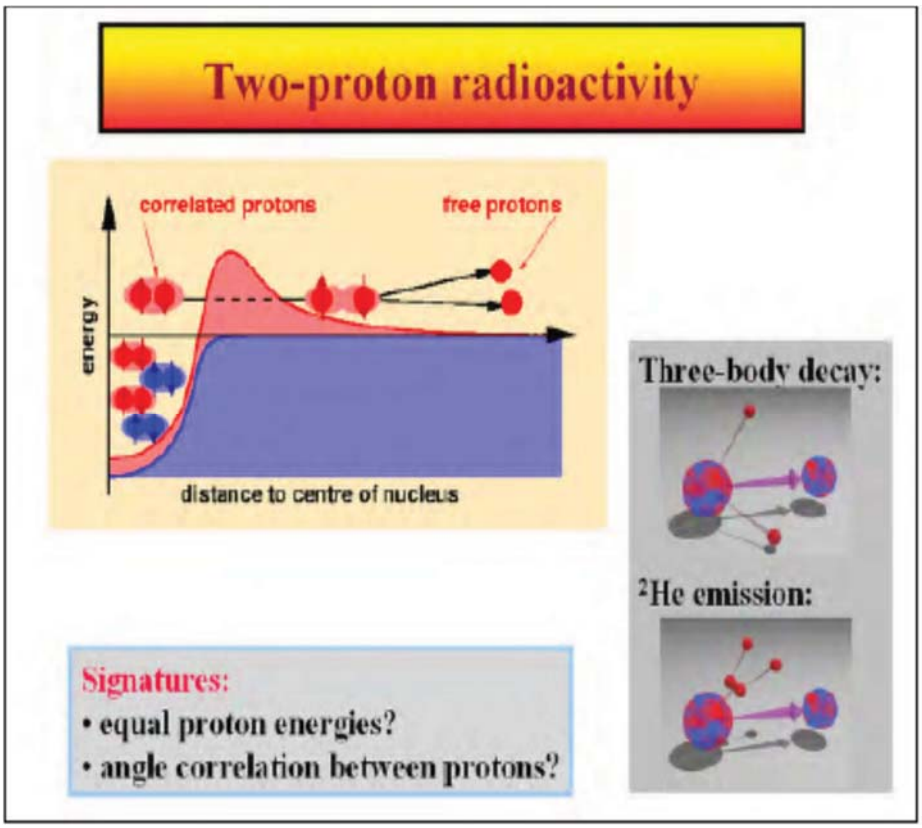

PRL 99, 102501 (2007) PHYSICAL REVIEW LETTERS week ending 7 SEPTEMBER 2007

First Direct Observation of Two Protons in the Decay of ^{45}Fe with a Time-Projection Chamber

J. Giovinazzo,[1] B. Blank,[1] C. Borcea,[1,*] G. Canchel,[1] J.-C. Dalouzy,[2] C. E. Demonchy,[1] F. de Oliveira Santos,[2] C. Dossat,[3] S. Grévy,[2] L. Hay,[1,†] J. Huikari,[1] S. Leblanc,[1] I. Matea,[1] J.-L. Pedroza,[1] L. Perrot,[2] J. Pibernat,[1] L. Serani,[1] C. Stodel,[2] and J.-C. Thomas[2]

[1]*Centre d'Etudes Nucléaires de Bordeaux Gradignan-Université Bordeaux 1-UMR 5797 CNRS/IN2P3, Chemin du Solarium, BP 120, F-33175 Gradignan Cedex, France*

[2]*Grand Accélérateur National d'Ions Lourds, CEA/DSM-CNRS/IN2P3, Bvd Henri Becquerel, BP 55027, F-14076 CAEN Cedex 5, France*

[3]*DAPNIA, CEA Saclay, F-91191 Gif-sur-Yvette Cedex, France*

(Received 5 March 2007; published 7 September 2007)

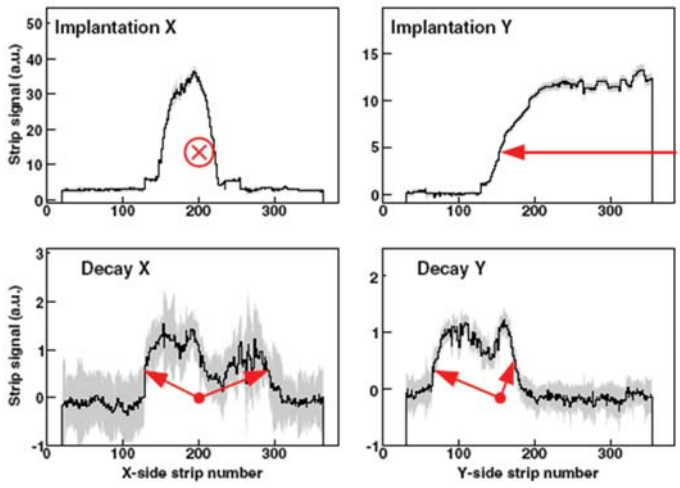

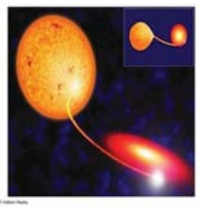

Cross section of astrophysical interest 18F(p,α)15O

Need to know rates of reactions creating and destroying ^{18}F

First direct measurement at GANIL via Spectroscopy of 19Ne using the reaction H(18F,p)18F

E ~ 4 AMeV

$2x10^4$ pps ^{18}F (a new beam at GANIL) Purity > 97 %

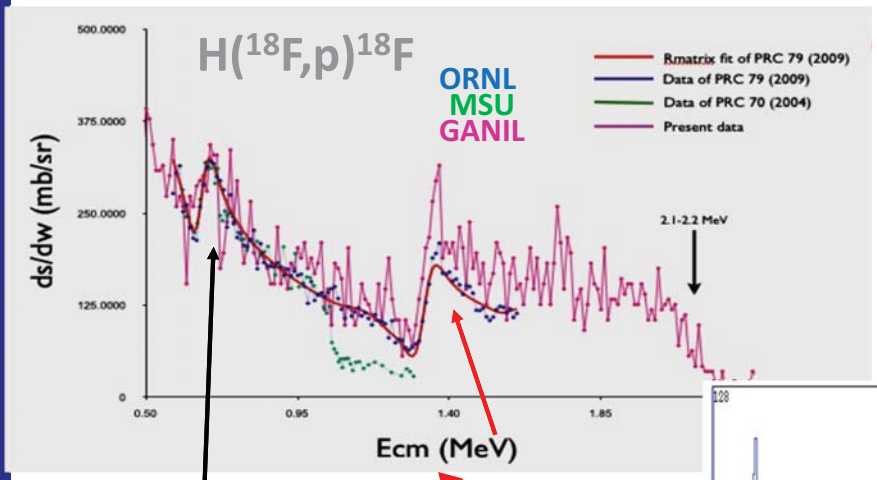

Orsay, LPC Caen,

- **Try to confirm the existence of a new broad ½+ state in ^{19}Ne**

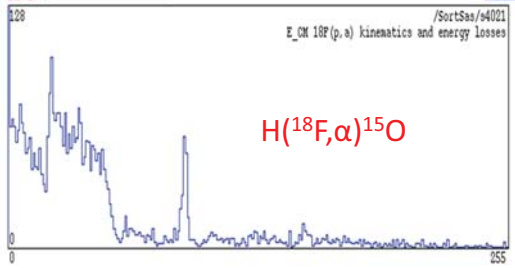

Other states detected in $H(^{18}F,\alpha)^{15}O$

GANIL Spiral2
International summer shcool on Subatomic Physics–Beijing Aug 27-31 2011

EXOGAM physics highlight

^{92}Pd: evidence for a new spin aligned np coupling scheme

End-point of the N=Z line and the heaviest doubly-magic core (^{100}Sn)

S.p. properties wrt ^{100}Sn core

Ideal « laboratory » for neutron-proton correlations in identical orbitals

Isovector (T=1, I=0) and (T=0, I=1) isoscalar np pairing

End point of the rp process path in X-ray bursts and steady-state hydrogen burning on accreting neutron stars

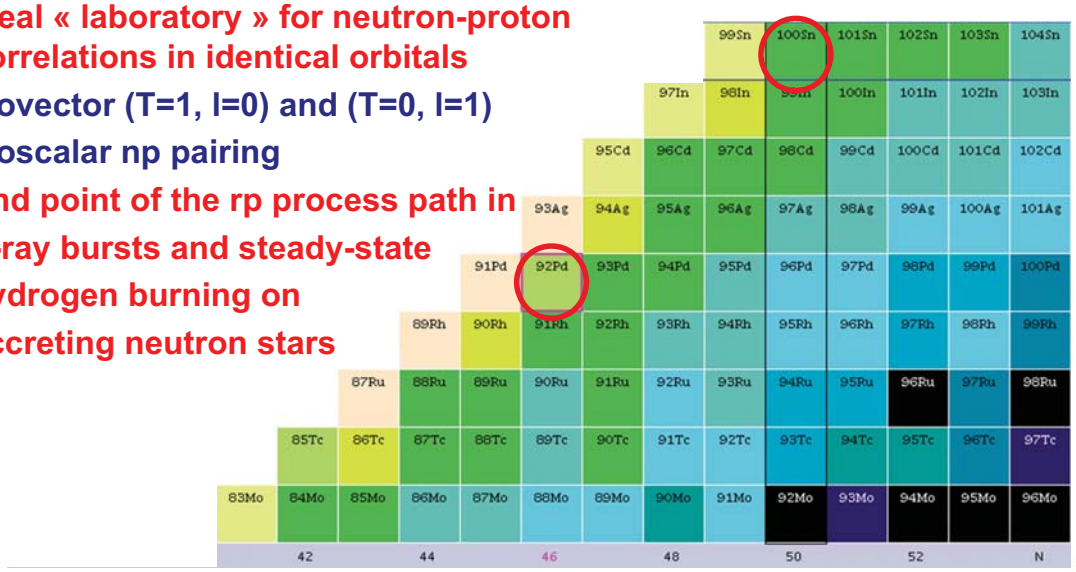

Sydney Gales

^{92}Pd: evidence for a new spin aligned np coupling scheme

*B Cederwall, F. Ghazi-Moradi, T Back, A Johnson, J. Blomqvist, E Clément, G. de France, R Wadsworth et al

EXOGAM-NWall-DIAMANT: The power of the coupling

EXOGAM: 11 Clovers. e_pw ~ 10% for E_g=1.3 MeV

DIAMANT: 80 CsI(Tl) dets. $e_{p \text{ or } a}$ ~ 66%

The Neutron Wall: 50 liquid scintillator detectors. e_{1n} ~ 23%

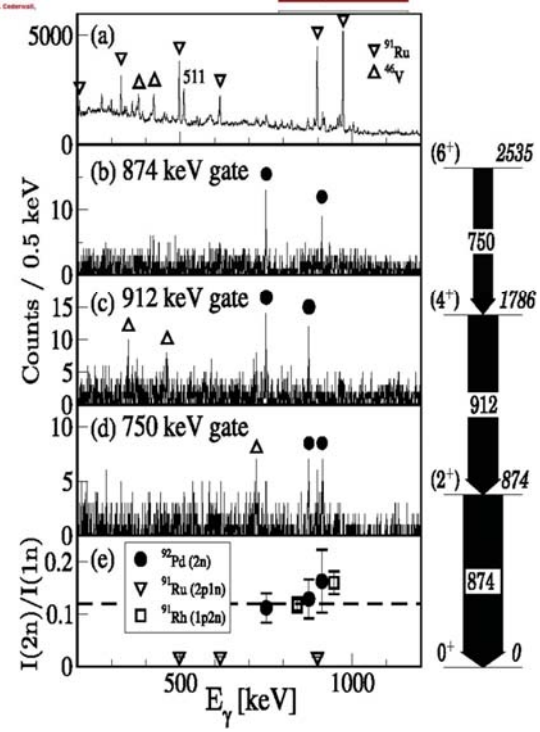

Upgrade SPIRAL 1

GANIL Spiral 2

GANIL 2015 study group

New beams from SPIRAL 1

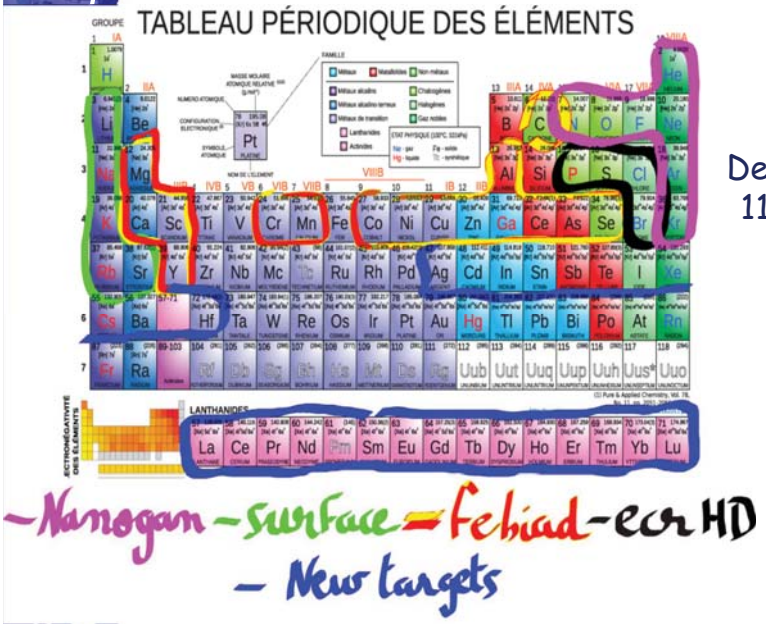

Developments driven by physics cases
11 LoIs were examined at the last PAC meeting (11/03/2010)

Already existing beams
$^{19}Ne^{1+}$, $^{35}Ar^{1+}$

Modifying the target configuration
^{118}Xe, ^{120}Xe, ^{15}C

Alkali beams
$^{8}Li^{1+}$, $^{21}Na^{1+}$, $^{37}K^{1+}$, ^{38}K

Metallic beams
$^{25}Al^{1+}$, ^{28}Mg, $^{39}Ca^{1+}$, $^{41}Sc^{1+}$, ^{68}Se

Non metallic beams
$^{29}P^{(1+/n+)}$, ^{30}P, $^{31}S^{1+}$, $^{33}Cl^{(1+/n+)}$

FEBIAD as first priority: VADIS (MoU ISOLDE)

Internatio Physics–B

Sydney Gales

AGATA physics campaigns 2010-15

AGATA MoU: at least 25% at GANIL, GSI and LNL
Campaigns decided by AGATA Steering Committee

2010/11
→ LNL
≥5 ATC

2012/13
→ GSI/FRS
≥5 ATC + 5 ADC

2014/15
→ GANIL/SPIRAL2
~10 ATC + 5 ADC

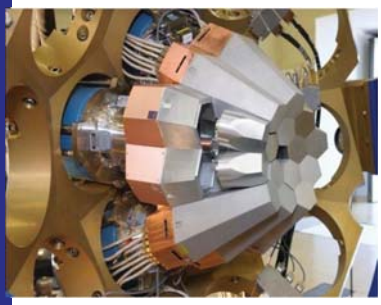

AGATA-5 + PRISMA

total eff. ε ~ 6%

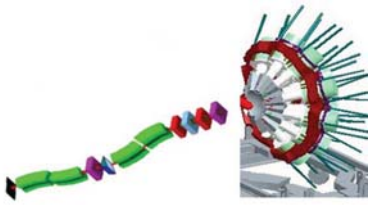

AGATA-10 @ FRS

total eff. ε > 10%

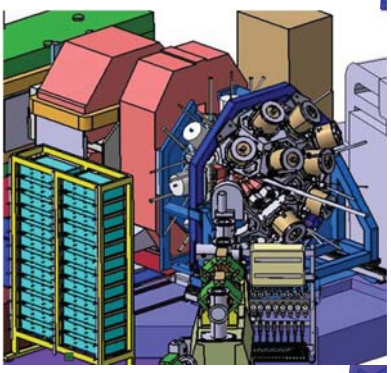

AGATA-15 + VAMOS

total eff. ε > 15 %

International summer shcool on Subatomic Physics–Beijing Aug 27-31 2011

Sydney Gales

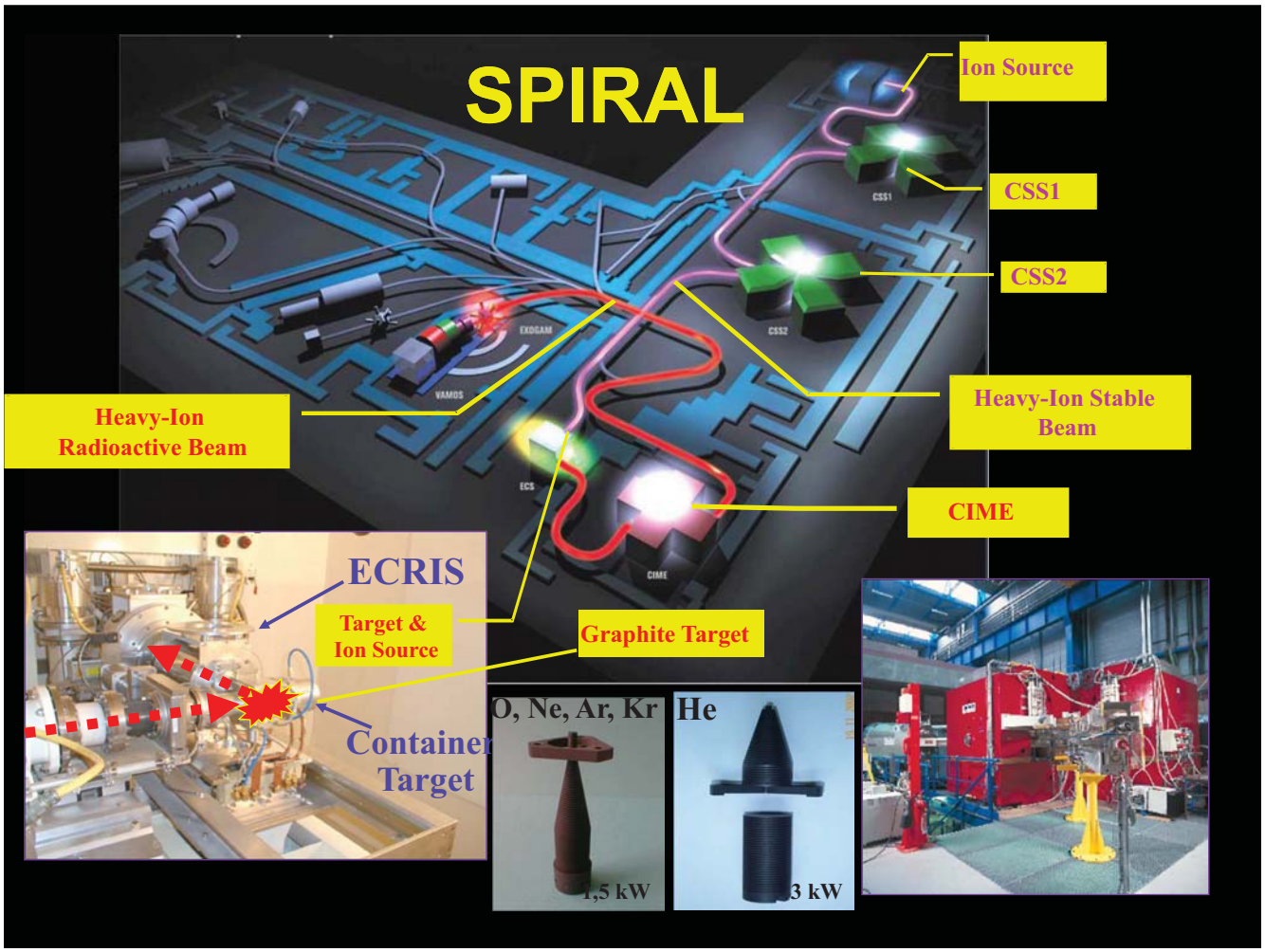

SPIRAL operation

(http://www.ganil.fr/operation/available_beams/radioactive_beams.htm)

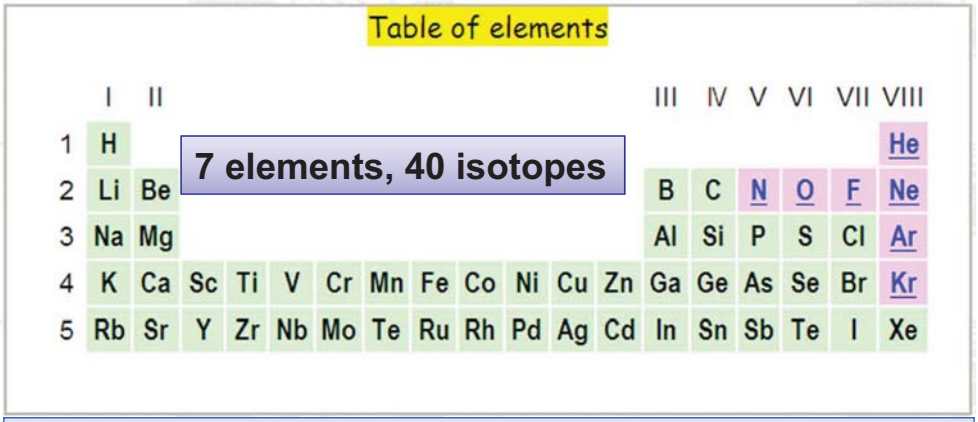

SPIRAL scientific production 2001 – 2008 :
70 physics articles
12 PhD Thesis
53 technical articles
7 PhD thesis

Recent overview article:
Navin Alahari et al.
J. Phys. G: Nucl. Part. Phys. 38 (2011) 024004.

Sydney Gales

GANIL laboratoire commun CEA/DSM Spiral2 CNRS/IN2P3

Heavy ion beams ,among the most intense in the world
From Carbone to Uranium
0 to 95 MeV/n
"Exotic" Beams In Flight and/or SPIRAL 0-25 MeV/n
An ensemble of detectors and spectrometers rather unique In the world !!

« Exotic Nuclei »

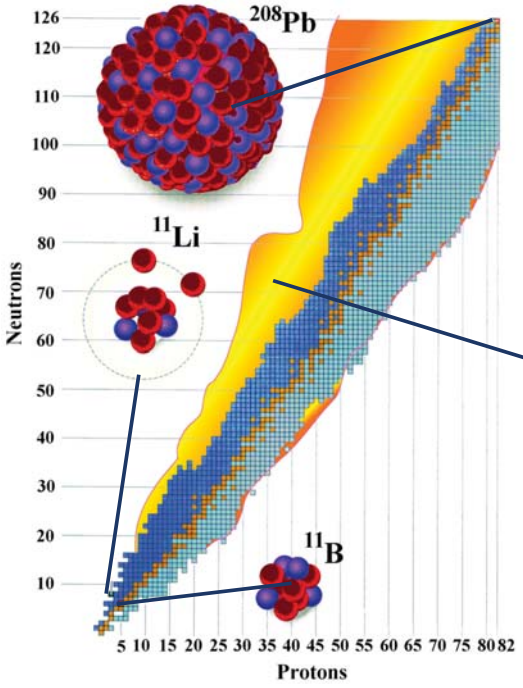

H. Rousseau, *Forêt Vierge ...*

A Typical Experiment with RIB (@ Ganil)

6,8He inverse kinematics reaction

MUST: Y. Blumenfeld et al., *NIM* **A366** (1999) 298
CATS: S. Ottini-Hustache et al., *NIM* **A431** (1999) 476

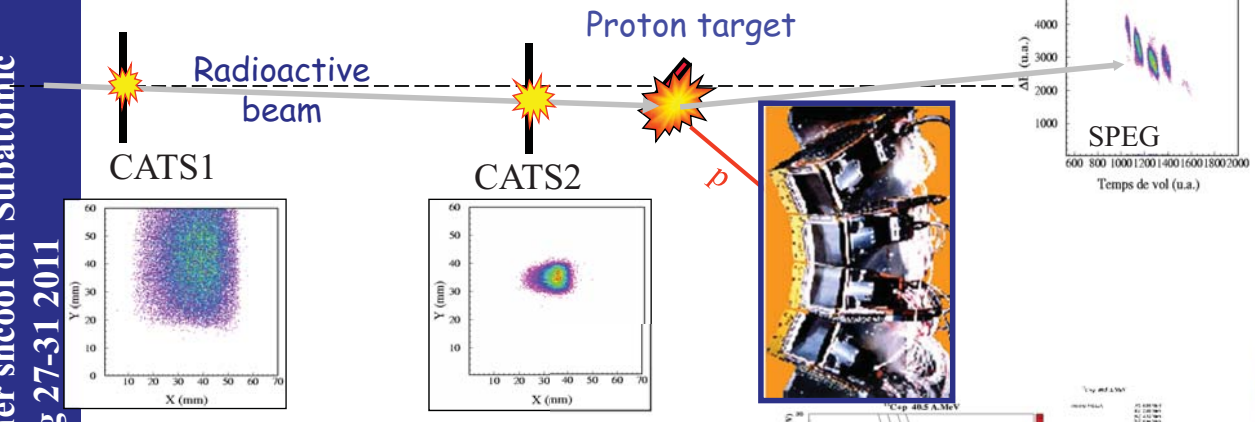

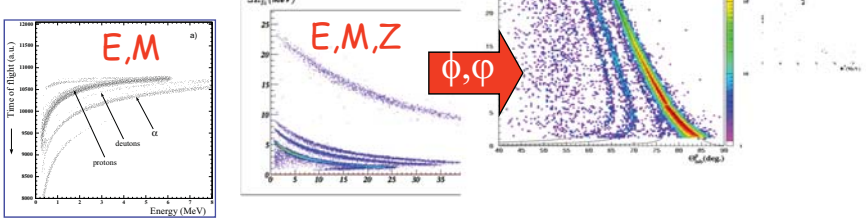

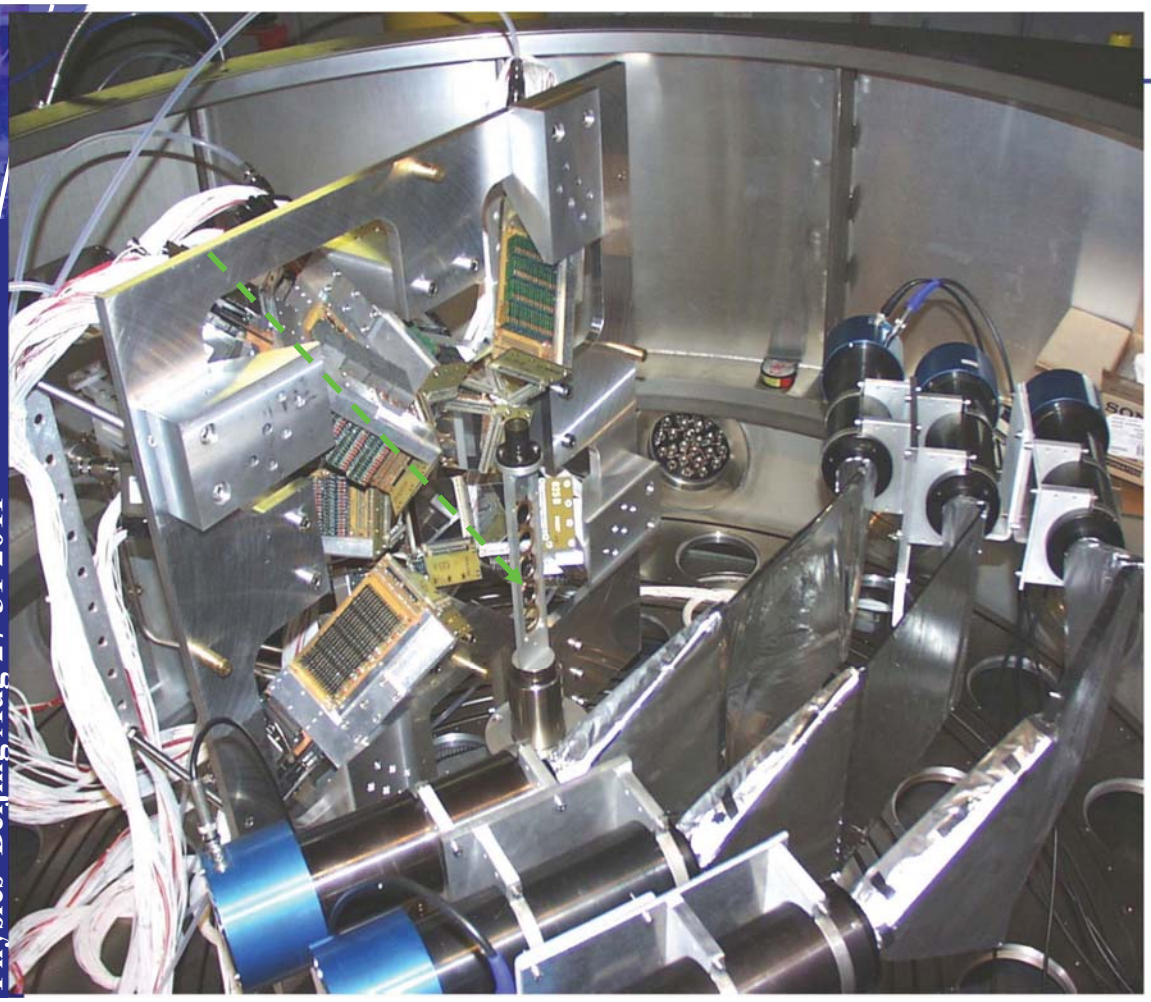

^{6}He (p,p') halo or skin?

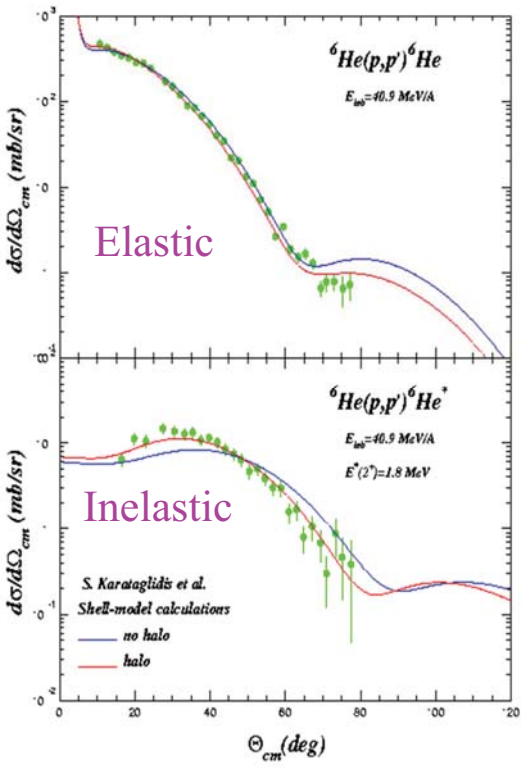

A. Lagoyannis et al PLB 518 (2001) 27

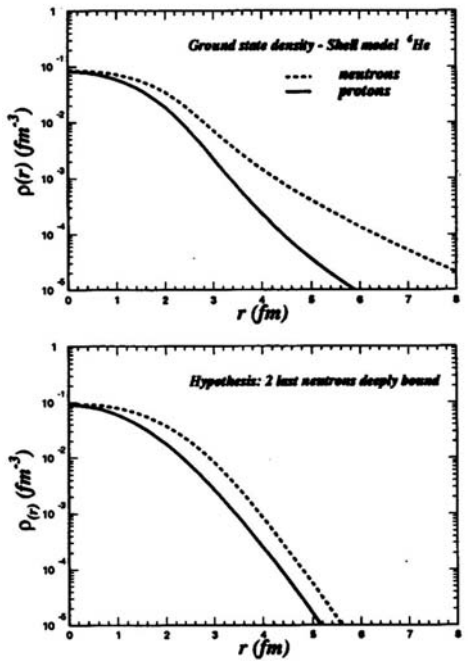

Sydney Gales

Universal Magic Numbers Mayer and Jensen (1949)

Shells N=28

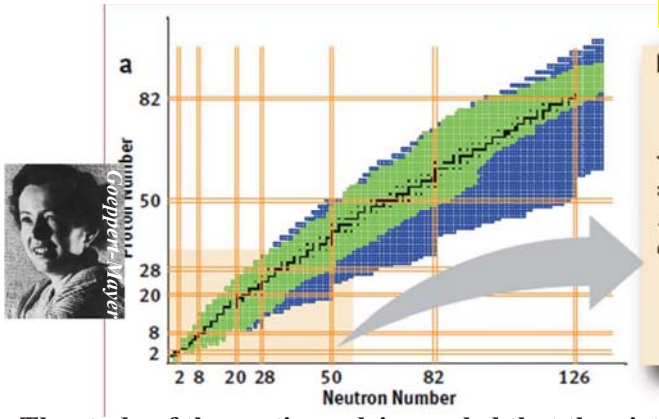

N=28

The study of the exotic nuclei revealed that the picture of "magic number" has to be refined…

At N=28, the ^{48}Ca is "magic" (spherical) but different experimental observations lead to the conclusion that the deformation plays an important role when Z≤20.

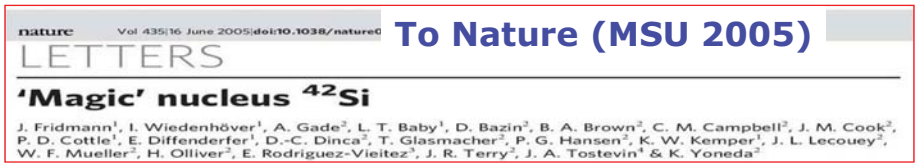

To Nature (MSU 2005)

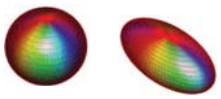

GANIL Spiral2

I) Motivations and goals "Key nucleus" 42Si

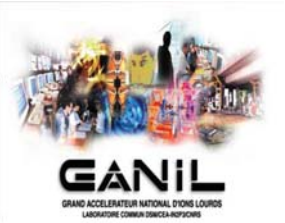

^{48}Ca (>10^{12} pps) → ^{44}S (100-150 pps) → ^{42}Si* (8/day) → ^{42}Si + γ

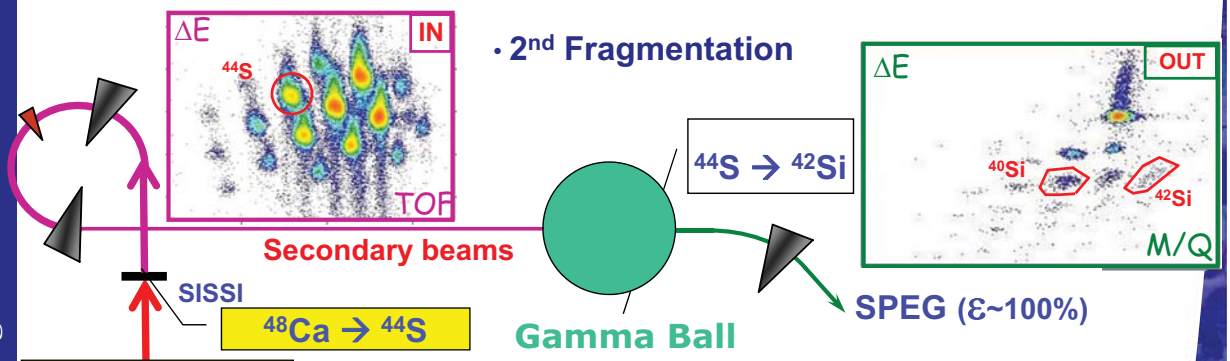

60 A.MeV
• I(^{48}Ca) ~ 4 μAe -
• First Fragmentation

Collaboration GANIL,IPNO,LPC Caen,SPhN/Dapnia
IFIN Roumanie, Univ Bonn, Univ Paisley, FLNR/JINR
Univ Surrey, IPHC, Univ Madrid

International summer shcool on Subatomic Physics–Beijing Aug 27-31 2011

Sydney Gales

GANIL "in flight" ^{42}Si Results

One example N=28 shell

GANIL+SISSI
« In beam gamma Spectroscopy »

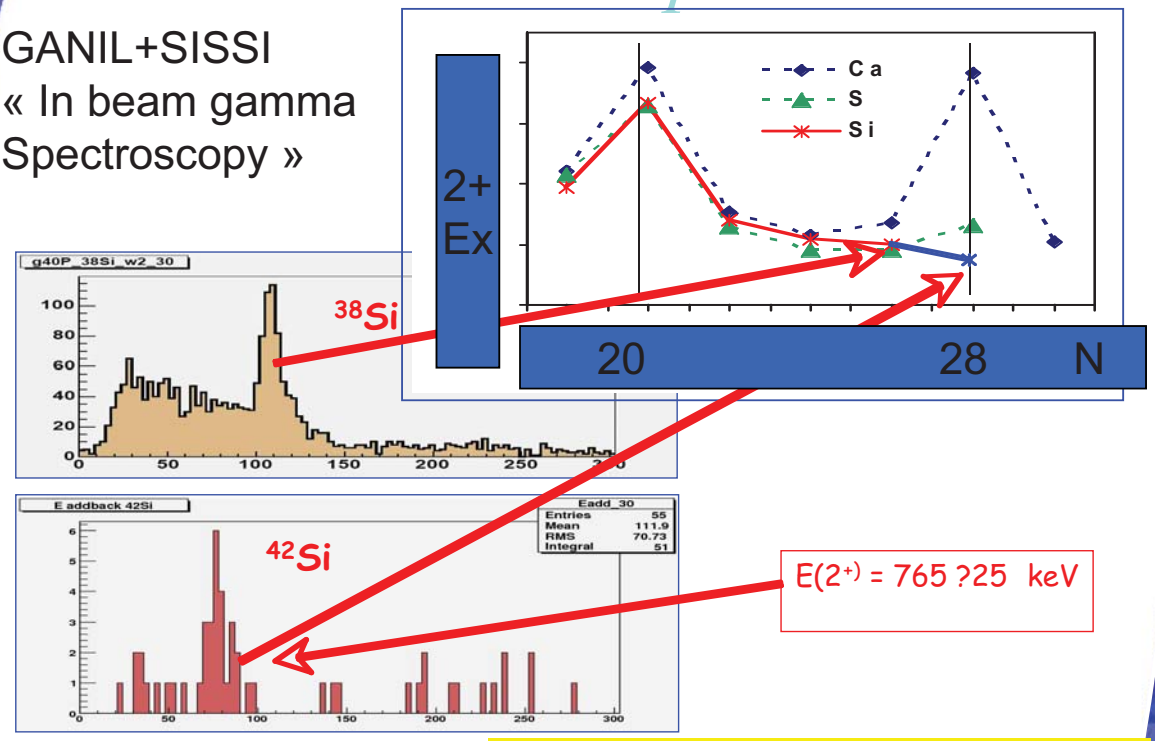

B. Bastin, S. Grévy et al.
PRL99,022503 (2007)

International summer shcool on Subatomic Physics–Beijing Aug 27-31 2011

Sydney Gales

Physics opportunities and Status of the SPIRAL2 Project

Outlines

5.SPIRAL2 Facility

5.1 International Context

5.2 Beams and Detectors

5.3 Physics Opportunities with high-intensity stable-ion and RI beams

6. Status of the Construction of SPIRAL2

7.Conclusions & Long(er) Range Plan

GANIL Spiral2

International summer shcool on Subatomic Physics–Beijing Aug 27-31 2011

The frontiers of nuclear science today require new tools, technologies, and accelerators. The quest is to understand the origin, evolution, and structure of the visible matter in the universe. Radioactive Ion Beams are central to this quest worldwide. GANIL is one of the leading facilities worldwide.

GANIL Spiral2

International summer shcool on Subatomic Physics–Beijing Aug 27-31 2011

GANIL/SPIRAL1/SPIRAL2

SPIRAL2 main goal
The high intensity frontier
both for stable heavy ions
and secondary Radioactive Ion Beams

The linac is a resonance accelerator

- An RF (80-120 MHz) source is used to generate an electric field in a region of a resonant metallic structure
- The particles of the beam need to be localized in *bunches* and properly phased with respect to the field so that the beam is accelerated

$$\frac{d(\gamma m_0 c^2)}{ds} = qE_z(s,t)$$

- In order to keep acceleration along the linac this synchronism condition needs to be maintained.

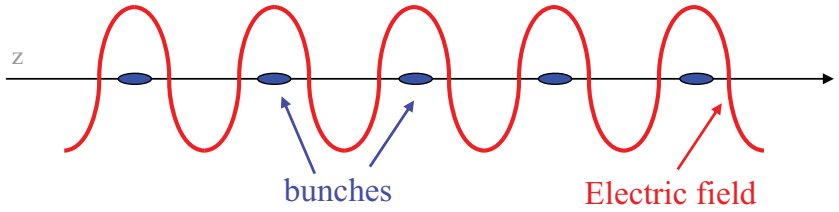

cnrs IN2P3 Les deux infinis

136 M€
2006-2014

Construction in 2 Phases

ceci

Phase 1 2013
Accelerator & S3, NFS

Phase 2 2014-2015
RIB production Building & DESIR

Civil construction: 2011 – 2014
Phase 1 permit granted
11Oct 2010

Investment (with 10% contingencies): 136 M€
CNRS, CEA, Local Region
Total cost: 196 M€ (136+60 Manpower)
In the investment budget 26M€ are expected to come from EU and international partners

SPIRAL 2 New Detectors

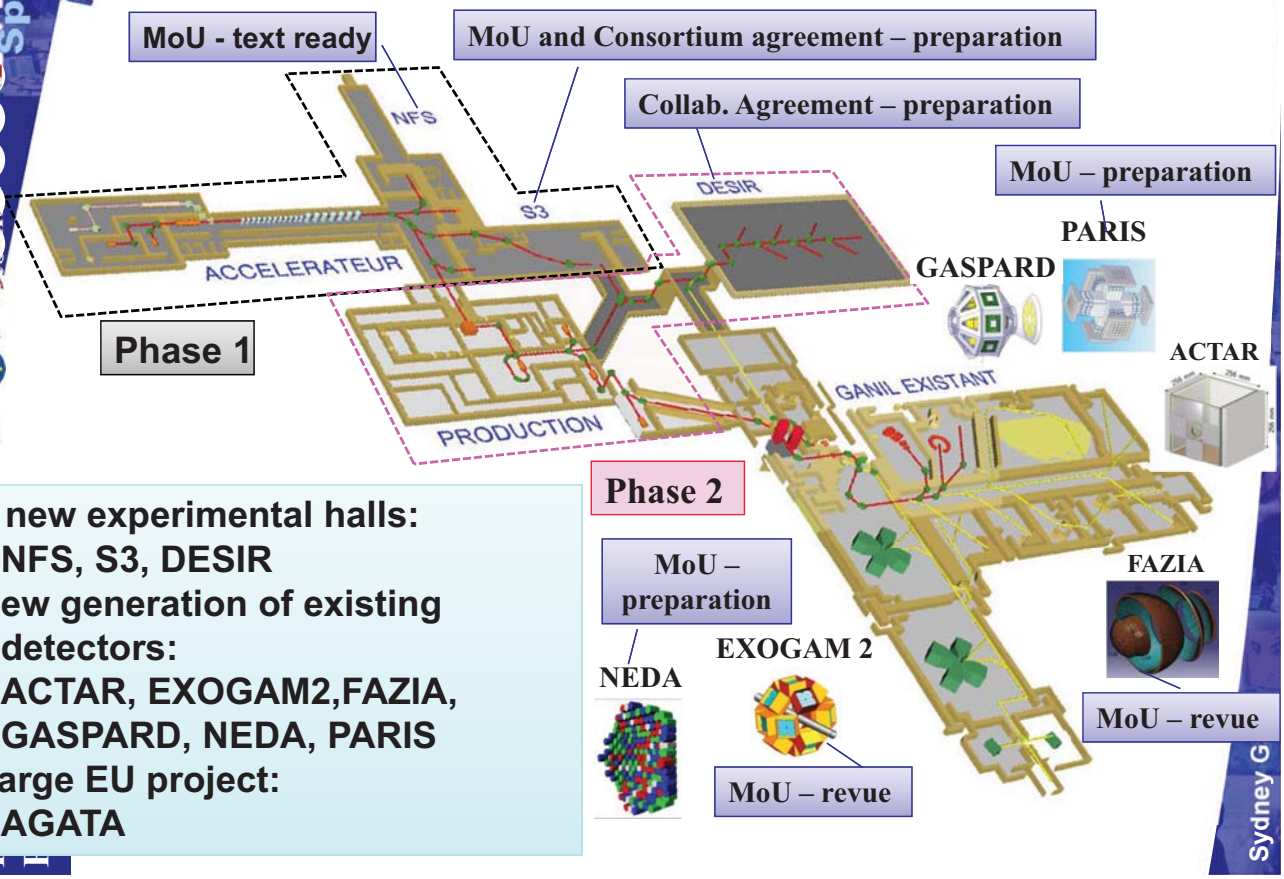

3 new experimental halls:
NFS, S3, DESIR
New generation of existing detectors:
ACTAR, EXOGAM2,FAZIA, GASPARD, NEDA, PARIS
Large EU project:
AGATA

Sydney G

Lol and Coll :New detectors to be used at SPIRAL 2

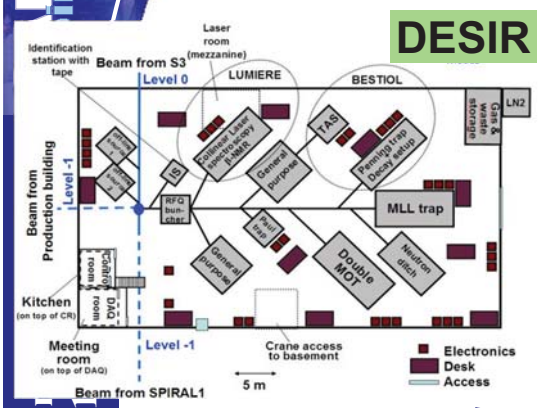

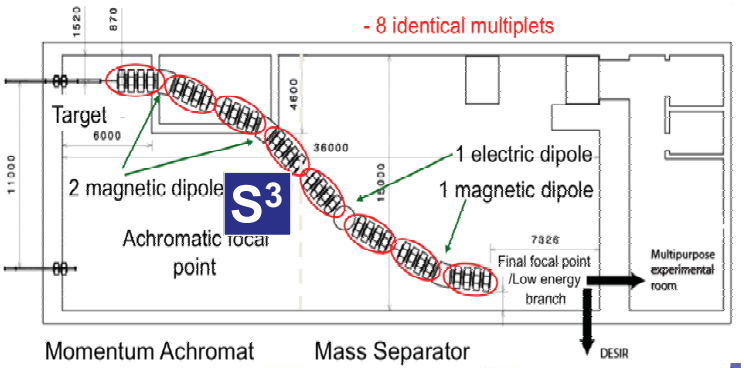

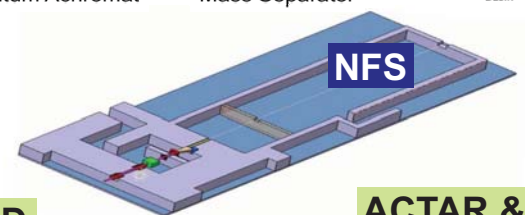

AGATA

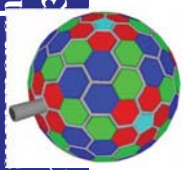

GASPARD

PARIS

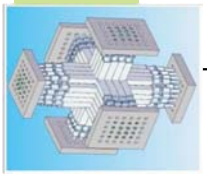

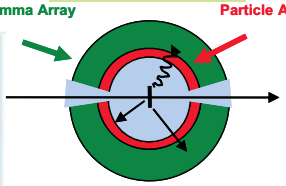

FAZIA

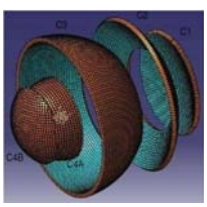

ACTAR & GET

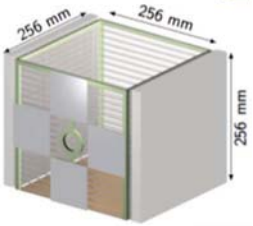

NEDA

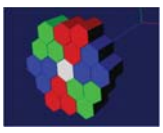

2011: MoUs, TDRs and follow-up

International Physics–Beijin

Syd

International Collaborations

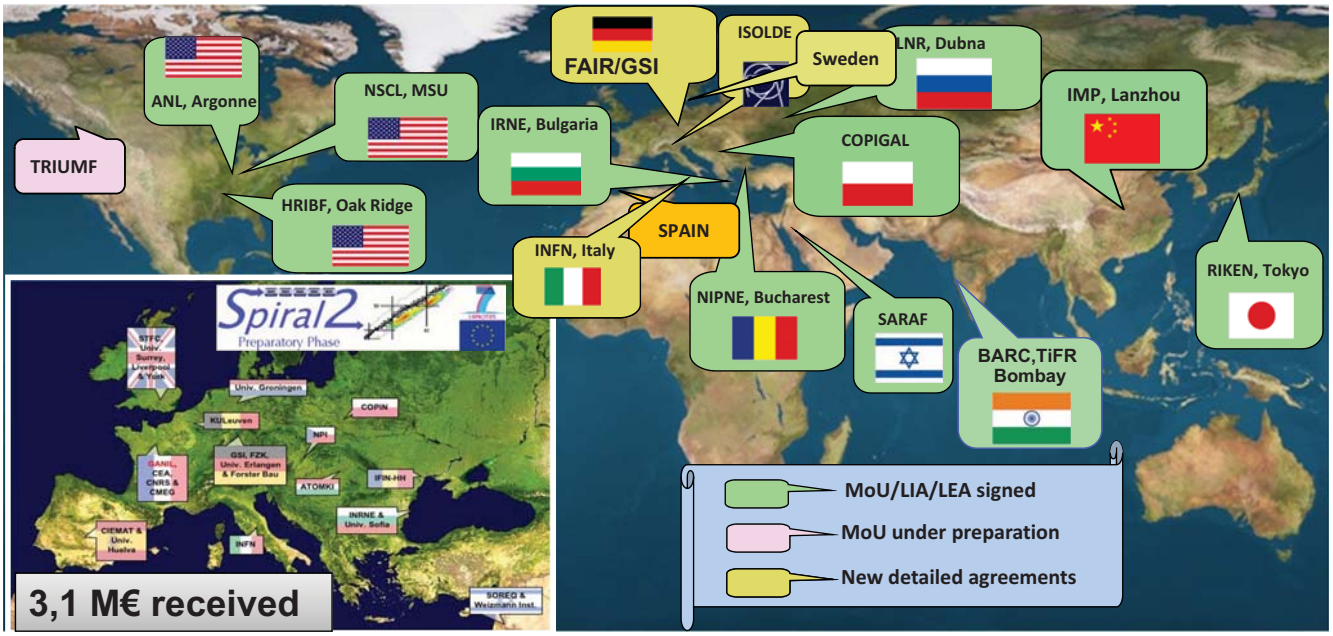

16 signed (LEA*, LIA**, MoU***) agreements
3 agreements under preparation:
- MoU with GSI (FAIR)
- MoU with Bilbao (RIB production module)

LINAC Stable beams for the Day 1 SPIRAL2 Phase 1 experiments*)
Based on the recommendations of SPIRAL2 SAC for the LoI

Energy = 0.75-15 *A.MeV*

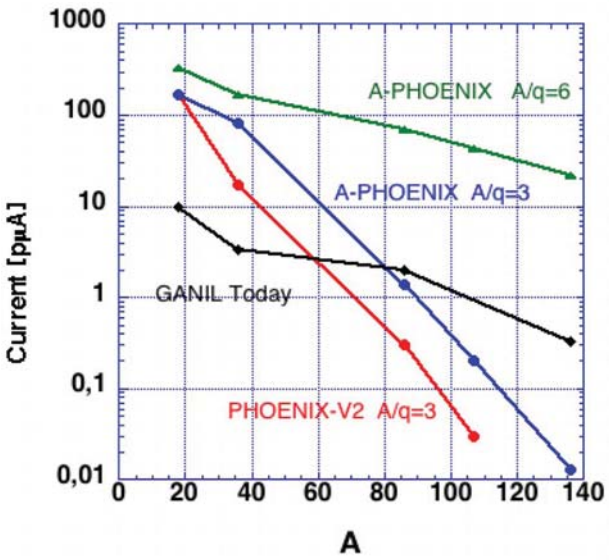

Ion(s)	Energy Range (MeV/nucleon)	Maximum Intensity (pμA)	Date of availability***)	Remarks
$^{1}H^{1+}$	20-33	2-10	December 2012	NFS beam line; Intensity with fast chopper 1/100
$^{2}H^{1+}$	10-20	2-10	December 2012	NFS beam line; Intensity with fast chopper 1/100
$^{4}He^{2+}$	10-20	2-10	December 2012	NFS beam line; Intensity with fast chopper 1/100
$^{12}C^{4+}$	5-7	≥10**)	February 2013	S3 beam line
$^{18}O^{6+}$	5-7	≥10**)	February 2013	S3 beam line
$^{22}Ne^{8+}$	5-7	≥10**)	February 2013	S3 beam line
$^{40}Ar^{14+}$	4-5	≥10**)	February 2013	S3 beam line
$^{28-30}Si^{10+}$ or $^{32-36}S^{12+}$	5-7	≥10**)	November 2013	S3 beam line
$^{40}Ca^{14+}$	5-7	≥10**)	November 2013	S3 beam line
$^{48}Ca^{16+}$	5-7	≥10**)	November 2013	S3 beam line
$^{58}Ni^{18+}$	4-14	≥1**)	November 2013	S3 beam line

*) The parameters indicated in this table are the first and the best approximations that can be done today.
**) Based on the order of magnitude of the expected best currents extracted from a high performance, fully operational, 28 GHz ECR Ion source.

http://pro.ganil-spiral2.eu/spiral2/spiral2-beams

GANIL Spiral2

on Subatomic

011

Liberté • Égalité • Fraternité
RÉPUBLIQUE FRANÇAISE
MINISTÈRE DE L'ENSEIGNEMENT SUPÉRIEUR ET DE LA RECHERCHE

INVESTISSEMENTS D'AVENIR

(S3)

Call for proposals « Equipments of excellence » (EQUIPEX)

76 Projects selected (all disciplines) out of 336 projects ranked by an international Jury

107 physicists, 30 institutions, 12 countries
Management Board
Hervé SAVAJOLS – GANIL, France (Project leader)Antoine DROUART – Irfu/SPhN (CEA), France (Spokesperson) Jerry A. NOLEN – Argonne National Laboratory, USA (Spokesperson)

SHE and N=Z Physics

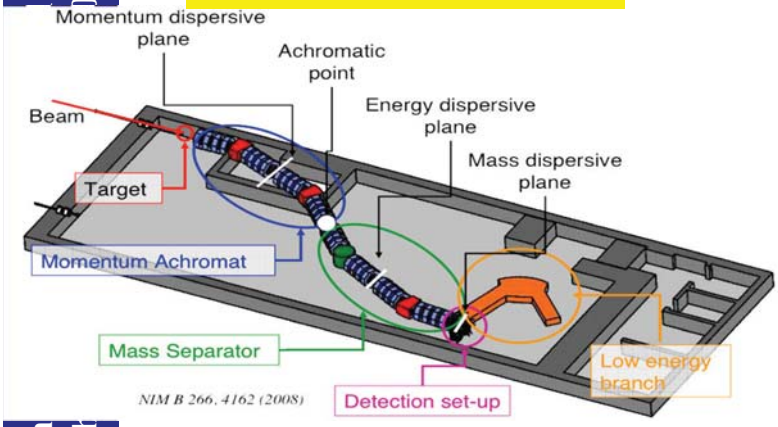

S3 Funded 8M€

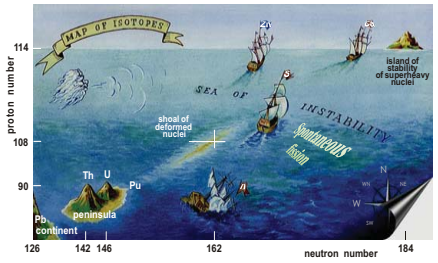

Sydney Gales

In Pl

Proton Dripline & N=Z nuclei

Lol_Day1_6, Lol_Day1_8, Lol_Day1_9 Lol_Day1_11, Lol_Day1_17
- Tests of Shell Model
- Single-Particle structure
- Development of Collectivity
- Shape coexistence

Lol_Day1_3, Lol_Day1_4, Lol_Day1_18
- Ground-State Properties

Lol_Day1_10
- Standard Model

S3 LoI Physics objectives

FISIC project

Lol_Day1_1

Heavy and Superheavy

Heavy and Superheavy Elements

Lol_Day1_2
- Synthesis
- Spectroscopy and Structure

Lol_Day1_5
- Ground-State Properties

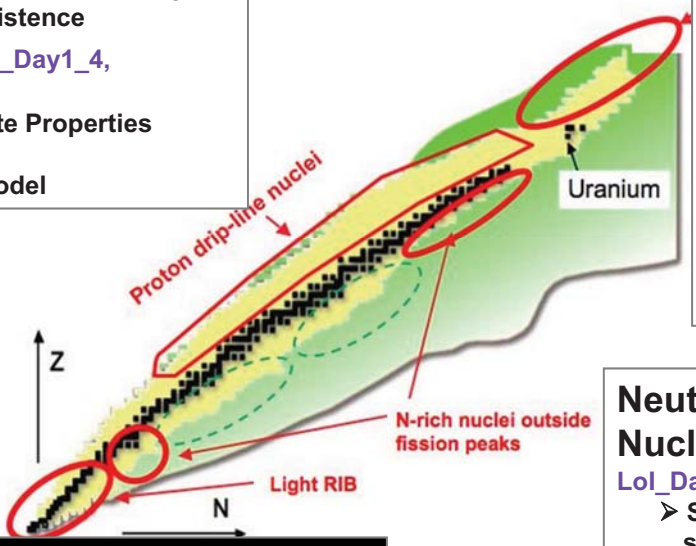

Neutron-Rich Nuclei

Lol_Day1_7
- Single-Particle structure
- Quenching of Shell Gaps

- 13 LoIs submitted
- LoIs signed by 170 physicists
- Requested beam time : 380 days

!!!

Production of SHE with Z=106-108-110-112

$^{40-48}Ca + ^{238}U$	$^{278-286}112^*$
$^{36-40}Ar + ^{238}U$	$^{274-278}Ds^*$
$^{32-36}S + ^{238}U$	$^{270-274}Hs^*$
$^{28-30}Si + ^{238}U$	$^{266-268}Sg^*$

Isotopic exploration
$^{40-48}Ca+^{238}U \rightarrow ^{275-283}112+3,4n$
S^3 (I=10pμA) ➔ 20evt/week/pb

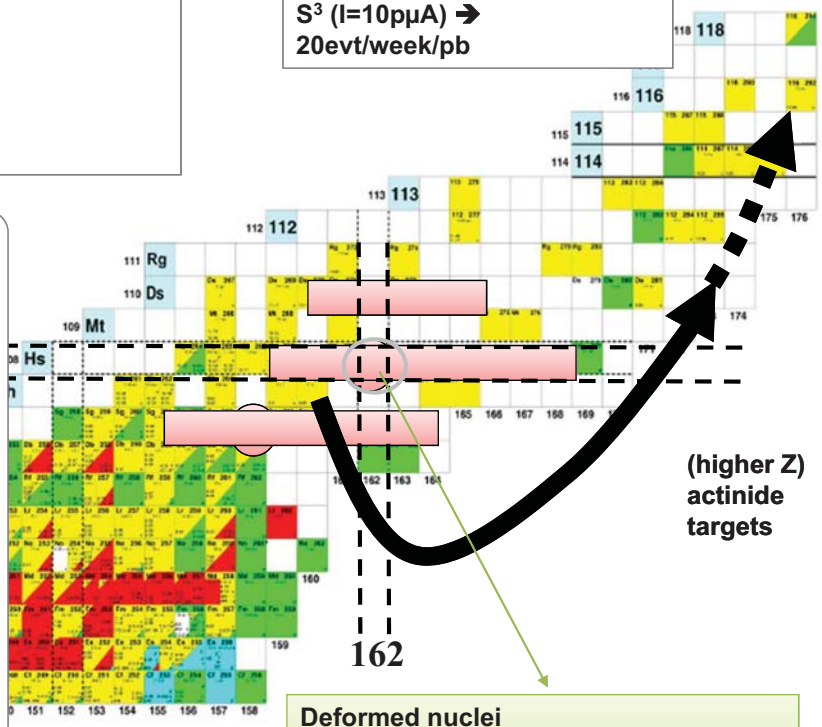

At the crossing road for

Reaction of synthesis :
- o Link hot to cold fusion
- o Isospin dependent reaction mechanism studies
- o X-section systematics

Decay properties :
- o K-isomers
- o SF decay (T_{SF} half-lives)
- o Alpha decays (Qa & half-lives)

Trans-actinide chemistry

GS properties
- o Mass measurements …

Deformed nuclei
$^{40}Ar+^{238}U \rightarrow ^{274}Ds$ (+4n) → $^{270}Hs + \alpha$
S^3 (I=50pμA) ➔190evt/week@σ_{th}=2pb

Neutrons For Science (NFS)

Collaboration

50 physicists, 18 institutions, 8 countries
Spokespersons:
Xavier Ledoux, CEA/DIF/DPTA/SPN, France
Stanislav Simakov, FZK, Germany

Physics topics

Fission
- Minor actinides, main isotopes
- Cross section
- Neutron spectrum, multiplicity
- Prompt fission gammas
- Detailed A and Z distributions
- Delayed neutron yields and precursor characteristics

Scattering
- Secondary neutron energy and angle differential cross sections
- Inelastic scattering

Fusion reactors

Astrophysics

Schematic layout

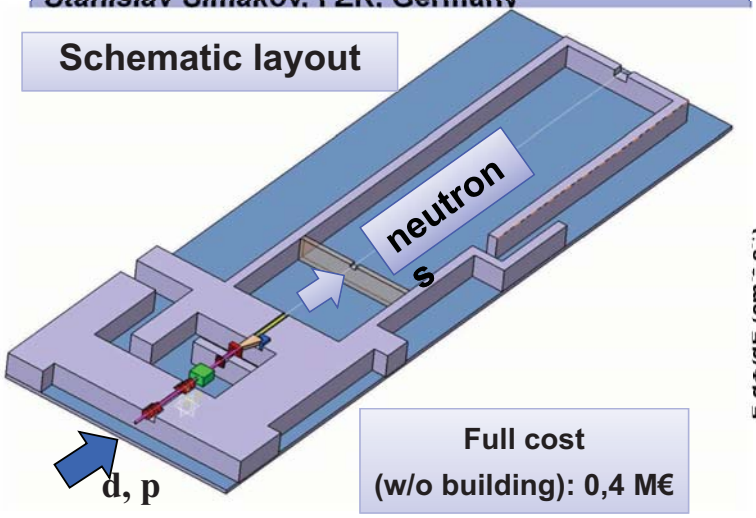

Full cost (w/o building): 0,4 M€

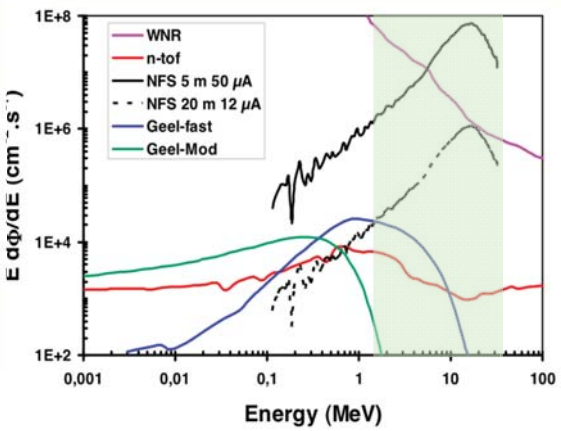

ISOL Rare Isotope Beams at SPIRAL 2

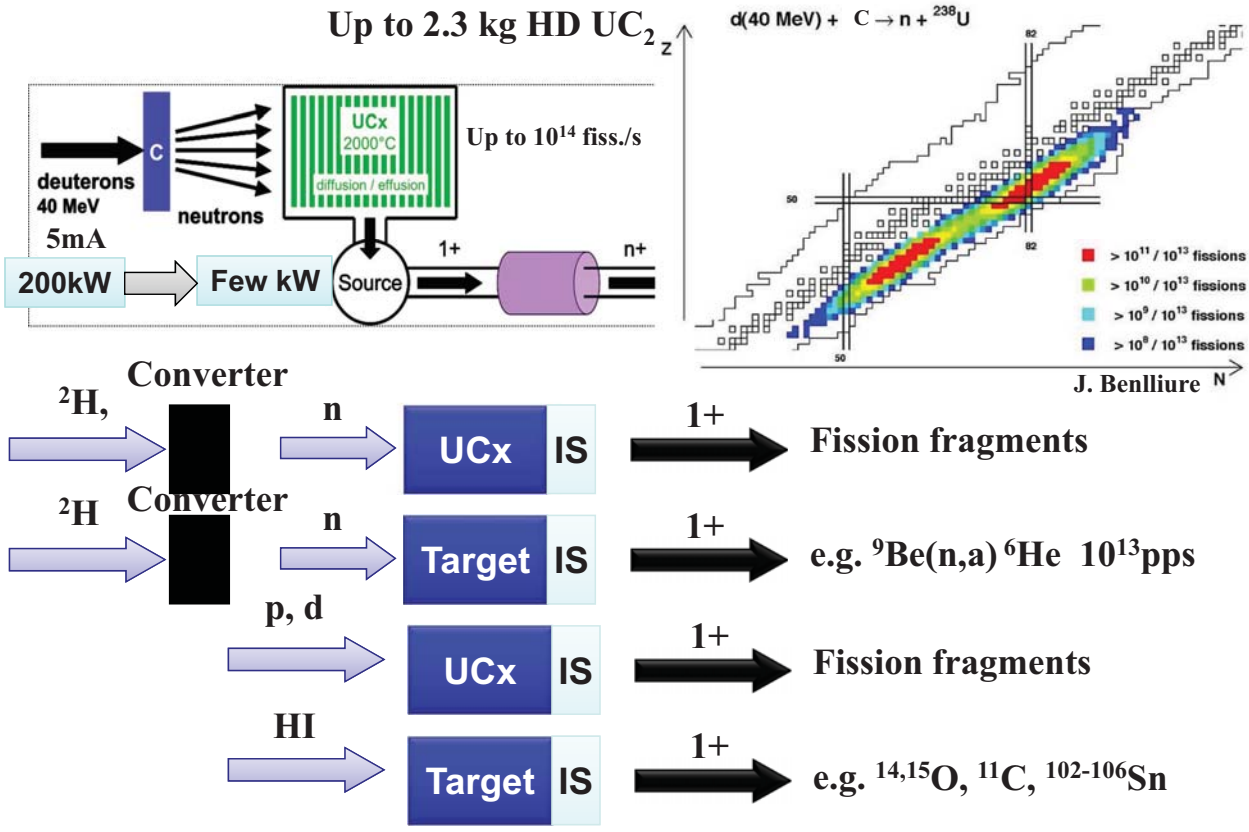

Acceleration of RIB - Beam Energies from CIME

Lower Energies

F. Chautard

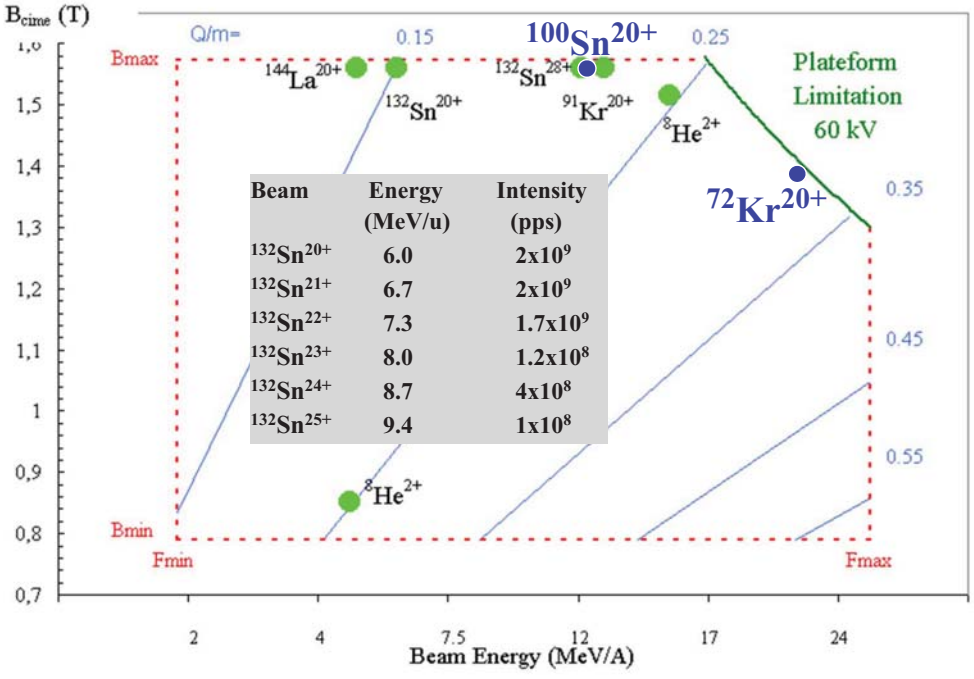

Beam	Energy (MeV/u)	Intensity (pps)
$^{132}Sn^{20+}$	6.0	$2x10^9$
$^{132}Sn^{21+}$	6.7	$2x10^9$
$^{132}Sn^{22+}$	7.3	$1.7x10^9$
$^{132}Sn^{23+}$	8.0	$1.2x10^8$
$^{132}Sn^{24+}$	8.7	$4x10^8$
$^{132}Sn^{25+}$	9.4	$1x10^8$

Energy range of SPIRAL2 RIB : < 30keV and 1-20 MeV/nucl.

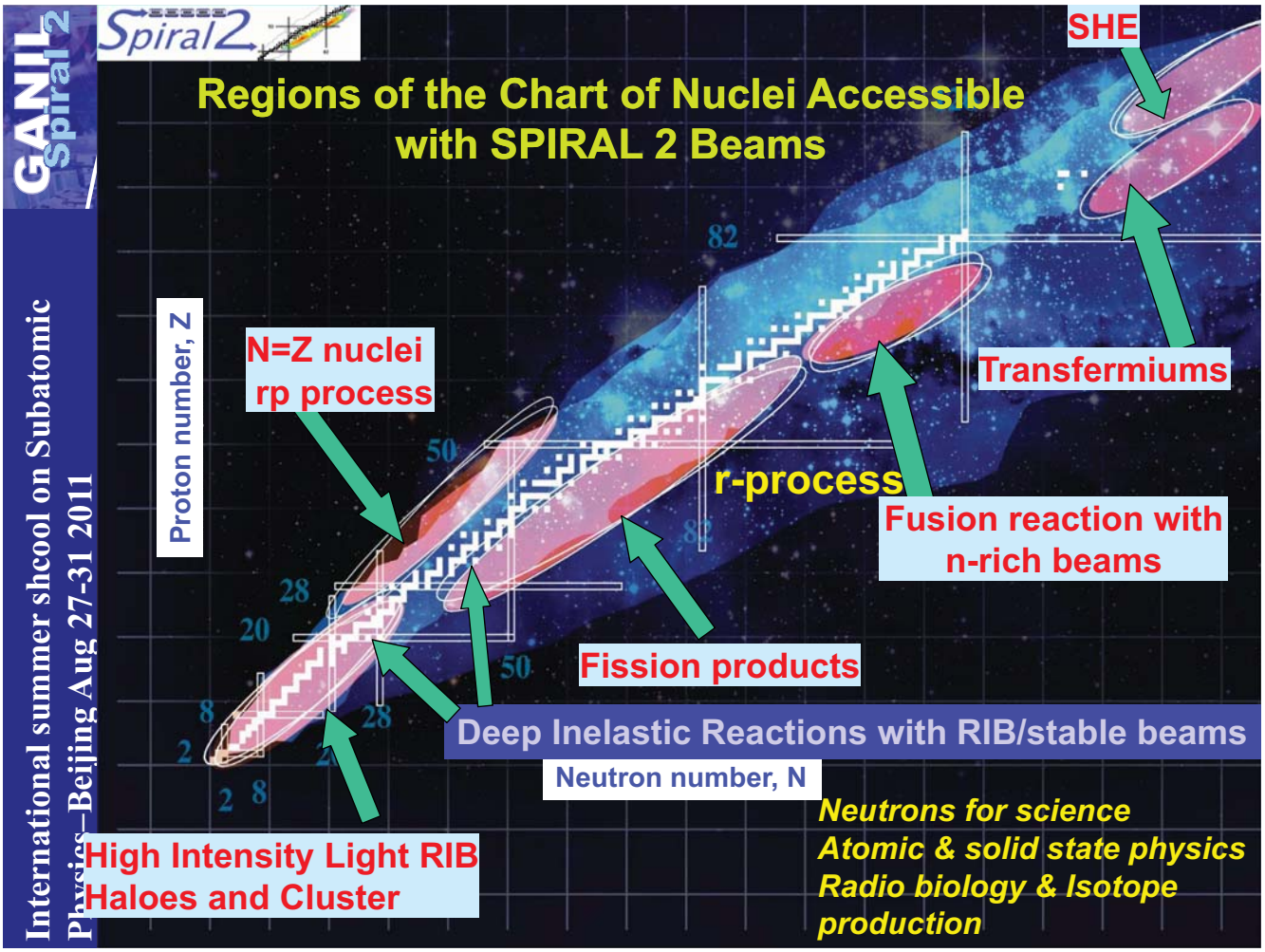

SPIRAL 2: Advanced ISOL RIB facility

SPIRAL 2: Experiments with RIB at low cross sections and very exotic nuclei at few MeV/nucleon

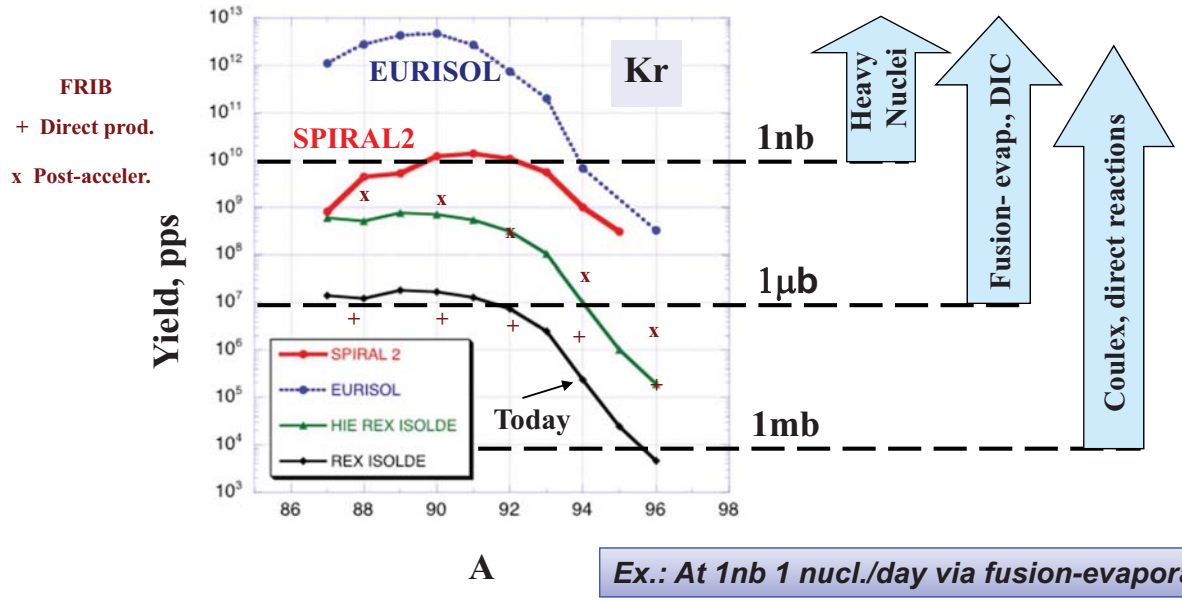

Ex.: At 1nb 1 nucl./day via fusion-evaporation

Examples of post-accelerated RIB with intensity ≥ 10^5 pps

Beam	54Ni	73Ni
N/Z	0,92	1,61
Max. Energy AMeV	15	9
Beam	**121Xe**	**146Xe**
N/Z	1,24	1,70
Max. Energy AMeV	12	8

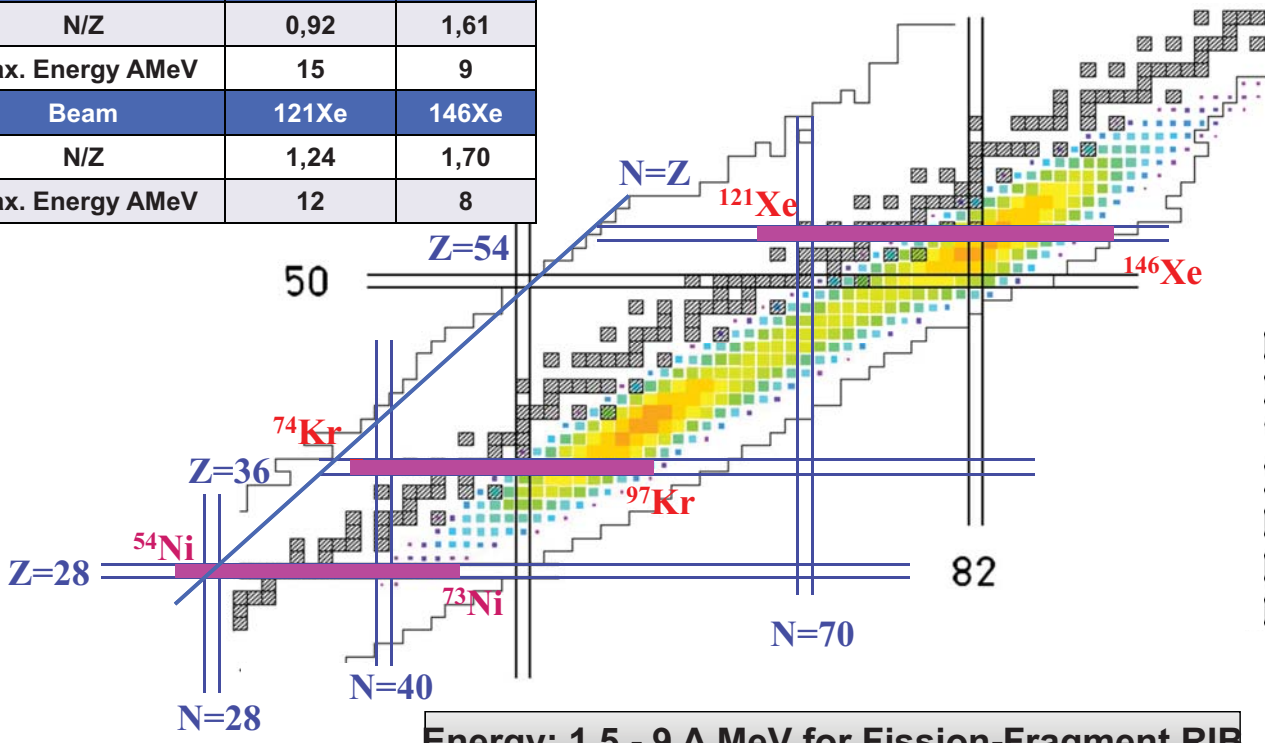

Energy: 1.5 - 9 A MeV for Fission-Fragment RIB

In the following:

A large National & International Collaboration

French Partners

CEN de Bordeaux-Gradignan

Centre de Spectro. Nucléaire et Spectro. de Masse Orsay

Institut de Physique Nucléaire Orsay

Institut de Physique Nucléaire Lyon

Institut Pluridisciplinaire Hubert Curien Strasbourg

Laboratoire Accélérateur Linéaire Orsay

Laboratoire de Physique Corpusculaire de Caen

Laboratoire de Physique Nucléaire et de Htes Energies Paris

Laboratoire de Physique Subatomatomique et de Cosmologie Grenoble

DSM		Irfu/SPhN
		Irfu/SACM
DSM		Irfu/SIS
DSM		Irfu/SENAC
DSM		Irfu/SEDI
DSM – Saclay		Expertise
DAM	DPTA	DASE et DP2I
DEN		Expertise
DPSN		Expertise

GANIL laboratoire commun CEA/DSM – CNRS/IN2P3 spiral2

Marcel Jacquemet

The first days of the civil construction of Phase 1

Dec. 2010

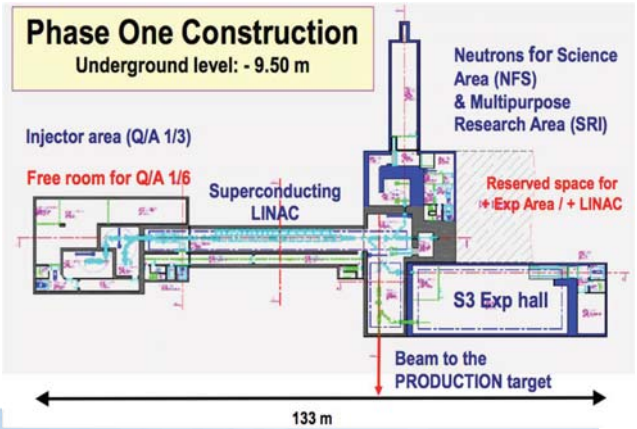

SPIRAL 2 Phase 1
Civil engineering started
Status April 22,2011

Accelerator

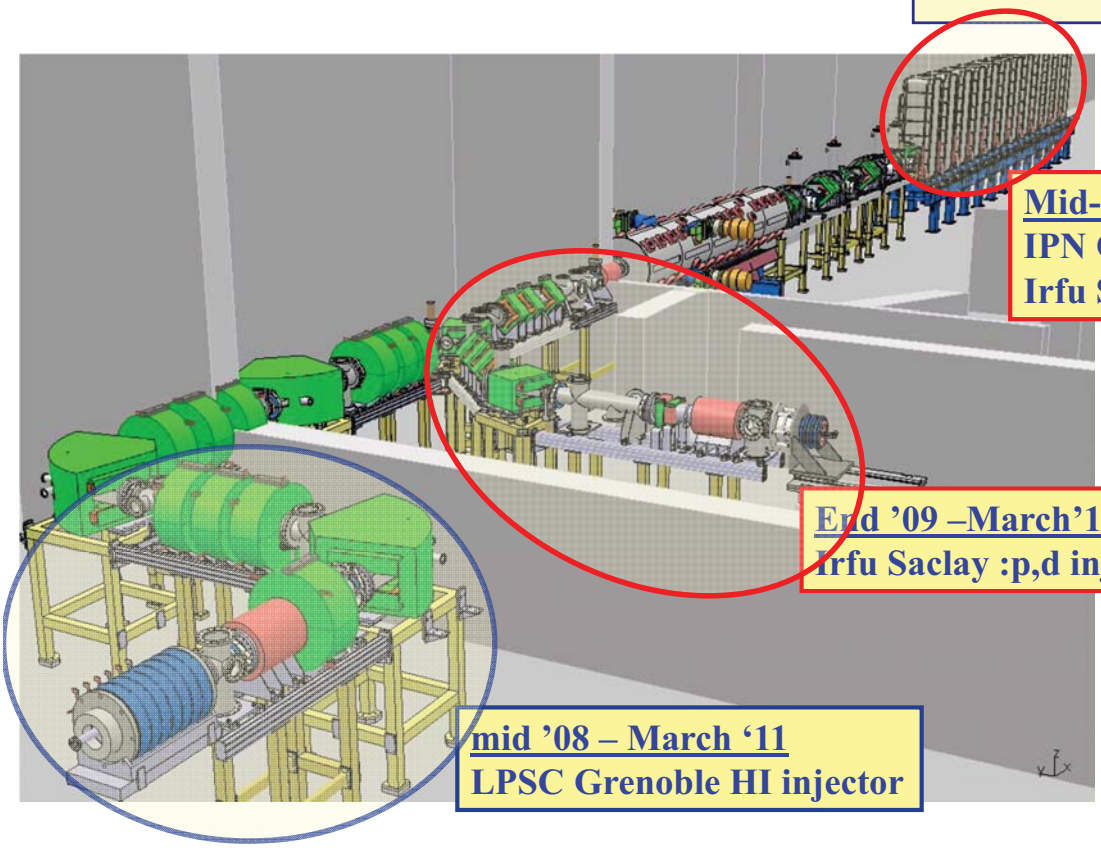

Mid-'08 – End-'10
IPN Orsay SC acc
Irfu Saclay

End '09 –March'11
Irfu Saclay :p,d injector

mid '08 – March '11
LPSC Grenoble HI injector

Heavy-ion injector of LINAC

LPSC, IRFU
GANIL, IPNL

Tests in Grenoble

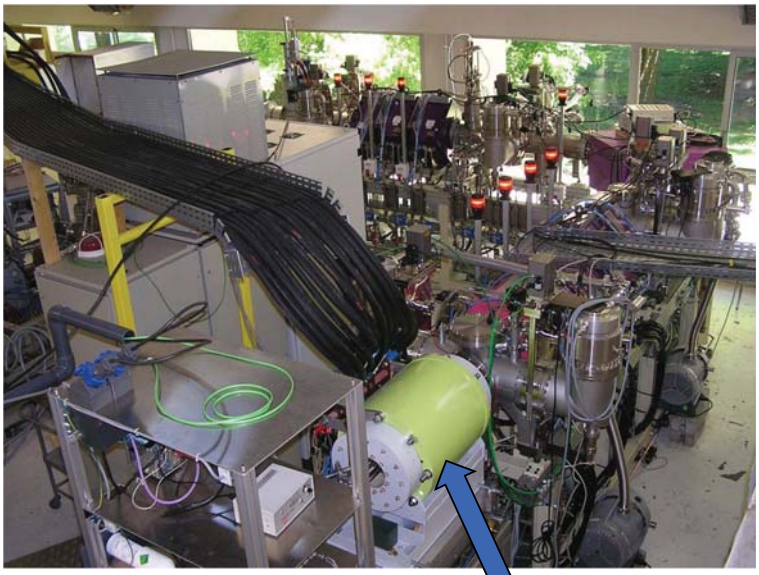

- $^{18}O^{6+}$ and $^{36}Ar^{12+}$ beams reached Day 1 intensity (≥10pmA) at Phoenix V2 at LPSC Grenoble
- Tests of metallic beams (Ca, S, Si, Ni) started
- Tests of the new generation SC ECR A-Phoenix source in the coming months

Accelerator

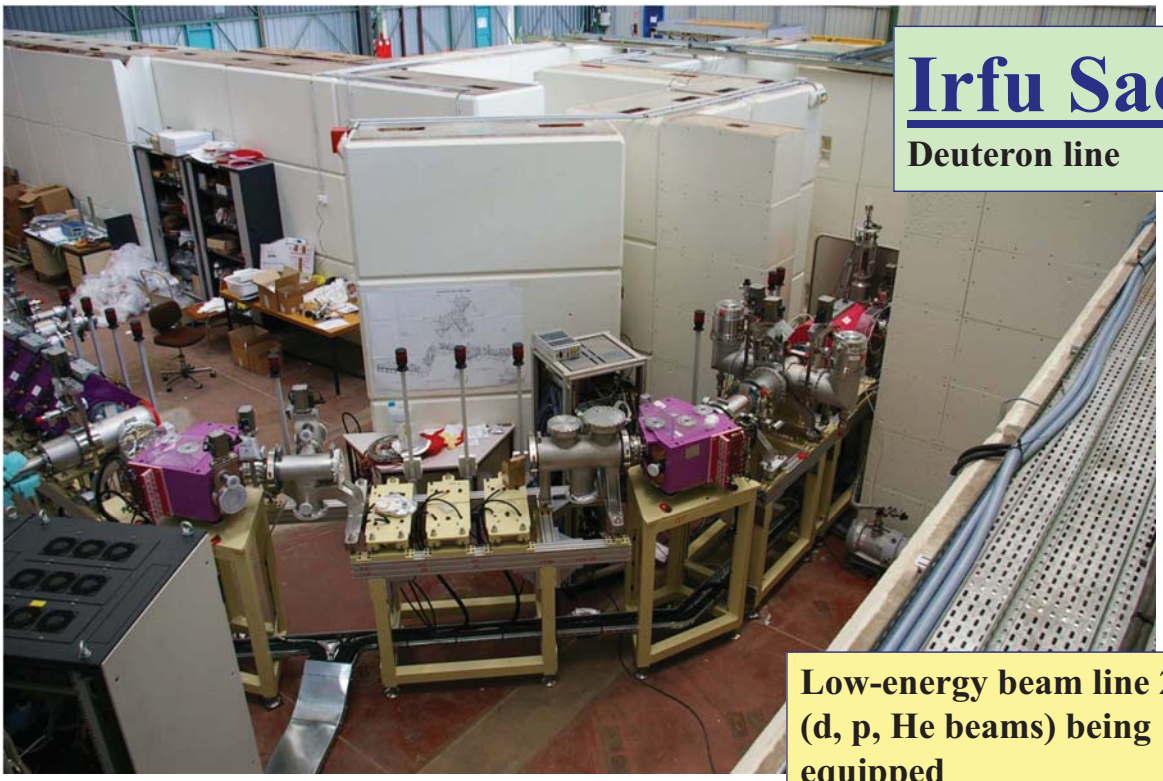

Irfu Saclay

Deuteron line

Low-energy beam line 2 (d, p, He beams) being equipped

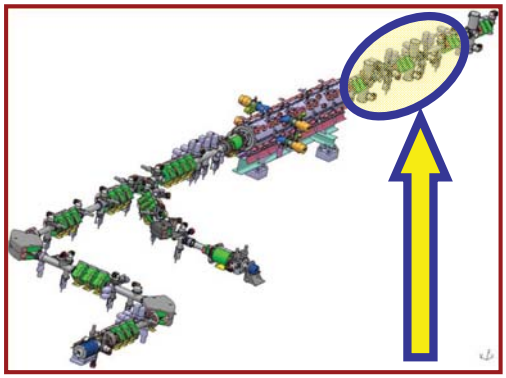

Accelerator

Ganil

Linac

Magnetic measurements

Series manufacturing by Tesla (UK)

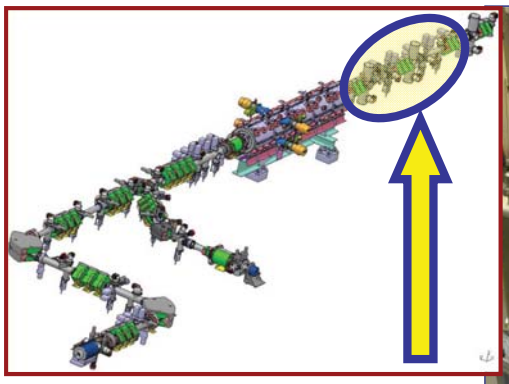

IPN Orsay

SC Cavities Type B

Status:
All cavities delivered and tested:
1st Cryomodule delivered in December

Tests of the SC cavities of type B at IPN Orsay

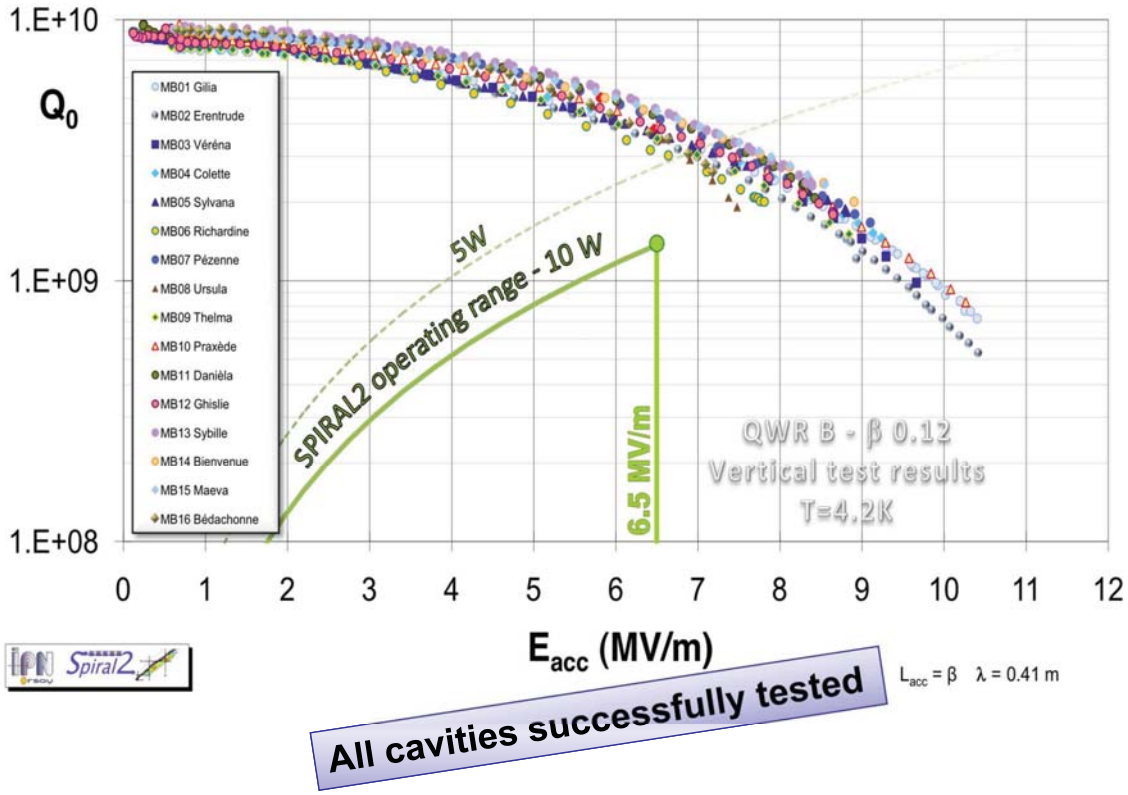

Detailed design of the RIB building

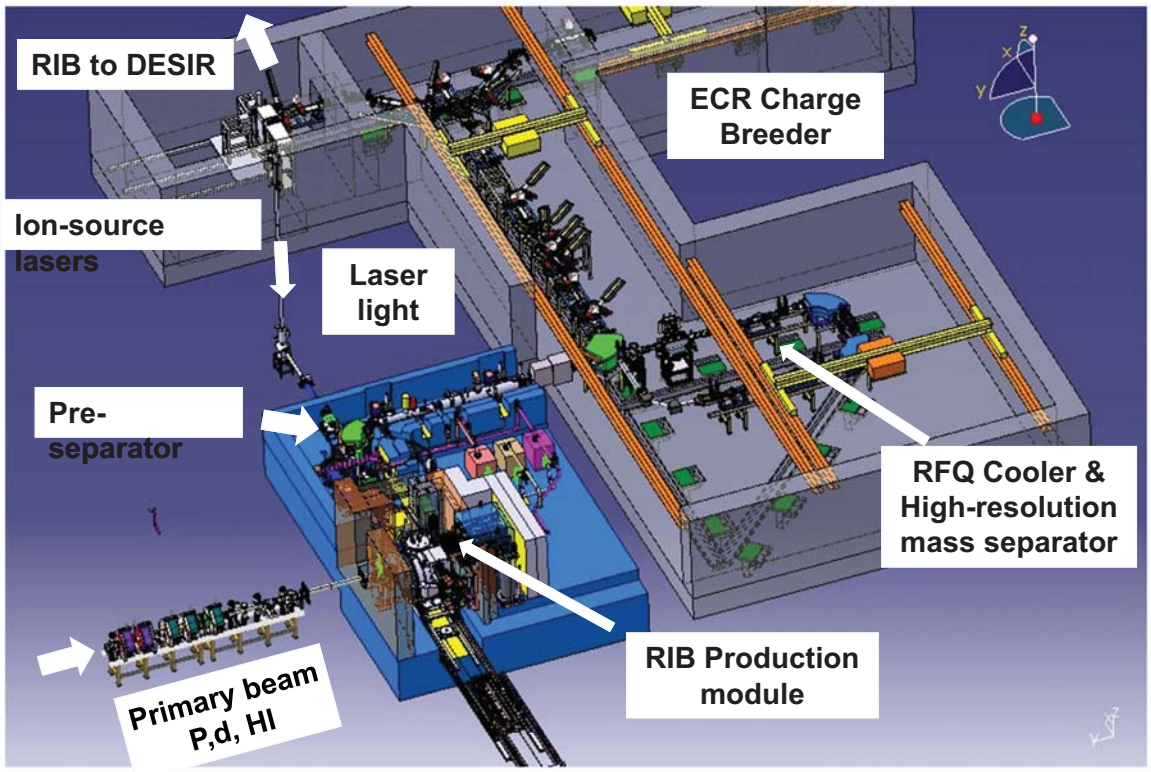

RIB production module

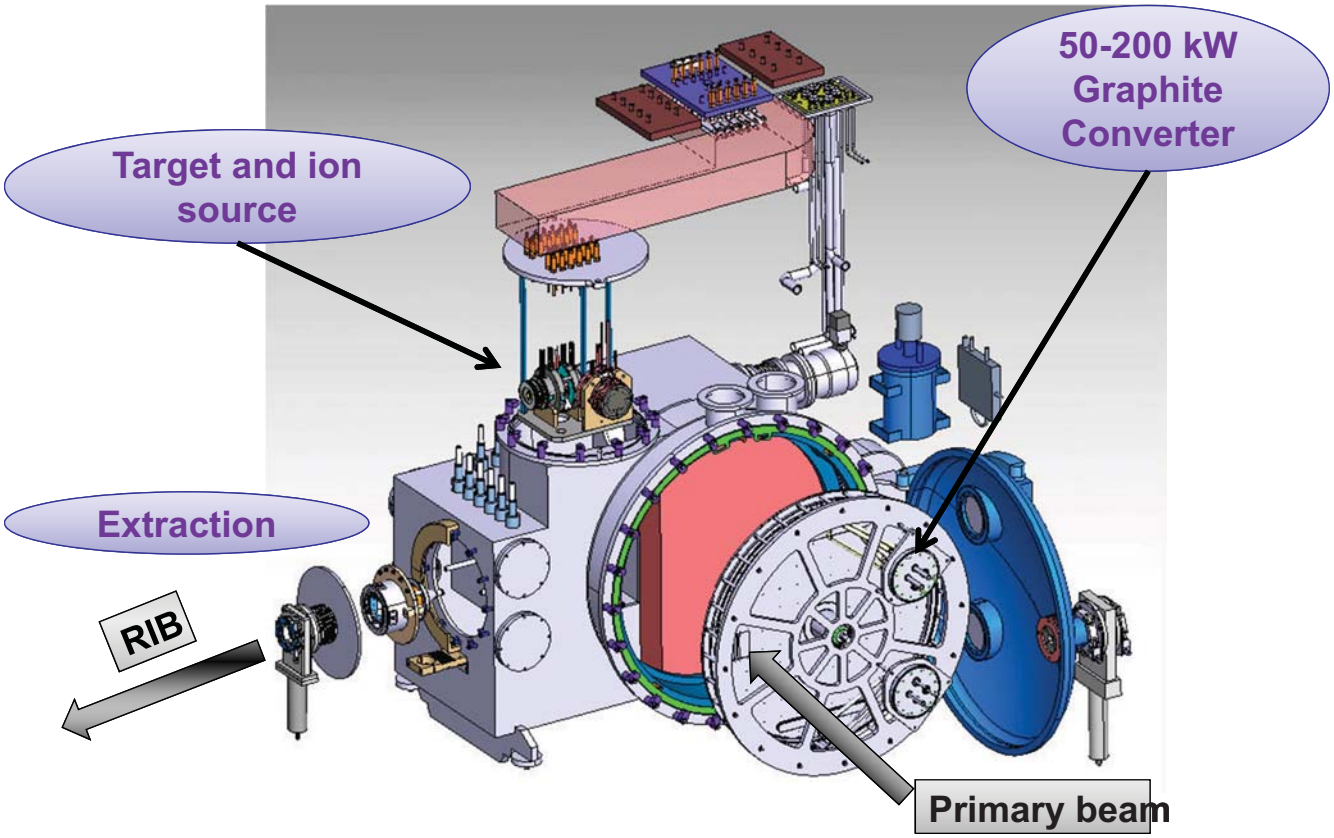

Conclusions & Long(er) Range Plan

- SPIRAL2 among the top priorities for the EU nuclear physics (NuPECC roadmap 2010)
- The civil construction of the SPIRAL2 Phase 1 started!
- Detailed design of the buildings SPIRAL2 Phase 2 to be ready in 2012.
- New detectors for SPIRAL2: R&D work and signatures of MoU entering in a final phase (to be accomplished by December 2011 as the EU SPIRAL2 PP deliverables)
- The first years of physics defined in:
  - 22 Letters of Intent for Day 1 experiments with high-intensity stable-ion beams with SPIRAL2 Phase 1 (NFS and S3 facilities) regularly updated & evaluated
  - 53 LoIs for Day One experiments at SPIRAL2 with RIB submitted recently (December 2010)
  - FUSTIPEN (Theory US-France collaboration) started on 01/10/2010, inauguration & workshop January 18-19, 2011: M. Ploszajczak and W. Nazarewicz among the leaders
  - European initiative in Theory in progress
- SPIRAL2 Week 2012 Caen,Jan 27,2012 (420 part in2011, 400 participants in 2010)

4

GANIL facility beyond 2015: 2+1options

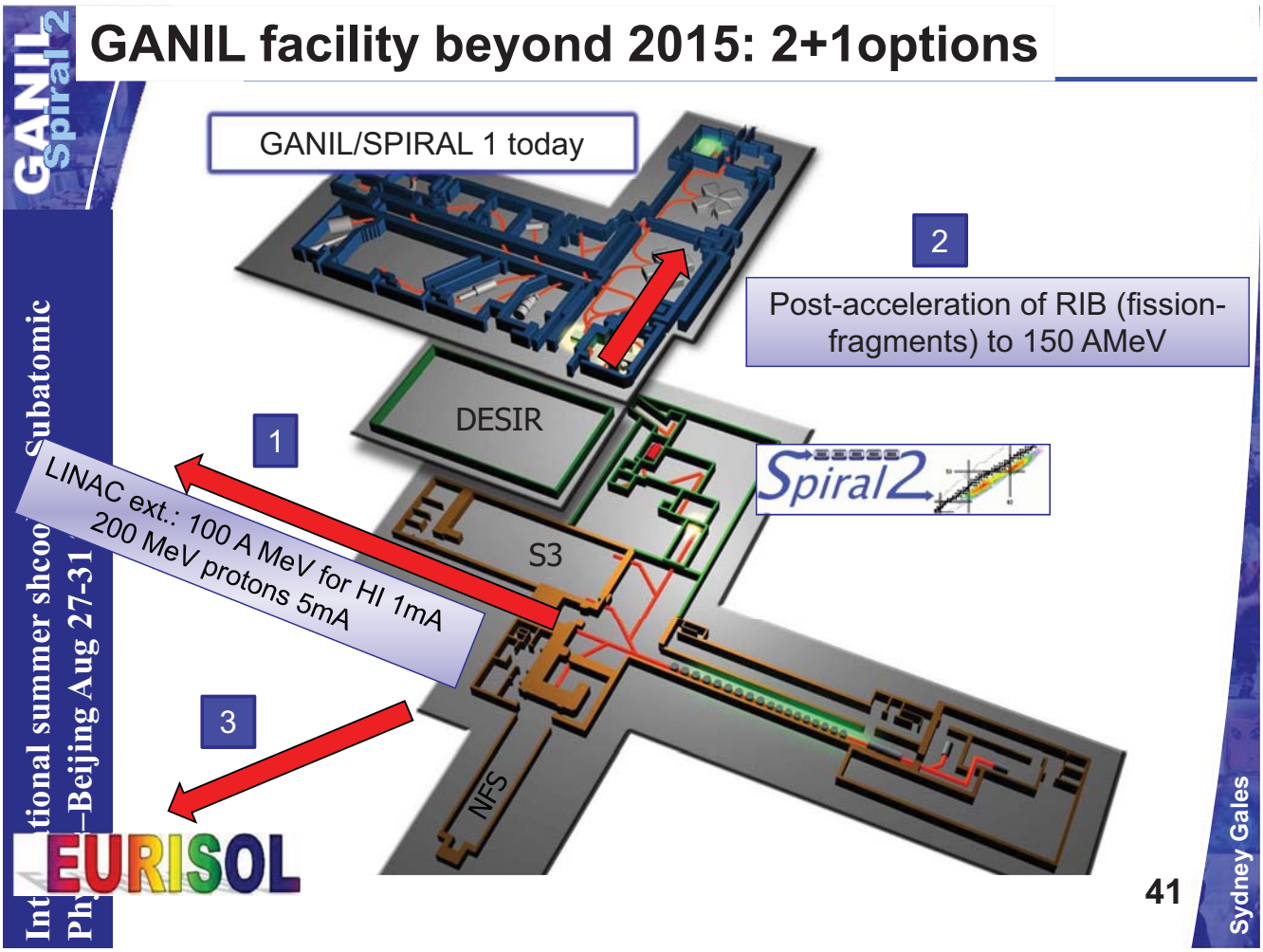

EURISOL @ GANIL…..2020?

SPIRAL2 will give a real advance in the technology of high power accelerators to GANIL and is an excellent step towards the next generation EURISOL . Possible and cost effective upgrade of SPIRAL2

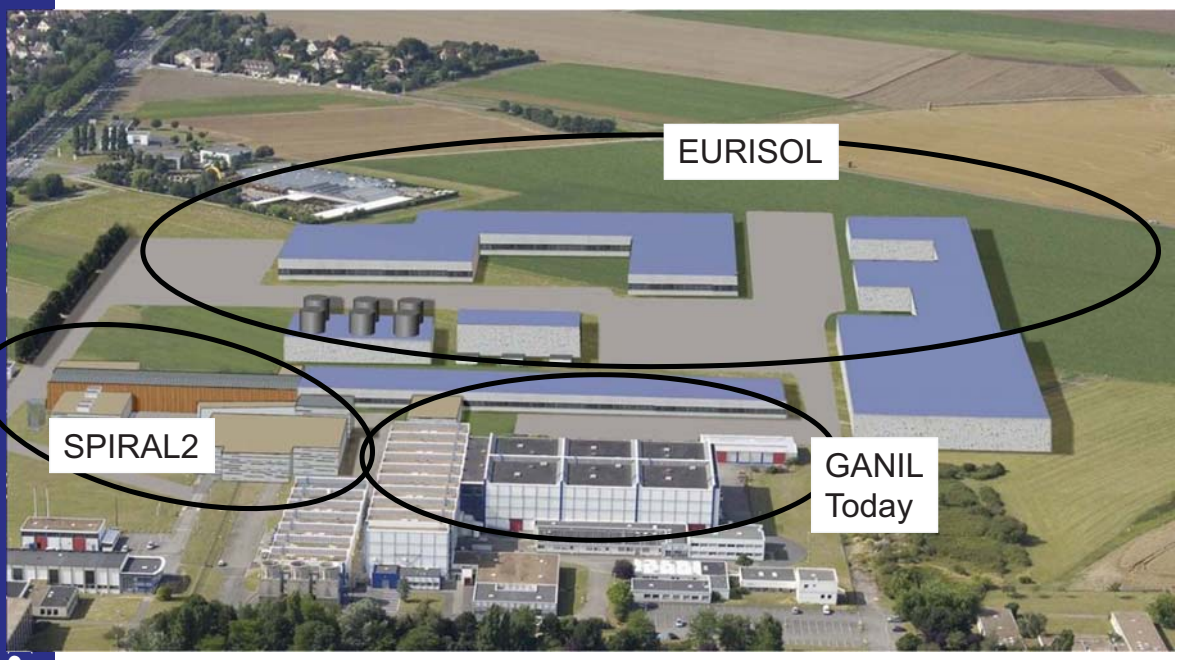

International summer shcool on Subatomic P

Sydney Gales

Civil engineering
SPIRAL2 ,May 20 2011

-10m Underground Floor Aug 2011

Infrastructure

Thanks to GANIL staff and SPIRAL2 Project group
Thanks for your patience and come to visit us
At GANIL-SPIRAL2 new facility

International summer shcool on Subatomic Physics–Beijing Aug 27-31 2011

Sydney Gales

END

GANIL Spiral2
International summer shcool on Subatomic Physics–Beijing Aug 27-31 2011

ISOL

at the highest power levels

- One stage :direct use of charged particles, minimize dE/dx (low Z, high E at 1 GeV max. 100 - 200 kW)

- Two stage :use neutral particles in second stage, i.e. neutrons & photons for neutrons 5 MW of proton beam (like spallation source)

Combine also (fragmentation + gas collection scheme) is also in this class

Sydney Gales

AGATA physics campaigns 2010-15

AGATA MoU: at least 25% at GANIL, GSI and LNL
Campaigns decided by AGATA Steering Committee

2010/11
→ LNL
≥5 ATC

2012/13
→ GSI/FRS
≥5 ATC + 5 ADC

2014/15
→ GANIL/SPIRAL2
~10 ATC + 5 ADC

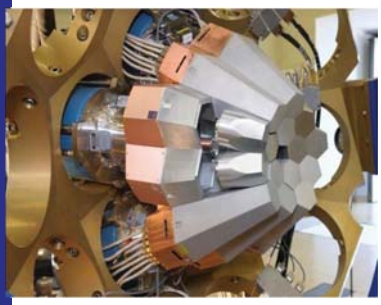

AGATA-5 + PRISMA

total eff. ε ~ 6%

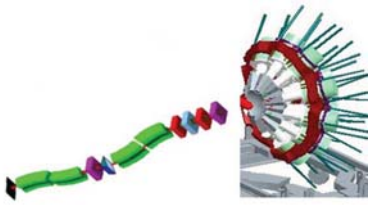

AGATA-10 @ FRS

total eff. ε > 10%

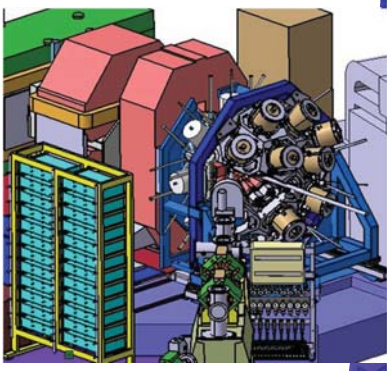

AGATA-15 + VAMOS

total eff. ε > 15 %

International summer shcool on Subatomic Physics–Beijing Aug 27-31 2011

Sydney Gales

RIB and nuclei far from stability accessible with SPIRAL1 & SPIRAL2

Energy range of SPIRAL1 & 2 ISOL RIB : ≤ 60keV and 1-15 MeV/nucl.

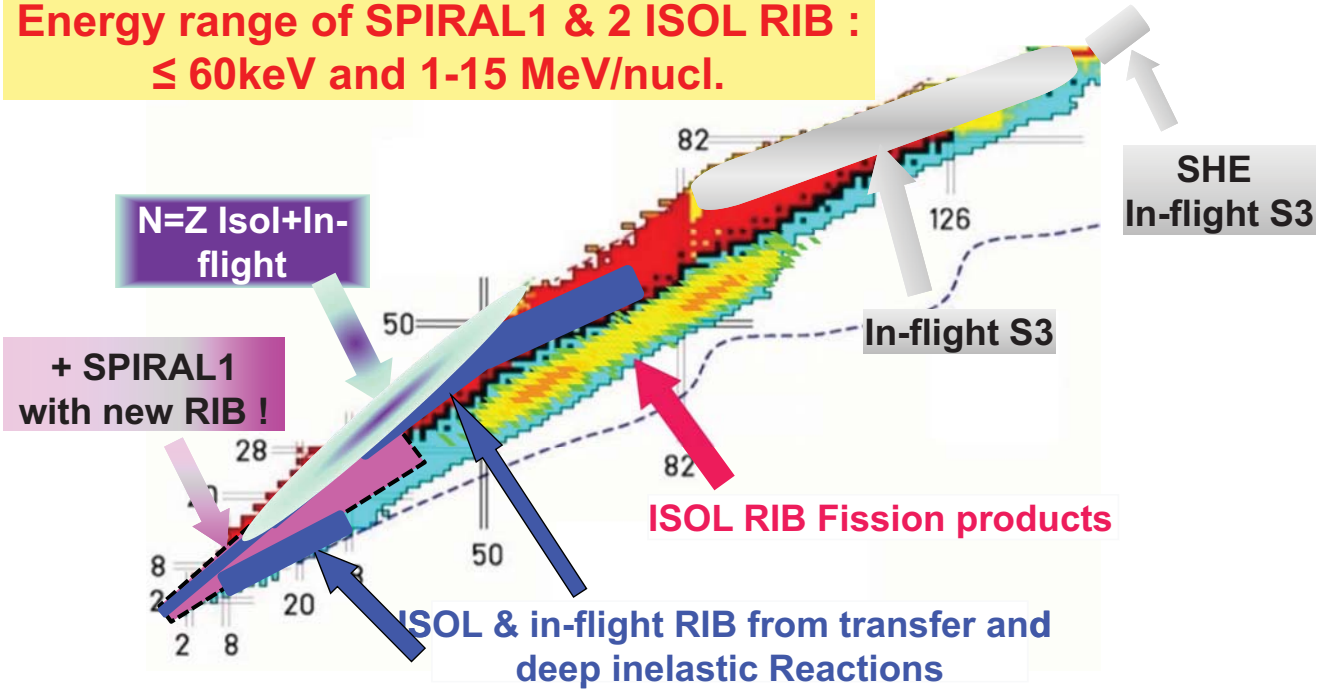

DESIR Facility

Collaboration

106 physicists, 34 institutions, 16 countries
Spokesperson:
Bertram Blank, CENBG, France
GANIL liaison: Jean-Charles Thomas

DESIR Layout

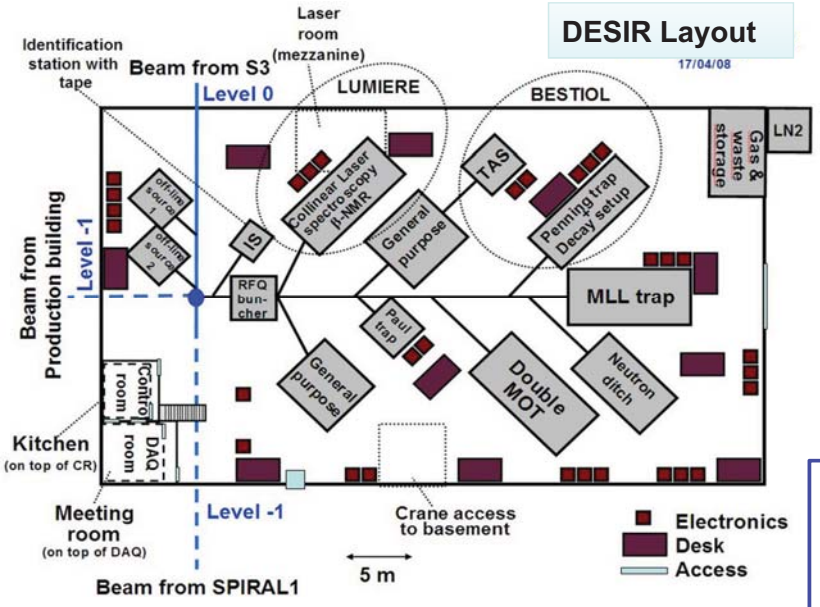

Topics:
- nuclear fine structure
- charge radii & moments
- masses, ion-purification
- weak interaction studies

Tools:
- keV RI Beams
- decay spectroscopy
- laser spectroscopy
- ion / atom trapping

DESIR time-line
- design: 2007 - 2010
- construction: 2012-13
- commissioning: 2014-15

GANIL Spiral2

International summer shcool on Subatomic Physics–Beijing Aug 27-31 2011

European Roadmad -ESFRI Process 2006

Nuclear Physics
FAIR &SPIRAL2
Selected!

Two Complementary approaches:

=> **FAIR @GSI** Darmstadt
Fragmentation at high energy , at the limit

=> SPIRAL-2 @GANIL-Caen
ISOL-method –Intense RIB – Good optics-
Post accelerated

Sydney Gales

Interactive chart of nuclides for GANIL and SPIRAL2 on Web

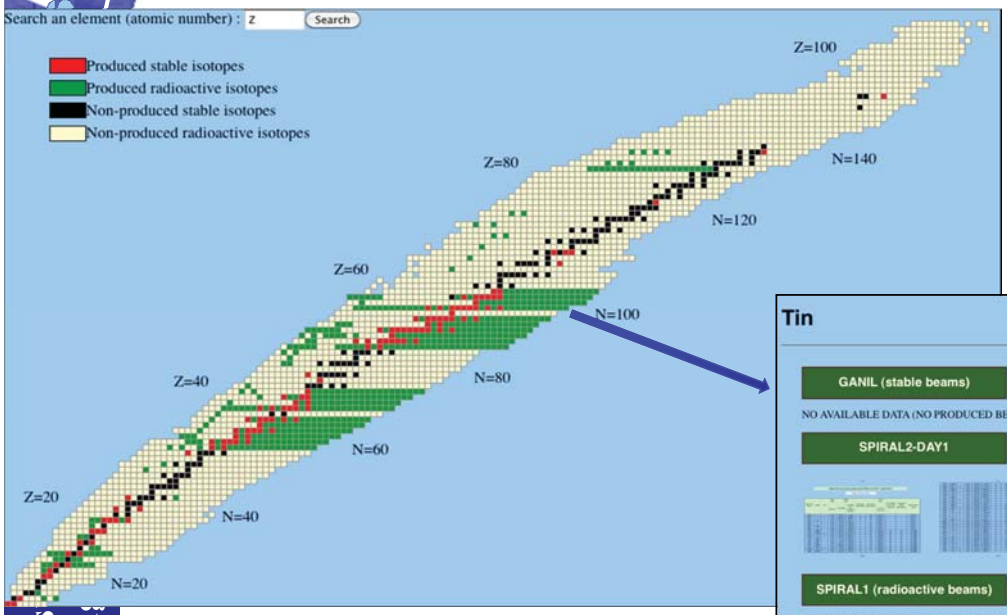

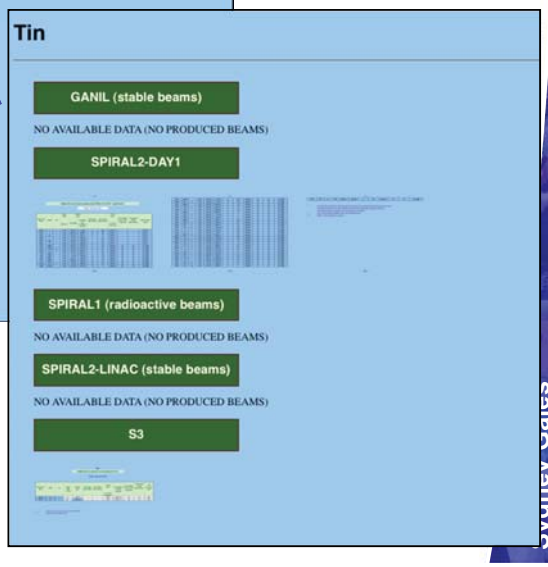

To be ready by end of June 2011

- *Hydrogen 7: the most "exotic" nuclear system ever observed*
- With the most intense ^{8}He beam from SP1

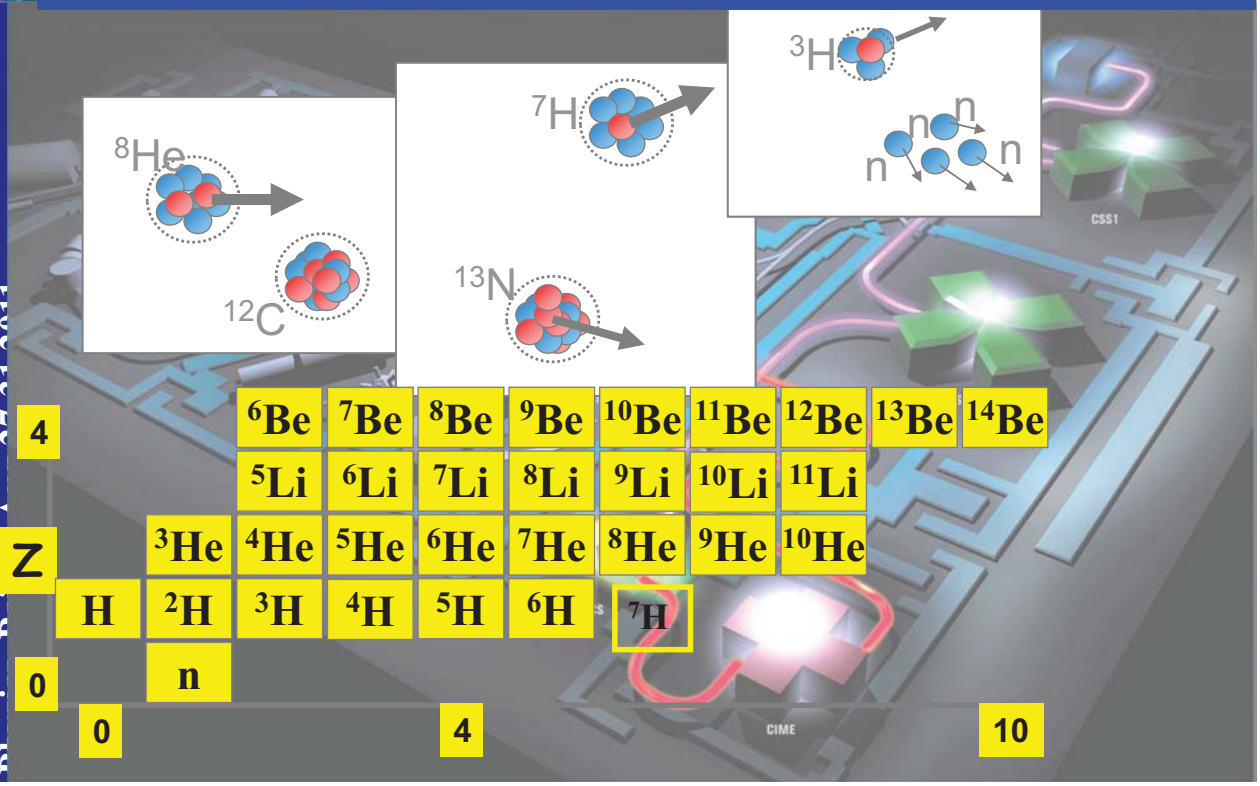

Active target MAYA

➲ The target is also the detector

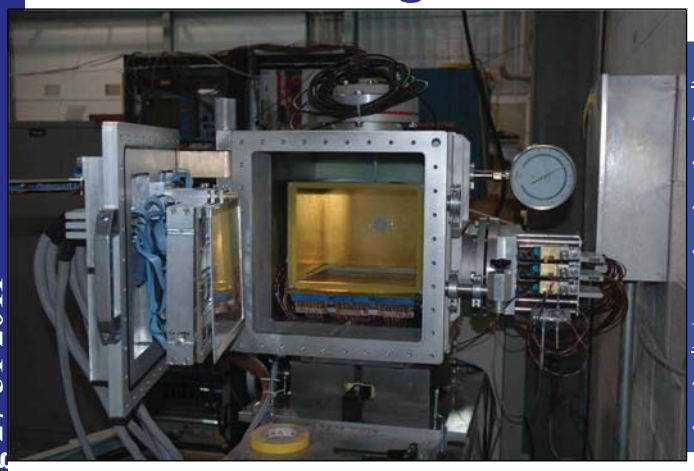

MAYA target-detector

Advantages:
- Thick target
- detection efficiancy 100%
- angular coverage 4π
- Very low energy threshold

Principle :
- 3D imaging of the reaction
- Identification of products

GANIL Spiral2
International summer shcool on Subatomic Physics–Beijing Aug 27-31 2011

From MAYA active target 3D detector

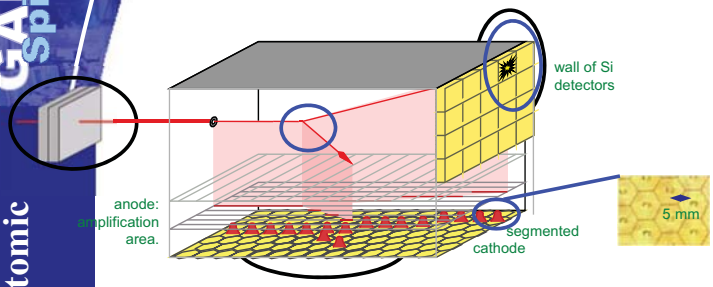

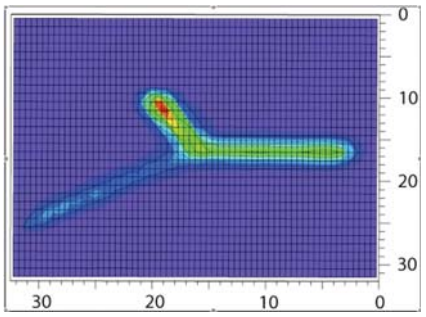

$^{12}C(^{8}He,^{7}H\text{->}^{3}H+4n)^{13}N$

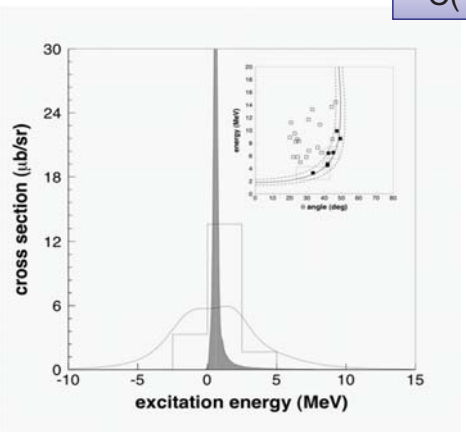

^{7}H observed

M. Caamaño *et al.*, Phys. Rev. Lett. 99, 062502 (2007)

Sydney Gales

Revisiting two proton radioactivity with TPC

B.Blank et al

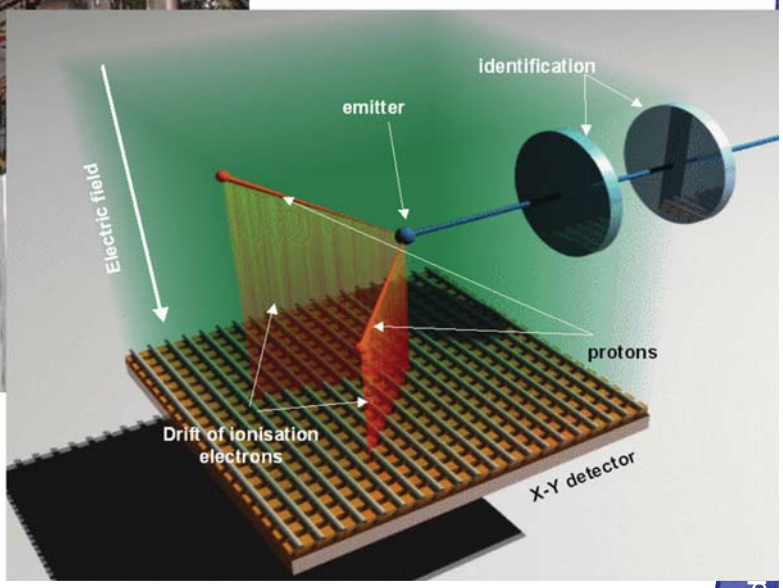

Search for Heavy and Super-Heavy nuclei (New Elements)

GSI Darmstadt, FLNR Dubna, RIKEN, LBL Berkeley,…

Upper part of the Chart of Nuclides

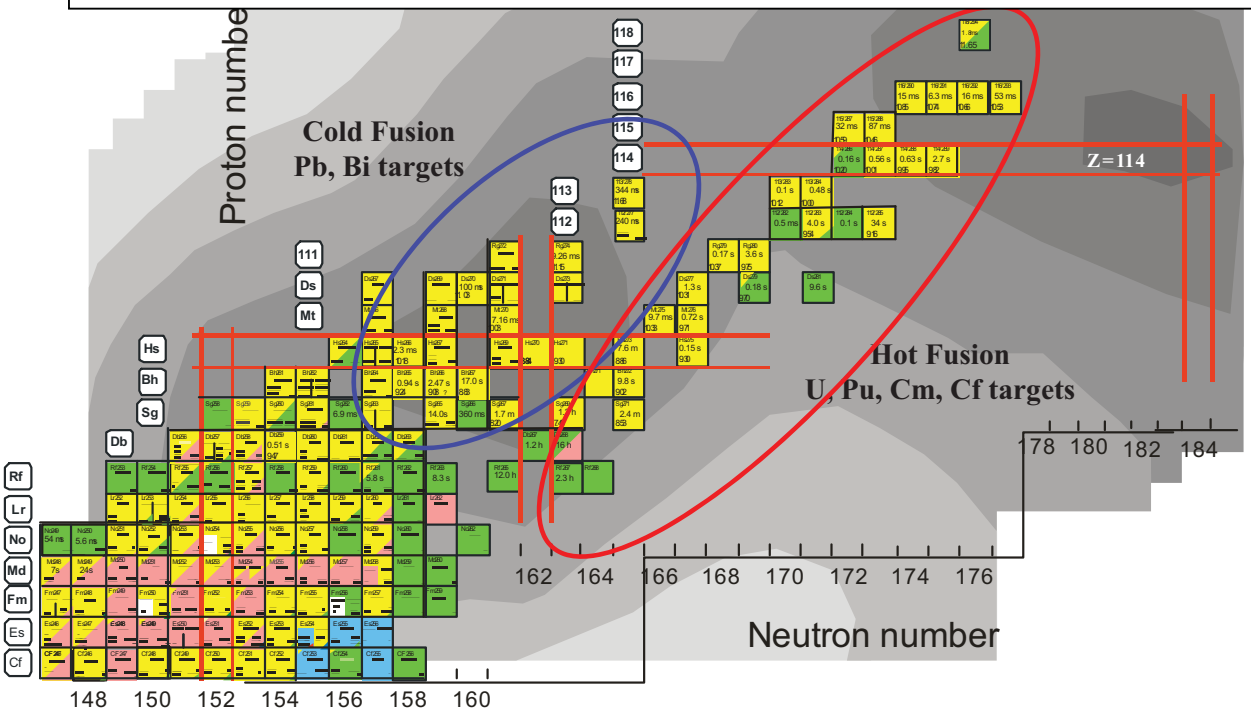

The heaviest elements found in nature: Uranium (Z=92) and Plutonium (Z=94)

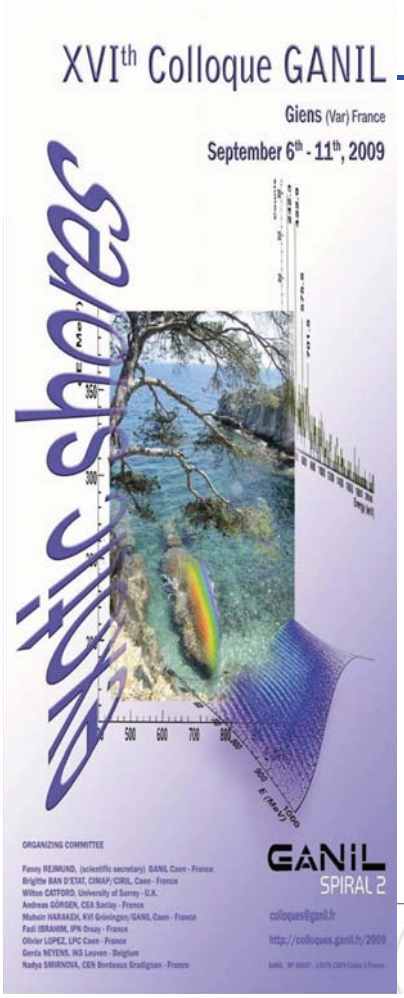

Post-acceleration of HI-RIB : Physics and perspectives On the road to EURISOL

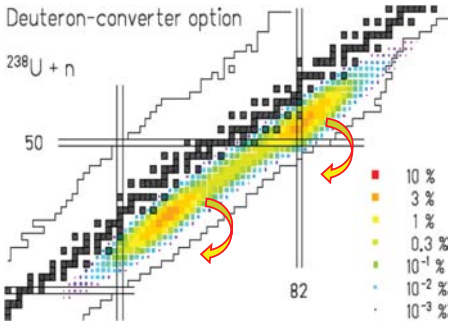

↳ **Fragmentation of *selected* n-rich fission fragments**

Sydney Gales

New Frontier with ^{238}U intense beams and VAMOS –EXOGAM

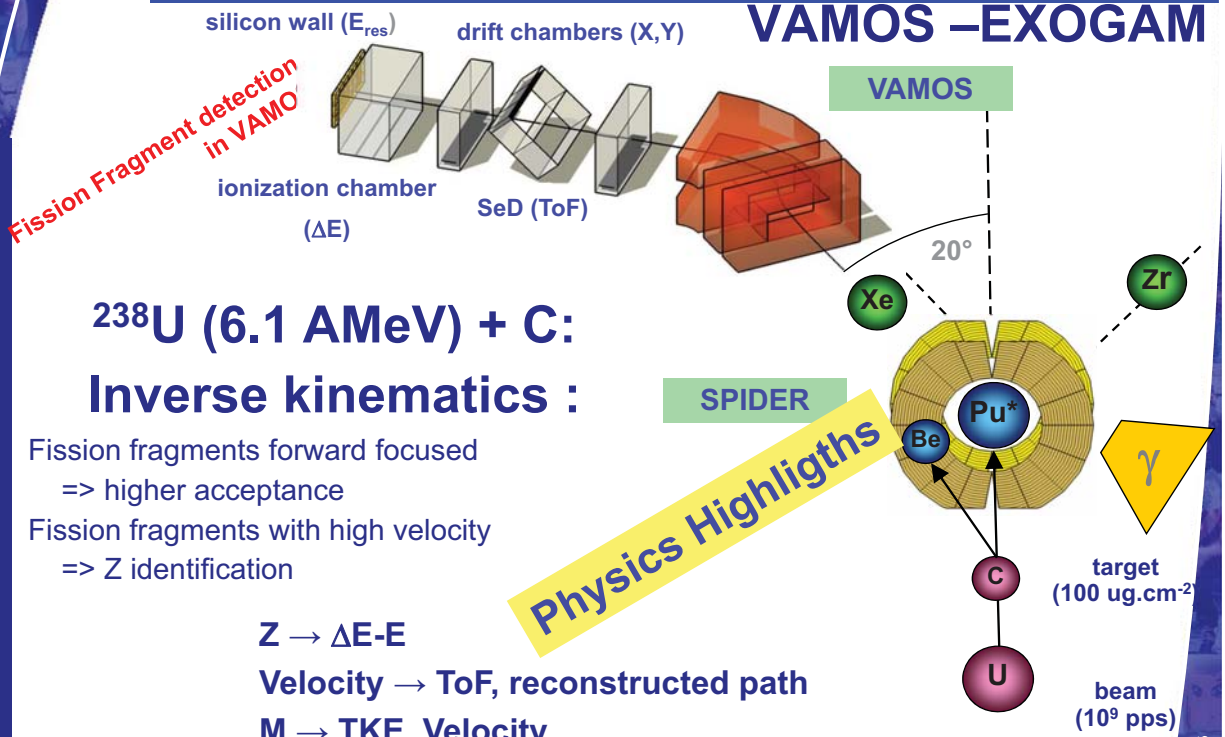

^{238}U (6.1 AMeV) + C:

Inverse kinematics :

Fission fragments forward focused
=> higher acceptance
Fission fragments with high velocity
=> Z identification

Physics Highligths

Z → ΔE-E
Velocity → ToF, reconstructed path
M → TKE, Velocity
M/Q → Bρ, Velocity
30 < Z < 60 **ΔZ/Z ~ 1.5 %**
70 < M < 160 **ΔM/M ~ 0.6 %**

International summer shcool on Subatomic Physics–Beijing Aug 27-31 2011

Sydney Gales

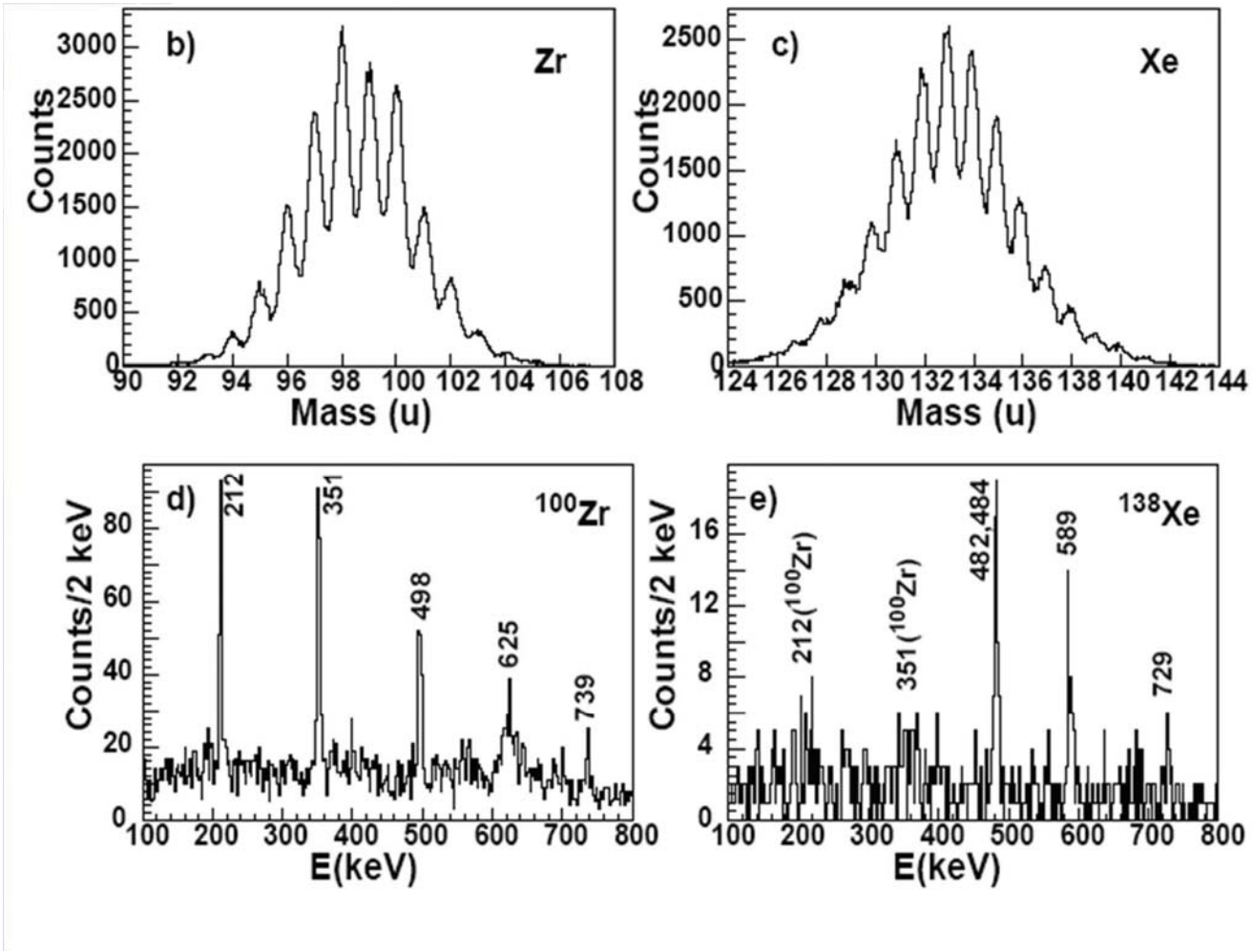

SPIRAL 2 timeline

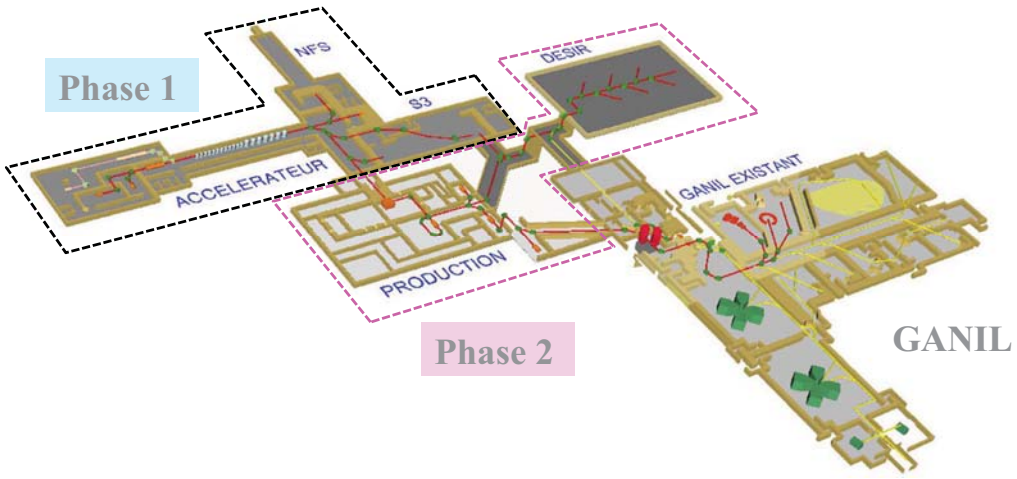

2007 2008 2009 2010 2011 2012 2013 2014 2015 2016

Construction Phase 1 LINAC, NFS, S3

Commis-sioning Phase 1

Stable ion beams from LINAC

Construction Phase 2 RIB, DESIR

Commis-sioning Phase 2

RIB

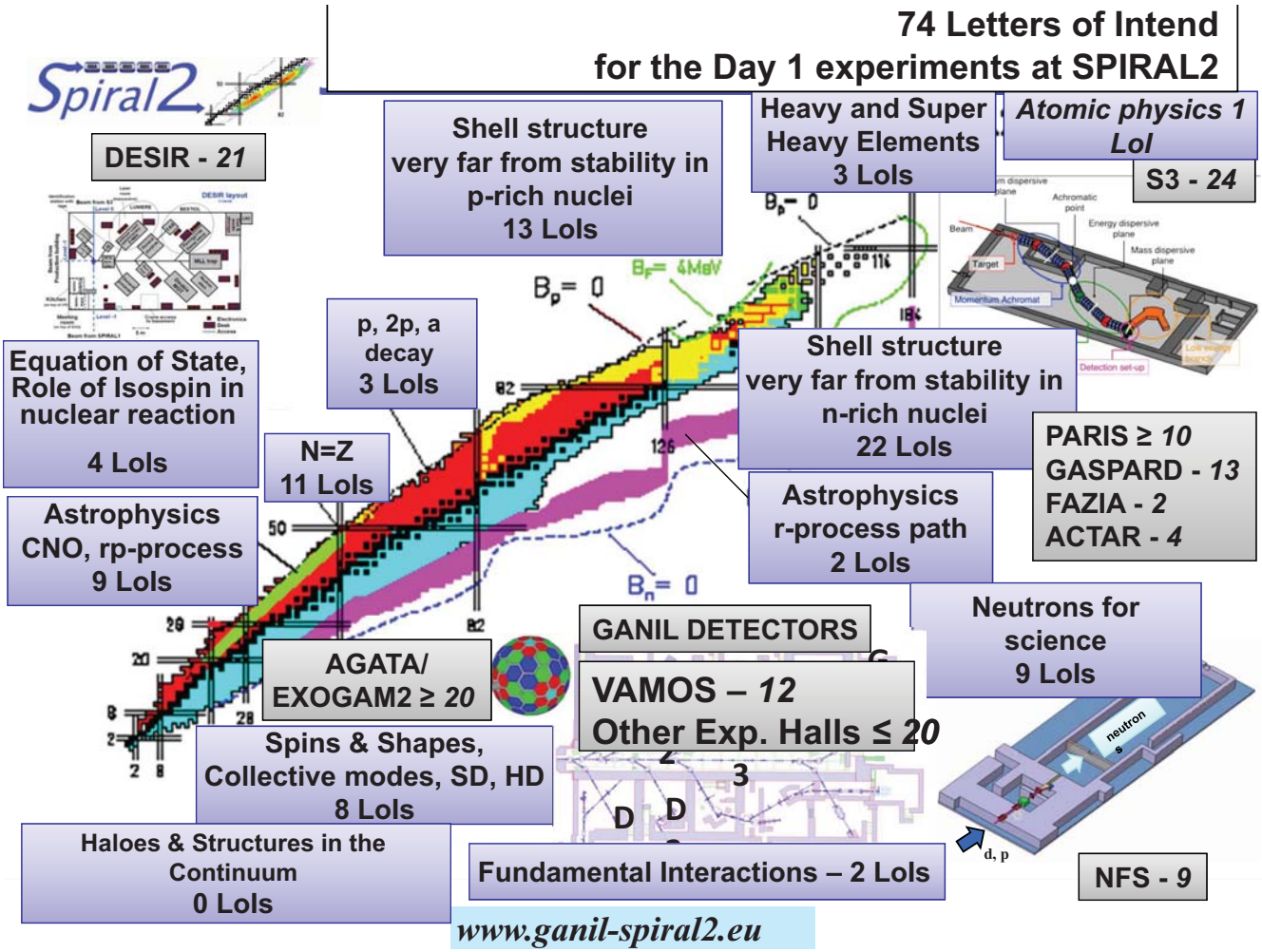
74 Letters of Intend
for the Day 1 experiments at SPIRAL2
Spiral2
DESIR - 21
Shell structure
very far from stability in
p-rich nuclei
13 LoIs
Heavy and Super
Heavy Elements
3 LoIs
Atomic physics 1
LoI
S3 - 24
Equation of State,
Role of Isospin in
nuclear reaction
4 LoIs
p, 2p, a
decay
3 LoIs
N=Z
11 LoIs
Shell structure
very far from stability in
n-rich nuclei
22 LoIs
PARIS ≥ 10
GASPARD - 13
FAZIA - 2
ACTAR - 4
Astrophysics
CNO, rp-process
9 LoIs
Astrophysics
r-process path
2 LoIs
Neutrons for
science
9 LoIs
GANIL DETECTORS
AGATA/
EXOGAM2 ≥ 20
VAMOS – 12
Other Exp. Halls ≤ 20
Spins & Shapes,
Collective modes, SD, HD
8 LoIs
Haloes & Structures in the
Continuum
0 LoIs
Fundamental Interactions – 2 LoIs
NFS - 9
www.ganil-spiral2.eu

Experimental progress in two-proton correlated emission

Two-proton (2*p*) correlated emission, also known as 2*p* radioactivity in a certain case, was first proposed by Goldanskii et al. [1] at the beginning of the1960s, and was first discovered in ^{45}Fe nucleus by DANIL [2] and GSI [3] at the beginning of this century. In this lecture, I would like to address the experimental progress in 2*p* correlated emission. It contains 6 sections, as followings,

1. Introduction: The history of radioactivity, the concepts of one-proton (1*p*) and 2*p* radioactivity, the discoveries of 1*p* and 2*p* radioactivity, the current progress in 1*p* radioactivity, and related concepts like 2*p* halo, BCS/BEC crossover will be briefly introduced in this section.

2. β-delayed 2*p* emitters: The β-delayed 2*p* (β2*p*) emission was also proposed by Goldanskii [4]. In this section, the β2*p* emitters ^{22}Al, ^{23}Si, ^{26}P, ^{27}S, ^{35}Ca, ^{31}Ar, ^{39}Ti, ^{43}Cr, ^{50}Ni, and so on, with their discoveries and the possibility of β-delayed three-proton (β3*p*) will be shortly reviewed in this section.

3. Ground-state 2*p* emitters: The direct 2*p* radioactivity was discovered first in ^{45}Fe, later in ^{54}Zn, and possibly in ^{48}Ni. In this section, the experimental procedures and subsequent progress will be presented in detail. The experimental research on other ground-state emitters (^{6}Be, ^{12}O, ^{16}Ne, ^{19}Mg, …) will be also presented.

4. Excited-state 2*p* emitters: 2*p* may also emit from an excited state as long as this state above the emission threshold. The experimental study on the candidate (^{14}O, ^{17,18}Ne, ^{28,29}S, …) and the possible signatures of ^{2}He emission will be discussed.

5. Technical developments: To introduce some remarkable experimental techniques like the complete-kinematics measurement, the in-flight particle identification, optical TPC detection, *etc*. in 2*p* emission experiments.

6. Summary and outlook: A short summary and outlook will be given to close this lecture.

Reference

[1] V. I. Goldansky, Nucl. Phys. **19**, 482 (1960); Y. B. Zel'dovich, Sov. Phys. – JETP **11**, 812 (1960); V. A. Karnaukhov and N. I. Tarantin, Sov. Phys. – JETP **12**, 771 (1961).

[2] J. Giovinazzo *et al*., Phys. Rev. Lett. **89**, 102501 (2002).

[3] Pf¨utzner M *et al*., Eur. Phys. J. A **14**, 279 (2002).

[4] V. I. Goldanskii, Sov. Phys. – JETP Lett. **32**, 554 (1980).

ISSSP2011

Experimental Progress in Two-proton Correlated emission

Cheng-Jian Lin
cjlin@ciae.ac.cn

China Institute of Atomic Energy

August 27-31, 2011, Beijing

Outline

1. Introduction:

History, discovery, concept, 2*p* correlation, experimental signatures, theoretic models, and related topics …

2. β-delayed 2*p* emitters (briefly)

β-delayed 2*p* (β2*p*): ^{22}Al, ^{23}Si, ^{26}P, ^{27}S, ^{35}Ca, ^{31}Ar, ^{39}Ti, ^{43}Cr, ^{50}Ni …

3. Ground-state 2*p* emitters

^{45}Fe, ^{54}Zn, ^{48}Ni (long lifetime); ^{6}Be, ^{12}O, ^{16}Ne, ^{19}Mg … (short lifetime)

4. Excited-state 2*p* emitters

^{14}O, ^{10}C, **^{17,18}Ne, ^{28,29}S** (in detail) … **Isomer-state:** ^{94}Ag^{m} (odd-Z)

Discussion: ^{2}He emission? & BCS/BEC crossover?

5. Technical developments

Kinematically complete measurement; In-flight identification

Optical TPC detection …

6. Summary and outlook

1. Introduction

1.1 History of radioactivity

First discovered in 1896

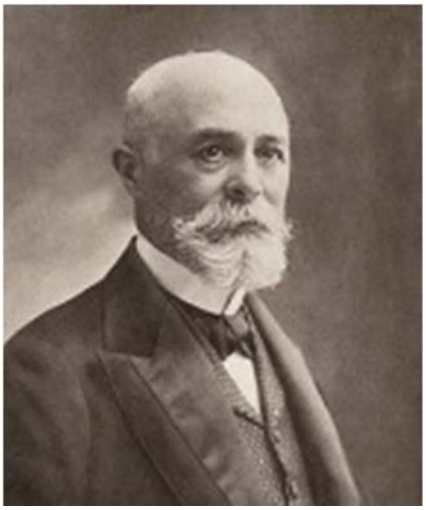

Antoine Henri Becquerel
(1852.12.15 -- 1908.8.25)

Becquerel Rays or Uranium Rays

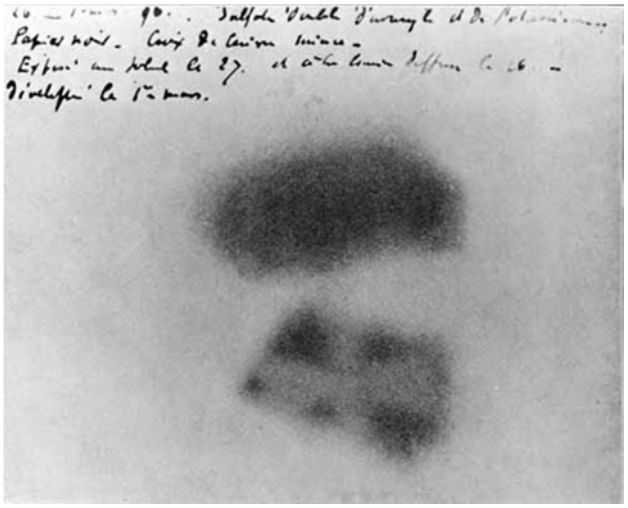

Image of Becquerel's **photographic plate** which has been fogged by exposure to radiation from a **uranium salt**.

α, β rays -- 1899

γ Ray -- 1900

Ernest Rutherford
(1871.8.30 – 1937.10.19)

Pierre Curie
(1859.5.15 – 1906.4.19)

Marie Curie
(1867.11.7 – 1934.7.4)

Paul Ulrich Villard
(1860.9.28 – 1934.1.13)

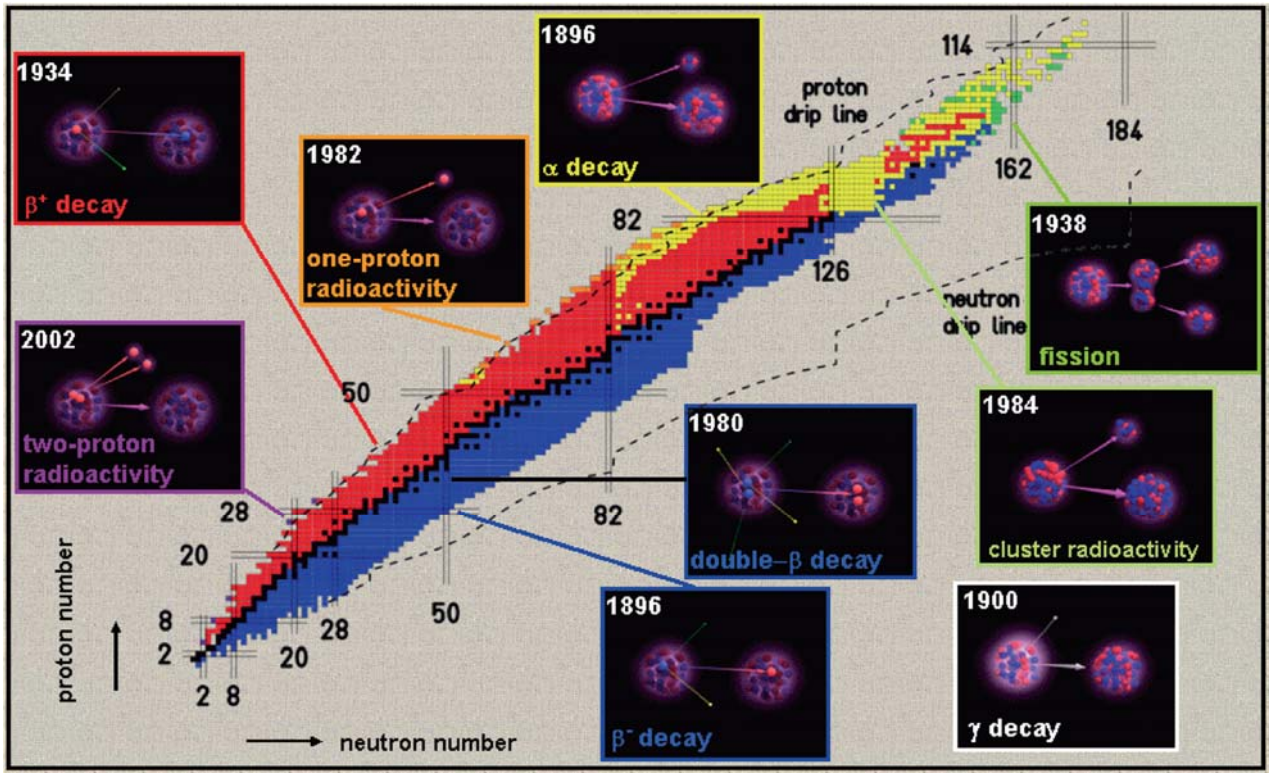

Figure: *Chart of the nuclides with all nuclei known today plotted as a function of neutron and proton numbers. B. Blank, Nuclear Physics News, Vol.19, No. 3, 14 (2009)*

1*p* & 2*p* radioactivity

(theory leading…)

♣ First proposed by **V.I. Goldanskii** & **Y.B. Zeldovich** in early of **1960**s

cf: V.I. Goldanskii, Nucl. Phys. **19**, 482 (1960); Y.B. Zeldovich, Sov. Phys.-JETP **11**, 812 (1960).

♣ **1*p*** (about 25 emitters were discovered.)

Isomer state – **^{53}Co^{m}** was observed in **1970**

cf: K.P. Jackson *et al.*, Phys. Lett. B **33** , 281 (1970); J. Cerny *et al.*, Phys. Lett. B **33**, 284 (1970).

Ground state – **^{151}Lu & ^{147}Tm** were observed in **1982**

cf: S. Hofmann *et al.*, Z. Phys. A **305**, 111 (1982); O. Klepper *et al.*, Z. Phys. A **305**, 125 (1982).

♣ **2*p*** (only 3 emitters were certified – **^{45}Fe, ^{48}Ni & ^{54}Zn**)

cf: M. Pfutnzer *et al.*, Eur. Phys. J. **A14**, 279 (2002); J. Giovinazzo *et al.*, Phys. Rev. Lett. **89**, 102501 (2002); C. Dossat et al., Phys. Rev. C **72**, 054315 (2005); B. Blank *et al.*, Phys. Rev. Lett. **94**, 232501 (2005).

Ground state – ^{6}Be, ^{12}O, ^{16}Ne, ^{19}Mg, ^{26}S … (short lifetime)

^{45}Fe, ^{48}Ni, ^{54}Zn … (long lifetime)

Excited state – ^{14}O, ^{17,18}Ne, ^{28,29}S, ^{94}Ag … (directly 2*p* emitters)

1.2 Concept of 1*p* & 2*p* radioactivity

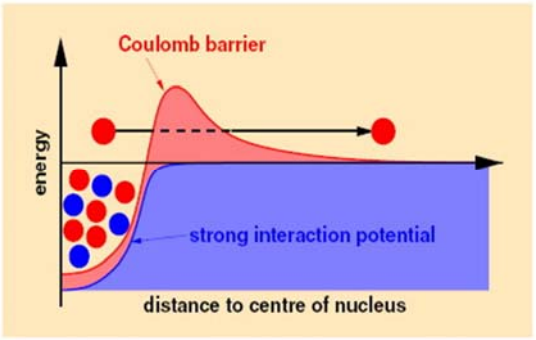

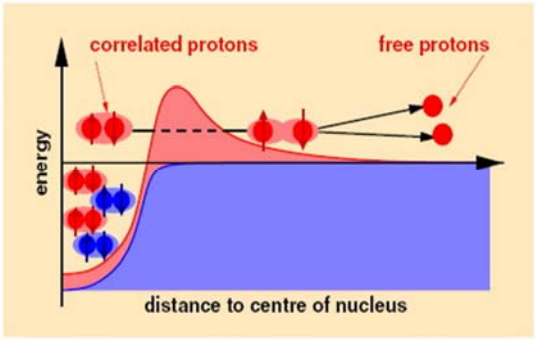

1*p* emission **2*p* emission**

cf: B. Blank and M. Ploszajczak, Rep. Prog. Phys. **71**, 046301 (2008).

2*p*:

- ♣ pair correlation: ^1S configuration (ISI -- initial state interaction)
- ♣ share the energy: $E_{p1} = E_{p2} = Q_{2p}/2$
- ♣ favors $l = 0$ orbit (s orbit)

Tunneling through the barrier:

$\lambda = S * \nu * P$

λ – decay probability ($\lambda \sim 1/T_{1/2}$)

S – spectroscopic factor

ν – frequency factor

P – penetration probability

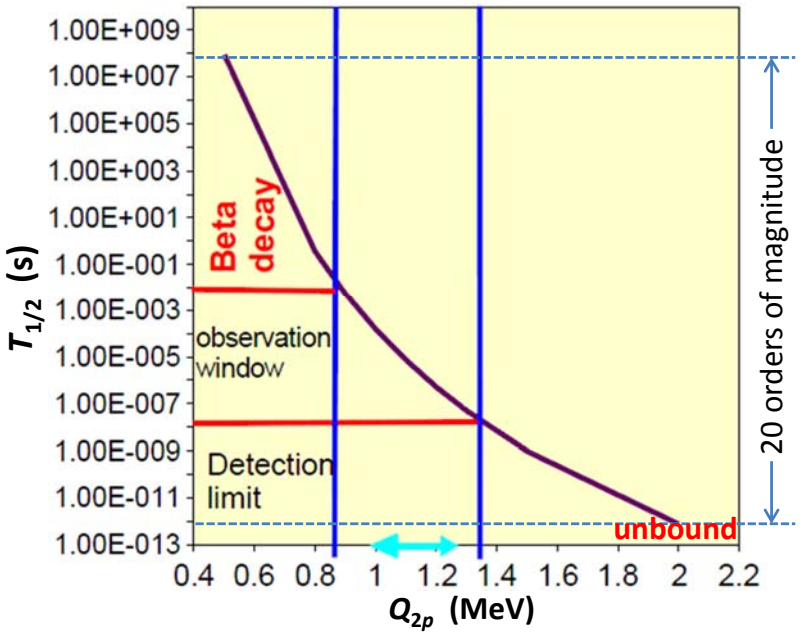

about 10 ns – 10 ms required in experiment

Penetrability strongly depends on the decay energy of 2*p*.

Possibly existing area

Heavy emitters: ^{39}Ti, ^{42}Cr, ^{45}Fe, ^{48,49}Ni, ^{54}Zn …
(A > 40)

- High Coulomb barrier
- Ground state
- Long lifetime (> ps)
- Offline decay measurement

Intermediate emitters: $^{22\text{-}24}$Si, $^{26\text{-}29}$S, ^{31,32}Ar, ^{34}Ca…
(20 < A < 40)

- Medium Coulomb barrier
- Ground state, lowly or highly excited state
- Short lifetime (~ fs/keV/MeV order)
- Online complete-kinematics measurement

Light emitters: ^{6}Be, ^{12,14}O, ^{16,17,18}Ne, ^{19}Mg …
(A < 20)

- Low Coulomb barrier
- Ground state or lowly excited state
- Short lifetime (~ keV order)
- Online complete-kinematics measurement

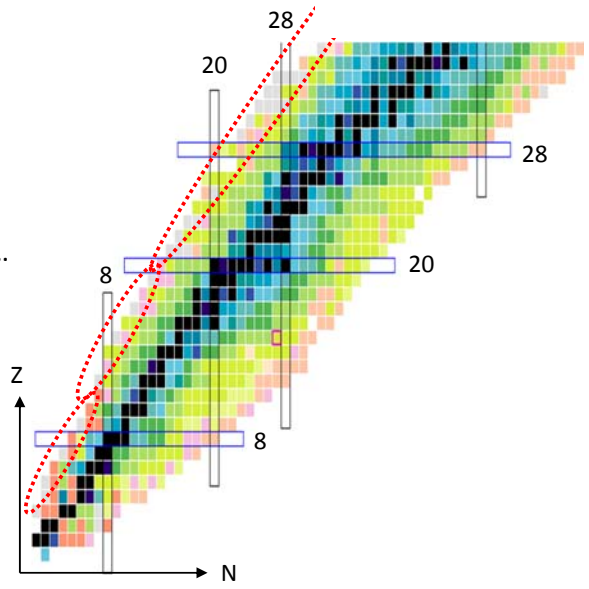

1.3 2*p* decay modes

Decay scheme

Sequential transitions through an intermediate state

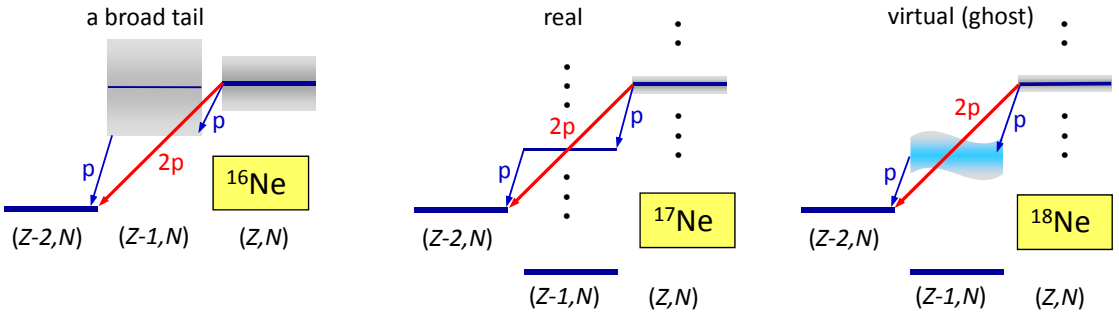

In each case a direct 3-body process may contribute,
but it is hard to distinguish it from the sequential one.

In special cases the pure 3-body mechanism
is expected to dominate – the 2p radioactivity.

➔Opportunity to study 3-body dynamics and probe
p-p correlations in the nucleus.

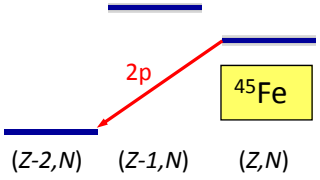

Decay dynamics

Sequential decay

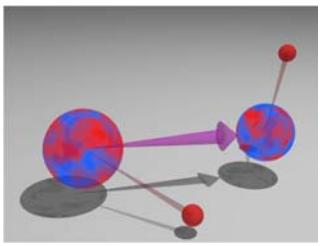

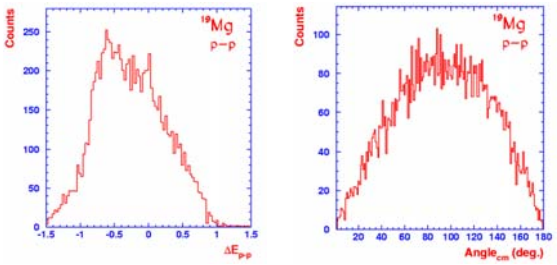

3-body breakup (uncorrelated)

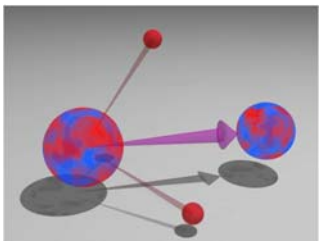

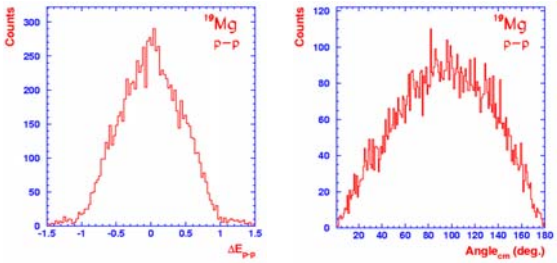

^{2}He emission (correlated)

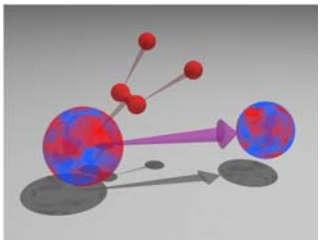

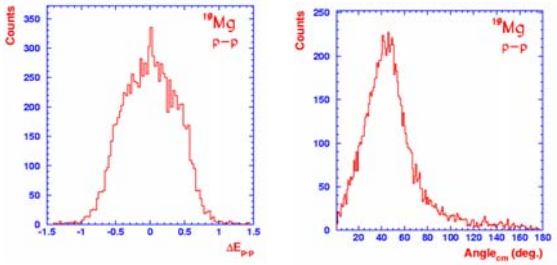

2p decay scenarios

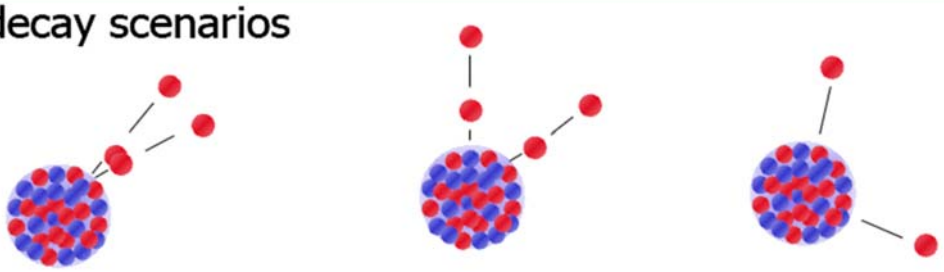

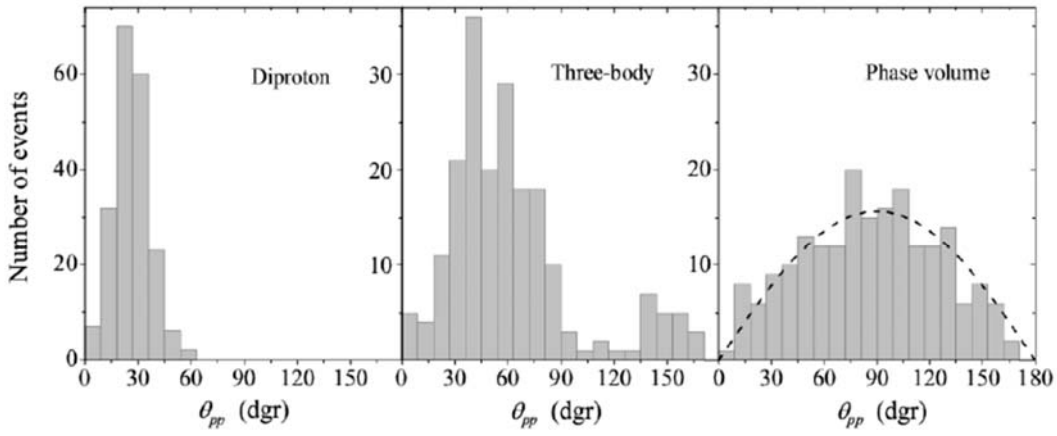

The Monte-Carlo simulations (200 events) of the opening angle pp between the protons emitted in the decay of 45Fe.

L. Grigorenko

1.4 Experimental measurements and signatures

Two protons are detected in an event …

- Decay Q-value: $Q_{2p} = E_{p1}+E_{p2}$, $\Delta E_p = E_{p1}-E_{p2} \approx 0$, $E_{p1} \approx E_{p2}$ (Ground state)
- Decay time (half-life): $T_{1/2}$ in agreement with theoretic prediction
- Opening angle: θ_{pp} NOT isotropic (< 90°)
- Invariance mass: $M = \sqrt{(\sum E_i)^2 - (\sum P_i c)^2}$ (four-momentum)

  Excitation Energy: $E_x = M\text{-}M_{G.S.}$ (in the 3-body system of final state)

- Relative momentum: $q_{pp} = \mu \left| \frac{\vec{p}_1}{m_1} - \frac{\vec{p}_2}{m_2} \right| = \frac{1}{2}|\vec{p}_1 - \vec{p}_2|$ peak at 20 MeV/c

  Relative energy: $E_{pp} = \frac{m_2 E_1 + m_1 E_2 - 2\sqrt{m_1 E_1 m_2 E_2}\cos\theta_{12}}{m_1+m_2} = \frac{1}{2}\left(E_1 + E_2 - 2\sqrt{E_1 E_2}\cos\theta_{12}\right)$

- Correlation function: $C(q) = \frac{N_2(q)}{N_1(p_1)N_1(p_2)}$ (HBT analysis)

(N_2: the relative momentum distribution of the proton pair measure in the experiment)

(N_1: the momentum distribution of single proton reconstructed by the MC simulation.)

2*p* configurations & Initial State Interaction (ISI)

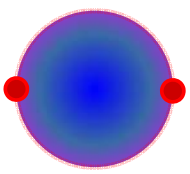

BCS

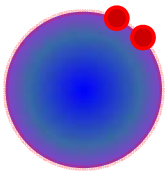

BEC

Copper pairing?

Bose-Einstein Condensation?

BCS/BEC crossover?

cf: K. Hagino *et al.*, Phys. Rev. Lett. 99, 022506 (2007). -- ^{6}He BCS/BEC crossover

C.A. Bertulani and M.S. Hussein, Phys. Rev. C 76, 051602R (2007). – ^{6}He, ^{11}Li, ^{14}Be, ^{17}Ne

HBT analysis & Final State Interaction (FSI)

Hanbury-Brown Twiss (HBT) interferometry

cf: R. Hanbury-Brown and R. Q. Twiss, Nature (London) **178**, 1046 (1956).

Two-neutron halo structure (^{6}He, ^{11}Li, ^{14}Be) – to probe space-time character

cf: F.M. Marques *et al.*, Phys. Lett. B **476**, 219 (2000); Phys. Rev. C **64**, 061301R (2001).

FSI & blurred femtoscopy

Cf: S.E. Koonin, Phys. Lett. **70B**, 43 (1979). -- FSI

C.A. Bertulani, M.S. Husseun, G. Verde, Phys. Lett. B 666, 86 (2008). -- blurred

1.5 Theoretic models

- R-matrix approach – recent formulation by F.C. Barker in PRC 59 (1999) 535 and PRC 63 (2001) 047303 replaced the simplified versions applied previously.
  Two extreme scenarios (2-body picture) :
  1) sequential decay through intermediate states (real or ghosts),
  2) di-proton decay through the s-wave p+p final state.
  Predicted p-p correlations (in the di-proton mode) are based on a simplified treatment of the final state interactions (Migdal-Watson approximation).

- 3-body model – founded by L.V. Grigorenko *et al*. in PRL 85 (2000) 22 and PRC 64 (2001) 054002. Accounts for the 3-body dynamics in a cluster approximation. Both widths and p-p correlations are calculated in the same framework.

- Shell Model Embedded in Continuum (SMEC) – initiated by J. Rotureau, J. Okołowicz and M. Płoszajczak in APPB 35 (2004) 1283 , and presented by J.R. at the PROCON03. Presently only widths calculated for the sequential and di-proton transitions.

2. β-delayed 2*p* emitters

cf: B. Blank and M.J.G. Borge,
Prog. In Part. and Nucl. Phys. 60, 403 (2008)

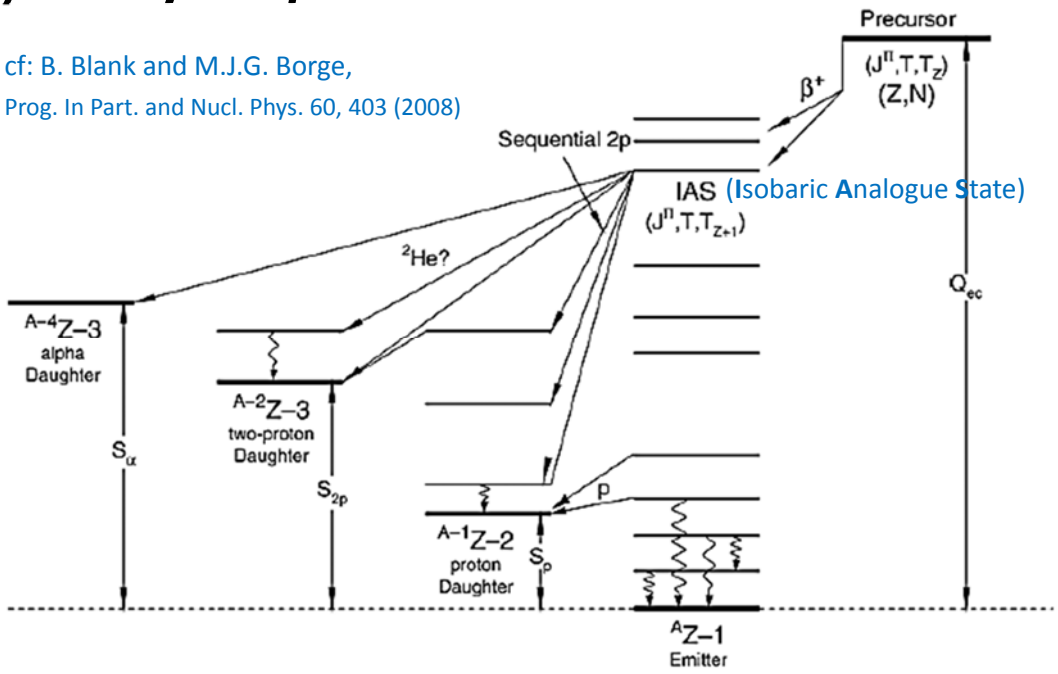

β-delayed decay scheme for proton-rich nucleus

The prediction:

Sov. Phys. JETP Lett. **32**, 554 (1980).

Emission of β^+-delayed pairs of protons and doubly β^+-delayed protons and α particles

V. I. Gol'danskiĭ
Institute of Chemical Physics, USSR Academy of Sciences

(Submitted 5 October 1980; resubmitted 23 October 1980)
Pis'ma Zh. Eksp. Teor. Fiz. **32**, No. 9, 572–574 (5 November 1980)

In addition to the two types of radioactive decay with the emission of nucleon pairs that were predicted in 1960—two-proton radioactivity so far not observed experimentally and the β^--delayed neutron pairs first observed in 1979—an emission of β^+-delayed proton pairs is possible. A list of probable examples is presented. The emission of doubly β^+-delayed protons and α particles, in particular, the doubly β^+-delayed, proton-radioactive decays from an excited nuclear state, should be observed after a chain of two β^+-decay events.

The discovery: -- ^{22}Al

M.D. Cable *et al.*, Phys. Rev. Lett. **50**, 404 (1983).

^{24}Mg(^{3}He,*p*4*n*)^{22}Al at 110 MeV @ LBL

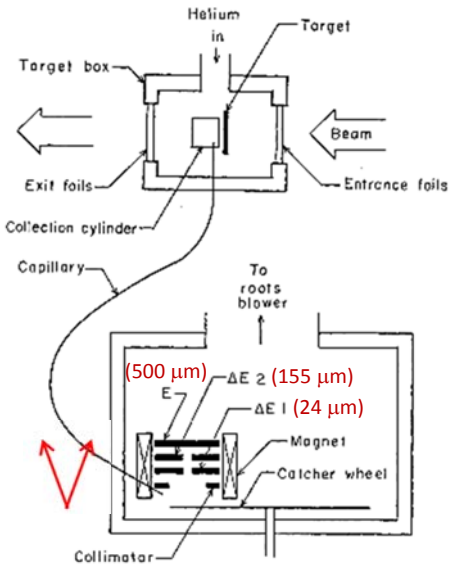

Experimental setup

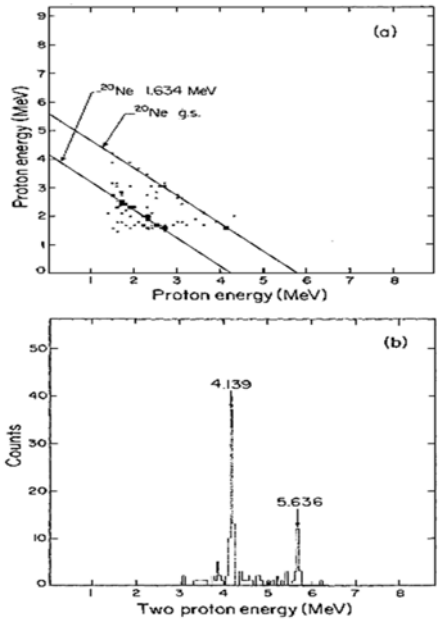

p-p coincidence spectrum

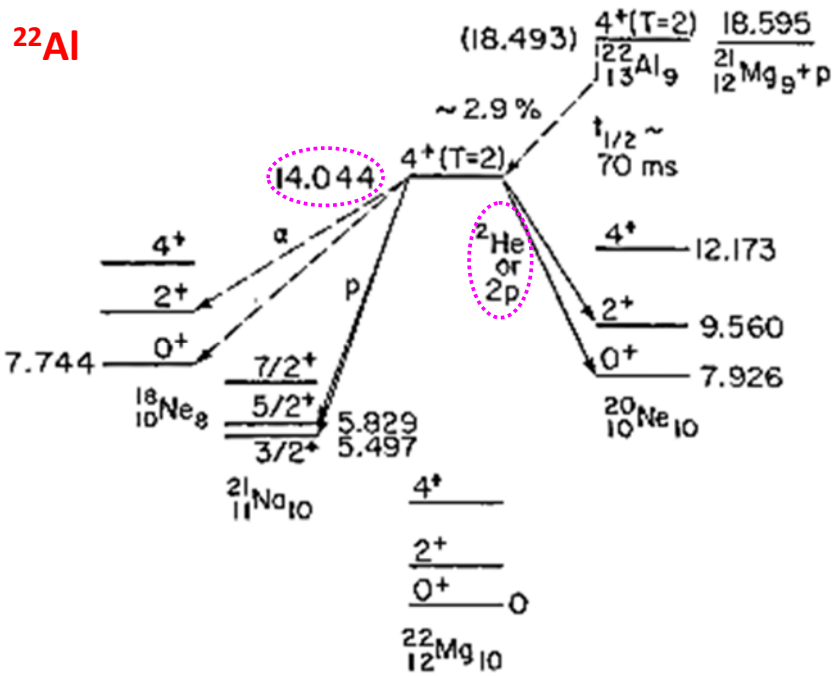

β-delayed decay scheme of ^{22}Al

Experiment: M.D. Cable *et al.*, Phys. Rev. Lett. **50**, 404 (1983).

Shell-model calculation: B.A. Brown, Phys. Rev. Lett. 65, 2753 (1990).

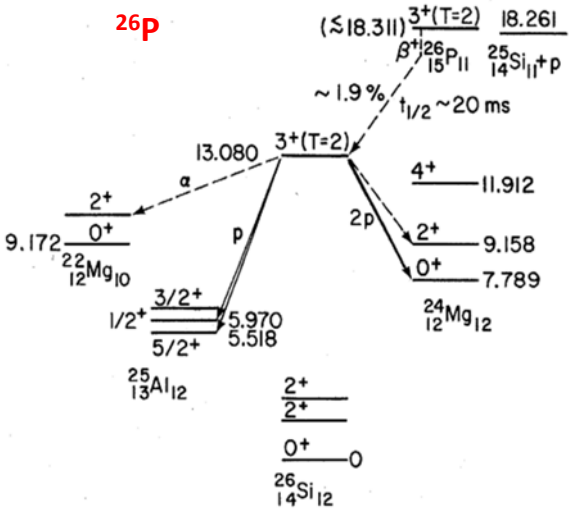

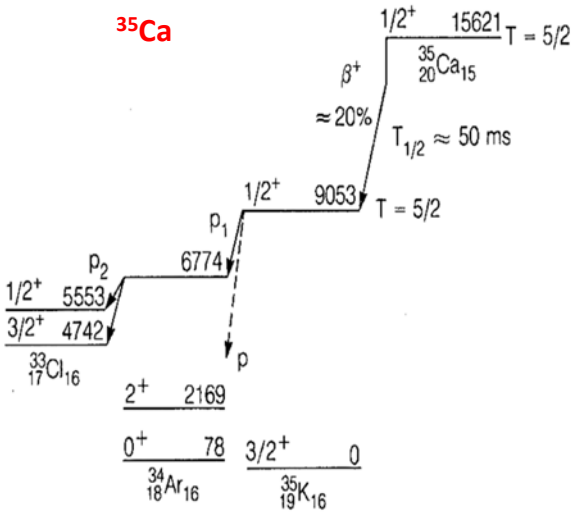

β-delayed decay scheme of ^{26}P

β-delayed decay scheme of ^{35}Ca

cf: J. Honkanen *et al.*, Phys. Lett. **133B**, 146 (1983).

M.D. Cable *et al.*, Phys. Rev. C **30**, 1276 (1984).

J. Aysto *et al.*, Phys. Rev. Lett. **55**, 1384 (1985).

List of $\beta 2p$ emitters & their references

^{22}Al – M.D. Cable *et al.*, Phys. Rev. Lett. **50**, 404 (1983).
^{26}P – J. Honkanen *et al.*, Phys. Lett. **133B**, 146 (1983).
^{35}Ca – J. Aysto *et al.*, Phys. Rev. Lett. **55**, 1384 (1985).
^{39}Ti – M.D. Moltz *et al.*, Z. Phys. A **342**, 273 (1992).

Berkeley helium-jet offline

^{31}Ar – J.E. Reiff *et al.*, Nucl. Inst. Meth. **A276**, 228 (1989).
^{27}S – V. Borrel *et al.*, Nucl. Phys. **A531**, 353 (1991).
^{43}Cr – V. Borrel *et al.*, Z. Phys. A **344**, 135 (1992).
^{23}Si – B. Blank *et al.*, Z. Phys. A **357**, 247 (1997).
^{50}Ni – C. Dossat *et al.*, Nucl. Phys. A **792**, 18 (2007).

LISEx@GANIL implanted online

Candidate: ^{22}Si, ^{42}Cr, ^{45}Fe, ^{48,49}Ni …

β-delayed multi-nucleon emission: $\beta 3p$ …, $\beta\alpha$, $\beta p\alpha$ …

3. Ground-state 2*p* emitters

3.1 The prediction:

Nucl. Phys. **19**, 482 (1960).

ON NEUTRON-DEFICIENT ISOTOPES OF LIGHT NUCLEI AND THE PHENOMENA OF PROTON AND TWO-PROTON RADIOACTIVITY

V. I. GOLDANSKY
P. N. Lebedev Physical Institute, USSR Academy of Sciences, Moscow

Received 14 March 1960

Abstract: Application of isobaric invariance principles to light nuclei leads to a very simple relation between the Z-th proton binding energy E_p in nucleus 1 ($_ZM_N^A$) and the Z-th neutron binding energy E_n in the mirror nucleus 2 ($_NM_Z^A$). With an accuracy of the order of a few per cent their difference $E_{n2} - E_{p1} = \Delta E_{np}$ is independent of N for a given Z and is given by

$$\Delta E_{np} \approx E_n(_ZM_Z^{2Z}) - E_p(_ZM_Z^{2Z}) \approx 1.2\,\frac{Z-1}{(2Z-1)^{\frac{1}{3}}},$$

which is more correct than the usual expression $1.2\,(Z-1)/(Z+N-1)^{\frac{1}{3}}$. By exploiting this fact one can predict the existence and properties of almost ninety new neutron-deficient isotopes of light nuclei (up to $Z = 34$) and establish the limits of stability of the isotopes with respect to decay with proton emission. Among the specific properties of neutron-deficient isotopes, proton and two-proton radioactivity effects which may occur are of special interest. Some nuclei are indicated in which these effects may be observed. The main features of a very curious phenomenon of two-proton radioactivity are discussed.

3.2 The discovery: -- ^{45}Fe

Two experiments:
- **GANIL in July 2000**
- **GSI in July 2001**

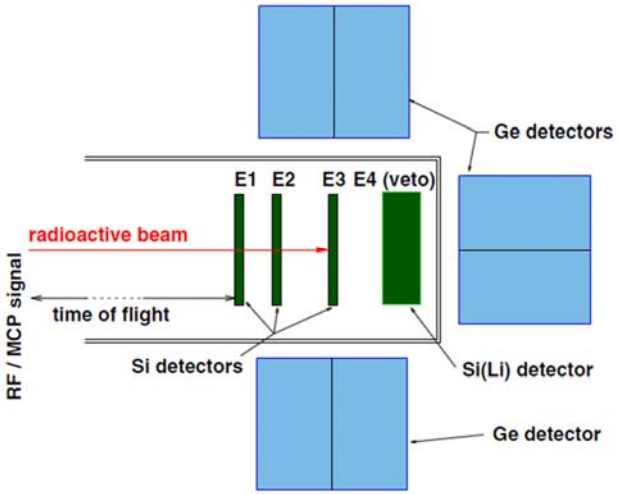

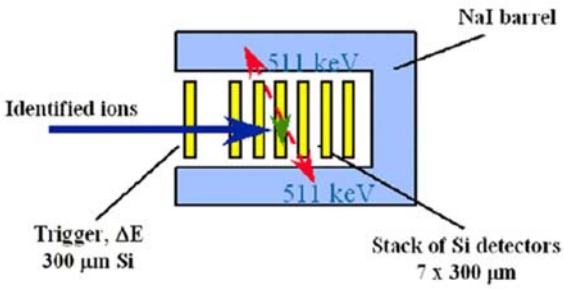

GANIL
- high production rate:
  15 ^{45}Fe per day
- standard data acquisition
  (CAMAC – VME)

GSI
- low production rate:
  6 ^{45}Fe implantations in 6 days
- fast data acquisition
  (XIA modules)

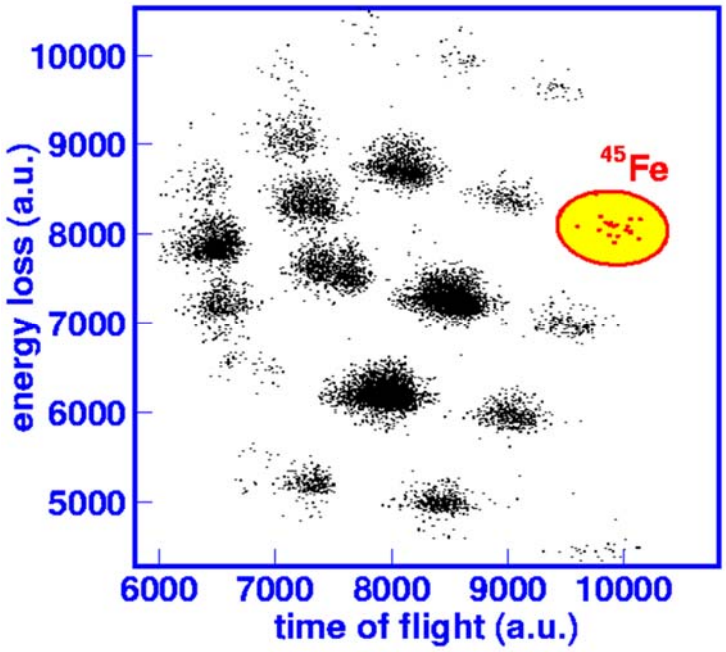

Particle identification of the secondary beam

Experiment at GANIL 2000 -- 22 events of ^{45}Fe implantation

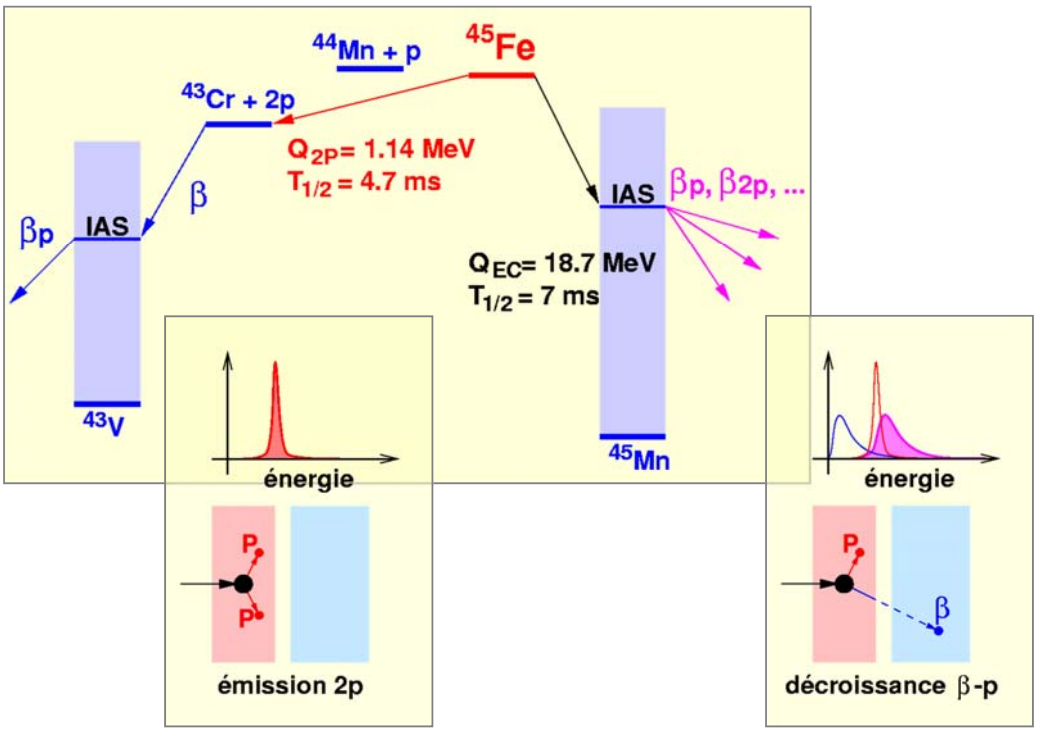

2*p* decay-energy spectrum

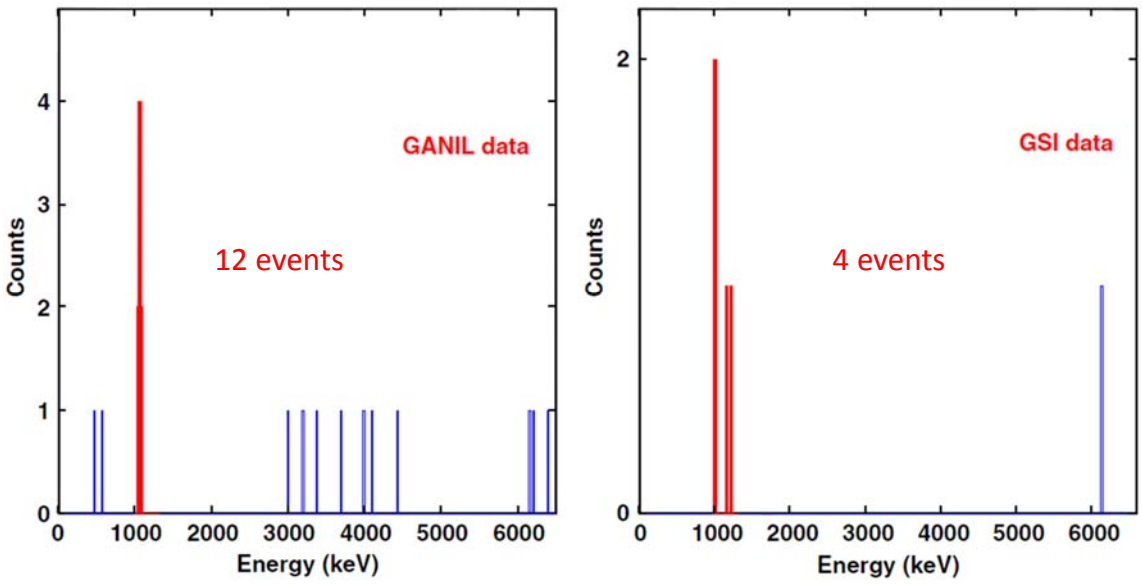

♣ No β-decay was observed → direct 2*p* emission.

GANIL result:

➔ E_{2p} = 1.14(5) MeV
$T_{1/2} = 4.7^{+3.4}_{-1.4}$ ms

J. Giovinazzo *et al.*, PRL **89**, 102501 (2002).

GSI results:

➔ 2*p* emission is the dominant (80%) decay mode of ^{45}Fe :
E_{2p} = 1.1(1) MeV
$T_{1/2} = 3.2^{+2.6}_{-1.0}$ ms

M. Pfutzner *et al.*, EPJ A **14** , 279 (2002).

M. Pfutzner *et al.*, NIM A **493**, 155 (2002).

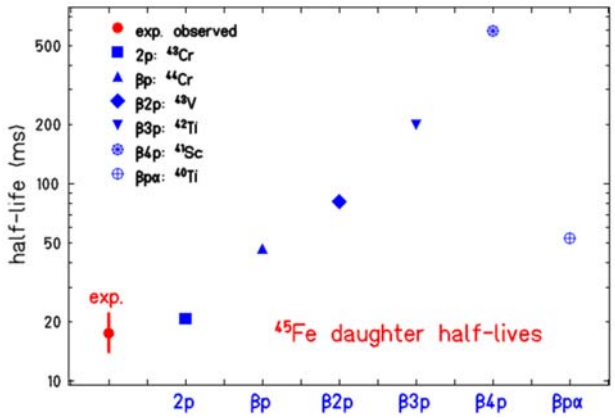

Predictions of 2p decay energy

Author	Q_{2p} [MeV]
Brown '91	1.15 ±0.09
Ormand '96	1.28 ±0.18
Cole '96	1.22 ±0.05
Goldansky '62	1.0

▶ **Only 2p decay hypothesis fits observations! !**

3.3 Confirmed by (O)TPC measurement – in 2007

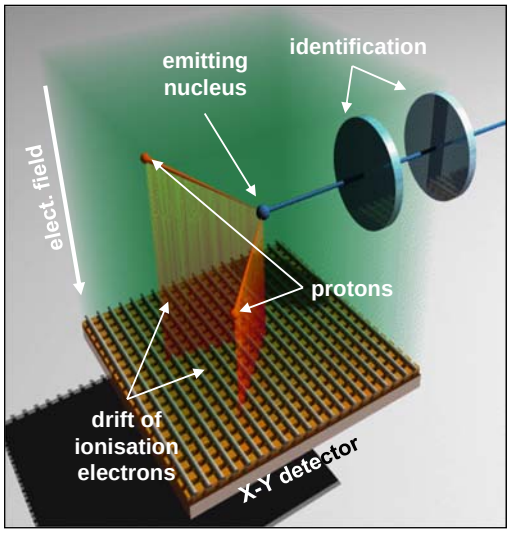

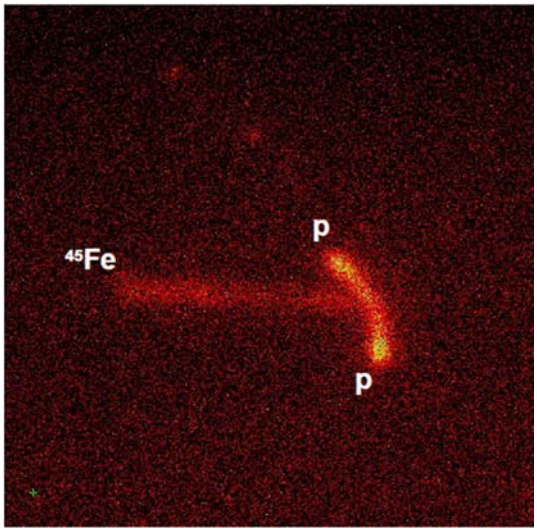

J. Giovinazzo et al.,
Phys. Rev. Lett. **99**, 102501 (2007).

K. Miernik et al.,
Phys. Rev. Lett. **99**, 192501 (2007).

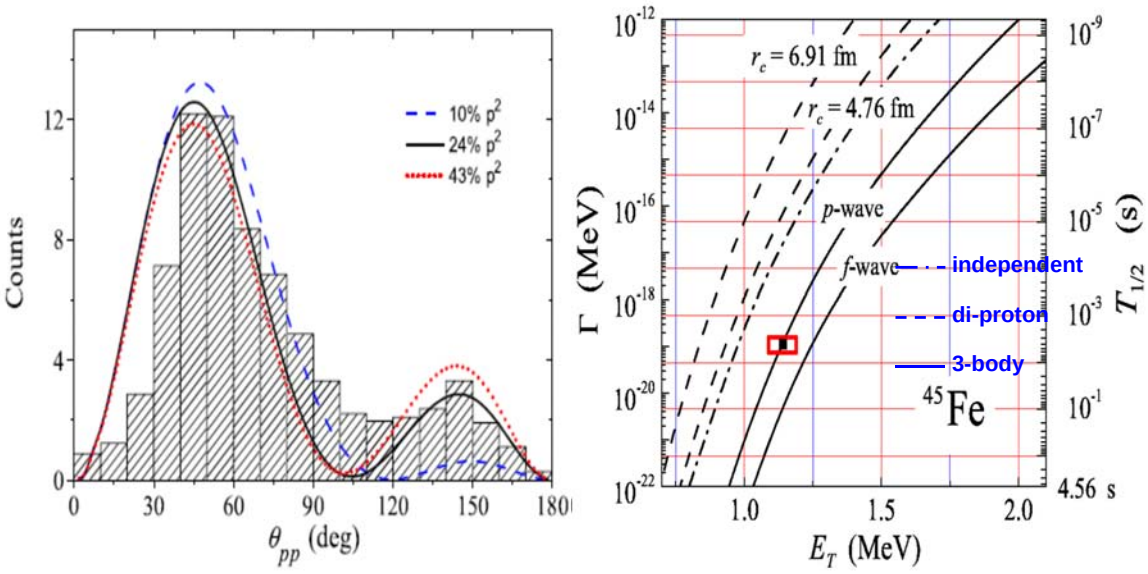

♣ Angular correlation: two-hump structure → strong p^2 contribution

♣ Decay width v.s. decay energy: *p*-wave configration

In good agreement with 3-body model (Grigorenko)

3.4 ^{54}Zn & ^{48}Ni -- in 2005

B. Blank et al., PRL 94, 232501 (2005)

C. Dossat et al., PRC 72, 054315 (2005).

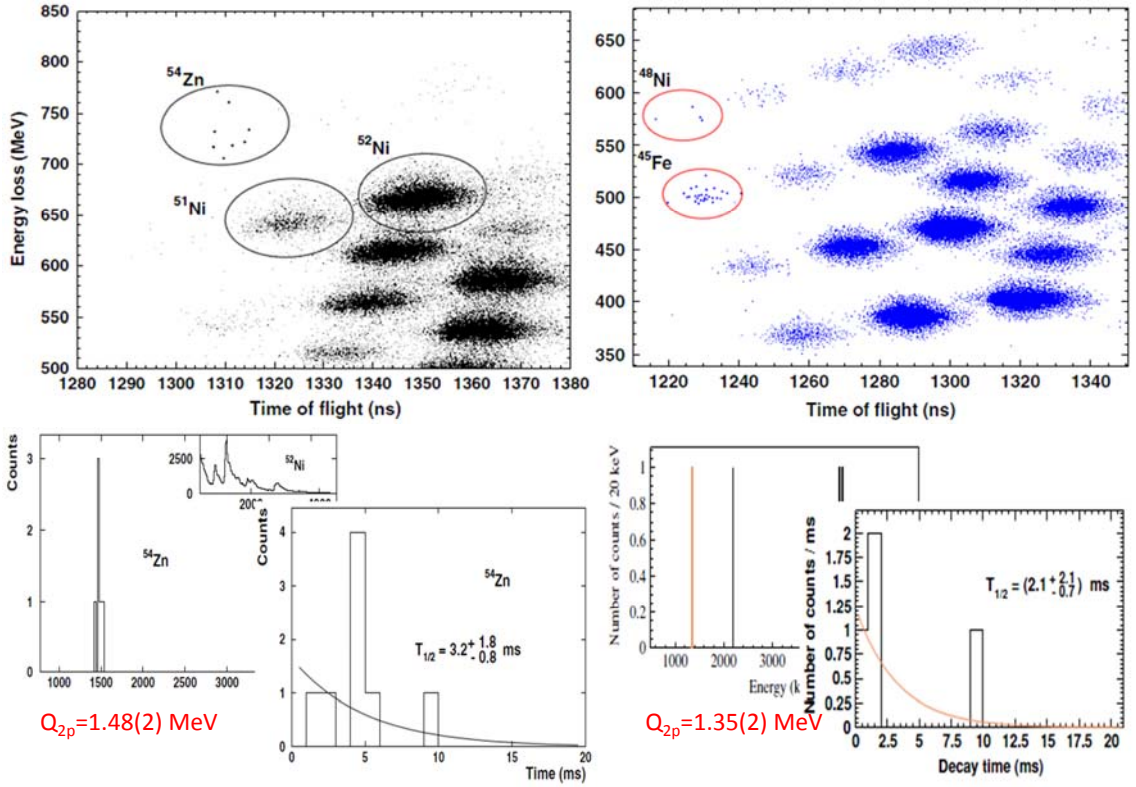

Q_{2p}=1.48(2) MeV

Q_{2p}=1.35(2) MeV

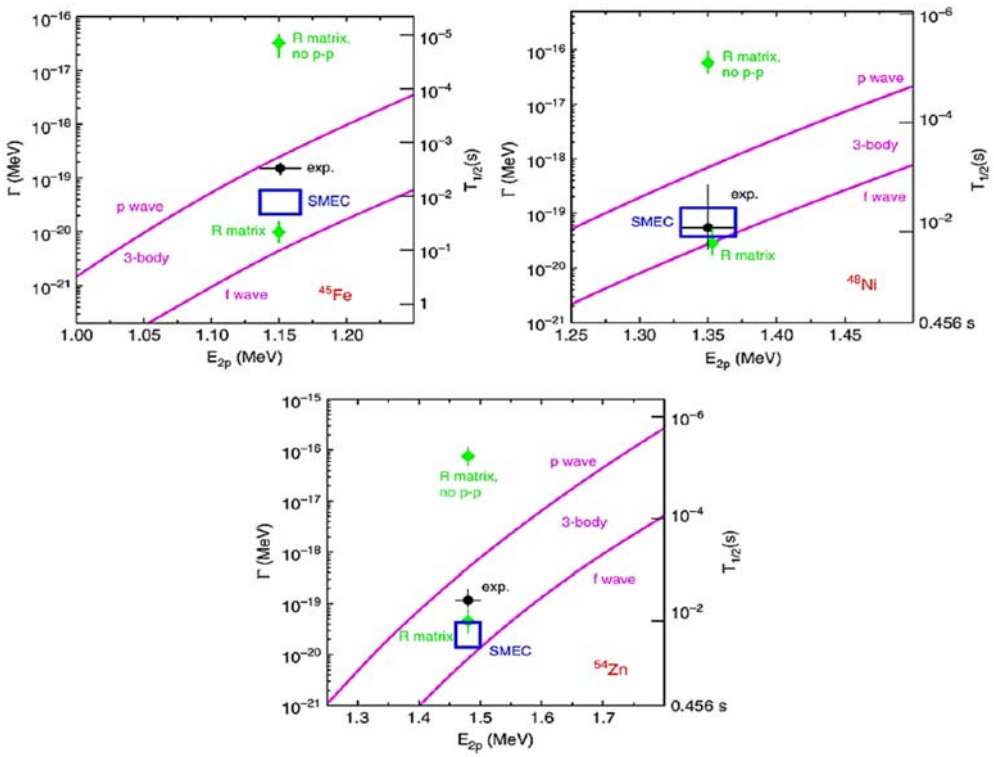

Compare with model predictions

cf: B. Blank and M.J.G. Borge, Prog. in Part. and Nulc. Phys. **60**, 403 (2008).

3.5 Light emitters

a) ^{6}Be

^{6}Li(^{3}He,t)^{6}Be

Kinematically complete measurement

A couple of ΔE-E telescopes

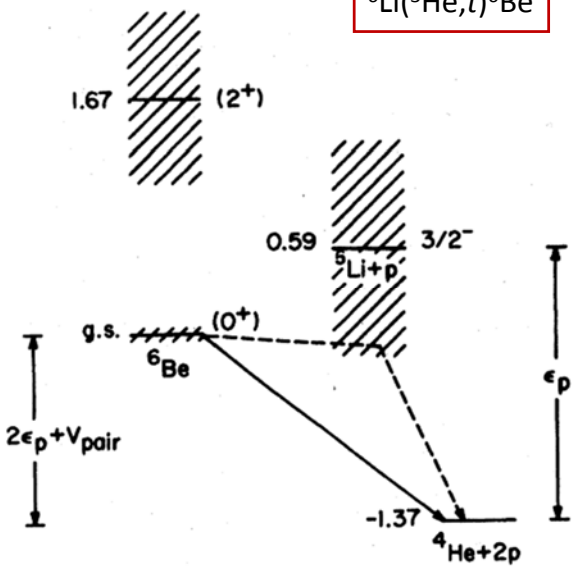

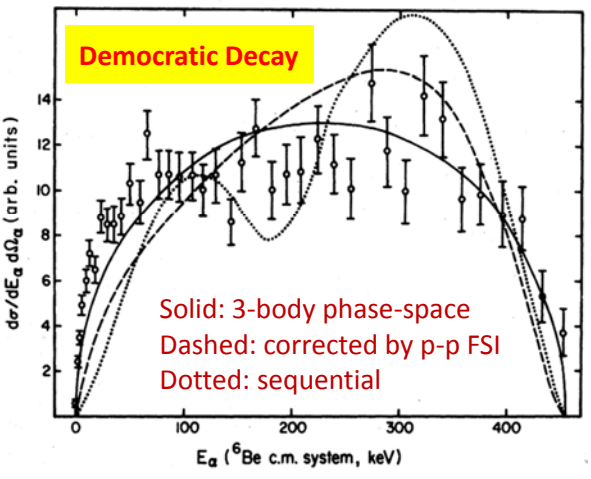

cf: D. F. Geesaman *et al.*, Phys. Rev. C **15**, 1835 (1977).
O. V. Bochkarev *et al.*, Nucl. Phys. **A505**, 215 (1989).

b) ^{12}O

R.A. Kryger et al., Phys. Rev. Lett. 74 (1995) 860

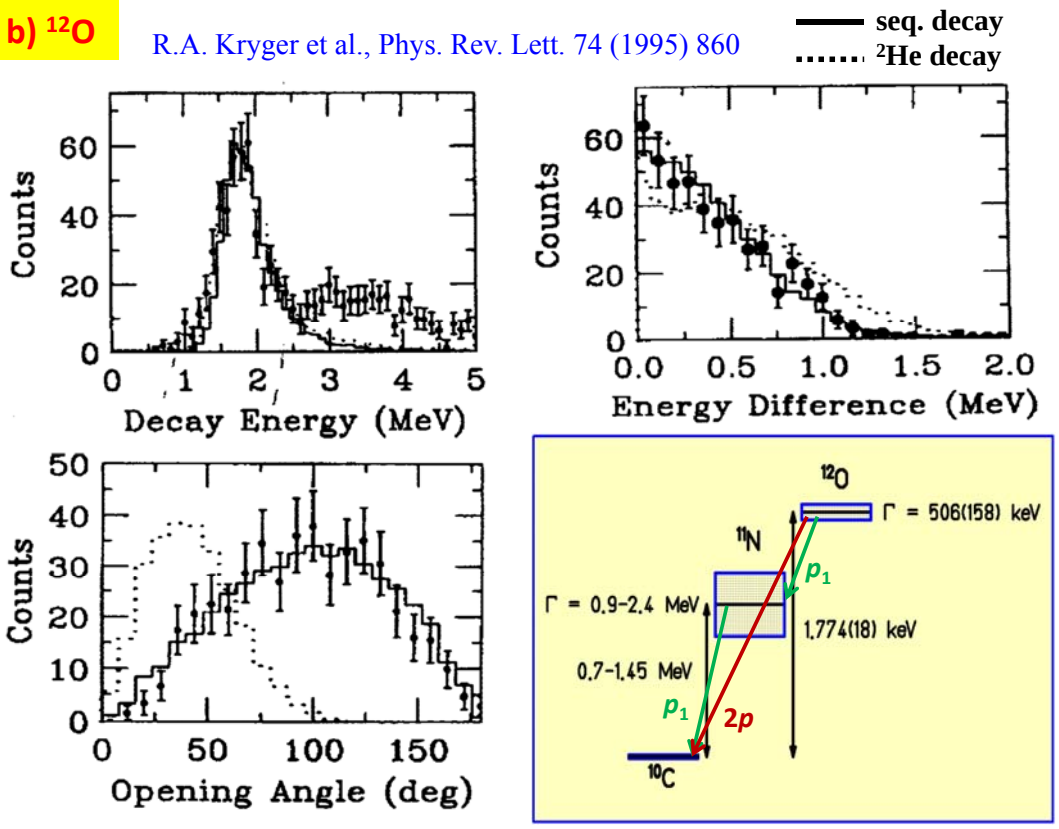

C) ^{16}Ne & ^{19}Mg

I. Mukha *et al.*, Phys. Rev. Lett. **99**, 182501 (2007);
Phys. Rev. C **77**, 061303(R) (2008).

^{16}Ne – $T_{1/2} \approx 4\times10^{-12}$ s

^{19}Mg – $T_{1/2} \approx 4\times10^{-19}$ s

The primary beam
^{24}Mg@591A MeV

½ FRS

The secondary beam
^{20}Mg@450A MeV
^{17}Mg@410A MeV

1n removal reaction

In-flight identification

The secondary's secondary beam
^{19}Mg & ^{16}Ne

½ FRS
MSD

Reaction products

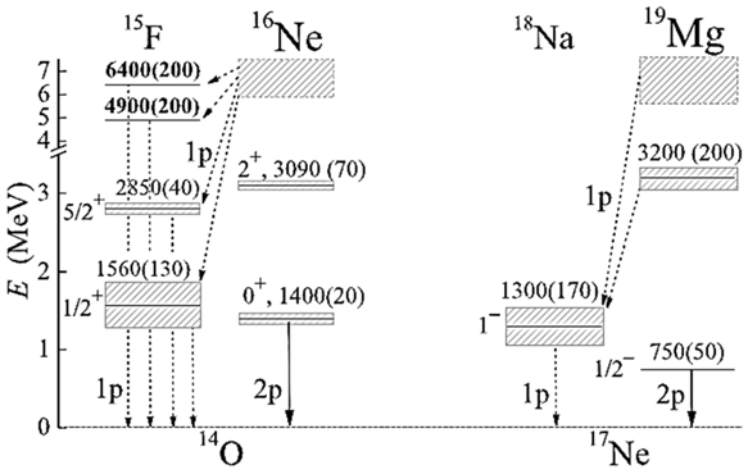

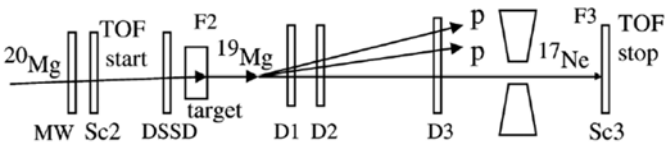

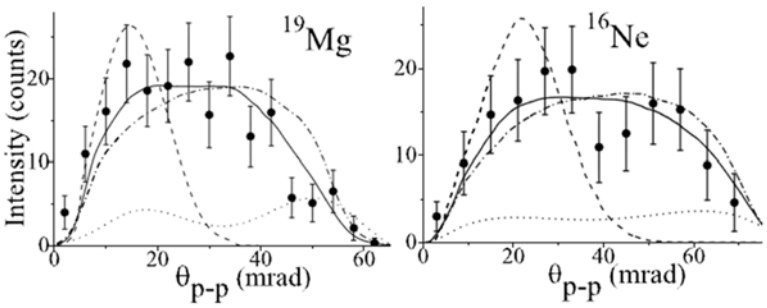

Angular p-p correlations

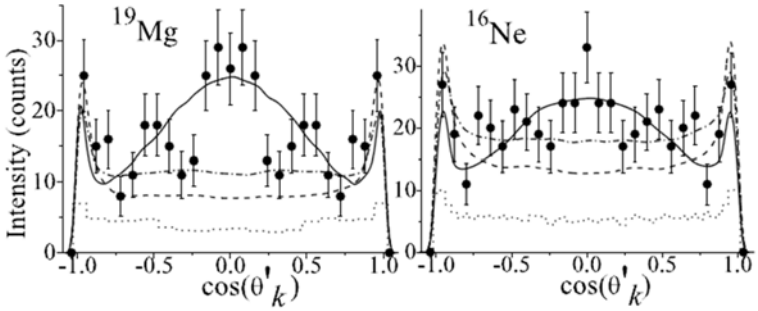

3-body correlations

Solid: 3-body (Grigorenko)

→ ^{16}Ne 54% d-wave

→ ^{19}Mg 88% d-wave

Dashed: diproton

Dash-dotted: phase-space (isotropic 2*p* emission)

Dotted: background

4. Excited-state 2*p* emitters

4.1 Light emitters

a) ^{14}O

C.R. Bain et al., Phys. Lett. B 373, 35 (1996).

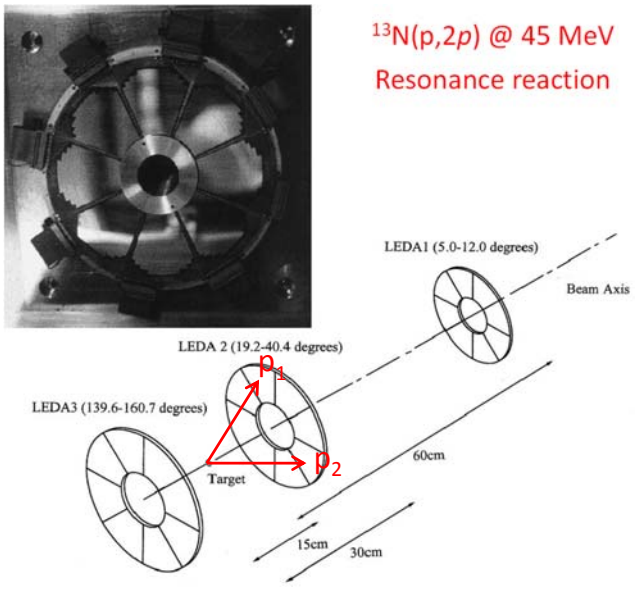

LEAD detector array

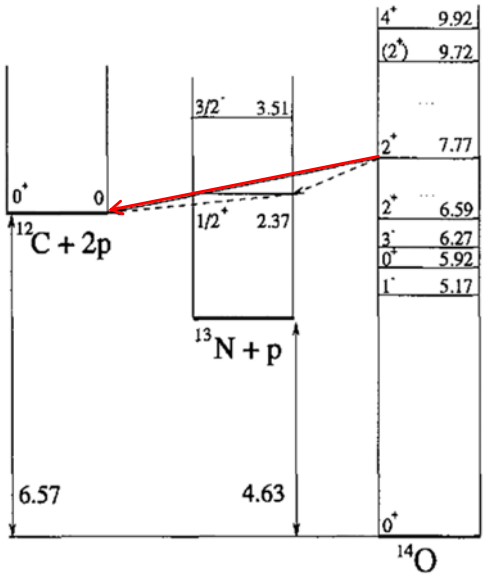

Decay scheme of ^{14}O

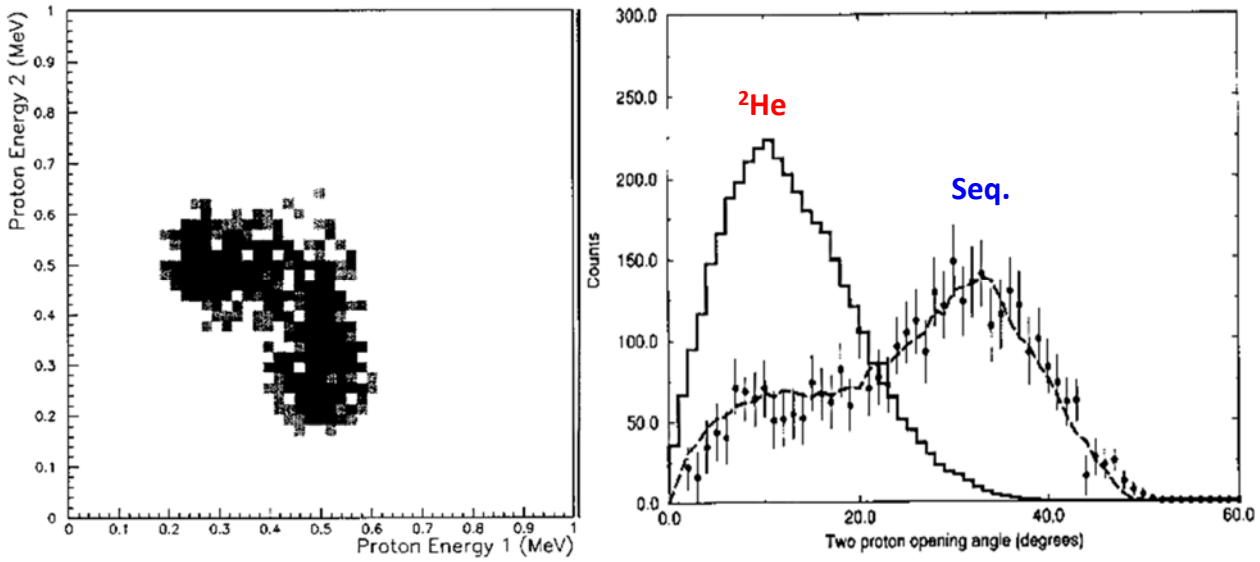

E_{p1} vs E_{p2} θ_{pp}

♣ Sequential emission; No ^{2}He emission.

b) ^{10}C

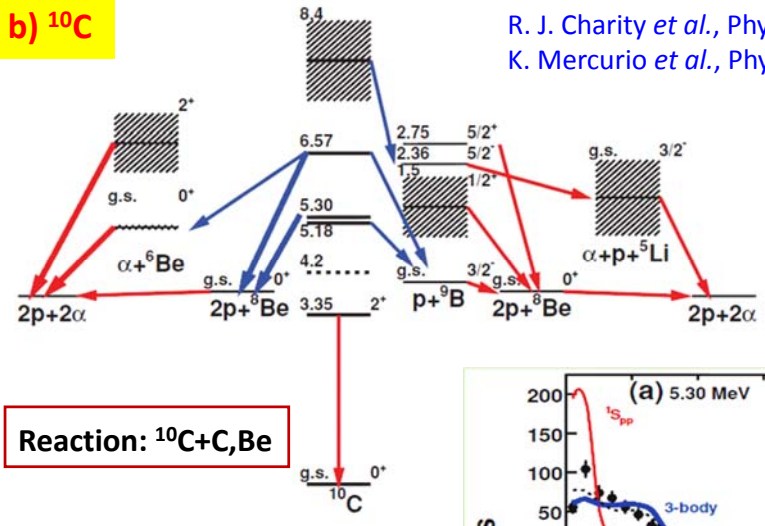

R. J. Charity *et al.*, Phys. Rev. C **75**, 051304(R) (2007).
K. Mercurio *et al.*, Phys. Rev. C **78**, 031602(R) (2008).

HiRA detector array

Kinematically complete measurement

Reaction: ^{10}C+C,Be

2*p* decay from 6.57 MeV state shows strong *p*-*p* correlation with the ^{1}S phase shift.

^{2}He decay?

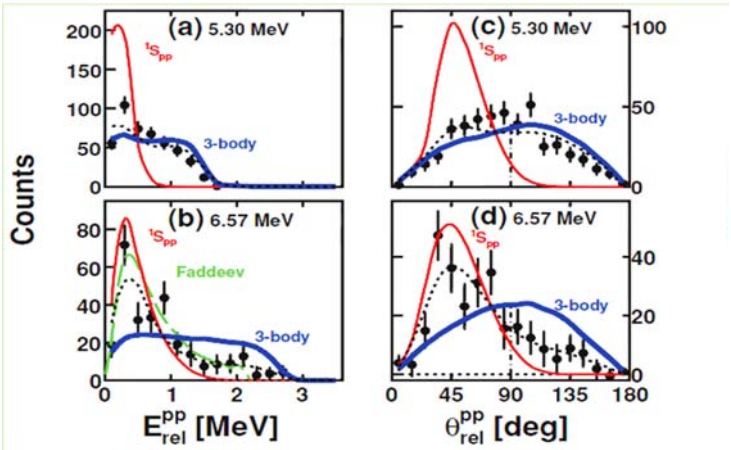

c) ^{17}Ne

M.J. Chromik et al., PRC**55**, 1676(1997); PRC **66**, 024313 (2002).

COULEX of 59 AMeV ^{17}Ne on Au target (**NSCL/MSU**)

Kinematically complete detection of reaction products

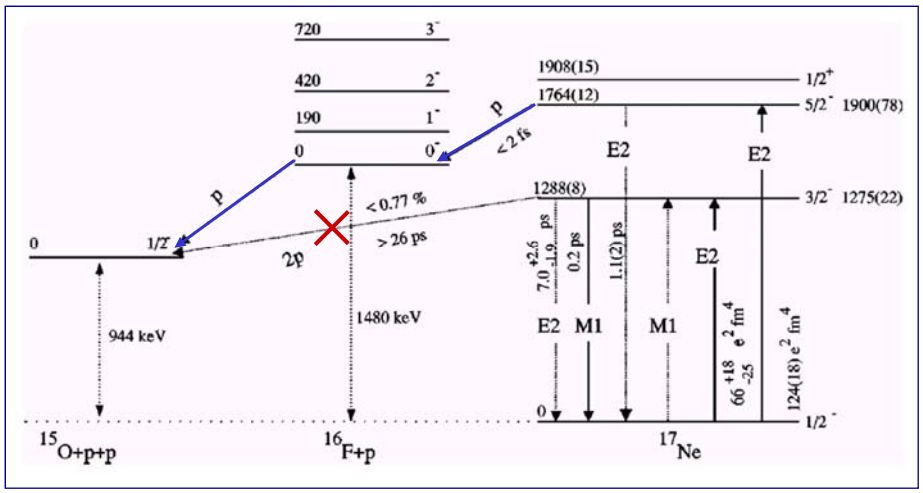

- Sequential 2p emission from the 5/2⁻ state was observed
- No evidence for the 2p branch from the 3/2⁻ state obtained

In agreement with prediction of Grigorenko, Mukha and Zhukov, NPA **713**, 372 (2003).

Evidence for the di-proton?

GANIL data

T. Zerguerras et al., EPJA **20**, 389 (2004) .

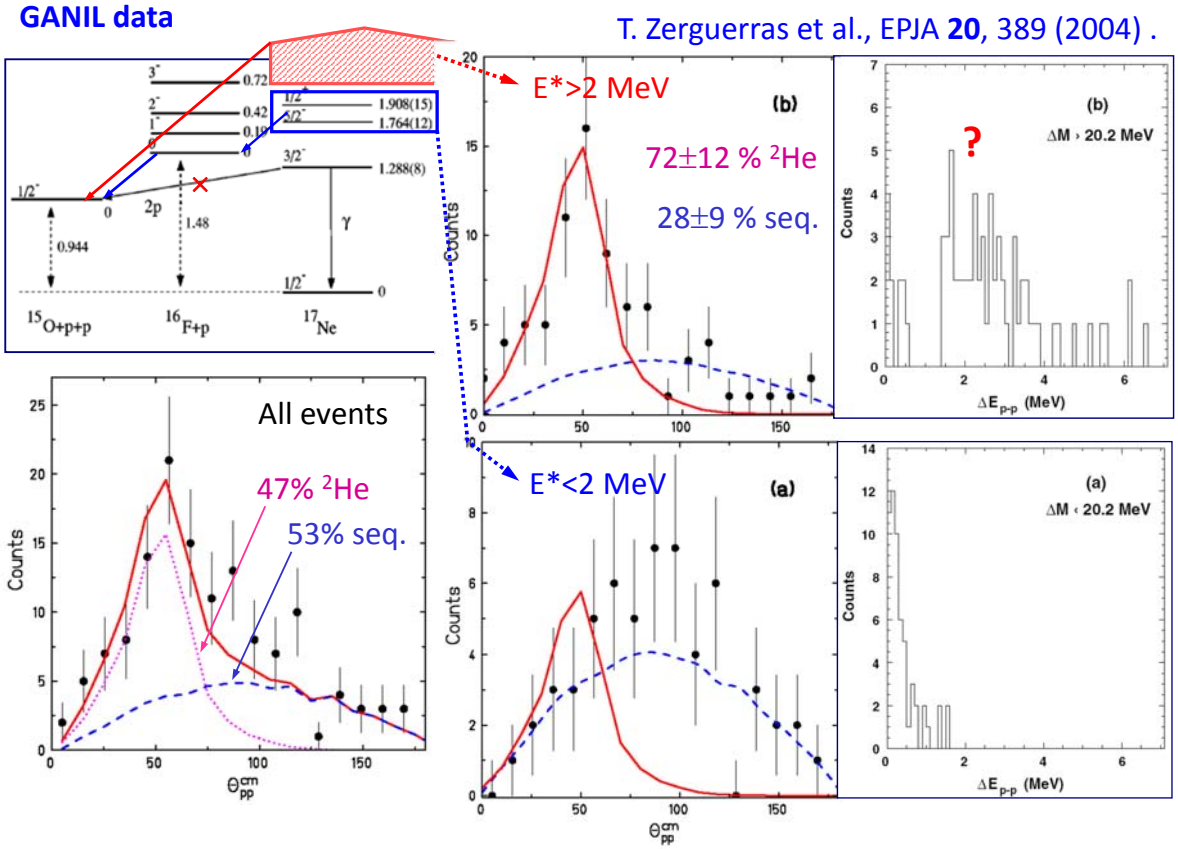

d) ^{18}Ne

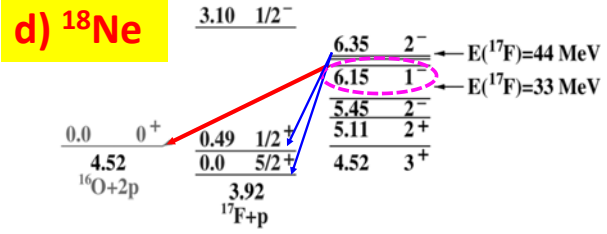

J. Gómez del Campo et al., PRL 86 (2001) 43

33/44 MeV ^{17}F(*p*,2*p*) (HRIBF@Oak Ridge)

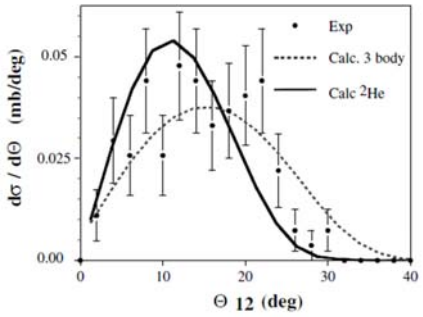

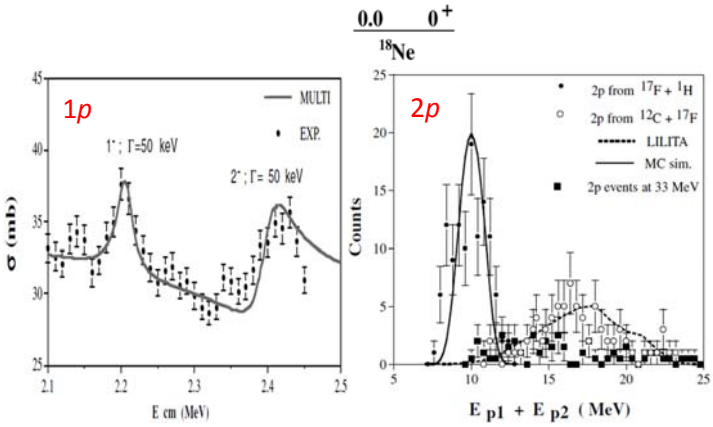

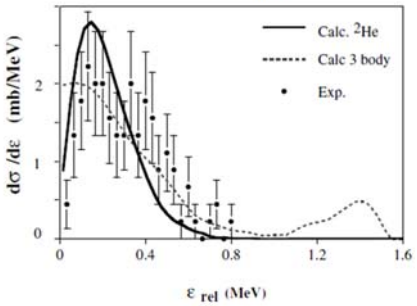

- Other processes : simultaneous (independent) emission via 2$^-$ state and direct breakup of ^{17}F on protons could contribute significantly! L.Grigorenko et al., PRC 65 (2002)044612

G. Raciti et al., Phys. Rev. Lett. ***100****, 192503 (2008).*

18Ne @ 33 AMeV -- FRIBs@Catania

Coulomb excitation (Pb target)

Kinematically complete measurement

31% ^{2}He decay

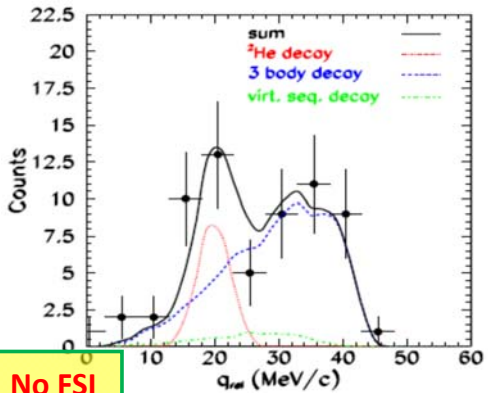

No FSI

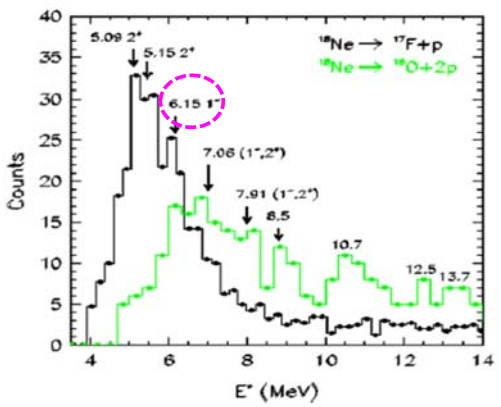

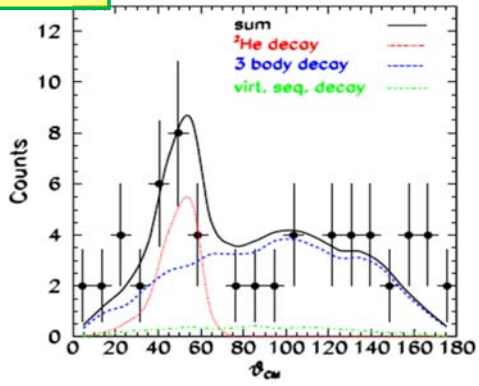

4.2 2*p* decay from odd-Z nucleus: $^{94}Ag^{m}$

1*p*: I. Mukha *et al.*, Phys. Rev. Lett. **95**, 022501 (2005).
2*p*: I. Mukha *et al.*, Nature (London) **439**, 298 (2006).

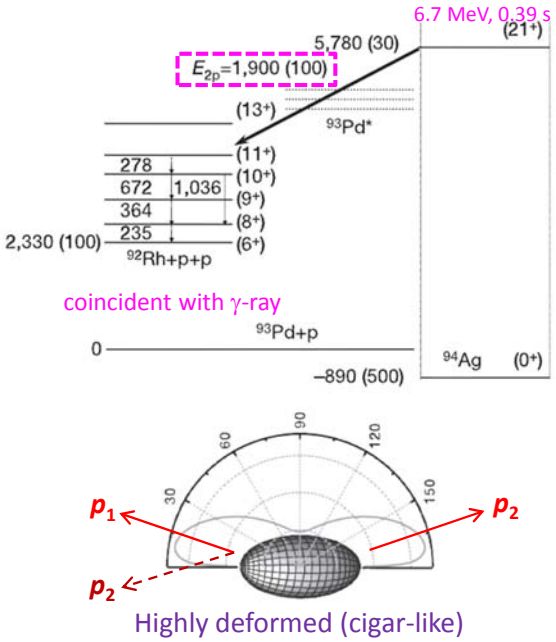

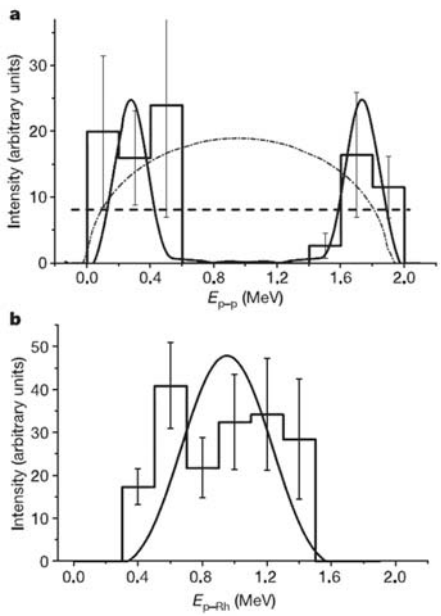

Latter …

LBNL

Directly measurement of proton emission from the isomer state of ^{94}Ag (21^+, 0.4s, 6.7 MeV).

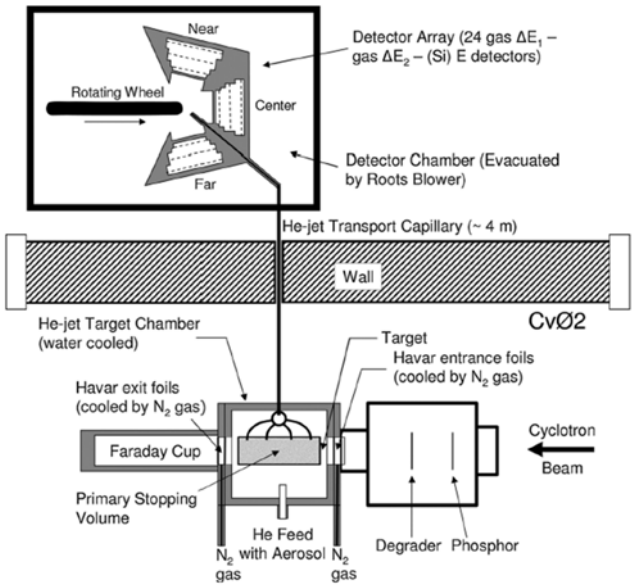

1*p* emission was confirmed, no 2*p* emission was observed!

cf: O.L. Pechenaya et al, Phys. Rev. C76, 011304(R) (2007).
D. G. Jenkins, Phys. Rev. C **80**, 054303 (2009).
J. Cerny, *et al.*, Phys. Rev. Lett. **103**, 152502 (2009).

2*p* decay from odd-Z nucleus?

4.3 Activities in China

1. ^{17,18}Ne & ^{28}P, ^{28,29}S – CIAE(Beijing) & IMP(Lanzhou)

   C.J. Lin's talk at the PROCON2011 conference.

2. ^{23}Al & ^{22}Mg – IAP(Shanghai) & RIKEN(Japan) …

   MA YuGang *et al*., Sci. China *Phys. Mech. Astron.* **54**(s1), 18-23 (2011).

5. Technical developments

Character of 2p-decay experiments:

- Radioactive ion beam (bad quality)
  low intensity — large solid-angle-covered detector array
  large beam spot — beam tracking
  low purity, strong background — high-efficiency rejection
- Rare decay — high-efficiency detection

Special methods:

- Kinematically complete measurement (KCM)
- In-flight identification – beam, reaction products, KCM
- Optical TPC detection
- … …

5.1 Kinematically complete measurement

Main task: to identify all the decay particles and determine their kinematics

- Stacks of silicon-strip detector – single-sided or double-sided
- Light-particle detector array – CsI+PIN scintillator array
- Zero-degree spectrometer
- Integrated electronics – ASIC (Application-Specific Integrated Circuit) or other types

Experimental setup at **GANIL**

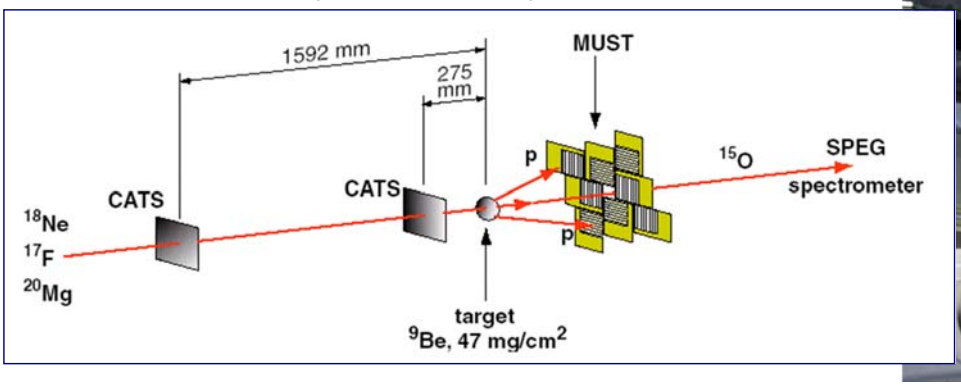

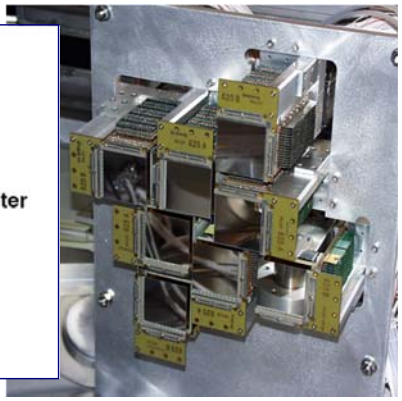

CIAE & IMP

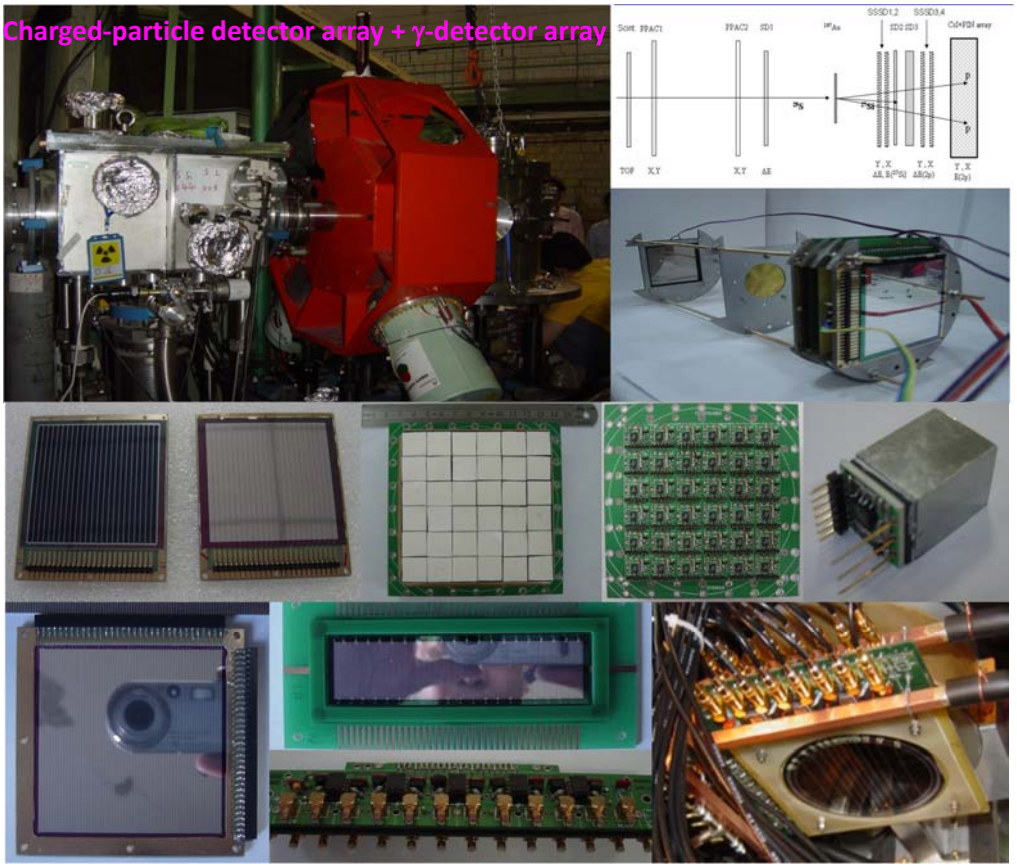

Nearly 4-π covered charged-particle detector array

Under construction at CIAE

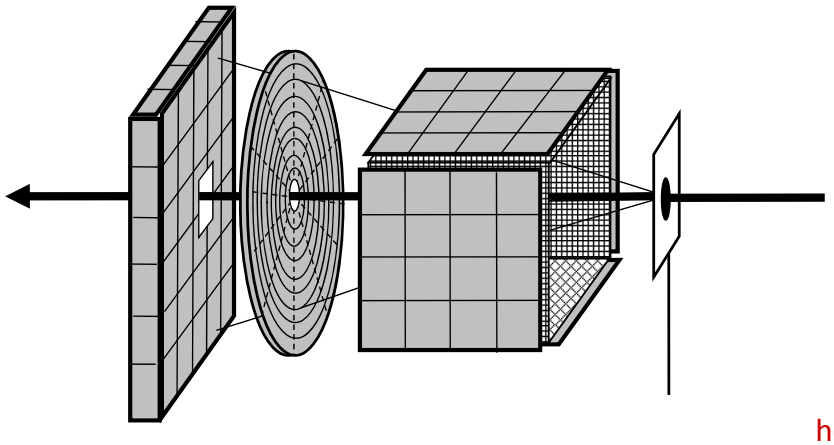

hodoscopes

Layer 1 -- DSSD, T: 64 / 300 μm, A: 64×64 mm², W: 0.96 mm, I: 0.04 μm.
D: 90 mm, H: ϕ10 mm, W: 0.96mm, I: 0.04mm, 12 sectors — heavy particle

Layer 2 – DSSD, T: 300 μm / 1 mm, same type of layer 1. — &

Layer 3 – CsI+PIN array, 4×4 (6×6) ×50 mm³ units. — Light particle

5.2 In-flight identification

Applied to the ^{19}Mg & ^{16}Ne experiment at **GSI** (I. Mukha *et al.*)

MSD -- Microstrip silicon detetor (strip: 100 μm, area: 70 × 40 mm²)

Sensitivity -- down to 10 ps

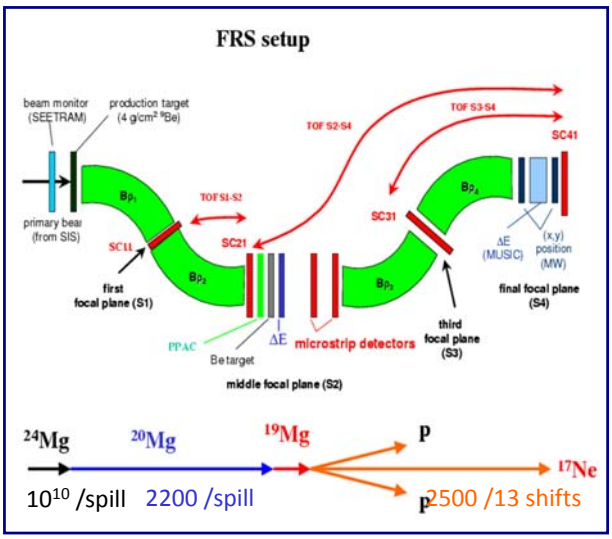

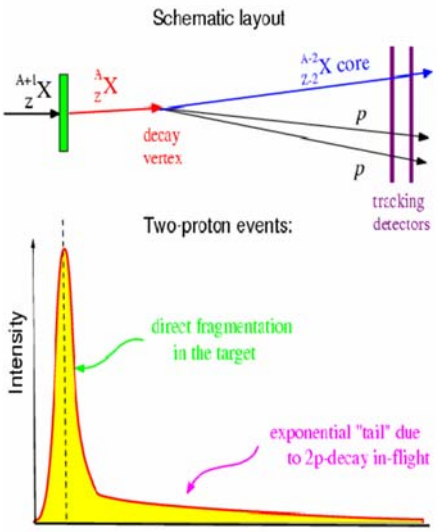

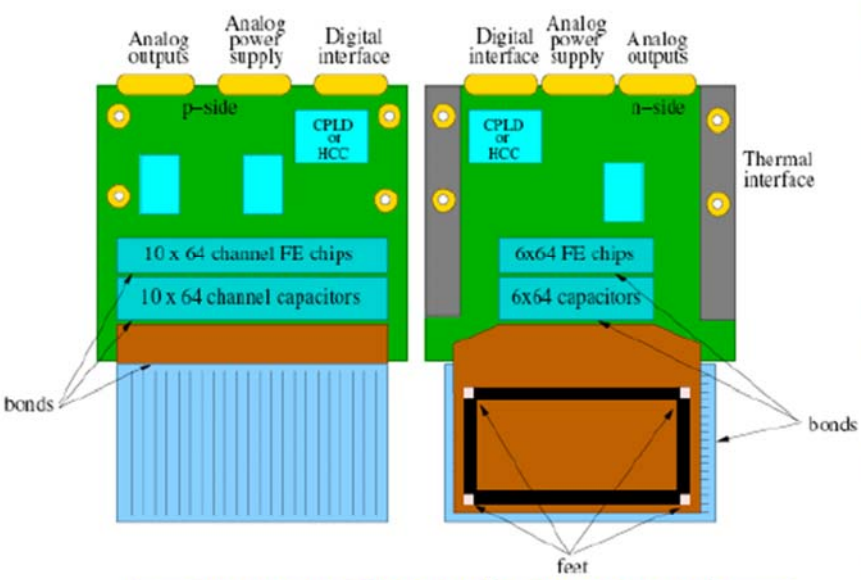

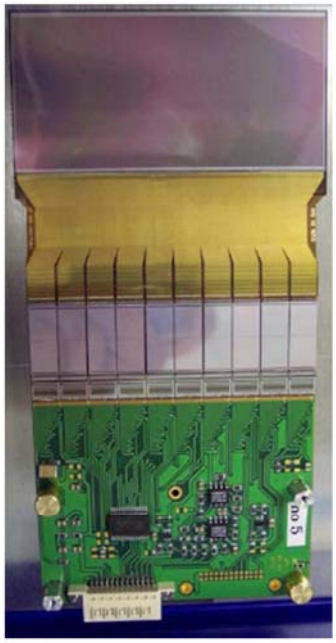

Dimensions 70x40 mm², 100m strip pitch, in total 1000 channels

http://dpnc.unige.ch/ams/GSItracker/www/

Front-end electronics: VA64_hdr9 chips from IDE AS. Serial read-out, digitalization, pedestal and common-noise subtraction made by GSI electronics and integration with GSI DAQ.

5.3 (O)TPC – (O)ptic Time Projection Chamber

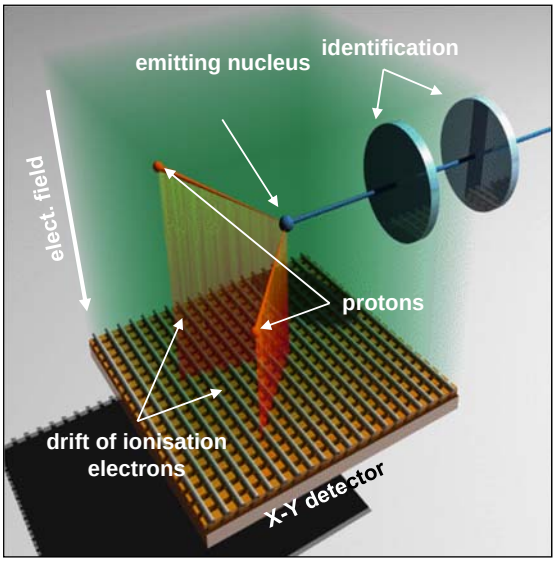

Technology:

- implantation in a gas cell
- integrated electronics (ASICs) or CCD camera

Measurement:

- 3D tracking of protons
  → X-Y detector
  → Z time projection

Results:

- Angular correlation
- Decay image

OTPC idea: G. Charpak et al., NIM A269, 142 (1988).

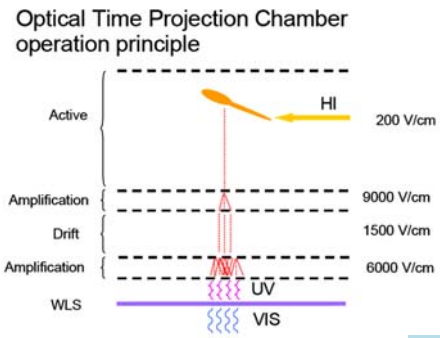

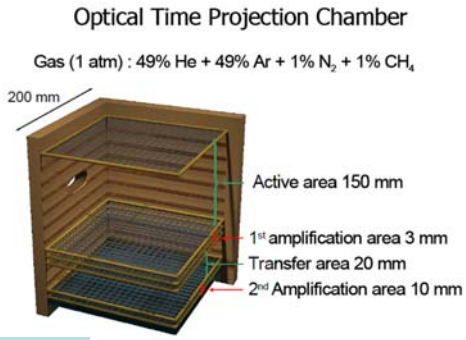

OTPC at NSCL

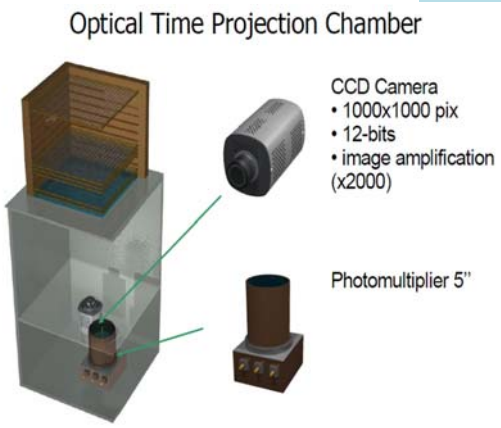

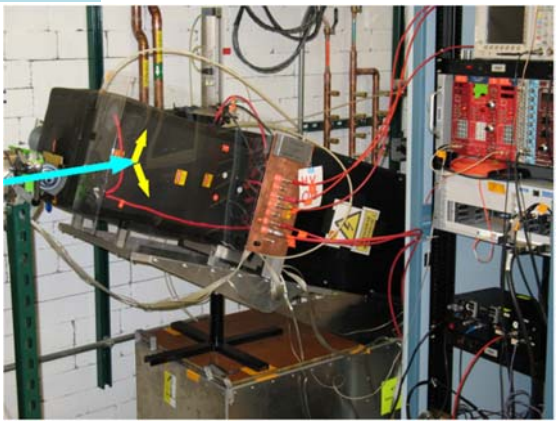

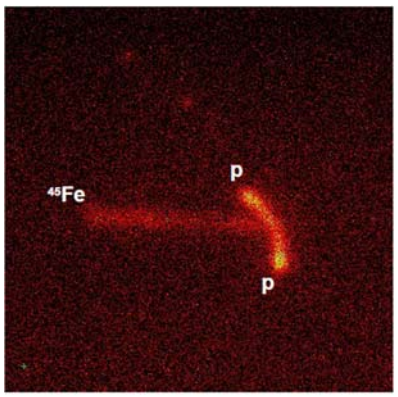

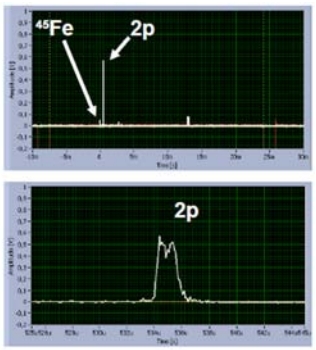

2p decay 0.53 ms after implantation

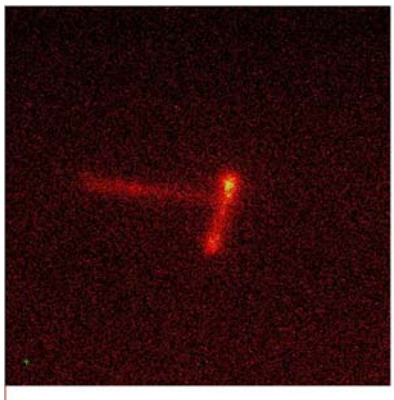

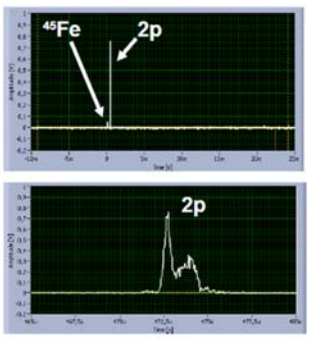

2p decay 0.47 ms after implantation

^{45}Fe 2*p* decay measurement
NSCL
2-11 Feb, 2007.

Bordeaux time projection chamber

TPC on LISE/GANIL

Drift volume

Hybrid card

Mount of electronics

GEM

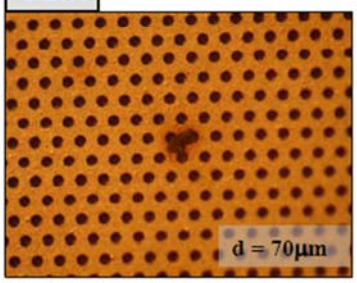

strip-strip detector

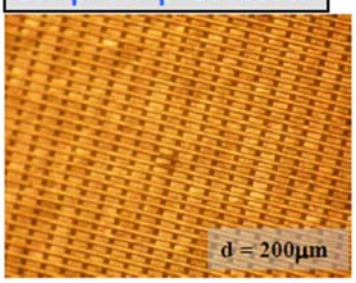

^{45}Fe two-proton event in CENBG TPC at GANIL

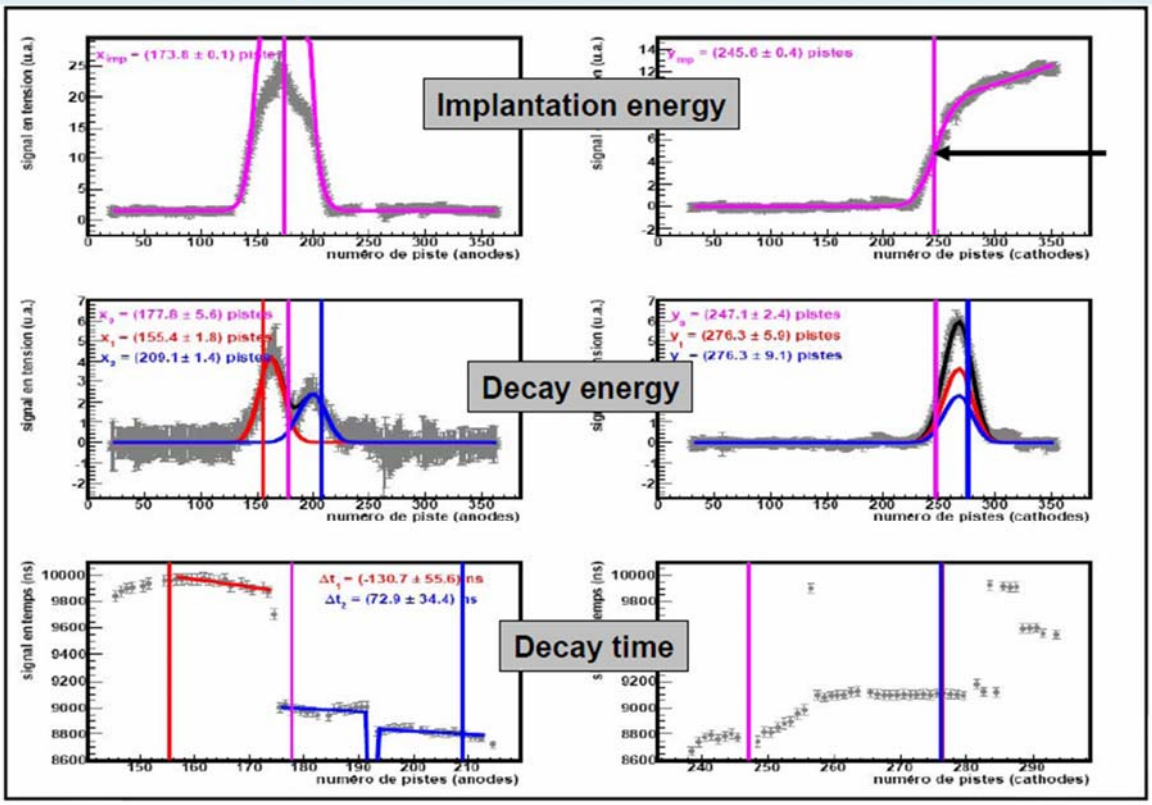

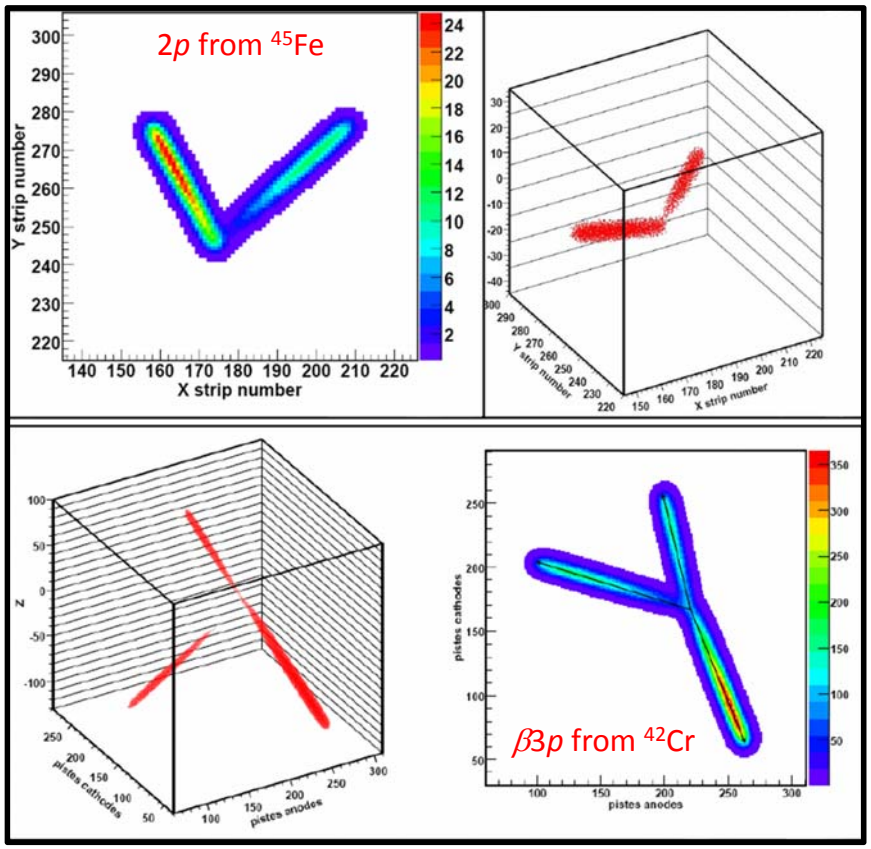

6. Summary and outlook

- **2*p* radioactivity was discovered in 2002.**
  more than 110 years after the discovery of radioactivity;
  more than 40 years after it was proposed.
- **3-body decay or sequential decay.**
  some experimental signatures show diproton decay;
  no conclusive evidence shows ^{2}He decay.
- **Need further study both in experiment and in theory.**
  exotic structure (2p halo) ←→ exotic decay (2p decay)
  exclude/include the FSI → 2*p* initial configuration (BCS/BEC)
- **Need powerful RIB facilities & Geniuses**

Next candidate: ^{26}S, ^{30}Ar, ^{34}Ca, ^{38}Ti, ^{48}Ni, ^{59}Ge, ^{63}Se, ^{67}Kr …

^{26}S: Dubuna 2009 negtive $T_{1/2} < 100$ ns → in-flight identification

^{59}Ge: GANIL & RIKEN in planning …

^{34}Ca: CIAE & IMP in a few months (welcome to join us)

Thanks!

Recent experimental results of two-proton correlated emission from the excited states of ^{17,18}Ne and ^{28,29}S

C. J. Lin, X. X. Xu, H. M. Jia, F. Yang, F. Jia, Z. D. Wu, S. T. Zhang, Z. H. Liu, and H. Q. Zhang

China Institute of Atomic Energy, P. O. Box 275(10), Beijing 102413, China

H.S. Xu, Z. Y. Sun, J. S. Wang, Z. G. Hu, M. Wang, R. F. Chen, X. Y. Zhang, C. Li, X. G. Lei, Z. G. Xu, and G. Q. Xiao

Institute of Modern Physics, The Chinese Academy of Science, Lanzhou 730000, China

PROCON 2011 Bordeaux, France 10th June 2011

Outline

1. Introduction

1.1 Basic idea: 2p halo/skin & 2p correlated emission

1.2 Previous knowledge on ^{17,18}Ne & ^{29}S

2. Experimental procedure and data analysis

2.1 Experimental setup -- RIBLL & detector array

2.2 Particle identification -- the secondary beams and reaction products

2.3 Trajectory reconstruction

3. Results

3.1 Monte-Carlo simulations

3.2 Relative momentum & opening angle -- ^{29}S

3.3 Momentum correlation functions & HBT analysis -- ^{17,18}Ne

4. Summary & outlook

1. Introduction

1.1 Basic idea: 2p halo/skin → 2p correlated emission

2p valence pair → above 2p emission threshold

weak link with core (decoupled)

Beyond 1p drip-line

Ground state

^{6}Be, ^{12}O, ^{16}Ne, ^{19}Mg,

^{45}Fe, ^{48}Ni, ^{54}Zn ……

2p resonance state

Excited state:

^{14}O, ^{17,18}Ne,

^{28,29}S, ……

Initial state configuration

BCS crossover? BEC

1.2 Previous studies:

the ^{17}Ne case

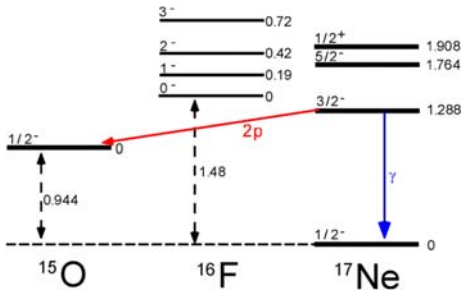

M. Chromik et al., Phys. Rev. C 55, 1676 (1997);
Phys. Rev. C 66, 024313 (2002).

MSU

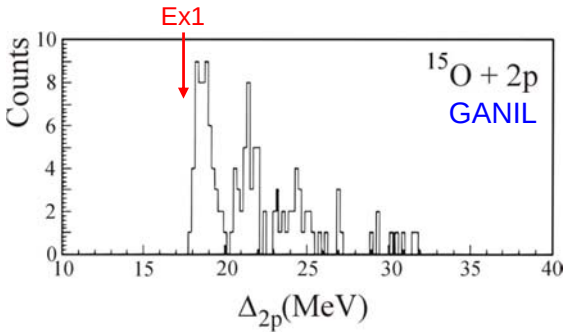

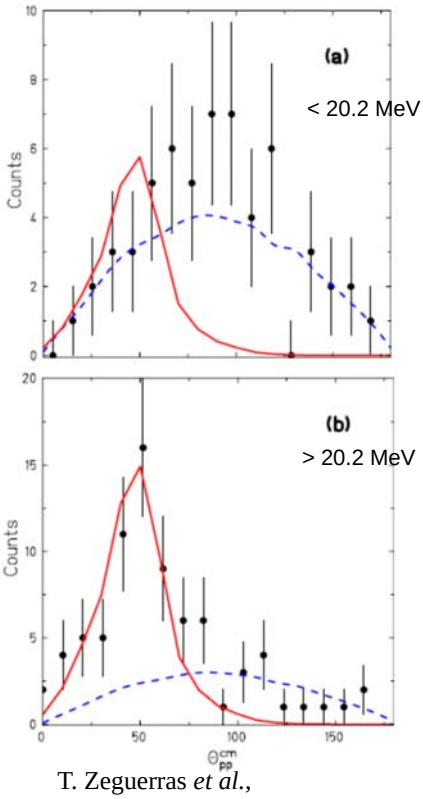

T. Zeguerras *et al.*,
Eur. Phys. J. A **20**, 389 (2004).

the ^{18}Ne case

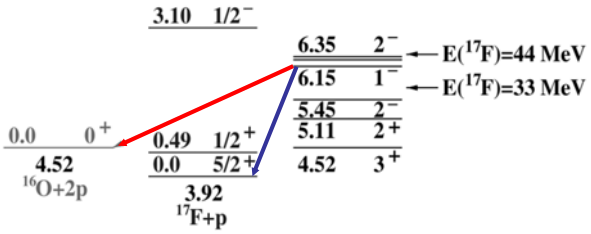

Oak Ridge

^{17}F(p,2p)

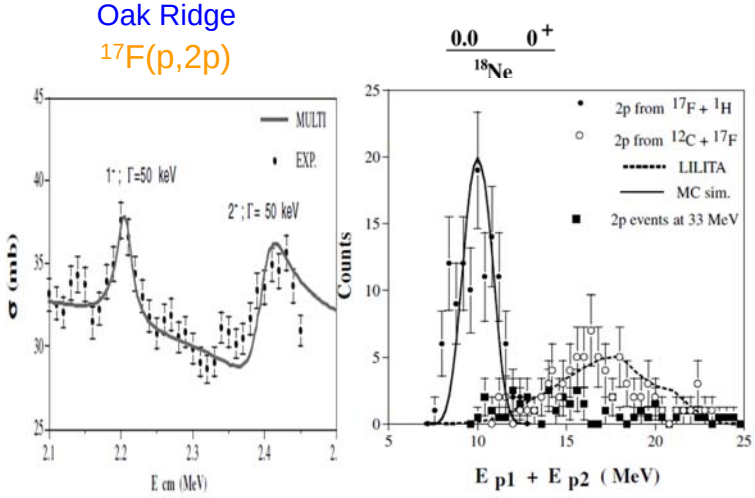

J. Gomez del Campo *et al.*, Phys. Rev. Lett. **86**, 43 (2001).

Catania

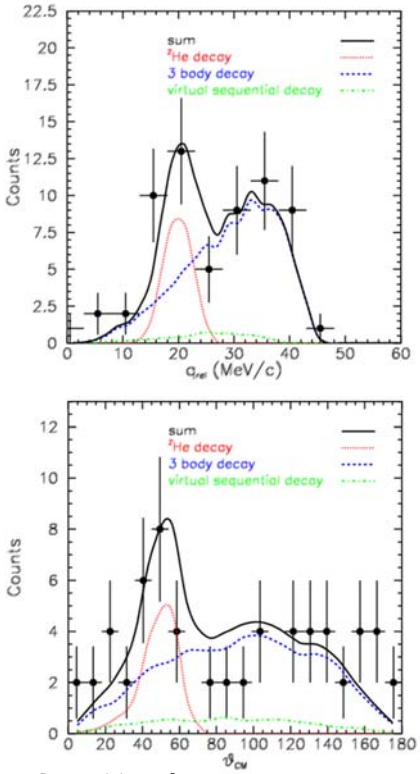

G. Raciti et al.,
Phys. Rev. Lett. ***100****, 192503 (2008)*

^{29}S+^{12}C

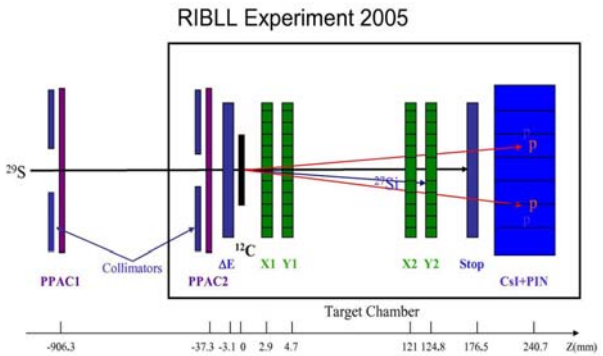

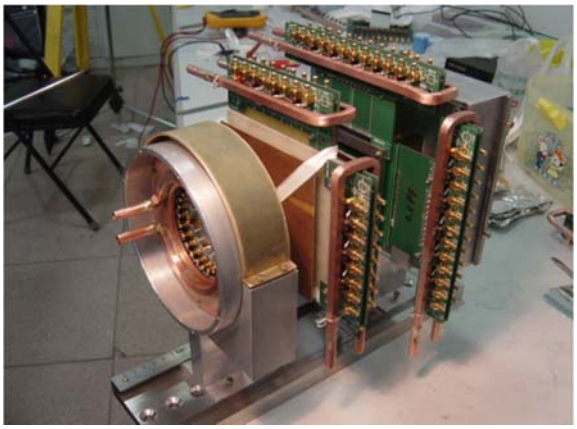

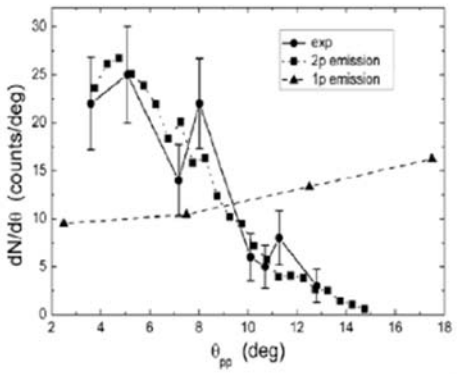

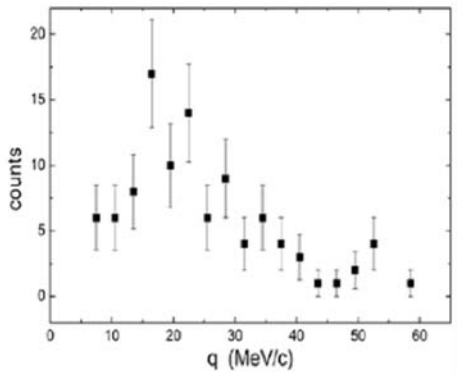

C. J. Lin et al., PROCON 07;
AIP 961, 117 (2007).

2. Experimental procedure and data analysis

2.1 Experimental setup

Primary beam: ^{32}S, 80.4 MeV/u, 100 enA

^{20}Ne, 78.2 MeV/u, 100 enA

Primary target: ^{9}Be, 1589 μm

Degrader: ^{27}Al, 489 μm (^{32}S)

1024 μm (^{20}Ne)

Secondary target: ^{197}Au, 100 μm (^{32}S)

200 μm (^{20}Ne)

Purification: Bρ-ΔE-Bρ method

Identification: ΔE-ToF method

HIRFL-RIBLL, Lanzhou, China

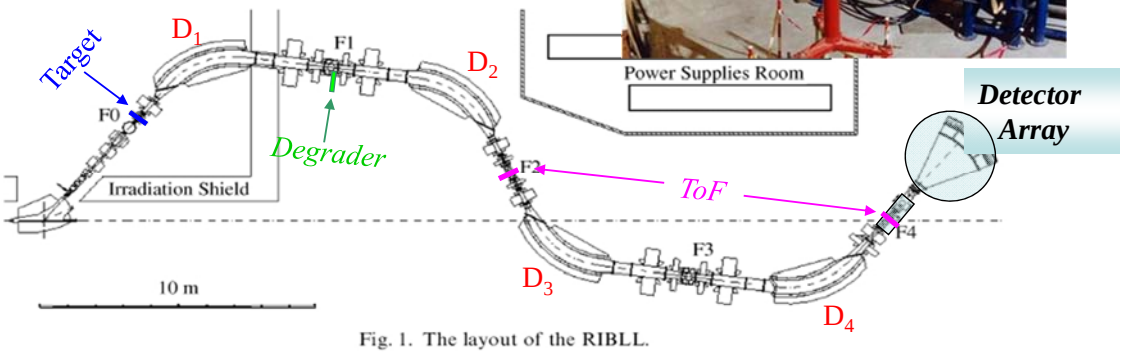

Fig. 1. The layout of the RIBLL.

Complete-kinematics measurement

Detector array for ^{17,18}Ne experiment

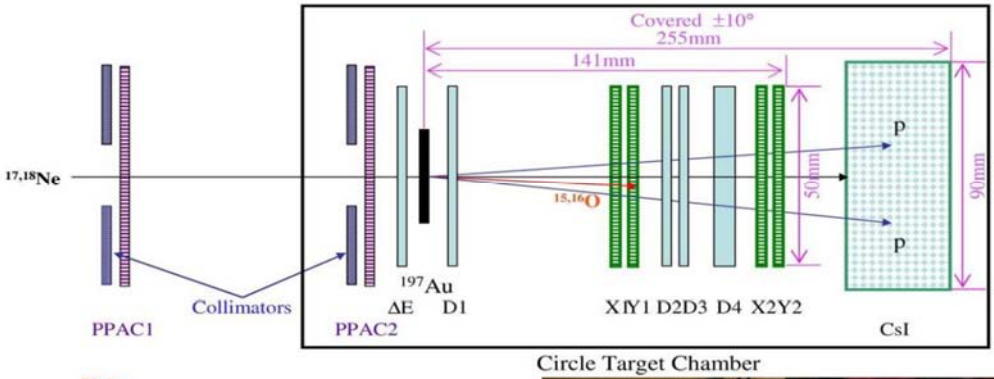

Circle Target Chamber

Note:
Collimators: PPAC1: ϕ30 mm; PPAC2: ϕ20 mm.
ΔE: 300μm Si ΔE detector, combined with TOF (PPA
^{197}Au: target, 200-250 μm, ϕ28 mm.
D1,D2,D3: 300μm Si, 48mm×48mm.
D4: 1000μm Si detector with 4 segments, 50mm×50m
X1,Y1,X2,Y2: 300μm Si strip detectors, each of 24 st
CSI: CSI(Tl)+PIN detectors, 20 mm length, total of 3

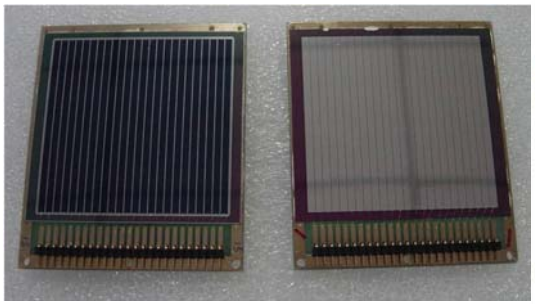

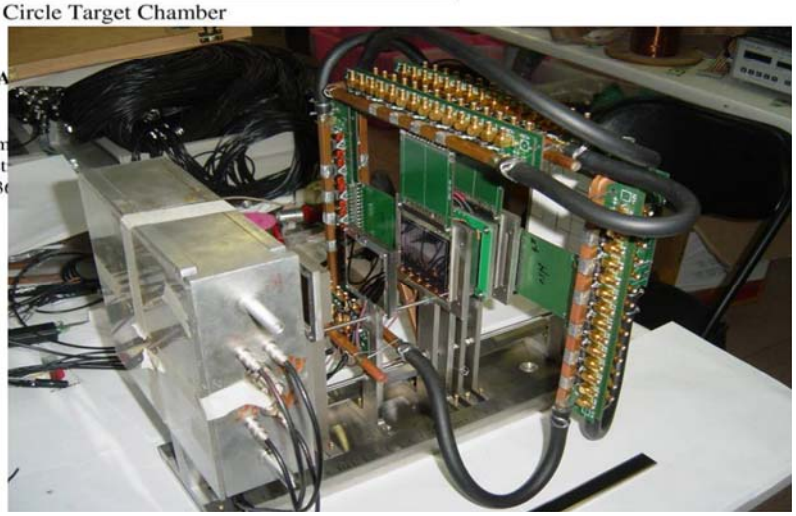

Detector array for ^{28,29}S experiment

Complete-kinematics measurements

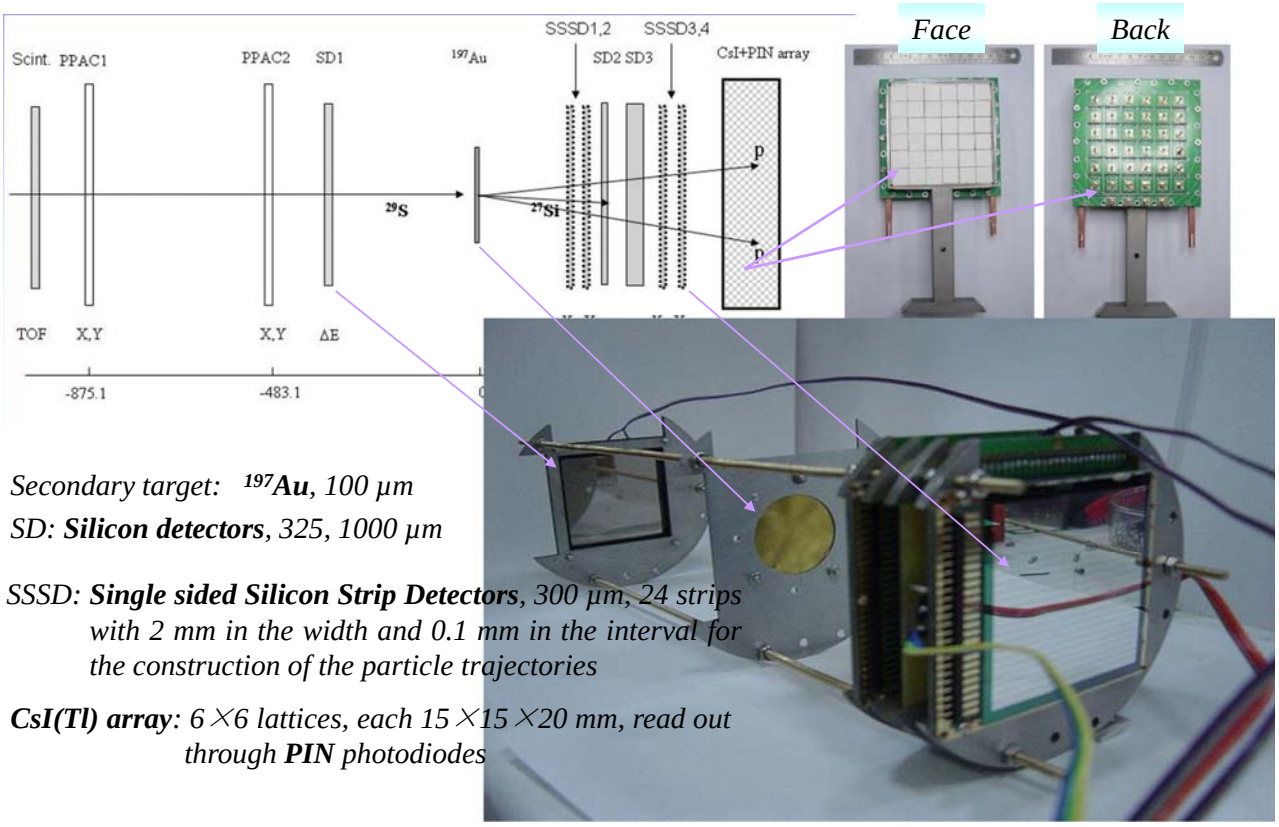

Secondary target: ***^{197}Au****, 100 μm*

SD: ***Silicon detectors****, 325, 1000 μm*

SSSD: ***Single sided Silicon Strip Detectors****, 300 μm, 24 strips with 2 mm in the width and 0.1 mm in the interval for the construction of the particle trajectories*

CsI(Tl) array*: 6×6 lattices, each 15×15×20 mm, read out through* ***PIN*** *photodiodes*

2.2 Particle identification

a) Identifications of the secondary beams

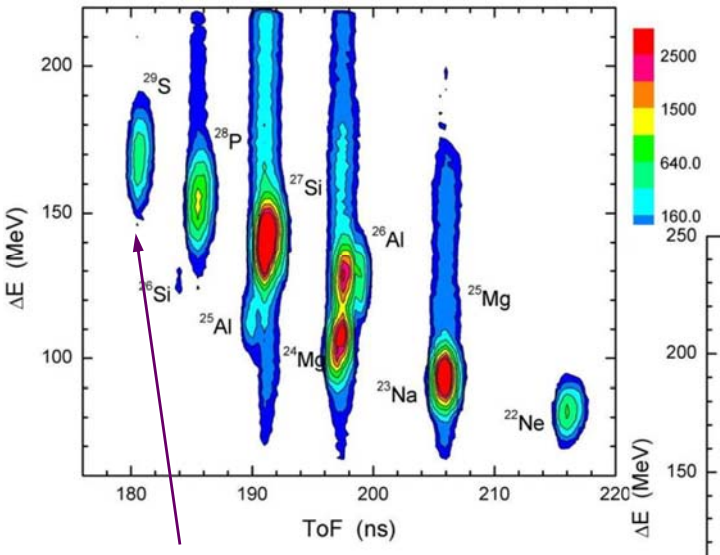

^{29}S: 49.2 MeV/u
Intensity: ~ 200 pps
Purity: ~ 3%
Dose: ~ 2.5×10^7

^{28}S: 48.0 MeV/u
Intensity: ~ 30 pps
Purity: ~ 1%
Dose: ~ 3×10^6

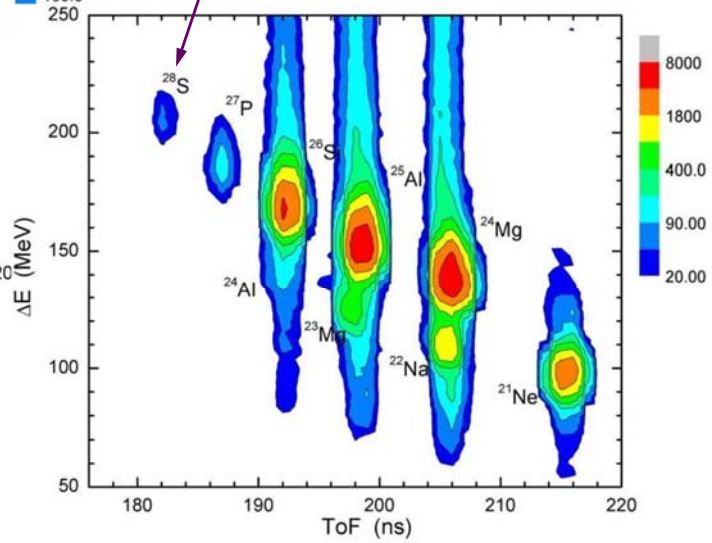

Primary beam: ^{20}Ne, 78.2 MeV/u; Primary target: ^{9}Be, 1590 μm

Degrader: ^{27}Al, 1024 μm; Secondary target: ^{197}Au, 200 μm

Secondary beam: **^{17}Ne**, 50.0 MeV/u, intensity: ~ 200 pps, purity: ~10%, dose: ~ 1.6×10^8

Secondary beam: **^{18}Ne**, 51.8 MeV/u, intensity: ~ 800 pps, purity: ~ 40%, dose: ~ 2.1×10^8

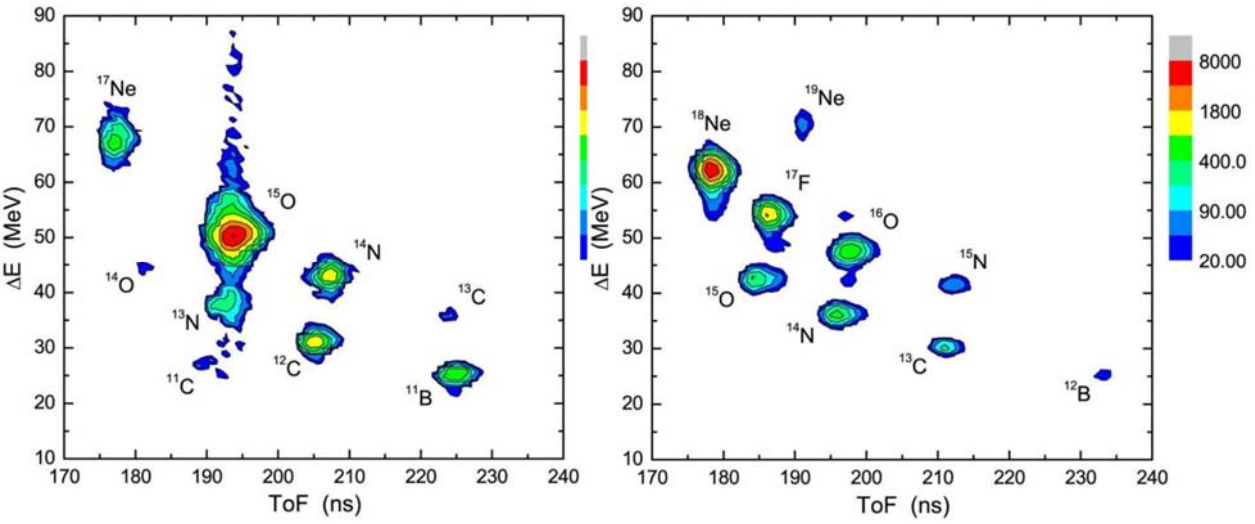

b) Selection of heavy fragments

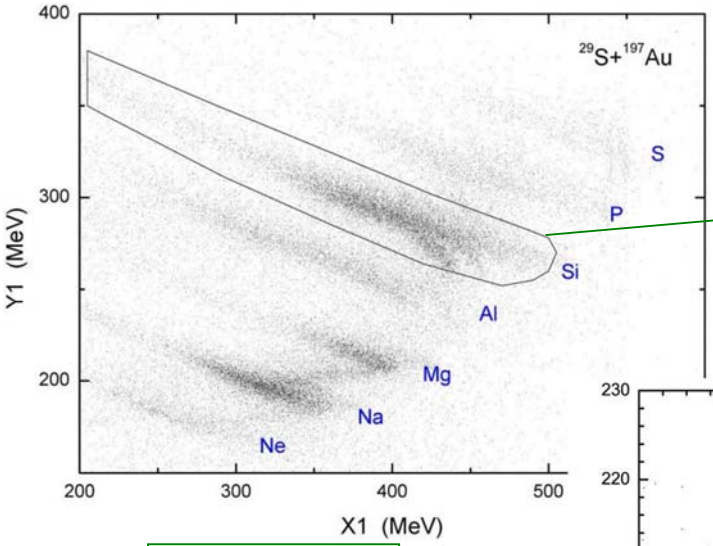

Si-isotope band

^{29}S time window

Events induced only by ^{29}S

Eliminate the contamination of ^{26,27}Si directly from the secondary beam and the accidental coincidences.

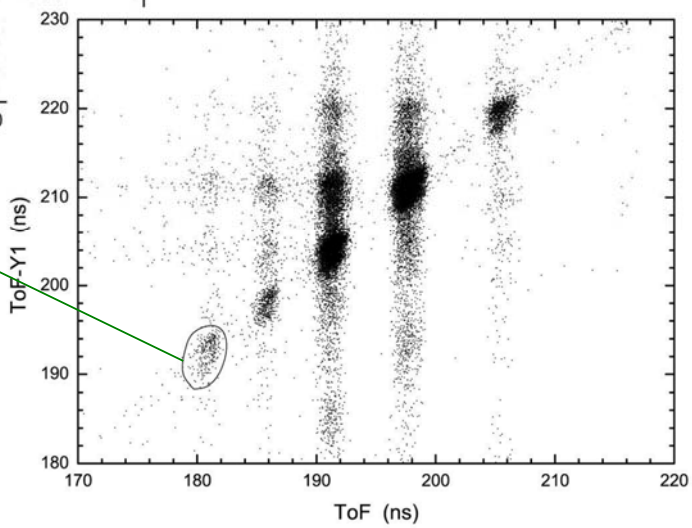

c) Selection of light particles

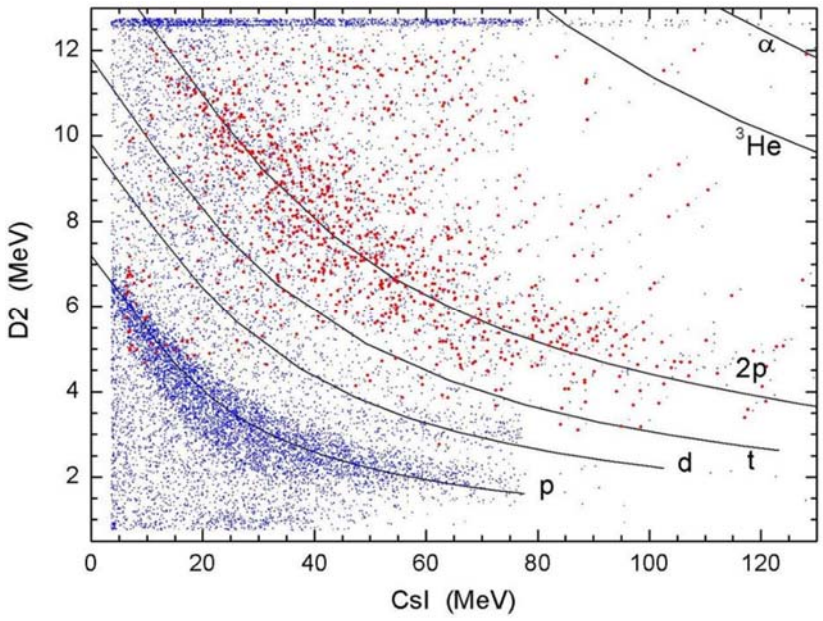

blue dots: single-hit events
red dots: double-hit events

In this way, the unmixed $^{29}S \rightarrow {}^{27}Si+p+p$ events are selected.

b) Identification of heavy fragments

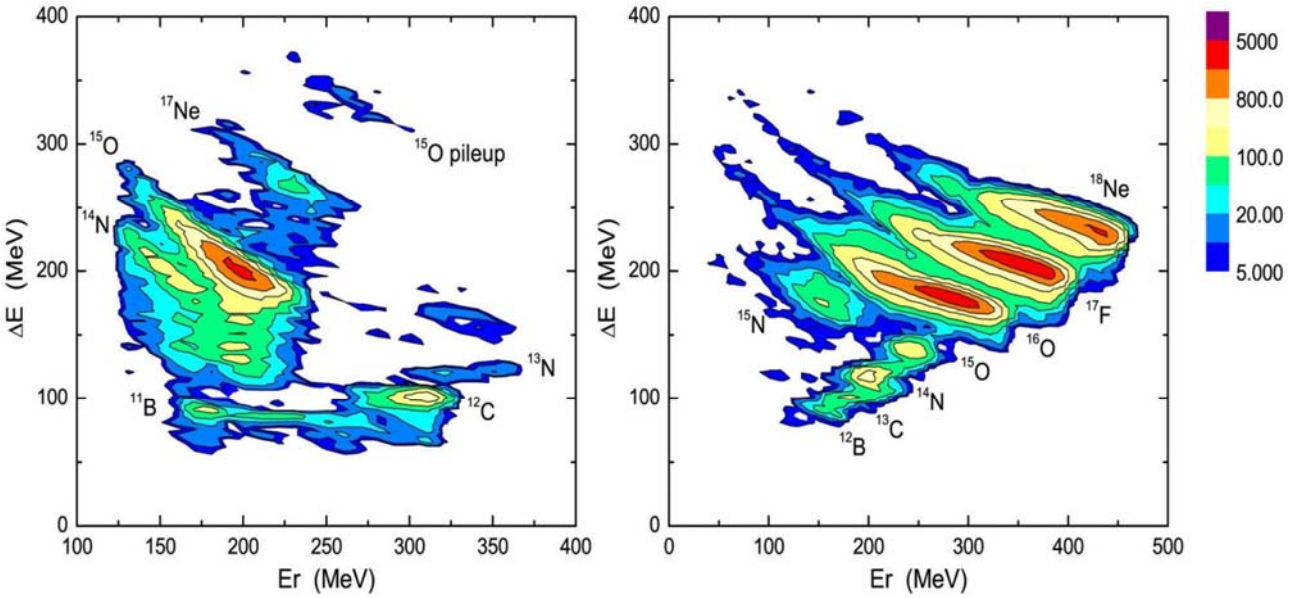

^{17}Ne ^{18}Ne

c) Identification of light particles

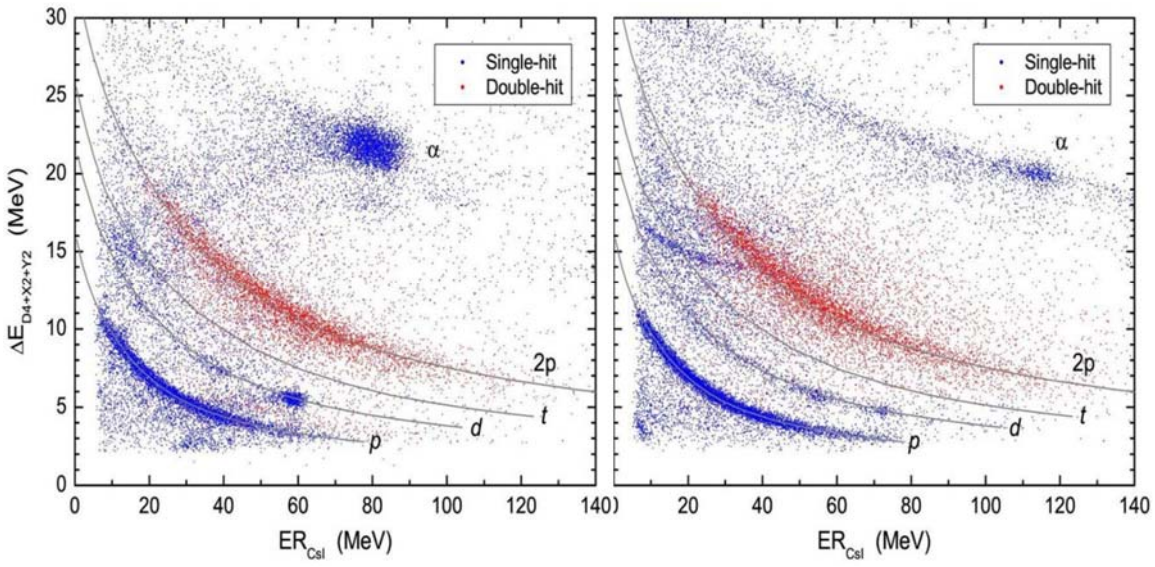

^{17}Ne ^{18}Ne

d) Trajectory tracking – selection of reactions in the target

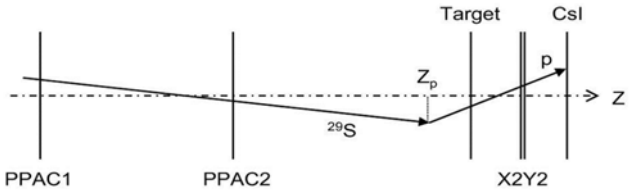

Cross point of trajectories before and after reaction

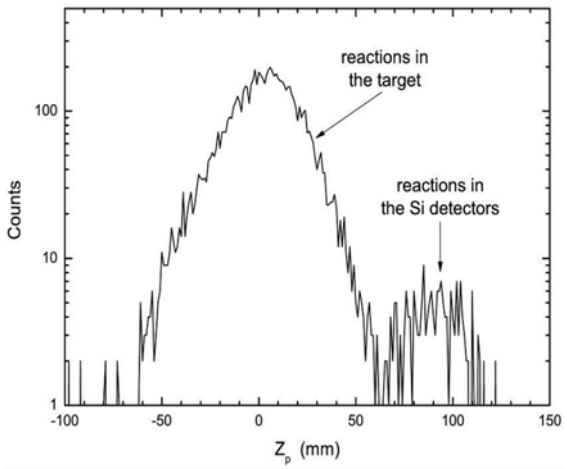

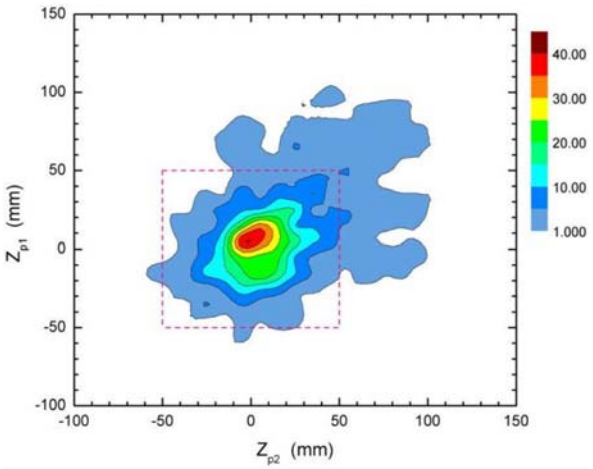

^{29}S → ^{28}P+*p* events ^{29}S → ^{27}Si+*p*+*p* events

3. Results

3.1 Monte-Carlo simulations

Three extreme decay modes

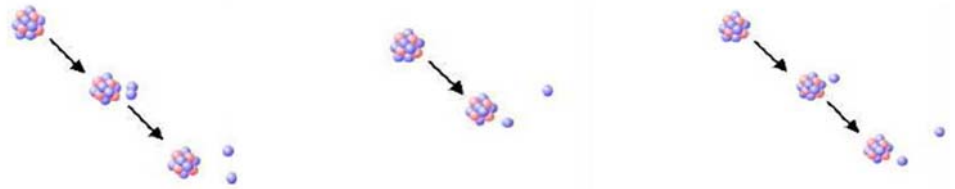

^{2}He cluster decay | 3-body democratic decay | 2-body sequential decay

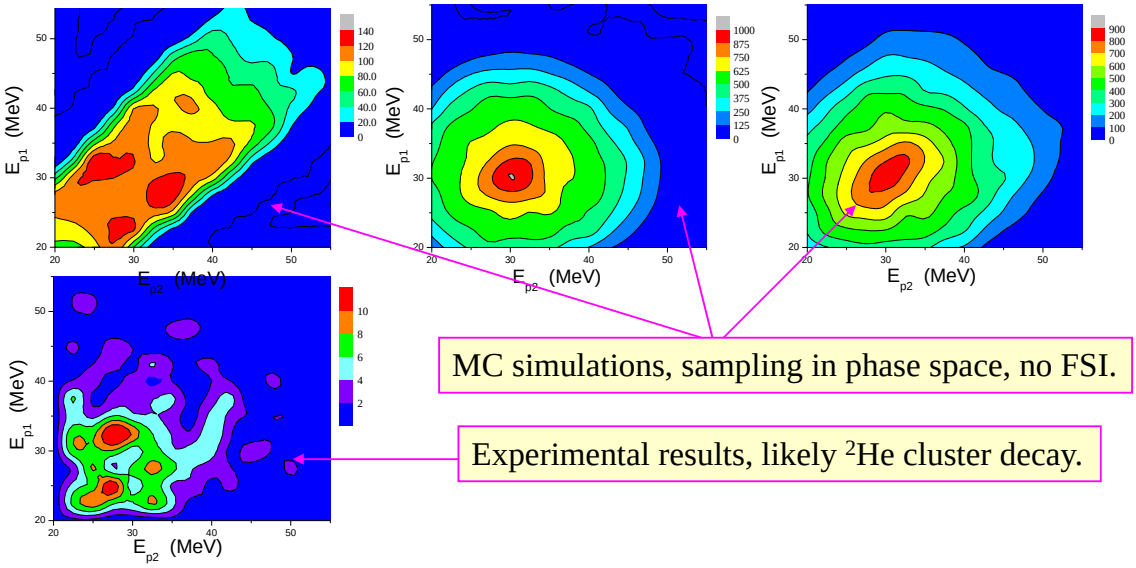

MC simulations, sampling in phase space, no FSI.

Experimental results, likely ^{2}He cluster decay.

3.2 ^{29}S results

Relativistic-kinematics reconstruction for ^{29}S → ^{27}Si+p+p events

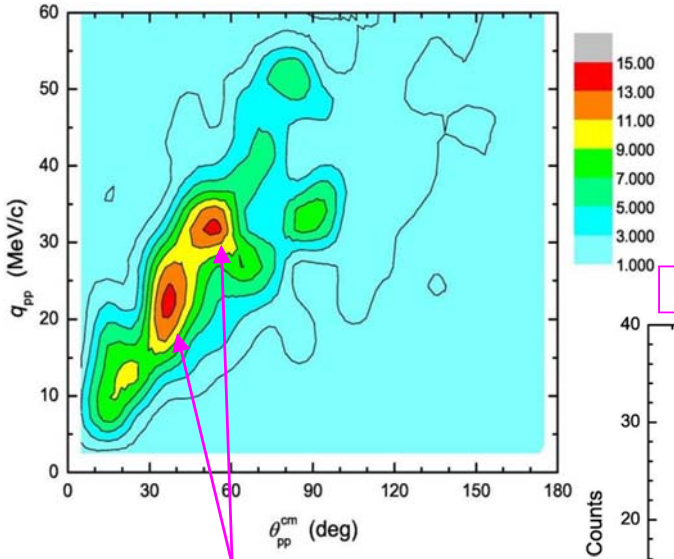

Relative momentum, $q_{pp} = |\boldsymbol{p}_1\text{-}\boldsymbol{p}_2|/2$

Feature 1: small q_{pp} (~ 20 MeV/c)

Opening angle, θ_{pp}^{cm}

Feature 2: small θ_{pp}^{cm} (< 90°)

Invariance mass $E^* = \sqrt{(\sum E_i)^2 - (\sum P_i c)^2} - M$

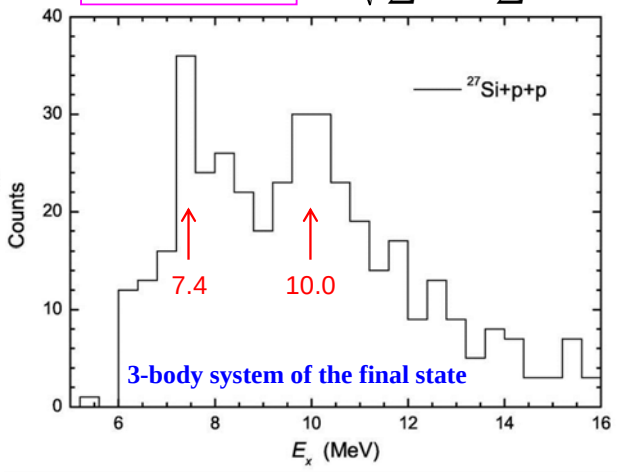

Excitation-energy spectrum of ^{29}S reconstructed by ^{27}Si+p+p

Strong p-p correlations

^{2}He cluster decay ?

3-body simultaneous decay ?

2-body sequential decay ?

or more complicated mode ?

Experimental evidences of ^{2}He emission from the 10 MeV excited states of ^{29}S

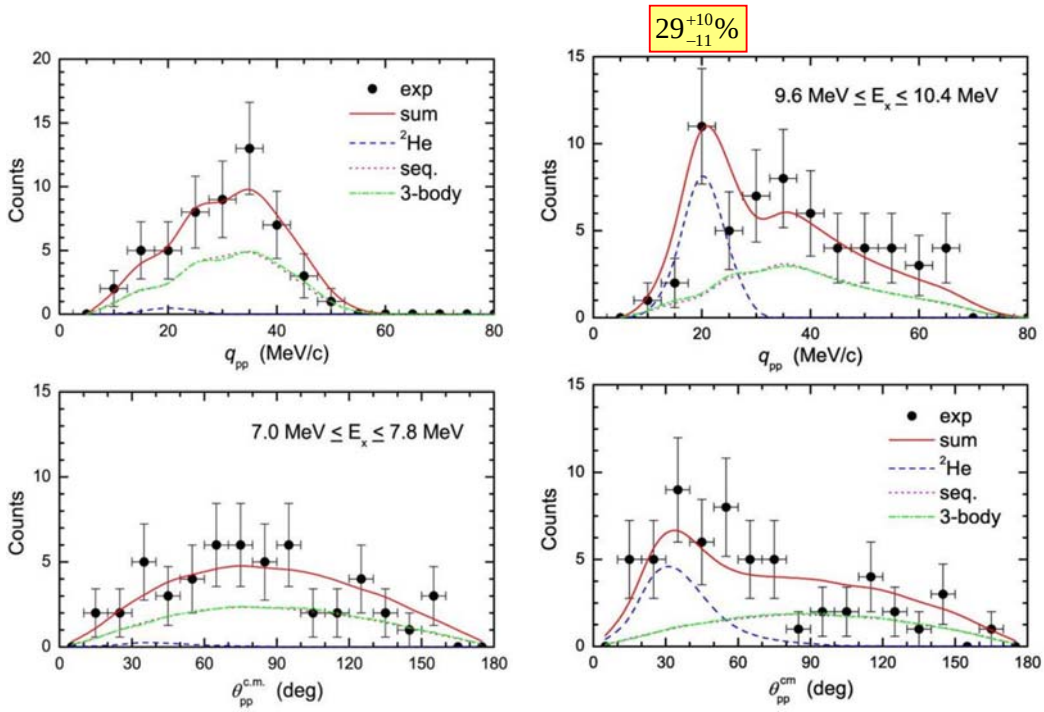

More evidences…

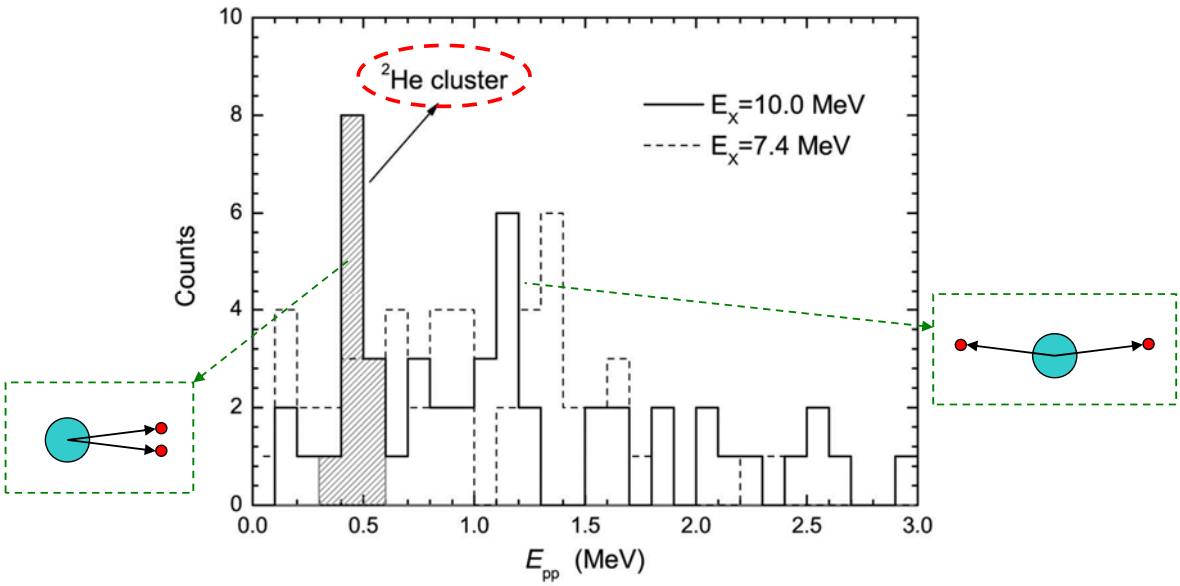

Relative energy of two protons, E_{pp}

Resonance of ^{2}He quasi-bound states ?

Precise theoretical description is required !

C. J. Lin *et al.*, Phys. Rev. C **80**, 014310 (2009).

Supplement:

1) 2*p* emission from ^{28}P* (odd-Z) X. X. Xu *et al.*, Phys. Rev. C **81**, 054317 (2010).

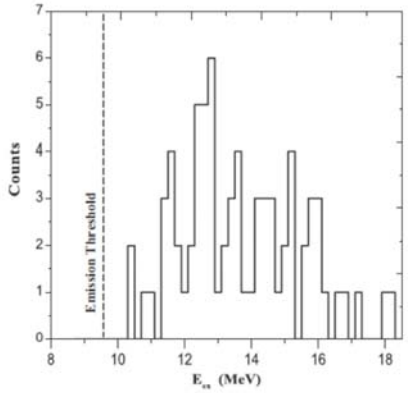

FIG. 5. Reconstructed excited energy spectrum for ^{28}P from three-body correlations of Al-*p*-*p* events.

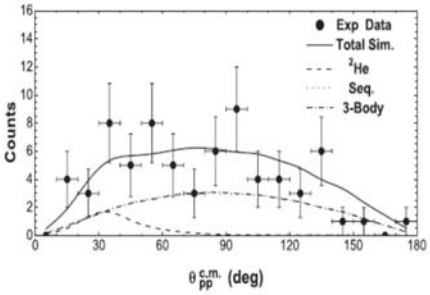

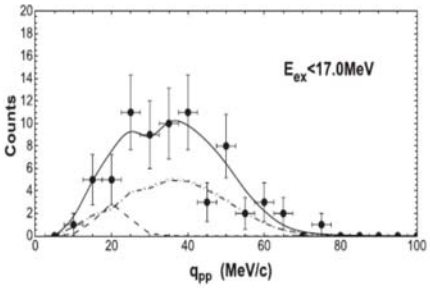

- ♣ No correlated 2*p* emission.
- ♣ No deformation effects.

2) 2α emission from ^{18}Ne* X. X. Xu, *et al.*, Phys. Rev. C **82**, 064316 (2010).

3.3 ^{17,18}Ne results

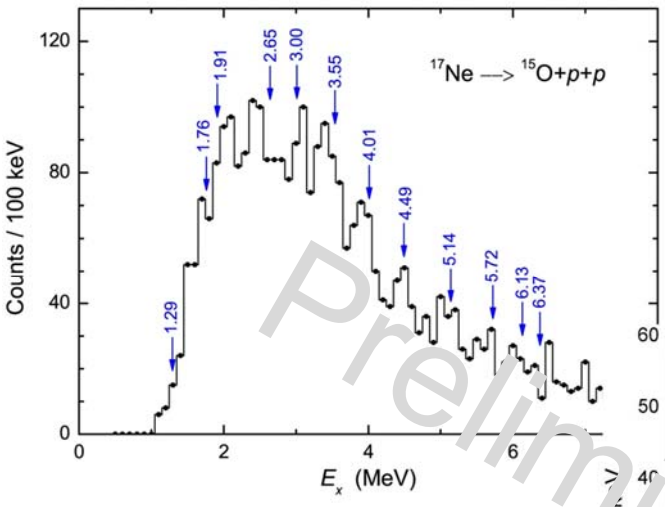

Excitation-energy spectra

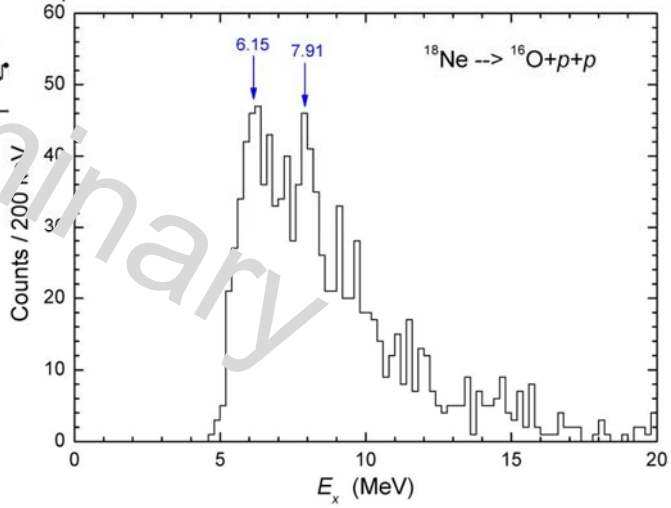

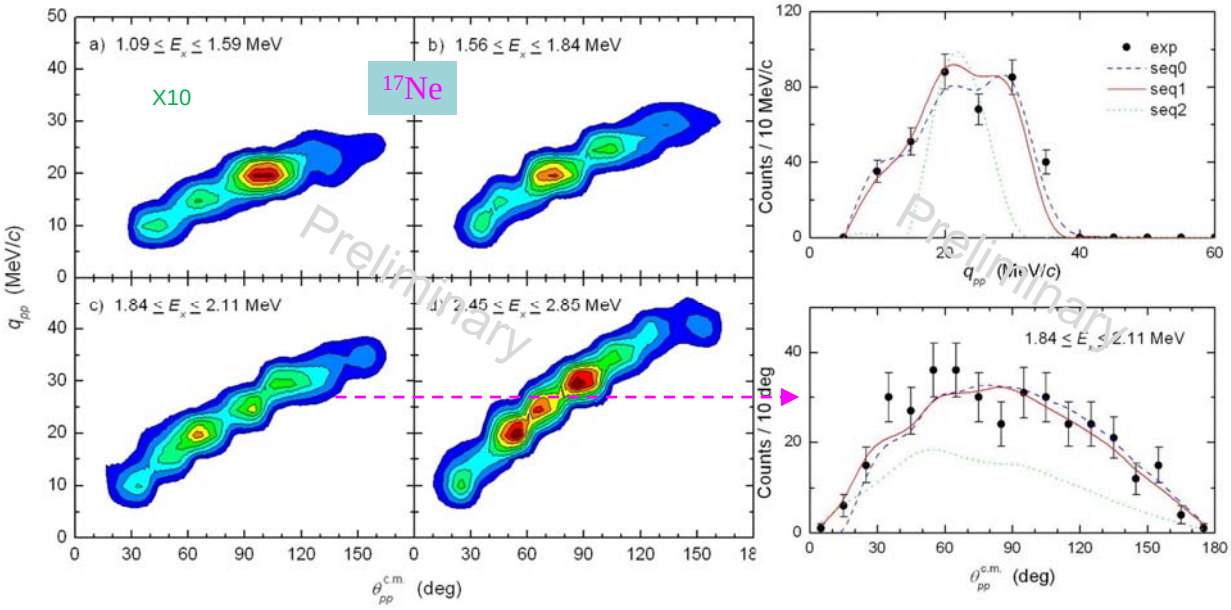

Main results from relative momenta & opening angles

1) No obvious ^{2}He emission from ^{17}Ne, at present.

2) ^{2}He emission from 6.15 MeV state of ^{18}Ne was confirmed.

Analyses are still in progress.

momentum correlation functions and HBT analyses

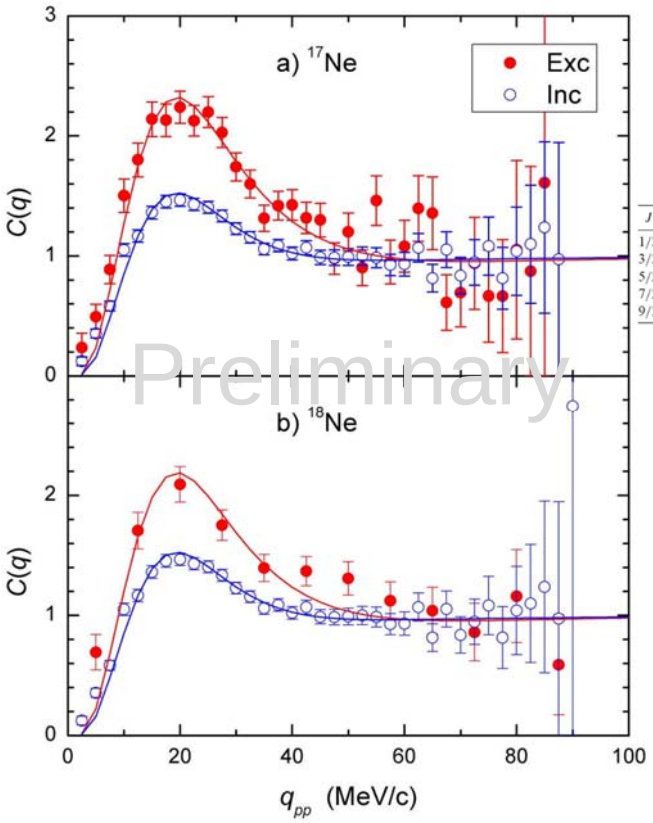

^{17}Ne	Exc: $5.17^{+0.09}_{-0.08}$ fm
	Inc: $7.50^{+0.09}_{-0.09}$ fm
^{18}Ne	Exc: $5.44^{+0.19}_{-0.17}$ fm
	Inc: $6.06^{+0.08}_{-0.09}$ fm

J^{π}	$\langle r_{pp}^2 \rangle^{1/2}$	$\langle r_{c.pp}^2 \rangle^{1/2}$	$\langle r_{cp}^2 \rangle^{1/2}$	$\langle r_{p.cp}^2 \rangle^{1/2}$	$\langle \rho^2 \rangle^{1/2}$	$\langle r^2 \rangle^{1/2}$
$1/2^-$	4.5	3.2	3.9	3.9	5.3	2.8
$3/2^-$	5.3	3.4	4.3	4.4	5.9	2.9
$5/2^-$	5.5	3.5	4.3	4.4	5.9	2.9
$7/2^-$	5.6	3.5	4.3	4.5	6.0	3.0
$9/2^-$	5.7	3.6	4.4	4.5	6.1	3.0

^{17}Ne: NPA733, 85(2004)

BCS or BEC ?

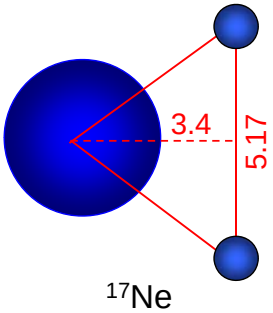

2p opening angel 74.5°

BCS/BEC crossover

Summary & outlook

- ♠ 2*p* correlated emission from the excited states of ^{17,18}Ne and ^{28,29}S have been investigated by means of complete-kinematics measurements.
- ♠ Signatures of ^{2}He emission from the 6.15 MeV excited state of ^{18}Ne and from ~10 MeV excited state of ^{29}S (branch ratio ~29%) were observed.
- ♠ 2*p* halo/skin may lead to ^{2}He emission with large probability.
- ♠ Rms of *p*-*p* pair in the excited states of ^{17,18}Ne have been derived as 5.17 and 5.44 fm, respectively, by HBT analyses. The BCS/BEC crossover may occur in the excited states of ^{17,18}Ne.

Pay attention to:

- ♠ The link between 2*p* halo and 2*p* emission & pygmy resonance.
- ♠ Explore the ground-state emitter: ^{26}S, ^{30}Ar, ^{34}Ca, ^{38}Ti, ^{48}Ni, ^{59}Ge, ^{63}Se, ^{67}Kr …
- ♠ Precise theoretical descriptions embedded in the MC simulations.

Production of ^{34}Ca

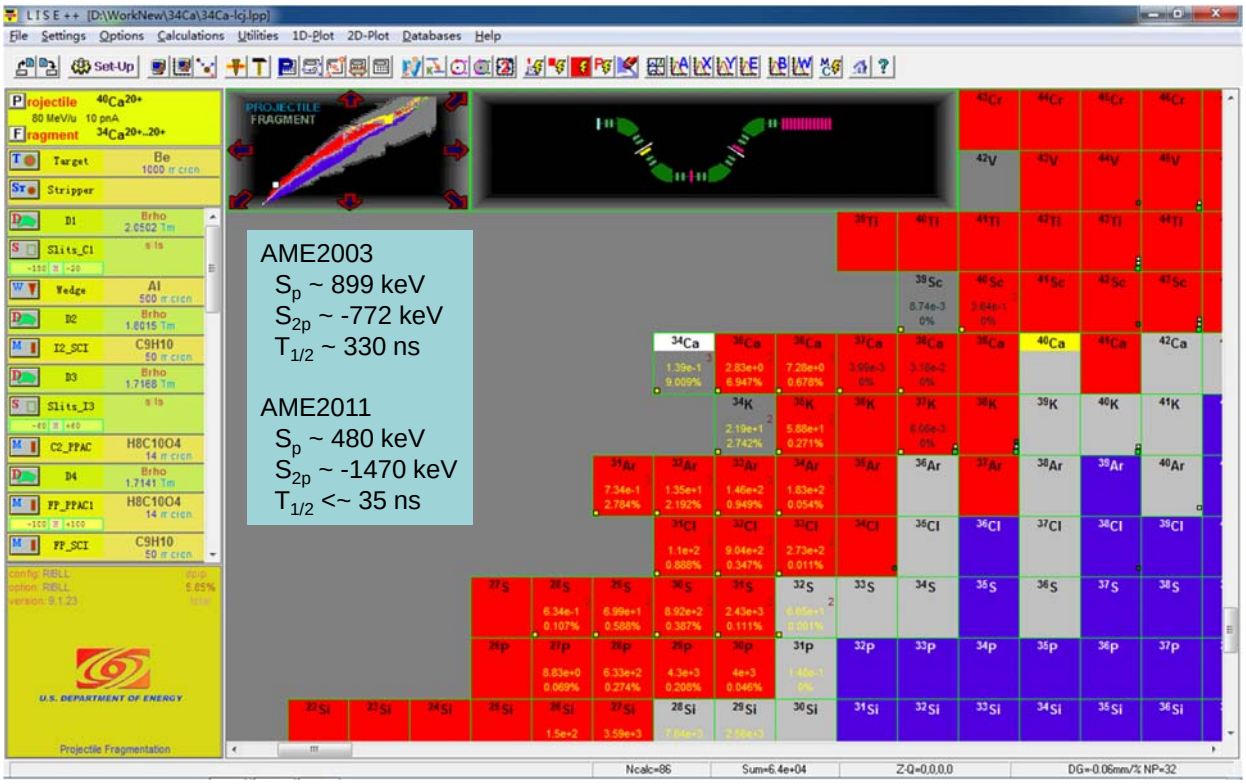

Thank you !

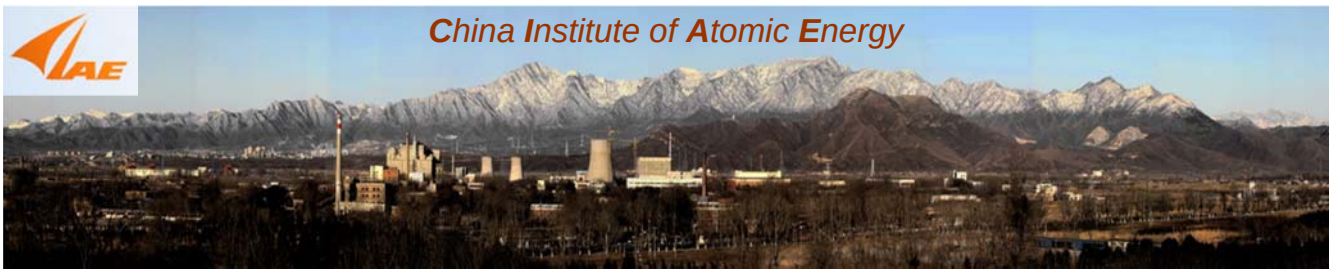

Add On

2p halo and 2p emission

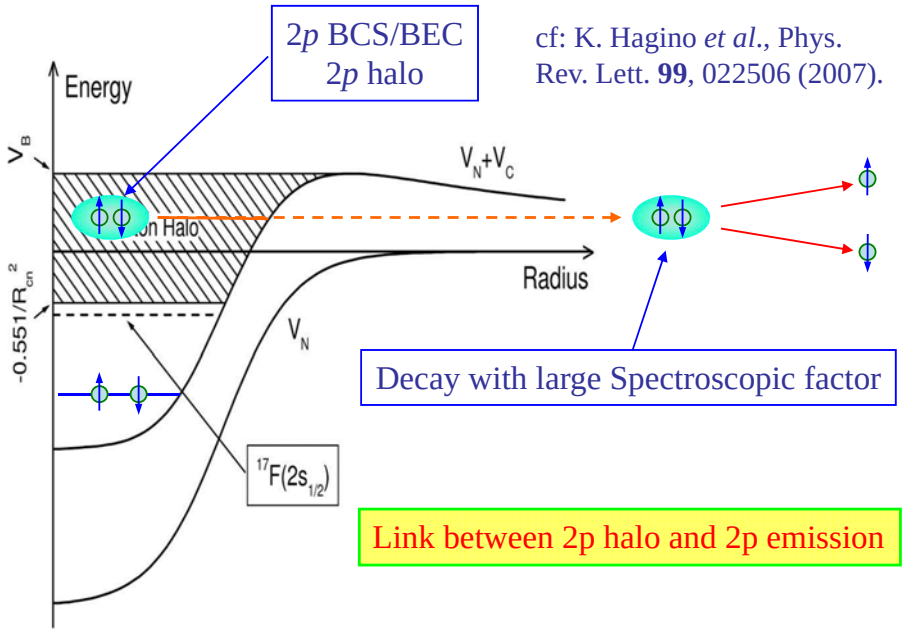

cf: C.J. Lin *et al.*, Phys. Rev. C **66**, 067302 (2002).

Two-proton halo/skins in $^{27\text{-}32}$S

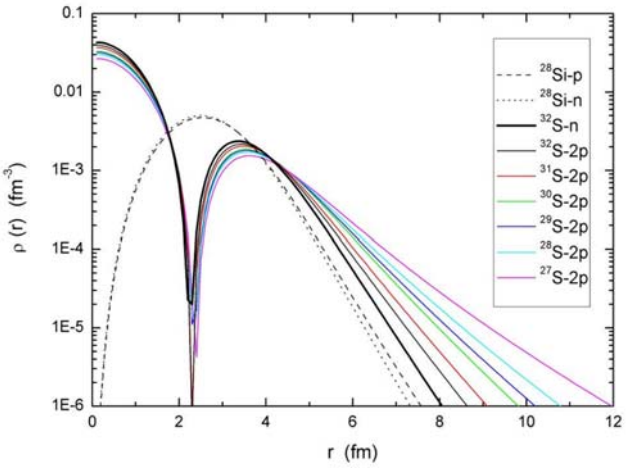

Figure: Density distributions of valence particles

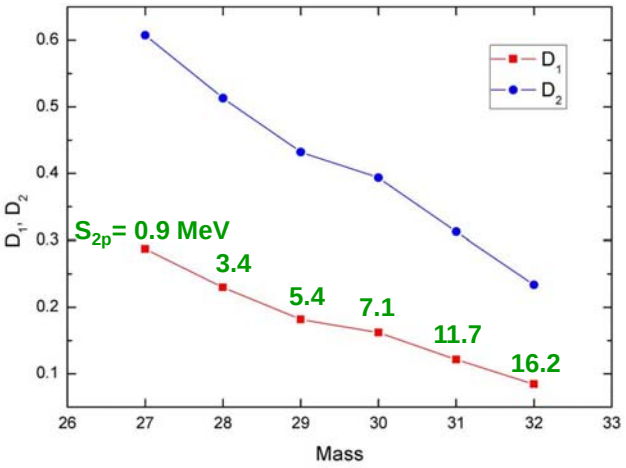

Figure: Contributions of valence particles

$$D_\lambda(R_N)=\left(\frac{\int_{R_N}^{\infty} r^{2\lambda}\Phi^2_{n_B l_B j_B}(r)dr}{\int_0^{\infty} r^{2\lambda}\Phi^2_{n_B l_B j_B}(r)dr}\right)^{1/\lambda}$$

with $\lambda=1,2$. The D_1 represents the probability of the last **2p** outside the range of the interaction radius R_N, and D_2 gives the contribution of the asymptotic part to the rms radius.

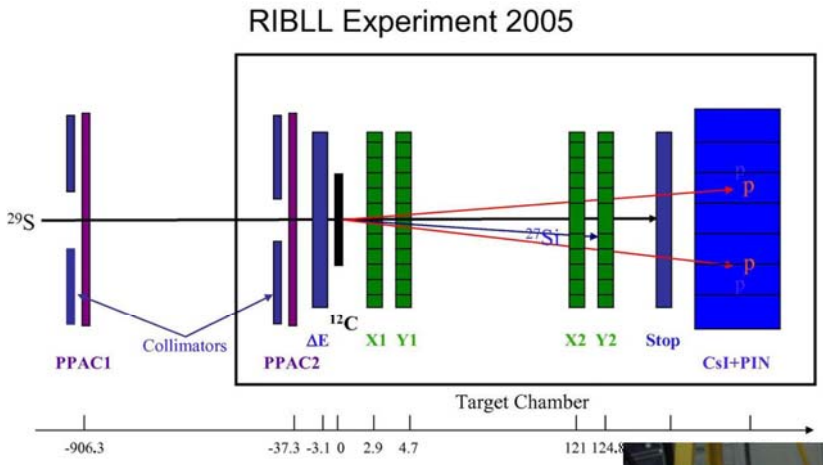

Collimators: ϕ30mm & ϕ20mm.
ΔE: 300μm Si ΔE detector, combined with **TOF** (upstream) for beam ide
^{12}C: target, 40.63 mg/cm^2.
X1, Y1, X2, Y2 : 300μm Si strip detectors, 18 strips each, 1.2mm/strip w
Stop: 300μm Si ΔE detector, for stopping all the heavy fragments.
CSI: CSI(Tl)+PIN array, 24 segments, for light particle (p, d, etc.) identi

^{29}S+^{12}C

Primary beam: ^{36}Ar, 80.4 MeV/u
Primary target: ^{9}Be, 512 μm
Degrader: ^{27}Al, 942 μm
Secondary beam: ^{29}S, 45.2 MeV/u,
intensity ~10 pps, purity ~1%
Secondary target: ^{12}C, 40.63 mg/cm2

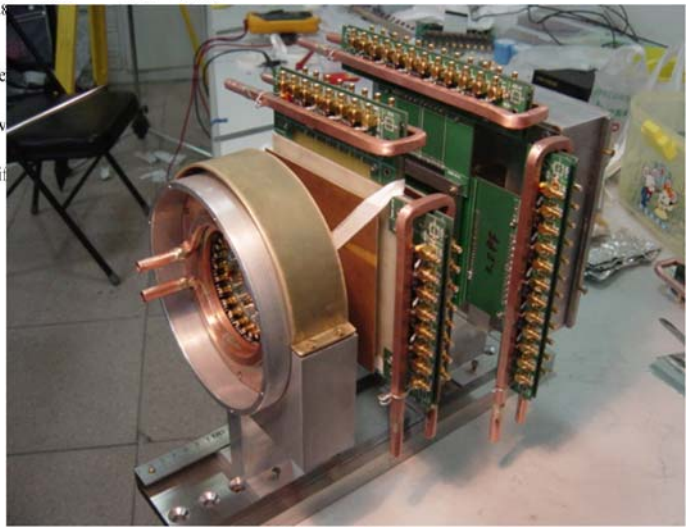

A few words on the HBT results

Introduction of nuclear astrophysics and related experimental techniques

Wei-ping Liu
China Institute of Atomic Energy
Lectrure notes for 2007 Shanghai nuclear structure summer school
wpliu@ciae.ac.cn

July 25, 2007

Contents

List of Tables

List of Figures

1 General aspects of nuclear astrophysics

Nuclear astrophysics is an inter-disciplinary research field, that combines the astrophysics(aiming at macroscopic objects) and nuclear physics(aiming at microscopic objects). In 1920，Eddington proposed that the solar energy is come from the Hydrogen to Helium fusion reaction inside[1]. In 1939, Bethe developed the above ideas, made clear that the pp reaction chain and CNO cycle related Hydrogen burning supply the energy of sun and star[2], and he won the Noble prize of 1967. After WWII, Fowler and his co-workers make more systematic theoretical and experimental studies on star evolution and the mechanism of producing elements other than Hydrogen and Helium. In 1957, Fowler, Burbidge and Hoyle together published the theory of star evolution, that is so called famous B^2FH paper [3]. Owing the outstanding contribution of Flower to nuclear astrophysics, he was honored Nobel prize of 1983. After those works, considerable progress have been made, and was summarized in the intensively cited book called "Cauldrons in the Cosmos" [4], the recent progress can also be found in the review article of Wallerstein [5].

In general, nuclear astrophysics uses the knowledge of nuclear physics to explain the energy production and element synthesis in star and universe. It is not only the energy to resist the gradational collapse, but also the only mechanism to produce elements other than Hydrogen. So it plays an important role in the time scale from a few second after big bang to the end of star life.

The sequence of star evolution is primarily determined by its intimal mass. For those star that has mass of $M < 0.08M_{\odot}$（$M_{\odot}$ means solar mass）, the gravitational collapse can not reach the ignition temperature of Hydrogen fusion, so those star is dying directly without Hydrogen burning. For those with mass range of $0.08M_{\odot} < M < M_{\odot}$, after the light elements burning, their core can not initiation the burning of next stage, so that dying to form the white dwarf. For those with mass range of $8M_{\odot} < M < 100M_{\odot}$, so call large mass isolated stars, they experienced a full stage burning of Hydrogen, Helium, Carbon, Neon, Oxygen and Silicon stellar process. This resulted a shell structure of above elements. After Silicon burning, the fusion energy can not balance the gravitation any more and resulted a super novae explosion, its shock wave drive large amount of material into inter star area, and some smaller part left become neutron star or black hole. The above picture is summarized in Fig.1. In above stellar burning, not only stable nuclei, but also unstable nuclei are involved. To explain the energy balance and abundance distribution, the nuclear physics contribution of nuclear mass or binding energy, reaction cross section and decay properties are needed. Because

of the extra low center of mass energy, the nuclear experiment and theory have to meet a strong challenge. In addition, most important astrophysical process are developed along the path of proton or neutron rich region of chart of nuclei, see Fig. 2. Indeed, the current nuclear astrophysics is one of the frontier of physics because of above reason.

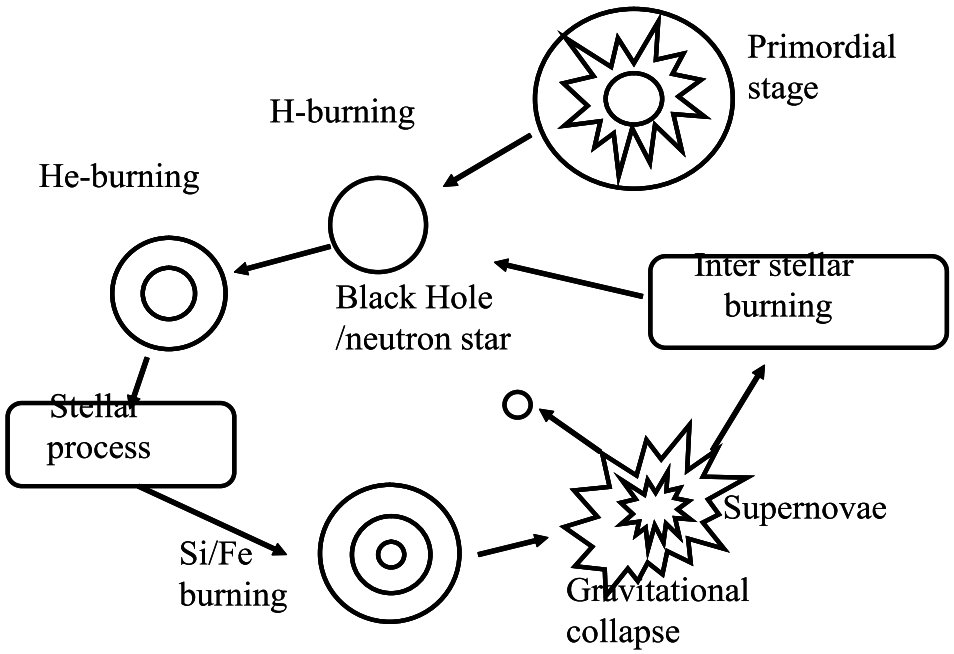

Figure 1: The primordial and stellar element syntheses.

2 Nuclear reaction rates in star

2.1 General remarks

The energy production and element abundance is directly determined by the speed of nuclear reaction or reaction rate. It is a convolution of Maxwell-Boltzmann

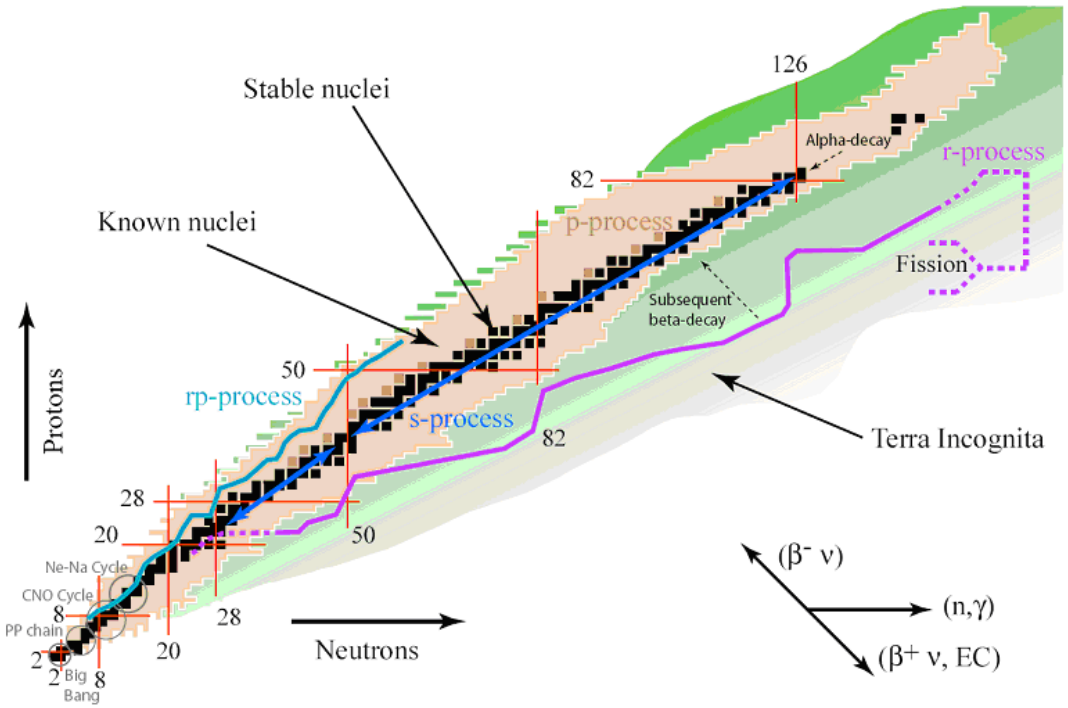

Figure 2: The astrophysical process in chart of nuclei.

distribution $\phi(v)$ and reaction cross section σ [4].

$$< \sigma v >= \int_0^\infty \phi(v)\sigma(v)v dv. \tag{1}$$

Maxwell-Boltzmann speed distribution is

$$\phi(v) = 4\pi v^2 (\frac{\mu}{2\pi kT})^{3/2} \exp(-\frac{\mu v^2}{2kT}), \tag{2}$$

In which, μ， k and T is reduced mass Boltzmann constant and star temperature respectively. It can be simplified into,

$$N_A < \sigma v >= 3.7313 \times 10^{10} \mu^{-1/2} T_9^{-3/2} \int_0^\infty \sigma(E) E \exp(-11.605 E/T_9) dE, \tag{3}$$

Where the reation rate $N_A < \sigma v >$ is in the unit of $\mathrm{cm^3 mol^{-1} s^{-1}}$ and center of mass energy E and corss section σ are in the unit of MeV and b.

2.2 Charged particle induced reactions

Charged particle induced reaction can be grouped into direct capture and resonance capture.

1. Direct capture

The reaction cross section can be re-scaled into astrophysical S-factor,

$$\sigma(E) = S(E) \exp(-2\pi\eta) \frac{1}{E}, \tag{4}$$

Where η is Sommerfeld constant，

$$\eta = \frac{Z_1 Z_2 e^2}{\hbar v} = 0.1575 Z_1 Z_2 (\frac{\mu}{E})^{1/2}, \tag{5}$$

Where $\hbar$ is reduced Plank constant, Z_1 and Z_2 are atomic number， E is the center of mass energy in MeV.

Because of Coulomb barrier, the cross section decrease violently with energy, making the extrapolation to astrophysical energy difficult. The S-factor is introduced to address this problem, because it separates the smooth part of energy dependence that contains the full nuclear information, as shown in Fig.3.

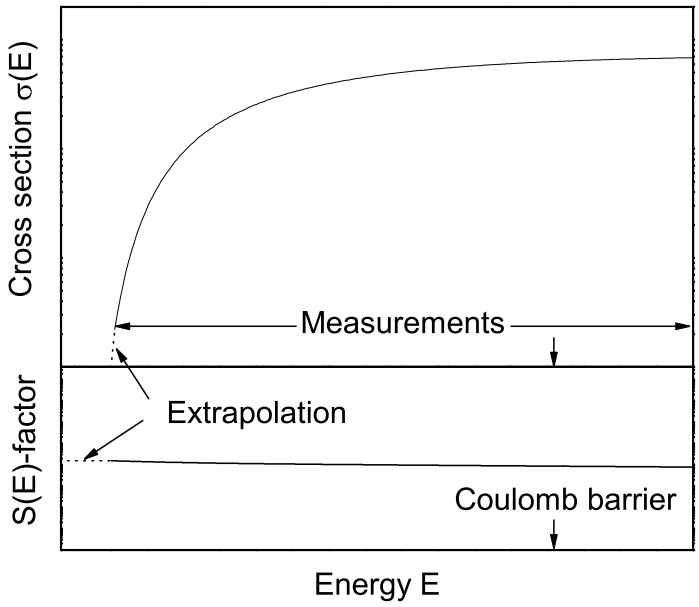

Figure 3: The energy dependence of reaction cross section and astrophysical s-factor.

One can get

$$N_A < \sigma v >= N_A(\frac{8}{\pi\mu})^{1/2}\frac{1}{(kT)^{3/2}}\int_0^\infty S(E)\exp(-\frac{E}{kT}-\frac{b}{E^{1/2}})dE, \qquad (6)$$

b come from Coulomb penetration

$$b = (2\mu)^{1/2}\pi e^2 Z_1 Z_2/\hbar = 0.989 Z_1 Z_2 \mu^{1/2}(\mathrm{MeV})^{1/2}. \qquad (7)$$

Its square is so called Gamow energy E_G.

In exponential part of Equ. 6, the first term come from Maxwell-Boltzmann velocity distribution, the second term is Coulomb term, the interplay of two terms reach a maximum in E_0, as shown in Fig. 4. Where the effective mean energy E_0 can be expressed as:

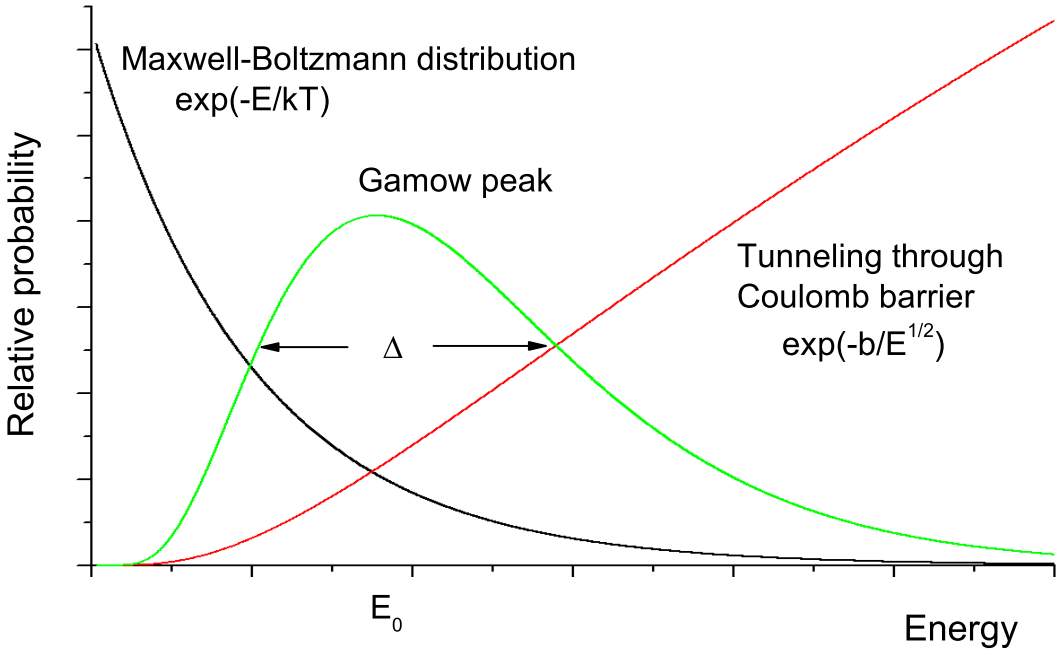

Figure 4: The GAMOW window.

$$E_0 = (bKT/2)^{2/3} = 1.22(Z_2^1 Z_2^2$$

$\mu T_6^2)^{1/3} keV(8)$

It is E_0 that is most important parameter for experimentalists to reach directly or in-directly. For system p+p, , for sun T_6=15, E_0 is only 5.9 keV!

2. Resonance capture reaction

The resonance capture reaction cross section can be expressed by Breit-Wigner formula [17],

$$\sigma_{BW}(E) = \pi \frac{\hbar^2}{2\mu E} \frac{2J_R + 1}{(2J_1 + 1)(2J_2 + 1)} \frac{\Gamma_{in}(E)\Gamma_{out}(E)}{(E - E_R)^2 + (\Gamma_{tot}/2)^2}, \tag{9}$$

Where J_1， J_2， J_R is the spin of beam, target and compound state respectively, Γ_{in}， Γ_{out} are entrance channel partial width，Γ_{tot} is the total width.

3 Experimental methods

3.1 Direct measurements

The direct measurement is the most reliable way. But in practice, in the energy around GAMOW window, the reaction cross section is extremely low, in some cases, even the beam itself is made of unstable nuclei, so that the intensity is a few order lower than stable beam. For direct measurement, not only one need more beam time, but also need to develop high beam reduction ratio devices and effective detection system.

One of such examples is the first measurement of CNO cycle reaction ^{13}N$(p,\gamma)^{14}$O in Louvain-la-Neuve 1991 [22]. This work gave the first excitation state width of $\Gamma_\gamma = 3.8 \pm 1.2$ eV. The DRAGON recoil mass spectrometer in TRIUMF is another good example[23]. Up to now many important reactions are measured, such as ^{21}Na$(p,\gamma)^{22}$Mg[24], ^{26}Al$(p,\gamma)^{27}$Si[25] and ^{12}C$(\alpha,\gamma)^{16}$O[26].

3.2 Indirect measurements

In many cases, the direct reaction is very difficult or impossible, due to technique limitations. People thus developed many methods of indirect measurement.

1. Elastic resonance scattering

Radiation capture reaction $A(a,\gamma)B$ can be studied by elastic resonance scattering excitation function of $a(A,a)A$. One can get excitation energy, spin and parity and energy width. In thin target experiment, the beam energy is varied by accelerator. One of such examples is Oak Ridge^{1}H(^{17}F, p) ^{17}F work[30], with new level of ^{17}F$(p,\gamma)^{18}$Ne found and the reaction rate of ^{17}F$(p,\gamma)^{18}$Ne was deduced.

In thick target experiment, the energy loss of beam gave a way to measure excitation function at same time, by detection the out-going light particles like proton, such as ^{1}H(^{11}C, p)^{11}C[32], recently, in CIAE, the ^{1}H(^{13}N, p)^{13}N excitation function[34] was also measured.

2. Coulomb dissociation

The study $A(a,\gamma)B$ reaction can be done by using ^{208}Pb$(B, a\ A)^{208}$Pb. It is a absorption process of virtual photon. This method was firstly used in RIKEN in studying ^{13}N$(p,\gamma)^{14}$O reaction [37], it gave the 1^-， 5.173 MeV level Γ_γ to be 3.1

±0.6 eV.

3. ANC method

It is believed that the $A(a,\gamma)B$ cross section can be determined by incident wave function and overlap wave function of bound state $B|A+a$. The asymptotic normalization constant (ANC) is the amplitude of overlap function outside nuclei, and is the main contribution of direct capture [38]. This means by using one proton transfer reaction such as (d,n), (^{3}He, d),(^{14}N,^{13} C), one can deduce ANC by DWBA, and then calculate (p,γ) reaction reliably. In 1996, CIAE used this method to deduce solar neutrino reaction^{7}Be$(p,\gamma)^8$B for the first time [126]. In 2003, another group in CIAE deduced ^{11}B$(n,\gamma)^{12}$B reaction corss section [40]. Recently, this method is widely used [41, 42, 43, 44].

4 Production of secondary radioactive nuclear beams

4.1 Introduction

Up to now, most knowledge in nuclear physics has been obtained from nuclear reactions induced by ion beams of stable isotopes. The isospin degree of freedom of those beams, however, was restricted so far. By broadening the range of isospin available in radioactive(or unstable) nuclei, it is now or will soon be possible to investigate the nuclear properties under very unsymmetrical conditions of the neutron or proton density distribution. This development coincides with increased interest in nuclear astrophysics. In a primordial and explosive stage, as well as r-process, the material of nuclear burning consists often of unstable nuclei, so that the experimental data on reactions induced by radioactive nuclear beams (RNB) have become of the fundamental importance in studying nuclear astrophysics. In fact, the production of RNB and the studies based on RNB are the most active fields in nuclear physics nowadays. Many laboratories invert a lot of efforts in producing RNB for nuclear physics research. There are many excellent review articles on this topic [106, 83].

To use RNB, one has to start from the design of a device that transforms a stable isotope beam provided by an accelerator into a secondary beam whose quality is good enough for nuclear physics experiments. Such an attempt was pioneered by Tanihata *et al.* in Berkeley in the 80's and resulted in the successful discovery

of a neutron halo in ^{11}Li. In the beginning of the 90's, the LISE spectrometer in GANIL was built and yielded the discovery of many new isotopes as well as the study of their exotic decay properties such as β-delayed 3-proton emission. Currently, many new devices are operational in the world, such as RIBF in Japan and CSR in Lanzhou.

4.2 Production mechanism

The general idea of producing RNB is to select a suitable nuclear reaction, which is capable of producing nuclei in a wide range of isospin. The production schemes can be classified according to the reaction mechanisms.

4.2.1 Projectile fragmentation reaction

The projectile fragmentation reaction occurs at a beam energy of 50 to 500·A MeV. The beams with these energies can be produced by a cyclotron (50-200·A MeV) or by a synchrotron (100-500·A MeV). The reaction mechanism was first studied by Goldhaber *et al.* [84] in the 70's. This reaction was used to produce RNB in Berkeley for the first time. Currently, there are a number of devices employing fragmentation reactions, such as LISE3 at GANIL, FRS at GSI, RIPS at RIKEN, A1200 at MSU, RIBLL at Lanzhou etc. The first advantage of this approach is that the fragments approximately reserve the same velocity as the primary beam with a limited momentum spread (discussed below in detail). As a result, the outgoing fragments, which are concentrated in a forward cone, can easily be collected, separated, and identified. A further advantage is that the fragments are produced in a wide isosping range extending to the proton or neutron drip line for light nuclei, which makes this reaction an ideal tool to produce very proton-rich or neutron-rich RNB.

According to the Goldhaber's work, the momentum distribution of projectile fragments is parameterized as follows:

$$\frac{d^3\sigma}{dp} \propto \exp\left[-\frac{p_\perp^2}{2\sigma_\perp^2} - \frac{(p_{//} - p_0)^2}{2\sigma_{//}^2}\right],$$

where the perpendicular momentum width is

$$\sigma_{//} = \sigma_0 \sqrt{A_F(A_P - A_F)/(A_P - 1)},$$

and the transverse momentum width is

$$\sigma_{\perp}^2 = \sigma_0^2 A_F(A_P - A_F)/(A_P - 1) + \sigma_1^2 A_F(A_F - 1)/A_P(A_P - 1),$$

with $\sigma_0 \approx 90 MeV/c$, $\sigma_1 \approx 200 MeV/c$, and $\sigma_0 = \frac{p_F}{\sqrt{5}}$, p_F being the Fermi momentum. For example, for A_P = 11 and A_F = 9, one obtains $\sigma_{//}$ = 133 MeV/c and $FWHM_{//}$ = 312 MeV/c.

The production cross section σ is usually estimated by the empirical code EPAX [117] as:

$\sigma(A,Z) = Y(A)\ n\ exp(-R|Z_p - Z|^U)$,

where n is a normalization factor, Y(A) the total yield of for the fragment mass number A, Z_p the peak position in the Z distribution of the cross section, R the width parameter, and U a parameter, which is assumed as 1.5 for $Z_p > Z$ and 2.0 for $Z_p < Z$.

It can be seen from the above equations that the cross section is basically independent of the projectile energy, whereas it strongly depends on the isospin of the projectile. The more proton (neutron)-rich the projectile is, the higher will be the production yield for the proton (neutron)-rich fragments.

One also needs to calculate the total reaction cross section σ_{tot}, e.g. in the case of estimating the reaction loss due to an energy degrader. This can also be done by using EPAX, based on the following formula developed by Kox *et al.* [93]:

$$\sigma_{tot} = \pi r_0^2 \left(A_P^{1/3} + A_T^{1/3} + a\frac{A_P^{1/3} A_T^{1/3}}{A_P^{1/3} + A_T^{1/3}} - c \right)^2 \left(1 - \frac{B_C}{E_{CM}} \right),$$

where B_c is Coulomb barrier energy:

$$B_c = \frac{Z_p Z_T e^2}{r_c(A_p^{1/3} + A_T^{1/3})}$$

The constants involved in these two equations are r_0 = 1.1 fm, and a = 1.85, c is increased linearly from 0.65 (at 30·A MeV) to 2.05 (at 200·A MeV), r_c = 1.3 fm, and E_{CM} is the center-of-mass energy of the projectile.

In practice, the more reliable empirical code called EPAX was developed by Summer at GSI, capable to calculate the production cross section of projectile fragments. This code was adapted into more flexible and versatile code called LISE++. This code is widely used to simulate the operation of a secondary beam line.

For example, the total reaction cross section for the system ^{58}Ni + ^{9}Be is 1.643 b at a ^{58}Ni beam energy of 500·A MeV, and the corresponding cross section for the production of ^{40}Ti is 1.6×10^{-5} mb.

4.2.2 Transfer reaction

The idea of using a transfer reaction to produce RNB can be traced back to the 70's when high precision spectrometers like Q3D were used to study such reactions. The device dedicated to RNB was firstly established in LLNL, where a QSBTS spectrometer was used to study the ^{7}Be(d,n)^{8}B reaction. Today, such devices are used in Notre Dame, in Beijing (GIRAFFE) and elsewhere. The transfer reaction has a simple exit channel, so that a simple separation device can achieve very high purity and intensity of the respective RNB.

In most cases, inverse geometry is adapted by using a heavy beam impinging on a light target. For example, to produce ^{7}Be beam in GIRAFFE, a ^{7}Li beam was guided to a H_2 gas target, in which ^{7}Li(d,n)^{7}Be reactions occurred. Such geometry compresses the reaction products ^{7}Be to a small angular cone of 9°. Because of the small momentum transfer from beam to target, the velocity of ^{7}Be is roughly the same as that of ^{7}Li, similar to projectile fragmentation reactions. Thus the resulting RNB is also easy to collect and to focus. The production cross section and angular distribution can be calculated by a DWBA program. In practice, one often uses the experimentally measured low-energy reaction data that have well established before. The charge-exchange reactions such as ^{7}Li(d,n)^{7}Be are frequently used, which have production cross sections of several tens of mb and result in a different atomic number (Z) of the reaction products compared to that of the primary beam. Such a Z difference results in a large magnetic rigidity difference, which in turn is a key factor to achieve a high RNB purity, see Fig. 5. To produce more exotic RNB, one may use two- or multi-nucleon transfer reaction, but production cross section is two- or multi-orders of magnitude lower, so in this case the projectile fragmentation is more attractive.

The reaction cross section can be calculated by distorted wave Bonn approximation (DWBA) code, provided the optical potential is well know. In the fortunate cases, some experimental data was available and can be directly used.

4.3 Separation methods

The principle of separation of RNB, regardless reaction mechanism, is based on electric and/or magnetic fields to select the desired isotope by its magnetic rigidity Bρ (electro-magnetic device), by its velocity v (velocity filter), or by its mass number A (mass separator). The principle of separation and particle identification can be summarized in the following formulae.

E = A(γ-1)

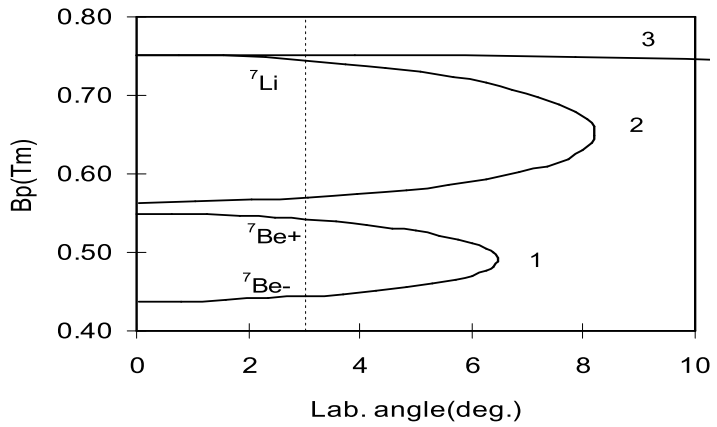

Figure 5: Rigidity vs. angle for ^{7}Be.

$B\rho = p/q = A\beta\gamma/q = B\rho_0(1 + x/d)$
with $\gamma = 1/(1-\beta^2)^{1/2}$,where E and ΔE are the total energy and energy-loss of the ion, Z and q its atomic number and charge state, x and d its position and the dispersion in the focal plane.

Under the condition of the small spectrometer acceptance $\Delta p/p$, β is constant. For the case of $q = Z$, which is valid in the energy of multi-hundred·A MeV,

$Z \propto (\Delta E)^{1/2}$,

$TOF \propto A/Z$.

where *TOF* is the time of flight of an ion.

In general, the atom is not fully stripped, so that $q = Z, Z-1, ...$ As a result,

$TOF \propto A/q$,

$q \propto E$.

The detailed treatment for partially stripped charge states can be found in [95].

For the velocity filter, $v \propto B/E$, where B and E stand for the magnetic field and electric field of the filter, respectively. Because this technique needs high electric field, it can only be applied to low energy transfer reaction.

4.3.1 Electromagnetic device

A general layout of an electromagnetic device is shown in Fig. **??**. According to the complexity of RNB, these devices are further categorized as subsequent arrays comprising one-stage such as GIRAFFE, two-stage such as FRS, or three-stage such as LISE.

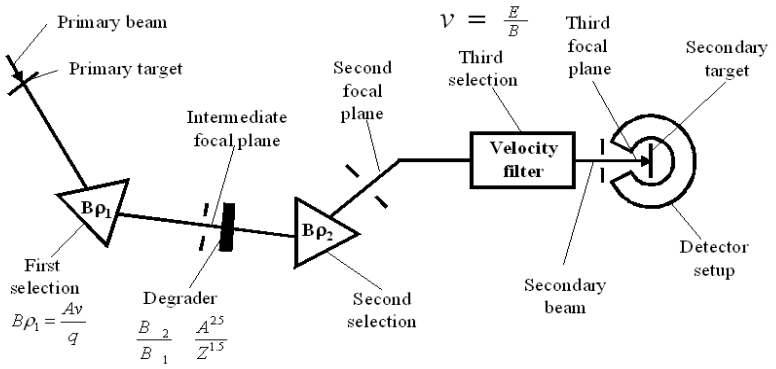

Figure 6: Basic components of a electromagnetic device.

4.3.2 Mass separator online

Mass separator online use fusion evaporation reactions or spallation reactions to produce RNB, which are stopped in a catcher in an ion-source. Different kinds of ion-sources are used to combine chemical selectivity with high efficiency even for short-lived nuclei. For example, laser ion-source can be applied to achieve more chemical selectivity. The RNB of interest are then extracted, accelerated, and mass separated for the final use.

4.4 Beam intensity and applications

The intensity of RNB can be obtained by using the following formulae.

$I = \varepsilon n_i N_t \sigma,$

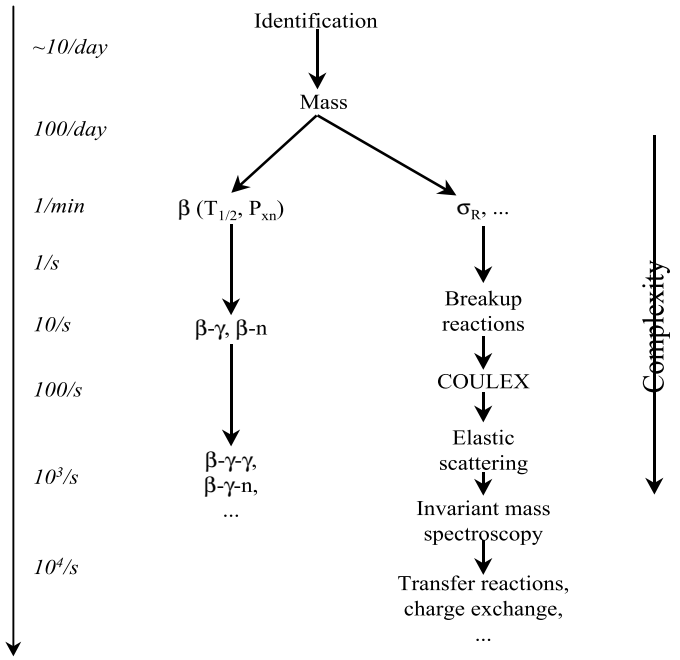

Figure 7: The relation between the intensity of RNB and its possible experiments.

where ε is the collection and separation efficiency of secondary beam line, n_i the beam intensity, N_t the effective target thickness, and σ the production cross section. The product of n_i and $N_t$is also called luminosity. Depending on the available RNB intensities, various nuclear physics experiments can be performed as illustrated in Fig. **??**. Of course, by the development of detection efficiency of modern detectors, such limits can be partially removed.

4.5 Example of the secondary beam line, FRS in GSI

Here an example is presented, i.e. the measurement of β-decay of ^{40}Ti and ^{41}Ti, was performed on the GSI fragment separator (FRS) [82]. It uses projectile fragmentation reaction and has a two-stage electromagnetic design. Because of the high magnetic rigidity of fragments (up to 18 Tm), it is not possible to include a

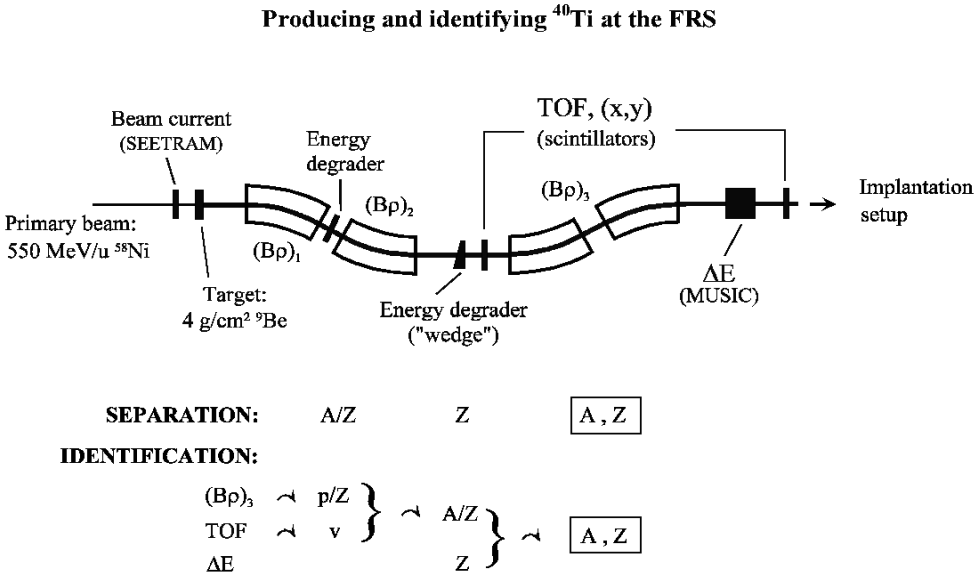

Figure 8: Layout of FRS.

third-stage separation, namely a velocity filter. This solution was ruled out due to the difficulties of reaching high electric fields.

4.5.1 General layout

The general layout of FRS is shown in Fig. **??**. It is a double achromatic device, so that ions with angular emitance of 3.4 mSr and a momentum distribution of 2 % can be focused at F_4 to a spot of 0.6 cm in diameter. Apart from the conventional energy degrader at F_2, an additional degrader was installed at F_1 in order to further suppress contaminants.

4.5.2 Beam diagnostics

In front of the primary target, an ionization chamber (SEETRAM) can be inserted to measure the primary beam intensity. In F_2, F_3, and F_4, scintillation counters

(SC), and MWPC's can be inserted to measure TOF and beam profile, respectively.

Furthermore, a MUSIC detector is used for measuring the energy-loss of RNB at F_4, in order to identify the projectile fragments by their atomic number. The SC and MWPC, can stand counting rates up to 10 kHz, whereas the counting rates in the MUSIC is limited to 1 kHz. It is therefore important to suppress the contaminants as much as possible at F_4.

4.5.3 Production of unstable beam: ^{40}Ti

The beam-target combination used to produce ^{40}Ti beam was ^{58}Ni on ^{9}Be. In the original proposal underlying this experiment, a ^{50}Cr beam was proposed, which unfortunately was not available at the time of the experiment. The ^{40}Ti production cross sections calculated by EPAX are 1.6×10^{-5} mb and 3.6×10^{-5} mb for ^{58}Ni and ^{50}Cr beam, respectively. Furthermore, the 1σ-widths of perpendicular momentum of ^{40}Ti are 320 MeV/c and 257 MeV/c for ^{58}Ni and ^{50}Cr beam, respectively, so that the FRS transmission for ^{50}Cr$\rightarrow^{40}$Ti is 20 % higher than that for ^{58}Ni$\rightarrow^{40}$Ti. Therefore, the ^{40}Ti beam intensity from ^{58}Ni fragmentation was lower than originally proposed.

To shift the center of the ^{40}Ti-range profile to the center of the silicon detector stack, an energy degrader of 1.14 g/cm^2 Al was inserted at F_4. As a result of this degrader, a secondary-reaction loss of ^{40}Ti ions has to be taken into account in the calculation of absolute proton branching ratio in ^{40}Ti decay. This can be either calculated or measured. According to the EPAX prediction [117], the total reaction cross section of 200·A MeV ^{40}Ti + ^{27}Al amounts to 2.0 b. Taking into account the degrader thickness, we estimated the secondary reaction loss to be 10 %. This is in good agreement with the measured value of 13(3) %.

4.6 Future development

The future developments are based on the idea of improving RNB, with respect to beam quality and/or intensity. This can be realized by coupling an accelerator after an electromagnetic ISOL device such as Louvain-la-Neuve in Belgium (ISOL method), or by building an accelerator with enhanced primary beam intensity followed by a projectile fragment separator (PF method) such as the RIBF factory in RIKEN. Presently, a large number of facilities base on ISOL or PF method are being constructed or planned. In the near future, considerably improved studies of the isospin degree of freedom and of phenomena of interest to nuclear astrophysics

will thus become possible. It is worthwhile to mention that the RIA project, which will be most probably constructed in Argon national lab or MSU in USA, can take advantage of both PF and ISOL method, by using gas stripper technology.

5 Beta-delayed proton emission, neutrino absorption rates, and shell-model calculation

Beta-decay half life is the most important nuclear data input to nuclear astrophysics. The decay mode known as β-delayed proton emission consists of two consecutive decay processes, i.e. β-decay and proton emission. The general decay scheme shown in Fig. **??** exemplifies this disintegration mode for a typical β^+-delayed proton precursor. The β-decay of the precursor populates states in the emitter, many of which lie above the proton separation energy (S_p). These levels then decay via proton emission to states in the daughter nucleus. Thus the experiment involves the observation of protons that exhibit the half-life of the precursor. The proton energies are determined by the excitation energy of the β-populated state in the emitter and by the S_p values of the states in the daughter. The observed proton intensities are used to obtain β^+-decay transition rates and to determine the relative reduced proton widths for proton emission to various final states. These observations provide a challenging test for shell-model calculations.

5.1 Allowed and super-allowed β-decay

By a standard application of time-dependent perturbation theory, the probability of emitting a β-particle with energy E and momentum p is given by

$$P(E)dE = \frac{1}{2\pi^3\hbar^7c^5}\left|M_{fi}\right|^2 F(Z,E)(E_0-E)^2pEdE,$$

where M_{fi} is the β-decay matrix element connecting the initial and final states, F(Z,E) is the Fermi function which takes into account the Coulomb distortion of the charged lepton's wave function form that describes a free particle (i.e., a plane wave) due to the nuclear charge and the surrounding atomic electrons, Z is the atomic number of the β-daughter, and E_0 is the maximum β-particle energy (for β^+-decay: $E_0 = Q_{EC} - E_x$- $2m_ec^2$). The β-decay constant (λ) for a particular transition is obtained by integrating this probability over all allowed energies

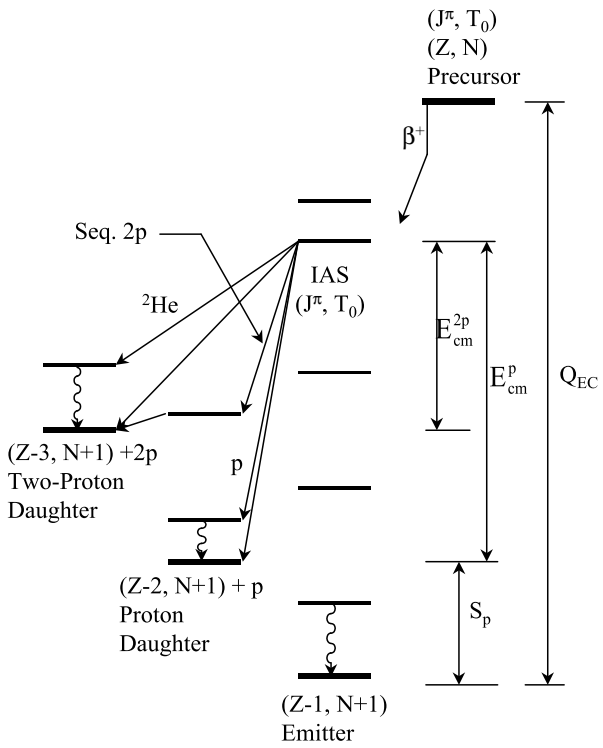

Figure 9: Schematic illustration of β-delayed proton emission process.

$$\lambda = \frac{1}{2\pi^3\hbar^7 c^5}\left|M_{fi}\right|^2 \int_0^{E_0} F(Z,E)(E_0 - E)^2 pEdE.$$

The integral in the above equation is known as the statistical rate function or phase space factor f. Substituting f, which can be expressed in units of $(m_e c^2)^5/c$, in this equation, and rewriting the relationship in terms of partial half-life, t = ln2/λ, one obtains the comparative half-life for the transition or its ft value.

$$ft = \frac{2\pi^3(\ln 2)\hbar^7/m_e c^4}{\left|M_{fi}\right|^2} \quad .$$

Comparative half-lives (often quoted as logft's) tend to fall into certain groups that enable β-transitions to be classified in terms of superallowed, allowed, or forbidden transitions, see Table 23 for detail. Once a particular decay is classified, the spin, parity, and isosping of the populated level is restricted to certain values governed by the selection rules for that type of transition. Since the present work only deals with superallowed and allowed transitions, the discussion will be limited to those decays.

Class	logft	L	Fermi transition		Gamow-Tellor transition	
			ΔI	$\Delta\pi$	ΔI	$\Delta\pi$
Super	2.9-3.7	0	0	No	(0), 1	No
Allowed	< 5.9	0	0	No	(0), 1	No
1^{st} forbidden	> 8.0	1	(0), 1	Yes	0, 1, 2	Yes
2^{nd} forbidden	> 10.6	2	(1), 2	No	2,3	No

Table 1: List of classification of β-transitions and corresponding selection roles.

For allowed and superallowed transitions, the β-decay matrix element can be divided into two parts, the Fermi matrix elements (l) and that of Gamow-Teller (GT) matrix elements (σ), together with their respective vector and axial vector coupling constants, g_v and g_A, as

$$\left|M_{fi}\right|^2 = g_V^2 \langle l\rangle^2 + g_A^2 \langle\sigma\rangle^2 ,$$

where the coupling constants have been renormalized to include electromagnetic corrections. Combing the above equations, one obtains the familiar relation

$$ft = \frac{2\pi^3(\ln 2)\hbar^7/m_e^5c^4}{g_V^2\langle l\rangle^2 + g_A^2\langle\sigma\rangle^2}.$$

Using the most recent values for the physical constants, together with the latest values of the renormalized coupling constants, leads to [124],

$$ft = \frac{6127(9)}{\langle l\rangle^2 + 1.567\langle\sigma\rangle^2}s.$$

The Fermi matrix element is given as

$$\langle l\rangle = \left\langle \psi_f \left| \sum_j \tau_\pm(j) \right| \psi_i \right\rangle = \left\langle \psi_f \left| T_\pm \right| \psi_i \right\rangle,$$

where i and f represent the initial and final wave functions, τ is the isosping raising or lowering operator for the j^{th} nucleon (i.e., for β^+-decay, τ_+p = n), and the sum of the j operator over all j nucleons is defined as the total isospin operator T. Analogous to the angular momentum raising and lowering operator J, the isospin operator raises or lowers the isosping projection, T_z, by one unit, thus

$$T_\pm \left|\psi\left(J^\pi, T, T_Z\right)\right\rangle = \left[\left(T \mp T_Z\right)\left(T \pm T_Z + 1\right)\right]^{1/2} \left|\psi\left(J^\pi, T, T_z + 1\right)\right\rangle$$

Correspondingly, the selection rules for allowed Fermi interactions are $\Delta J^{\Delta\pi}=0^{(no)}$ and $\Delta T = 0$. Neglecting the small isosping impurities in the final wave function, the Fermi matrix element becomes

$$\langle l\rangle^2 = T(T+1) - T_{Z_i}T_{Z_f},$$

where T_{zi} and T_{Zf} are the initial and final isospin projections.

The GT matrix element is given by

$$\langle l\rangle = \left\langle \psi_f \left| \sum_j \sigma(j)\tau_\pm(j) \right| \psi_i \right\rangle,$$

where σ(j) is the Pauli spin operator. The selection rules for allowed GT interactions are $\Delta J^{\Delta\pi}= 0,1^{(no)}$ and $\Delta T = 0,1$. Unlike the Fermi matrix element, this matrix element depends upon the explicit details of the initial and final wave functions.

Within the simplest shell-model, where initial and final states are described by a single particle coupled to an inert J = 0 core (i.e.,$\left[l_j \otimes \left(l_j^{|}\right)_{J=0}^{n}, the GT matrix element is given by\right.$

$$\langle\sigma\rangle^2 = 6(2J_f + 1) \left\{ \begin{array}{ccc} 1/2 & 1/2 & 1 \\ J_i & J_f & l \end{array} \right\}^2 ,$$

where the term enclosed by brackets is a Wigner 6j symbol. This expression applies to allowed transitions between single particle state where J_i= l + 1/2 such as a $1d_{5/2}$ $1d_{3/2}$ transition.

Unfortunately, due to configuration mixing, most nuclear states can not be accurately expressed by only one shell-model configuration, but require wave functions consisting of several different shell-model configurations. Shell-model calculations, which allow configuration mixing between a large variety of different configurations restricted by the basis space covered, have proven to be very successful in predicting various experimental observables.

5.2 IMME mass predictions

From the observed proton decay energy of the Isospin Analogue States (IAS) as measured in this work, one can determine the mass excess of the IAS (if the ground state mass excess is known), which can then be used to predict the precursor's mass through the use of isobaric multiplet mass equation (IMME). As shown by Wigner, the mass of an isobaric multiplet member with isospin T and isosping projection T_z is given by the following quadratic relation

$$M(T_Z) = a + bT_Z + cT_Z^2$$

Thus if one knows the masses of all but one members of a multiplet, one can calculate the mass of the remaining members.

In the following, this method is used to deduce the ground state mass excess of ^{40}Ti and the Q_{EC} value of ^{40}Ti β-decay, based our measured ^{40}Sc IAS state excitation energy. Table 24 summarized the list of input data for the IMME fit procedure.

[a]Measured in this work and the work of Trinder et al. .

Based on these data, the polynomial fits were performed, which yielded the coefficients as listed in Table **??**.

Using the constants from Set I, the excitation energy of ^{40}Sc IAS state was calculated to be 4365 keV, compared with experimental value of 4365(8) keV. The

Nucleus	T_z	G.S. mass excess (keV)	E_x of T=2 states (keV)	T=2 states mass excess (keV)
^{40}Ar	2	-35039.891(5)	0	-35039.891(5)
^{40}K	1	-33535.0(3)	4384.0(3)	-29151.0(4)
^{40}Ca	0	-34846.0(3)	11988(2)	-22858(2)
^{40}Sc	-1	-20526(4)	4365(8)[a]	-16161(9)
^{40}Ti	-2	To be determined	0	To be determined

Table 2: Masses and T=2 excited states of A = 40, T = 2 series.

Set	Fit condition	a (keV)	b (keV)	c (keV)
I	^{40}Ar, ^{40}K, ^{40}Ca (this work)	-22858.0(16)	-6495.2(24)	202.0(8)
II	^{40}Ar, ^{40}K, ^{40}Ca, and ^{40}Sc (this work)	-22858.0(16)	-6495.1(24)	202.1(8)
III	^{40}Ar, ^{40}K, ^{40}Ca, and ^{40}Sc [**?**]	-22857.9(16)	-6495.2(24)	202.1(8)

Table 3: List of polynomial fit constants.

excellent agreement shows that the IMME prediction is reliable enough to predict the ^{40}Ti ground state mass excess. The fit procedure was extended by including the measured ^{40}Sc IAS excitation energy. This resulted the constants marked as Set II, which is supported by the results in [**?**] (Set III). By using these constants, the ground state mass excess was predicted and the Q_{EC} value for ^{40}Ti was determined to be -9060(12) keV and 11466(13) keV, respectively. These values are considerably more precise than the previous values of -8850(160) keV and 10680(160) keV given in [60], which were based on a systematic mass evaluation.

5.3 Spherical Shell-Model

Shell model is an indispensable tool of understanding direct reaction and decay process. The increased binding of certain combinations of neutrons and protons was pointed out by Elsasser [75] in 1934, and this effects for light nuclei with N or Z values of 2 (^{4}He), 8 (^{16}O), and 20 (^{40}Ca) were already known in these early days of nuclear physics. In 1948 Mayer [100] observed strong evidence for additional "magic numbers" at 50 and 82 for protons, and 50, 82, and 126 for neutrons. This phenomenon can be clearly seen from the 2p or 2n separation energies along lines of constant isospin for even-even nuclei. Mayer and Jensen [102] explained this in terms of a "shell-model", where nucleons are bound by a spherically symmetric potential well. If a harmonic oscillator of the form

V(r) =g−V0 [1t(r /R)^2]

is used, where V(r) is the potential at a distance r from the center of the nucleus and R is the nuclear radius, the resulting quantum states can be characterized by n, the principal quantum number related to the number of radial nodes in the wave function, and by l, the orbital angular momentum of the particle. By analogy to atomic spectroscopy, states with l = 0, 1, 2, 3, 4, 5, 6, ... are designated as s, p, d, f, g, h, i, ..., respectively. The states are identified by as 1s, 2f, 3p, etc, where, unlike in atomic spectroscopy, n is defined so that each state has nt1 radial nodes.

The evolution of shell-model states from the harmonic oscillator model is showed in Fig. below.

In the shell-model calculation, the interaction between the valence particles and the core nucleus is treated by the perturbation theory. Because of the large valence space of ^{40}Ti, the two major oscillator shells must be included in the calculation, e.g. the $1d_{5/2}2s_{1/2}1d_{3/2}$ (sd) and the $1f_{7/2}2p_{3/2}1f_{5/2}2p_{1/2}$ (fp) shells. Correspondingly, the number of possible configurations of the model space in the shell-model calculation is as large as 10^6. To truncate the model space, the nhω truncation was imposed [109].

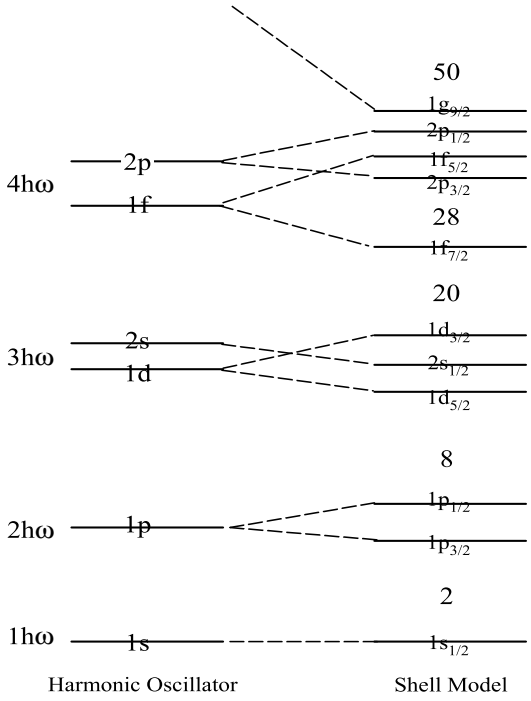

Figure 10: Evolution of nuclear shell model from the harmonic oscillator to the shell structure.

6 Production of unstable beams at HI-13 Tandem Accelerator in CIAE

6.1 Introduction

A radioactive nuclear beam (RNB) facility (GIRAFFE) has been built at the HI-13 tandem accelerator of China Institute of Atomic Energy (CIAE). The facility makes use of the inverse kinematics. It was designed for yielding low energy ^{6}He, ^{7}Be, ^{8}Li, ^{11}C, ^{12}B, ^{13}N, ^{15}O and ^{17}F secondary beams with intensities of 10^{4}-10^{6} ions/s and for studying reactions of nuclear physical and astrophysical interest. The facility and experimental results in producing RNB will be described.

6.2 General Description of the Facility

As a starting point towards studies with RNB at CIAE, the facility GIRAFFE for producing and for utilizing low energy beams of unstable nuclei such as ^{6}He, ^{7}Be, ^{8}Li, ^{11}C, ^{12}B, ^{13}N, ^{15}O and ^{17}F has been constructed at the HI-13 tandem laboratory. GIRAFFE was designed for studying a number of reactions of astrophysical interest and charge-exchange reactions among several $T_z = \pm 1/2$ pairs of mirror nuclei.

GIRAFFE makes use of the inverse kinematics. The general feature of the facility is schematically shown in Figure 4. It comprises a primary reaction chamber, a dipole-quadrupole doublet (D-Q-Q) beam transport system and a secondary reaction chamber. The primary beams of ^{7}Li, ^{11}B, ^{12}C, and ^{16}O ions from the HI-13 tandem accelerator were used for bombarding a hydrogen or deuterium gas cell in the primary reaction chamber to produce unstable nuclei of interest via reactions such as ^{1}H(^{7}Li,^{7}Be)n. Because of the kinematic effect, the desired unstable nuclei are compressed into a forward cone. Fig. **??**shows the differential cross section of the ^{7}Be ions from the ^{1}H(^{7}Li, ^{7}Be)n reaction at E(^{7}Li) = 35 MeV. The RNB of interest were then magnetically separated from the scattered ^{7}Li beam and unwanted reaction products, and finally focused onto a secondary reaction target by using the D-Q-Q system. Fig. **??** shows the result of beam optics calculation. The basic parameters of the secondary beam line are summarized in the following Table.

Downstream of the secondary reaction target, a detector telescope was mounted on a rotatable arm for observing the reaction products of interest. It was found in the initial RNB tuning experiments that the appropriate choice of the acceptance

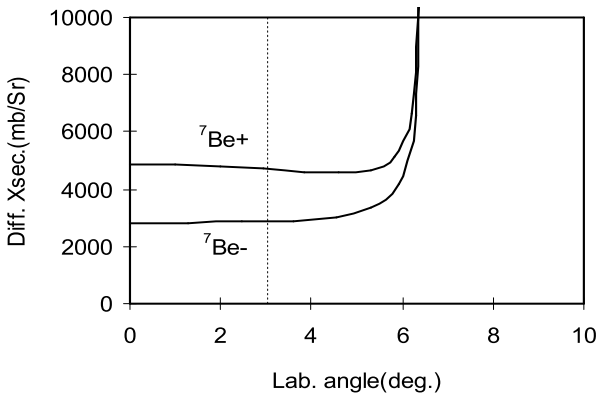

Figure 11: Cross section vs. lab. angle for ^{7}be beam.

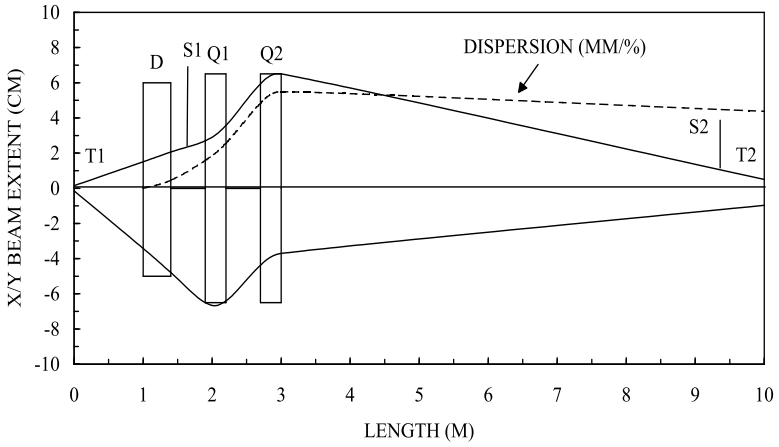

Figure 12: The GIRAFFE beam optics.

Maximum solid angle	$\Delta\Omega$ = 1.8msr ($\Delta\theta$ = ±16.4 mrad, $\Delta\phi$ = ±34.8 mrad)
Maximum rigidity	$B\rho$ = 1.4 Tm
Total length	L = 9.8 m
Focal plane dispersion	$\Delta X/(\Delta p/p)$ = 0.47 cm/%
Acceptance angle	3°
Deflection angle	13°

Table 4: The basic parameters of GIRAFFE.

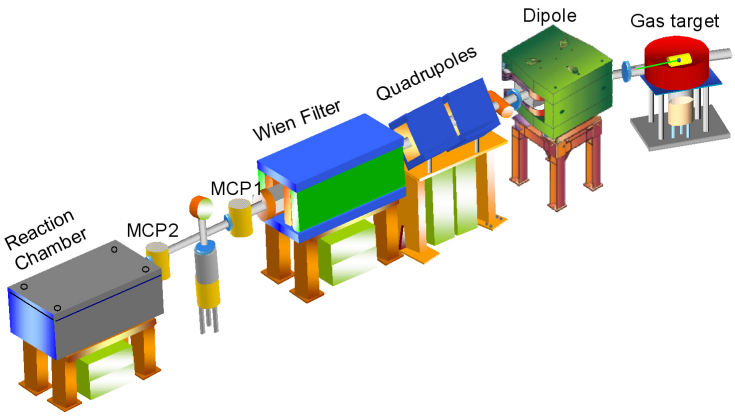

Figure 13: Sketch of GIRAFFE.

angle for each of the desired RNB plays a critical role in purifying secondary beams. So far a value of 3° has been chosen for this angle. It is planed to install a beam swinger at upstream of the primary reaction chamber for optimizing the incident angles.

GIRAFFE comprises a primary reaction chamber, a dipole-quadrupole doublet (D-Q-Q) magnetic separation and focusing system, as well as a secondary reaction chamber, as shown in Fig. 13. Up to now, the ion beams of ^{6}He, ^{7}Be, ^{8}Li, ^{11}C, ^{13}N, ^{15}O, ^{17}F and ^{10}C etc have been delivered. A Wien filter is installed between quadrupole doublet and focal plane by the end of 2004, which greatly improved the secondary beam purity.

6.3 Choice of direct reactions

Taking the beam energy and the beam intensity at HI-13 Tandem accelerator into account, the RNB production reactions were selected based on the following con-

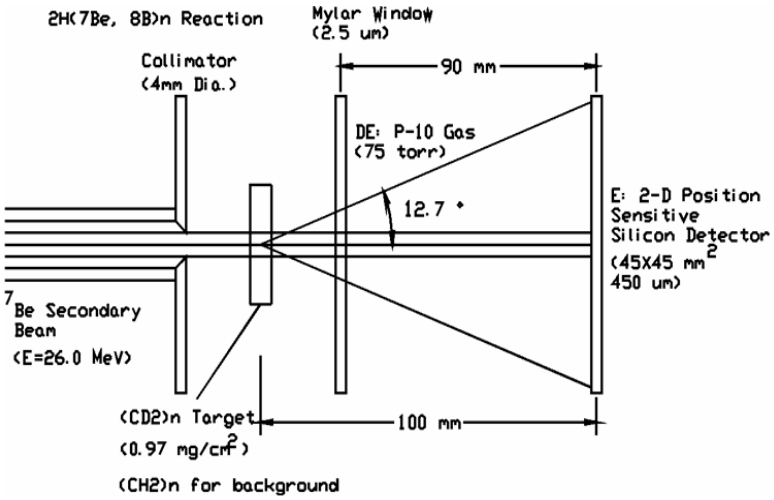

Figure 14: Experimental setup.

siderations:

The reaction products should have high differential cross sections. Consequently the reactions of inverse kinematics, such as ^{1}H(^{7}Li,^{7}Be)n, were selected, in which the reaction products of interest were compressed into a forward cone.

The reactions should have large total cross sections. The charge exchange and single nucleon transfer reactions were adapted. As a result, RNB are limited to the isotopes near the β-stability line.

The magnetic rigidities of the desired RNB should be considerably different from those of the primary beams and the products from other reaction channels. The (p,n) and (d,n) reactions are most suitable for this purpose, since the RNB of interest and the primary beam have different magnetic rigidities due to the differences in atomic numbers.

In order to sustain the high current of the primary beam, a H_2 or D_2 gas target with titanium windows was adopted.

For a specific reaction, one can select either the positive or negative group of center-of-mass angular distribution, depending on the compromise between magnetic rigidity difference and the differential cross sections.

Some reactions that meet the above criteria are summarized in the following.

*Values calculated by assuming a primary beam intensity of 1.0 pμA, gas cell

RNB	Production reaction	E_{beam} (MeV)	$d\sigma/d\Omega$ (mb/Sr)	E_{RNB} (MeV)	$\Delta B\rho/B\rho$ (%)	Intensity* (pps)
^{6}He	^{2}H(^{7}Li,^{6}He)^{3}He	42.0	160+	34.0±1 .0	17.3	2.2×10^{5}
^{7}Be	^{1}H(^{7}Li,^{7}Be)n	35.0	5000+	33.0±0.5	-3.1	1.4×10^{7}
^{8}Li	^{2}H(^{7}Li,^{8}Li)^{1}H	42.0	900+	40.0±0.5	5.2	1.2×10^{6}
^{11}C	^{1}H(^{11}B,^{11}C)n	78.1	6700-	57.0±1.0	-17.5	4.5×10^{6}
^{12}B	^{2}H(^{11}B,^{12}B)^{1}H	66.0	1100+	65.0±1.0	6.3	1.5×10^{6}
^{13}N	^{2}H(^{12}C,^{13}N)n	70.8	3000+	70.0±1 .0	-9.7	2.1×10^{6}
^{15}O	^{2}H(^{14}N,^{15} O)n	84.0	8300+	82.0±1 .0	-12.7	3.7×10^{6}
^{17}F	^{2}H(^{16}O,^{17}F)n	88.0	28000+	85.0±0.3	-10.8	1.3×10^{7}

Table 5: Summary of some of the production reactions for the secondary beams and the estimated characteristics of resulted beams.

pressure of 1 atm, and differential cross sections at their optimum angles. The marks + and - refer to the forward and backward center-of-mass angular group selected, respectively.

6.4 Purification of unstable beam

It can be seen from the energy spectra of RNB that the contaminants come from secondary products of other reaction channels and from the low energy tail of the primary beam, which fall into the selected rigidity window due to multiple coulomb scattering. In order to study the purity of RNB, two acceptance angle settings of GIRAFFE (0˚ and 3˚) were used and a shadow bar was installed in the case of 0˚ setting. The corresponding results are listed below:

In the 0˚ setting, the installation of the shadow bar allows to eliminate low energy beam contaminant. This results from the fact that the primary beam components have smaller emmitance than that of secondary beam. The purity of ^{11}C beam was increased from 6 % to 14 % by installing the shadow bar.

In the 3˚ setting, the purity of RNB (with the shadow bar removed) is higher than that obtained at 0˚ with the shadow bar. This is due to the Coulomb scattering cross section, which is proportional to $\sin^4(\theta/2)$, θ being the acceptance angle. Setting acceptance angle values other than 0˚ can greatly reduce the accepted scattering primary beam, whereas the differential cross section of RNB is similar to that at 0˚. Another advantage of such a setting is that the shadow bar is not necessary, since the center of primary beam and scattered component is automatically

avoided, thus increasing the transmission for RNB. The drawback of the 3° setting is the slightly lower energy resolution of RNB, which is due to the kinematics.

6.5 Production of secondary beams

In the RNB production experiments, a gas cell at 1.2 atm pressure was used as the target, the entrance and exit windows being made of ~2.5 mg/cm^2 thick titanium foils. The RNB were measured by using a ΔE-E counter telescope consisting of an ionization chamber filled with P-10 gas backed by a 45×45 mm^2 Hamamatsu two-dimensional position-sensitive silicon detector (PSSD) of 450 μm in thickness. So far, the production of the ^{6}He, ^{7}Be, ^{11}C, ^{13}N, and ^{17}F etc. beams has been tested. The characteristics of these beams are summarized below. The position profile for ^{7}Be beam is presented in Fig. **??**.

6.6 Future developments

The possible improvements of GIRAFFE are planned into two phases.

For the phase I, a beam swinger will be installed in front of the primary target chamber. It was designed for altering the incident angle of the primary beam on target, so that one can select the optimal acceptance angle for each RNB. Velocity filter and beam-switcher are planned to be installed in front of the focal plane. In addition, a velocity filter will be used to enhance the secondary beam selection, see Section 5.3 of Appendix 1. Taking the ^{7}Be-beam production as an example, the velocity filter will effectively filter out ^{7}Li contaminants, since the ^{7}Li ions have the same magnetic rigidity but different charge states, thus different velocity. The beam switcher will be used to serve for the decay measurement. During such a measurement, RNB itself will be switched off, so that background will be effectively reduced.

A detector setup for decay measurement was also considered in phase I. This setup will include implantation/detection silicon detectors and germanium detectors to detect the γ-rays in the decay process. A helium-jet technique can be used to transport the RNB to a detector station with lower background. This measure will also improve the implantation profile in range and in beam spot.

The GIRAFFE improvement phase II consists of adding a second-stage magnetic separation, so that an energy degrader can be placed in the intermediate focal plane, which will allow double achromatic operation with isotopic selection.

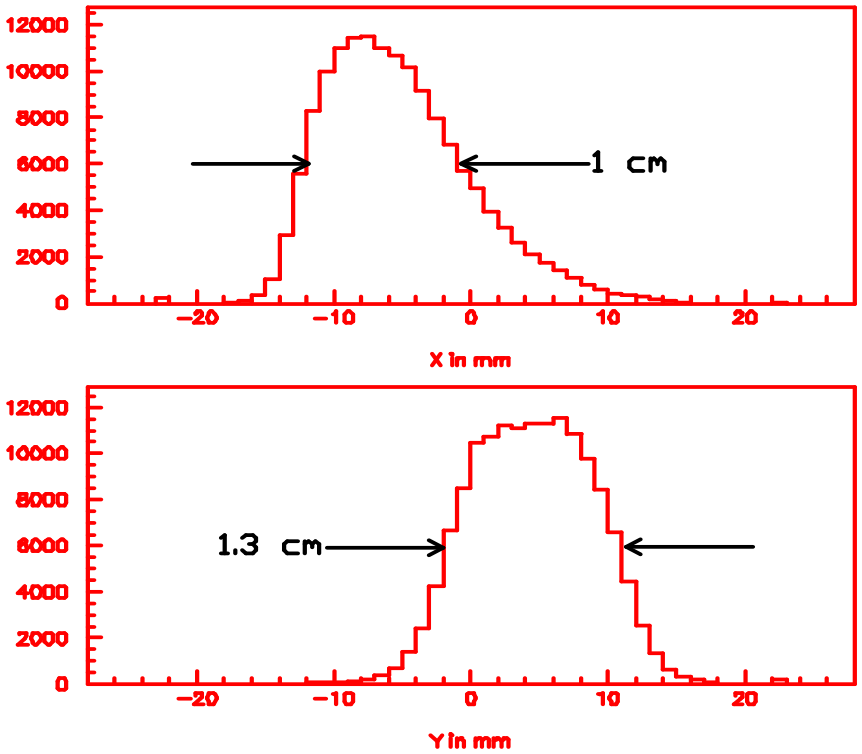

Figure 15: Position profile of ^{7}Be beam.

Table 6: Summary of produced RNB in GIRAFFE.

RNB	Reaction	Energy±Spread（MeV）	Purity（%）	intensity（pps）[†]
^{6}He	^{2}H(^{7}Li,^{6}He)^{3}He	35.7 ± 0.5	92	500
^{7}Be	^{1}H(^{7}Li,^{7}Be)n	30.8 ± 1.3	99	900
^{8}Li	^{2}H(^{7}Li,^{8}Li)^{1}H	40.0 ± 0.5	88	500
^{10}C	^{1}H(^{10}B,^{10}C)n	55.9 ± 3.5	96	200 [‡] [§]
^{11}C	^{1}H(^{11}B,^{11}C)n	63.4 ± 2.7	80	1000
^{13}N	^{2}H(^{12}C,^{13}N)n	57.8 ± 2.1	92	1200 [‡]
^{15}O	^{2}H(^{14}N,^{15}O)n	66.0 ± 3.6	91	800 [‡]
^{17}F	^{2}H(^{16}O,^{17}F)n	76.1 ± 3.7	90	2000 [‡]
^{18}F	^{3}He(^{16}O,^{18}F)^{1}H	75.7 ± 2.2	85	800 [‡]
^{19}Ne	^{4}He(^{16}O,^{19}Ne)n	56.6 ± 3.4	47	120 [‡] [§]
	^{3}He(^{19}F,^{19}Ne)^{3}H	68.6 ± 3.8	42	70 [‡] [§]
^{22}Na	^{4}He(^{19}F,^{22}Na)n	52.9 ± 1.9	57	100 [‡] [¶]

[†] With ϕ3 mmdiameter collimator.
[‡] With velocity filter.
[§] Primary beam intensity can be increased by a factor of 2.
[¶] Primary beam intensity can be increased by a factor of 10.

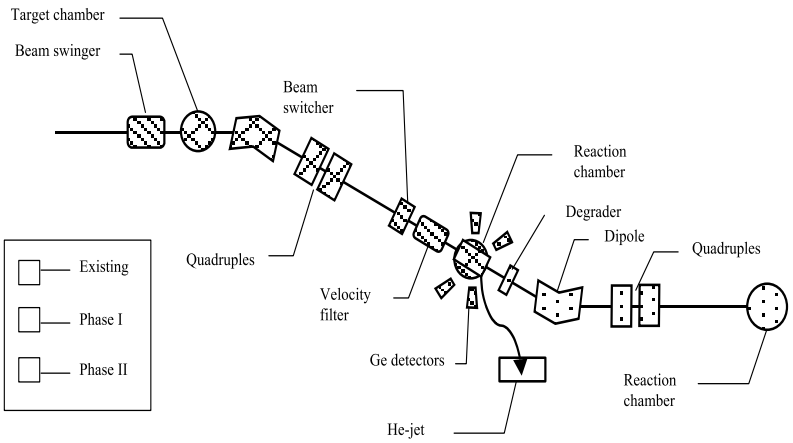

Figure 16: Sketch of future GIRAFFE

The upgrading of the focal plane detector is also planned. A general detector chamber was designed, which will cover larger angular range than current setup. In addition, the use of a MUSIC detector is planned. This detector has better ΔE resolution and provides the possibility of measuring the excitation function in a single setting of GIRAFFE, by using the gas of the MUSIC both for detection and as a secondary target.

All the above-proposed improvements are summarized in the Figure 11. In 2006, the velocity filter was installed successfully, and yielded more pure secondary beams.

7 Using RNB's for the determination of key nuclei properties for nuclear astrophysics

7.1 Solar neutrino problem

The neutrinos that are produced by fusion reactions in the interior of sun provide most valuable information on our understanding of the physical processes inside the sun and of the electroweak interaction theory concerning the basic properties

of neutrino [63]. For more than 20 years, the comparison between experimental results (Homestake, Kamiokande, Gallex and Sage, see Table 5) and the theoretical predictions (Standard solar model, SSM, see, e.g., Bahcall *et al.* (In the following, I shall call it BP95) [63] or Dar *et al.* (I will call it DS95) [73]) have yielded the so-called solar neutrino problem [64]. It refers to the fact that the measured solar neutrino flux is significantly lower than that of the solar model predictions, as shown in the following.

Figure 13: Energy spectrum of solar neutrinos predicted by Bahcall and Ulrich.

Over the years, the large communities of astrophysics and of nuclear physics took enormous efforts in solving this problem [68]. Based on all the information available experimentally and theoretically, it seems that a solution can only be found by introducing a new physics [64]. On the new physics explaining the missing solar neutrinos, especially the complete missing of ^{7}Be neutrinos after evaluating the results of the available experiments, the most promising scenario is based on neutrino oscillation. It can be either oscillation in mater (MSW) or vacuum oscillation (VO) as indicated in Table 6 [69]. Very recently, the Super-Kamiokande group announced the finding of neutrino oscillation - the first experimental observation of non-zero neutrino mass [80]. In the year 2001, the SNO neutrino detection collaboration in Canada, combined with Super Kamiokande data, announced the solid experimental proof of solar neutrino oscillation, their results was generally accepted by the physics community in 2001 Nuclear Physics Conference, thus the final solution of the long problem is with high confidence.

In this context, nuclear physics can make a significant contribution. In a solar model calculation, the uncertainties of nuclear reaction cross sections, such as those of ^{7}Be(p,γ)^{8}B, contribute significantly to the uncertainties associated with the solar model prediction of neutrino fluxes. However, in order to compare the prediction of a given solar model with the solar neutrino experiments, the neutrino fluxes predicted by this model have to be translated into reaction rates by using the nuclear absorption cross section of the detector material. Therefore, another important nuclear physics contribution consists in an accurate determination of the absorption cross section in the relevant detector material. The Homestake experiment (neutrino detection via ^{37}Cl inverse β-decay) and the proposed ICARUS experiment (neutrino detection using ^{40}Ar inverse β-decay) may serve as examples. This argument is expressed in the following simple formula:

Predicted reaction rates = Absorption cross section (nuclear physics input, e.g. ^{37}Ca or ^{40}Ti β-decay)$\times$ Solar neutrino flux (solar model + nuclear physics input, e.g. ^{7}Be(p,γ)^{8}B reaction)

In the present lecture note, I shall give a detailed description of contributions to two experiments which both yield to the nuclear physics data relevant to the solar neutrino problem. The first one is the determination of the ^{7}Be(p,γ)^{8}B cross section [97], responsible for the ^{8}B neutrino flux, the second one is the measurement of ^{40}Ti β-decay [98, 99], which is related to the ^{40}Ar absorption cross section in the ICARUS detector.

7.2 ^{7}Be(p,γ)^{8}B reaction

The high energy neutrinos from the β^+ decay of ^{8}B produced via the ^{7}Be(p, γ)^{8}B reaction at solar energies play a very important role in the solar neutrino problem [63], as explained in Section .1. Therefore, the astrophysical $S_{17}(0)$ factor for the ^{7}Be(p, γ)^{8}B reaction has attracted an increasing attention for many years. There were a number of considerable efforts to study the $S_{17}(0)$ factor through both direct radiative capture reaction [79, 87] and Coulomb dissociation reaction of ^{8}B [105]. However, the obvious disagreement among the experimental results is still a challenging puzzle. Therefore further experiments were called for to reduce the uncertainties of the $S_{17}(0)$. Recently, the proton pickup reactions of ^{7}Be were proposed as an indirect way to extract the $S_{17}(0)$ factor by introducing a simple relation between the asymptotic normalization constant (ANC) and the $S_{17}(0)$ factor [**?**]. This approach was expected to yield the $S_{17}(0)$ factor with an accuracy at least comparable to that of direct radiative capture or Coulomb dissociation reactions, and could thus provide a valuable cross examination as an independent method. We carried out a measurement of cross section and angular distribution of the proton-pickup ^{7}Be(d,n)^{8}B reaction using a radioactive ^{7}Be beam.

The detailed description of this work has already been published [97]. To the best of my knowledge, only two experiments were dedicated to this reaction, which were performed at different energies and presented only cross sections with large uncertainties without the measurement of angular distributions [86].

7.3 ^{40}Ti β-decay and ICARUS detector

In the ICARUS detector [90], the energy and the directions of the electrons scattered by the incoming solar neutrinos, as well as of the electrons produced in the inverse β-decay ^{40}Ar(ν_e,e$^-$)^{40}K, can be measured in a large-volume liquid argon time-projection chamber, see Table 10. Since the inverse β-decay to the ^{40}K ground state is forbidden, each neutrino-absorption event is accompanied by γtrays emitted from excited ^{40}K levels, which produce Compton electrons, as

shown in Figure 14. In this way the electron multiplicity distinguishes scattering and absorption events, making it possible to measure the ratio between these two types of events. This ratio is independent of the total neutrino flux impinging on a terrestrial detector whereas it depends significantly on possible neutrino oscillations. This is due to electrons being scattered by electron neutrinos as well as by μ and τ neutrinos while the production of electrons via neutrino absorption is restricted to only electron neutrinos. Furthermore, quantitative information on the oscillation probability $\upsilon_e \rightarrow \upsilon_{\mu s \tau g}$an be obtained from the experimental ratios.

As indicated in Section .1, the cross sections for the different interaction processes must be known very well for a reliable evaluation of the ICARUS data. The scattering rates can be accurately calculated by using the standard electroweak theory [62], whereas the situation is more complicated for the case of neutrino absorption. While the value for the Fermi transition strength $B(F)$ between the ^{40}Ar ground state and the isobaric analog state (IAS) in ^{40}K is given by the model-independent sum-rule [70], it is more difficult to determine the transition strengths *B(GT)* for the individual contribution of allowed Gamow-Teller (GT) transitions to the neutrino-capture rate. In principle, the *B(GT)* values for the inverse β-decay can be deduced by using shell-model theory or from data measured for the zero-degree charge-exchange reaction ^{40}Ar(p,n)^{40}K. However, as has recently been shown, shell-model calculations failed to reproduce the *B(GT)* distributions measured in the region around ^{40}Ca [56, 123, 124, **?**]. Furthermore, the proportionality of β-decay transition strengths and zero-degree (p,n) reaction rates has been questioned, because a comparison of the β-decay of ^{37}Ca with the ^{37}Cl(p,n)^{37}Ar mirror reaction [57] showed that the differences were probably not entirely due to isospin-violating effects [108, 71]. Hence, a calibration of the neutrino absorption rate based on shell-model calculations or on (p,n)-reactions might jeopardize the quality of the ICARUS results.

An alternative possibility of calibrating the ^{40}Ar neutrino capture rate is to use, under the assumption of isospin symmetry, the *B(GT)* values of the mirror β-decay of ^{40}Ti, as can be seen in Figure 14 (see Appendix 2 for a general description of a β-decay process). In principle, the large energy release of the ^{40}Ti decay (Q_{EC} = 11680(160) keV [60]) enables one to extract all information that is relevant for the GT contributions to the rate of solar neutrinos absorbed by ^{40}Ar, provided sufficiently accurate half-life and branching-ratio data are available. It is interesting to note that the efficiency calibration for the ^{37}Cl experiment has recently been achieved in a similar way by using the *B(GT)* values measured in the β-decay of ^{37}Ca (see [**?**] for a recent review).

7.4 Selected example of indirect measurements and theoretical analysis

The astrophysical S-factor for the ^{7}Be(p,γ)^{8}B reaction at solar energies is a crucial nuclear physics input for the "solar neutrino problem". The S-factor can be indirectly determined through the asymptotic normalization coefficient (ANC) [38] extracted from the proton pickup reaction of ^{7}Be, with accuracy comparable to that from direct radiative capture or Coulomb Dissociation reaction, and thus can provide a significant cross examination. We measured the ^{7}Be(d,n)^{8}B angular distribution in inverse kinematics at $E_{\rm cm}$ = 5.8 MeV and extracted the ANC for the virtual decay ^{8}B $\rightarrow$ ^{7}Be + p based on DWBA [125] analysis. The astrophysical S-factor for the ^{7}Be(p,γ)^{8}B reaction at zero energy was found to be $S_{17}(0)$ = 27.4 $\pm$ 4.4 eV b [126]. Our experimental data were re-analyzed by other groups, as shown in Fig. 20.

One of the key reactions in the hot pp chains is the ^{11}C(p,γ)^{12}N which is believed to play an important role in the evolution of Pop III stars. As a result of the low Q-value, its cross section at astrophysically relevant energies is likely dominated by the direct capture into the 1^{+} ground state of ^{12}N, and the resonant captures into the first and second excited states of ^{12}N at 2^{+} 0.960 MeV and 2^{-} 1.191 MeV, respectively. Angular distribution of the ^{11}C(d,n)^{12}N reaction at $E_{\rm cm}$ = 9.8 MeV was measured with the secondary ^{11}C beam. The experimental data were analyzed with DWBA calculations and thereby the (ANC)^{2} was extracted to be 2.86 $\pm$ 0.91 fm^{-1} for the virtual decay ^{12}N $\rightarrow$ ^{11}C + p. The zero energy astrophysical S-factor for the direct capture ^{11}C(p,γ)^{12}N reaction was then derived to be 157 $\pm$ 50 eV b. We have also estimated the contributions from resonant captures into the first and second excited states of ^{12}N and the interference between direct capture into the ground state and resonant capture into the second excited state. The astrophysical S-factor of ^{11}C(p,γ)^{12}N in the astrophysically relevant energies are illustrated in Fig. 17. The temperature dependence of the direct capture, resonant capture and total reaction rates for ^{11}C(p,γ)^{12}N were derived [127]. This work shows that the direct capture dominates the ^{11}C(p,γ)^{12}N in the wide energy range of astrophysical interest except the ranges corresponding to two resonances.

In the baryon inhomogeneous big-bang models for primordial nucleosynthesis, (IBBNs) [128], many nuclear reactions of unstable nuclei are involved, which can bridge the stability gap at mass number A = 8, and predict a higher production of elements beyond ^{7}Li and a larger universal mass-density parameter of baryons Ω_B. The reaction chains involving unstable nuclei ^{8}Li, ^{9}Li, ^{8}B, etc. are

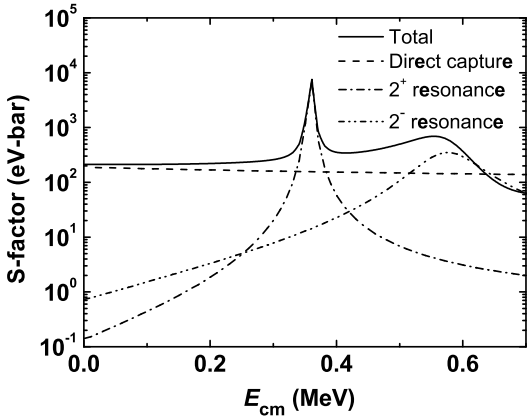

Figure 17: Deduced $^{11}C(p,\gamma)^{12}N$ astrophysical S-factors.

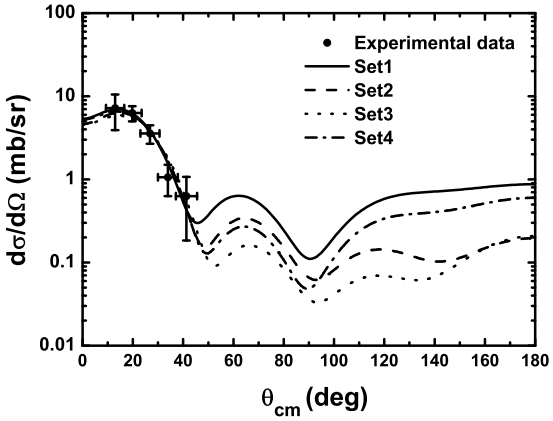

Figure 18: Angular distribution of $^{8}Li(d,p)^{9}Li$ at E_{cm} = 7.8 MeV.

found to play a pivotal role in IBBNs. The production of succeeding heavier elements scales with the abundances of these unstable isotopes during primordial nucleosynthesis and thus all the reactions for generating or destroying them are of importance. We have measured the angular distribution of ^{8}Li(d,p)^{9}Li reaction at $E_{\rm cm}$ = 7.8 MeV, through coincidence detection of ^{9}Li and recoil proton, and obtained the cross section and astrophysical S-factor. By using spectroscopic factor deduced from the ^{8}Li(d,p)^{9}Li$_{g.s.}$ angular distribution, we have successfully derived the ^{8}Li(n,γ)^{9}Li direct capture cross section and astrophysical reaction rate for the first time [132].

The typical experimental setup for the ^{8}Li(d,p)^{9}Li reaction is shown in Fig. **??**, the setup of ^{7}Be(d,n)^{8}B reaction and that of ^{11}C(d,n)^{12}N were described elsewhere [126, 127], respectively. Two Multi-Ring Semiconductor Detectors (MRSDs) with center hole were used in this experiment. The upstream one aimed at detection of the recoil protons, and the downstream one served as a residue energy (E_r) detector which composed a $\Delta E - E_r$ silicon counter telescope. This setup enabled the ^{9}Li -recoil proton coincidence measurement. We applied the similar experimental setup to other reactions except upstream MRSD. Such a detector configuration covered the full laboratory angular region. This setup also facilitated to precisely determine the accumulated quantity of incident unstable beams because the beams themselves were recorded by the counter telescope simultaneously.

As examples, Fig. 18 demonstrates the angular distribution of ^{8}Li(d,p)^{9}Li reaction, where set1 to set4 refer to four sets of optical potential parameters; Fig. 20 shows the comparison of ^{7}Be(p,γ)^{8}B $S_{17}(0)$ factor with other measurements described in Ref. [129] and references therein; Fig. 21 displays the reaction rate of ^{8}Li(n,γ)^{9}Li derived through transfer reaction approach and those of theoretical calculations and Coulomb dissociation measurements presented in Ref. [130] and references therein. This data was also used to extract the ANC of mirror system, by assuming the identical nuclear spectroscopic factor as a result of mirror symmetry [133].

^{13}N$(p,\gamma)^{14}$O is important reaction in the hot CNO cycle which occurs at stellar temperatures around $T_9 \geq 0.1$. But some uncertainties still exist for the direct capture component. The angular distribution of the ^{13}N$(d,n)^{14}$O reaction at $E_{\rm c.m.}$ = 8.9 MeV has been measured in inverse kinematics, for the first time, as shown in Fig. 22. Based on DWBA analysis, the ANC, $C^{^{14}O}_{1,1/2}$, for the ground state of ^{14}O $\rightarrow$ ^{13}N + p is derived to be 5.42 $\pm$ 0.74 fm$^{-1/2}$. The ^{13}N$(p,\gamma)^{14}$O reaction was analyzed with the R-matrix approach, its astrophysical S-factors and reaction

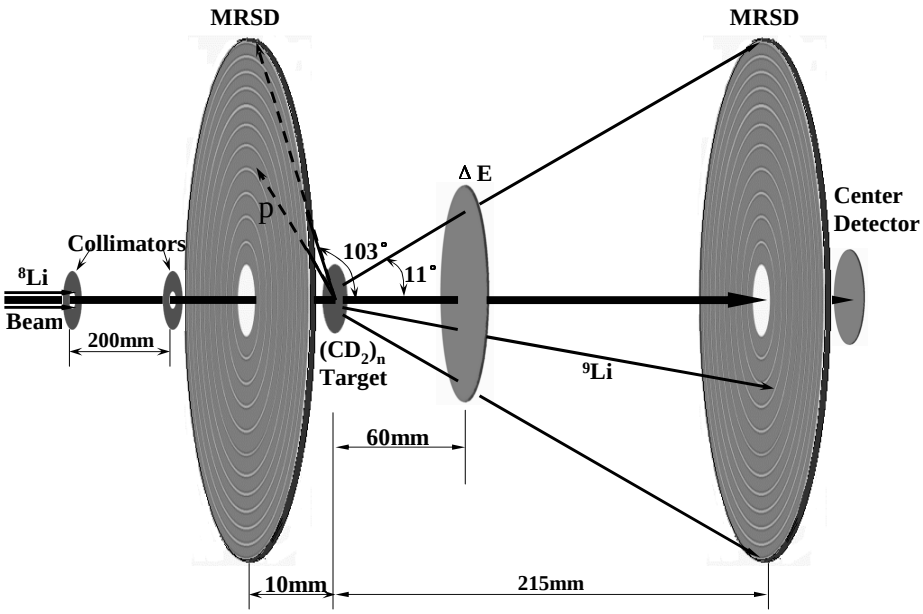

Figure 19: The experimental setup for the ^{8}Li(d,p)^{9}Li reaction

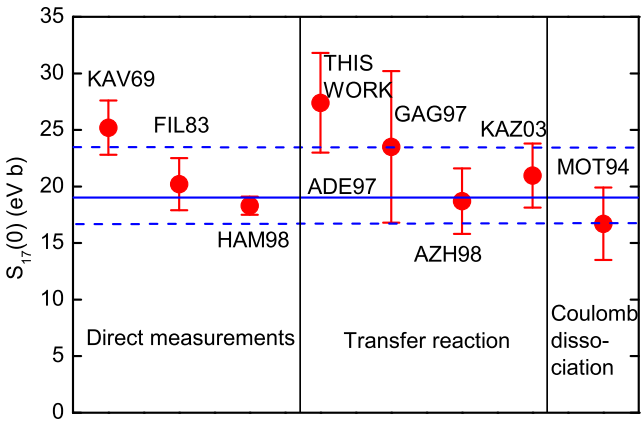

Figure 20: The ^{7}Be(p,γ)^{8}B S-factor by different approach.

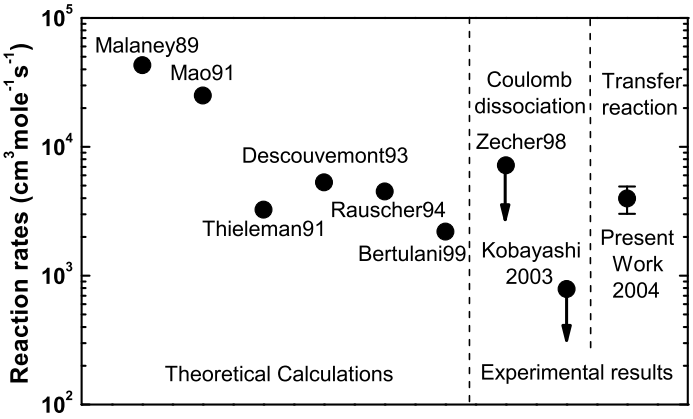

Figure 21: Comparison for reaction rates of ^{8}Li(n,γ)^{9}Li.

Figure 22: The angular distribution of the $^{13}N(d,n)^{14}O$ reaction at $E_{c.m.}$ = 8.9 MeV, together with DWBA calculations using different optical potential parameters.

rates at energies of astrophysical relevance are then determined with the ANC. The present result is in good agreement with that extracted from the ^{14}N (^{13}N,^{14}O)^{13}C transfer reaction [134]. S-factors for direct and resonant captures is then derived, as demonstrated in Fig. 23, and reaction rate is deduced [135]. The implications of the present reaction rates on the evolution of novae are then obtained with the reaction network calculations.

More over, a direct measurement of nuclear astrophysical reaction will be conducted. Excitation function of the ^{11}C(p,γ)^{12}N at $E_{\rm cm}$=0.2-1.0 MeV will be measured in inverse kinematics with the ISAC accelerated ^{11}C beam at DRAGON. There are large discrepancies in the existing indirect measurements and theoretical calculations of this reaction for both direct and resonant captures. The approved proposal [136] aims at clarifying these discrepancies through the direct measurement of excitation function by using high precision DRAGON spectrometer. Based on the measured excitation function, we will be able to derive the energy dependence of astrophysical S-factors for direct capture into the ground state of ^{12}N and resonant captures into the first and second excited states of ^{12}N at 2^+ 0.960 MeV and 2^- 1.191 MeV, as well as the interference between the direct capture into the ground state and resonant capture into the second excited state. The temperature dependence of direct capture-, resonant capture- and total reaction rates will be given. Recently, a proof of principle approach for the production

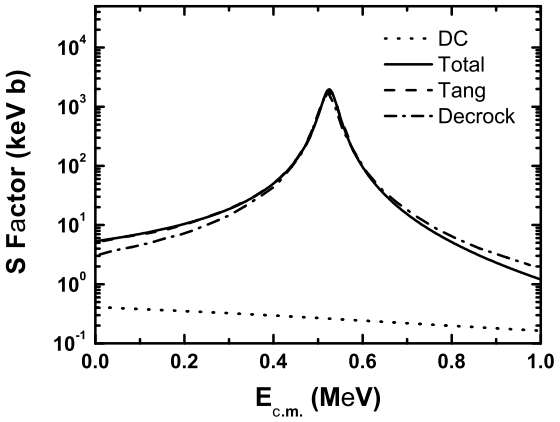

Figure 23: Astrophysical S-factors as a function of $E_{\mathrm{c.m.}}$ for the $^{13}\mathrm{N}(p,\gamma)^{14}\mathrm{O}$ reaction.

Reaction	E_{cm} (MeV)	σ_{tot} (mb)	$(\mathrm{ANC})^2$ (fm^{-1})	Indirect Reaction	S(0) (eV b) or rate	reference
^{7}Be(d,n)^{8}B	5.8	58 ± 8	0.711 ± 0.090	(p,γ)	27 ± 4	[126]
^{7}Be(d,n)^{8}B	8.3	28 ± 3	0.62 ± 0.12	(p,γ)	24 ± 5	[131]
^{11}C(d,n)^{12}N	9.8	23 ± 5	2.86 ± 0.91	(p,γ)	157 ±	[127]
^{8}Li(d,p)^{9}Li	7.8	7.9 ± 2.0	1.25 ± 0.25	(n,γ)	3970 ± 950	[132]
^{8}Li(d,p)^{9}Li	7.8	7.9 ± 2.0	1.10 ± 0.23	^{8}B mirror	42 ± 9	[133]
^{13}N(d,n)^{14}O	8.9	7.4 ± 1.1	29.4 ± 5.3	(p,γ)	417 ± 74	[135]

Table 7: Summary of astrophysics experiment results

of intense (10 ^{8}/s) radioactive ion beams, which differs from the standard ISOL (Isotope Separation On-Line), has been demonstrated successfully taking ^{11}C at the TRIUMF facility [137], as a test case. This approach uses 13 MeV protons and should be useful for a range of radioisotopes of interest to the nuclear astrophysics research program.

All astrophysical reactions and their deduced parameters are summarized in Table below.

References

[1] A.S. Eddington, The Internal Constitution of the Stars, Rept. Brit. Assoc. Adv. Sci. (Cardiff), 34 (1920); Nature 106, 14 (1920).

[2] H.A. Bethe, Energy Production in Stars, Phys. Rev. 55, 103 (1939); Phys. Rev. 55, 434 (1939).

[3] E.M. Burbidge, G.R. Burbidge, W.A. Fowler and F. Hoyle, Synthesis of the elements of stars, Rev. Mod. Phys. 29, 547 (1957).

[4] C.E. Rolfs and W.S. Rodney, Cauldron in the Cosmos, The University of Chicago Press, (1988).

[5] G. Wallerstein, I.I. Jr., P. Parker et al., Synthesis of the elements in stars: forty years of progress, Rev. Mod. Phys. 69, 995 (1997).

[6] J.N. Bahcall, W.F. Huebner and S.H. Lubow et al., New solar-neutrino flux calculations and implications regarding neutrino oscillations, Phys. Rev. Lett. 45, 945 (1980).

[7] G.M. Fuller, S.E. Woosley and T.A. Weaver, The evolution of radiation-dominated stars, Astrophys. J. 307, 675 (1986).

[8] M. Wiescher, J. Görres, S. Graff et al., The hot proton-proton chains in low-metallicity objects, Astrophys. J. 343, 352 (1989).

[9] A. Redder, H.W. Becker, H. Lorenz-Wirzba et al., The ^{15}N$(p,\alpha_0)^{12}$C reaction at stellar energies, Z. Phys. A 305, 325 (1982).

[10] J. Zyskind and P.D. Parker, Remeasurement of the low-energy cross section for the ^{15}N$(p,\alpha_0)^{12}$C reaction, Nucl. Phys. A 320, 404 (1979).

[11] C.E. Rolfs and W.S. Rodney, Proton capture by ^{15}N at stellar energies, Nucl. Phys. A 235, 450 (1974).

[12] D.F. Hebbard, Proton capture by ^{15}N, Nucl. Phys. 15, 289 (1960).

[13] C.E. Rolfs, Spectroscopic factors from radiative capture reactions, Nucl. Phys. A 217, 29 (1973).

[14] C.E. Rolfs and W.S. Rodney, Hydrogen burning of ^{17}O in the CNO cycle, Nucl. Phys. A 250, 295 (1975).

[15] H. Lorenz-Wirzba, P. Schmalbrock, H.P. Trautvetter et al., The ^{18}O$(p,\alpha)^{15}$N reaction at stellar energies, Nucl. Phys. A 313, 346 (1979).

[16] M. Wiescher, H.W. Becker, J. Goerres et al., Nuclear and astrophysical aspects of $^{18}O(p,\gamma)^{19}F$, Nucl. Phys. A 349, 165 (1980).

[17] 卢希庭，江栋兴，叶沿林，原子核物理，原子能出版社，(2000).

[18] P. Decrock, M. Gaelens, M. Huyse et al., Study of the $^{13}N(d,n)^{14}O$ reaction cross section and its astrophysical implications for the ^{13}N proton capture reaction, Phys. Rev. C 48, 2057 (1993).

[19] L. Buchmann, J.M. D'Auria and P. Mccorquodale, Stellar reaction rates of alpha capture on light nuclei and their astrophysical implications, Astrophys. J. 324, 953 (1988).

[20] X. Bai, W. Liu, J. Qin et al., A facility for production and utilization of radioactive beams, Nucl. Phys. A 588, 273c (1995).

[21] W. Liu, Z. Li, X. Bai et al., Current progress of nuclear astrophysics study and BRNBF at CIAE, Nucl. Instrum. Methods Phys. Res. B 204, 62 (2003).

[22] P. Decrock, Th. Delbar, P. Duhamel et al., Determination of the $^{13}N(p,\gamma)^{14}O$ reaction cross section using a ^{13}N radioactive ion beam, Phys. Rev. Lett. 67, 808 (1991).

[23] D.A. Hutcheon, S. Bishop, L. Buchmann et al., The DRAGON facility for nuclear astrophysics at TRIUMF-ISAC: design, construction and operation, Nucl. Instrum. Methods Phys. Res. A 498, 190 (2003).

[24] S. Bishop, R.E. Azuma, L. Buchmann et al., $^{21}Na(p,\gamma)^{22}Mg$ reaction and Oxygen-Neon novae, Phys. Rev. Lett. 90, 162501 (2003).

[25] C. Ruiz, A. Parikh, J. José et al., Measurement of the $E_{c.m.}$=184 keV resonance strength in the $^{26g}Al(p,\gamma)^{27}Si$ reaction, Phys. Rev. Lett. 96, 252501 (2006).

[26] C. Matei, L. Buchmann, W.R. Hannes et al., Measurement of the cascade transition via the first excited state of ^{16}O in the $^{12}C(\alpha,\gamma)^{16}O$ reaction, and its S factor in stellar helium burning, Phys. Rev. Lett. 97, 242503 (2006).

[27] H. Utsunomiya, Y. Yonezawa, H. Akimune et al., Photodisintegration of ^{9}Be with laser-induced Compton backscattered γ rays, Phys. Rev. C 63, 018801 (2000).

[28] R.D. Page, G. Vancraeynest, A.C. Shotter et al., First experimental limit on the ^{19}Ne$(p,\gamma)^{20}$Na resonance strength of astrophysical interest, Phys. Rev. Lett. 73, 3066 (1994).

[29] C. Michotte, C.R. Bain, F. Binon, et al., New limits for the ^{19}Ne$(p,\gamma)^{20}$Na astrophysical reaction rate from direct measurements using radioactive beams, Phys. Lett. B 381, 402 (1996).

[30] D.W. Bardayan, J.C. Blackmon, C.R. Brune et al., Observation of the astrophysically important 3^+ state in ^{18}Ne via elastic scattering of a radioactive ^{17}F beam from ^{1}H, Phys. Rev. Lett. 83, 45 (1999).

[31] C. Ruiz, F. Sarazin, L. Buchmann et al., Strong resonances in elastic scattering of radioactive ^{21}Na on protons, Phys. Rev. C 65, 042801(R) (2002).

[32] T. Teranishi, S. Kubono, S. Shimoura et al., Study of resonance states in ^{12}N using a radioactive ion beam of ^{11}C, Phys. Lett. B 556, 27 (2003).

[33] 王友宝，王宝祥，白希祥等, 高能物理与核物理 30, 202s (2006).

[34] Y.B. Wang et al, to be submitted.

[35] G. Baur, C.A. Bertulani and H. Rebel, Coulomb dissociation as a source of information on radiative capture processes of astrophysical interest, Nucl. Phys. A 458, 188 (1986).

[36] C.A. Bertulani and G. Baur, Electromagnetic processes in relativistic heavy ion collisions, Phys. Rep. 163, 299 (1988).

[37] T. Motobayashi, T. Takei, S. Kox et al., Determination of the astrophysical ^{13}N$(p,\gamma)^{14}$O cross section through the Coulomb dissociation method, Phys. Lett. B 264, 259 (1991).

[38] H.M. Xu, C.A. Gagliardi, R.E. Tribble et al., Overall normalization of the astrophysical S factor and the nuclear vertex constant for ^{7}Be$(p,\gamma)^8$B reactions, Phys. Rev. Lett. 73, 2027 (1994).

[39] W. Liu, X. Bai, S. Zhou et al., Angular distribution for the ^{7}Be$(d,n)^8$B reaction at $E_{c.m.}$=5.8 MeV and the $S_{17}(0)$ factor for the ^{7}Be$(p,\gamma)^8$B reaction, Phys. Rev. Lett. 77, 611 (1996).

[40] C.J. Lin, H.Q. Zhang ande Z.H. Liu et al., Nonresonant capture cross sections of ^{11}B(n,γ) and ^{12}C(n,γ) at stellar energies, Phys. Rev. C 68, 047601 (2003).

[41] A. Azhari, V. Burjan, F. Carstoiu et al., The ^{10}B(^{7}Be,^{8}B)^{9}Be reaction and the ^{7}Be$(p,\gamma)^{8}$B S factor, Phys. Rev. Lett. 82, 3960 (1999).

[42] A. Azhari, V. Burjan, F. Carstoiu et al., The ^{14}N(^{7}Be,^{8}B)^{13}C reaction and the ^{7}Be$(p,\gamma)^{8}$B S factor, Phys. Rev. C 60, 055803 (1999).

[43] W. Liu, Z. Li, X. Bai et al., Determination of ^{11}C$(p,\gamma)^{12}$N astrophysical S-factor via measurement of ^{11}C$(d,n)^{12}$N reaction, Nucl. Phys. A 728, 275 (2003).

[44] Z.H. Li, B. Guo, S.Q. Yan et al., ^{13}N$(d,n)^{14}$O reaction and the astrophysical ^{13}N$(p,\gamma)^{14}$O reaction rate, Phys. Rev. C 74, 035801 (2006).

[45] J. Enders, T. Baumann, B.A. Brown et al., Spectroscopic factors measured in inclusive proton-knockout reactions on ^{8}B and ^{9}C at intermediate energies, Phys. Rev. C 67, 064301 (2003).

[46] L. Trache, F. Carstoiu, C.A. Gagliardi et al., Asymptotic Normalization Coefficient of ^{8}B from Breakup Reactions and the S_{17} Astrophysical Factor, Phys. Rev. Lett. 87, 271102 (2001).

[47] P.B. Fernandez, E.G. Adelberger and A. Garcia, γ width of the unbound 5.17 MeV level of ^{14}O and the hot CNO cycle, Phys. Rev. C 40, 1887 (1989).

[48] S. Kubono, C.C. Yun, R.N. Boyd et al., High resolution study of ^{24}Mg$(p,d)^{23}$Mg for the Ne-E problem, Z. Phys. A 348, 59 (1994).

[49] S. Schmidt, C. Rolfs, W.H. Schulte et al., ^{22}Na(^{3}He,d)^{23}Mg reaction studies of states near the proton threshold and hydrogen burning of ^{22}Na, Nucl. Phys. A 591, 227 (1995).

[50] J.A. Caggiano, D. Bazin, W. Benenson et al., Spectroscopy of ^{23}Al and ^{27}P using the (^{7}Li,^{8}He) reaction and the implications for ^{22}Na and ^{26}Al nucleosynthesis in explosive hydrogen burning, Phys. Rev. C 64, 025802 (2001).

[51] D.W. Bardayan, J.C. Blackmon, A.E. Champagne et al., Astrophysically important ^{26}Si states studied with the ^{28}Si$(p,t)^{26}$Si reaction, Phys. Rev. C 65, 032801(R) (2002).

[52] M.S. Smith, P.V. Magnus, K.I. Hahn et al., Gamma width of ^{14}O*(5.17 MeV) and the stellar ^{13}N$(p,\gamma)^{14}$O reaction rate, Phys. Rev. C 47, 2740 (1993).

[53] W.P. Tan, J.L. Fisker, J. Görres, et al., ^{15}O$(\alpha,\gamma)^{19}$Ne Breakout Reaction and Impact on X-Ray Bursts, Phys. Rev. Lett. 98, 242503 (2007).

[54] D.G. Jenkins, C.J. Lister, R.V.F. Janssens et al., Reevaluation of the ^{22}Na(p,γ) reaction rate: implications for the detection of ^{22}Na Gamma rays from novae, Phys. Rev. Lett. 92, 031101 (2004).

[55] D. Seweryniak, P.J. Woods, M.P. Carpenter et al., Level structure of ^{22}Mg: implications for the ^{21}Na$(p,\gamma)^{22}$Mg astrophysical reaction rate and for the ^{22}Mg mass, Phys. Rev. Lett. 94, 032501 (2005).

[56] E.G. ADELBERGER *ET AL.*, PHYS. REV. LETT. 67 (1991) 3658.

[57] E.G. ADELBERGER *ET AL.,* IN *SOLAR FUSION RATES* (1997) UNPUBLISHED.

[58] B. D. ANDERSON *ET AL.*, PHYS. REV. C54 (1996) 602.

[59] B. D. ANDERSON, PRIVATE COMMUNICATION

[60] G. AUDI *ET AL.*, NUCL. PHYS. A624 (1997) 1.

[61] A. AZHARI *ET AL.*, PROGRESS IN RESEARCH, 1997-1998, CYCLOTRON INSTITUTE, TEXAS A&M UNIVERSITY.

[62] J.N. BAHCALL *ET AL.*, PHYS. LETT. B178 (1986) 324.

[63] J. N. BAHCALL, REV. MOD. PHYS. 67 (1995) 781.

[64] J. N. BAHCALL, NUCL. PHYS. B (PROC. SUPPL.) 48 (1996) 309.

[65] X. BAI *ET AL.,* NUCL. PHYS. A588, (1995) 273C.

[66] F. C. BARKER, AUST. J. PHYS. 33 (1980) 177.

[67] F.C. BARKER AND R.H. SPEAR, ASTROPHYS. J. 307 (1986) 807.

[68] G. BELLINI, 1997, NUPECC REPORT, NUCLEAR PHYSICS IN EUROPE: HIGHLIGHTS AND OPPERTUNITIES, EDITED BY J. VERVIER *ET AL.,* P. 93.

[69] E. BELLOTTI, 1997, IN PROCEDINGS OF THE 8^{TH}INTERNATIONAL CONFERENCE ON NUCLEAR REACTION MECHANISMS, EDITED BY E. GADIOLI, SUPPLEMENTO N. 111, P. 666.

[70] B.A. BROWN *ET AL.*, AT. DATA NUCL. DATA S 33 (1985) 347.

[71] B.A. BROWN, PHYS. REV. LETT. 69 (1992) 1034.

[72] E. CAURIER ET AL., PHYS. REV. C57 (1998) 2316.

[73] A. DAR AND G. SHAVIV, NUCL. PHYS. B (PROC. SUPPL.) 48 (1996) 335.

[74] C. DéTRAZ *ET AL.*, NUCL. PHYS. A519 (1990) 529.

[75] W. ELSASSER, J.PHYS. RAD.5 (1934) 625.

[76] P.M. ENDT, NUCL. PHYS. A521 (1990) 1.

[77] L. FAUX *ET AL.*, NUCL. PHYS. A602 (1996)167.

[78] J.C. FERNANDES *ET AL.*, 1998, IN PROCEDINGS OF THE 2^{ND}INTERNATIONAL CONFERENCE ON EXOTIC NUCLEI AND ATOMIC MASSES (TO BE PUBLISHED).

[79] B.W. FILIPPONE *ET AL.*, PHYS. REV. LETT. 50 (1983) 412

[80] Y. FUKUDA *ET AL.*, HEP-EX/9807003, SEE ALSO HTTP://WWW.PS.UCI.EDU/~SUPERK/

[81] C.A. GAGLIARDI *ET AL.,* PHYS. REV. LETT. 80 (1998) 421.

[82] H. GEISSEL *ET AL.*, NUCL. INSTR. METH. B70 (1992) 286.

[83] H. GEISSEL *ET AL.*, ANN. REV. NUCL. PART. SCI. 45 (1995) 163.

[84] A. S. GOLDHABER, PHYS. LETT. B53 (1974) 396.

[85] S. A. GONCHAROV *ET AL.*, SOV. J. NUCL. PHYS. 35(3) (1982) 383.

[86] R.C. HAIGHT *ET AL.*, NUCL. INST. METHODS 212 (1983) 245.

[87] H. HAMMACHE *ET AL.,* PHYS. REV. LETT. 80 (1998) 929.

[88] O. HAXEL, J.H.D. JENSEN, AND H.E. SUESS, Z. PHYSIK128 (1950) 295.

[89] A. HONKANEN *ET AL.*, NUCL. PHYS. A621(1997) 689.

[90] ICARUS COLLABORATION, ICARUS II PROPOSAL, LNGS REPORT 95/99-I(1993), SEE ALSO *HTTP://WWW.AQUILA.INFN.IT:80/ICARUS/MAIN.HTML.*

[91] M. JUNKER, 1998, IN PROCEDINGS OF THE INTERATIONAL WORKSHOP XXVI ON GROSS PROPERTIES OF NUCLEI AND NUCLEAR EXCITAIONS, EDITED BY M. BABALLA *ET AL.* (GSI, DARMSTADT), P. 271.

[92] N. I. KALOSKAMIS *ET AL.*, PHYS. REV. C55 (1997) 630.

[93] S. KOX *ET AL.*, PHYS. LETT. 159B (1985) 15.

[94] P.D. KUNZ, COMPUTER CODE DWUCK4.

[95] W. LIU *ET AL*, NUCL. INSTRUM. METHODS, A (1988) .

[96] W. LIU *ET AL*, NUCL. INSTRUM. METHODS, A287 (1990) 476.

[97] W. LIU *ET AL.,* PHYS. REV. LETT 77 (1996) 611.

[98] W. LIU *ET AL.*, Z. PHYS. A359 (1997)1.

[99] W. LIU *ET AL.,* PHYS. REV. C (IN PRESS).

[100] M.G. MAYER, PHYS. REV.74 (1948) 235.

[101] M.G. MAYER, PHYS. REV.78 (1950) 16.

[102] M.G. MAYER AND J.H.D. JENSEN, IN ELEMENTARY THEORY OF NUCLEAR SHELL STRUCTURE, JOHN WILEY & SONS, INC., NEW YORK (1955).

[103] V. METAG *ET AL.*, COMMENTS NUCL. PART. PHYS. 16 (1986) 213.

[104] D.R.O. MORRISON, 1994, IN 27^{TH} INTERNATIONAL CONFERENCE ON HIGH ENERGY PHYSICS.

[105] T. MOTOBAYASHI *ET AL.*, PHYS. REV. LETT. 73 (1994) 2680.

[106] A.C. MUELLER *ET AL.*, ANN. REV. NUCL. PART. SCI. 45 (1993) 529.

[107] L. OBERAUER, 1998, IN PROCEDINGS OF THE INTERATIONAL WORKSHOP XXVI ON GROSS PROPERTIES OF NUCLEI AND NUCLEAR EXCITAIONS, EDITED BY M. BABALLA *ET AL.* (GSI, DARMSTADT), P. 262.

[108] W.E. ORMAND *ET AL.*, NUCL. PHYS. A491 (1989) 1.

[109] W.E. ORMAND *ET AL.*, PHYS. LETT. B345 (1995) 343.

[110] C. M. PEREY, ATOMIC DATA AND NUCLEAR DATA TABLES 17(1) (1976) 2.

[111] A. PIECHACZEK, PH.D. THESIS, TECHNISCHE HOCHSCHULE DARMSTADT 1994.

[112] A. PIECHACZEK *ET AL.*, NUCL. PHYS. A584 (1995) 509.

[113] F. POUGHEON *ET AL.,* Z. PHYS. A327 (1987) 17.

[114] G.R. SATCHLER, IN *DIRECT NUCLEAR REACTIONS* (OXFORD UNIVERSITY PRESS, OXFORD, 1983), P. 786.

[115] C. SCHEIDENBERGER, COMPUTER CODE ATIMA.

[116] R.G. SEXTRO *ET AL.*, NUCL. PHYS. A234 (1974)130.

[117] K. SüMMERER *ET AL.*, PHYS. REV. C42 (1990) 2546.

[118] Y. TAKEEUCHI, 1997, IN '97 ELECTROWEAK INTERACTIONS & UNIFIED THEORIES, EDITED BY J. TRAN THANH VAN (EDITIONS FRONTIERES, PARIS), P. 335.

[119] X. TANG, MASTER THESIS, CHINA INSTITUTE OF ATOMIC ENERGY, 1997.

[120] Y. TOTSUKA, NUCL. PHYS. B (PROC. SUPPL.) 48 (1996) 547.

[121] I.S. TOWNER, NUCL. PHYS. A216 (1973) 589.

[122] W. TRINDER, COMPUTER CODE EFFPROT.

[123] W. TRINDER *ET AL.*, PHYS. LETT. B348 (1995) 331.

[124] W. TRINDER *ET AL.*, PHYS. LETT. B349 (1995) 267.

[125] P. Kunz, computer code DWUCK4.

[126] W. Liu, X. Bai, S. Zhou et al., Phys. Rev. Lett. 77 (1996) 611.

[127] W. Liu, Z. Li, X. Bai et al., Nucl. Phys. A 728 (2003) 275.

[128] T. Kajino and R. N. Boyd, Astrophys. J. 359 (1990) 267.

[129] K. Ogata, M. Yahiro, Y. IseriH et al., Phys. Rev. C 67 (2003) 011602(R).

[130] H. Kobayashi, K. Ieki, A. Horvath et al., Phys. Rev. C 67 (2003) 015806.

[131] Y. Wang, W. Liu, X. Bai et al., Chin. Phys. Lett. 16 (1999) 873.

[132] Z. H. Li, W. P. Liu, Z. H. Li et al., Phys. Rev. C 71 (2005) 052801(R)

[133] B. Guo, Z. H. Li, W. P. Liu et al., Nucl. Phys. A 761 (2005) 162

[134] X. Tang et al., Phys. Rev. C **69**, 055807 (2004)

[135] Z. H. Li et al., submitted to Phys. Rev. C.

[136] W. P. Liu et al., TRIUMF proporsal E983.

[137] B. Guo, W. P. Liu et al.,High Ene. Phys. and Nucl. Phys. 30,(2006)675 (In Chinese.)

Introduction of nuclear astrophysics and related experimental techniques

Weiping Liu
wpliu@ciae.ac.cn
China Institute of Atomic Energy
August 27-31, 2011

Related lectures in this school

- Prof. Sherrill, An introduction to nuclear astrophysics, Monday
- Prof. Sakurai, New generation of nuclear physics with RIBF, Saturday-Sunday
- Prof. Zhang, Mass measurement of short-lived nuclides using CSRe in Lanzhou, Saturday

Contents

- Saturday
- Introduction
- Nuclear astrophysics basic
  - Experimental approach: direct and in-direct
- Production of unstable beams
  - PF method
  - ISOL method
- Sunday
- Some remarks about nuclear decay
- Examples of reaction: $^{7}Be(p,\gamma)^{8}B$
- Examples of decay: ^{40}Ti β-decay
- Some other selected examples

What is Nuclear Astrophysics

- Extending between macro and micro world: nuclear physics and astrophysics
- Application of nuclear physics in energy production and element synthesis in star
- Determining time scales of evolution, star environment, isotope abundance
- In combination with astrophysical model and observation
- Using nuclear mass, cross section, half-life as input
- Difficulty: low cross section due to low energy and high isospin

Contribution of nuclear physicist, Nobel prize of physics winner

- 1930, Hans Bethe, pp chain, CNO cycle, 1967

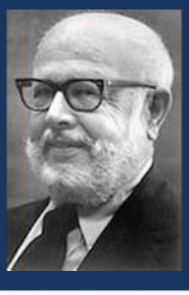

- 1957, William Fowler, star evolution, B^2FH, 1983

- 1960, Raymond Davis and Masatoshi Koshiba, neutrino detection, 2002

Some of the great discovery of astrophysics

- 3K microwave background radiation,1965, experimental support for Big-Bang theory
- Detection of solar neutrino, 1960, gave the hints of neutrino oscillation
- Detection of ^{26}Al γ-ray, 1980, direct support of explosive nuclear synthesis, and triggering γ-ray astronomy
- Detection of SN1987A supernova explosion,1987
- Experimental explanation of solar neutrino missing, 2003

Nuclear reaction: alchemist in universe

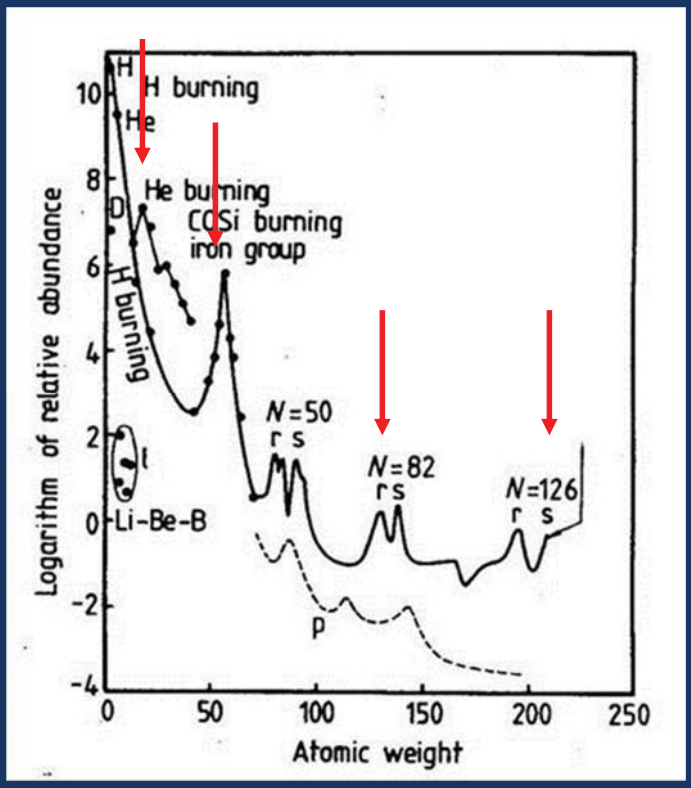

Peak: finger print of nuclear physics: Shell model magic number

Primordial and stellar elements syntheses

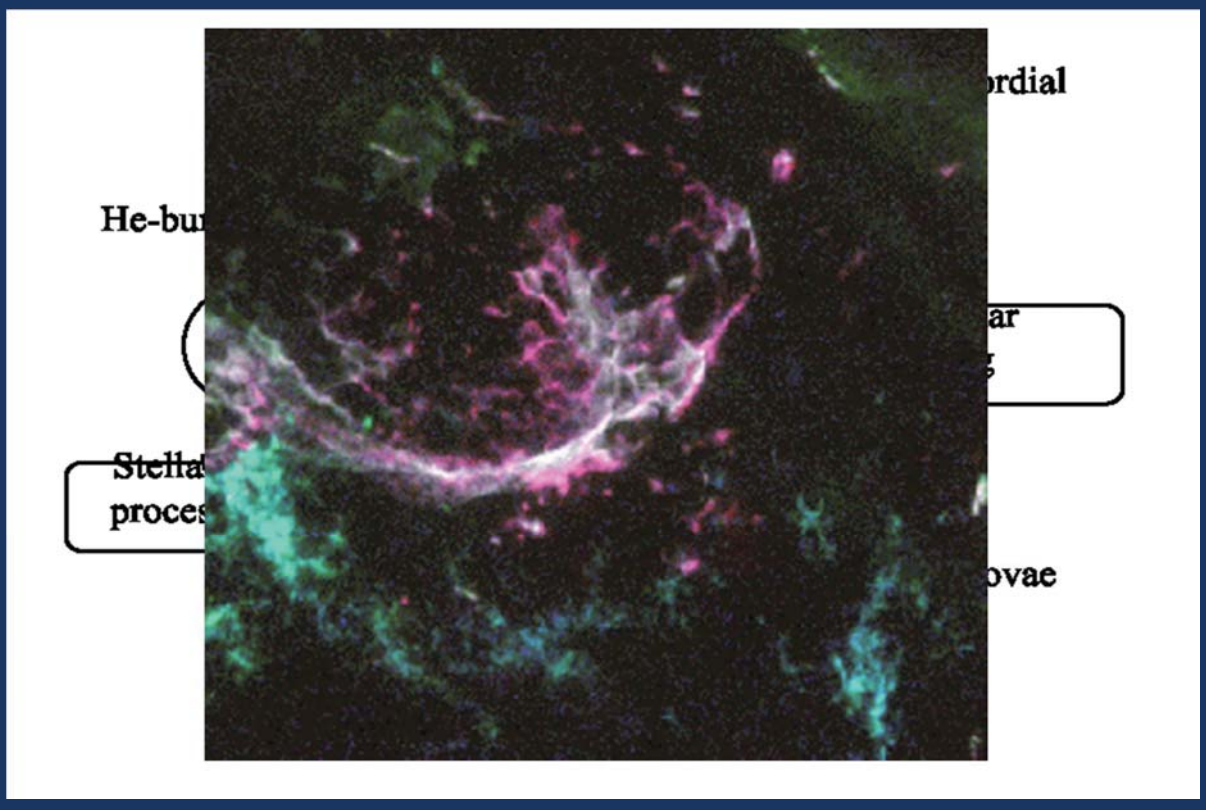

Astrophysical process in chart of nuclei

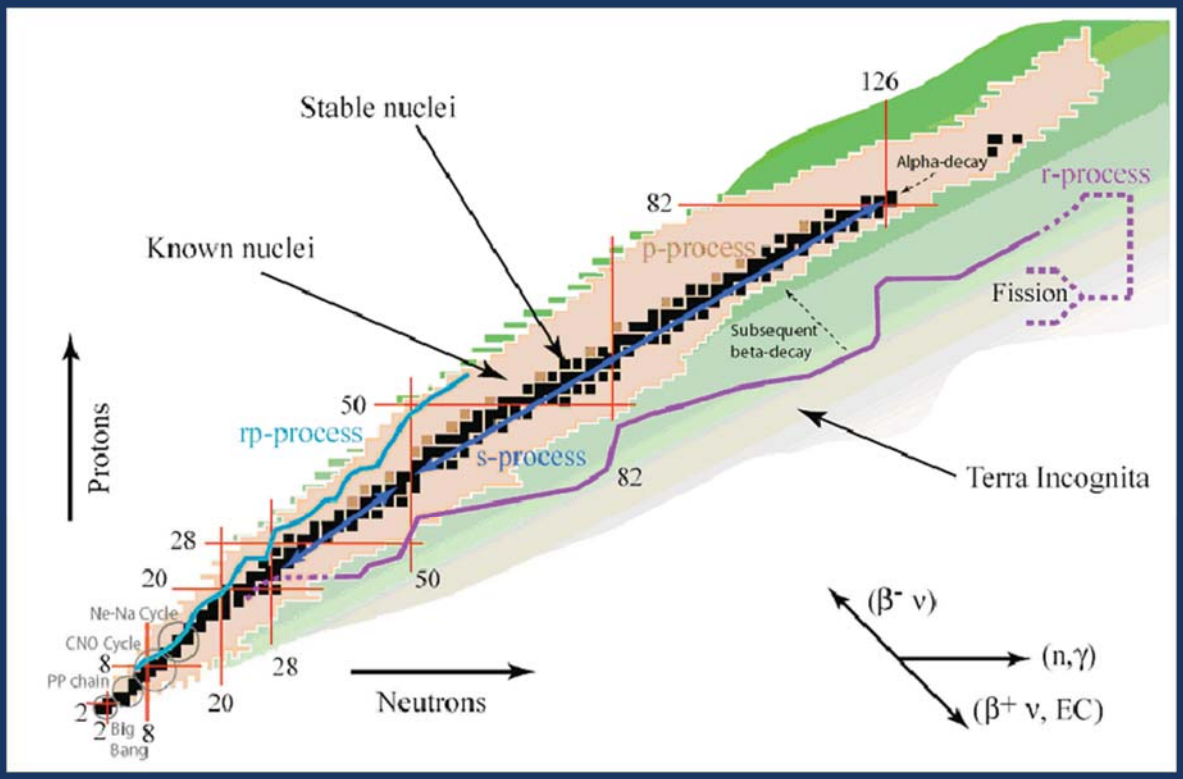

The interplay between nuclear physics and astrophysics

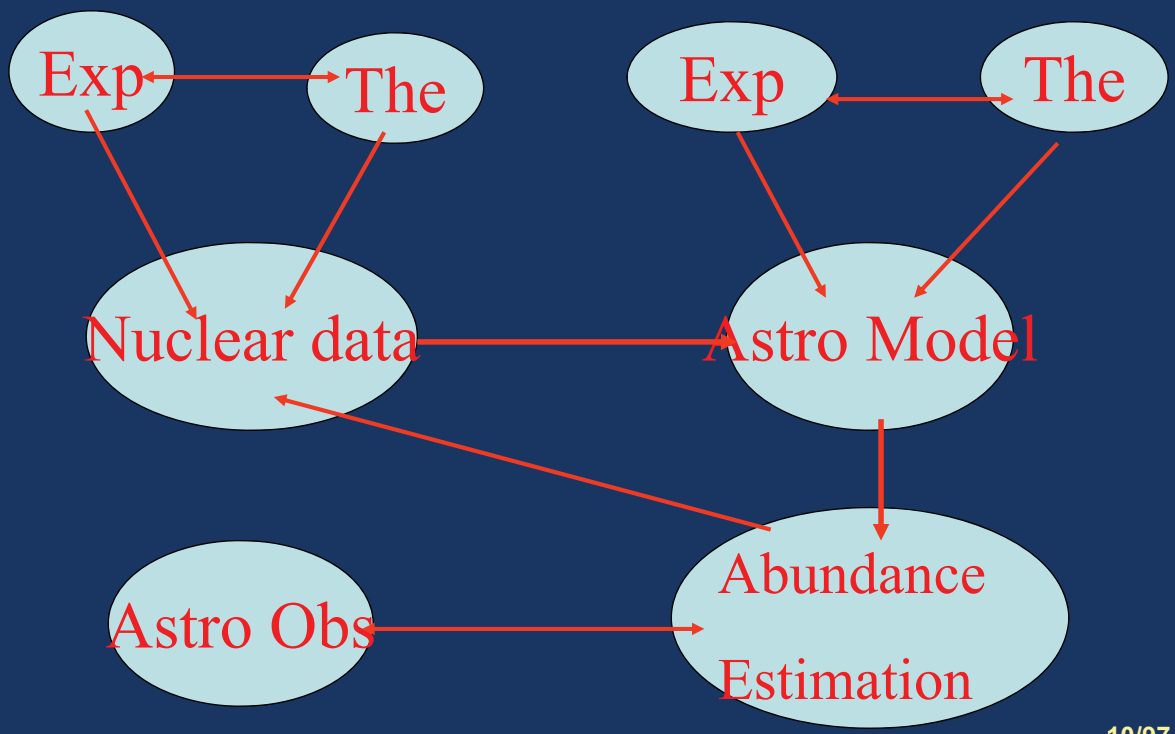

Element synthesis network

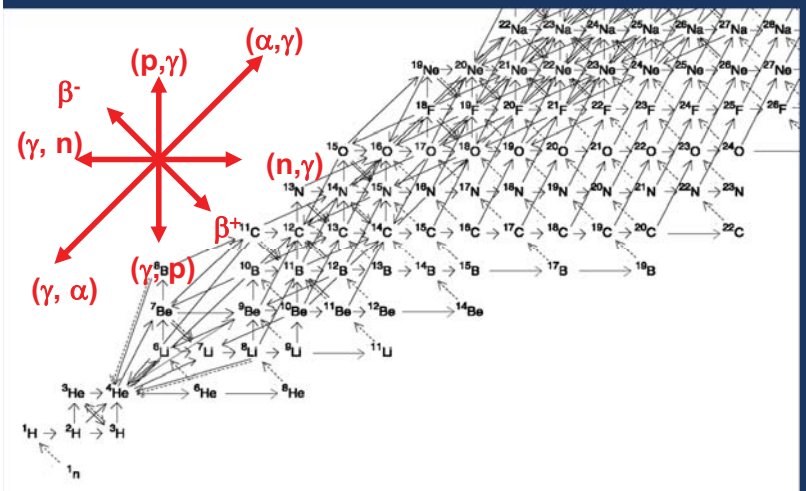

Cross section

$$\frac{dY_i}{dt} = \sum_j N_i^j \lambda_j Y_j + \sum_{j,k} N_{j,k}^i \rho N_A < \sigma V >_{jk,i} Y_j Y_k$$

$$+ \sum_{j,k,l} N_{j,k,l}^i \rho^2 N_A^{\,2} < \sigma V >_{jkl,i} Y_j Y_k Y_l$$

Decay half-life

Abundance curve

NUCLEAR ASTROPHYSICS is concerned with

- the origin of elements in stellar burning
- the production of energy in stars and stellar explosions

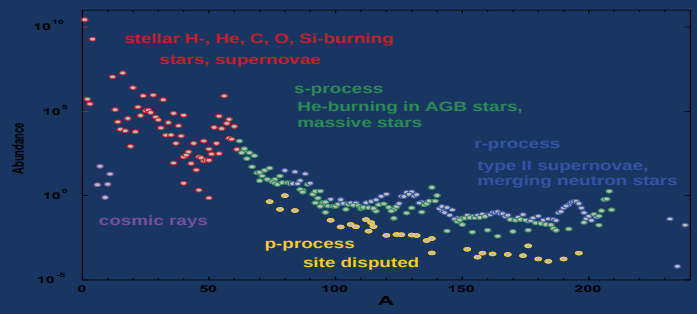

observational signatures are

- abundance distributions
- luminosities

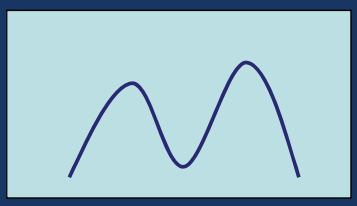

Light curve

↓ /$\sigma_{\text{atomic transition}}$

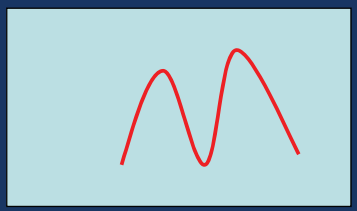

Abundance curve

From DOE 2007 plan

- Nuclei and Nuclear Astrophysics
  - What is the nature of the nuclear force that binds protons and neutrons into stable nuclei and rare isotopes?
  - What is the origin of simple patterns in complex nuclei?
  - What is the nature of neutron stars and dense nuclear matter?
  - What is the origin of the elements in the cosmos?
  - What are the nuclear reactions that drive stars and stellar explosions?

The importance of one and more experiments

- Key reaction, most difficult, like $^{12}C(\alpha,\gamma)^{16}O$, $^{7}Be(p,\gamma)^{8}B$
- Supporting reaction, large numbers, like $^{11}C(p,\gamma)$, $^{8}Li(\alpha,n)$
- Importance of international collaboration, data evaluation and compilation
- Importance of theoretical calculation, fill the impossible

Status of China

- Th
- O aya Ba
- Nu La
- M roup fu
- Ne
- In Bochum, JINA, RIKEN, GSI, MSU…)

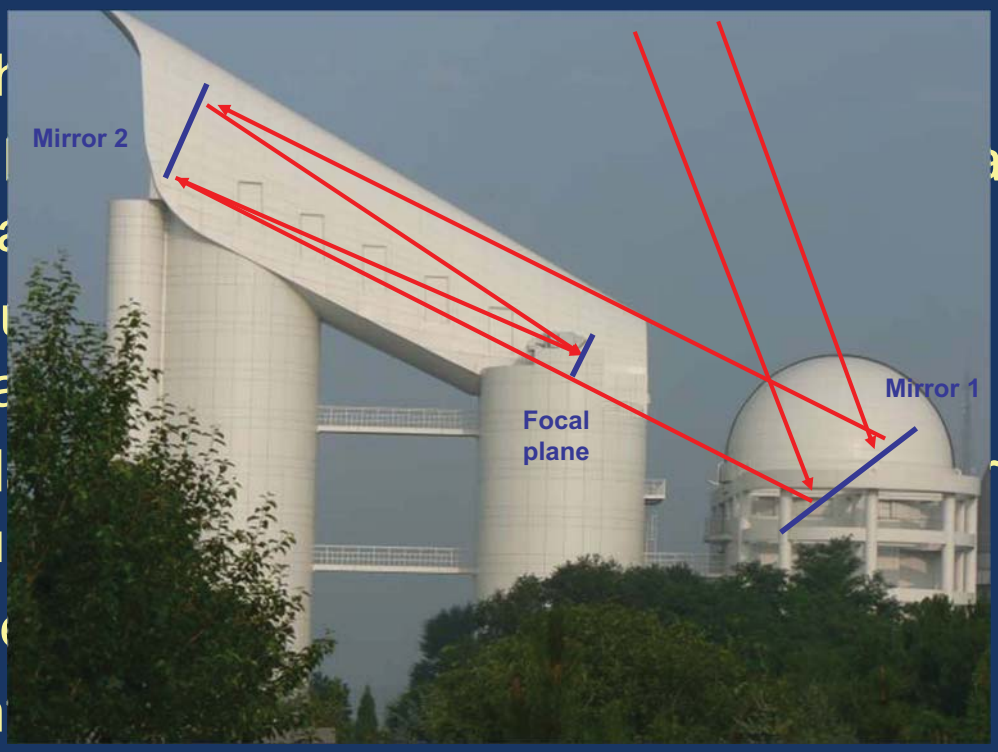

Important nuclear physics data

- S-factor, focus on NP, down to astrophysics energies
- Reaction rates, direct input to network calculation
- Direct capture, direct reactions
- Resonance, level scheme, level width, and partial width
- Mass and decay half-life and branching ratio

Nuclear astrophysics basics

- Reaction rates
- Gamow window
- S-factor
- Direct reaction
- Resonance

Reaction rates

$$< \sigma v >= \int_0^\infty \phi(v)\sigma(v)v dv. \quad (1)$$

Maxwell-Boltzmann speed distribution is

$$\phi(v) = 4\pi v^2 (\frac{\mu}{2\pi kT})^{3/2} \exp(-\frac{\mu v^2}{2kT}), \quad (2)$$

In which, μ, k and T is reduced mass Boltzmann constant and star temperature respectively. It can be simplified into,

$$N_A < \sigma v >= 3.7313 \times 10^{10} \mu^{-1/2} T_9^{-3/2} \int_0^\infty \sigma(E) E \exp(-11.605 E/T_9) dE, \quad (3)$$

Where the reation rate $N_A < \sigma v >$ is in the unit of $cm^3 mol^{-1} s^{-1}$ and center of mass energy E and corss section σ are in the unit of MeV and b.

C.E. Rolfs and W.S. Rodney, Cauldron in the Cosmos, The University of Chicago Press, (1988).

Astrophysical S-factor

The reaction cross section can be re-scaled into astrophysical S-factor,

$$\sigma(E) = S(E)\exp(-2\pi\eta)\frac{1}{E}, \quad (4)$$

Where η is Sommerfeld constant,

$$\eta = \frac{Z_1 Z_2 e^2}{\hbar v} = 0.1575 Z_1 Z_2 (\frac{\mu}{E})^{1/2}, \quad (5)$$

Where $\hbar$ is reduced Plank constant, Z_1 and Z_2 are atomic number, E is the center of mass energy in MeV.

C.E. Rolfs and W.S. Rodney, Cauldron in the Cosmos, The University of Chicago Press, (1988).

Energy dependence of cross section and astrophysical S-factor

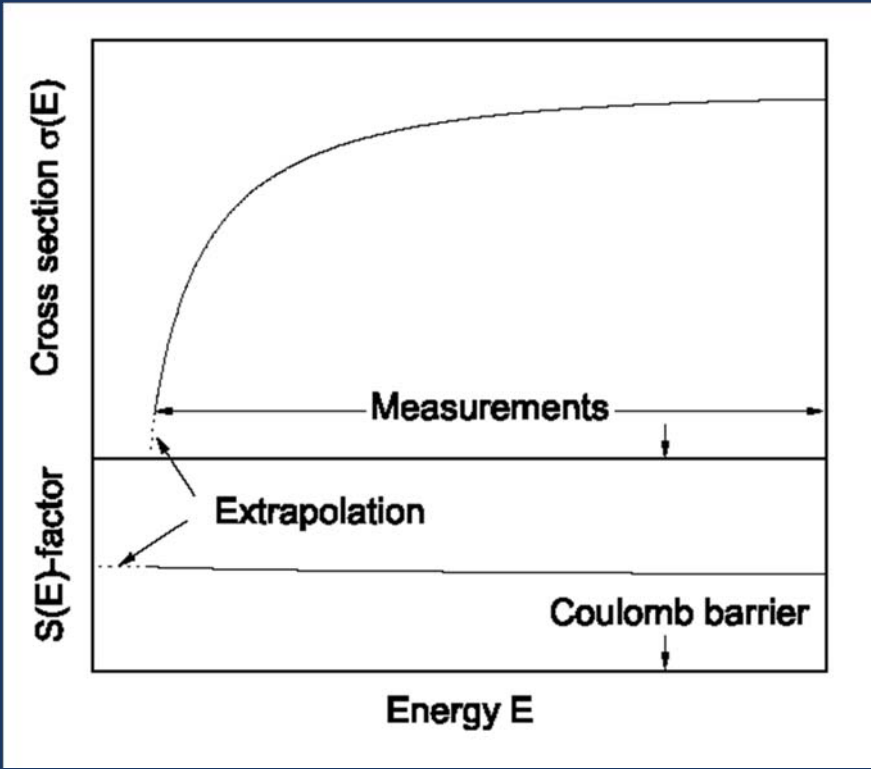

Gamow window

$$N_A < \sigma v >= N_A(\frac{8}{\pi\mu})^{1/2}\frac{1}{(kT)^{3/2}}\int_0^\infty S(E)\exp(-\frac{E}{kT}-\frac{b}{E^{1/2}})dE, \qquad (6)$$

b come from Coulomb penetration

$$b = (2\mu)^{1/2}\pi e^2 Z_1 Z_2/\hbar = 0.989 Z_1 Z_2 \mu^{1/2}(\mathrm{MeV})^{1/2}. \qquad (7)$$

Its square is so called Gamow energy E_G.

In exponential part of Equ. 6, the first term come from Maxwell-Boltzmann velocity distribution, the second term is Coulomb term, the interplay of two terms reach a maximum in E_0, as shown in Fig. 4. Where the effective mean energy E_0 can be expressed as:

$$E_0 = (bKT/2)^{2/3} = 1.22(Z_2^1 Z_2^2$$

$\mu T_6^2)^{1/3} keV(8)$

It is E_0 that is most important parameter for experimentalists to reach directly or in-directly. For system p+p, , for sun T_6=15, E_0 is only 5.9 keV!

The Gamow window

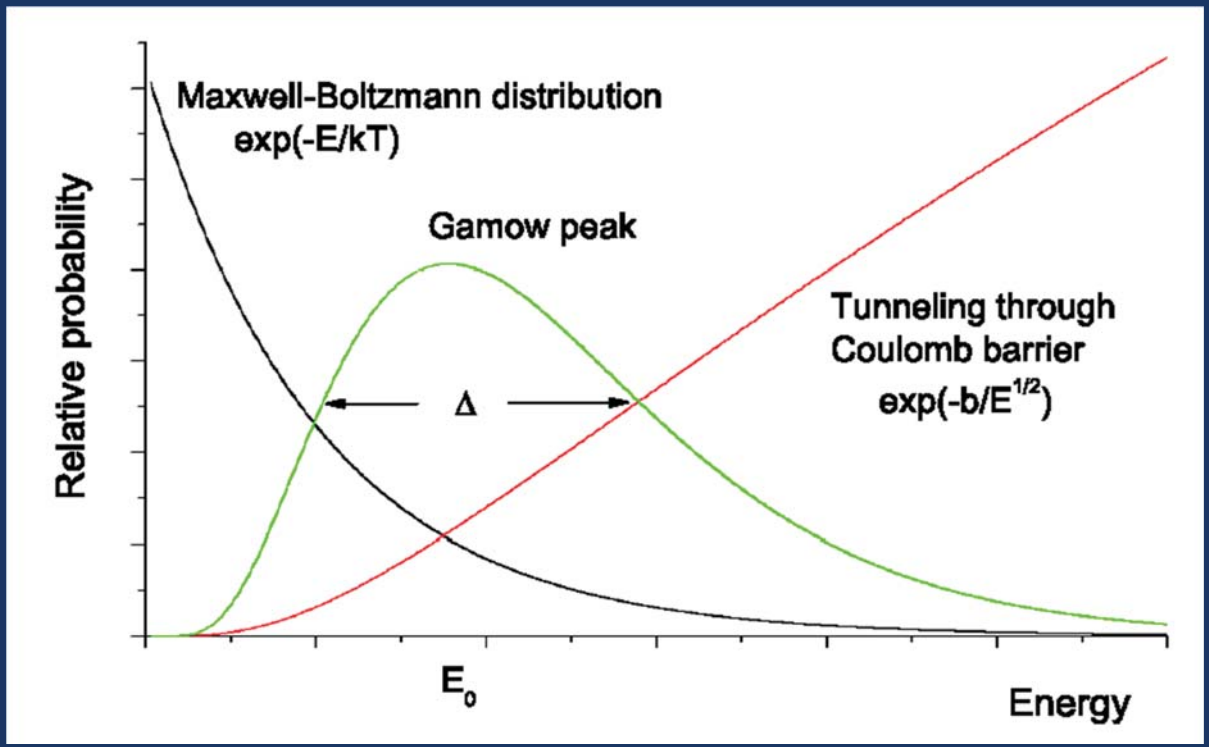

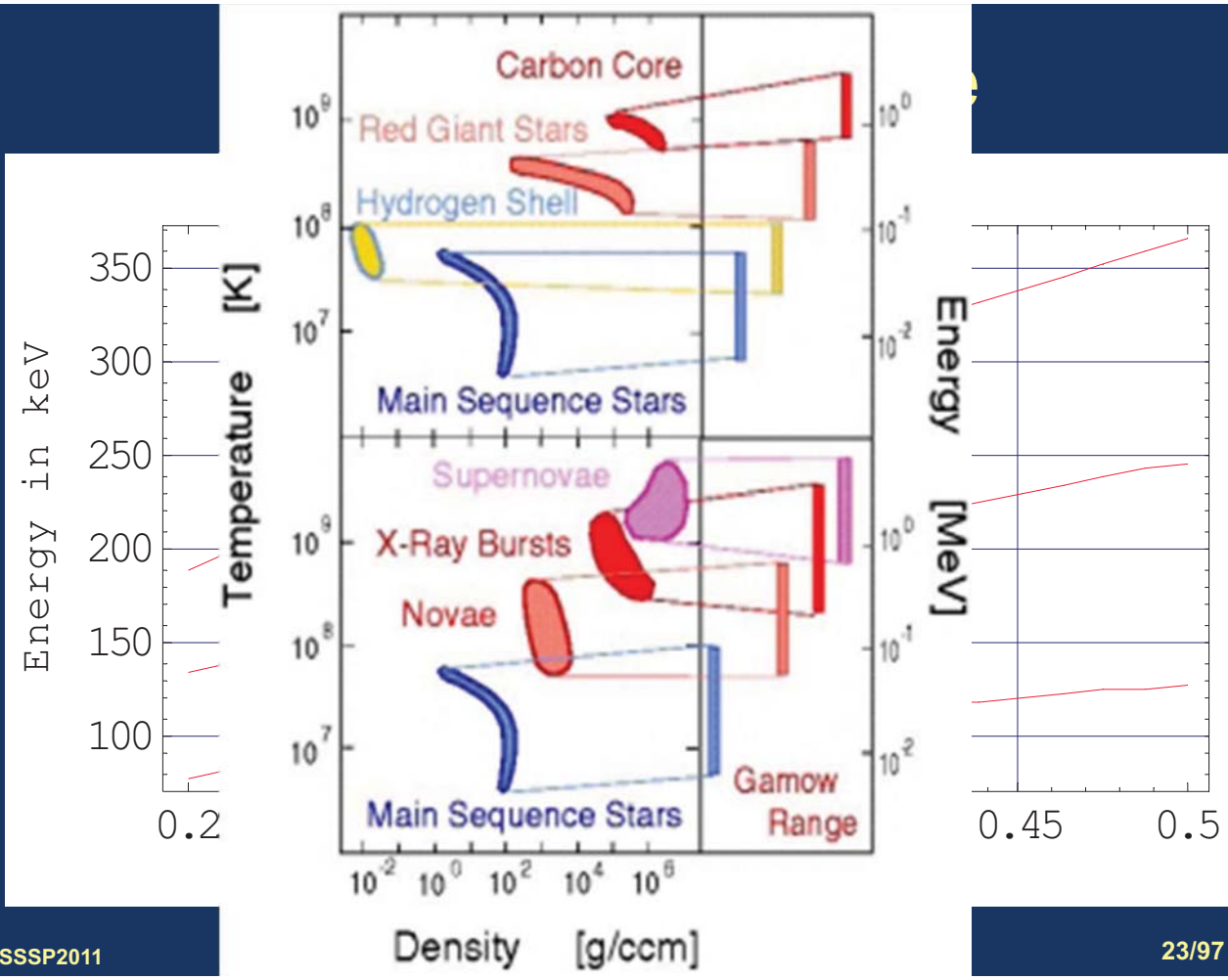

Resonance capture

The resonance capture reaction cross section can be expressed by Breit-Wigner formula [17],

$$\sigma_{BW}(E) = \pi \frac{\hbar^2}{2\mu E} \frac{2J_R + 1}{(2J_1 + 1)(2J_2 + 1)} \frac{\Gamma_{in}(E)\Gamma_{out}(E)}{(E - E_R)^2 + (\Gamma_{tot}/2)^2}, \quad (9)$$

Where J_1, J_2, J_R is the spin of beam, target and compound state respectively, Γ_{in}, Γ_{out} are entrance channel partial width, Γ_{tot} is the total width.

Experimental approach

- Direct

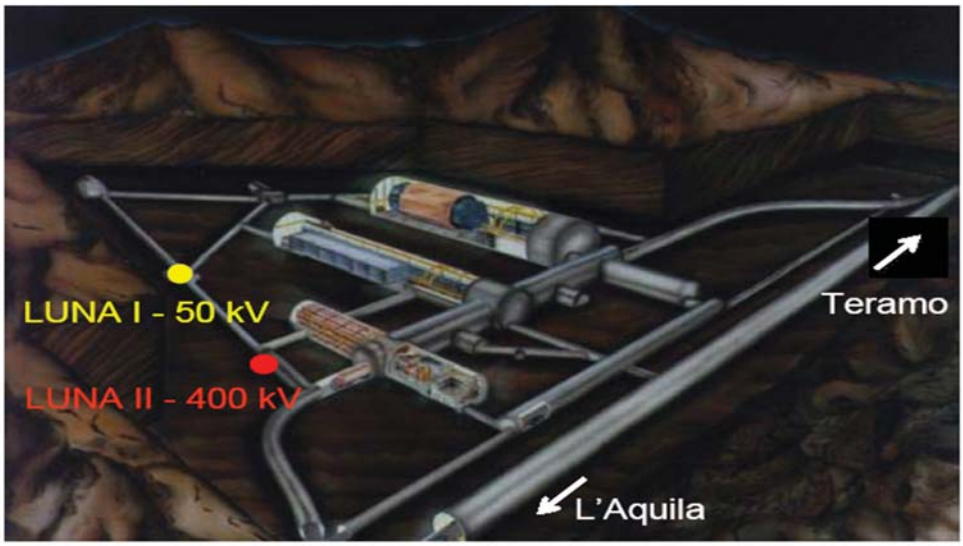

- I
- D

all for

- R
  - CIAE
  - (d,p) and the like, ORNL

Why unstable beam

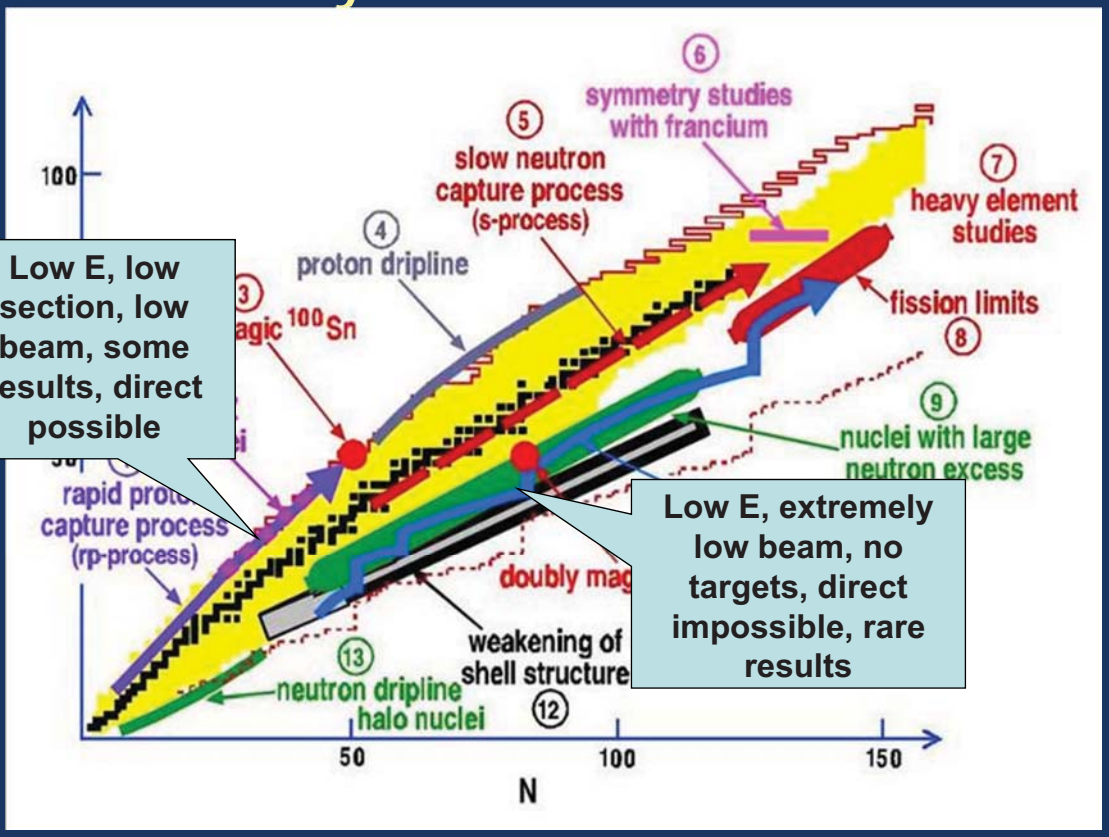

Experimental technique of unstable beam physics

产生 Production → 初级加速器或反应堆+靶 Acc. or reactor+target

电离 Ionization → 离子源系统 剥离 Ion source

纯化 Purification → 离子分离separation E, B, ΔE/Δx, 离子井

加速/减速/储存 Acc. Decc./storage → 后加速器/储存环/离子井 Post acc. ring, trap

测量Measurement: 鉴别Identification 反应/衰变/基态性质 reaction/decay → 谱仪/探测器/数据获取和分析 Spect. Det. DAQ, analysis

Wei-ping Liu, E983 Proposal@DRAGON

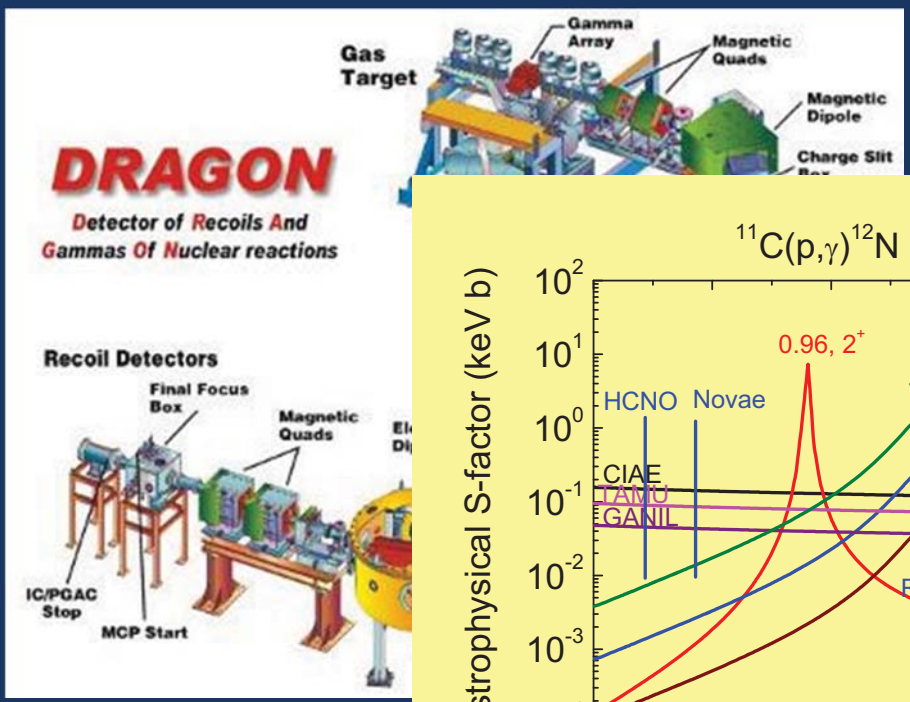

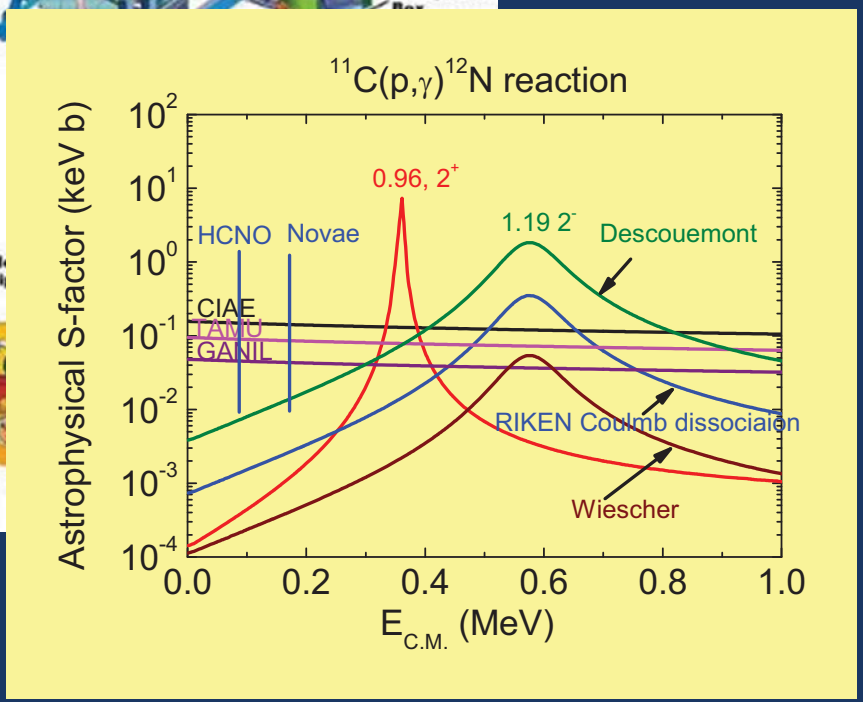

Production of unstable beams

- PF method
  - Formulae
  - FRS example
  - Transfer as special case, CIAE example
- ISOL method
  - Comparison
  - GSI example

Some essential about fragmentation I

- $V_{frag}=V_{beam}$
- A momentum broadening of Fermi momentum
- Memory effect of beam iso-spin
- A broad distribution of fragments with a narrow angular range due to inverse kinematics

$$\sigma_{||} = \sigma_0 \sqrt{A_F\left(A_P - A_F\right)\left(A_P - 1\right)}$$

$$\sigma_0 \approx 90 MeV/c$$

$$\sigma\left(A_F, Z_F\right) = Y(A) e^{-R\left(Z_P - Z_F\right)^{1.5}}$$

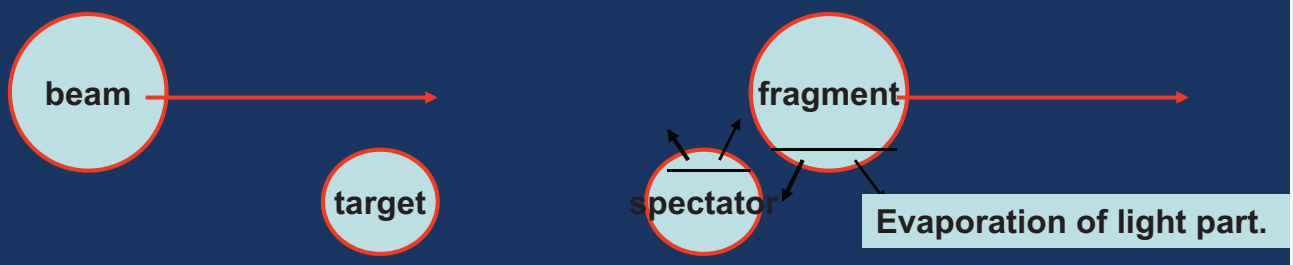

Particle identification

$B\rho = p/q = A\beta\gamma/q = B\rho_0(1 + x/d)$

with $\gamma = 1/(1-\beta^2)^{1/2}$, where E and ΔE are the total energy and energy-loss of the ion, Z and q its atomic number and charge state, x and d its position and the dispersion in the focal plane.

For the case of $q = Z$, which is valid in the energy of multi-hundred·A MeV,

$Z \propto (\Delta E)^{1/2}$,

$TOF \propto A/Z$.

where *TOF* is the time of flight of an ion.

In general, the atom is not fully stripped, so that $q = Z, Z-1, \ldots$ As a result,

$TOF \propto A/q$,

$q \propto E$.

The detailed treatment for partially stripped charge states can be found in [95].

For the velocity filter, $v \propto B/E$, where B and E stand for the magnetic field and electric field of the filter, respectively. Because this technique needs high electric field, it can only be applied to low energy transfer reaction.

Basic components of a electromagnetic device

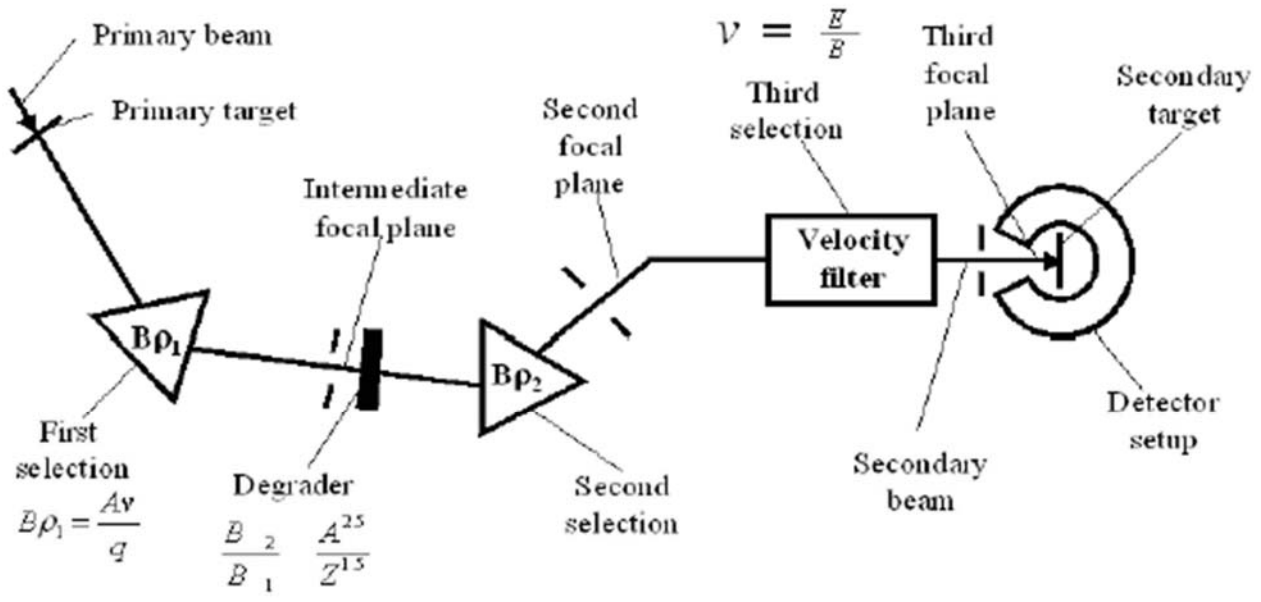

FRS example

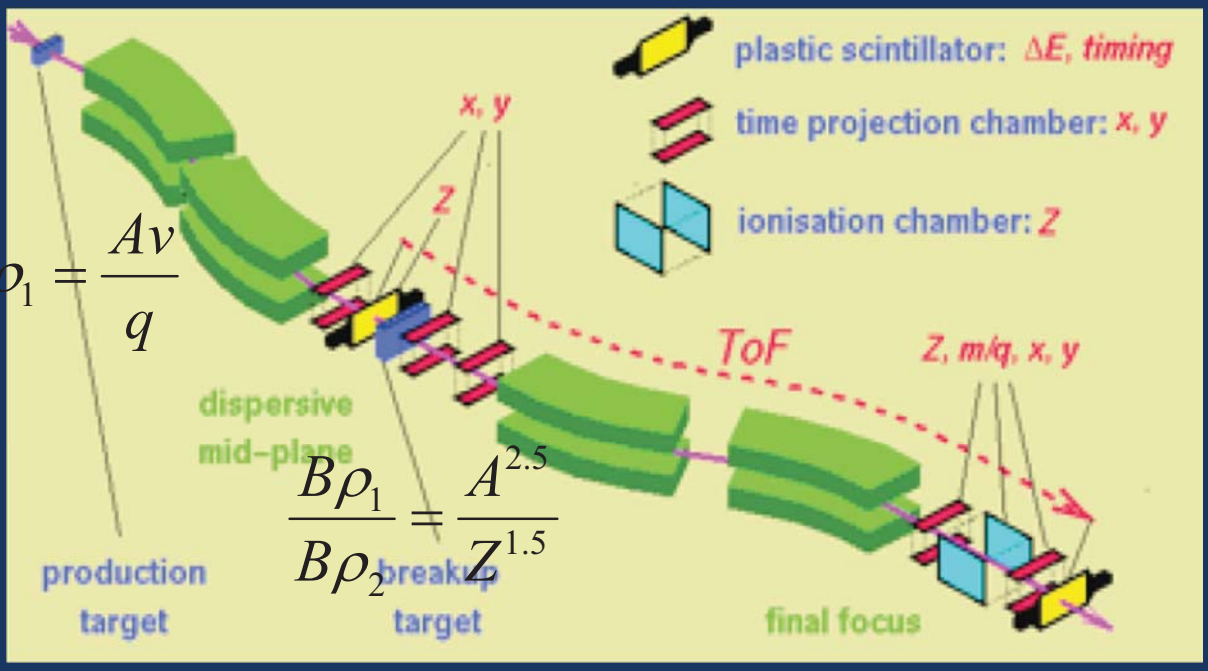

$$B\rho_1 = \frac{Av}{q}$$

$$\frac{B\rho_1}{B\rho_2} = \frac{A^{2.5}}{Z^{1.5}}$$

Some essential about fragmentation III

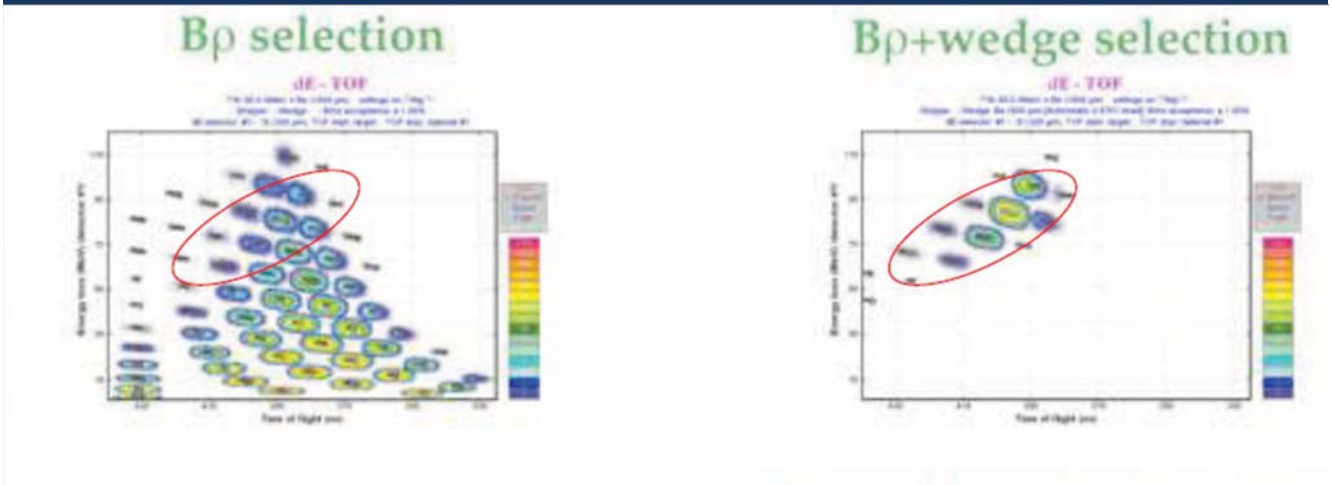

The relation between the intensity of RNB and its possible experiments

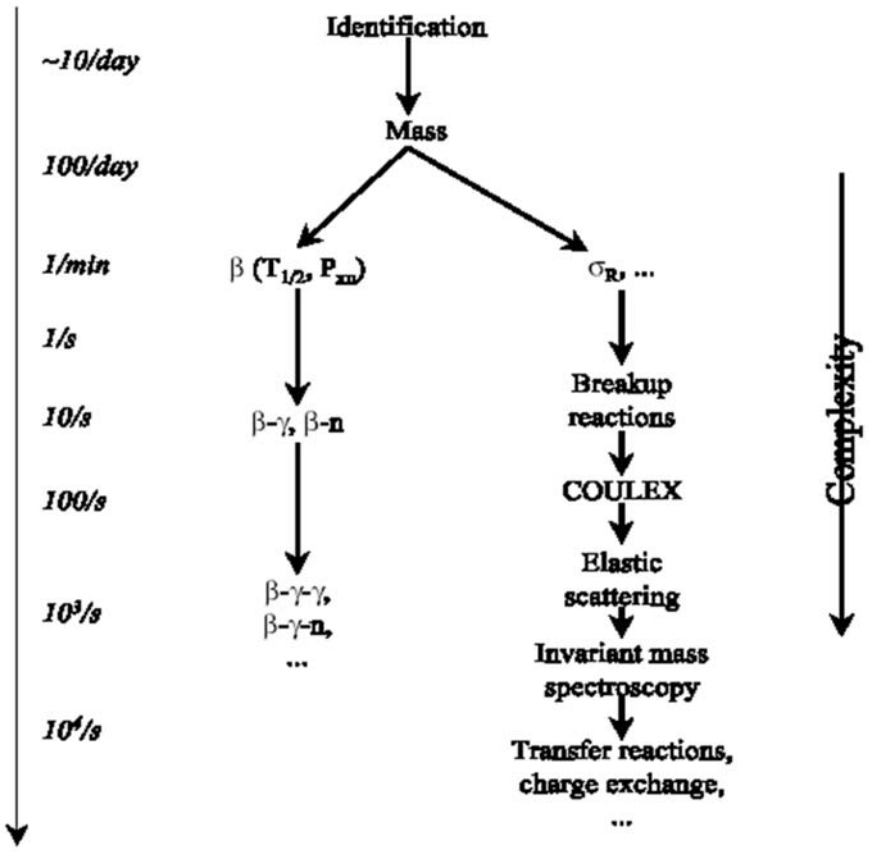

Inverse kinematics

$$\theta_{lab}^{\max} = \sin^{-1}\left(\frac{1}{\gamma}\right), \gamma > 1 \,(A_{\text{beam}} > A_{\text{target}})$$

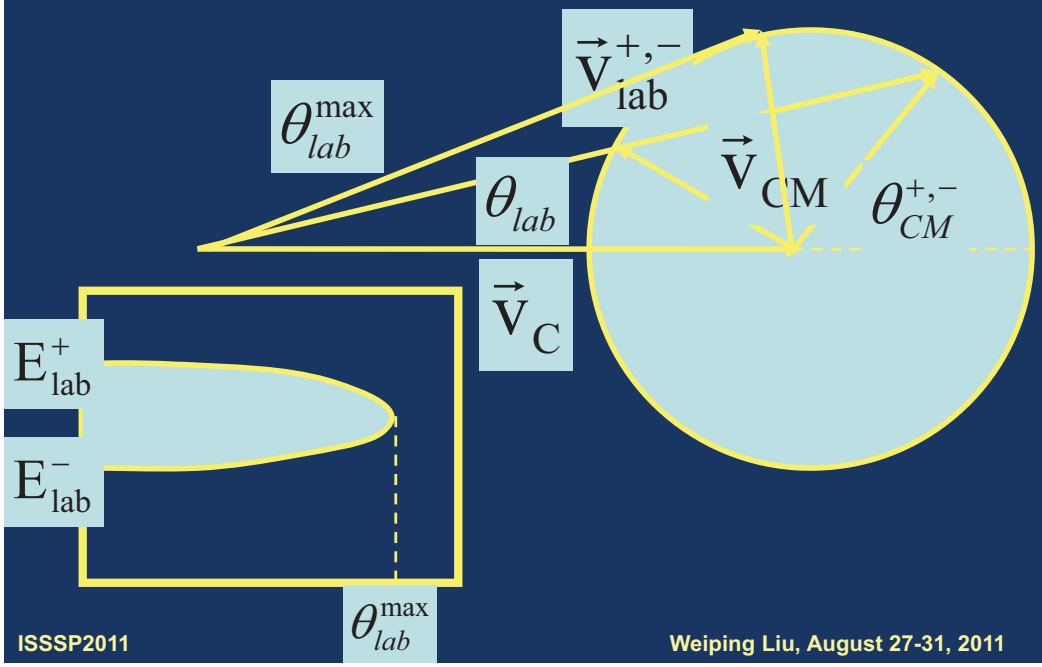

Bρ and dσ/dΩ vs. θ_{lab} of ^{7}Be

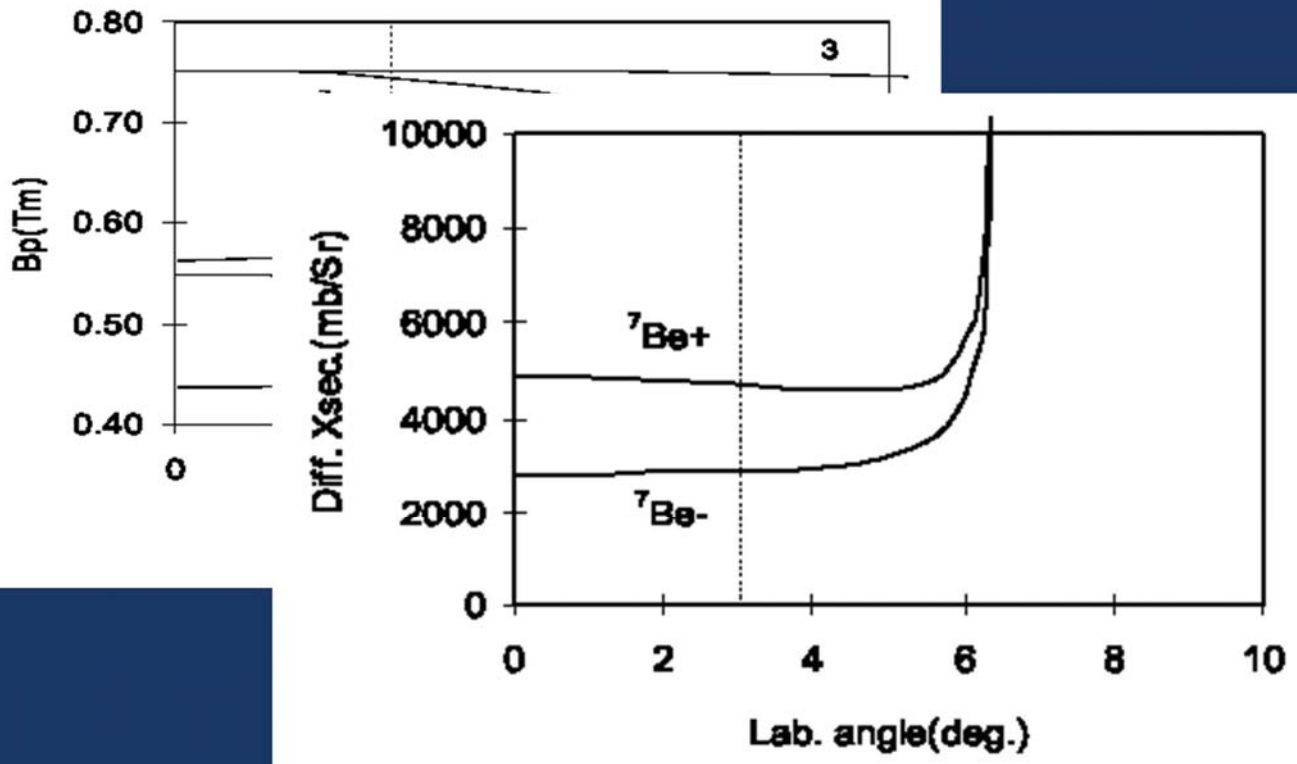

Beam optics of GIRAFFE

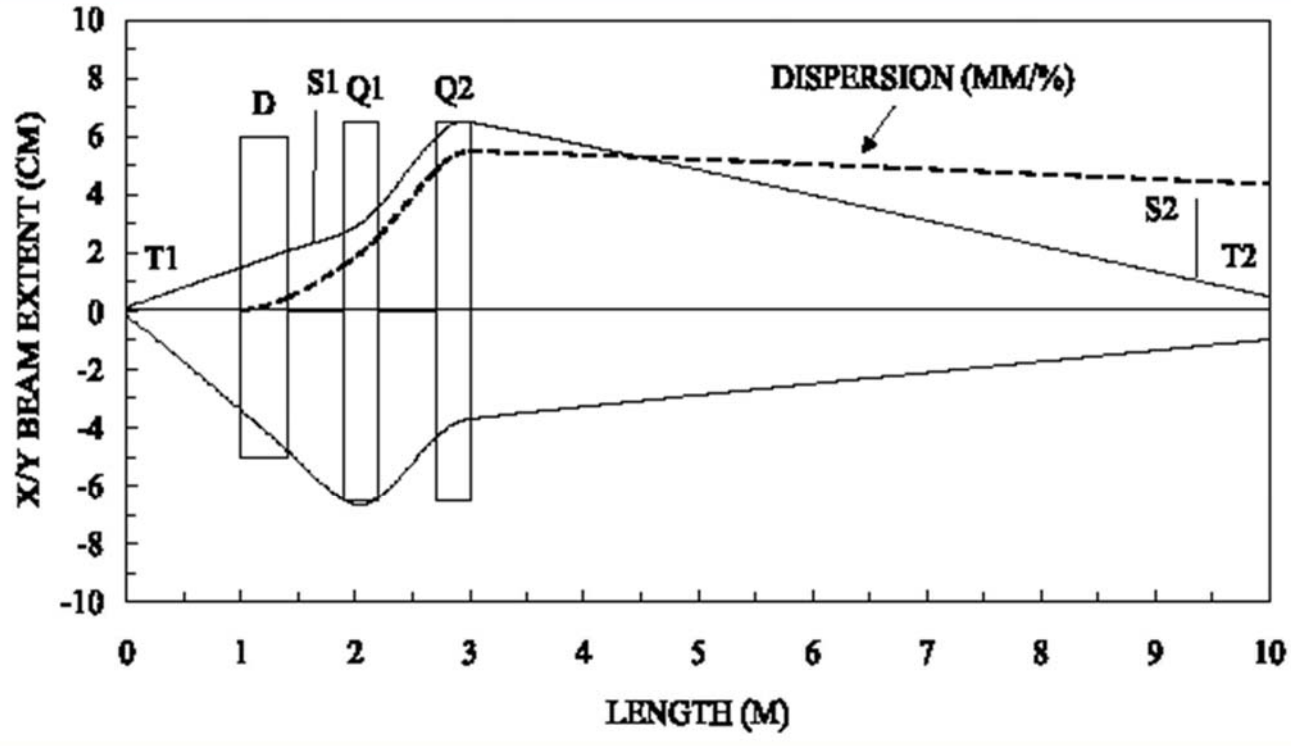

The sketch of GIRAFFE

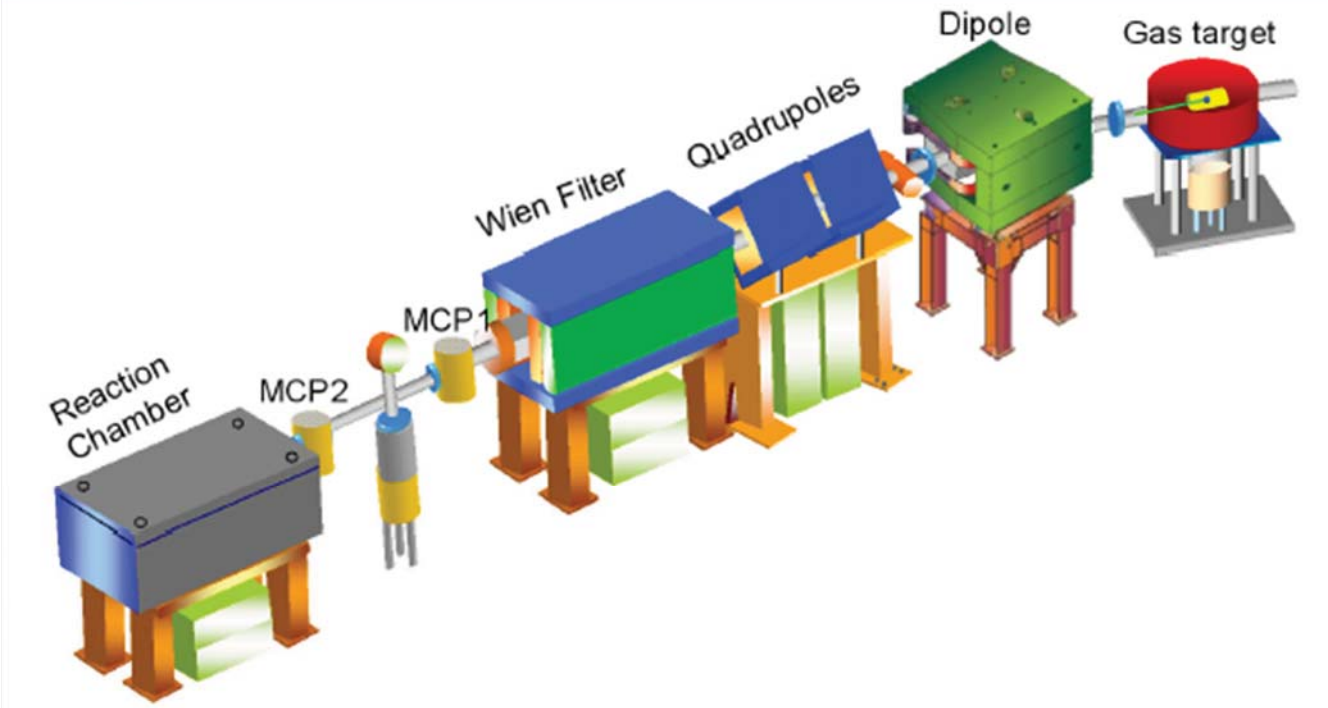

Some of the production reaction for secondary beams and the estimated characteristics of resulted beams

RNB	Production reaction	E_{beam} (MeV)	$d\sigma/d\Omega$ (mb/Sr)	E_{RNB} (MeV)	$\Delta B\rho/B\rho$ (%)	Intensity* (pps)
^{6}He	^{2}H(^{7}Li,^{6}He)^{3}He	42.0	160+	34.0±1 .0	17.3	2.2×10^{5}
^{7}Be	^{1}H(^{7}Li,^{7}Be)n	35.0	5000+	33.0±0.5	-3.1	1.4×10^{7}
^{8}Li	^{2}H(^{7}Li,^{8}Li)^{1}H	42.0	900+	40.0±0.5	5.2	1.2×10^{6}
^{11}C	^{1}H(^{11}B,^{11}C)n	78.1	6700-	57.0±1.0	-17.5	4.5×10^{6}
^{12}B	^{2}H(^{11}B,^{12}B)^{1}H	66.0	1100+	65.0±1.0	6.3	1.5×10^{6}
^{13}N	^{2}H(^{12}C,^{13}N)n	70.8	3000+	70.0±1 .0	-9.7	2.1×10^{6}
^{15}O	^{2}H(^{14}N,^{15} O)n	84.0	8300+	82.0±1 .0	-12.7	3.7×10^{6}
^{17}F	^{2}H(^{16}O,^{17}F)n	88.0	28000+	85.0±0.3	-10.8	1.3×10^{7}

Summary of produced RNB in GIRAFFE

RNB	Reaction	Energy±Spread (MeV)	Purity (%)	intensity (pps) †
^{6}He	^{2}H(^{7}Li,^{6}He)^{3}He	35.7 ± 0.5	92	500
^{7}Be	^{1}H(^{7}Li,^{7}Be)n	30.8 ± 1.3	99	900
^{8}Li	^{2}H(^{7}Li,^{8}Li)^{1}H	40.0 ± 0.5	88	500
^{10}C	^{1}H(^{10}B,^{10}C)n	55.9 ± 3.5	96	200 ‡ §
^{11}C	^{1}H(^{11}B,^{11}C)n	63.4 ± 2.7	80	1000
^{13}N	^{2}H(^{12}C,^{13}N)n	57.8 ± 2.1	92	1200 ‡
^{15}O	^{2}H(^{14}N,^{15}O)n	66.0 ± 3.6	91	800 ‡
^{17}F	^{2}H(^{16}O,^{17}F)n	76.1 ± 3.7	90	2000 ‡
^{18}F	^{3}He(^{16}O,^{18}F)^{1}H	75.7 ± 2.2	85	800 ‡
^{19}Ne	^{4}He(^{16}O,^{19}Ne)n	56.6 ± 3.4	47	120 ‡ §
	^{3}He(^{19}F,^{19}Ne)^{3}H	68.6 ± 3.8	42	70 ‡ §
^{22}Na	^{4}He(^{19}F,^{22}Na)n	52.9 ± 1.9	57	100 ‡ ¶

† With ϕ3 mmdiameter collimator.
‡ With velocity filter.
§ Primary beam intensity can be increased by a factor of 2.
¶ Primary beam intensity can be increased by a factor of 10.

Next generation RI facility

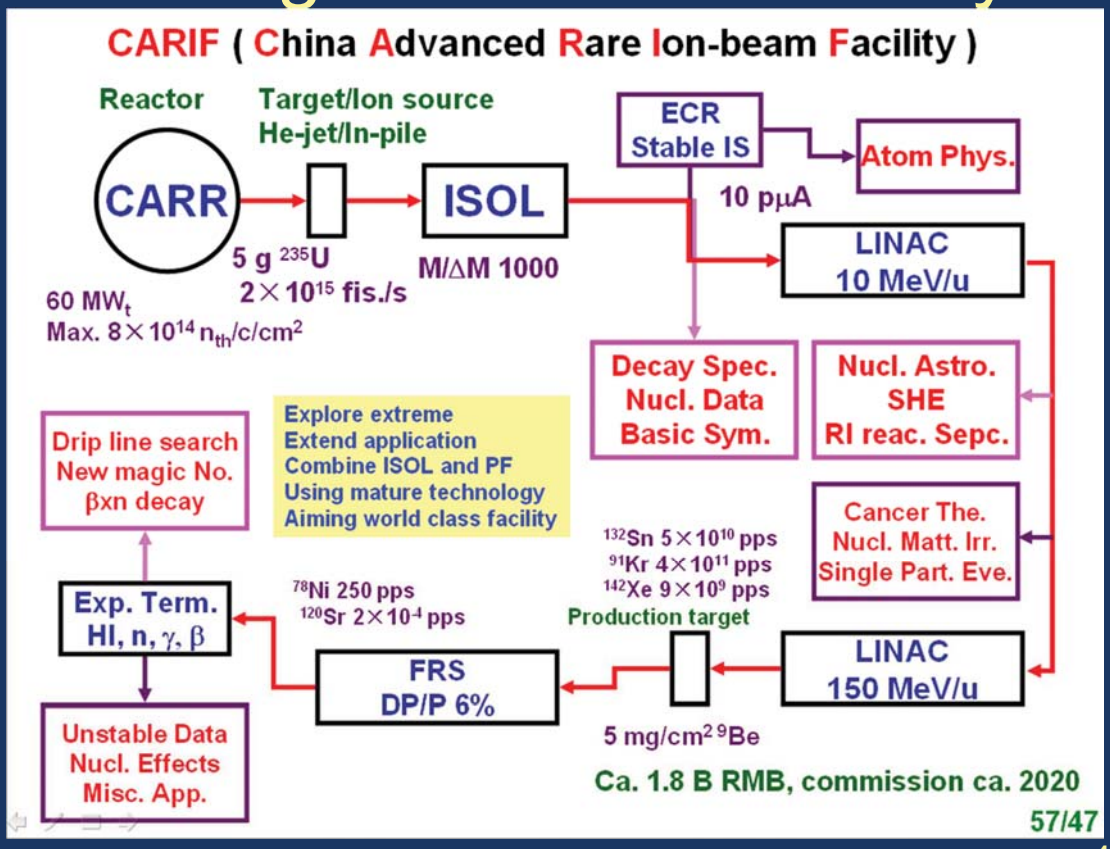

End of the first part, discussion, questions

Some remarks about nuclear decay

- Selection role
- Fermi and Gamow-Teller
- Shell model basic

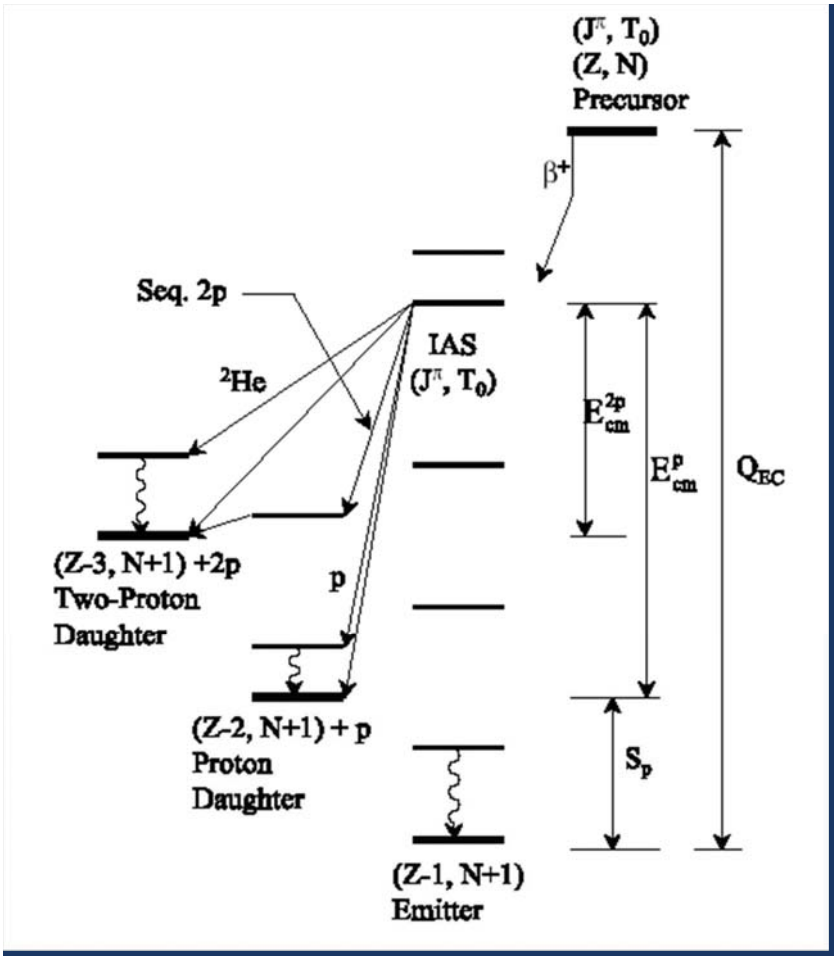

Schematic illustration of b-delayed proton emission process

Some basics about β-decay

$$\lambda = \frac{1}{2\pi^3\hbar^7 c^5}\left|M_{fi}\right|^2 \int_0^{E_0} F(Z,E)(E_0 - E)^2\, pEdE$$

$$\left|M_{fi}\right|^2 = g_V^2\langle l\rangle^2 + g_A^2\langle\sigma\rangle^2$$

$$ft = \frac{2\pi^3(\ln 2)\hbar^7 / m_e c^4}{\left|M_{fi}\right|^2}$$

$$ft = \frac{2\pi^3(\ln 2)\hbar^7 / m_e{}^5 c^4}{g_V^2\langle l\rangle^2 + g_A^2\langle\sigma\rangle^2}$$

$$\langle l\rangle^2 = T(T+1) - T_{Z_i}T_{Z_f}$$

$$\langle l\rangle = \left\langle \psi_f \left| \sum_j \sigma(j)\tau_{\pm} \right| \psi_i \right\rangle$$

List of classification of β-transition and corresponding selection roles

Class	logft	L	Fermi transition		Gamow-Tellor transition	
			ΔI	Δπ	ΔI	Δπ
Super	2.9-3.7	0	0	No	(0), 1	No
Allowed	< 5.9	0	0	No	(0), 1	No
1^{st} for-bidden	> 8.0	1	(0), 1	Yes	0, 1, 2	Yes
2^{nd} for-bidden	> 10.6	2	(1), 2	No	2,3	No

Evolution of nuclear shell model from the harmonic oscillator to the shell structure

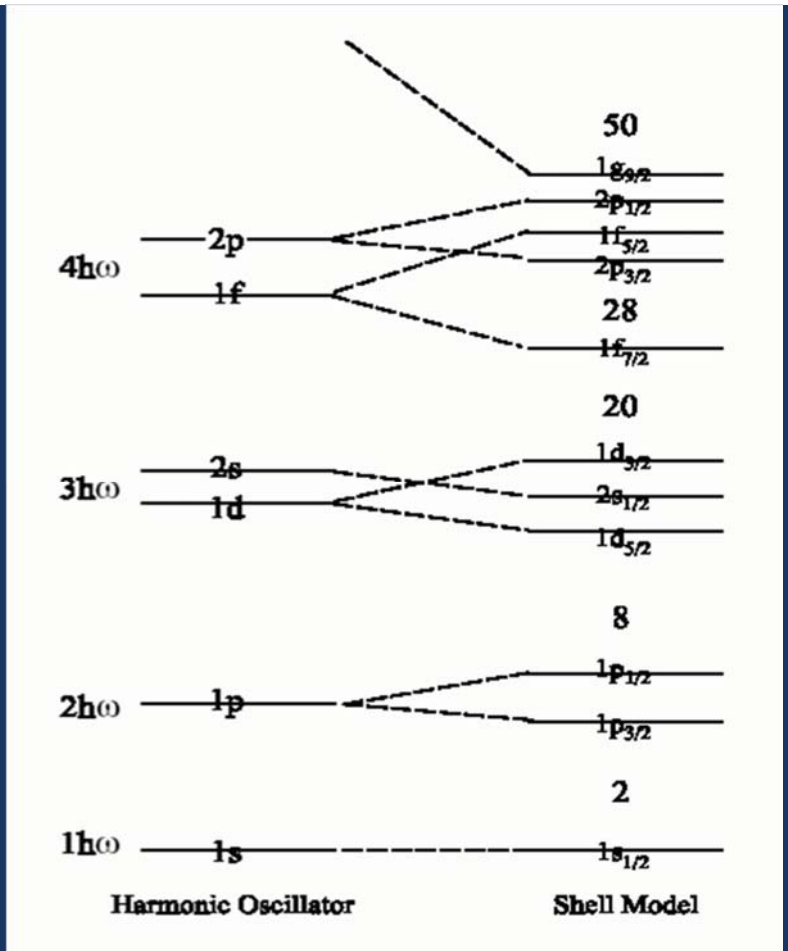

Shell quenching and r-process

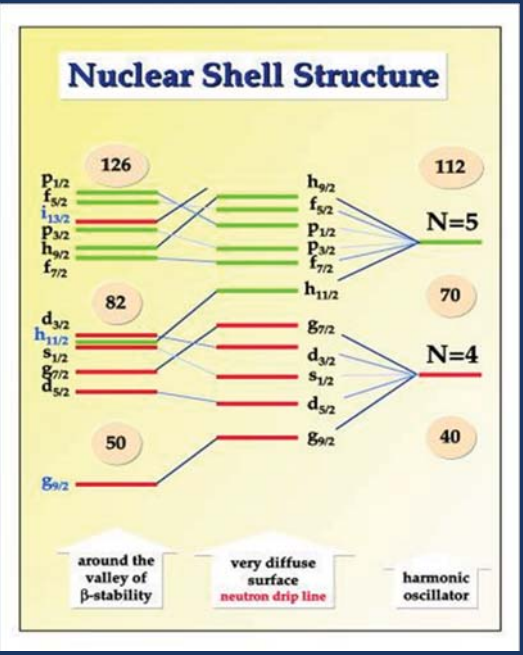

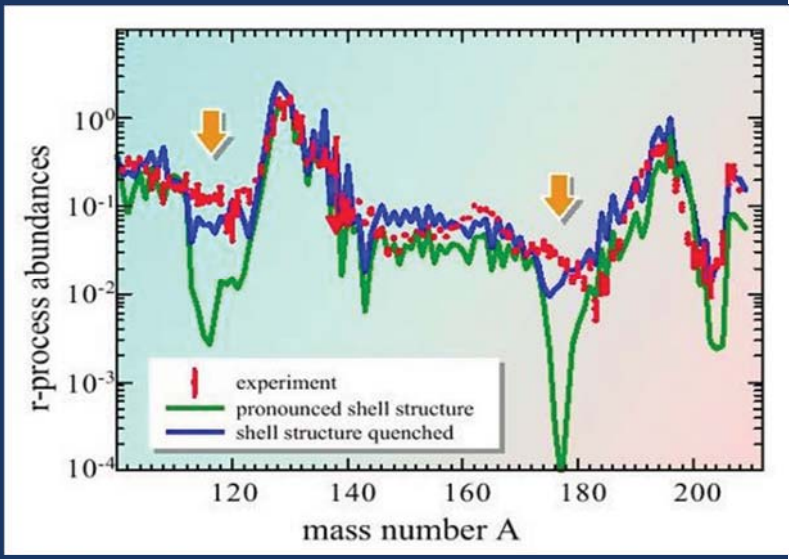

Examples of reaction: $^{7}Be(p,\gamma)^{8}B$

- Motivation
- Beam production
- Detection
- Data analysis
- DWBA calculation
- From ANC to S-factor
- Astrophysical implication
- Other recent examples

Where does neutrino come from?

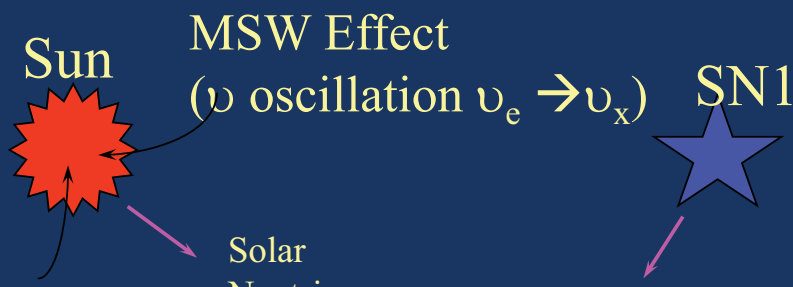

Nuclear Reaction

pp: $p + p \rightarrow {}^2H + e^+ + u_e$

pep: $p + e^- + p \rightarrow {}^2H + u_e$

^7Be: $^7Be + e^- \rightarrow {}^7Li + u_e$

^8B: $^8B \rightarrow {}^8B^* + e^+ + u_e$

Neutrinos form Supernovae

Detector
(Homestake, Gallex, SNO
Sage, Kamiokande, ICARUS)

Neutrino detection

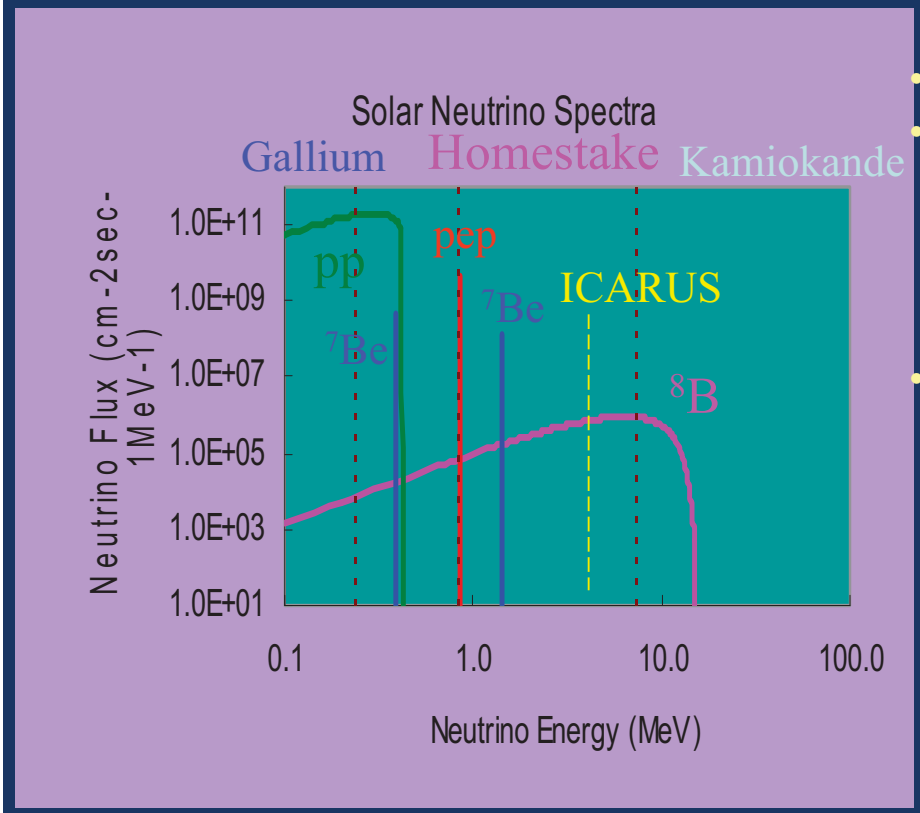

- Radiochemical
- Homestake exp.

  $\upsilon_e + {}^{37}Cl \rightarrow {}^{37}Ar + e^-$
- Gallex and Sage

  $\upsilon_e + {}^{71}Ga \rightarrow {}^{71}Ge + e$

- Direct measurement
- Kamioka, SNO
- Exp.

  $\upsilon + e \rightarrow \upsilon + e$
- ICARUS Exp.

  $\upsilon_e + {}^{40}Ar \rightarrow {}^{40}K + e^-$

  $\upsilon_x + e^- \rightarrow \upsilon_\xi + e^-$

Solar neutrino experiments

- Past: mainly sensitive to υ_e
  - Super Kamiokande
  - Gallex, Sage
  - Homestake
    - SNO (also to other flavor)
- Now: Neutrino of all flavor
  - Super Kamiokande
  - SNO
  - Underground Lab
  - ...

How nuclear physics connected with solar neutrino problem

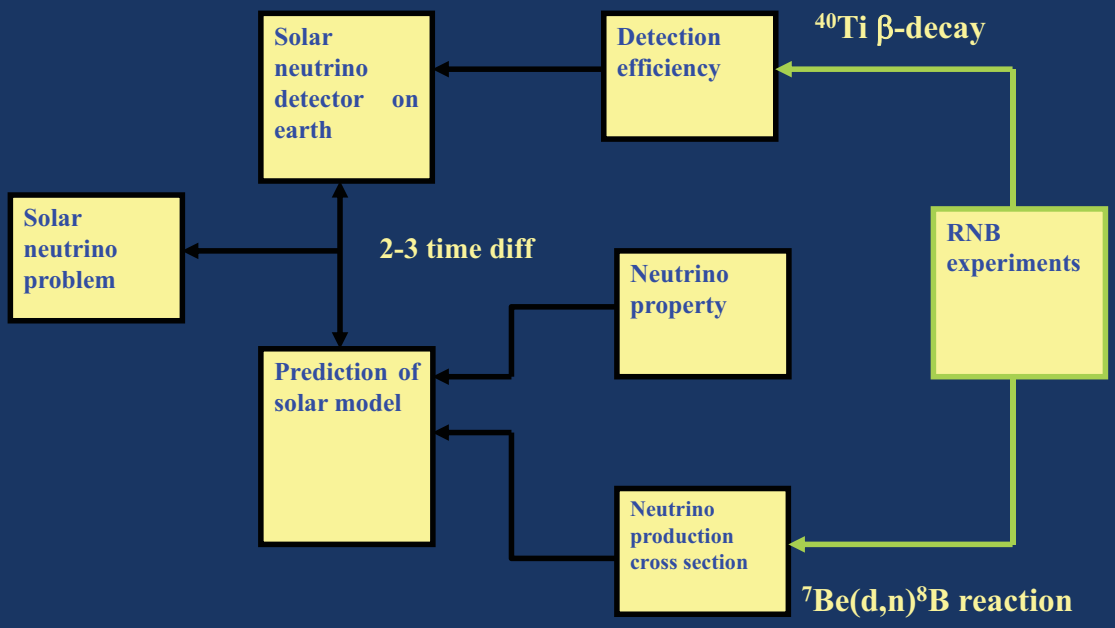

Predicted reaction rates = Absorption cross section (nuclear physics input, e.g. ^{37}Ca or ^{40}Ti β-decay)× Solar neutrino flux (solar model + nuclear physics input, e.g. ^{7}Be(p,γ)^{8}B reaction)

100 MeV 200 μA compact proton cyclotron
20000 mass resolution ISOL, 2 MeV/u super-conducting LINAC

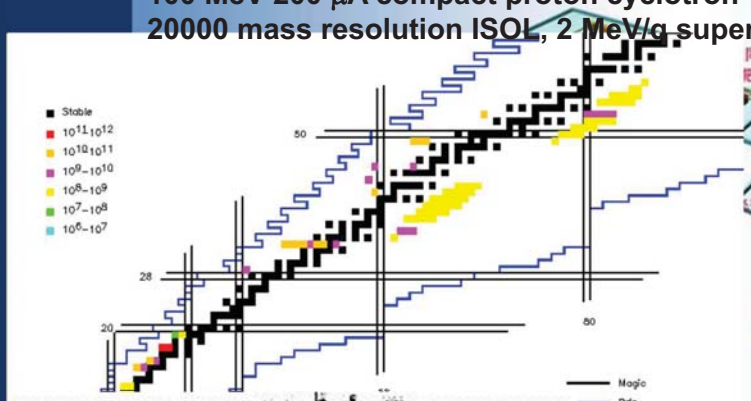

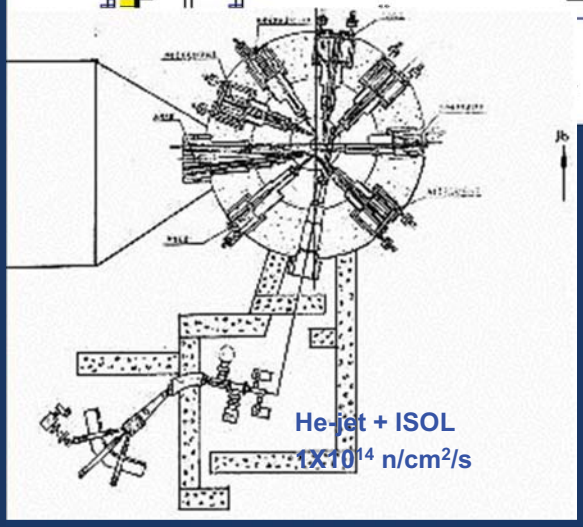

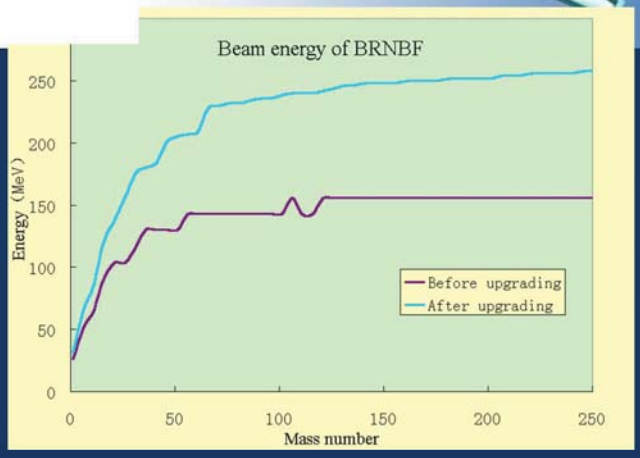

Indirect method for ^{7}Be(p,γ)^{8}B

RIB production

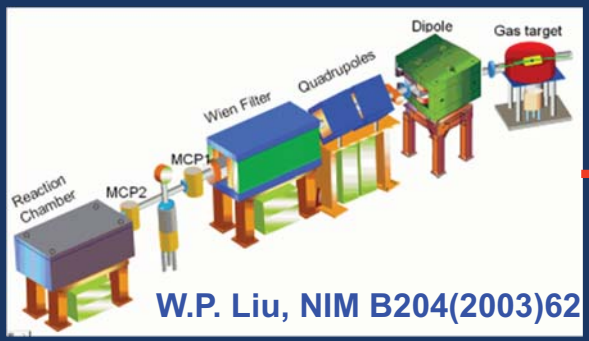

W.P. Liu, NIM B204(2003)62

(d,n) or (d,p) measurement

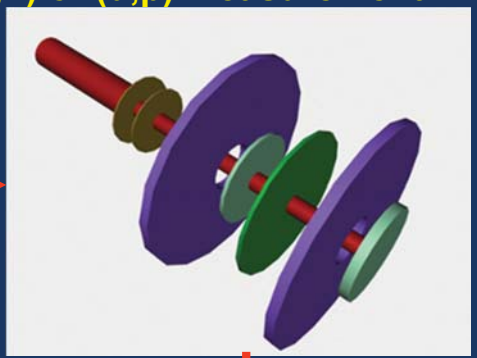

W.P. Liu, PRL77(1996)611

$$\left(\frac{d\sigma}{d\Omega}\right)_{exp} - \left(\frac{d\sigma}{d\Omega}\right)_{CN} = \sum_{j_i j_f} (C^{d}_{l_i j_i})^2 (C^{^{12}N}_{l_f j_f})^2 \frac{d\sigma^{DW}_{l_f j_f l_i j_i}/d\Omega}{b^2_{l_i j_i} b^2_{l_f j_f}},$$

$$\sigma_t = \frac{16\pi}{9}\left(\frac{E_\gamma}{\hbar c}\right)^3 \frac{1}{\hbar v}\frac{e^2_{eff}}{k^2}\frac{(2j_f+1)}{(2I_1+1)(2I_2+1)} C^2_{\ell_f j_f} \times \left| \int_{R_N}^{\infty} r^2 dr \, f_{\ell j}(kr) W_{\eta,\ell_f+1/2}(2\kappa r) \right|^2,$$

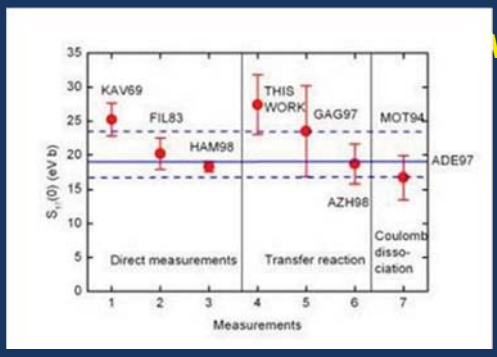

Astrophysical reaction rates

ANC or Spec factor

$^{7}Be(d,n)^{8}B$ experimental setup

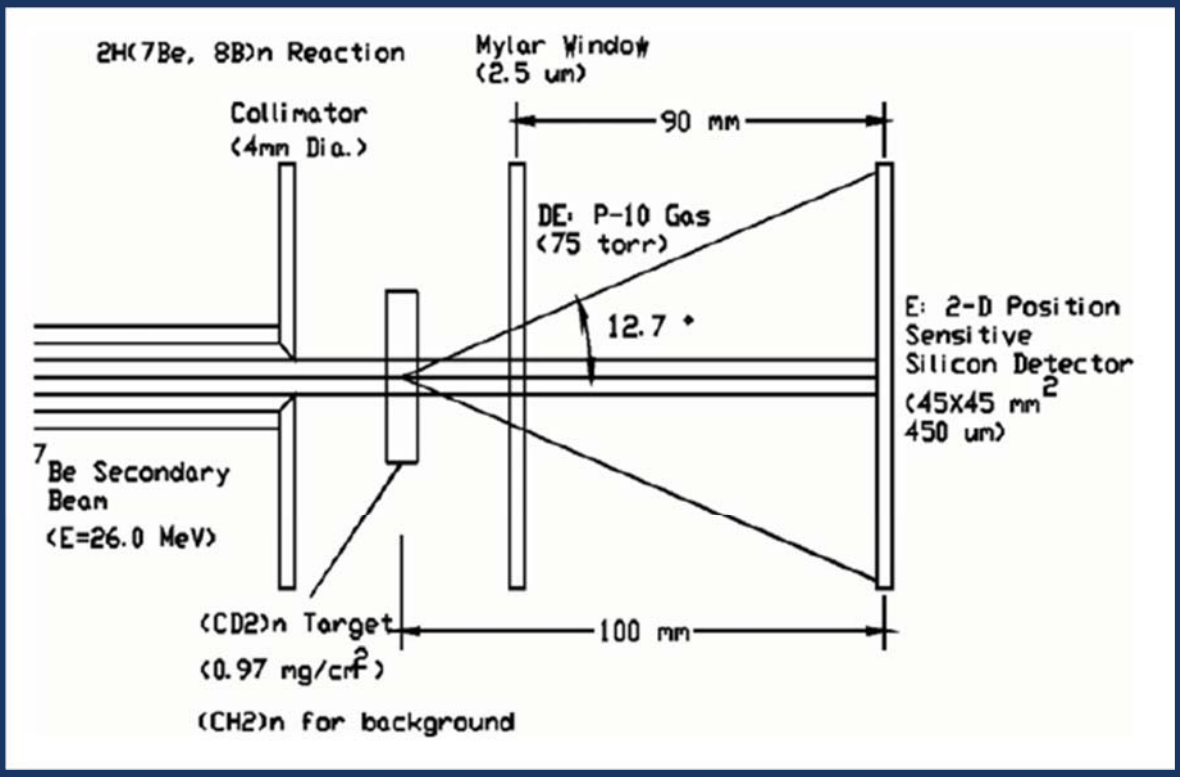

Results—^{7}Be

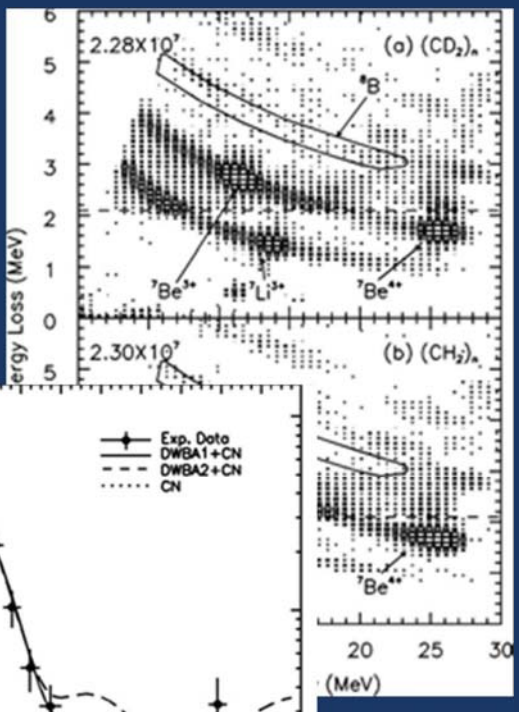

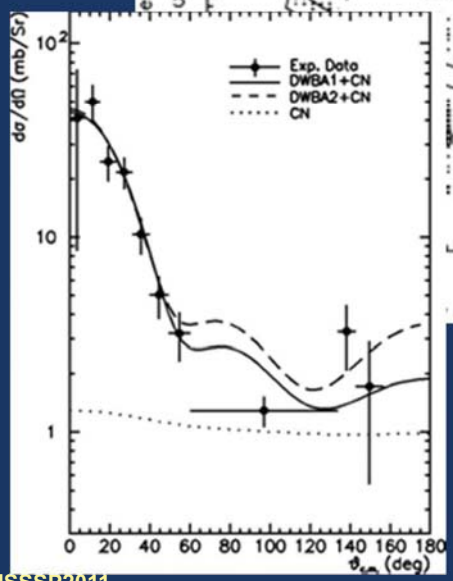

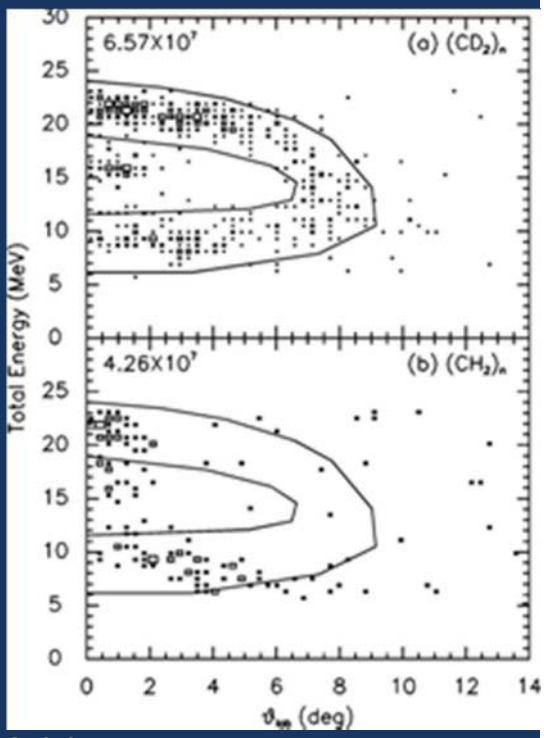

W. P. Liu
PRL77(1996)611
NPA 616(1997)131c

ANC method

For peripheral transfer reaction: B(d,n)A

two virtual captures:

$$B + p \rightarrow A$$
$$n + p \rightarrow d$$

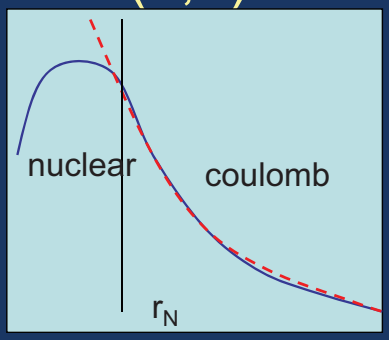

two ANC's : C^A_{Bp} and C^d_{np}

$$\frac{d\sigma}{d\Omega} = \sum \frac{(C^A_{Bpl_Aj_A})^2 (C^d_{npl_dj_d})^2}{b^2_{Bpl_Aj_A} b^2_{npl_dj_d}} \sigma^{DWBA}_{l_Aj_Al_dj_d}$$

$(C^d_{np})^2 = 0.76\, fm^{-1}$ known value

$(C^A_{Bp})^2$ can be obtained from $(\frac{d\sigma}{d\Omega})_{\exp}$

The Cross Section for E1 capture

$$B(E1; j\pi \rightarrow j_f\pi_f) = \frac{1}{(2I_1+1)(2I_2+1)} \sum_m \sum_{I\, m_I} |T_{1m}|^2 =$$

$$\frac{e_{eff}^2}{k^2} \sum_{\ell jI} \lambda(\ell j \ell_f j_f I) C_{\ell_f j_f I}^2 \left| \int_{R_N}^{\infty} r^2 dr f_{\ell jI}(kr) W_{\eta,\ell_f+1/2}(2\kappa r) \right|^2$$

ANC or spec factor

$\lambda(\ell j \ell_f j_f I)$ is the kinetic factor

$e_{eff} = eN/A$ for Protons

$-eZ/A$ for Neutrons

(p,γ) vs. (n,γ)

- (p,γ)
- One p transfer like (d,n)
- Easy PID, no coin.
- Get ANC
- Peripheral

- (n,γ)
- One n transfer like (d,p)
- Hard PID, coin. with p
- Get spec. factor
- Fix V_0 by known data

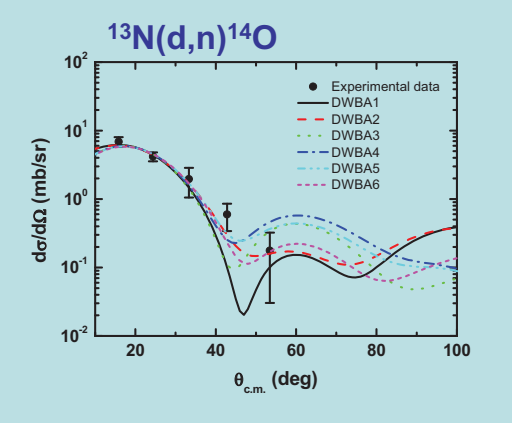

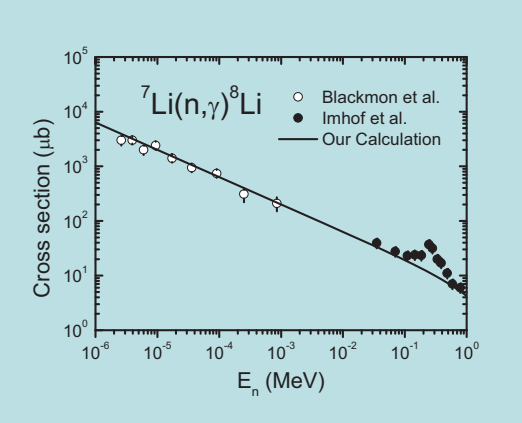

Experimental setup for the ^{8}Li(d,p)^{9}Li reaction

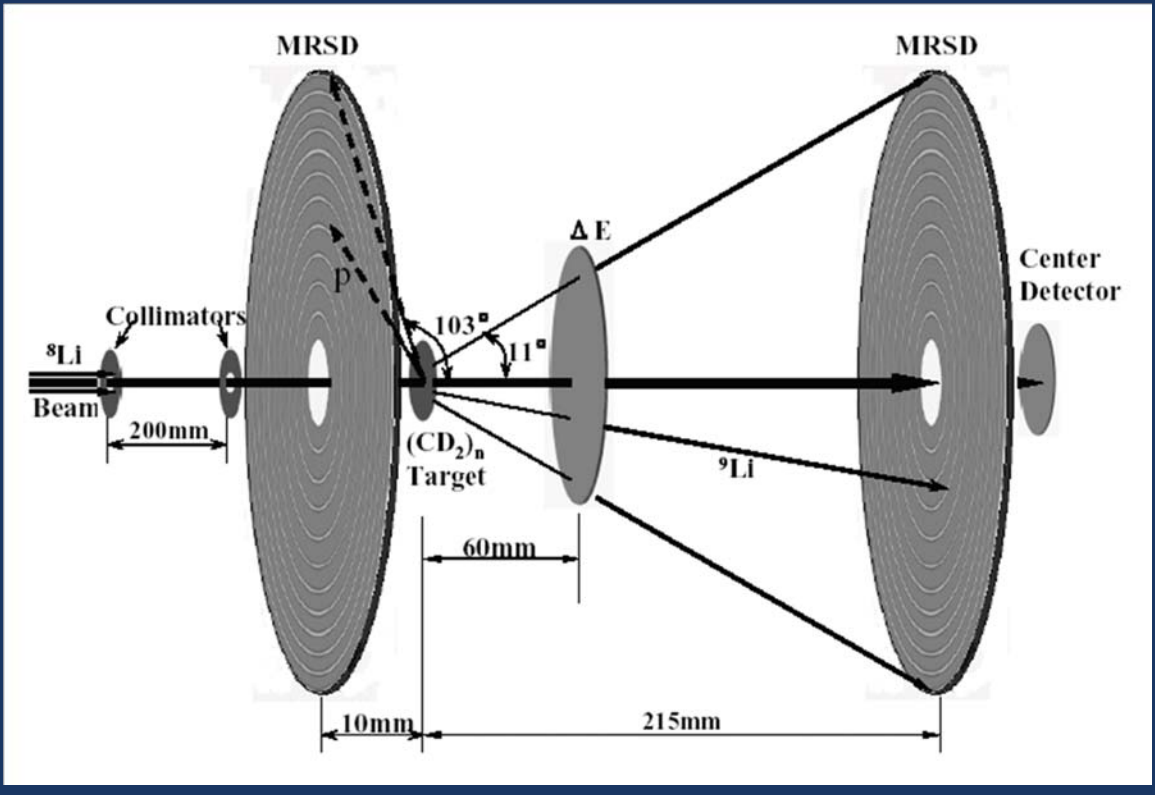

From (d,p) to (n,γ): the detail

$$\left(\frac{d\sigma}{d\Omega}\right)_{exp} = S_d \sum_{lj} S_{lj}\sigma_{lj}^{DWBA}(\theta)$$

$$\sigma_{n,\gamma} = \frac{8\pi}{9}\left(\frac{E_\gamma}{\hbar c}\right)^3 \frac{e_{eff}^2}{\hbar v}\frac{(2j_f+1)}{(2I_t+1)}\frac{S_{l_f j_f}}{k^2}\left|\int_0^\infty u_{l_f}(r) r^2 w_{l_i}(kr) dr\right|^2$$

Z. H. Li, W. P. Liu et al., The ^{8}Li(d,p)^{9}Li Reaction and the Astrophysical ^{8}Li(n,γ)^{9}Li Reaction Rate, Phys. Rev. C 71 (2005) 052801(R)

First measurement of primordial ^{8}Li(n,γ)^{9}Li reaction rate

- Destroy reaction of 8Li: ^{8}Li(n,γ)^{9}Li, ^{8}Li(d,p)^{9}Li in inhomogeneous big bang，APJ429(1994)499
- Half-life of ^{8}Li: 0.83 s，direct (n,γ) exp. impossible

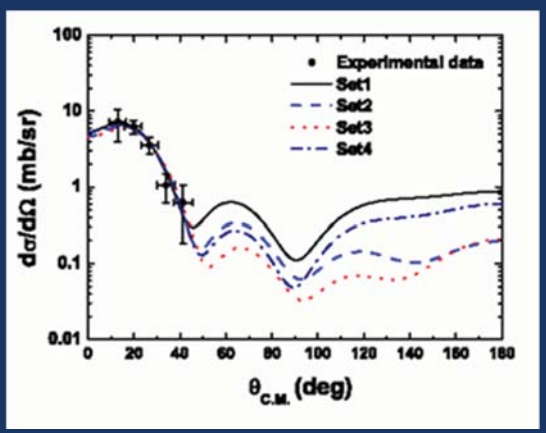

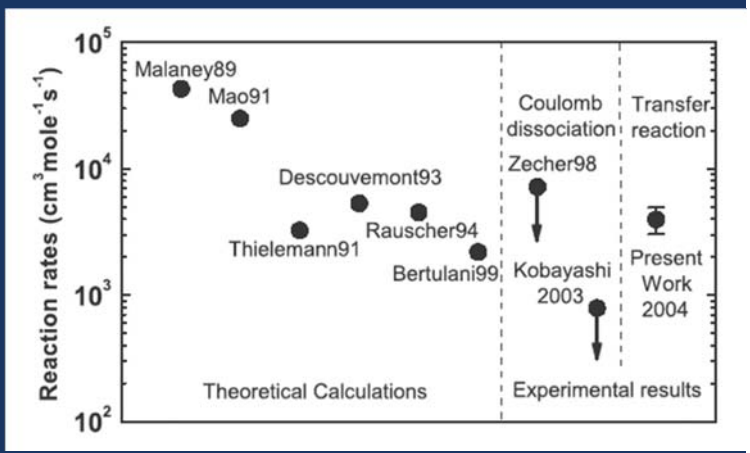

Z. H. Li, W.P. Liu et al.，PRC 71, 052801(R) (2005)

Summary of astrophysics experimental results

Reaction	E_{cm} (MeV)	σ_{tot} (mb)	$(ANC)^2$ (fm^{-1})	Indirect Reaction	S(0) (eV b) or rate
$^{7}Be(d,n)^{8}B$	5.8	58 ± 8	0.711 ± 0.090	(p,γ)	27 ± 4
$^{7}Be(d,n)^{8}B$	8.3	28 ± 3	0.62 ± 0.12	(p,γ)	24 ± 5
$^{11}C(d,n)^{12}N$	9.8	23 ± 5	2.86 ± 0.91	(p,γ)	157 ±
$^{8}Li(d,p)^{9}Li$	7.8	7.9 ± 2.0	1.25 ± 0.25	(n,γ)	3970 ± 950
$^{8}Li(d,p)^{9}Li$	7.8	7.9 ± 2.0	1.10 ± 0.23	^{8}B mirror	42 ± 9
$^{13}N(d,n)^{14}O$	8.9	7.4 ± 1.1	29.4 ± 5.3	(p,γ)	417 ± 74

- **Method used**
  - **ANC, $^{7}Be(p,\gamma)^{8}B$, $^{11}C(p,\gamma)^{12}N$, $^{13}N(p,\gamma)^{14}O$, $^{8}Li(p,\gamma)^{9}Be$**
  - **Spec-factor, $^{8}Li(n,\gamma)^{9}Li$, $^{6}Li(n,\gamma)^{7}Li$, $^{12}C(n,\gamma)^{13}N$**
  - **Charge symmetry, $^{8}B(p,\gamma)^{9}C$, $^{26}Si(p,\gamma)^{27}P$**
- **Direct method, $^{11}C(p,\gamma)^{12}N$, DRAGON, in progress**
- **Indirect method, $^{12}N(p,\gamma)^{13}O$, CRIB, analysis in progress**

y of reaction studied

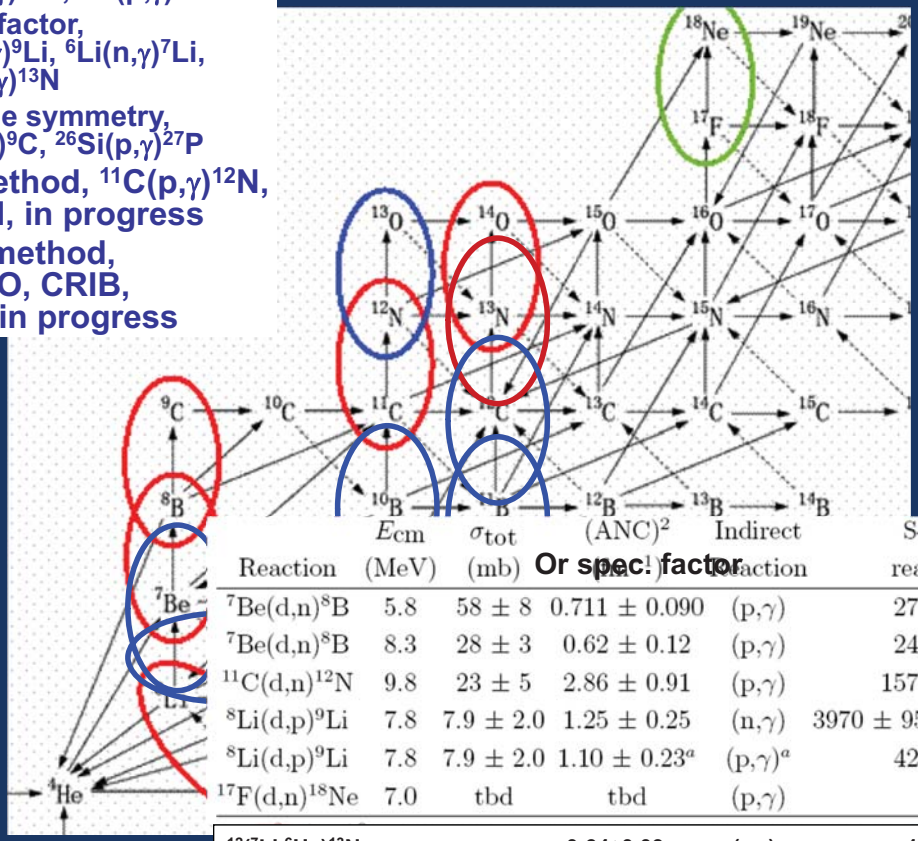

Or spec. factor

Reaction	E_{cm} (MeV)	σ_{tot} (mb)	$(ANC)^2$	Indirect Reaction	S-factor or reaction rate
$^{7}Be(d,n)^{8}B$	5.8	58 ± 8	0.711 ± 0.090	(p,γ)	27 ± 4 eV b
$^{7}Be(d,n)^{8}B$	8.3	28 ± 3	0.62 ± 0.12	(p,γ)	24 ± 5 eV b
$^{11}C(d,n)^{12}N$	9.8	23 ± 5	2.86 ± 0.91	(p,γ)	157 ± 50 eV b
$^{8}Li(d,p)^{9}Li$	7.8	7.9 ± 2.0	1.25 ± 0.25	(n,γ)	3970 ± 950 cm $^{3}mole^{-1}s^{-1}$
$^{8}Li(d,p)^{9}Li$	7.8	7.9 ± 2.0	1.10 ± 0.23[a]	(p,γ)[a]	42 ± 9 eV b
$^{17}F(d,n)^{18}Ne$	7.0	tbd	tbd	(p,γ)	tbd
$^{12}(^{7}Li,^{6}He)^{13}N$			**0.64±0.09**	**(n,γ)**	**1.87 kev b**

Examples of decay: ^{40}Ti β-decay

- Motivation
- Beam production
- Experiment
- Data analysis
- Implication

ICARUS and neutrino oscillation

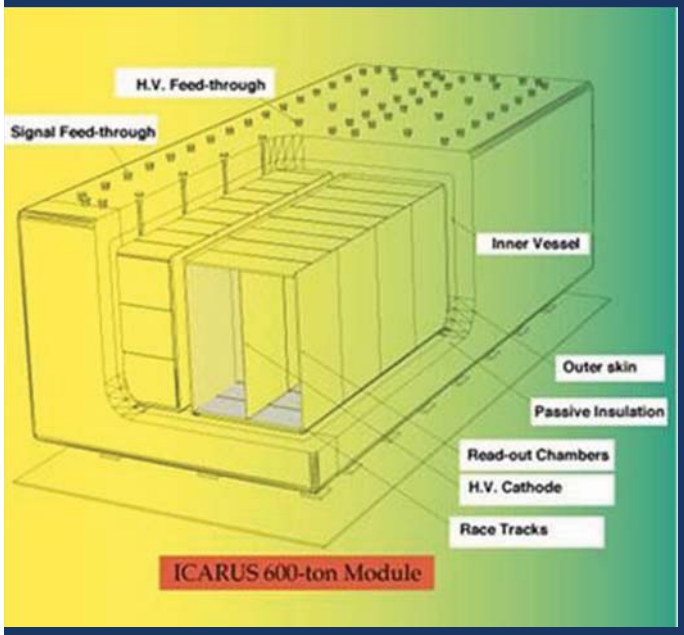

Two process:

Absorption

$\upsilon_e + {}^{40}Ar \rightarrow {}^{40}K^* + e^-$

${}^{40}K^* \rightarrow {}^{40}K + \gamma$

$\gamma + e^- \rightarrow \gamma' + e^{-'}$

$M(e^-) = 2$

Scattering

$\upsilon_x + e^- \rightarrow \upsilon_x' + e^{-'}$

$M(e^-) = 1$

®ICARUS homepage

^{40}Ti and ^{40}Ar Mirror symmetry

Mirror symmetry in mass 40

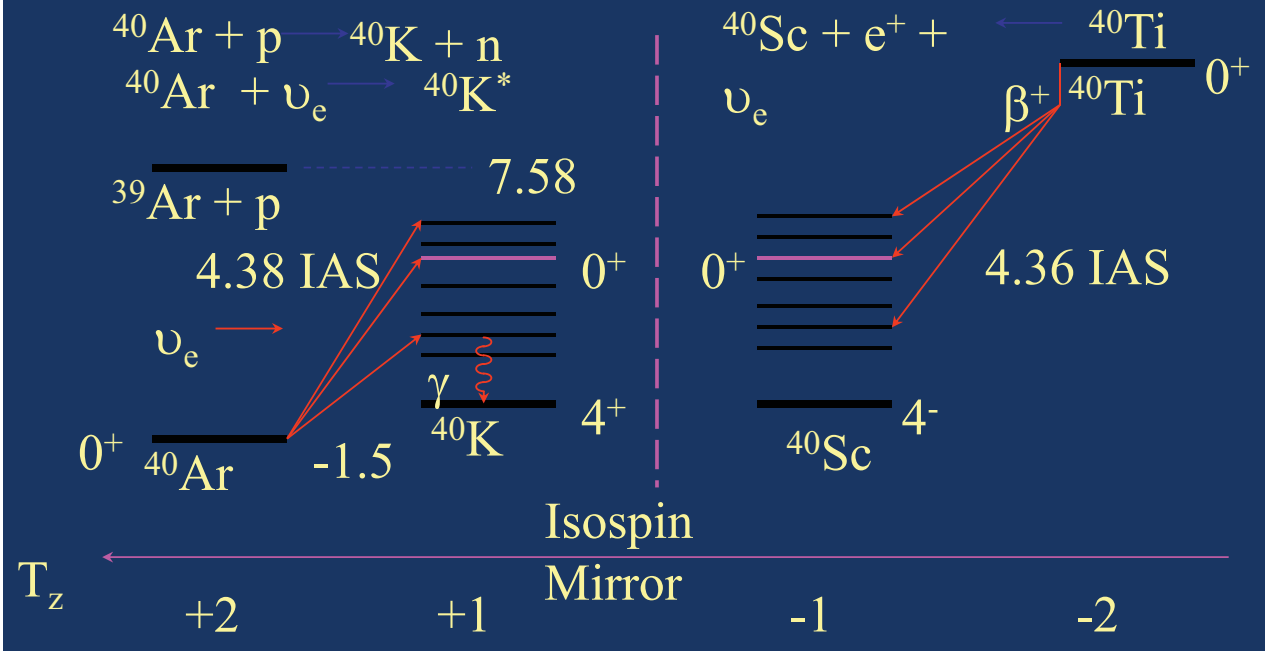

Focal plane detectors

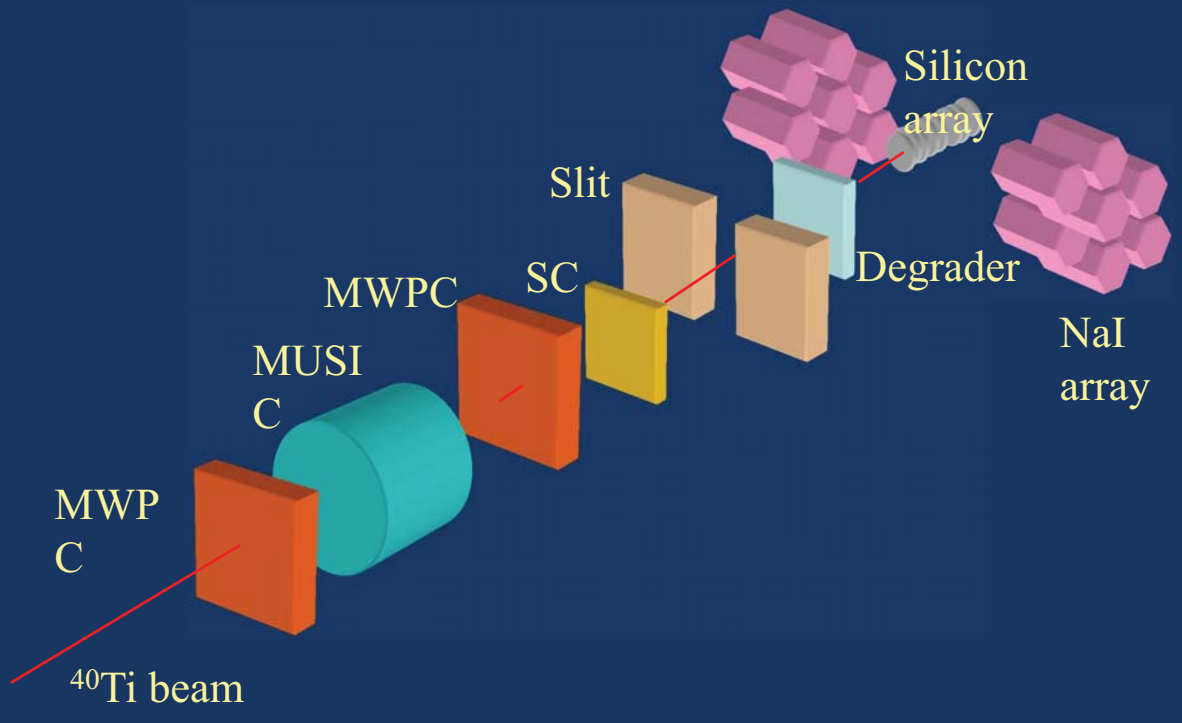

^{40}Ti selection

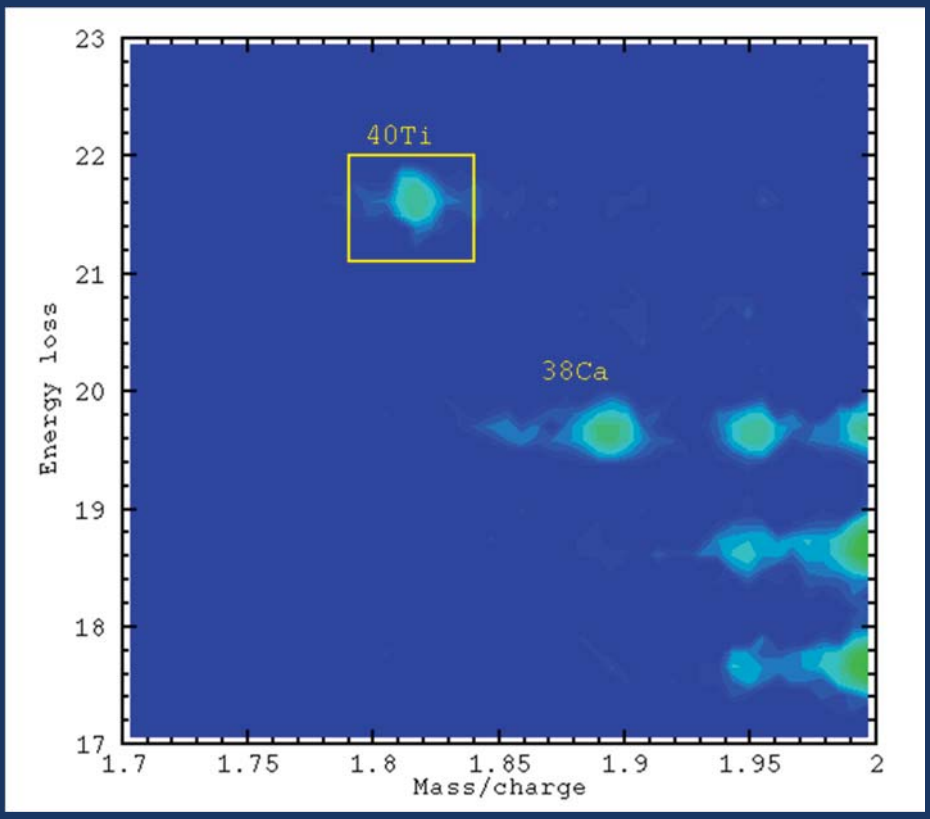

Delayed coincidence technique

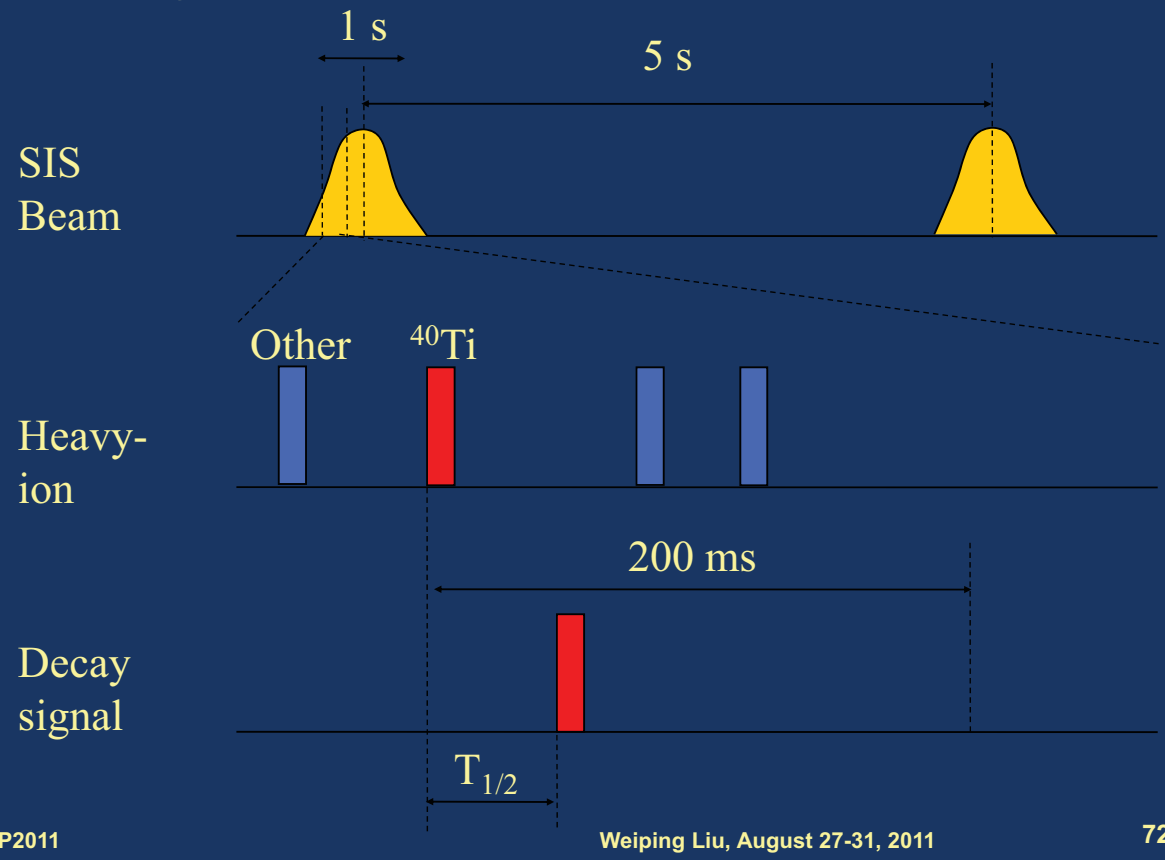

^{40}Ti β-delayed protons

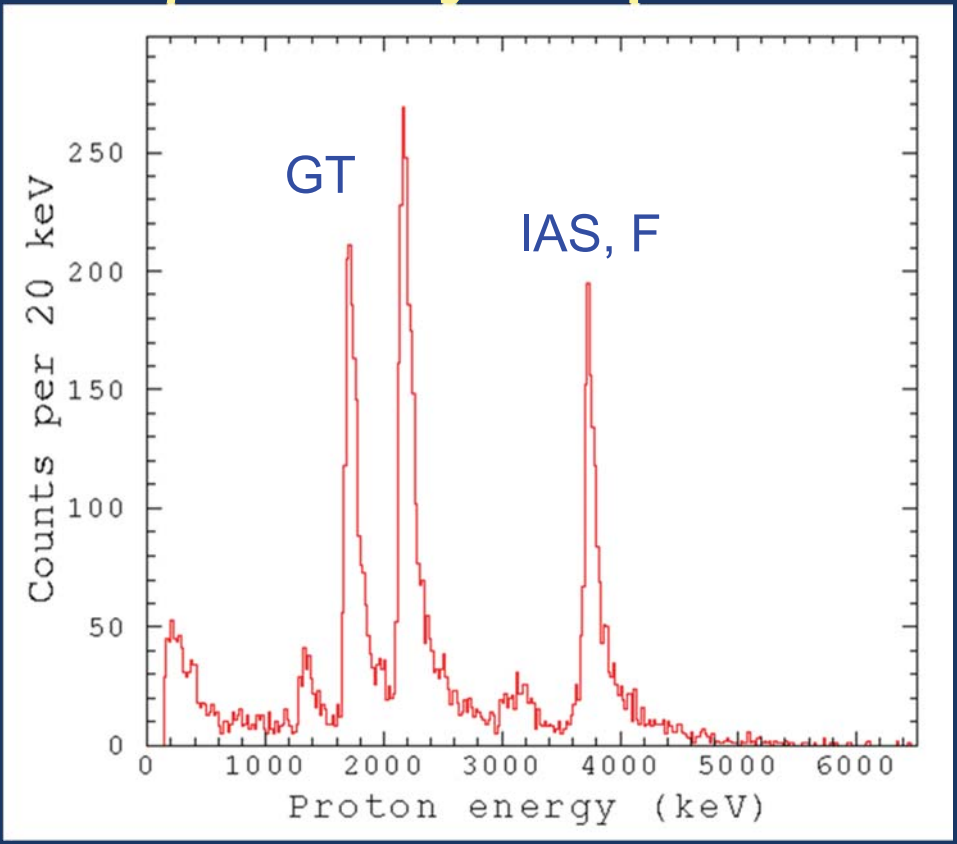

Mass determination for ^{40}Ti by IMME

Mass and Q_{EC} for ^{40}Ti by IAS level energy in ^{40}Sc using IMME: $M(T_Z) = a + b\,T_Z + c\,T_Z^2$

Old: DM = -8850(160) keV , Q_{EC} = 11680(160) keV

Now: DM = -9096(10) keV , Q_{EC} = 11466(13) keV

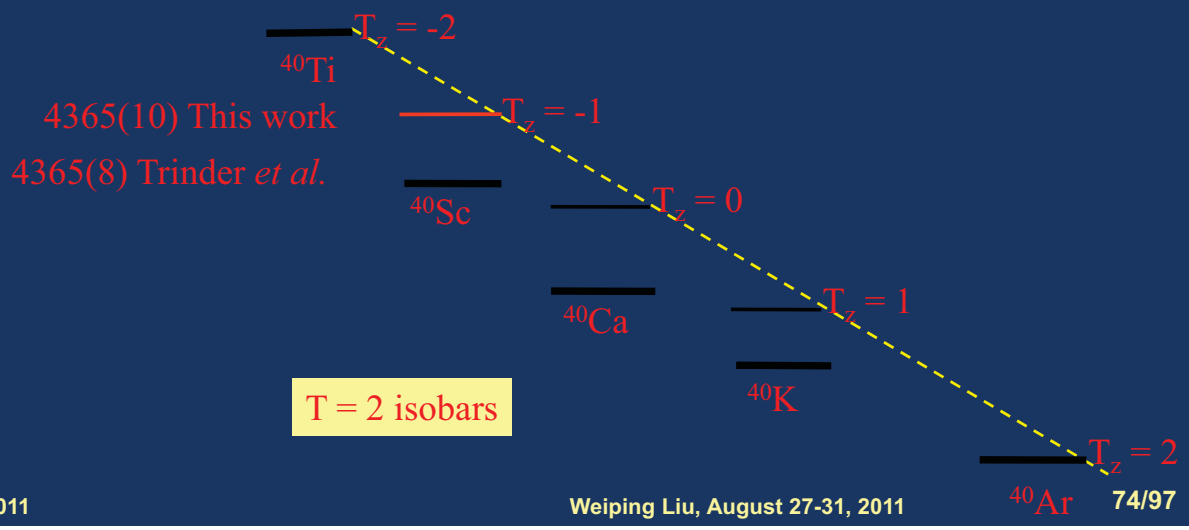

F/GT distributions

W. Liu et al., PRC58(1998)2677

- ^{40}Ti β-delayed proton→ Half-life
- ^{40}Sc IAS level → ^{40}Ti mass
- Full energy, p-γ coin, secondary reaction corrections
- →F and GT decay strength distributions

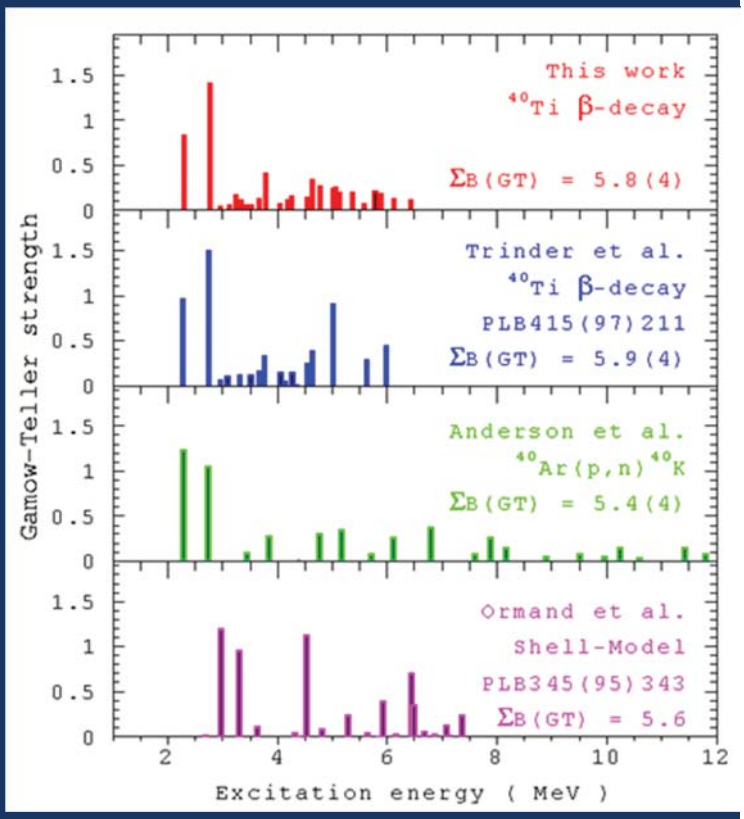

Reaction rates for ICARUS

B(GT) + B(F) from this work
σ/B-E_x relation from
Ormond et al., Phys. Lett. B345(1995)343.
→Absorption cross section = 13.8(6)×10^{-10} pb
with Bahcall et al. ^{8}B solar neutrino flux of
F = 6.6(1.0) × 10^6 $cm^{-2}s^{-1}$
→ICARUS reaction rate
9.1(1.4) SNU (once for two days)
=2.6 (Fermi) + 6.5 (Gamow-Teller)
→ 3 times larger than Bahcall predictions
W. Liu et al., PRC58(1998)2677

Some more recent examples

Contents

- ^{7}Be(d,p)2α, C. Angulo, to be appear in APJ letter
- ^{16}N β-decay$\rightarrow$^{12}C(α,γ)^{16}O, X. D. Tang, PRL**99**, 052502 (2007)

^{7}Be(d,p)2α

- ^{7}Li abundance related to baryon density of BBN
- For ^{7}Li, more than 100 reactions, 40 are not precise enough, ^{7}Be(d,p)2α is one of them
- Now observed ^{7}Li 2 times more than theory
- So if this reaction 100 times larger can explain
- No experiment at GW of 1 MeV measured
- C. Angulo, LLN, May 2004(exp) to end of 2006(pub)

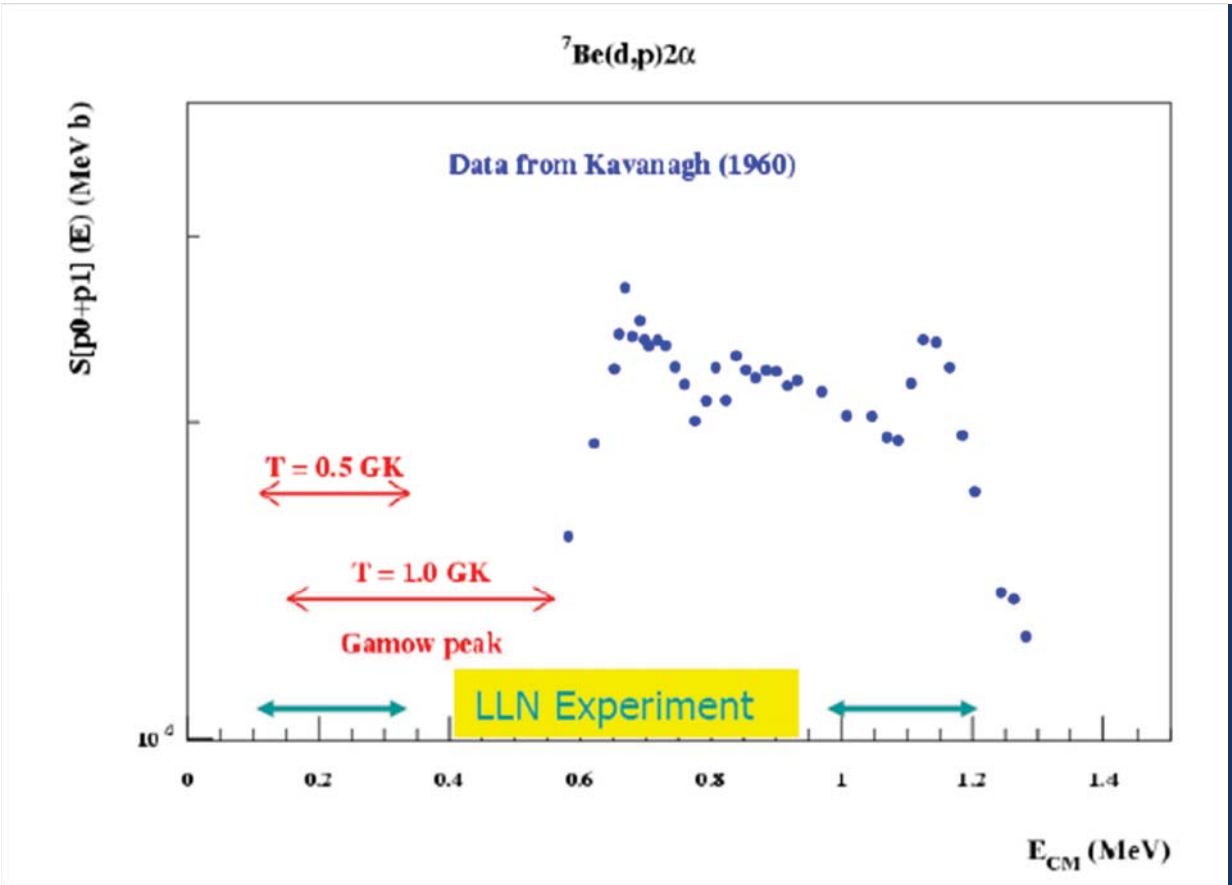

Motivation

Beam energies: 5.545 and 1.710 MeV (c.m. range: 1.2-0.96 MeV and 0.38-0.15 MeV)

Experiment

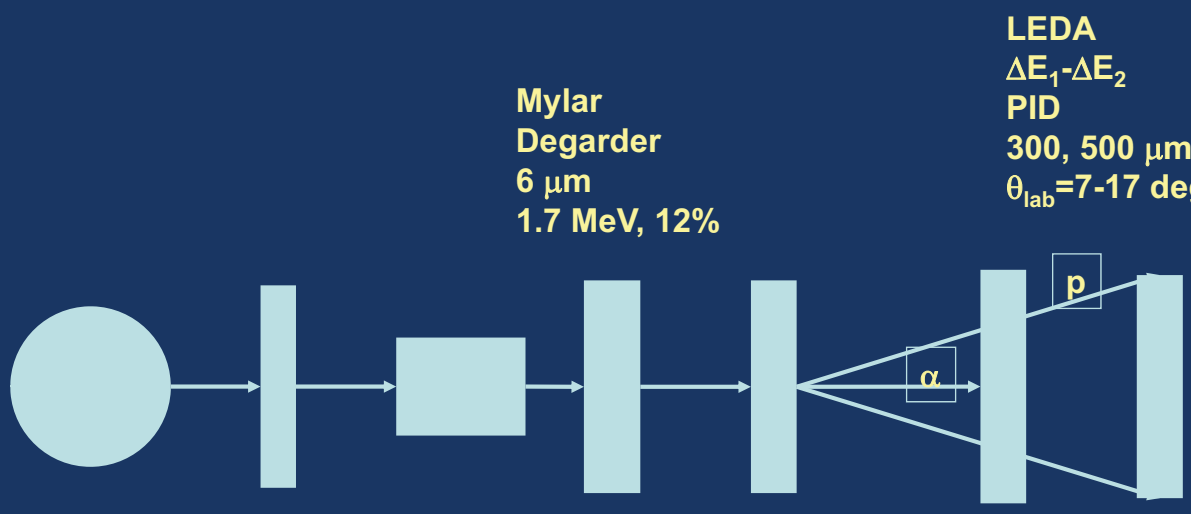

Beam development

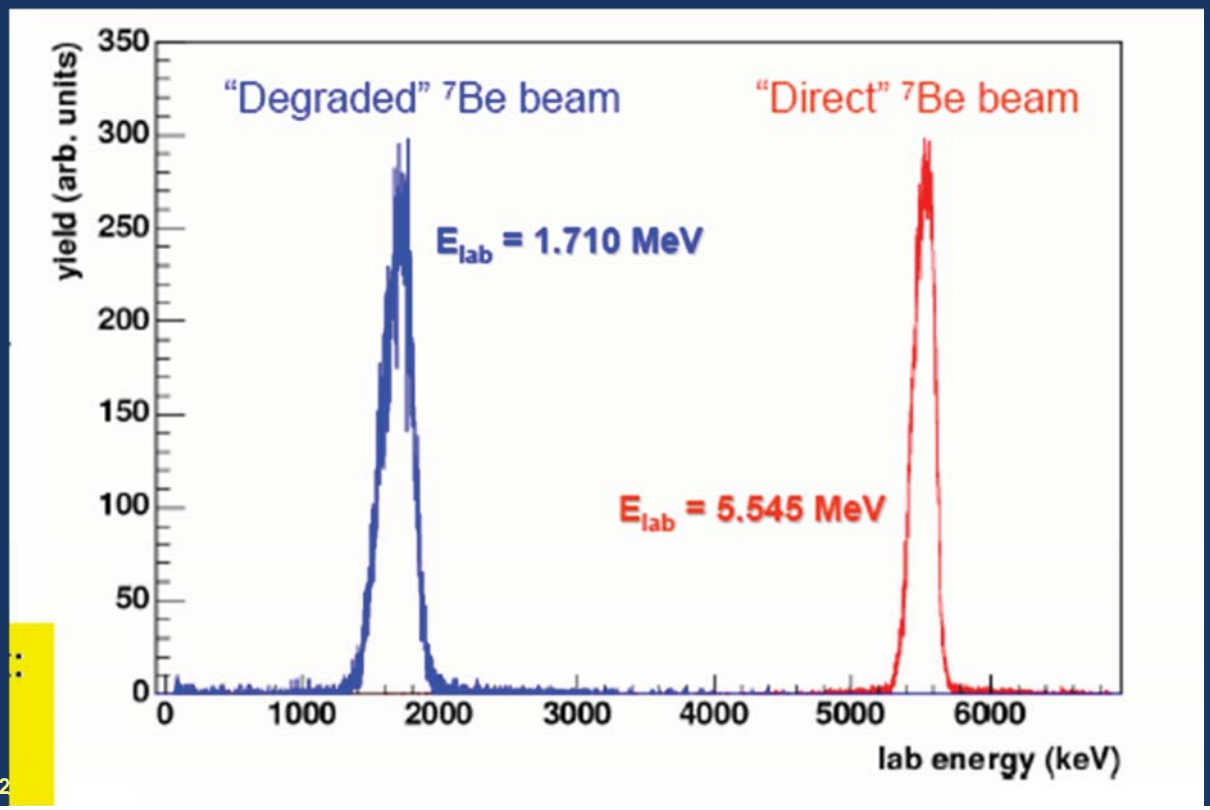

Data

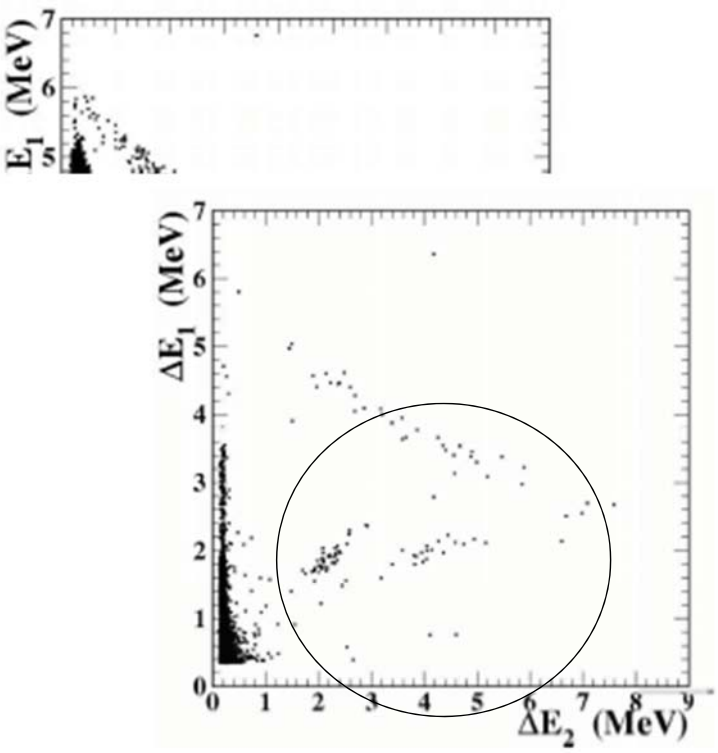

100 proton
Counts
In 26 hour

FIG. 2.—
a 200 μgr/
1.0 to 1.23

FIG. 3.— Same as Fig. 3 for a beam energy of 1.71 MeV, corresponding to a c.m. energy range of 0.13 to 0.38 MeV.

results

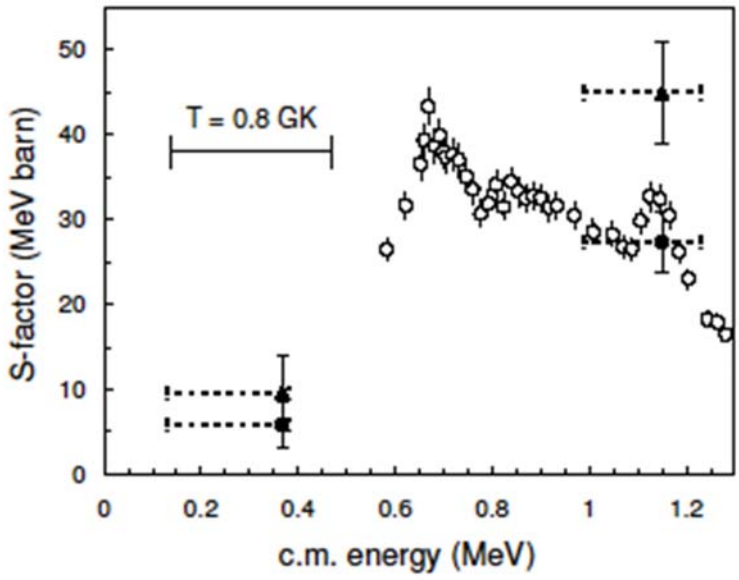

FIG. 4.— Astrophysical S factor of the ^{7}Be(d,p)^{8}Be reaction. Open circles: data from Kavanagh (1960); filled circles: present data including contributions from the ground and first excited states of ^{8}Be only; filled triangles: total S-factor derived from the present experiment. The vertical error bars are the total error. The horizontal dotted bars indicate the energy range covered at each data point. The Gamow window for a typical BBN temperature T=0.8 GK is also shown.

Findings

- Current data factor of 2 smaller
- Can not explain ^{7}Li difference further
- Other reason have to be found
- This paper to be appeared in APJ letter

^{16}N β-decay

- 1
- C
- 3
- 1

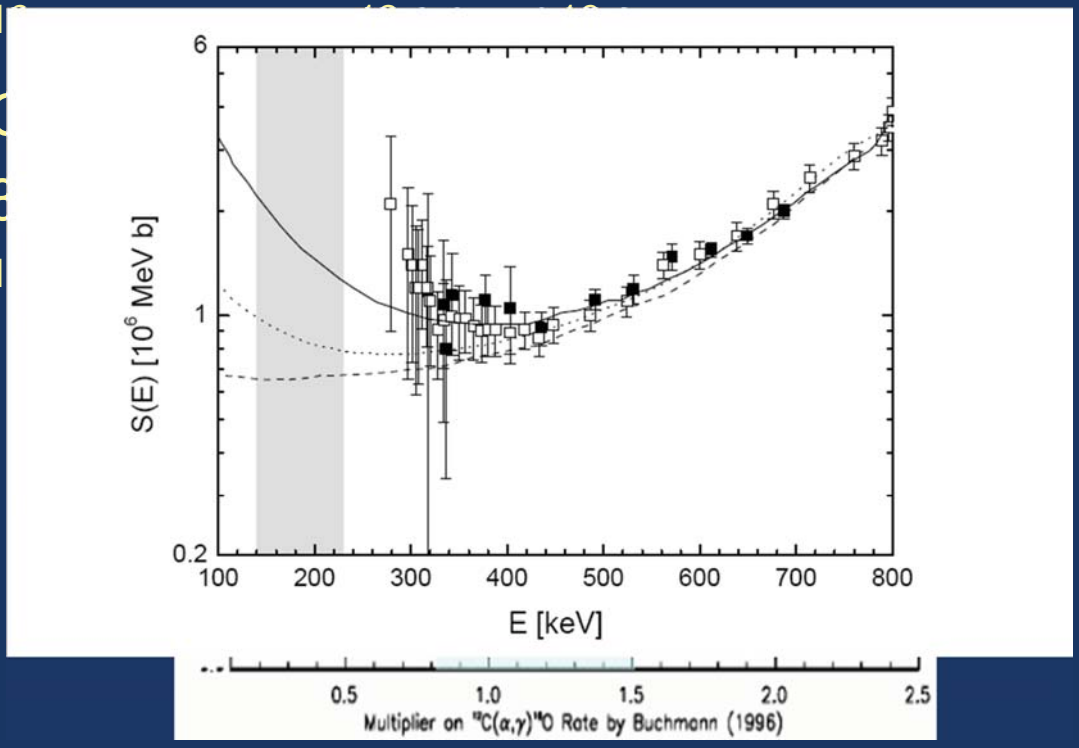

X. D. Tang, PRL99, 052502 (2007)

Complications and solutions

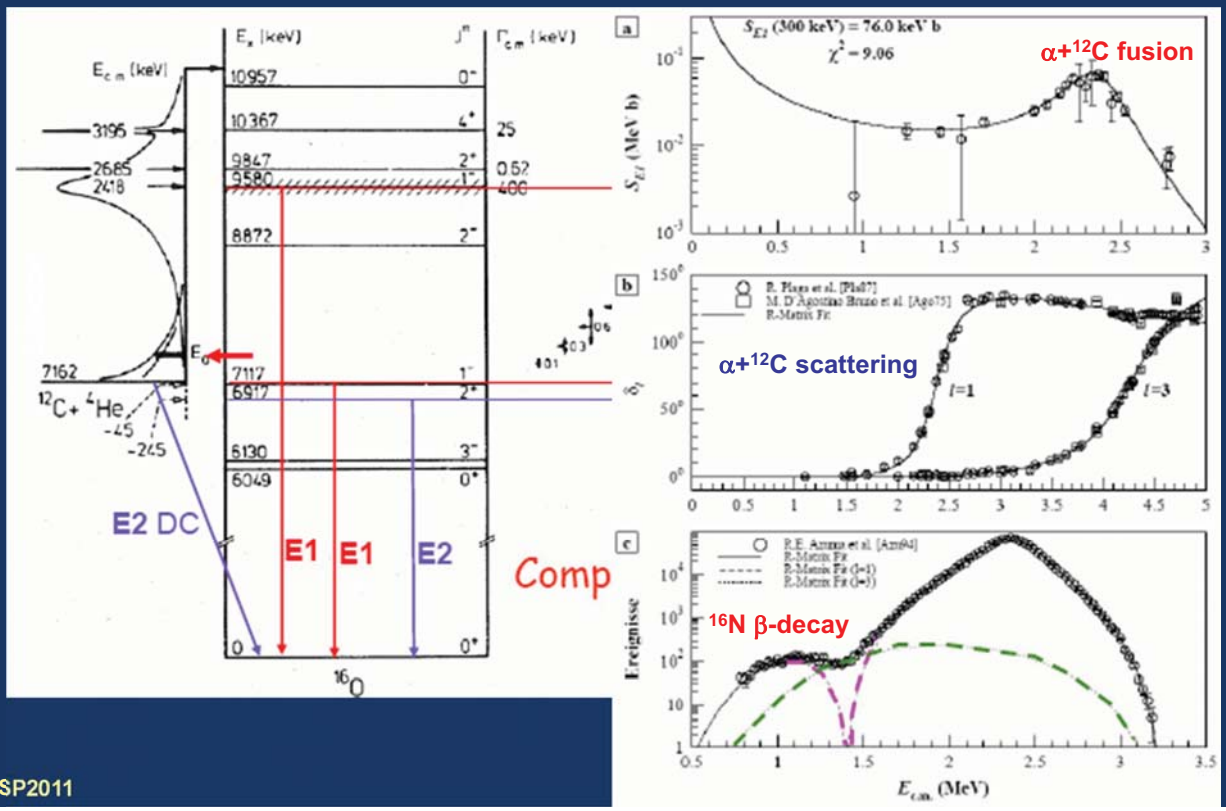

Why β-decay?

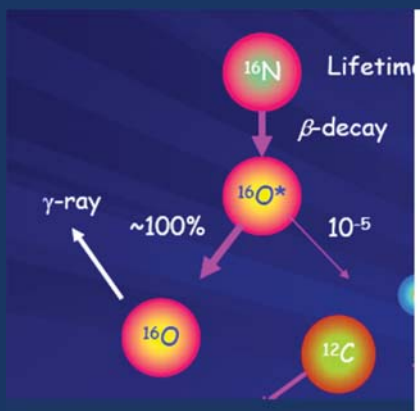

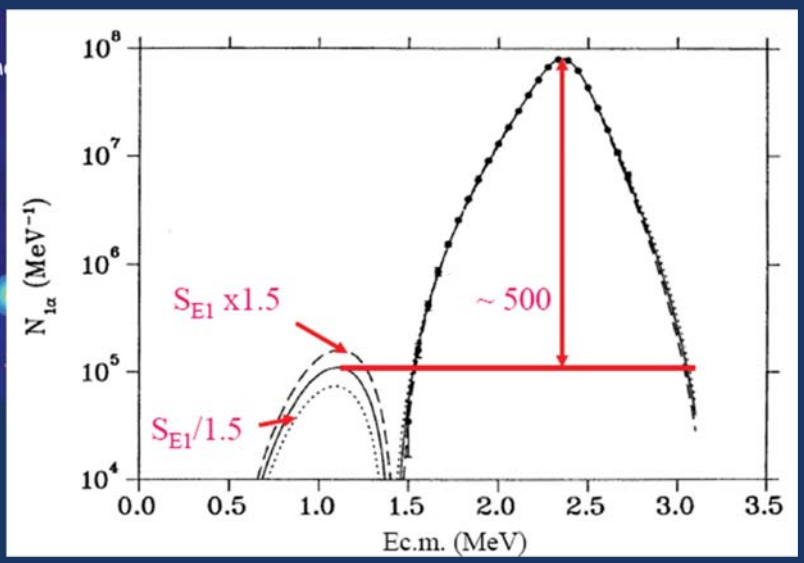

How to do it?

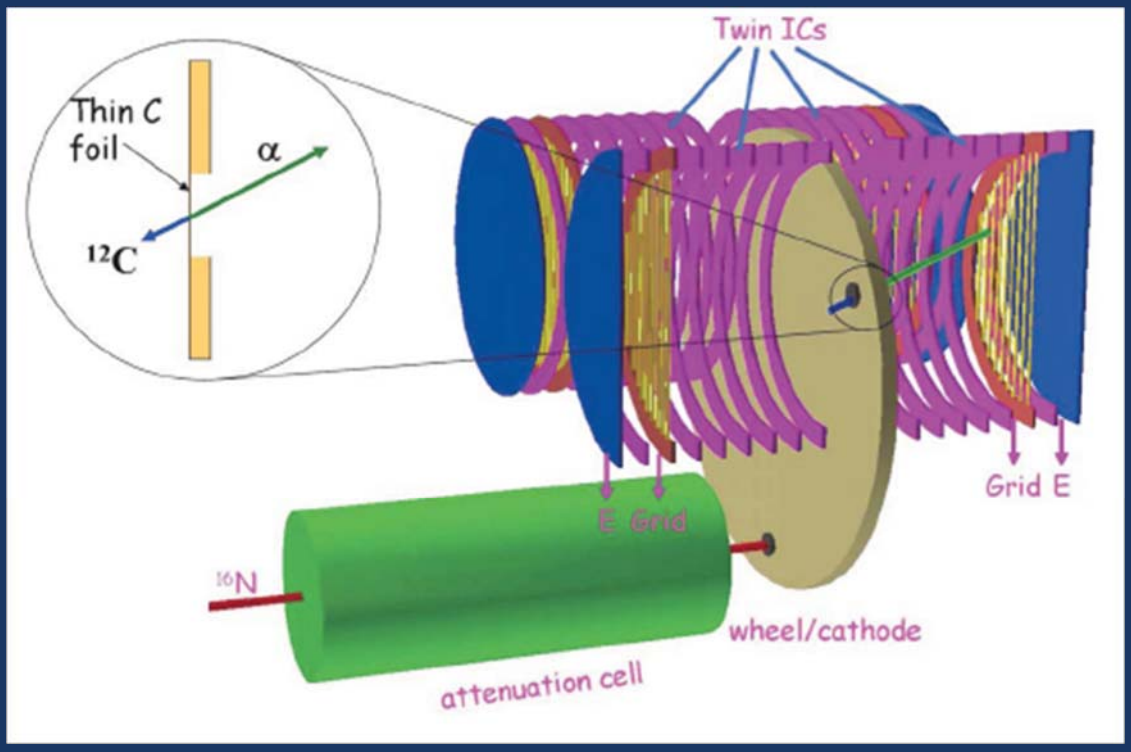

The results

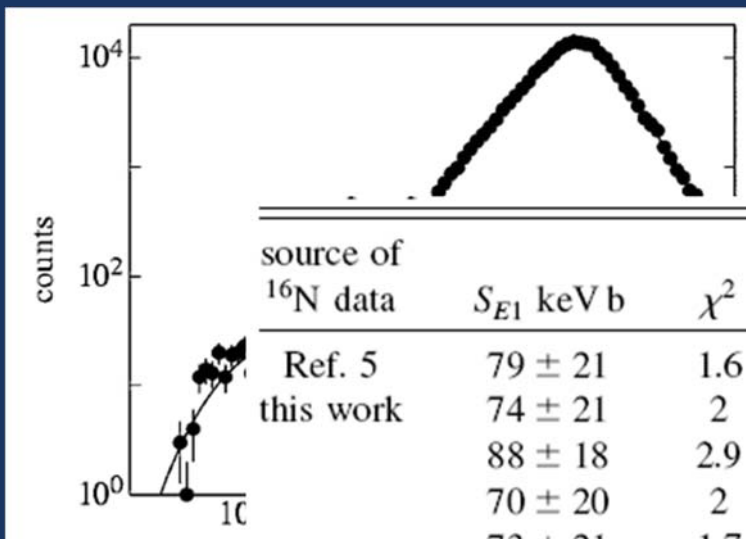

source of ^{16}N data	S_{E1} keV b	χ^2	other data used in fits
Ref. 5	79 ± 21	1.6	
this work	74 ± 21	2	standard input
	88 ± 18	2.9	phase shifts from [21]
	70 ± 20	2	new β-branching ratio [23]
	73 ± 21	1.7	with (α, γ) data from [8]
	77 ± 23	2	constant + linear term
	85 ± 18	2.7	Ref. [8,21,23]

Lesson for us

- Even with simple device we can still today attack most important problems
- But, one should be very careful and should work hard (sometimes for long time) experimental developments, everyone knows physics, but the key is to get more precise and background free data

Important reference

卢希庭，江栋兴，叶沿林，原子核物理，原子能出版社，(2000)

C.E. Rolfs and W.S. Rodney, Cauldron in the Cosmos, The University of Chicago Press, (1988).

G. Wallerstein, I.I. Jr., P. Parker et al., Synthesis of the elements in stars: forty years of progress, Rev. Mod. Phys. 69, 995 (1997).

W. Liu, X. Bai, S. Zhou et al., Angular distribution for the ^{7}Be$(d,n)^{8}$B reaction at $E_{c.m.}$=5.8 MeV and the $S_{17}(0)$ factor for the ^{7}Be$(p,\gamma)^{8}$B reaction, Phys. Rev. Lett. 77, 611 (1996).

Z. H. Li, W. P. Liu, Z. H. Li et al., Phys. Rev. C 71 (2005) 052801(R)

李宗伟，天体物理学，高等教育出版社，2001年

Outlook

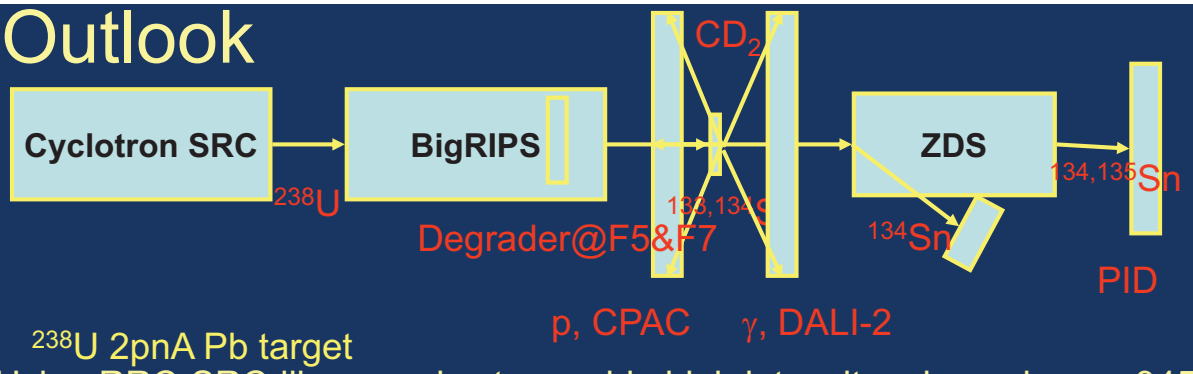

^{238}U 2pnA Pb target

- Using RRC-SRC-like complex to provide high intensity primary beam, 345 MeV/u, 2 pnA and more
- Applying BigRIPS-like to select a cocktail secondary beam using in-flight fission and fragmentation that just pass r-process path and neutron magic number chain, ^{134}Sn 100 MeV/A (after degrader), 100-1000 pps
- Put CD_2 or liquid D reaction target in F3 of BigRIPS and backed by ring silicon detector and gamma detector to tag proton and/or deuteron from $(d,p_{0,1})$
- Function ZDS-like as a recoil mass separator to accept and identify the residuals and make coincidence with proton and gamma
- d,p) angular distribution →spectroscopic factor →microscopic calculation →(n,γ) cross section
- (d,p_0) and (d,p_1) for even-even nuclei→$E(2^+)$ and B(E2)
- But now, beam intensity? The huge energy broadening when degrading the secondary beam down to 10 MeV/u?

Summary

- Nuclear astrophysics is an active and frontier part of nuclear physics research
- To do such kind of research, the production of unstable beam and novel experiment methods is a key to success
- Novel theoretical consideration, like in-direct method, is sometimes the only solution

Single-particle and collective motions in nuclei: The basics of nuclear mean-field models*

Takashi Nakatsukasa

RIKEN Nishina Center, Wako 351-0198, Japan

http://www.nishina.riken.jp/lab/TNP/

Abstract

Basic concepts of nuclear mean-field models are briefly reviewed. The mean-filed picture with any phenomenological interaction without the state dependence cannot account for the nuclear saturation. This state dependence is successfully taken into account by the density dependence, leading to the energy density functional. Then, I show the time-dependent density-functional approach to the giant resonances.

I insert five "Problems" enclosed by the box in the following text. Try to solve them for yourselves before the lecture. That will help you to understand my lecture and most of the problems do not assume any advanced knowledge. The answers will be given in my lecture.

*This work is supported by Grant-in-Aid for Scientific Research in Japan (Nos. 21340073 and 20105003).

Contents

I. INTRODUCTION

The nucleus is a self-bound quantum system which presents a rich variety of phenomena. It is composed of fermions of spin 1/2 and isospin 1/2, called nucleons (protons and neutrons), interacting with each other through a complex interaction with a short-range repulsive core. Extensive studies have been made in the past, to introduce models and effective interactions to describe a variety of nuclear phenomena and to understand basic nuclear dynamics behind them (Bohr and Mottelson, 1969; Ring and Schuck, 1980). Simultaneously, significant efforts have been made in the microscopic foundation of those models.

For light nuclei, the "first-principles" large-scale computation, starting from the bare nucleon-nucleon (two-body & three-body) forces, is becoming a current trend in theoretical nuclear physics. Although the ab-initio-type approaches have recently shown a significant progress, they are still limited to nuclei with the small mass number. In contrast, the mean-field model is a leading theory for describing nuclear properties of heavy nuclei and perhaps the only theory capable of describing all nuclei and nuclear matter with a single universal energy density functional. The nuclear mean-field models are not based on the mean-field

approach to the Hamiltonian with the bare nucleon-nucleon forces. Instead, its concept is closer to the density functional theory and it is based on a historical development of the Brueckner-Hartree-Fock theory and introduction of the effective interaction. In either way, the nuclear properties are well described by the self-consistent single-particle equations (the Hartree-Fock (HF) equation or the Kohn-Sham (KS) equation).

$$h[\rho]|\phi_i\rangle = \epsilon_i|\phi_i\rangle, \quad \text{or} \quad i\frac{\partial}{\partial t}|\psi_i(t)\rangle = h[\rho(t)]|\psi_i(t)\rangle, \quad i = 1, \cdots, A. \tag{1}$$

In this lecture note, I adopt the natural unit, $\hbar = c = 1$.

I briefly review basic properties of nuclei and discuss whether those properties can be understood by a simple independent-particle model. Then, I recapitulate developments in the microscopic many-body theory leading to the nuclear density functional model. Here, the saturation property plays a key role to understand the nuclear force and the effective interaction. Then, if I have enough time, I will present some result of our recent study with the time-dependent density functional approach. Intensive studies in nuclear density functional models in recent years have produced numerous results and new insights into nuclear structure. You may find these developments in other lecturers in this summer school and in references (Bender *et al.*, 2003; Lunney *et al.*, 2003).

II. NUCLEAR MEAN-FIELD MODELS (DENSITY FUNCTIONAL MODEL)

Nuclei are known to be well characterized by the saturation property. Namely, they have an approximately constant density $\rho_0 \approx 0.16$ fm^{-3}, and a constant binding energy per particle $B/A \approx 16$ MeV.[1] In this section, I show that the nuclear saturation property has a great impact on nuclear models. Especially, it is inconsistent with the independent-particle model of nuclei with a "naive" average (mean-field) potential.

There are many evidences for the fact that the mean-free path of nucleons is larger than the size of nucleus. In fact, the mean free path depends on the nucleon's energy, and becomes larger for lower energy (Bohr and Mottelson, 1969). Therefore, it is natural to assume that the nucleus can be primarily approximated by the independent-particle model with an average one-body potential. The crudest approximation is the degenerate Fermi

[1] This is the extrapolated value for the infinite nuclear matter without the surface and the Coulomb energy. The observed values for finite nuclei are $B/A \approx 8$ MeV.

gas of the same number of protons and neutrons ($Z = N = A/2$). The observed saturation density of $\rho_0 \approx 0.16$ fm^{-3} gives the Fermi momentum, $k_F \approx 1.35$ fm^{-1}, that leads to the Fermi energy (the maximum kinetic energy), $T_F = k_F^2/2M \approx 40$ MeV.

Problem 1

Show the relation between the density ρ and the Fermi momentum k_F, for symmetric nuclear matter ($N = Z = A/2$) and for the neutron matter.

A. Simple independent particle model

First, I show that the independent-particle model with a constant attractive potential $V < 0$ cannot describe the nuclear saturation property. It follows from the simple arguments. The constancy of B/A means that it is approximately equal to the separation energy of nucleons, S. In the independent-particle model, it is estimated as

$$S \approx B/A \approx -(T_F + V). \tag{2}$$

Since the binding energy is $B/A \approx 16$ MeV, the potential V is about -55 MeV. It should be noted that the relatively small separation energy is the consequence of the significant cancellation between kinetic and potential energies. The total (binding) energy is given by

$$-B = \sum_{i=1}^{A} \left(T_i + \frac{V}{2} \right) = A \left(\boxed{?}\, T_F + \frac{V}{2} \right), \tag{3}$$

where we assume that the average potential results from a two-body interaction. The two kinds of expressions for B/A, Eqs. (2) and (3), lead to $T_F \approx -5V/4 \approx 70$ MeV, which is different from the previously estimated value (~ 40 MeV). Moreover, it contradicts the fact that the nucleus is bound ($T_F < |V|$).

Problem 2

Calculate the factor $\boxed{?}$ in front of T_F in Eq. (3). Then, show that this factor is independent from the number of spin-isospin degeneracy.

To reconcile the independent-particle motion with the saturation property of the nucleus, the nuclear average potential should be state dependent. Allowing the potential V_i depend on the state i, the potential V should be replaced by that for the highest occupied orbital V_F in Eq. (2), and by its average value $\langle V \rangle$ in the right-hand side of Eq. (3). Then, we obtain the following relation:

$$V_F \approx \langle V \rangle + T_F/5 + B/A. \tag{4}$$

Therefore, the potential V_F is shallower than its average value.

Weisskopf suggested the momentum-dependent potential V, which can be expressed in terms of an effective mass m^* (Weisskopf, 1957):

$$V_i = U_0 + U_1 \frac{k_i^2}{k_F^2}. \tag{5}$$

Actually, if the mean-field potential is non-local, it can be expressed by the momentum dependence. Equation (5) leads to the effective mass, $m^*/m = (1 + U_1/T_F)^{-1}$. Using Eqs. (2), (4), and (5), we obtain the effective mass as

$$\frac{m^*}{m} = \left\{ \boxed{?} + \boxed{?} \frac{B}{A} \frac{1}{T_F} \right\}^{-1} \approx 0.4. \tag{6}$$

Quantitatively, this value disagrees with the experimental data. The empirical values of the effective mass vary according to the energy of nucleons, $0.7 \lesssim m^*/m \lesssim 1$, however, they are almost twice larger than the value in Eq. (6). As far as we use a normal two-body interaction, this discrepancy should be present in the mean-field calculation with any interaction, because Eq. (6) is valid in general for a saturated self-bound system. Therefore, the conventional models cannot simultaneously reproduce the most basic properties of nuclei; the binding energy and the single-particle property. This suggest the importance of the state-dependent effective interaction, which will be discussed in Sec. II.C.

Problem 3

Calculate the factors $\boxed{?}$ in Eq. (6).

B. Nucleon-nucleon interaction

The saturation property of nuclear density indicates the balance between attractive and repulsive contributions to nuclear binding energy. One source of such repulsive effects is the nucleonic kinetic energy of the Fermi gas. However, its contribution per particle is proportional to $\rho^{2/3}$, which is not strong enough to resist against the collapse caused by the attractive force between nucleons. Therefore, the nucleonic interaction must contain a repulsive element. Indeed, the phase-shift analysis on the nucleon-nucleon scattering at high energy ($E > 250$ MeV) reveals a short-range strong repulsive core in the nucleonic force. The radius of the repulsive core is approximately $c \approx 0.5$ fm. This strong repulsive core prevents the nucleons approaching closer than the distance c, which produces a strong

two-body correlation, $\rho^{(2)}(\vec{r}_1, \vec{r}_2) \approx 0$ for $|\vec{r}_1 - \vec{r}_2| < c$. The attractive part of the interaction has a longer range, which can be characterized by the pion's Compton wave length λ_π, and is significantly weaker than the repulsion. Thus, a naive application of the mean-field calculation fails to bind the nucleus, since the mean-field approximation cannot take account of such strong two-body correlations.

At first sight, this seems inconsistent with the experimental observations. As I mentioned in Sec. II, there are many experimental evidences for the independent-particle motion in nuclei. We may intuitively understand that it is due to the fact that the nucleonic density is significantly smaller than $1/c^3$. Therefore, the collisions by the repulsive core rarely occur and the system can be approximately described in terms of the independent-particle motion. Furthermore, the effects of the Pauli principle hinder the collisions, since the nucleons cannot be scattered into occupied states. Although the repulsive-core collisions are experienced by only a small fraction of nucleons ($\sim \rho_0 c^3$), each collision carries a large amount of energy. Therefore, the repulsive core provides an important contribution to the total energy and are responsible for the saturation.

Another important factor for the independent particle motion is the strong quantum nature due to the weakness of the attractive part of the nuclear force. The importance of the quantum nature can be measured by the magnitude of the zero-point kinetic energy compared to that of the interaction. If the attractive part of the nuclear force were much stronger than the unit of $\hbar^2/Mc^2$, the quantum effect would disappear and each nucleon would stay at the bottom of the interaction potential (cf. Fig. 2-36 in Ref. (Bohr and Mottelson, 1969)). Then, the nucleus would crystallize at low temperature. In reality, the attraction of the nuclear force is so weak that it barely produces many-nucleon bound states at the relatively low density. In Sec. II.A, I have shown that, in nuclear binding energy, there is a strong cancellation between the positive kinetic energy and the negative potential energy. The nucleonic kinetic energy plays an important role in many phenomena in nuclei, which can be described in terms of the independent-particle motion.

C. Density-dependent Hartree-Fock method and energy density functional

The nuclear matter theory pioneered by Brueckner gives a hint for a solution for the inconsistency between the nuclear saturation and the independent-particle model. Details

of the theory can be found at Refs. (Day, 1967; Ring and Schuck, 1980). The independent-particle motion under the presence of the interaction with a repulsive core was qualitatively discussed in Sec. II.B. The Brueckner theory may provide a first step toward the quantitative treatment to understand the saturation property and the independent-particle motion in nuclei.

The basic ingredient of the Brueckner theory is a two-body scattering matrix of particle 1 and 2 inside nucleus caused by the nuclear force v,

$$G(\omega) \equiv v + v\frac{Q}{\omega - Q(T_1 + T_2)Q}G(\omega), \tag{7}$$

where T_i is the kinetic energy of particle i, Q is the Pauli-exclusion operator to restrict the intermediate states, and ω is called a starting energy that depends on energies of particle 1 and 2. This is called G-matrix (Bethe and Goldstone, 1957). The G-matrix renormalizes high-momentum components in the bare nuclear force and becomes an effective interaction in nuclei under the independent-pair approximation. The G-matrix reflects an underlying structure of the independent many-nucleon system through the operator Q and the starting energy ω. Inevitably, the G-matrix becomes state (structure) dependent.

Since the short-range singularity is renormalized in the G-matrix, we can calculate the total energy in the independent-particle (mean-field) model, analogous to Eq. (3).

$$-B = \sum_{i=1}^{A}\left\{T_i + \frac{1}{2}\sum_{j=1}^{A}\bar{G}_{ij,ij}(\omega_{ij})\right\} \tag{8}$$

where $\omega_{ij} = \epsilon_i + \epsilon_j$, defines the self-consistency condition for the Brueckner's single-particle energies, and $\bar{G}_{ij,ij} \equiv G_{ij,ij} - G_{ij,ji}$. This is called Brueckner-Hartree-Fock (BHF) theory. The validity of the BHF theory is measured by the wound integral $\kappa = \langle\psi - \phi|\psi - \phi\rangle$, where $|\phi\rangle$ is an unperturbed two-particle wave function and $|\psi\rangle$ is a correlated two-particle wave function in nucleus. κ is known to be of the order of 15 %. The BHF calculation was successful to describe the nuclear saturation, however, could not reproduce simultaneously B/A and ρ_0, known as a problem of the Coester band (Day, 1981). Its applications to finite nuclei also quantitatively failed to reproduce the energy, radius, and density in the ground state.

These problems are somewhat miraculously solved by the density-dependent Hartree-Fock (DDHF) theory by Negele (Negele, 1970). Starting from a realistic G-matrix, first, the

local density approximation is introduced, using the expressions for the Pauli operator

$$\langle \vec{r}_1 \vec{r}_2 | Q | \vec{r}_1' \vec{r}_2' \rangle = \{\delta(\vec{r}_1 - \vec{r}_1') - \rho(\vec{r}_1 - \vec{r}_1')\} \{\delta(\vec{r}_2 - \vec{r}_2') - \rho(\vec{r}_2 - \vec{r}_2')\}, \tag{9}$$

and the average single-particle energy $\epsilon[\rho(\vec{r})]$. Then, a short-range part of the G-matrix, which is not fully understood, is phenomenologically added to the energy expression to quantitatively fit the saturation property, and finally, the total energy is treated variationally. This procedure is called the density matrix expansion (DME) (Negele and Vautherin, 1972). The state dependence of the G-matrix is now replaced by the density dependence. The final result for the energy is of the form

$$E[\rho] = \int d\vec{R} H(\vec{R}), \quad H(\vec{R}) = H[\rho(\vec{R})] = H[\psi^*, \psi], \tag{10}$$

which is completely analogous to the Hamiltonian density of the Skyrme energy functional (Vautherin and Brink, 1972).

The essential aspect of the DDHF comes from the density dependence and the variational treatment. The variation of the total energy with respect to the density contains re-arrangement potential, $\partial V_{\rm eff}[\rho]/\partial\rho$, which appear due to the density dependence of the effective force $V_{\rm eff}[\rho]$. These terms turn out to be crucial to obtain the saturation condition. Now, the expression for the total energy, Eq. (3), should be modified to include the re-arrangement effect. This resolves the previous issue, then provides a consistent independent-particle description for the nuclear saturation.

In summary, the failure in the mean-field description of nuclei using phenomenological effective interactions can be traced back to the missing state (structure) dependence. The DDHF takes into account the state dependence in terms of the density dependence. This provides a foundation for the nuclear energy functional.

D. Skyrme-Hartree-Fock-Bogoliubov calculation

The solution of the DDHF requires a complicated task. However, the energy functional obtained by the DME is essentially identical to the Skyrme energy functional. Vautherin and Brink (Vautherin and Brink, 1972) revived the effective interaction originally proposed by Skyrme in 1959 and showed that the HF calculation with the Skyrme interaction can be a feasible alternative to the DDHF. The feasibility is very important when we want to

extend the approach to dynamical problems, such as the time-dependent Hartree-Fock and the random-phase approximation.

A modern energy functional for nuclei is a functional of many kinds of density, such as kinetic $\tau(\vec{r})$ and spin-orbit density $\vec{J}(\vec{r})$. In addition, to describe superfluid nuclei with pairing correlation, we need to add the pair (abnormal) density $\kappa(\vec{r})$. It is convenient to define the generalized density R for the many-body state $|\Phi\rangle$ as

$$\begin{aligned} R(\vec{r}\sigma\tau, \vec{r'}\sigma'\tau') &\equiv \langle\Phi| \begin{pmatrix} \psi^\dagger_{\sigma'\tau'}(\vec{r'})\psi_{\sigma\tau}(\vec{r}) & \psi^\dagger_{\sigma'\tau'}(\vec{r'})\psi_{\sigma\tau}(\vec{r}) \\ \psi^\dagger_{\sigma'\tau'}(\vec{r'})\psi^\dagger_{\sigma\tau}(\vec{r}) & \psi_{\sigma'\tau'}(\vec{r'})\psi^\dagger_{\sigma\tau}(\vec{r}) \end{pmatrix} |\Phi\rangle \\ &= \begin{pmatrix} \rho(\xi,\xi') & \kappa(\xi,\xi') \\ -\kappa^*(\xi,\xi'') & 1-\rho^*(\xi,\xi') \end{pmatrix}, \end{aligned} \tag{11}$$

where $\xi = (\vec{r}, \sigma, \tau)$. The Skyrme energy density functional $E[R]$ depends on the densities with some derivatives which can be expressed as a diagonal limit of the off-diagonal density. For instance, the kinetic density is given by $\tau(\xi) = \lim_{\xi'\to\xi} \nabla\cdot\nabla'\rho(\vec{\xi},\vec{\xi'})$. Together with constraints on the average number and the generalized Slater determinant ($R^2 = R$), variation of the total energy with respect to the density R, $\mathcal{H} \equiv \delta E[R]/\delta R$, leads to the Hartree-Fock-Bogoliubov (HFB) equation: $[\mathcal{H}, R] = 0$. Introducing the quasi-particle orbitals that simultaneously diagonalize R and $\mathcal{H}$, the HFB equation can be rewritten as

$$\mathcal{H}[R]|\phi_\mu\rangle = E_\mu|\phi_\mu\rangle, \qquad \text{with} \quad \mathcal{H}[R] \equiv \begin{pmatrix} h-\lambda & \Delta \\ -\Delta^* & -(h-\lambda)^* \end{pmatrix}, \tag{12}$$

where E_μ and $|\phi_\mu\rangle$ are the quasi-particle energies and states, respectively (Blaizot and Ripka, 1986; Ring and Schuck, 1980). $|\phi_\mu\rangle$ is composed of two components; the upper $|U_\mu\rangle$ and the lower one $|V_\mu\rangle$. The solution of Eq. (12) defines the normal density $\rho(\vec{r}) = \sum_\mu V_\mu(\vec{r})V^*_\mu(\vec{r})$, the pair density $\kappa(\vec{r}) = \sum_\mu U_\mu(\vec{r})V_\mu(\vec{r})$, and other densities at the ground state. Since $\mathcal{H}[R]$ depends on these densities, Eq. (12) must be solved in a self-consistent way.

When the quasi-particle state $|\phi_\mu\rangle = (|U_\mu\rangle, |V_\mu\rangle)^T$ is a solution of Eq. (12), it is easy to prove that the state $|\bar{\phi}_\mu\rangle \equiv (|V^*_\mu\rangle, |U^*_\mu\rangle)^T$ is also a solution with the quasi-particle energy $-E_\mu$. Thus, we need to solve only the positive (negative) energy solutions of Eq. (12). Those with the positive (negative) quasi-particle energies are often called "unoccupied" ("occupied") states. However, you should not take these words so seriously, because they are not related to real occupation probabilities. The generalized density R can be expressed

as

$$R(\xi,\xi') = \sum_\mu \begin{pmatrix} V_\mu^*(\xi) \\ U_\mu^*(\xi) \end{pmatrix} \Big(V_\mu(\xi') \;\; U_\mu(\xi') \Big) = \sum_\mu \bar{\phi}_\mu(\xi)\bar{\phi}_\mu^\dagger(\xi'), \tag{13}$$

using the "occupied" orbitals, $\bar{\phi}_\mu$. This expression is analogous to the HF case ($\Delta = 0$): $\rho(\xi,\xi') = \sum_{i=1}^A \phi_i(\xi)\phi_i^*(\xi')$, where ϕ_i are occupied (hole) single-particle orbitals. It should be noted that these properties of the HFB are true not only in the static case but also in the time-dependent case discussed in Sec. III.B.

Minimization of the energy density functional may lead to a spontaneous breaking of symmetry. An example is given in Fig. 1 for Nd isotopes (Yoshida and Nakatsukasa, 2011). The intrinsic quadrupole moment calculated with the Skyrme functional of SkM* is compared with the experimental data. At $N = 82$, the nucleus at the ground state is spherical $Q_0 = 0$, while for $N = 86 \sim 92$, the deformation gradually develops. The observed ground-state deformations deduced from the transition probability $B(E2; 2^+ \to 0^+)$ are nicely reproduced. Note that there are no adjustable parameters in this calculation. It should be noted that the finite pair density is also a consequence of the spontaneous breaking of the gauge symmetry. At $N = 82$, the neutron pair density is zero, while it becomes finite for $N = 84 \sim 92$.

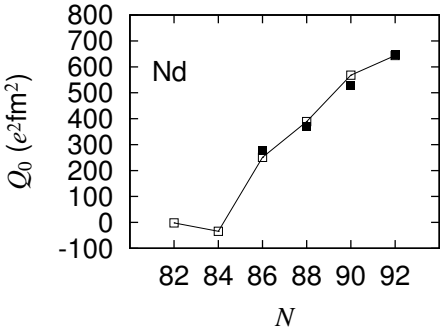

FIG. 1 Calculated (open squares) and experimental (filled) intrinsic quadrupole moment for Nd isotopes (Yoshida and Nakatsukasa, 2011).

Problem 4

Prove that the states $|\phi_\mu\rangle$ and $|\bar{\phi}_\mu\rangle$ are simultaneous solutions of the HFB equation with the eigenenergies of E_μ and $-E_\mu$, respectively.

III. GIANT RESONANCES

A. Nuclear matter and giant resonances

The giant resonance (GR) is a typical collective motion in nuclei, which exhausts a major part of the sum-rule value. They are also related to the basic properties of nuclear matter, such as incompressibility K_∞, effective mass m^*, etc.

The nuclear matter incompressibility is extracted from properties of the isoscalar giant monopole resonances (Blaizot, 1980),

$$K_\infty = 210 \pm 30 \text{ MeV}. \tag{14}$$

This gives a restriction on the density dependence of the phenomenological short-range repulsive part of the energy functional. In the Skyrme energy functional, this density-dependent repulsive part has a form of

$$E_{\rm DD}[\rho] = \int d\vec{r} \left[\frac{1}{12} t_3 \left(1 + \frac{x_3}{2}\right) \rho^{\alpha+2}(\vec{r}) - \frac{1}{12} t_3 \left(\frac{1}{2} + x_3\right) \rho^{\alpha}(\vec{r}) \left\{ \rho_n^2(\vec{r}) + \rho_p^2(\vec{r}) \right\} \right]. \tag{15}$$

Here, the parameter α consistent with the saturation property and the incompressibility of Eq. (14) is known to be $\alpha = 1/6 \sim 1/3$.

The effective mass deduced from the analysis on the giant quadrupole resonances is (Blaizot, 1980)

$$m^*/m \approx 0.8 \sim 1. \tag{16}$$

As we have seen in Eq. (6), this value is inconsistent with the naive mean-field value of $m* \approx 0.4m$. We need a state-dependent (density-dependent) interaction to make the observed effective mass compatible with the saturation.

The bulk properties of the nuclear matter can be well characterized by the Landau parameters of the Fermi liquid theory. For the Landau's Fermi liquid theory, I want to refer you to textbooks, for instance the one by Negele and Orland (Negele and Orland, 1988). The Landau parameters specify the interaction between the quasi-particles $f(\vec{k}_1, \vec{k}_2)$ on the Fermi surface ($|\vec{k}_1| = |\vec{k}_2| = k_F$). When we expand $f(\vec{k}_1, \vec{k}_2)$ with the Legendre function $P_l(\hat{k}_1 \cdot \hat{k}_2)$, the Landau parameters F_l are defined by their coefficients. The isospin-dependent, spin-dependent, spin-isospin-dependent parts are defined in the same way, giving the Landau parameters of F'_l, G_l, G'_l, respectively. The incompressibility and the effective mass are related to the Landau parameters F_0 and F_1 as follows:

$$K_\infty = \frac{3k_F^2}{m^*}(1 + F_0), \qquad \frac{m^*}{m} = 1 + \frac{F_1}{3}. \tag{17}$$

From these relations, we can estimate the values as $F_1 \approx -0.9 \sim 0$ and $F_0 \approx -0.4 \sim 0$. Observed properties of the Gamow-Teller resonances and the spin excitations give us a hint for the G'_0 and G_0 ($G'_0 \approx 0.9 \sim 1.2$, $G_0 \lesssim 0.3$). The value of F'_0 is estimated from the symmetry energy as $F'_0 \approx 0.6 \sim 1.5$. These Landau parameters provide an additional constraint on the energy functional.

B. Time-dependent density functional approaches to GR

The giant resonances can be reasonably described by a small-amplitude approximation of the time-dependent version of the DDHF. In this approach, again, the re-arrangement terms, such as $\partial V_{\rm eff}[\rho]/\partial\rho$ and $\partial^2 V_{\rm eff}[\rho]/\partial\rho^2$ should be consistently taken into account. The theory can be regarded as the time-dependent density-functional theory, founded by Runge and Gross (Runge and Gross, 1984).

For a study of the giant resonances, we need to extend the energy functional to include the time-odd densities, such as the spin density $\vec{s}(\vec{r})$ and the current density $\vec{j}(\vec{r})$. Now, these densities are time dependent. The time-dependent version of Eq. (12) is

$$i\frac{\partial}{\partial t}|\phi_\mu(t)\rangle = H[R(t)]|\phi_\mu(t)\rangle. \tag{18}$$

This equation automatically conserves the average total energy and average particle number (Blaizot and Ripka, 1986). Thus, the chemical potential λ in Eq. (12) is not necessary for the time-dependent equation. Actually, the pair potential $\Delta(t)$ and the abnormal density $\kappa(t)$ depends on the choice of the gauge λ, while the density $\rho(t)$ and the single-particle Hamiltonian $h(t)$ are independent from λ. The different choice of λ changes the phases of $|\phi_\mu(t)\rangle$, the pair potential $\Delta(t)$, and the abnormal density $\kappa(t)$.

Problem 5

A static solution of Eq. (12), $|\phi_\mu^{(0)}\rangle$, corresponds to a solution of Eq. (18) as $|\phi_\mu(t)\rangle = |\phi_\mu^{(0)}\rangle e^{-iE_\mu t}$, adopting the same value of the chemical potential λ. If we adopt a gauge of $\lambda = 0$, how should we modify the phases of $|\phi_\mu(t)\rangle$, $\kappa(t)$, and $\Delta(t)$?

Assuming the oscillation with a fixed frequency, this equation is linearized with respect to the fluctuation of the densities around those at the ground state. This leads to the matrix form of the equation identical to the quasi-particle random-phase approximation (QRPA) (Blaizot and Ripka, 1986; Ring and Schuck, 1980).

$$\sum_{\gamma\delta}\begin{pmatrix} A_{\alpha\beta,\gamma\delta} & B_{\alpha\beta,\gamma\delta} \\ -B_{\alpha\beta,\gamma\delta} & -A_{\alpha\beta,\gamma\delta}\end{pmatrix}\begin{pmatrix} X_{\gamma\delta} \\ Y_{\gamma\delta}\end{pmatrix} = \hbar\omega\begin{pmatrix} X_{\alpha\beta} \\ Y_{\alpha\beta}\end{pmatrix}. \tag{19}$$

The QRPA matrix, A and B, are calculated in the quasi-particle basis, then the normal modes of excitation and their energies are obtained from Eq. (19).

It is quite tedious task to calculate all the matrix elements of $A_{\alpha\beta,\gamma\delta}$ and $B_{\alpha\beta,\gamma\delta}$, because it requires the calculation of the two-body(-like) operators. To simplify the calculation and

numerical cost, we have developed a feasible approach to avoid calculation of these two-body matrix elements, which is named as "finite amplitude method". In this new approach, instead of explicit calculation of the QRPA matrix, we resort to an iterative approach to the QRPA without construction of the QRPA matrix in Eq. (19). The details of the method and its applications can be found in our recent papers (Avogadro and Nakatsukasa, 2011; Inakura *et al.*, 2009, 2011; Nakatsukasa *et al.*, 2007).

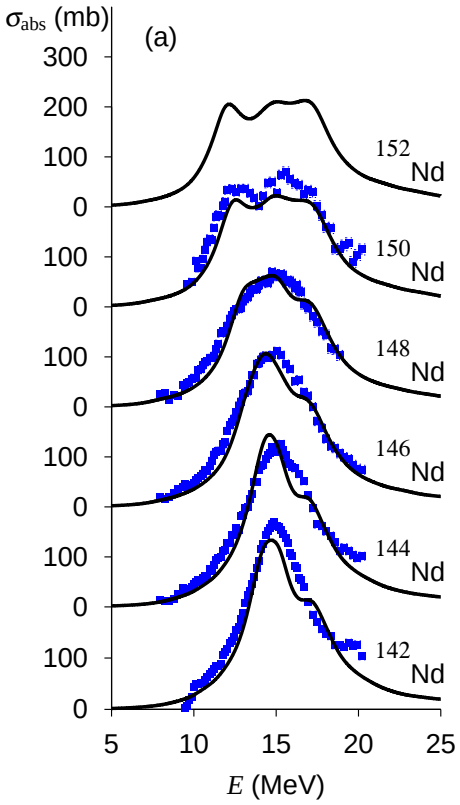

FIG. 2 Calculated (lines) and experimental (symbols) photoabsorption cross sections for Nd isotopes (Yoshida and Nakatsukasa, 2011).

As an example of the QRPA calculation, the calculated photoabsorption cross sections for Nd isotopes are shown in Fig. 2. We use the same energy functional as that for Fig. 1. For spherical nuclei ($N = 82$ and 84), the photoabsorption has a single peak for the photon energy of $E \approx 15$ MeV. The increase of the neutron number results in the broadening of the peak, which well agree with the experimental data. This is due to the increase of the ground-state deformation shown in Fig. 1. The calculated energy-weighted sum-rule values for these isotopes are about 40 % larger than the classical Thomas-Reiche-Kuhn sum-rule value, because of the momentum and isospin dependence of the mean field (Kohn-Sham) potential. This enhancement factor κ is related to the Landau parameter F_1' as

$$1 + \kappa = \frac{m}{m^*}\left(1 + \frac{F_1'}{3}\right). \tag{20}$$

The value of κ is also related to the increment of the orbital g factor as $\delta g_l = -\kappa\tau_z/2$ (Bohr and Mottelson, 1975). The observed value is qualitatively consistent with the enhancement factor for the giant dipole resonances.

Here, I have discussed the small-amplitude dynamics in the time-dependent mean-field theory, namely the QRPA. For low-lying vibrational states in nuclei, this approximation is often broken down. Furthermore, heavy nuclei such as uranium show a spontaneous fission, which is a quantum tunneling phenomenon and a typical example of the large-amplitude

collective motion in nuclei. There have been extensive studies for developments in theories of the large-amplitude collective motion in nuclear physics (Negele, 1982; Ring and Schuck, 1980). However, this is beyond the scope of this lecture. You could be referred to our recent article on open problems related to this issue (Matsuyanagi *et al.*, 2010).

IV. TEXTBOOKS AND REVIEWS

Most of the contents of this lecture can be found in the following textbooks and review ariticles.

- Section II.A, II.B (Bohr and Mottelson, 1969; Negele, 1982)
- Section II.C, II.D (Blaizot and Ripka, 1986; Negele, 1982; Ring and Schuck, 1980)
- Section III (Blaizot, 1980; Blaizot and Ripka, 1986; Bohr and Mottelson, 1975; Negele, 1982; Ring and Schuck, 1980)

References

Avogadro, P., and T. Nakatsukasa, 2011, phys. Rev. C in press; arXiv:1104.3692.

Bender, M., P. H. Heenen, and P.-G. Reinhard, 2003, Rev. Mod. Phys. **75**, 121.

Bethe, H. A., and J. Goldstone, 1957, Proc. Roy. Soc. (London) **A238**, 551.

Blaizot, J. P., 1980, Phys. Rep. **64**, 171.

Blaizot, J.-P., and G. Ripka, 1986, *Quantum Theory of Finite Systems* (MIT Press, Cambridge).

Bohr, A., and B. R. Mottelson, 1969, *Nuclear Structure, Vol. I* (W. A. Benjamin, New York).

Bohr, A., and B. R. Mottelson, 1975, *Nuclear Structure, Vol. II* (W. A. Benjamin, New York).

Day, B. D., 1967, Rev. Mod. Phys. **39**, 719.

Day, B. D., 1981, Phys. Rev. Lett. **47**, 226.

Inakura, T., T. Nakatsukasa, and K. Yabana, 2009, Phys. Rev. C **80**(4), 044301.

Inakura, T., T. Nakatsukasa, and K. Yabana, 2011, preprint: arXiv:1106.3618.

Lunney, D., J. M. Pearson, and C. Thibault, 2003, Rev. Mod. Phys. **75**, 1021.

Matsuyanagi, K., M. Matsuo, T. Nakatsukasa, N. Hinohara, and K. Sato, 2010, J. Phys. G **37**, 064018.

Nakatsukasa, T., T. Inakura, and K. Yabana, 2007, Phys. Rev. C **76**(2), 024318.

Negele, J. W., 1970, Phys. Rev. C **1**, 1260.

Negele, J. W., 1982, Rev. Mod. Phys. **54**, 913.

Negele, J. W., and H. Orland, 1988, *Quantum Many-Particle Systems* (Addison-Wesley, Reading).

Negele, J. W., and D. Vautherin, 1972, Phys. Rev. C **5**, 1472.

Ring, P., and P. Schuck, 1980, *The nuclear many-body problems*, (Springer-Verlag, New York).

Runge, E., and E. K. U. Gross, 1984, Phys. Rev. Lett. **52**, 997.

Vautherin, D., and D. M. Brink, 1972, Phys. Rev. C **5**, 626.

Weisskopf, V. F., 1957, Nucl. Phys. **3**, 423.

Yoshida, K., and T. Nakatsukasa, 2011, Phys. Rev. C **83**(2), 021304.

Single-particle and collective motions in nuclei
--- The basics of nuclear mean-field models ---

Takashi Nakatsukasa (中務　孝)
RIKEN NiSHiNA CENTER 独立行政法人 理化学研究所 仁科加速器研究センター

- Single-particle motion in nuclei
  - –Experimental evidences
  - –Simple model: inconsistent with experiments
  - –How can we reconcile them?
  - –Nuclear mean-field model (Density functional model)
    - Cf) Lecture by Peter Ring
- Collective motion in nuclei
  - –How can it co-exist with the single-particle motion?
  - –Time-dependent density functional model

2011.8.27--31 ISSSP @Beijing, China

Three faces of nuclei

Liquid

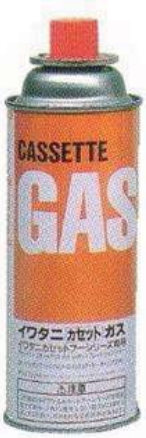

Gas

Chaos

First, “Chaos” picture

- To explain properties of resonances observed in thermal neutron scattering, Niels Bohr introduced a kind of “quantum-chaos” picture for the compound nuclei.
  - Nucleons’ mean free path is shorter than the nuclear size

$$\lambda << R$$

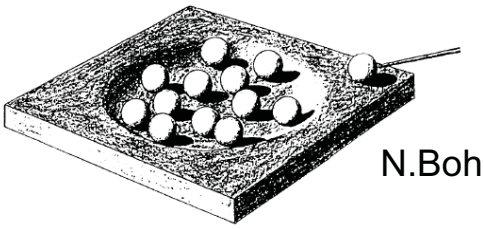

N.Bohr (1936)

  - Is this correct?

Second: “Gas” picture

- Single-particle motion in nuclei
  - Nucleons’ mean free path must be larger than the nuclear size

$$\lambda >> R$$

  - Use the quantum mechanics
- Experimental evidences?

Evidence of the single-particle motion

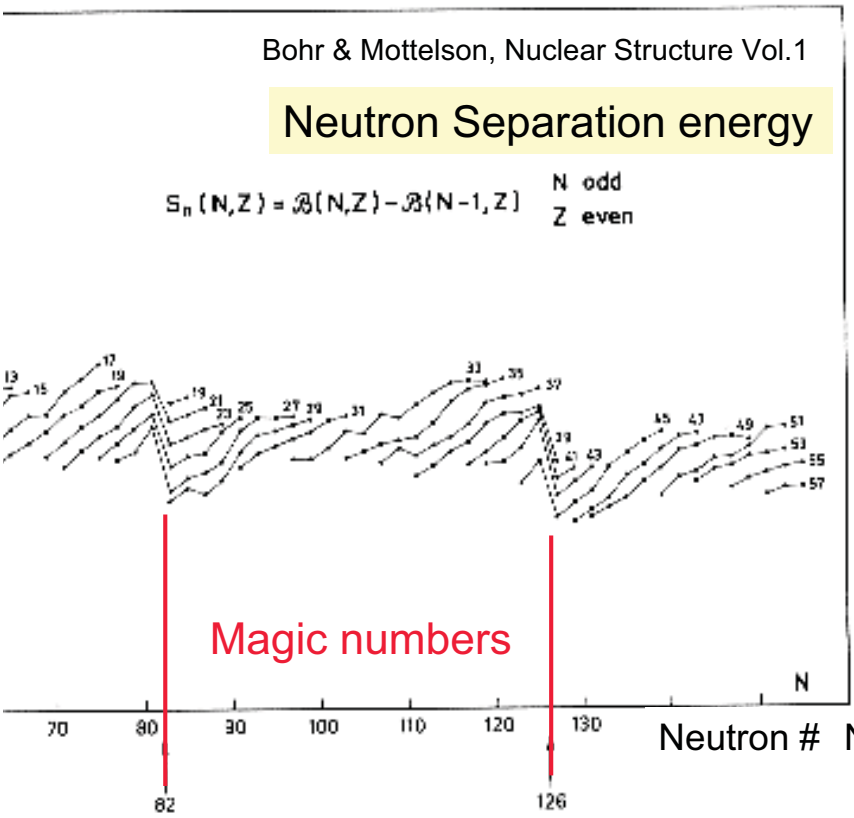

Shell Model
(Mayer-Jensen)

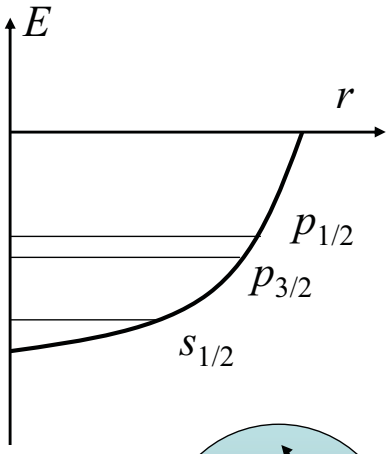

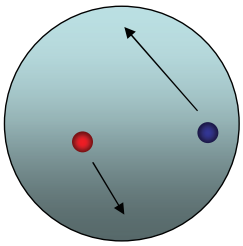

Energy required to remove two neutrons from nuclei

(2-neutron binding energies = 2-neutron "separation" energies)

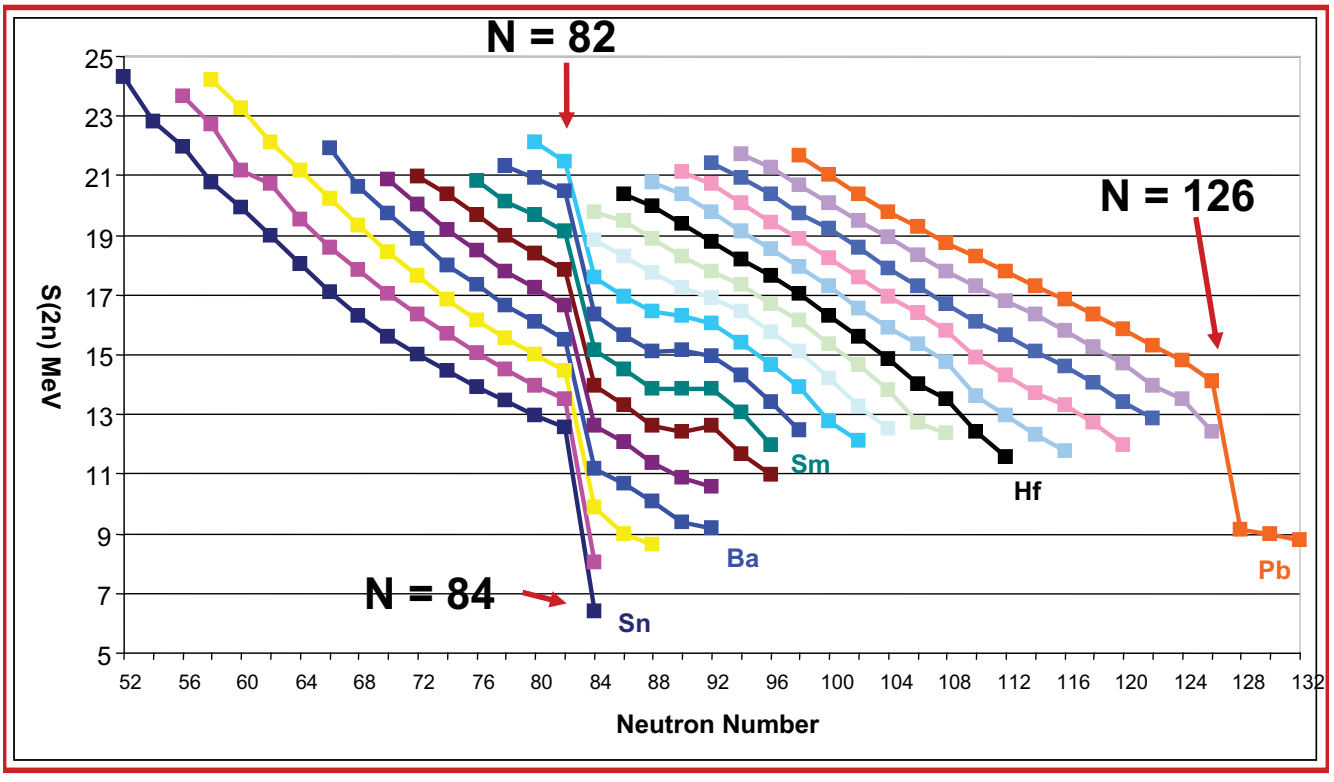

From a lecture by R. Casten

Electronic single-particle motion in atoms

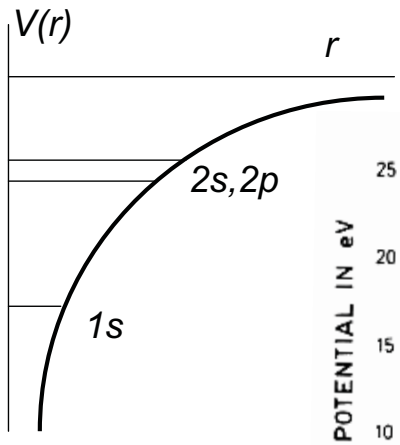

Single-particle orbitals in the Coulomb potential → Magic number

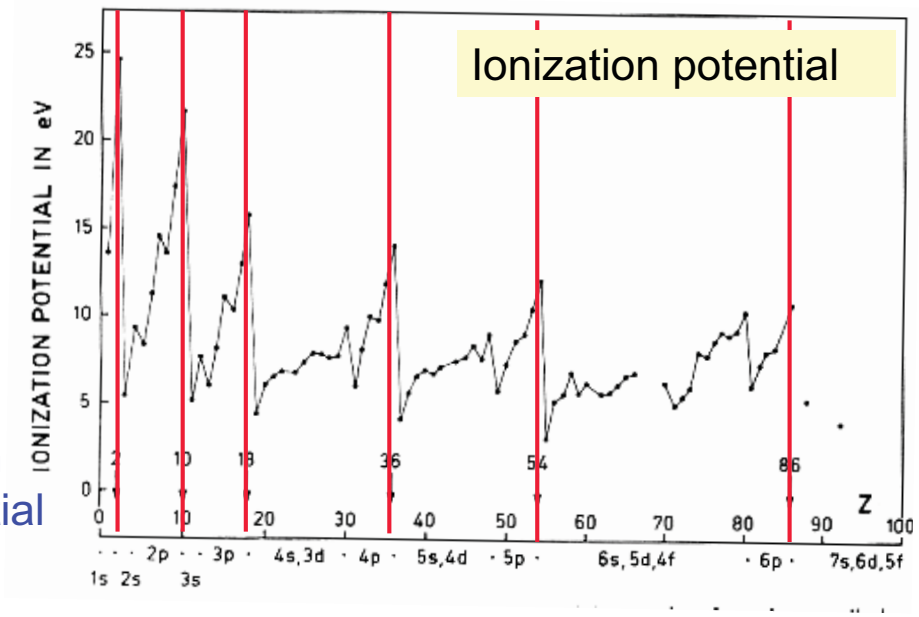

Free particles in Coulomb potential

Mayer-Jensen's Shell Model

Harmonic oscillator potential + spin-orbit force

$$V(r) = \frac{1}{2} M\omega^2 r^2 + v_{ll}\ell^2 + v_{ls}\vec{\ell}\cdot\vec{s}$$

→ Correct magic numbers:

(N,Z)=2, 8, 20, 28, 50, 82, 126

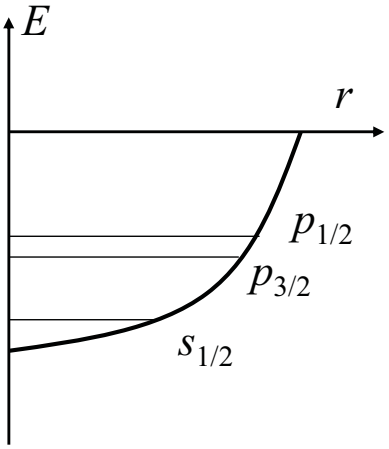

Spin-parity of odd nuclei

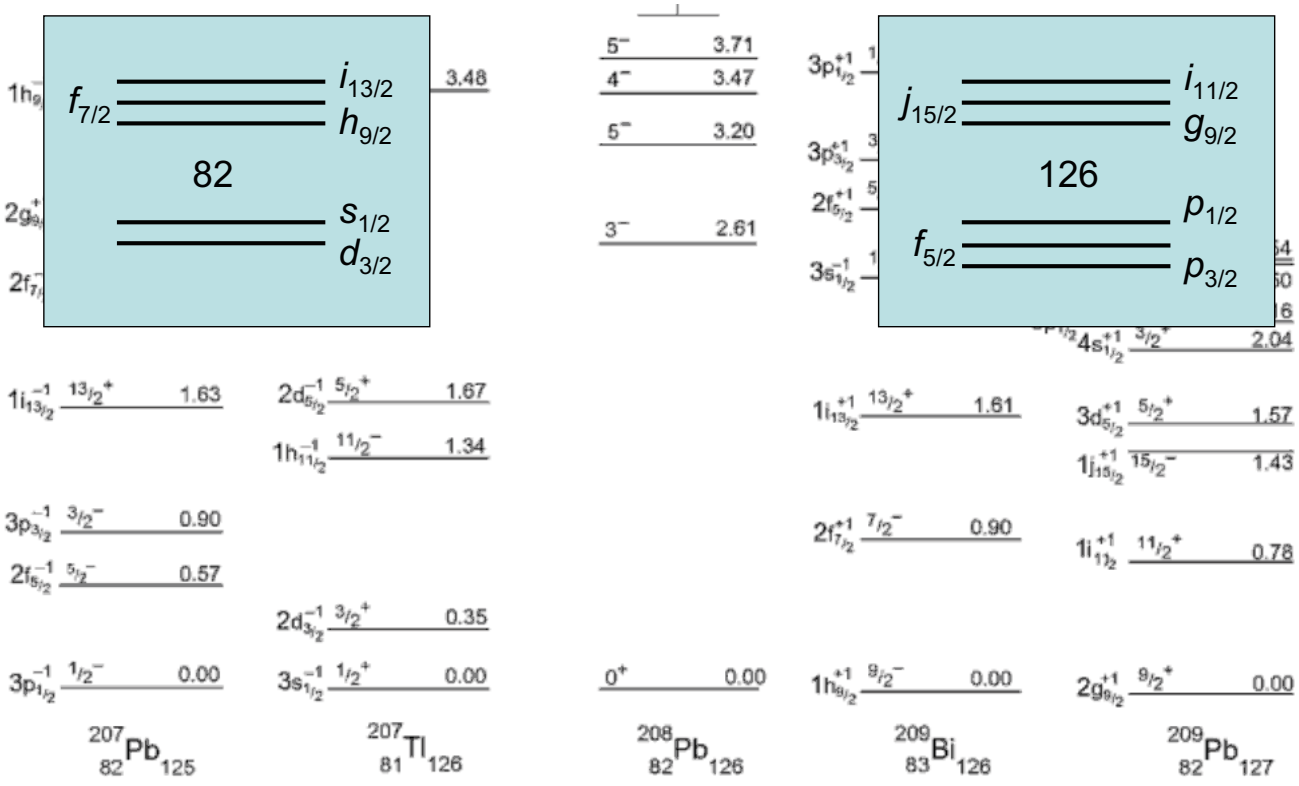

Gas (Shell-model/Mean-field) picture

Phenomenlogical shell-model potential

$$V(r) = \frac{1}{2} M\omega^2 r^2 + v_{ll}\ell^2 + v_{ls}\vec{\ell}\cdot\vec{s}$$

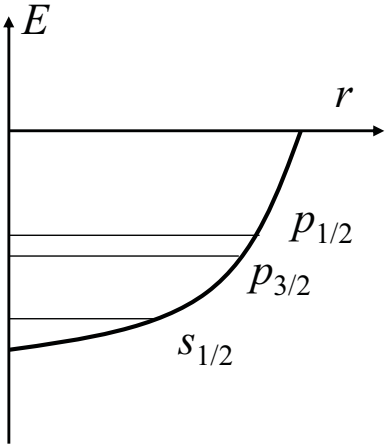

How large is the nucleons' mean free path?

$$\lambda >> R\,?$$

Neutron scattering cross section

From Bohr and Mottelson,
Nuclear Structure Vol.1

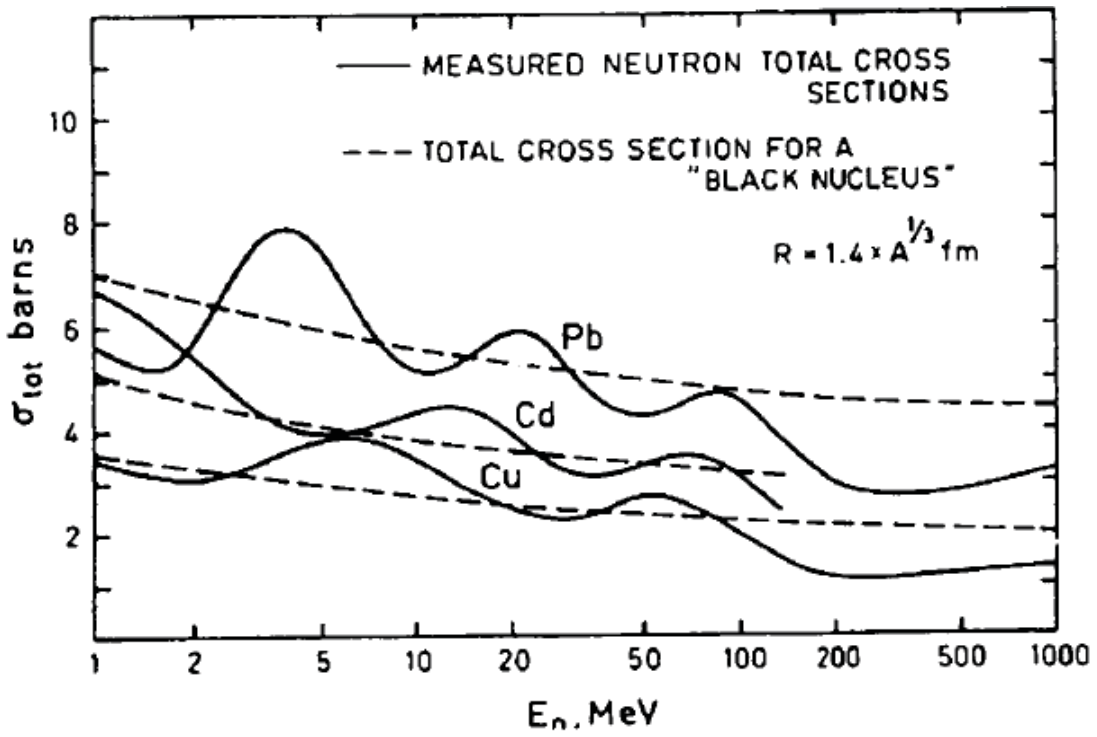

Phase shift & optical theorem

Phase shift

$$\delta(k) \approx 2(k_{in} - k)R$$

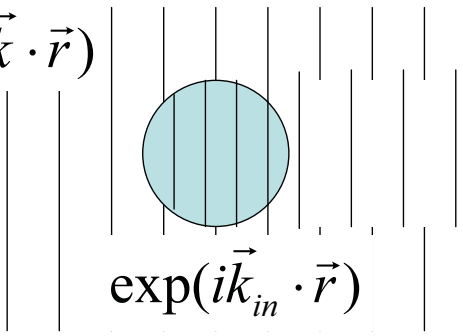

Scattering amplitude

$$f(\theta) = \frac{1}{2ik}\sum_l (2l+1)\left(\exp(2i\delta_l) - 1\right)$$

Total cross section

$$\eta_l = \exp(2i\delta_l), \quad |\eta_l| = 1$$

$$\sigma_{tot} = \frac{4\pi}{k}\,\mathrm{Im}\, f(0) = \frac{4\pi}{k^2}\sum_l (2l+1)\sin^2\delta_l$$

→ Oscillation as a function of energy

cf) Ramsauer-Townsend effect

Neutron scattering cross section

From Bohr and Mottelson,
Nuclear Structure Vol.1

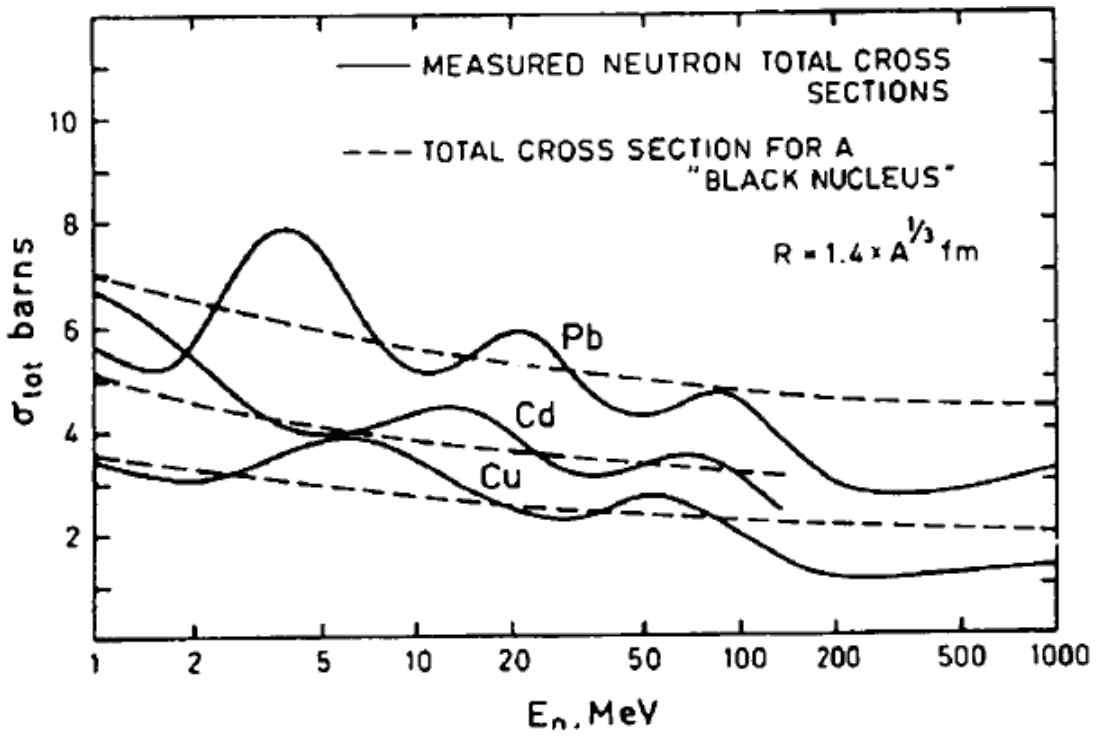

Nuclear transparency

Optical potential

$$V + iW \Rightarrow k_{in} + \frac{i}{2\lambda}$$

Complex phase shift

$$\eta_l = \exp(2i\delta_l), \quad |\eta_l| \le 1$$

Total cross section

$$\sigma_{tot} = \frac{4\pi}{k}\,\mathrm{Im}\, f(0) = \frac{2\pi}{k^2}\sum_l (2l+1)(1-\mathrm{Re}\,\eta_l)$$

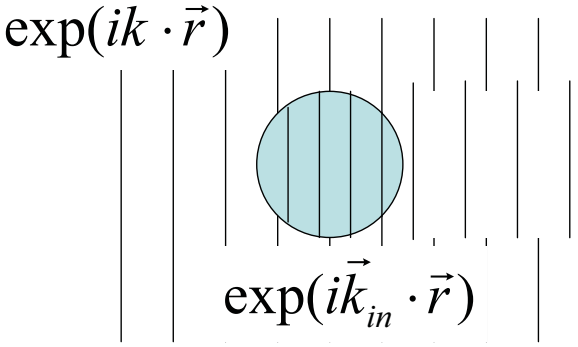

Oscillation frequency → Real part: V

Oscillation amplitude → Imaginary part: W → Mean free path: λ

$-V \approx 50 - 0.3E, \quad -W \approx (0 \sim 2) + 0.1E$ in units of MeV

$\Rightarrow \quad \lambda \approx \alpha R, \quad [\alpha \approx 1 \sim 10 \text{ or more}]$

Energy dependence of the imaginary part

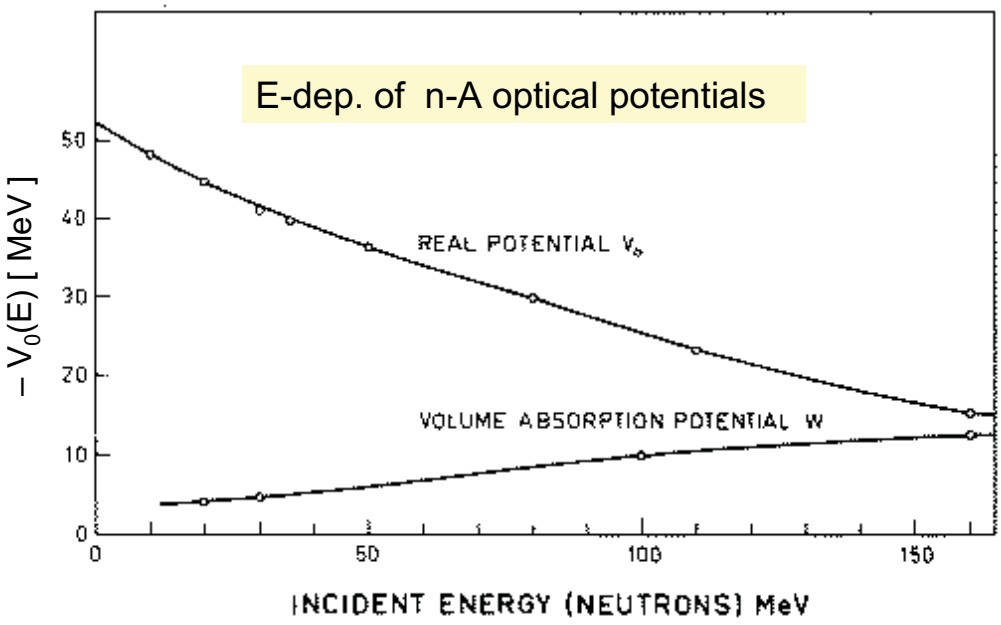

The imaginary potential becomes smaller for lower-energy neutrons.

Third: "Liquid" picture

- Experimental evidences?
  - Saturation property
  - Liquid drop mass formula
  - Fission: fissility parameter

Nuclear Saturation

The most basic property of nucleus

B/A ~ 8 MeV

(B/A ~ 16 MeV for nuclear matter)

Density $\rho \approx 0.16$ fm^{-3}

Liquid drop model

Bethe-Weizsäcker mass formula

$$B(N,Z) = a_V A - a_S A^{2/3} - a_{sym}\frac{(N-Z)^2}{A} - a_C \frac{Z^2}{A^{1/3}} + \delta(A)$$

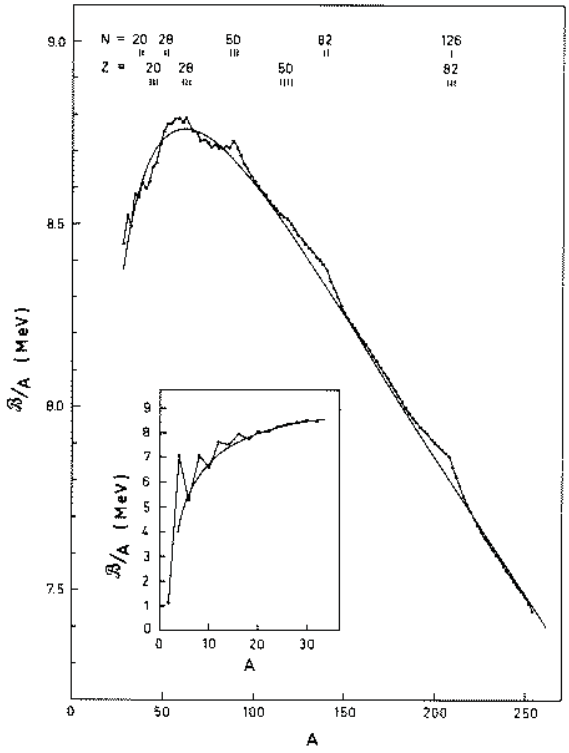

Saturated gas?

- Is the mean-field (gas or single-particle) picture consistent with the saturation property?
  - Analysis with a simple potential model for infinite nuclear matter

$$h = -\frac{\hbar^2}{2m}\nabla^2 + V$$

Saturation properties of nuclear matter

- Symmetric nuclear matter w/o Coulomb
  - $N = Z = A/2$
- Constant binding energy per nucleon
  - Constant separation energy

$$B/A \approx S_{n(p)} \approx 16\ \text{MeV}$$

- Saturation density

$$\rho \approx 0.16\ \text{fm}^{-3} \quad \Rightarrow \quad k_F \approx 1.35\ \text{fm}^{-1}$$

  - Fermi energy

$$T_F = \frac{\hbar^2 k_F^2}{2m} \approx 40\ \text{MeV}$$

A constant mean-field potential

- Separation energy

$$S = -(T_F + V), \quad V \approx -55\ \text{MeV}$$

- Binding energy in the mean field

$$-B = \sum_{i=1}^{A}\left(T_i + \frac{V}{2}\right), \quad T_i = \frac{\hbar^2 k_i^2}{2m}$$

$$= A\left(\frac{3}{5}T_F + \frac{V}{2}\right)$$

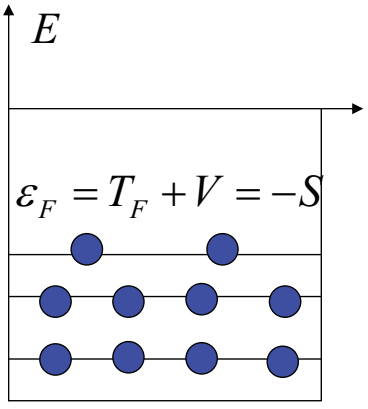

- $S = B/A \quad \Rightarrow \quad T_F = -\frac{5}{4}V$

Inconsistent with nuclear binding

Momentum-dependent potential

- State-dependent potential

$$V_F = \langle V \rangle + {}^{T_F}\!/_{5} + {}^{B}\!/_{A}$$

  – The potential becomes shallower for particles with a weaker binding

- Momentum dependence
  – The lowest order → "Effective mass"

$$V = U_0 + U_1 k^2 \quad \Rightarrow {}^{m^*}\!/_{m} = \left(1 + {}^{U_1 k_F^2}\!/_{T_F}\right)^{-1}$$

$$= \left(\frac{3}{2} + \frac{5}{2}\frac{B}{A}\frac{1}{T_F}\right)^{-1} \approx 0.4$$

Nucleons' effective mass

Energy dependence of optical potential

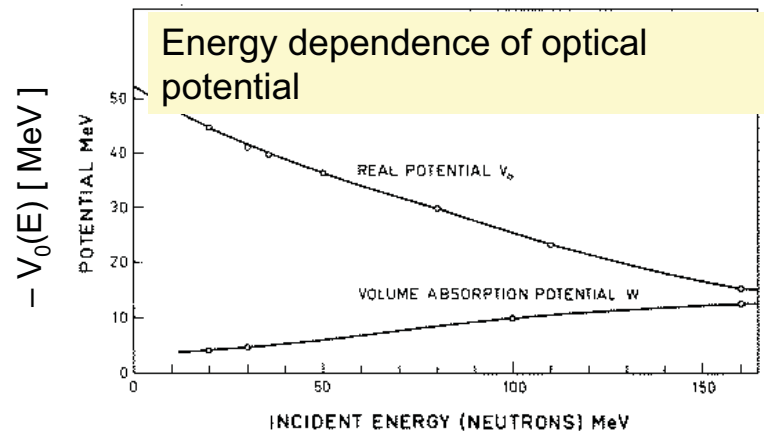

$$V_0 = -52 + 0.3E\,[\,\mathrm{MeV}\,]$$

$$\frac{m^*}{m} = 1 - \frac{dV_0}{dE} \approx 0.7$$

$$\left|E - \varepsilon_F\right| > 20\mathrm{MeV}$$

GQR's analysis → 0.9~1(?)

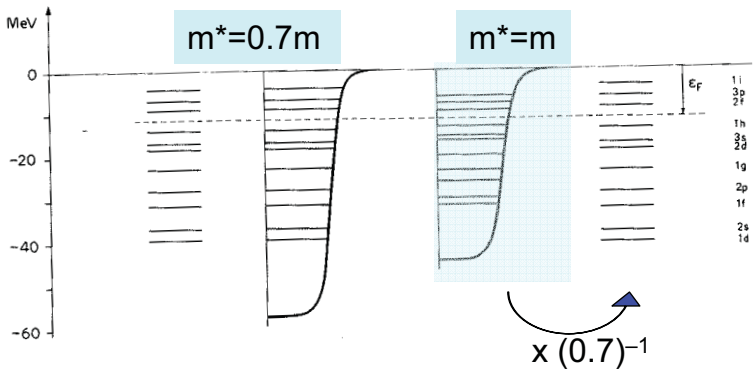

Single-particle level spacings are proportional to m*

Experiments suggest m=m*

$$\frac{m^*}{m} \approx 1 \quad \left|E - \varepsilon_F\right| < 10\mathrm{MeV}$$

Failure of the mean-field models

- In order to explain the nuclear saturation within the mean-field picture, we need an extremely small value of the effective mass.

$$\frac{m^*}{m} = \left(\frac{3}{2} + \frac{5}{2} \frac{B}{A} \frac{1}{T_F} \right)^{-1} \approx 0.4$$

  - This is inconsistent with the experimental data.

$$\frac{m^*}{m} = 0.7 \sim 1$$

A possible solution for the inconsistency

- State-dependent effective interaction
  - Rearrangement terms
- Energy density functional

$$E[\rho] \Rightarrow \quad h[\rho] |\phi_i\rangle = \varepsilon_i |\phi_i\rangle$$

$$h[\rho] \equiv \frac{\delta E}{\delta \rho}$$

Single-particle and collective motions in nuclei
--- The basics of nuclear mean-field models ---

Takashi Nakatsukasa (中務　孝)
RIKEN NISHINA CENTER 独立行政法人 理化学研究所 仁科加速器研究センター

- Single-particle motion in nuclei
  - –Experimental evidences
  - –Simple model: inconsistent with experiments
  - –How can we reconcile them?
  - –Nuclear mean-field model (Density functional model)
    - Cf) Lecture by Peter Ring
- Collective motion in nuclei
  - –How can it co-exist with the single-particle motion?
  - –Time-dependent density functional model

2011.8.27--31 ISSSP @Beijing, China

Nuclear force

Range: Pion Compton wavelength λ_π

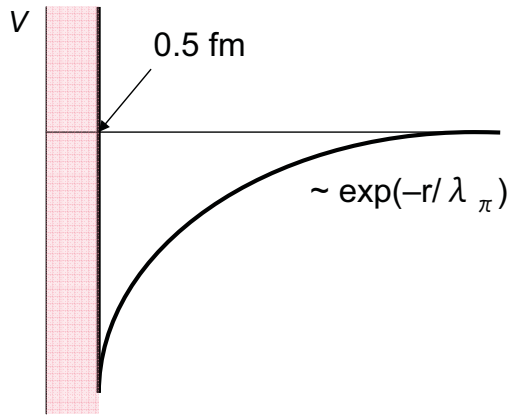

Repulsive core

Hamada-Johnston (HJ) interaction

V_C V_T V_{LS} V_{L2}

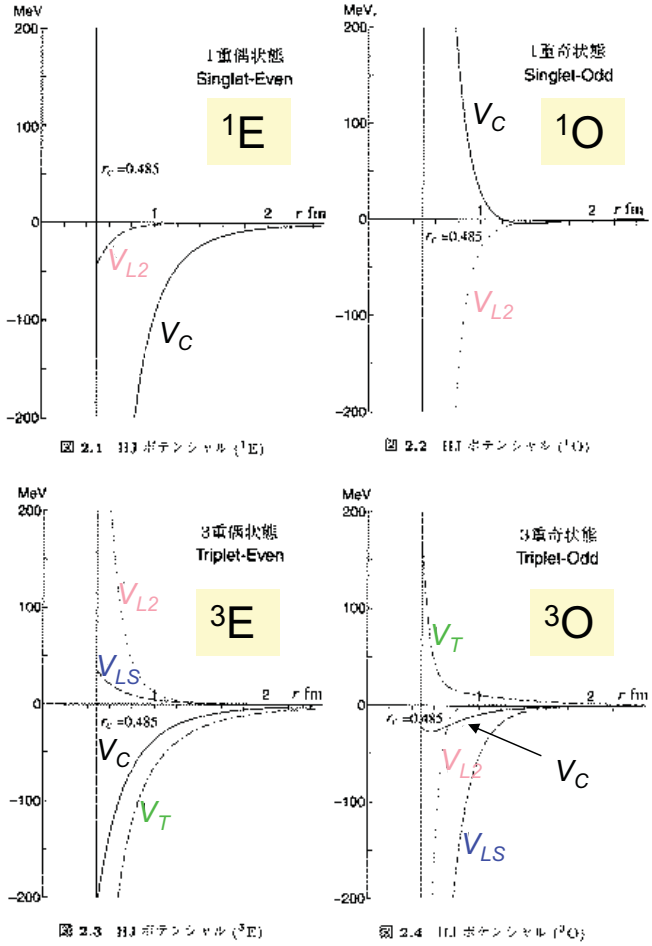

Mean-field approximation (Hartree-Fock)

$$\delta \frac{\langle \Phi | H | \Phi \rangle}{\langle \Phi | \Phi \rangle} = 0, \qquad |\Phi\rangle = \det\{\phi_1 \cdots \phi_N\}: \text{ Slater determinant}$$

Electrons in atoms

	HF	Exp
He	–2.86	–2.90
Li	–7.43	–7.48
Ne	–128.55	–128.94
Ar	–526.82	–527.60

(Energy in atomic unit: 27.2 eV)

Nucleus cannot be bound in the HF approx.

$$\langle \Phi | V | \Phi \rangle = \int d\mathbf{r}\, d\mathbf{r}'\, \rho(\mathbf{r}) V(\mathbf{r}-\mathbf{r}') \rho(\mathbf{r}') = +\infty$$

Two-body correlations are indispensable!

$$\rho_2(\mathbf{r}_1, \mathbf{r}_2) = 0, \qquad \text{for } |\mathbf{r}_1 - \mathbf{r}_2| < c$$

Brueckner Theory

G-matrix, Low-k interaction

Brueckner Theory

T-matrix

$$T(E) = V + V \frac{1}{E - H_0 + i\eta} T(E)$$

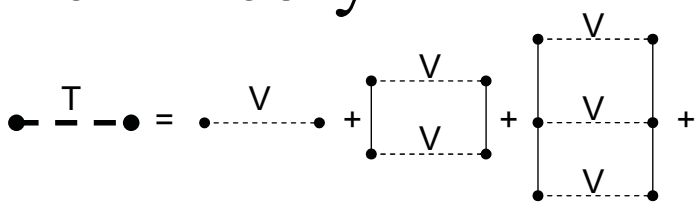

$$= (E - H_0) \frac{1}{E - H_0 - V} V \quad : \text{Regular}$$

$$V \left| \Psi_{\mathbf{k}}^{(+)} \right\rangle = T |\mathbf{k}\rangle$$

G-matrix (E < 2 ε_F)

$$\tilde{G}(E) = V + V\hat{Q} \frac{1}{E - H_0} \hat{Q} \tilde{G}(E)$$

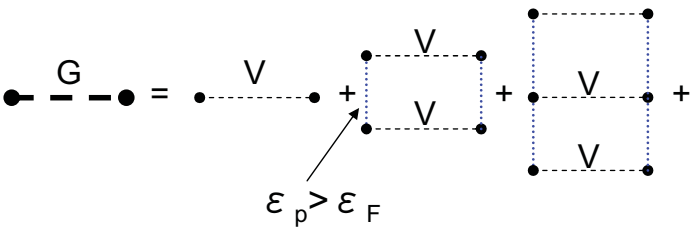

$$Q = 1 - \sum_{i,j<F} |ij\rangle\langle ij|$$

$$V |\Psi\rangle = \tilde{G} |\Phi\rangle$$

With 2-body correlation

Without 2-body correlation (Slater det.)

Brueckner-Hartree-Fock (BHF)

Self-energy

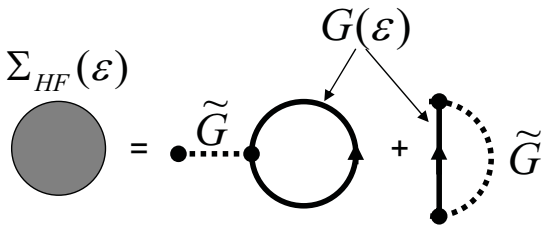

1-particle Green's function

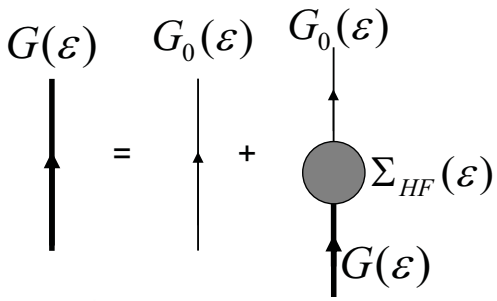

Mean-field pontential

$$\hat{U} = \sum_{\alpha\beta}\left(\sum_{i<F}\widetilde{G}_{\alpha i\beta i}(\varepsilon_i+\varepsilon_\beta) - \widetilde{G}_{\alpha ii\beta}(\varepsilon_i+\varepsilon_\beta)\right)c^+c$$

→ Nuclear saturation

Strong state-dependence

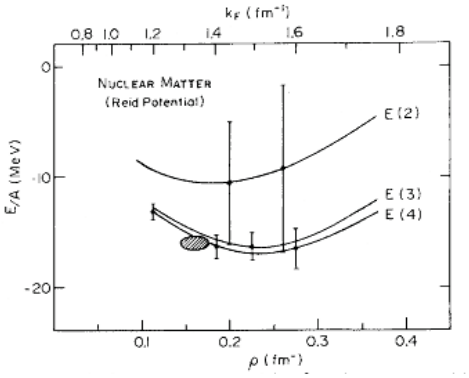

Day. PRC **24** (1981) 1203

Brueckner-Hartree-Fock (BHF)

Success/Achievements

Qualitative understanding of the nuclear saturation

Foundation of the shell model (Indep. Part. Model)

Nucleons' effective mass: m*/m =0.7～0.8

Failures/problems

- Quantitative saturation (Coester line)
- Nuclear central density
- Spin-orbit potential

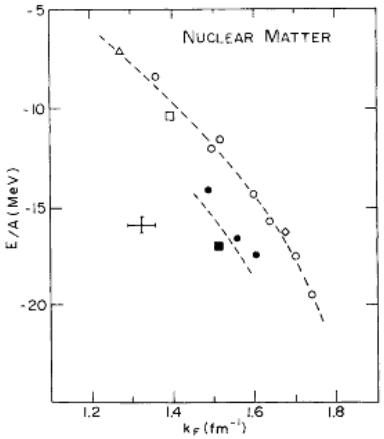

Higher-order (rearrangement) terms

ph matrix elements of MF pot.

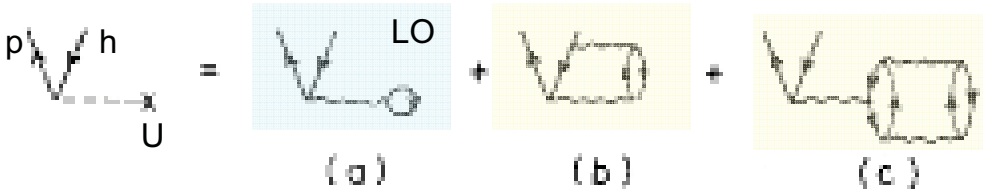

Importance of diagrams (b), (c)

cf) CC calculations (Kummel et al, 1978)

DME calculations (Negele 1970)

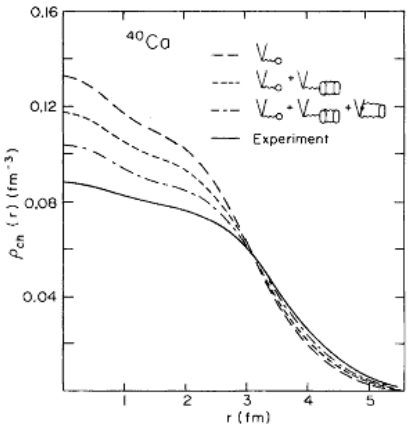

The effects may be taken into account by variation.

$$\frac{\partial G}{\partial Q}\frac{\partial Q}{\partial \varphi_i^*} \rightarrow \text{(b)} \qquad \frac{\partial G}{\partial E}\frac{\partial E}{\partial \varphi_i^*} \rightarrow \text{(c)}$$

Density Matrix Expansion (DME)

Negele 1970, Negele & Vautherin 1972

Local density approximation (LDA) + Variational principle

$$\langle \mathbf{r}_1\mathbf{r}_2 | Q | \mathbf{r}_1\mathbf{r}_2 \rangle = \{\delta(\mathbf{r}_1-\mathbf{r}_1') - \rho(\mathbf{r}_1,\mathbf{r}_1')\}\{\delta(\mathbf{r}_2-\mathbf{r}_2') - \rho(\mathbf{r}_2,\mathbf{r}_2')\}$$

$$\rho\left(\mathbf{R}+\frac{\mathbf{r}}{2},\mathbf{R}-\frac{\mathbf{r}}{2}\right) = \frac{3j_1(k_F r)}{k_F r}\rho(\mathbf{R}) + \cdots \qquad \varepsilon \Rightarrow \bar{\varepsilon}(\rho(\mathbf{R}))$$

$$E_{BHF} = \sum_{i<F}\langle i|T|i\rangle + \frac{1}{2}\sum_{i,j<F}\langle ij|\tilde{G}(\varepsilon_i+\varepsilon_j)|ij-ji\rangle$$

$$E = \int d\mathbf{R} H(\mathbf{R})$$

$$H(\mathbf{R}) = H[\rho(\mathbf{R}),\tau(\mathbf{R}),\cdots]$$

Energy functional of local densities.

Often called “density-dependent Hartree-Fock (DDHF) theory”

DDHF vs BHF

		BHF	DME	Exp
^{16}O	B/A [MeV]	3.91	7.59	7.98
	$(Z\langle r^2\rangle)^{1/2}$ [fm]	2.50	2.75	2.73
^{40}Ca	B/A [MeV]	3.88	7.99	8.55
	$(Z\langle r^2\rangle)^{1/2}$ [fm]	3.04	3.46	3.48
^{208}Pb	B/A [MeV]	2.52	7.83	7.87
	$(Z\langle r^2\rangle)^{1/2}$ [fm]	4.51	5.49	5.50

	$\langle r^2\rangle_{ch}^{1/2}$ Theory	$\langle r^2\rangle_{ch}^{1/2}$ Experiment	$\langle r^2\rangle_n^{1/2}-\langle r^2\rangle_p^{1/2}$ Theory	$\langle r^2\rangle_n^{1/2}-\langle r^2\rangle_p^{1/2}$ Experiment
^{16}O	2.79	2.71±0.01	−0.03	0.00 a
^{40}Ca	3.50	3.48	−0.05	−0.03 a −0.04 c
^{48}Ca	3.50	3.47	0.18	0.16 a 0.19 c
^{58}Ni	3.80	3.78	0.00	0.01 d
^{90}Zr	4.29	4.28±0.02	0.07	0.13 b
^{116}Sn	4.63	4.62±0.01	0.12	0.15 d
^{208}Pb	5.49	5.50	0.20	0.21 c 0.16 d

Density distribution

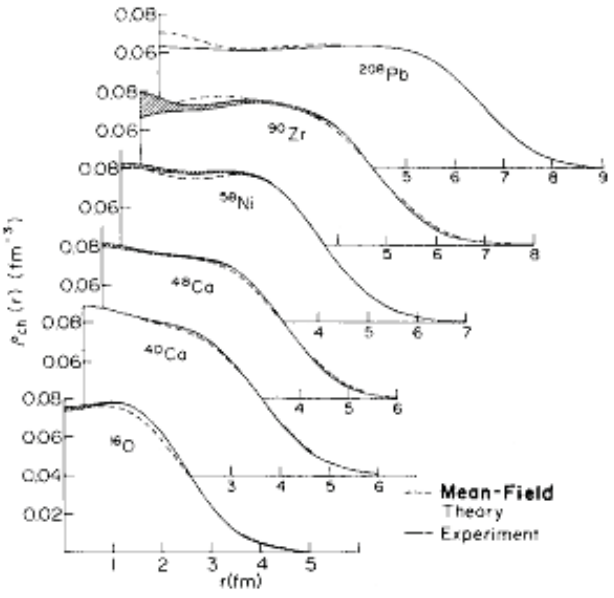

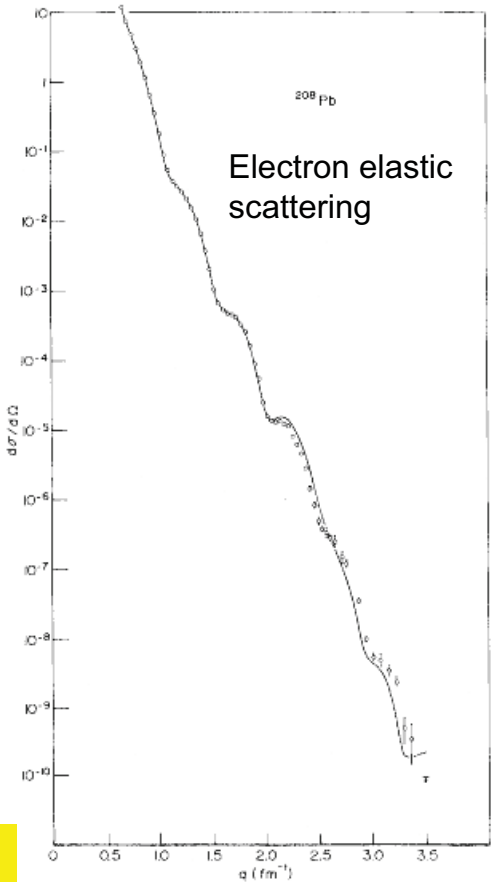

The strong & complex state-dependence of the effective nuclear interaction is nicely replaced by the Energy density functionals.

⇒ Made possible a universal description

Essence of DDHF

- Naïve Hartree-Fock

$$E = \langle \Phi | T + V | \Phi \rangle \quad \Rightarrow \quad m^*/m \approx 0.4$$

- Density-dependent Hartree-Fock (DDHF)

$$E = \langle \Phi | T + V[\rho] | \Phi \rangle \quad \Rightarrow \quad m^*/m = 0.7 \sim 1$$

  – Energy density functional

$$E[\rho] \Rightarrow \quad h[\rho] | \phi_i \rangle = \varepsilon_i | \phi_i \rangle, \quad h[\rho] \equiv \frac{\delta E}{\delta \rho}$$

  – Almost identical to the Skyrme energy functional

Nuclear energy density functional

- Energy functional for the intrinsic states
- Spin & isospin degrees of freedom
  – Spin-current density is indispensable.
- Nuclear superfluidity → Kohn-Sham-Bogoliubov eq.
  – Pair density (tensor) is necessary for heavy nuclei.

$$E\left[\rho_q, \tau_q, \overleftrightarrow{J}_q; \kappa_q\right]$$

kinetic

spin-current

pair density

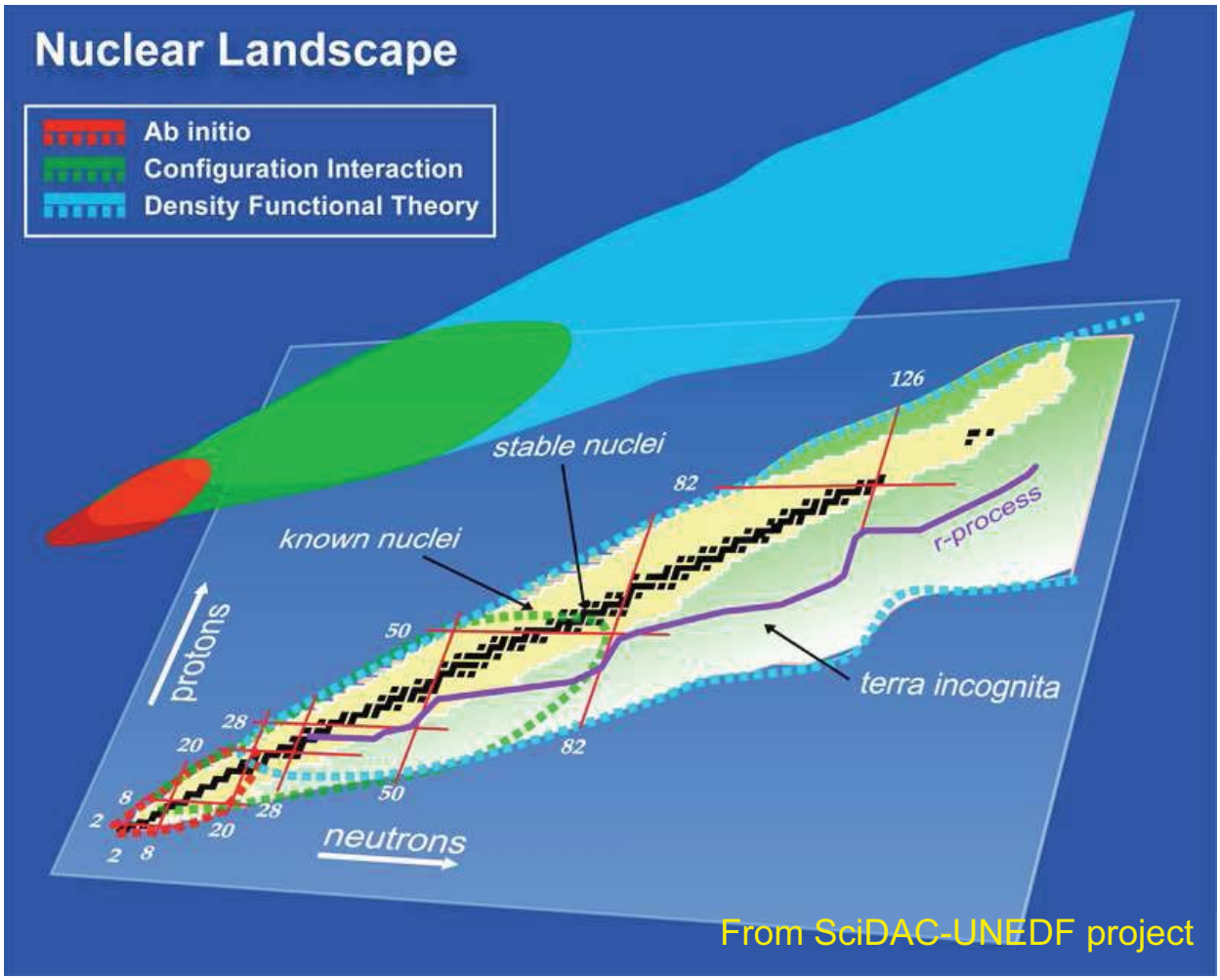

Nuclear deformation as symmetry breaking

$$e^{i\phi J}\left|\Psi\right\rangle \neq \left|\Psi\right\rangle$$

$$e^{i\phi N}\left|\Psi\right\rangle \neq \left|\Psi\right\rangle$$

Quadrupole deformation

$$\beta_{2\mu} = \left\langle \Psi \left| r^2 Y_{2\mu} \right| \Psi \right\rangle$$

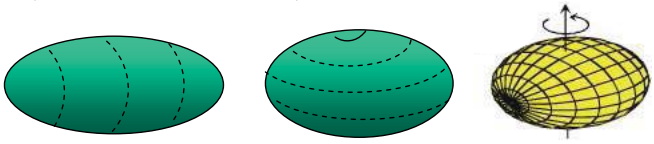

prolate oblate triaxial

Octupole deformation

$$\beta_{30} = \left\langle \Psi \left| r^3 Y_{30} \right| \Psi \right\rangle$$

$$\hat{P}\left|\Psi\right\rangle \neq \pm\left|\Psi\right\rangle$$

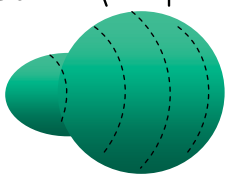

Pear shape (μ =0)

Pairing deformation (superfluidity)

$$\Delta = \left\langle \Psi \left| \hat{\psi}\hat{\psi} \right| \Psi \right\rangle$$

Deformation in the gauge space

Nuclear Superconductivity
Nuclear Superfluidity

Nuclear deformation as phonon condensation

$|\Phi_0\rangle$ Ground state

$B^+_{2^+}|\Phi_0\rangle$ Excited state (2^+)

Away from the closed-shell

$$|\Phi_{\text{def}}\rangle = \exp(cB^+_{2^+})|\Phi_0\rangle$$

$$\beta \equiv \langle\Phi_{\text{def}}|r^2 Y_{20}(\hat{r})|\Phi_{\text{def}}\rangle$$

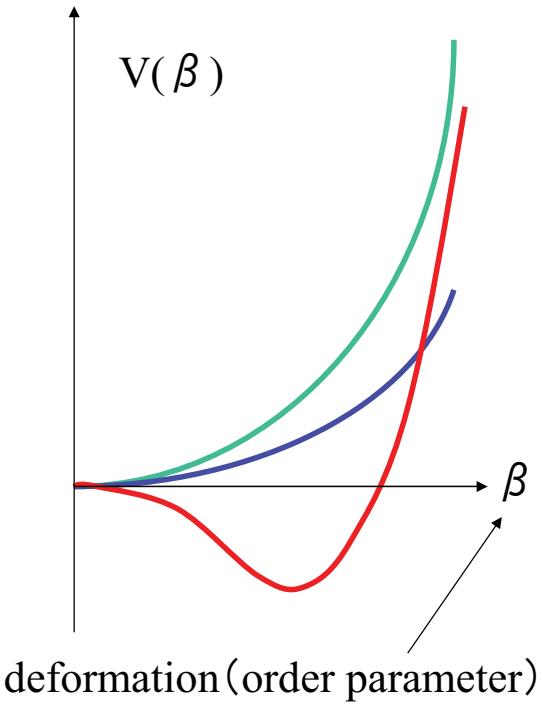

Shape phase transition

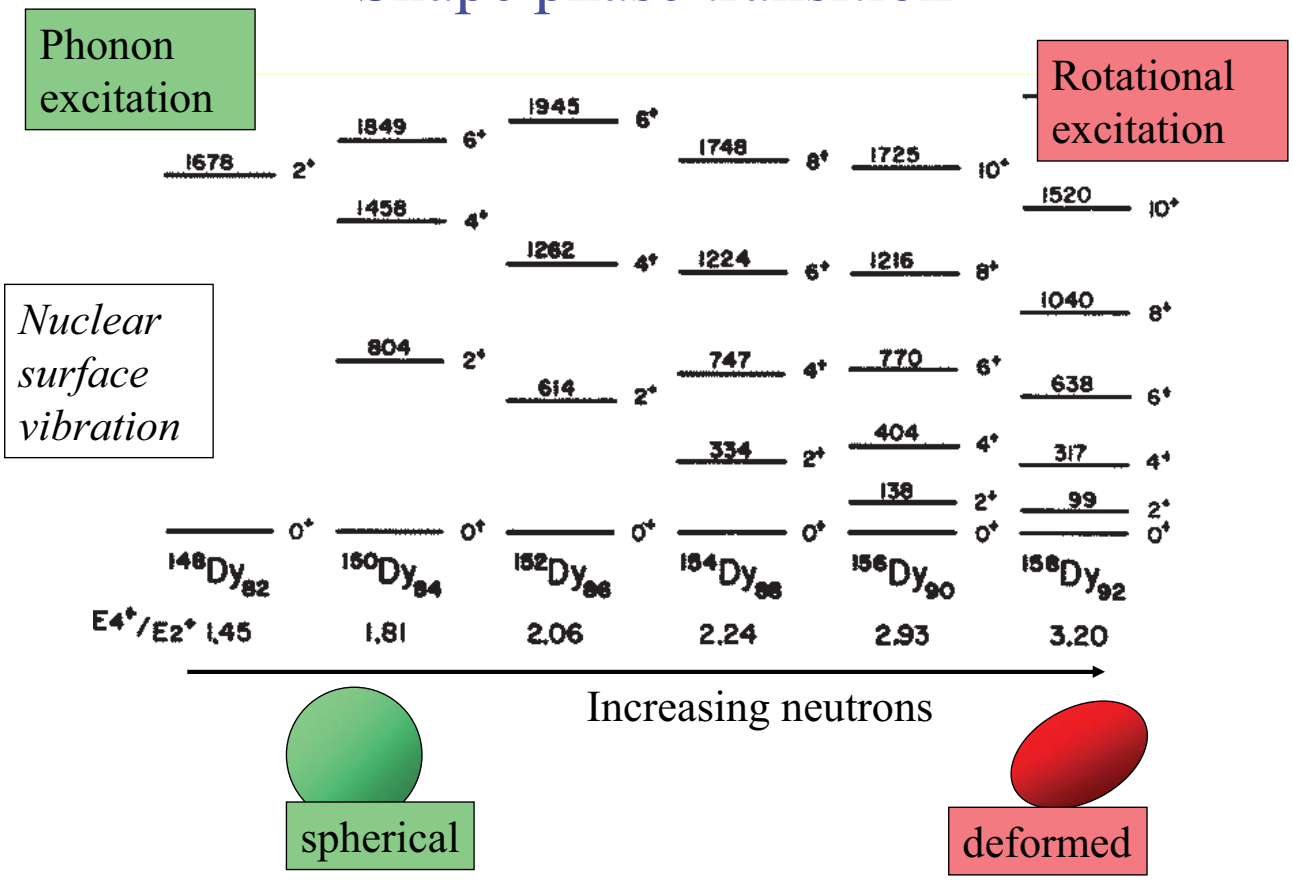

Nuclear deformation predicted by DFT

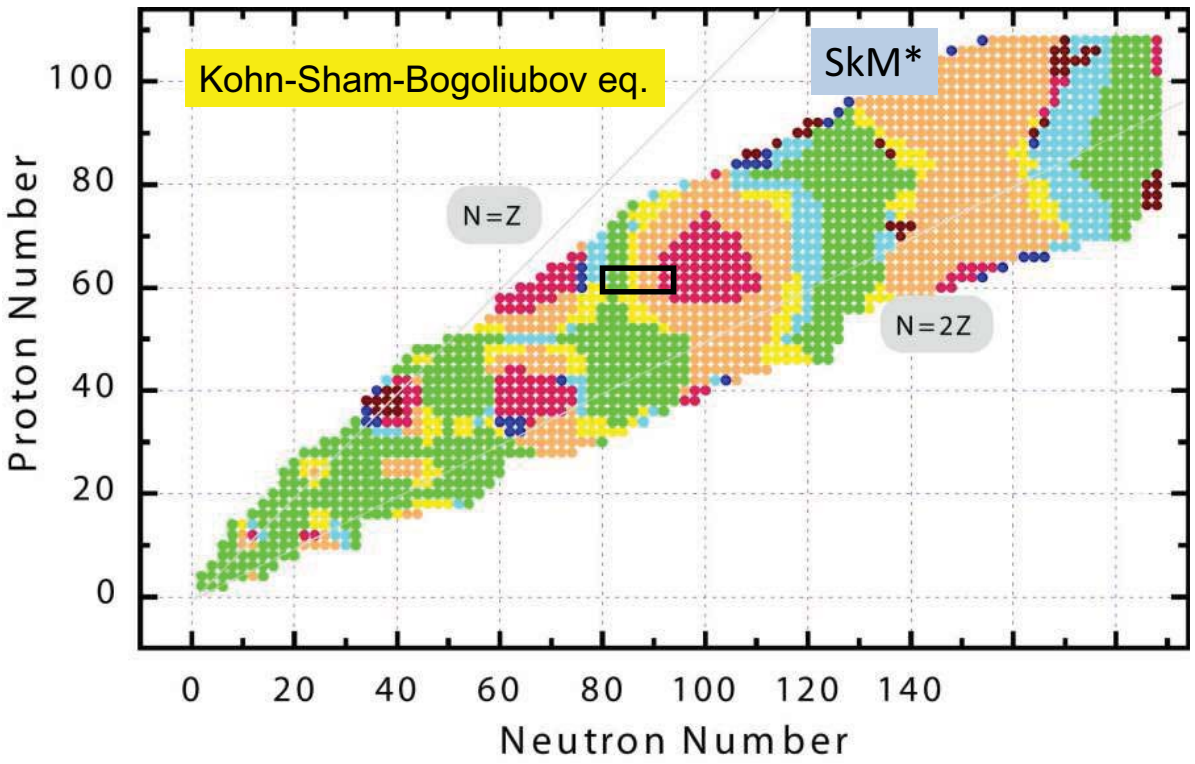

M.V. Stoitsov *et al.*, Phys. Rev. C68(2003) 054312

Nuclear deformation is prevalent in the nuclear chart

Nuclear deformation predicted by DFT

Intrinsic Q moment

$\langle \hat{Q}_{20} \rangle$

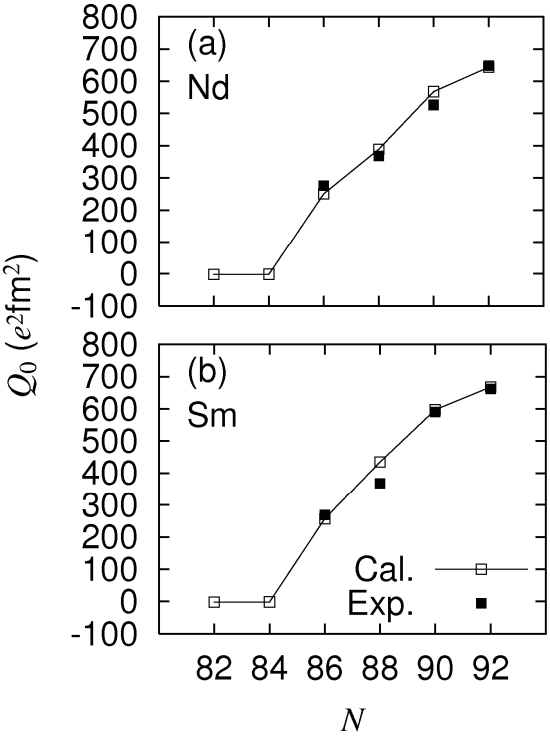

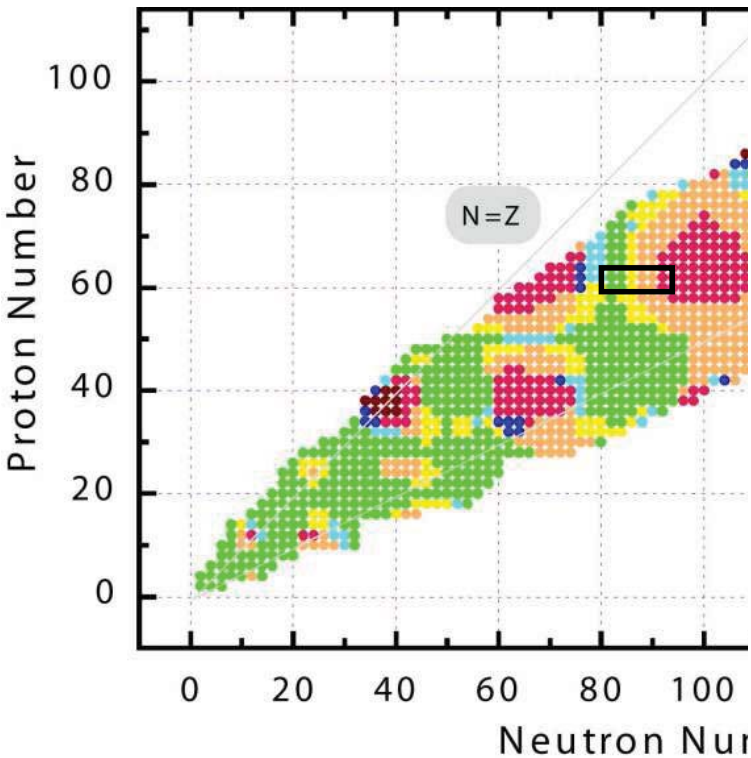

Time-dependent density functional theory (TDDFT) for nuclei

- Time-odd densities (current density, spin density, etc.)

$$E\left[\rho_q(t),\tau_q(t),\vec{\vec{J}}_q(t),\vec{j}_q(t),\vec{s}_q(t),\vec{\vec{T}}_q(t);\kappa_q(t)\right]$$

kinetic, spin-current, current, spin, spin-kinetic, pair density

- Time-dependent Kohn-Sham-Bogoliubov eq.

$$i\frac{\partial}{\partial t}\begin{pmatrix}U_\mu(t)\\V_\mu(t)\end{pmatrix}=\begin{pmatrix}h(t)-\lambda & \Delta(t)\\-\Delta^*(t) & -\left(h(t)-\lambda\right)^*\end{pmatrix}\begin{pmatrix}U_\mu(t)\\V_\mu(t)\end{pmatrix}$$

Linear response calculation

Small amplitude limit

- Starting from the TDKS equation

$$i\frac{\partial}{\partial t}\phi_i(t)=\left\{-\frac{\hbar^2}{2m}\nabla^2+V\left[\rho(t)\right]\right\}\phi_i(t)$$

- Assuming the external field is small, linearize the equation:

$$i\frac{\partial}{\partial t}\delta\phi_i(t)=\frac{\delta V}{\delta\rho}\delta\rho(t)\phi_i^0+\left\{-\frac{\hbar^2}{2m}\nabla^2+V_0-\varepsilon_i\right\}\delta\phi_i(t)$$

$$\phi_i(t)=\left\{\phi_i^0+\delta\phi_i(t)\right\}\exp(-i\varepsilon_i^0 t)$$

Induced (screening) field

$$\delta\rho(t)=\sum_i\phi_i^0\delta\phi_i^*(t)+h.c.,\quad V\left[\rho(t)\right]=V_0+\frac{\delta V}{\delta\rho}\delta\rho(t)$$

Single-particle/collective excitation

- If the induced field is negligibly small,

$$i\frac{\partial}{\partial t}\delta\phi_i(t) = \left\{-\frac{\hbar^2}{2m}\nabla^2 + V_0 - \varepsilon_i\right\}\delta\phi_i(t)$$

these equations are NOT coupled.

$$\delta\phi_i(t) = \eta\phi_m^0 \exp(-i(\varepsilon_m - \varepsilon_i)t)$$
$$\delta\phi_j(t) = 0 \quad \text{for} \quad j \neq i$$

$$\left\{-\frac{\hbar^2}{2m} + V_0\right\}\phi_m^0 = \varepsilon_m\phi_m^0$$

Single-particle motion

- The induced field is essential for collective excitations to which many particles coherently contribute.

Collective motion in the time-dependent mean-field picture

$$\delta V(t) = \frac{\delta V}{\delta\rho}\delta\rho(t)$$

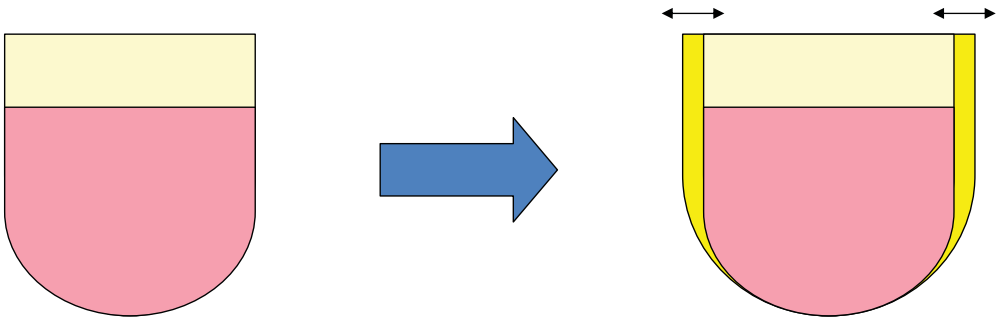

The collective motion is induced by the motion of the potential.

Analogous to the unified model by Bohr and Mottelson

Linear response (RPA) equation

Assuming the external field with a fixed frequency and expanding $\delta\phi_i$ in terms of particle (unoccupied) orbitals,

$$\delta\phi_i(t) = \sum_{m>A} \phi_m^0 \left\{ X_{mi} \exp(-i\omega t) + Y_{mi}^* \exp(i\omega t) \right\}$$

$$\left\{ \begin{pmatrix} A & B \\ B^* & A^* \end{pmatrix} - \omega \begin{pmatrix} 1 & 0 \\ 0 & -1 \end{pmatrix} \right\} \begin{pmatrix} X_{mi}(\omega) \\ Y_{mi}(\omega) \end{pmatrix} = - \begin{pmatrix} (V_{\text{ext}})_{mi} \\ (V_{\text{ext}})_{im} \end{pmatrix}$$

$$A_{mi,nj} = (\varepsilon_m - \varepsilon)\delta_{mn}\delta_{ij} + \left\langle \phi_m \left| \frac{\partial V}{\partial \rho_{nj}} \right|_{\rho_0} \right| \phi_i \right\rangle$$

$$B_{mi,nj} = \left\langle \phi_m \left| \frac{\partial V}{\partial \rho_{jn}} \right|_{\rho_0} \right| \phi_i \right\rangle$$

- Tedious calculation of residual interactions
- Computationally very demanding, especially for deformed systems.

Deformation effects for photoabsorption cross section

SkM* functional

K.Yoshida and TN, PRC83, 021404 (2011).

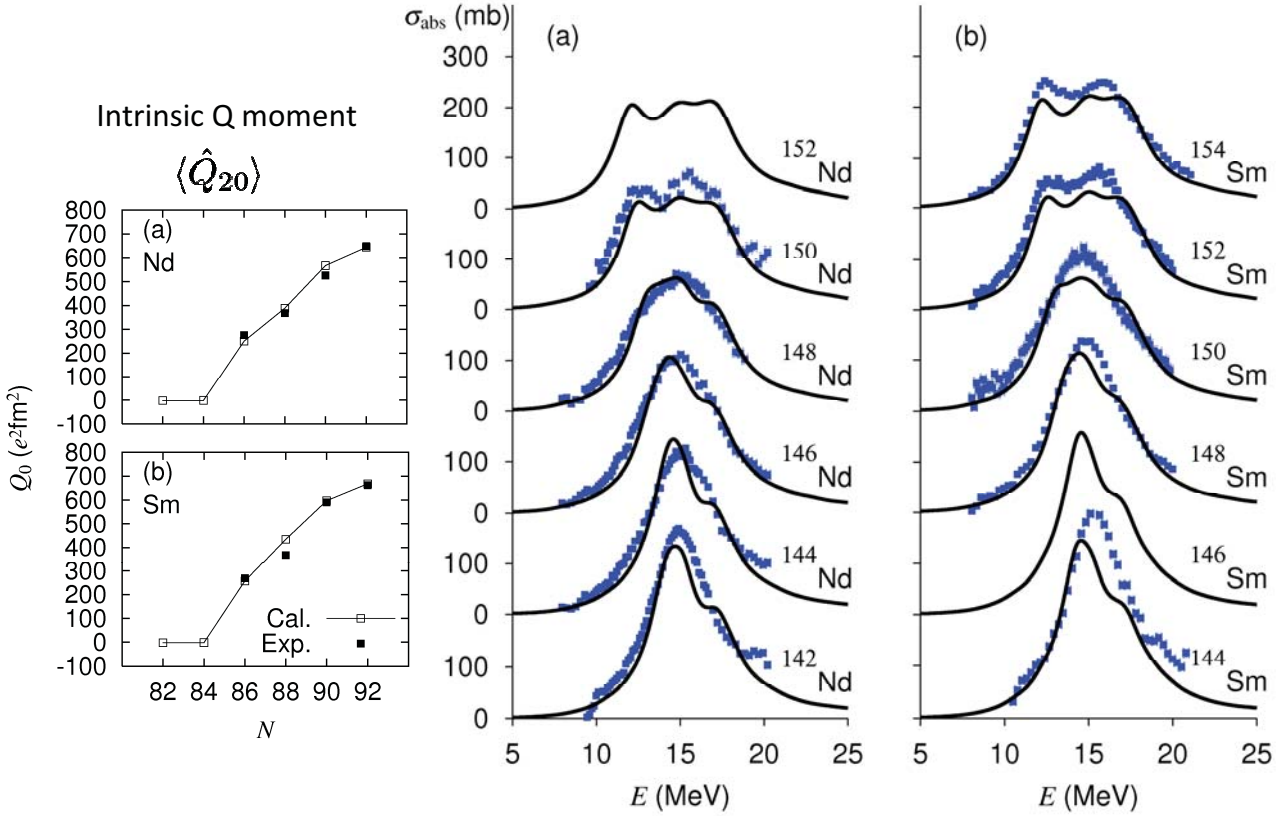

Summary

- Nuclear saturation is inconsistent with a naive mean-field picture.
  - A solution: “State-dependent” effective interaction
  - A common choice is the density-dependent interaction
    ⇨ “Energy density functional”
- Modern energy density functionals reproduce (predict) nuclear mass, radius, deformation, etc. with high accuracy and for the entire nuclear chart.
- A variety of nuclear excitations are studied with the time-dependent DFT.
- Current issues & Future perspectives:
  - Missing correlations
  - Odd nuclei, precise determination of drip lines (higher accuracy)
  - Large-amplitude collective dynamics (fusion/fission, etc.)
  - Nuclear reaction studies by combining DFT with quantum scattering theory
  - The density dependence (functional) is really the best choice for nuclear physics?

Shell Model for Open Quantum Systems*

Marek Płoszajczak[1]

[1]*Grand Accélérateur National d'Ions Lourds (GANIL), CEA/DSM - CNRS/IN2P3, BP 55027, F-14076 Caen Cedex, France*

Abstract

Resonances are commonly found in various quantum systems, independently of their building blocks and the kinematic regime of their appearance. Resonances are genuine intrinsic properties of quantum systems, associated with their natural frequencies, and describing preferential decays of unbound states. The effect of resonances and the non-resonant scattering states can be considered in the open quantum system extension of the nuclear interacting shell model. In these lectures, we will review the fascinating adventure of the last decade associated with the development and applications of the continuum shell model approach to bound and unbound nuclear states, nuclear decays, and reactions.

*These lectures are based on results of GANIL-ORNL-Kraków Theory Collaboration. Authors wish to thank its members for the long-term stimulating efforts and the collaborative research.

Nuclear shell model has been proposed almost sixty years ago [1, 2]. Soon afterwards, the interacting shell model (ISM) has been developed by Lane, Kurath, and others (see [3] for a recent review). The ISM-based description of an evolution of the nucleonic coupling scheme from the LS to jj coupling with increasing mass number, provided foundations of modern nuclear structure theory and helped to understand a wealth of data on nuclear levels, moments, collective excitations, electromagnetic and β decays, and various particle decays [4].

In its traditional form, ISM describes the nucleus as a closed quantum system: nucleons occupy bound, hence well localized, single particle orbits of an infinite (e.g., harmonic oscillator) potential and are isolated from the environment of unbound scattering states that are not square integrable. Since the scattering continuum is not considered explicitly, the presence of branch points (decay thresholds) and double-poles of the scattering matrix is neglected. The divide between the discrete states and the scattering continuum, i.e., the focus on one or another, has unfortunately become a kind of paradigm. In the long term, this has led to an artificial separation of nuclear structure from nuclear reactions, and hindered a deeper understanding of nuclear properties. Indeed, many structural properties of the nucleus are determined by means of nuclear collisions. Hence, the knowledge of nuclear structure depends on nuclear reactions and *vice versa*, and this cries for a unified theoretical framework.

At low excitation energies, well-bound nuclei can be considered as closed quantum systems, well described by the standard ISM or its modern versions such as the no-core shell model [5–7]. Moving towards drip lines, or higher in excitation energy, the continuum coupling becomes gradually more important, changing the nature of weakly bound states. (Properties of unbound states are directly impacted by couplings to reaction channels.) In this regime, the chemical potential has a similar magnitude as the pairing gap; hence, the system is dominated by many-nucleon correlations which no longer cannot be considered as small perturbations atop the average potential [8]. Many-body states in neighboring nuclear systems with different proton and neutron numbers become interconnected via continuum, forming correlated domains (clusters) of quantum states.

The first attempt towards unification nuclear structure and nuclear reactions came from Feshbach [9, 10] who expressed the collision matrix of the optical model using matrix ele-

ments of the Hamiltonian. This development gave a strong push to the ISM approach to nuclear reactions [11–14] (see introduction in Ref.[15] for detailed historical account) and led to various formulations of the continuum shell model [16–20]. A modern version of continuum shell model in the Hilbert space, the Shell Model Embedded in the Continuum (SMEC) [20–23], provides a unified description of the structure and reactions with up to two nucleons in the scattering continuum using realistic ISM Hamiltonians. Nevertheless, the fully symmetric treatment of bound and scattering states in the multiparticle wave function is still too ambitious a goal [24].

The advantage of SMEC is that effects of the continuum coupling ('external' couplings) can be separated from effects of the 'internal' configuration mixing, hence providing an insight into the configuration mixing in open quantum system. The model has been applied to study: (i) the statistical aspects of the continuum coupling [25], (ii) the radiative capture reactions [20, 26–28], (iii) the elastic scattering cross-sections [27], (iv) the first-forbidden β-decays [29], (v) the Coulomb dissociation at relativistic energies [30], (vi) the continuum correction to binding energies [31], (vii) the two-proton radioactivity [23, 32, 33], (viii) the exceptional points in the scattering continuum [34], and (ix) the near-threshold configuration mixing [35].

A different attempt to formulate the ISM for open quantum systems has been proposed recently [36–39] within the Berggren ensemble [40]. The resulting complex-energy open quantum system extension of the ISM, the Gamow Shell Model (GSM), can be conveniently formulated in the Rigged Hilbert Space (Gel'fand triple) [41, 42] which encompasses Gamow states [43, 44], and is suitable for extending the quantum mechanics into the domain of time-asymmetric processes (e.g. decays). The GSM offers a fully symmetric treatment of bound, resonance, and scattering single-particle states but, until now, has been primarily used in the context of nuclear structure (for a recent review of the complex-energy shell model, see Ref. [45]). In nuclear structure application, solutions of the GSM can be found by diagonalizing a complex-symmetric Hamiltonian matrix. The 'dimensional catastrophe' in GSM when increasing number of active particles has been alleviated by a recent progress in the generalization of the Density Matrix Renormalization Group [46–48] method to non-Hermitian, complex-symmetric matrix problems [49, 50].

A significant progress has also been made in applications of realistic interactions in GSM

[51]. Finally, powerful techniques for a selection of physical resonances, based on the overlap method, have been developed [36, 38]. The GSM has allowed to understand: (i) the role of continuum in the binding mechanism of helium isotopes binding [36] and (ii) spin-orbit splitting [52], (iii) the role of antibound states in halo formation [53], (iv) the threshold effects in spectroscopic factors [54] and (v) radial overlap integrals [55], and (vi) the isospin mixing in weakly-bound mirror nuclei due to continuum coupling [56].

GSM is the open quantum system formulation of ISM for a self-adjoint Hamilton operator. This formulation offers a number of conceptual advantages. For instance, the transition from a bound to unbound regime, either within a single nucleus or in the long chain of isotopes (isotones), can be viewed as an opening in the configuration space and described without changing the Hamiltonian. The many-body nuclear Hamiltonian in this formulation does not describe just one isolated nucleus (N, Z), but all nuclei and all nuclear states that are coupled through various decays and captures. This idealization offers a right physical picture of the many-body system and its interactions.

Many challenging problems remain that could be illuminated with GSM — thanks to its ability to follow a quantum transition from a bound-state regime to unbound one. For instance, GSM is an excellent tool to explain an 'alignment' of a many-body wave function with a channel wave function in the vicinity of a channel threshold [8, 57]. This mechanism, which is a likely source of clustering effects seen near different threshold openings, can be studied in GSM. A near-threshold behavior of pairing correlations is an example from another domain where systematic GSM studies could be most helpful. That is probably a most transparent illustration of a near-threshold clustering.

The developments reviewed in these lectures are not solely limited to nuclei; they can be of interest in various fields of physics (atomic and molecular physics, nanoscience, quantum optics, etc.) where small quantum systems whose properties are profoundly affected by continuum of scattering and decay channels are intensely studied. To describe such systems, one has to give up either the concept of the Hilbert space or the self-adjoint nature of the Hamiltonian if one wants to keep the simplicity and conceptual and practical advantages of

the standard ISM framework.

---

[1] M. Göppert-Mayer, Phys. Rev. **75**, 1969 (1949)

[2] O. Haxel, J.H.D. Jensen and H.E. Süss, Phys. Rev. **75**, 1766 (1949)

[3] E. Caurier, G. Martinez-Pinedo, F. Nowacki, A. Poves and A.P. Zuker, Rev. Mod. Phys. **77**, 427 (2005)

[4] A. Bohr and B.R. Mottelson, *Nuclear Structure, Vol. II* (Benjamin, Reading, MA), (1975)

[5] P. Navratil and B.R. Barrett, Phys. Rev. C **54**, 2986 (1996)

[6] P. Navratil and B.R. Barrett, Phys. Rev. C **62**, 054311 (2000)

[7] R. Roth and P. Navratil, Phys. Rev. Lett. **99**, 092501(2007)

[8] J. Dobaczewski, N. Michel, W. Nazarewicz, M. Płoszajczak and J. Rotureau, Prog. Part. Nucl. Phys. **59** , 432 (2007)

[9] H. Feshbach, Annals of Physics (NY) **5**, 357 (1958)

[10] H. Feshbach, Annals of Physics (NY) **19**, 287 (1962)

[11] W. Brenig, Nucl. Phys. **13**, 333 (1959)

[12] L.S. Rodberg, Phys. Rev. **124**, 210 (1961)

[13] W.M. Macdonald, Nucl. Phys. **54**, 393 (1964); ibid. **56**, 636

[14] U. Fano, Phys. Rev. **124**, 1866 (1961)

[15] R.F. Barrett, L.C. Biedenharn, M. Danos, P.P. Delsanto and W. Greiner, Rev. Mod. Phys. **45**, 44 (1973)

[16] C. Mahux and H.A. Weidenmüller, *Shell Model Approach to Nuclear Reactions* (North-Holland, Amsterdam) (1969)

[17] H.W. Barz, I. Rotter and J. Höhn, Nucl. Phys. **A 275**, 111 (1977)

[18] R.J. Philpott, *Fizika* **9**, 109 (1977);
D. Halderson and R.J. Philpott, Nucl. Phys. **A 321**, 295 (1979); ibid. **A 359**, 365 (1981)

[19] I. Rotter, H.W. Barz and J. Höhn, Nucl. Phys. **A 297**, 237 (1978)

[20] K. Bennaceur, F. Nowacki, J. Okołowicz and M. Płoszajczak, Nucl. Phys. **A 651**, 289 (1999)

[21] A. Volya and V. Zelevinsky, 2006 Phys. Rev. C **74** 064314;
A. Volya and V. Zelevinsky, Phys. Rev. Lett. **94**, 052501 (2005)

[22] J.-B. Faes and M. Płoszajczak, Nucl. Phys. **A 800**, 21 (2008)

[23] J. Rotureau, J. Okołowicz and M. Płoszajczak, Nucl. Phys. **A 767**, 13 (2006)

[24] J. Okołowicz, M. Płoszajczak and I. Rotter, Phys. Reports **374**, 271 (2003)

[25] S. Drożdż, J. Okołowicz, M. Płoszajczak and I. Rotter, Phys. Rev. **62**, 24313 (2000)

[26] K. Bennaceur, F. Nowacki, J. Okołowicz and M. Płoszajczak, Nucl. Phys. **A 671**, 203 (2000)

[27] K. Bennaceur, N. Michel, F. Nowacki, J. Okołowicz and M. Płoszajczak, Phys. Lett. **B 488**, 75 (2000)

[28] R. Chatterjee, J. Okołowicz and M. Płoszajczak, Nucl. Phys. **A 764**, 528 (2006)

[29] N. Michel, F. Nowacki, J. Okołowicz and M. Płoszajczak, Nucl. Phys. **A 703**, 202 (2002)

[30] R. Shyam, K. Bennaceur, J. Okołowicz and M. Płoszajczak, Nucl. Phys. **A 669**, 65 (2000)

[31] Y. Luo, J. Okołowicz, M. Płoszajczak and N. Michel, ArXiv:nucl-th/0211068;
J. Okołowicz, M. Płoszajczak and Y. Luo, Acta Phys. Pol. **39**, 389 (2008)

[32] J. Rotureau, J. Okołowicz and M. Płoszajczak, Phys. Rev. Lett. **95**, 042503 (2005)

[33] B. Blank and M. Płoszajczak, Rep. Prog. Phys. **71**, 046301 (2008)

[34] J. Okołowicz and M. Płoszajczak, Phys. Rev. C **80**, 034619 (2009)

[35] J. Okołowicz and M. Płoszajczak, Acta Phys. Pol. **42**, 451 (2011)

[36] N. Michel, W. Nazarewicz, M. Płoszajczak and K. Bennaceur, Phys. Rev. Lett. **89**, 042502 (2002)

[37] R. Id Betan, R.J. Liotta, N. Sandulescu and T. Vertse, Phys. Rev. Lett. **89**, 042501(2002)

[38] N. Michel, W. Nazarewicz, M. Płoszajczak and J. Okołowicz, Phys. Rev. C **67**, 054311(2003)

[39] N. Michel, W. Nazarewicz and M. Płoszajczak, Phys. Rev. C **70**, 064313 (2004)

[40] T. Berggren, Nucl. Phys. **A 109**, 265 (1968)

[41] I.M. Gel'fand and N.Ya. Vilenkin, *Generalized Functions, Vol. 4* (Academic Press, New York) (1961)

[42] K. Maurin, *Generalized Eigenfunction Expansions and Unitary Representations of Topological Groups* (Polish Scientific Publishers, Warsaw) (1968)

[43] G. Gamow, Z. Phys. **51**, 204 (1928)

[44] R.W. Gurney and E.U. Condon, Phys. Rev. **33**, 127 (1929)

[45] N. Michel, W. Nazarewicz, M. Płoszajczak and T. Vertse, J. Phys G: Nucl. Phys. (Topical Review) **36**, 013101 (2009)

[46] S.R. White, Phys. Rev. Lett. **69**, 2363 (1992)

[47] S.R. White, Phys. Rev. B **48**, 10345 (1993)

[48] E. Carlon, M. Henkel and J. Schollwöck, Eur. J. Phys. B **12**, 99 (1991)

[49] J. Rotureau, N. Michel, W. Nazarewicz, M. Płoszajczak and J. Dukelsky, Phys. Rev. Lett. **97**, 110603 (2006)

[50] J. Rotureau, N. Michel, W. Nazarewicz, M. Płoszajczak and J. Dukelsky, Phys. Rev. C **79**, 014304 (2009)

[51] G. Hagen, M. Hjorth-Jensen and N. Michel, Phys. Rev. C **73**, 064307 (2006)

[52] N. Michel, W. Nazarewicz, J. Okołowicz and M. Płoszajczak, Nucl. Phys. **A 752**, 335c (2005)

[53] N. Michel, W. Nazarewicz, M. Płoszajczak and J. Rotureau, Phys. Rev. C **74**, 054305 (2006)

[54] N. Michel, W. Nazarewicz and M. Płoszajczak, Phys. Rev. C **75**, 031301 (2007)

[55] N. Michel, W. Nazarewicz and M. Płoszajczak, Nucl. Phys. **A 794**, 29 (2007)

[56] N. Michel, W. Nazarewicz and M. Płoszajczak, Phys. Rev. C **82**, 044315 (2010)

[57] K. Ikeda, N. Takigawa, and. H. Horiuchi, Prog. Theor. Phys. Suppl. Extra Number, 464 (1968)

Shell Model for Open Quantum Systems (Part I)

M. Płoszajczak
GANIL, Caen, France

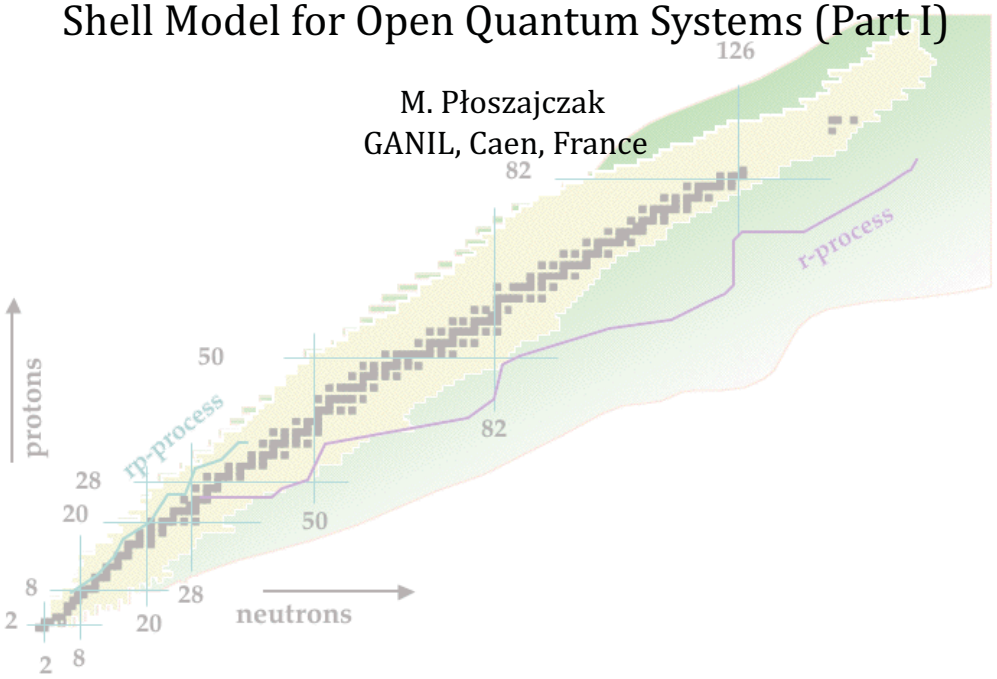

Outline

1

1. Introduction
   - Pioneering age of the nuclear Shell Model
   - Nuclei as open quantum systems
2. Phenomena related to the openness: nuclear decays, halos
   - Impact of scattering states on structural properties
3. Configuration mixing approach (I)
   - Complex-energy quantum mechanics (Rigged Hilbert Space)
   - Quasi-stationary Shell Model: Gamow Shell Model (GSM)
4. GSM spectra, density distribution, overlap integrals
   - Threshold anomalies, configuration mixing in mirror systems

2

5. Introduction: threshold phenomena
6. Configuration mixing approach (II)
   - Real-energy quantum mechanics (Hilbert space)
   - Continuum Shell Model
7. Unified approach to nuclear structure and reactions
   - Continuum coupling correction to Shell Model eigenfunctions/eigenvalues
   - Exceptional points in the scattering continuum, entangled wave functions, configuration mixing in the vicinity of the elastic threshold, ...
   - Higher up in the continuum: the segregation of time-scales
8. Short résumé

Nuclei are Open Quantum Systems

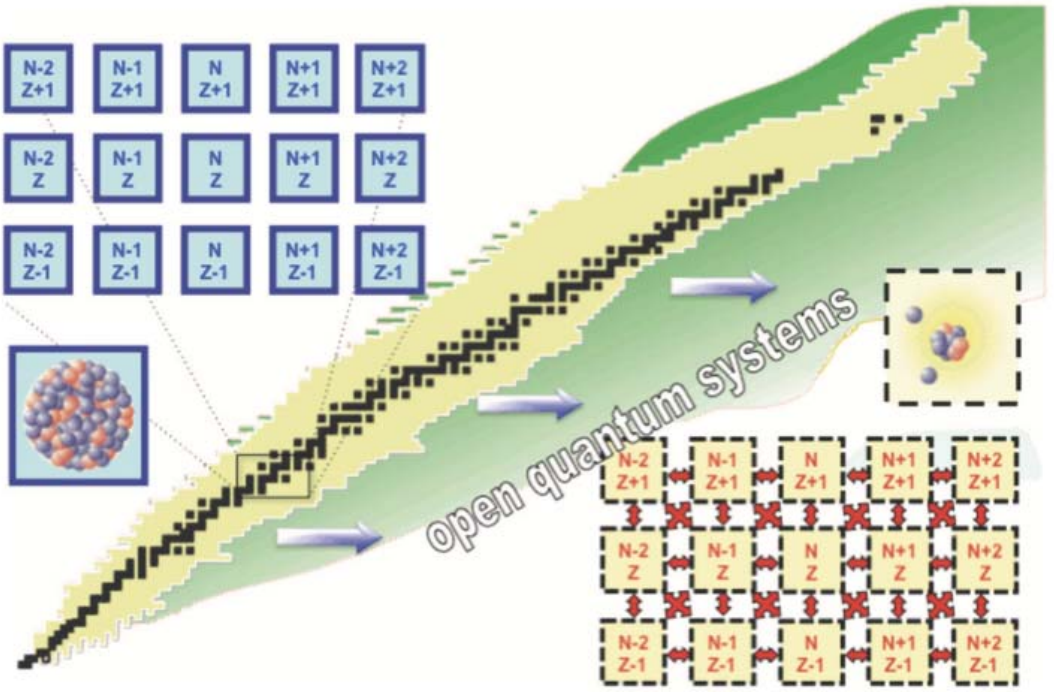

On Closed Shells in Nuclei. II

MARIA GOEPPERT MAYER
Argonne National Laboratory and Department of Physics, University of Chicago, Chicago, Illinois
February 4, 1949

THE spins and magnetic moments of the even-odd nuclei have been used by Feenberg[1,2] and Nordheim[3] to determine the angular momentum of the eigenfunction of the odd particle. The tabulations given by them indicate that spin orbit coupling favors the state of higher total angular momentum. If strong spin-orbit coupling, increasing with angular momentum, is assumed, a level assignment different from either Feenberg or Nordheim is obtained. This assignment encounters a very few contradictions with experimental facts and requires no major crossing of the levels from those of a square well potential. The magic numbers 50, 82, and 126 occur at the place of the spin-orbit splitting of levels of high angular momentum.

Thanks are due to Enrico Fermi for the remark, "Is there any indication of spin-orbit coupling?" which was the origin of this paper.


Enrico Fermi


Maria Goeppert-Mayer


J. Hans D. Jensen

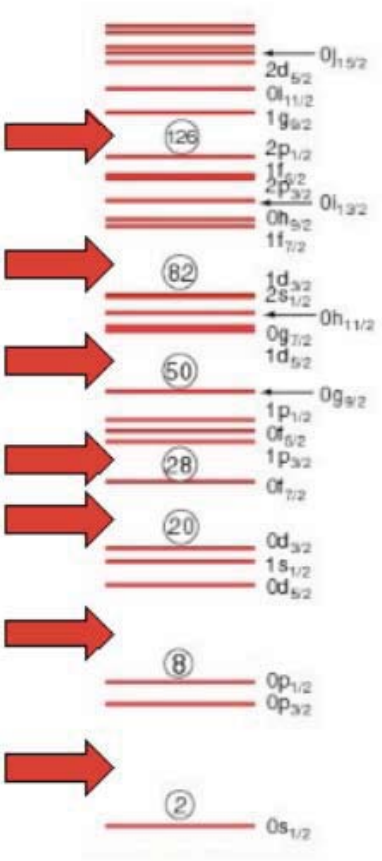

Shell Model of Nuclei

On Closed Shells in Nuclei. II

MARIA GOEPPERT MAYER
Argonne National Laboratory and Department of Physics, University of Chicago, Chicago, Illinois
February 4, 1949

THE spins and magnetic moments of the even-odd nuclei have been used by Feenberg[1,2] and Nordheim[3] to determine the angular momentum of the eigenfunction of the odd particle. The tabulations given by them indicate that spin orbit coupling favors the state of higher total angular momentum. If strong spin-orbit coupling, increasing with angular momentum, is assumed, a level assignment different from either Feenberg or Nordheim is obtained. This assignment encounters a very few contradictions with experimental facts and requires no major crossing of the levels from those of a square well potential. The magic numbers 50, 82, and 126 occur at the place of the spin-orbit splitting of levels of high angular momentum.

Closed Quantum System

No coupling with external decay channels

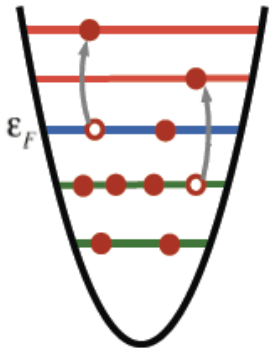

Is the closed quantum system formulation of the Shell Model justified?

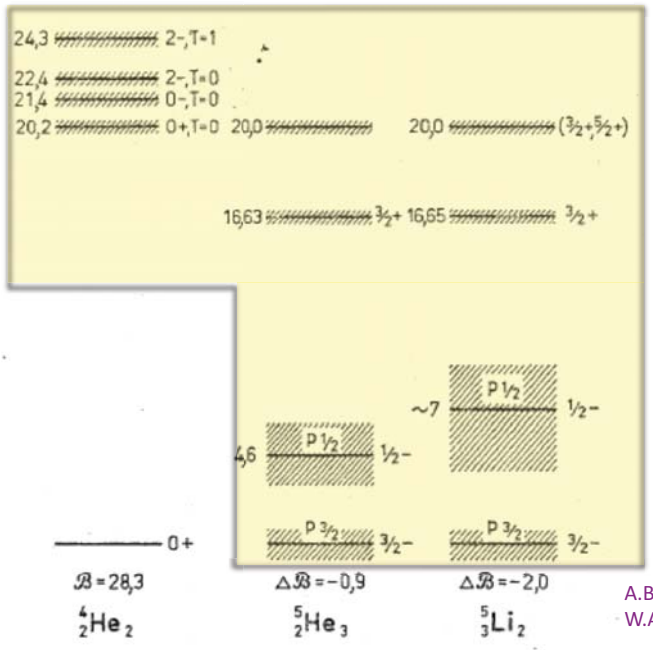

A.Bohr, B.R. Mottelson, *Nuclear Structure*, W.A. Benjamin, Inc. 1969

Is it justified to neglect couplings to decay channels (continuum)?

PHYSICAL REVIEW VOLUME 81, NUMBER 3 FEBRUARY 1, 1951

On the Displacement of Corresponding Energy Levels of C^{13} and N^{13}

JOACHIM B. EHRMAN*
Princeton University, Princeton, New Jersey
(Received July 17, 1950)

It is investigated to what extent the change in boundary conditions at the nuclear surface due to Coulomb wave function distortion in the external region can explain the relative displacement of the first excited states of C^{13} and N^{13}. It is found that the calculated displacement is in the right direction and of a sufficiently large magnitude, but rather sensitively dependent on the definition of nuclear radius.

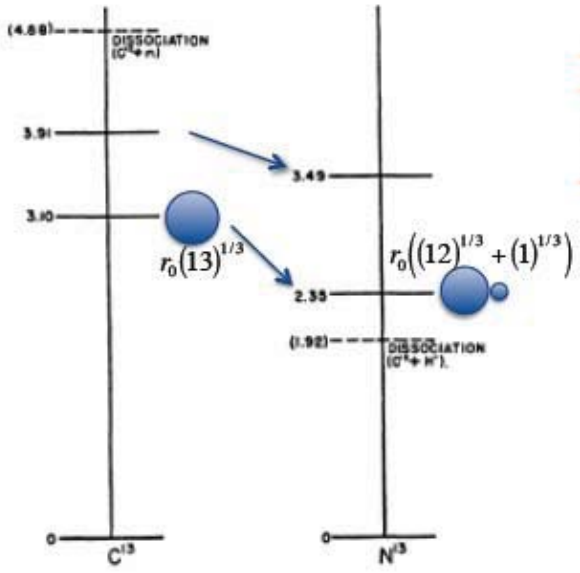

FIG. 1.

The boundary condition postulate predicts a shift in the positions of the energy levels of C^{13} with respect to the corresponding levels of N^{13}, in addition to the ordinary Coulomb energy difference and the neutron-hydrogen mass difference, especially for states near the dissociation energy.

It is a pleasure to thank Professor Wigner for suggesting this problem, and for continued advice and encouragement.

Eugene P. Wigner

On the Displacement of Corresponding Energy Levels of C^{13} and N^{13}

JOACHIM B. EHRMAN*
Princeton University, Princeton, New Jersey
(Received July 17, 1950)

It is investigated to what extent the change in boundary conditions at the nuclear surface due to Coulomb wave function distortion in the external region can explain the relative displacement of the first excited states of C^{13} and N^{13}. It is found that the calculated displacement is in the right direction and of a sufficiently large magnitude, but rather sensitively dependent on the definition of nuclear radius.

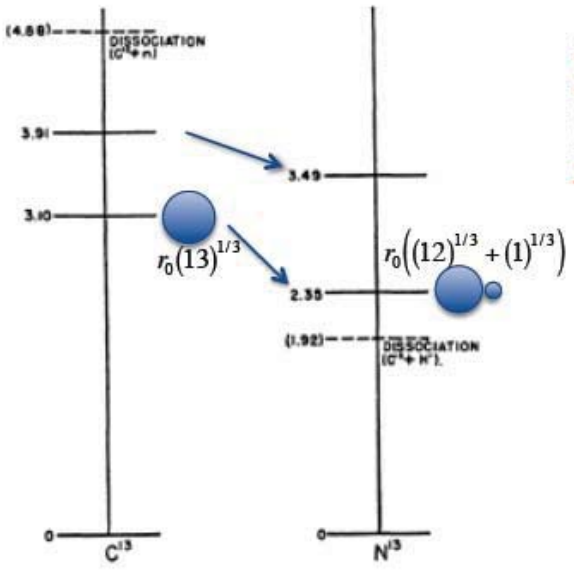

FIG. 1.

The boundary condition postulate predicts a shift in the positions of the energy levels of C^{13} with respect to the corresponding levels of N^{13}, in addition to the ordinary Coulomb energy difference and the neutron-hydrogen mass difference, especially for states near the dissociation energy.

Fundamental assumption of Shell Model is dubious!

PHYSICAL REVIEW VOLUME 101, NUMBER 1 JANUARY 1, 1956

Intermediate Coupling in the 1*p*-Shell*

DIETER KURATH
Argonne National Laboratory, Lemont, Illinois
(Received August 31, 1955)

The region between He^4 and O^{16} is treated for the case of intermediate strength of spin-orbit coupling and central two-body interaction. Energy levels are presented as a function of the relative coupling strength parameter, a/K. Static electromagnetic moments are also computed as functions of a/K. Comparison with experimental results gives a fairly good picture, and determines a definite behavior for a/K as a function of mass number. A possible interpretation of this behavior is suggested.

$A = 7$

$$H = H_{HO} + a(\mathbf{l}\cdot\mathbf{s}) + A_0 \exp\left[-(r_{12}/r_0)^2\right]$$

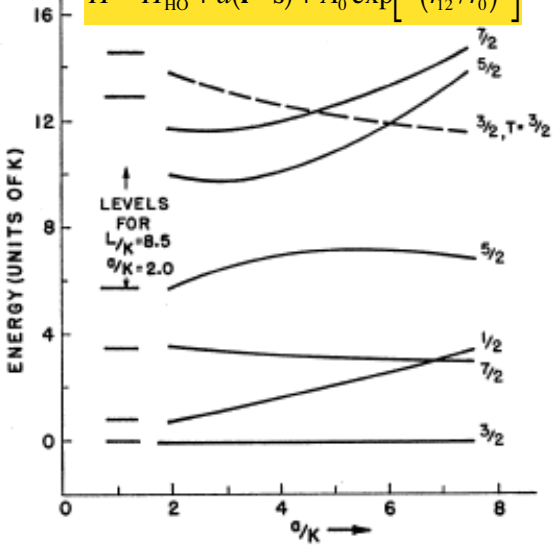

The contributions of the central two-body interaction to the energy matrices are usually expressed in terms of two integrals,[4] L and K, which are linear combinations of the two Slater integrals involved. These integrals are functions of the strength of two-body interaction A_0, and the ratio $\rho = r_p/r_0$ which is a measure of the ratio of nuclear radius to range of nuclear forces.

a/K, measures the relative spin-orbit and central energy contributions and turns out to be the most important for the computation.'

Today ~ 10^{10} configurations

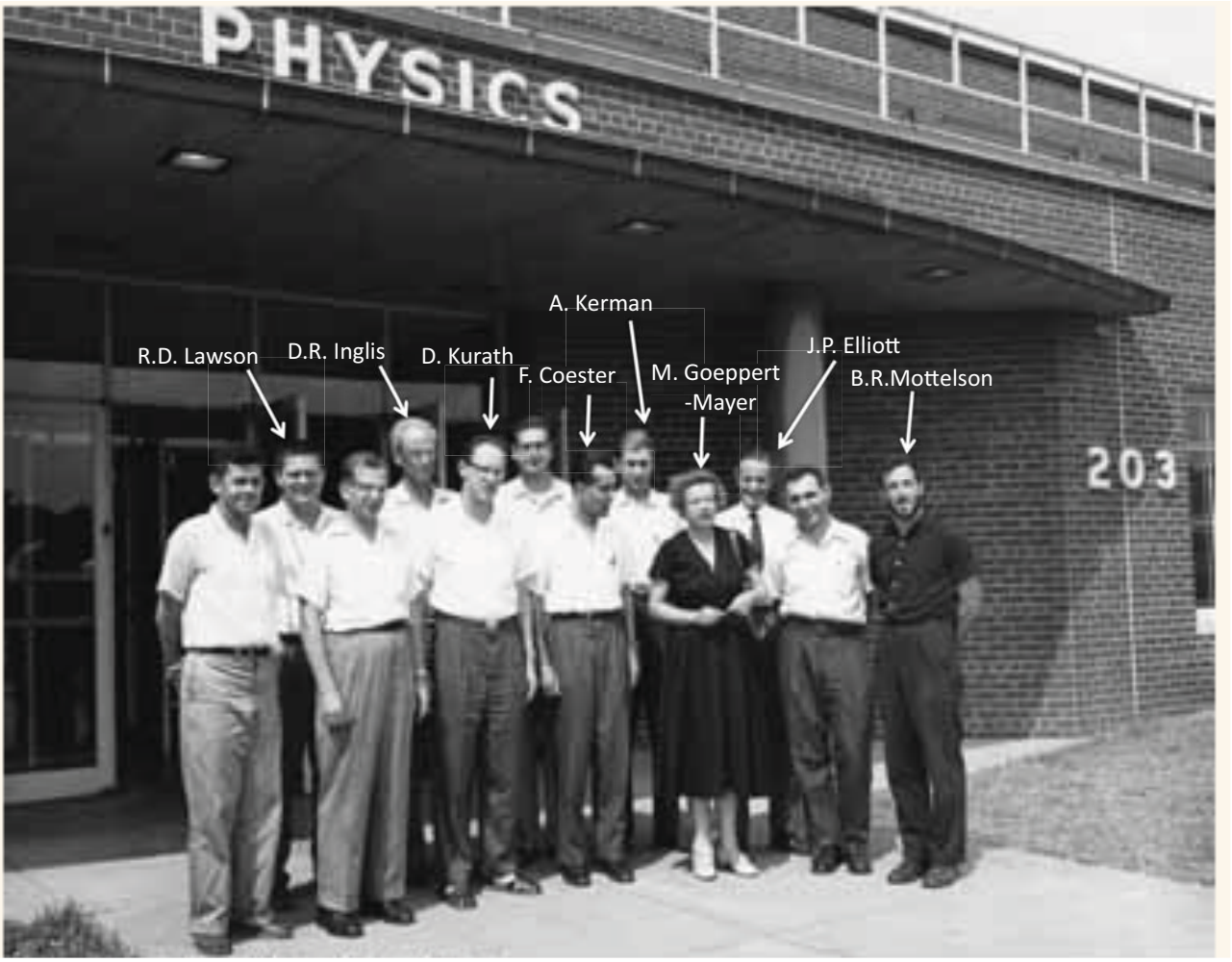

PHYSICAL REVIEW VOLUME 124, NUMBER 6 DECEMBER 15, 1961

Effects of Configuration Interaction on Intensities and Phase Shifts*

U. FANO
National Bureau of Standards, Washington, D. C.
(Received July 14, 1961)

The actual stationary states may be represented as superpositions of states of different configurations which are "mixed" by the "configuration interaction," i.e., by terms of the Hamiltonian that are disregarded in the independent-particle approximation. The effects of configuration interaction are particularly conspicuous at energy levels above the lowest ionization threshold, where states of different configurations coincide in energy exactly since at least some of them belong to a continuous spectrum. The mixing of a configuration belonging to a discrete spectrum with continuous spectrum configurations gives rise to the phenomenon of *autoionization*. The exact coincidence of the energies of different configurations makes the ordinary perturbation theory inadequate, so that special procedures are required for the treatment of autoionization and of related phenomena.

The achievement of this program took ~40 years!

Open Quantum System

An Open Quantum System (OQS) is a quantum system which is found to be in interaction with an external quantum system, the environment.
The OQS can be viewed as a distinguished part of a larger Closed Quantum System, the other part being the environment.

Resonance refers to the energy distribution of the outgoing particles in a scattering process, and it is characterized by its energy and width.
Decaying state is described in a time dependent setting by its energy and lifetime.
Both concepts are related by: $T_0=\hbar/\Gamma$, as verified in precision experiments

R. de la Madrid, NPA 812, 13 (2008)

Resonances are genuine intrinsic properties of quantum systems but they do not belong to the Hilbert space

Resonances find a natural description within the rigged Hilbert space

For a pedagogical description see: R. de la Madrid, AIP Conf. Proc. 885, 3 (2007)

Example: Nuclear decays

α – decay

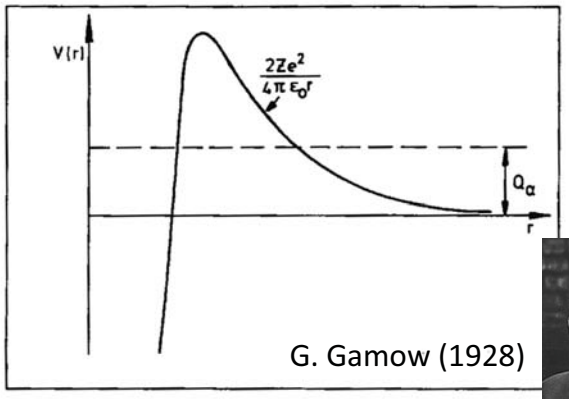

G. Gamow (1928)

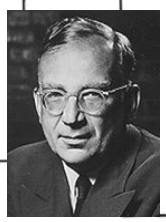

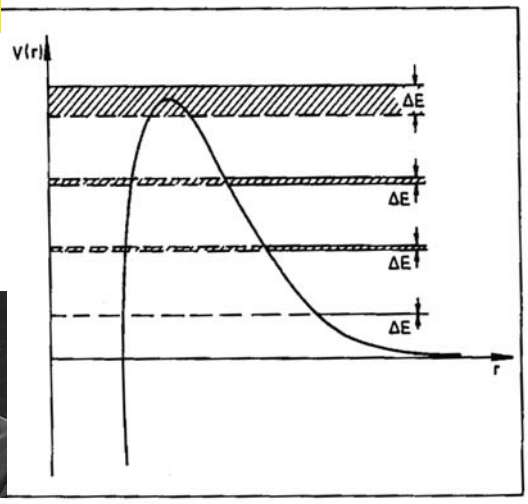

Electromagnetic decays

Emission of γ-ray is caused by the interaction of the nucleus with an external electromagnetic field

$$V = -\frac{1}{c} j_\mu A^\mu$$

Nuclear current — External EM field

6^+

E2, (M3, E4,…)

4^+

Example: Radii of halo systems

^{2}H (deuteron)
S_n=2.2 MeV, r_{np}=4 fm

$^3H_\Lambda$ (hypertriton)
S_L=0.08 MeV

$^4He_2$ (atomic helium dimer)
S=0.13 meV, r=100 Å

A. Cobis et al., J. Phys. G23, 401 (1997)
K. Riisager et al., Europhys. Lett. 49, 547 (2000)

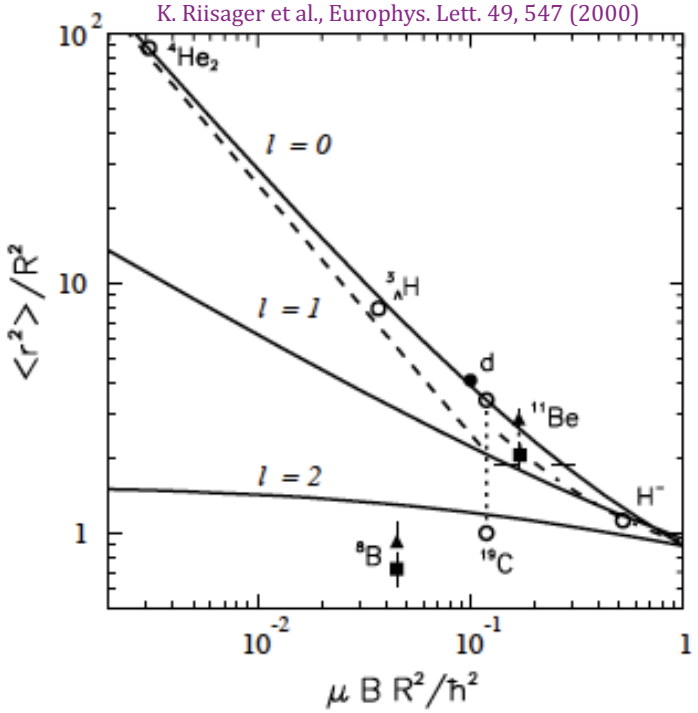

K. Riisager et al, NP A548 (1992) 393
T. Misu et al, NP A614 (1997) 44

One-body Schrödinger equation:

$$\left[\nabla^2 - \frac{2m}{\hbar^2}U(r) - \kappa_\nu^2\right]\psi_\nu(r) = 0$$

$$\kappa_\nu = \sqrt{-2m\epsilon_\nu/\hbar^2}$$

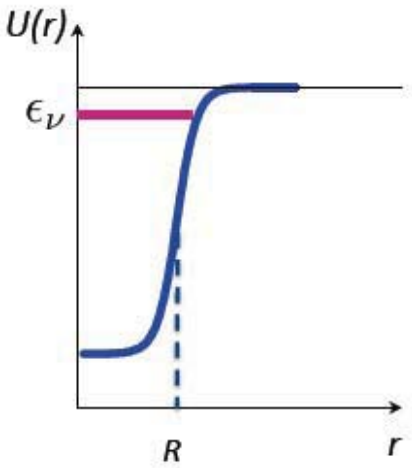

at large distances:

$$\left[\frac{d^2}{dr^2} + \frac{2}{r}\frac{d}{dr} - \kappa_\nu^2 - \frac{\ell(\ell+1)}{r^2}\right]R_{\ell\nu}(r) = 0.$$

$R_{\ell\nu}(r) = B_\ell h_\ell^+(i\kappa_\nu r)$ for r→∞

$$\langle r^n \rangle = \int_0^\infty r^n R_{\ell\nu}^2(r) r^2 dr \equiv I_n + O_n$$

inner part outer part

$$O_n = \int_R^\infty r^{n+2}|B_\ell|^2\left|h_\ell^+(i\kappa_\nu r)\right|^2 dr = |B_\ell|^2 \kappa_\nu^{-(n+3)} \int_{R\kappa_\nu}^\infty \left|h_\ell^+(ix)\right|^2 x^{2+n} dx$$

In the limit of weak binding: $B_\ell \approx \frac{i^{\ell+1}}{1\times 3\times \ldots(2\ell-1)} R_{\ell\nu}(R)(R\kappa_\nu)^{\ell+1}$

$n > 2\ell - 1$: O_n diverges as $(-\varepsilon_\nu)^{(2\ell-n-1)/2}$

$n = 2\ell - 1$: O_n diverges as $-(1/2)\ln(-\varepsilon_\nu)$

$n < 2\ell - 1$: O_n remains finite

⇒

$\ell = 0$: $\langle r^2 \rangle$ diverges as $(-\varepsilon_\nu)^{-1}$

$\ell = 1$: $\langle r^2 \rangle$ diverges as $(-\varepsilon_\nu)^{-1/2}$

$\ell > 1$: $\langle r^2 \rangle$ remains finite

What happens if pairing is present? K. Bennaceur et al, PL B496 (2000)154

In even-N nuclei, the paired densities decrease faster than the unpaired densities

⇒ pairing anti-halo effect

Pairing correlations do not prevent a divergence of the neutron radii for odd-N

Impact of scattering states on structural properties

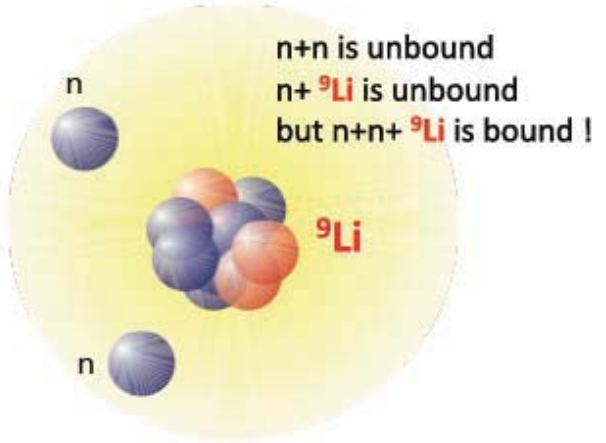

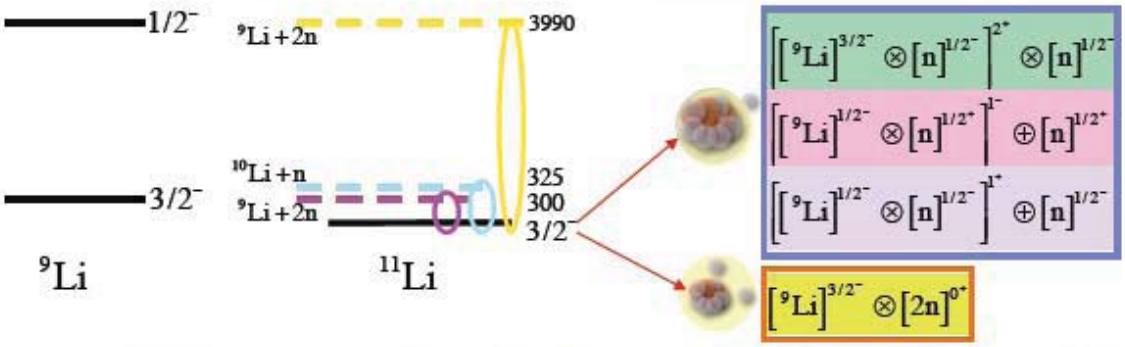

The structure of ^{11}Li is a tremendous challenge to both experiment and theory!

The nucleus is a correlated open quantum many-body system.
Environment: the continuum of decay channels

The configuration mixing (shell model) approach for open quantum systems

Continuum (real-energy) Shell Model
(1977 - 1999 - 2005)

H.W.Bartz et al, NP A275 (1977) 111
R.J. Philpott, NP A289 (1977) 109
K. Bennaceur et al, NP A651 (1999) 289
N. Michel et al, APP B35 (2004) 1249
J. Rotureau et al, NP A767 (2006) 13
J-B. Faes, M.P., NP A800 (2008) 21
J. Okolowicz et al, APP B39 (2008) 389
J. Okolowicz, M.P., PRC 80 (2009) 034619
J. Okolowicz et al., Phys. Rep. 374 (2003) 271
B. Blank, M.P., Rep. Prog. Phys. 71 (2008) 046301

Gamow (complex-energy) Shell Model
(2002 -)

N. Michel et al, PRL 89 (2002) 042502
R. Id Betan et al, PRL 89 (2002) 042501
N. Michel et al, PRC 70 (2004) 064311
G. Hagen et al, PRC 71 (2005) 044314
J. Rotureau et al, PRL 97 (2006) 110603
N. Michel et al, PRC 75 (2007) R031301
N. Michel et al, NP Au794 (2007) 29
K. Tsukiyama et al, PR C80 (2009) 051301
N. Michel et al, PRC 82 (2010) 044315
N. Michel et al., J. Phys. G: Nucl. Part. Phys. (Topical Review) 36 (2009) 013101

(Gamow-) Coupled Cluster Approach
(2007 -)

G. Hagen et al, PL B656 (2007) 169
G. Hagen et al, PRL 103 (2009) 062503
G. Hagen et al, PRL 104 (2010) 182501
Ø. Jensen et al, PRC 82 (2010) 014310
Ø. Jensen et al, arXiv:1104.1552

Rigged Hilbert Space

The Hilbert space includes bound and scattering states, because the Hilbert space spectrum of an observable is real ⟹ resonance spectrum is discarded as unphysical

But… radioactive nuclei and unstable elementary particles are physical objects!

Rigged Hilbert Space (RHS) is the natural setting of Quantum Mechanics in which resonance spectrum, Dirac bra-ket formalism (and Heisenberg uncertainty relations) have place

In mathematics, RHS (Gel'fand triple, nested Hilbert space, equipped Hilbert space): $\Phi \subset \mathcal{H} \subset \Phi^{\times}$ and $\Phi \subset \mathcal{H} \subset \Phi'$ ($\mathcal{H}$ - Hilbert space, Φ - (dense) space of test functions, $\Phi^{\times}$- (dense) space of distributions, and Φ' - space of linear functionals over Φ) is a construction designed to link the distribution and square-integrable aspects of functional analysis.

I.M. Gel'fand and N. J. Vilenkin. *Generalized Functions*, vol. 4: *Some Applications of Harmonic Analysis. Rigged Hilbert Spaces*, Academic Press, New York, 1964
G. Ludwig, *Foundation of Quantum Mechanics*, Vol. I and II, Springer-Verlag, New York, 1983

The resonance amplitude associated with the Gamow states is proportional to the complex δ-function and such amplitude can be approximated in the near resonance region by the Breit-Wigner amplitude:

$$\mathcal{A}(E_n \to E) \propto i\sqrt{2\pi}\delta(E - E_n) \approx -\frac{1}{2\pi}\frac{1}{E - E_n}$$

R. de la Madrid, Nucl. Phys. 885, 3 (2007)
R. de la Madrid, Eur. J. Phys. 26, 287 (2005)

Question: Can one apply the time-dependent Schrödinger equation for the description of resonances?

$$i\hbar\frac{\partial\psi}{\partial t} = \hat{H}\psi$$

$$T_{1/2} = \ln 2\frac{\hbar}{\Gamma}, \qquad \hbar = 6.58 \cdot 10^{-22}\ \text{MeV} \cdot \text{sec}$$

Can one calculate Γ with sufficient accuracy?

$$T_{s.p.} \approx 3 \cdot 10^{-22}\ \text{sec} = 3\,\text{baby sec}$$

^{238}U: $T_{1/2}=10^{16}$ years
^{256}Fm: $T_{1/2}$=3 hours

For very narrow resonances explicit time-propagation impossible!

Quasi-stationary open quantum system extension of the Shell Model

$$i\hbar\frac{\partial}{\partial t}\Phi(r,t)=\hat{H}\Phi(r,t)\quad \Phi(r,t)=\tau(t)\Psi(r)$$

$$\hat{H}\Psi=\left(e-i\frac{\Gamma}{2}\right)\Psi \rightarrow \tau(t)=\exp\left(-i\left(e-i\frac{\Gamma}{2}\right)\right)$$

$$\Psi(0,k)=0\ ,\ \begin{cases}\Psi(\vec{r},k)\underset{r\to\infty}{\rightarrow}O_l(kr)\\ \Psi(\vec{r},k)\underset{r\to\infty}{\rightarrow}I_l(kr)+O_l(kr)\end{cases}$$

$k_n=\sqrt{\frac{2m}{\hbar^2}\left(e_n-i\frac{\Gamma_n}{2}\right)}$ (poles of the S-matrix)

Bound states	$k_n=i\kappa_n$
Antibound states	$k_n=-i\kappa_n$
Resonances	$k_n=\pm\gamma_n-i\kappa_n$

Only bound states are integrable!

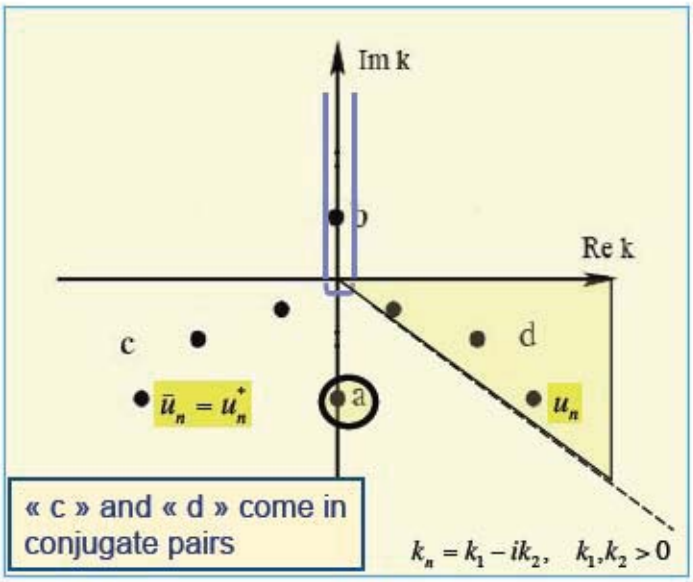

Quasi-stationary open quantum system extension of the Shell Model

$$i\hbar\frac{\partial}{\partial t}\Phi(r,t)=\hat{H}\Phi(r,t)\quad \Phi(r,t)=\tau(t)\Psi(r)$$

$$\hat{H}\Psi=\left(e-i\frac{\Gamma}{2}\right)\Psi \rightarrow \tau(t)=\exp\left(-i\left(e-i\frac{\Gamma}{2}\right)\right)$$

$$\Psi(0,k)=0\ ,\ \begin{cases}\Psi(\vec{r},k)\underset{r\to\infty}{\rightarrow}O_l(kr)\\ \Psi(\vec{r},k)\underset{r\to\infty}{\rightarrow}I_l(kr)+O_l(kr)\end{cases}$$

$k_n=\sqrt{\frac{2m}{\hbar^2}\left(e_n-i\frac{\Gamma_n}{2}\right)}$ (poles of the S-matrix)

Bound states	$k_n=i\kappa_n$
Antibound states	$k_n=-i\kappa_n$
Resonances	$k_n=\pm\gamma_n-i\kappa_n$

Only bound states are integrable!

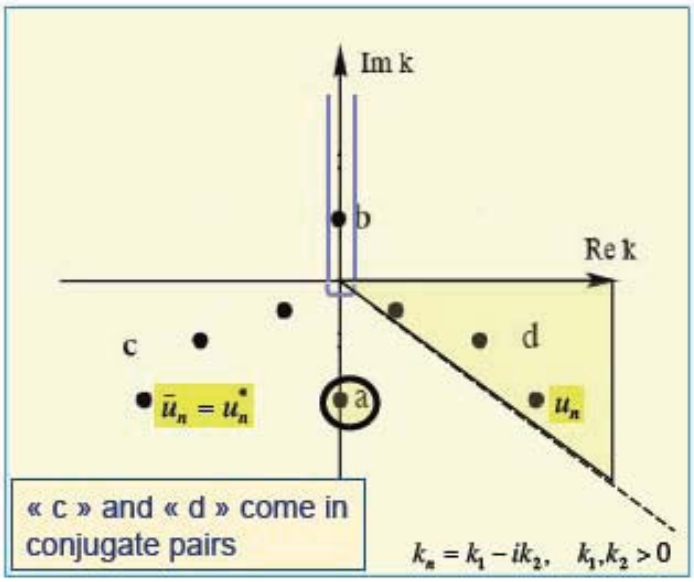

Euclidean inner product

$$\langle u_n|u_n\rangle=\int_0^\infty dr u_n^*(r)u_n(r)$$

$$\xrightarrow[r\to\infty]{} e^{2k_2r}$$

RHS inner product

$$\langle \bar{u}_n|u_n\rangle=\int_0^\infty dr \bar{u}_n^*(r)u_n(r)$$

$$\xrightarrow[r\to\infty]{} e^{2ir(k_1-ik_2)}$$

Completeness relations in Gamow Shell Model

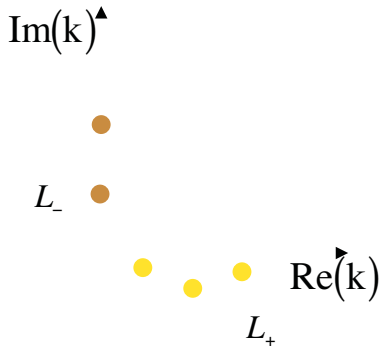

T. Berggren, NPA 109, 265 (1968); A389, 261 (1982)
T. Lind, Phys. Rev. C47, 1903 (1993)

$$\sum_n |u_n\rangle\langle\tilde{u}_n| + \int_{L_+} |u_k\rangle\langle\tilde{u}_k| dk = 1 \; ; \; \langle u_i|\tilde{u}_j\rangle = \delta_{ij}$$

bound states, resonances — non-resonant continuum

$$|SD_i\rangle = |u_{i_1} \ldots u_{i_A}\rangle$$

$$\sum_k |SD_k\rangle\langle\widetilde{SD}_k| \cong 1$$

N. Michel et al, PRL 89 (2002) 042502

$$H \rightarrow [H]_{ij} = [H]_{ji}$$

Gamow Shell Model

complex-symmetric eigenvalue problem for hermitian Hamiltonian

Interacting Shell Model respecting unitarity in weakly-bound/unbound states

The long-term goal of Fano (1961) finally achieved!

VOLUME 89, NUMBER 4 PHYSICAL REVIEW LETTERS 22 JULY 2002

Gamow Shell Model Description of Neutron-Rich Nuclei

N. Michel,[1] W. Nazarewicz,[2,3,4] M. Płoszajczak,[1] and K. Bennaceur[2,5]
[1]*GANIL, CEA/DSM-CNRS/IN2P3, BP 5027, F-14076 Caen Cedex 05, France*
[2]*Department of Physics and Astronomy, The University of Tennessee, Knoxville, Tennessee 37996*
[3]*Physics Division, Oak Ridge National Laboratory, P.O. Box 2008, Oak Ridge, Tennessee 37831*
[4]*Institute of Theoretical Physics, Warsaw University, ul. Hoża 69, PL-00681, Warsaw, Poland*
[5]*Institut de Physique Nucleaire de Lyon, Université Claude Bernard–Lyon 1, F-69622 Villeurbanne Cedex, France*
(Received 25 January 2002; published 3 July 2002)

This work presents the first continuum shell-model study of weakly bound neutron-rich nuclei involving multiconfiguration mixing. For the single-particle basis, the complex-energy Berggren ensemble representing the bound single-particle states, narrow resonances, and the nonresonant continuum background is taken. Our shell-model Hamiltonian consists of a one-body finite potential and a zero-range residual two-body interaction. It is demonstrated that the residual interaction coupling to the particle continuum is important; in some cases, it can give rise to the binding of a nucleus.

- The correct formulation in rigged Hilbert space
  M. Gel'fand and N. J. Vilenkin, *Generalized Functions*, vol. 4: Academic Press, New York, 1964
  K. Maurin, *Generalized Eigenfunction Expansions and Unitary Representations of Topological Groups*, Polish Scientific Publishers, Warsaw (1968)

- Definition of a complete single-particle basis
  T. Berggren, NPA 109, 265 (1968)

Gamow Shell Model Hamiltonian

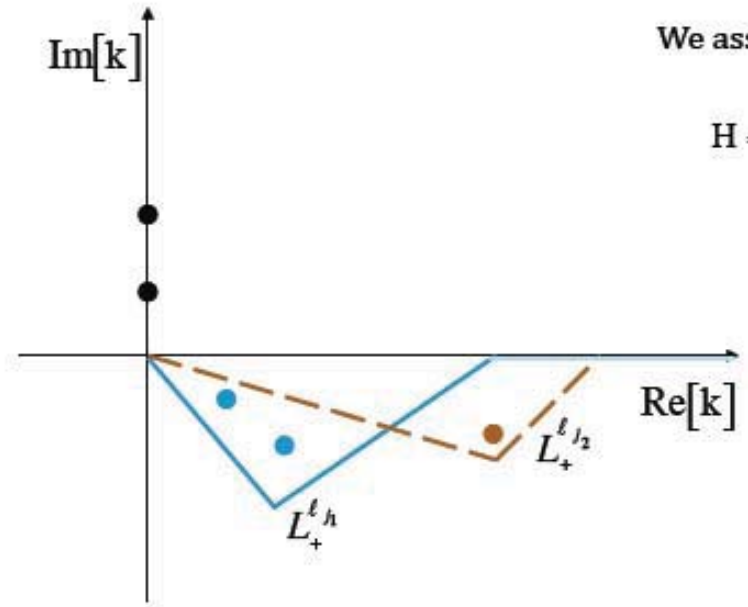

We assume a core:

$$H = \sum_{i=1}^{A_v}\left(\frac{\mathbf{p}_i^2}{2\mu} + U_i\right) + \sum_{i<j}^{A_v}\left(V_{ij} + \frac{\mathbf{p}_i\mathbf{p}_j}{A_c}\right)$$

"Recoil" term coming from the expression of H in the COSM coordinates. No spurious states

COSM coordinates

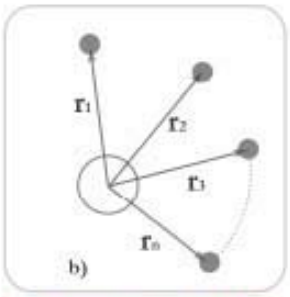

Y.Suzuki and K.Ikeda PRC 38,1 (1988)

(i) two-step diagnalization: $|\Psi_0^{(J)}\rangle \rightarrow \{|\Psi^{(J)}\rangle\}$
- selection of states: $\max\{|\langle\Psi_i^{(J)}|\Psi_0^{(J)}\rangle|\}$

(ii) Density Matrix Renormalization Group method

J. Rotureau et al., PRL 97, 110603 (2007); PRC 79, 014304 (2009)

Results (I)

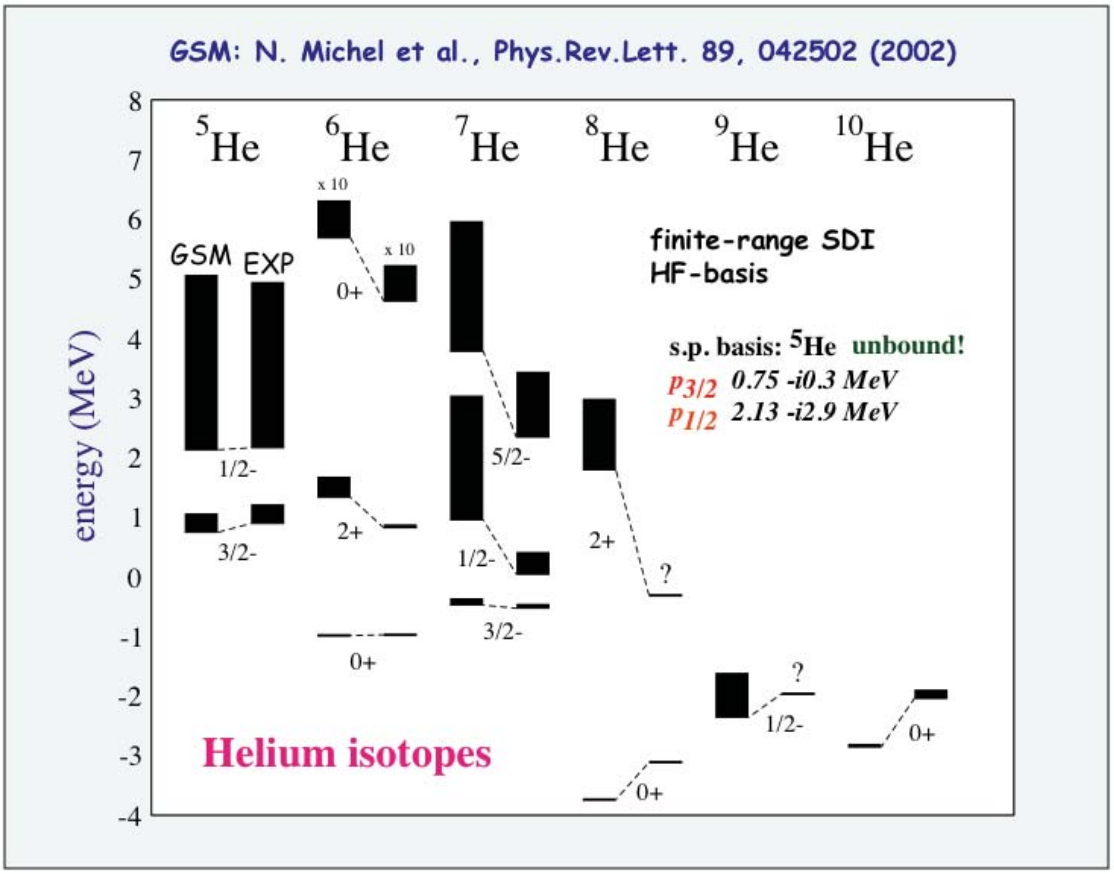

Density distribution of valence neutrons in ^{6}He

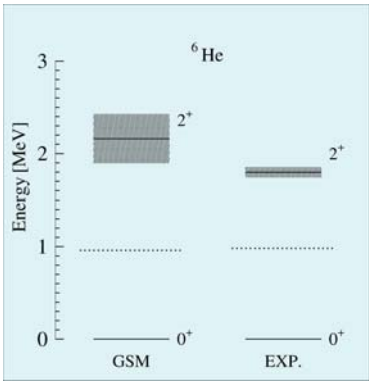

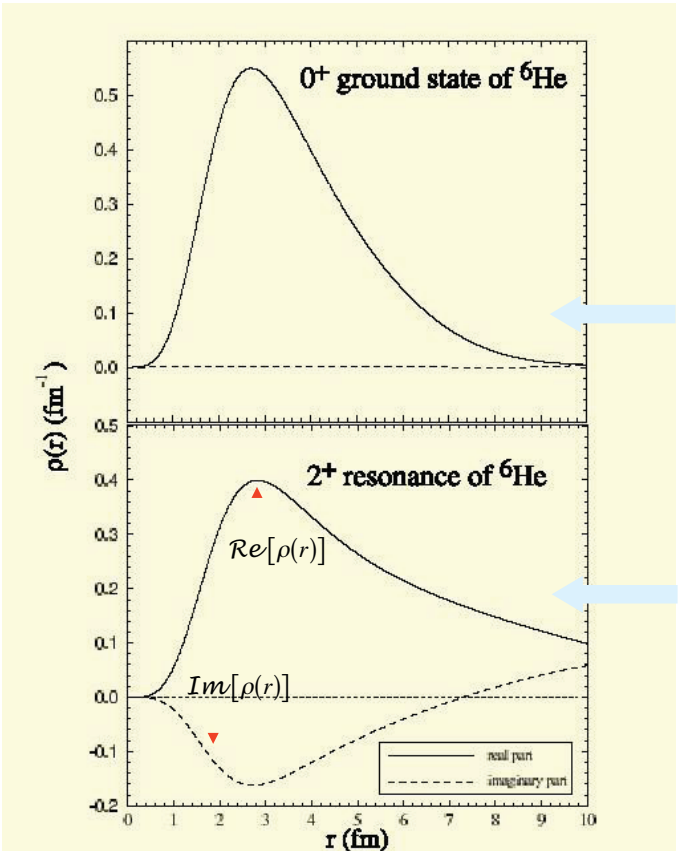

weakly bound state

broad resonance

One-neutron radial overlap integral

Provide a connection to the reaction theory

$$u_{\ell j}(r) = \sum_{\mathcal{B}} \langle \widetilde{\Psi}_A^{J_A} || a^+_{\ell j}(\mathcal{B}) || \Psi_{A-1}^{J_{A-1}} \rangle \ \langle r \ell j | u_{\mathcal{B}} \rangle$$

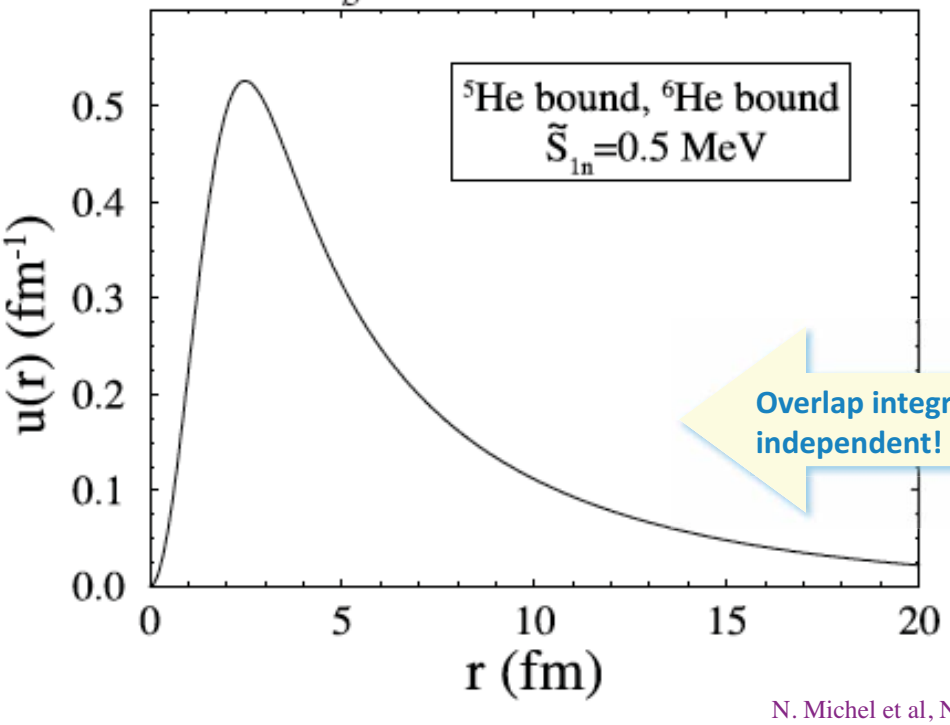

Overlap integral, basis independent!

N. Michel et al, NPA 794, 29 (2007)

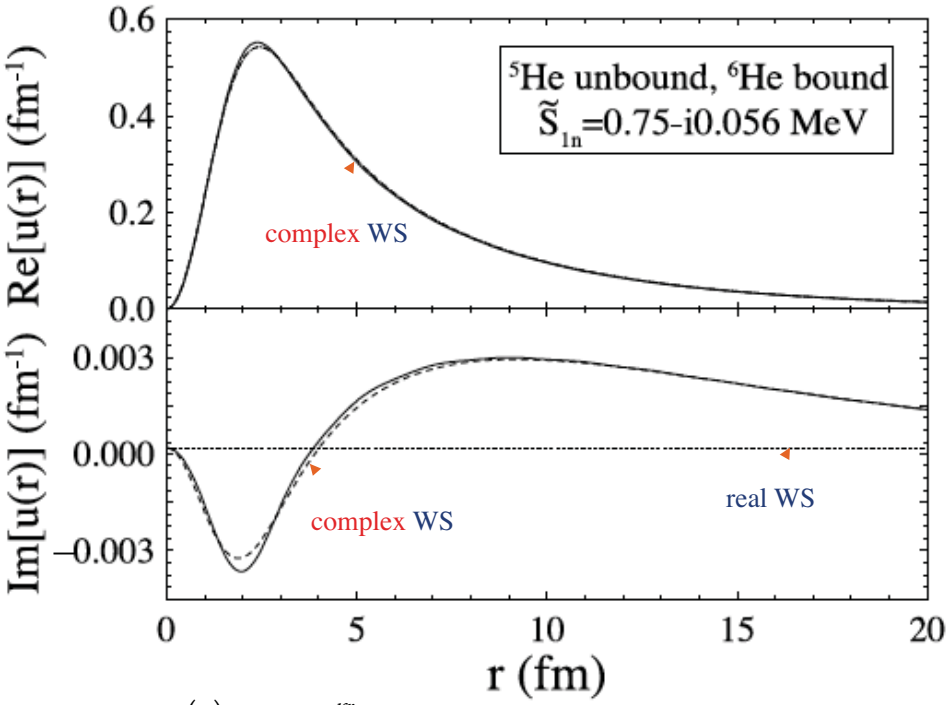

$$O(r) \to C_0 e^{-\kappa r}$$

$$\kappa = \sqrt{2\mu \tilde{S}_{1n}} / \hbar$$

$$\tilde{S}_{1n} = \left(E(N-1) - E(N)\right) - \frac{i}{2}\left(\Gamma(N-1) - \Gamma(N)\right)$$

S_{1n} $\quad$ $\frac{i}{2}\Sigma_{1n}$

Relevant quantities:
complex separation energies

Threshold anomalies

- Threshold is a branching point which originates in the unitarity

$$X + a \rightarrow a + X$$
$$X + a \leftrightarrow a_1 + X_1 \quad \text{at } E_1^{(th)}$$
$$X + a \leftrightarrow a_2 + X_2 \quad \text{at } E_2^{(th)}$$
$$\ldots \qquad \ldots$$

  - for $E < E^{(th)}$ a single solution: $X(a,a)X$
  - for $E > E^{(th)}$ two independent solutions: $X(a,b)Y$ and $Y(b,a)X$

Wave function has a singularity at the threshold

- If a new channel opens, a redistribution of the flux in other open channels appears

- The shape of the cusp depends on charge and orbital angular momentum:

$$Y(b,a)X : \sigma_\ell \sim k^{2\ell-1}$$
$$X(a,b)Y : \sigma_\ell \sim k^{2\ell+1}$$

E.P. Wigner, PR 73, 1002 (1948)
G. Breit, PR 107, 923 (1957)

Example: Coupling between analog states in (d,p) and (d,n) C.F. Moore et al., PRL 17, 926 (1966)

Configuration mixing in weakly bound/unbound many-body states

$$S^2 \equiv \int u_{\ell j}^2(r)dr = \sum_{\mathcal{B}} \langle \widetilde{\Psi}_A^{J_A} || a_{\ell j}^+(\mathcal{B}) || \Psi_{A-1}^{J_{A-1}} \rangle^2$$

$$\left\langle {}^6\mathrm{He}(\mathrm{g.s.}) \middle| \left[{}^5\mathrm{He}(\mathrm{g.s.}) \otimes p_{3/2} \right]^{0^+} \right\rangle$$

bound — weakly bound/unbound

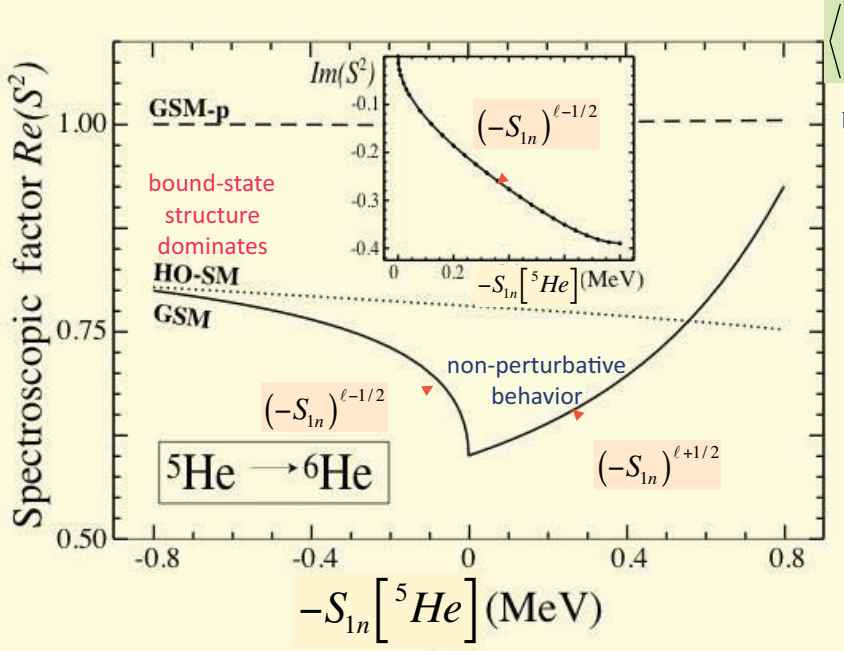

$$Y(b,a)X : \sigma_\ell \sim k^{2\ell-1} \quad \leftrightarrow \quad (-S_n)^{\ell-1/2} \text{ for } S_n < 0$$
$$X(a,b)Y : \sigma_\ell \sim k^{2\ell+1} \quad \leftrightarrow \quad (-S_n)^{\ell+1/2} \text{ for } S_n > 0$$

Analogy with the Wigner threshold phenomenon for reaction cross-sections E.P. Wigner, PR 73, 1002 (1948)

Configuration mixing in mirror systems

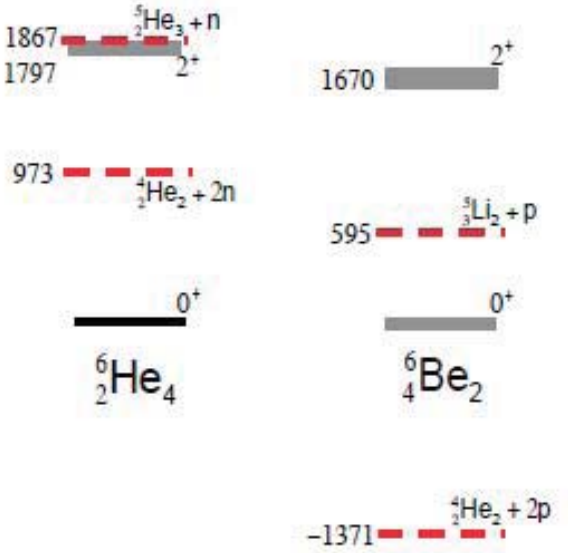

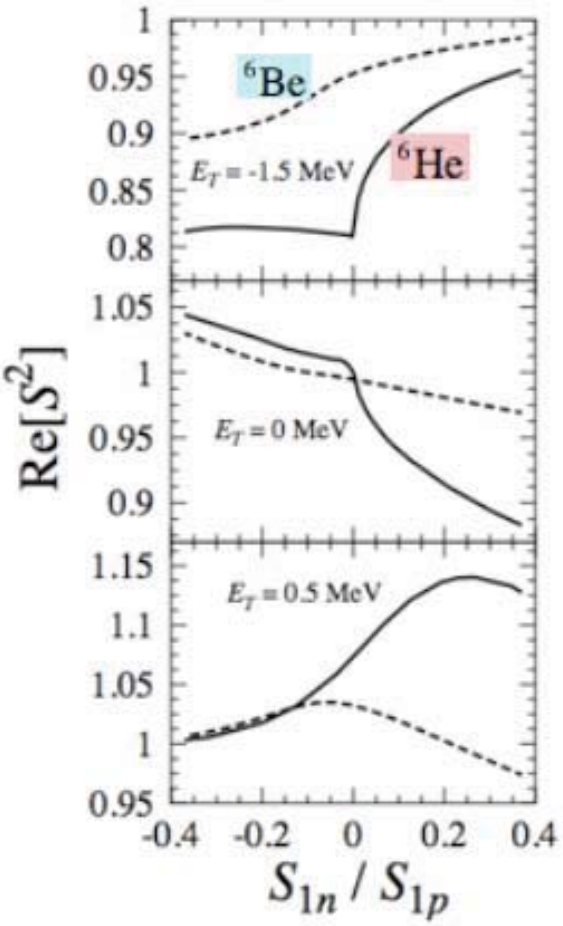

For experimental S_{1n}/S_{1p}, S_{2n}/S_{2p}:

$$S^2_{^6\mathrm{He}}[0^+] = 0.88 - i0.386$$

$$S^2_{^6\mathrm{Be}}[0^+] = 1.057 - i0.181$$

End of Part I

Shell Model for Open Quantum Systems (Part II)

M. Płoszajczak
GANIL, Caen, France

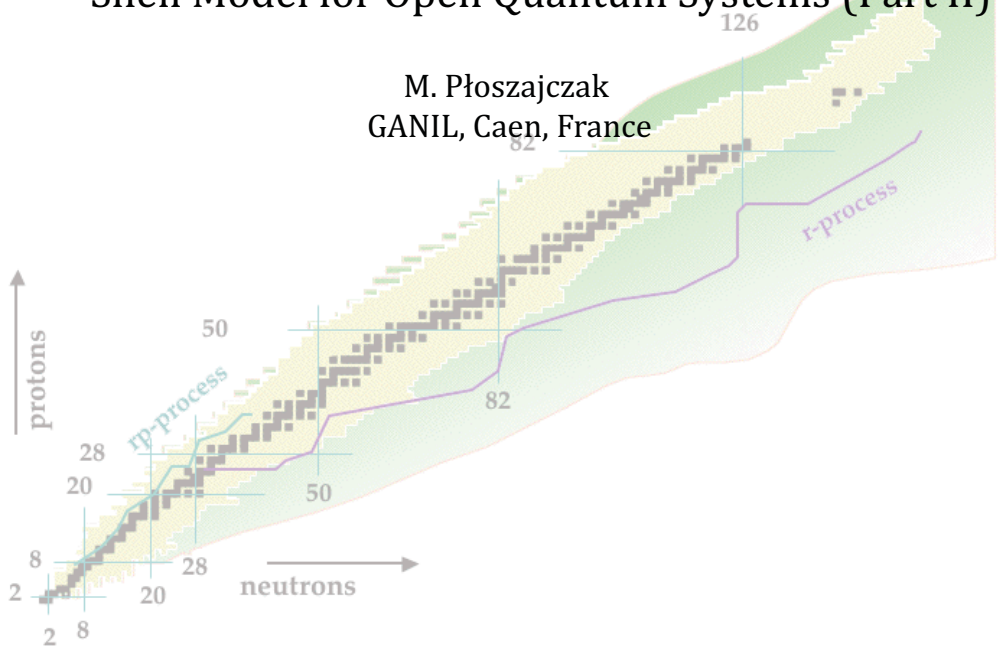

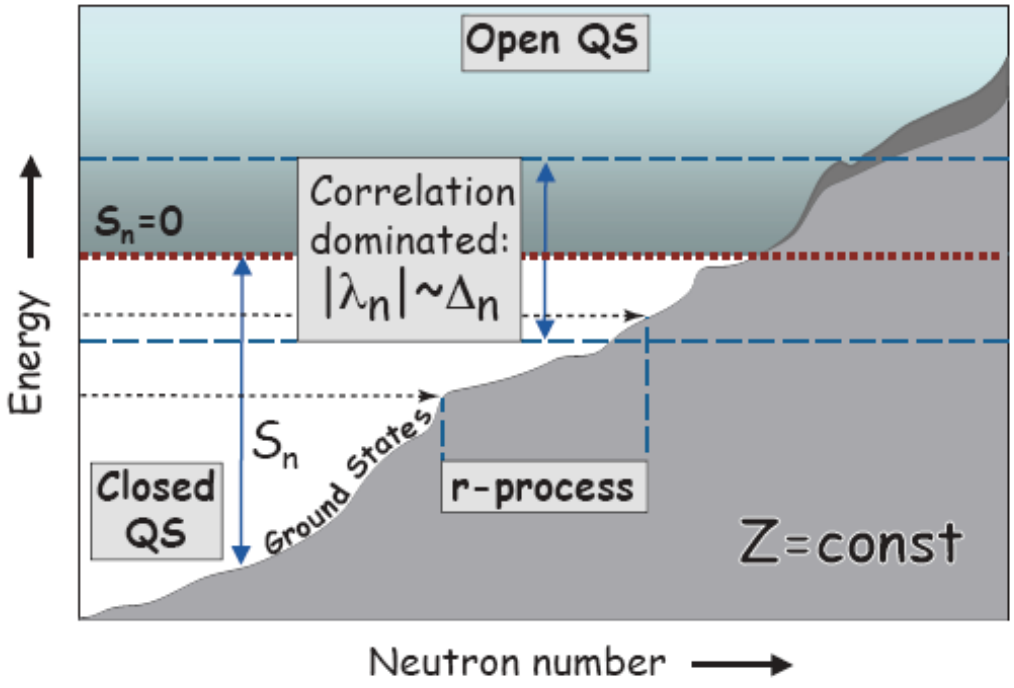

- Majority of nuclear systems are affected by the continuum coupling even in their ground state

Cluster states close to the threshold

α - cluster states

2n - states
'halo' states

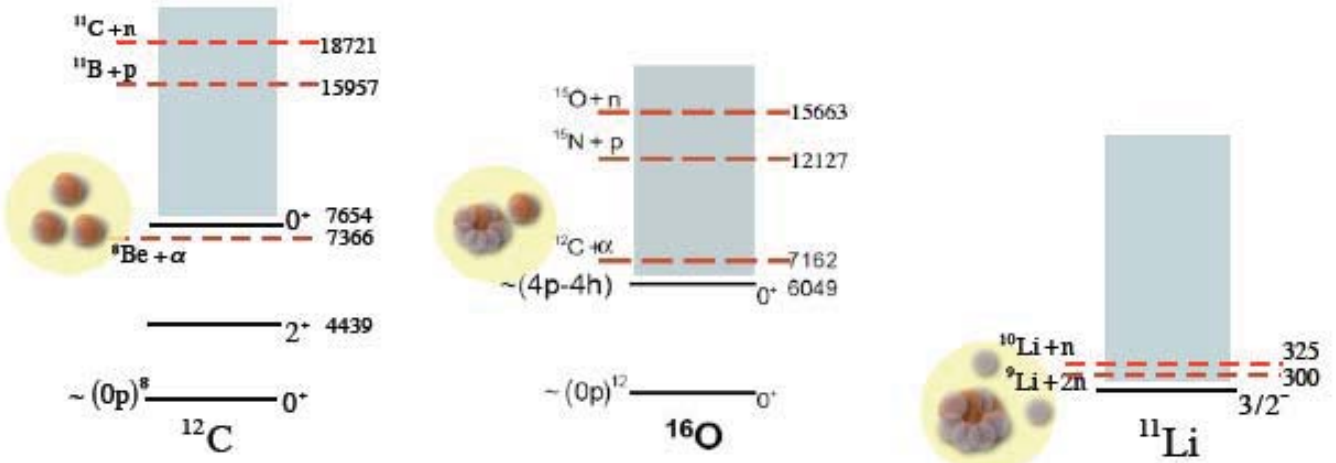

Cluster states close to the threshold

α - cluster states

2n - states
'halo' states

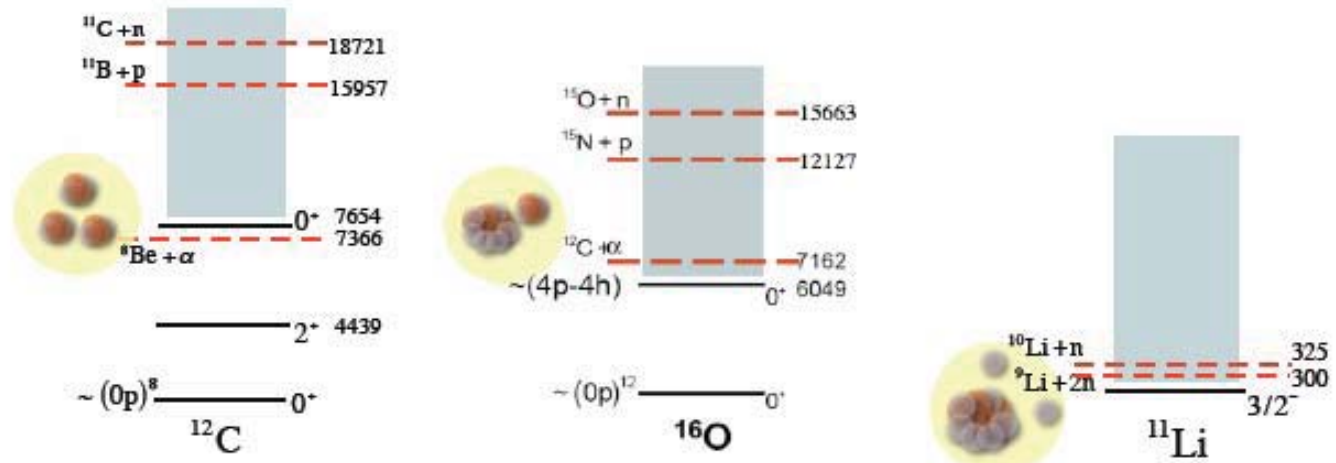

The coupling of 'internal' and 'external' states determines the structure of near-threshold states ➡ the unification of structure and reaction aspects of weakly bound and unbound nuclei, based on the open quantum system formalism is a major challenge for nuclear theory

The configuration mixing (shell model) approach for open quantum systems

Gamow (complex-energy) Shell Model in rigged Hilbert space

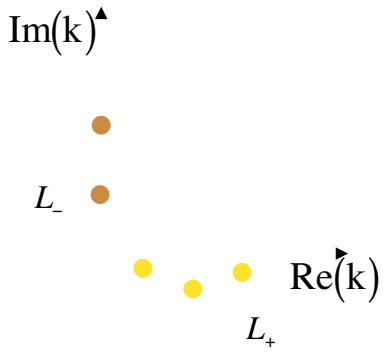

T. Berggren, NPA 109, 265 (1968)

$$\sum_n |u_n\rangle\langle\tilde{u}_n| + \int_{L_+} |u_k\rangle\langle\tilde{u}_k| dk = 1 \; ; \; \langle u_i|\tilde{u}_j\rangle = \delta_{ij}$$

bound states resonances — non-resonant continuum

$$|SD_i\rangle = |u_{i_1} \ldots u_{i_A}\rangle$$

$$\sum_k |SD_k\rangle\langle\widetilde{SD}_k| \cong 1$$

N. Michel et al, PRL 89 (2002) 042502

Interacting Shell Model respecting unitarity in weakly-bound/unbound states

Shell Model Embedded in the Continuum
- Continuum (real-energy) Shell Model -

K. Bennaceur et al. NPA 671, 203 (2000)
J. Rotureau et al., PRL 95, 042503 (2005); NPA 767, 13 (2006)

Resonances are genuine intrinsic properties of quantum systems but they do not belong to the Hilbert space

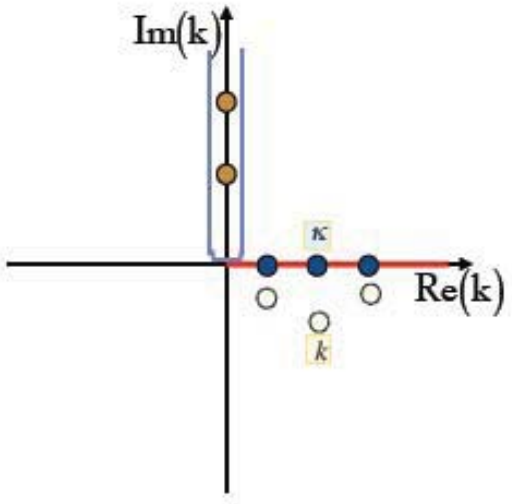

J.-B. Faes, M. Ploszajczak, NPA 800, 21 (2008)

Shell Model Embedded in the Continuum
- Continuum (real-energy) Shell Model -

K. Bennaceur et al. NPA 671, 203 (2000)
J. Rotureau et al., PRL 95, 042503 (2005); NPA 767, 13 (2006)

Resonances are genuine intrinsic properties of quantum systems but they do not belong to the Hilbert space

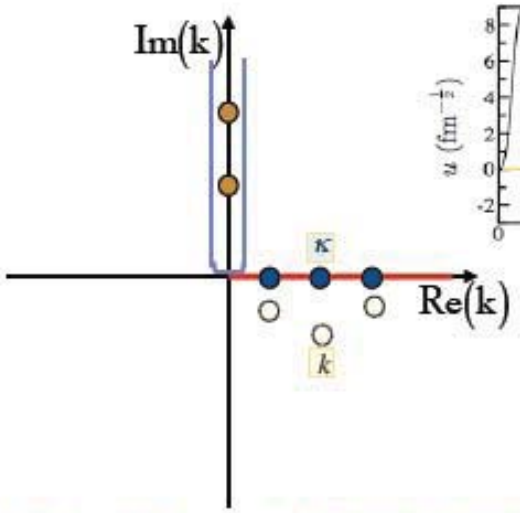

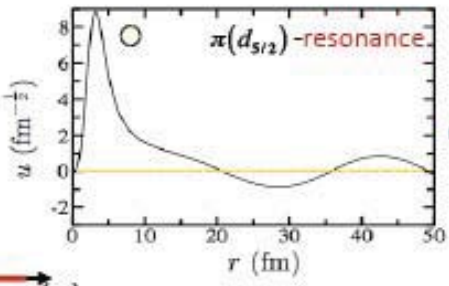

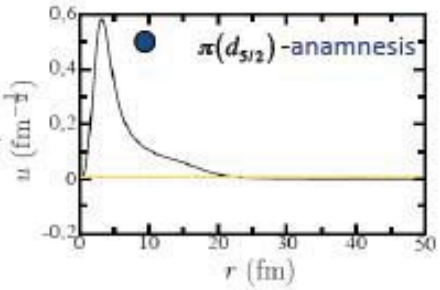

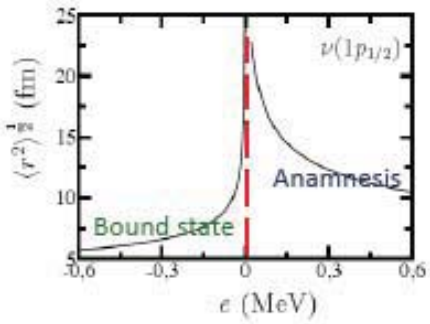

$$v_\kappa(r) \sim u_\kappa^{(reg)}(r) \quad \text{on} \quad [0,R]$$
$$v_\kappa(r) \sim H_{i\kappa}^{+}(r) \quad \text{on} \quad [R,\infty[$$
$$W\left(u_\kappa^{(reg)}, H_{i\kappa}^{+}\right)(r)\Big|_{r=R} = 0$$

J.-B. Faes, M. Ploszajczak, NPA 800, 21 (2008)

Scattering continuum becomes non-resonant if anamneses are projected out:

$$\mathcal{P} = 1 - \sum_n |\tilde{u}_n\rangle\langle\tilde{u}_n| \;, \quad \{\tilde{u}_n\} \equiv \{\{u_n\},\{v_n\}\}$$

discrete states; anamneses

$$h = \sum_n |\tilde{u}_n\rangle \tilde{e}_n \langle\tilde{u}_n| + \mathcal{P}h^{(0)}\mathcal{P}$$

new basis-generating potential

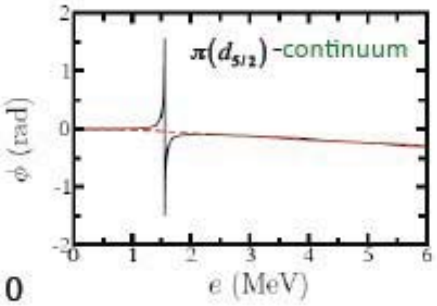

Discrete states: $\left(\tilde{e}_n - h\right)|\tilde{u}_n\rangle = 0$

Continuum states: $\mathcal{P}\left(\tilde{e} - h^{(0)}\right) = 0$

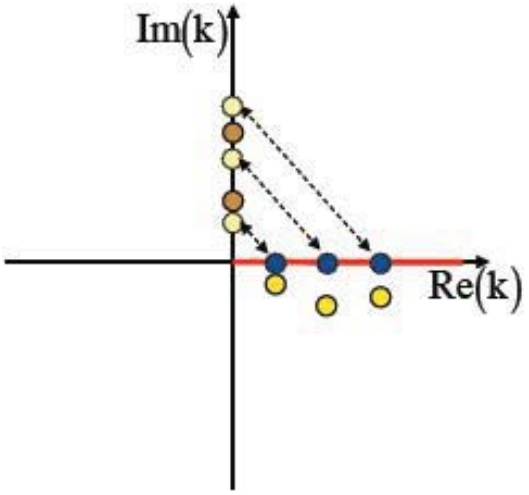

$$\sum_n |\bar{u}_n\rangle\langle\bar{u}_n| + \int_{R_+} |\bar{u}_k\rangle\langle\bar{u}_k| dk = 1; \quad \langle\bar{u}_i|\bar{u}_j\rangle = \delta_{ij}$$

bound states res. anamneses; non-resonant continuum

$$|SD_i\rangle = |u_{i_1} \ldots u_{i_A}\rangle$$

$$\sum_j |SD_j\rangle\langle SD_j| \cong 1$$

Basic idea:

Choice of « relevant » subspaces in the A-particle system depends on the order of particle emission thresholds

↓

QM in Hilbert space using projected subspaces

↓

Real-energy continuum SM (SMEC)

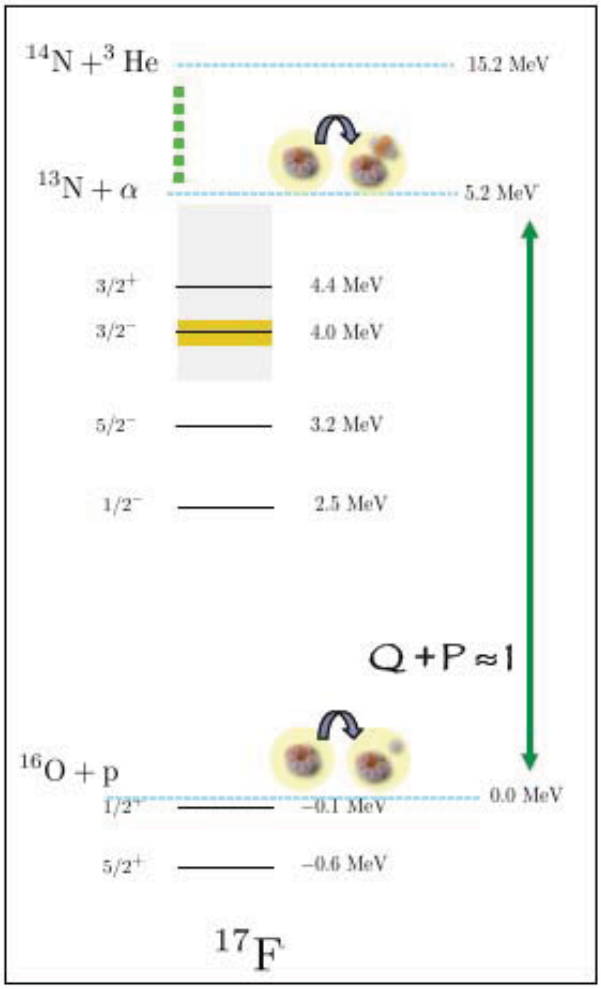

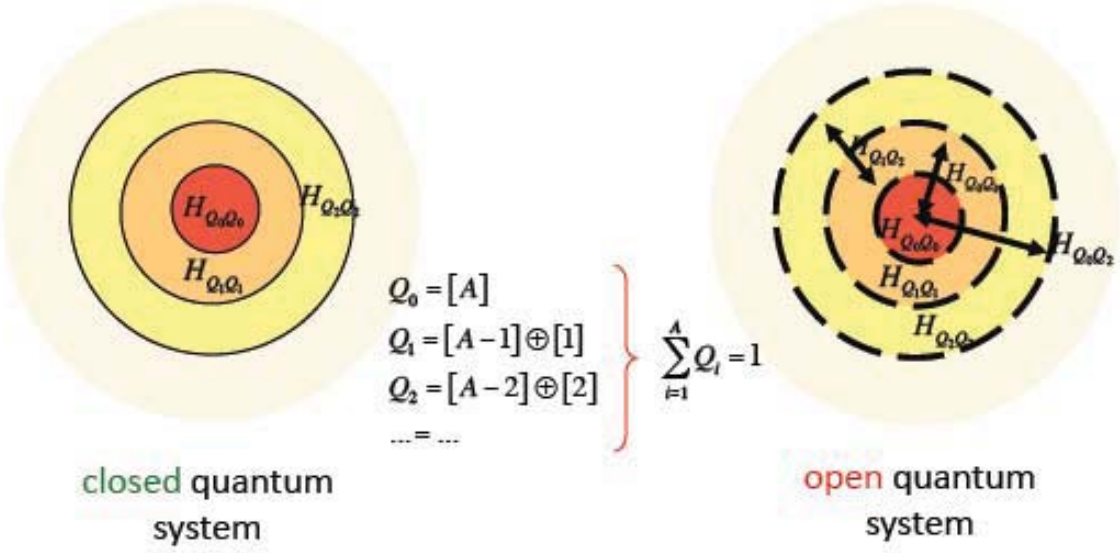

closed quantum system

open quantum system

$$H_{Q_0Q_0} \rightarrow \mathcal{H}_{Q_0Q_0}(E) = H'_{Q_0Q_0}(E) - \frac{i}{2}V(E)V^T(E)$$

$[M \times M]$ $[M \times \Lambda]$

Example: One-nucleon continuum

$$\mathcal{H}_{Q_0Q_0}(E) = H_{Q_0Q_0} + H_{Q_0Q_1}G^{(+)}_{Q_1}(E)H_{Q_1Q_0}$$

Structure of many-body states is determined by the coupling of 'internal' (in Q_0) and 'external' (in Q_i ($i = 1,2...$)) states

Open QS solution in Q:

$$\mathcal{H}_{Q_0Q_0}|\Psi_\alpha\rangle = \mathcal{E}_\alpha|\Psi_\alpha\rangle$$
$$\langle\Psi_{\tilde\alpha}|\mathcal{H}_{Q_0Q_0} = \mathcal{E}^*_\alpha\langle\Psi_{\tilde\alpha}|$$

biorthogonal basis

$$\langle\Psi_{\tilde\alpha}|\Psi_\beta\rangle = \delta_{\alpha\beta}$$
$$\langle\mathcal{O}\rangle_{\alpha\beta} = \langle\Psi_{\tilde\alpha}|\mathcal{O}|\Psi_\beta\rangle$$

$$\Psi_\alpha = \sum_i a^i_\alpha \Phi^A_i \quad ; \quad \Psi_{\tilde\alpha} = \Psi^*_\alpha$$

For bound states: $\mathcal{E}_\alpha(E)$ is real and $\mathcal{E}_\alpha(E) = E$

For unbound states: physical resonances ≡ poles of S-matrix

$$E_\alpha = \mathrm{Re}\left(\mathcal{E}_\alpha(E)\right)\Big|_{E=E_\alpha}$$
$$\Gamma_\alpha = -2\mathrm{Im}\left(\mathcal{E}_\alpha(E)\right)\Big|_{E=E_\alpha}$$

The scattering function (in $\mathrm{I} = \mathrm{Q}_0 + (\mathrm{Q}_1 + \ldots)$)

$$\Psi^c_E = \varsigma^c_E + \sum_\alpha c_\alpha \tilde\Psi_\alpha \quad ; \quad c_\alpha = \frac{\langle\Psi_\alpha|H_{Q_0Q_1}|\varsigma^c_E\rangle}{E - \mathcal{E}_\alpha}$$
$$\tilde\Psi_\alpha \equiv \left(1 + G^{(+)}_{Q_1} H_{Q_1Q_0}\right)\Psi_\alpha$$

Inside of the interaction region :

$$\Psi^c_E \sim \sum_\alpha c_\alpha \Psi_\alpha$$

eigenfunctions of $\mathcal{H}_{Q_0Q_0}(E)$

$$\mathcal{E}_{ij} = \langle\Phi^{SM}_i|\mathcal{H}_{Q_0Q_0}(E)|\Phi^{SM}_j\rangle = \langle\Phi^{SM}_i|H_{Q_0Q_0}|\Phi^{SM}_j\rangle\delta_{ij} + \sum_{c=1}^{\Lambda} P\left(\int_{\varepsilon_c}^{\infty} dE' \frac{\gamma^c_i\gamma^c_j}{E - E'}\right) - \frac{i}{2}\sum_{c=1}^{\Lambda}\gamma^c_i\gamma^c_j$$

real — imaginary

$$\gamma^c_i(E, E') = \langle i|H - E|c; E'\rangle$$
$$\gamma^c_i(E) = \gamma^c_i(E, E)$$

Competition between Hermitian and non-Hermitian parts of Hamiltonian may lead to the coalescence of eigenvalues

Results (II)

Unified approach to nuclear structure and reactions

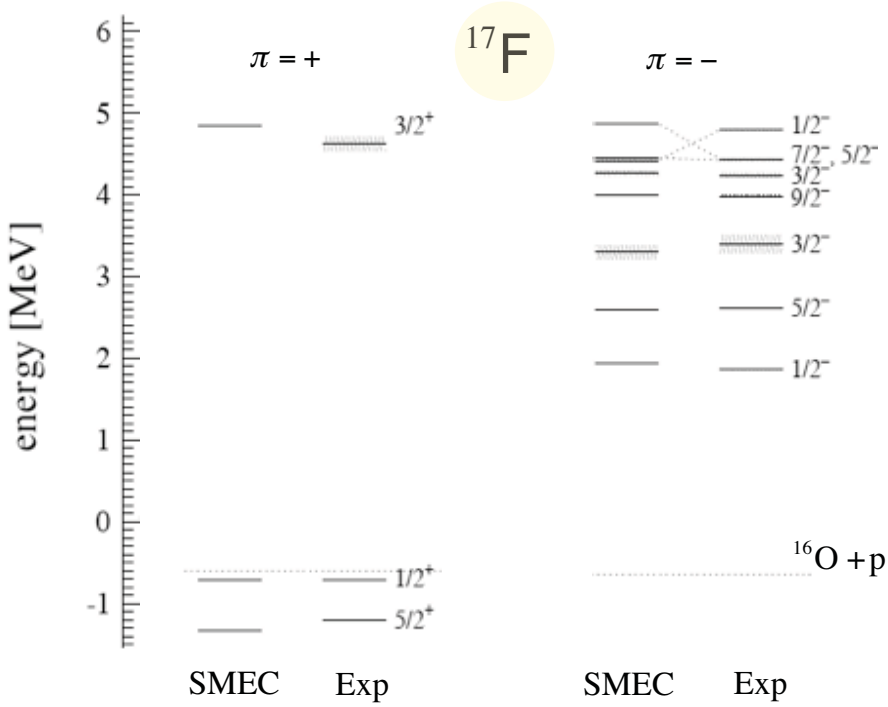

ZBM: $(p_{1/2}, s_{1/2}, d_{5/2})$

K. Bennaceur et al., Phys. Lett. B488, 75 (2000)
K. Bennaceur et al., Nucl. Phys. A671, 203 (2000)

Radiative capture : $^{16}\mathrm{O}(\mathrm{p},\gamma)^{17}\mathrm{F}$

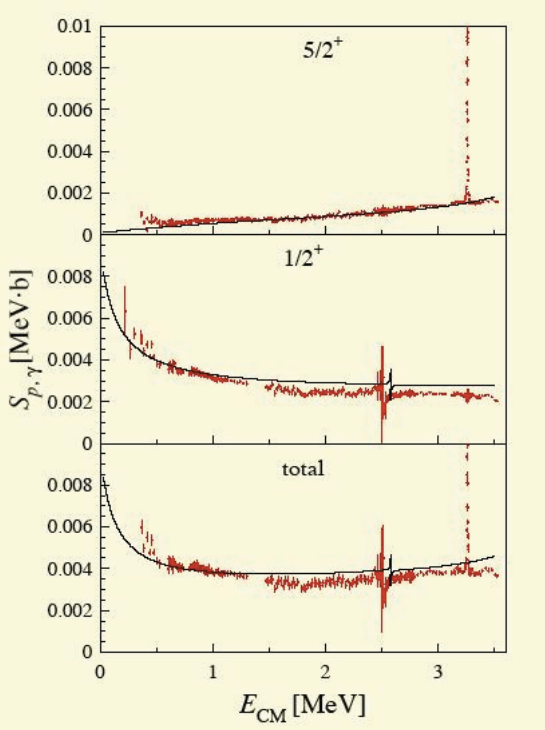

$$\sigma(E) = \frac{1}{E} e^{-2\pi\eta} S(E) \qquad \eta = \frac{Z_1 Z_2 e^2}{\hbar v}$$

Exp.: Morlock et al., Phys. Rev. Lett. 79 (1997) 3837

Elastic scattering : $^{16}\mathrm{O}(\mathrm{p},\mathrm{p})^{16}\mathrm{O}$

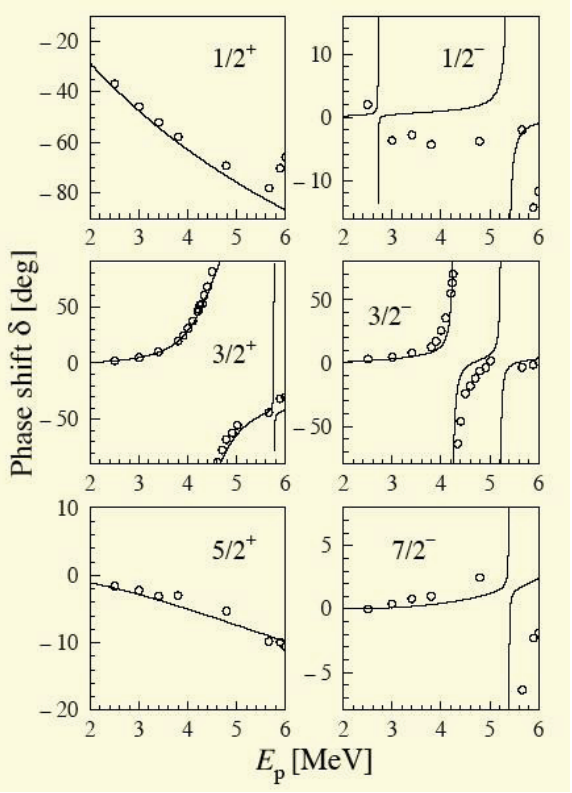

Exp.: Blue and Haeberli, Phys. Rev. 137 (1965) B284

Continuum coupling correction to Shell Model eigenstates

$$E_{corr} = \left\langle \Phi_i^A \middle| \mathcal{H}_{Q_0Q_0} - H_{Q_0Q_0} \middle| \Phi_i^A \right\rangle$$

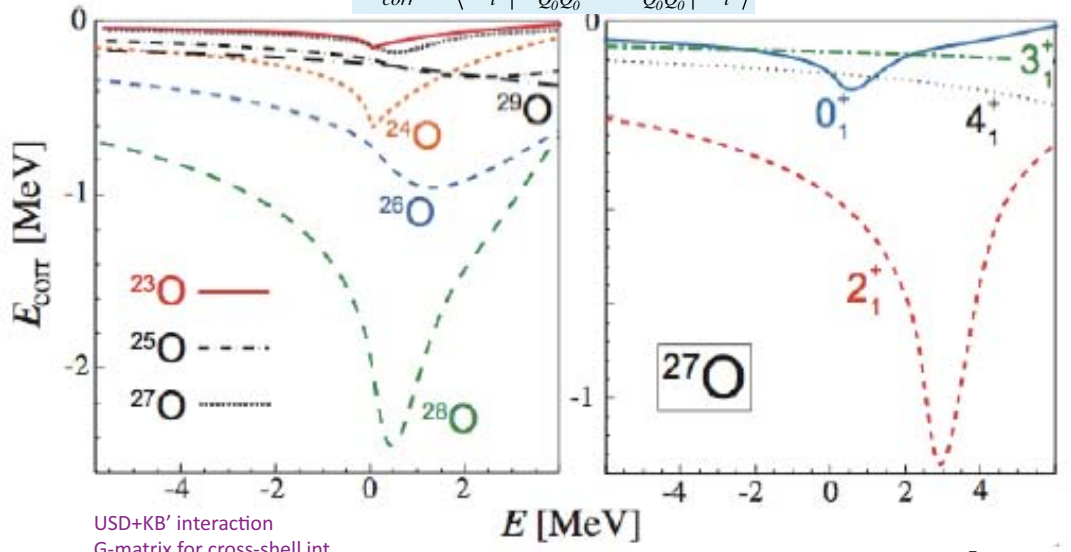

USD+KB' interaction
G-matrix for cross-shell int.
WB continuum coupling

Coupling to a single channel: $\left[{}^{A-1}\mathrm{O}(\mathrm{g.s.}) \otimes {}^{1}\mathrm{n}(\ell j)\right]^{J^\pi_{\mathrm{g.s.}}}_{E^*}$

Threshold effects 0.1-3 MeV → at the intersection between energy scales of pairing and collective excitations

Binding energy ~8 MeV/nucl

Continuum-coupling correction to binding energies

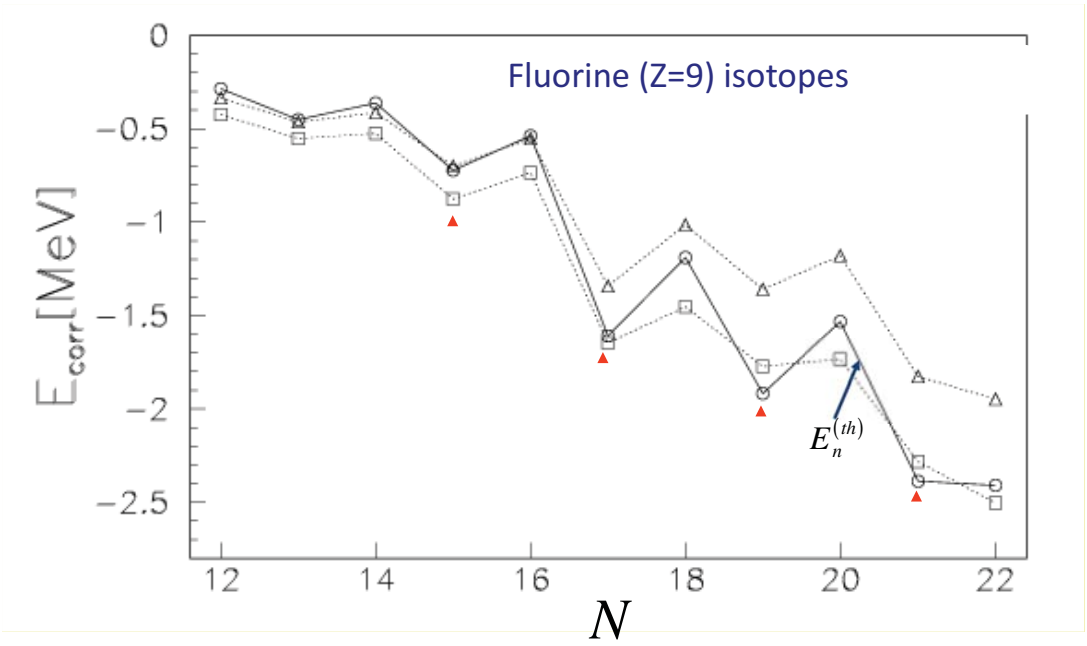

Anti-odd-even staggering of E_{corr}

'Incompatible symmetries' of $H_{Q_0Q_0}$ and $\mathcal{H}_{Q_0Q_0}(E)$: $\begin{cases} [A] \rightarrow [A-1] \otimes [1] \\ \text{[odd-N]} \rightarrow \text{[even-N]} \otimes [1] \end{cases}$

J. Okolowicz, et al., Physics Reports 374, 271 (2003)

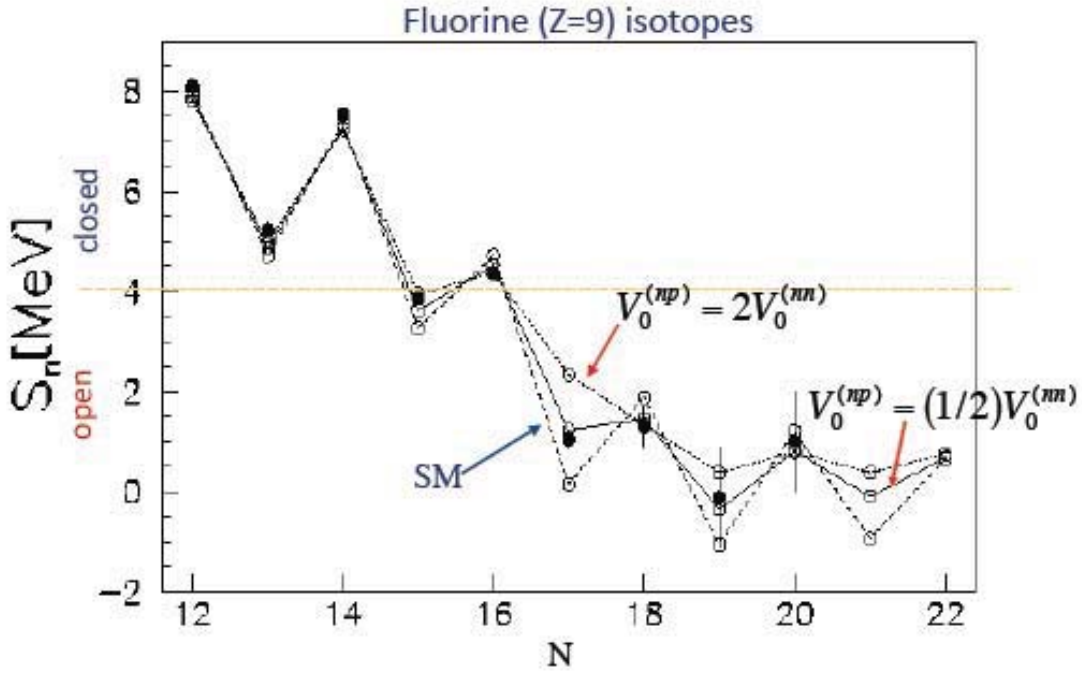

- $\left\langle \Phi^{A-2}_{g.s.} \middle| [a_\nu a_\nu]^{J=0} \middle| \Phi^{A}_{g.s.} \right\rangle$ in SM and SMEC are similar
- Blocking mechanism gradually disappears: $\Delta(N) \rightarrow \text{const}(N)$
- Strong reduction of the np continuum coupling

Y. Luo et al., arXiv:nucl-th/0211068

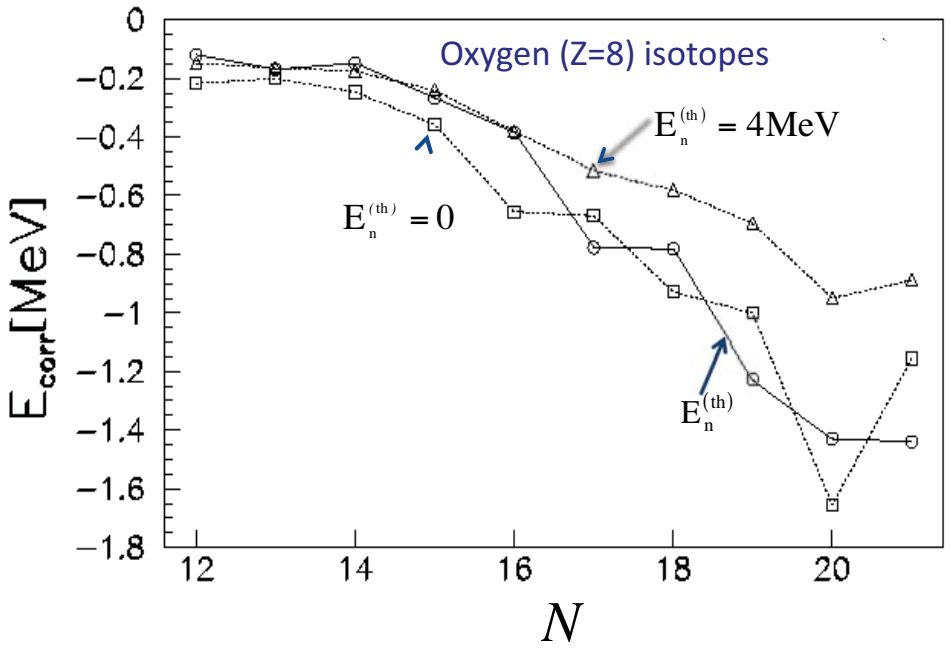

$E_{\text{corr}}(N) \propto \alpha(N)N \approx (\alpha_0 + \beta N)N$ ⟹ effective 3-body interaction

nn-coupling favors $\begin{cases} [A] \to [A-1] \otimes [1] \\ \text{[even-N]} \to \text{[odd-N]} \otimes [1] \end{cases}$

Instability of SM eigenstates at channel threshold?

Continuum coupling correction
to shell model eigenstates

$\blacktriangle \left| E_{\text{corr}}^{(\ell)} \right|$

$\blacktriangleleft \varepsilon \blacktriangleright$

$i_1 \quad 0 \quad i_2$ $\qquad$ $e \blacktriangleright e^{(th)}$

Admixture of many-body continuum states

$\Psi^{(SM)}_{[A-1],\mu} \otimes \varphi^{(c)}_{[1],i} \quad \Psi^{(SM)}_{[A-2],\nu} \otimes \varphi^{(c)}_{[2],j}$ with $E > E_{th}$

Is it a collective phenomenon?
or
a specific coupling of two SM eigenstates?

Exceptional points in the scattering continuum

Bound states (Hermitian problem)

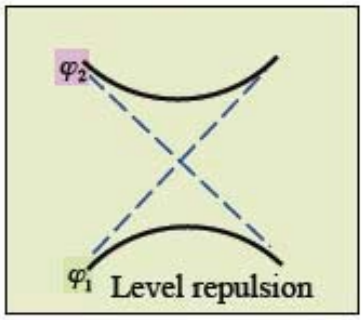

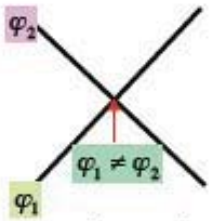

Level crossing

Exceptional points in the scattering continuum

Bound states (Hermitian problem)

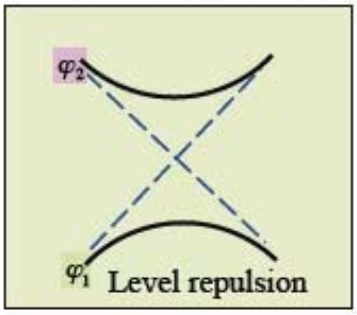

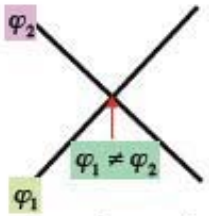

Level crossing

Resonances (non-Hermitian problem)

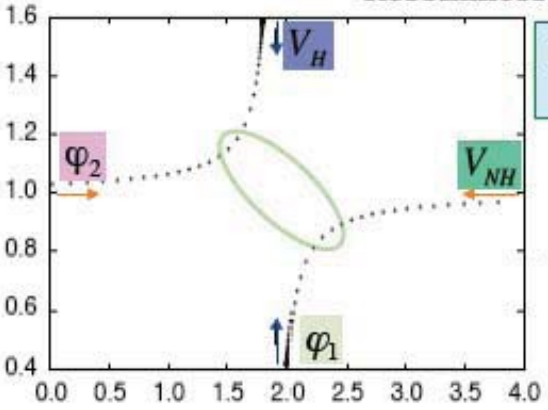

Exceptional point: $\varphi_1 = \varphi_2$, $\varphi_1 = \varphi_1^*$

$\omega = v_{in} + iw_{ex}$

$$\mathscr{H} = \begin{pmatrix} \epsilon_1 & \omega \\ \omega & \epsilon_2 \end{pmatrix} \equiv \begin{pmatrix} e_1 - \frac{i}{2}\gamma_1 & 0 \\ 0 & e_2 - \frac{i}{2}\gamma_2 \end{pmatrix} + \begin{pmatrix} 0 & \omega \\ \omega & 0 \end{pmatrix}$$

M.R. Zimbauer et al., NPA 411, 161 (1983)
J. Okolowicz et al., Phys. Reports 374, 271 (2003)

Example: Continuum Shell Model

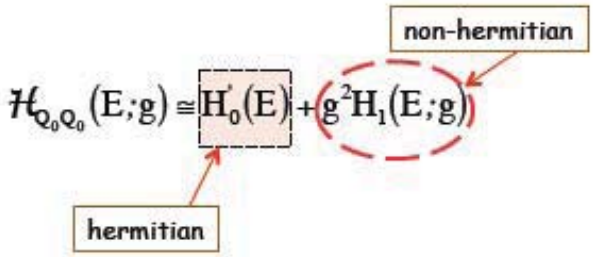

Exceptional point $\varphi_1 = \varphi_2$ $(\varphi_1 = \varphi_1^*)$ is a generic situation in non-hermitian problems

In the N-dim Hilbert space, number of exceptional points is: $n_{EP} \le N(N-1)/2$
At the EP, the dimension of Hilbert space is reduced: N⇒N-1

Example: Continuum Shell Model

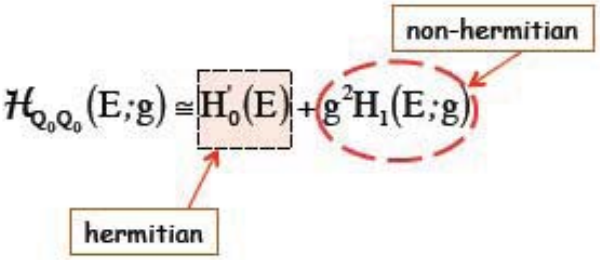

Exceptional point $\varphi_1 = \varphi_2$ $(\varphi_1 = \varphi_1^*)$ is a generic situation in non-hermitian problems

In the N-dim Hilbert space, number of exceptional points is: $n_{EP} \le N(N-1)/2$
At the EP, the dimension of Hilbert space is reduced: N⇒N-1

Avoided crossing of two eigenvalues of the (hermitian) Hamiltonian is caused by a nearby exceptional point of the complex-extended Hamiltonian

The configuration mixing of resonances is characterized by lines $\mathcal{E}_{\alpha_1}(E) = \mathcal{E}_{\alpha_2}(E)$ of coalescing eigenvalues (exceptional threads) of the complex-extended CSM Hamiltonian (complex g).

Experiment: Avoided crossing of resonances

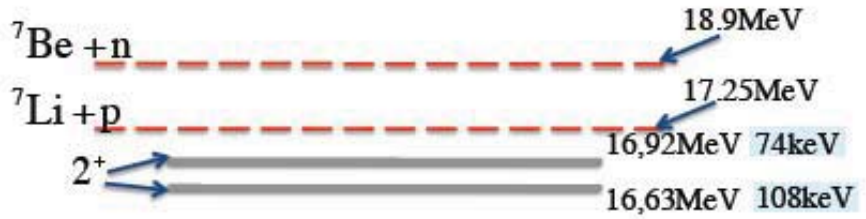

^{8}Be

P. Von Brentano, Phys. Lett. B246,320(1990)
E. Hernandez, A. Mondragon, Phys. Lett. B326,1(1994)
F. Hinterberger et al., Nucl. Phys. A299,397(1978)
J.B. Marion, Phys. Lett. 14,315(1965)
P. Paul, Z. Naturf. 21a,914(1966)

Entanglement of wave functions at the exceptional point

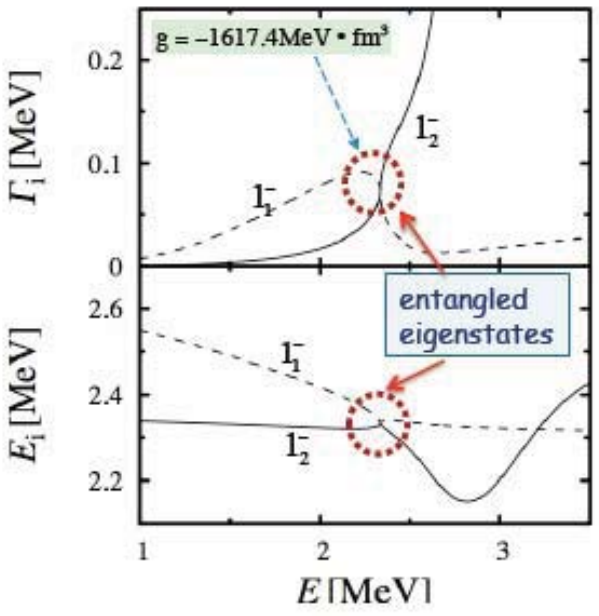

J. Okolowicz, et al, PRC 80, 034619 (2009)

^{16}Ne

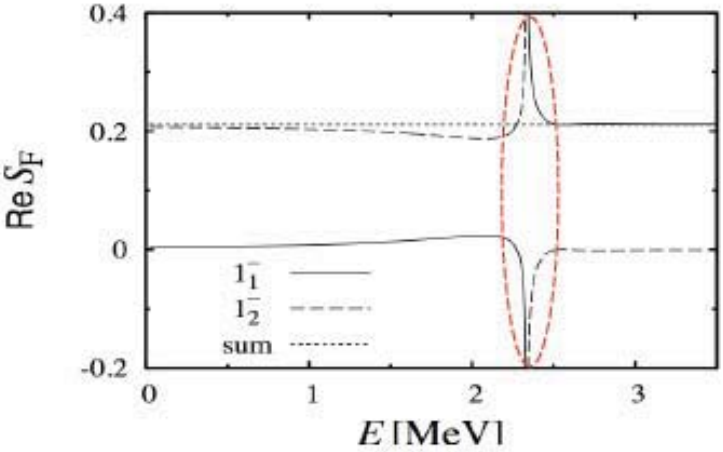

- defect of the vector space: $D_H = N - 1$
- appearance of a topological phase:

$$\Phi_1 \rightarrow i\Phi_2$$
$$\Phi_2 \rightarrow -i\Phi_1$$

Exp.:
C. Dembowski et al., PRL 86 (2001) 787
(microwave cavity)
H. Catarius et al., PRL 99 (2007) 173003
(hydrogen atom in external field)

Experimental signatures of the exceptional point

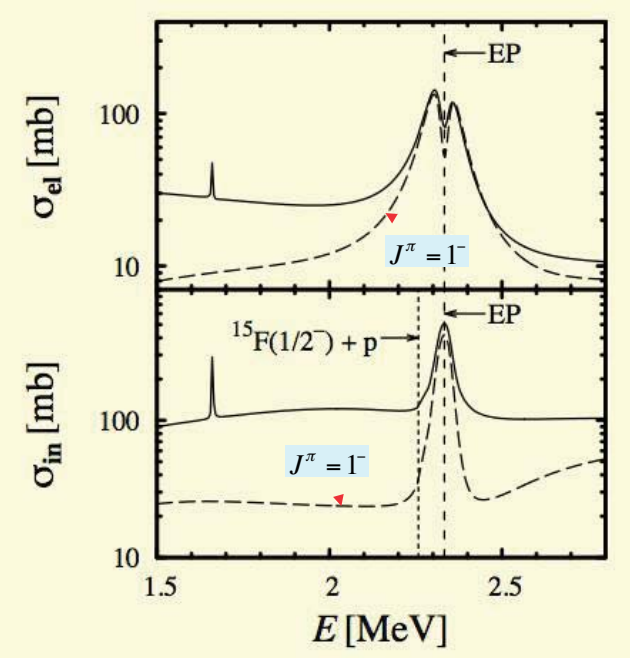

^{16}Ne

J. Okolowicz, et al, PRC 80, 034619 (2009)

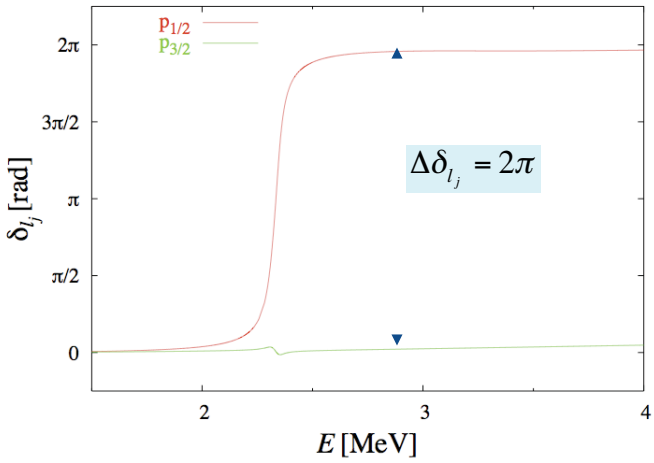

EPs (double-poles of the S-matrix) can appear in the low-energy continuum. Their experimental observation would provide a stringent test of configuration mixing in nuclear open quantum system.

Configuration mixing in the vicinity of the elastic threshold

^{8}He

$J^\pi = 0^+$; 2 levels

$l = 1$ channel :

$\left[{}^7\mathrm{He}\left(3/2^-\right) \oplus \nu p_{3/2}\right]^{0^+}$

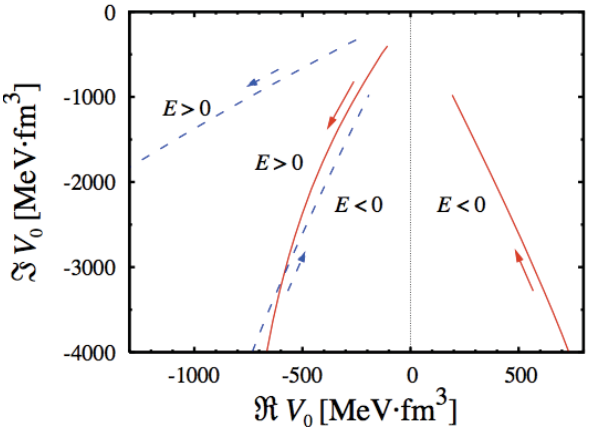

$g \leftrightarrow -g$

For $E < 0 : g \leftrightarrow g^*$

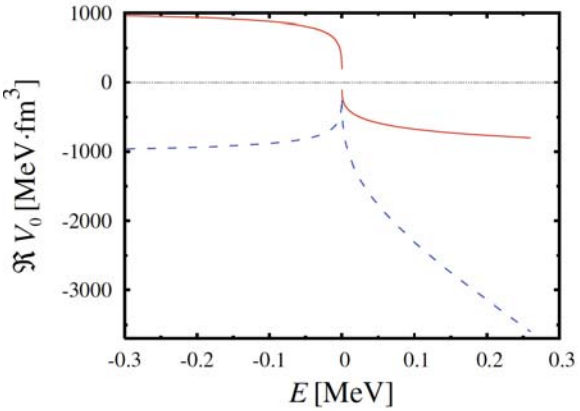

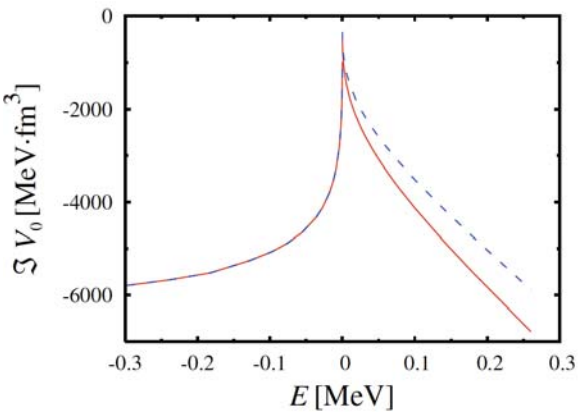

^{8}He

$J^{\pi} = 0^{+}$; 2 levels

$l = 1$ channel :

$\left[{}^{7}\mathrm{He}\left(3/2^{-}\right) \oplus \nu p_{3/2} \right]^{0^{+}}$

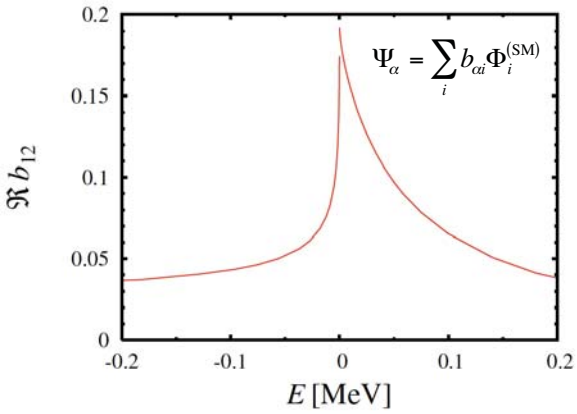

Energies and widths of eigenstates of $\mathcal{H}_{\mathrm{eff}}$

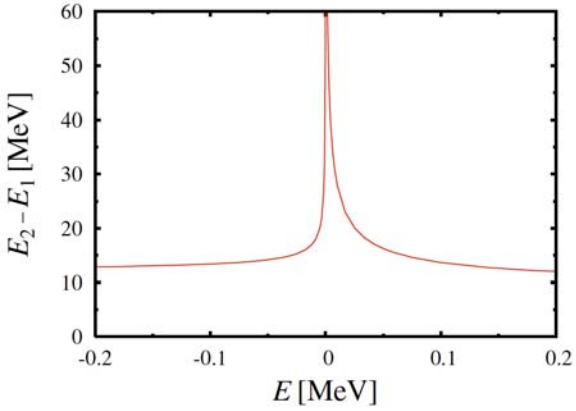

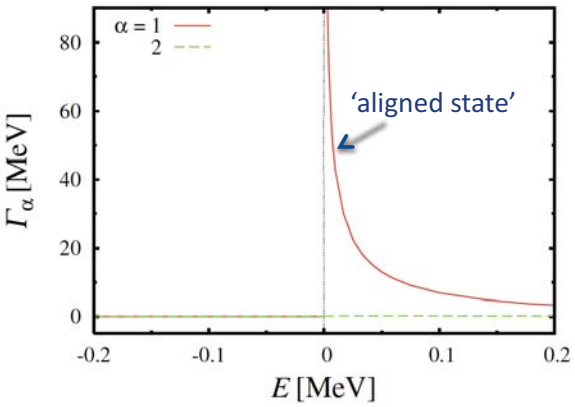

^{16}C

$J^{\pi} = 0^{+}$; 4 levels

$l = 1$ channel :

$\left[{}^{15}\mathrm{C}\left(1/2^{-}\right) \oplus \nu p_{1/2} \right]^{0^{+}}$

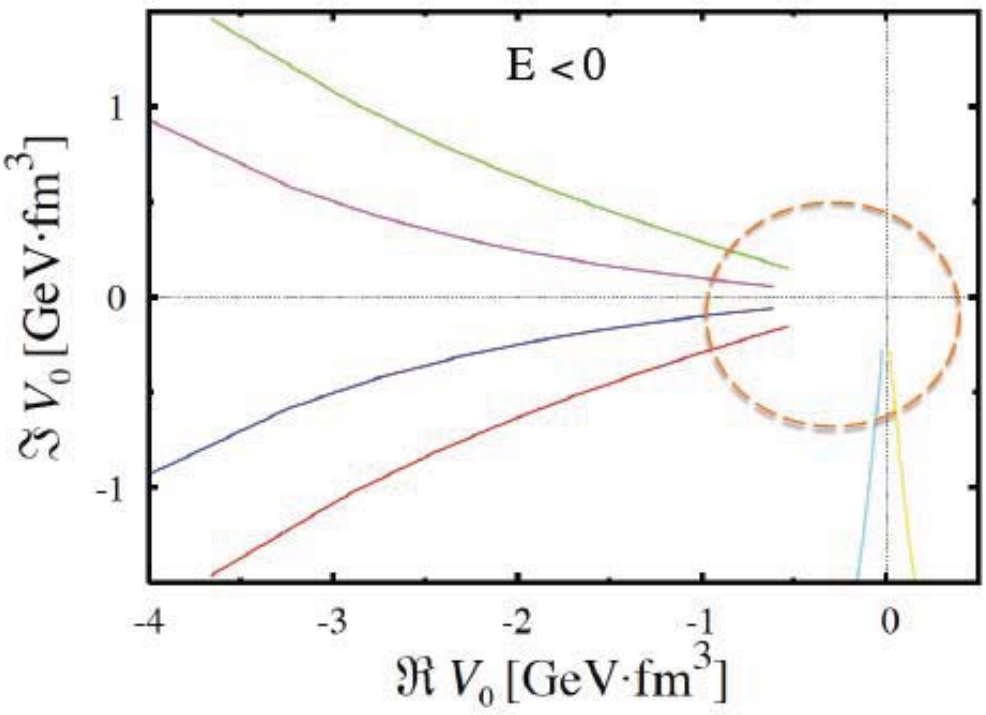

- For a system of n states $\Psi_{\alpha}^{J^{\pi}}$ $(\alpha = 1,\ldots,n)$ coupled to a common decay channel one finds an accumulation of (n-1) exceptional threads
- This collective configuration mixing effect depends strongly on the nature of the decay channel involved

Higher up in the continuum: the segregation of time scales

$J^{\pi}=0^{+}$, $T=0$ states in ^{24}Mg (sd-shell), $Q_0 \leftrightarrow Q_1$ coupling, $\Lambda=10$ channels

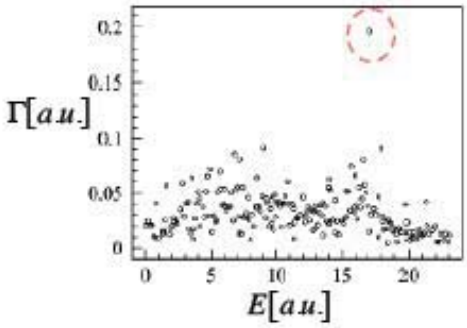

'physical' coupling strength

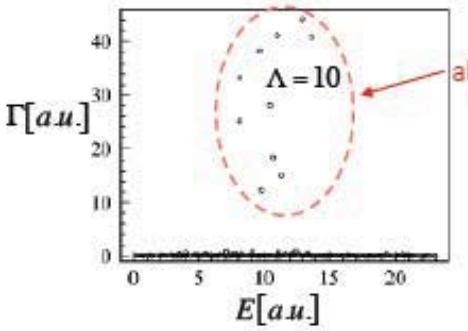

strong coupling limit

'Bound states' in the continuum

Anti-aligned narrow state

closed cavity

opened cavity

‘Superradiant states’ in the continuum

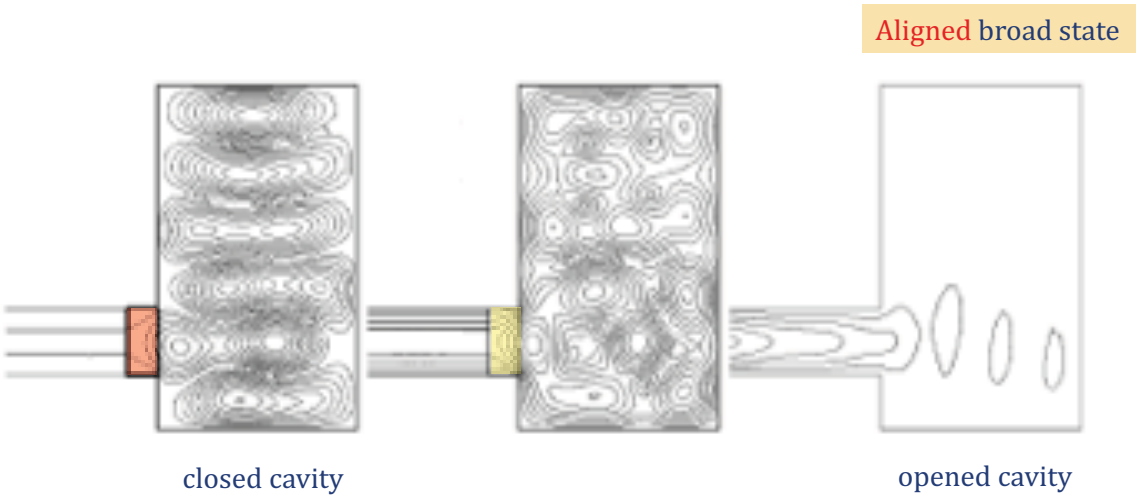

Summary

Coupling of nuclear structure and reaction theory

Tying nuclear structure directly to nuclear reactions within a coherent framework is an important goal. For light nuclei, *ab-initio* methods hold the promise of direct calculation of low-energy scattering processes. In nuclear structure for heavier nuclei, the continuum shell model allows for the consistent treatment of open channels, thus linking the description of bound and unbound nuclear states and direct reactions. On the reaction side, better treatment of nuclear structure aspects is equally crucial. The battleground in this task is the territory of weakly bound nuclei where the structure and reaction aspects are interwoven.

End of Part II

Density functional theory for ground states and excited states in nuclei

P. Ring
Physikdepartment, Technische Universität München, D-85748 Garching, Germany and
State Key Laboratory of Nuclear Physics and Technology, School of Physics,
Peking University, Beijing 100871, People's Republic of China

9. **Broken symmetries and their restoration [12]**

   (a) Projection techniques [36]

   (b) Projection before and after the variation [37]

10. **The Generator Coordinate Method (GCM) and nuclear spectroscopy [12, 38]**

   (a) Shape coexistence [39–41]

   (b) Quantum phase transitions [42]

   (c) Derivation of a collective Hamiltonian [43, 44]

11. **Conclusions and outlook**

References:

---

[1] P. Hohenberg and W. Kohn, Phys. Rev. **136**, B864 (1964).
[2] W. Kohn and L. J. Sham, Phys. Rev. **137**, A1697 (1965).
[3] J. Engel, Phys. Rev. **C75**, 014306 (2007).
[4] B. G. Giraud, Phys. Rev. **C77**, 014311 (2008).
[5] J. D. Walecka, Ann. Phys. (N.Y.) **83**, 491 (1974).
[6] P.-G. Reinhard, Rep. Prog. Phys. **52**, 439 (1989).
[7] P. Ring, Prog. Part. Nucl. Phys. **37**, 193 (1996).
[8] J. Meng, H. Toki, S.-G. Zhou, S.-Q. Zhang, W.-H. Long, and L.-S. Geng, Prog. Part. Nucl. Phys. **57**, 470 (2006).
[9] D. Vretenar, A. V. Afanasjev, G. A. Lalazissis, and P. Ring, Phys. Rep. **409**, 101 (2005).
[10] M. A. L. Marques *et al*, *Time-Dependent Density Functional Theory* (Springer, Heidelberg, 2006).
[11] E. Runge and E. K. U. Gross, Phys. Rev. Lett. **52**, 997 (1984).
[12] P. Ring and P. Schuck, *The Nuclear Many-Body Problem* (Springer-Verlag, Berlin, 1980).
[13] P. Ring, Z.-Y. Ma, N. Van Giai, D. Vretenar, A. Wandelt, and L.-G. Cao, Nucl. Phys. **A694**, 249 (2001).
[14] J. Boguta and A. R. Bodmer, Nucl. Phys. **A292**, 413 (1977).
[15] G. A. Lalazissis, J. König, and P. Ring, Phys. Rev. **C55**, 540 (1997).
[16] G. A. Lalazissis, T. Nikšić, D. Vretenar, and P. Ring, Phys. Rev. **C71**, 024312 (2005).
[17] P. W. Zhao, Z. P. Li, J. M. Yao, and J. Meng, Phys. Rev. **C82**, 054319 (2010).
[18] T. Nikšić, D. Vretenar, and P. Ring, Phys. Rev. **C78**, 034318 (2008).
[19] J. E. Drut, R. J. Furnstahl, and L. Platter, Progr. Part. Nucl. Phys. **??**, in print (2009).
[20] Y. K. Gambhir, P. Ring, and A. Thimet, Ann. Phys. (N.Y.) **198**, 132 (1990).
[21] J. Meng and P. Ring, Phys. Rev. Lett. **77**, 3963 (1996).
[22] J. Meng, Nucl. Phys. **A635**, 3 (1998).
[23] G. A. Lalazissis, D. Vretenar, and P. Ring, Phys. Rev. **C69**, 017301 (2004).
[24] A. Sobiczewski and K. Pomorski, Prog. Part. Nucl. Phys. **58**, 292 (2007).
[25] H. Abusara, A. V. Afanasjev, and P. Ring, Phys. Rev. **C82**, 044303 (2010).
[26] W. Koepf and P. Ring, Nucl. Phys. **A493**, 61 (1989).
[27] A. V. Afanasjev, J. König, and P. Ring, Phys. Rev. **C60**, 051303(R) (1999).
[28] J. Peng, J. Meng, P. Ring, and S. Q. Zhang, Phys. Rev. **C78**, 024313 (2008).
[29] N. Paar, P. Ring, T. Nikšić, and D. Vretenar, Phys. Rev. **C67**, 034312 (2003).
[30] N. Paar, T. Nikšić, D. Vretenar, and P. Ring, Phys. Rev. **C69**, 054303 (2004).
[31] N. Paar, D. Vretenar, E. Khan, and G. Coló, Rep. Prog. Phys. **70**, 691 (2007).
[32] J. Daoutidis and P. Ring, Phys. Rev. **C80**, 024309 (2009).
[33] P. Ring and E. Litvinova, Phys. At. Nuclei **72**, 1285 (2007), translated from Yadernaya Fisika **72** (2009) No. 8, 1.
[34] E. Litvinova and P. Ring, Phys. Rev. **C73**, 044328 (2006).
[35] E. Litvinova, P. Ring, and V. I. Tselyaev, Phys. Rev. **C75**, 064308 (2007).
[36] J.-M. Yao, J. Meng, P. Ring, and D. Peña Arteaga, Phys. Rev. **C79**, 044312 (2009).
[37] J. A. Sheikh and P. Ring, Nucl. Phys. **A665**, 71 (2000).
[38] D. L. Hill and J. A. Wheeler, Phys. Rev. **89**, 1102 (1953).
[39] T. Nikšić, D. Vretenar, and P. Ring, Phys. Rev. **C73**, 034308 (2006).
[40] T. Nikšić, D. Vretenar, and P. Ring, Phys. Rev. **C74**, 064309 (2006).
[41] J. M. Yao, H. Mei, H. Chen, J. Meng, P. Ring, and D. Vretenar, Phys. Rev. **C83**, 014308 (2011).
[42] T. Nikšić, D. Vretenar, G. A. Lalazissis, and P. Ring, Phys. Rev. Lett. **99**, 092502 (2007).
[43] T. Nikšić, Z. P. Li, D. Vretenar, L. Próchniak, J. Meng, and P. Ring, Phys. Rev. **C79**, 034303 (2009).
[44] T. Nikšić, D. Vretenar, and P. Ring, Prog. Part. Nucl. Phys. **66**, 519 (2011).

Density Functional Theory for ground states and excited states in nuclei.

Beijing, Aug. 27/29, 2011

Peter Ring

Technical University Munich
Peking University

TECHNISCHE UNIVERSITÄT MÜNCHEN

Motivation:

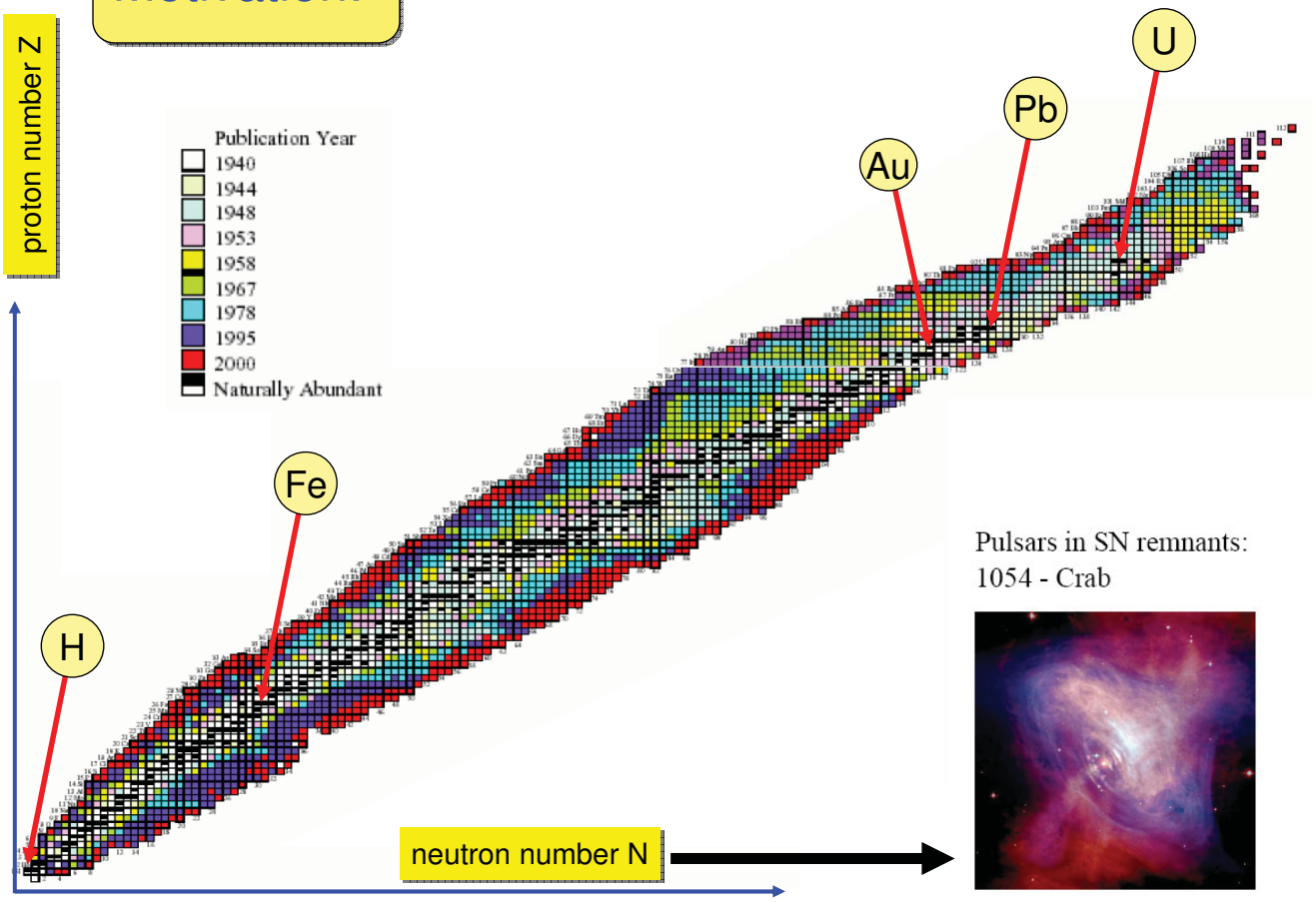

What data does astrophysics need ?

- nuclear masses (bindung energies – Q-values): 100 keV
- equation of state (EOS) of nuclear matter: $E(\rho)$
- isospin dependence $E(\rho_p, \rho_n)$
- nuclear matrix elements (life times of β-decay ..)
- cross section for neutron or electron capture ….
- fission probabilities
- cross sections for neutrino reactions
- …..
- …..

ab-initio: 3 scales

- **QCD:** non-linear gauge theory, **quarks, gluons**
- confinement
- running coupling constant
- at low energies **non-perturbative**
- effective degrees of freedom: nucleon, pion

> 1 GeV

- effective Lagrangian in **nucleons and pions**
- parameters (LEC) so far phenomenological
- non renormalizable
- at low momenta: **chiral perturbation theory: χPT**
- → bare nucleon-nucleon interaction: NNNL **N3LO**

~ 200 MeV

- effective forces within the nucleus
- density dependent
- configuration mixing, **density functional theory**

~ 100 keV

The bare nucleon-nucleon interaction:

distance > 1 fm: attractive

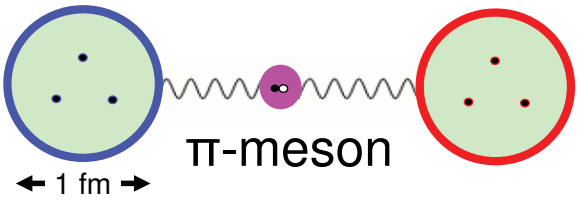

distance < 0.8 fm: repulsive

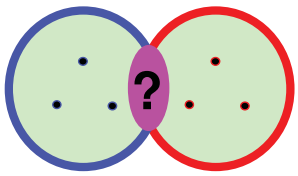

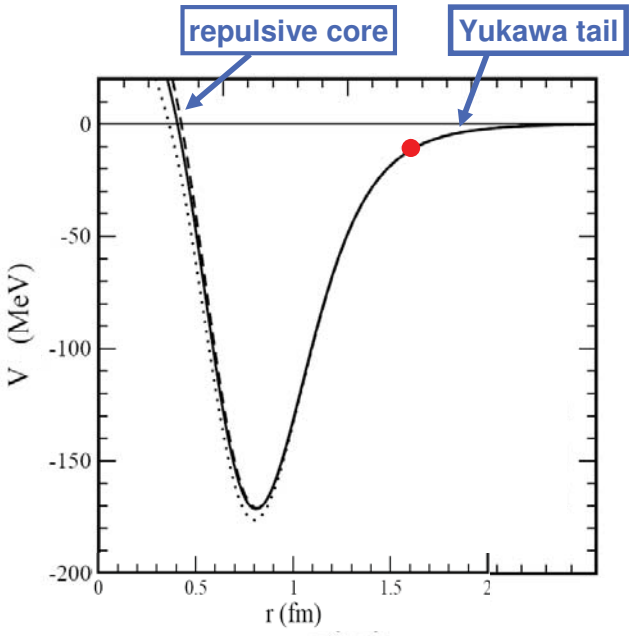

Three-body forces

What is special in nuclei?

- size: nuclei are very small objects: Uncertainty relation

$$\Delta x^2 \Delta p^2 \geq \frac{\hbar^2}{4} \qquad E_{kin} \geq 10 \frac{\mathrm{fm}^2}{r^2}\ \mathrm{MeV} = 10^{-5} \frac{\mathrm{nm}^2}{r^2}\ \mathrm{eV}$$

- degrees of freedom: spin and isospin: 4^A possibities
- very complicated interaction: strongly repulsive
  tensor forces
  3-body forces
- many particles: Pauli principle:
  effective interaction inside the nucleus is quenched (Brueckner)
- required accuracy (for masses):
  100 keV / 1000 MeV ≈ 10^{-4}

Content:

- Motivation
- Density Functional Theory
- The Nuclear Density Functional
- Covariant Density Functionals
- Ground state properties
- Nuclear dynamics and excitations
- Beyond mean field
- Outlook

Hohenberg-Kohn theorem (1964):


Hohenberg


Kohn

The exact energy of a quantum mechanical many body system is a functional of the local density $\rho(\mathbf{r})$

$$E[\rho] = \langle \Psi | H | \Psi \rangle$$

This functional is universal. It does not depend on the system, only on the interaction.

One obtains the exact density $\rho(\mathbf{r})$ by a variation of the functional with respect to the density

note:

$\rho(\mathbf{r})$ is a function of 3 variables.

$\Psi(\mathbf{r}_1 \ldots \mathbf{r}_N)$ is a function of $3N$ variables.

Many-body system in an external field U(r):

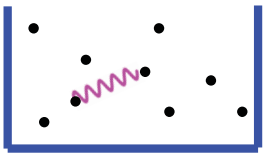

We consider a realistic many-body system in an external field U(r) and a two- (or three-) body interaction $V(r_i,r_k)$. The total energy E_{tot} of the system depends on U(r): It is a functional of U(r):

$$E_{\rm tot} = \langle \hat{T}+\hat{V}+\hat{U} \rangle = \langle \hat{T}+\hat{V} \rangle + \int \rho(\mathbf{r}) U(\mathbf{r}) d^3r = E_{\rm tot}[U(\mathbf{r})]$$

in the same way we obtain the density: $\rho(\mathbf{r}) = \rho[U(\mathbf{r})]$

Inverting this relation we can introduce a Legendre transformation replacing the independent function U(r) by the density ρ(r):

$$\rho = \rho[U] \quad \Rightarrow \quad U = U[\rho]$$

Legendre transformations in thermodynamics:

Free energy: $F(T,V)$ depends on the volume

$$dF = -SdT - PdV \qquad \text{Pressure:} \qquad P(V) = -\frac{\partial F}{\partial V}$$

Inversion: $V = V(P)$

Gibbs energy: $G(T,P) = F(T,V(P)) + PV(P)$

$$F(T,V) \Rightarrow G(T,P)$$

$$dG = -SdT + VdP \qquad \text{Volume} \qquad V(P) = \frac{\partial G}{\partial P}$$

In many-body systems:

$$V \Rightarrow -U(\mathbf{r}), \qquad F(V) \Rightarrow E_{\rm tot}[U]$$

$$P \Rightarrow \rho(\mathbf{r}), \qquad G(P) \Rightarrow E_{\rm HK}[\rho] = E_{\rm tot} - \int \rho U d^3r$$

Many-body system in an external field U(r):

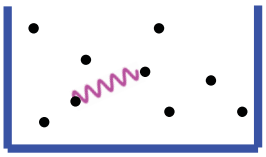

We consider a realistic many-body system in an external field U(r) and a two- (or three-) body interaction $V(r_i,r_k)$. The total energy E_{tot} of the system depends on U(r): It is a functional of U(r):

$$E_{\text{tot}} = \langle \hat{T}+\hat{V}+\hat{U} \rangle = \langle \hat{T}+\hat{V} \rangle + \int \rho(\mathbf{r}) U(\mathbf{r}) d^3r = E_{\text{tot}}[U(\mathbf{r})]$$

in the same way we obtain the density: $\rho = \rho[U]$

Inverting this relation we can introduce a Legendre transformation replacing the independent function U(r) by the density ρ(r): $U = U[\rho]$

$$E_{\text{tot}}[U] \Rightarrow E_{\text{HK}}[\rho]$$

F(V) → G(P) = F + PV

$$E_{\text{HK}}[\rho] = E_{\text{tot}}[U] - \int \rho(\mathbf{r}) U(\mathbf{r}) d^3r$$

$$= \langle \hat{T} + \hat{V} + \hat{U} \rangle - \langle \hat{U} \rangle = \langle \hat{T} + \hat{V} \rangle = E$$

Decomposition of the HK-functional:

In practical applications the functional $E_{HK}[\rho]$ is decomposed into three parts:

$$E_{HK}[\rho] = E_{ni}[\rho] + E_H[\rho] + E_{xc}[\rho]$$

The Hartree term is simple: $E_H[\rho] = \frac{1}{2} \int \rho(\mathbf{r}) V(\mathbf{r},\mathbf{r}') \rho(\mathbf{r}') d^3r d^3r'$

The non interacting part: $E_{ni}[\rho] = E_{HK}[\rho]_{V=0}$

The exchange-correlation part is the rest: $E_{xc}[\rho] = E_{HK}[\rho] - E_{ni}[\rho] - E_H[\rho]$

E_{xc} is less important and often approximated, but for modern calculations it plays an essential rule.

Thomas Fermi approximation:

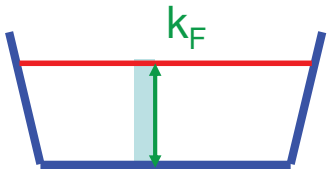

Thomas and Fermi used the local density approximation (LDA) to get an analytical expression for the non-interacting term. They start with the constant density of a homogeneous system

$$\varphi_i(\mathbf{r}) = \frac{1}{(2\pi)^{3/2}} e^{i\mathbf{kr}}, \qquad \rho(\mathbf{r}) = \sum_i^A |\varphi_i(\mathbf{r})|^2$$

$$\sum_i^A .. \rightarrow \gamma \int_{|k|<k_F} .. \, d^3k, \qquad \rho = \frac{\gamma}{(2\pi)^3} \frac{4\pi}{3} k_F^3$$

where γ is the spin/isospin degeneracy, i.e. $k_F \approx \rho^{1/3}$

Thomas Fermi approximation:

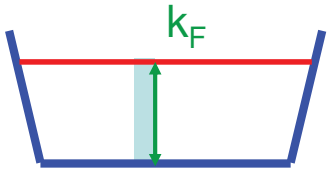

Thomas and Fermi used the local density approximation (LDA) to get an analytical expression for the non-interacting term. They calculated the kinetic energy density of a homogeneous system with constant density ρ

$$\frac{E}{V} = \gamma \int_{k<k_F} \frac{(\hbar k)^2}{2m} d^3k = \frac{\hbar^2}{2m} \frac{3}{5} \left(\frac{6\pi^2}{\gamma}\right)^{\frac{2}{3}} \rho^{\frac{5}{3}}$$

where γ is the spin/isospin degeneracy. One finds:

$$E_{ni}^{(TF)}[\rho] = \frac{\hbar^2}{2m} \frac{3}{5} \left(\frac{6\pi^2}{\gamma}\right)^{\frac{2}{3}} \int \rho^{\frac{5}{3}}(r) d^3r$$

This is not very good (molecules are never bound) and therefore one added later on gradient terms containing ∇ρ and Δρ. This method is called Extended Thomas Fermi (ETF) theory. However, these are all asymptotic expansions and one always ends up with semi-classical approximations. Shell effects are never included.

Example for Thomas Fermi approximation:

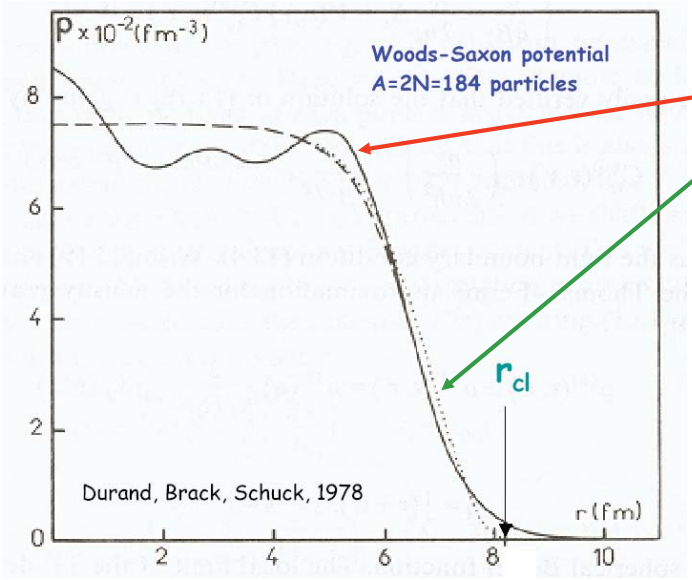

Kohn-Sham theory:

In order to reproduce shell structure Kohn and Sham introduced a auxiliary single particle potential $V_{\text{eff}}(r)$, which is defined by the condition, that after the solution of the single particle eigenvalue problem

$$\left\{-\frac{\hbar^2}{2m}\Delta + V_{\text{eff}}(\mathbf{r})\right\}\varphi_i(\mathbf{r}) = \varepsilon_i\varphi_i(\mathbf{r})$$

the density obtained as $\sum_{i=1}^{A}|\varphi_i(\mathbf{r})|^2 = \rho(\mathbf{r})$ is the exact density

Obviously to each density $\rho(r)$ there exist such a potential $V_{\text{eff}}(r)$.

We define the non interacting part of the energy functional as:

$$E_{\text{ni}}[\rho] = \int \frac{\hbar^2}{2m}\tau(\mathbf{r})d^3r = \int \frac{\hbar^2}{2m}\sum_{i=1}^{A}|\nabla\varphi_i(\mathbf{r})|^2 d^3r = \sum_{i=1}^{A}\varepsilon_i - \int V_{\text{eff}}(\mathbf{r})\rho(\mathbf{r})d^3r$$

and obviously we have:

$$V_{\text{eff}}(\mathbf{r}) = -\frac{\delta}{\delta\rho}E_{\text{ni}}[\rho] = -\frac{\delta}{\delta\rho}\left(E_{\text{HK}} - E_{\text{H}} - E_{\text{xc}}\right)$$

Determinaton of $V_{eff}(r)$:

In principle we can find $V_{eff}(r)$ by calculating the functional derivatives:

$$V_{\text{eff}}(\mathbf{r}) = -\frac{\delta}{\delta\rho}E_{\text{HK}} + \frac{\delta}{\delta\rho}E_{\text{H}} + \frac{\delta}{\delta\rho}E_{\text{xc}}$$

$$V_{\text{eff}}(\mathbf{r}) = U(\mathbf{r}) + V_H(\mathbf{r}) + V_{\text{xc}}(\mathbf{r})$$

with the Hartree potential: $V_H(\mathbf{r}) = \int V(\mathbf{r},\mathbf{r}')\rho(\mathbf{r}')d^3r$

and the exchange-correlation potential: $V_{\text{xc}}(\mathbf{r}) = \frac{\delta}{\delta\rho}E_{\text{xc}}$

of course it all depends on the knowledge or on the approximation of the functional for the exchange-correlation energy

Kohn-Sham functional:

$$E_{\text{KS}}[\rho,\tau] = \int \frac{\hbar^2}{2m}\tau(\mathbf{r})d^3r + E_{\text{H}}[\rho] + E_{\text{xc}}[\rho]$$

Practical applications:

The Kohn-Sham scheme involves the following steps

a) determine a good approximation for the functional $E_{XC}[\rho]$

b) start with some initial guess for ρ_0

c) calculate from this ρ_0 the potentials $V_H(r)$ and $V_{xc}(r)$ and $V_{eff}(r)$

d) solve the single particle Schrödinger equation for $V_{eff}(r)$ and obtain the wave functions $\phi_i(r)$

e) use these single particle wave functions to calculate the density $\rho_1(r)$ in the next step of the iteration

f) repeat this cycle until convergence is achieved:

$$E[\rho] \Rightarrow \boxed{\hat{h} = \frac{\delta E}{\delta\rho}} \Rightarrow \boxed{\hat{h}\varphi_i = \varepsilon_i\varphi_i} \Rightarrow \boxed{\rho = \sum_{i=1}^{A}|\varphi_i|^2}$$

Caveat:

The Kohn Sham potential has to be understood as

$$\hat{h} = \frac{\delta E}{\delta \hat{\rho}} = -\frac{\hbar^2}{2m}\Delta + \frac{\delta E_{\mathrm{H}}}{\delta \hat{\rho}} + \frac{\delta E_{\mathrm{xc}}}{\delta \hat{\rho}} + U$$

where the kinetic term is non-local

$$h(\mathbf{r},\mathbf{r}') = T(\mathbf{r},\mathbf{r}') + \delta(\mathbf{r}-\mathbf{r}')V_{\mathrm{eff}}(\mathbf{r})$$

and $$T(\mathbf{r}.\mathbf{r}') = \frac{\delta E_{\mathrm{ni}}}{\delta \rho(\mathbf{r}',\mathbf{r})} = \frac{\hbar^2}{2m}\overrightarrow{\nabla}\delta(\mathbf{r}-\mathbf{r}')\overleftarrow{\nabla}'$$

Here the non-local density matrix: $$\rho(\mathbf{r},\mathbf{r}') = \sum_i \varphi_i(\mathbf{r})\varphi_i^*(\mathbf{r}')$$

is not exact ($\rho^2=\rho$). Only its diagonal term is exact!

Remarks to the Kohn-Sham method:

We have the following remarks to the Kohn-Sham method

1) The method is exact under the condition that $V_{xc}[\rho]$ is known.
2) The single particle wave functions $\phi_i(r)$ and the single particle energies ε_i are only auxiliary quantities. They have nothing to do with experiment. We only obtain the exact total energy and the exact density, i.e. quantities accessible by the density $\rho(r)$.
3) The method works rather well even for shell structures

Methods to get a good approximation for the functional $E_{XC}[\rho]$:

1) phenomenological formulas with parameters determined by fits.
2) Monte-Carlo techniques allow to calculate $E_{xc}[\rho]$ for a homogeneous electron gas. In the inhomogeneous system the LDA is used.
3) there exist many more sophisticated techniques nowadays
4) In Coulomb-Systems one has now the exact functional (Perdue)

An example: The binding energy of the Ar-atom is reproduced
by Thomas Fermi method with an accuracy of 20 %,
by Kohn-Sham method with LDA approximation of 0.5 %.

DFT: density of the Ar-atom:

N.Argaman, G. Makov,
Am. J. Phys. 68, 69 (2000)

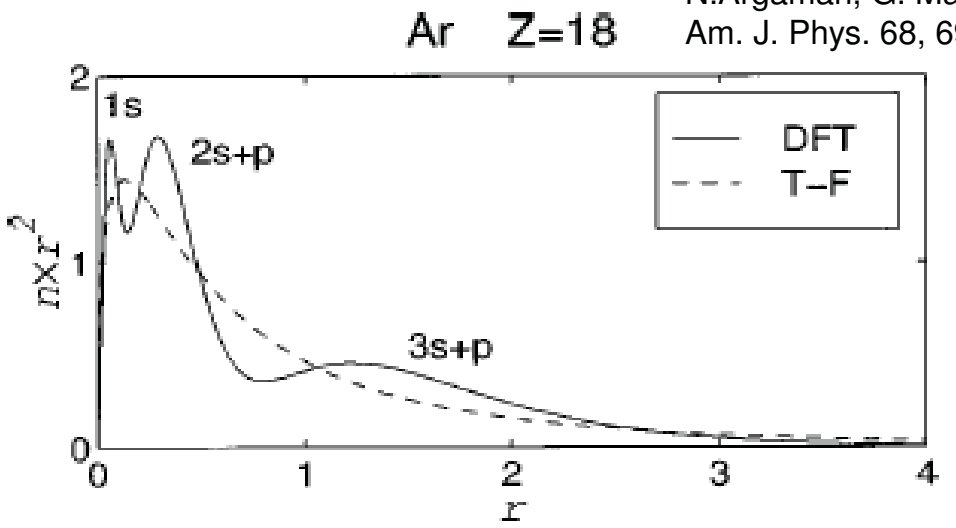

units: radius: Bohr radii
densities x r^2 in inverse Bohr radii

Limitations of exact density functionals:

	formally exact	in practice
Hohenberg-Kohn:	$E[\rho(\mathbf{r})]$	no shell effects
Kohn-Sham:	$E[\rho(\mathbf{r}),\tau(\mathbf{r})]$	no l·s,
Skyrme:	$E[\rho(\mathbf{r}),\tau(\mathbf{r}),J(\mathbf{r})]$	no pairing
Gogny:	$E[\rho(\mathbf{r}),\tau(\mathbf{r}),J(\mathbf{r}),\kappa(\mathbf{r})]$	no config.mixing

generalized mean field: **no configuration mixing, no two-body correlations**

local density: $\rho(\mathbf{r}) = \langle a^\dagger(\mathbf{r})a(\mathbf{r})\rangle = \sum_i^A |\varphi_i(\mathbf{r})\rangle\langle\varphi_i(\mathbf{r})|$

kinetic energy density: $\tau(\mathbf{r}) = \sum_i^A |\nabla\varphi_i(\mathbf{r})\rangle\langle\nabla\varphi_i(\mathbf{r})|$

pairing density: $\kappa(\mathbf{r}) = \langle a^\dagger(\mathbf{r},s)a^\dagger(\mathbf{r},-s)\rangle$

twobody density: $\rho(\mathbf{r},\mathbf{r}') = \langle a^\dagger(\mathbf{r})a(\mathbf{r})a^\dagger(\mathbf{r}')a(\mathbf{r}')\rangle$

Content:

- Motivation
- Density Functional Theory
- The Nuclear Density Functional
- Covariant Density Functionals
- Ground state properties
- Nuclear dynamics and excitations
- Beyond mean field
- Outlook

Density functional theory in nuclei

- In nuclei DFT has been introduced by **effective Hamiltonians**: by Vautherin and Brink (1972)

$$E = \langle\Psi|H|\Psi\rangle \approx \langle\Phi|\hat{H}_{eff}(\hat{\rho})|\Phi\rangle \stackrel{?}{=} E[\hat{\rho}]$$

Skyrme
Gogny
Rel. MF

- Nuclei are **self-bound systems**.
  The exact density is a constant. ρ(r) = const
  Hohenberg-Kohn theorem is true, but useless
  ρ(r) has to be replaced by the intrinsic density:

$$\rho_I(\vec{r}) = \rho(\vec{r} + \vec{R}_{CM}) \quad \text{with} \quad \vec{R}_{CM} = \frac{1}{A}\sum_i \vec{r}_i$$

- Density functional theory in nuclei is probably **not exact**, but it is a very good approximation.

Density functional theory in nuclei

- **Symmetry breaking** is important: Janus

Advantage:
Correlations can be
taken into account
in simple wave functions

Problems:
no good quantum numbers
no spectroscopy
projection required

translational,	rotational,	gauge symmetry,	…….
momentum P	spin J	particle number N	

- More degrees of freedom: **spin, isospin, relativistic, pairing**
- nuclei are **relativistic systems** !
- at present all successful functionals are **phenomenological**

General properties of nuclear density functionals

- At present the nuclear energy functionals are **phenomenological** and not connected to any NN- or NNN-interaction.
- There is a large **spin-orbit term**
- The functionals are expressed in terms of **powers** and **gradients** of the ground state density and of currents using the principles of **symmetry** and **simplicity**
- **Relativistic functionals** (Covariant DFT) include the spin orbit automatically. Therefore they have considerable less parameters
- For zero range forces **Fock terms** can be absorbed in the parameters
- The remaining parameters are adjusted to characteristic properties of **nuclear matter** and **finite nuclei** and in future (more and more) to **ab initio** results

Virtues of the mean field descprition:

- the intuitive interpretation of mean fields results in terms of **intrinsic shapes** and of shells with **single particle states**

- the **full model space** is used: no distinction between core and valence nucleons, **no need for effective charges**

- the functional is **universal**: it can be applied to all nuclei throughout the periodic chart, light and heavy, spherical and deformed

3 types of functionals are presently used:

- **non-relativistic zero range forces (Skyrme)**
- **non-relativistic finite range forces of Gaussian shape (Gogny)**
- **relativistic density functionals (RMF)**

Non-relativistic density functional theory in nuclei:

The building blocks of the nuclear energy density functional are various densities and currents:

For $x = (\mathbf{r}, \sigma, \tau)$ we have the density matrix:

$$\rho(x, x') = \sum_{i}^{A} |\varphi_i(x)\rangle\langle\varphi_i(x')|$$

$$= \frac{1}{4}\{ \quad \rho_{00}(x, x') + \rho_{0i}(x, x')\sigma_i \qquad \text{isoscalar}$$

$$+ (\rho_{q0}(x, x') + \rho_{qi}(x, x')\sigma_i)\tau_q \quad \} \qquad \text{isovector}$$

Local quantities:

$$\rho_0(\mathbf{r}) = \rho_{00}(\mathbf{r},\mathbf{r}) = \sum_{st} \rho(\mathbf{r}st,\mathbf{r}st)$$ isoscalar density: $\rho_0 = \rho_n + \rho_p$

$$\rho_1(\mathbf{r}) = \rho_{30}(\mathbf{r},\mathbf{r}) = \sum_{st} \rho(\mathbf{r}st,\mathbf{r}st)\tau_{tt}^{(3}$$ isovector density: $\rho_0 = \rho_n - \rho_p$

$$\mathbf{s}_0(\mathbf{r}) = \sum_{ss't} \rho(\mathbf{r}st,\mathbf{r}s't)\sigma_{ss'}$$ isoscalar spin density

$$\mathbf{s}_1(\mathbf{r}) = \sum_{ss't} \rho(\mathbf{r}st,\mathbf{r}s't)\sigma_{ss'}\tau_{tt}^{(3)}$$ isovector spin density

$$\mathbf{j}_T(\mathbf{r}) = \frac{i}{2}(\nabla' - \nabla)\rho_T(\mathbf{r},\mathbf{r}')|_{\mathbf{r}=\mathbf{r}'}$$ current density T=0,1

$$\mathbf{J}_T(\mathbf{r}) = \frac{i}{2}(\nabla' - \nabla) \times \mathbf{s}_T(\mathbf{r},\mathbf{r}')|_{\mathbf{r}=\mathbf{r}'}$$ spin current density

$$\tau_T(\mathbf{r}) = (\nabla \cdot \nabla')\rho_T(\mathbf{r},\mathbf{r}')|_{\mathbf{r}=\mathbf{r}'}$$ kinetic energy density

$$\mathbf{T}_T(\mathbf{r}) = (\nabla \cdot \nabla')\mathbf{s}_T(\mathbf{r},\mathbf{r}')|_{\mathbf{r}=\mathbf{r}'}$$ kinetic spin density

The Skyrme functional can be derived from a density dependent two-body force:

$$V_{Sk}(1,2) = t_0\left(1 + x_0\hat{P}_\sigma\right)\delta(\vec{r}_{12})$$
$$+ \frac{1}{2}t_1\left(1 + x_1\hat{P}_\sigma\right)\left[\hat{k}^{+2}\delta(\vec{r}_{12}) + \delta(\vec{r}_{12})\hat{k}^2\right]$$
$$+ \frac{1}{2}t_2\left(1 + x_2\hat{P}_\sigma\right)\left[\hat{k}^{+}\delta(\vec{r}_{12})\hat{k}\right]$$

zero-range limit of a finite-range force up to second order in derivatives (finite range = momentum dependence!)

$$+ iW_0(\vec{\sigma}_1 + \vec{\sigma}_2)\cdot\hat{k}^{+} \times \delta(\vec{r}_{12})\hat{k}$$

two-body spin-orbit

$$+ \frac{1}{6}t_3\left(1 + x_3\hat{P}_\sigma\right)\delta(\vec{r}_{12})\rho^{\alpha}\left(\frac{\vec{r}_1 + \vec{r}_2}{2}\right)$$

density dependent term (3-body,...)

$$\hat{P}_\sigma = \frac{1}{2}(1 + \vec{\sigma}_1\cdot\vec{\sigma}_2),\ \hat{k} = \frac{1}{2i}\left(\vec{\nabla}_1 - \vec{\nabla}_2\right)$$

Energy functional: $$E_{tot} = \int \mathcal{H}\ (\vec{r})\ d^3r$$

Content:

- Motivation
- Density Functional Theory
- The Nuclear Density Functional
- Covariant Density Functionals
- Ground state properties
- Nuclear dynamics and excitations
- Beyond mean field
- Outlook

Relativistic densities

In the relativistic treatment, one has to deal with four-component Dirac spinor wave functions. Consequently, there are 16 independent bilinear covariants:

$$\bar{\psi}(\mathbf{r})\Gamma\psi(\mathbf{r})$$

This gives the following local densities:

$\Gamma^s = 1$	scalar density
$\Gamma^v_\mu = \gamma_\mu$	vector density
$\Gamma^t_{\mu\nu} = (i/2)\left(\gamma_\mu\gamma_\nu - \gamma_\nu\gamma_\mu\right)$	tensor density
$\Gamma^p = \gamma_5$	pseudoscalar density
$\Gamma^a_\mu = \gamma_\mu\gamma_5$	axial density

(which have isoscalar and isovector components.) In most applications, only three densities are required:

$\bar{\psi}\psi$ (σ) $\quad \bar{\psi}\gamma^\mu\psi$ (ω) $\quad \bar{\psi}\gamma^\mu\vec{\tau}\psi$ (ρ)

Relativistic Kohn-Sham equations:

$$\begin{pmatrix} m+S+V & \boldsymbol{\sigma p} \\ \boldsymbol{\sigma p} & -m-S+V \end{pmatrix} \begin{pmatrix} f_i \\ g_i \end{pmatrix} = \varepsilon_i \begin{pmatrix} f_i \\ g_i \end{pmatrix}$$

scalar potential: $S(r) \approx -400$ MeV vector potential: $V(r) \approx 350$ MeV

$$\begin{pmatrix} m+S+V & \boldsymbol{\sigma p} \\ \boldsymbol{\sigma p} & -m-S+V \end{pmatrix} \begin{pmatrix} f_i \\ g_i \end{pmatrix} = \varepsilon_i \begin{pmatrix} f_i \\ g_i \end{pmatrix}$$

scalar potential: $S(r) \approx -400$ MeV vector potential: $V(r) \approx 350$ MeV

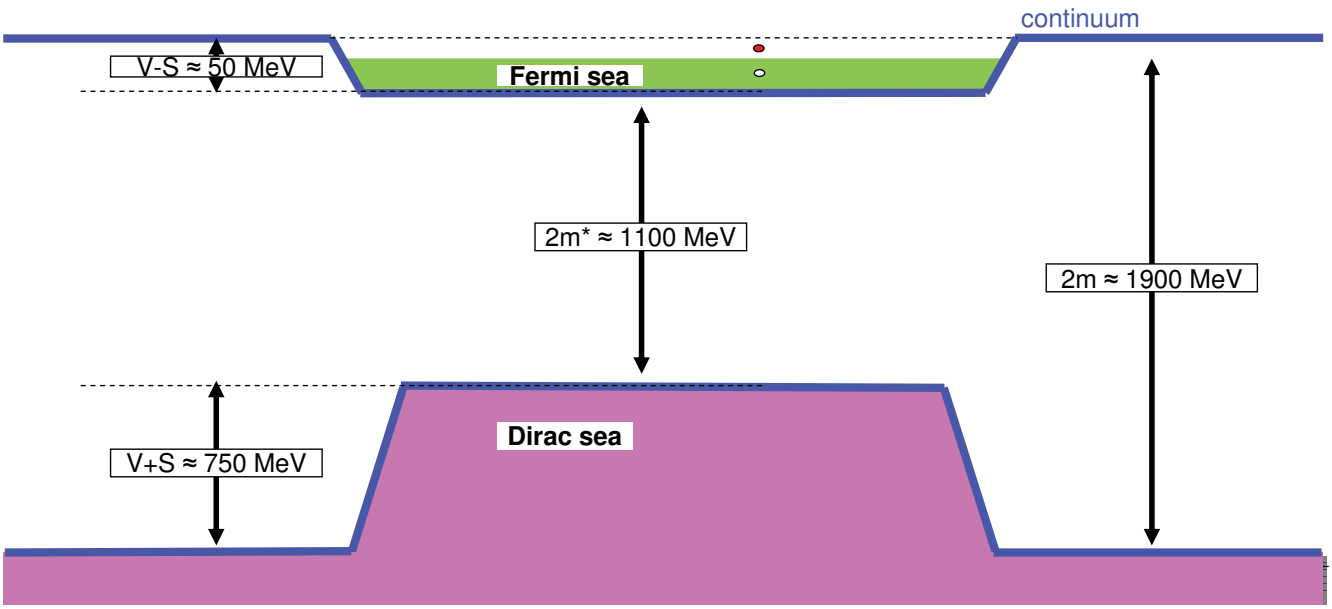

Relativistic Kohn-Sham equations:

$$\begin{pmatrix} m+S+V & \boldsymbol{\sigma p} \\ \boldsymbol{\sigma p} & -m-S+V \end{pmatrix} \begin{pmatrix} f_i \\ g_i \end{pmatrix} = \varepsilon_i \begin{pmatrix} f_i \\ g_i \end{pmatrix}$$

scalar potential: $S(r)$ vector potential: $V_0(r)$ time-like, $V_i(r)$ space-like

$$\begin{pmatrix} m+S+V & \boldsymbol{\sigma}(\boldsymbol{p}-\boldsymbol{V}) \\ \boldsymbol{\sigma}(\boldsymbol{p}-\boldsymbol{V}) & -m-S+V \end{pmatrix} \begin{pmatrix} f \\ g \end{pmatrix} = \varepsilon \begin{pmatrix} f \\ g \end{pmatrix}$$

The Walecka model

Dürr and Teller, Phys.Rev 101 (1956)
Walecka, Phys.Rev. C83 (1974)
Boguta and Bodmer, Nucl.Phys. A292 (1977)

The nuclear fields are obtained by coupling the nucleons through the exchange of effective mesons through an effective Lagrangian.

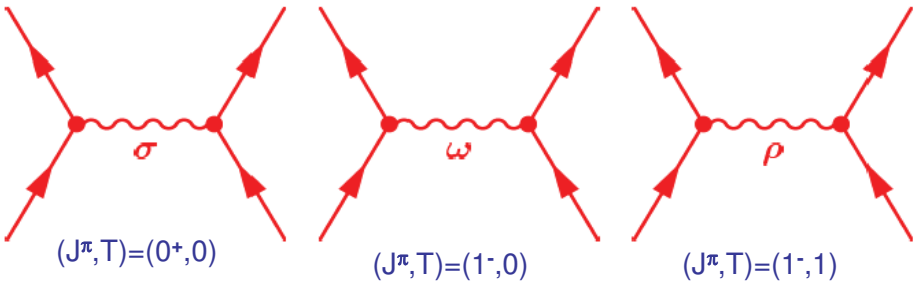

$$S(\mathbf{r}) = g_\sigma \sigma(\mathbf{r}) \qquad V(\mathbf{r}) = g_\omega \omega(\mathbf{r}) + g_\rho \vec{\tau}\vec{\rho}(\mathbf{r}) + eA(\mathbf{r})$$

sigma-meson: attractive scalar field

omega-meson: short-range repulsive

rho-meson: isovector field

Lagrangian density:

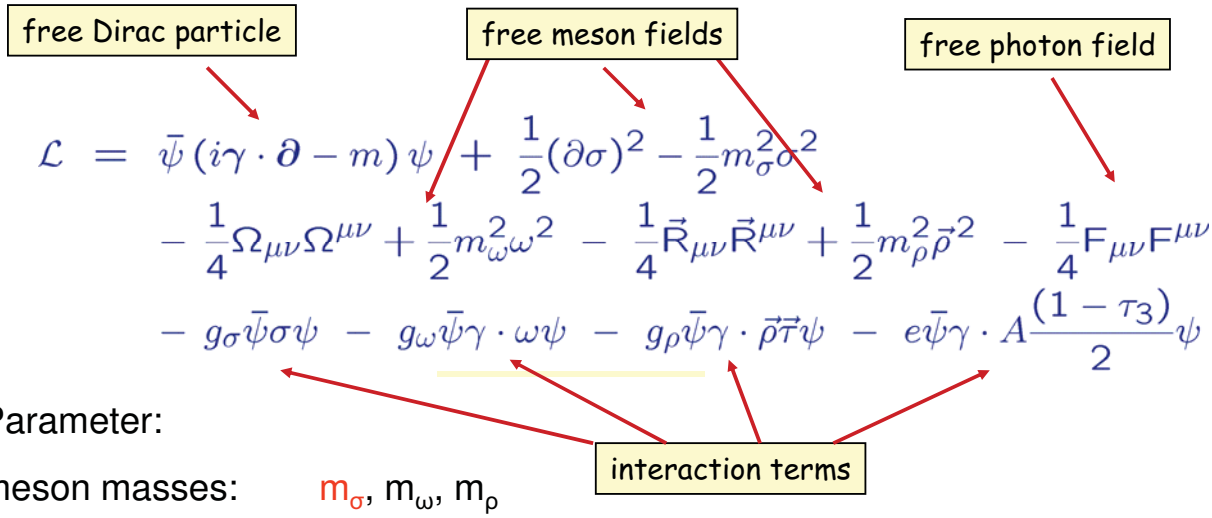

Parameter:

meson masses: m_σ, m_ω, m_ρ

meson couplings: g_σ, g_ω, g_ρ

Static limit (with time reversal invariance)

for the nucleons we find the static Dirac equation

$$(\boldsymbol{\alpha p} + V + \beta(m + S))\,\psi_i = \varepsilon_i\psi_i$$

$$S = -g_\sigma\rho_s, \qquad V = g_\omega\omega_0 + g_\rho\rho_0 + eA_0$$

No-sea approxim. !

for the mesons we find the Helmholtz equations:

$$\left(-\Delta + m_\sigma^2\right)\sigma = -g_\sigma\rho_s,$$

$$\left(-\Delta + m_\omega^2\right)\omega_0 = +g_\omega\rho,$$

$$\ldots$$

$$\rho_s = \sum_{i=1}^{A}\bar{\psi}_i\psi_i$$

$$\rho = \sum_{i=1}^{A}\psi_i^\dagger\psi_i$$

Symmetric nuclear matter:

$$[\alpha \mathrm{k} + \beta (m + S)]\psi = [E - V]\psi$$

with $m^* = m + S$ and $E^* = \sqrt{\mathrm{k}^2 + m^{*2}}$ and $E = E^* + V$

we have plane wave solutions of the Dirac equation:

$$\psi(\mathrm{k}) = \sqrt{\frac{E^* + m^*}{2m^*}} \begin{pmatrix} 1 \\ \frac{\sigma \mathrm{k}}{E^* + m^*} \end{pmatrix} \chi$$

the ω-field is given by the density:

$$V = g_\omega \omega_0 = \left(\frac{g_\omega}{m_\omega}\right)^2 \rho_B$$

the σ-field has to be determined from a non-linear equation, which gives saturation:

$$S = -g_\sigma \sigma = m - m^* = \frac{g_\sigma^2}{m_\sigma^2} \rho_s = \gamma \frac{g_\sigma^2}{m_\sigma^2} \int \frac{d^3k}{(2\pi)^3} \frac{m^*}{E^*(k)}$$
$$= \frac{\gamma}{4\pi^2} \frac{g_\sigma^2}{m_\sigma^2} m^* \left[k_F E_F^* - m^{*2} \ln\left(\frac{k_F}{m^*} + \frac{E_F^*}{m^*} \right) \right]$$

One needs only 2 constants: $G_\sigma = \left(\frac{g_\sigma}{m_\sigma}\right)^2 = 11{,}75\ \mathrm{fm}^2$ $G_\omega = \left(\frac{g_\omega}{m_\omega}\right)^2 = 8{,}61\ \mathrm{fm}^2$

Why covariant ?

1) no relativistic kinematics necessary: $\sqrt{p_F^2 + m_N^2} = m_N \sqrt{1 + 0.075}$

2) non-relativistic DFT works relatively well

3) technical problems:
   - no harmonic oscillator
   - no exact soluble models
   - double dimension
   - huge cancellations between V and S
   - no variational method ?

4) conceptual problems:
   - treatment of Dirac sea (no-sea approx.)
   - no well defined many-body theory

Why covariant ?

1) Relativistic kinematic is not important in nucl. structure
2) Large fields V ≈ 350 MeV , S ≈ – 400 MeV
3) Large spin-orbit splittings in nuclei
4) Success of relativistic Brueckner calculations
5) Success of intermediate energy proton scattering
6) Relativistic saturation mechanism
7) Consistent treatment of time-odd fields
8) Natural explanation of pseudospin symmetry
9) Connection to underlying theories ?
10) Use as many symmetries as possible in phenomenology

Why covariant ?

1) Large fields V ≈ 350 MeV , S ≈ – 400 MeV

Why covariant ?

1) Large fields V ≈ 350 MeV, S ≈ – 400 MeV

In medium QCD-sum rules
relate the scalar condensate $\langle \bar{q}q \rangle$ and the quark density $\langle q^\dagger q \rangle$
to the scalar and vector self-energies of the nucleon in the medium:

scalar self-energy: $S \sim \langle \bar{q}q \rangle_{\text{vac}} - \langle \bar{q}q \rangle_{\rho_N}$

vector self-energy: $V \sim \langle q^\dagger q \rangle_{\rho_N}$

$$V \approx -S \approx 400 \text{ MeV} \quad (\pm 20\%)$$

Cohen, Furnstahl, Griegel, PRC 67 (1992) 961

Why covariant ?

1) Large fields V ≈ 350 MeV, S ≈ – 400 MeV

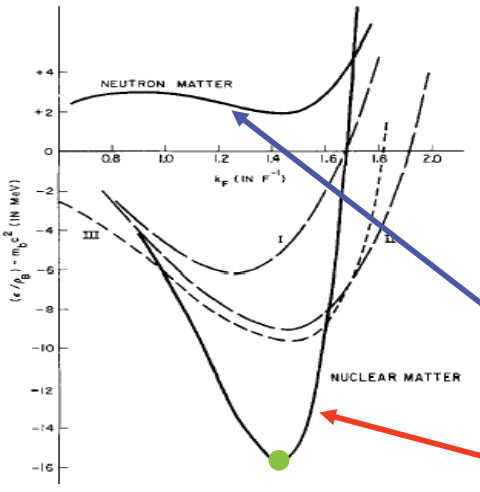

The EoS in the σω-model depends on two parameters G_σ and G_ω. They are determined by the density ρ_0 and the binding energy E/A at saturation

This gives the proper spin-orbit splitting

σω - model

J.D. Walecka, Ann.Phys. (NY) 83, (1974) 491

Why covariant ?

1) Large fields V ≈ 350 MeV, S ≈ – 400 MeV
2) Large spin-orbit splittings in nuclei

$$\begin{pmatrix} M+W_+ & \sigma p \\ \sigma p & -M+W_- \end{pmatrix} \begin{pmatrix} f \\ g \end{pmatrix} = \varepsilon \begin{pmatrix} f \\ g \end{pmatrix}$$

$$W_\pm(r) = V(r) \pm S(r) \qquad M_\pm(r,\varepsilon) = M \pm \varepsilon \mp W_\mp(r)$$

Eliminate small components:

$$\left\{ p \frac{1}{2M_+} p - \frac{1}{4M_+^2} \frac{1}{r} \frac{\partial W_-}{\partial r} \ell s + M + W_+ \right\} f = \varepsilon f$$

W_ ≈ 750 MeV

W$_+$ ≈ 50 MeV

Why covariant ?

1) Large fields V ≈ 350 MeV, S ≈ – 400 MeV
2) Large spin-orbit splittings in nuclei
3) Success of relativistic Brueckner calculations

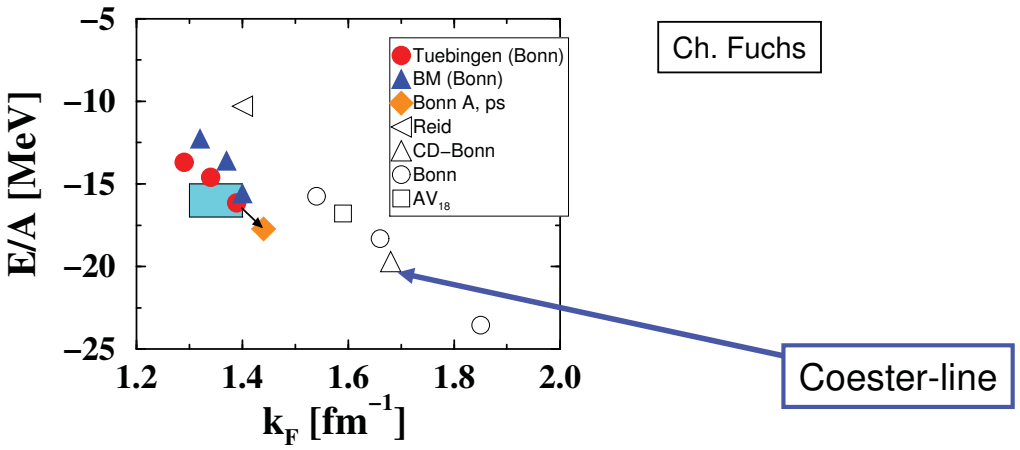

Why covariant ?

1) Large fields V ≈ 350 MeV ,S ≈ -400 MeV
2) Large spin-orbit splittings in nuclei
3) Success of relativistic Brueckner calculations
4) Success of intermediate energy proton scattering (spin observables)

Why covariant ?

1) Large fields V ≈ 350 MeV, S ≈ – 400 MeV
2) Large spin-orbit splittings in nuclei
3) Success of relativistic Brueckner calculations
4) Success of intermediate energy proton scattering (spin observables)
5) A relativistic saturation mechanism:

The σ-field is the origin of attraction. Its source is the scalar density:

$$m_\sigma^2\,\sigma = -g_\sigma \sum_{i=1}^{A} \overline{\psi}_i \psi_i = -g_\sigma \sum_{i=1}^{A} \left(f_i^+ f_i - g_i^+ g_i \right)$$

$$m_\sigma^2\,\sigma \approx -g_\sigma \rho \; -2\sum_{i=1}^{A} f_i^+ f_i = -g_\sigma \rho \; + \frac{1}{\tilde{m}} \sum_{i=1}^{A} \nabla f_i^+ \nabla f_i$$

In the non-rel. case, Hartree with Yukawa forces would lead to collapse

Why covariant ?

1) Large fields V ≈ 350 MeV, S ≈ – 400 MeV
2) Large spin-orbit splittings in nuclei
3) Success of relativistic Brueckner calculations
4) Success of intermediate energy proton scattering (spin observables)
5) Relativistic saturation mechanism
6) Consistent treatment of time-odd fields

$$\begin{pmatrix} m + V + S & \vec{\sigma}(\vec{\mathbf{p}} + \vec{\mathbf{V}}) \\ \vec{\sigma}(\vec{\mathbf{p}} + \vec{\mathbf{V}}) & -m + V - S \end{pmatrix} \begin{pmatrix} g_i \\ f_i \end{pmatrix} = \varepsilon_i \begin{pmatrix} g_i \\ f_i \end{pmatrix}$$

scalar potential $S(\mathbf{r})$
vector potential (time-like) $V(\mathbf{r})$
vector potential (space-like) $\vec{V}(\mathbf{r})$

Nuclear magnetism

Superdeformed bands in the Hg-Pb region:

$$\left[\boldsymbol{\alpha} \cdot (-i\boldsymbol{\nabla} - \mathbf{V}) + \beta\,(m + S) + V - \boldsymbol{\Omega} \cdot \hat{\mathbf{J}}\right] \psi_i \;=\; \varepsilon_i \psi_i$$

Cranked
RHB calculations:

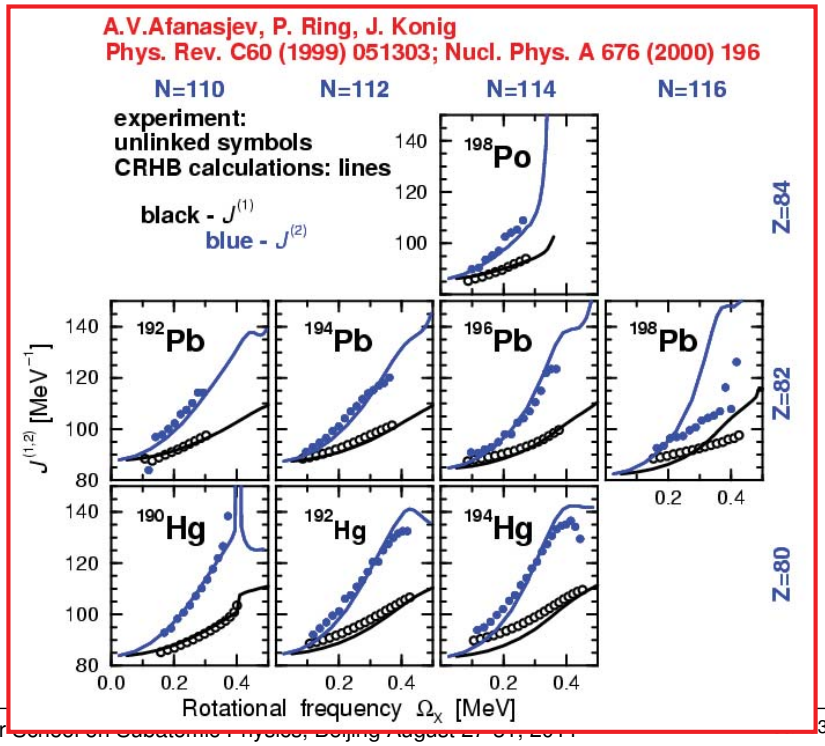

Moments of inertia in rotating nuclei:

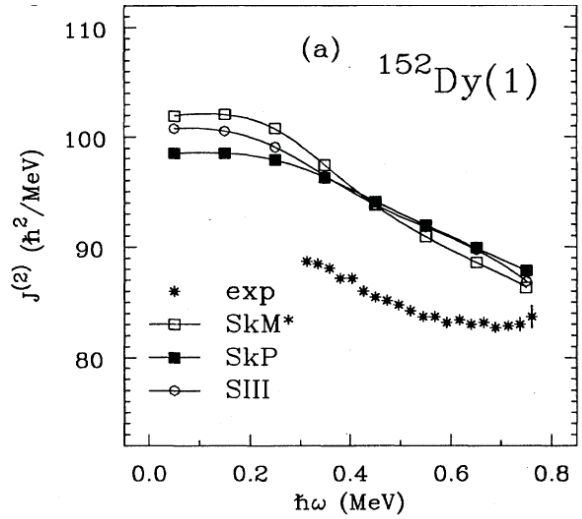

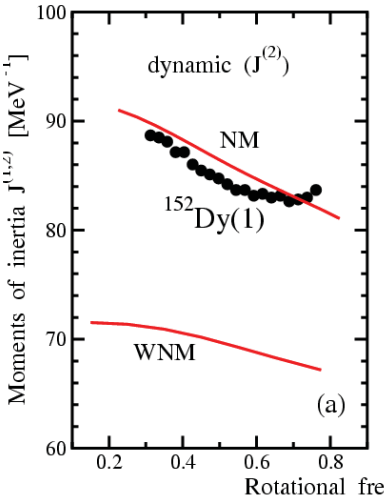

Skyrme

RMF NL1

Dobaczewski, Dudek, PRC (1995)

Afanasjev, P.R. PRC (1996)

Why covariant ?

1) Large fields V ≈ 350 MeV, S ≈ – 400 MeV
2) Large spin-orbit splittings in nuclei
3) Success of relativistic Brueckner calculations
4) Success of intermediate energy proton scattering (spin observables)
5) Relativistic saturation mechanism
6) Consistent treatment of time-odd fields
7) Natural explanation of pseudospin symmetry

Pseudospin symmetry found 1969

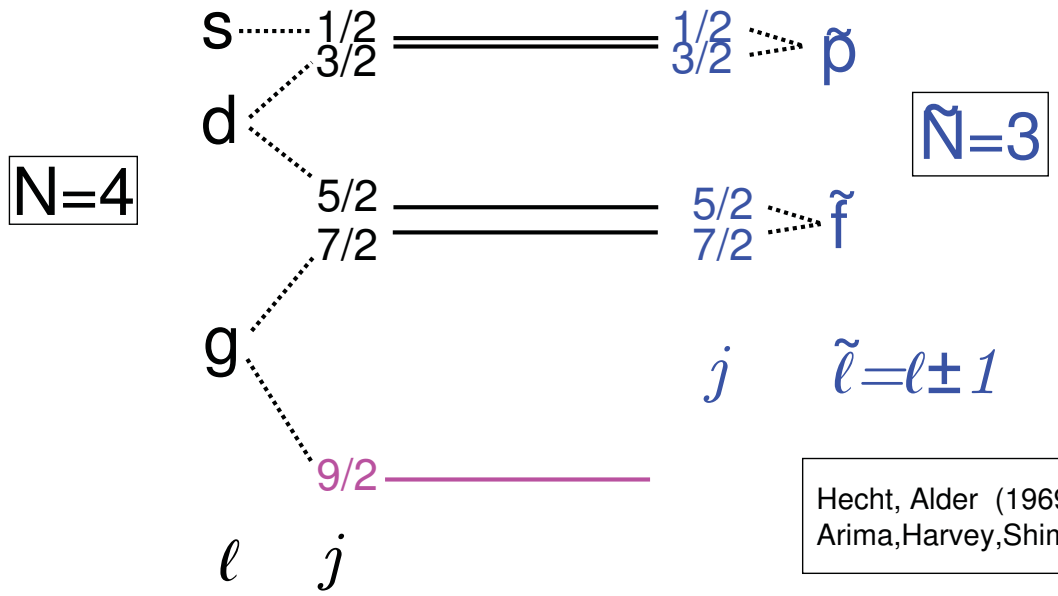

Hecht, Alder (1969)
Arima,Harvey,Shimizu (1969)

Ginocchio, (1997)

$$\psi_{njm}(\boldsymbol{r}) = \begin{pmatrix} f_{nj}(r)\mathcal{Y}_{\ell jm} \\ g_{\tilde{n}j}(r)\mathcal{Y}_{\tilde{\ell}jm} \end{pmatrix}$$

Spin and pseudo-spin splitting for nucleons:

$$\begin{pmatrix} M+W_+ & \boldsymbol{\sigma p} \\ \boldsymbol{\sigma p} & -M+W_- \end{pmatrix} \begin{pmatrix} f \\ g \end{pmatrix} = \varepsilon \begin{pmatrix} f \\ g \end{pmatrix}$$

$$W_\pm(r) = V(r) \pm S(r)$$
$$M_\pm(r,\varepsilon) = M \pm \varepsilon \mp W_\mp(r)$$

g eliminated:

$$\left\{ \boldsymbol{p}\frac{1}{2M_+}\boldsymbol{p} - \frac{1}{4M_+^2}\frac{1}{r}\frac{\partial W_-}{\partial r}\boldsymbol{\ell s} + M + W_+ \right\} f = \varepsilon f$$

f eliminated:

$$\left\{ \boldsymbol{p}\frac{1}{2M_-}\boldsymbol{p} + \frac{1}{4M_-^2}\frac{1}{r}\frac{\partial W_+}{\partial r}\boldsymbol{\ell s} + M - W_- \right\} g = -\varepsilon g$$

$W_+ = V+S = 0$ → **pseudospin symmetry**
$W_- = V-S = 0$ → **spin symmetry**

Ginocchio, PRL 78 (1997) 436

Why covariant ?

1) Large fields V ≈ 350 MeV , S ≈ – 400 MeV
2) Large spin-orbit splittings in nuclei
3) Success of relativistic Brueckner calculations
4) Success of intermediate energy proton scattering
5) Relativistic saturation mechanism
6) Consistent treatment of time-odd fields
7) Natural explanation of pseudospin symmetry
8) Connection to underlying theories ?

Why covariant ?

1) Large fields V ≈ 350 MeV , S ≈ – 400 MeV
2) Large spin-orbit splittings in nuclei
3) Success of relativistic Brueckner calculations
4) Success of intermediate energy proton scattering
5) Relativistic saturation mechanism
6) Consistent treatment of time-odd fields
7) Natural explanation of pseudospin symmetry
8) Connection to underlying theories ?
9) **Use as many symmetries as possible in phenomenology**

Effective density dependence:

non-linear potential:

Boguta and Bodmer, NPA 431, 3408 (1977)

NL1, NL3, PK1 . .

$$\frac{1}{2}m_\sigma^2\sigma^2 \quad \Rightarrow \quad U(\sigma)=\frac{1}{2}m_\sigma^2\sigma^2+\frac{1}{3}g_2\sigma^3+\frac{1}{4}g_3\sigma^4$$

density dependent coupling constants:

R.Brockmann and H.Toki, PRL 68, 3408 (1992)
S.Typel and H.H.Wolter, NPA 656, 331 (1999)
T. Niksic, D. Vretenar, P. Finelli, and P. Ring, PRC 56 (2002) 024306

$$g_o, g_\omega, g_\rho \Rightarrow g_o(\rho), g_\omega(\rho), g_\rho(\rho)$$

g → g(ρ(r))

DD-ME1, DD-ME2

Effective density dependence:

The basic idea comes from ab initio calculations
density dependent coupling constants include Brueckner correlations
and threebody forces

non-linear meson coupling: **NL3**

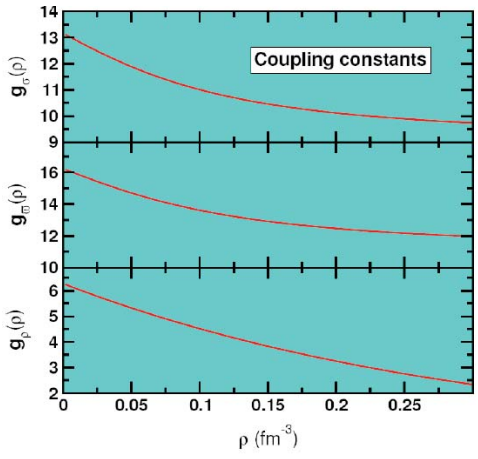

Effective interactions with medium-dependent couplings:

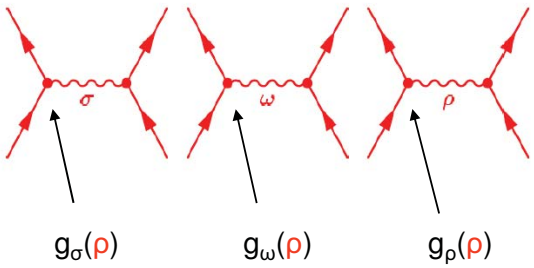

adjusted to ground state properties of finite nuclei

Typel, Wolter, NPA **656**, 331 (1999)
Niksic, Vretenar, Finelli, P.R., PRC **66**, 024306 (2002): **DD-ME1**
Lalazissis, Niksic, Vretenar, P.R., PRC 78, 034318 (2008): **DD-ME2**

Effective density dependence:

The basic idea comes from ab initio calculations
density dependent coupling constants include Brueckner correlations
and threebody forces

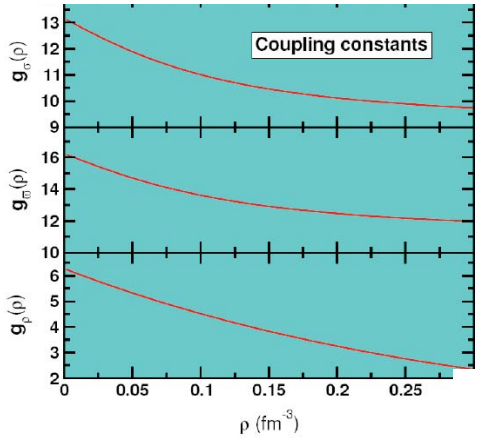

Point-coupling models
with derivative terms:

$g_\sigma(\rho)$ $g_\omega(\rho)$ $g_\rho(\rho)$

adjusted to ground state properties of finite nuclei

Manakos and Mannel, Z.Phys. **330**, 223 (1988)	
Bürvenich, Madland, Maruhn, Reinhard, PRC **65**, 044308 (2002):	**PC-F1**
Niksic, Vretenar, P.R., PRC 78, 034318 (2008):	**DD-PC1**
Zhao, Li, Yao, Meng, J. Meng, archiv 1002.1789	**PC-PK1**

How many parameters ?

4 + 3 parameters

symmetric nuclear matter: E/A, ρ_0 → G_σ G_ω

finite nuclei (N=Z): E/A, radii → m_σ
spinorbit for free

Coulomb (N≠Z): a_4 → G_ρ

density dependence: T=0 K_∞ → g_2 g_3

T=1 $r_n - r_p$ → a_ρ

Comparison with ab initio calculations:

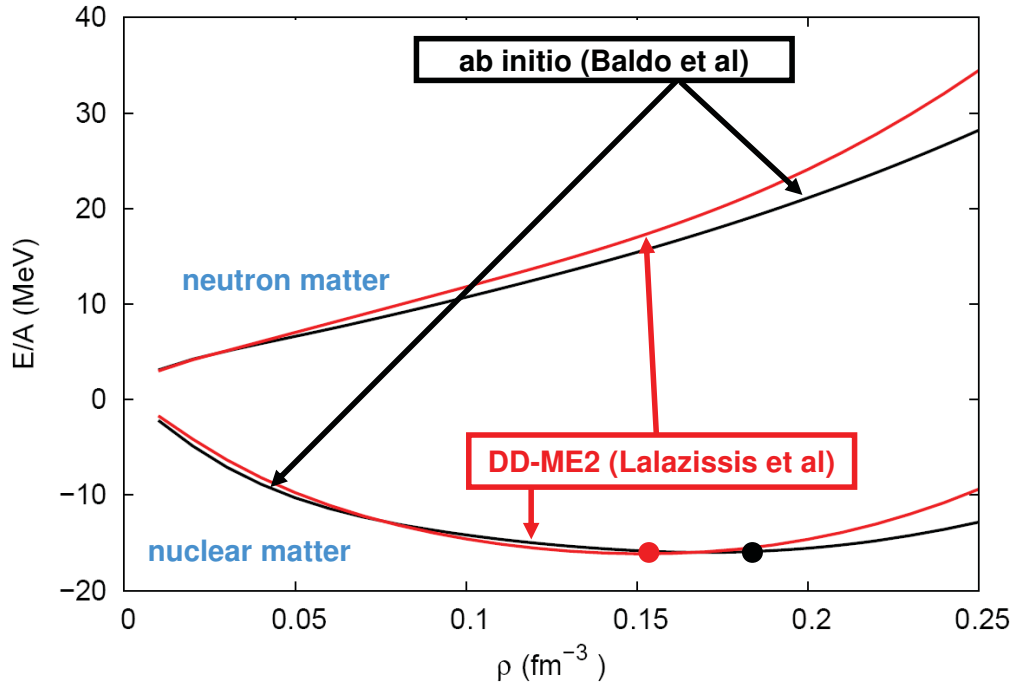

we find excellent agreement with ab initio calculations of Baldo et al.

Using ab initio data for the fit

point coupling model is fitted to microscopic nuclear matter
and to masses of 64 deformed nuclei:

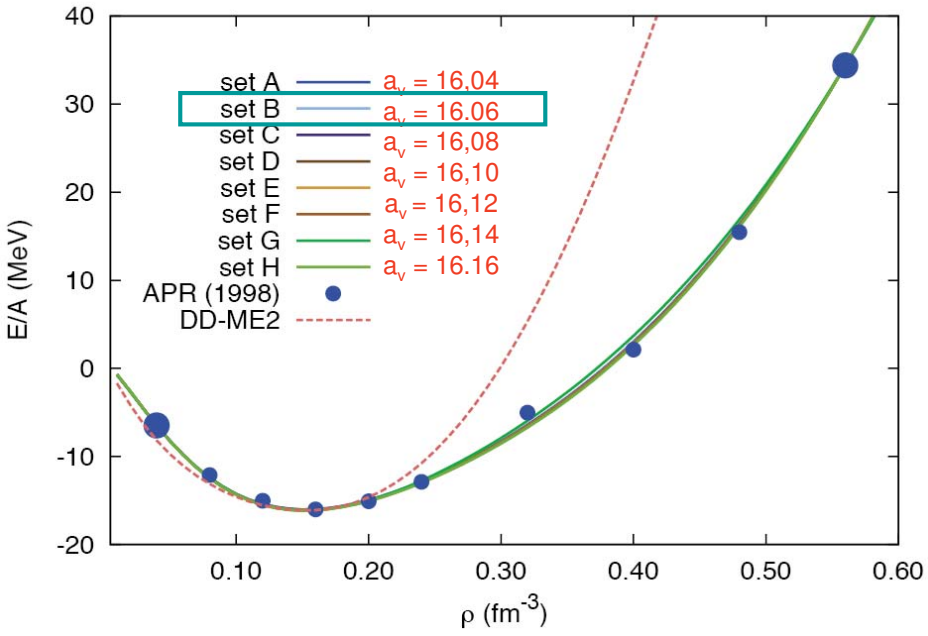

ρ_{sat} = 0.152 fm^{-3}
m^* = 0.58m
K_{nm} = 230 MeV
a_4 = 33 MeV

DD-PC1

A. Akmal, V.R. Pandharipande, and D.G. Ravenhall, PRC. 58, 1804 (1998).

Adjusting the model parameters

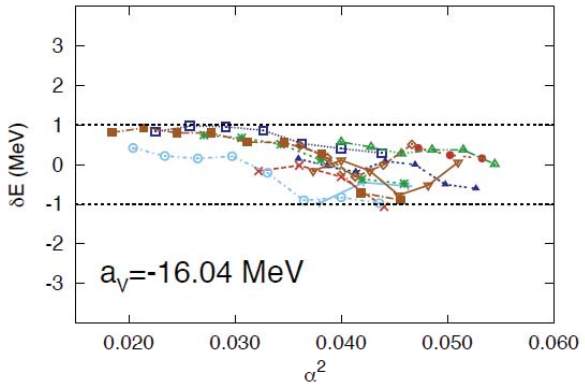

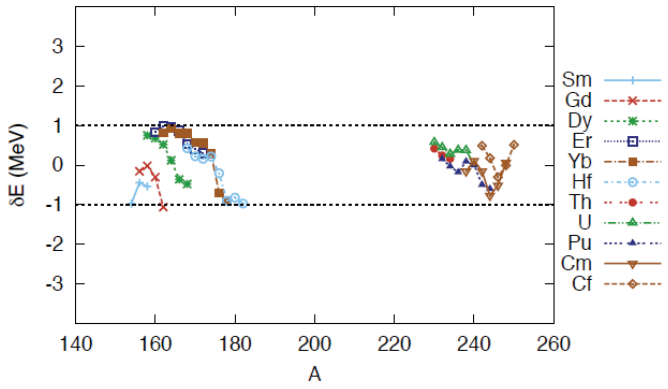

Rare-earth region

Sm (Z=62), Gd (Z=64), Dy (Z=66), Er (Z=68), Yb (Z=70), Hf (Z=72)

Actinides

Th (Z=90), U (Z=92), Pu (Z=94), Cm (Z=96), Cf (Z=98)

Total

64 isotopes

T. Niksic

Adjusting the model parameters

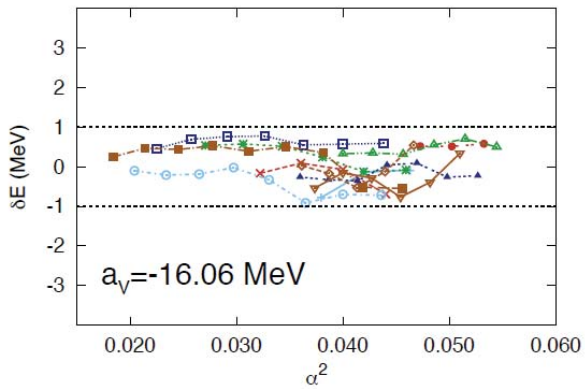

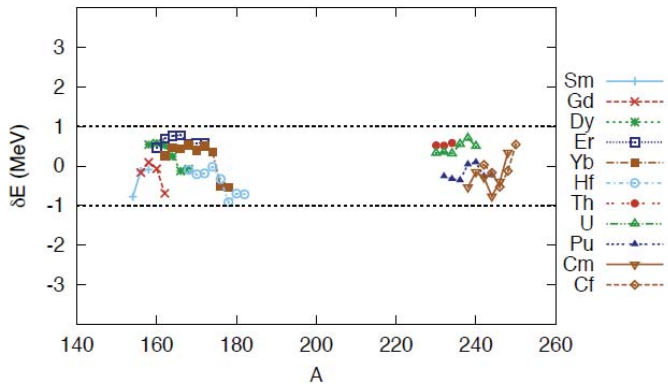

Rare-earth region

Sm (Z=62), Gd (Z=64), Dy (Z=66), Er (Z=68), Yb (Z=70), Hf (Z=72)

Actinides

Th (Z=90), U (Z=92), Pu (Z=94), Cm (Z=96), Cf (Z=98)

Total

64 isotopes

T. Niksic

Adjusting the model parameters

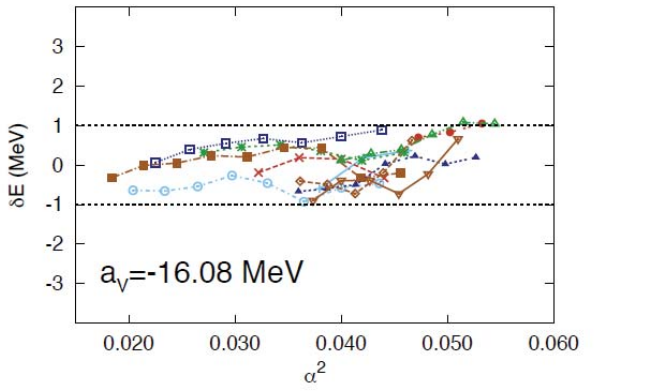

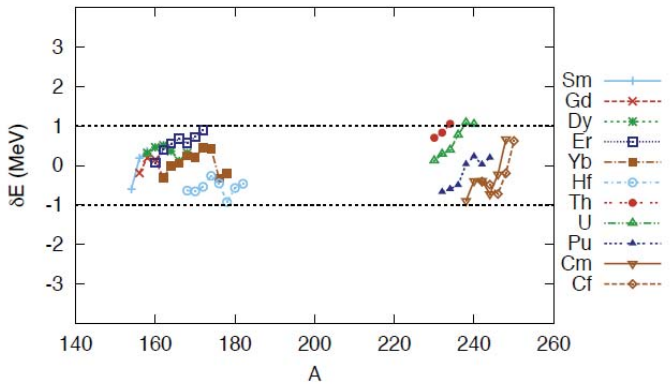

Rare-earth region

Sm (Z=62), Gd (Z=64), Dy (Z=66), Er (Z=68), Yb (Z=70), Hf (Z=72)

Actinides

Th (Z=90), U (Z=92), Pu (Z=94), Cm (Z=96), Cf (Z=98)

Total

64 isotopes

T. Niksic

Adjusting the model parameters

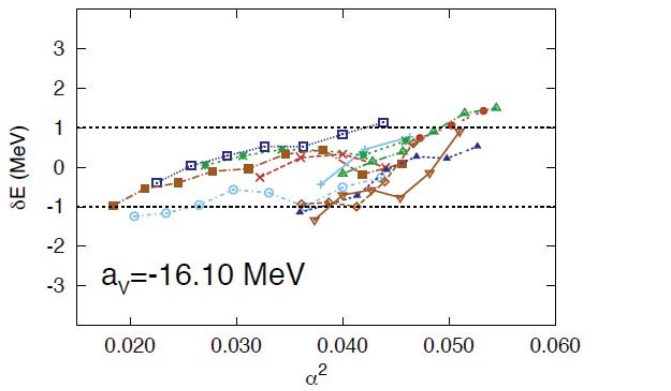

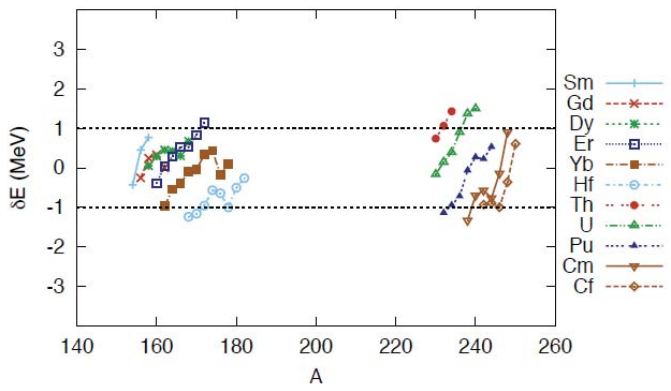

Rare-earth region

Sm (Z=62), Gd (Z=64), Dy (Z=66), Er (Z=68), Yb (Z=70), Hf (Z=72)

Actinides

Th (Z=90), U (Z=92), Pu (Z=94), Cm (Z=96), Cf (Z=98)

Total

64 isotopes

T. Niksic

Adjusting the model parameters

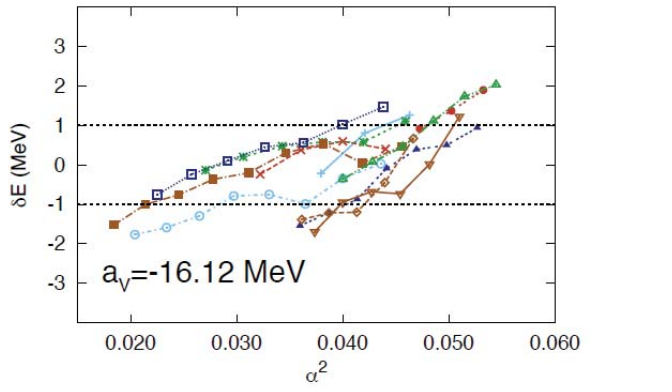

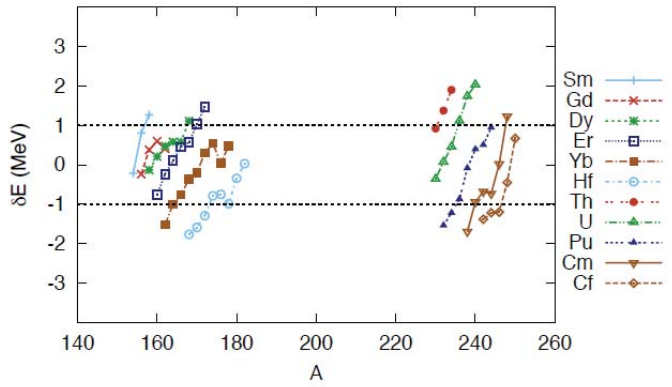

Rare-earth region

Sm (Z=62), Gd (Z=64), Dy (Z=66), Er (Z=68), Yb (Z=70), Hf (Z=72)

Actinides

Th (Z=90), U (Z=92), Pu (Z=94), Cm (Z=96), Cf (Z=98)

Total

64 isotopes

T. Niksic

Adjusting the model parameters

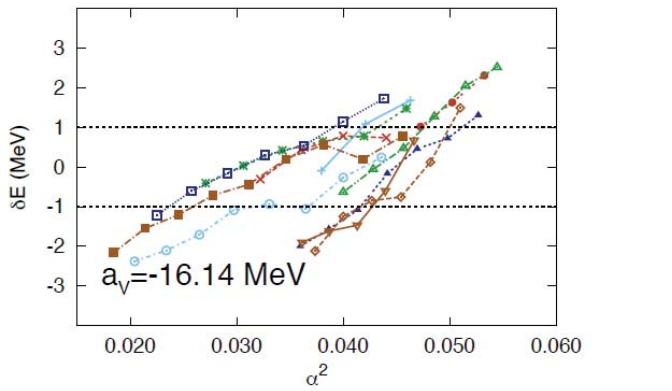

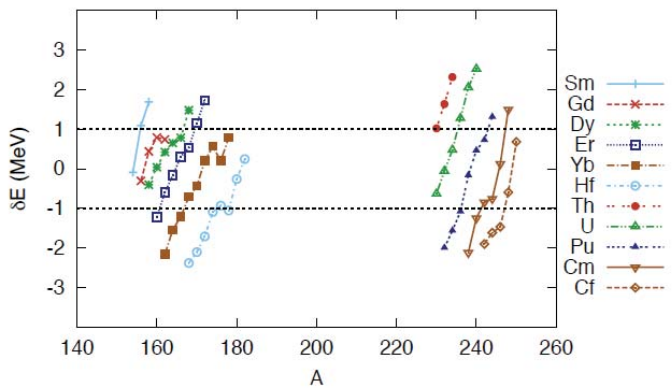

Rare-earth region

Sm (Z=62), Gd (Z=64), Dy (Z=66), Er (Z=68), Yb (Z=70), Hf (Z=72)

Actinides

Th (Z=90), U (Z=92), Pu (Z=94), Cm (Z=96), Cf (Z=98)

Total

64 isotopes

T. Niksic

Successes of relativistic investigations:

- Masses and radii
- Isotope shifts
- Neutron halo's
- Proton emitters
- Collective vibrations
- Pygmy modes
- Beyond mean field: transitional nuclei
- Beyond mean field: complex configurations

rms-deviations: masses: $\Delta m = 900$ keV
radii: $\Delta r = 0.015$ fm

Lalazissis, Niksic, Vretenar, Ring, PRC 71, 024312 (2005)

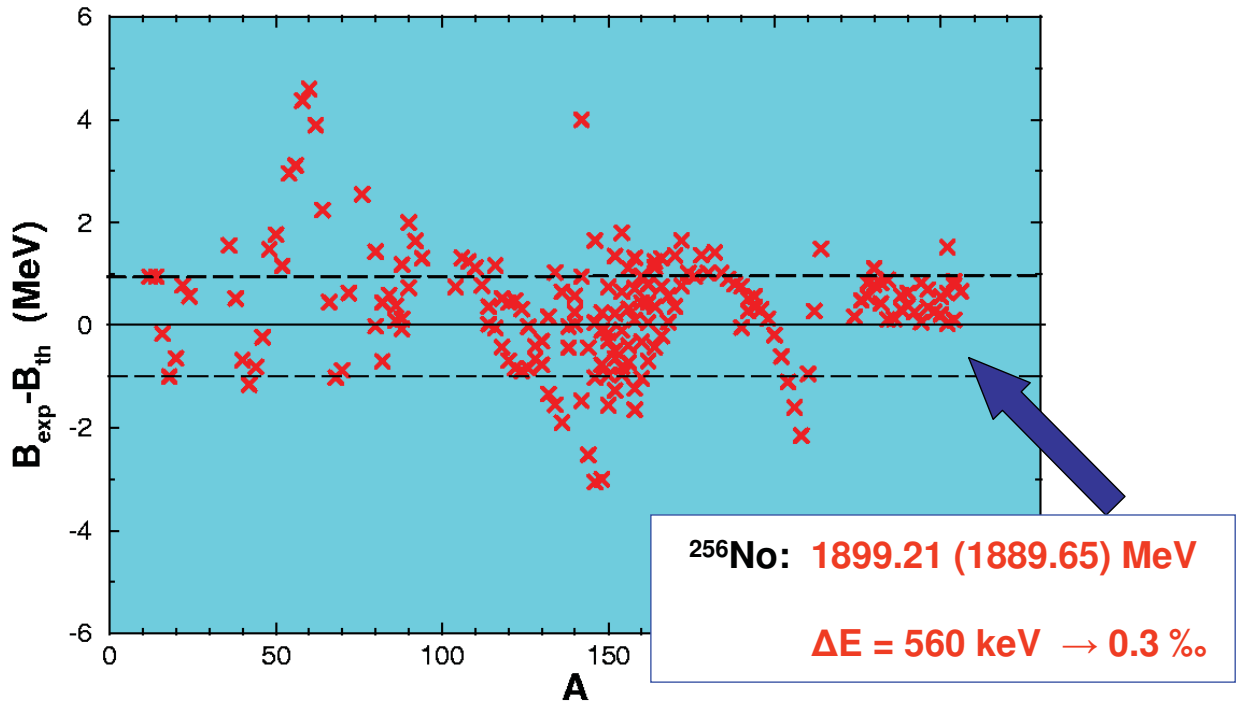

Kink in the isotopic shifts of radii: relativistic

Pb isotopes

- differences between neutron and proton radii
- charge isotope shifts

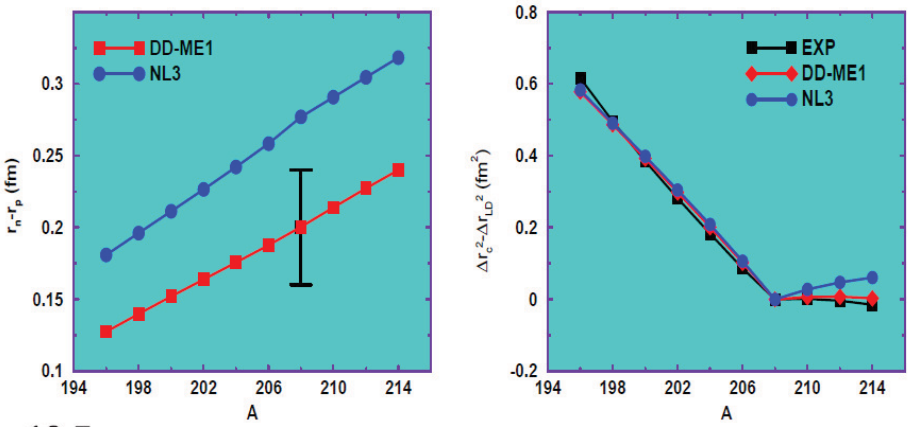

NL3: Isotope shifts in deformed nuclei:

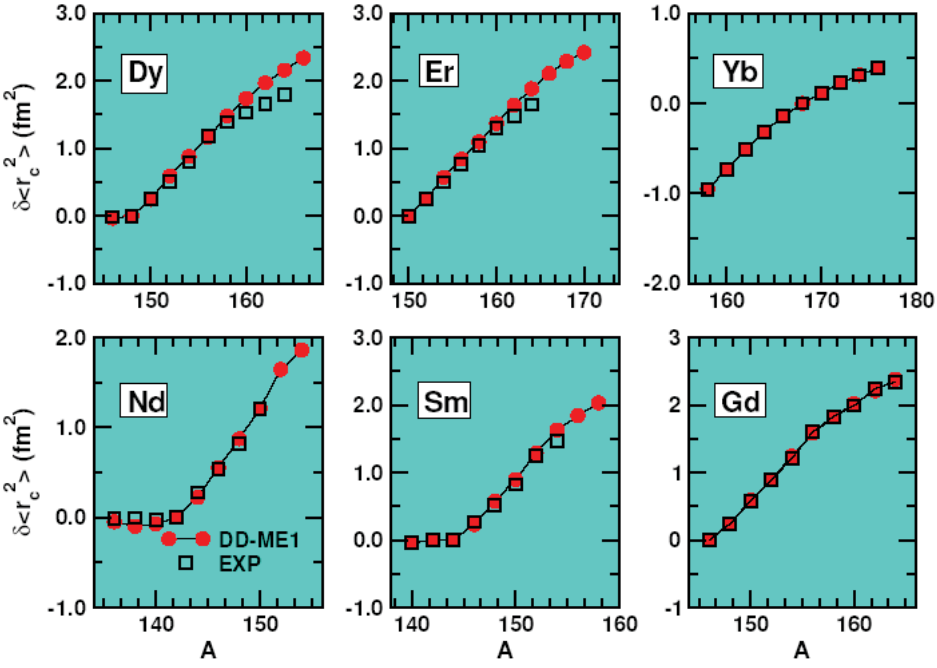

Empirical data: E.G. Nadjakov et al., At. Data Nucl. Data Tables 56, 133(1994)

Kink in the isotopic shifts of radii: Skyrme

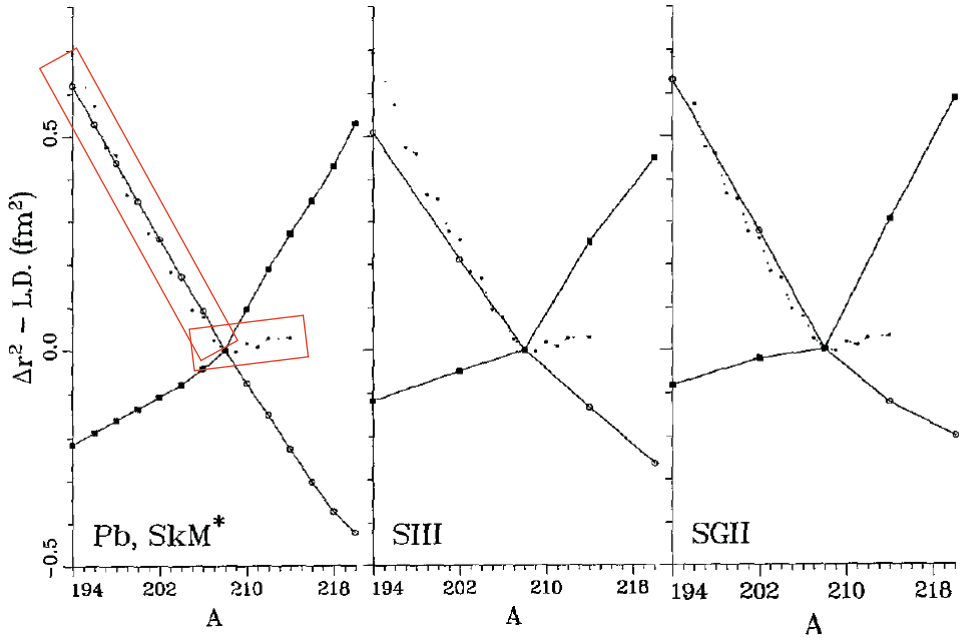

Tajima, Bonche, Flocard, Heenen, Weiss, NPA 551 (1993)

Neutron halo:

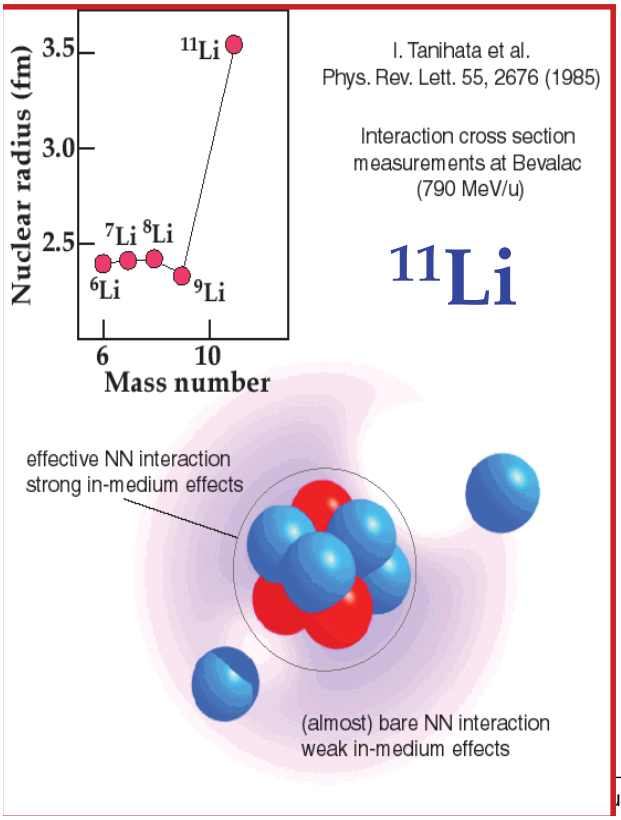

Mean field theory of halo's: (RHB in the continuum)

advantages:

* residual interaction by pairing
* self-consistent description
* universal parameters
* polarization of the core
* treatment of the continuum

problems:

*center of mass motion

*boudary conditions at infinity

Density distribution in Li-nuclei

J. Meng and P. Ring , PRL 77, 3963 (1996)

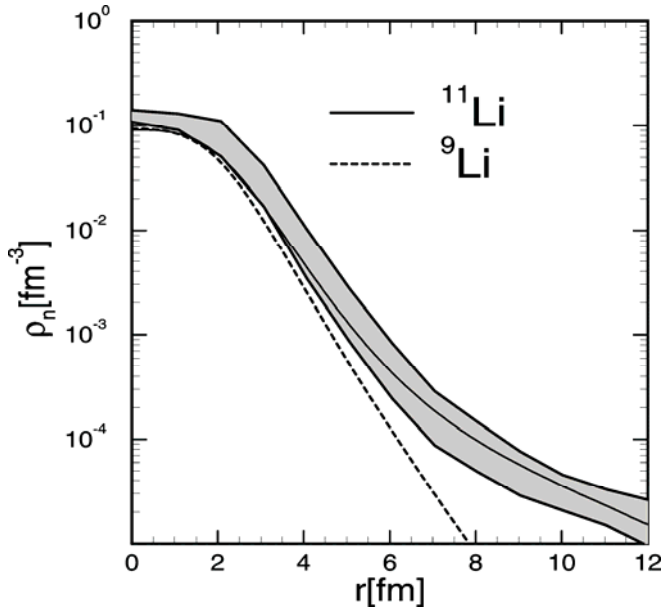

rel. Hartree-Bogoliubov,
with continuum
parameter set NL2
density dependent d-pairing

Density distribution in Li-nuclei

J. Meng and P. Ring , PRL 77, 3963 (1996)

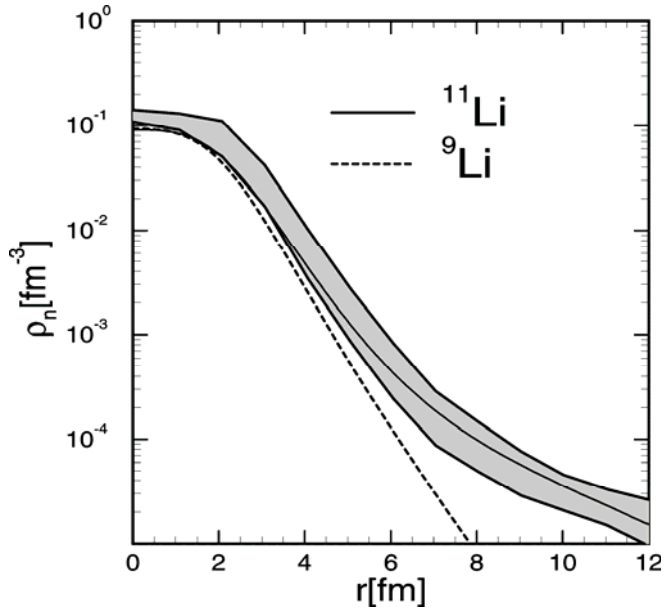

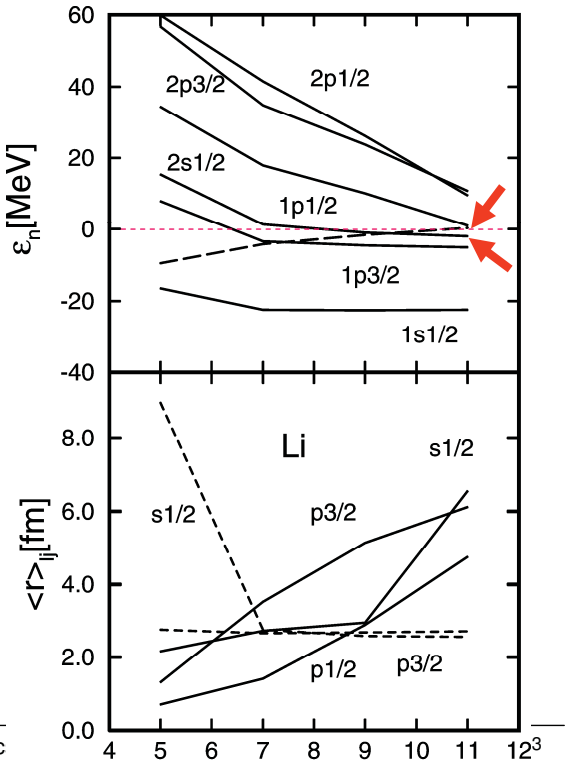

Proton emitters at the proton dripline

Vretenar, Lalazissis, Ring, Phys.Rev.Lett. 82, 4595 (1999)

characterized by exotic ground-state decay modes such as the direct emission of charged particles and β -decays with large Q-values.

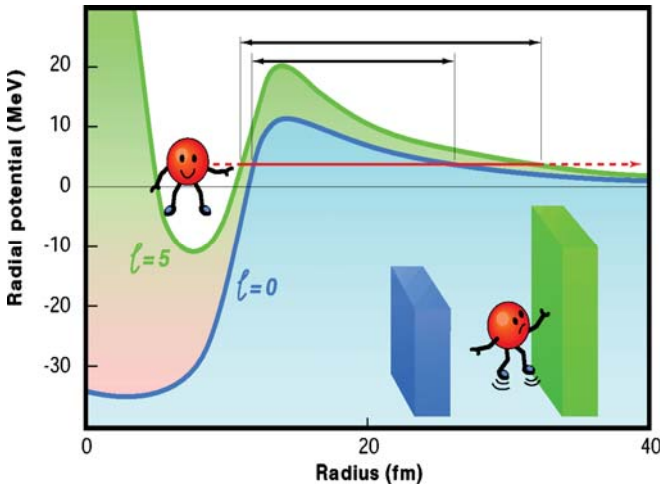

Ground-state proton emitters

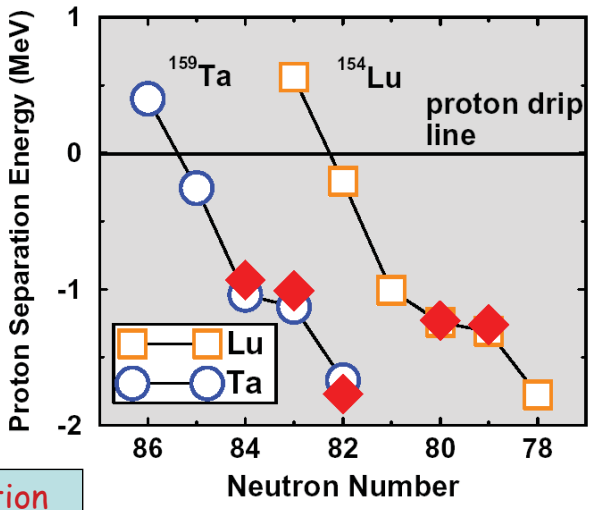

Self-consistent RHB calculations -> separation energies, quadrupole deformations, odd-proton orbitals, spectroscopic factors

Lalazissis, Vretenar, Ring
Phys.Rev. C60, 051302 (1999)

Fission barriers for triaxially deformed shapes:

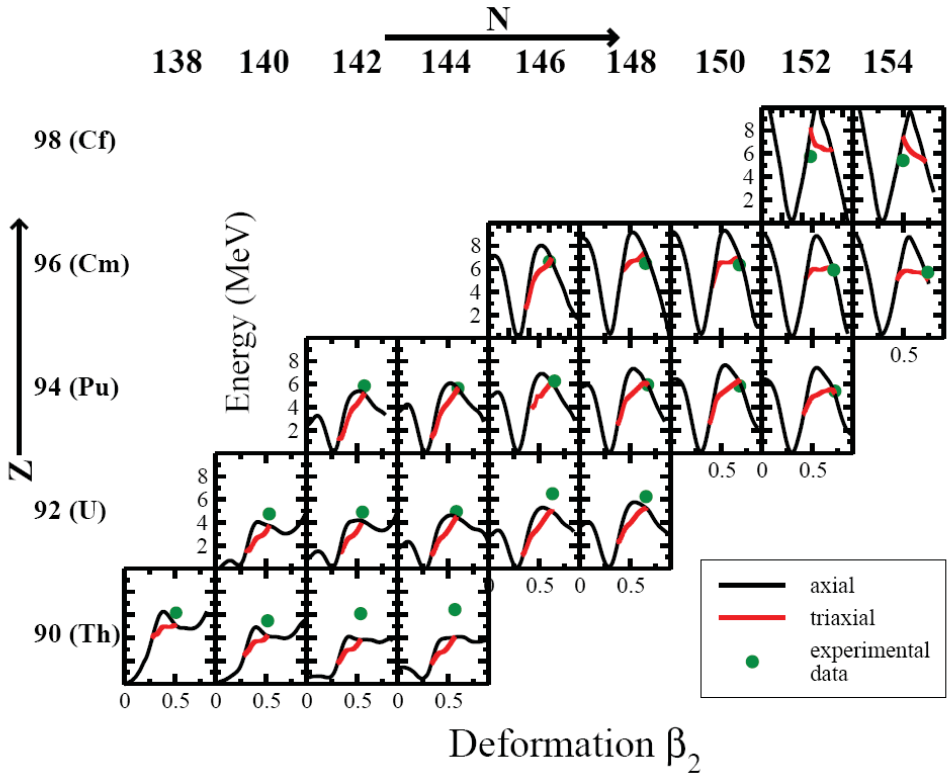

Afanasjev

Superheavy Elements: Q_α-values

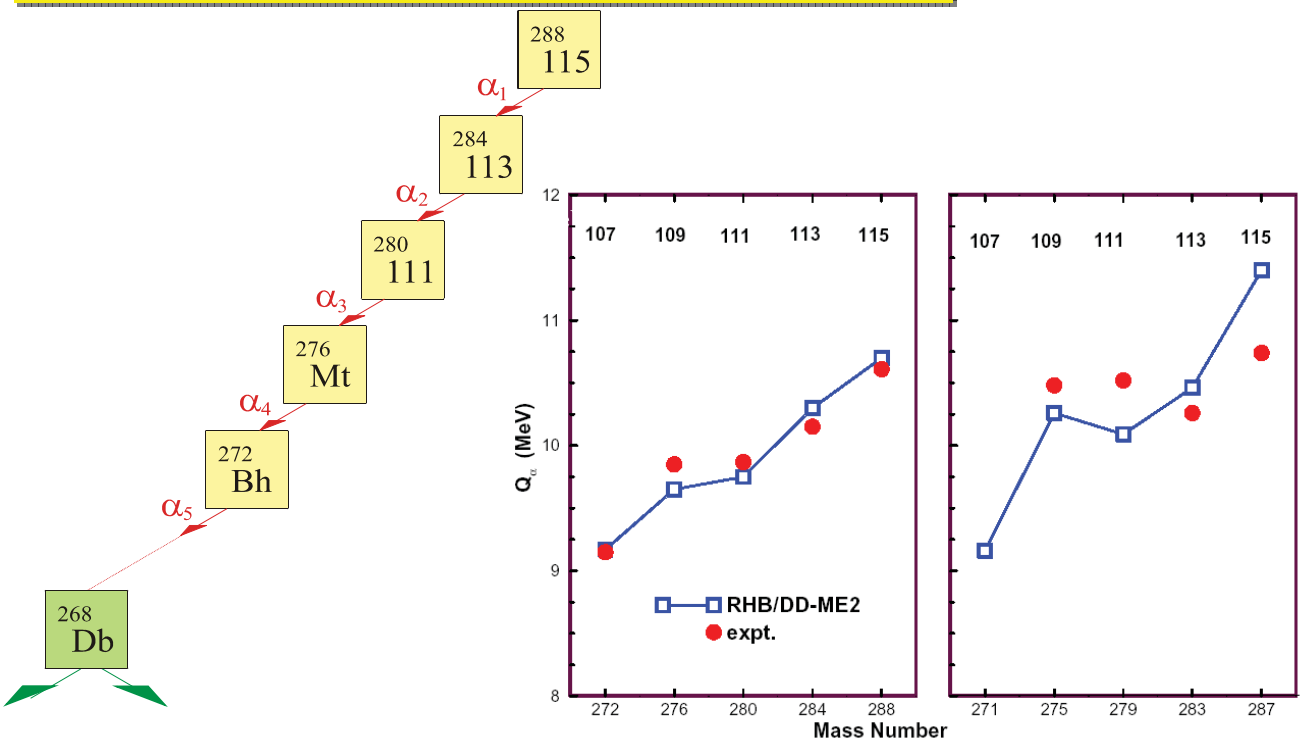

- Exp: Yu.Ts.Oganessian *et al*, PRC 69, 021601(R) (2004)
- Lalzissis

Content:

- Motivation
- Density Functional Theory
- The Nuclear Density Functional
- Covariant Density Functionals
- Ground state properties
- Nuclear dynamics and excitations
- Beyond mean field
- Outlook

Time dependent density functional theory:

Runge-Gross Theorem (1984):

$$\int dt \{\langle \Phi(t)|i\partial_t|\Phi(t)\rangle - E[\rho(t),t]\} = 0$$

quasi-static approx: $E[\rho(t),t] = E_{HK}[\rho(t)]$

$$i\partial_t\hat{\rho} = \left[\hat{h}(\hat{\rho}) + \hat{f}, \hat{\rho}\right]$$

time-dependent mean field equatios

Interaction:

$$\hat{V} = \frac{\delta^2 E}{\delta\hat{\rho}\,\delta\hat{\rho}}$$

$$\langle \Phi(t)|r^2|\Phi(t)\rangle$$

Breathing mode: ^{208}Pb

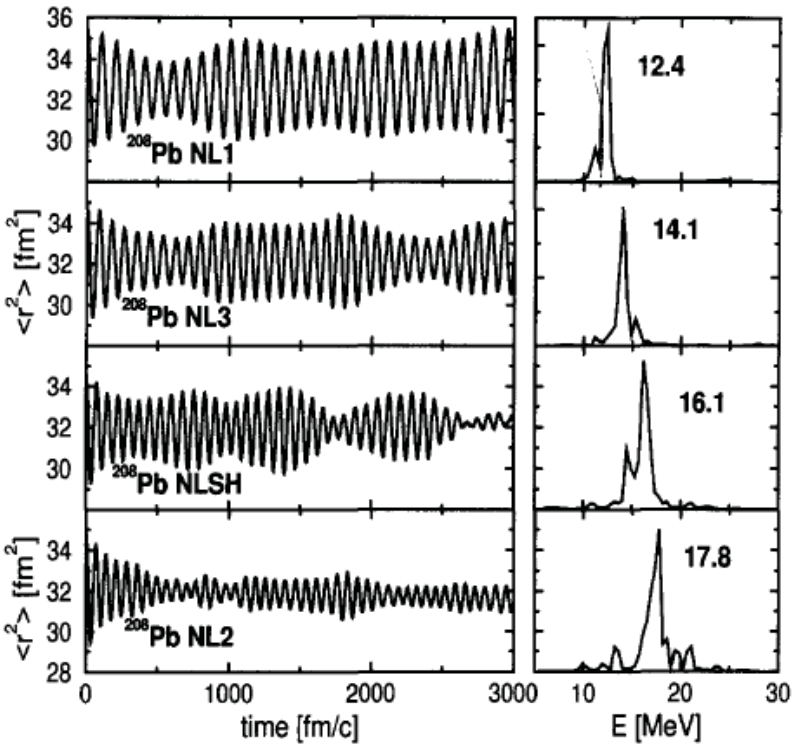

K_∞=211

K_∞=271

K_∞=355

Interaction:

$$\hat{V} = \frac{\delta^2 E}{\delta\hat{\rho}\,\delta\hat{\rho}}$$

Relativistic (Q)RPA calculations of giant resonances

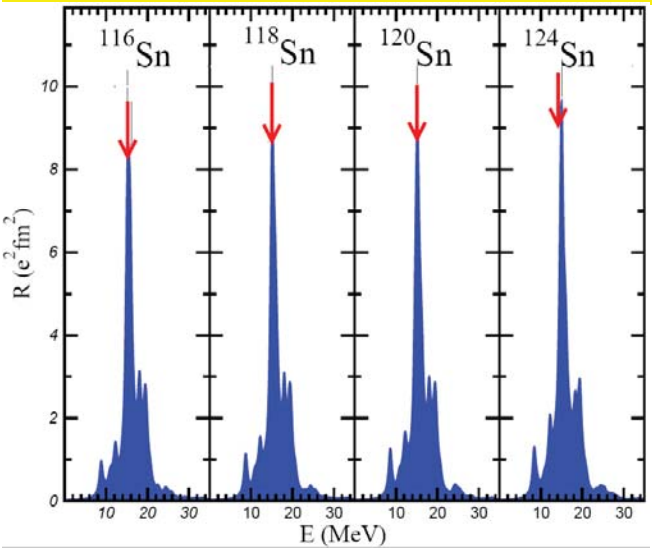

Sn isotopes: DD-ME2 effective interaction + Gogny pairing

Isovector dipole response

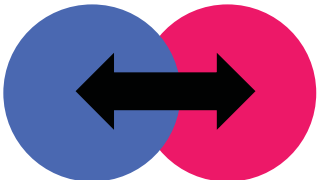

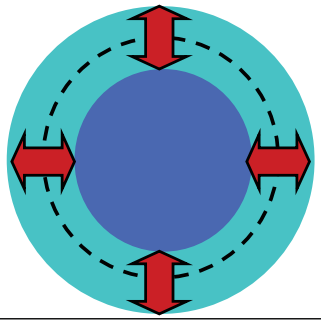

Isoscalar monopole response

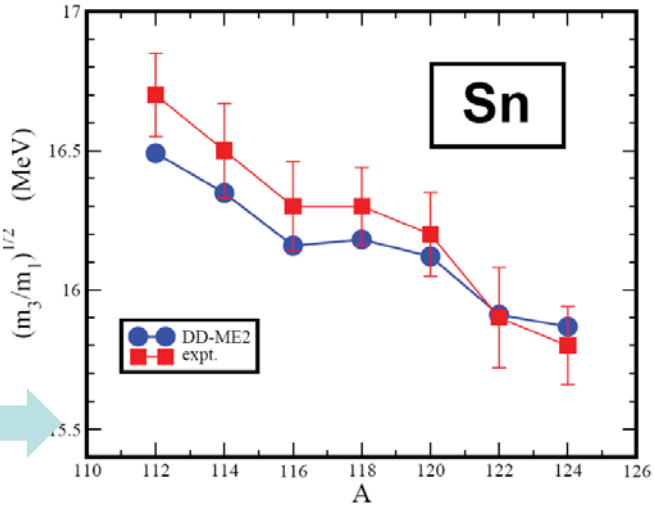

U.Garg: Monopole-resonance and compressibility:

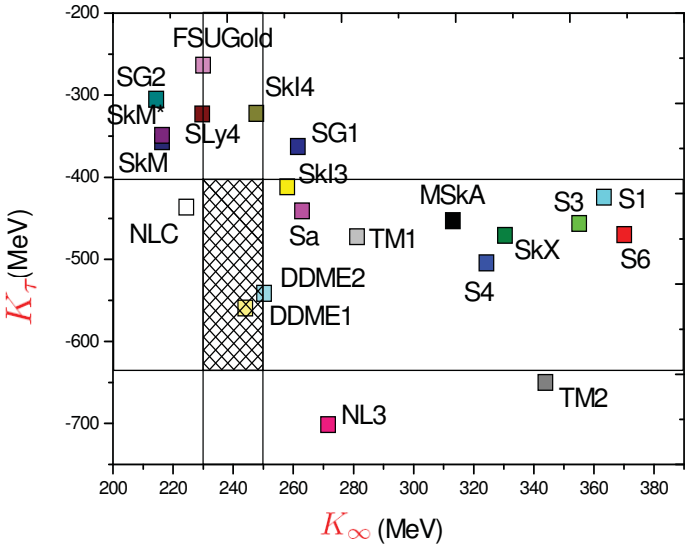

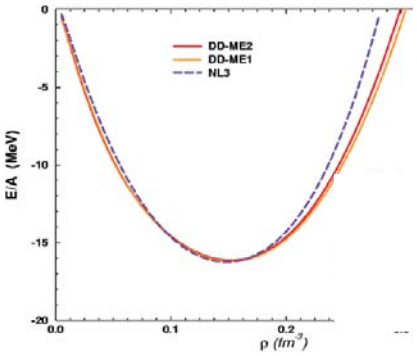

$$E_{GDR} = \hbar\sqrt{\frac{K_A}{m\langle r^2\rangle}}$$

$$K_A \approx K_\infty(1+cA^{-1/3})+K_\tau((N-Z)/A)^2+K_{\text{coul}}Z^2A^{-4/3}$$

c ≈ -1

Soft dipole modes and neutron skin:

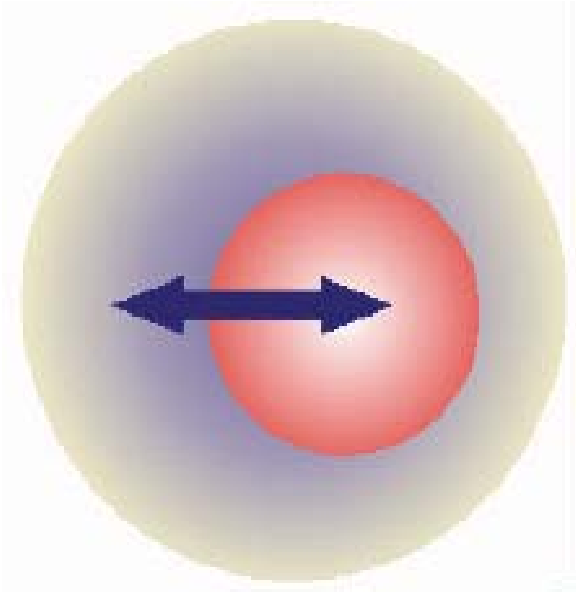

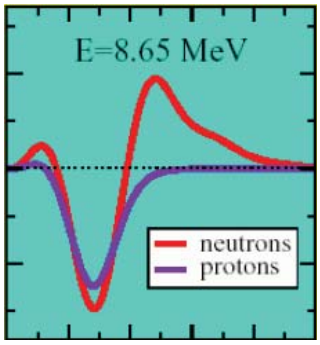

IV Dipole Strength for ^{208}Pb and transition densities for the peaks at 7.29 MeV and 12.95 MeV

Vretenar, Paar, Ring, Lalazissis, Phys. Rev. C63, 047301 (2001)

Exp GDR at 13.3 MeV

Exp PYGMY centroid at 7.37 MeV

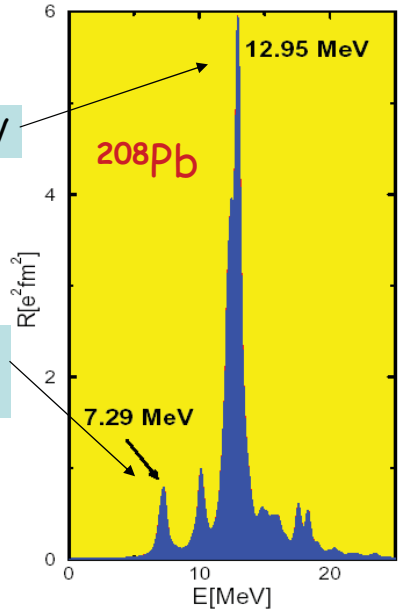

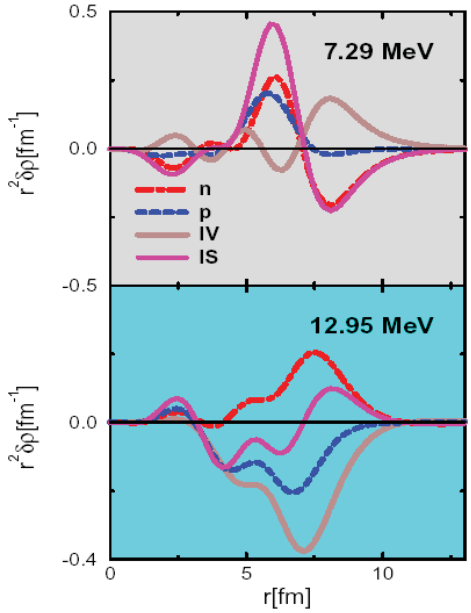

In heavier nuclei low-lying dipole states appear that are characterized by a more distributed structure of the RQRPA amplitude.

Among several single-particle transitions, a single collective dipole state is found below 10 MeV and its amplitude represents a coherent superposition of many neutron particle-hole configurations.

Evolution of isovector dipole strength in Sn isotopes:

Transition densities

Transition densities

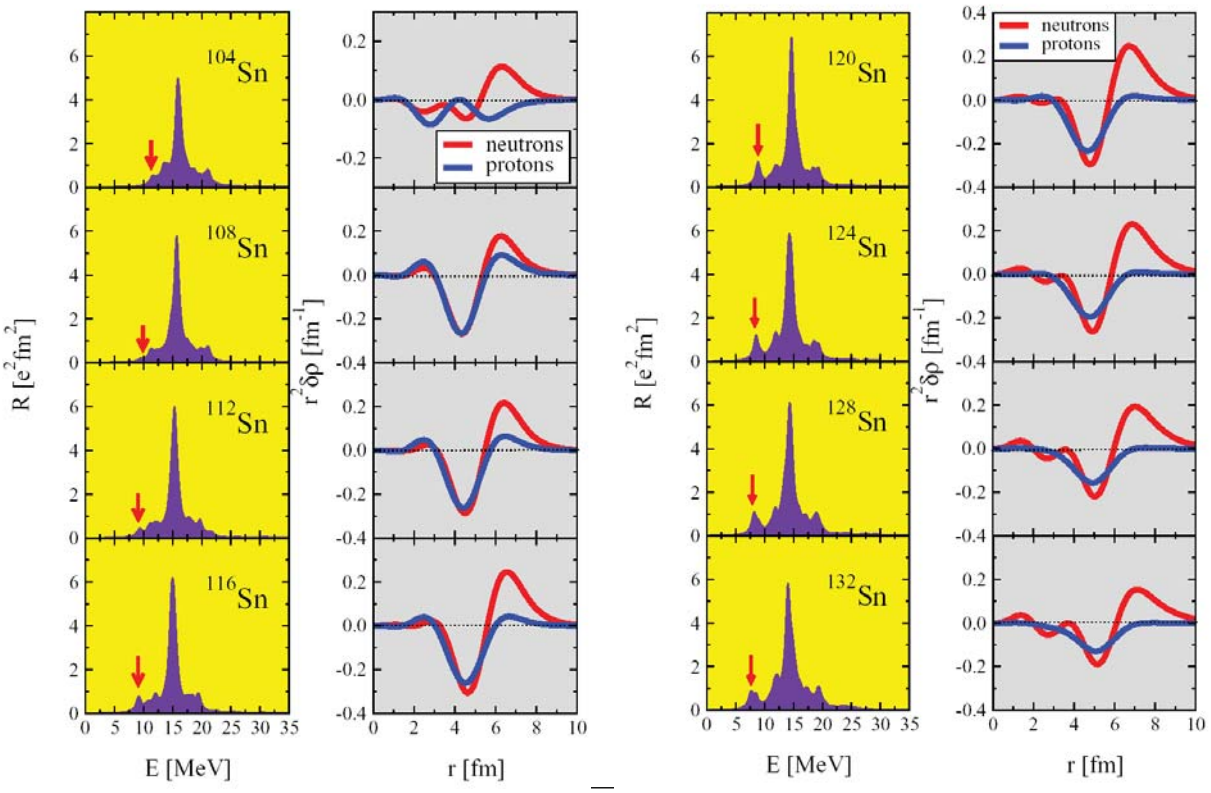

Model dependence of the results for the PDR

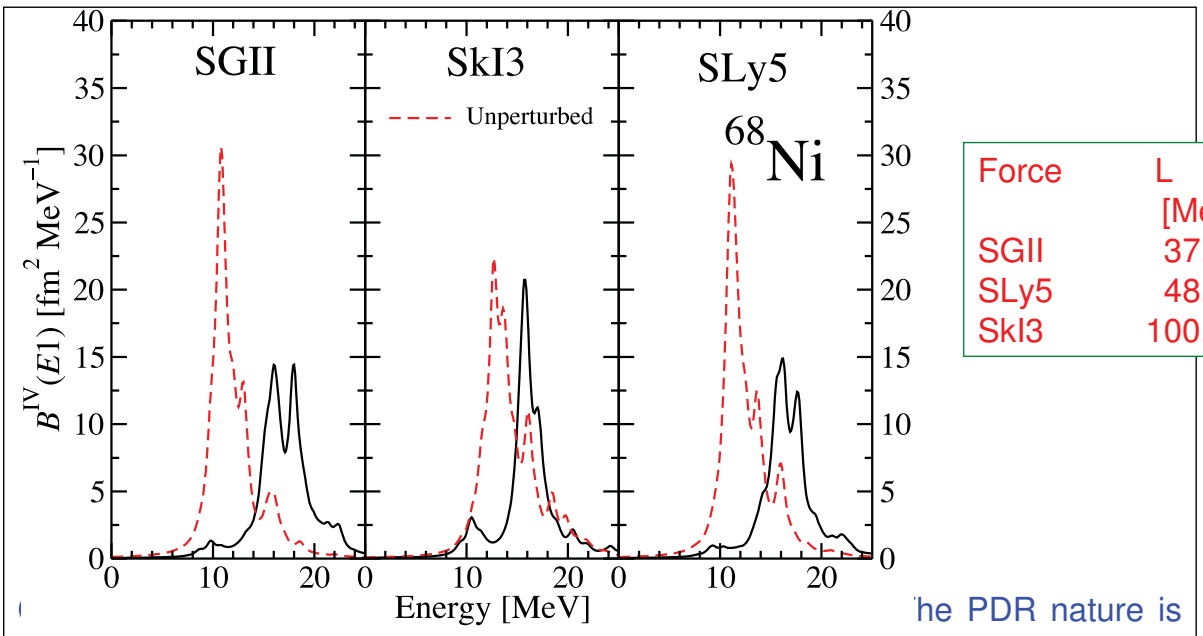

Force	L [MeV]
SGII	37.6
SLy5	48.3
SkI3	100.5

(…) he PDR nature is model-dependent. DD-ME2 calculations show even more collective low-E peak (cf. N. Paar).

Gianluca Colo, Primosten 2011

Pygmy dipole resonance

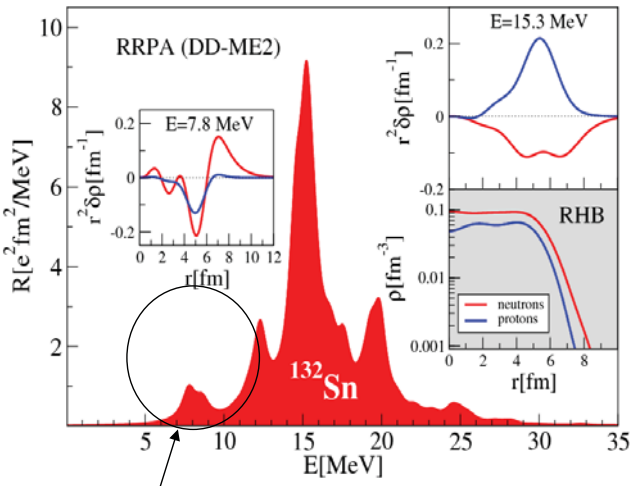

^{132}Sn at 7.6 MeV	
28.2%	$2d_{3/2} \rightarrow 2f_{5/2}$
21.9%	$2d_{5/2} \rightarrow 2f_{7/2}$
19.7%	$2d_{3/2} \rightarrow 3p_{1/2}$
10.5%	$1h_{11/2} \rightarrow 1i_{13/2}$
3.5%	$2d_{5/2} \rightarrow 3p_{3/2}$
1.9%	$1g_{7/2} \rightarrow 2f_{5/2}$
1.5%	$1g_{7/2} \rightarrow 1h_{9/2}$
0.6%	$1g_{7/2} \rightarrow 2f_{7/2}$
0.6%	$2d_{3/2} \rightarrow 3p_{3/2}$

Opening of the closed neutron shell increases collectivity !

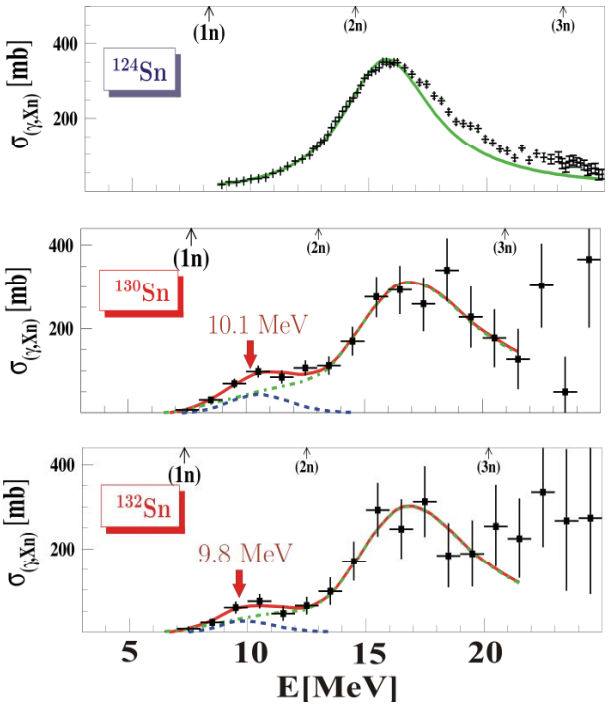

P.Adrich et al., Phys. Rev. Lett. 95, 132501(2005).

response of the nucleus to an incoming particle

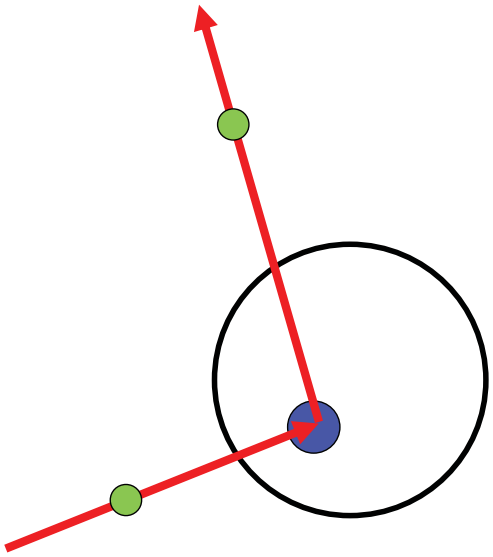

scattering at a single nucleon

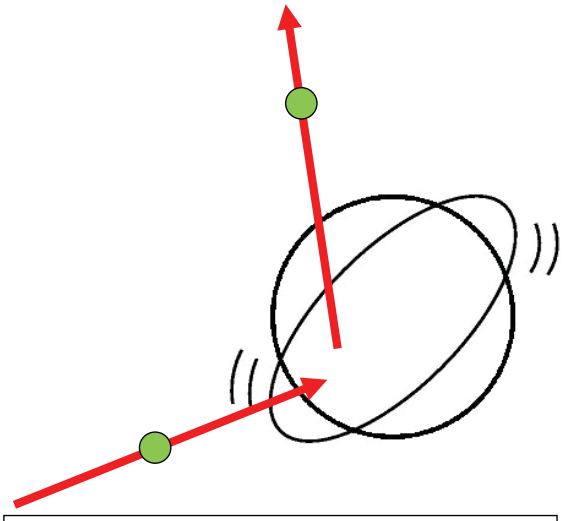

excitation of the entire nucleus
we need the nuclear spectrum

neutrino scattering

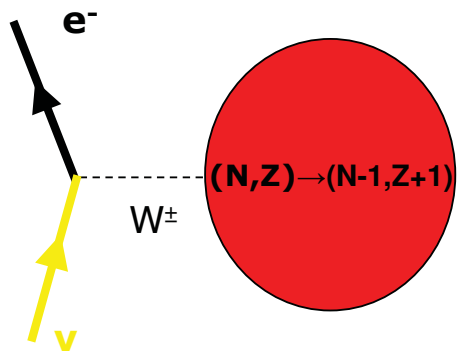

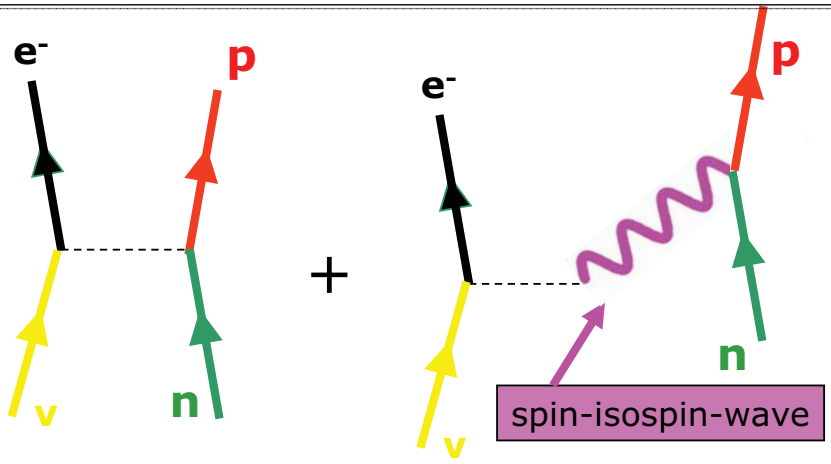

Spin-Isospin Resonances: IAR - GTR

Z,N **Z+1,N-1**

$$|GTR\rangle = S_- T_+ |Z,N\rangle$$

spin flip σ

$$|Z,N\rangle \longrightarrow |IAR\rangle = T_+ |Z,N\rangle$$

isospin flip τ

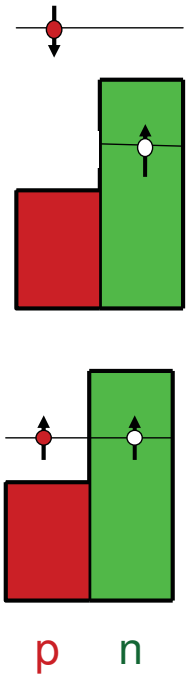

$$E_{GTR} - E_{IAR} \sim \Delta(l \cdot s) \sim \frac{dV}{dr} \sim \text{neutron skin} = r_n - r_p$$

Spin-Isospin Resonances: IAR - GTR

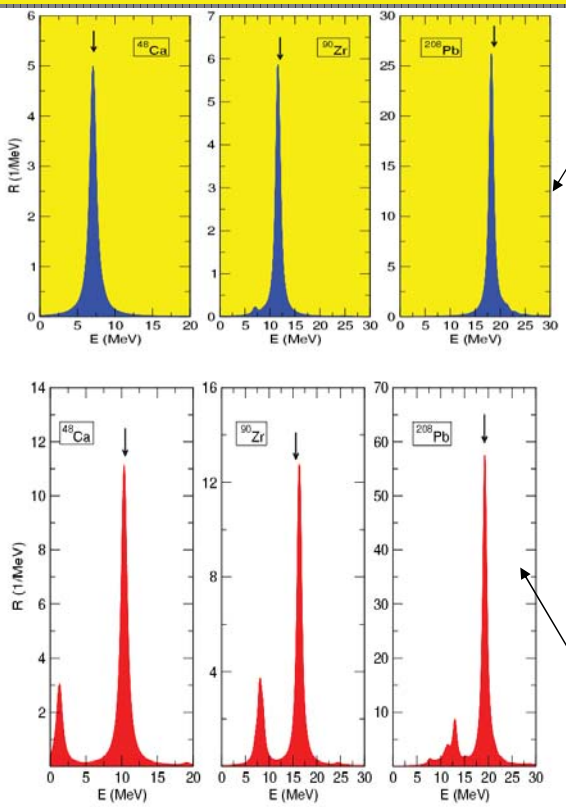

ISOSPIN-FLIP EXCITATIONS

$T^F_{\beta^\pm} = \sum_{i=1}^{A} \tau_\pm$

S=0 T=1 $J^\pi = 0^+$

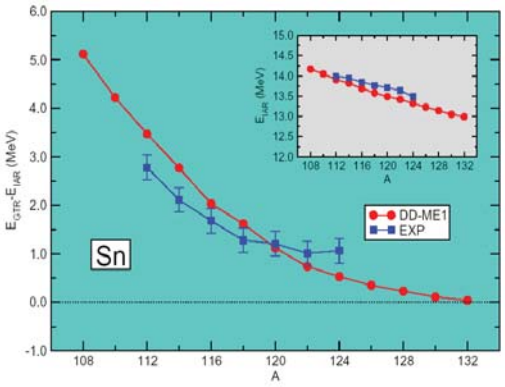

S=1 T=1 $J^\pi = 1^+$

SPIN-FLIP & ISOSPIN-FLIP EXCITATIONS

$T^{GT}_{\beta^\pm} = \sum_{i=1}^{A} \Sigma\tau_\pm$

PR C69, 054303 (2004)

Distribution of neutrino cross section over multipolarities:

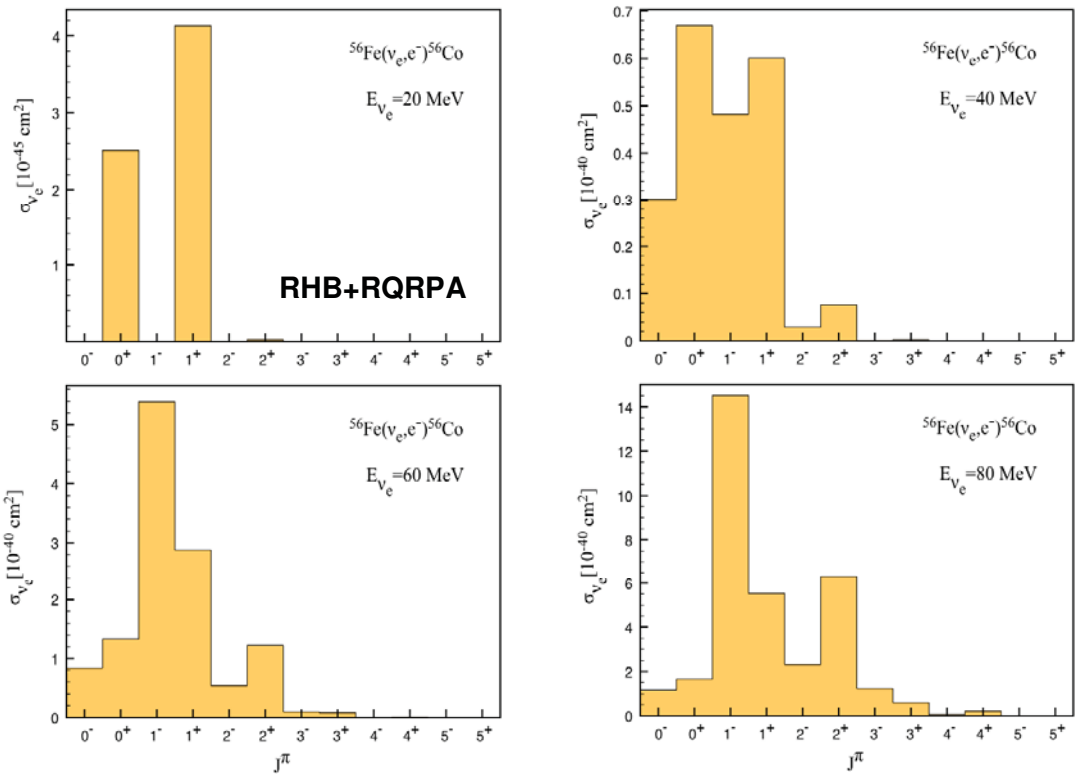

Cross section (ν_e,e^-) averaged over the supernova neutrino flux

$$\langle \sigma_\nu \rangle = \frac{\int dE_\nu \sigma_\nu(E_\nu) f(E_\nu)}{\int dE'_\nu f(E'_\nu)}$$

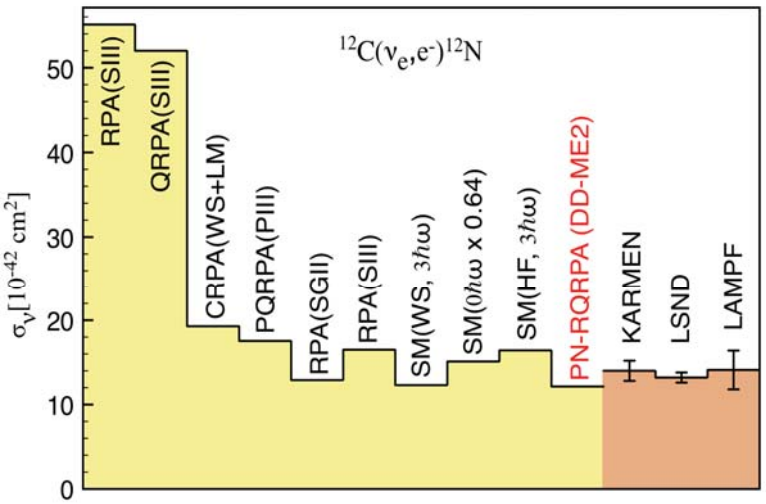

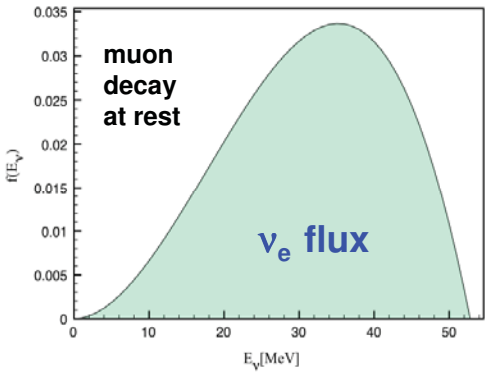

Content:

- Motivation
- Density Functional Theory
- The Nuclear Density Functional
- Covariant Density Functionals
- Ground state properties
- Nuclear dynamics and excitations
- Beyond mean field
- Outlook

Problems with the mean field description:

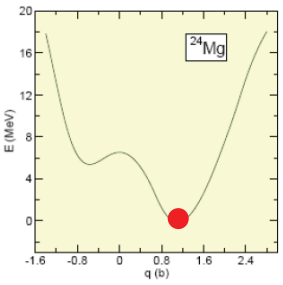

- **Fluctuations** are neglected
  solution: **GCM:** configuration mixing in transitional nu

J.M. Yao

- **Symmetries** are broken
  no spectroscopy
  solution: **Projection** to good quantum numbers
  derivation of a **Bohr Hamiltonian**

$$|\Psi\rangle = \int dq\, f(q)\,|q\rangle$$

Niksic, Z.P. Li

- **Energy dependence** of the self-energy is neglected
  low level density at the Fermi surface (arches in the masses)
  no coupling to many-particle many-hole states in Giant Resonances

  solution: **PVC**: coupling to surface vibrations
  and complex configurations

Litvinova

Particle-vibrational coupling: energy dependent self-energy

$$\Sigma = S + V + \Sigma(\omega)$$

mean field | pole part

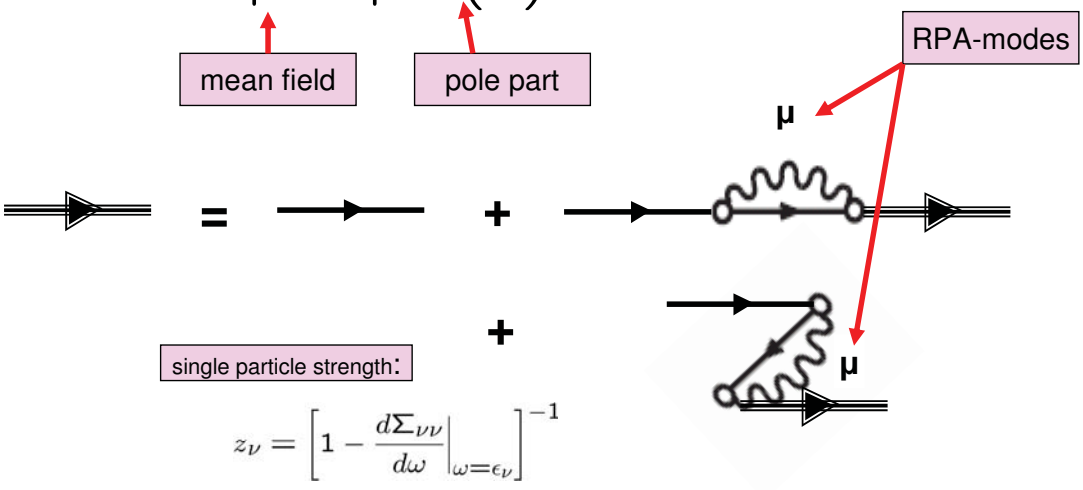

single particle strength:

$$z_\nu = \left[1 - \left.\frac{d\Sigma_{\nu\nu}}{d\omega}\right|_{\omega=\epsilon_\nu}\right]^{-1}$$

Density functional theory - Landau-Migdal theory

Coupling to complex configurations in the GDR:

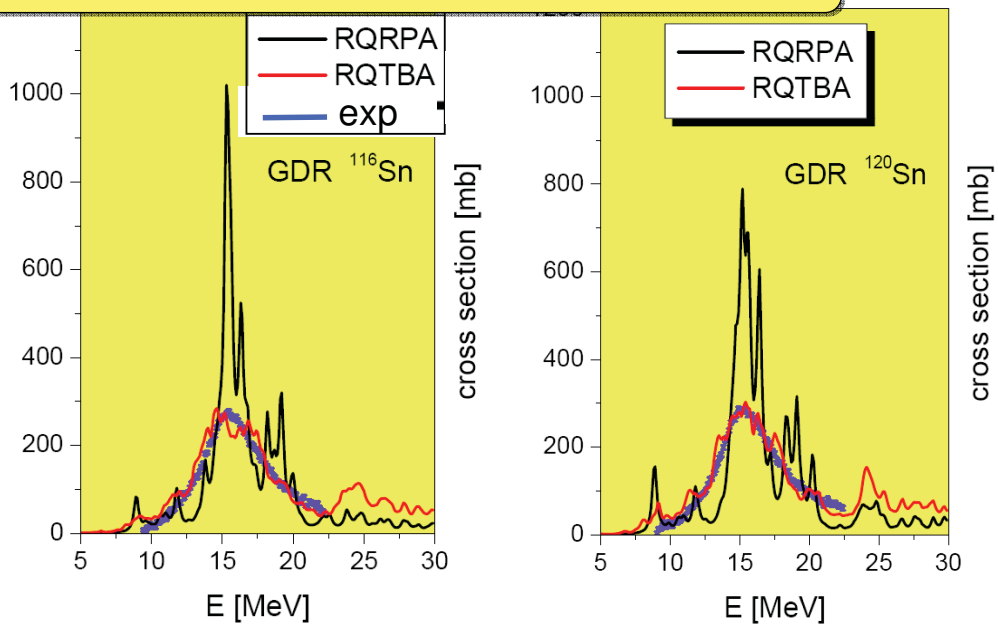

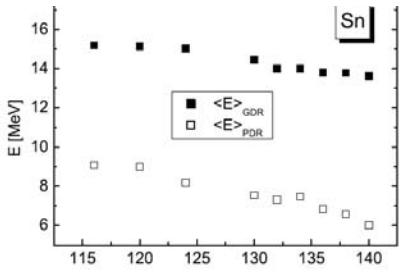

centroid energies for
GDR and PDR

Litvinova, P.R. Tselyaev, PRC 78, 14312 (2008)
Litvinova, P.R. Tselyaev, Langanke, PRC 79, 054312 (2009)

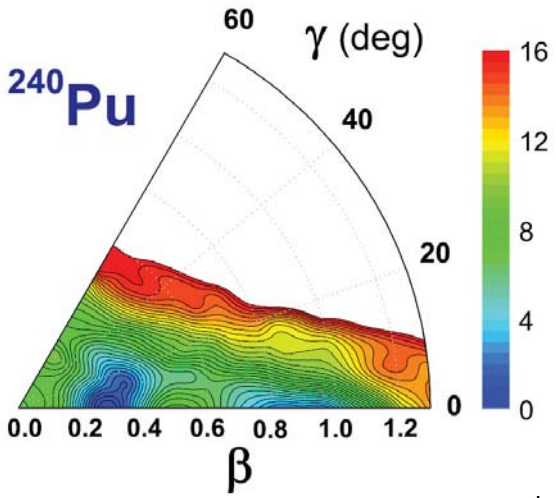

Fission barrier and super-deformed bands in ^{240}Pu

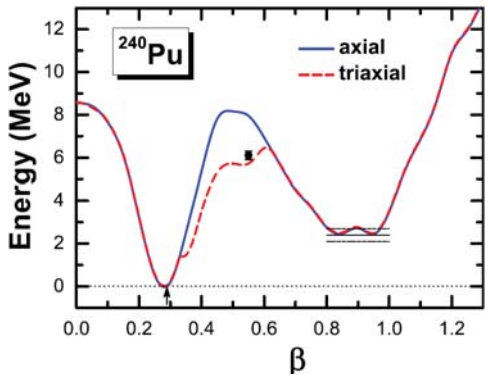

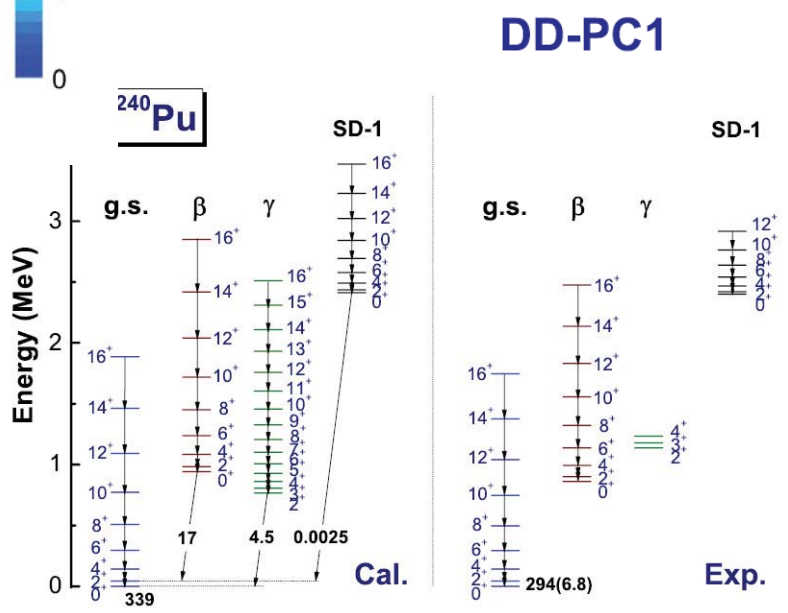

Conclusions:

Covariant density functional theory is technically more complicated

There are many good reasons to treat relativity seriously.

Relativistic kinematics is not amongst them.

Relativistic effects can be represented also in a non-relativistic functional, e.g. spin-orbit.

This leads to an increased number of parameters, difficult to handle

Present rel. functionals have a sophisticated density dependence

There is still a long way to go for an ab initio derivation

Collaborators:

A. Afanasjev (Mississippi)
A. Ansari (Bhubaneshwar)
I. Daoutidis (Brussels)
D. Peña (Orsay)

G. A. Lalazissis (Thessaloniki)

E. Litvinova (GSI)
V. Tselayev (St. Petersburg)

T. Niksic (Zagreb)
N. Paar (Zagreb)
D. Vretenar (Zagreb)

Z.-P. Li (Chonqing)
J.M. Yao (Chonqing)

W.H. Long (Lanchow)

L.L. Li (Beijing)
Z.-P. Li (Beijing)
H.Z. Liang (Beijing)
J. Peng (Beijing)
J. Meng (Beijing)
L.F. Yu (Beijing)
S.Q. Zang (Beijing)
P.-W. Zhao (Beijing)
S.-G. Zhou (Beijing)

Literature:

Gambhir et al, Ann. Phys. NY. 198, 132 (1990)
Ring, Prog. Part. Nucl. Phys. 37, 193 (1996)
Vretenar et al, Phys. Rep. 409, 101 (2005)
Meng et al, Prog. Part. Nucl. Phys. 57, 470 (2006)
Paar et al, Rep. Prog. Phys. 79, 691 (2007)
Ring et al, Phys. At. Nucl. 72, 1285 (2007)
Niksic et al, Prog. Part. Nucl. Phys. 66, 519 (2011)

„Extended Density Functional Theory in Nuclear Structure Physics“
Lecture Notes in Physics, Vol 641, Eds. Lalazissis et al
Springer Verlag Heidelberg, 2004

New generation of Nuclear Physics with RIBF

H. Sakurai
櫻井　博儀

Univ. of Tokyo/ RIKEN

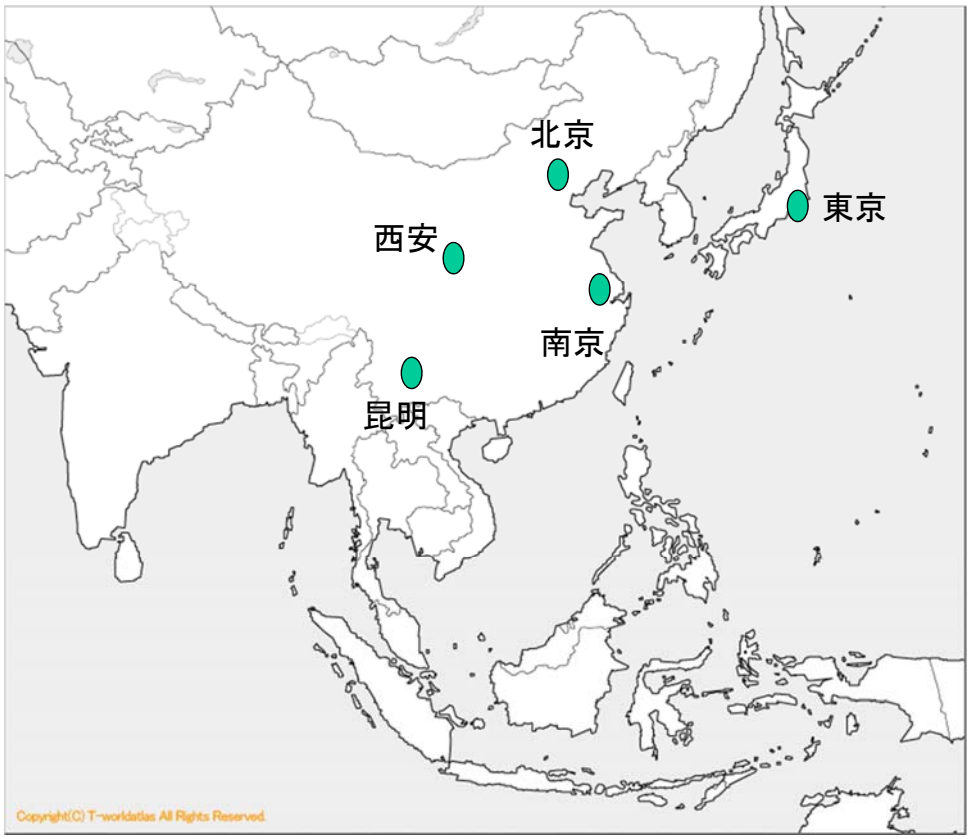

RI=Radioactive Isotope B=Beam F=Factory
Mass production of radioactive isotopes as secondary beams

Exploration of the Limit of Existence

stable nuclei	~300 nuclei
unstable nuclei observed so far	~2700 nuclei
drip-lines (limit of existence)（theoretical predictions)	~6000 nuclei
magic numbers	

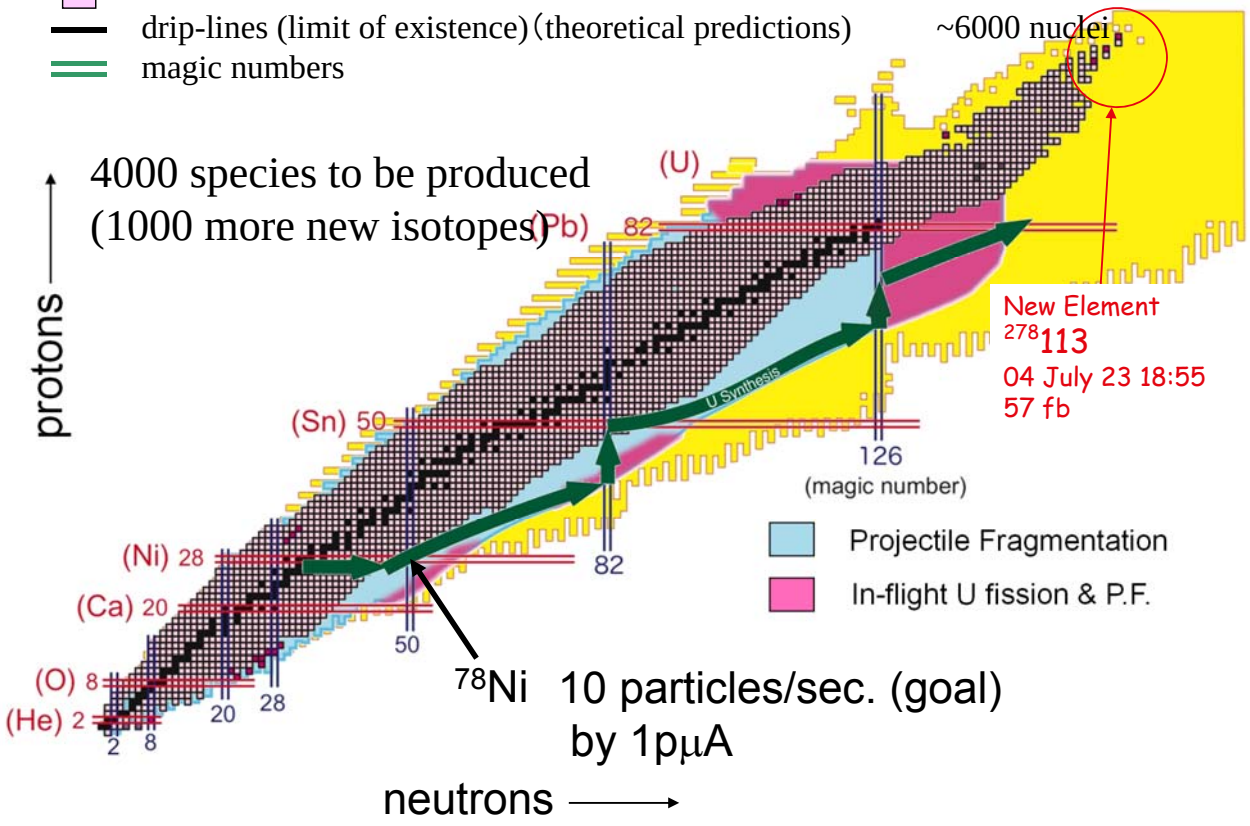

In-flight Production Method of RI beam

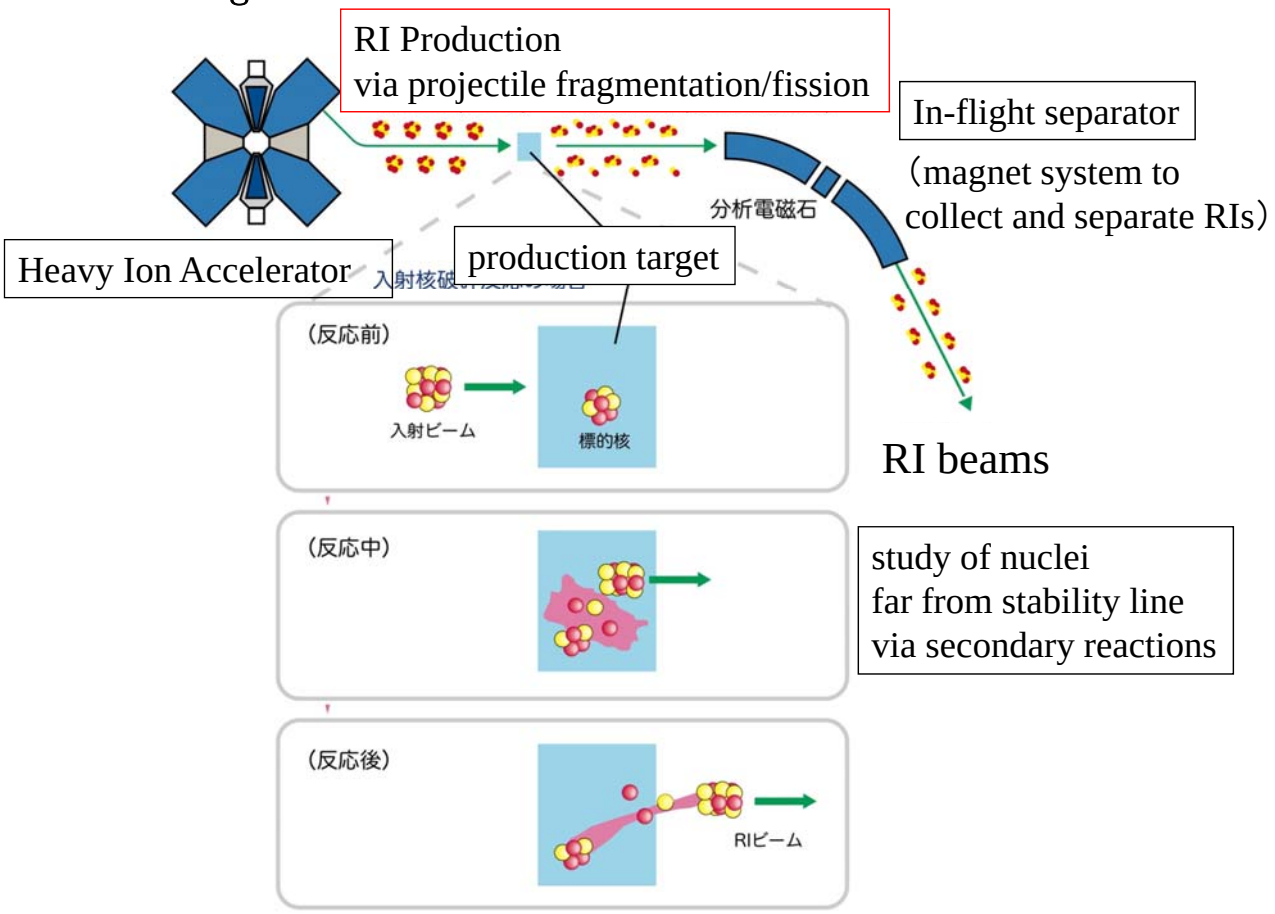

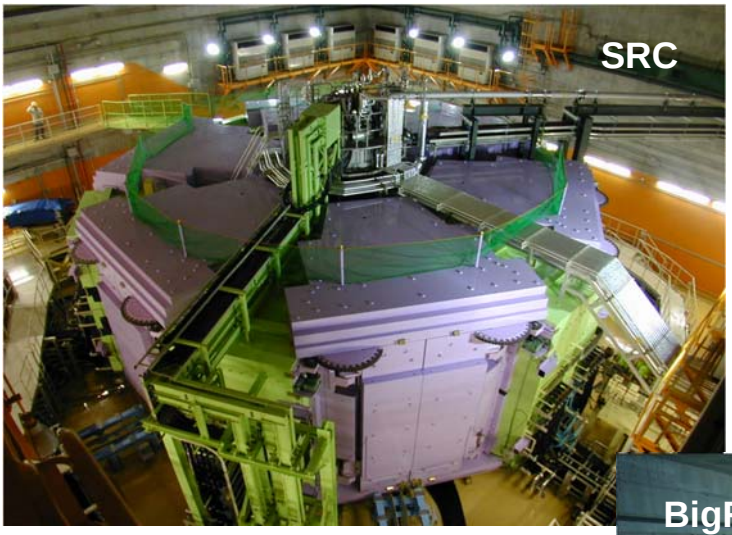

Superconducting Ring Cyclotron

World's First and Strongest K2600MeV

400 MeV/u Light-ion beam
345 MeV/u Uranium beam

BigRIPS In-flight Separator

World's Largest Acceptance
9 Tm
Superconducting RI beam Separator

~250-300 MeV/nucleon RIB

History of In-flight Method

0th Generation (70's) LBL
"Discovery" of Projectile Fragmentation

1st Generation (80's) GANIL/LISE LISE was originally designed for atomic-physics
Establishment of Separation Technique Bρ-ΔE-Bρ Method

2nd Generation (90's) GSI/FRS, NSCL/A1200-1900, GANIL/SISSI, RIKEN/RIPS
High-Collection Technique

Max. Bρ and Large Acceptances	RIKEN/RIPS
Emittance-transformation	GANIL/SISSI
Further Purification Methods	
ExB filter	GANIL/LISE
rf-deflector	RIKEN/RIPS
In-flight Fission for neutron-rich nuclei	GSI/FRS
Combination of Separator+Spectrometer	GANIL, NSCL, GSI

3rd Generation (00's-10's) RIKEN/RIBF, GSI/FAIR, USA/RIA
High-Power Heavy-Ion Beams up to U

Energy Dependence of RI Yields

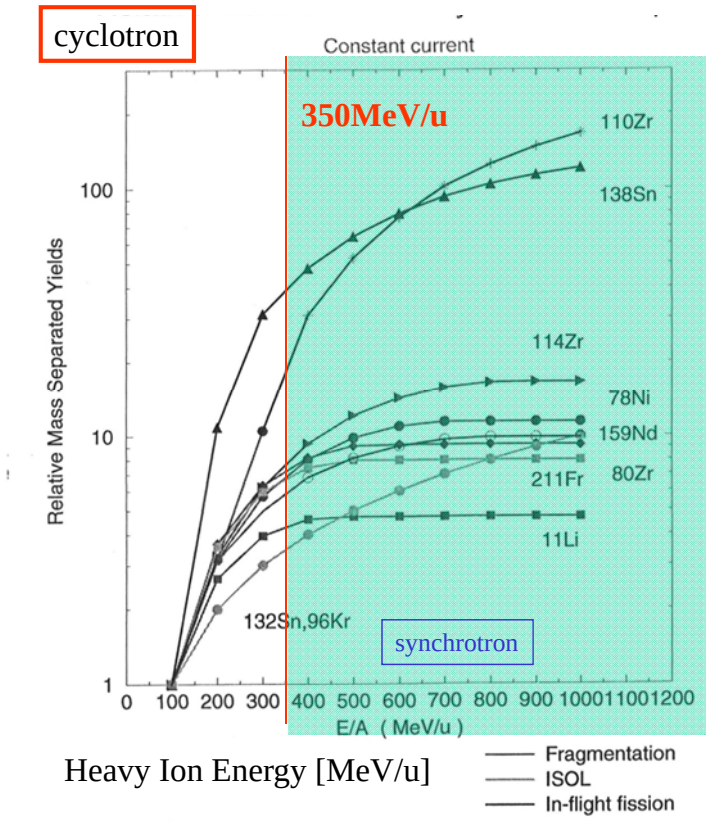

Heavy Ion Energy [MeV/u]

Cyclotron provides more intense beams than synchrotron.

Acceleration Flow in RI Beam Production

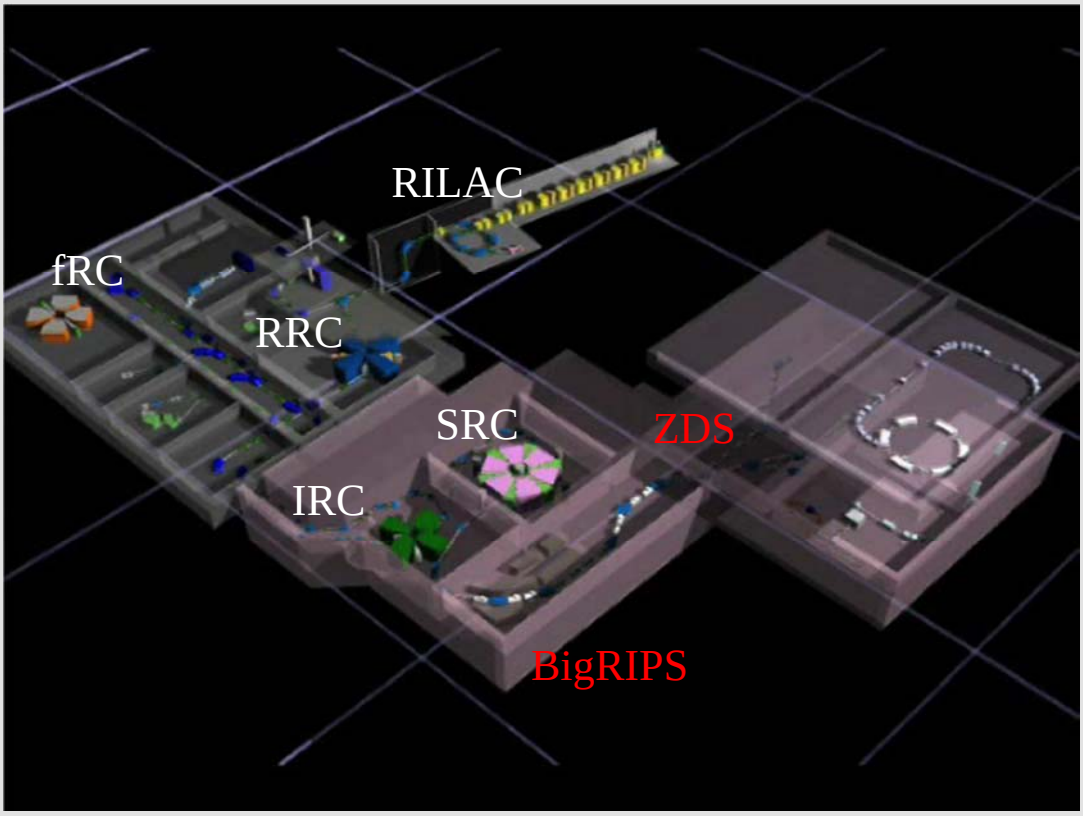

by Narumasa Miyauchi

First beam accelerated at SRC K2600MeV

16:00 28th Dec., 2006 $^{27}Al^{10+}$ 345MeV/u

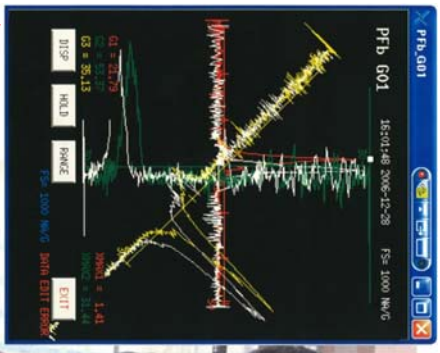

Large-scaled Facilities in the world

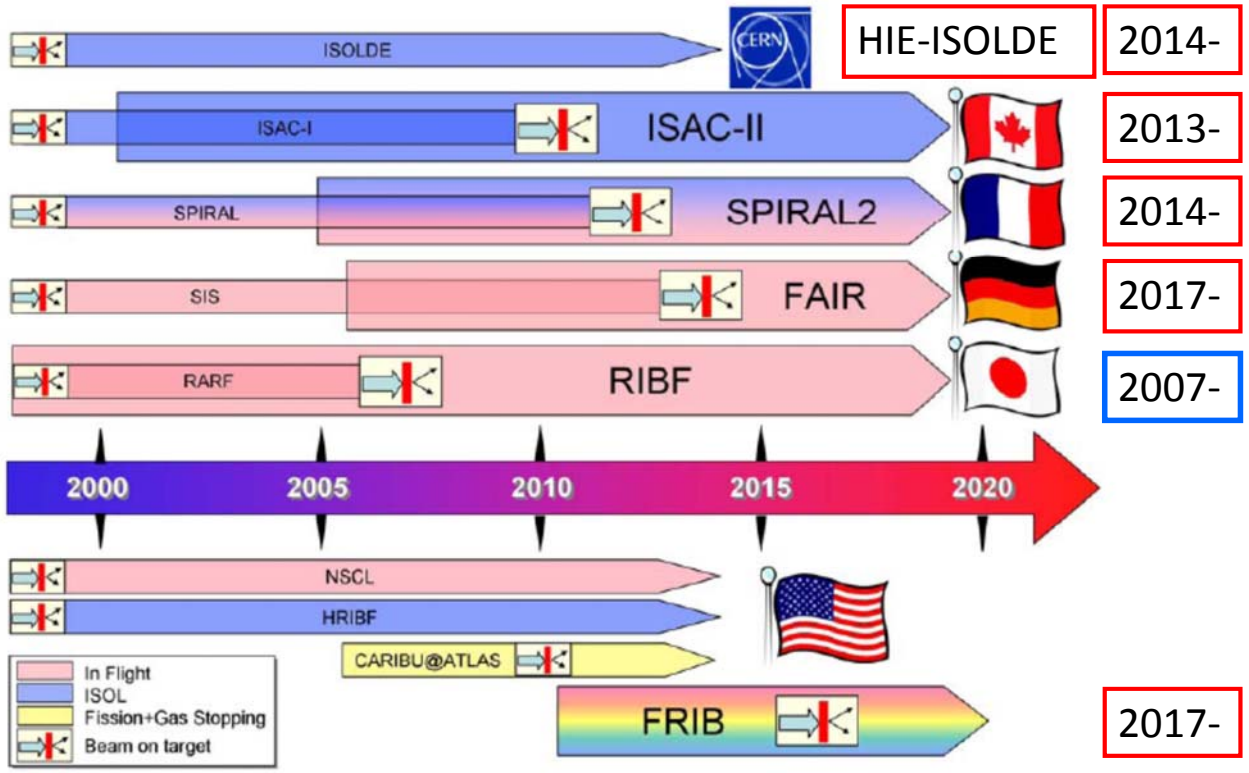

In-flight and ISOL methods to produce radioactive ions

In-Flight Method

High energy, large variety of species, Poor optical qualities

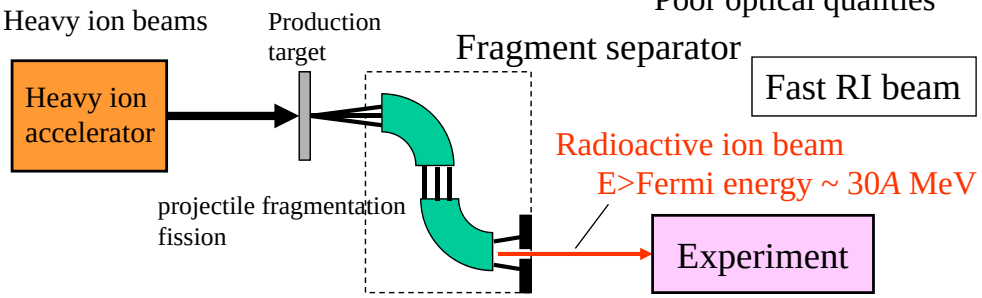

ISOL Method

Low energy, chemistry is difficult, good beam qualities

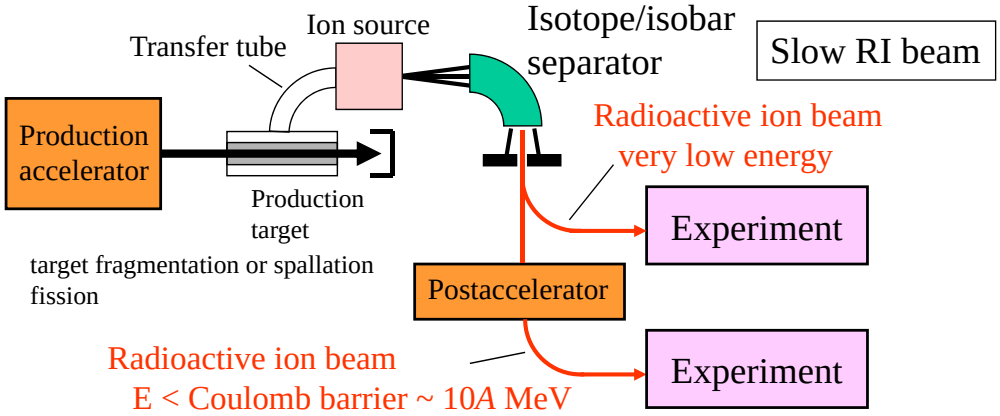

New experimental techniques to have very slow RI beams

RIKEN, NSCL/MSU, ANL

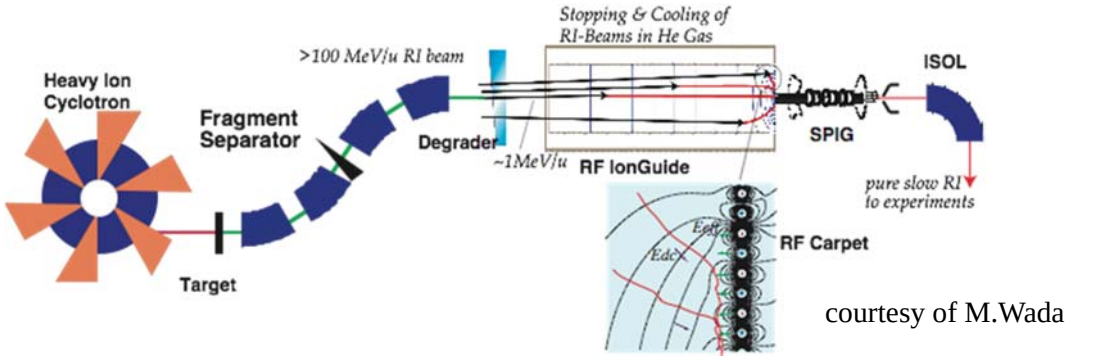

In-flight Method | Gas-catcher system | ISOL

High energy, large variety of species,
Poor optical qualities → large variety of species, good optical qualities, nice purity

Large-scaled facilities in operation and proposed in East Asia

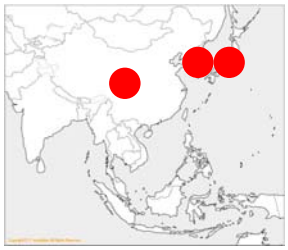

RIBF (RIKEN)
In-flight

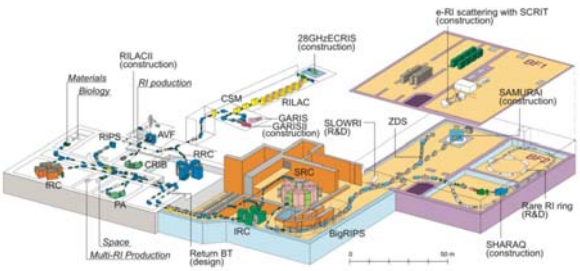

IMP

HIRFL (IMP)
In-flight + Ring

BRIF project (CIAE) ISOL
HIAF project(IMP) In-flight
ADS project (CAS)

KoRIA Project
ISOL+In-Flight+ISOL

RIKEN RI Beam Factory (RIBF)

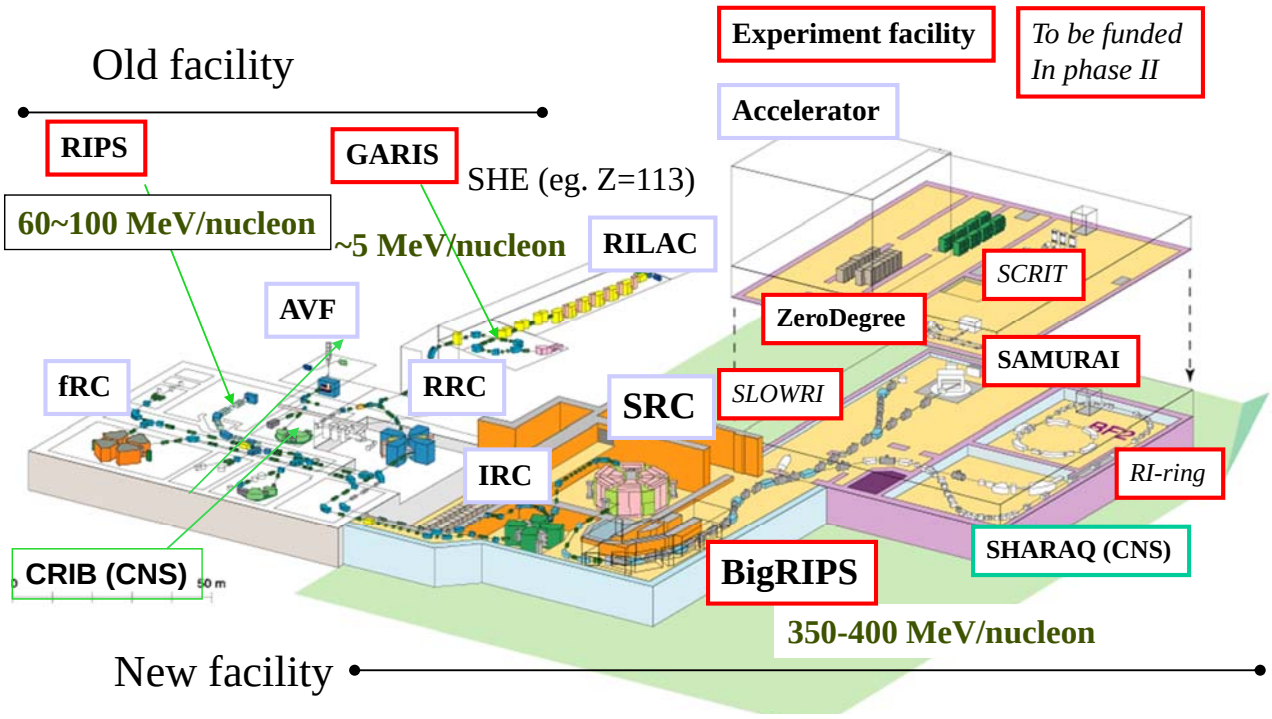

Intense (80 kW max.) H.I. beams (up to U) of 345*A*MeV at SRC
Fast RI beams by projectile fragmentation and U-fission at BigRIPS
Operation since 2007

Three Challenges of RIBF

1 To Establish New Framework of Nuclear Physics

2 To Elucidate the Origin of Elements

3 To Explore New Applications with fast RI Beams

Exploration of the Limit of Existence

stable nuclei ~300 nuclei
unstable nuclei observed so far ~2700 nuclei
drip-lines (limit of existence)（theoretical predictions) ~6000 nuclei
magic numbers

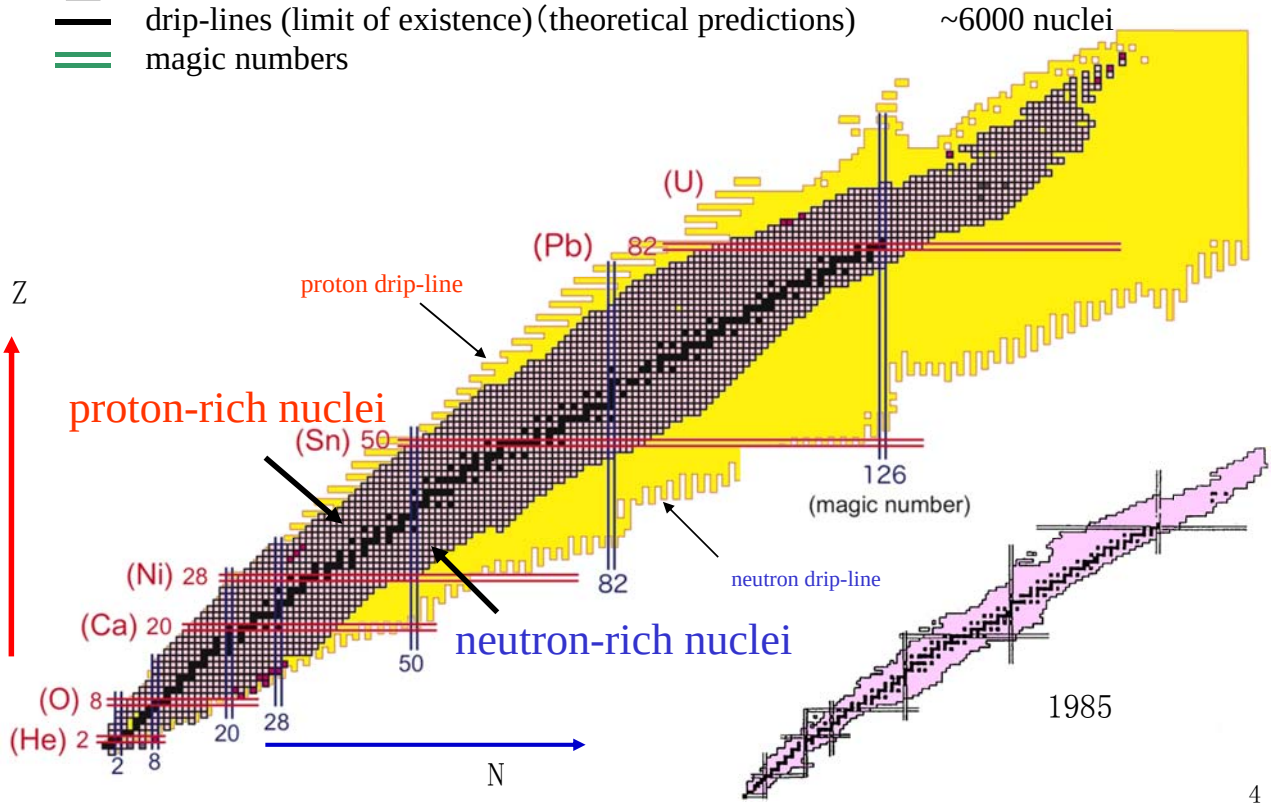

New frameworks for the new region of nuclear chart

Nuclear Structure: Shell evolution

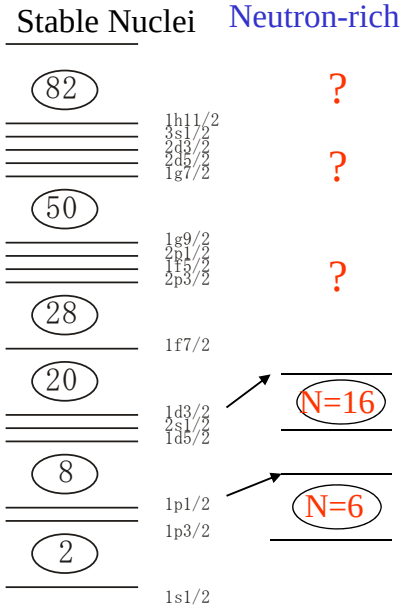

Nuclear Matter: New forms

neutron-skin nuclei

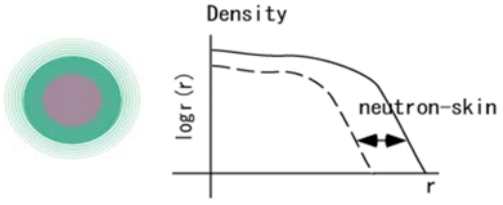

neutron-halo nuclei

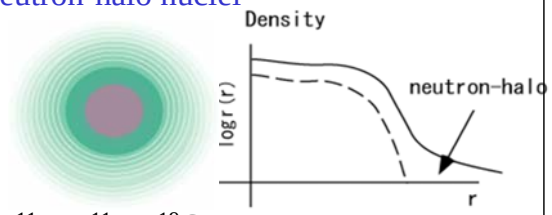

^{11}Be, ^{11}Li, ^{19}C...

To write up new text book： Exotic phenomena, Systematics, etc.
Isospin-, density-dependences of effective interactions, nucleon-corrections
Microscopic system (nuclei) to Macroscopic system (neutron stars)

Liberation from Stable Region and Exotic Nuclei

Shell Evolution : magicity loss and new magicity

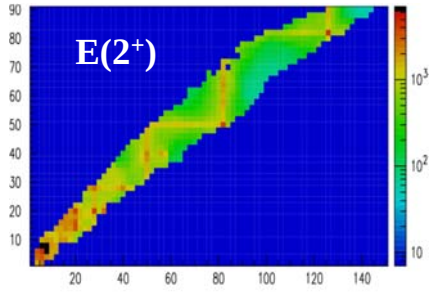

Shape ?
Shell gap ?
Single particle level ?
Cluster formation?
Role of 3NF ?
Magicity loss ?
50、82、126、184

Spherical Deformed

Dynamics of new "material" : Neutron-skin（halo）

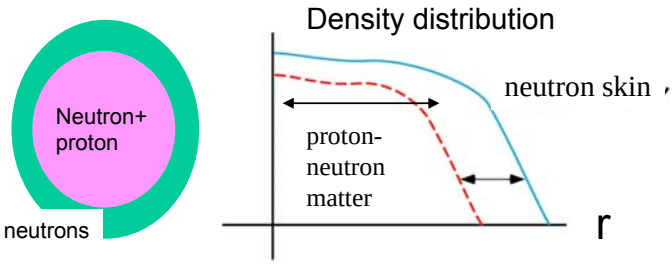

Skin thickness ? Density distribution ?
Role of skin in reactions ?
Pairing in skin ? di-neutrons?
Exotic modes of skin ?

RIBF provides data for nuclei far from the stability line

Challenges in establishing new frame work of nuclear physics

Challenge for r-process path and explosion in supernovae

Synthesis up to U （r-process）

unknown neutron-rich nuclei
theoretical predictions only

Necessary of experimental investigation for nuclear properties of heavy and neutron-rich nuclei
Mass, life-time, decay mode

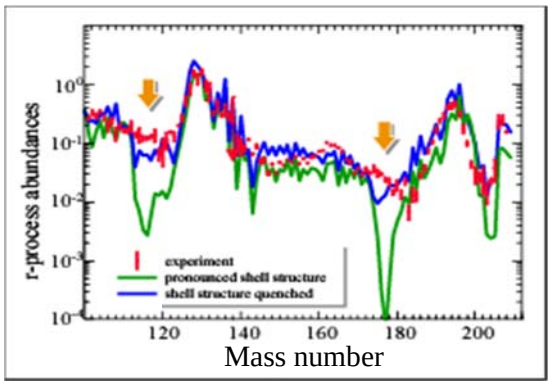

Explosion mechanism of supernova

No explosion in theoretical works
Outer clast of neutron star

Necessary of experimental study for Equation-of-State for nuclear matter

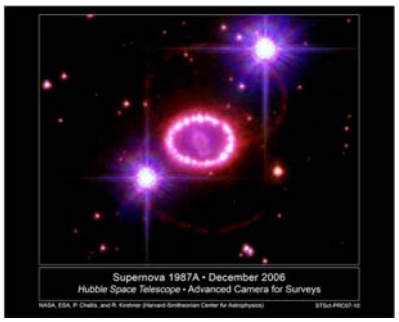

1987A

Challenge to investigate EOS of neutron matter

from nuclei to neutron stars

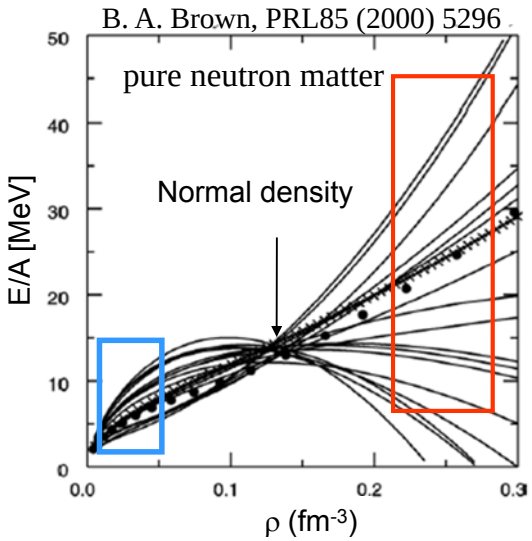

3NF
T=3/2 channels?
density dependence?

Elastic d+p for T=1/2
Nuclear structure in
very neutron-rich nuclei for T=3/2?
Heavy-ion Collisions to achieve ρ~2-3ρ0 ?

$^3P_2$ correlation
pairing gap?
Density depencence?

????

^1S correlation
BCS-BEC crossover
in dilute system ($\rho \sim 0.1\rho_0$) ?

Role of di-neutron in skin? : collectivity, transfer reactions

New Devices of RIBF

To maximize the potentials of intense RI beams available at RIBF

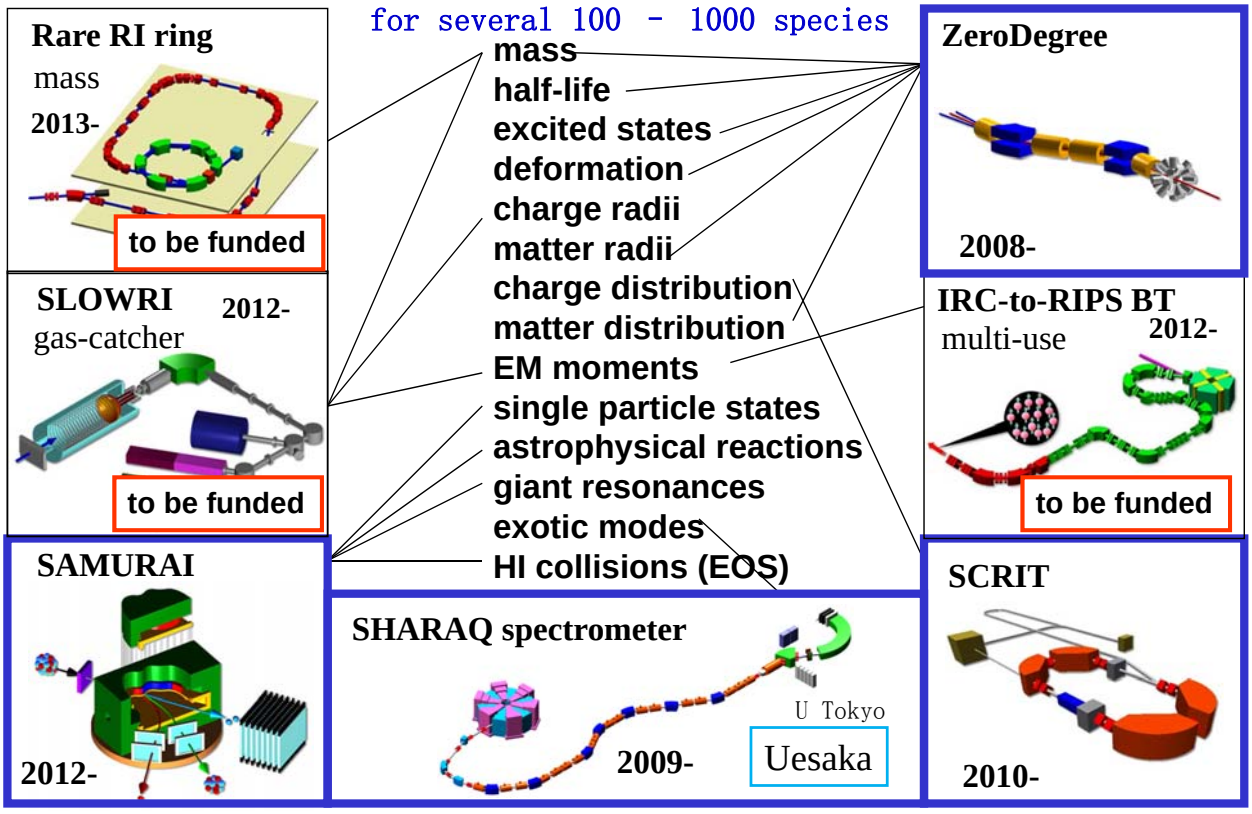

Program for nuclear structure and matter at RIBF

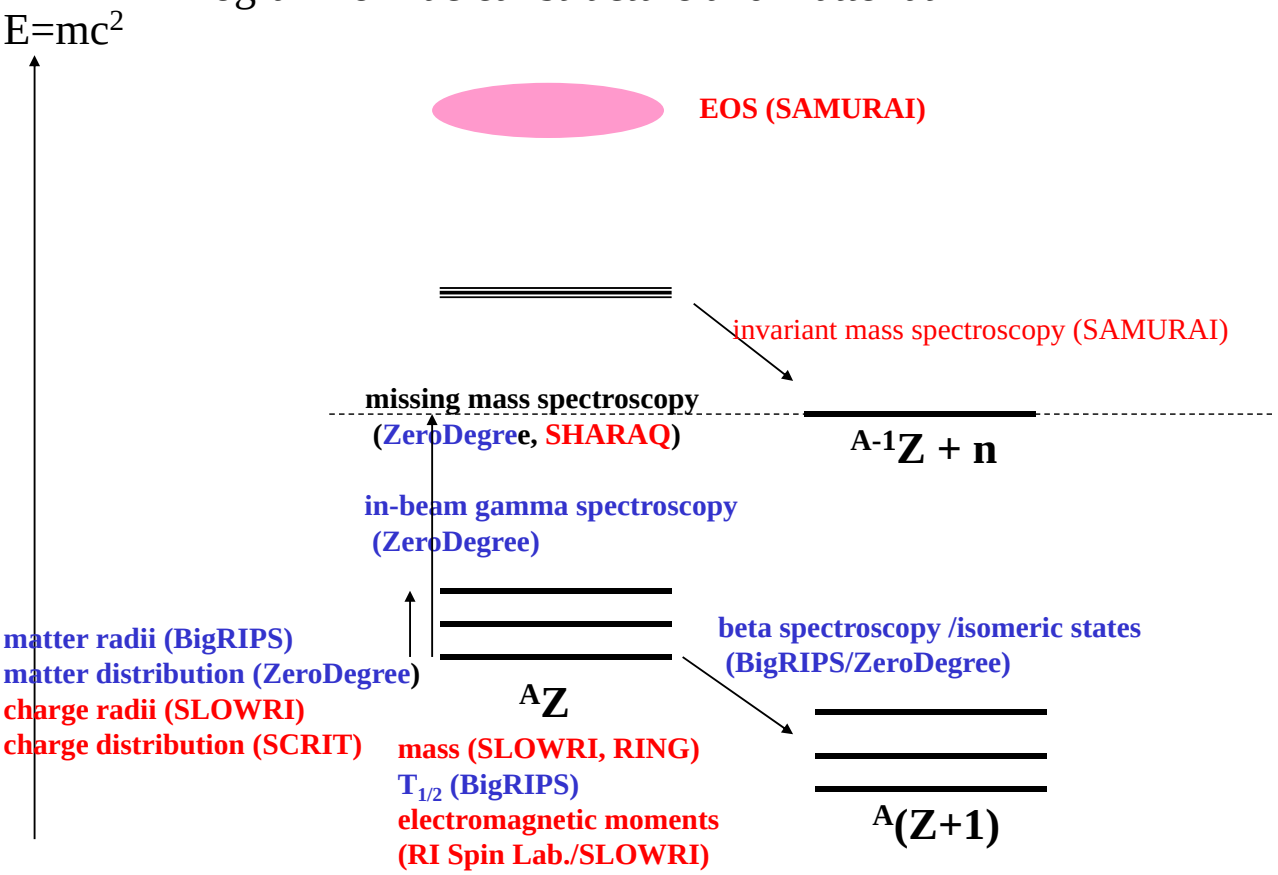

Experimental Devices available at the new facility in 2009

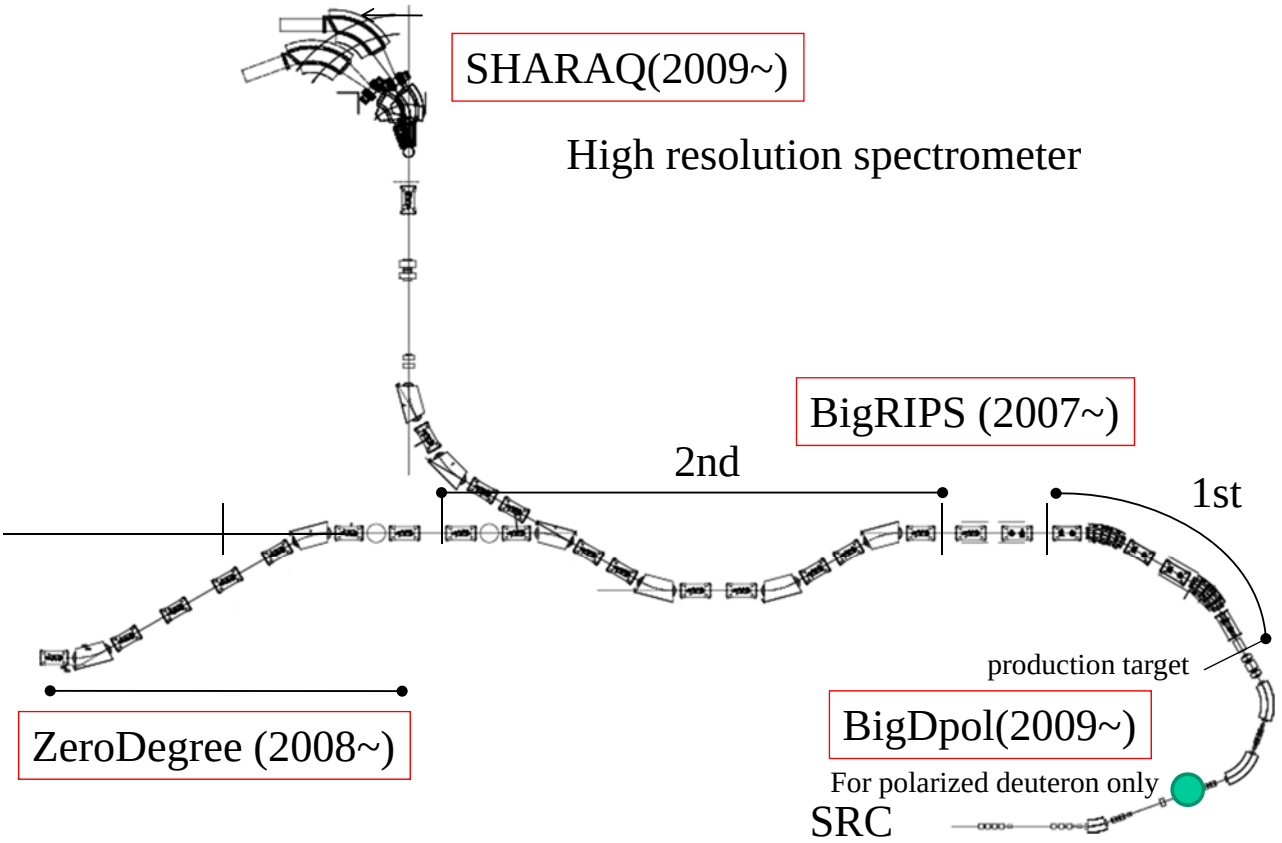

Programs at BigRIPS/ZeroDegree 2007~

Rare-Isotope Physics Programs

Fast RI beam production to search for new isotopes

Global survey to search for anomalous regions

Specific programs with deuteron beams

BigRIPS in-flight production of fast rare-isotope beams

Ground state properties and low lying excited states via decay spectroscopy / transmission method:
particle stability, $T_{1/2}$, Q_β, σ_R, Ex.(2^+)...

Deeply bound pionic states via (d, ^{3}He) at 500 MeV

Three-body force via pol. d+p elastic scattering at 700 MeV

ZeroDegree multi-function beam line for inclusive/semi-inclusive measurements
production of 3rd RI beams

Collectivity and matter distribution via in-beam gamma / missing mass spectroscopy

One step energy regime 200~300 A MeV
B(E2), B(M1), (p,p), (p,p'), Ex....

Iso-diffusion

ICW06

Delivery of tagged RI-beam

Based on two-stage separator scheme

T. Kubo et al.

Identify RI-beam species Z, A/Q by measuring ΔE, Bρ, TOF in an event-by-event mode using beam-line detectors on the 2nd stage. Aim at tagging rate up to 1 x 10^6 pps.

Standard		New Scheme
Bρ-TOF-dE-**E**	⟶	Bρ-TOF-dE
Z, A, Q		Z, A/Q

PID to determine Z and A

Standard Technique

Z=Q case

TOF $1/\beta$

ΔE Z^2/β^2 (non-relativistic approx.)

$B\rho$ $A/Z*\beta$

If $\Delta Br/Br < 1/A$, Br may not be measured.

But, you may lose intensity of RIB.

Z≠Q case

$B\rho$ $A/Q*\beta$

+E $A\beta^2$

We have to stop beams? No reaction studies??

BigRIPS was designed

to have nice resolving power to determine A/Q without E measurement.

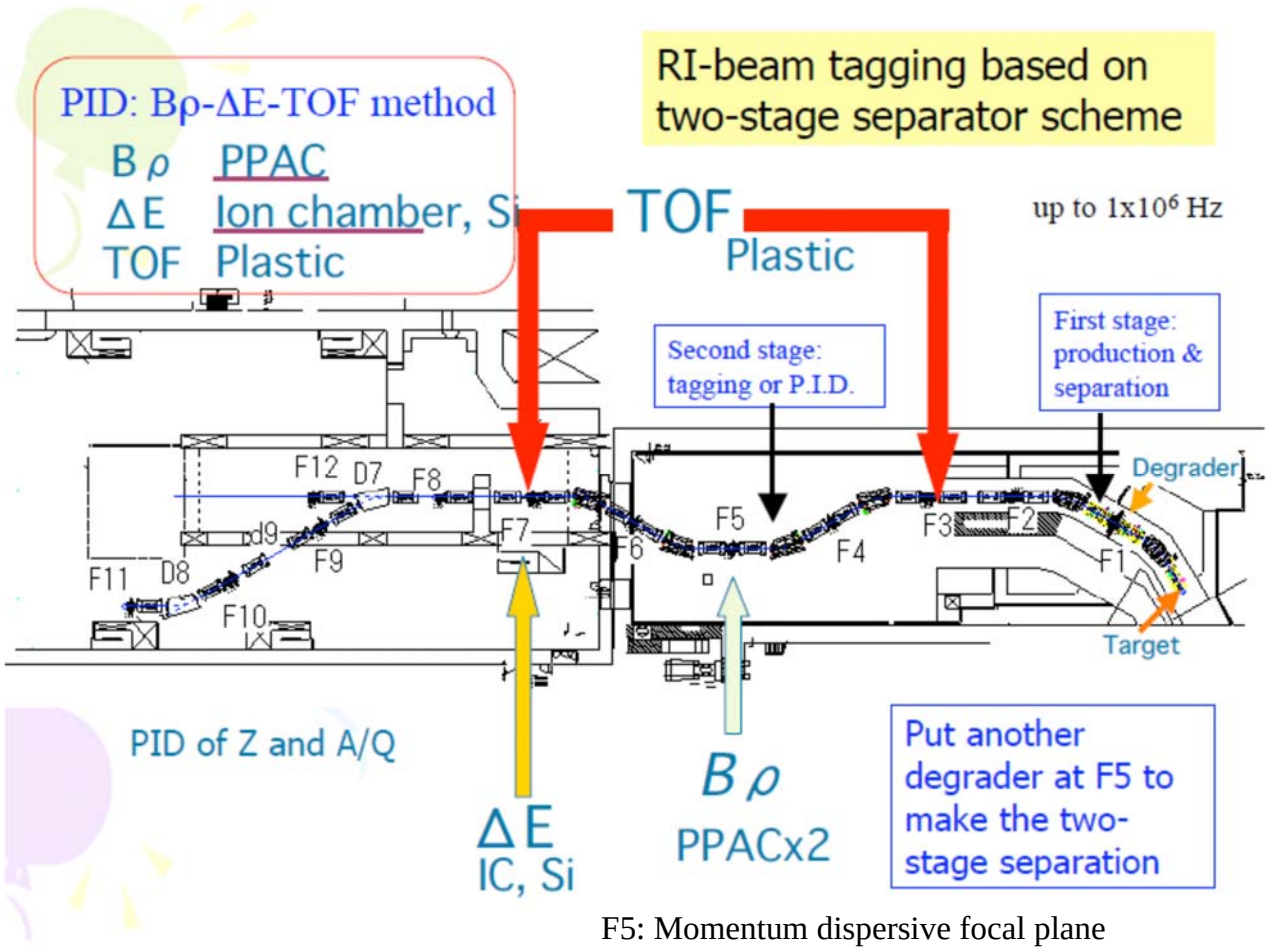

F5: Momentum dispersive focal plane

New isotopes of $^{125,\ 126}$Pd

T. Onishi et al, JPSJ 77 (08)083201.

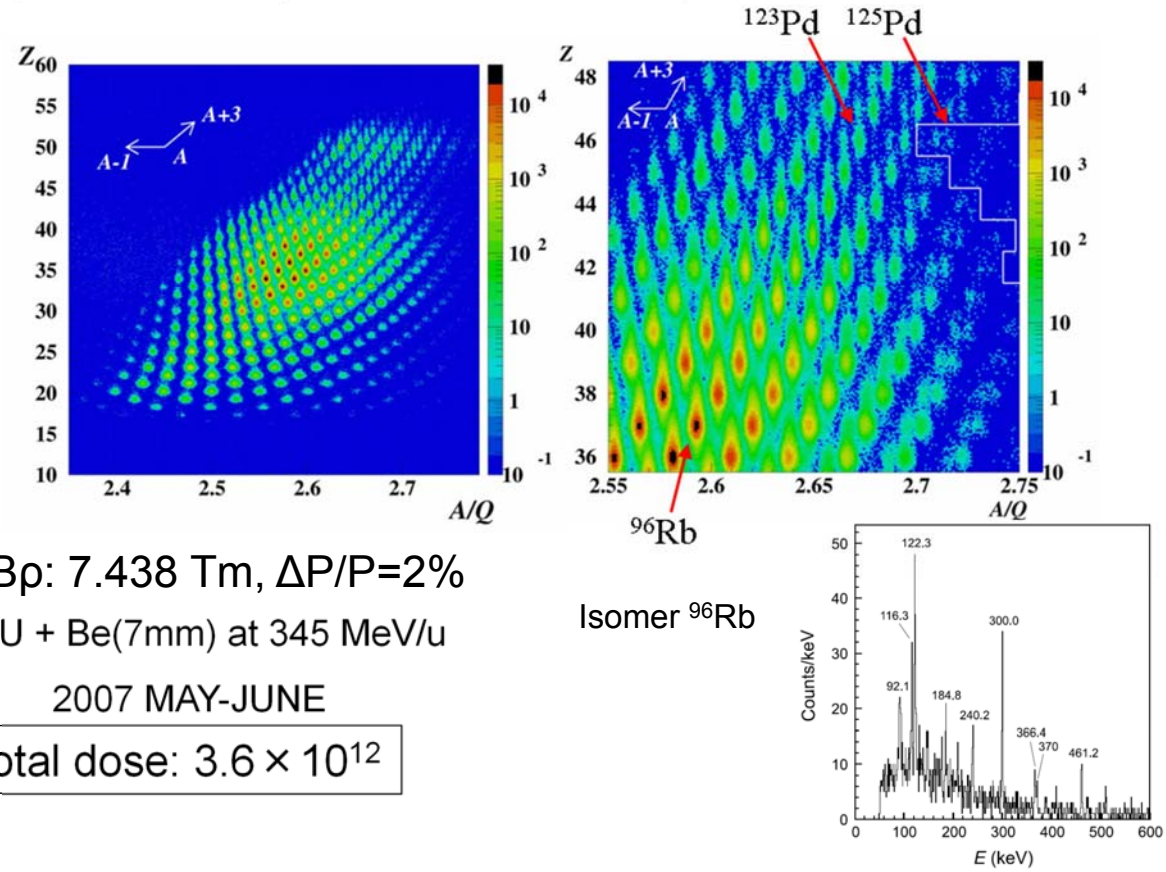

Bρ: 7.438 Tm, ΔP/P=2%

^{238}U + Be(7mm) at 345 MeV/u

2007 MAY-JUNE

Total dose: 3.6×10^{12}

Isomer ^{96}Rb

Identification of new isotopes ^{125,126}Pd

RIKEN NISHINA CENTER

T. Onishi et al, JPSJ 77 (08)083201.

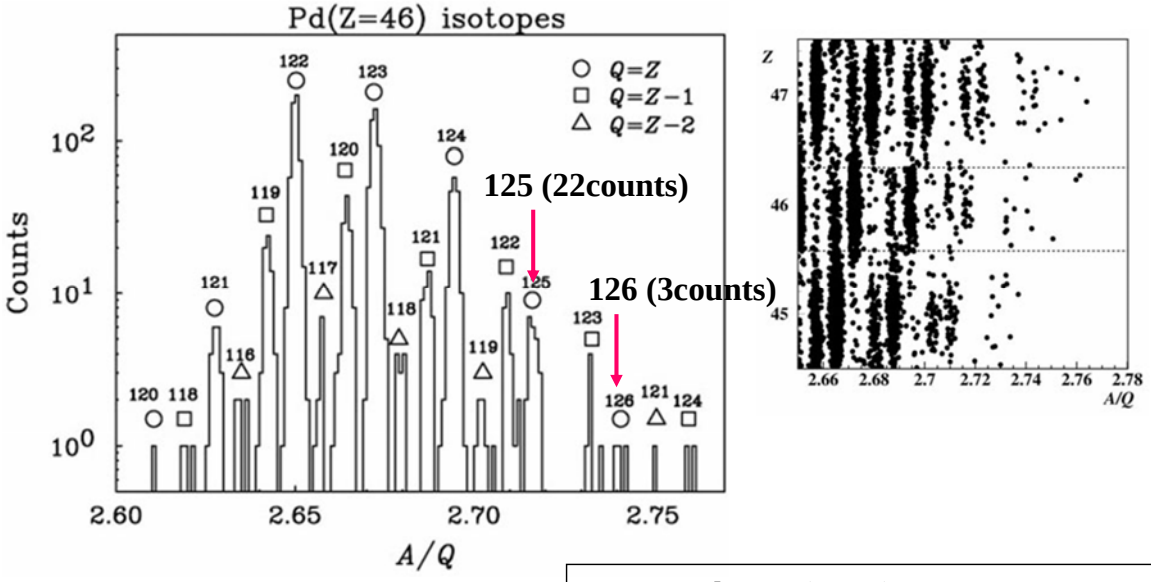

Total dose 3.6×10^{12} for 25 hrs
I ~0.01 pnA on average

A/Q resolution(r.m.s): 0.041% at Z=46
Bρ resolution (r.m.s): 0.02%
ΔT resolution (r.m.s.): 40 psec

Cf. ^{124}Pd 19 counts, ^{125}Pd(cand.) 1count at GSI, 1997
PLB 415, 111 (97); total dose ~1×10^{12}

Identification of 45 New Neutron-Rich Isotopes Produced by In-Flight Fission of a ^{238}U Beam at 345 MeV/nucleon

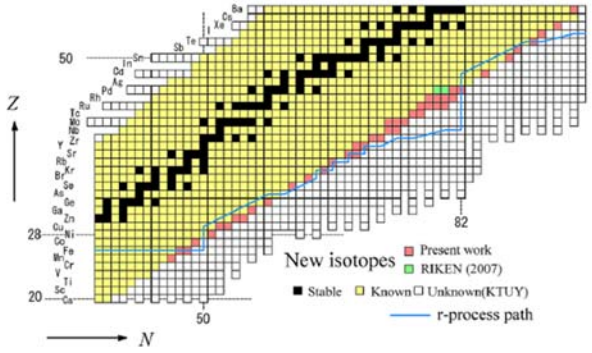

T. Ohnishi, et al., JPSJ 79, 073201 (2010).

Nov., 2008
Averaged beam intensity ~0.2 pnA
Maximum intensity 0.4 pnA

Mn (Z=25) to Ba (Z=56)
Covered by three Brho settings
Be and Pb targets
Total dose 1-2x10^{14} for each Brho setting

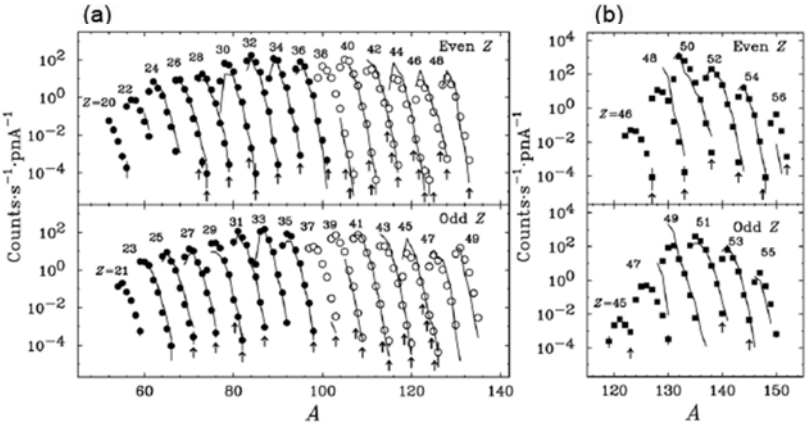

Yield rates reasonably reproduced by LISE++

RIKEN

Press-Conference on June 8th, 2010

June 8, 2010
RIKEN

Scientists discover 45 new radioisotopes in 4 days


毎日新聞 2010年(平成22年)6月22日(火)

23

放射性同位元素 効率的発見

4日で新たに45種


2010年(平成22年)6月9日(水曜日) 3

同位元素45種
一度に発見

加速器施設 世界最高の性能


日刊工業新聞

2010年(平成22年)6月9日 水曜日 21

中性子多い放射性同位元素

新たに45種類発見

理研など

IOP physicsworld.com
"Radioisotopes galore at RIKEN"
http://physicsworld.com/cws/article/news/42915

Spectroscopy on nuclei in “island-of-inversion” and beyond

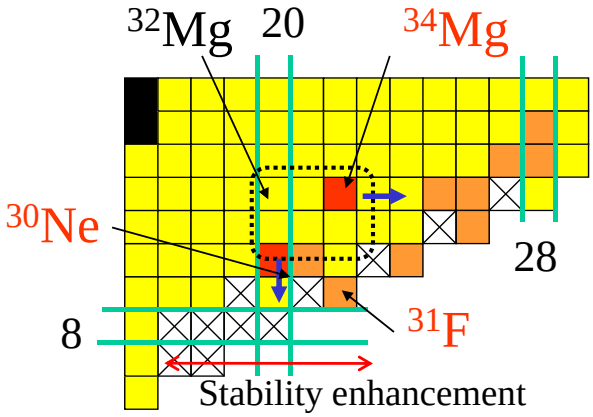

How the deformation region expands toward the drip line?

Deformed halo nuclei?
- deformed core + valence n in a low L orbit
- M. Misu et al., Nucl. Phys. A 614 (97) 44
- I. Hamamoto, Phys. Rev. C69 (04) 041306R

Something new associated with weakly bound natures?
- pairing gap ~ separation energy
- di-neutron ?
- cluster formation?

Total interaction cross sections
Inclusive Coulomb breakup
In-beam gamma spectroscopy
1st Dec. 2008
2nd Dec. 2009
3rd Nov/Dec 2010
20days for 6 programs
+ decay (parasitic)

Experiment setup at BigRIPS/ZDS

In-beam gamma spectroscopy
Coulomb breakup
BigRIPS+ZDS

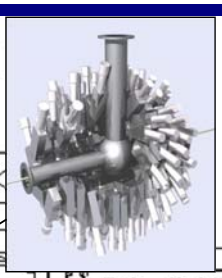

DALI-II
NaI-based gamma Detectors

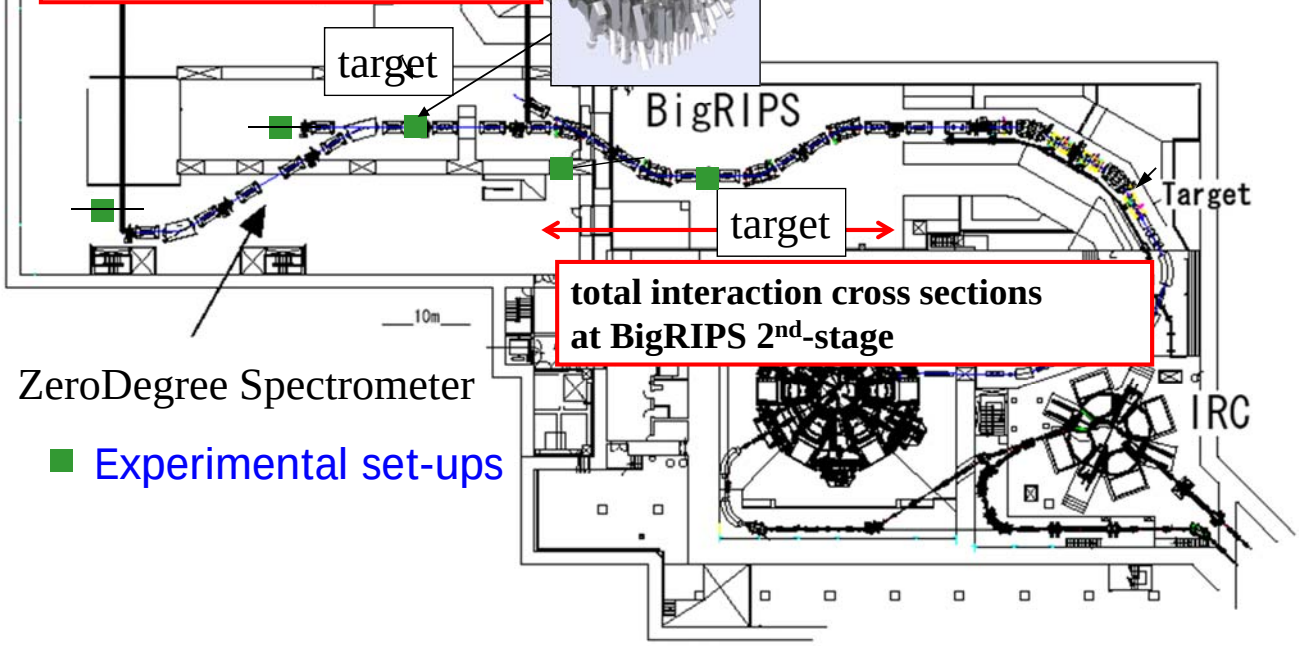

total interaction cross sections at BigRIPS 2nd-stage

ZeroDegree Spectrometer

- Experimental set-ups

YAKITORI “焼き鳥”

ICW06

“YAKITORI”-Setup for RI beams

RI beams are “rare” and “expensive” !
Usually, reaction rates at 2ndary targets are 1% or less.
At most, three users could perform experiments at the same time via the Yakitori-setup.
Main user + Main user
Main user + Parasite user

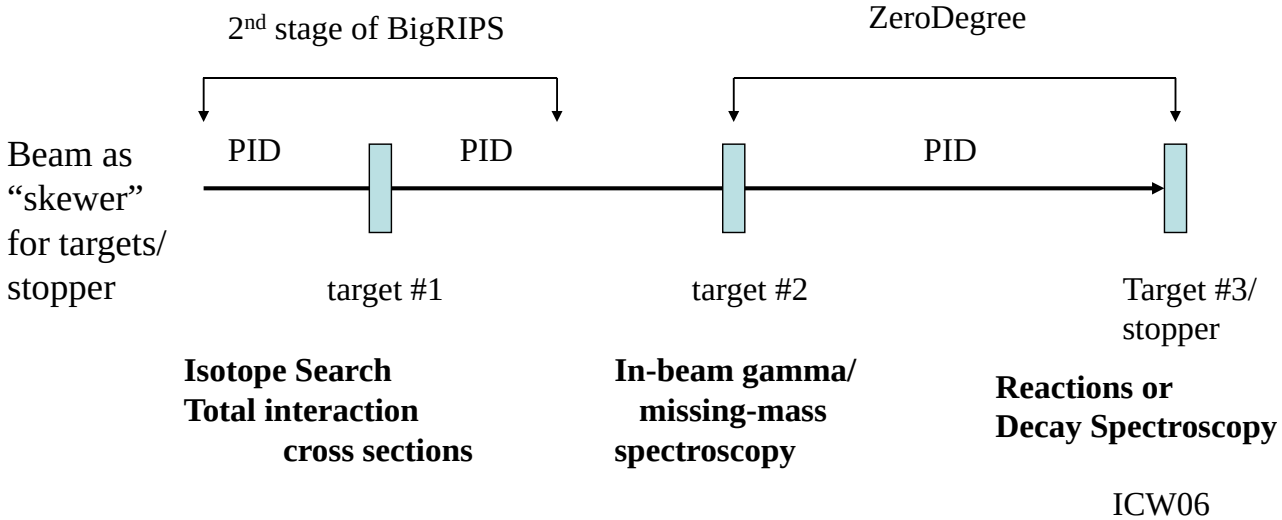

ICW06

DayOne Experiments in Dec., 2008
-The first data in the “island-of-inversion” -

RIKEN NISHINA CENTER

Coordinated by Aoi

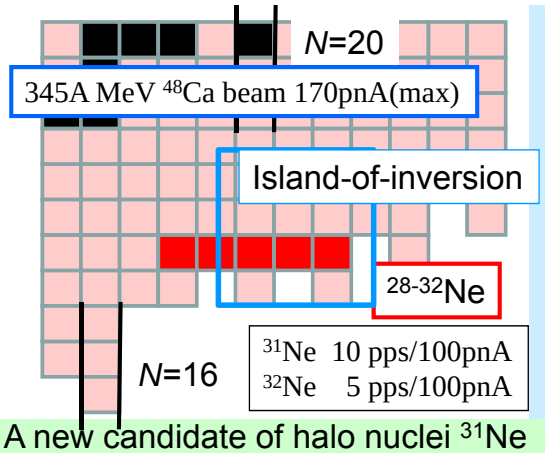

A new candidate of halo nuclei ^{31}Ne via Coulomb breakup

Nakamura et al., PRL 103, 262501(2009)

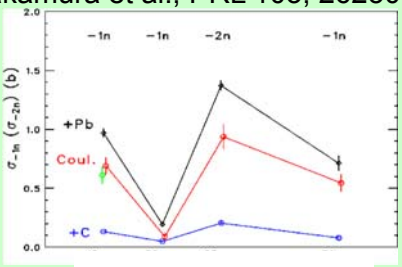

^{19}C ^{20}C ^{22}C ^{31}Ne

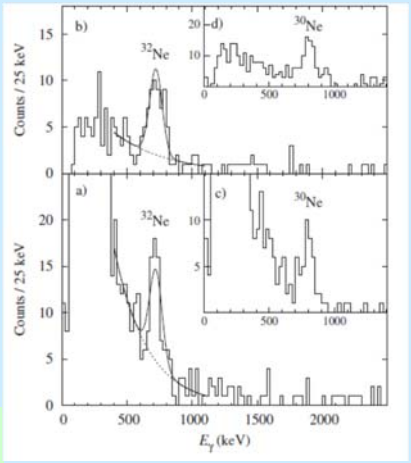

Spectroscopy of ^{32}Ne and the “island-of-inversion”

E(2+) = 722 keV

Doornenbal, Scheit et al. PRL 103, 032501 (2009)

New states in ^{31,32,33}Na PRC 81, 041305R (2010)

Total interaction cross sections for the neutron-rich Ne isotopes

Takechi, Otsubo et al., Niigata 2010 symposium

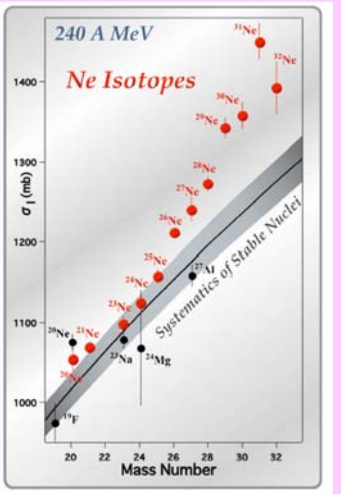

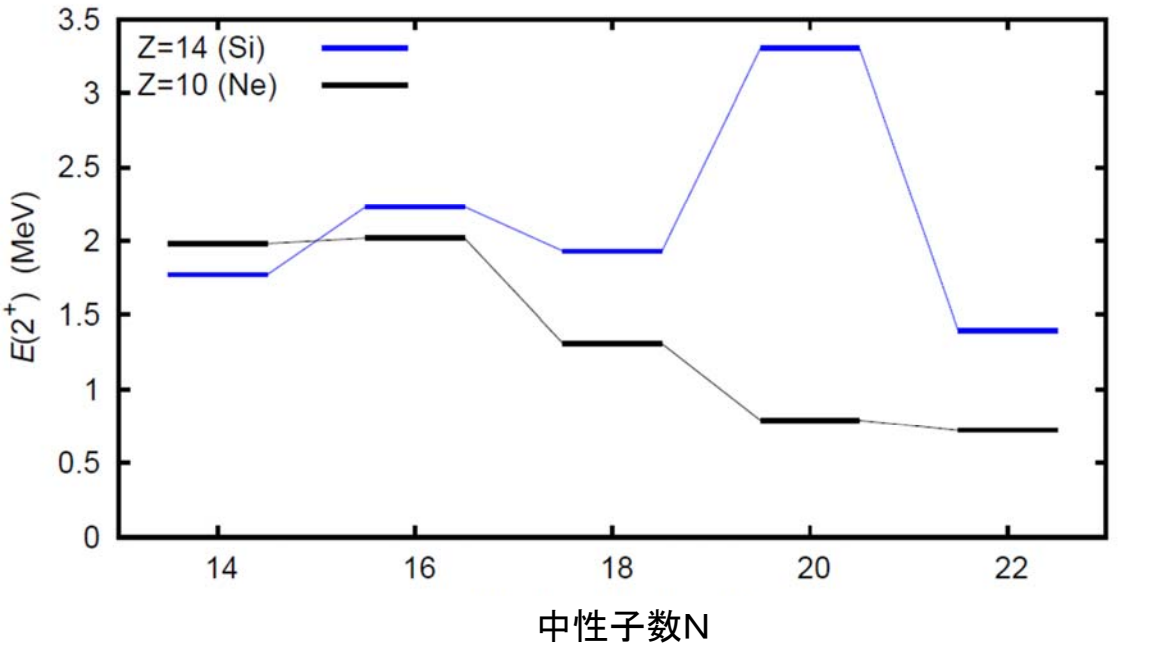

DayOne Experiments in Dec., 2008
-The first data in the "island-of-inversion" -

RIKEN NISHINA CENTER

Coordinated by Aoi

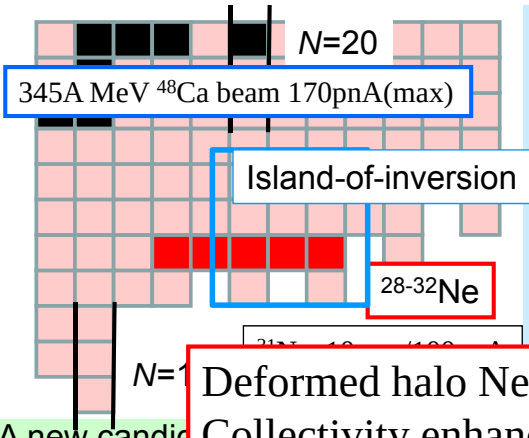

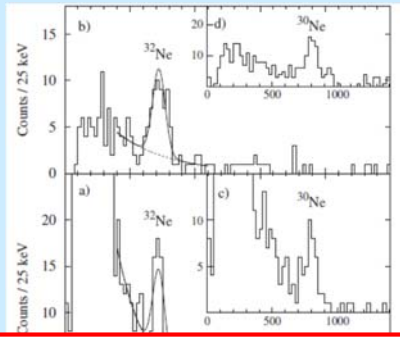

Spectroscopy of ^{32}Ne and the "island-of-inversion"

E(2+) = 722 keV

Doornenbal, Scheit et al. PRL 103, 032501 (2009)

New states in ^{31,32,33}Na PRC 81, 041305R (2010)

Deformed halo Ne-31

Collectivity enhancement toward the drip line

A new candid
via Coulomb breakup

Nakamura et al., PRL 103, 262501(2009)

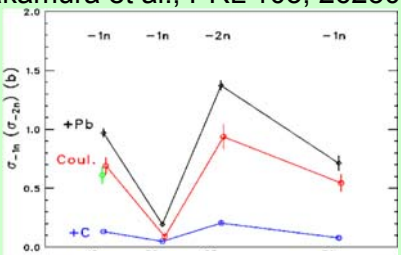

^{19}C ^{20}C ^{22}C ^{31}Ne

Total interaction cross sections for the neutron-rich Ne isotopes

Takechi, Otsubo et al., Niigata 2010 symposium

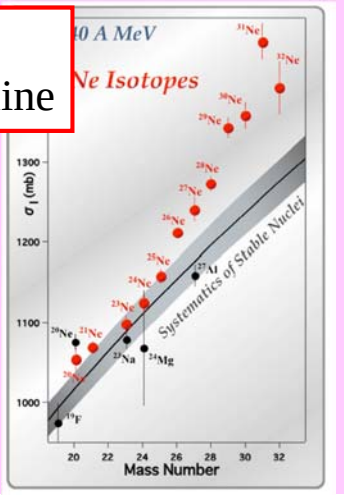

Third Ca-48 beam Campaign

RIKEN NISHINA CENTER

Nov.- Dec., 2010

H. Scheit et al.	3 days	in-beam gamma for Ne, Mg
P. Fallon et al.	1 day	feasibility study for ^{40}Mg
S. Takeuchi et al.	6 days	in-beam gamma for Si
D. Bazin et al.	4 days	one n-knockout towards ^{33}Mg
T. Nakamura et al.	4.5 days	search for halo nuclei
M. Takechi et al.	4 days	total interaction cs for Mg, Al

Low-lying Excited States in ^{24}O via (p,p')
- The First Missing Mass Spectroscopy at RIBF -

RIKEN NiSHiNA CENTER

Spokespersons : Valerie Lapoux and Hideaki Otsu

May, 2010

The state-of-art detector MUST2 from France coupled with BigRIPS/ZDS setup

GOAL

Characteristics of the N=16 new magic number ?
… in O isotopes
Structure of a drip-line nucleus,
possible neutron-skin or halo

EXCITATION ENERGY SPECTRUM
FOR ^{24}O ➔ ^{24}O(p,p')^{24}O*

^{24}O E(2+) > S_n = 3.7 MeV
+ states above S_{2n} = 6.35 MeV ?

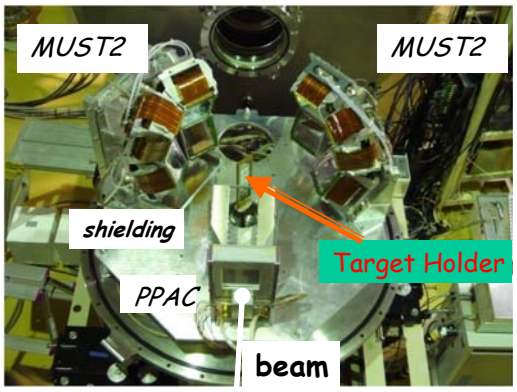

TOOLS

Particle spectroscopy of
UNBOUND states

SET- UP

Kinematics,
(p,p') reactions
Beam time

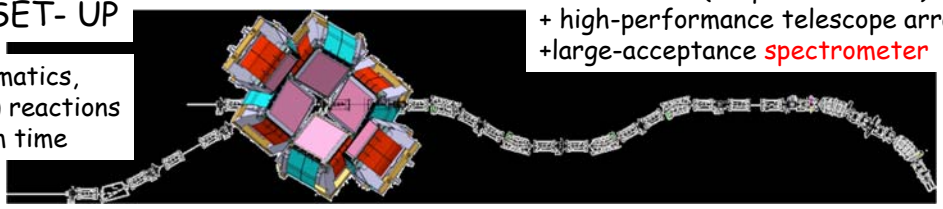

RIBF beam (unique intensities)
+ high-performance telescope array
+large-acceptance spectrometer

Next Generation Gamma-Detector System SHOGUN

Scintilator based High resOlution Gamma-ray spectrometer for Unstable Nuclei

H. Scheit et al.

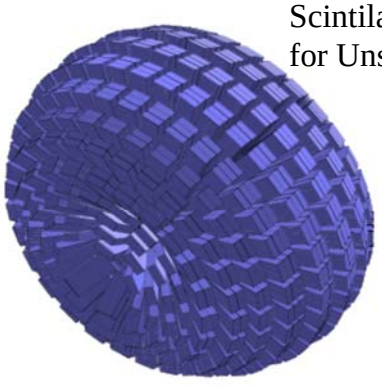

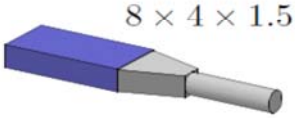

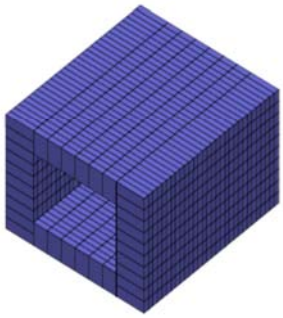

fast beam setup ($v = 0.6c$)	$\frac{\Delta E}{E}$ (%)	ϵ_γ (%)	$\epsilon_{\gamma\gamma}$ (%)
NaI(Tl) DALI2	10.0	23.5	5.5
RISING	1.9	2.8	0.08
$LaBr_3$(Ce) 1000	**3.2**	**42.0**	**17.6**
slow/stopped beam setup			
RISING	0.2	15.0	2.25
$LaBr_3$(Ce) 1000	2.4	**56.0**	**31.3**

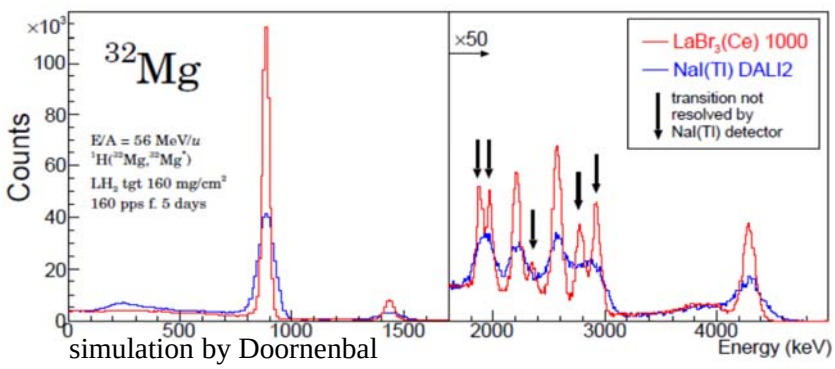

simulation by Doornenbal

The First Decay Spectroscopy at RIBF

2009 Dec.

U beam to access A~110 region

Intensity 0.8 pnA max.

0.1-0.2 pnA on average

Sumikama, Nishimura, et al.

Half life measurements for r-process nuclei
Nishimura et al., PRL 106 (11) 052502

Beta-gamma spectroscopy on Zr-106,108
Sumikama et al., PRL 106 (11) 202501

Delayed gamma spectroscopy for isomers
H.Watanabe et al., PLB 696 (11) 186

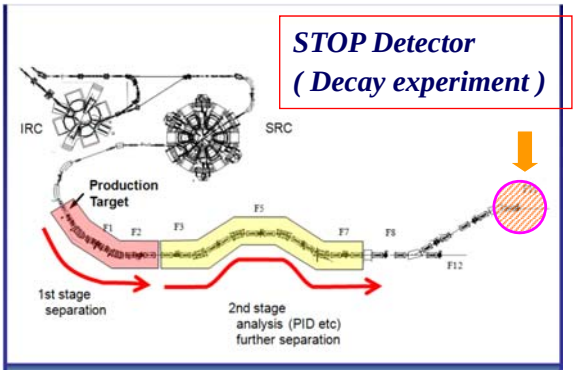

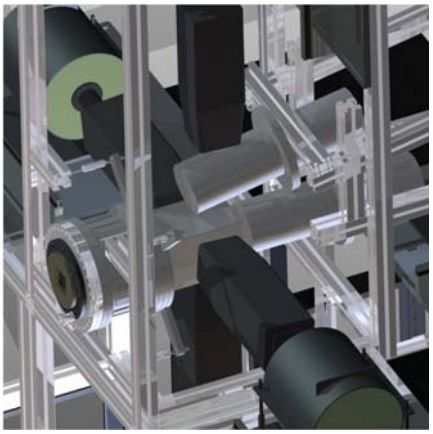

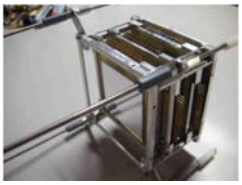

Clovers (RIKEN)

$LaBr_3$ (Milano)

9 layers of DSSD (RIKEN, TUS)

Half-Lives of Very Neutron-Rich Nuclei

S. Nishimura et al.

(Kr,Rb,Sr,Y,Zr,Nb,Mo,Tc) around 2nd R-Process Peak

T.Ohnishi, JPSJ 79 (2010).. 45 new isotopes

New half-lives (18 nuclei) are measured !

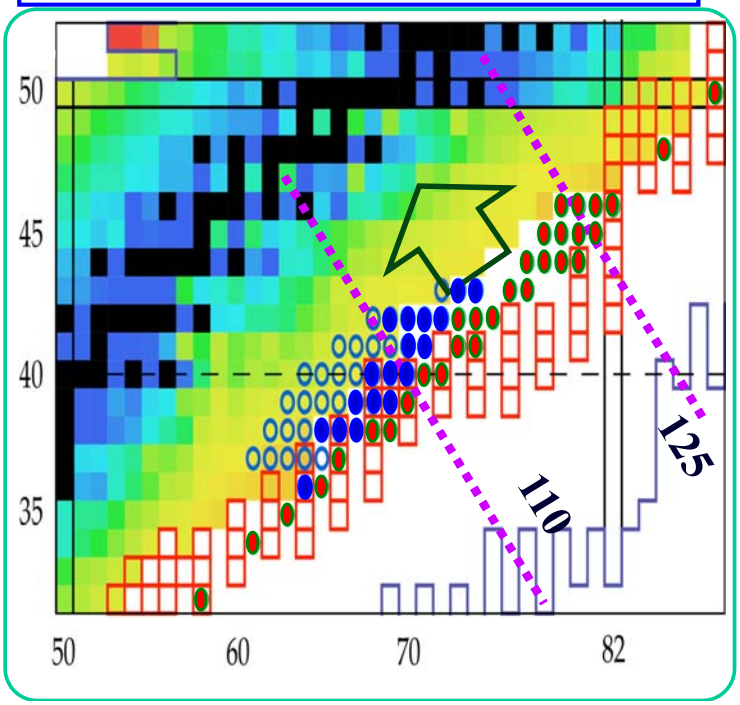

B.Pfeiffer et al. Z. Phys. A357 (1997)

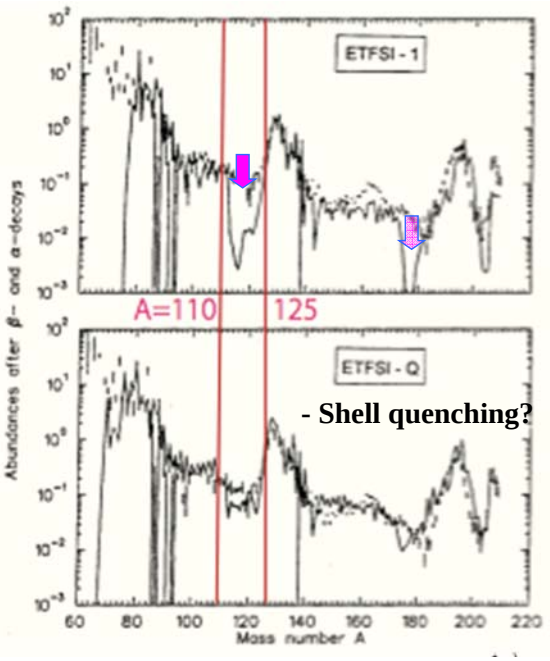

Brand-new half-life data for 18 isotopes

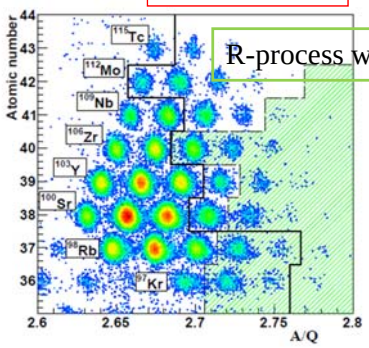

8 hour data acquisition
T1/2 data of 38 isotopes including first data for 18 isotopes
FRDM may underestimate Q-value for Zr and Nb by 1 MeV at A~110
More rapid flow in the rapid neutron-capture process than expected

S. Nishimura et al., PRL 106 (11) 052502

1/3 ~ 1/2 Shorter Half-lives of Zr and Nb (A~110)

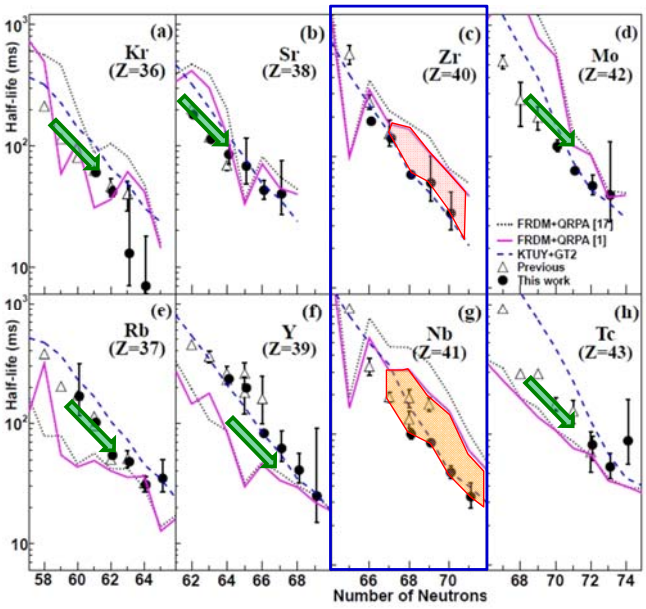

Press-Conference on February 1st, 2011

Faster r-process synthesis in supernova explosion ?
－new half-life data for 18 neutron-rich nuclei

超新星爆発で重元素 再現

超新星爆発で重い元素が作られる様子を地上で再現したところ、一部の元素はこれまでの理論よりも多く作られることがわかった。理化学研究所が発表した。太陽系にあるいくつかの元素は理論予想より10倍多く、どう作られたのか20年間議論が続いていたが、超新星爆発が重元素の工場だった可能性が高まった。

理研の西村俊二先任研究員らは、埼玉県和光市の大強度重イオン加速器施設「ＲＩＢＦ」で、ウランを光速の70％に加速しベリリウムに毎秒10億個ぶつけた。ウランが分裂してできた元素のうち、18種類は世界で初めて寿命が調べられたという。（フィジカル・レビュー・レターズ）

重元素は短時間で合成

超新星爆発の再現は世界初

2011年（平成23年）2月11日（金曜日）

38個の中性子過剰なＲＩの寿命を測定 理研

理論予想より2～3倍速く崩壊

EUROBALL-RIKEN Cluster Array (EURICA)

Decay + in-beam gamma with E-degraded RI beams

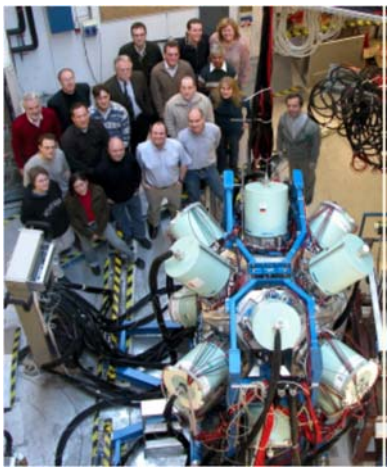

+

Experimental Devices available at the new facility in 2012

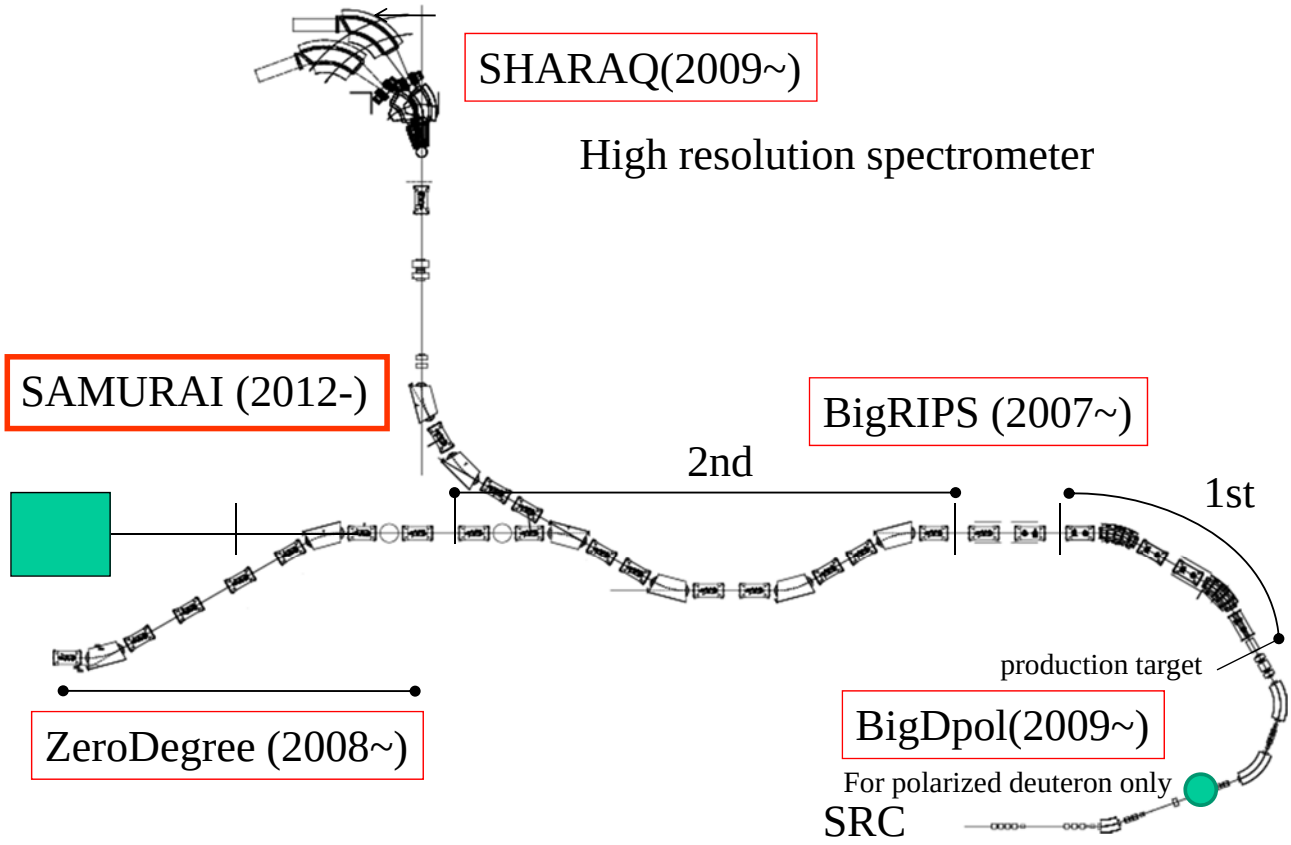

SAMURAI Spectrometer Kobayashi et al 2012-

versatile spectrometer with a large superconducting magnet

Spectroscopy of
Unbound States e.g. (γ,n)
(p,2p) Missing Mass
Nucl. Astrophys. (p,γ)
Deuteron expts for 3NF
Nucl. Matter

15M$ covers
SC-Magnet 9M$
Detectors
neutron counter
electronics, software
STQ for BT

Bending Magnet
Superconducting
Large B·L (7Tm)
Large pole gap (80cm)
Weight ~ 600 ton

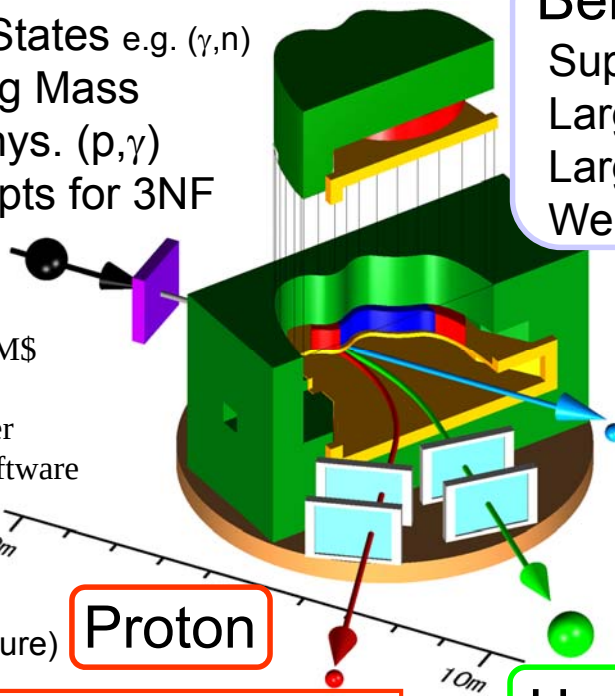

Neutron

TPC
(not shown in picture)

d setup
(not shown in picture)

Proton

Heavy Ion

NSCL, TA&M joining this project

SAMURAI under construction

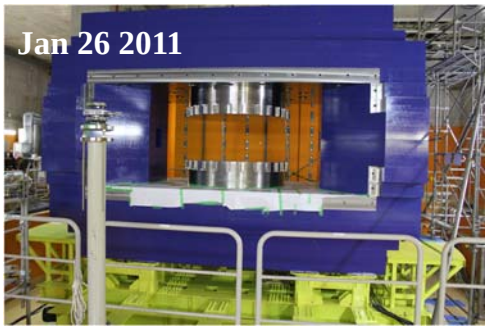

New Injector RILAC2
to deliver more intense beam and more opportunities for SHE

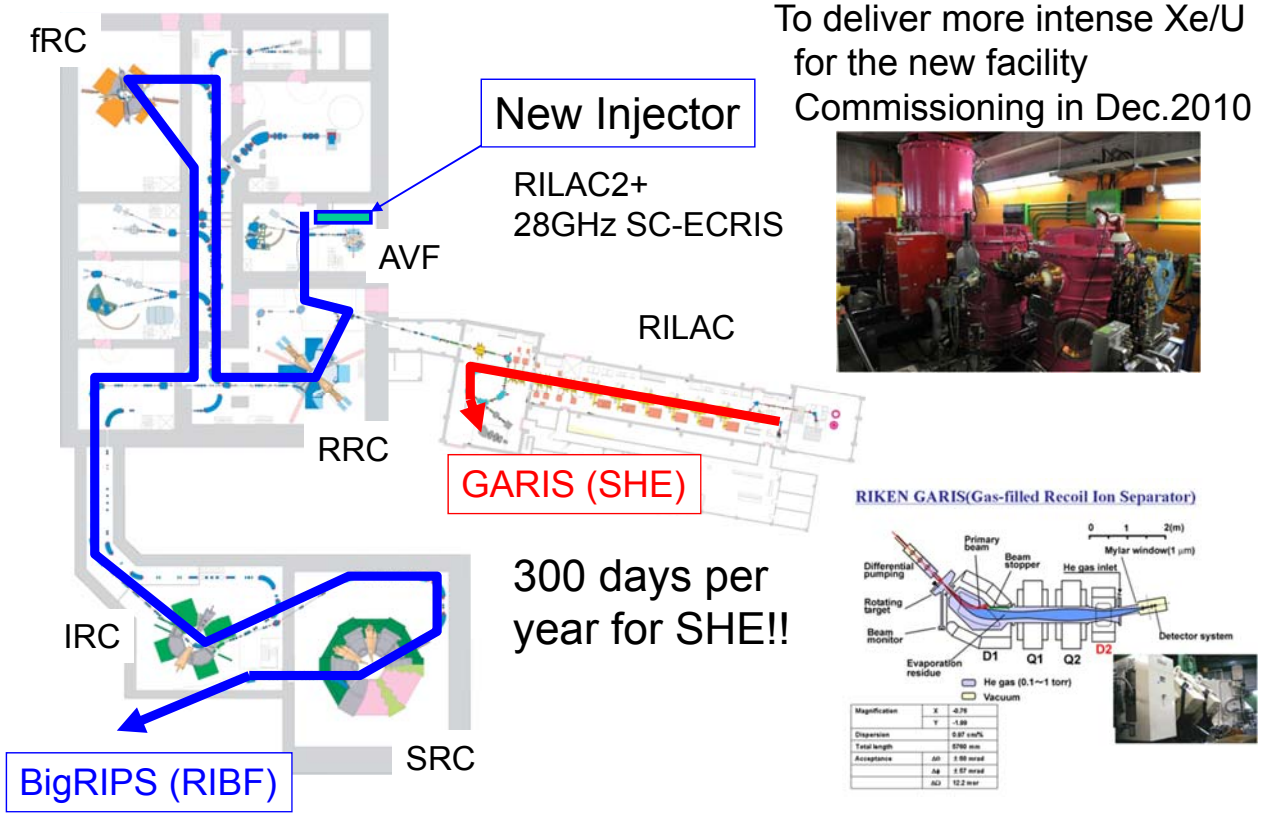

Summary

RIBF In-flight RIB facility with a powerful accelerator complex and several experimental devices

Many experimental programs / projects

Many works to discover something new

The RIB physics is very promising.
You could enjoy the research.

Recoiled proton tagged knockout reaction for He-8 at RIPS

PKU-RIKEN-IMP-TITech-Seaul

Ye et al., July 2009

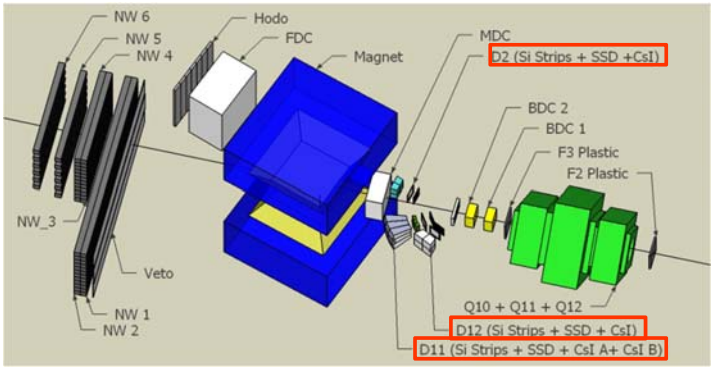

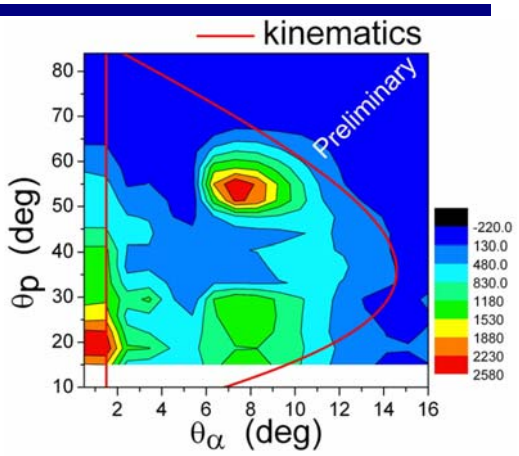

"Quasi-elastic scattering of He-6 from C-12"
Lou and Ye et al., PRC 83, 034612 (2011)

Cao and Ye et al., in preparation

Nuclear Collective Motion

closed shell ⟷ open shell

at magic number

spherical nuclei — surface vibration — deformed nuclei

|β|~0 ← Quadrupole deformation parameter β → |β| large

degree of collectivity

Quantum Liquid Drop Model

Even-Even Nuclei

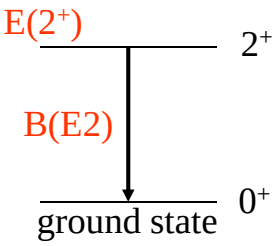

Energy of the first excited state

$E(2^+) \propto 1/\beta^2$

E2 transition probability between 2^+ and 0^+

$B(E2) \propto \beta^2$

$E(2^+) \propto B(E2)^{-1}$

Nuclear Collective Motion

closed shell ⟷ open shell

at magic number

spherical nuclei — surface vibration — deformed nuclei

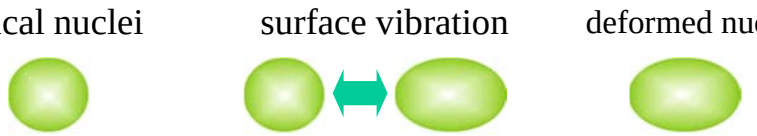

|β|~0 ← Quadrupole deformation parameter β → |β| large

degree of collectivity

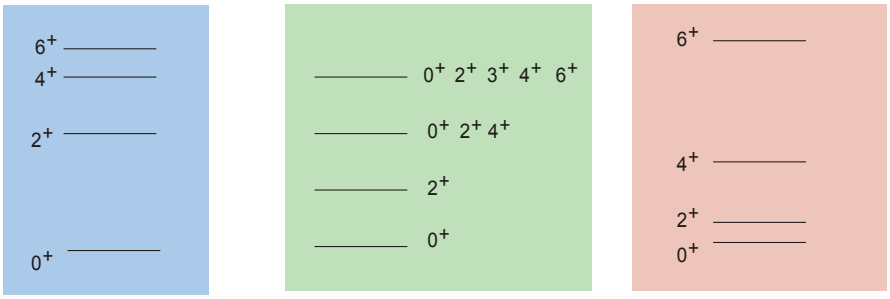

$E(4^+)/E(2^+)$ | ~ 1.8 | ~ 2.2 | ~ 3.3

Nuclear Structure and Collectivity

Energy of the first 2+ state in even-even isotopes

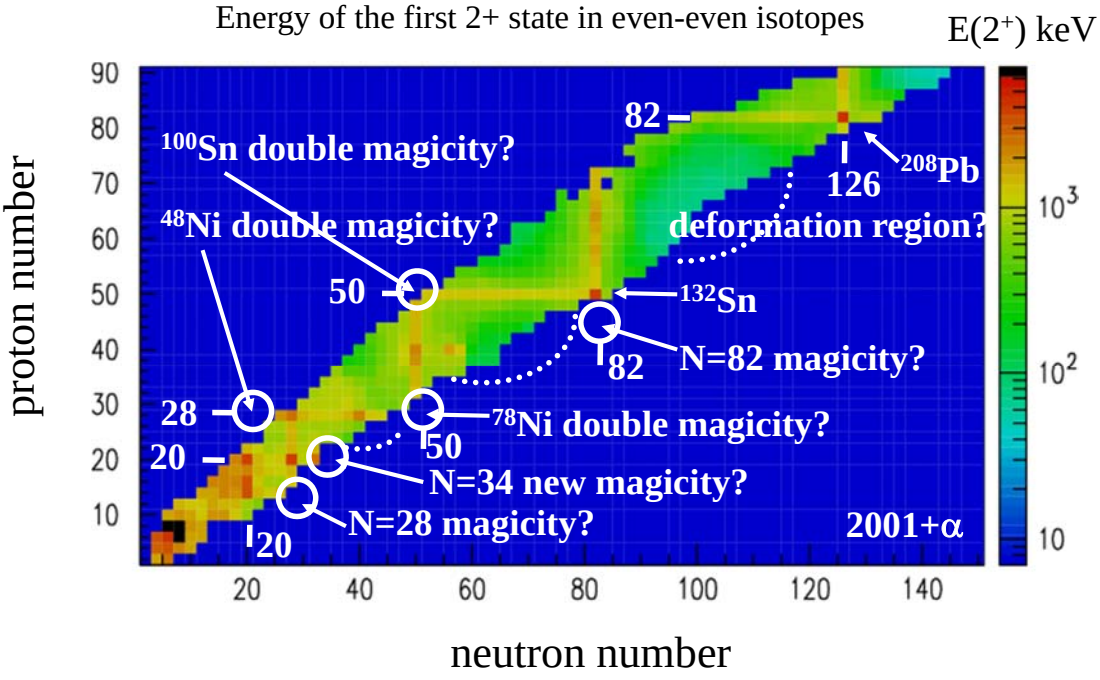

Programs at the RIBF since 2007

RIKEN NISHINA CENTER

2007	May	345A MeV U-238	Search for new isotopes	BigRIPS
2008	Nov.	345A MeV U-238	Search for new isotopes/isomers	BigRIPS
			ZeroDegree Commissioning	
	Dec.	345A MeV Ca-48	Spectroscopy at N~20	BigRIPS/ZDS
2009	April	250A MeV pol.-d	3NF in d+p elastic	BigDpol
			cross section, tensor analyzing power	
	May	250A MeV N-14	SHARAQ Commissioning	SHARAQ
20days	Oct	320A MeV He-4	(t,3He) IVSMR	SHARAQ
	Nov	345A MeV U-238	Decay Spectroscopy	ZDS
	Dec	345A MeV Ca-48	total cs	BigRIPS
			test for in-beam gamma	ZDS
2010	May	345A MeV Ca-48	Missing mass spectroscopy	ZDS
			Two-step Alignments	BigRIPS
	June	345A MeV O-18	(p,2p)	Kappa Spec.
	Oct.	250A MeV N-14	Charge exchange	SHARAQ
70days		250A MeV d	($d,^3He$) deeply-bound	BigRIPS
			pionic states Itagaki et al.	
	Nov.-	345A MeV Ca-48	in-beam gamma, total cs.	BigRIPS/ZDS
	Dec.		Inclusive Coulomb breakup	
			Decay-spectroscopy	

Achieved beam intensities

- pol-d(250 MeV/u) : 120 pnA : May2009
- ^{4}He(320 MeV/u) : 1000 pnA : Oct2009
- ^{14}N(250 MeV/u) : 80 pnA : May2009
- ^{18}O(MeV/u) : 500 pnA : Jun2010
- ^{48}Ca(345 MeV/u) : 230 pnA : Jun2010
- ^{86}Kr(345 MeV/u) : 30 pnA(<1min) : Nov2007
- ^{238}U(345 MeV/u) : 0.8 pnA(short time) : Dec2009

Expected beam intensities

- ^{70}Zn(345 MeV/u) : 50 pnA
- ^{124}Xe(345 MeV/u) : 10 pnA => FY2011
- ^{238}U(345 MeV/u) : 5 pnA => FY2011

Two Other Outputs from the Decay Campaign

RIKEN NiSHiNA CENTER

Phys. Lett. B 696 (2011) H.Watanabe
Oblate shape isomer for ^{109}Nb?

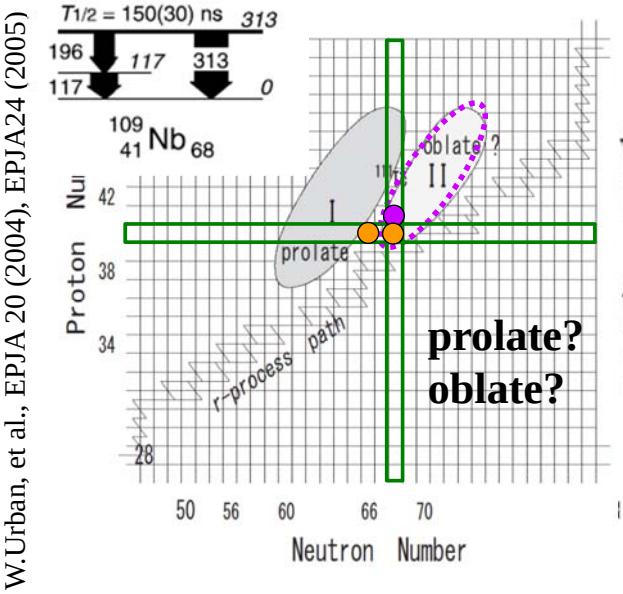

W.Urban, et al., EPJA 20 (2004), EPJA24 (2005)

- Beta-delayed gamma : ^{106}Y → ^{106}Zr
- Isomeric states : ^{108}Zr

Phys. Rev. Lett. 106, 202501 (2011) T.Sumikama
Shell Evolution : 106Zr and 108Zr

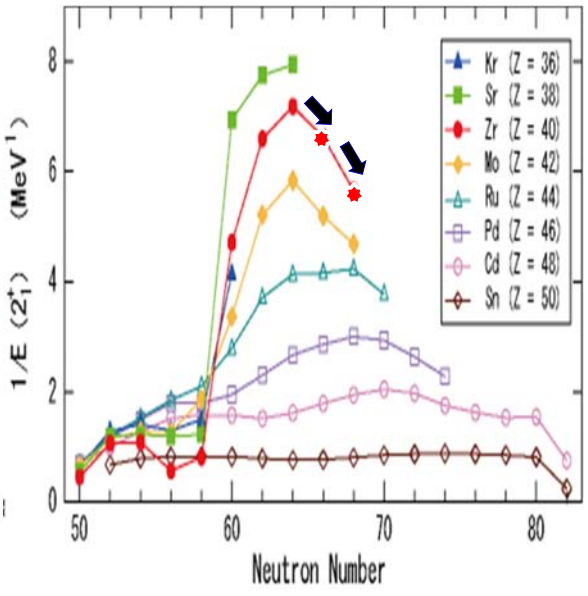

Deformed sub-shell closure at N=64 ?

Sumikama

Chiral effective field theory and nuclear structure

Achim Schwenk

TECHNISCHE UNIVERSITÄT DARMSTADT

EMMI

International Summer School on Subatomic Physics 2011
"New Frontiers of Nuclear Physics", Beijing University

S-DALINAC

DFG

HELMHOLTZ ASSOCIATION

Minerva Stiftung

Bundesministerium für Bildung und Forschung

Outline

Chiral effective field theory for nuclear forces

Epelbaum, Hammer, Meissner, Rev. Mod. Phys. 81, 1773 (2009). Overview.
Epelbaum, Prog. Part. Nucl. Phys. 57, 654 (2006). Many useful details.
Bogner, Furnstahl, AS, Prog. Part. Nucl. Phys. 65, 94 (2010). Renormalization Group.

3N forces and neutron-rich nuclei

Otsuka, Suzuki, Holt, AS, Akaishi, Phys. Rev. Lett. 105, 032501 (2010).
Holt, Otsuka, AS, Suzuki, arXiv:1009.5984.
Holt, AS, arXiv:1108.2680.

3N forces and neutron matter, impact on neutron stars

Hebeler, AS, Phys. Rev. C 82, 014314 (2010).
Hebeler, Lattimer, Pethick, AS, Phys. Rev. Lett. 105, 161102 (2010).

3N forces and electroweak currents

Menendez, Gazit, AS, Phys. Rev. Lett. 107, 062501 (2011).

The nuclear forces frontier

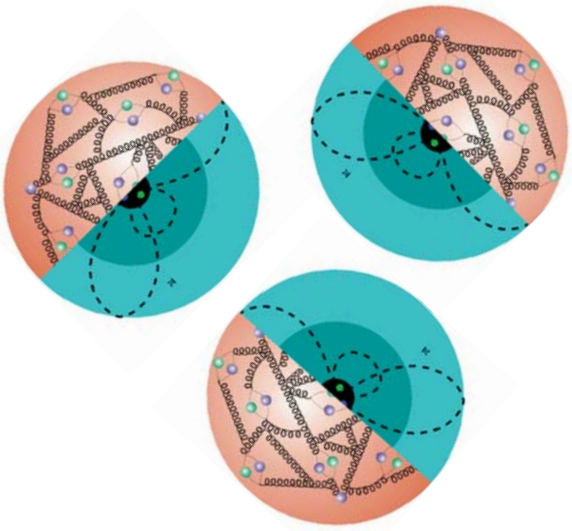

Λ / Resolution dependence

with high-energy probes:
quarks+gluons

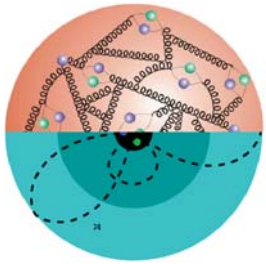

at low energies:
complex QCD vacuum

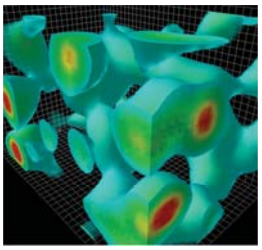

lowest energy excitations:
pions, nearly massless, m_π=140 MeV
'phonons' of QCD vacuum

Λ / Resolution dependence of nuclear forces

with high-energy probes:
quarks+gluons

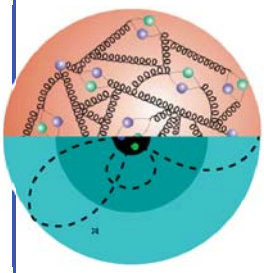

at low energies:
complex QCD vacuum

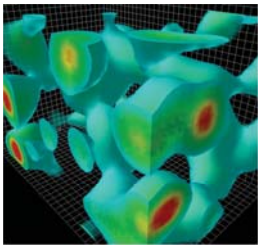

lowest energy excitations:
pions, nearly massless, m_π=140 MeV
'phonons' of QCD vacuum

Λ_{chiral}
momenta $Q \sim \lambda^{-1} \sim m_\pi$

$\Lambda_{pionless}$
momenta $Q << m_\pi$

Λ / Resolution dependence of nuclear forces

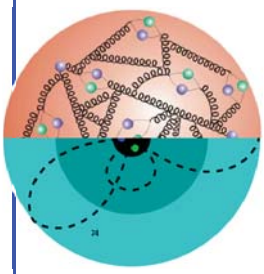

$\Lambda_{pionless}$
momenta $Q << m_\pi$: pionless effective field theory

large scattering length physics and corrections

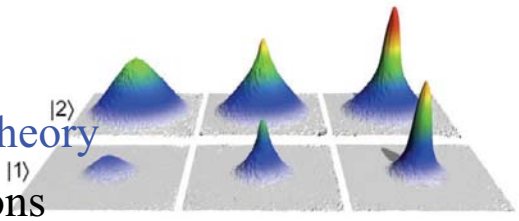

Λ / Resolution dependence of nuclear forces

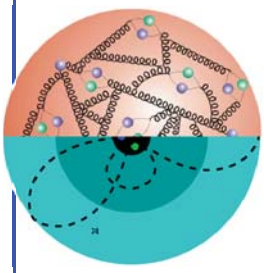

Λ_{chiral}
momenta $Q \sim \lambda^{-1} \sim m_\pi$: chiral effective field theory

neutrons and protons interacting via pion exchanges
and shorter-range contact interactions

typical momenta in nuclei ~ m_π

$\Lambda_{\text{pionless}}$
momenta $Q \ll m_\pi$

Λ / Resolution dependence of nuclear forces

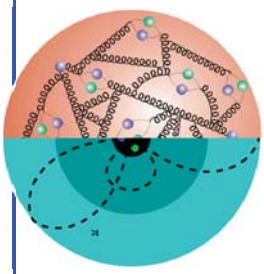

Effective theory for NN, 3N, many-N interactions and electroweak operators: resolution scale/Λ-dependent

$$H(\Lambda) = T + V_{\text{NN}}(\Lambda) + V_{\text{3N}}(\Lambda) + V_{\text{4N}}(\Lambda) + \ldots$$

Λ_{chiral}
momenta $Q \sim \lambda^{-1} \sim m_\pi$: chiral effective field theory

Λ ↓

$\Lambda_{\text{pionless}}$
momenta $Q \ll m_\pi$

Chiral Effective Field Theory for nuclear forces

Separation of scales: low momenta $\frac{1}{\lambda} = Q \ll \Lambda_b$ breakdown scale ~500 MeV

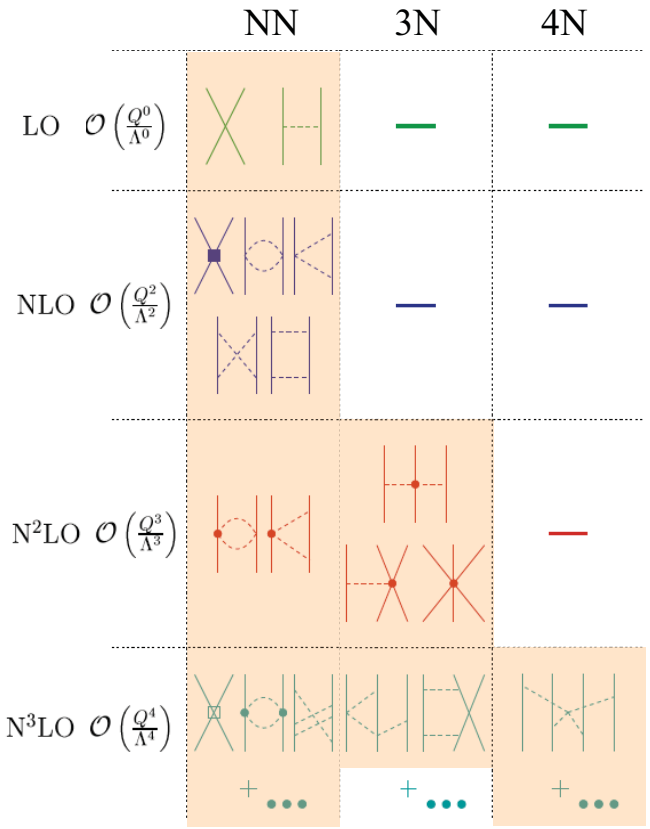

limited resolution at low energies,
can expand in powers $(Q/\Lambda_b)^n$

LO, n=0 - leading order,
NLO, n=2 - next-to-leading order,…

expansion parameter ~ 1/3

(compare to multipole expansion for a charge distribution)

Weinberg, van Kolck, Kaplan, Savage, Wise, Epelbaum, Kaiser, Meissner,…

Chiral Effective Field Theory for nuclear forces

Separation of scales: low momenta $\frac{1}{\lambda} = Q \ll \Lambda_b$ breakdown scale ~500 MeV

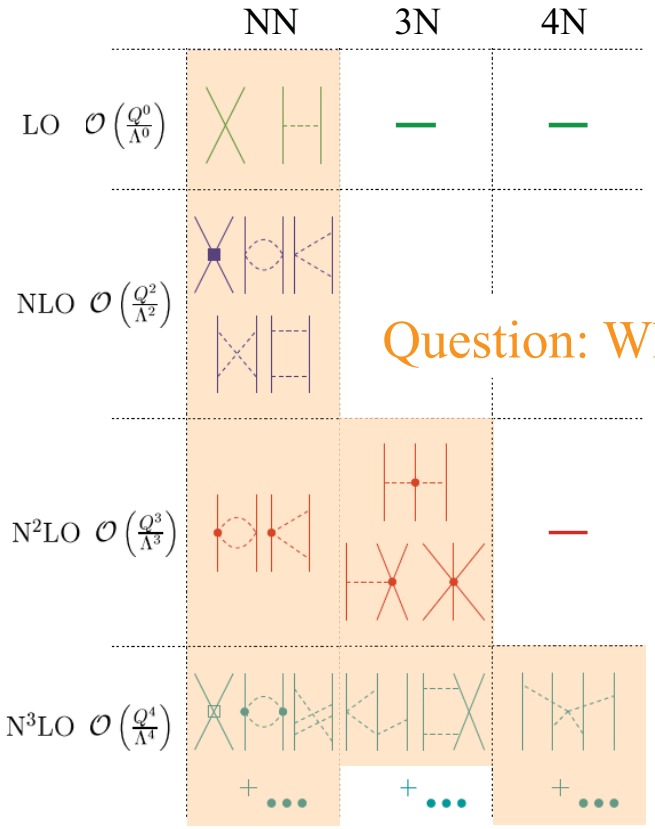

limited resolution at low energies,
can expand in powers $(Q/\Lambda_b)^n$

LO, n=0 - leading order,
NLO, n=2 - next-to-leading order,…

Question: Why is there no n=1 contribution?

Weinberg, van Kolck, Kaplan, Savage, Wise, Epelbaum, Kaiser, Meissner,…

Chiral Effective Field Theory for nuclear forces

Separation of scales: low momenta $\frac{1}{\lambda} = Q \ll \Lambda_b$ breakdown scale ~500 MeV

include long-range pion physics

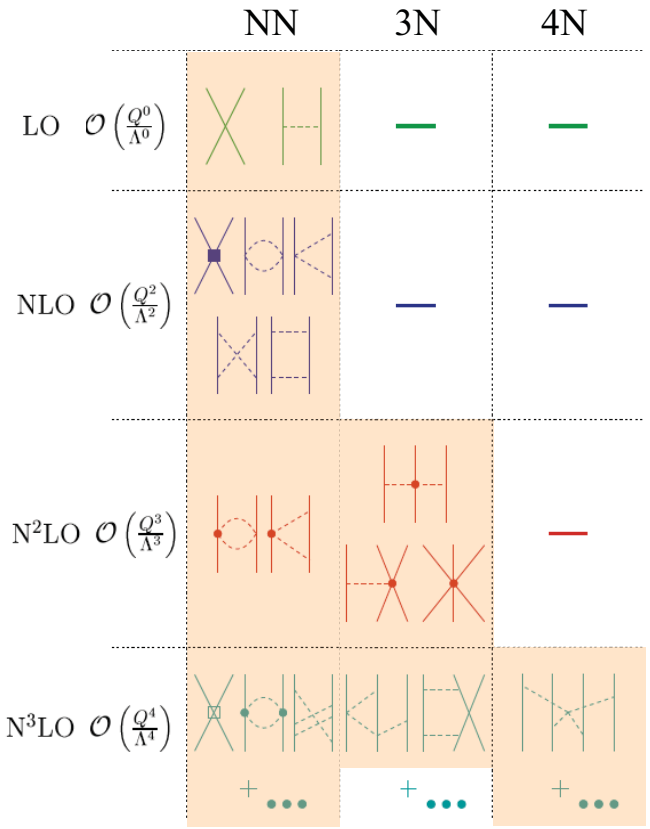

Weinberg, van Kolck, Kaplan, Savage, Wise, Epelbaum, Kaiser, Meissner,…

Chiral Effective Field Theory for nuclear forces

Separation of scales: low momenta $\frac{1}{\lambda} = Q \ll \Lambda_b$ breakdown scale ~500 MeV

include long-range pion physics

details at short distance not resolved

capture in few short-range couplings, fit to experiment once, Λ-dependent

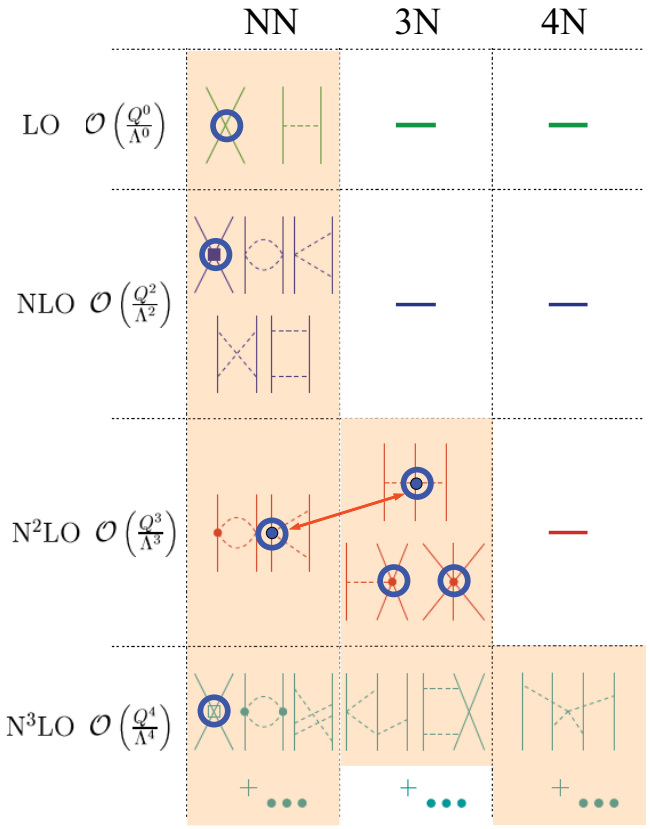

Weinberg, van Kolck, Kaplan, Savage, Wise, Epelbaum, Kaiser, Meissner,…

Chiral Effective Field Theory for nuclear forces

Separation of scales: low momenta $\frac{1}{\lambda} = Q \ll \Lambda_b$ breakdown scale ~500 MeV

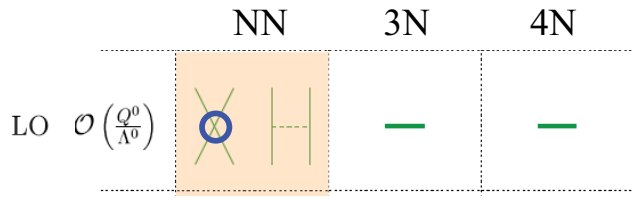

Question: What is V(r) for NN interactions at LO?

Hint: One-pion exchange + contact interaction
but with resolution scale Λ~500 MeV (cutoff on momenta)

Chiral Effective Field Theory for nuclear forces

Separation of scales: low momenta $\frac{1}{\lambda} = Q \ll \Lambda_b$ breakdown scale ~500 MeV

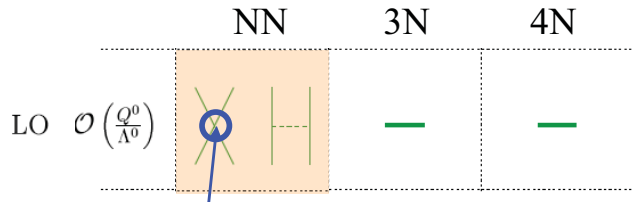

large scattering length physics

^{6}Li fermions
2 spin states

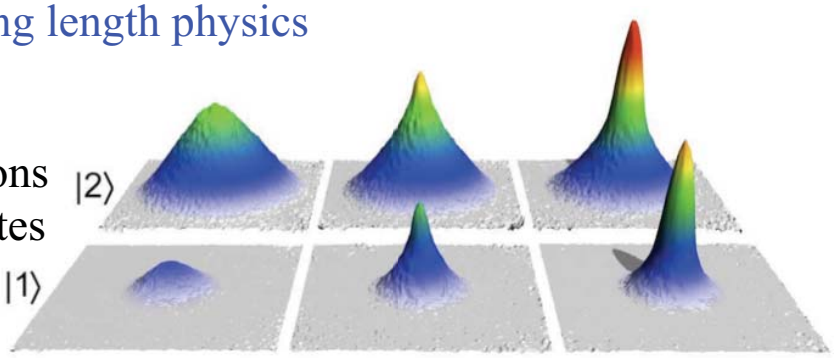

from M. Zwierlein

neutrons with same density and temperature
have the same properties!

Chiral Effective Field Theory for nuclear forces

Separation of scales: low momenta $\frac{1}{\lambda} = Q \ll \Lambda_b$ breakdown scale ~500 MeV

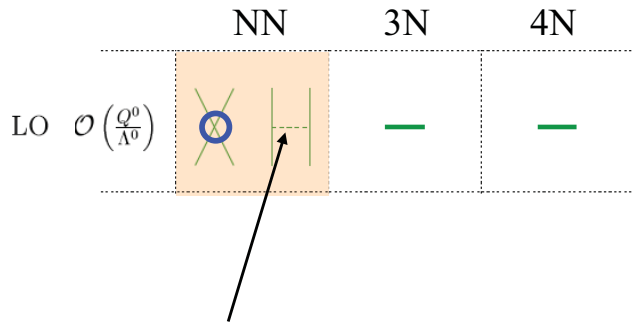

pion tensor/dipole interactions + …
→ compare to cold polar molecules

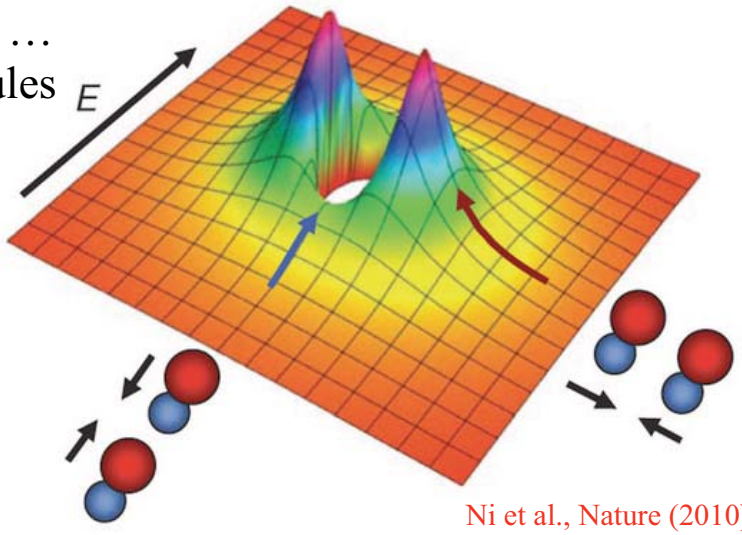

Ni et al., Nature (2010)

Chiral Effective Field Theory for nuclear forces

Separation of scales: low momenta $\frac{1}{\lambda} = Q \ll \Lambda_b$ breakdown scale ~500 MeV

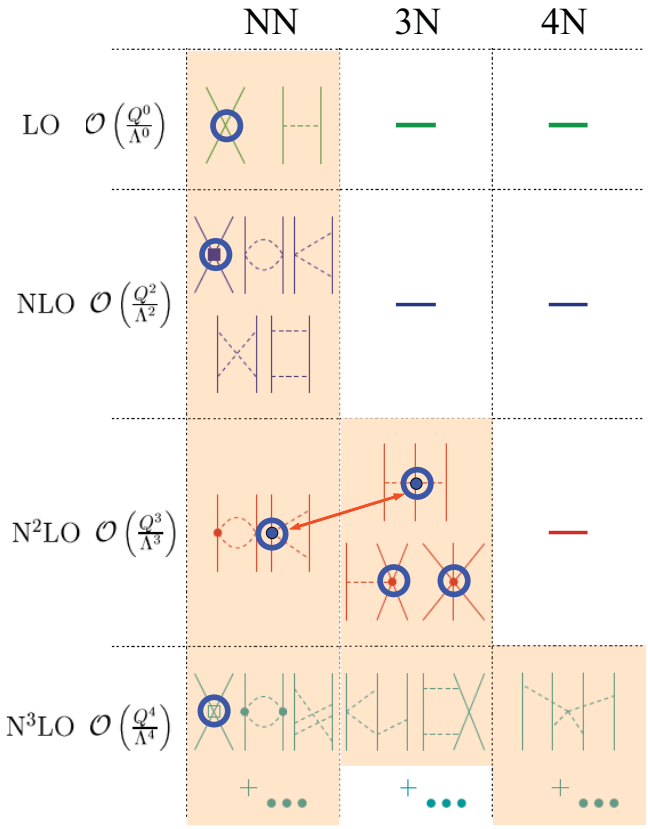

systematic: can work to desired accuracy and obtain error estimates from truncation order and Λ variation

accurate reproduction of
low-energy NN scattering at N³LO

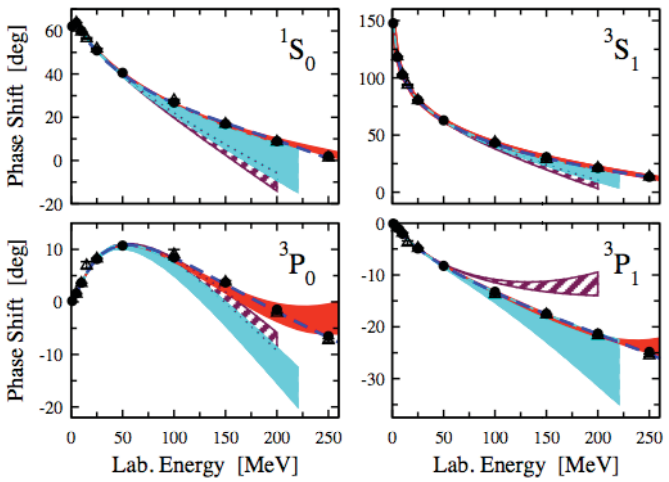

Weinberg, van Kolck, Kaplan, Savage, Wise, Epelbaum, Kaiser, Meissner,…

Chiral Effective Field Theory for nuclear forces

Separation of scales: low momenta $\frac{1}{\lambda} = Q \ll \Lambda_b$ breakdown scale ~500 MeV

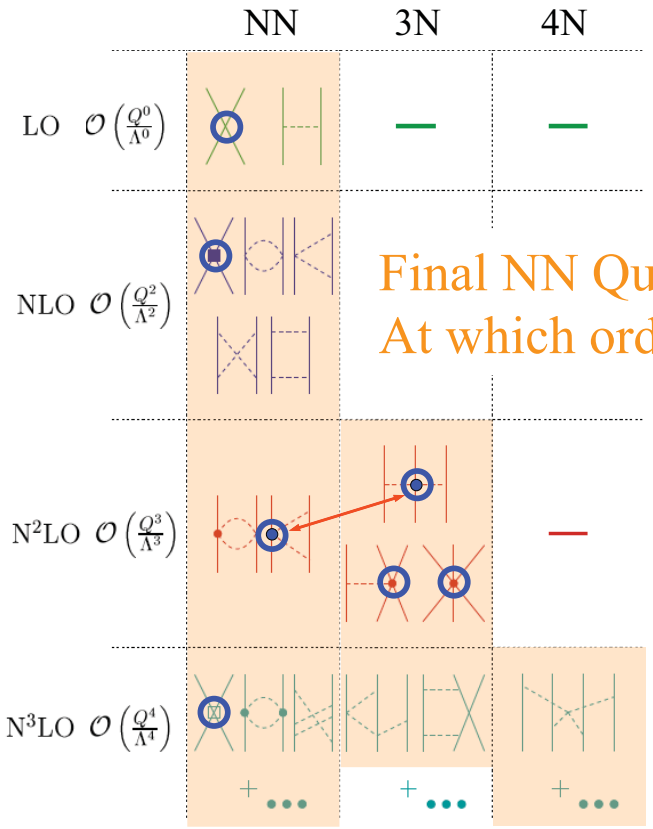

Final NN Question:
At which order do spin-orbit forces come in?

Weinberg, van Kolck, Kaplan, Savage, Wise, Epelbaum, Kaiser, Meissner,…

Nuclear forces and the Renormalization Group (RG)

RG evolution to lower resolution/cutoffs Bogner, Kuo, AS, Furnstahl,…

$$H(\Lambda) = T + V_{\rm NN}(\Lambda) + V_{\rm 3N}(\Lambda) + V_{\rm 4N}(\Lambda) + \ldots$$

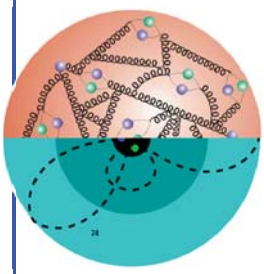

$\Lambda_{\rm chiral}$

Λ

Nuclear forces and the Renormalization Group (RG)

RG evolution to lower resolution/cutoffs Bogner, Kuo, AS, Furnstahl,…

$$H(\Lambda) = T + V_{\rm NN}(\Lambda) + V_{\rm 3N}(\Lambda) + V_{\rm 4N}(\Lambda) + \ldots$$

for NN interactions (preserves NN observables)

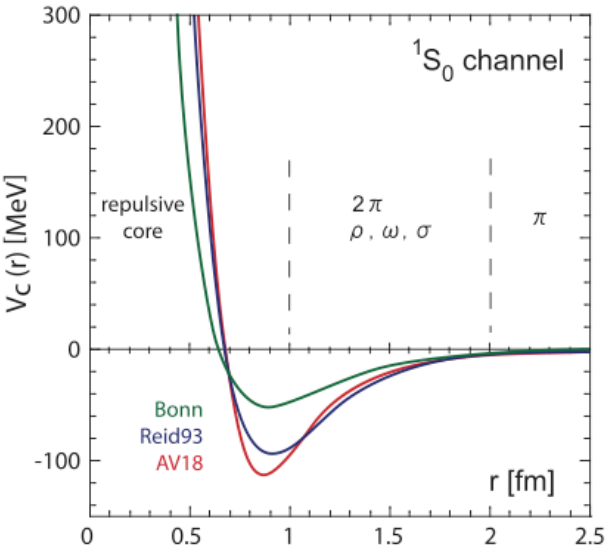

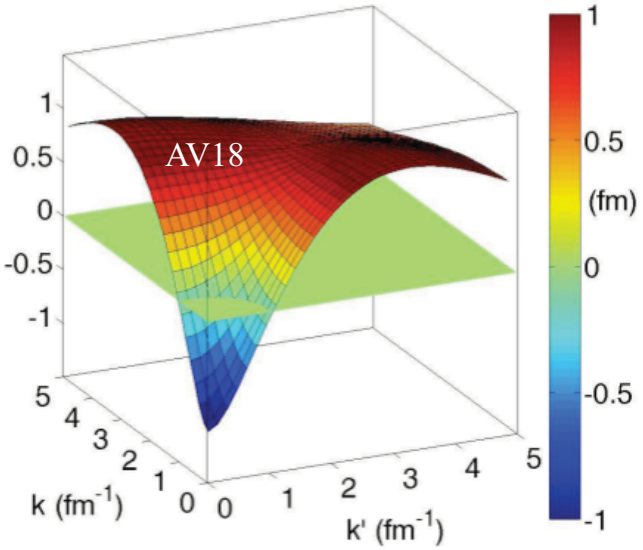

red = short-range repulsion

Nuclear forces and the Renormalization Group (RG)

RG evolution to lower resolution/cutoffs Bogner, Kuo, AS, Furnstahl,…

$$H(\Lambda) = T + V_{\rm NN}(\Lambda) + V_{\rm 3N}(\Lambda) + V_{\rm 4N}(\Lambda) + \ldots$$

for NN interactions (preserves NN observables)

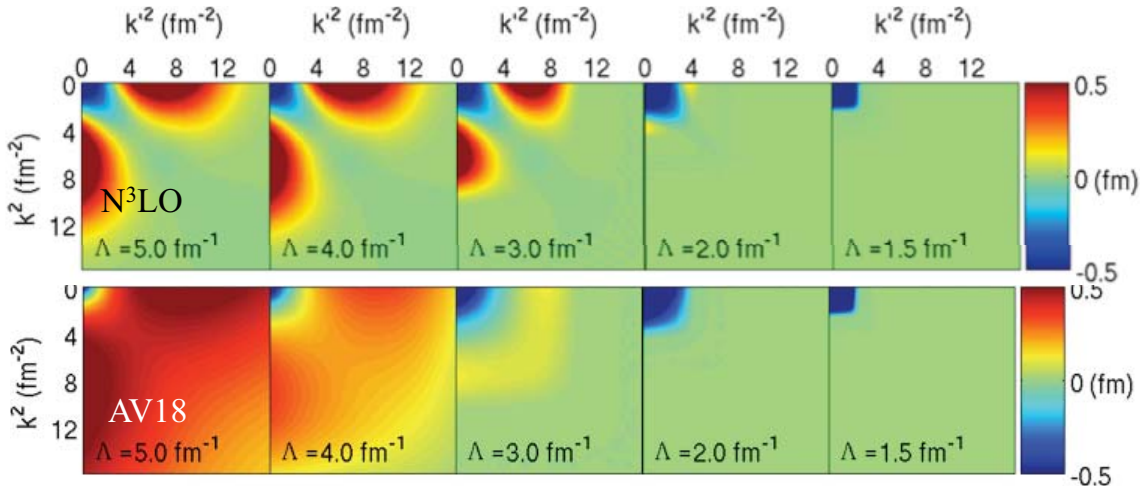

low-momentum interactions $V_{\text{low } k}(\Lambda)$

RG decouples low-momentum physics from high momenta

Nuclear forces and the Renormalization Group (RG)

RG evolution to lower resolution/cutoffs Bogner, Kuo, AS, Furnstahl,…

$$H(\Lambda) = T + V_{\rm NN}(\Lambda) + V_{\rm 3N}(\Lambda) + V_{\rm 4N}(\Lambda) + \ldots$$

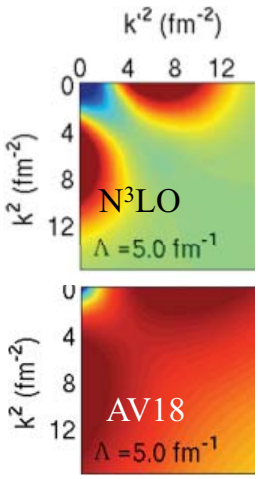

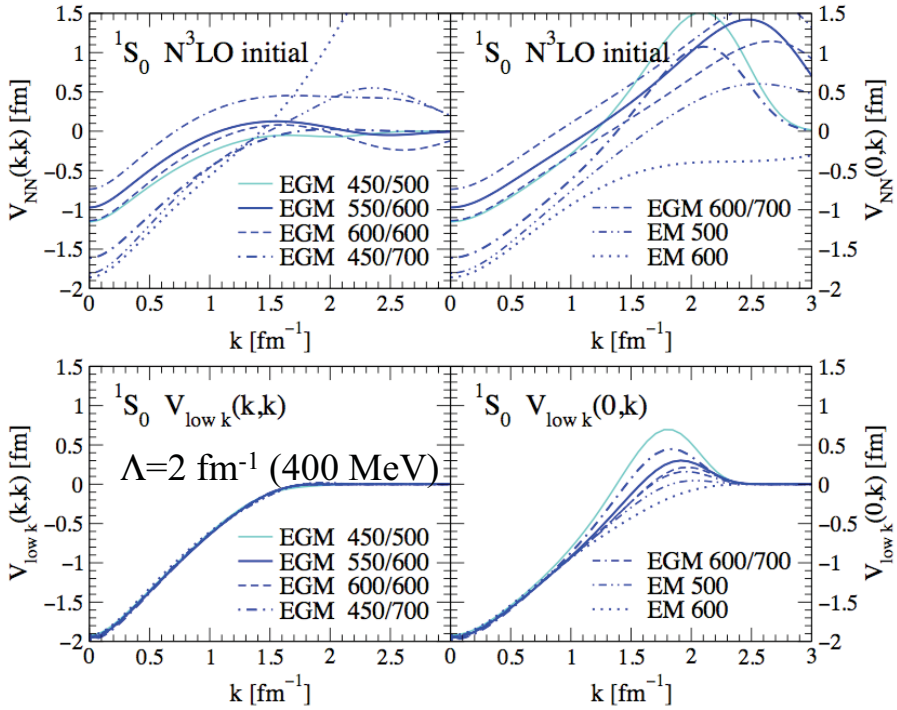

low-momentum i

RG decouples lov

low-momentum universality from different chiral N³LO potentials

Nuclear forces and the Renormalization Group (RG)

RG evolution to lower resolution/cutoffs Bogner, Kuo, AS, Furnstahl,…

$$H(\Lambda) = T + V_{\rm NN}(\Lambda) + V_{\rm 3N}(\Lambda) + V_{\rm 4N}(\Lambda) + \ldots$$

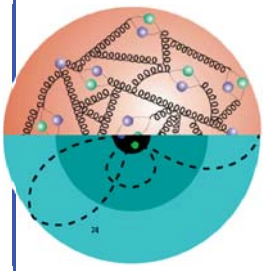

Question: Where else have you seen the Renormalization Group in Nuclear Physics?

$\Lambda_{\rm chiral}$

Λ

Chiral Effective Field Theory for nuclear forces

Separation of scales: low momenta $\frac{1}{\lambda} = Q \ll \Lambda_b$ breakdown scale ~500 MeV

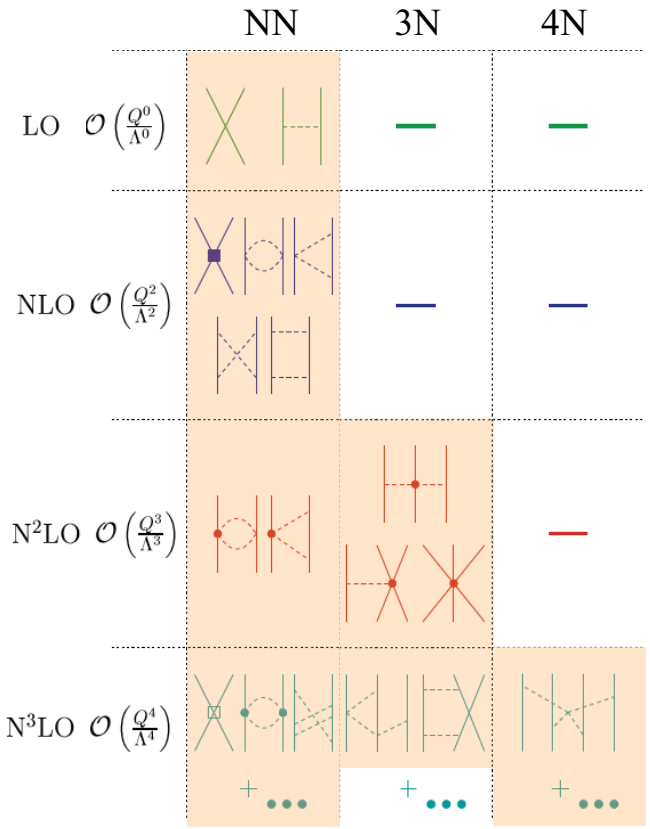

limited resolution at low energies,
can expand in powers $(Q/\Lambda_b)^n$

LO, n=0 - leading order,
NLO, n=2 - next-to-leading order,…

expansion parameter ~ 1/3

(compare to multipole expansion
for a charge distribution)

Weinberg, van Kolck, Kaplan, Savage, Wise, Epelbaum, Kaiser, Meissner,…

Why are there three-body forces?

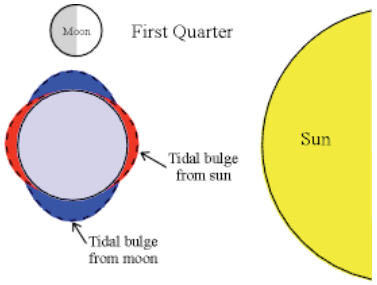

tidal effects lead to 3-body forces
in earth-sun-moon system

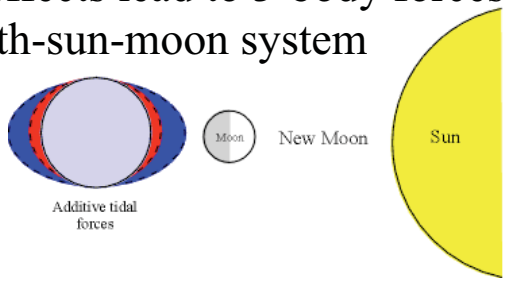

Why are there three-nucleon (3N) forces?

Nucleons are finite-mass composite particles, can be excited to resonances

dominant contribution from Δ(1232 MeV)

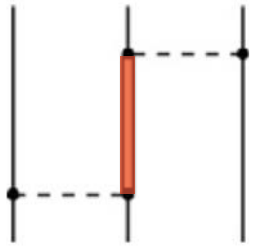

+ many shorter-range parts

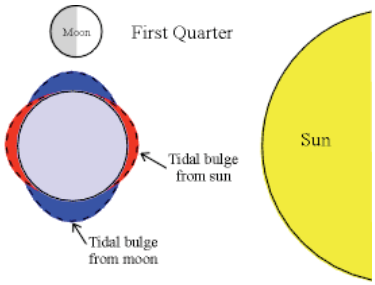

tidal effects lead to 3-body forces in earth-sun-moon system

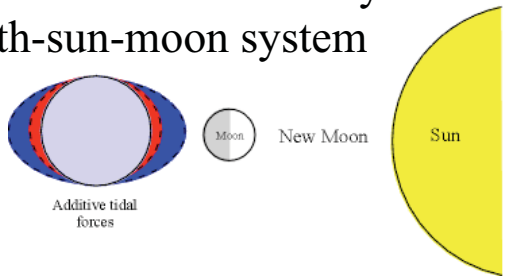

in chiral EFT (Delta-less): 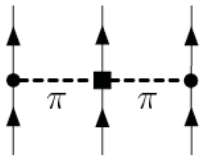 + shorter-range parts

in pionless EFT: 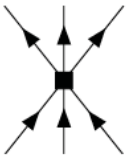 + higher-order parts

Chiral Effective Field Theory for nuclear forces

Separation of scales: low momenta $\frac{1}{\lambda} = Q \ll \Lambda_b$ breakdown scale ~500 MeV

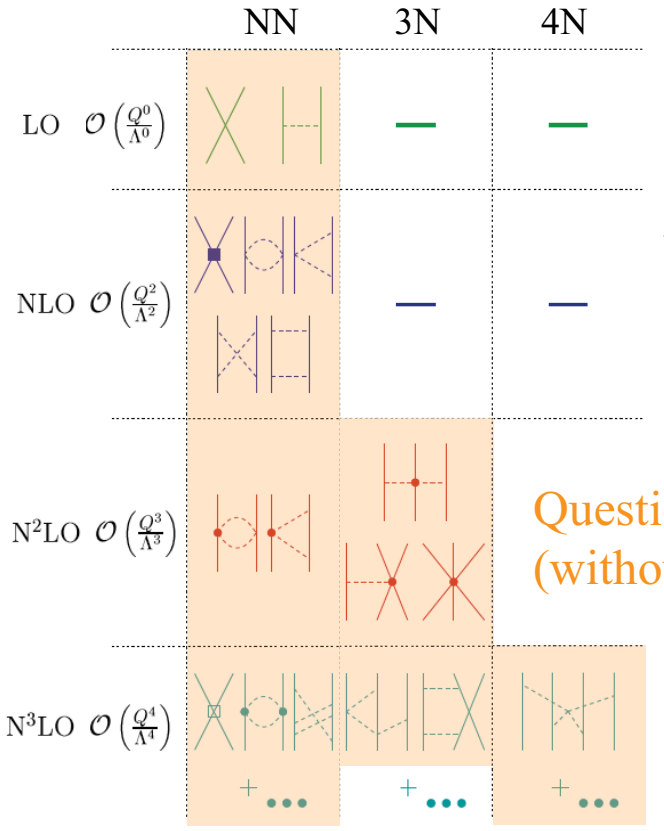

limited resolution at low energies, can expand in powers $(Q/\Lambda_b)^n$

LO, n=0 - leading order,
NLO, n=2 - next-to-leading order,…

Question: Why do 3N forces start at n=3 (without explicit Deltas)?

Weinberg, van Kolck, Kaplan, Savage, Wise, Epelbaum, Kaiser, Meissner,…

Chiral Effective Field Theory for nuclear forces

Separation of scales: low momenta $\frac{1}{\lambda} = Q \ll \Lambda_b$ breakdown scale ~500 MeV

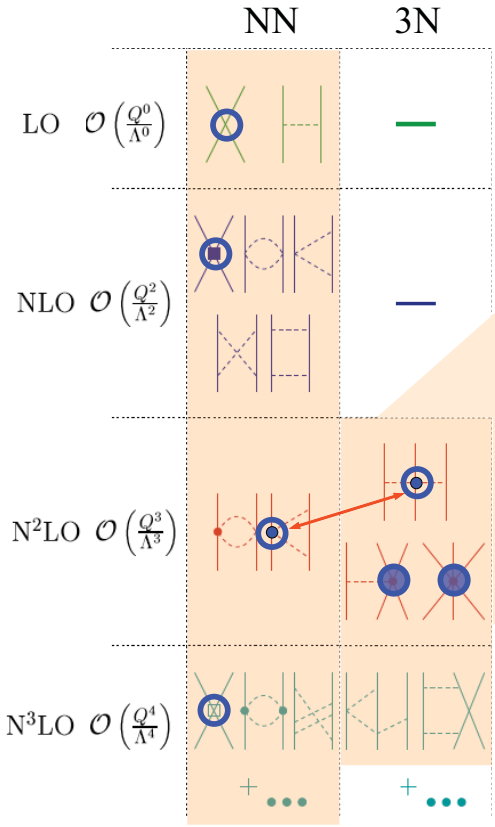

consistent NN-3N interactions

3N,4N: only 2 new couplings to N³LO

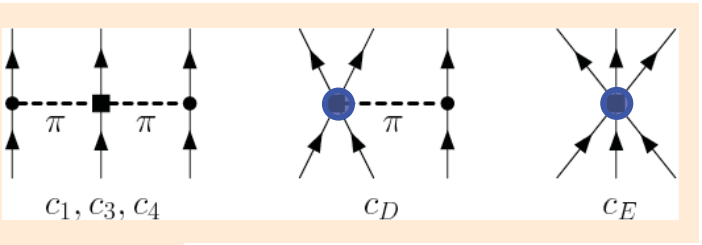

c_i from πN and NN Meissner et al. (2007)

$$c_1 = -0.9^{+0.2}_{-0.5}\,,\; c_3 = -4.7^{+1.2}_{-1.0}\,,\; c_4 = 3.5^{+0.5}_{-0.2}$$

single-Δ: c_1=0, c_3=-c_4/2=-3 GeV^{-1}

c_D, c_E fit to ^{3}H binding energy and ^{4}He radius (or ^{3}H beta decay half-life)

Weinberg, van Kolck, Kaplan, Savage, Wise, Epelbaum, Kaiser, Meissner,…

Chiral Effective Field Theory for nuclear forces

Separation of scales: low momenta $\frac{1}{\lambda} = Q \ll \Lambda_b$ breakdown scale ~500 MeV

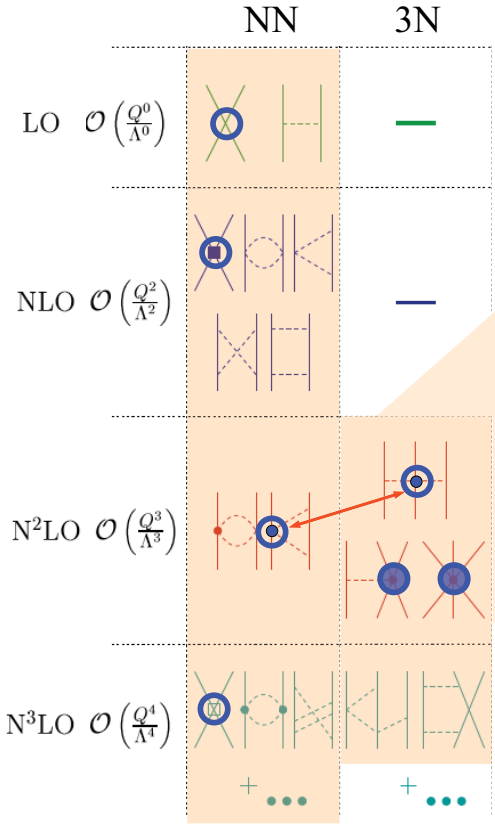

consistent NN-3N interactions

3N,4N: only 2 new couplings to N³LO

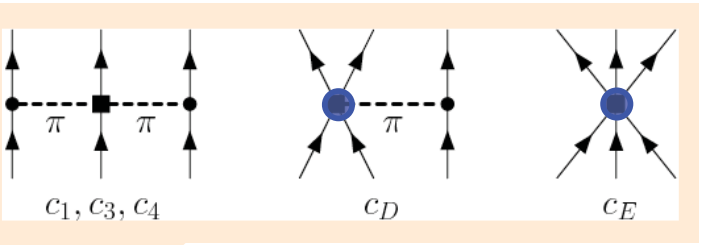

Question: Why are the next order 3N forces (n=4) parameter-free (without new 3N contact interactions)?

Weinberg, van Kolck, Kaplan, Savage, Wise, Epelbaum, Kaiser, Meissner,…

Subleading chiral 3N forces

parameter-free N^{3}LO from Epelbaum et al.; Bernard et al. (2007), Ishikawa, Robilotta (2007)

one-loop contributions:
2π-exchange, 2π-1π-exchange, rings, contact-1π-, contact-2π-exchange

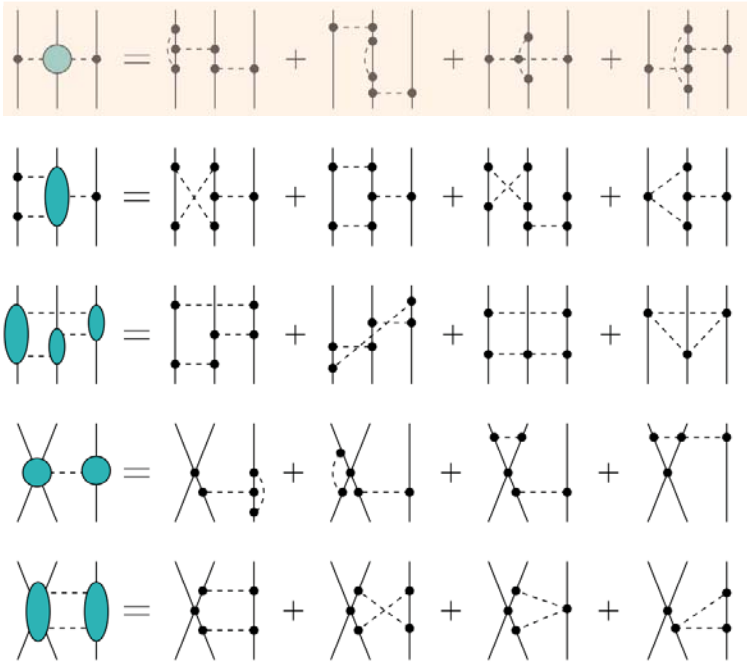

decrease c_i strengths
comparable to N^{2}LO uncertainty

$\delta c_1 = -g_A^2 M_\pi / 64\pi F_\pi^2$, $\delta c_3 = -\delta c_4 = g_A^4 M_\pi / 16\pi F_\pi^2$

$\delta c_3 = -\delta c_4 = 1$ GeV^{-1}

1/m corrections: spin-orbit parts, interesting for A_y puzzle

Chiral Effective Field Theory for nuclear forces

Separation of scales: low momenta $\frac{1}{\lambda} = Q \ll \Lambda_b$ breakdown scale ~500 MeV

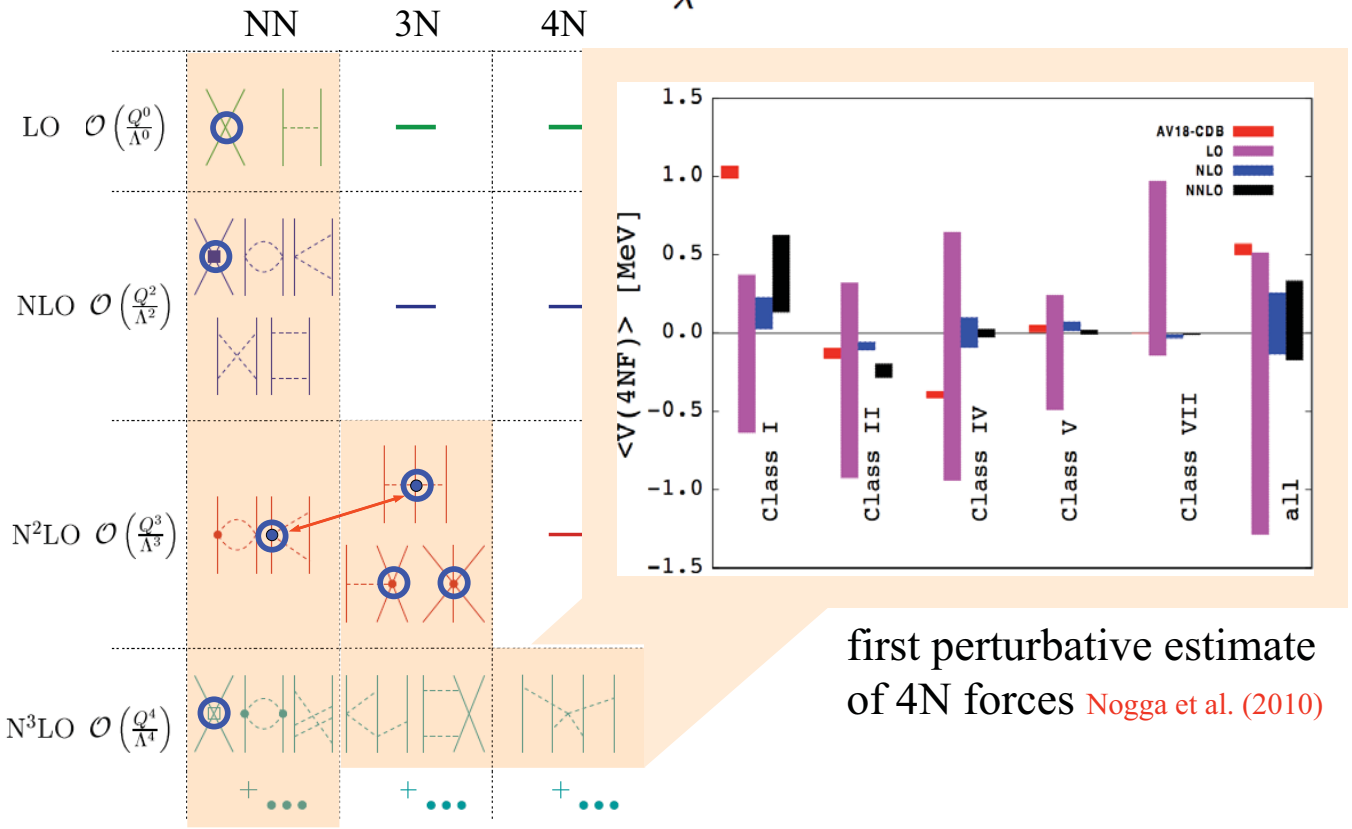

first perturbative estimate of 4N forces Nogga et al. (2010)

Weinberg, van Kolck, Kaplan, Savage, Wise, Epelbaum, Meissner,…

Outline

Chiral effective field theory for nuclear forces
Epelbaum, Hammer, Meissner, Rev. Mod. Phys. 81, 1773 (2009). Overview.
Epelbaum, Prog. Part. Nucl. Phys. 57, 654 (2006). Many useful details.
Bogner, Furnstahl, AS, Prog. Part. Nucl. Phys. 65, 94 (2010). Renormalization Group.

3N forces and neutron-rich nuclei
Otsuka, Suzuki, Holt, AS, Akaishi, Phys. Rev. Lett. 105, 032501 (2010).
Holt, Otsuka, AS, Suzuki, arXiv:1009.5984.
Holt, AS, arXiv:1108.2680.

3N forces and neutron matter, impact on neutron stars
Hebeler, AS, Phys. Rev. C 82, 014314 (2010).
Hebeler, Lattimer, Pethick, AS, Phys. Rev. Lett. 105, 161102 (2010).

3N forces and electroweak currents
Menendez, Gazit, AS, Phys. Rev. Lett. 107, 062501 (2011).

Chiral Effective Field Theory for nuclear forces

Separation of scales: low momenta $\frac{1}{\lambda} = Q \ll \Lambda_b$ breakdown scale ~500 MeV

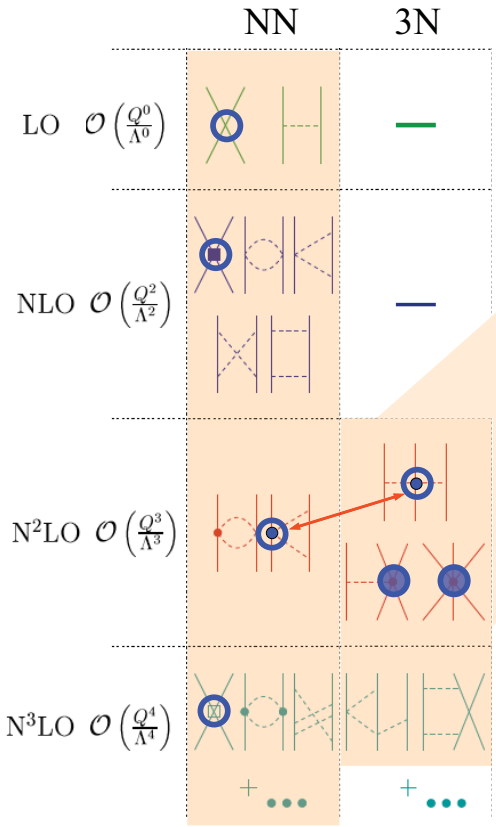

consistent NN-3N interactions

3N,4N: only 2 new couplings to N³LO

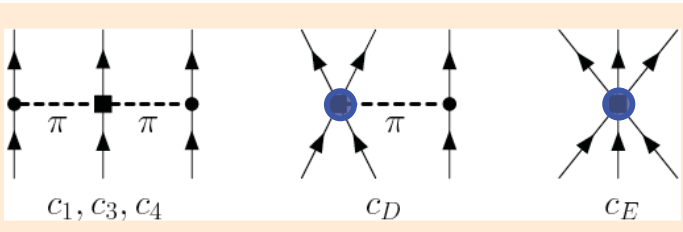

c_i from πN and NN Meissner et al. (2007)

$$c_1 = -0.9^{+0.2}_{-0.5}\,,\; c_3 = -4.7^{+1.2}_{-1.0}\,,\; c_4 = 3.5^{+0.5}_{-0.2}$$

single-Δ: c_1=0, c_3=-c_4/2=-3 GeV^{-1}

c_D, c_E fit to ^{3}H binding energy and ^{4}He radius (or ^{3}H beta decay half-life)

Weinberg, van Kolck, Kaplan, Savage, Wise, Epelbaum, Kaiser, Meissner,…

Towards the limits of existence - the neutron drip-line

Discovery of ^{40}Mg and ^{42}Al suggests neutron drip-line slant towards heavier isotopes

Nature (2007)

T. Baumann[1], A. M. Amthor[1,2], D. Bazin[1], B. A. Brown[1,2], C. M. Folden III[1], A. Gade[1,2], T. N. Ginter[1], M. Hausmann[1], M. Matoš[1], D. J. Morrissey[1,3], M. Portillo[1], A. Schiller[1], B. M. Sherrill[1,2], A. Stolz[1], O. B. Tarasov[1,4] & M. Thoennessen[1,2]

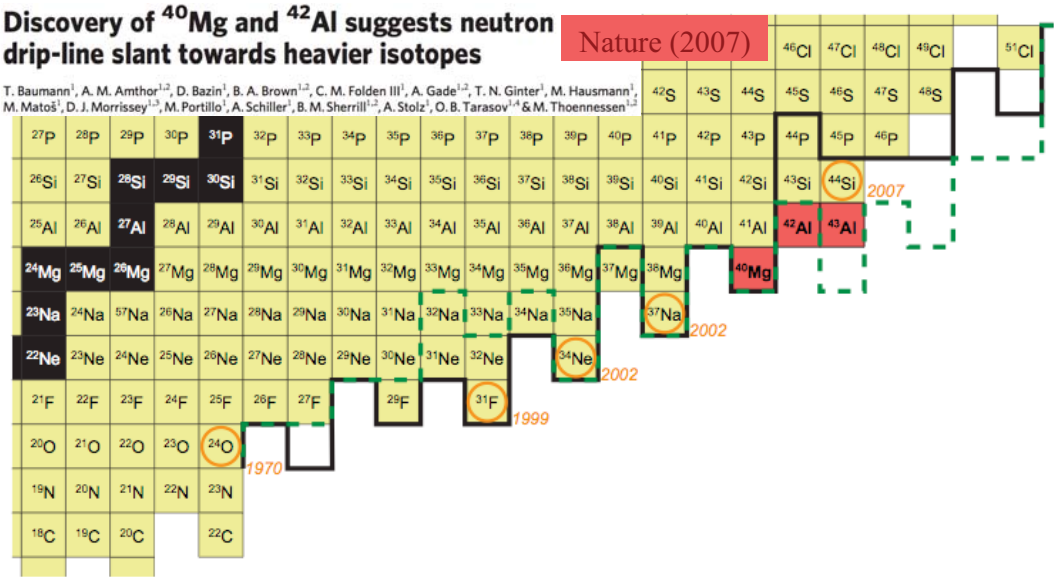

The oxygen anomaly

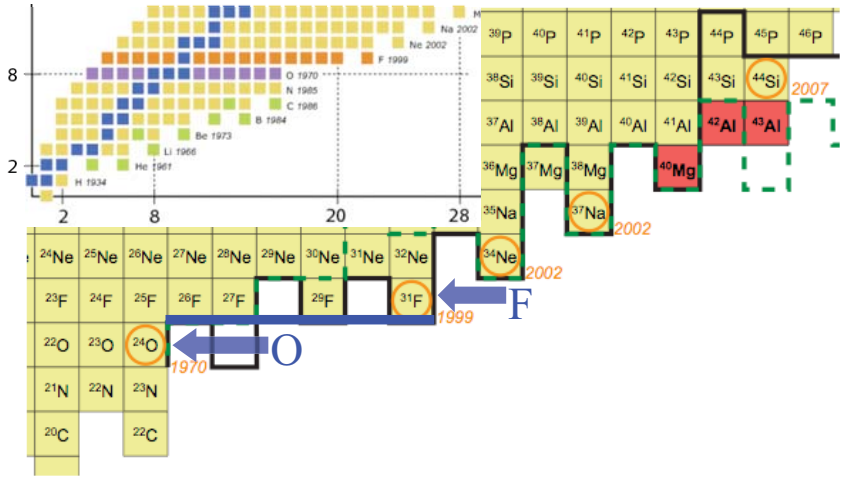

The oxygen anomaly

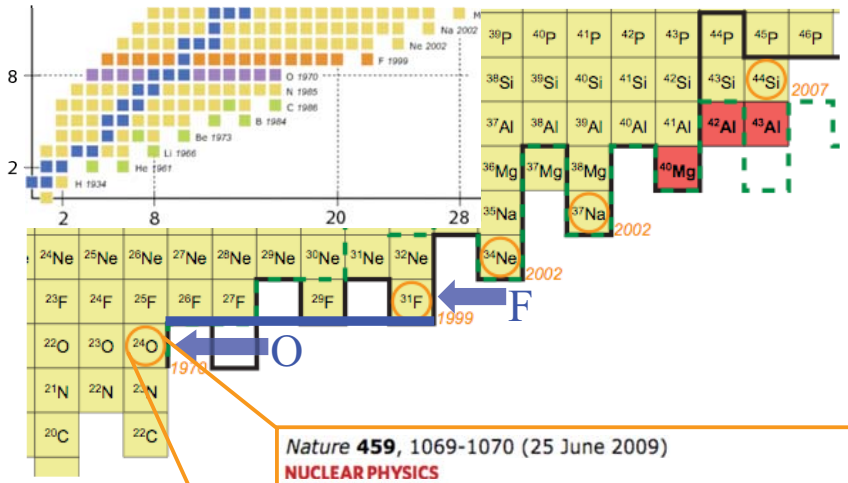

Nature **459**, 1069-1070 (25 June 2009)

NUCLEAR PHYSICS

Unexpected doubly magic nucleus

Robert V. F. Janssens

Nuclei with a 'magic' number of both protons and neutrons, dubbed doubly magic, are particularly stable. The oxygen isotope ^{24}O has been found to be one such nucleus — yet it lies just at the limit of stability.

The oxygen anomaly - not reproduced without 3N forces

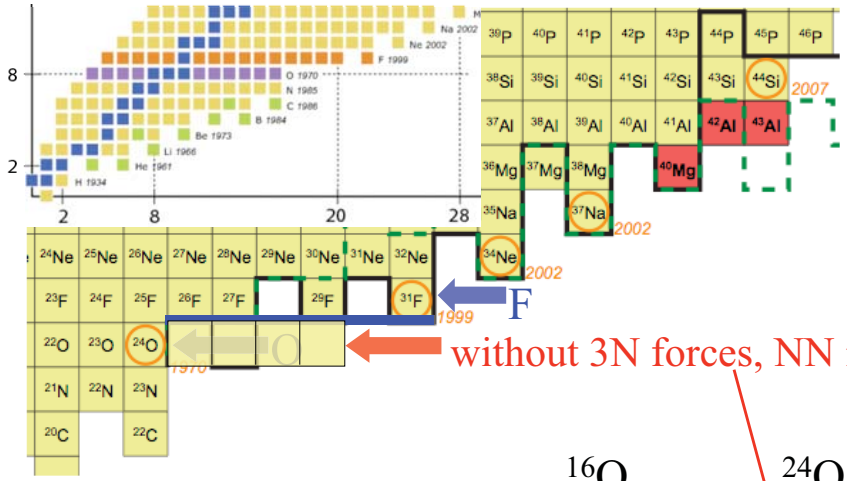

without 3N forces, NN interactions too attractive

many-body theory based on two-nucleon forces: drip-line incorrect at ^{28}O

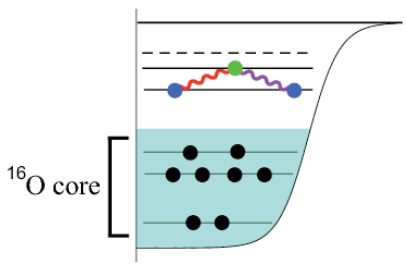

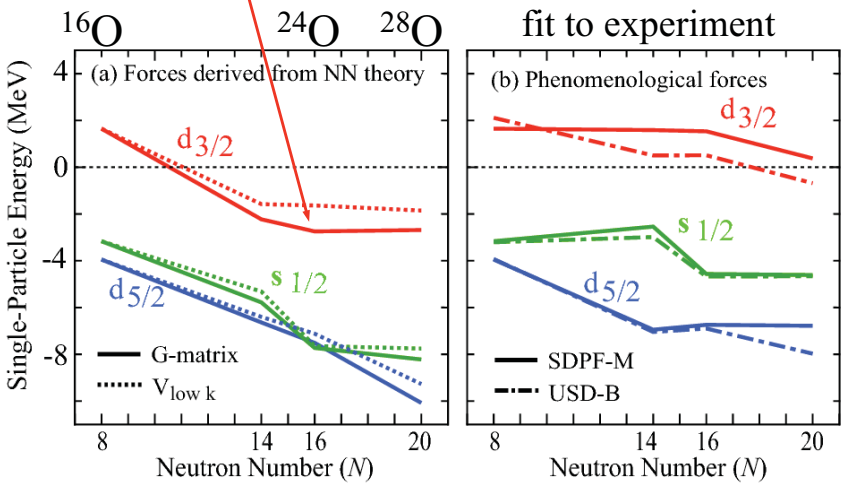

The oxygen anomaly - impact of 3N forces

include ‘normal-ordered’ 2-body part of 3N forces (enhanced by core A)

leads to repulsive interactions between valence neutrons

contributions from residual three valence-nucleon interactions suppressed by $E_{ex}/E_F \sim N_{valence}/N_{core}$

Friman, AS, arXiv:1101.4858.

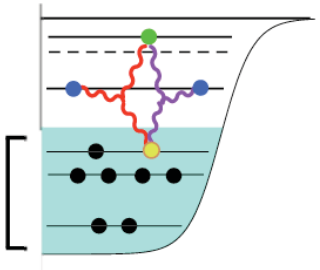

The oxygen anomaly - impact of 3N forces

include ‘normal-ordered’ 2-body part of 3N forces (enhanced by core A)

leads to repulsive interactions between valence neutrons

contributions from residual three valence-nucleon interactions suppressed by $E_{ex}/E_F \sim N_{valence}/N_{core}$

Friman, AS, arXiv:1101.4858.

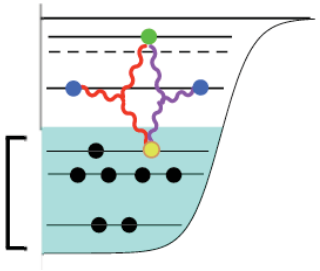

$d_{3/2}$ orbital remains unbound from ^{16}O to ^{28}O

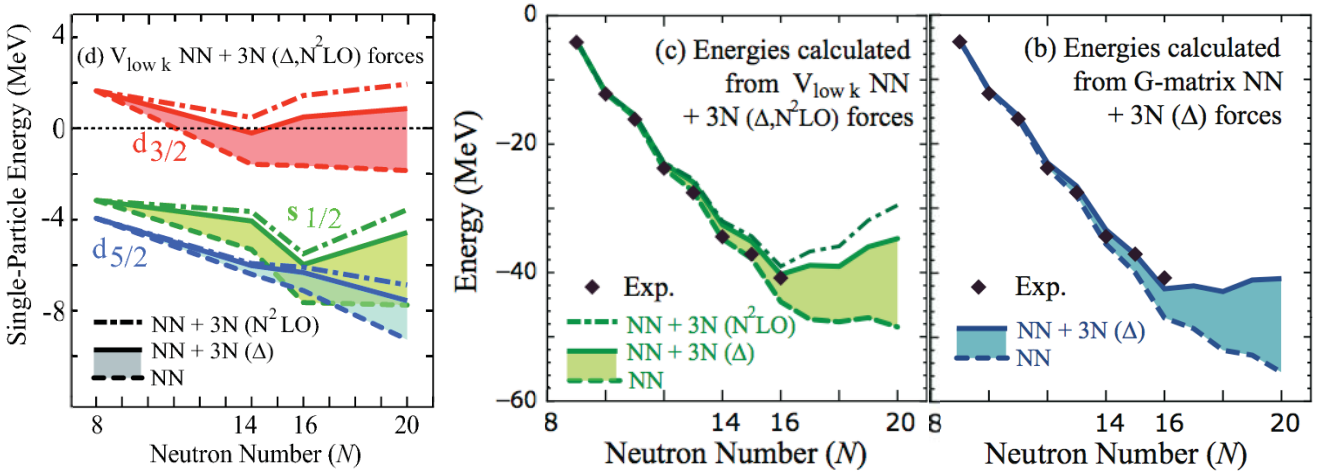

microscopic explanation of the oxygen anomaly Otsuka et al., PRL (2010)

Oxygen spectra

focused on bound excited states

Holt, AS, arXiv:1108.2680.

NN only too compressed

3N contributions and extended valence space are key to reproduce excited states

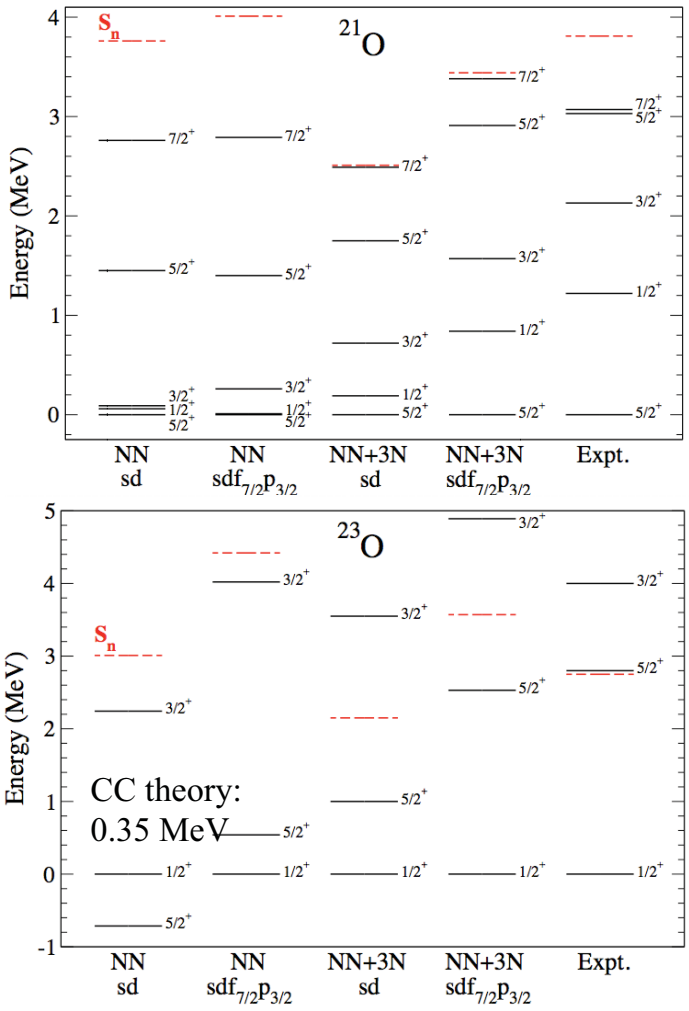

Evolution to neutron-rich calcium isotopes

repulsive 3N contributions also key for calcium ground-state energies

Holt et al., arXiv:1009:5984

mass measured to ^{52}Ca

shown to exist to ^{58}Ca

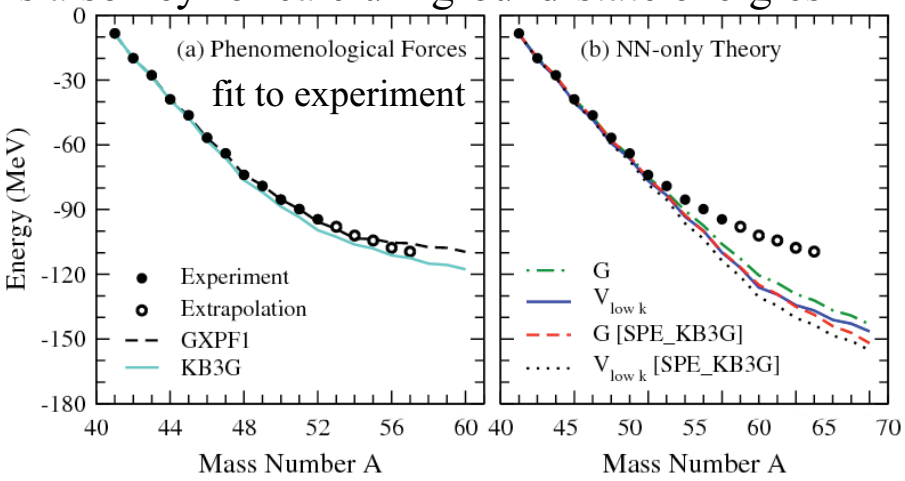

Evolution to neutron-rich calcium isotopes

repulsive 3N contributions also key for calcium ground-state energies

Holt et al., arXiv:1009:5984

mass measured to ^{52}Ca
shown to exist to ^{58}Ca

predict drip-line
around ^{60}Ca,
continuum contributions
will be key

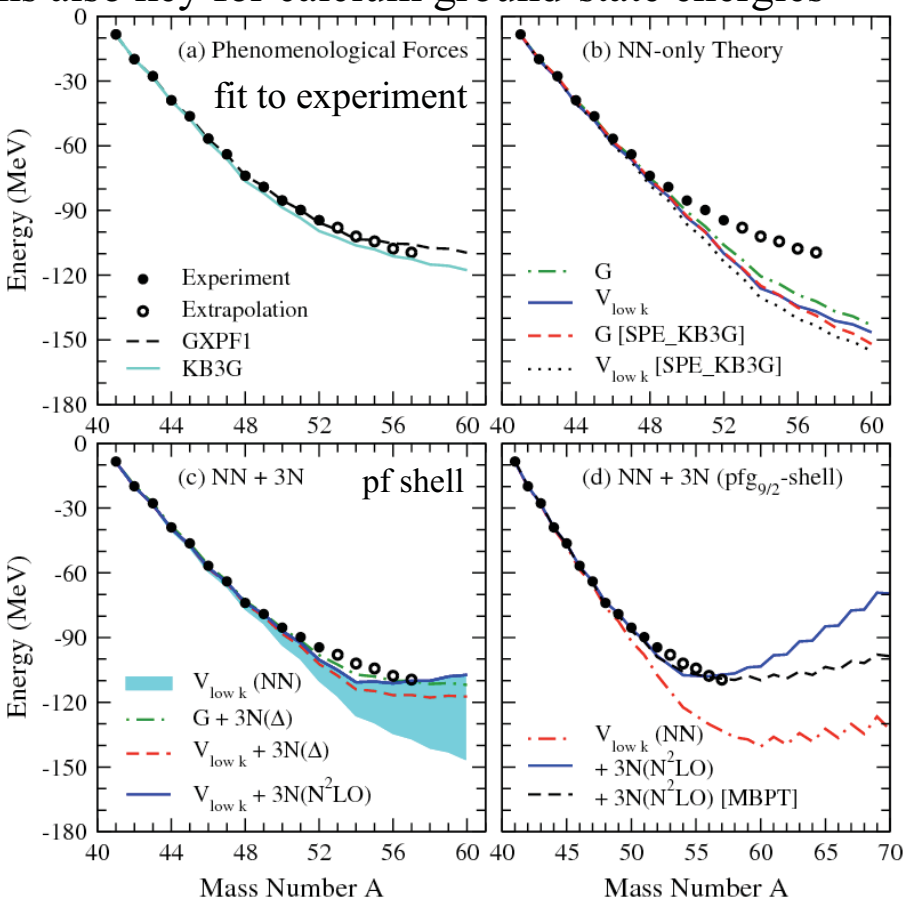

Three-body forces and magic numbers

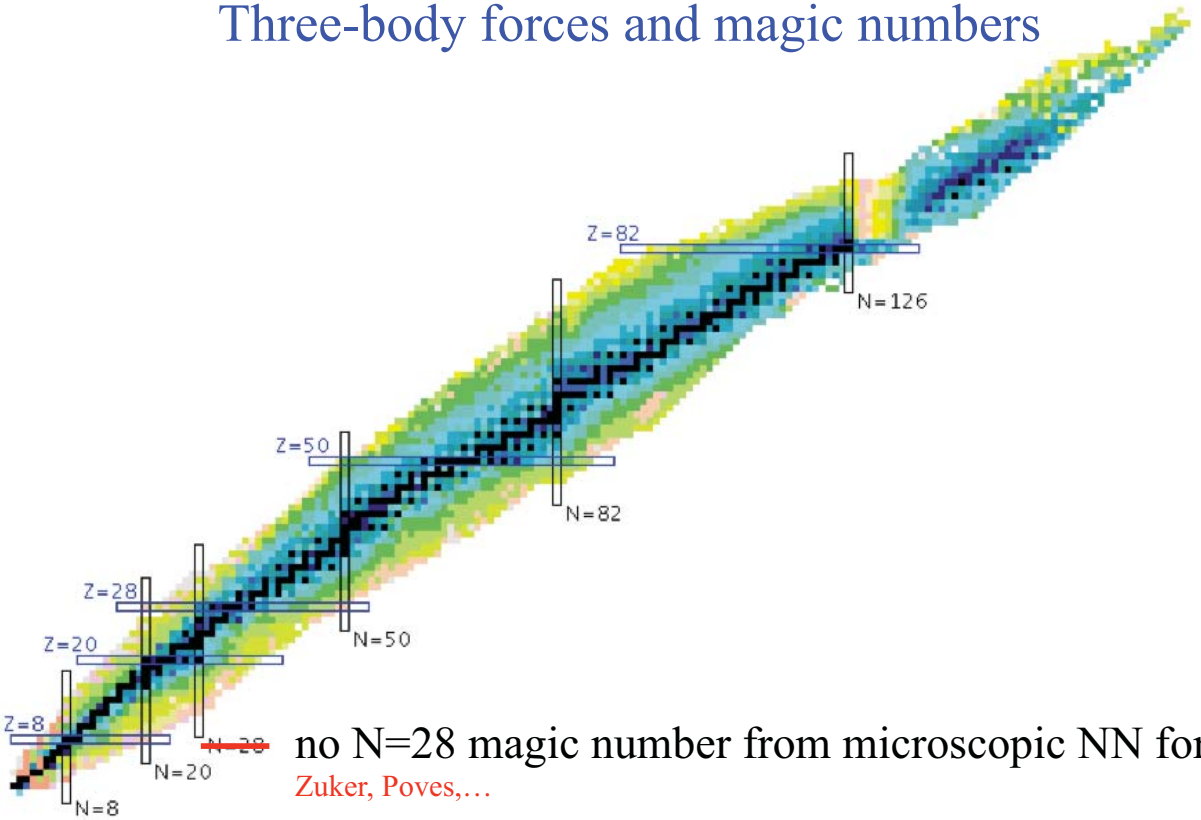

no N=28 magic number from microscopic NN forces

Zuker, Poves,…

Three-body forces and magic numbers

3N mechanism important for shell structure

Holt et al., arXiv:1009:5984

N=28 shell closure due to 3N forces and single-particle effects (^{41}Ca)

N=34: predict high 2^+ excitation energy in ^{54}Ca at 3-5 MeV

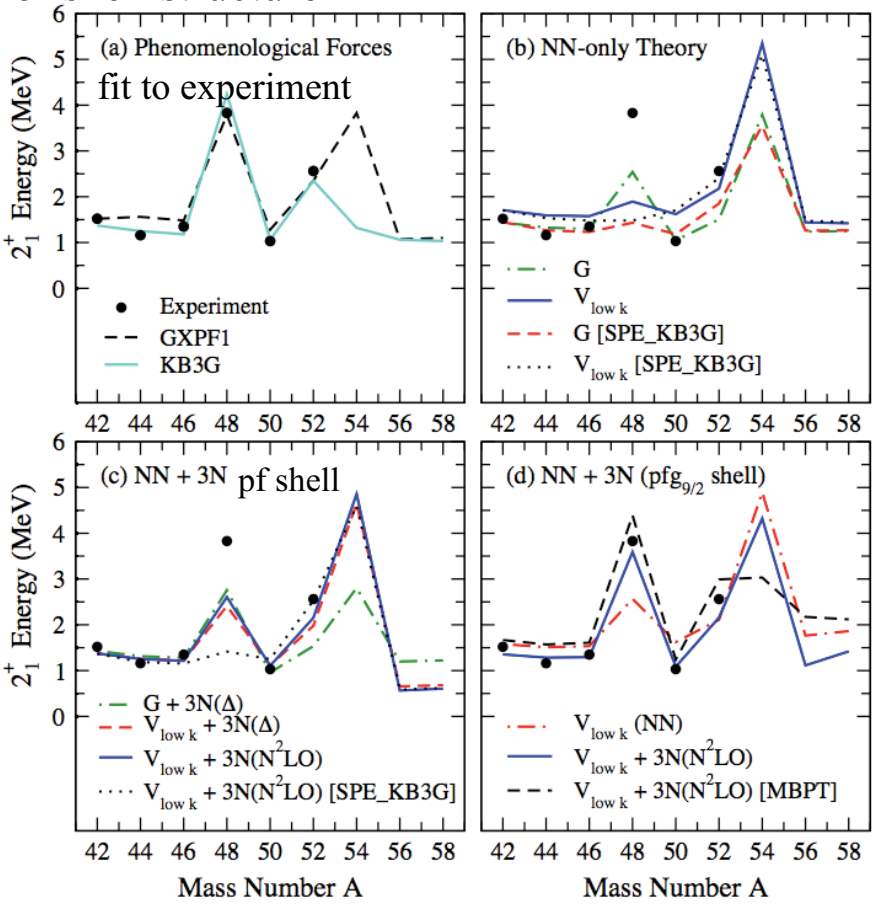

Extreme neutron-rich matter in stars

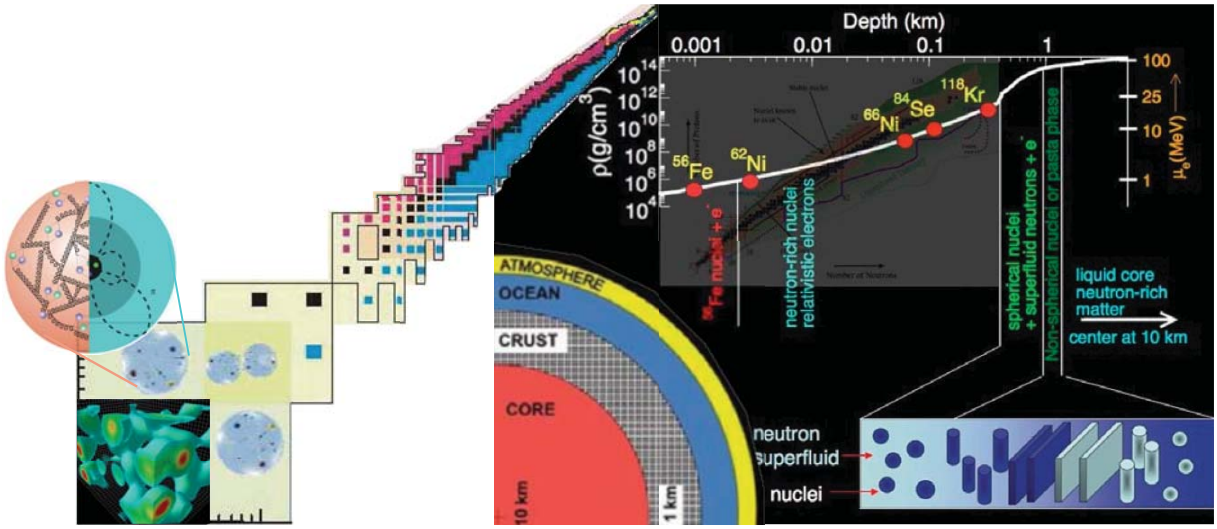

Convergence with low-momentum interactions

large cutoffs lead to flipped-potential bound states, even for small -λV
requires nonperturbative expansion, leads to slow convergence for nuclei

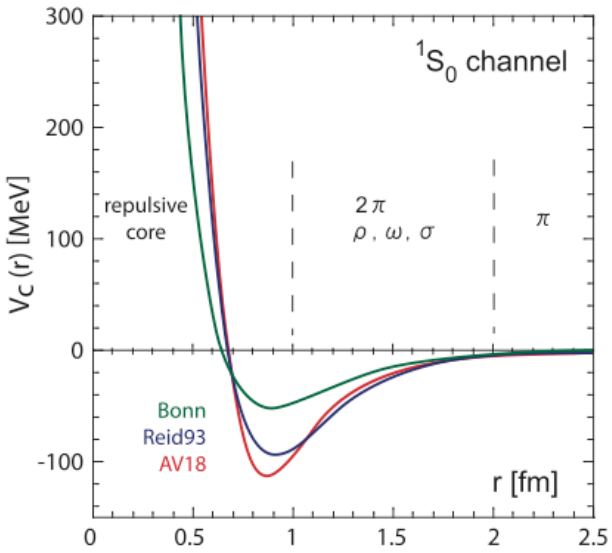

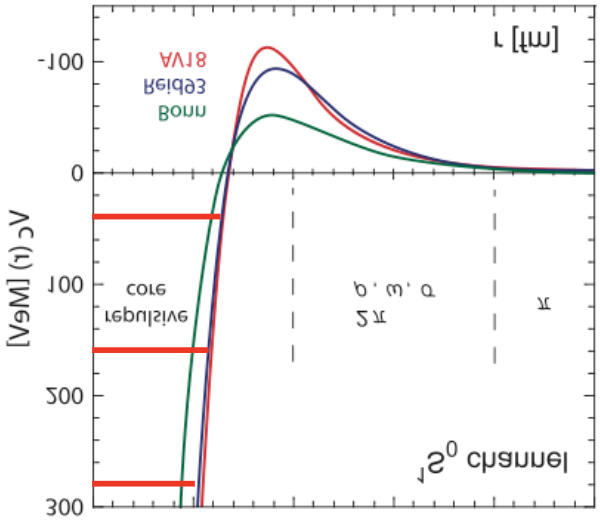

Weinberg eigenvalue analysis: two-body scattering becomes perturbative after RG evolution, except in channels with bound states

EFT and RG leads to improved convergence for nuclei and nuclear matter

Advances in nuclear matter theory

Is nuclear matter perturbative with chiral EFT and RG evolution?

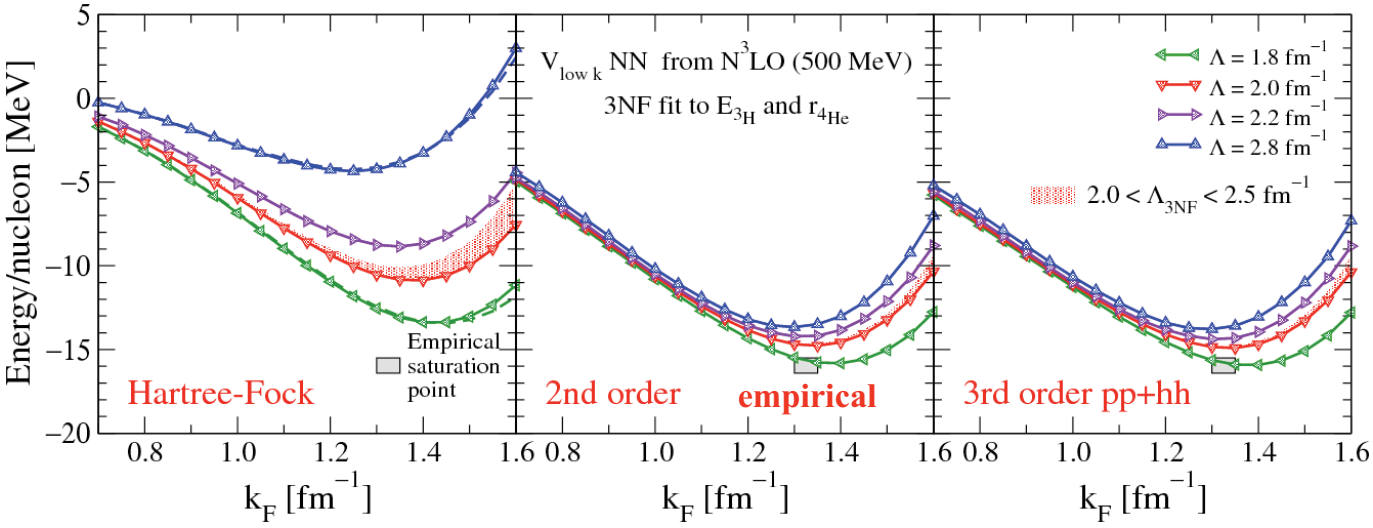

Hebeler, Bogner, Furnstahl, Nogga, AS (2009, 2010)

exciting: empirical saturation with theoretical uncertainties
improved 3N treatment see also Holt, Kaiser, Weise (2010)

input to develop a universal energy density functional for all nuclei

UNEDF SciDAC Collaboration
Universal Nuclear Energy Density Functional

Impact of 3N forces on neutron matter

Hebeler, AS (2010); Tolos, Friman, AS (2007)

only long-range parts of 3N forces contribute to neutron matter (c_1 and c_3)

neutron matter: many-body forces are predicted to N^{3}LO!

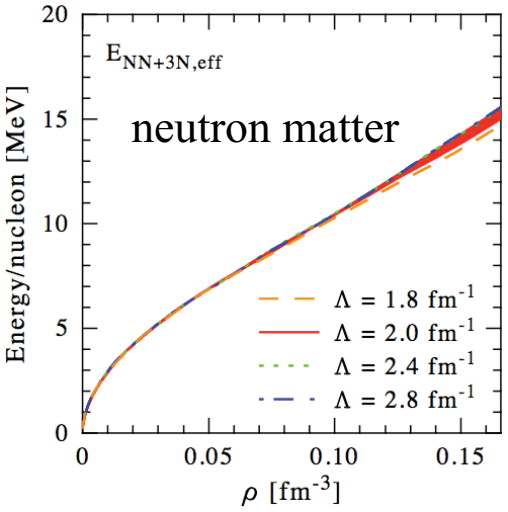

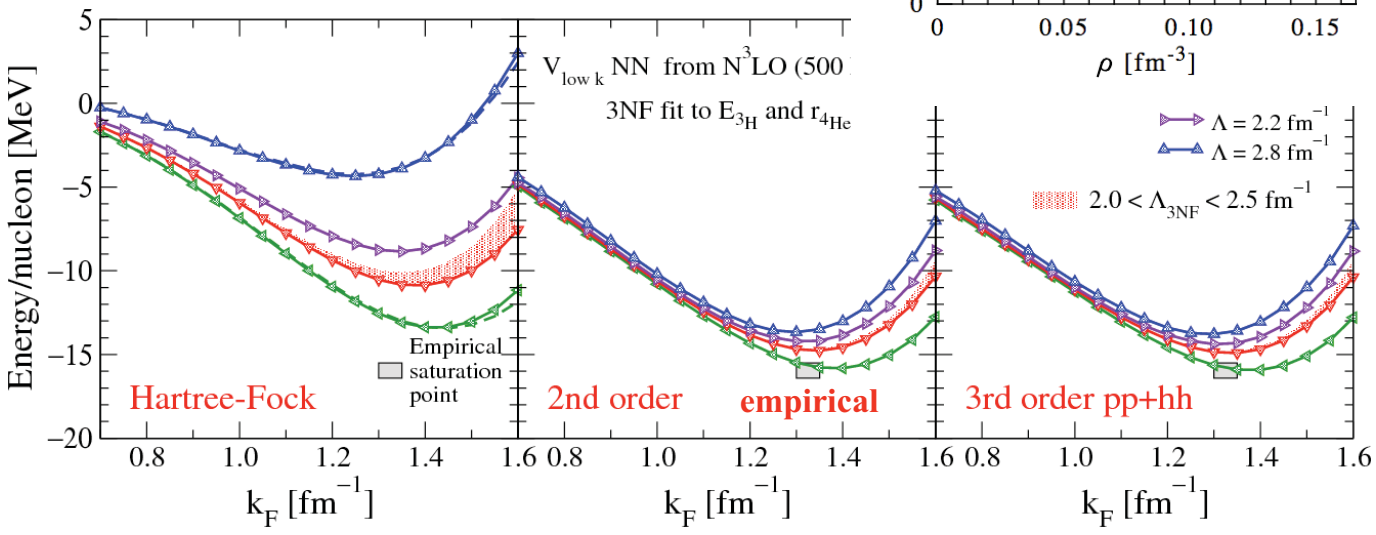

Chiral Effective Field Theory for nuclear forces

Separation of scales: low momenta $\frac{1}{\lambda} = Q \ll \Lambda_b$ breakdown scale ~500 MeV

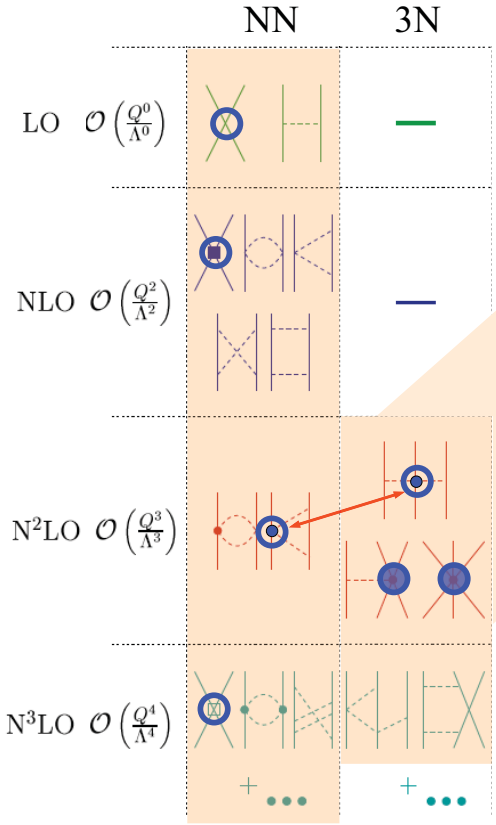

consistent NN-3N interactions

3N,4N: only 2 new couplings to N^{3}LO

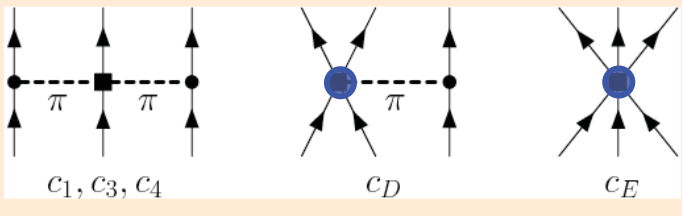

Question: Why do the c_D and c_E terms not contribute to neutron matter?

Weinberg, van Kolck, Kaplan, Savage, Wise, Epelbaum, Kaiser, Meissner,…

Chiral Effective Field Theory for nuclear forces

Separation of scales: low momenta $\frac{1}{\lambda} = Q \ll \Lambda_b$ breakdown scale ~500 MeV

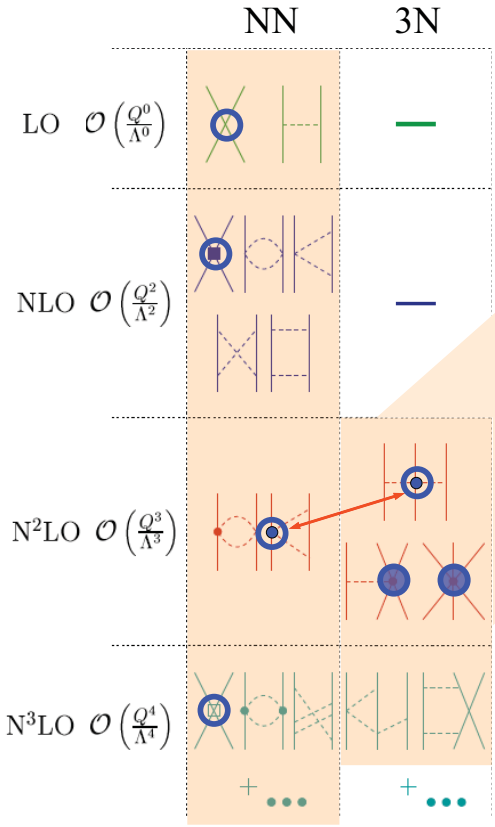

consistent NN-3N interactions

3N,4N: only 2 new couplings to N³LO

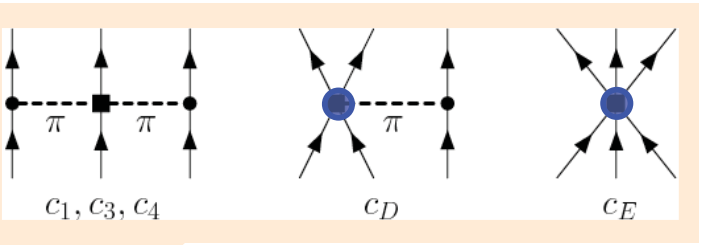

c_i from πN and NN Meissner et al. (2007)

$$c_1 = -0.9^{+0.2}_{-0.5}\,,\; c_3 = -4.7^{+1.2}_{-1.0}\,,\; c_4 = 3.5^{+0.5}_{-0.2}$$

single-Δ: c_1=0, c_3=-c_4/2=-3 GeV^{-1}

Weinberg, van Kolck, Kaplan, Savage, Wise, Epelbaum, Kaiser, Meissner,…

Impact of 3N forces on neutron matter

Hebeler, AS (2010); Tolos, Friman, AS (2007)

only long-range parts of 3N forces contribute to neutron matter (c_1 and c_3)

uncertainties dominated by c_3 coupling

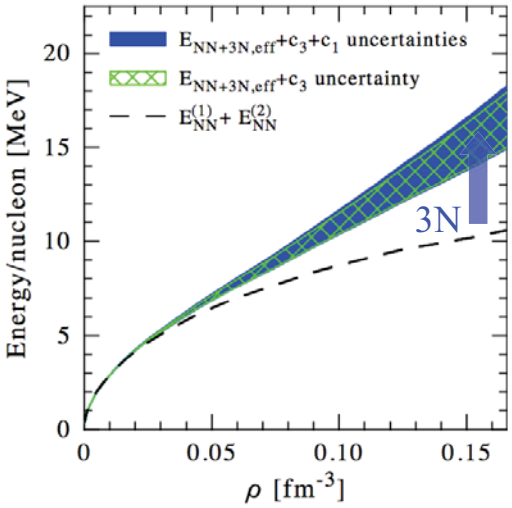

Impact of 3N forces on neutron matter

Hebeler, AS (2010); Tolos, Friman, AS (2007)

only long-range parts of 3N forces contribute to neutron matter (c_1 and c_3)

uncertainties dominated by c_3 coupling

microscopic calculations within band

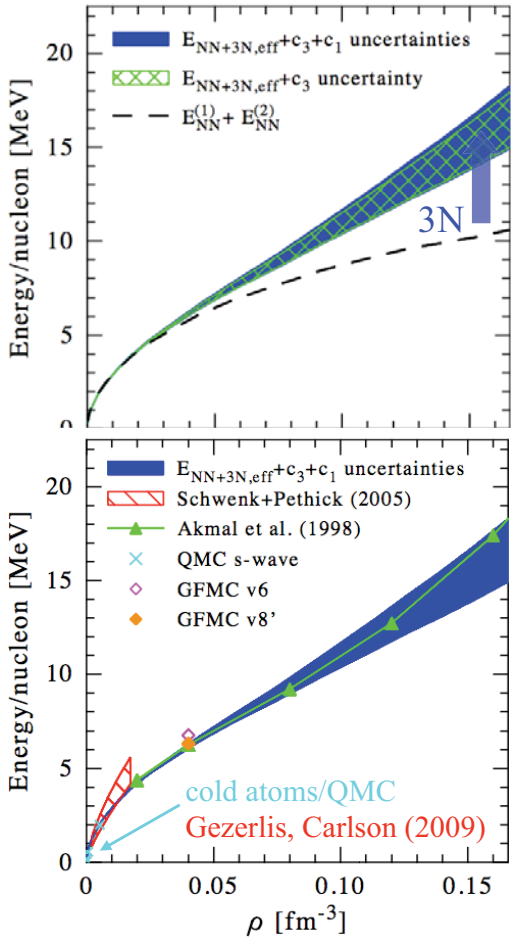

Symmetry energy and neutron skin Hebeler et al. (2010)

neutron matter band predicts range for symmetry energy 30.1-34.4 MeV

c_1 [GeV^{-1}]	c_3 [GeV^{-1}]	$\overline{S}_2$ [MeV]
−0.7	−2.2	30.1
−1.4	−4.8	34.4
NN-only EM		26.5
NN-only EGM		25.6

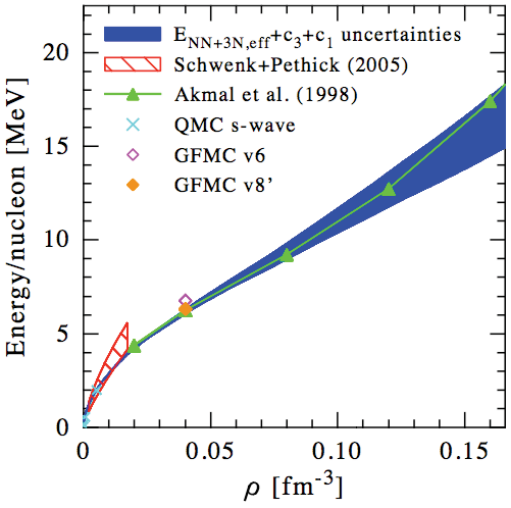

and neutron skin of ^{208}Pb to 0.17±0.03 fm

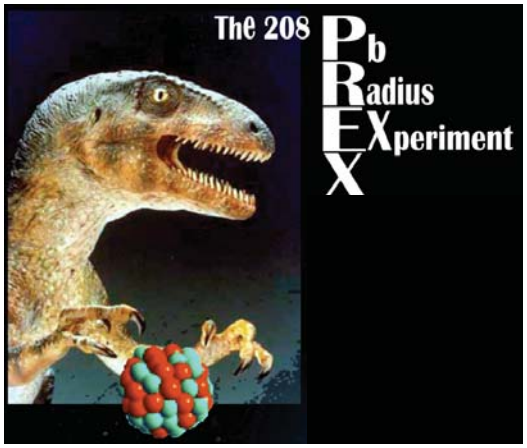

compare to ±0.05 fm future PREX goal
first result: 0.34+0.15-0.17 fm

from complete E1 response
0.156+0.025-0.021 fm Tamii et al., PRL (2011).

Discovery of the heaviest neutron star

A two-solar-mass neutron star measured using Shapiro delay

P. B. Demorest[1], T. Pennucci[2], S. M. Ransom[1], M. S. E. Roberts[3] & J. W. T. Hessels[4,5]

Nature (2010)

direct measurement of neutron star mass from increase in signal travel time near companion

J1614-2230
most edge-on binary pulsar known (89.17°) + massive white dwarf companion (0.5 M_{sun})

heaviest neutron star with 1.97±0.04 M_{sun}

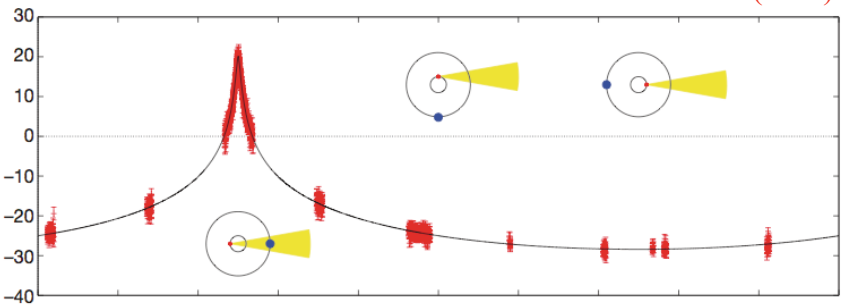

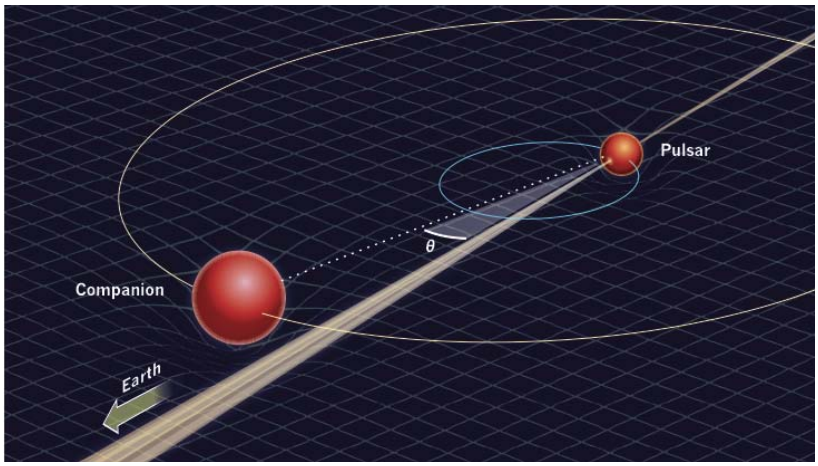

Impact on neutron stars

Neutron star structure determined by Tolman-Oppenheimer-Volkov eqn

$$\frac{dP}{dr} = -\frac{GM\epsilon}{r^2}\left[1+\frac{P}{\epsilon c^2}\right]\left[1+\frac{4\pi r^3 P}{Mc^2}\right]\left[1-\frac{2GM}{c^2 r}\right]^{-1}$$

with equation of state/pressure for neutron-star matter

Hebeler et al., (2010)

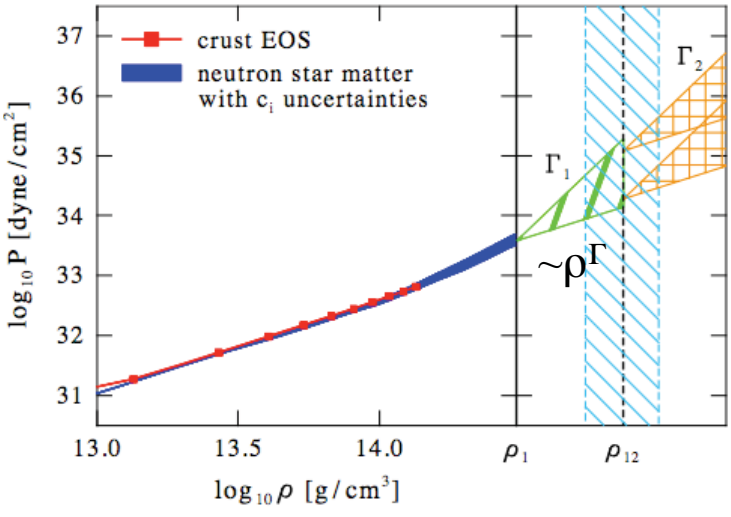

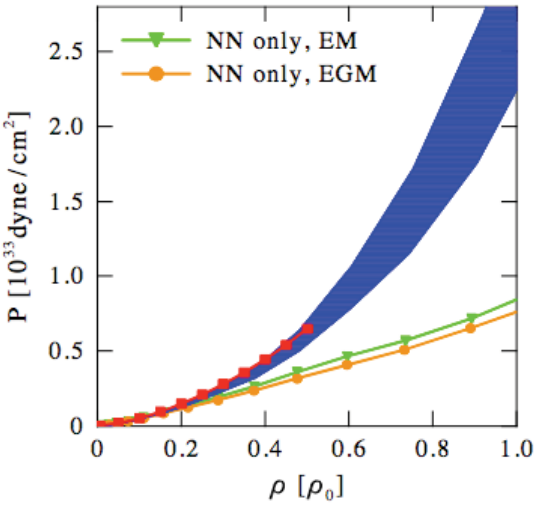

pressure below nuclear densities agrees with standard crust equation of state only after 3N forces are included

extend uncertainty band to higher densities using piecewise polytropes

Pressure of neutron star matter Hebeler et al. (2010)

constrain polytropes by causality and require to support 1.97 M_{sun} star

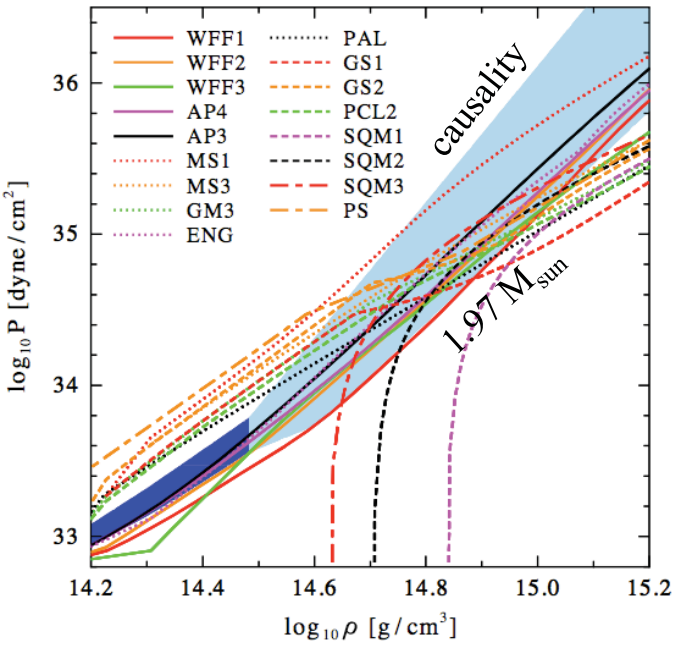

low-density pressure sets scale, chiral EFT interactions provide strong constraints, ruling out many model equations of state

Neutron star radius constraints Hebeler et al. (2010)

constrain polytropes by causality and require to support 1.97 M_{sun} star

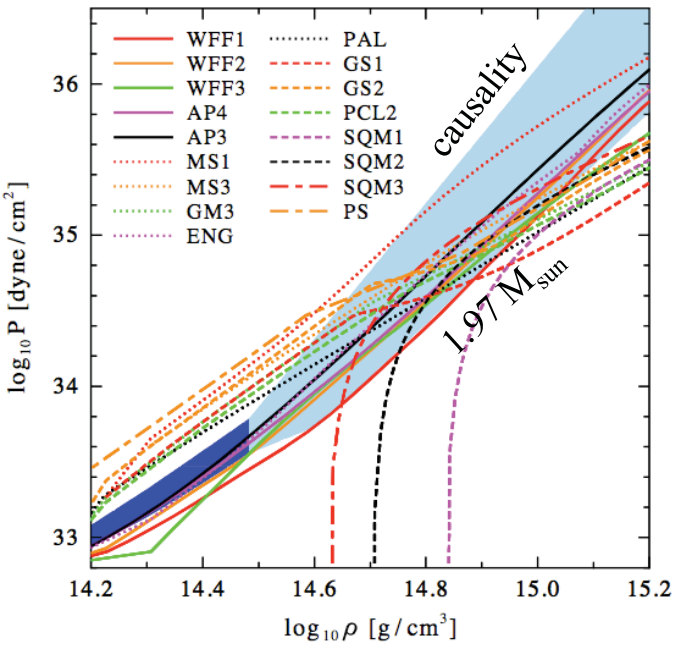

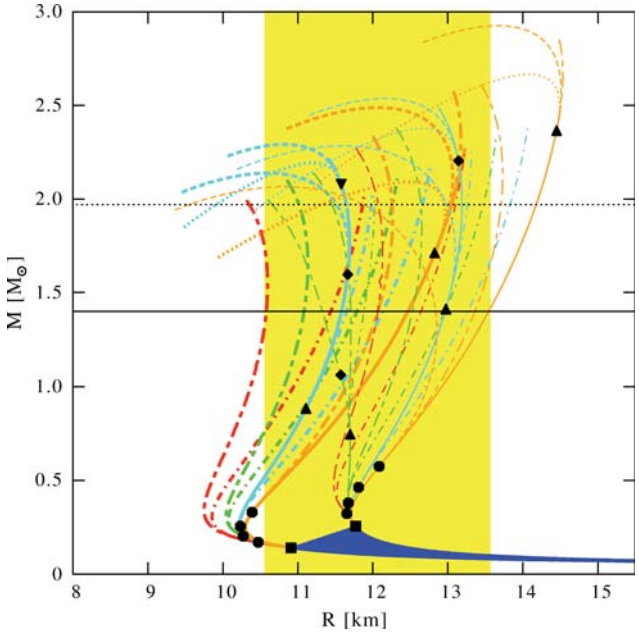

low-density pressure sets scale, chiral EFT interactions provide strong constraints, ruling out many model equations of state

constrains neutron star radius: 10.9-13.9 km for M=1.4 M_{sun} (±12% !)

Neutron star radius constraints Hebeler et al. (2010)

constrain polytropes by causality and require to support 1.97 M_{sun} star

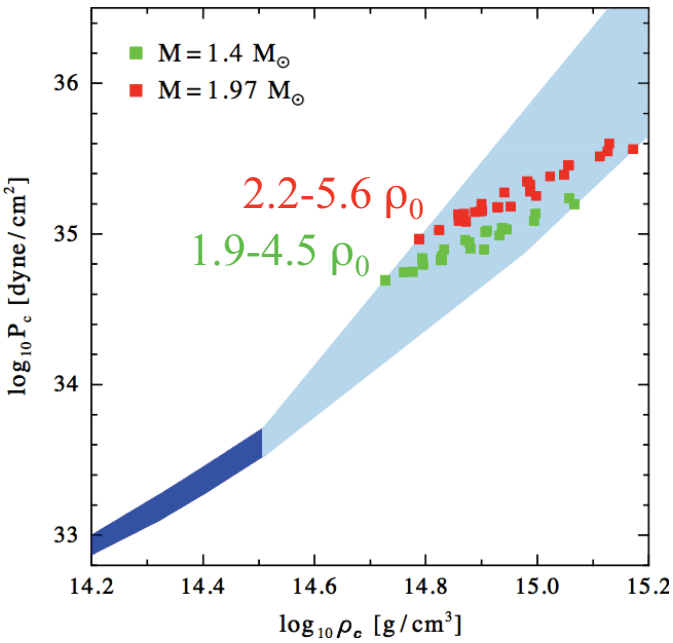

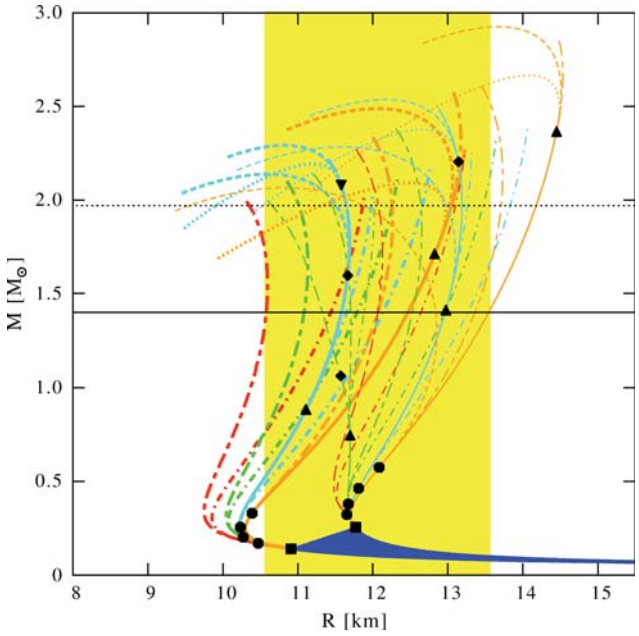

low-density pressure sets scale, chiral EFT interactions provide strong constraints, ruling out many model equations of state

constrains neutron star radius: 10.9-13.9 km for M=1.4 M_{sun} (±12% !)

Comparison to astrophysics

constrain polytropes by causality and require to support 1.97 M_{sun} star

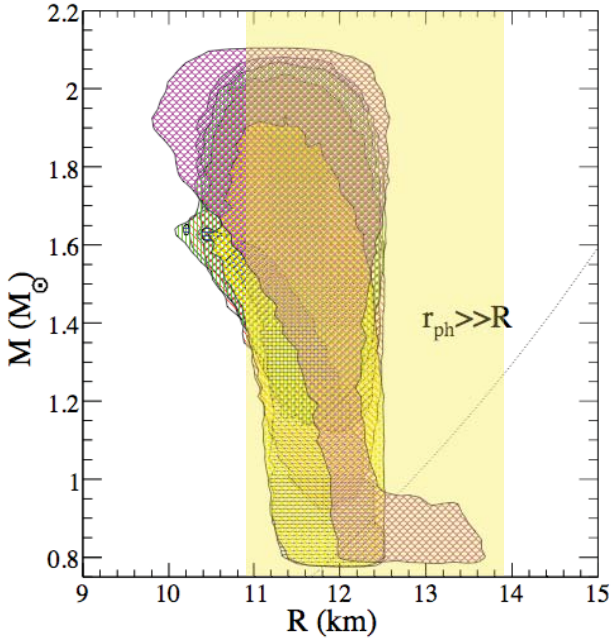

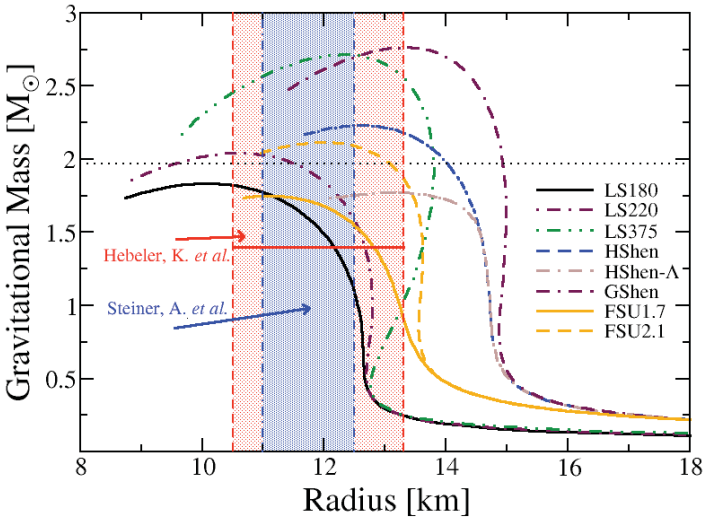

from Evan O'Connor

constrains neutron star radius: 10.9-13.9 km for M=1.4 M_{sun} (±12% !)

consistent with extraction from X-ray burst sources Steiner et al., ApJ (2010)
provides important constraints for EOS for core-collapse supernovae

Chiral EFT for electroweak transitions Menendez, Gazit, AS (2011).

two-body currents lead to important contributions in nuclei (Q~100 MeV) especially for Gamow-Teller transitions

two-body currents determined by NN, 3N couplings to N^{3}LO
Park et al., Phillips,…

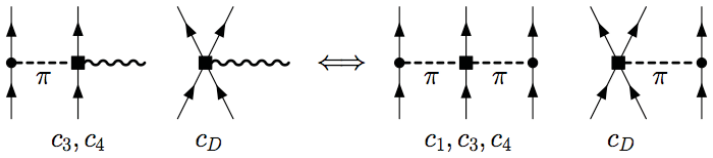

explains part of quenching of g_A (dominated by long-range part)

+ predict momentum dependence (weaker quenching for larger p)

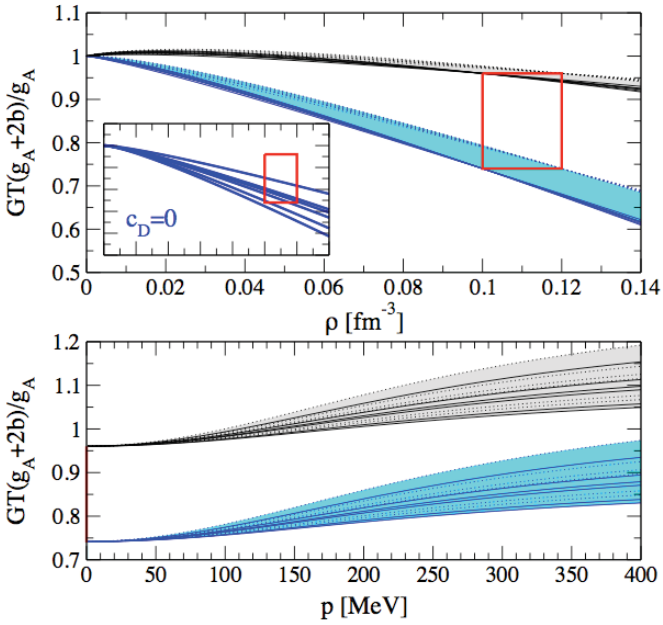

Chiral EFT for electroweak transitions Menendez, Gazit, AS (2011).

two-body currents lead to important contributions in nuclei (Q~100 MeV) especially for Gamow-Teller transitions

two-body currents determined by NN, 3N couplings to N^{3}LO
Park et al., Phillips,…

explains part of quenching of g_A

+ predict mom. dependence

+ nuclear matrix elements for 0νββ decay based on chiral EFT operator

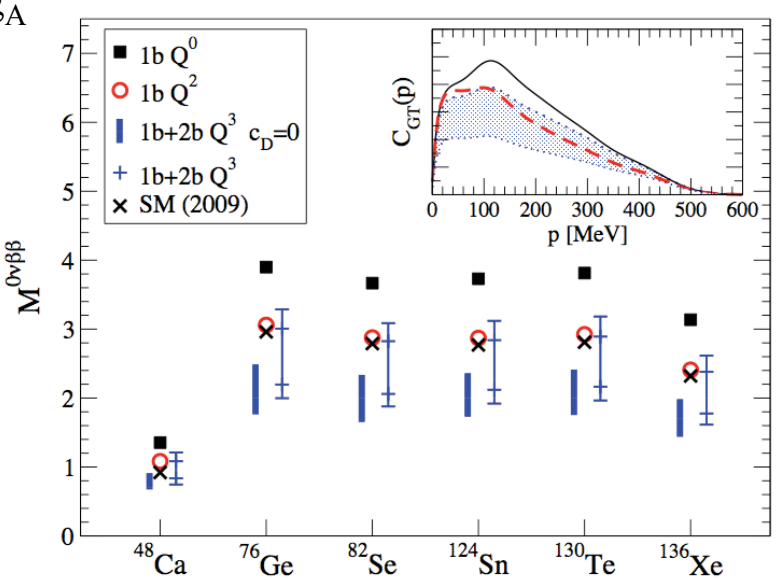

Thanks to collaborators!

T. Krüger, J. Menendez

S.K. Bogner

R.J. Furnstahl,
K. Hebeler

A. Nogga

J.D. Holt

T. Otsuka


T. Suzuki

Y. Akaishi

C.J. Pethick

J.M. Lattimer

D. Gazit

Summary

Exciting era with advances on many fronts:
development of effective field theory and the renormalization group

enables a unified description from nuclei to matter in astrophysics

3N forces are a frontier for neutron-rich nuclei/matter:

key to explain why ^{24}O is the heaviest oxygen isotope

Ca isotopes and N=28 magic number, key for neutron-rich nuclei

dominant uncertainty of neutron (star) matter below nuclear densities,
constraints on neutron star radii

exciting interactions with experiments and observations!


Thank you very much for an unforgettable school!

International Summer School on Subatomic Physics: An Overview of Nuclear Astrophysics

August, 2011

Bradley M. Sherrill

FRIB Chief Scientist

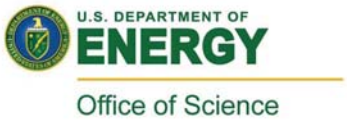

Goals of Nuclear Astrophysics

- Understand the origin and history of atoms in the Universe
  - Model the chemical history of the Milky Way
  - Trace the chemical history of the Universe back to the first stars
  - Learn about the early Universe from what atoms were produced in the Big Bang
- Use the chemical nature of a star, cluster or galaxy to infer something about its origin and history
- Allow accurate modeling of astrophysical objects and allow observations to be used to infer conditions at the site
  - For example, using the light as a function of time (called a light curve) of an X-ray burst to determine the size of emitting region.
  - Use observations to tell us about extreme environments in the universe; neutron stars, supernovae, novae, black holes, the Big Bang, etc.

Example: The lightest elements were made in the Big Bang

- BBN – Big Bang Nucleosynthesis
- H, He, Li were made in the Big Bang (BBN is one of the three main pieces of evidence for the Big Bang; expansion, cosmic microwave radiation, big Bang nucleosynthesis)
- The reaction network and the conditions during the Big Bang allow the elemental abundances to be calculated

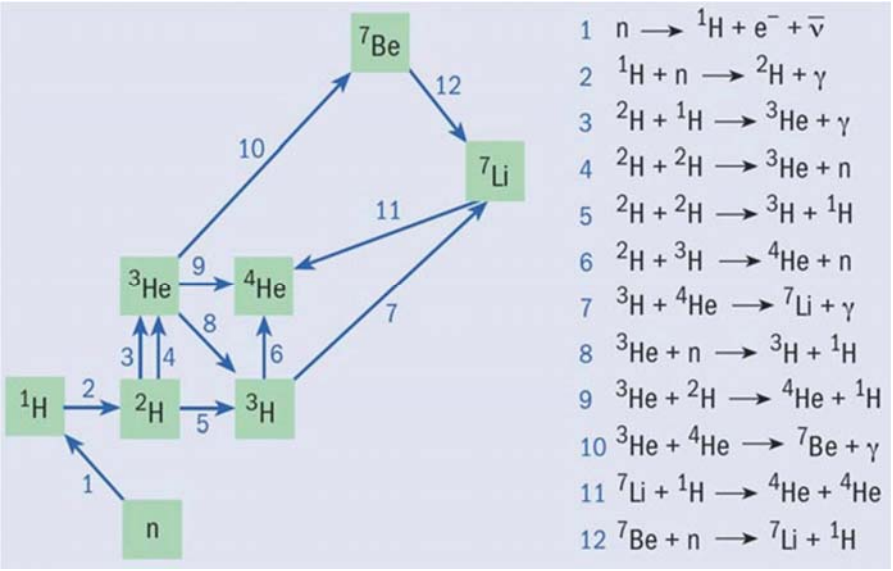

Sample of a Reaction Network Physics World

Example: Predicted versus Observed BBN

- The abundances following the Big Bang can be calculated from measured nuclear reaction rates (NACRE website: http://pntpm.ulb.ac.be/Nacre/nacre_d.htm)
- The abundance of ^{7}Li relative to H does not agree
- Does this tell us something about the structure of the Universe, or the nature of fundamental particles in the Universe?
- Most people agree it is not due to inaccurate or missing nuclear astrophysics data.
- Summary of BBN(Fields and Sarkar) at http://pdg.lbl.gov/2011/reviews/rpp2011-rev-bbang-nucleosynthesis.pdf

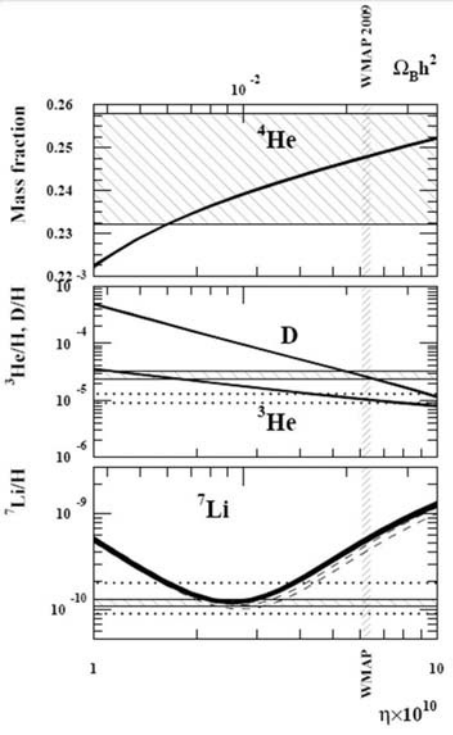

A. Coc and E. Vangioni, 2010 J. Phy. Conf. Ser. 202 012001; IOP Publishing

Zoom Out: Structure and History of the Universe

- 13.6 billion years old
- 200 Billion Galaxies (each with on average 200 billion stars)

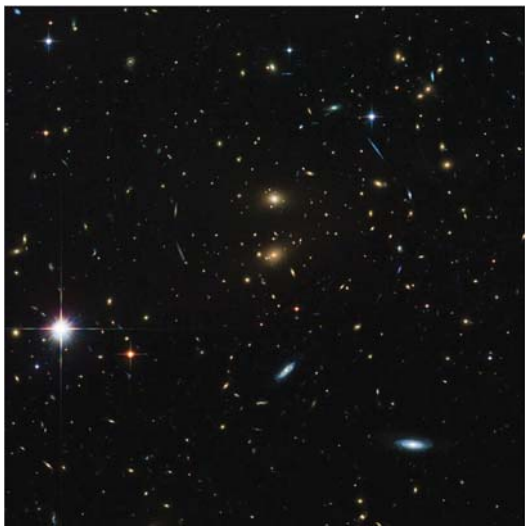

Hubble Deep Field

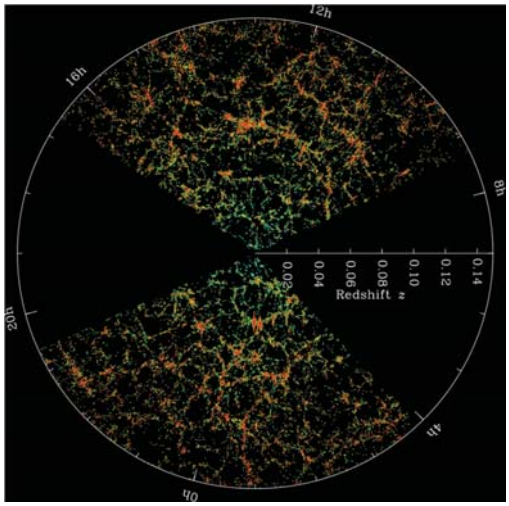

Sloan Digital Sky Survey, SDSS

Structure of the Milky Way

- Our Galaxy is thought to be a barred spiral.
- We know it formed from the merger of other galaxies
- Structure
  - Flat disk 3000 ly
  - Nuclear bulge at center (black hole)
  - Nearly spherical halo extending out 50,000 ly from the center

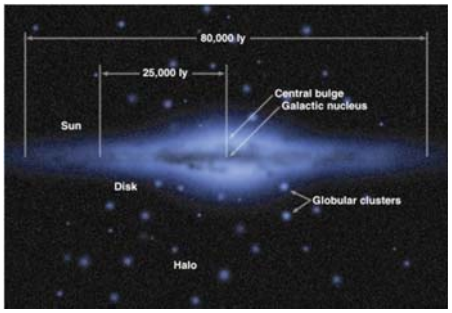

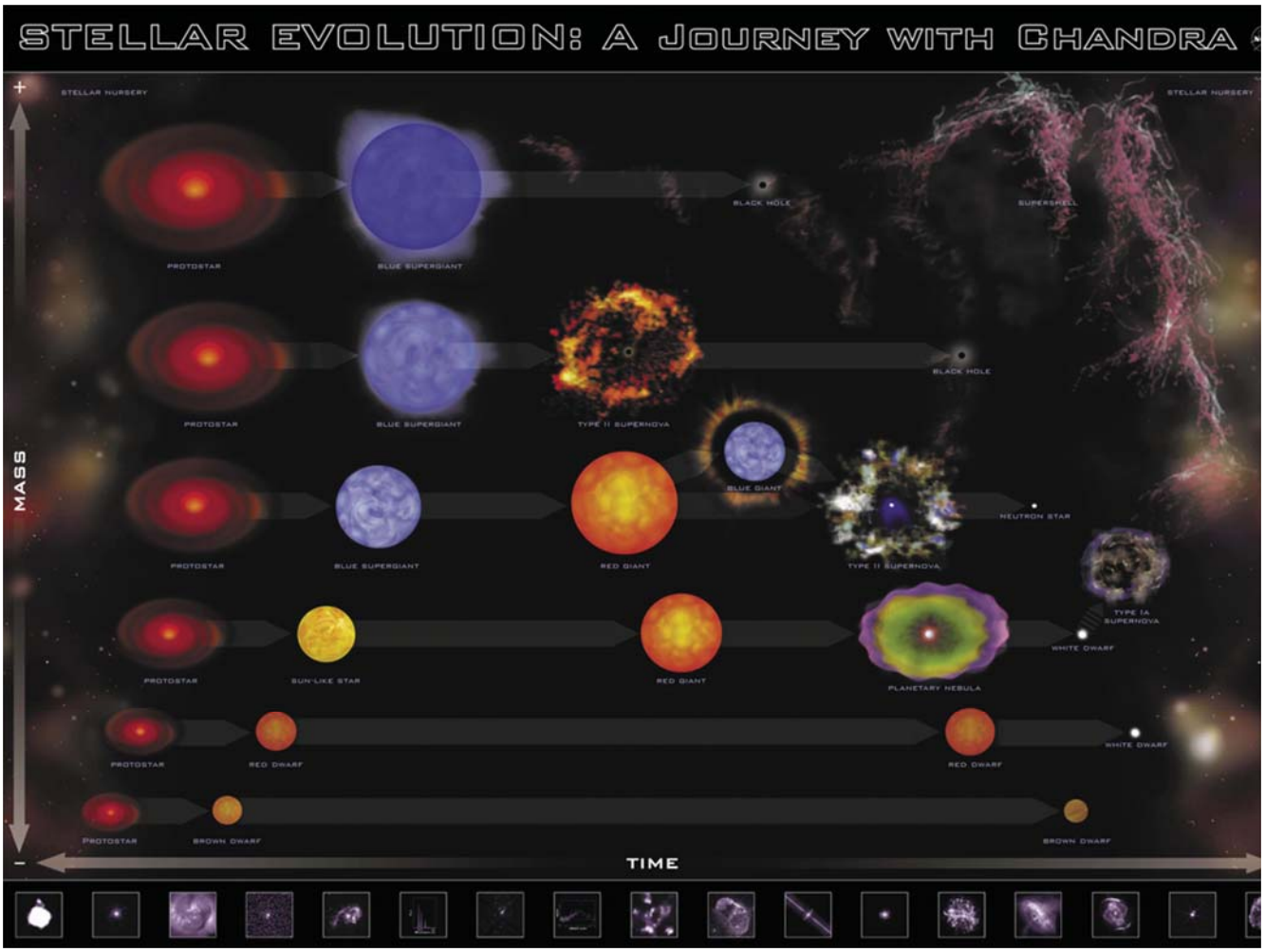

Hertzsprung-Russel Diagram

- Diagram used by astronomers to categorize stars

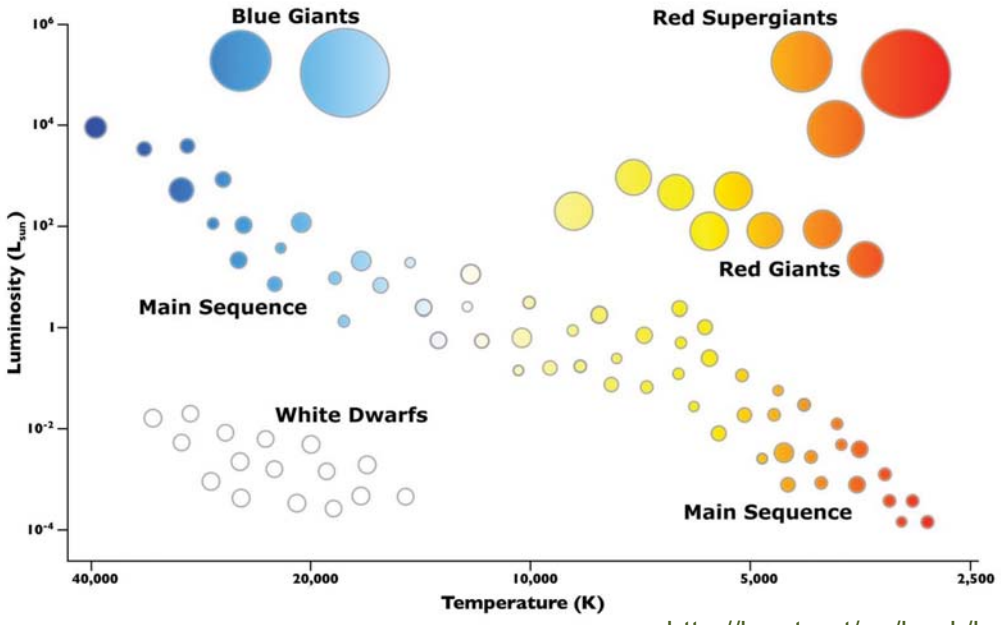

http://lcogt.net/en/book/h-r-diagrams

47 Tuc Globular Cluster

- Globular clusters are gravitationally bound collections of thousands of normally old stars
- See Stellar evolution in progress

$$\frac{brightness}{brightness_{ref}} = (2.512)^{m-m_{ref}}$$

Visual Image
Copyright Daniel Verschatse,
Observatorio Antilhue, Chile

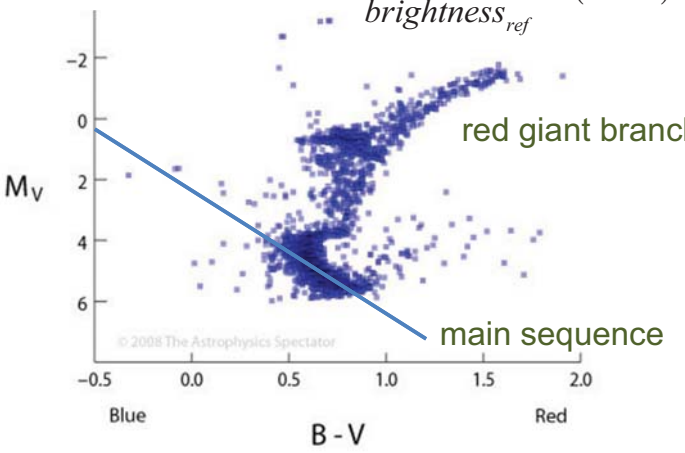

Mv – visual absolute magnitude (apparent magnitude, m, of a star if it were 33 ly away)
B – V blue magnitude minus visual

Stellar evolution of massive stars

- Stars with more than 8 times the mass of our Sun develop the following layers
- Hydrogen to helium
- Helium to carbon
- Carbon to oxygen, neon, magnesium
- Oxygen to neon
- Neon to magnesium
- Magnesium to Silicon
- Silicon to Iron
- Iron is the most bound nucleus and has no exothermic nuclear reactions

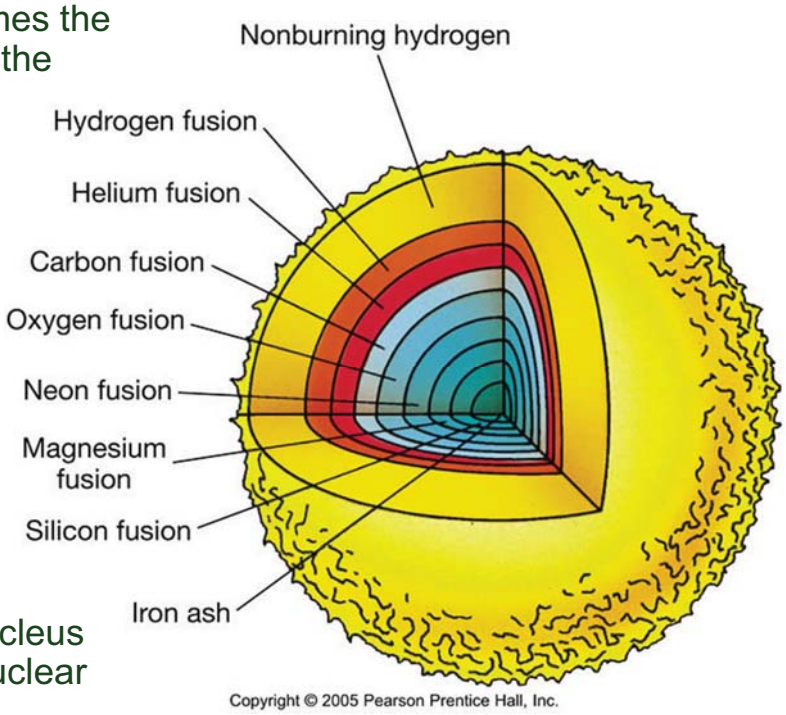

The Problem of Chemical Evolution of the Milky Way – Coupled Problems

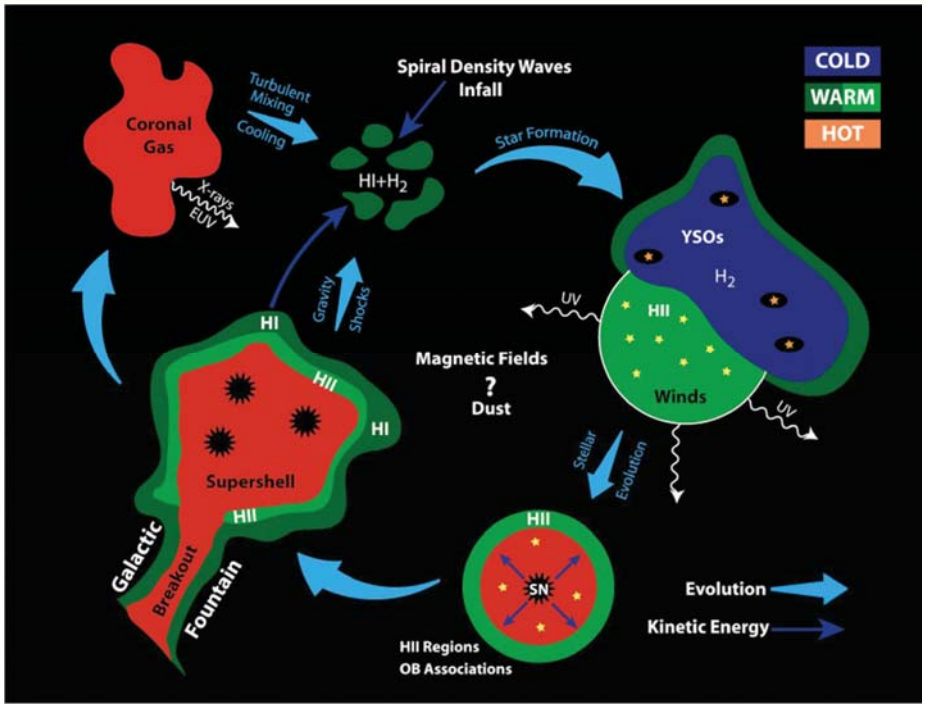

Nuclear reactions
+ Stellar evolution and explosive scenarios
+ Evolution of the Universe and Galactic collisions

Figure illustrates all the steps and the difficulty of the problem. For example, no one can explain why the Milky Way looks like it does.

Jason Tumlinson STSCI

Solar Abundances of the Elements

- Stars are mostly made of hydrogen and helium, but the patter of other metals can be very different
- The abundance of elements tell us about the history of events prior to the formation of our sun
- The plot at the right shows the composition in the visible surface layer of the Sun (photosphere)

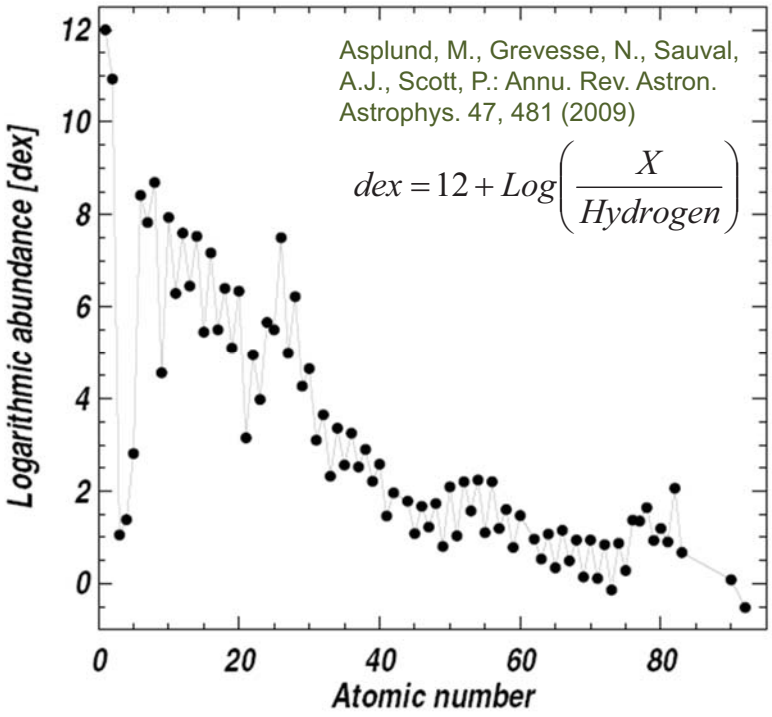

Abundances are inferred from stellar absorption spectra

- Stellar absorption spectra

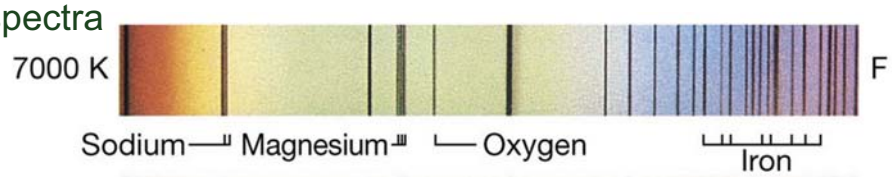

- Not all stellar absorption spectra of the same surface temperature are identical

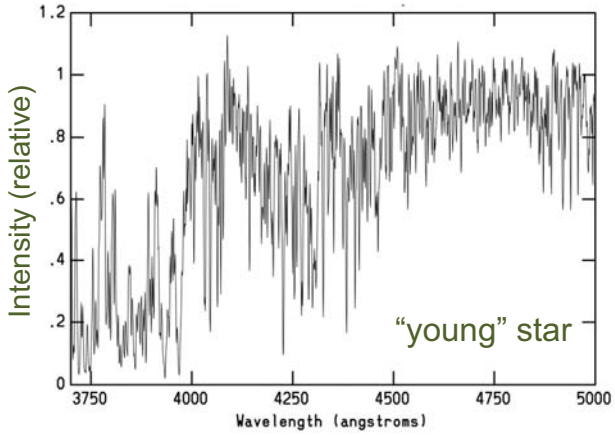

T=4800 K; elements like our sun

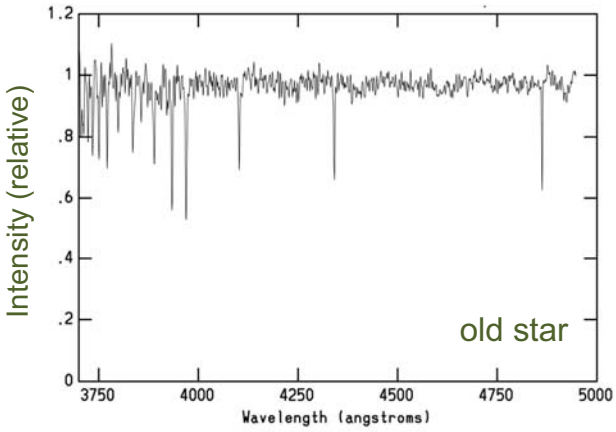

T=4700 K; only 1/10,000 heavy elements

Abundances can also com from Presolar Grains Meteorite Grains

- Another wealth of new data come from the isotopic measurements of individual meteorite grains (pictures from Washington Univ website)
- Other data will come from isotopic analysis cosmic rays
- Measured by Secondary Ion Mass Spectroscopy

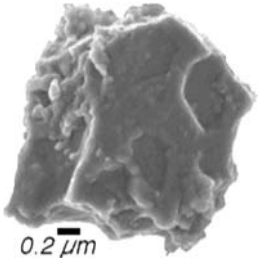

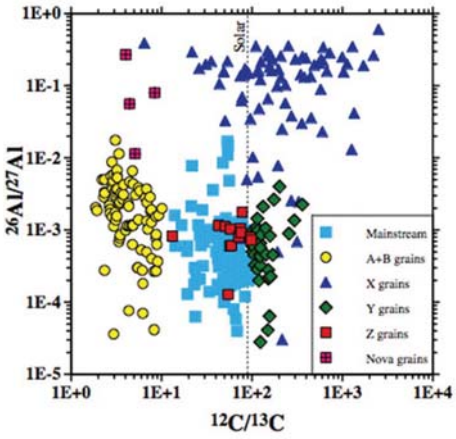

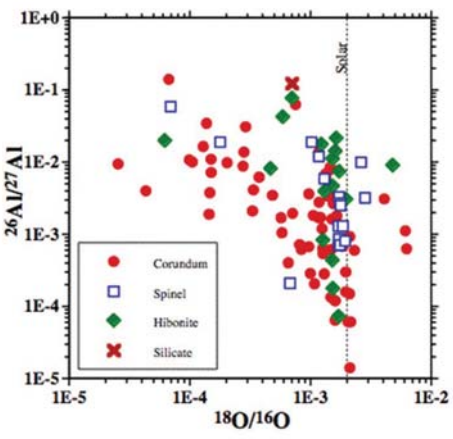

Radioactive ^{26}Al in the Milky Way

^{26}Al half-life 7.8x10^5 y
Stars are still making atoms

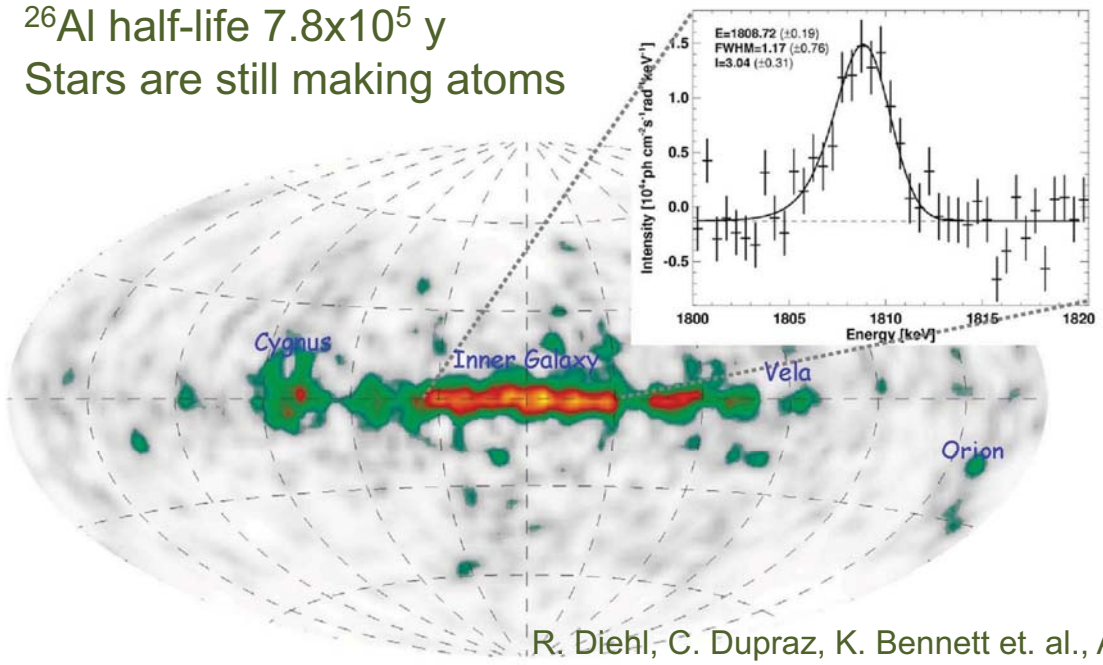

COMPTEL

R. Diehl, C. Dupraz, K. Bennett et. al., A&A 298 (June, 1995) 445.

Forefront of Observational Astronomy: High Resolution Telescopes

- The measurement of elemental abundances is at the forefront of astronomy using large telescopes
- Large mirrors enable high resolution spectroscopic studies in a short time (Hubble, LBT, Keck, …)
- Surveys provide large data sets (LAMOST,SDSS, SEGUE, RAVE, LSST, …)
- Future missions: JWST - "is specifically designed for discovering and understanding the formation of the first stars and galaxies, measuring the geometry of the Universe and the distribution of dark matter, **investigating the evolution of galaxies and the production of elements by stars,** and the process of star and planet formation."

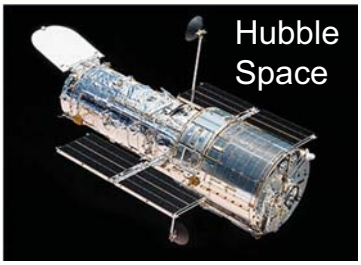

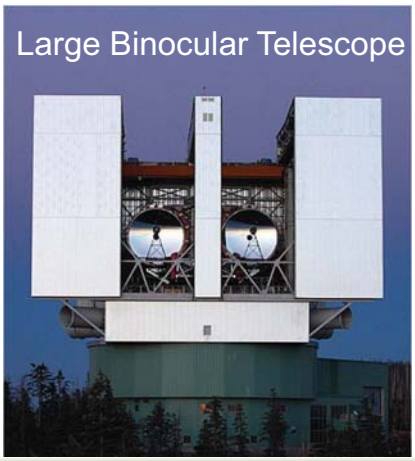

Chemical History of the Universe – the Fossil Evidence of the first Stars

- The process that makes Ba must be different from the main process that makes Fe
- There are many mysteries, e.g., the [Ba/Fe] is not understood

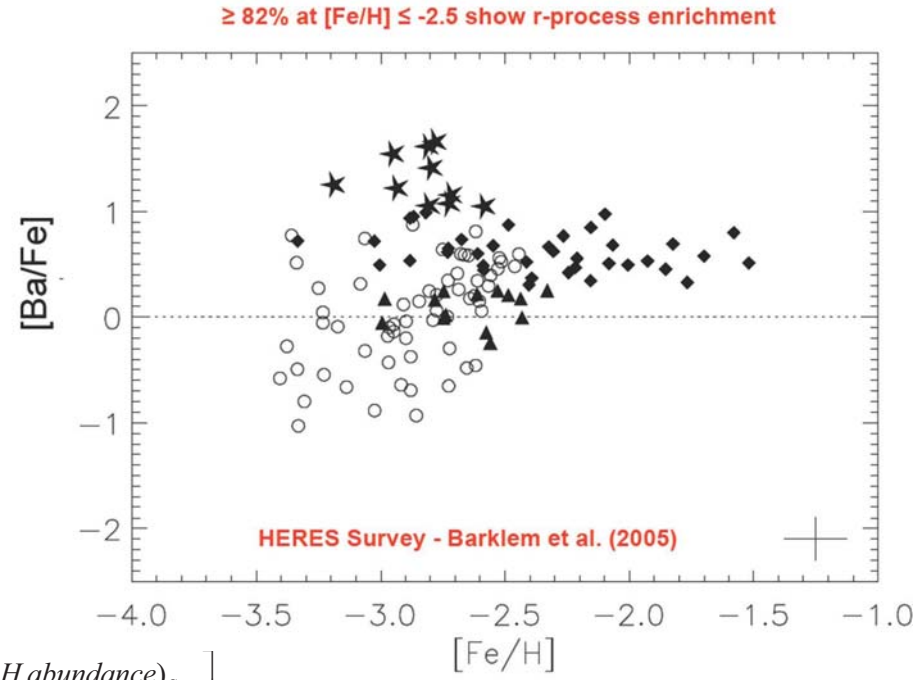

$$[\mathrm{Fe/H}] = LOG\left[\frac{(Fe\,abundance\,/\,H\,abundance)_{Star}}{(Fe\,abundance\,/\,H\,abundance)_{Sun}}\right]$$

There are a number of nucleosynthesis processes that must be modeled

- Big Bang Nucleosynthesis
- pp-chain
- CNO cycle
- Helium, C, O, Ne, Si burning
- s-process
- r-process
- rp-process
- vp – process
- p – process
- α - process
- fission recycling
- Cosmic ray spallation
- pyconuclear fusion
- + others

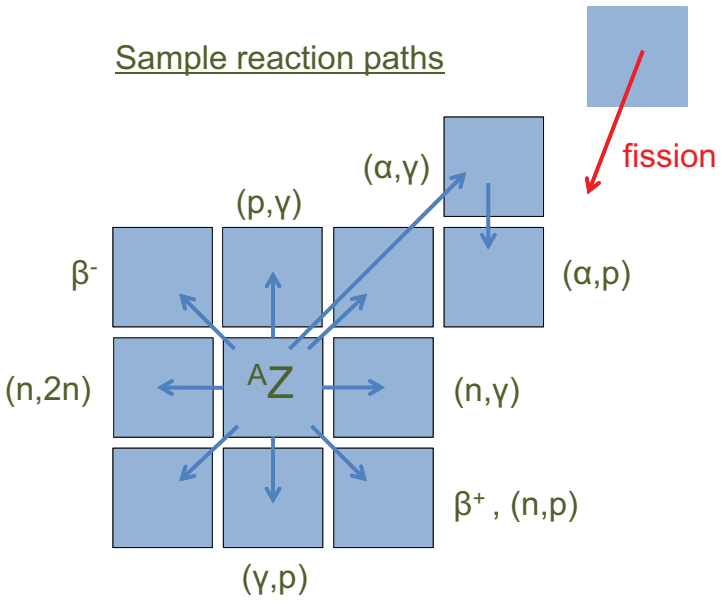

C. Iliadis, **Nuclear Physics of Stars** (WILEY, 2007)
R. Boyd, **An Introduction to Nuclear Astrophysics** (Univ of Chicago press, 2008)

Types of Nuclear Reactions

- Transfer (strong interaction
  - $^{15}N(p,\alpha)^{12}C$ σ~0.5 b at E= 2.0 MeV
- Capture (electromagnetic interaction)
  - $^{3}He(\alpha,\gamma)^{7}Be$ σ~10^{-6} b at E= 2.0 MeV
- β-decay or electron capture (weak interaction)
  - $p(p,e^{+}\nu)d$ σ~10^{-20} b at E= 2.0 MeV

Slide adopted from KH Langanke

Stellar Reaction Rates

Consider N_a and N_b particles per cubic centimeter of particle types *a* and *b*. The rate of nuclear reactions is given by:

$$r = N_a N_b \sigma(v) v$$

In stellar environment the velocity (energy) of particles follows a thermal distribution that depends on the type of particles.

- Nuclei (Maxwell-Boltzmann): $\phi(v) = N 4\pi v^2 \left(\frac{m}{2\pi kT}\right)^{3/2} \exp\left(-\frac{mv^2}{2kT}\right)$

The product σv has to be averaged over the velocity distribution $\phi(v)$

$$\langle \sigma v \rangle = \int_0^\infty \int_0^\infty \phi(v_a)\phi(v_b)\sigma(v) v dv_a dv_b$$

Changing to center-of-mass coordinates, integrating over the cm-velocity and using $E = \mu v^2/2$

$$\langle \sigma v \rangle = \left(\frac{8}{\pi\mu}\right)^{1/2} \frac{1}{(kT)^{3/2}} \int_0^\infty \sigma(E) E \exp\left(-\frac{E}{kT}\right) dE$$

KH Langanke

Astrophysical S-Factor

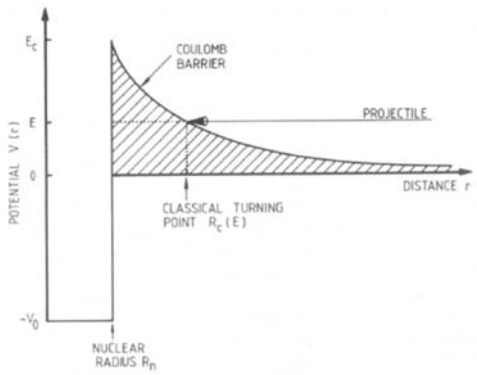

Rolfs and Rodney, **Cauldrons in the Cosmos**, (University of Chicago Press, 1988)

cross section: $\sigma(E) = \frac{1}{E} S(E) e^{-2\pi\eta}; \quad \eta = \frac{Z_1 Z_2 e^2}{\hbar} \sqrt{\frac{\mu}{2E}} = \frac{b}{E^{1/2}}$

S-factor Example

Review of Underground Nuclear Astrophysics - Broggini, Bemmerer, Guglielmetti, Menegazzo Ann Rev Nucl Part Sci 60, 53 (2010)

^{3}He(^{3}He,2p)^{4}He
LUNA

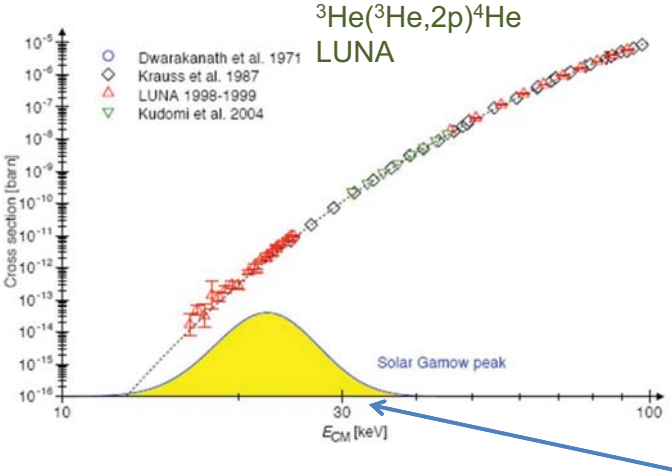

^{3}He(^{4}He,γ)^{7}Be
LUNA

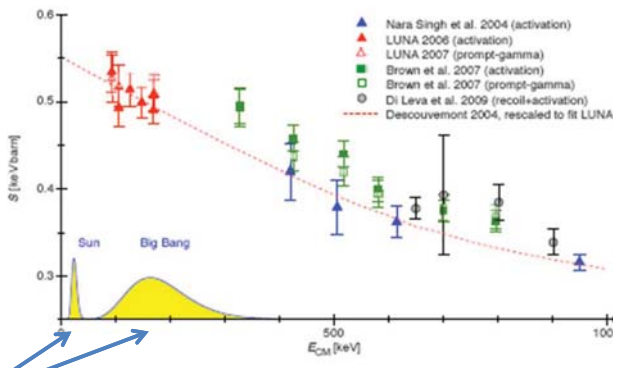

Gamow Peak

Gamow Window (Peak)

$$\langle \sigma v \rangle = \left(\frac{8}{\pi\mu}\right)^{1/2} \frac{1}{(kT)^{3/2}} \int_0^\infty S(E) \exp\left[-\frac{E}{kT} - \frac{b}{E^{1/2}}\right] dE$$

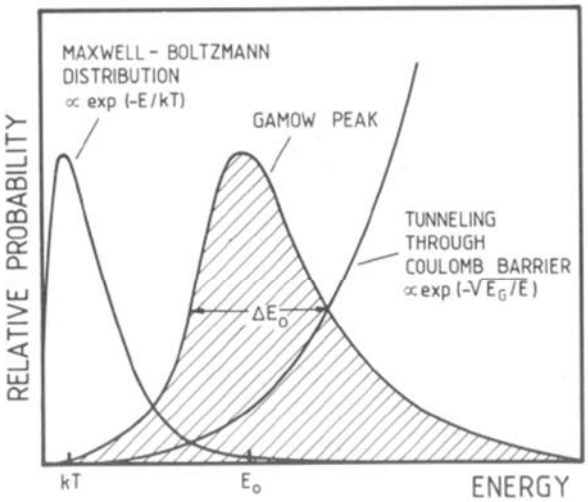

Rolfs and Rodney, **Cauldrons in the Cosmos**, (University of Chicago Press, 1988)

KH Langanke

Solar Abundances Plotted versus Atomic Number (Z)

- The plot at the right shows the composition in the visible surface layer of the Sun (photosphere)

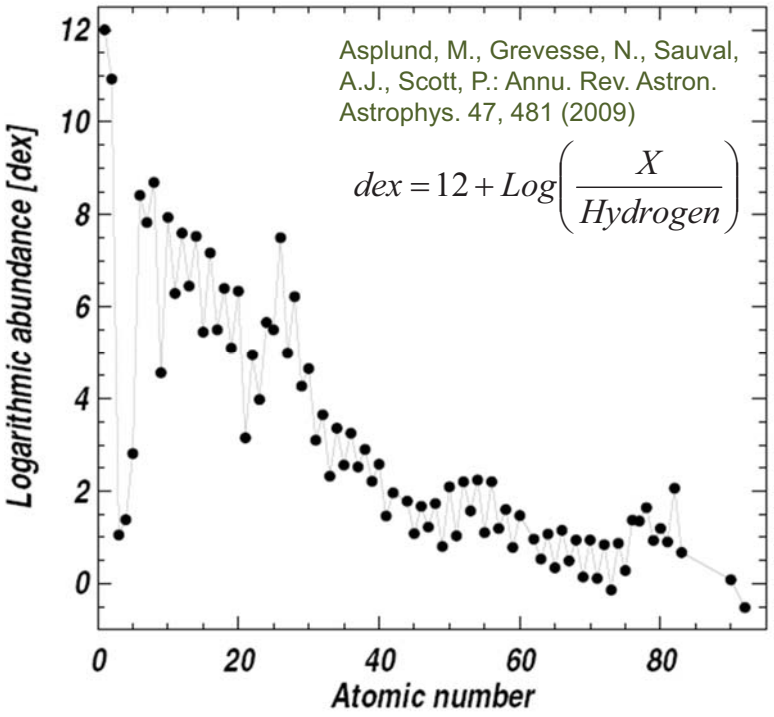

Asplund, M., Grevesse, N., Sauval, A.J., Scott, P.: Annu. Rev. Astron. Astrophys. 47, 481 (2009)

$$dex = 12 + Log\left(\frac{X}{Hydrogen}\right)$$

Plotted versus Mass Number (A)

- The pattern plotted versus mass number shows the origin of some of the processes more clearly
- For clarity, not all process contributing to element synthesis are listed

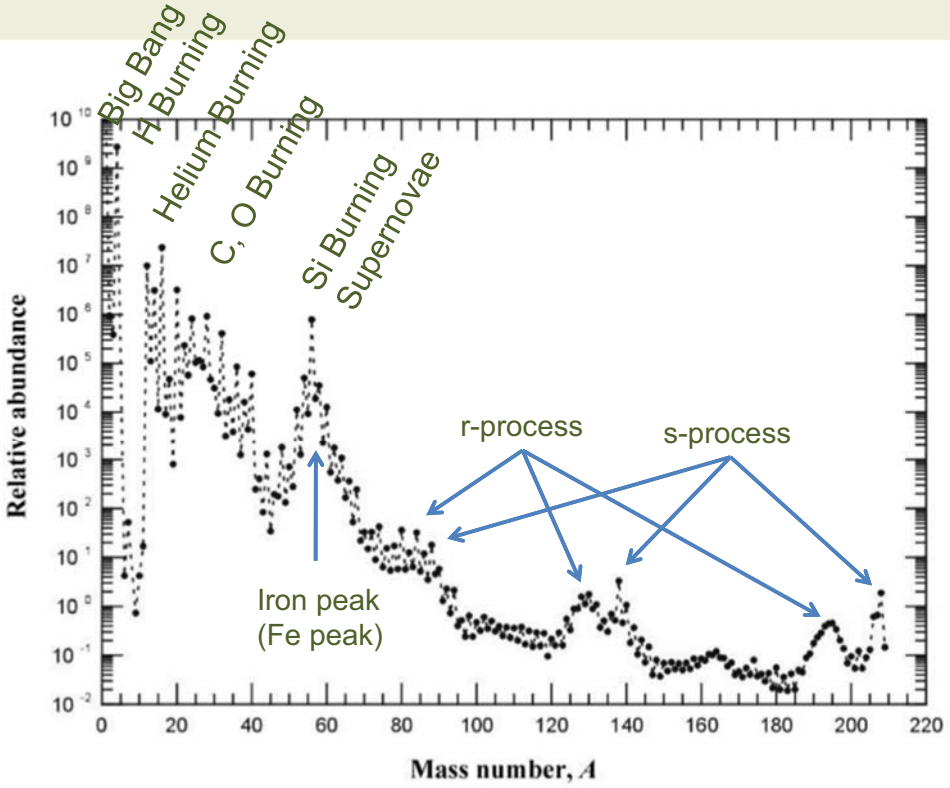

Not all stars have the same pattern

- Abundances from Sneden, *et al.,* Asto. Phy. Jour 2003, Cowan *et al.,* Asto. Phy. Jour 2006
- This is an example of a very metal poor star with only .1% of the metal abundance of our Sun
- It is an old star in the halo of the Milky Way

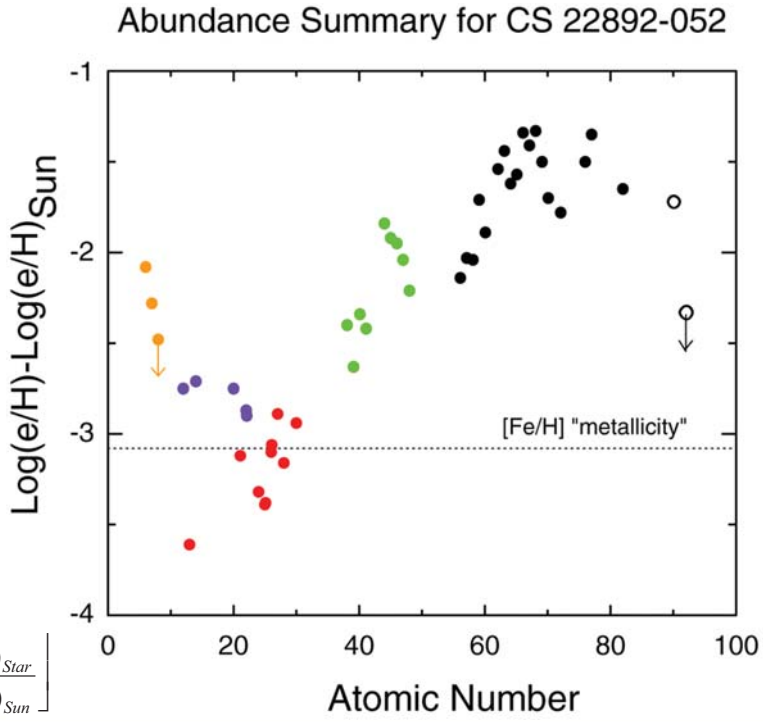

$$[\mathrm{Fe/H}] = LOG\left[\frac{(Fe\,abundance/H\,abundance)_{Star}}{(Fe\,abundance/H\,abundance)_{Sun}}\right]$$

Simulation of Solar System Abundances

Parameters:

- Supernovae type Ia and II
- Number (77 supernovae with M_s 11-40 M_{sun})
- Progenitor mass distributions
- Age of the galaxy
- …

Results:

- SN rate1/3 comes from type Ia
- They reproduce measured ^{7}Li abundance metalicity vs. time etc.

Timmes, Woosley, Weaver
Astrophysical Journal 1995

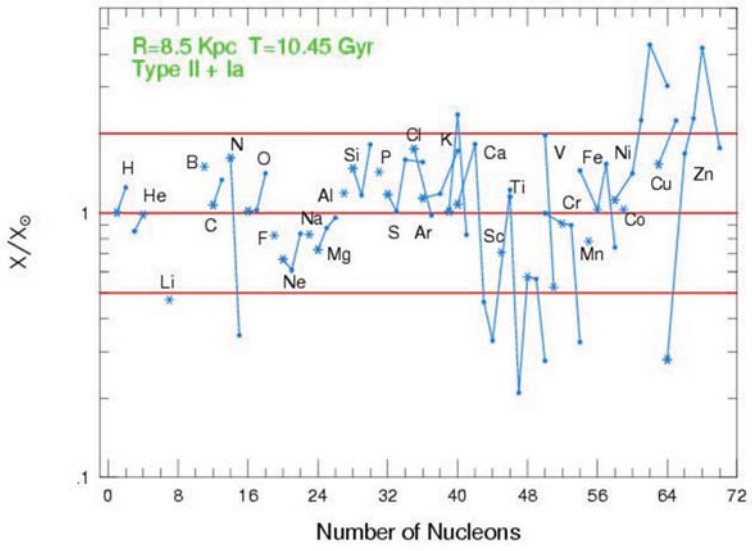

Success ! ? Above 72 we can't model well

Example: Where do gold atoms come from? More than half of Z>28 from an r-process

- E. M. Burbidge, G. R. Burbidge, W. A. Fowler, and F. Hoyle. (1957). "Synthesis of the Elements in Stars". Rev Mod Phy 29: 547, must be an r-procees (10% of gold from s-process)
- We know they must be made in a neutron-rich environment T > 10^9 K, $\rho_{neutron} \approx 10^{20\text{-}28}$ cm^{-3} , that lasts for about 1 second; called the rapid-neutron capture process, r-process
- Type II supernovae are a possible site (variants)
  - Neutrino driven shock wave, however models do not produce the entropy and neutron flux needed to match abundance data (although we can't say that for sure)
  - Shock waves in C-O layers
  - Magnetic outflows
- Colliding neutron stars would also work, but there does not seem to be enough of these in the early universe to explain how much heavier elements we see
- Once the underlying physics is known, we can infer information of the site from observational data

About Half of Heavier Elements must be made in an r-Process

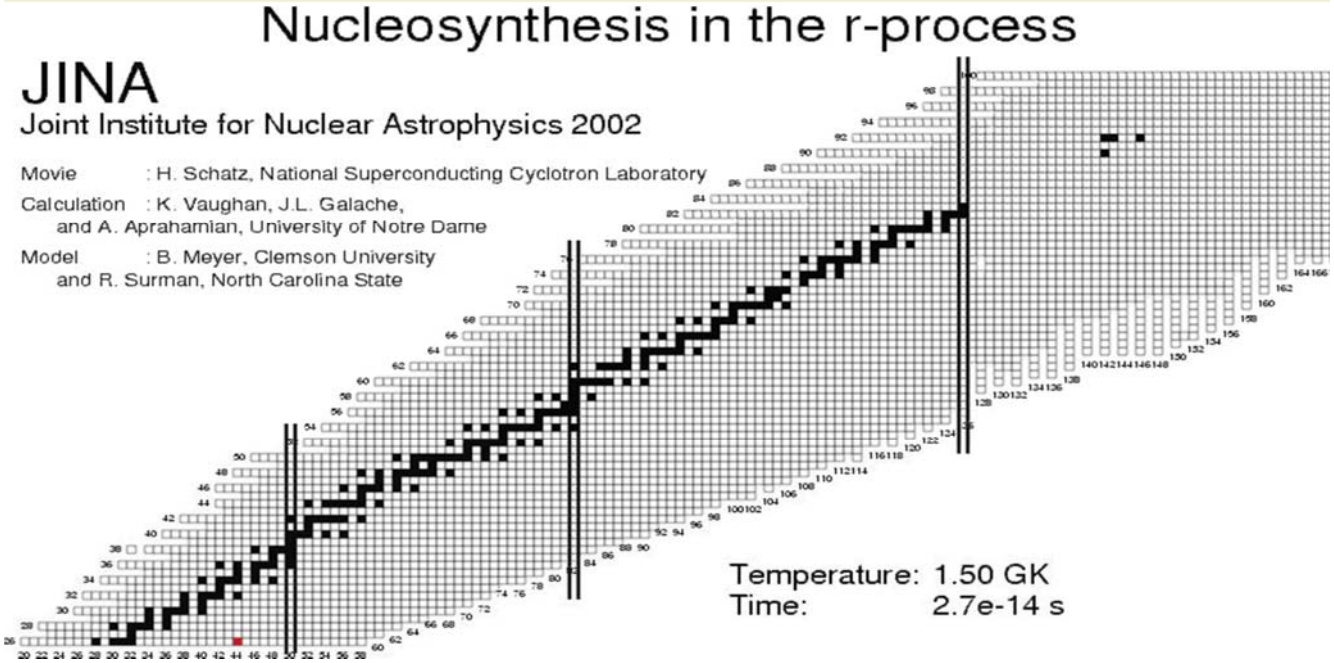

Nuclear physics shapes the characteristic final abundance pattern for a given r-process model

Neutrino Heated Wind in Supernovae

- Review: Woosley and Janka Nature Physics 1, 147 (2005)

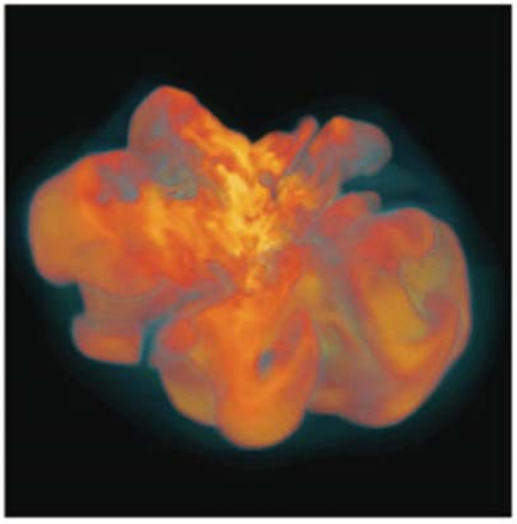

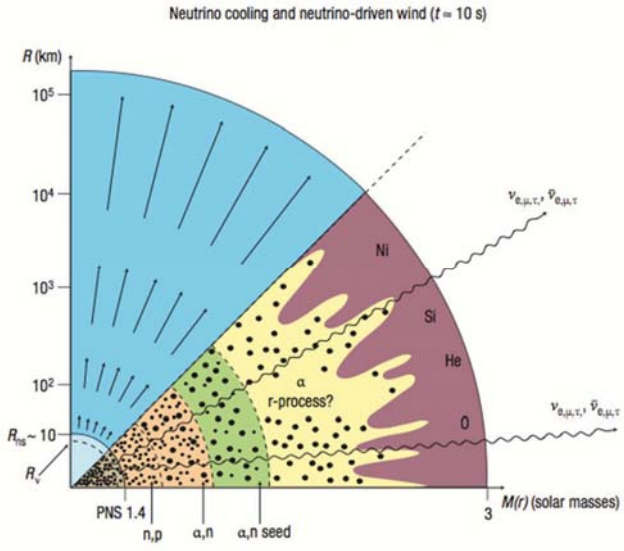

- Problem: The entropy is not high enough!

Uncertainty between models and nuclear properties

Astrophysics

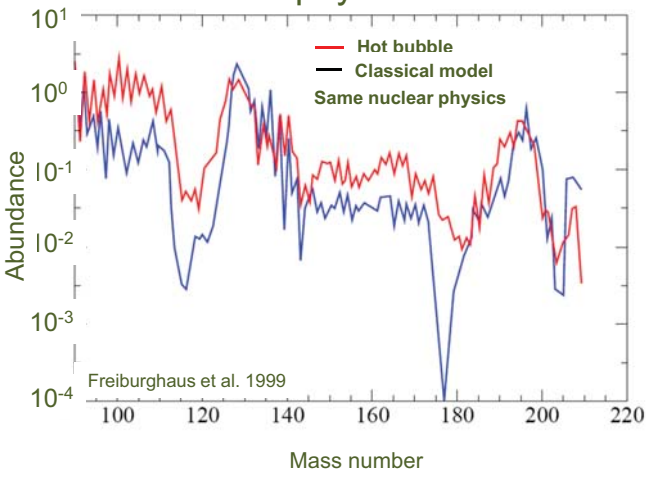

Nuclear physics

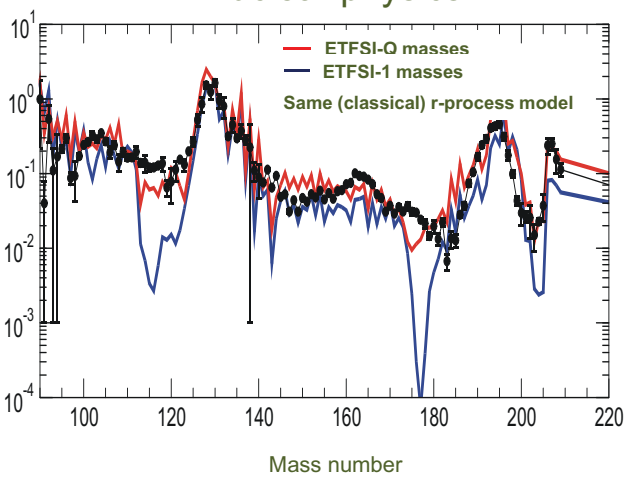

Goal: Understanding of Astrophysical Environments

- Use observational data to infer conditions at the site by modeling
- Accurate modeling requires
  - that we make the same isotopes that participate in astrophysical environments
  - reproduce the nuclear reactions that occur in those environments
- The hard part is that nature produces isotopes in environments like the r-process with $T > 10^9$ K, $\rho_{neutron} \approx 10^{20\text{-}28}$ cm^{-3}

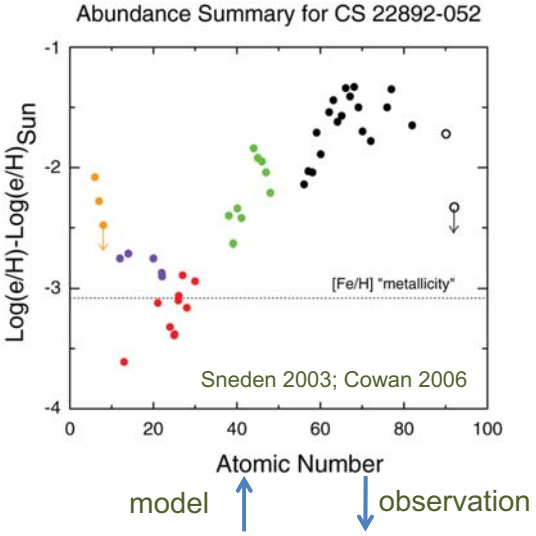

model ↑ ↓ observation

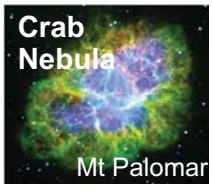

Reach of FRIB (see first lecture) – Will Allow Modeling of the r-Process

- β-decay properties
- masses (Trap + TOF)
- (d,p) to constrain (n,γ)
- fission barriers, yields

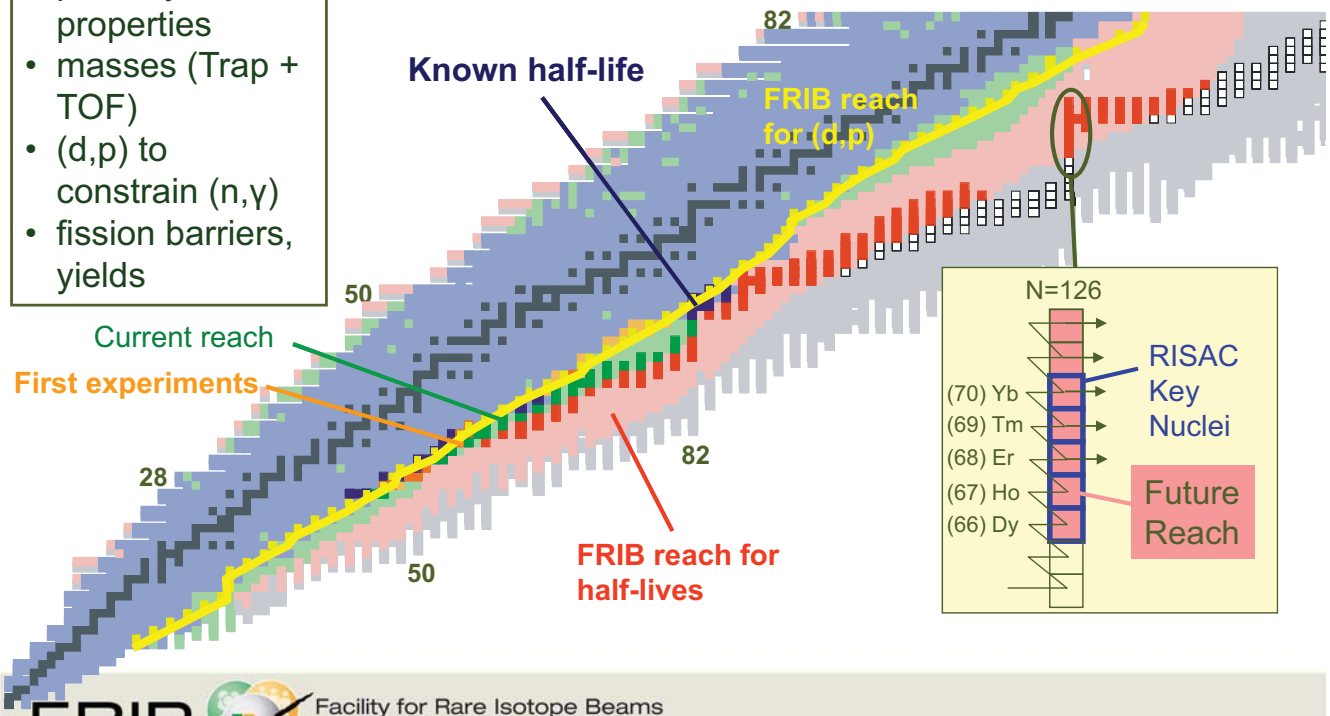

Rare Isotope Crusts of Accreting Neutron Stars

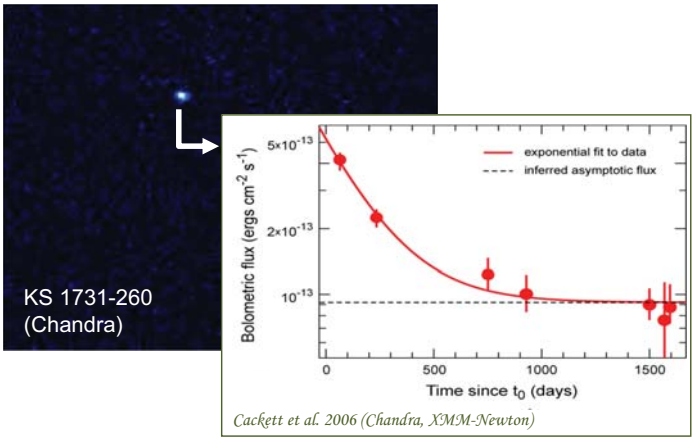

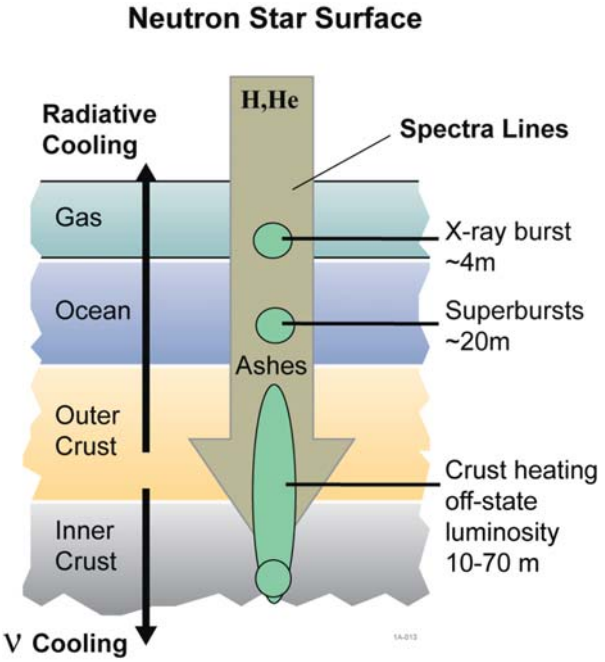

- Nuclear reactions in the crust set thermal properties
- Can be directly observed in transients
- Directly affects superburst ignition

Understanding of crust reactions offers possibility to constrain neutron star properties (core composition, neutrino emission…)

H-fraction in surface from X-ray burst light curves

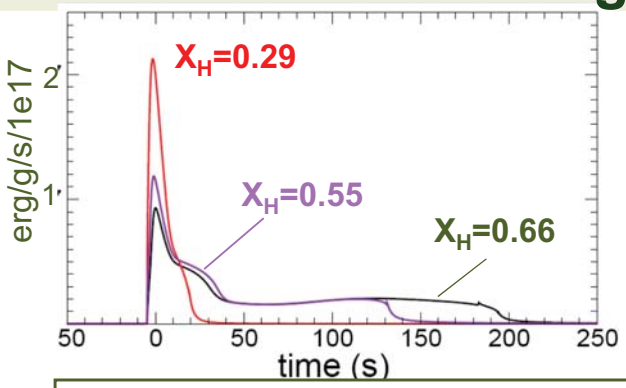

→ **Fix one key parameter**
(more meaningful model comparisons)
→ **Determine Eddington Luminosity**
(apparent L_{edd} from PRE bursts)
→ Standard candle/distance
→ Constrain EOS
→ model atmosphere in transients
H. Schatz, Brown 2002, Schatz 2001

Mass uncertainties in ^{64}Ge – ^{74}Sr region:

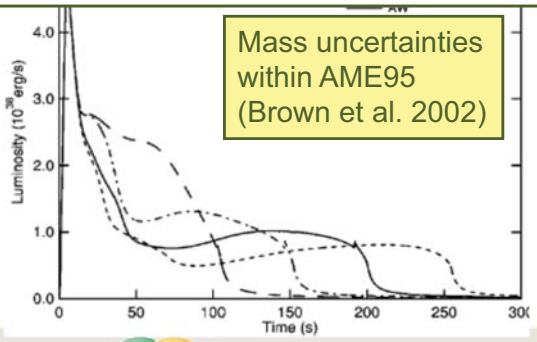

Mass uncertainties within AME95 (Brown et al. 2002)

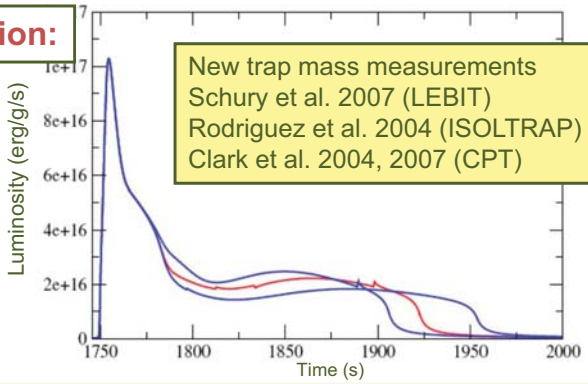

New trap mass measurements
Schury et al. 2007 (LEBIT)
Rodriguez et al. 2004 (ISOLTRAP)
Clark et al. 2004, 2007 (CPT)

FRIB Reach for Novae and X-ray burst reaction rate studies

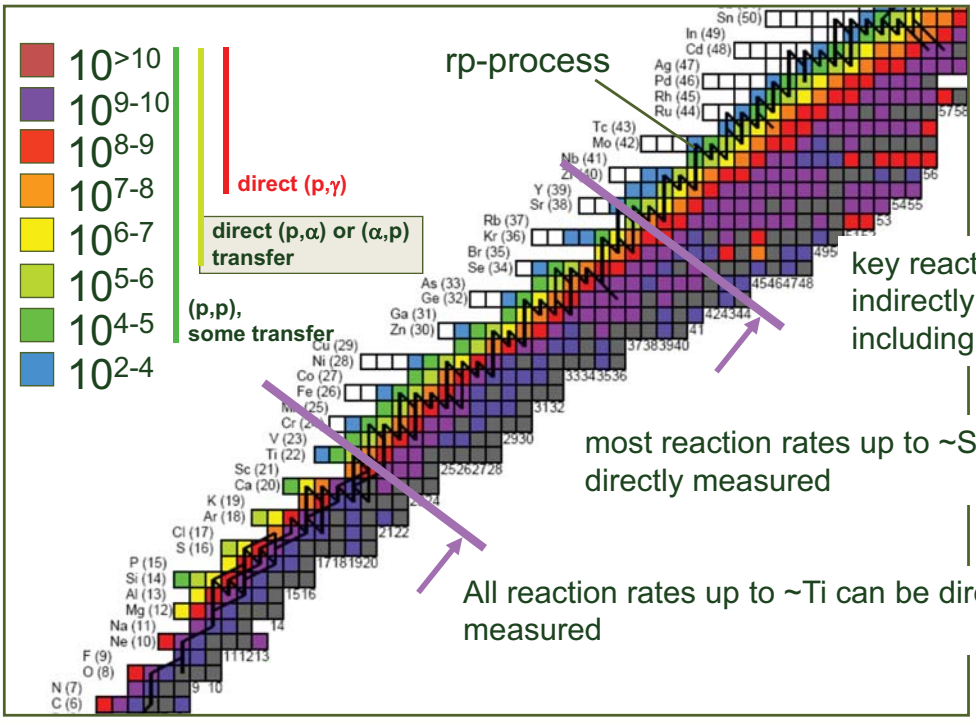

key reaction rates can be indirectly measured including ^{72}Kr waiting point

most reaction rates up to ~Sr can be directly measured

All reaction rates up to ~Ti can be directly measured

Summary

- Nuclear astrophysics attempts to model the creation of the elements in the universe and the chemical history over time
- The field is closely tied to astronomical observation – I covered some of the observational language in the talk
- The elements were created in a variety of astrophysical process involving nuclear reactions (both strong and weak)
- Examples
  - r – process
  - rp – process

Hubble Space Telescope image of the face-on spiral galaxy Messier 101 (M101)

International Summer School on Subatomic Physics: Rare Isotope Production Methods and Facilities

August, 2011

Bradley M. Sherrill

FRIB Chief Scientist

U.S. DEPARTMENT OF ENERGY
Office of Science

Accelerators are used to produce important isotopes and make beams of them

Start with the stable isotopes (black) and make all the others

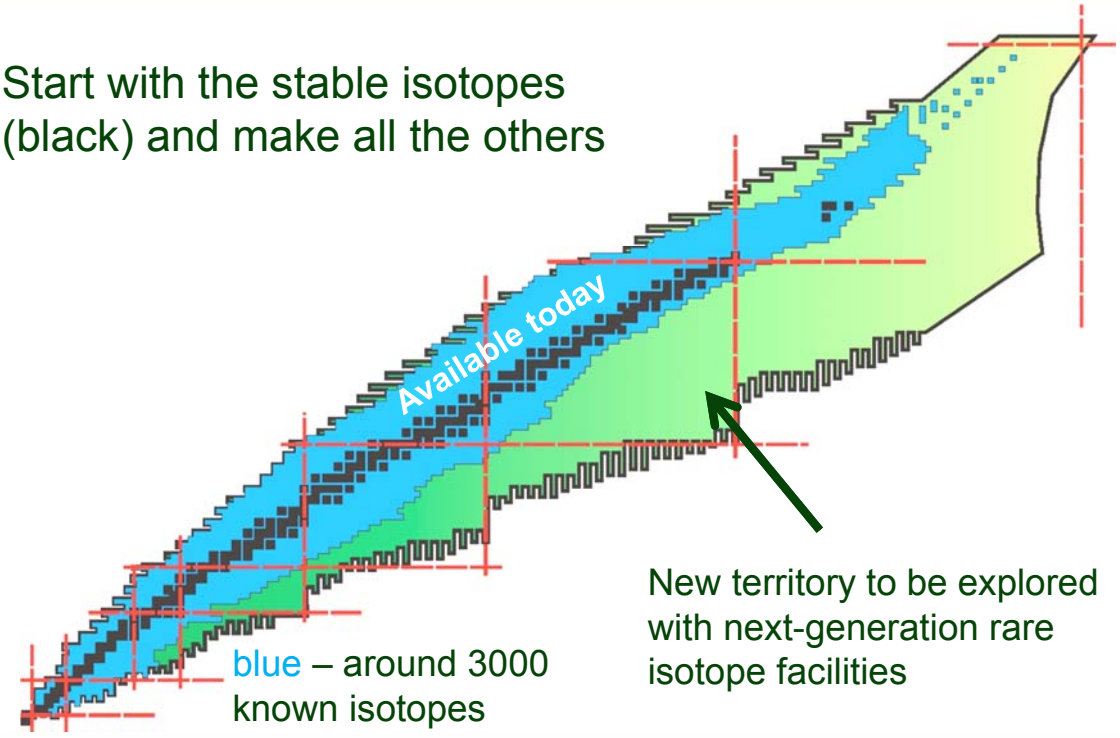

blue – around 3000 known isotopes

New territory to be explored with next-generation rare isotope facilities

Rare Isotope Production Mechanisms

- There are a variety of nuclear reaction mechanisms used to add or remove nucleons (jargon)
- Spallation
- Fragmentation
- Coulomb fission (photo fission)
- Nuclear induced fission
- Light ion transfer
- Fusion-evaporation (cold, hot, incomplete, …)
- Fusion-Fission
- Deep Inelastic Transfer
- Charge Exchange

There is no best method. Many still have interesting physics question relevant to their application to produce rare isotopes.

Production Probability

- The probability of production of a fragment is related to its production cross section:

$$P = \frac{N(\tau)}{N_0} = \left(1 - e^{-\frac{\tau N_a \sigma}{A_t}}\right)$$

τ target thickness (g/cm^2)
N_a Avagodro's number
A_t target mass number
σ production cross section

- For production cross sections of 1 mb and ^{9}Be target thickness of 1 g/cm^2 the production probability (and fragment rate) is high:

$$P = \frac{N(\tau)}{N_0} = \left(1 - e^{-\frac{1 \cdot 6.022 \times 10^{23} \cdot 1 \times 10^{-27}}{9}}\right) = 7 \times 10^{-5}$$

- Beam of 10^{14}/s beam would yield 7x10^9 /s

Cross Section for Production

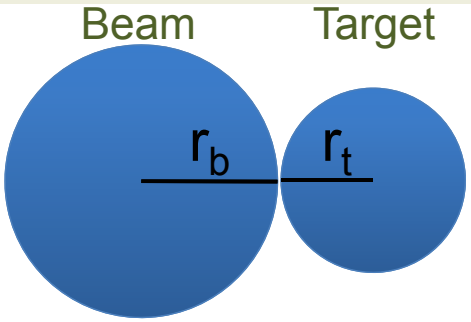

$$\sigma = \pi\left(r_t + r_b\right)^2 \approx 600\ mb$$

Actual: ^{16}O +^{12}C interaction cross section: 1000 mb (measured at 970 MeV/u)

Note: Above around 300 MeV/u the interaction length is shorter than the electronic stopping range of the ^{16}O so most beam particles can interact

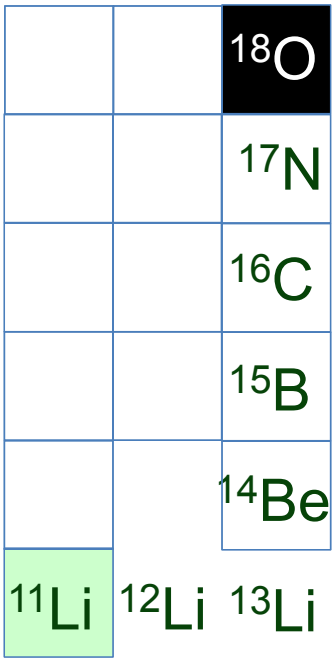

One nucleon removal
Around 50 mb (light nuclei)

P ≈ 5%

2n removal
5 mb
P = .5%

And so on
Rule of thumb
.1 x for each neutron removed

Rare Isotope Production Mechanisms

- There are a variety of nuclear reaction mechanisms used to add or remove nucleons (items for the jargon page)
- Spallation
- Fragmentation
- Coulomb fission (photo fission)
- Nuclear induced fission
- Light ion transfer
- Fusion-evaporation (cold, hot, incomplete, …)
- Fusion-Fission
- Deep Inelastic Transfer
- Massive transfer

There is no best method. Many still have interesting physics question relevant to their application to produce rare isotopes.

Production Methods – Low Energy

- (p,n) (p,nn) etc.
  - E_p < 50 MeV
  - Used for the production of medical isotopes.
  - Selective, large production cross sections (100 mb), and intense (500 mA) primary beams.
  - Used at HRIBF(ISOL), LLN (ISOL), ANL (in-flight) and Notre Dame (in-flight), Texas A&M (in-flight with MARS, e.g. ^{23}Al)
- Fusion-Evaporation
  - Low energy 5-15 MeV/A and "thin" targets (mg/cm^2)
  - Selective with fairly large production cross sections.
  - Used at for example ANL(in-flight), JYFL (Jyväskylä)
- Fusion-Fission – ^{238}U+^{12}C (basis of Laser acceleration idea D. Habs et al.)

Example of production by fusion-evaporation

- Beam and target fuse (post fusion nucleons may be evaporated)
- Variant – Incomplete fusion where particles are lost prior to the complete fusion of the participants
- High, specific production cross sections
- Example: ^{3}He (^{58}Ni, ^{60}Zn) n, E_{Ni} = 250 MeV
  - Production cross section from PACE4 (A.Gavron, Phys.Rev. C21 (1980) 230-236): 60 mb
  - 1 g/cm^2 target
  - Yield of ^{60}Zn is 7x10^7/pμA (LBL 88-inch has 10 pμA of ^{58}Ni)
  - 1 pμA = 6x10^{12} /s (particle microAmp – current if the charge is e = 1)

Low Energy - Continued

- Multi-Nucleon Transfer reactions (two body final state)
  - Significant cross section between 10 - 50 MeV/A
  - High production of nuclei near stability.
  - Multi-nucleon reactions can be used to produce rare or more neutron rich nuclei, e.g. GSI mass separator had a program to study neutron rich f-p shell nuclei using neutron transfer.
- Deeply inelastic reactions (10 - 50?/A MeV/u range)
  - Deep inelastic - KE of the beam is deposited in the target. Products are emitted away from the beam axis.
  - Was used to first produce many of the light neutron rich nuclei
  - Is used to study neutron rich nuclei since the products are "cooler" and fewer neutrons are evaporated than in fusion reactions.
  - Large cross sections for production of some exotic isotopes

Deep Inelastic Transfer Example

R Broda J Phys G 32, R151-R192 (2006) – work at ANL, recent with GAMMASPHERE

I = 10^6/s
σ = 1 mb
20 mg/cm^2
Yield = 700/hr

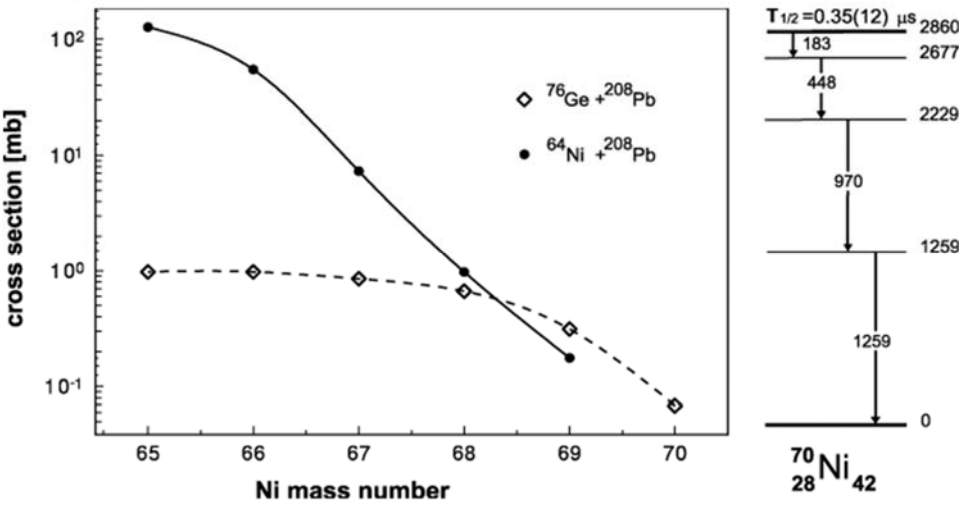

Models by Tasson-Got based on Monte Carlo (L. Tassan-Got and C. Stefan, Nucl. Phys. A524, 121 (1991)) and statistical decay of the product GEMINI (R. Charity et al., Nucl. Phys. A483, 371 (1988))

Production Mechanisms – High Energy

- Fragmentation (FRIB, RIBLL Lanzhou, NSCL, GSI, RIKEN, GANIL)
  - Projectile fragmentation of high energy (>50 MeV/A) heavy ions
  - Target fragmentation of a target with high energy protons or light HIs. In the heavy ion reaction mechanism community this would include *intermediate mass fragments*.
- Spallation (ISOLDE, TRIUMF-ISAC, EURISOL, SPES, …)
  - Name comes from spalling or cracking-off of target pieces.
  - One of the major ISOLDE mechanisms, e.g. ^{11}Li made from spallation of Uranium.
- Fission (HRIBF, ARIEL, ISAC, JYFL, BRIF,…)
  - There is a variety of ways to induce fission (photons, protons, neutrons (thermal, low, high energy)
  - The fissioning nuclei can be the target (HRIBF, ISAC) or the beam (GSI, NSCL, RIKEN, FAIR, FRIB).
- Coulomb Breakup (GSI)
  - At beam velocities of 1 GeV/n the equivalent photon flux as an ion passes a target is so high the GDR excitation cross section is many barns.

Spallation

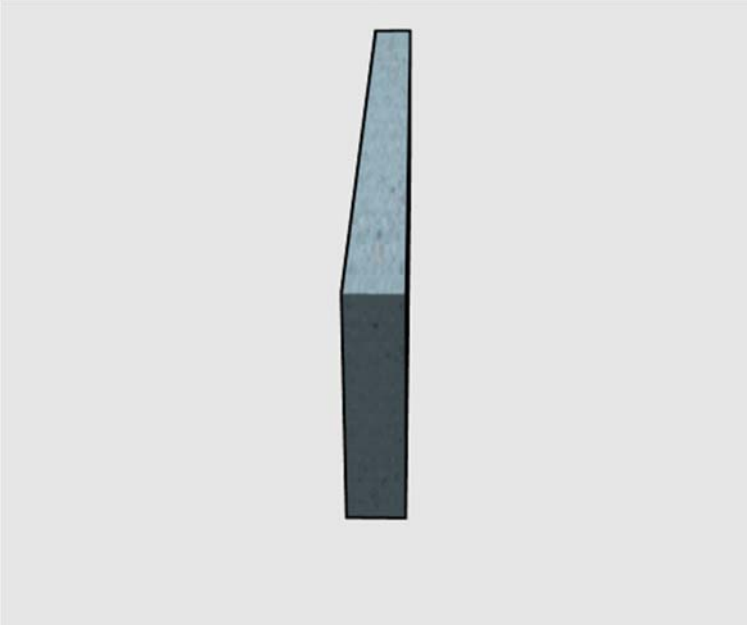

From Wikimedia Commons: http://en.wikipedia.org/wiki/File:Spallation.gif

Fragmentation (Projectile)

- Pictorial model (above 50 MeV/u)

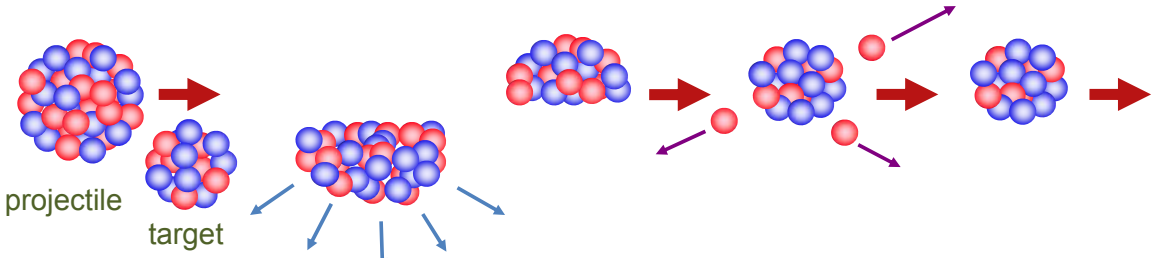

- Parameterization of cross sections (EPAX 2 Sümmerer and Blank, Phys.Rev. C61(2000)034607)
  - Close related to Silverberg-Tso parameterization
  - Parameters fit to experimental data (exponential form function of removed nucleons)
  - Energy independent cross sections
  - Production cross section does not depend on the target
- More detailed models (e.g. ABRABLA (K-H Schmidt *et al.* - See http://www-win.gsi.de/charms/)
- Internuclear Cascade

Production of Rare Isotopes by Projectile Fragmentation

- Cartoon of the production process – projectile fragmentation (fission)

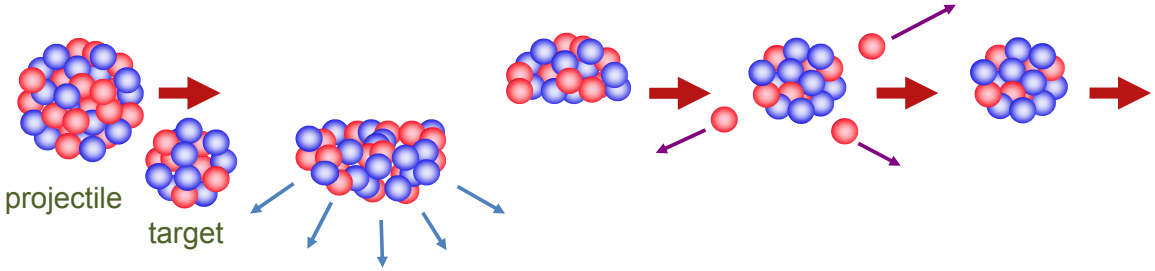

- To produce a key nucleus like ^{122}Zr from ^{136}Xe, the production cross is estimated to be 2×10^{-18} b (2 attobarns, 2×10^{-46} m^2)
- Nevertheless with a ^{136}Xe beam of power 400 kW ($\cong 8\times10^{13}$ ion/s) and modern separation techniques (fragment separators can select 1 out of 10^{18} produced), a few atoms per week can be made and studied
- For comparison: Element 117 production cross section was 1.3 (+1.5 - 0.6) pb (Oganessian, Yu. Ts. et al. Phy Rev Lett 104 (2010) 142502)

Limiting Fragmentation

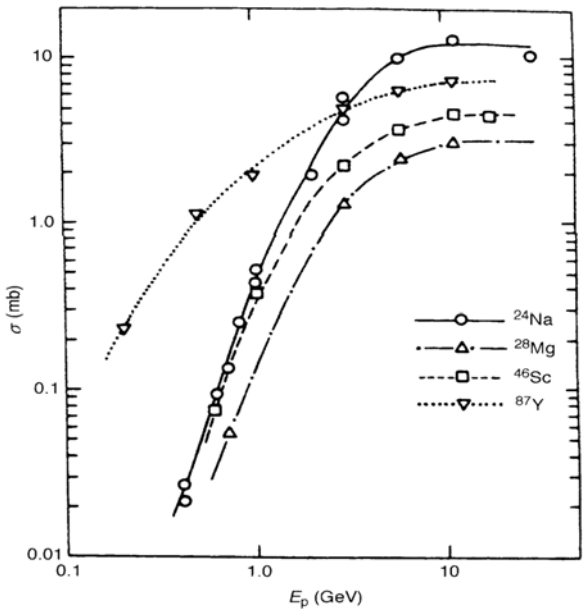

Kaufman and Steinberg, PRC 22 (80) 167.

The production yield of residues saturates with a total beam energy of a few GeV. **Limiting Fragmentaton**

H. Ravn - "The saturation cross-section for more exotic species may well first be reached beyond 5 GeV."

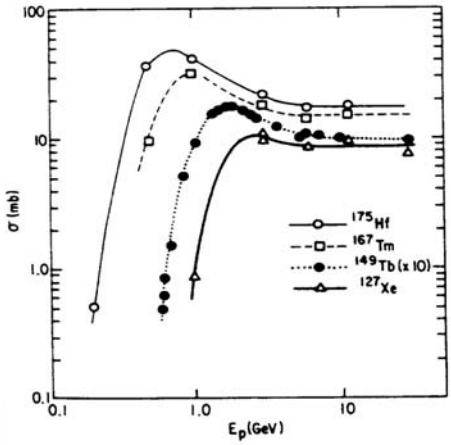

Universality of Production Cross Sections

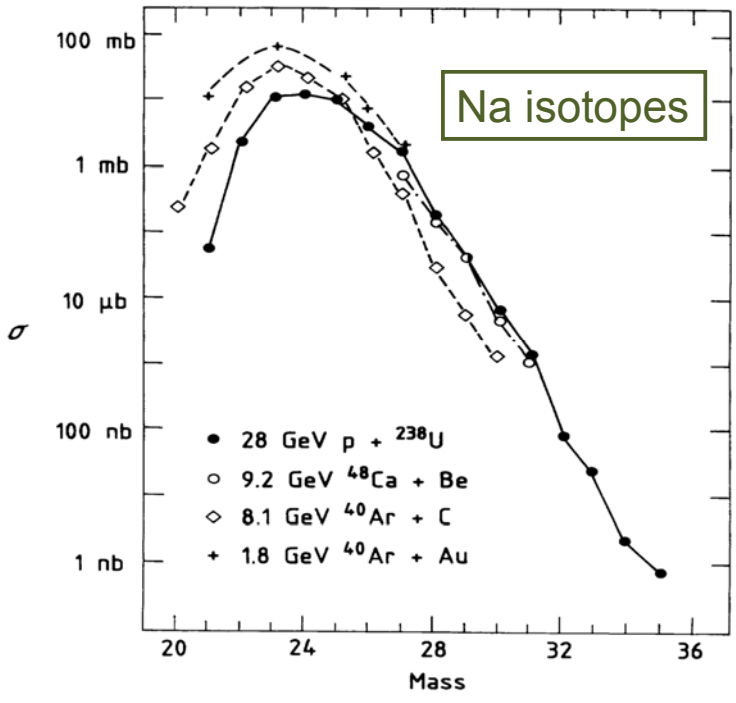

H Ravn, CERN

Production cross section depends on mass

- Cross section logarithmic with Q_g (Tarasov PRC75)
- Q_g = ME(beam) – ME(fragment)
- This provides a means to determine (roughly) the binding energy (M.B. Tsang et al., Phy Rev C DOI:10.1103/PhysRevC.76.041302)
- NOTE: The magnitude of the production cross sections do depend on the target

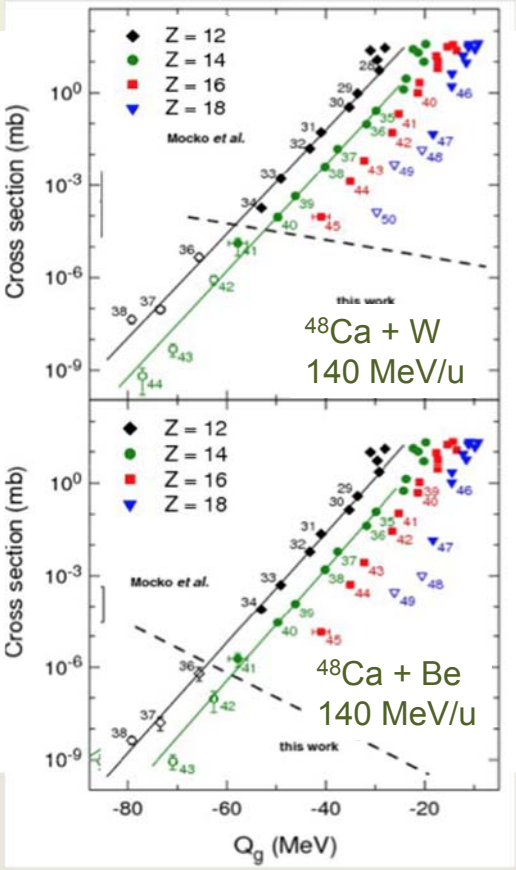

FRIB Facility for Rare Isotope Beams
U.S. Department of Energy Office of Science
Michigan State University

Production Cross Sections Measured ^{76}Ge Fragmentation at 130 MeV/u

Tarasov et al. Phys. Rev. Lett. 102, 142501 (2009)

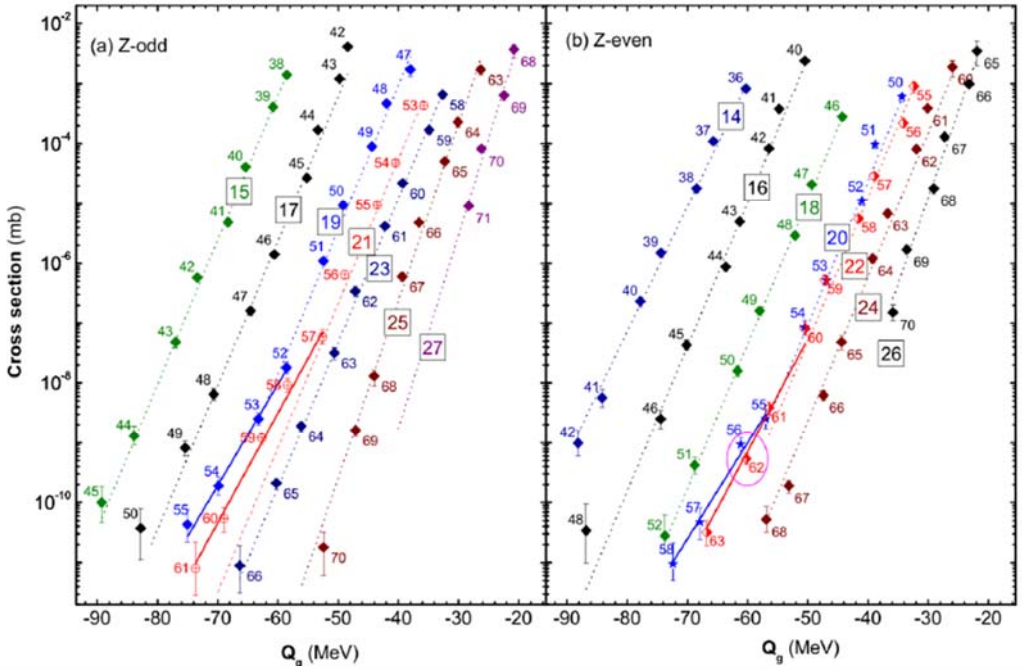

FRIB Facility for Rare Isotope Beams
U.S. Department of Energy Office of Science
Michigan State University

Fission

- Pictorial Model

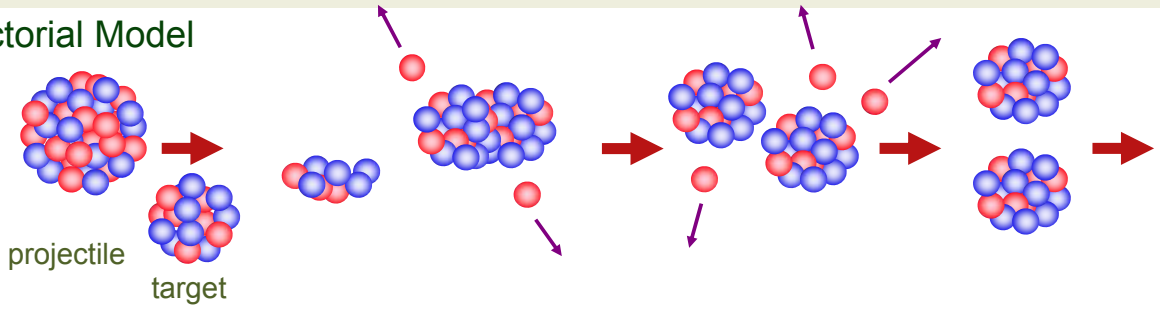

- ABRABLA - See http://www-win.gsi.de/charms/ for excellent details (Schmidt et al.) – J. Benlluire et al. Phy. Rev. C 78 054605 (2008)
- LISE++ Fission Models (Tarasov et al.) LISE++
- The initial fragmentation step produces a wide range of excitation energies
- Can use photons, protons, nuclei, etc. to induce the fission
- Observation: For 500 MeV/u ^{238}U the fragmentation and fission cross sections are approximately equal

Fission Cross Sections

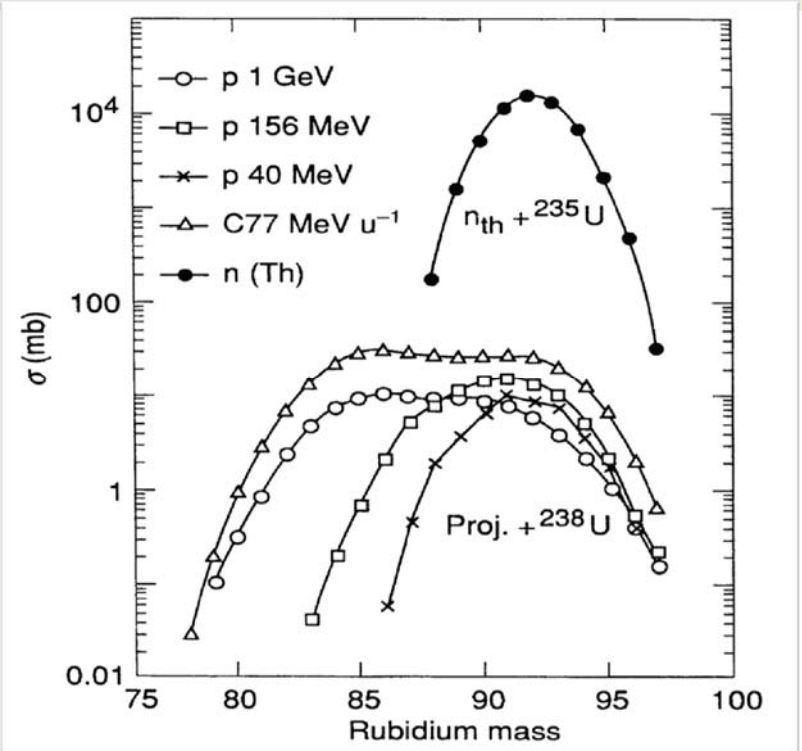

Low energy fission can lead to higher yields for certain nuclides.
This is the basis for one idea for the BRIF upgrade, and the electron driver upgrade of the TRIUMF (ARIEL).

Summary of High Energy Production Mechanisms

- CHARMS http/www.gsi.de/charms

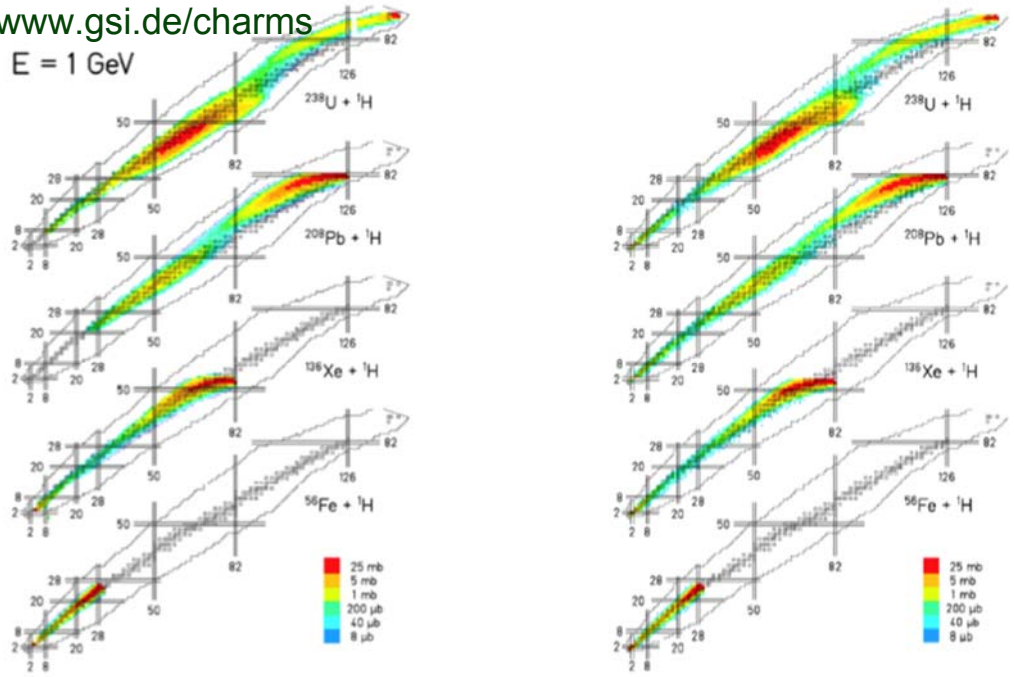

Experiment (FRS) ABRABLA07

A. Kelić, S. Lukić, M. V. Ricciardi, K.-H. Schmidt

LISE++ Simulation Code

The code operates under Windows and provides a highly user-friendly interface. It can be downloaded from the following internet address:

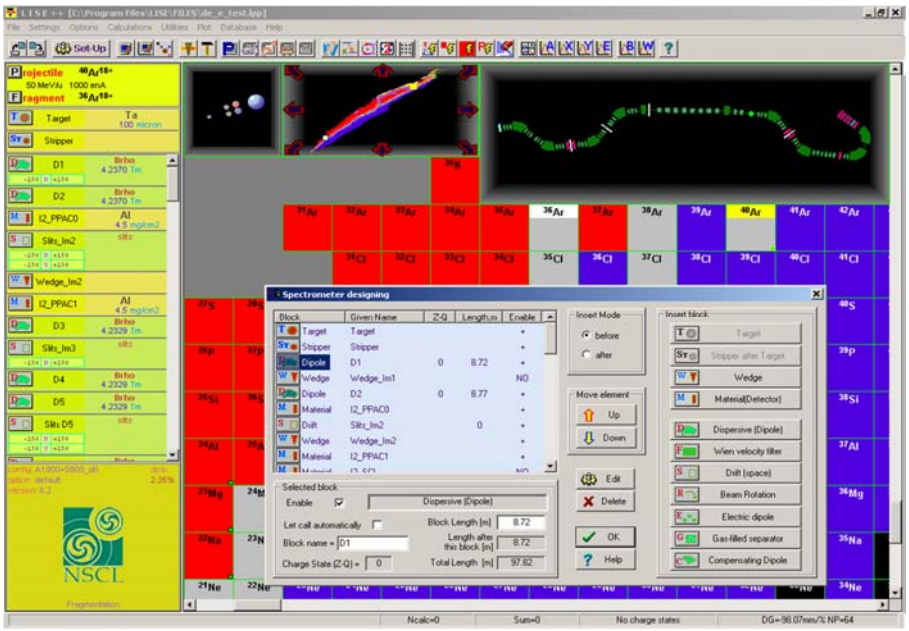

http://www.nscl.msu.edu/lise O. Tarasov, D. Bazin *et al.*

RINEN - Production rates of fission fragments and comparison with LISE++ simulation

Fairly well reproduced by the LISE++ simulations (Oleg Tarasov et al.) in which an abrasion fission (AF) model is used.

——— LISE++(ver. 8.4.1)

$^{238}U^{86+}$ 345MeV/u + Be Abrasion fission

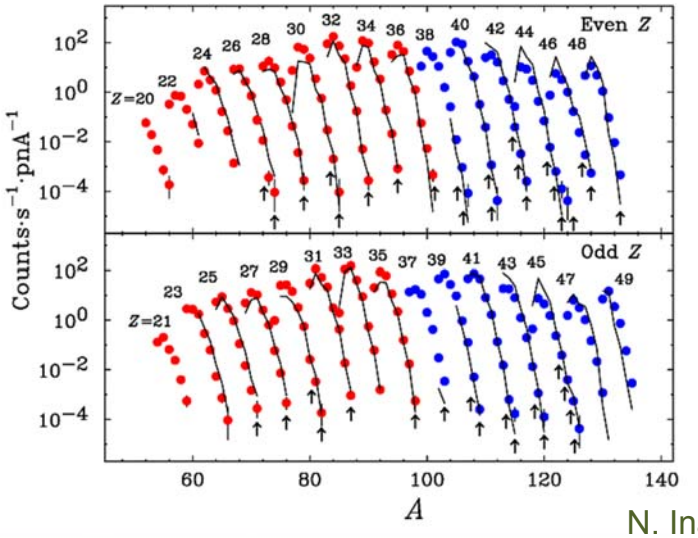

$^{238}U^{86+}$ 345MeV/u + Pb Coulomb fission

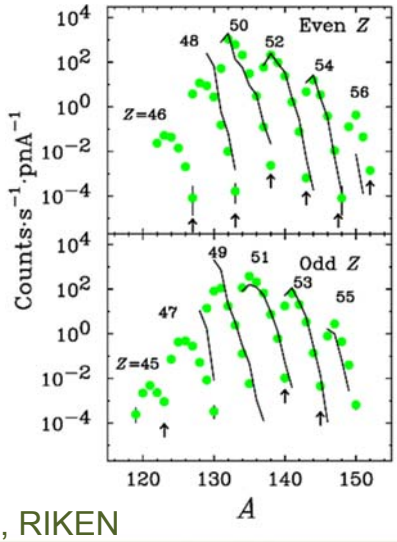

N. Inabe, RIKEN

The availability of rare isotopes over time

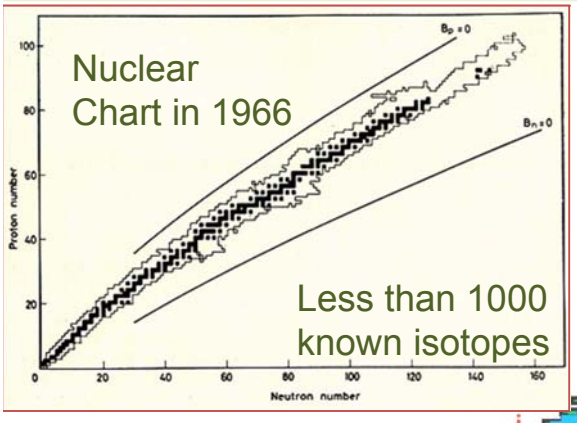

The good old days

Available today

New territory to be explored with next-generation rare isotope facilities

blue – around 3000 known isotopes

Rare Isotope Production Techniques

- Target spallation and fragmentation by light ions (ISOL – Isotope separation on line)

- Photon or particle induced fission

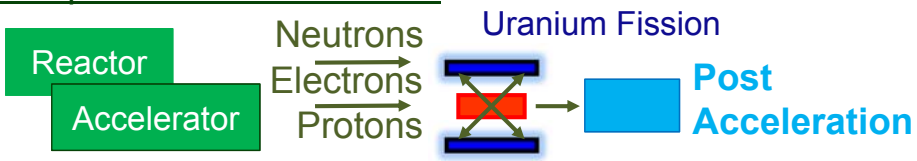

- In-flight Separation following nucleon transfer, fusion, projectile fragmentation/fission

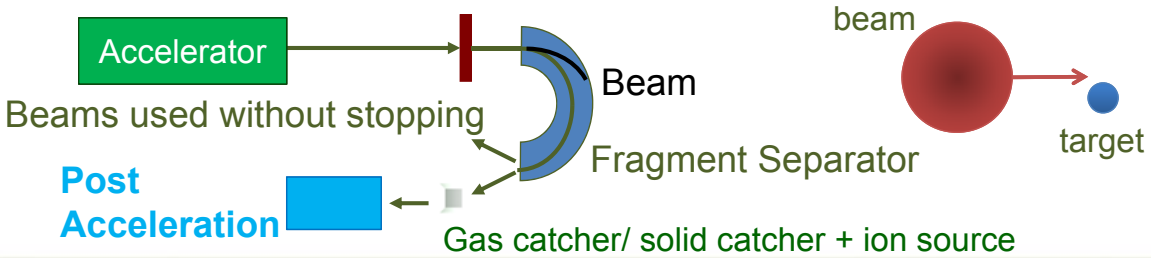

Accelerators

- The particle accelerator used for production is often called the "driver"
- Types
  - Cyclotron (NSCL, GANIL, TRIUMF (proton driver), HRIBF (proton driver), RIKEN RIBF)
  - Synchroton (GSI, FAIR-GSI)
  - LINAC (LINear ACcelerator) (FRIB, ATLAS - ANL
  - Others like FFAGs (Fixed-Field Alternating Gradient) are currently not used
- Main Parameters
  - Top Energy (e.g. FRIB will have 200 MeV/u uranium ions)
  - Particle range (TRIUMF cyclotron accelerates hydrogen, hence is used for spallation)
  - Intensity or Beam Power (e.g. 400 kW = $8x6x10^{12}$/s x 50GeV
  - Power = pμA x Beam Energy (GeV) (1pμA = $6x10^{12}$ /s)

Cyclotrons

- Relatively easy to operate and tune (only a few parts.
- Tend to be used for isotope production and places where reliable and reproducible operation are important
- Intensity is moderately high, acceleration efficiency is high, cost low
- Relativity is an issue, so energy is limited to a few hundred MeV/u.
- RIKEN Superconducting Ring Cyclotron 350 MeV/u

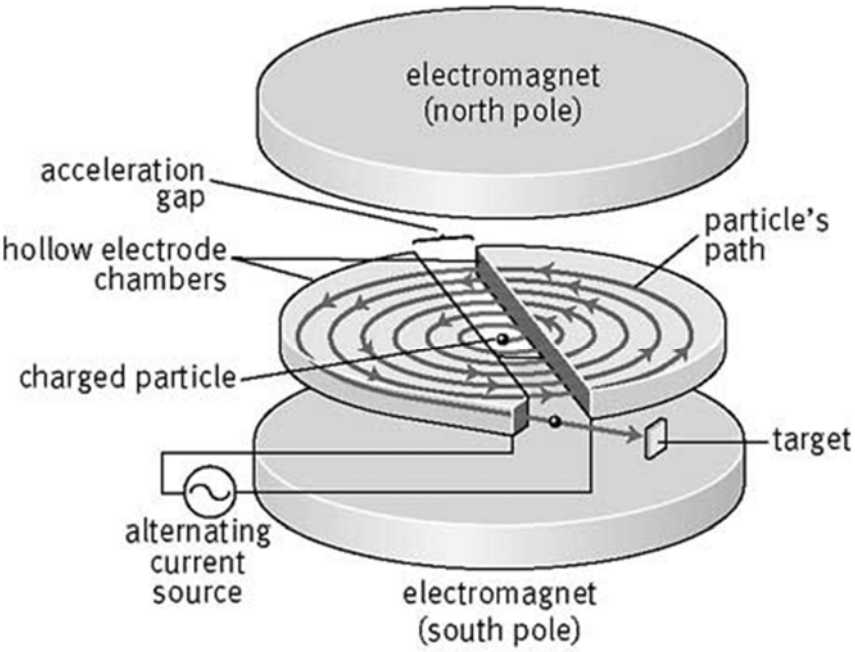

http://images.yourdictionary.com/cyclotron

Synchrotron

- Can achieve high energy at modest cost – tend to be used to deliver the highest energies
- Beam is accelerated in bunches
- Beam is accelerated internally and then ejected
- Intensity is limited by the Coulomb force of particles within a bunch (Space Charge)
- The magnets must ramp and this can be difficult to do quickly for superconducting magnets

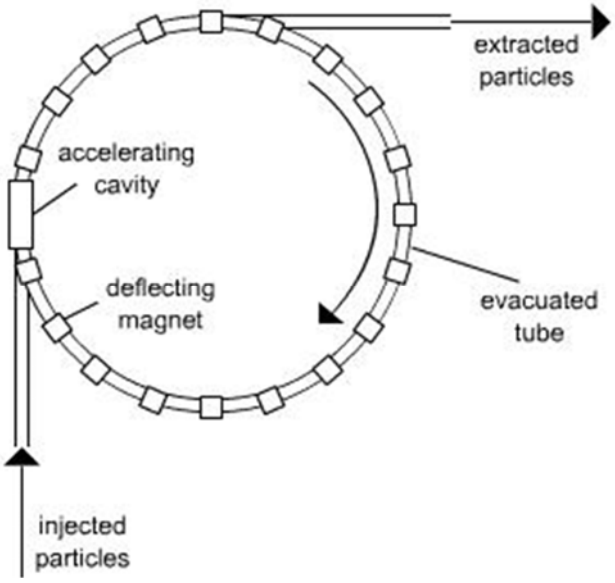

http://universe-review.ca/R15-20-accelerators.htm

Linear Accelerator - LINAC

- There are many difference types
- At the right is the principle behind the drift tube linac introduced by Alverz
- Intensity can be very high
- Tuning can be difficult and complicated
- FRIB will have around 400 separate cavities
- Cost can be high
- Used to provide the highest intensities
- Electron linacs are widely used for medical applications

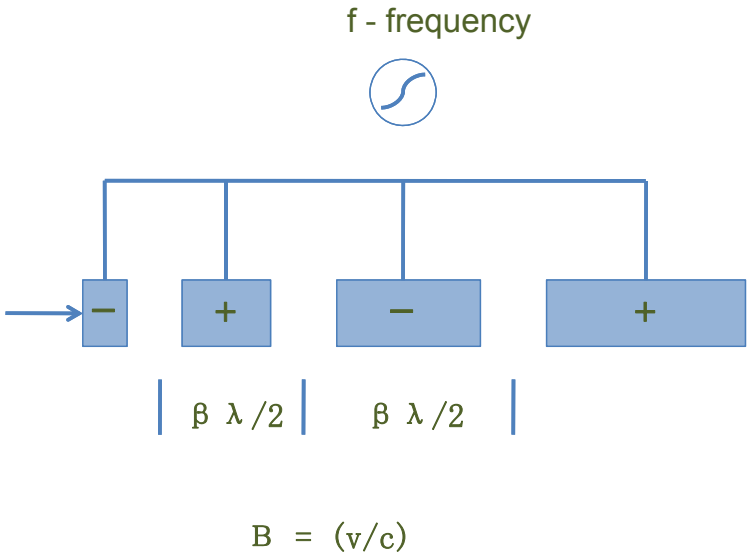

$$B = (v/c)$$

Jargon

- ISOL

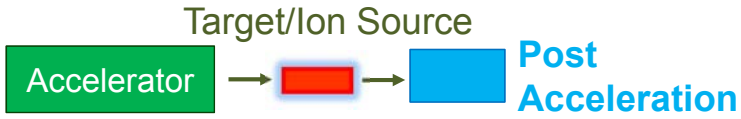

- In-flight (projectile fragmentation is one production mechanism)

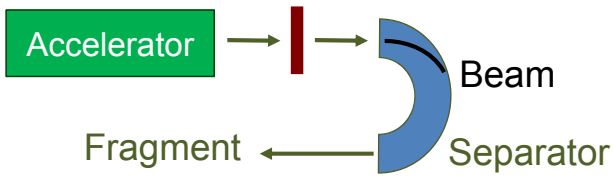

Types of ISOL Ion Sources

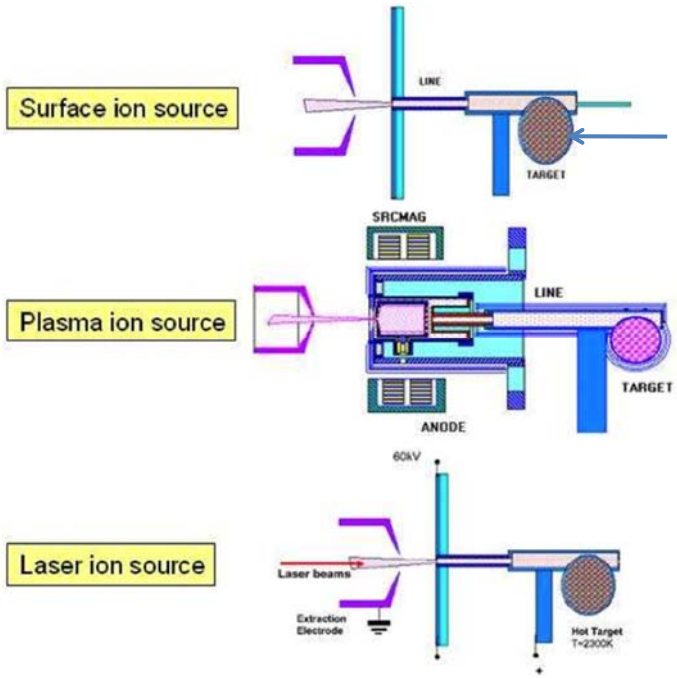

P. Butler

Production is only one part of the equation

H. Ravn

$$I = \sigma I_b T_{useable} \varepsilon_{diff} \varepsilon_{des} \varepsilon_{eff} \varepsilon_{is\_eff} \varepsilon_{accel\_eff}$$

- σ - production cross section
- I_b - beam intensity
- $T_{useable}$ - usable target thickness
- ε_{diff} – diffusion efficiency
- ε_{des} – desorption efficiency
- ε_{eff} – effusion efficiency
- ε_{is_eff} - ionization efficiency
- ε_{accel_eff} - acceleration efficiency

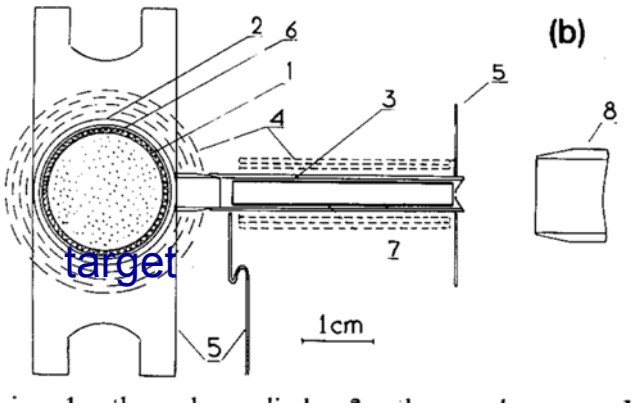

In-Flight Production Example: NSCL's CCF

D.J. Morrissey, B.M. Sherrill, Philos. Trans. R. Soc. Lond. Ser. A. Math. Phys. Eng. Sci. 356 (1998) 1985.

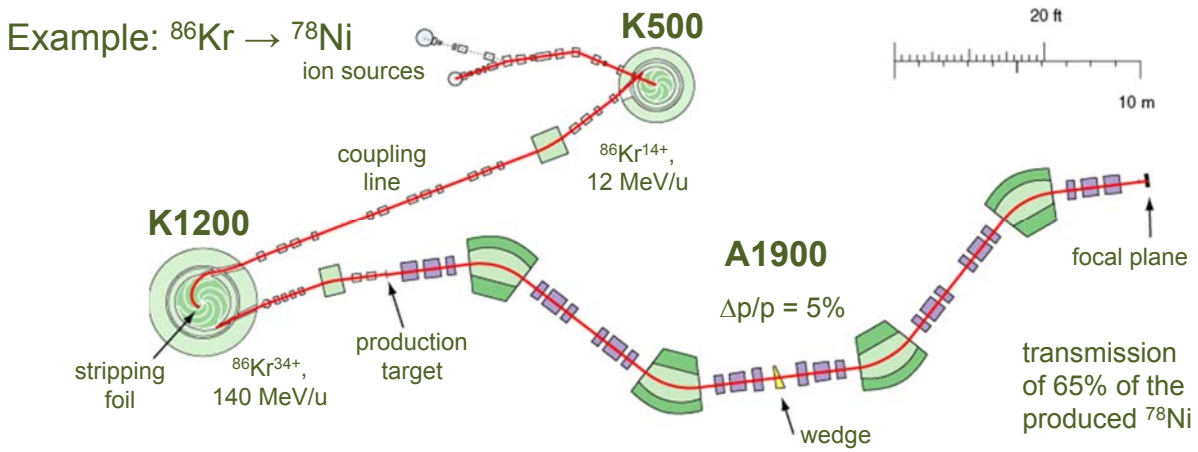

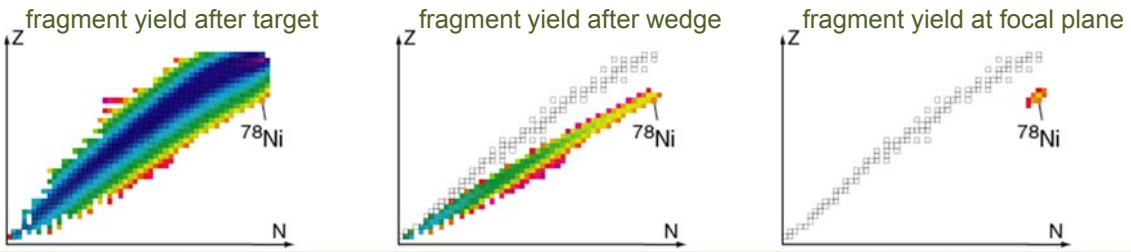

Exotic Beams Produced at NSCL

More than 1000 RIBs have been made – more than 830 RIBs have been used in experiments

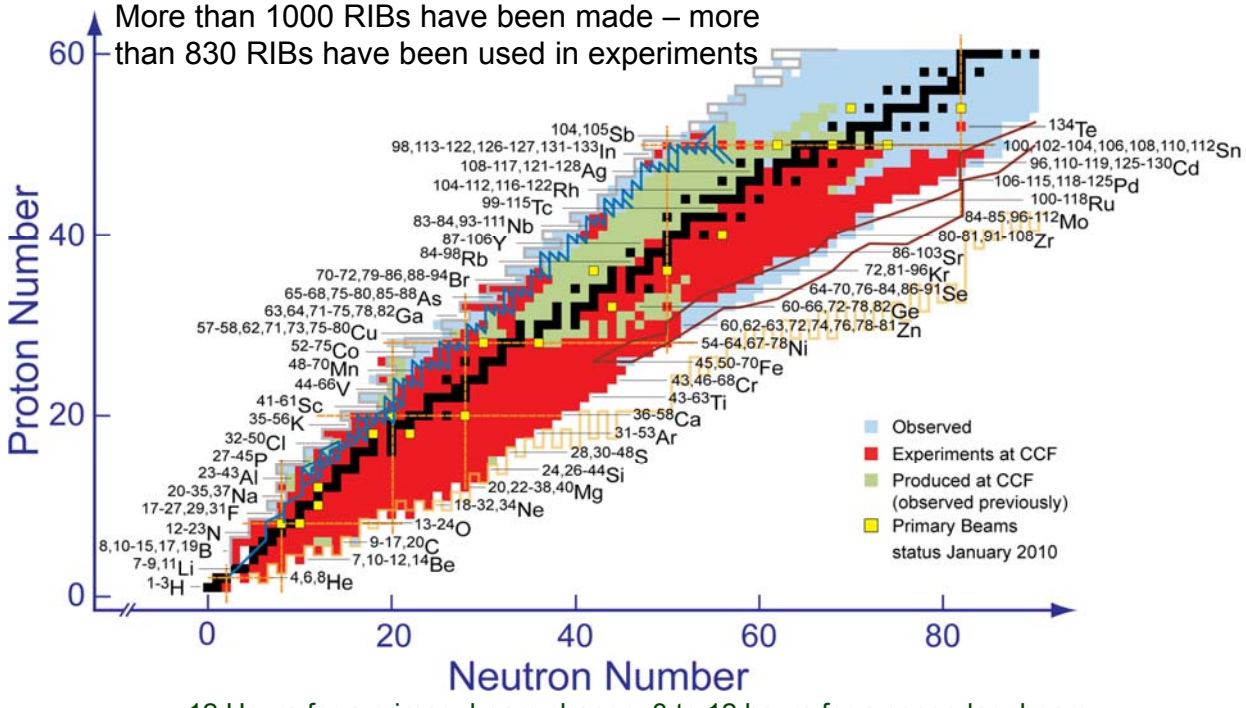

12 Hours for a primary beam change; 3 to 12 hours for a secondary beam

Advantages/Disadvantages of ISOL/In-Flight

In-flight:
GSI
RIKEN
NSCL
FRIB
GANIL
ANL
RIBBAS …

- Provides beams with energy near that of the primary beam
  - For experiments that use high energy reaction mechanisms
  - Luminosity (intensity x target thickness) gain of 10,000
  - Individual ions can be identified
- Efficient, Fast (100 ns), chemically independent separation
- Production target is relatively simple

ISOL:
HRIBF
ISAC
SPIRAL
ISOLDE
SPES
EURIOSOL

- Good Beam quality (π mm-mr vs. 30 π mm-mr transverse)
- Small beam energy spread for fusion studies
- Can use chemistry (or atomic physics) to limit the elements released
- 2-step targets provide a path to MW targets
- High beam intensity leads to 100x gain in secondary ions

400kW protons at 1 GeV is 2.4×10^{15} protons/s

World view of rare isotope facilities

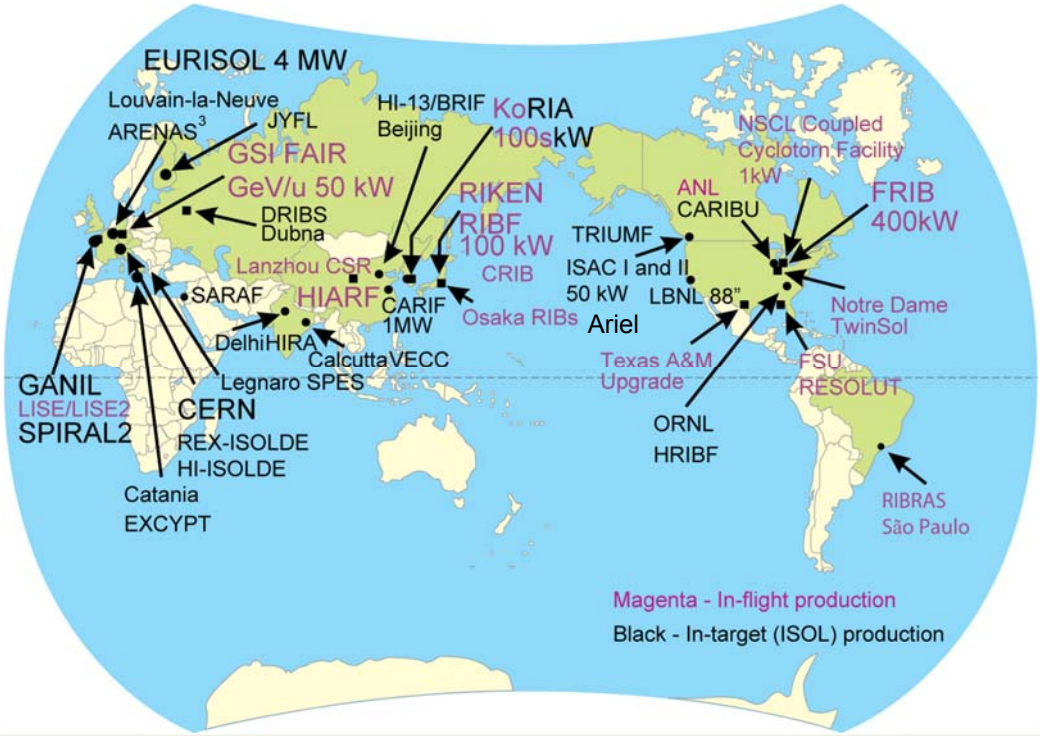

The Five-Minute Rap Version

Rare Isotope Rap by Kate McAlpine (also did the LHC Rap)

Facility for Rare Isotope Beams, FRIB - USA

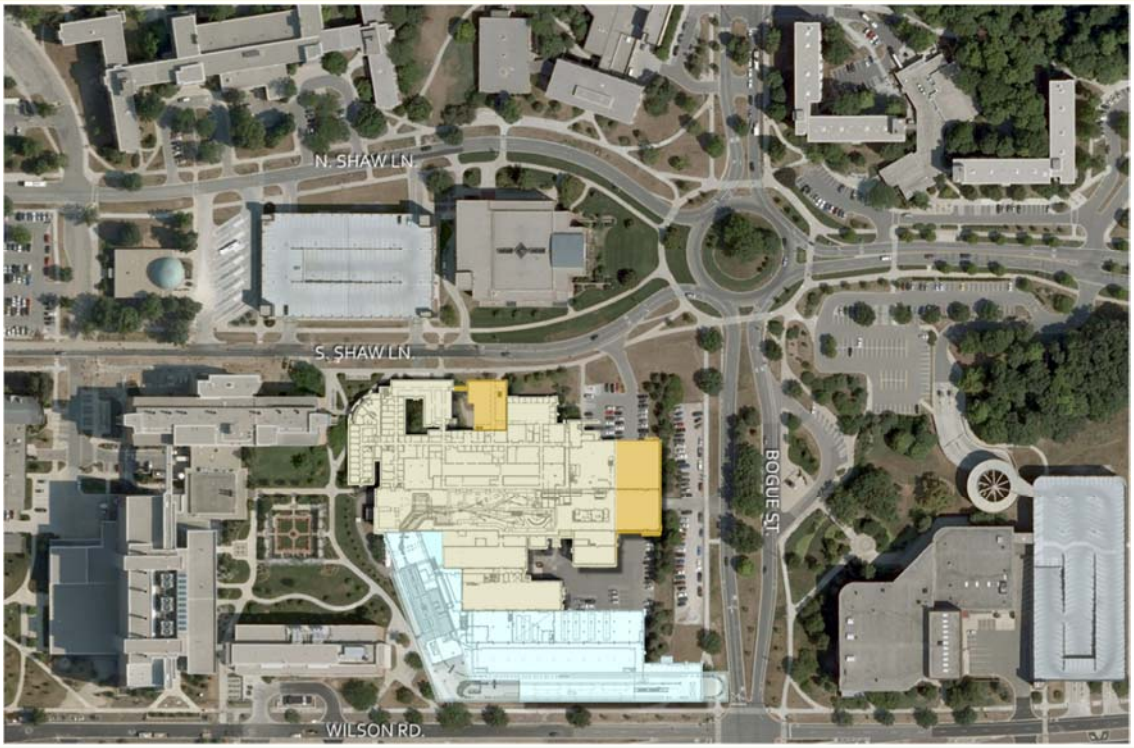

US Community's Major New Initiative – Facility for Rare Isotope Beams

- Laboratory Director Konrad Gelbke, Project Director Thomas Glasmacher
- Estimate of TPC $614.5M
- Project completion in 2020, managed for early completion in 2018
- Key features (unique)
  - 400 kW heavy ion beams
  - Efficient acceleration (multiple charge states)
  - Stopped and reaccelerated, separated beams
- Space for
  - Reaccelerated beams, uranium to 12 (15) MeV/u
  - Isotope harvesting

FRIB

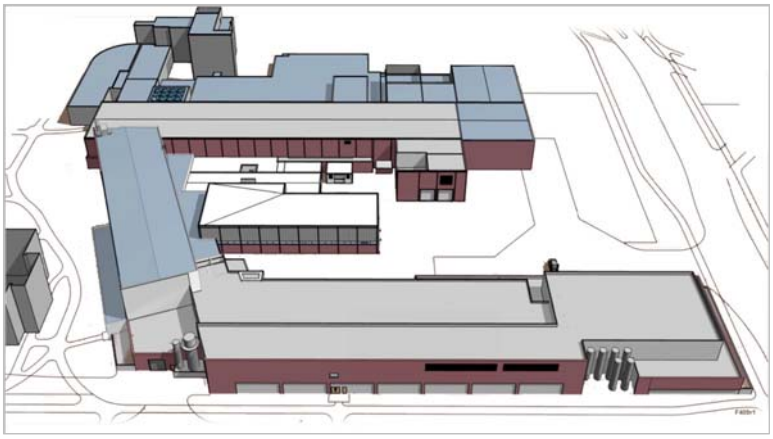

FRIB Facility for Rare Isotope Beams
U.S. Department of Energy Office of Science
Michigan State University

FRIB External Overview

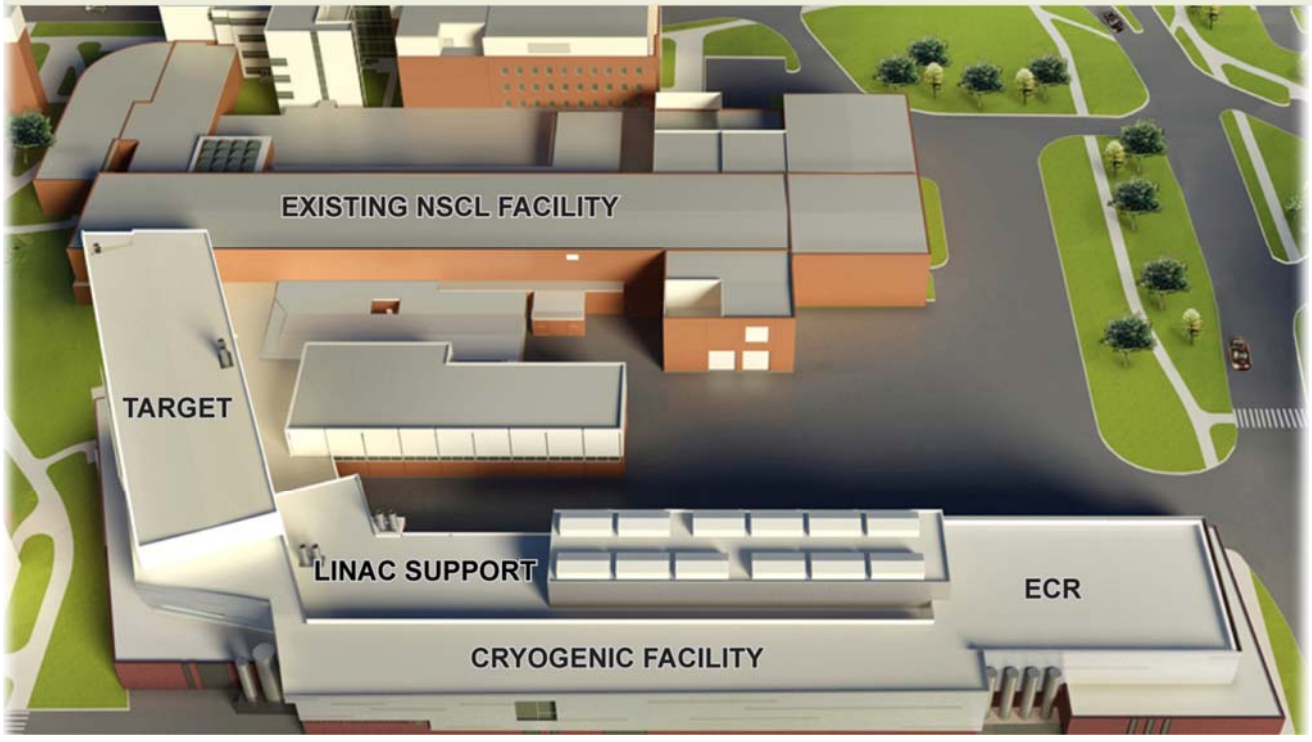

FRIB Facility for Rare Isotope Beams
U.S. Department of Energy Office of Science
Michigan State University

FRIB Facility Layout

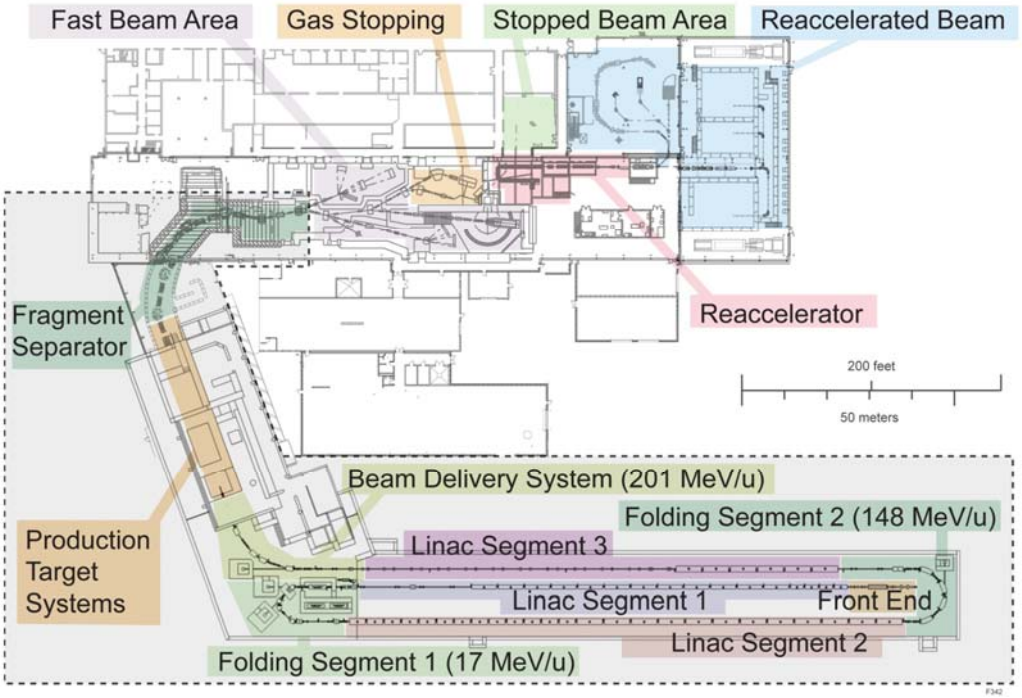

FRIB Driver Linac

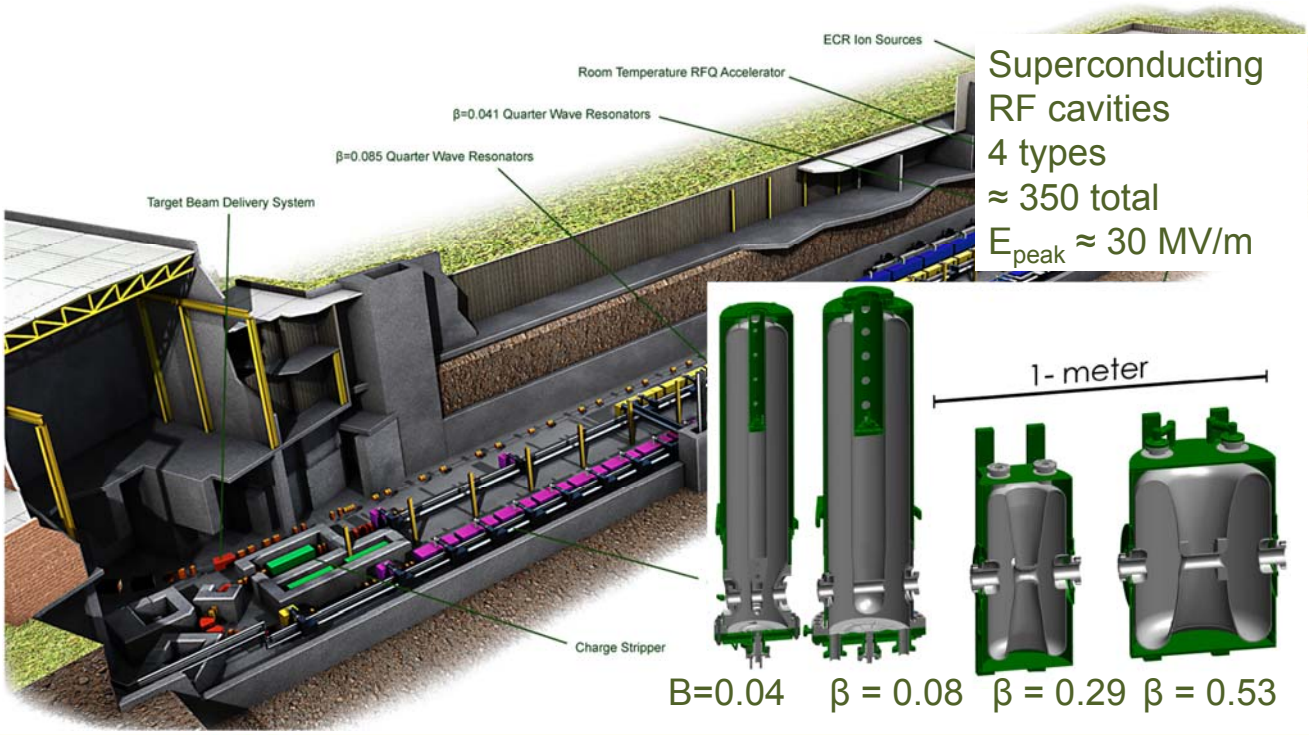

FRIB Fragment Separator

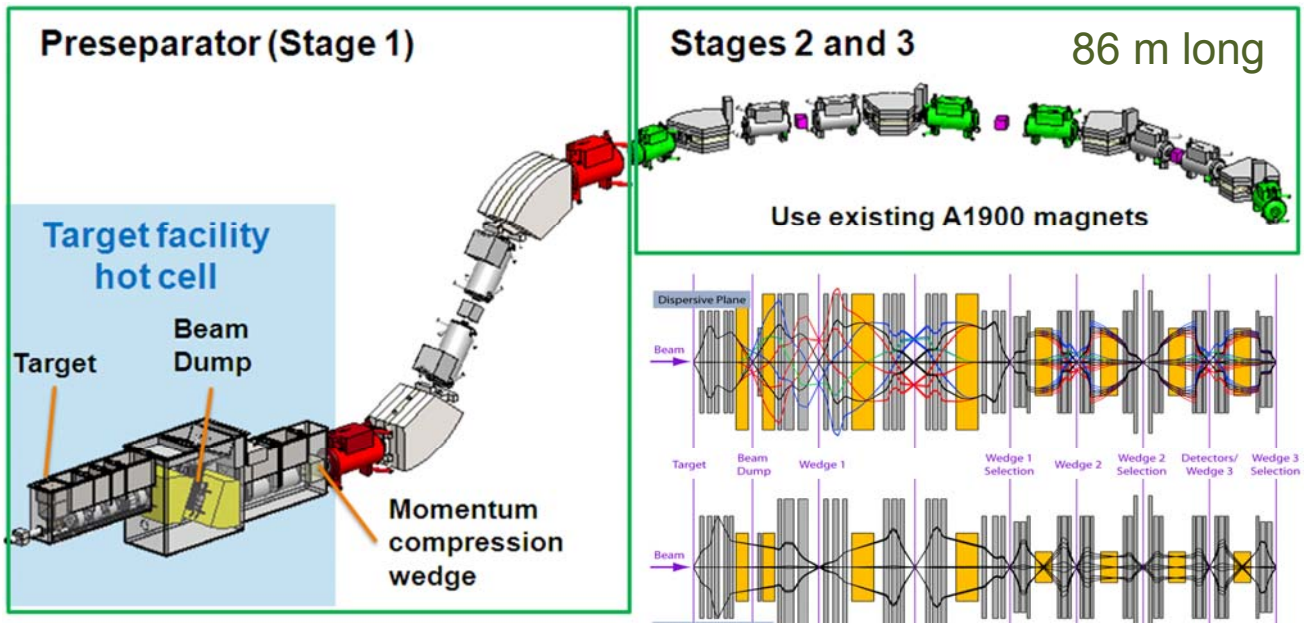

Target and beam dump capable to handle 400 kW beams

5th Order Ion Optical Design

Production Target and Beam Dump Area

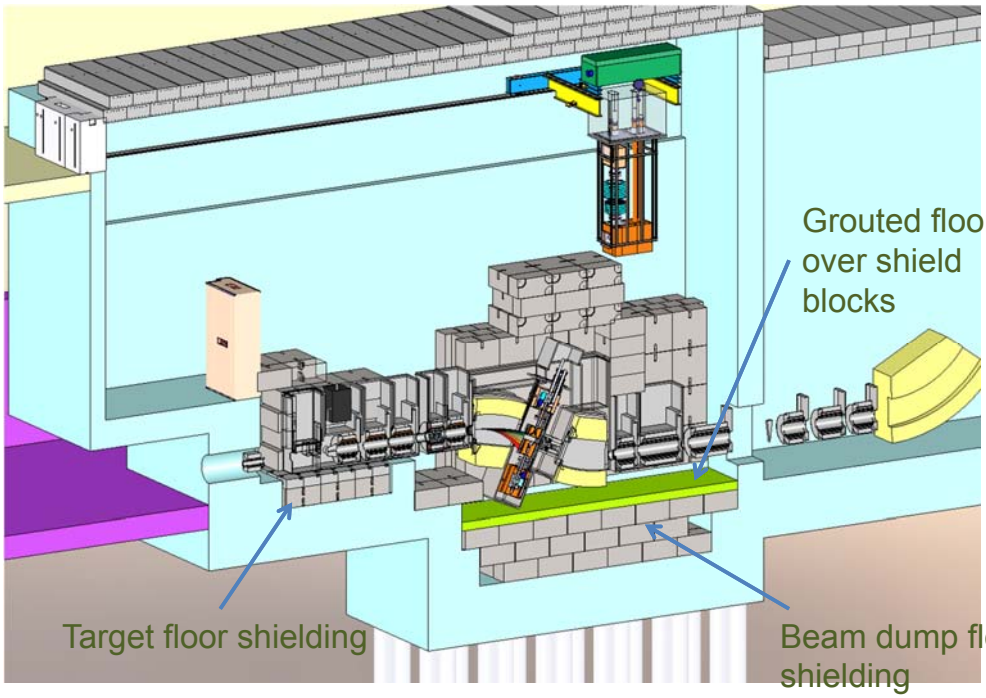

Notional Equipment Layout for Fast, Stopped, and ReA3-ReA12

- FRIB experimental areas will use existing NSCL augmented by a new ReA12 experimental area (funded by MSU, to be completed Sept 1, 2011)
- ReA12 Upgrade is essential for much of the science of FRIB

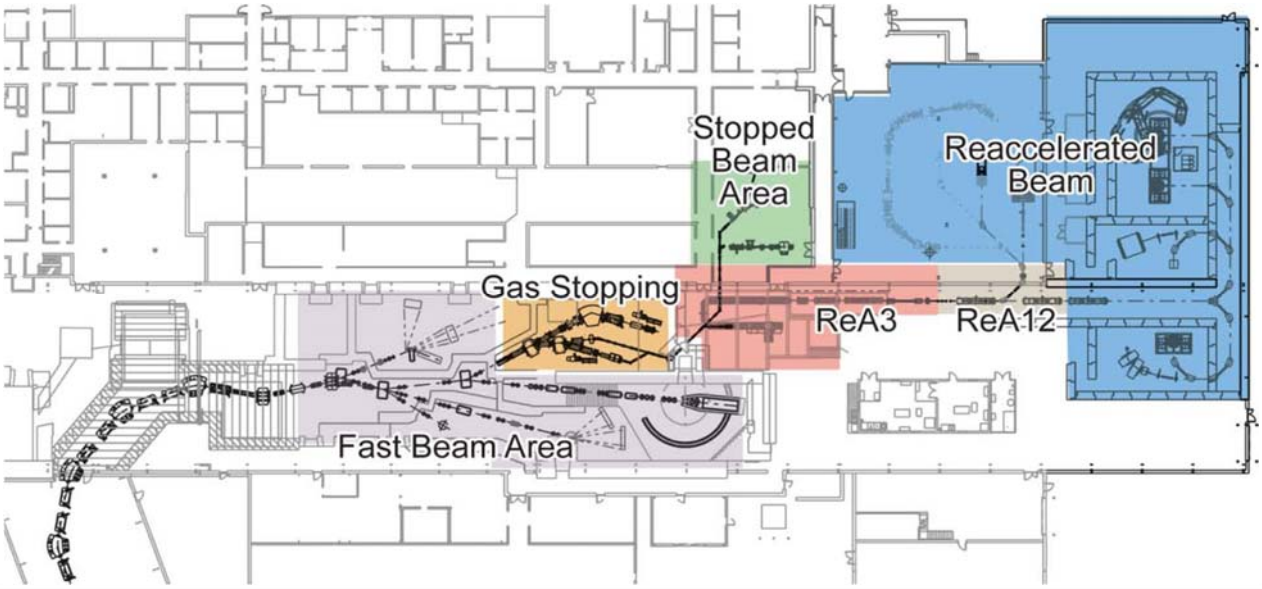

Key FRIB component: Beam Stopping

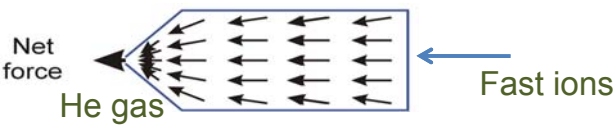

G. Savard, ANL, D. Morrissey NSCL
LLN, GSI, et al.

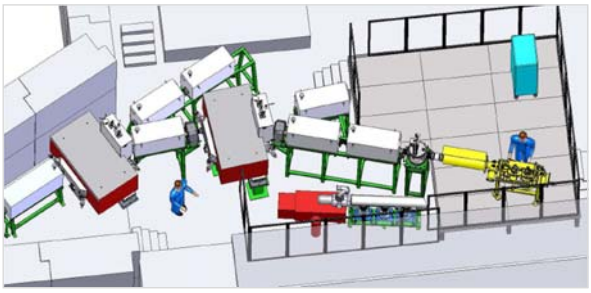

Beams for precision experiments at very low-energies or at rest and for reacceleration

- Cyclotron gas stopper
- Linear gas stopper
- Solid stopper (LLN (Belgium), KVI (Netherlands))

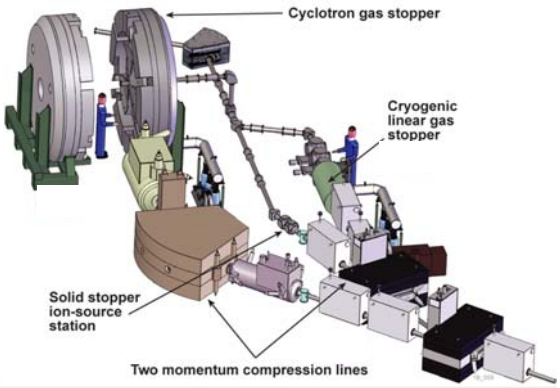

ReA12 - Reaccelerator 12 MeV/u

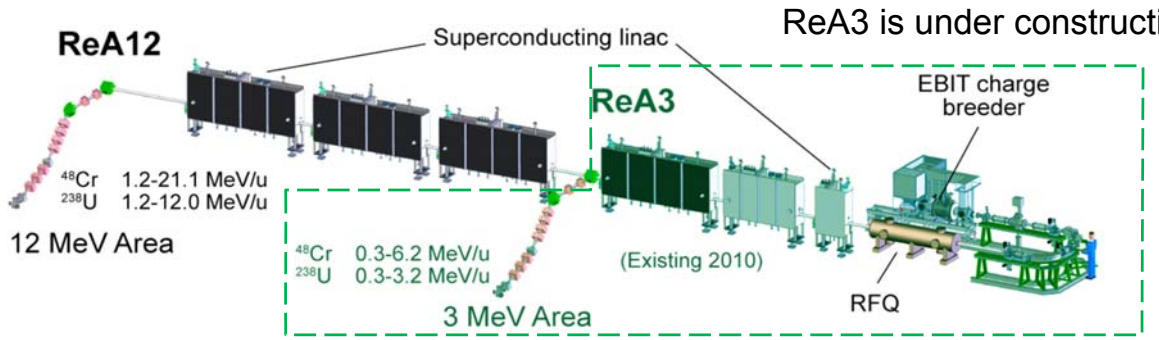

- ReA3 in operation by 2011
  - 0.3-3.2 MeV/u for uranium
- Upgrade to ReA12 by adding cryomodules already designed and previously constructed
  - 1.2-12 MeV/u for uranium
- Priority to fund outside the FRIB project

What New Nuclides Will FRIB Produce?

- FRIB will produce more than 1000 NEW isotopes at useful rates (4500 available for study)
- Theory is key to making the right measurements
- Exciting prospects for study of nuclei along the drip line to mass 120 (compared to 24)
- Production of most of the key nuclei for astrophysical modeling
- Harvesting of unusual isotopes for a wide range of applications

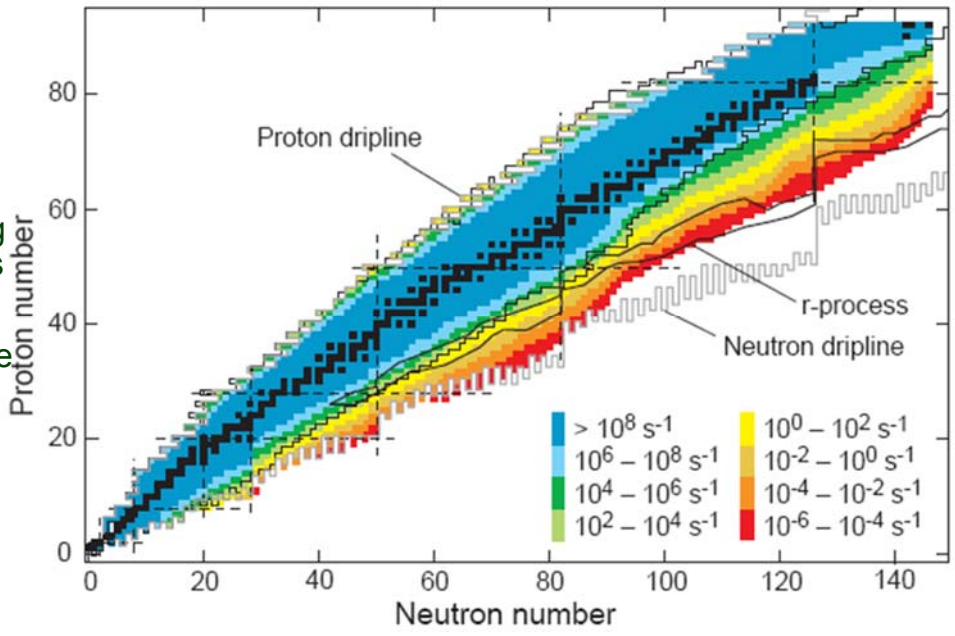

Rates are available at http://groups.nscl.msu.edu/frib/rates/

Summary

- We have entered the age of designer atoms – new tool for science
- FRIB (and other facilities) will allow production of a wide range of new designer isotopes
  - Necessary for the next steps in accurate modeling of atomic nuclei
  - Necessary for progress in astronomy (chemical history, mechanisms of stellar explosions)
  - Opportunities for the tests of fundamental symmetries
  - Important component of a future U.S. isotopes program
- There are significant challenges remaining in modeling and understanding the best production mechanism

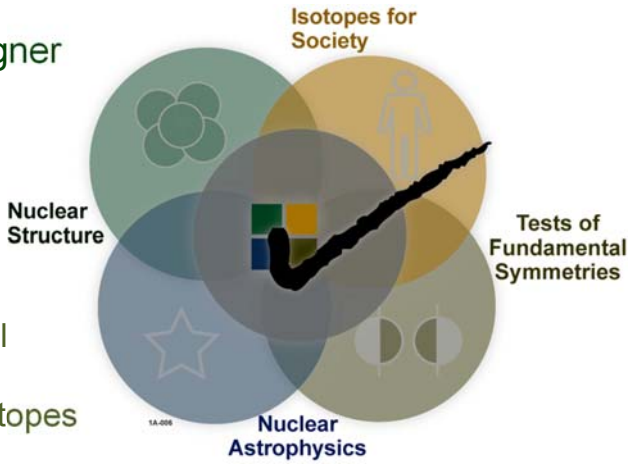

Fragmentation at 400MeV/u

- LISE++ Simulation for ^{124}Xe and ^{208}Pb fragmentation

Relatively 'easy' to collect due to small phase space

^{100}Sn

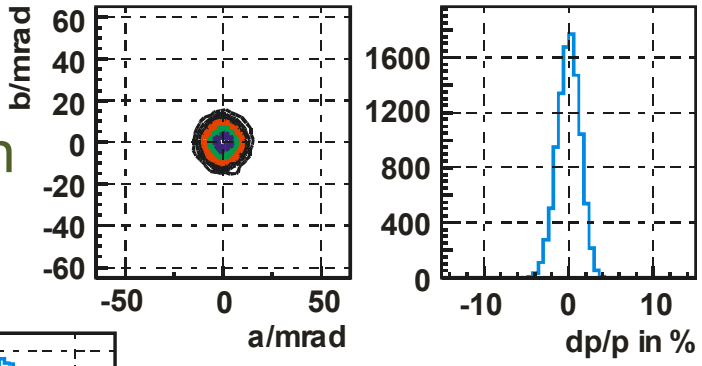

Momentum distrib.

^{200}W

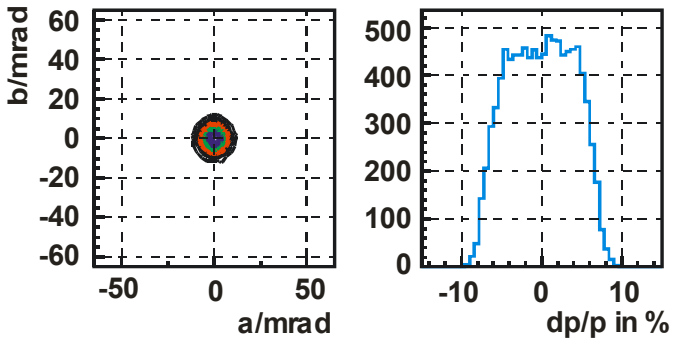

- Angles ≤ ± 20 mrad
- Momentum ± 3 - 8 %

M. Hausmann, T. Nettleton

In-Flight Fission at 400 MeV/u

• LISE++ Fission model for ^{238}U

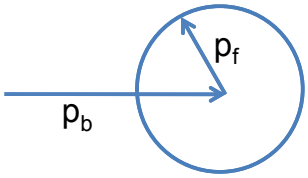

^{132}Sn

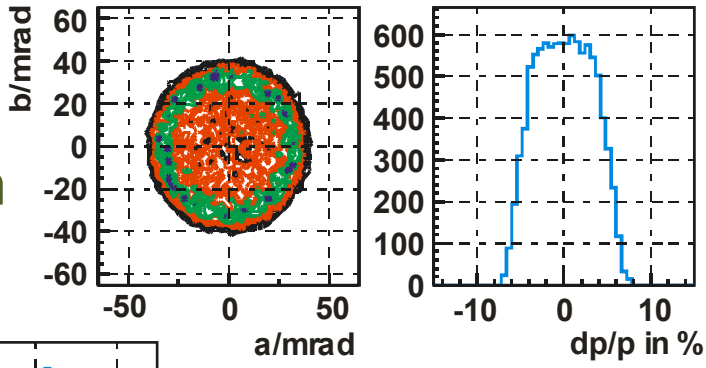

^{76}Ni

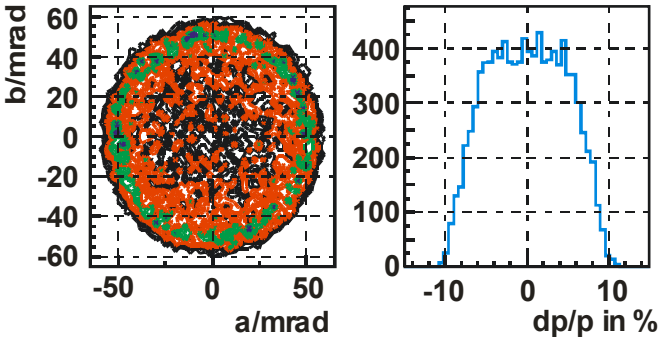

- Angles ± 40 - 60 mrad
- Rigidity ± 6 - 10 %
- Plus correlations due to fission kinematics

M. Hausmann, T. Nettleton

FRIB Facility for Rare Isotope Beams
U.S. Department of Energy Office of Science
Michigan State University

TRIUMF

ISAC @ TRIUMF

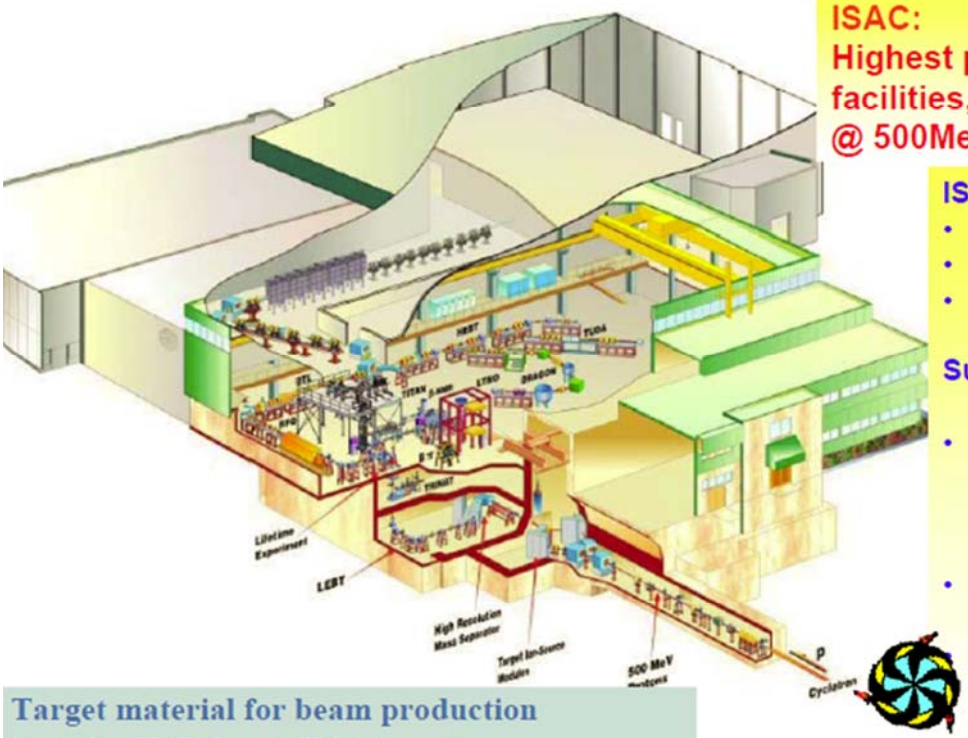

ISAC:
Highest power for On-Line facilities, we go up to 100μA @ 500MeV DC proton

ISAC has 3 exper. areas:
- Low energy (60keV)
- ISAC I (up 1.8 MeV/u)
- ISAC II (up to 16MeV/u, presently upgraded)

Suite of experimental stations:
- TRINAT, Beta-NMR, 8pi, tape-station, TITAN, Co-linear laser spec, polarised beam line, etc
- DRAGON, TUDA, TACTIC, GPS, TIGRESS, EMMA (2011), HERACLES

Target material for beam production includes U (UO and UC license)
Ion sources: surface, laser, FEBIAD, ECR (test)
TRIUMF part of collaborations for target and ion source R&D

Gordon Ball, TRIUMF

Present status of the Ariel Project

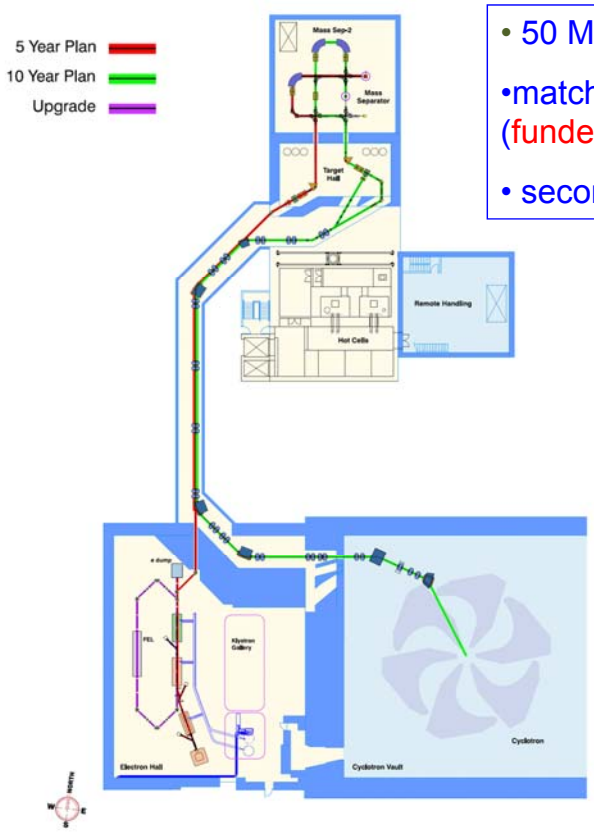

- 50 MeV, 500 kW superconducting e-linac funded
- matching funding from BC province for buildings (funded June 2010)
- second proton beamline deferred until next 5YP

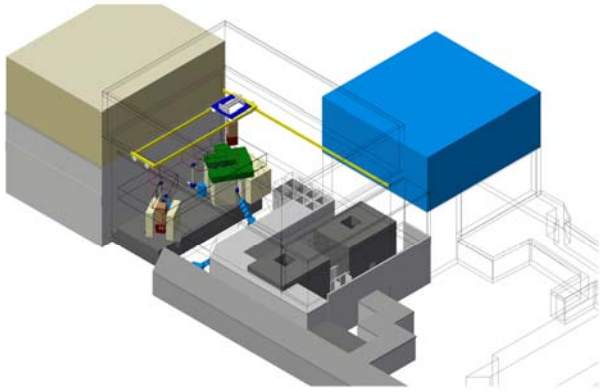

Gordon Ball, TRIUMF

Argonne National Laboratory: CARIBU & Energy Upgrade & HELIOS: Unique Synergy

- **Fission products of ^{252}Cf spontaneous fission stopped in gas and accelerated**
- **CARIBU gives access to exotic beams not available elsewhere.**
- **Physics with beams from CARIBU (1 & 2 nucleon transfer reactions) needs the new energy regime opened by the Energy Upgrade (12 MeV/u) .**
- **Solenoid Spectrometer greatly expands the effectiveness of both the fission fragment beams and the existing in-flight RIB program at these higher energies.**

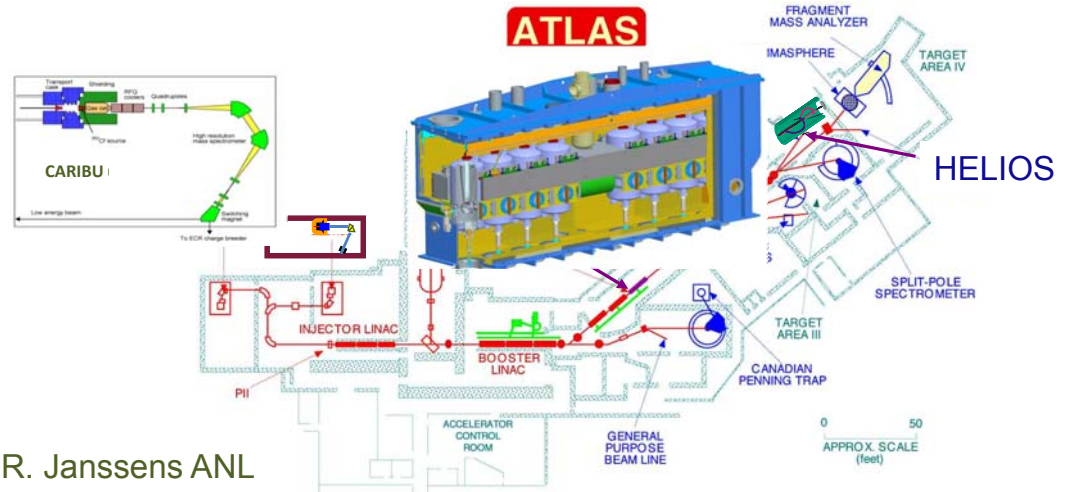

R. Janssens ANL

FRIB Facility for Rare Isotope Beams
U.S. Department of Energy Office of Science
Michigan State University

Yields from the ANL Upgrade

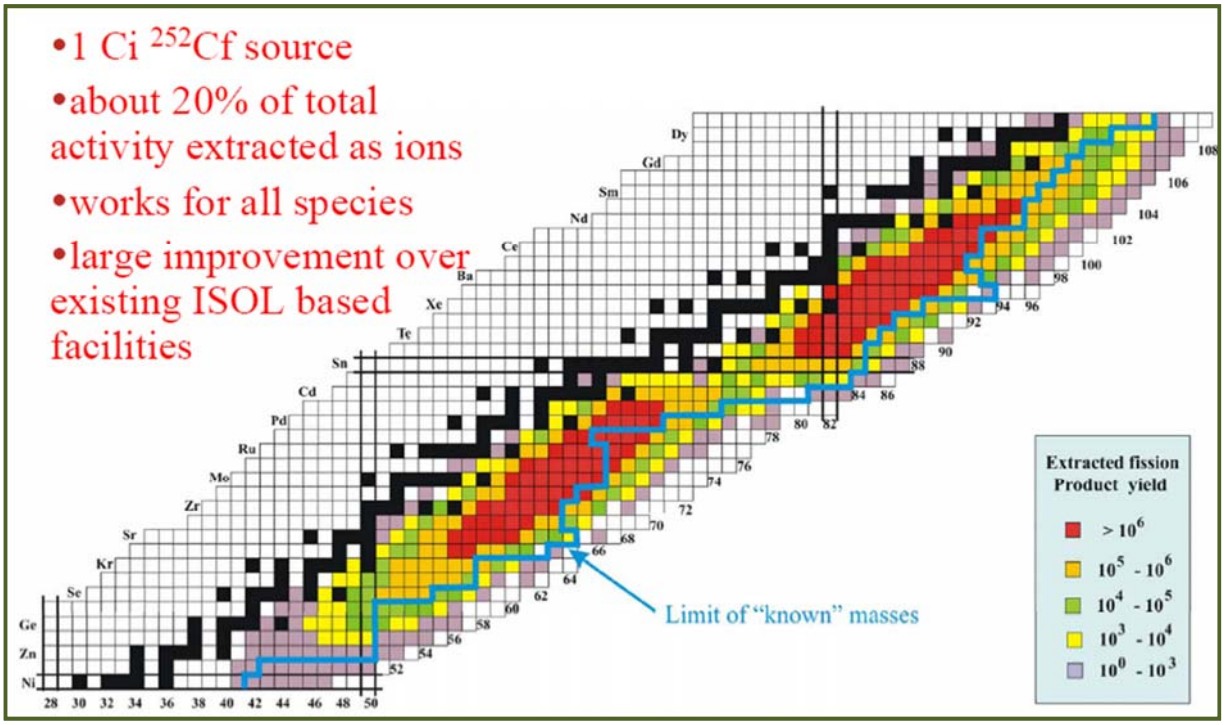

Guy Savard, ANL

Brad Sherrill ISSSP August 2011, Slide 55

RIKEN RI Beam Factory (RIBF)

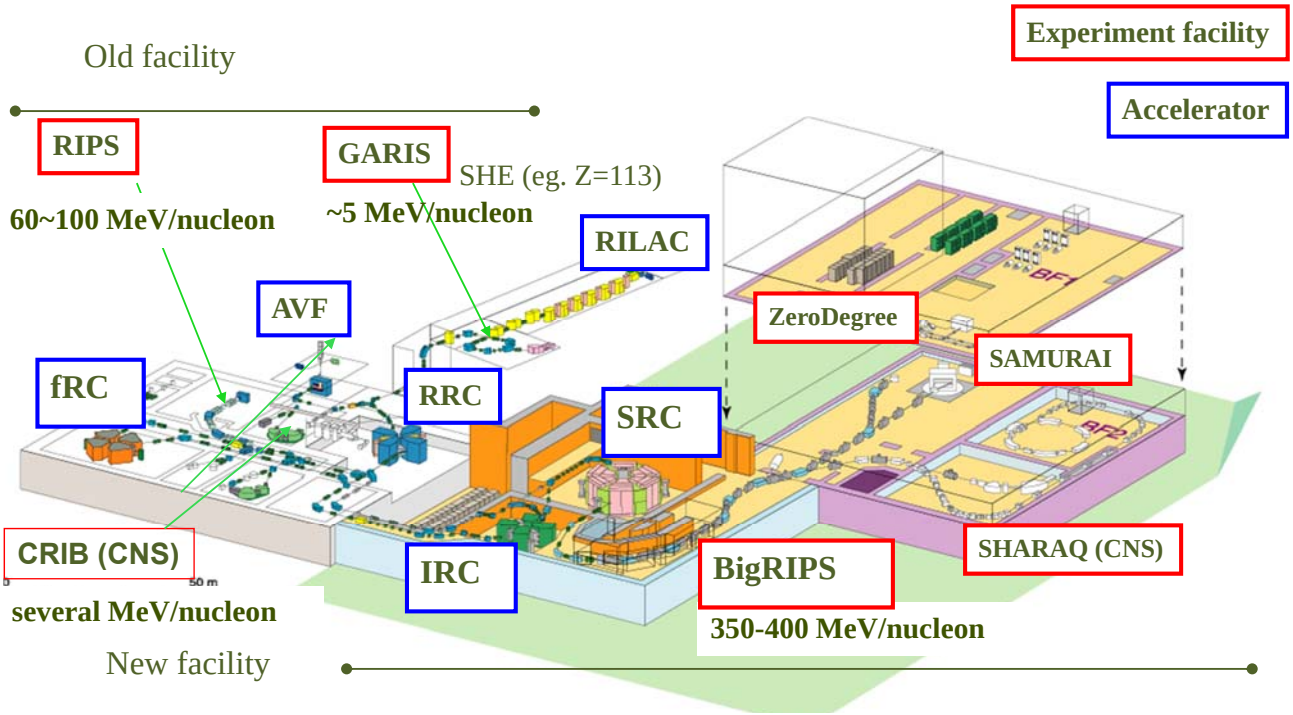

Intense Heavy Ion beams (up to U) up to 345*A*MeV at SRC
Fast RI beams by projectile fragmentation and U-fission at BigRIPS
Operation since 2007

Brad Sherrill ISSSP August 2011, Slide 56

SRC: World Largest (Heaviest) Cyclotron

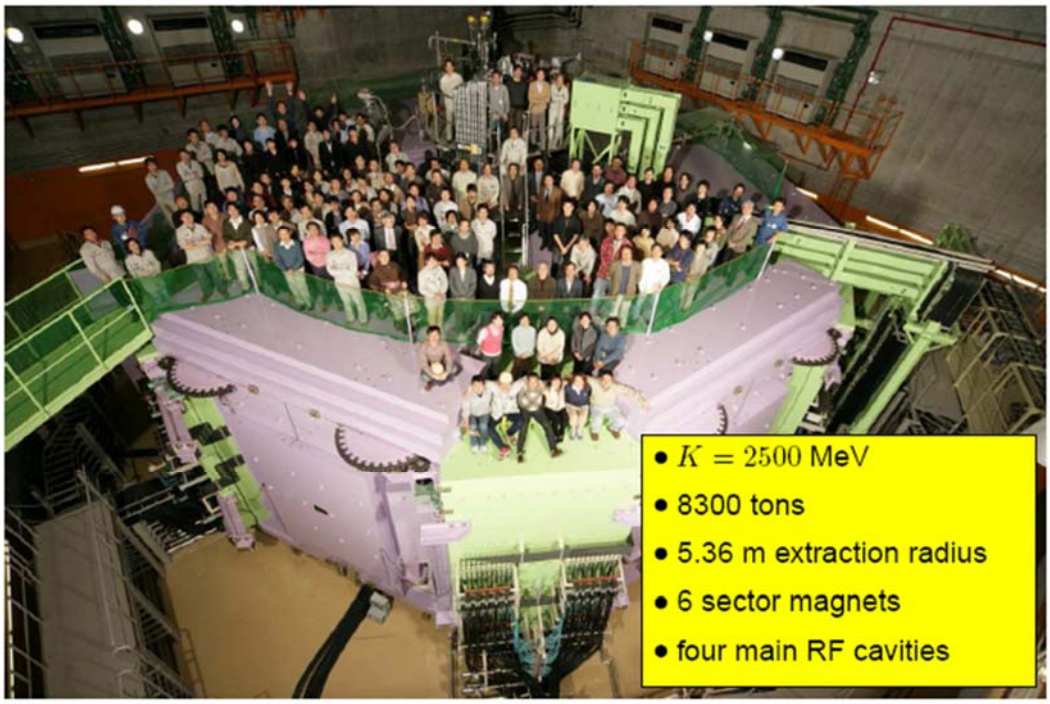

Example of Other In-Target Production Facilities

- SPRIRAL2 – European Project Located at GANIL in France

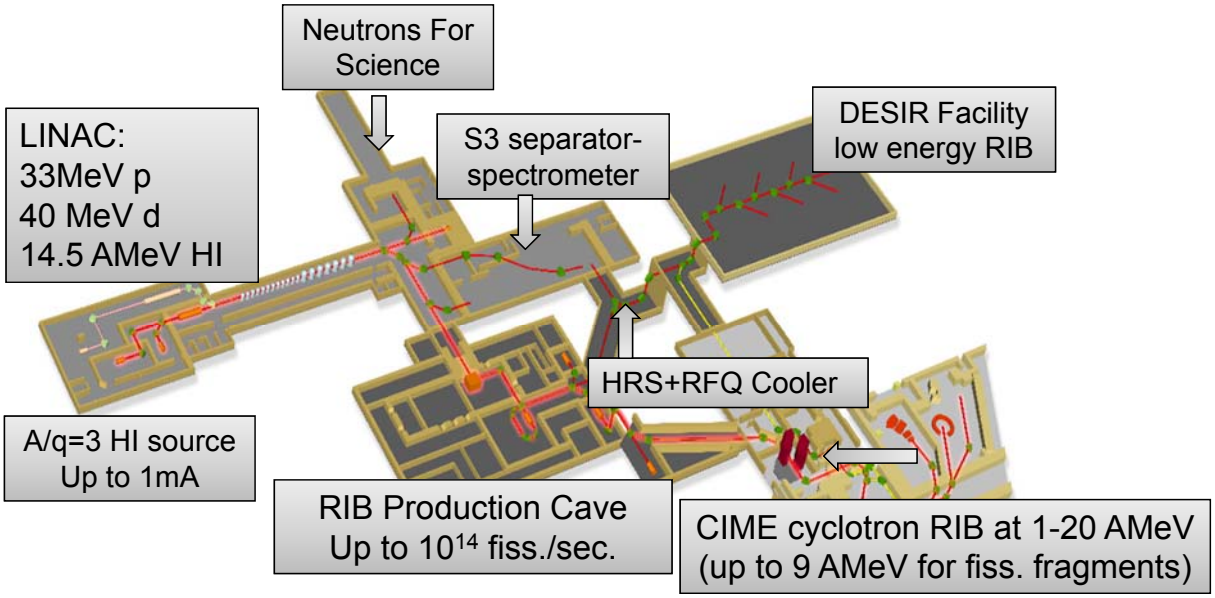

Facility for Antiproton and Ion Research

- Beams at 1.5 GeV/u
- 10^{12}/s Uranium
- Research
  - Compressed matter
  - Rare isotopes
  - Antiproton
  - Plasma
  - Atomic physics
- Completion of the first stages are planned around 2018

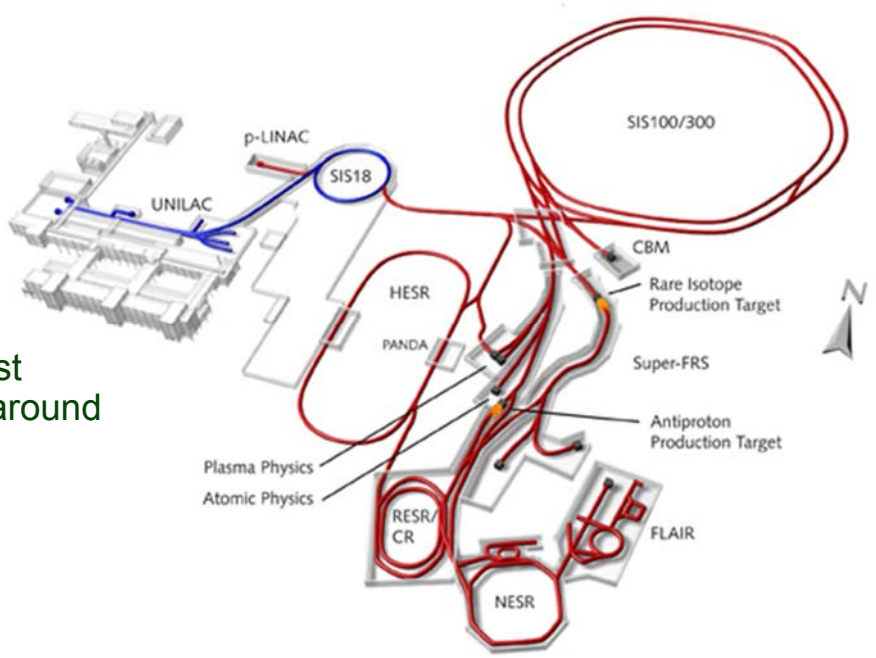

http://www.fair-center.de/index.php?id=1

Heavy Ion Research Facilities in Lanzhou HIRFL

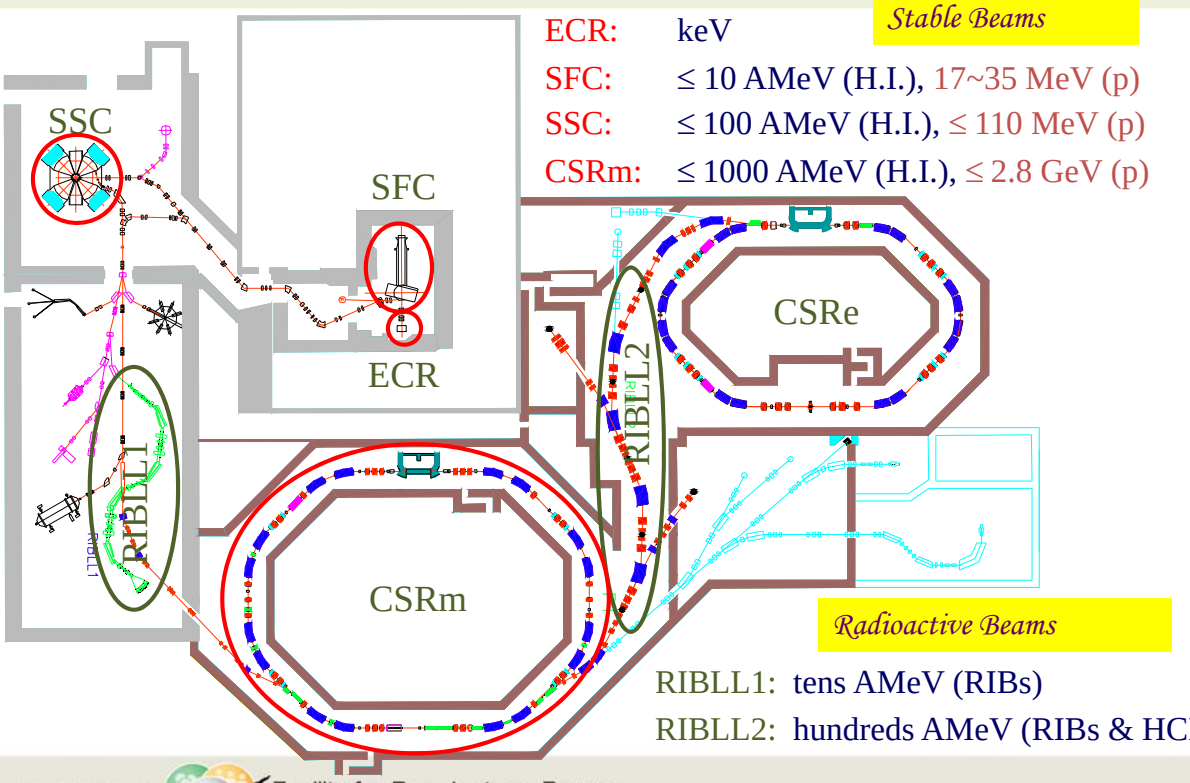

Stable Beams

ECR: keV

SFC: ≤ 10 AMeV (H.I.), 17~35 MeV (p)

SSC: ≤ 100 AMeV (H.I.), ≤ 110 MeV (p)

CSRm: ≤ 1000 AMeV (H.I.), ≤ 2.8 GeV (p)

Radioactive Beams

RIBLL1: tens AMeV (RIBs)

RIBLL2: hundreds AMeV (RIBs & HCI)

BRIF
(Beijing rare ion beam facility)

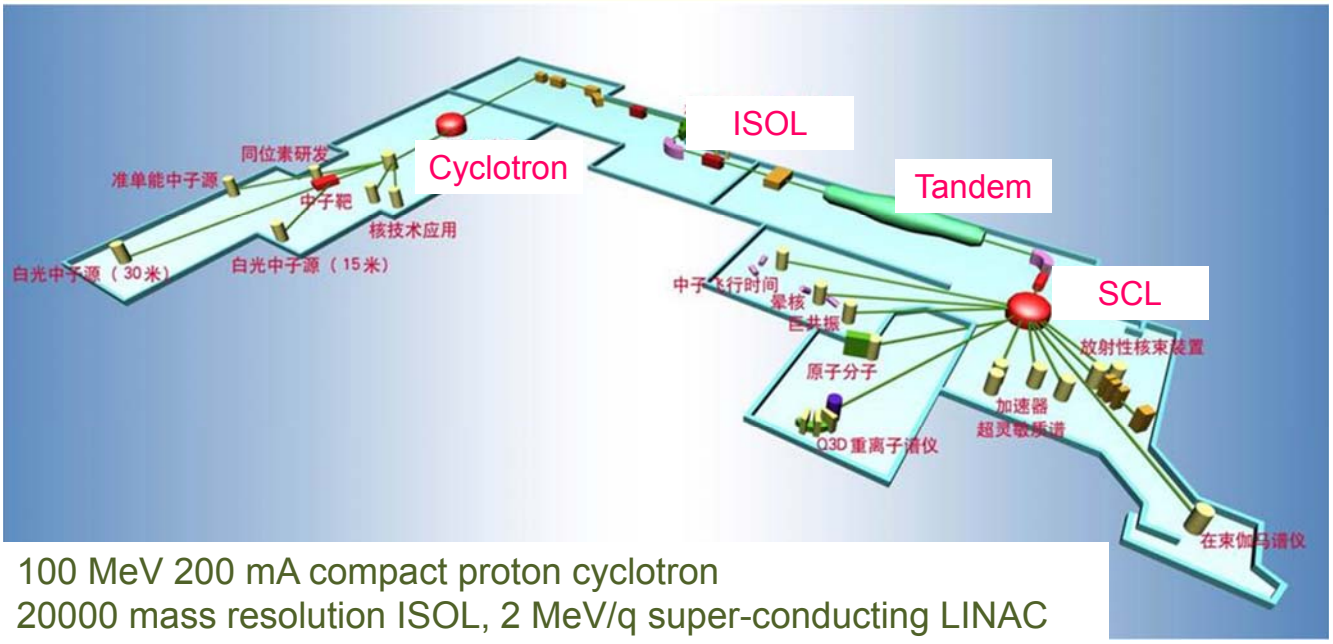

100 MeV 200 mA compact proton cyclotron
20000 mass resolution ISOL, 2 MeV/q super-conducting LINAC
Already funded, but requiring additional supplement
Brief idea in 1990, supported in 2004 Available in 2011-2012

W. Liu

KoRIA Schematic Layout

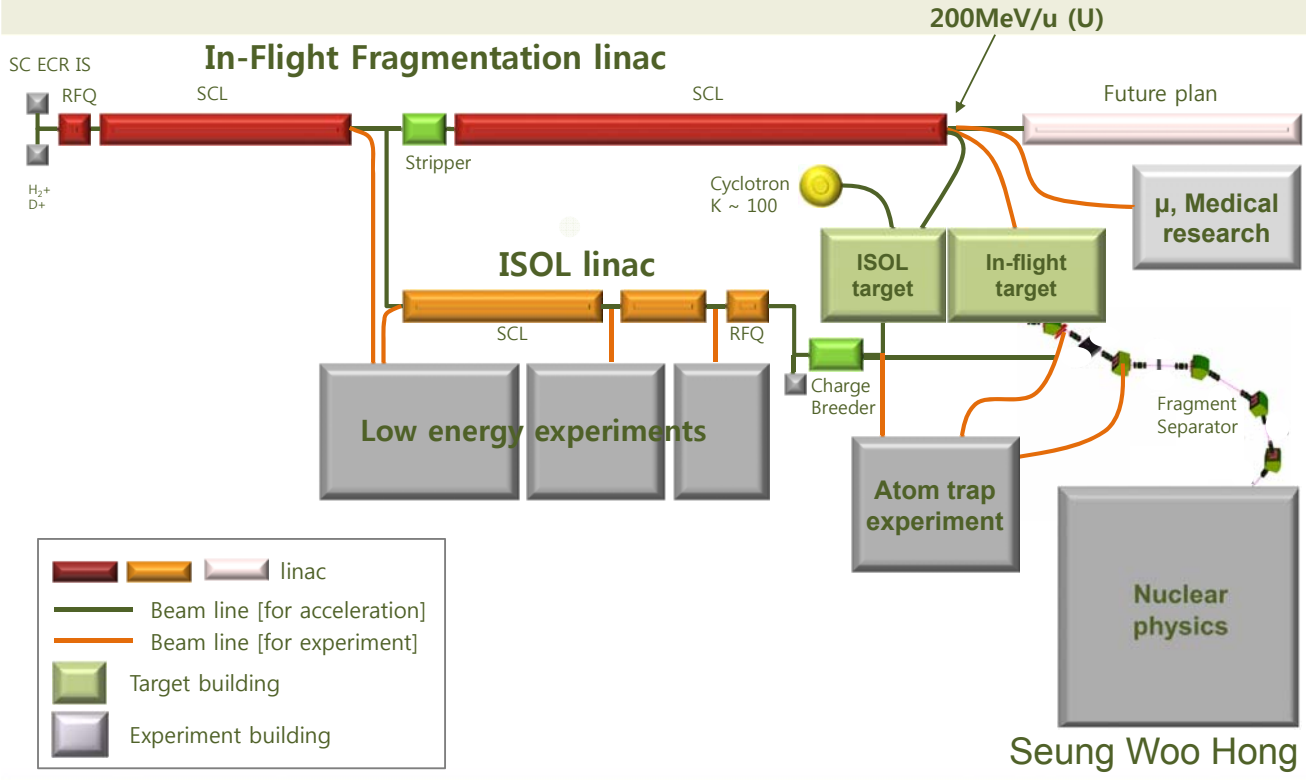

Seung Woo Hong

International Summer School on Subatomic Physics

Neutron halo and tensor forces in nuclei

at Peking University
26-31 August 2011
Lecture by Isao Tanihata
Beihang University, Osaka University

1

2011年8月31日水曜日

Neutron halo and tensor forces in nuclei Lecture I

- **Neutron halo**
  - *What is neutron halo*
  - *Nuclear matter radii and appearance of halo*
  - *Density distribution of neutron halo*
  - *Proton distribution radii of neutron halo nuclei*
  - *A model of neutron halo nuclei and its limit.*
  - *New magic numbers and change of single particle orbital*
  -

Density distribution of a halo nucleus

11Li density

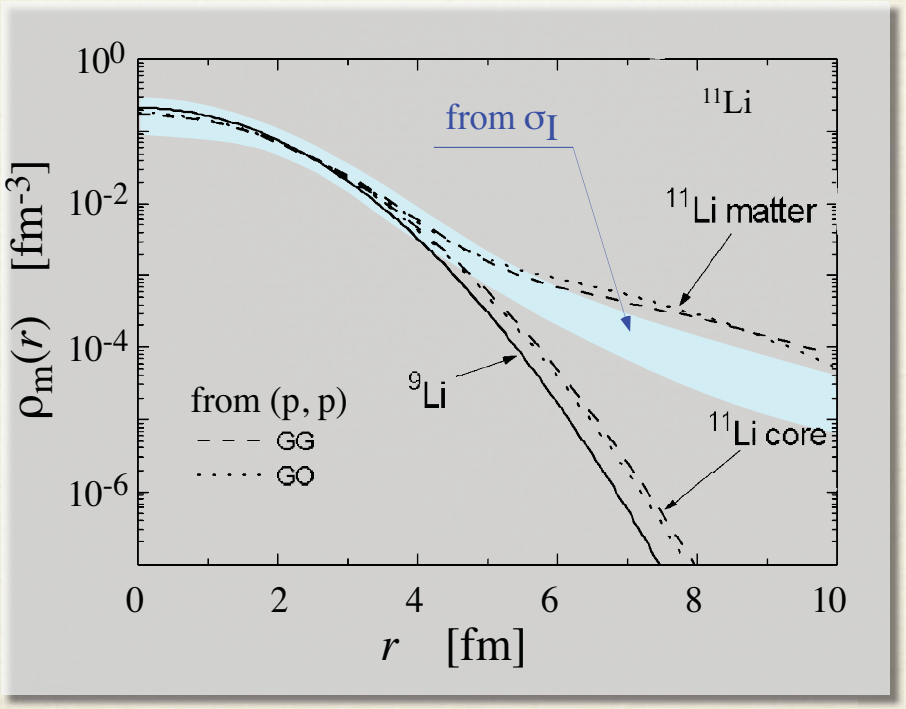

2011年8月31日水曜日

What is a neutron halo?

- A Loosely bound nucleon in a potential
  - *A square well potential*
  - *A density distributions of nucleon in WS potential*

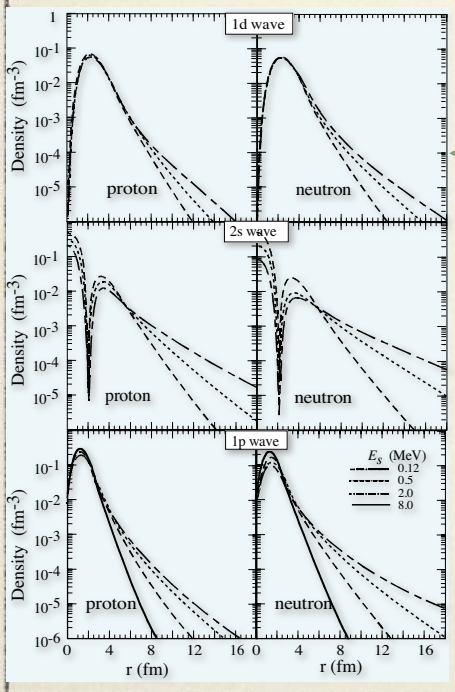

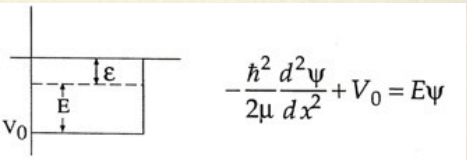

$$-\frac{\hbar^2}{2\mu}\frac{d^2\psi}{dx^2}+V_0=E\psi$$

$$(\hbar\kappa)^2=2\mu(V_0-E)=2\mu\varepsilon$$

$$\psi(r)\propto\frac{e^{-\kappa r}}{r} \qquad F(p)=\frac{c}{(P^2+\kappa^2)}$$

ε -> smaller then ψ(r) -> longer tail
F(p) -> narrower

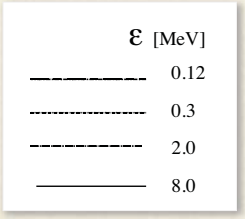

2011年8月31日水曜日

What is a neutron halo (continued)

- *RMS radii of neutron density distribution*

$$rms\ \text{radius} = \left\langle r^2 \right\rangle^{1/2} \equiv \frac{\int r^2 \rho(\mathbf{r}) d\mathbf{r}}{\int \rho(\mathbf{r}) d\mathbf{r}} = \frac{\int r^4 \rho(r) dr}{\int r^2 \rho(r) dr}$$

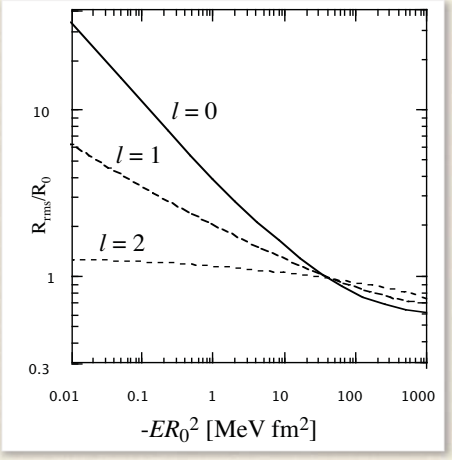

Riisager et al, NP A **548** (1992) 393.

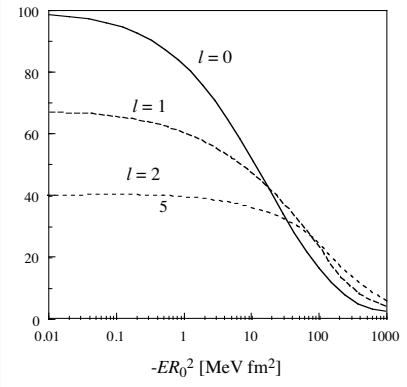

D. V. Fedorov et al., PR C **49** (1994) 201.

Lecture in Peking University Summer School 2011

2011年8月31日水曜日

What is a neutron halo (continued)

- *RMS radii of neutron density distribution*

$$rms\ \text{radius} = \left\langle r^2 \right\rangle^{1/2} \equiv \frac{\int r^2 \rho(\mathbf{r}) d\mathbf{r}}{\int \rho(\mathbf{r}) d\mathbf{r}} = \frac{\int r^4 \rho(r) dr}{\int r^2 \rho(r) dr}$$

Rms radii of two-neutron halo

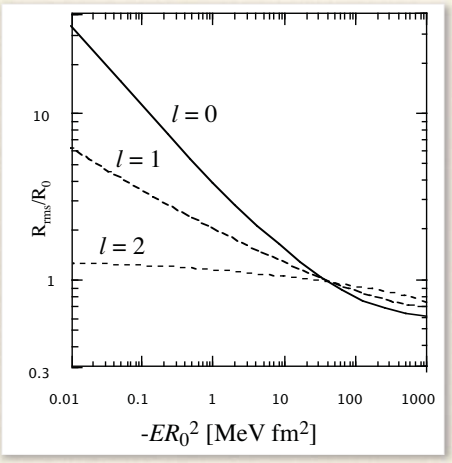

Riisager et al, NP A **548** (1992) 393.

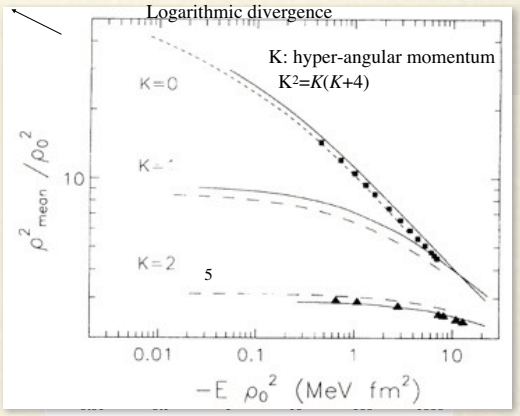

D. V. Fedorov et al., PR C **49** (1994) 201.

Lecture in Peking University Summer School 2011

Nuclear matter radii

- **Matter (nucleon), Neutron, Proton radii**

$\rho_m(r)$: point nucleon density distribution.

mean-square radius: $< r^2 >= \int r^2 \rho(r) d\mathbf{r} / \int \rho(r) d\mathbf{r}$

root-mean-square (rms) radius: $<r^2>^{1/2}$

$$\rho_m(r) = \rho_p(r) + \rho_n(r)$$

$$\int \rho_m(r) d\mathbf{r} = A, \quad \int \rho_p(r) d\mathbf{r} = Z, \quad \int \rho_n(r) d\mathbf{r} = N$$

$$A<r_m^2>=Z<r_p^2> + N <r_n^2>$$

2011年8月31日水曜日

Nuclear Density Distribution

- **Electron elastic scattering**
- **Proton elastic scattering**

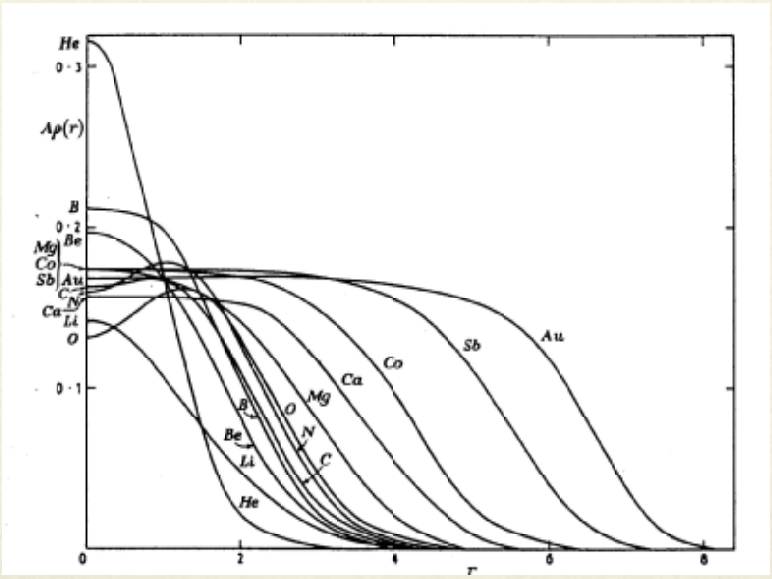

2011年8月31日水曜日

General properties of stable nuclei

- Nucleus is like a liquid drip with diffused surface

Density distribution of stable nuclei

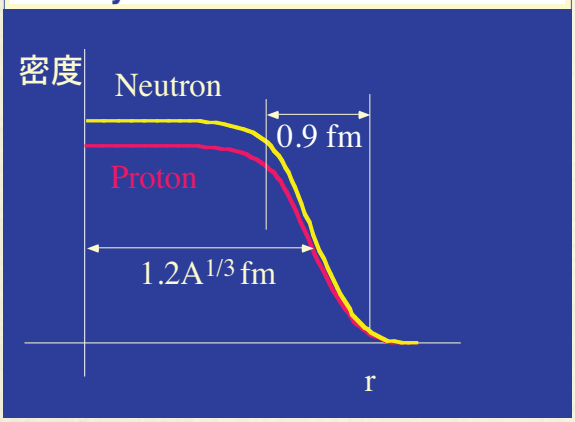

1. $R = r_0 A^{1/3}$
2. Surface diffuseness is constant
3. $\rho_p(r) \propto \rho_n(r)$

- **1. Saturation of nuclear density**
- **2. range of nuclear forces**
- **3. strong p-n attraction**

2011年8月31日水曜日

Atomic Radii

Effective Radius in Metallic Crystal

金属の結晶では金属結合によって原子が結びつけられている．この場合に隣接する原子間の距離はつぎの有効半径の和となっている．

原子	半径	原子	半径	原子	半径	原子	半径
Na	1.91	Al	1.43	Pt	1.39	Zn	1.37
K	2.35	Fe	1.26	Cu	1.28	Hg	1.55
Mg	1.60	Co	1.25	Ag	1.44	Sn	1.58
Ca	1.97	Ni	1.25	Au	1.44	Pb	1.75

Ion Radius

イオン半径（単位 Å）

イオン	半径	イオン	半径	イオン	半径	イオン	半径
Li^+	0.90	Ba^{2+}	1.49	Sn^{4+}	0.83	O^{2-}	1.28
Na^+	1.16	Al^{3+}	0.68	Cu^{2+}	0.87	S^{2-}	1.70
K^+	1.52	$Fe^{2+}l^*$	0.75	Zn^{2+}	0.88	Cl^-	1.67
Mg^{2+}	0.86	$Fe^{3+}l^*$	0.69	Hg^{2+}	1.16	Br^-	1.82
Ca^{2+}	1.14	Ni^{2+}	0.83	Pb^{2+}	1.33	I^-	2.06

l^*：低スピン状態．

R (^{4}He) = 1.4 , R(^{208}Pb) = 7.3 fm

2011年8月31日水曜日

Break of 'general property'

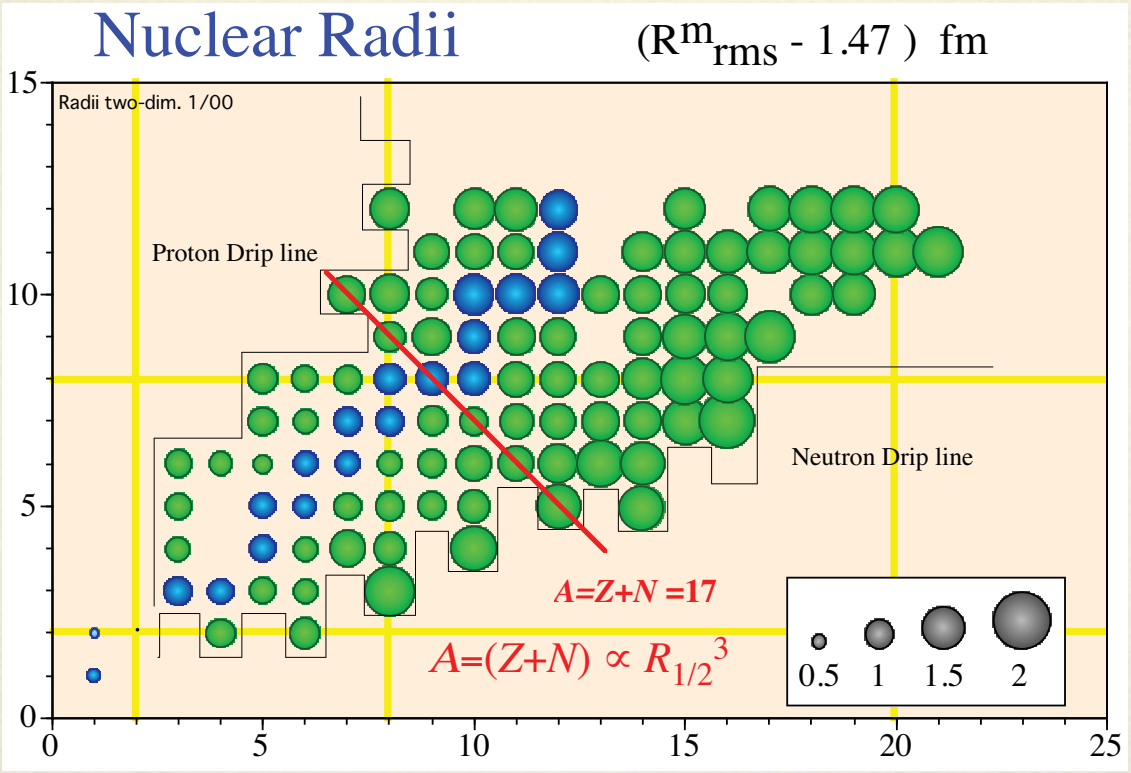

10

2011年8月31日水曜日

Nuclear density distributions

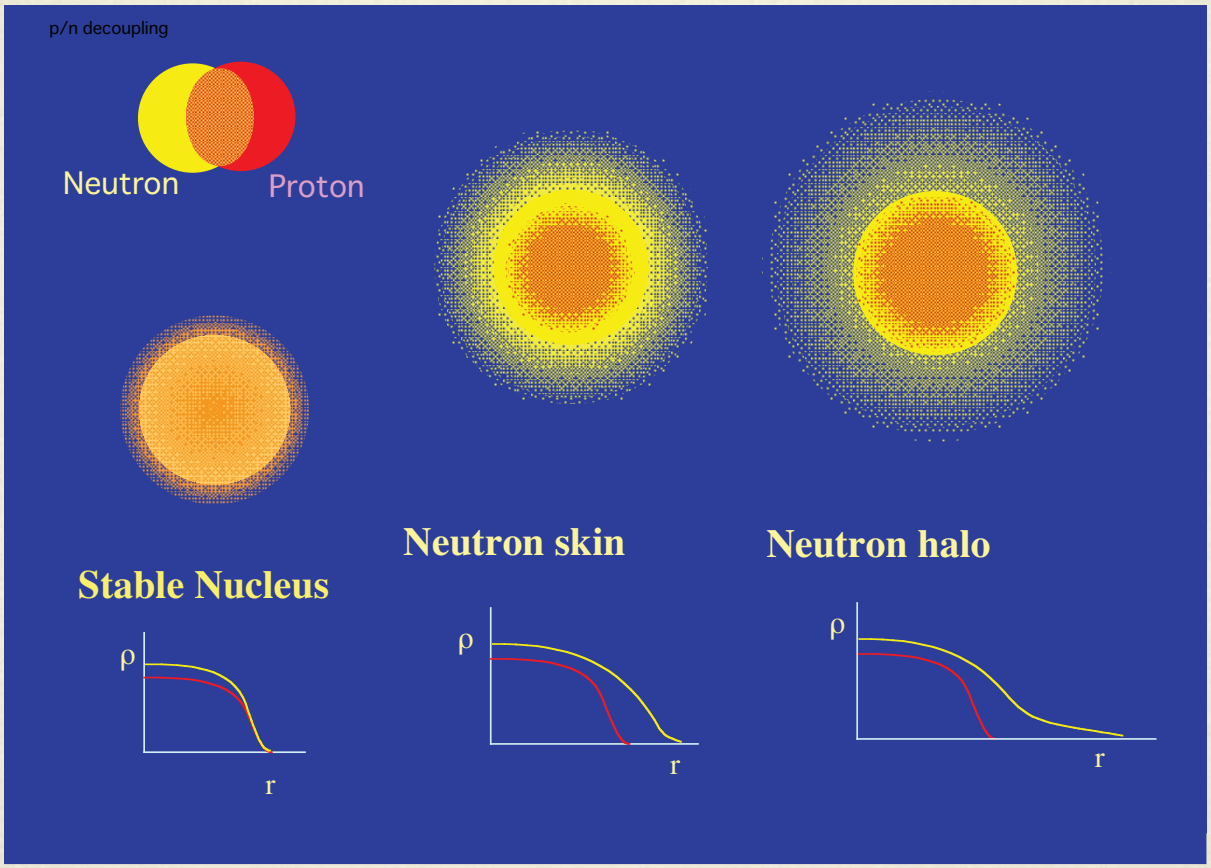

11

Density distribution of a halo nucleus

11Li density

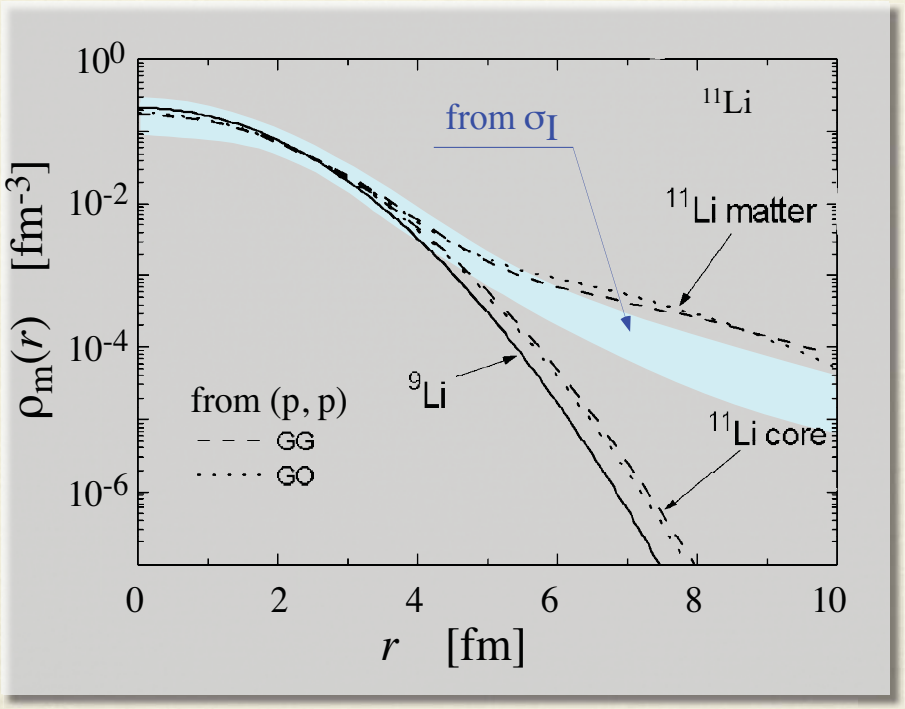

2011年8月31日水曜日

Li、Be isotope radii

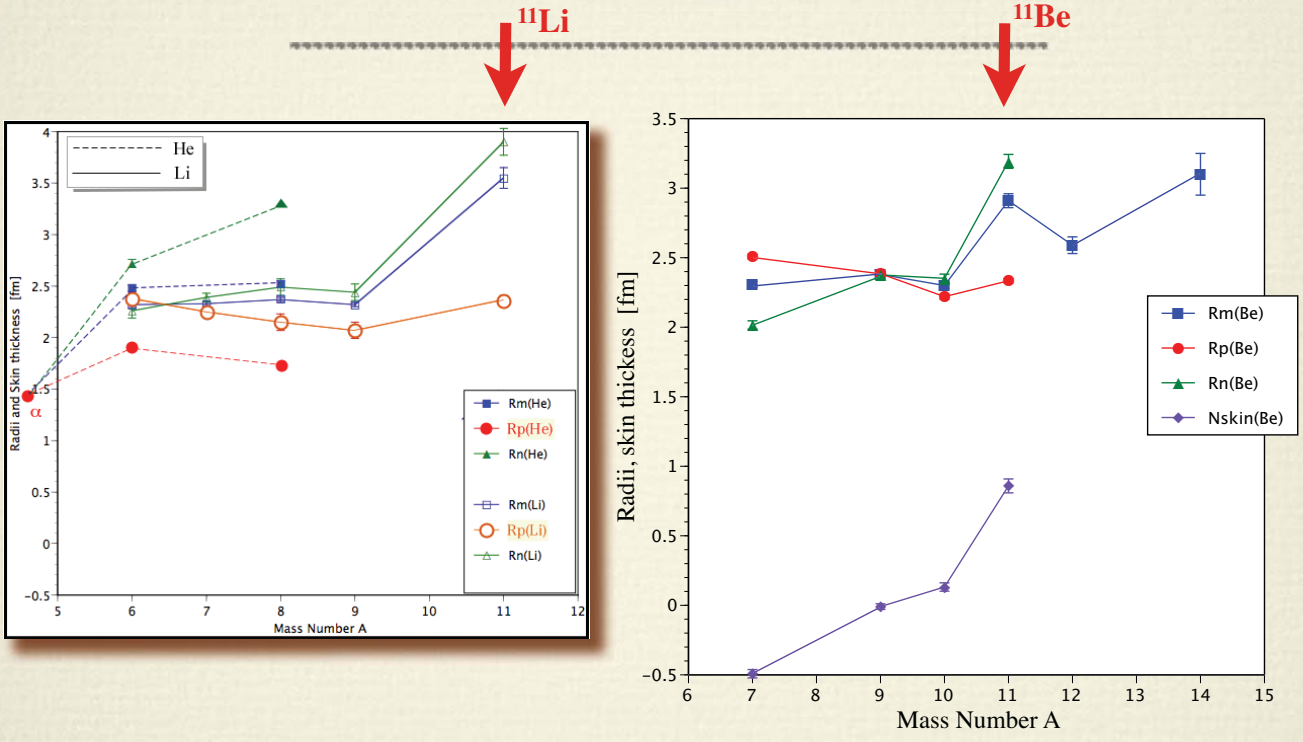

2011年8月31日水曜日

A model of a halo nucleus

(single neutron) ^{11}Be

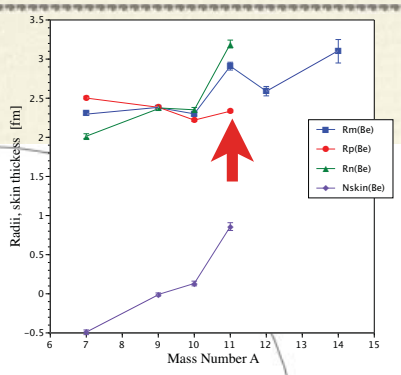

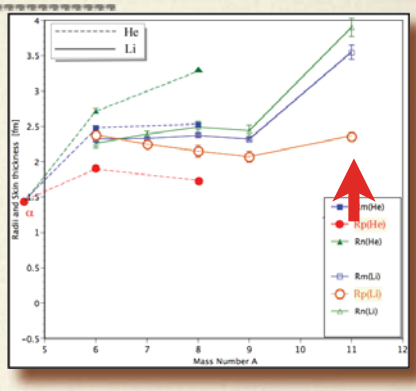

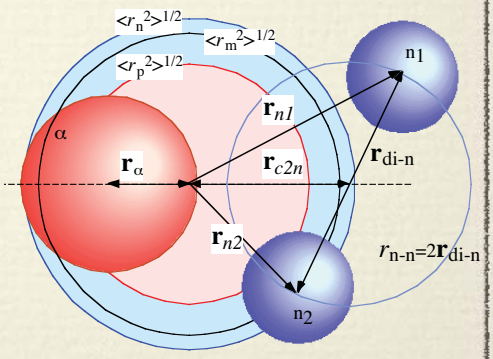

two neutron halo

Specialty of s- and p-waves

=the basic reason of halo formation=

- ***E* = kinetic energy(*K*)**
  - potential energy(*V*)
  (*E*<0 for bound nucleus)

- **Near the limit of binding**
  When *V* ↘
  K has to ↘ to make bound state.
  When *V* is constant,
  K(larger *l*) > *K* (smaller *l*)

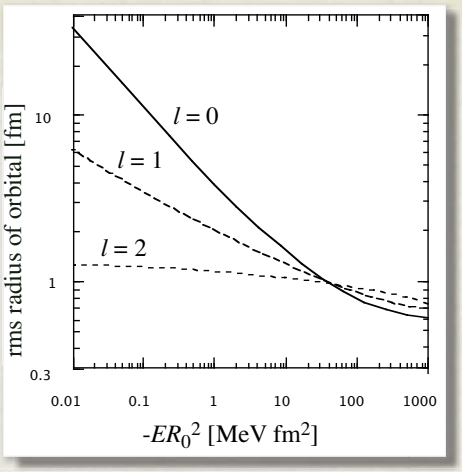

Riisager et al, NP A **548** (1992) 393.

larger *l* smaller *l*

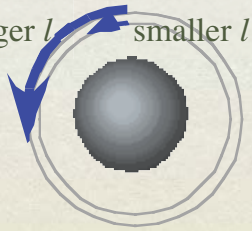

$\Delta x \cdot \Delta p \approx h$

s-wave and p-wave diverges when *E* goes to 0.

Specialty of s- and p-waves
=the basic reason of halo formation=

- E = kinetic energy(K)
  - potential energy(V)

  (E<0 for bound nucleus)
- **Near the limit of binding**

When V is constant,

K(larger l) > K (smaller l)

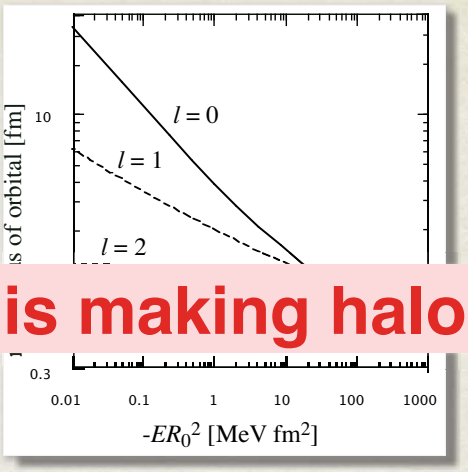

Riisager et al, NP A **548** (1992) 393.

Loosely bound s-wave is making halos!

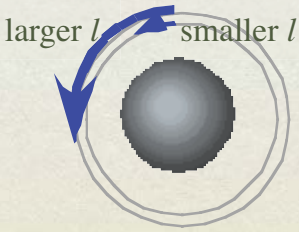

$\Delta x \cdot \Delta p \approx h$

s-wave and p-wave diverges when E goes to 0.

2011年8月31日水曜日

S wave contribution to the interaction cross sections

- **"Normal" Orbitals**

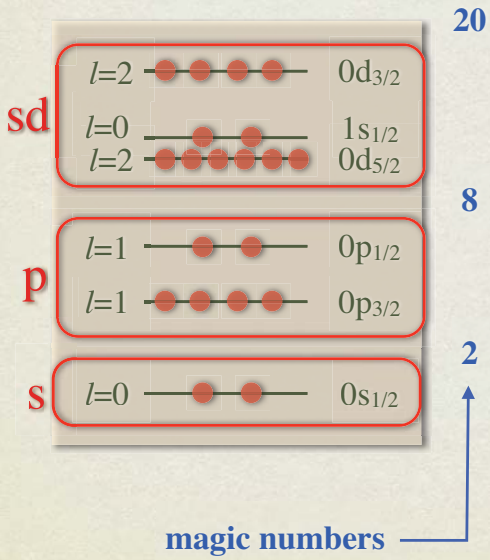

2011年8月31日水曜日

S wave contribution to the interaction cross sections

- "Normal" Orbitals

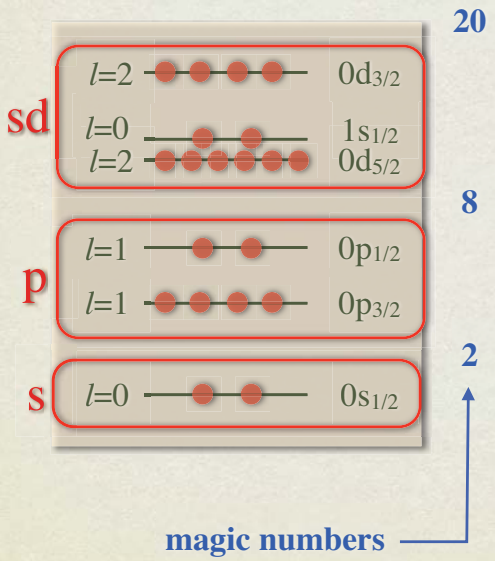

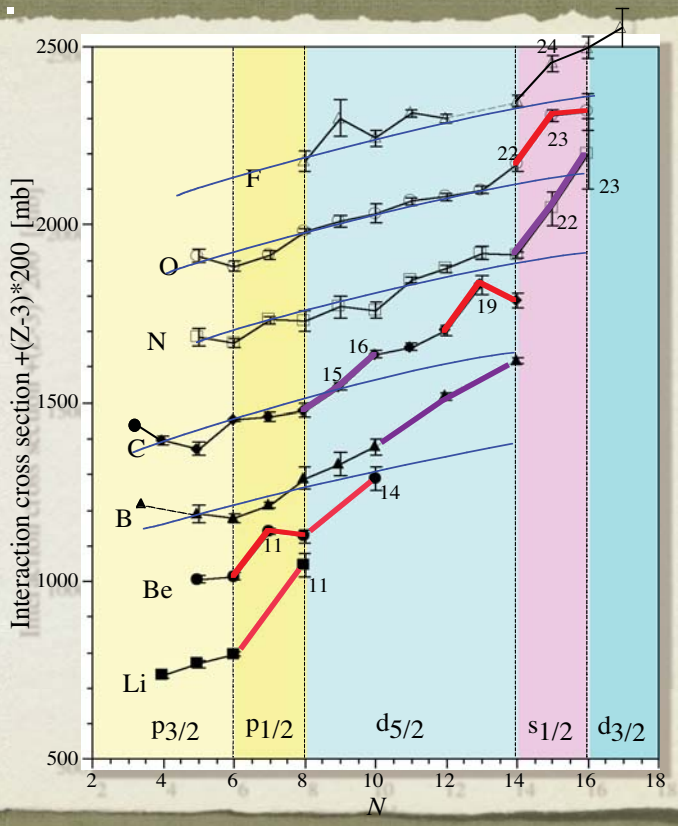

2011年8月31日水曜日

Orbitals in a region around ^{11}Li

- s-wave everywhere at neutron drip line.

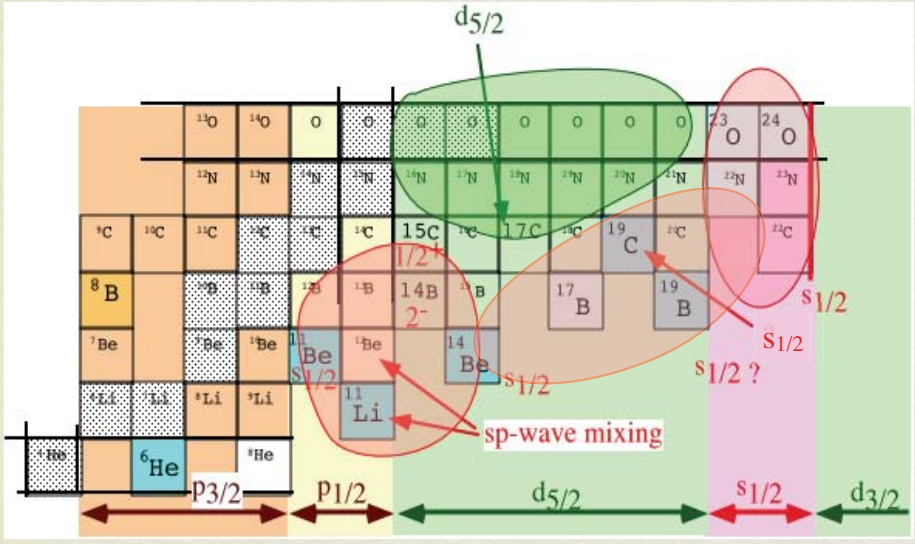

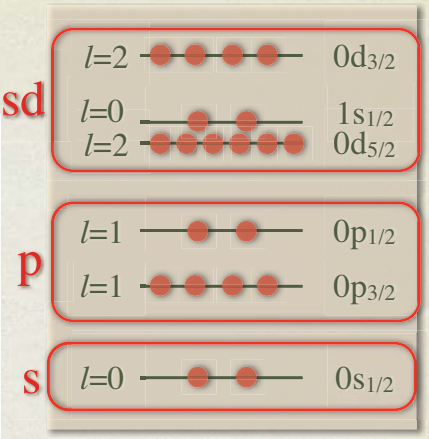

2011年8月31日水曜日

Orbitals in a region around ^{11}Li

- s-wave everywhere at neutron drip line.

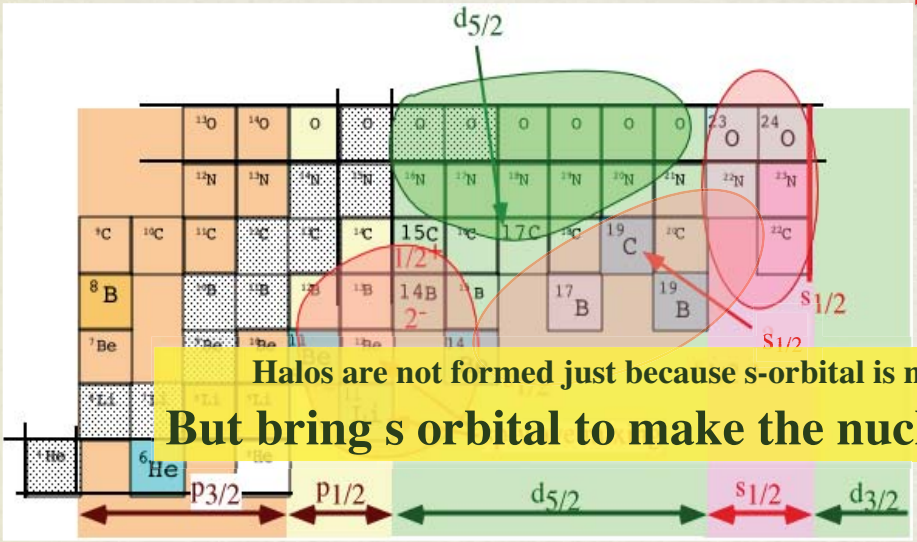

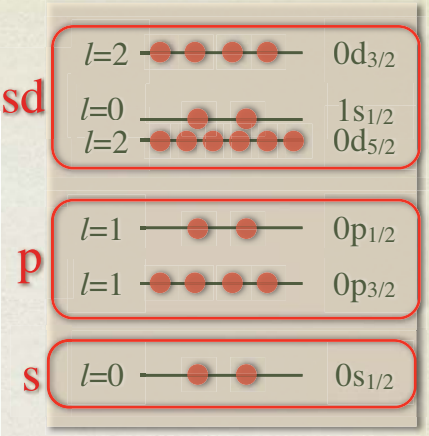

Halos are not formed just because s-orbital is near at the drip line.

But bring s orbital to make the nucleus more bound.

2011年8月31日水曜日

Neutron halo and tensor forces in nuclei
Lecture II

- **Tensor forces in nuclei**
  - *What is tensor forces*
  - *Effects of tensor forces in nuclei (d, α...)*
  - *Behavior of $2s_{1/2}$ orbitals and s-p mixing in ^{11}Li halo*
  - *Two-particle two-hole excitation and high momentum components*
  - *Observation of high-momentum tail originated by tensor forces*

Tensor Forces in Nuclei

- **Nucleon-nucleon interactions contain the central forces and the tensor forces in almost equal weight.**

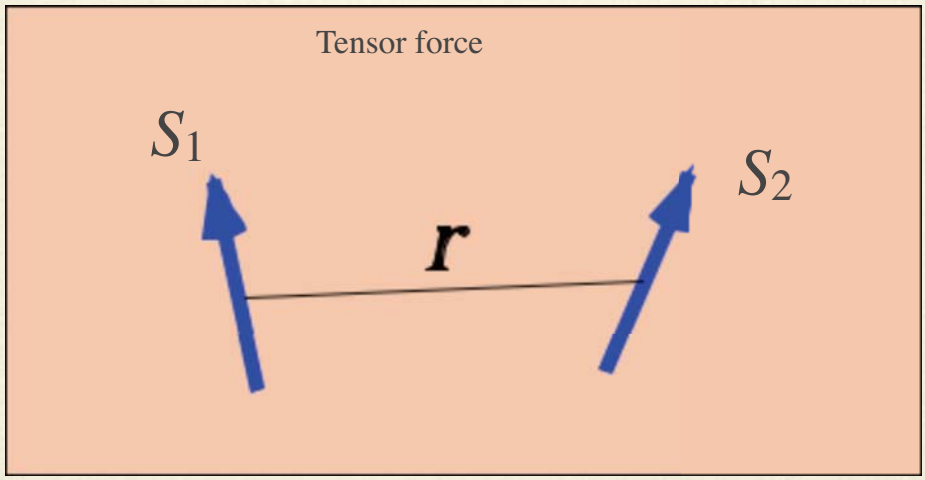

2011年8月31日水曜日

Effects of tensor forces in nuclear structure

- As major part of the binding energy of nuclei.
  - *D-wave mixing in d, α... nucleus*

2011年8月31日水曜日

An importance of tensor forces in a light nuclei

Contributions of various energies to the binding energy of ^{4}He nucleus.

M. Sakai, I. Shimodaya, Y. Akaishi, J. Hiura, and H. Tanaka, Prog. Theor. Phys. 56(1974)32.

Deuteron

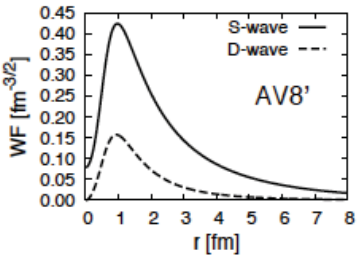

Fig. 6 Deuteron s-wave and d-wave functions obtained using the AV8' nucleon-nucleon potential.

Table 2 Deuteron properties using the AV8' nucleon-nucleon potential.

Energy	−2.24 [MeV]
Kinetic	19.88
(SS)	11.31
(DD)	8.57
Central	−4.46
(SS)	−3.96
(DD)	−0.50
Tensor	−16.64
(SD)	−18.93
(DD)	2.29
LS	−1.02
P(*D*)	5.78 [%]
Radius	1.96 [fm]
(SS)	2.00 [fm]
(DD)	1.22 [fm]

Alpha	H-J
Energy	-20.6 (MeV)
Kin. E	131.1
Pot. E	-151.7
Central forces	
C ^{1}E	-51.3
C ^{3}E	-26.2
C ^{1}O+^{3}O	-0.4
Tensor forces	
T ^{3}E	-69.7
T ^{3}O	-0.5
LS+QLS	-3.6
P(D)%	12.8

Effects of tensor forces in nuclear structure

Effects of tensor forces in nuclear structure

- As major part of the binding energy of nuclei.
  - *D-wave mixing in d, α... nucleus*
  - *Deviation of the magnetic moments of (doubly-closed ±1) nuclei*
    - H. Hyuga, A, Arima, and K. Shimizu (Nucl. Phys. **A 336** (1980) 363.

Effects of tensor forces in nuclear structure

- As major part of the binding energy of nuclei.
  - *D-wave mixing in d, α... nucleus*
  - *Deviation of the magnetic moments of (doubly-closed ±1) nuclei*
    - H. Hyuga, A, Arima, and K. Shimizu (Nucl. Phys. **A 336** (1980) 363.

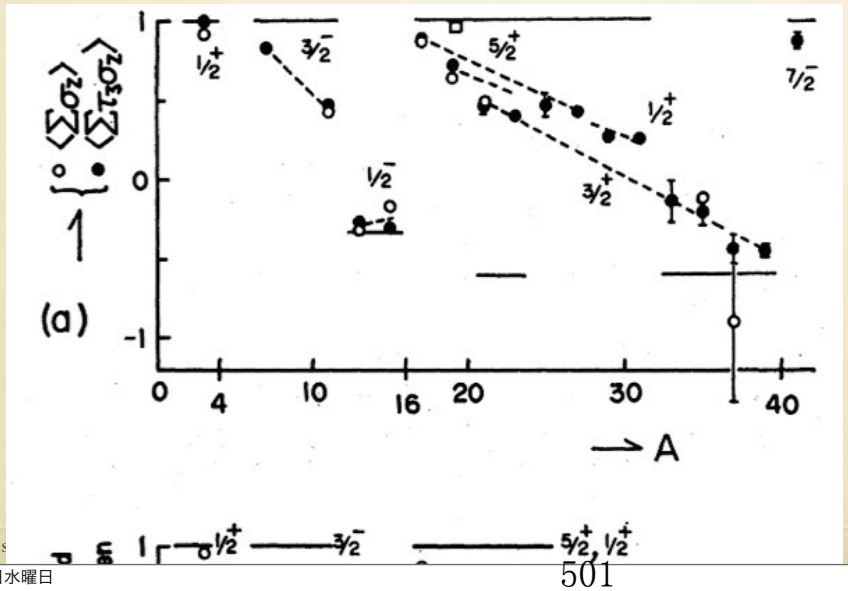

Effects of tensor forces in nuclear structure

- As major part of the binding energy of nuclei.
  - *D-wave mixing in d, α... nucleus*
  - *Deviation of the magnetic moments of (doubly-closed ±1) nuclei*
    - H. Hyuga, A, Arima, and K. Shimizu (Nucl. Phys. **A 336** (1980) 363.

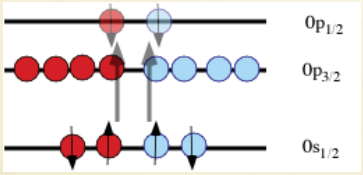

$\Delta L=2$, $\Delta S=2$
p-n pair: yes
n-n, p-p pair: no

Effects of tensor forces in nuclear structure

- As major part of the binding energy of nuclei.
  - *D-wave mixing in d, α... nucleus*
  - *Deviation of the magnetic moments of (doubly-closed ±1) nuclei*
    - H. Hyuga, A, Arima, and K. Shimizu (Nucl. Phys. **A 336** (1980) 363.

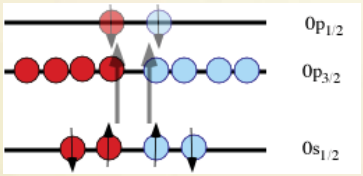

$\Delta L=2$, $\Delta S=2$
p-n pair: yes
n-n, p-p pair: no

- As changes of single particle orbitals (magic numbers)
  - *Changes of magic numbers in nuclei far from the stability line.*

Effects of tensor forces in nuclear structure

- As major part of the binding energy of nuclei.
  - *D-wave mixing in d, α... nucleus*
  - *Deviation of the magnetic moments of (doubly-closed ±1) nuclei*
    - H. Hyuga, A, Arima, and K. Shimizu (Nucl. Phys. **A 336** (1980) 363.

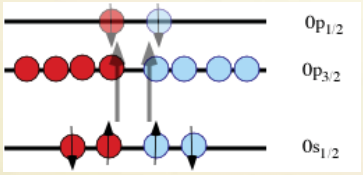

$\Delta L=2$, $\Delta S=2$
p-n pair: yes
n-n, p-p pair: no

- As changes of single particle orbitals (magic numbers)
  - *Changes of magic numbers in nuclei far from the stability line.*

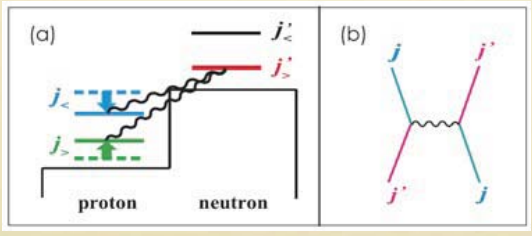

Difference between Shell model treatment and reality

pion exchange: $\propto S_{12}\dfrac{q^2}{m^2+q^2}$

Shell Model Approach

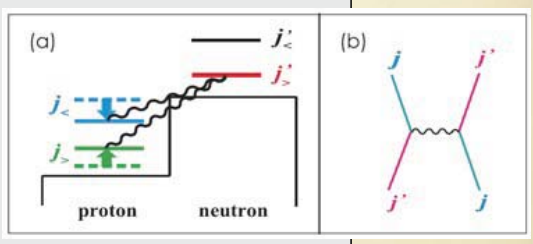

One pion

Model wave function without high momentum

G matrix

Two pions ✓

Model wave function without high momentum

✓ **High Momentum Component**

Difference between Shell model treatment and reality

pion exchange: $\propto S_{12} \frac{q^2}{m^2 + q^2}$

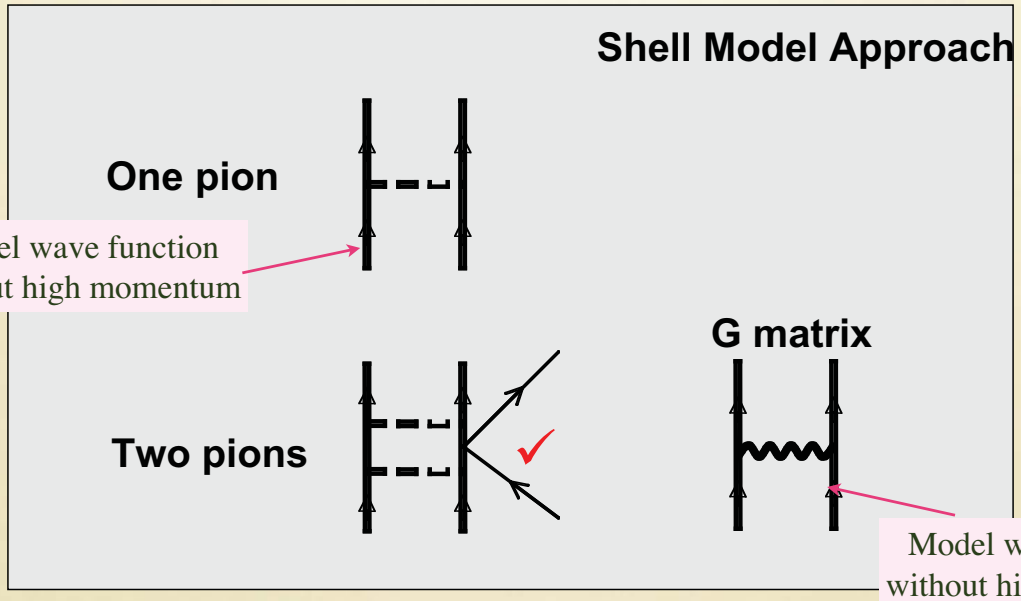

✓ High Momentum Component

2011年8月31日水曜日

Search for Direct evidence of tensor forces

- s-d mixing in ^{11}Li ground state by transfer reaction
- To see the high-momentum components specific to tensor forces

2011年8月31日水曜日

s- and p- waves mixing in ^{11}Li

$$\Psi_{3/2+}(^{11}\mathrm{Li}) = \Psi_{3/2+}(^{9}\mathrm{Li}) + \Psi_{0+}(2n \text{ in } 2s_{1/2}) + \Psi_{0+}(2n \text{ in } 1p_{1/2}) + \ldots$$

$0p_{1/2}$

$1s_{1/2}$

2011年8月31日水曜日

s- and p- waves mixing in ^{11}Li

- **Momentum distribution of fragments ^{10}Li**
  - *Equal amount of $p_{1/2}$ and $s_{1/2}$. (Simon 1999)*
- **Beta-decay**
  - *30-40% $s_{1/2}$ wave and small amount of $p_{1/2}$ (Borge 1997)*
- **two-neutron transfer reaction**
  - *(^{11}Li+p --> ^{9}Li+t)*
  - *31-45% $s_{1/2}$ and $p_{1/2}$*
  - *(2008)*

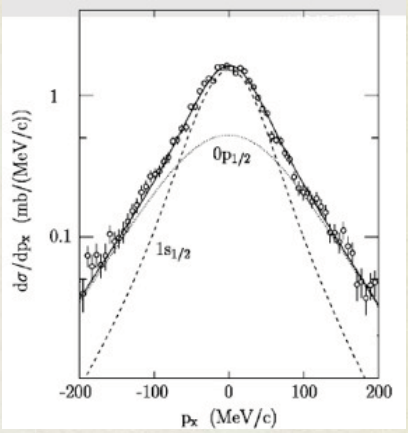

41% s

35% s

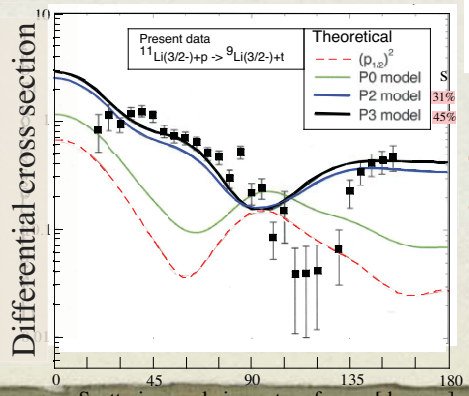

I. Tanihata et al., Phys. Rev. Lett 100 (2008) 192502..

PKU summer school on subatomic physics 2022 25

2011年8月31日水曜日

How s-, p- are mixed?

Consider from the view of single particle orbitals

- 1. Weak binding
- 2. Deformation
- 3. Tensor interactions I
- 4. Tensor interactions II

Mixing of ground and sky

2011年8月31日水曜日

How s-, p- are mixed?

Why magic numbers changes?

Consider from the view of single particle orbitals

- 1. Weak binding
- 2. Deformation
- 3. Tensor interactions I
- 4. Tensor interactions II

Mixing of ground and sky

PKU summer school on subatomic physics 2022 26

Changes of Magic Numbers

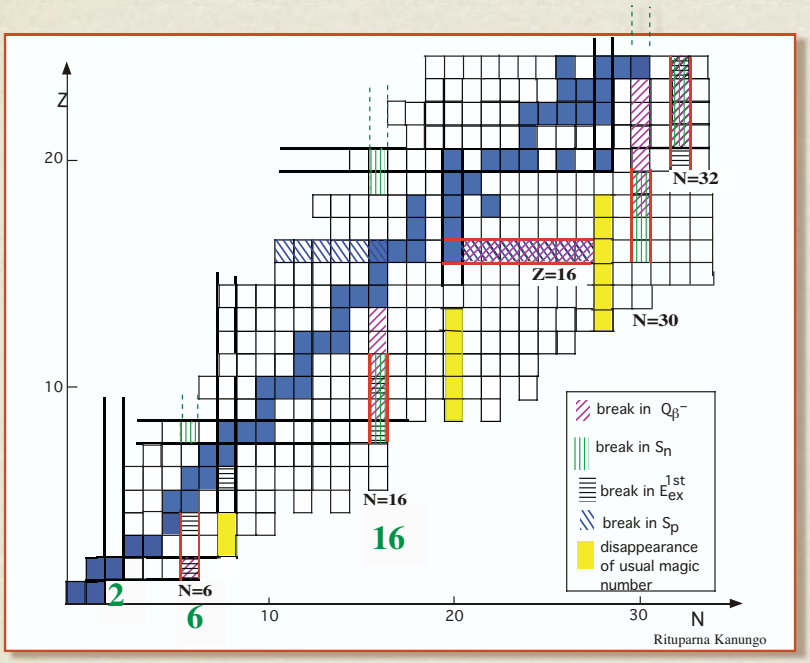

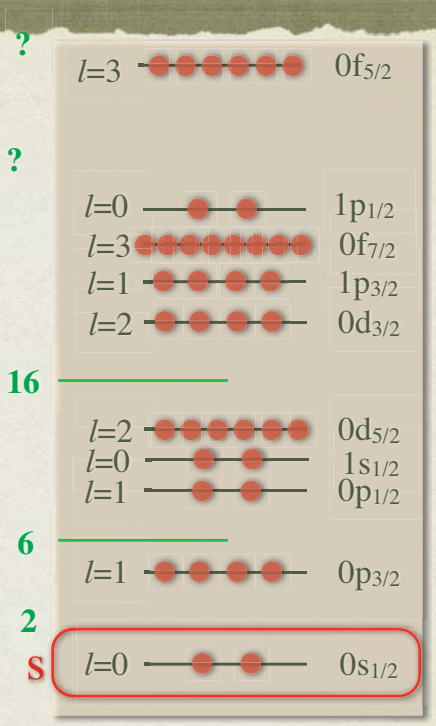

2011年8月31日水曜日

1. Effect of weak binding

- **Binding of low angular momentum orbitals become relatively stronger for loosely bound nuclei..**

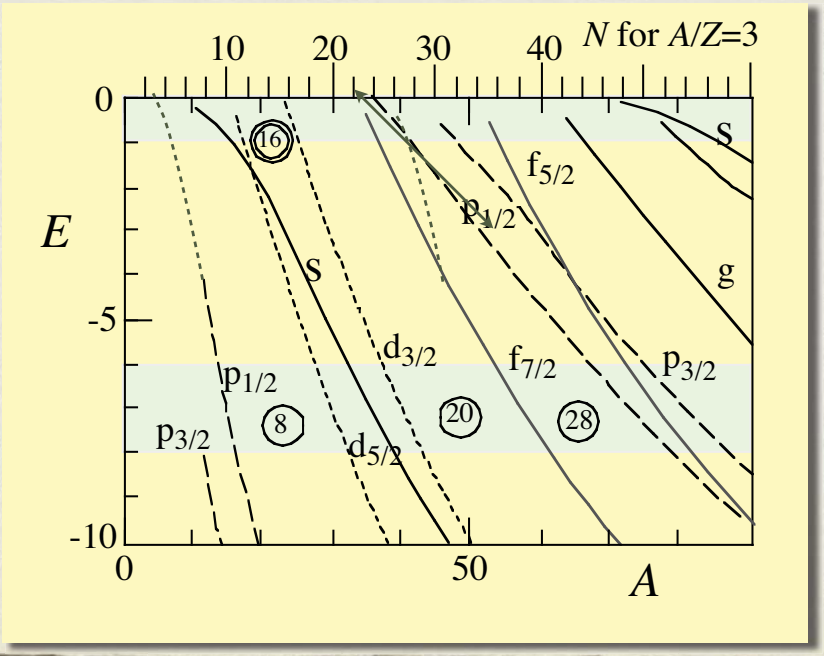

2011年8月31日水曜日

1. Effect of weak binding

- Binding of low angular momentum orbitals become relatively stronger for loosely bound nuclei..

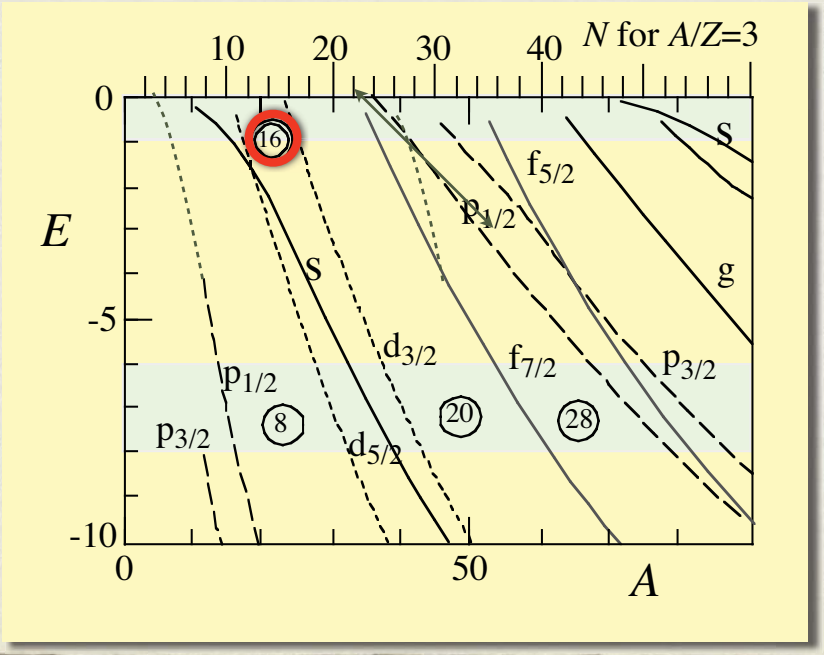

2011年8月31日水曜日

1. Effect of weak binding

- Binding of low angular momentum orbitals become relatively stronger for loosely bound nuclei..

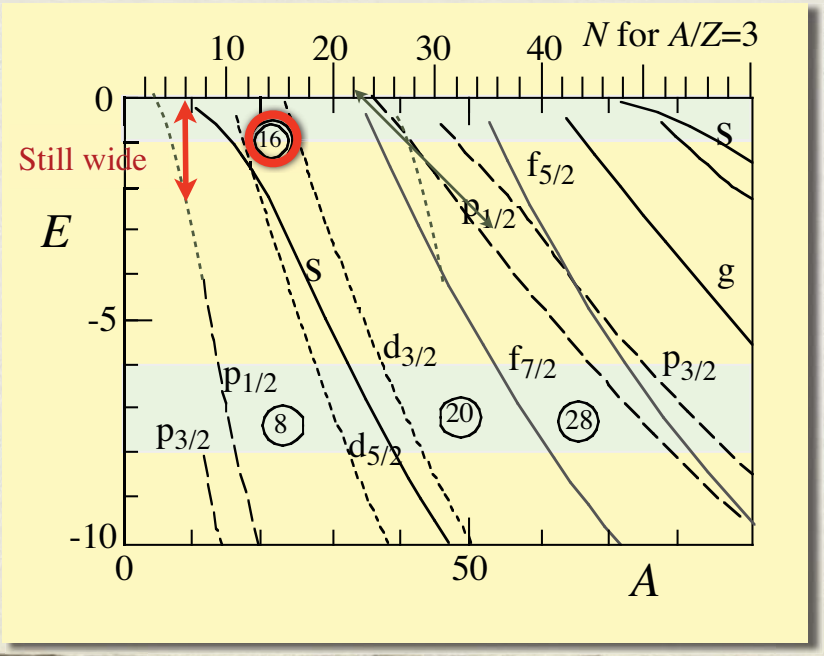

PKU summer school on subatomic physics 2022
28

2011年8月31日水曜日

2. Deformation (important in ^{11}Be)

- Nilsson diagram (Deformation does not change s-wave very much)

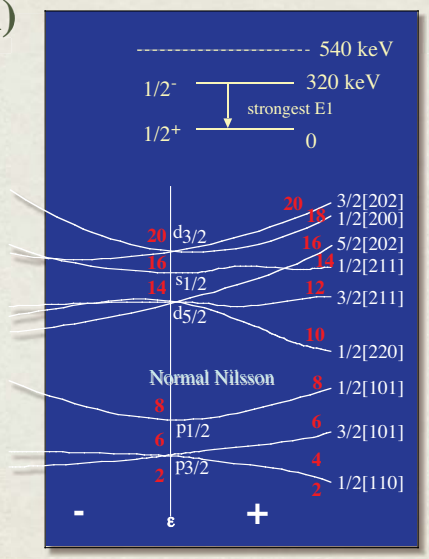

But if combined with weak binding

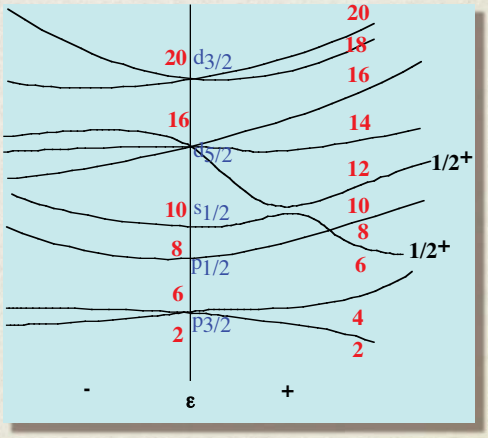

2011年8月31日水曜日

2. Deformation (important in ^{11}Be)

- Nilsson diagram (Deformation does not change s-wave very much)

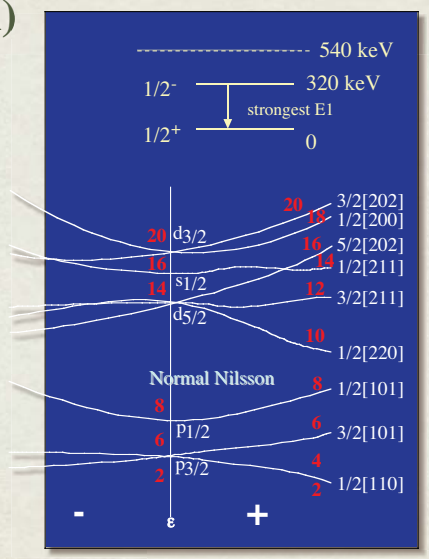

But if combined with weak binding

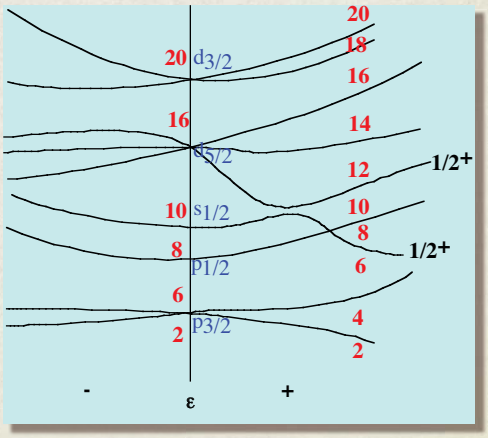

Probably not important for ^{11}Li

PKU summer school on subatomic physics 2022 29

2011年8月31日水曜日

3. Tensor Interactions I

Otsuka et al.

- Important for *N*=16 and 20 magic numbers

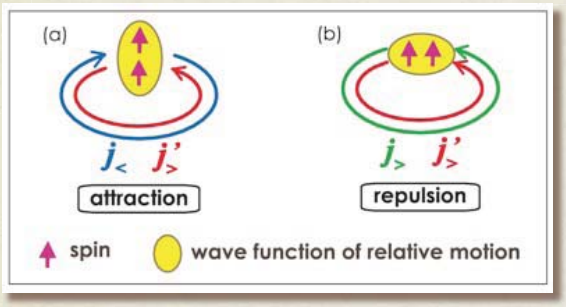

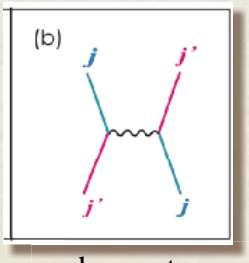

exchange term

2011年8月31日水曜日

3. Tensor Interactions I

Otsuka et al.

- Important for *N*=16 and 20 magic numbers

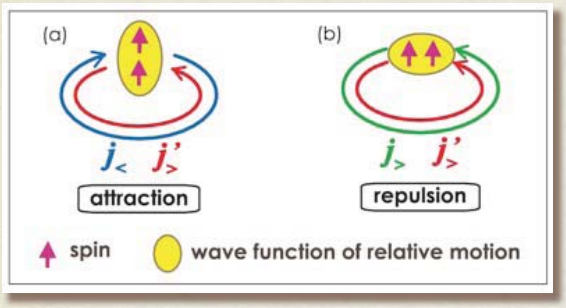

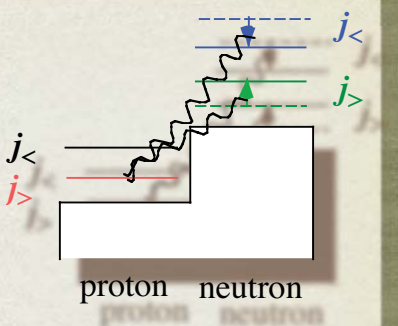

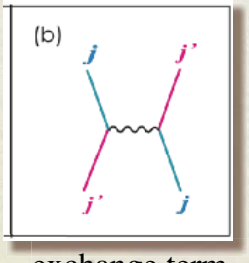

exchange term

2011年8月31日水曜日

3. Tensor Interactions I

Otsuka et al.

- Important for *N*=16 and 20 magic numbers

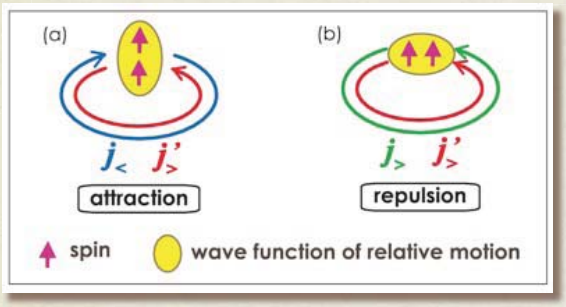

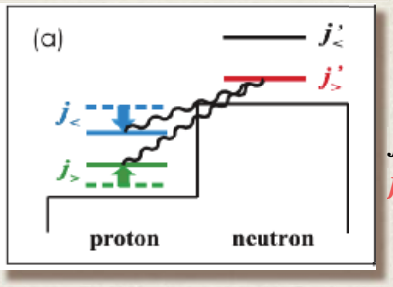

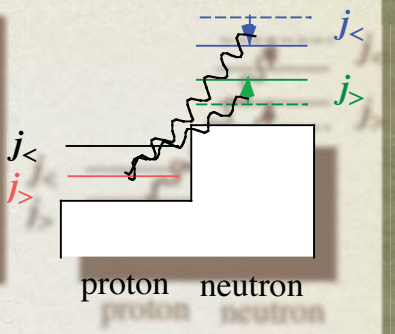

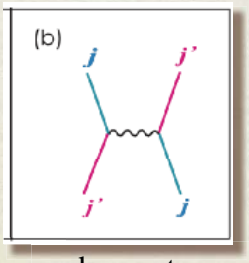

exchange term

2011年8月31日水曜日

3. Tensor Interactions I

Otsuka et al.

- Important for *N*=16 and 20 magic numbers

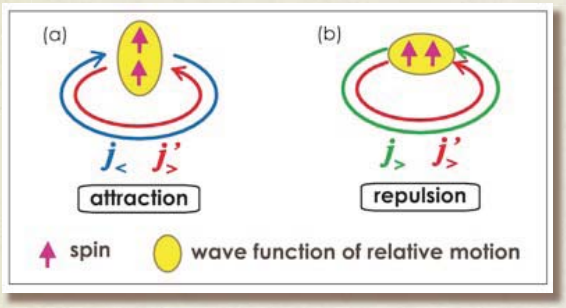

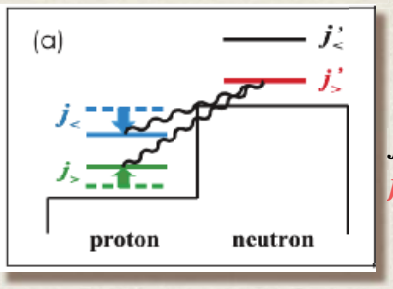

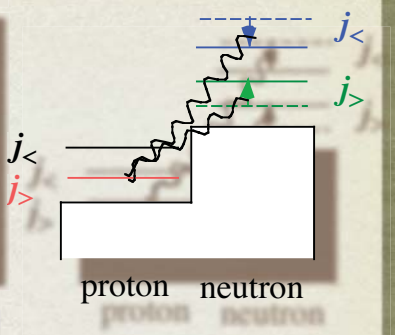

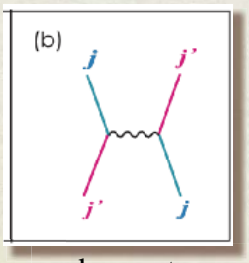

exchange term

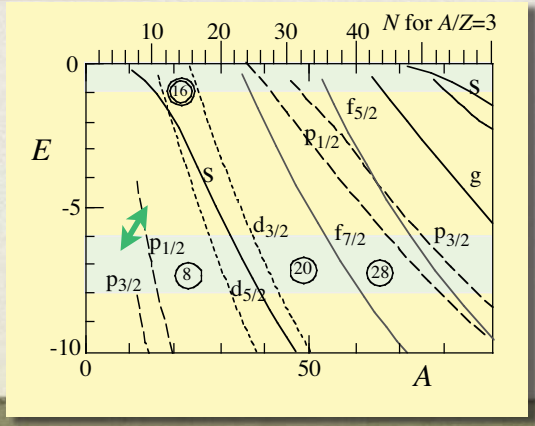

PKU summer school on subatomic physics 2022 30

2011年8月31日水曜日

3. Tensor Interactions I

Otsuka et al.

- Important for *N*=16 and 20 magic numbers

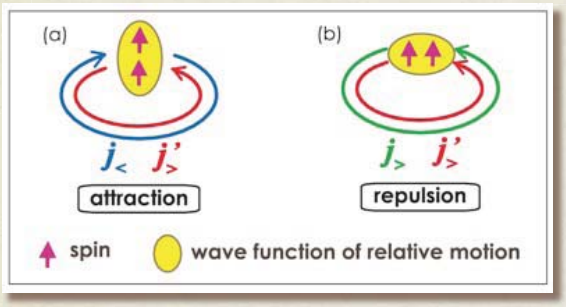

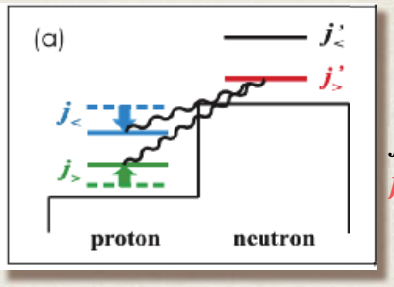

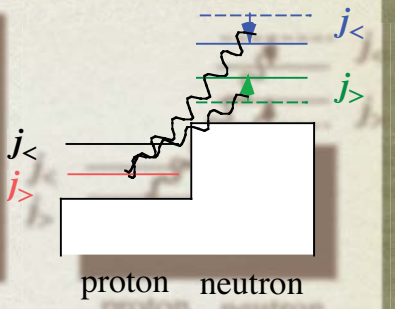

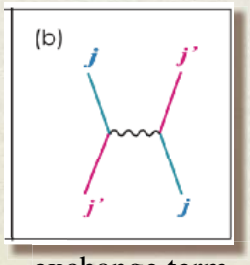

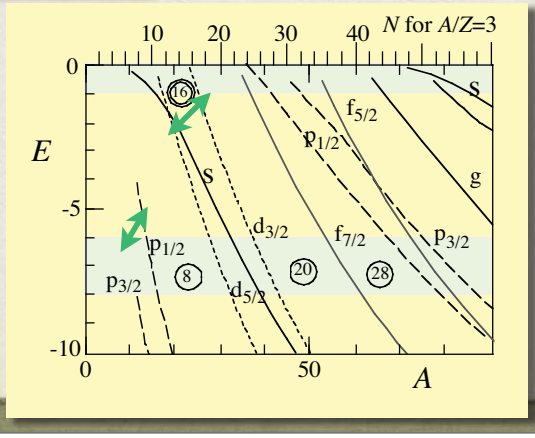

2011年8月31日水曜日

3. Tensor Interactions I

Otsuka et al.

- Important for *N*=16 and 20 magic numbers

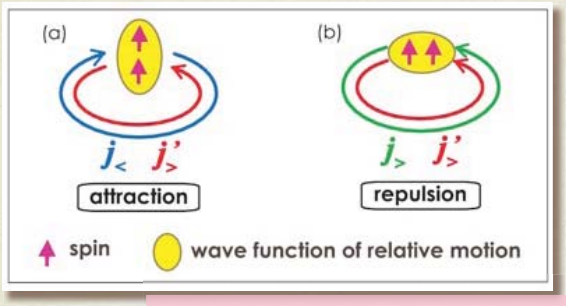

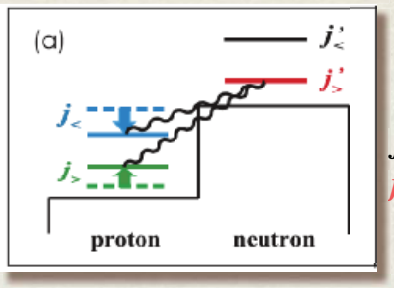

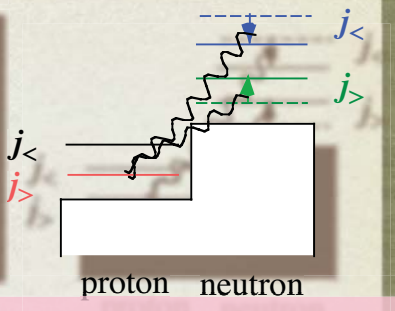

Still s-wave does not get close to p-wave!

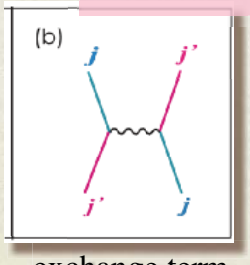

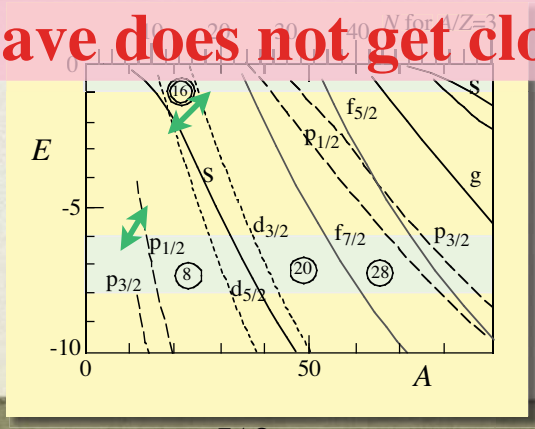

PKU summer school on subatomic physics 2022
30

2011年8月31日水曜日

4. Tensor Interactions II

- 2p-2h excitation in ^{11}Li
  - *Excitation by the tensor force is blocked if neutrons are in $p_{1/2}$ orbital.*
  - *^{11}Li can gain energy by opening the $0p_{1/2}$ orbital and putting neutrons in s orbital.*

Two pions 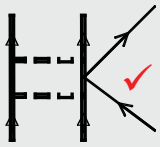

✓High-momentum component

2011年8月31日水曜日

4. Tensor Interactions II

- 2p-2h excit… in ^{11}Li
  - *Excitation …*
  - *^{11}Li can gai… …ital.*

Two pions 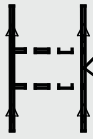

✓High-momentum co…

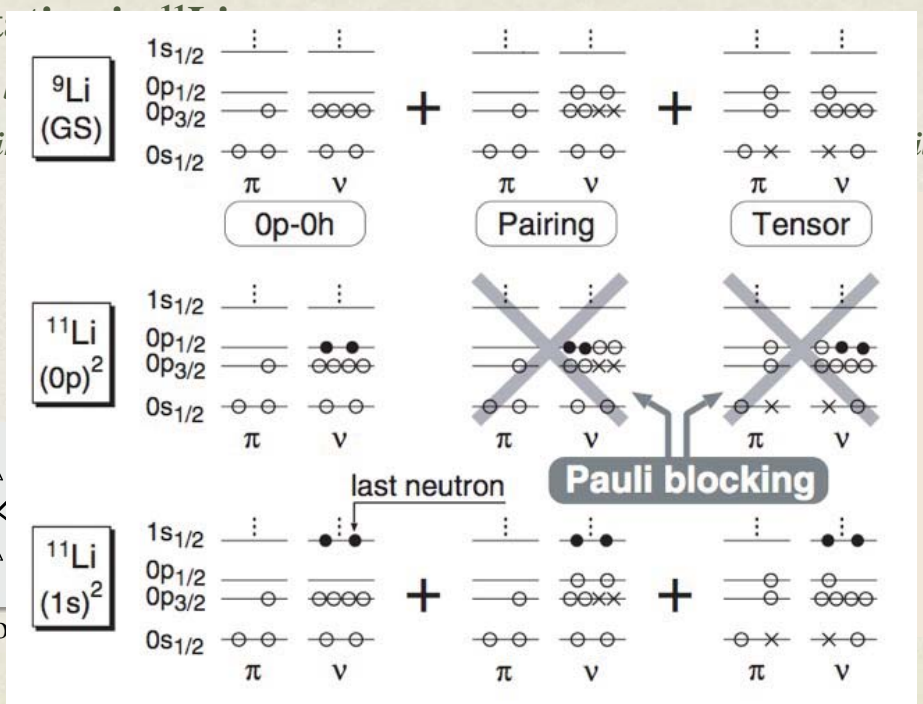

T. Myo, K. Kato, H. Toki, K. Ikeda, Phys. Rev. 76 (2007) 024305.

PKU summer school on subatomic physics 2022 31

2011年8月31日水曜日

How s-, p- are mixed?

All of them seems important for the change of orbitals

- **1. Weak binding**
- **2. Deformation**
- **3. Tensor interactions I**
- **4. Tensor interactions II**

2011年8月31日水曜日

How s-, p- are mixed?

All of them seems important for the change of orbitals

- **1. Weak binding**
- **2. Deformation**
- **3. Tensor interactions I**
- **4. Tensor interactions II**

But 1. and 4. seems like most important for s-p mixing in ^{11}Li

PKU summer school on subatomic physics 2022 Mixing of ground and sky 32

2011年8月31日水曜日

Wave functions

Wave functions

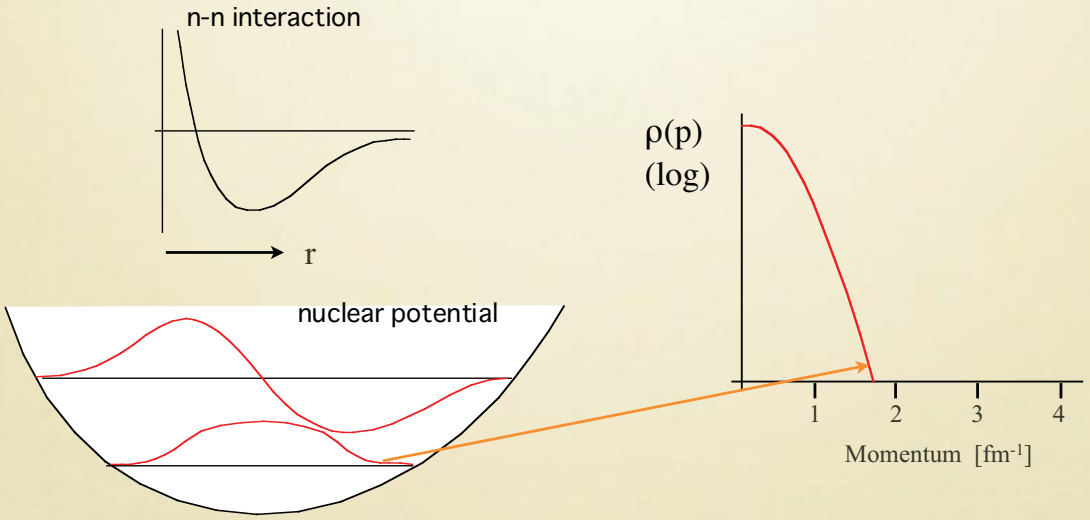

2011年8月31日水曜日

Wave functions

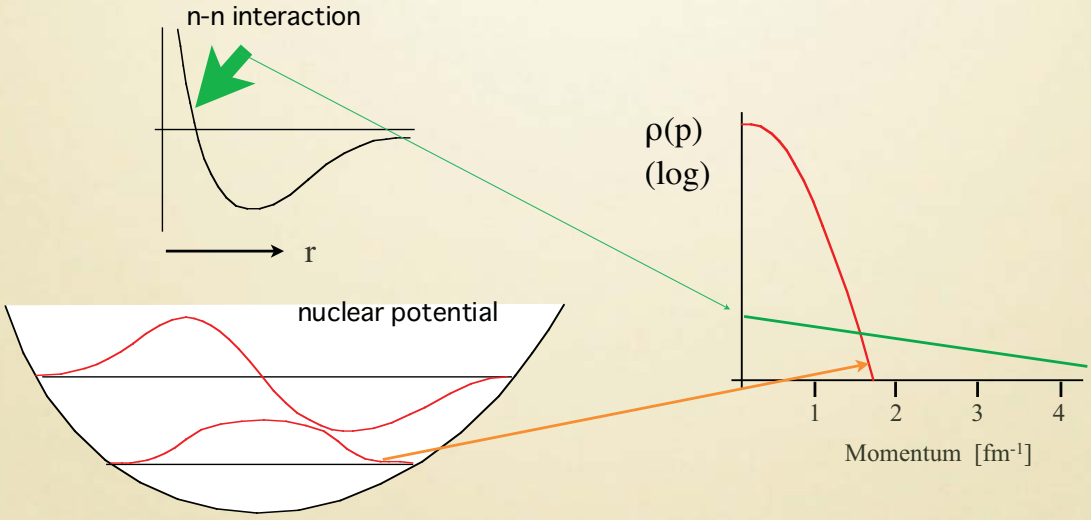

2011年8月31日水曜日

Wave functions

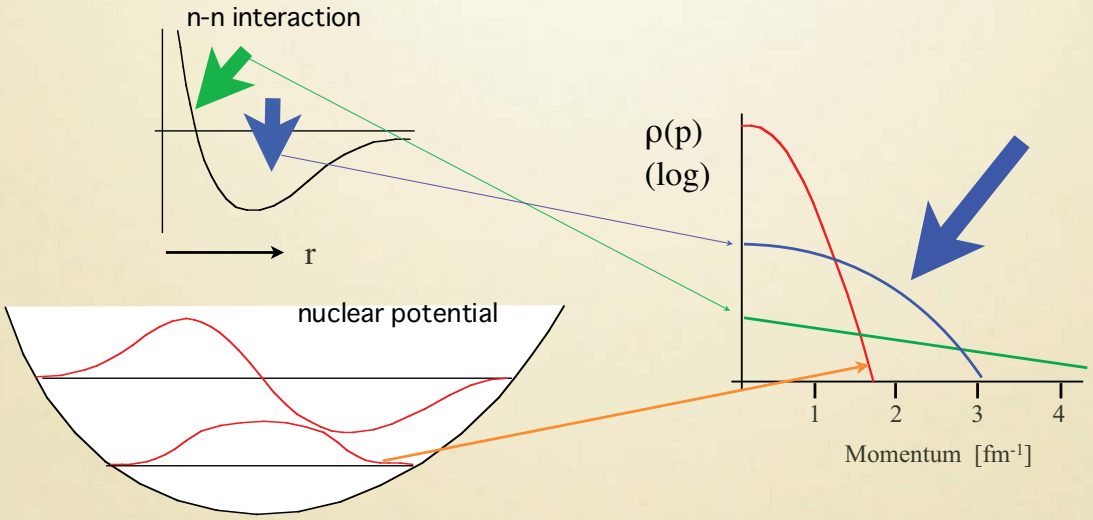

2011年8月31日水曜日

Wave functions

- **Range of tensor force is about the distance of pion exchange, and thus gives momentum component specific to it.**

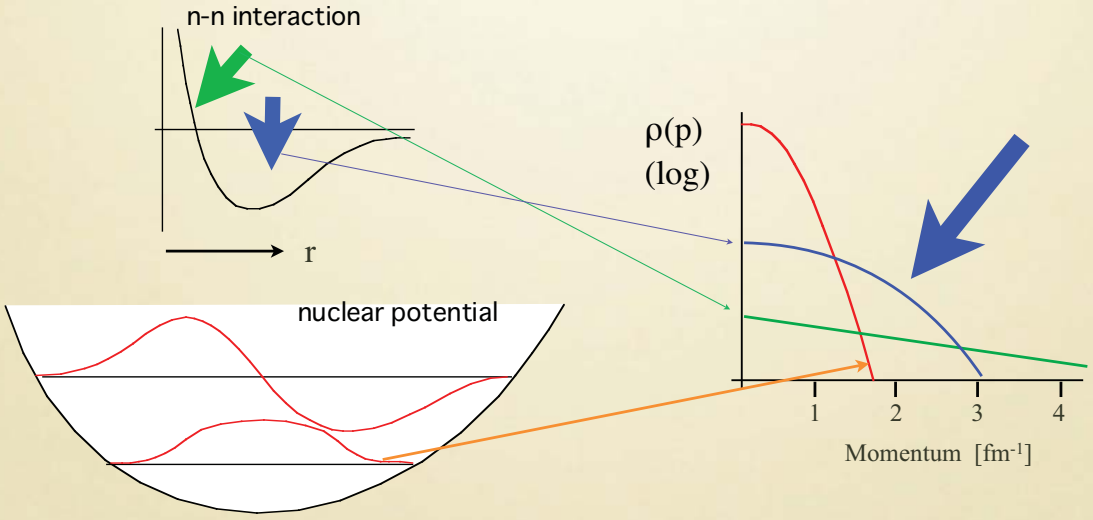

2011年8月31日水曜日

Predictions

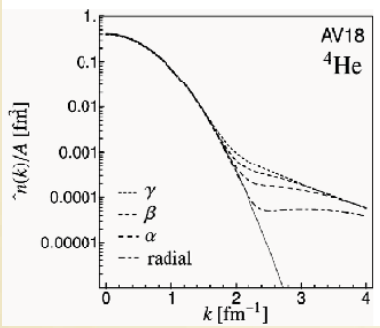

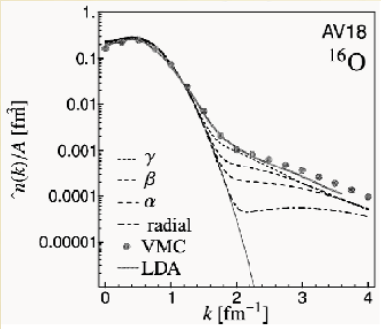

T. Neff and H. Feldmeier, NPA713, 311(2003)

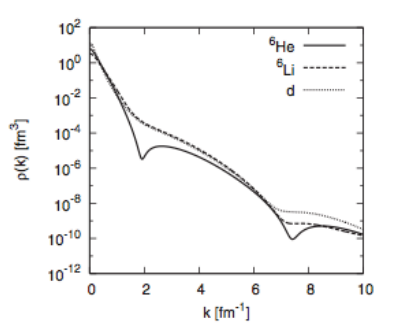

W. Horiuchi and Y. Suzuki, PRC76, 024311(2007)

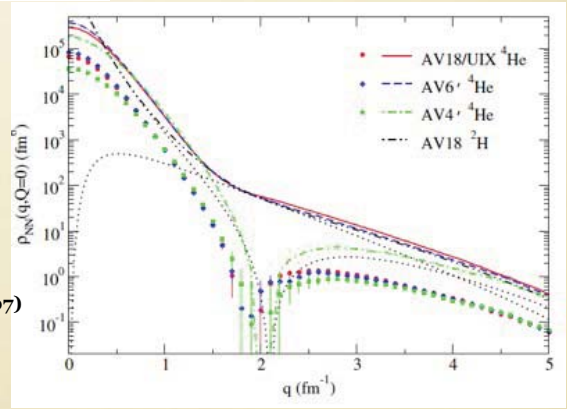

R. Schiavilla et al., PRL 98 132501 (2007)

2011年8月31日水曜日

(p,d) scattering

= suitable to pick up high momentum neutron =

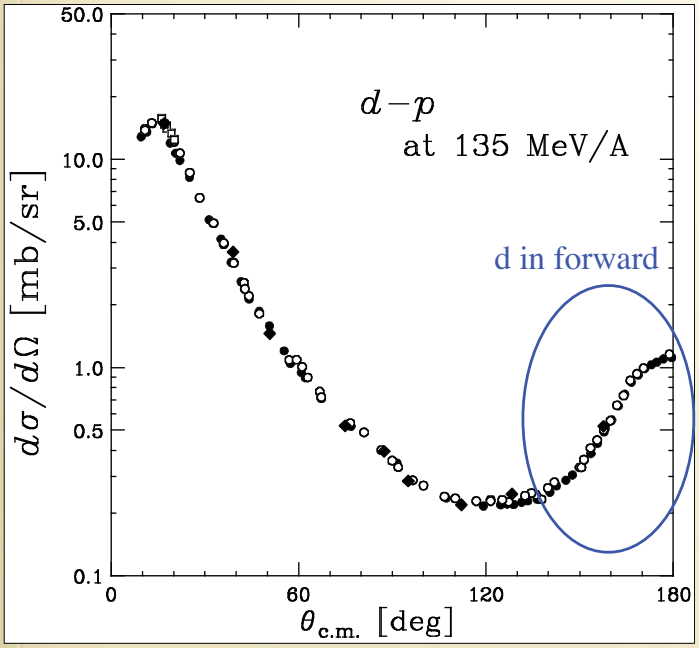

K. Sekiguchi et al., PRL 95 (2004) 162301

2011年8月31日水曜日

(P,D) SCATTERING

= SUITABLE TO PICK UP HIGH MOMENTUM NEUTRON =

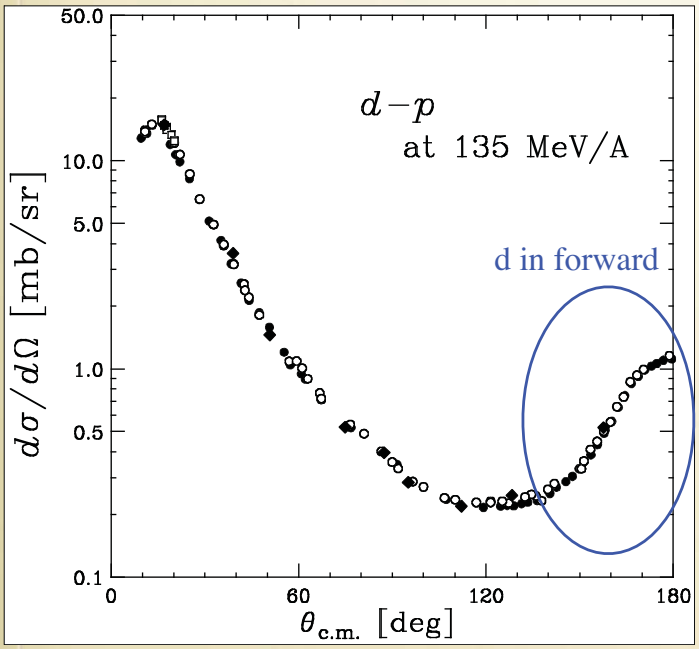

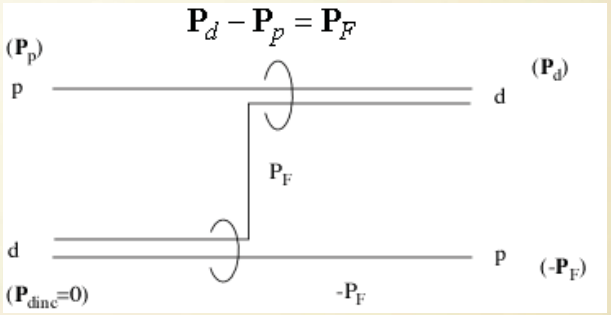

K. Sekiguchi et al.,
PRL **95** (2004) 162301

2011年8月31日水曜日

(P,D) SCATTERING

= SUITABLE TO PICK UP HIGH MOMENTUM NEUTRON =

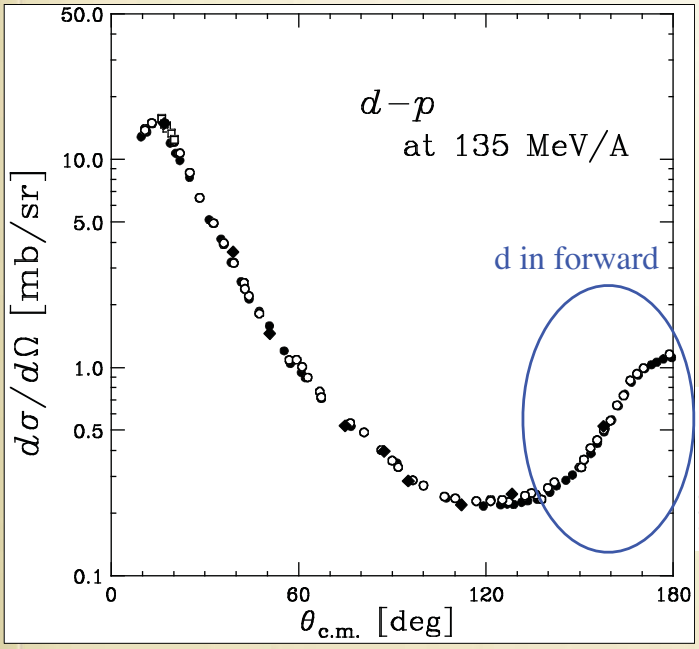

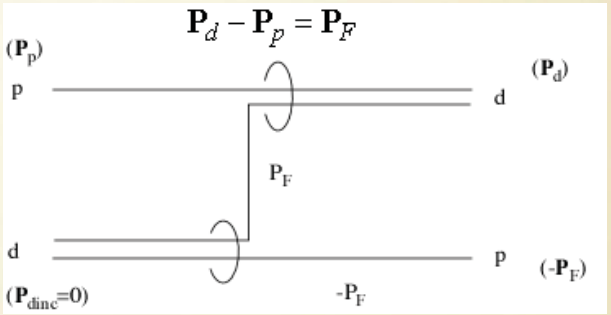

$$\sigma_F = K\frac{P_d}{p}N(P_F)\left[B_D + \frac{\hbar^2}{M}(\mathbf{p} - \mathbf{P}_d/2)^2\right]^{-2}\left|\langle\varphi(r), e^{i(\mathbf{p}-\mathbf{P}_d\cdot\mathbf{r}/2)}\rangle\right|^2$$

K: phase space constant, B_D: deutron binding energy, M: nucleon mass
by G. F Chew and M.L. Goldberger Phys. Rev. **77** (1950) 470.

Reaction at backward occurs by the high-momentum component.

K. Sekiguchi et al.,
PRL **95** (2004) 162301

2011年8月31日水曜日

Experiment at RCNP

$^{16}O(p,d)^{15}O$ at E_p=200 - 400 MeV at θ_s=10°

2011年8月31日水曜日

Necessary beam energies

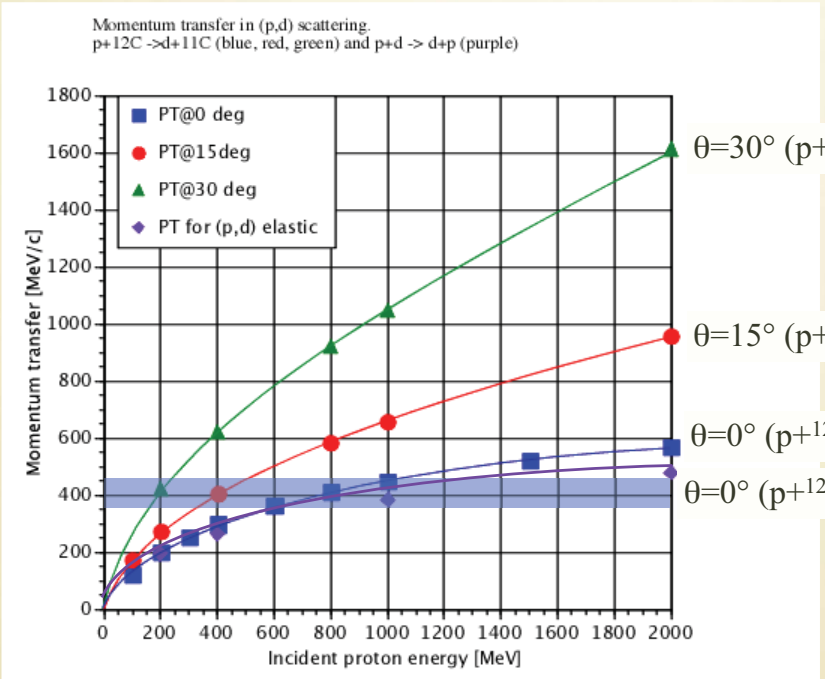

θ=30° (p+^{12}C -> d+^{11}C)

θ=15° (p+^{12}C) -> d+^{11}C

θ=0° (p+^{12}C) -> d+^{11}C

θ=0° (p+^{12}C) -> p+d+^{11}C

2011年8月31日水曜日

^{16}O, ^{15}O CONFIGURATIONS

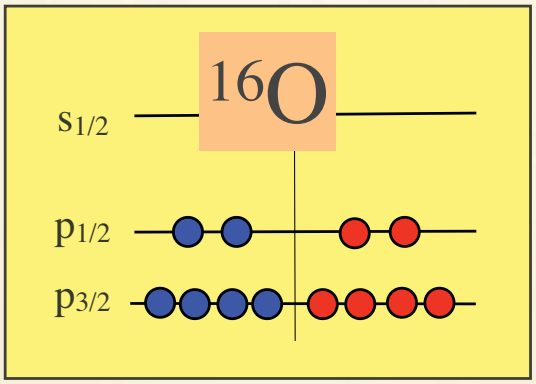

^{15}O

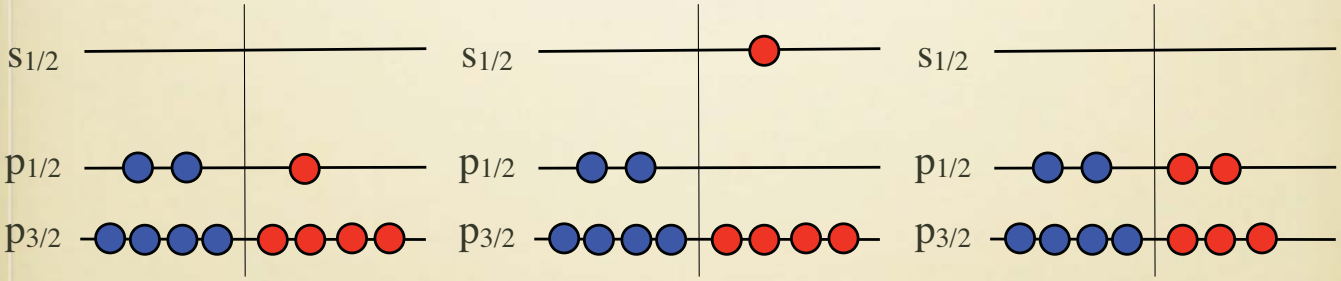

gs $1/2^-$ 1st $1/2^+$ 2nd $3/2^-$

2011年8月31日水曜日

POSITIVE PARITY STATE IN ^{15}O

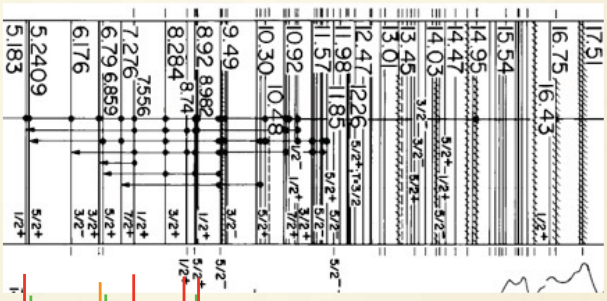

$^{15}O_{gs}$

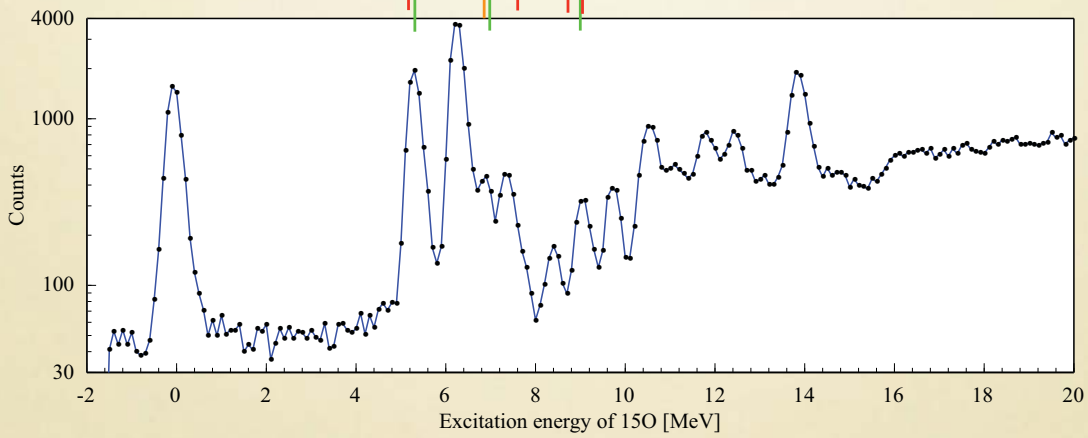

Transition to $1/2^+$ is as strong as to that to the ground state.

2011年8月31日水曜日

At 45 MeV

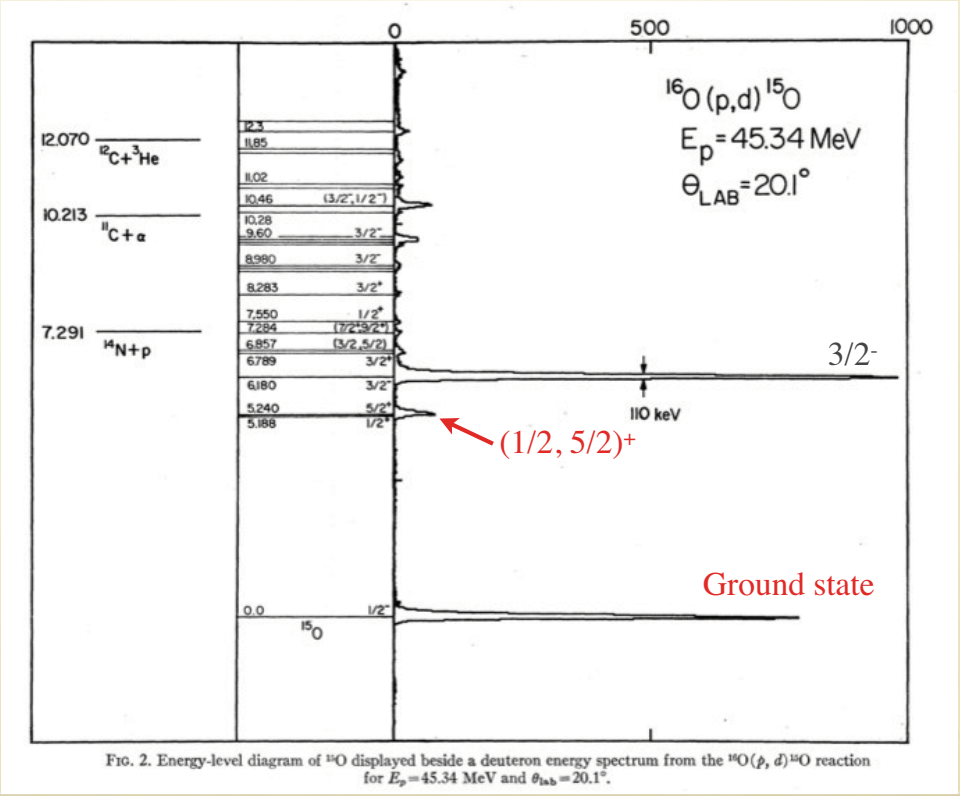

FIG. 2. Energy-level diagram of ^{15}O displayed beside a deuteron energy spectrum from the $^{16}O(p, d)^{15}O$ reaction for $E_p = 45.34$ MeV and $\theta_{lab} = 20.1°$.

2011年8月31日水曜日

Energy dependence of the cross section ratio

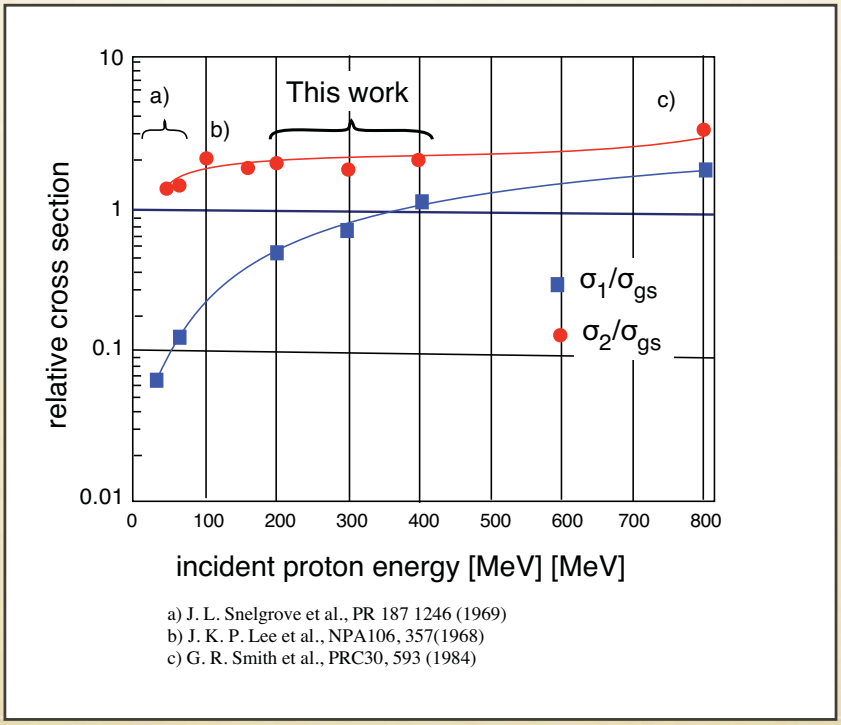

a) J. L. Snelgrove et al., PR 187 1246 (1969)
b) J. K. P. Lee et al., NPA106, 357(1968)
c) G. R. Smith et al., PRC30, 593 (1984)

2011年8月31日水曜日

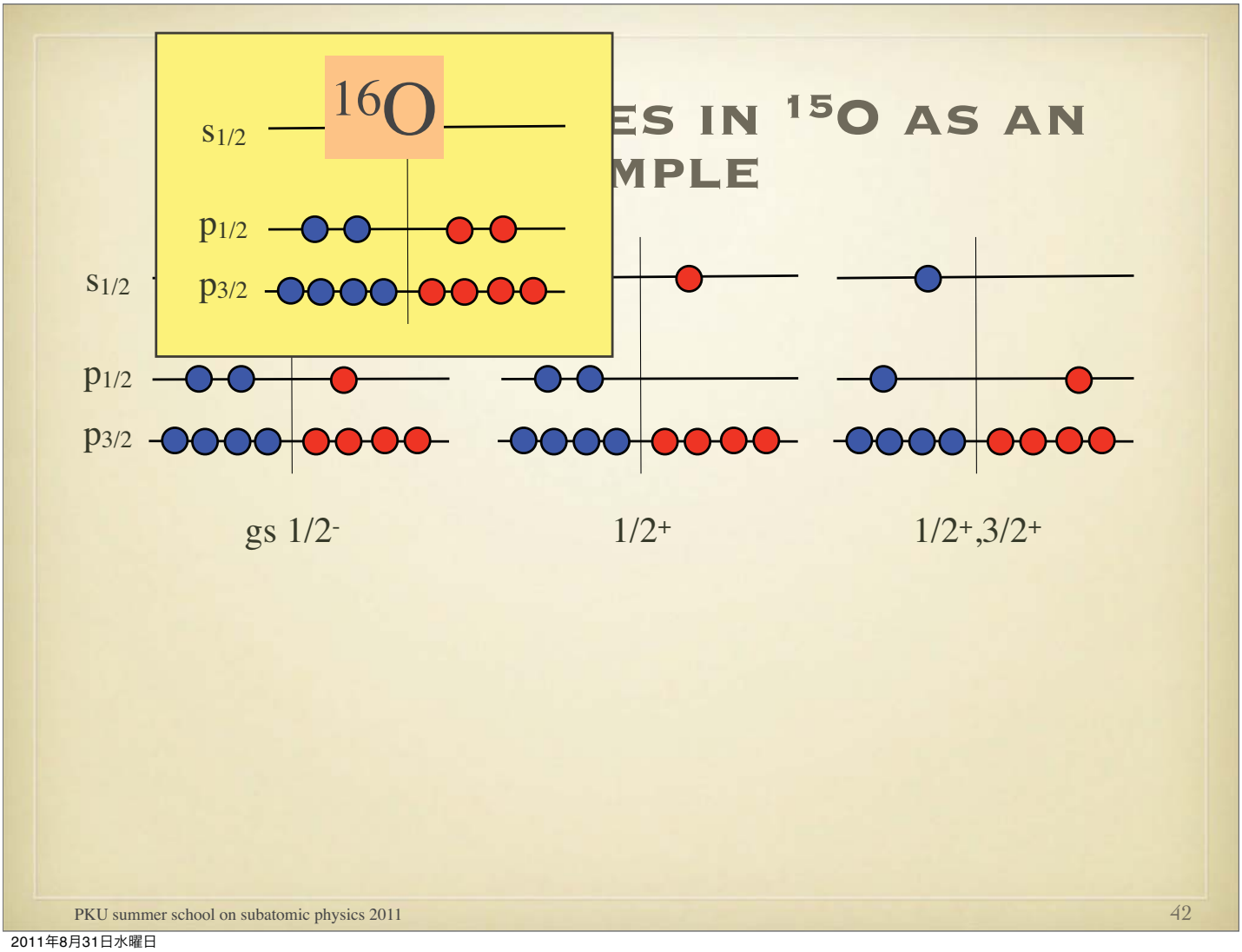

2011年8月31日水曜日

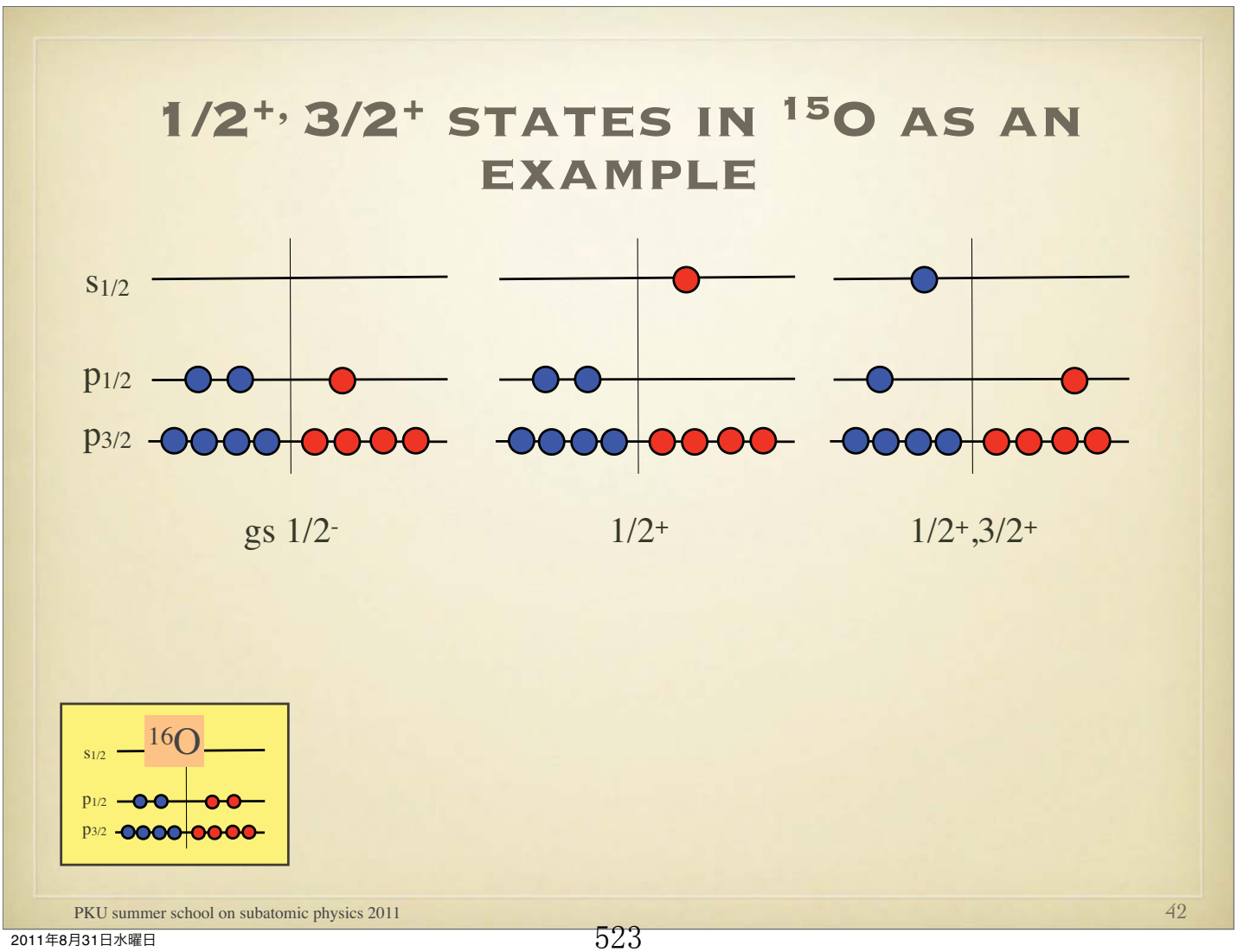

2011年8月31日水曜日

$1/2^+, 3/2^+$ states in ^{15}O as an example

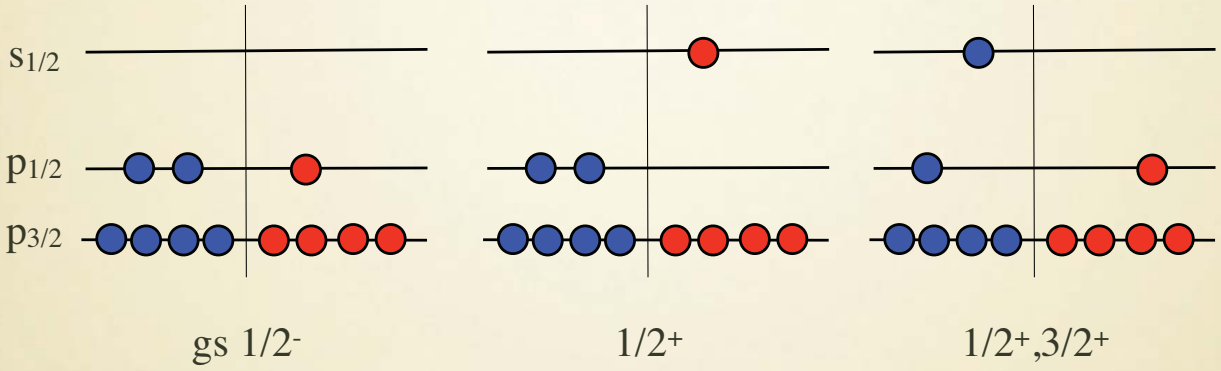

Tensor interaction in ^{16}O

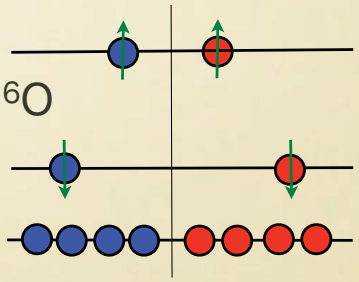

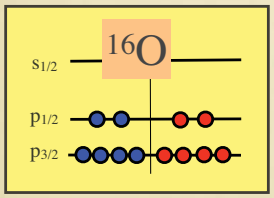

2011年8月31日水曜日

Experiment at Lanzhou

(p,d) reaction at 0°

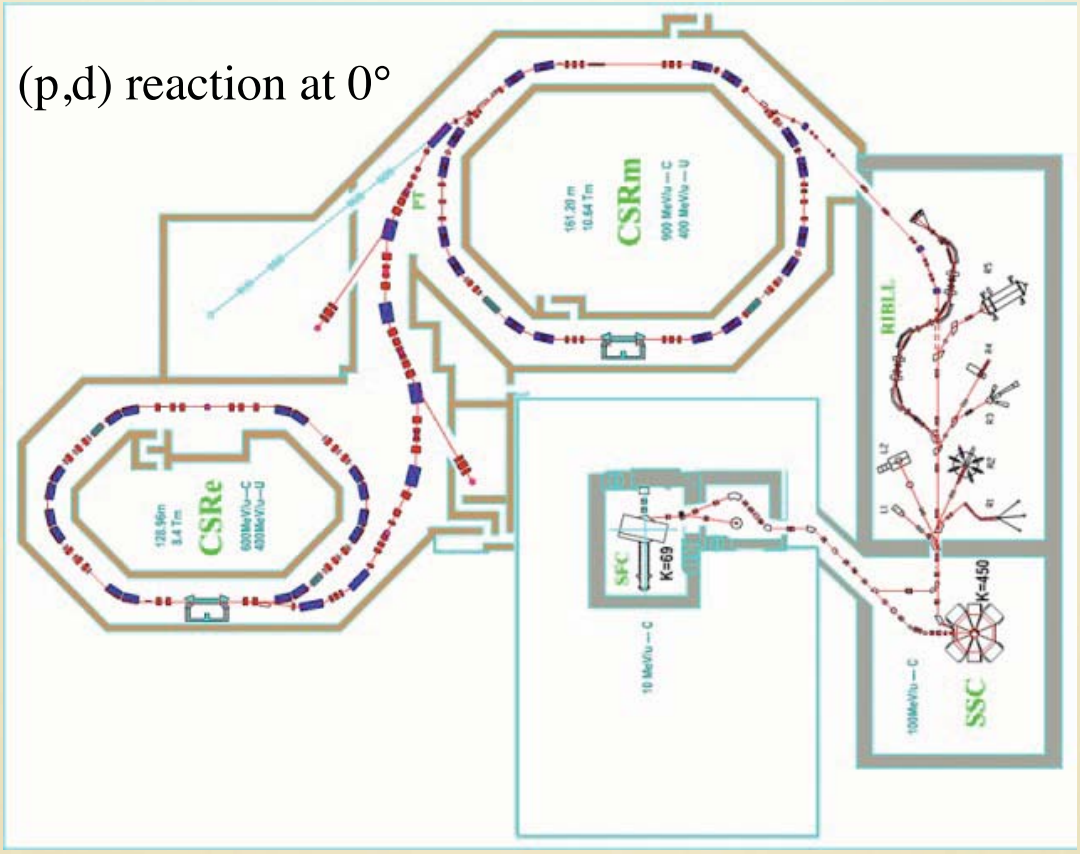

2011年8月31日水曜日

Experiment at Lanzhou

(p,d) reaction at 0°

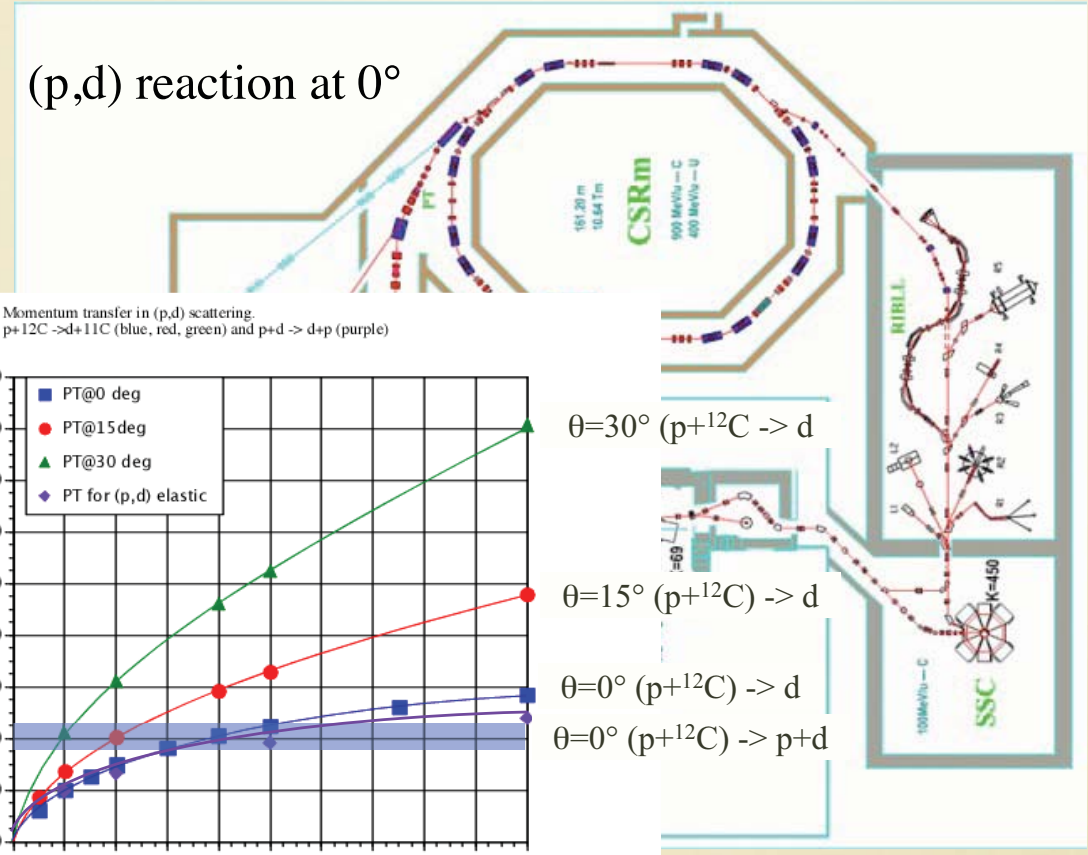

θ=30° (p+^{12}C -> d

θ=15° (p+^{12}C) -> d

θ=0° (p+^{12}C) -> d

θ=0° (p+^{12}C) -> p+d

2011年8月31日水曜日

Experiment at Lanzhou

(p,d) reaction at 0°

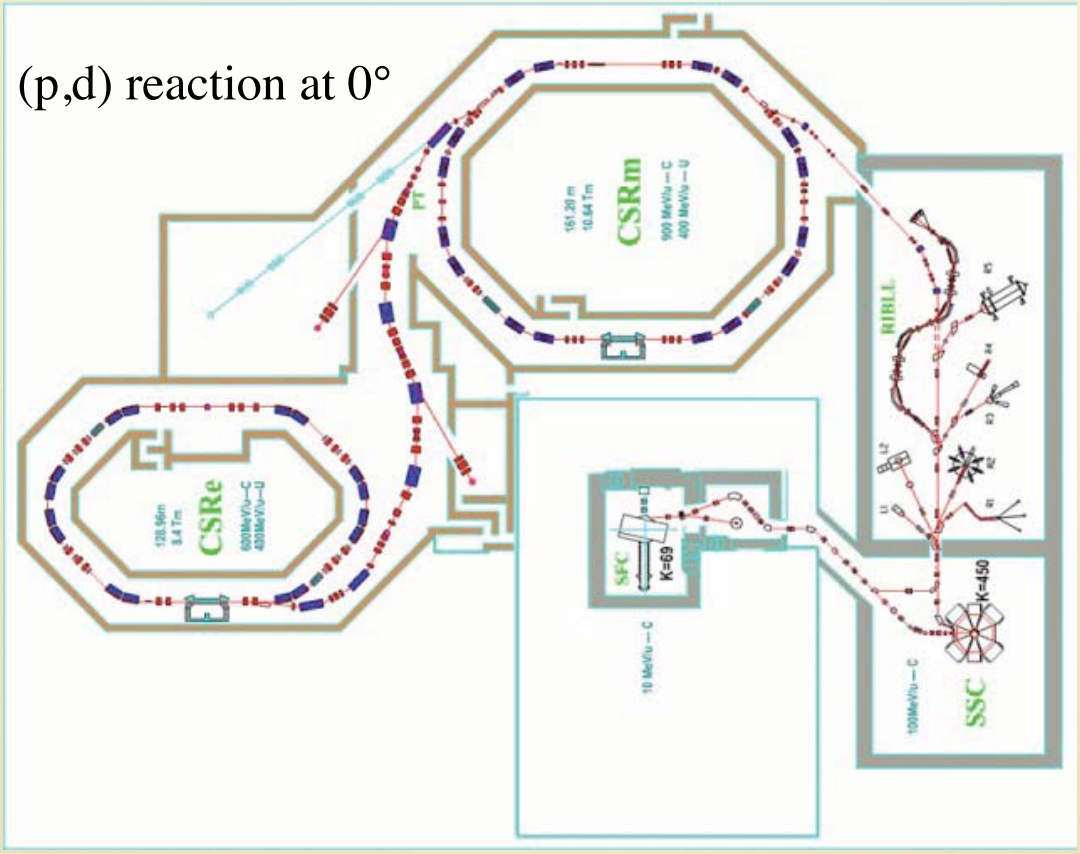

PKU summer school on subatomic physics 2011 43

CSR-RIBLL2

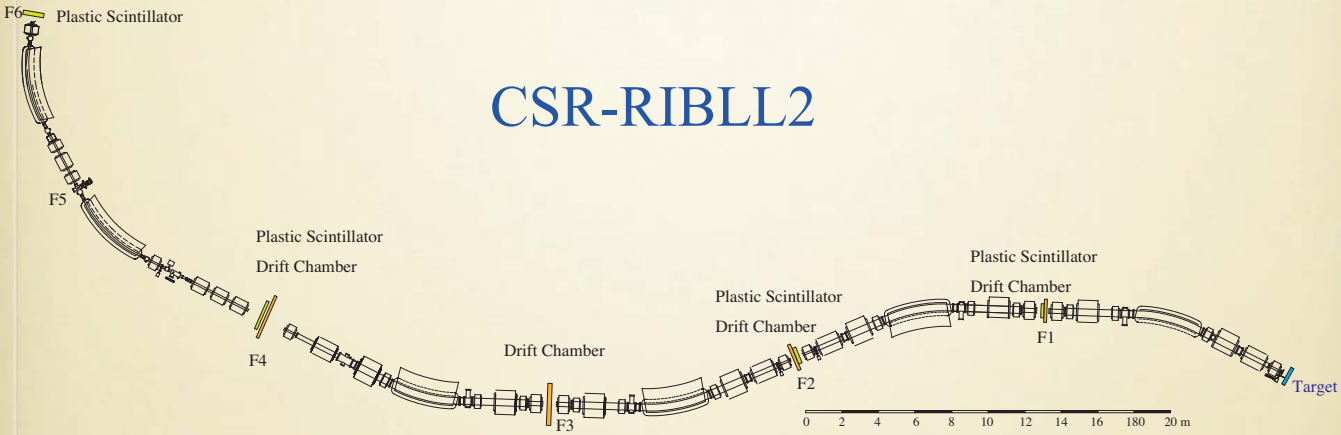

Beihang/Beijing - IMP/Lanzhou - RCNP/Osaka collaboration

2011年8月31日水曜日

STILL THING TO WORK TOGETHER

- **Effect of tensor forces that are not included in the mean field could be studied experimentally.**
- **We need a model that include the tensor forces and high momentum components explicitly.**

Thank you for your attention.

2011年8月31日水曜日

Collaborators

Active target exp's

TRIUMF

M. Alcorta, D. Bandyopadhyay
R. Bieri, L. Buchmann
B. Davids, N. Galinski
D. Howell, W. Mills
S. Mythili, R. Openshaw
E. Padilla-Rodal, G. Ruprecht
G. Sheffer, A.C. Shotter
M. Trinczek, P. Walden

GANIL

H. Savajols, T. Roger
M. Caamano, W. Mittig
P. Roussel-Chomaz

St. Mary's Univ.

R. Kanungo
A. Gallant

ANL

M. Notani
G. Savard

LLNL

I. J. Thompson

(p,d) (p,pd) reaction

RCNP, Osaka U.

H. J. Ong, A. Tamii
H. Okamura, M. Yosoi
K. Suda, T. Adachi
Y. Tameshige, H. Matsubara
D. Ishikawa, H. Sakaguchi
H. Toki, T. Myo
Y. Ogawa

Dep. Phys., Osaka Univ.

K. Matsuta, M. Fukuda
M. Mihara, D. Nishimura

Tsukuba Univ.

A. Ozawa

RIKEN

K. Sekiguchi
K. Ikeda

Breakup and knockout reactions for probing the structure of unstable nuclei

Y. L. Ye

School of Physics and State Key Laboratory of Nuclear Physics and Technology, Peking University, Beijing, China, 100871

Abstract

Exotic structure of unstable nuclei are among the most fascinating phenomena of nowadays nuclear physics. From experimental point of view selection of the proper reaction tool is important in order to extract correct structure information. Since the past twenty years breakup and knockout reactions have been used intensively to investigate the exotic nuclear structure in a spectroscopic way, thanks to the development of the new RIB facilities and experimental techniques. In this lecture we briefly describe the concept and historical development of the breakup and knockout reactions. Latest progress related to unstable projectiles are introduced.

1. Introduction

Breakup reaction was initially observed in Deuteron induced reaction and theoretically studied by Oppenheimer [1] in 1935. He proposed a method to calculate the breakup rate of deuterons in a Coulomb field. This is also the initial idea of the so called Coulomb excitation. In 1947, Based on the "Sudden approximation" Serber proposed another major reaction mechanism, the stripping, for deuterons, in which part of the projectile is absorbed or knocked out by the target while the remaining part of the projectile flight out by carrying on its original momentum in the mother nucleus [2]. it is obvious that Coulomb excitation is more effective when heavy targets (such as Au or Pb) were applied whereas stripping is more probable for light targets (such as C or Be) and at higher energies. Later in the 1970s, heavy ion reaction had becoming a main trend of nuclear physics research. At high energies it was demonstrated that breakup fragments are forward focused and maintain a momentum distribution basically reflecting their Fermi motion property within the mother nucleus [3], consistent with the Serber model [2]. Heavy ion breakup has also provided one of the main tools, the so called projectile fragmentation (PF), to generate the radioactive ion beams (RIB)in the following decades.

Breakup reaction may be classified as elastic breakup and inelastic breakup. Elastic breakup is also called diffractive breakup or diffractive dissociation, indicating that each component of the projectile interact elastically with the target and flight out to the forward angles. According to the interaction properties, elastic breakup is further divided into nuclear breakup and Coulomb excitation. Inelastic breakup is also called stripping or knockout or absorption process, indicating that part of the projectile interacts strongly with the target while the remaining part behaves like a spectator carrying on the original structure information of the mother nucleus. Inelastic breakup can be divided into direct breakup and sequential breakup. The former means a sudden breakup to the final state, whereas the latter means a production of an intermediate state of the spectator, often a resonant state, which decays sequentially to the final state quite long after the initial breakup.

We will give a briefly overview of the historical development of the breakup reaction for unstable nuclei and then focus more on the inelastic breakup reactions for studying halo and cluster structure of nuclei close to the neutron drip-line.

2. A historical development

In mid-1980s radioactive beams were produced and separated in LBL, and used to study the properties of unstable nuclei [4]. Interaction (particle removal) cross sections were measured at about 800 MeV/u for He, Li and Be isotope chains. Extremely large radius of certain nuclei, such as ^{6}He and ^{11}Li were observed. This exotic phenomenon has stimulated the world wide growth of a new field of nuclear physics, namely the radioactive nuclear physics. Soon after that, Kobayashi et al. [5] measured the transverse momentum distribution of the core fragment of the unstable projectile and find extremely narrows peak for those exotic nuclei, which in turn helped to establish the concept of halo nucleus. Using the structure configuration with an inert core plus valence nucleons, Glauber model calculations were implemented to extract the proton and neutron matter distributions and to illustrate the neutron skin and neutron halo pictures. Another important new phenomenon for unstable nuclei is the extremely large Coulomb excitation cross section for halo nucleus [6], based on which the idea of the soft (or pigmy) giant dipole resonance (Soft GDR or PDR) was established. This is thought as a new mode of collective resonant motion of the core fragment against the halo neutrons.

After the first phase of fast development, several new facilities of RIB lines were constructed in the 1990s in several major nuclear physics laboratories. For instance A1200 beam line was built in NSCL [7], FRS in GSI [8] and RIPS in RIKEN [9]. Since the measurement of transverse momentum distribution is inevitably affected by the diffraction, Coulomb scattering and so on, a special method was developed at NSCL to detect precisely the longitudinal momentum ($p_{//}$) distribution. The key

technology is to use the dispersion-matched mode of magnetic spectrograph to compensate the energy spread of the incident beam and to achieve a momentum resolution of less than 0.025% [10]. In China the radioactive beam lines GIRAFFE [11] in CIAE and RIBLL in IMP [12] were also commissioned in that period.

Breakup and knockout are relatively simple direct reactions with large cross sections and sensitive to the surface of the colliding nuclei. It is especially suitable for investigating the weakly binding exotic nuclei and has gained special attention world wide. Therefore since this century new generation of RIB facilities are emerged which allow to make spectroscopic study of unstable nuclei. In NSCL, together with the upgrade of the accelerator system, a new beam line (A1900) was constructed which is characterized by very large angular and momentum acceptance, large deflection power with the super-conducting magnet, high transmission efficiency and so on [13]. Also a new magnetic spectrograph S800 was also constructed allowing to run in dispersion matching mode with very high momentum resolution (0.02%) [14]. In-beam γ-ray detection was also implemented in order to identify various states of the spectator fragment. On the theoretical side, Glauber model calculations for both diffractive and stripping breakup processes were largely advanced, together with CDCC calculations for diffractive process only. Based on all these progresses breakup, and especially knockout reaction has been developed into a powerful spectroscopic tool to investigate the exotic structure of unstable nuclei [15] .

In the following we are going to focus on knockout reaction but leave the Coulomb excitation as a reading material [16, 17]

3. Knockout reaction for probing the single particle state

Hansen et al. [15] has summarized the advantages of the knockout reaction as a spectroscopic tool to probe the single-particle state of unstable nuclei. It includes the large cross section, full solid angle detection due to the inverse kinematics, applicability of thick target, event by event tracking, relatively simple theoretical treatment and so on. As a result even a beam intensity of few tens of particle per second (pps) is enough to make spectroscopic measurement.

We pick up a simple and early example of ^{11}Be to illustrate the method . The ground state of ^{11}Be has an abnormal spin-parity of $1/2^+$. Theoretically it might be interpreted as a ^{10}Be core at the 0^+ state plus a valence neutron at the $1s_{1/2}$ state, or a ^{10}Be core at the 2^+ excited state coupled to a valence neutron at the $0d_{5/2}$ state. The probability of the excited 2^+ core ranges from 7% to 40%. Aumann et al. [18] used a ^{11}Be secondary beam of 60 MeV/u at NSCL, impinged on a Be target, and measured the parallel momentum distribution of the core fragment ^{10}Be by the dispersion matched magnetic spectrograph S800. In-beam γ rays were also measured by an array of NaI(Tl) scintillator in coincidence with the core fragments. Fig.1 shows the measured γ ray spectrum and the fitting results. IN Fig.2 and Fig.3 are momentum distributions of the ^{10}Be fragment corresponding to various excited states determined by the coincidence with corresponding γ rays. The analysis showed an admixture of the core excited states in ^{11}Be at a level of only 6%. In addition the angular momentum assignment for each excited state of the core fragment can be obtained by comparing the measured parallel momentum distribution to the calculated one. This spectroscopic method was then well established and used intensively in NSCL and GSI over the last decade. Recent Examples can be find in Ref.[19, 20, 21, 22]. On the theoretical side Glauber and CDCC models have been developed to perform the calculation of the reaction cross section. The experimental spectroscopic factor (SF) can be obtained by comparing the measure cross section to the calculated one. the results are then used to check the various shell model predictions for SF.

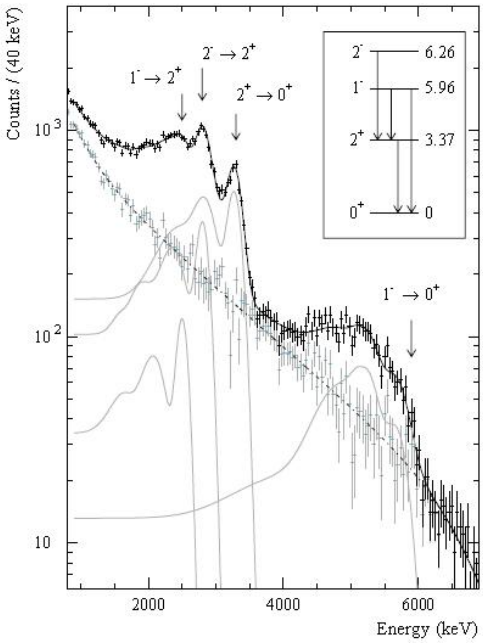

Figure 1: Taken from Ref.[18]. Doppler-corrected energy spectrum measured with the NaI array in coincidence with ^{10}Be fragments. The solid curve is a fit to the experimental spectrum (black error bars) and contains the sum of the simulated response functions (grey curves) for the four g energies indicated by arrows and a background parametrization (dashed-dotted curve). The experimental spectrum after subtraction of the simulations for the four g lines is shown by the grey error bars. The absolute g energies in MeV and intensities (percent after correction for acceptance) for the observed transitions are 2.59 (2.4), 2.89 (9.1), 3.37 (17.6), and 5.96 (4.2).

But very recently it was reported that, for nuclei with large neutron-proton asymmetry, the experimental SF obtained from knockout reactions exhibit very large reduction factor and deviate systematically from those obtained from transfer reactions [23, 24]. Some non-direct reaction processes were proposed to account for this discrepancy [25]. This is an important problem which needs to be understood in-depth in order to obtain unambiguous structure information and to further benefit from the powerful knockout reaction tool [26].

4. Probing the halo and cluster structure of exotic nuclei

Nucleus used to be regarded as a deeply bound and compact quantum system. But since the advent of radioactive nucleus

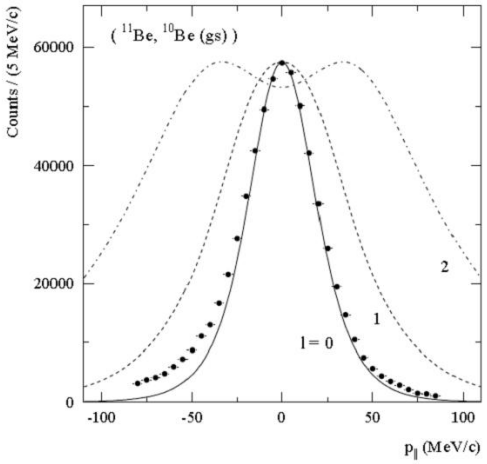

Figure 2: Taken from Ref.[18]. $p_{//}$ distribution of the ^{10}Be fragments in the rest frame of the projectile. Only the contribution leading to the ground state of ^{10}Be is shown. The curves are calculations assuming a knockout reaction from s, p, and d states.

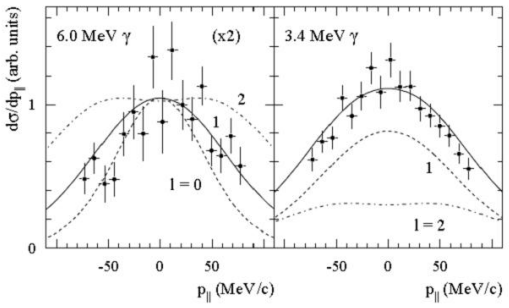

Figure 3: Taken from Ref.[18]. ^{10}Be $p_{//}$ distributions for the excited states. Left panel: in coincidence with 6.0 MeV γ rays, compared with a calculation (solid line) assuming knockout of a neutron from a $p_{3/2}$ core state. Right panel: in coincidence with the 3.4 MeV γ ray, compared with our calculation (solid curve) representing the sum of individual contributions with l = 2 (direct feeding, dotted-dashed curve) and with l = 1 (dashed curve).

beam, many new phenomena have been observed, including the emergence of new degrees of freedom, such as halo and cluster configuration at ground state for nuclei closed to the drip-line [27, 28].

So far Halo structure was identified for ^{6}He, ^{11}Li, ^{11}Be, ^{14}Be, ^{19}C at neutron rich side and for ^{8}B at proton rich side [29]. In addition evidence of halo structure was reported for ^{15}C, ^{17}B, ^{19}B, ^{22}N, ^{23}N, ^{23}O., ^{24}O, ^{24}F and ^{17}Ne. Very recently halo properties were also observed for ^{22}C [30] and ^{31}Ne [31]. Halo nuclei are characterized by very small nucleon separation energy, s or p wave for valence nucleons, few-body clusterization and extraordinary large sizes. Halo structure causes many interesting features in the nuclear reaction, such as extremely large interaction cross section and very narrow parallel momentum distribution for the core fragment compared with its neighbor nucleus, very large Coulomb excitation cross section due to the pygmy dipole resonances (PDR), strong coupling between various reaction channels including continuum states and so on (see Ref.[27] and references therein).

The clustering is a popular phenomena in heavy nuclei and in highly excited states of $N = Z$ nuclei. In the past decades it has been found that cluster structure develops in very neutron rich unstable nuclei even at or close to the ground state [32, 28]. Excess neutrons tend to play the role like chemical bond to stabilize the nucleus in a molecular configuration. Furthermore even the chain or ring configuration was predicted for a nuclide composed of many clusters and valence neutrons [33]. Various theoretical models have been developed to describe the cluster formation and decay [36, 35, 36, 37]. Effort has been made also to incorporate the single-particle degree of freedom and the cluster degree of freedom into one theoretical framework [28]. Clustering effect appears also between valence neutrons. For two neutron halo nucleus, the di-neutron configuration may be built on certain nuclear matter density provided by the core fragment [38, 39, 40]. Strong neutron coupling is also predicted for heavy nuclei due to the so called size effect [41]. Neutron coupling has attracted wide interests since it is related to the BCS and BEC pairing crossover and the possible BES condensation in neutron matter.

Although theoretical work has been largely advanced over past years, experimental investigation of the cluster structure of unstable nuclei is still very limited, especially for ground and low-lying excited states. Reaction tools are especially useful here due to the short life time and the lack of the decay γ rays. We describe here the knockout reaction mechanism which has been the most powerful tool to extract the halo and cluster structure information of unstable nuclei. Also some care will be paid to the newly developed "towing mode" reaction tool.

4.1. explicit knockout reaction mechanisms

Early in 1990's the knockout reaction mechanism of a fast moving Borromean type projectile was sketched into four classes [43, 44], as shown in Fig.4: (A) sudden breakup of the projectile nucleus in the field provided by the target nucleus (diffractive breakup); (B) knockout of a valence nucleon followed by sudden breakup of the spectator fragment; (C) knockout of a valence nucleon followed by strong final state interaction (FSI or resonance decay), and (D) knockout of the core fragment (cluster) followed by emission of valence nucleons with FSI. In the subsequent studies using knockout reaction it was realized that the mechanism (C) is dominating over (B) [45], whereas class (D) was often ignored based on the strong absorption assumption for experiments employing complex targets (such as Beryllium or Carbon targets) and measuring only the spectator fragments at forward angles [15]. Later on it was demonstrated in a quasi-free scattering experiment with ^{6,8}He beams impinging on non-absorptive Hydrogen target [46], the coincident measurement of the forward moving fragment together with the recoiled target proton allows to clearly identify the process (D), which in turn could be used to study the cluster structure of the projectile at ground state, similar to the traditional (p, pα) experiment with normal kinematics for studying stable nuclei [42]. This is of great importance since clustering phenomenon seems growing at around neutron drip-line and spectroscopic investigation of this new degree of freedom is badly needed

[28]. The reported experiment was carried-out at very high energy (717 and 671 MeV/u for ^{6}He and ^{8}He, respectively) and without implementation of neutron detection. It would be interesting to investigate if this recoiled proton tagging method was valid also at energies around 100 MeV/u where most knockout reaction experiments for unstable nuclei were performed and a lot of spectroscopic information were generated. This study of the reaction mechanism, together with neutron detection, might also shed light on the puzzles concerning the SF for asymmetric system and the reconstructed resonance peak as mentioned above.

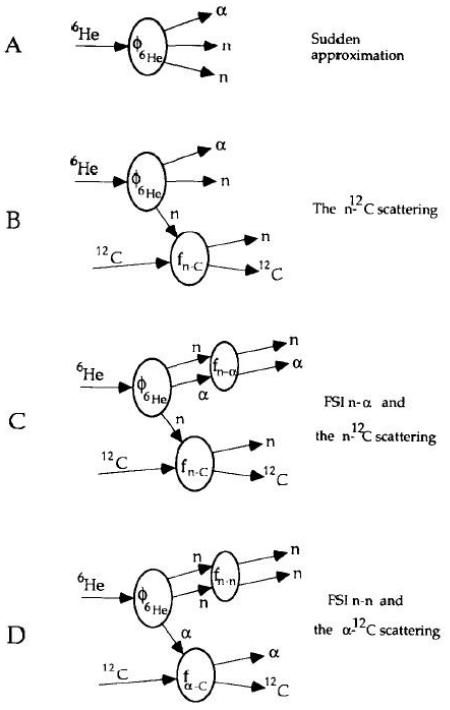

Figure 4: Explicit knockout reaction mechanisms of a fast moving Borromean type projectile. Classifications are described in the text.

To validate the knockout reaction concept, it is required that the collision between the target and the constituent of the projectile obeys the quasi-free condition so that the remaining part of the projectile behaves like a good spectator. It is then mandatory to make the reaction mechanism related kinematics analysis in order to design a sensitive experiment. In the case with the recoiled proton tagging we have developed a formula to be used for quantitative evaluation [47]. Assuming that the projectile A is composed of B and C (A=B+C) and B makes a quasi-free collision with the target (proton target as an example), according to the momentum conservation the magnitude of the momentum of the recoiled proton p_p in the laboratory system is equal to that transferred to the constituent B, the latter is exactly the same as the relative momentum $p_{B,rel}$ of B seen in the projectile rest frame. After the sudden collision, B tends to leave the spectator C by overcoming the attraction force between them and will loss part of its momentum according to:

$$\Delta p_{B,rel} = \int f dt = \int \frac{d\Phi}{dr} dt = \int \frac{d\Phi}{v_r} \approx \frac{m_B S_B}{p_{B,rel}} = \frac{m_B S_B}{p_P} \quad (for \quad \Delta p_{B,rel} \ll p_P) \tag{1}$$

where f is the interaction force along the direction of the field gradient, Φ the potential between B and C, and S_B the separation (or binding) energy of the B+C system. The quasi-free condition is equivalent to require that the momentum loose of B on its way leaving the remnant C is much smaller than the momentum it acquired from the sudden collision ($\Delta p_{B,rel} << p_p$). It is evident that this condition is better satisfied for higher momentum transfer p_p, lighter knockout component (B) and smaller banding energy S_B. We note that p_p is a function of recoiled proton emission angle with respect to the beam axis. Smaller proton angle, corresponding to smaller impact parameter, would lead to larger p_p value. We empirically set the ratio R=$\Delta p_{B,rel}$ /p_p < 0.15 as a quasi-free collision condition. This criteria should be verified by experimental observations. In addition the influence of $\Delta p_{B,rel}$ to the emission angle of the spectator C may also be checked. As a matter of fact, since the force f acts between constituents B and C, the momentum of C ought also change by the same quantity of $\Delta p_{B,rel}$ relative to its original momentum in the projectile. The transverse component of $\Delta p_{B,rel}$ divided by the incident parallel momentum of C gives the deviation angle of C. This deviation angle must be substantially smaller than the scattering angle of B. Otherwise the C component would stick on B, in contradiction to the knockout concept.

For the GSI experiment with 717MeV/u ^{6}He and 671 MeV/u ^{8}He impinged on proton target, the above criteria is satisfied even at angles very close to 90° [46]. But at medium energy such as about 80 MeV/u [47], the proton detection must be moved to some smaller angles, especially when core fragment knockout is concerned. We plot in Fig.5 the calculation of the ratio R as a function of the recoiled proton angle relative to the beam axis, for knockout of the ^{6}He core fragment from a ^{8}He projectile at 80 MeV/u. The requirement of R < 0.15 would put an upper limit of about 62° for the recoiled proton angle. According to this estimation we see that the quasi-free feature of the knockout reaction can well be retained at around 100 MeV/u, as long as the projectile is loosely bound and recoiled proton angle is limited in an appropriate range. We should note that the detection of protons at medium energy is much easier than at very high energy, due to the penetrability of the particle. This is one of the advantages of performing experiment at medium energies.

4.2. Discrimination of the knockout reaction mechanisms through the recoil proton tagging

As indicated above, the recoiled proton tagging may provide a good way to discriminate the core fragment and valence nucleon knockout mechanisms. This discrimination was initially realized at very high energy [46]. Fig.6 shows the polar angle correlation between the recoiled protons and the α-core fragments, detected in an knockout reaction experiment induced by

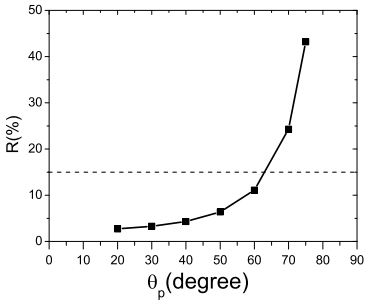

Figure 5: The ratio R, defined in the text, is plotted as a function of the recoiled proton angle relative to the beam axis for knockout of the ^{6}He core fragment from a ^{8}He projectile at 80 MeV/u. The 0.15 requirement for R corresponds to a an upper limit of the recoiled proton angle at about 62 °.

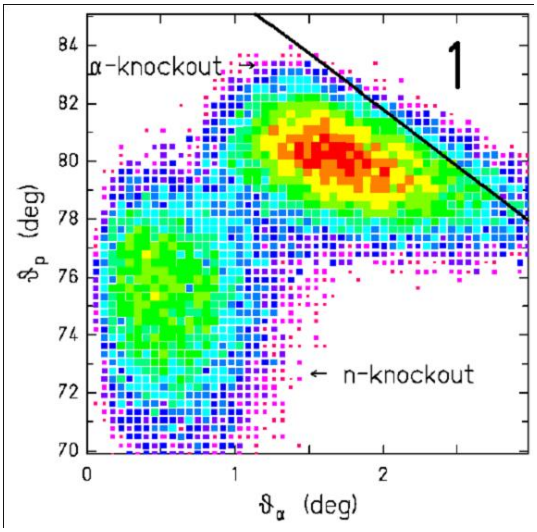

Figure 6: Correlation between the polar angles of the recoiled protons and the α-core fragments in the knockout reaction induced by 717 MeV/u ^{6}He on proton target.

^{6}He at 717 MeV/u on proton target. As explained above the proton detection was set very closed to 90°. Two components appear in the Figure, one with larger proton and ^{6}He angles corresponding to core knockout mechanism whereas another with smaller angles corresponding to valence nucleon knockout. These mechanisms were verified by other quantities, such as azimuthal angle correlation, energy-angle correlation, differential cross section and so on [46] .

The same kind of discrimination may also be realized at much lower energies, such as at around 80 MeV/u as demonstrated by our recent experiment data [47]. Based on above kinematics analysis the proton detection now must move to smaller angular region, as shown in Fig.7. We note that the distribution in Fig.7 is just preliminary by using only the signals taken by the CsI(Tl) crystals in particle telescopes. Much finer presentation will be obtained by using the Silicon strip detector information. Verifications with other quantities are also successful, supporting the validity of quasi-free knockout at the medium energy around 100 MeV/u and the applicability of the recoiled proton tagging technique.

Discrimination of the knockout reaction mechanisms is not only important for its own seek but also for the correct spectroscopic investigation of the relevant structure configuration. For instance by selecting the pure valence nucleon knockout events the single-particle state (either bound or resonant state) can be probed without contamination from other reaction mechanism. On the other hand, by selecting the core fragment knockout events the cluster structure at ground state may be analyzed quantitatively [47]. In addition, after the core knockout, the correlation between the remaining valence neutrons may be studied by directly detecting the emitted neutrons. All these topics are actually very interesting and experiments of these kind are largely demanding.

4.3. The towing mode reaction

Knockout reaction is effective at relatively high energies, typically above 50 MeV/u [15]. Another well known spectroscopic tool is the transfer reaction which is effective at around fermi energy, namely 10-30 MeV/u [49]. In between of these energy regions a new mode of direct nuclear reaction, the so called "towing mode" reaction, was discovered [50, 51] and gradually applied to extract the single particle and cluster structure SF for both stable and unstable nuclei [52, 53, 54, 55].

The towing phenomenon was observed when carrying on heavy ion collision experiment at around 40 MeV/u. By selecting events with one light particle emission together with the ejectile and target nucleus staying basically on their ground or low-lying excited states, the emission may be treated as a direct towing process. If we call the mother nucleus of the emitted particle as the emitter, the collision counterpart as the probe, the "towing" mode is characterized by emitting the particle to the same side of the probe with relatively large emission angle and rapidity. This is in contradiction to the knockout process in which the knocked out particle and the probe nucleus go to the opposite sides of the beam axis. It has been demonstrated that the angular and energy (or momentum vector) distributions of the towed particle depend sensitively on its original quantum state in the mother nucleus (emitter), providing a good spectroscopic tool to extract the structure information of the emitter. It is understandable that "towing" could only happen within in an energy window. It will switch to knockout process when energy is higher or merged into transfer or collective excitation process when energy is lower down to fermi energy range.

Simple but effective theoretical tool has been developed corresponding to the "towing" process [51]. The emitted particle is supposed to move in time-dependent two center nuclear potentials provided by the emitter and the probe, respectively. The calculation is done in the framework of Time-Dependent Schrodinger Equation (TDSE) with structure wave function as its input.

This experimental method together with the theoretical model has been applied to investigate the structure of exotic nucleus such as ^{11}Be [52]. It was also exercised to study the di-

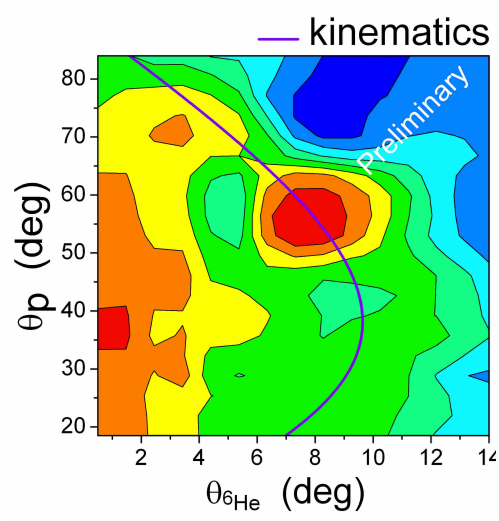

Figure 7: Correlation between the polar angles of the recoiled protons and the ^{6}He-core fragments in the knockout reaction induced by 82.3 MeV/u ^{8}He.

neutron configuration of borromean type halo nucleus by using the towing mode breakup reaction [54], and theoretical tool for two particle emission was also implemented accordingly [53]. More amazingly the cluster SF at ground state can also be extracted by properly towing the cluster out of its mother nucleus [55]. Based on the systematic development over a decade or so, we anticipate that the "towing mode" reaction will become an complementary spectroscopic tool at transition energies with important applications.

5. Summary and conclusion

Exotic structure of unstable nuclei are among the most fascinating phenomena of nowadays nuclear physics. Much efforts have been made to observe and describe these exotic structure. From experimental point of view selection of proper reaction tool is mandatory in order to extract correct structure information. Since the past twenty years breakup and knockout reactions have been used intensively to investigate these exotic structure in a spectroscopic way, thanks to the development of the new RIB facilities and experimental techniques. But some ambiguities still exist which require more precise understanding of various knockout processes. In this lecture we have outlined the history and latest development of these reaction tools. Emphasis is given to the knockout reaction, especially that with the recoil proton tagging. The newly developed "towing mode" reaction tool is also introduced and its applicability at transit energies is discussed.

References

[1] J.R. Oppenheimer, Phys. Rev. 47 (1935)845.
[2] R.Srber Phys. Rev. 72(1947)1008.
[3] D.E. Greiner, P.J. Lindstrom, H.H. Heckman, et al., Phys. Rev. Lett. 35(1975)152.
[4] I. Tanihata, H. HAMAGAKI, O. HASHIMATO, et al., Phys. Lett. B 160(1985)380 and Phys. Rev. Lett. 55(1985)2676.
[5] T. Kobayashi, O. Yamakawa, K. Omata, et al., Phys. Rev. Lett. 60(1988)2599.
[6] T. Kobayashi, S. Shimoura, I. Tanihata, et al., Phys. Lett. B 232(1989)51.
[7] B.M. Sherrill, D.J. Morrissey, J.A. Nolen, et al., Nucl. Instr. Meth. B 56-57(1991)1106.
[8] H. Geissel, P. Armbruster, K.H. Behr, et al., Nucl. Instr. Meth. B70(1992)286.
[9] T. Kubo, M. Ishihara, N. Inabe, et al., Nucl. Instr. Meth. B70(1992)309.
[10] N.A. Orr, N. Anantaraman, S.M. Austin, et al., Phys. Rev. Lett., 69(1992)2050.
[11] W.P. Liu, X.X. Bai, S.H. Zhou, et al., Phys. Rev. Lett. 77(1996)611.
[12] Z.Y. Sun, W.L. Zhan, Z.Y. Guo, et al., Nucl. Instr. Meth. A 503(2003)496.
[13] D.J. Morrisey, B.M. Sherrill, M. Steiner, et al., Nucl. Instr. Meth. B 204(2003)90.
[14] D. Bazin£J.A. Caggiano, B.M. Sherrill, et al., Nucl. Instr. Meth. B 204(2003)629.
[15] P.G. Hansen and J.A. Tostevin, Annu. Rev. Nucl. Part. Sci. 53 (2003) 219.
[16] T. Nakamura, A.M. Vinodkumar, T. Sugimoto, et al., Phys. Rev. Lett., 96(2006)252502.
[17] N. Paar, J. Phys. G: Nucl. Part. Phys. 37 (2010) 064014.
[18] T. Aumann, A. Navin, D.P. Balamuth, et al., Phys. Rev. Lett. 84(2000)35.
[19] L.A. Riley, P. Adrich, T.R. Baugher, et al., Phys. Rev. C 78(2008)011303.
[20] R. Kanungo, C. Nociforo, A. Prochazka, et al., Phys. Rev. Lett. 102(2009)152501.
[21] C. Rodriguez-Tajes, et al., Phys. Rev. C 82 (2010)024305.
[22] G.F. Grinyer, et al., Phys. Rev. Lett. 106(2011)162502.
[23] J. Lee, M.B. Tsang, D. Bazin, et al., Phys. Rev. Lett. 104 (2010) 112701.
[24] J. Lee, M.B. Tsang, D. Bazin, et al., Phys. Rev. C 83(2011)014606 and references therein.
[25] C. Louchart et al., Phys. Rev. C 83(2011)011601(R).
[26] W.H. Dickhoff, J. Phys. G: Nucl. Part. Phys. 37 (2010)064007.
[27] S.N. Ershov, et al., J. Phys. G 37(2010)064026.
[28] H. Horiuchi, J. Phys. G 37(2010)064021.
[29] D. Baye, et al., Nucl. Phys. News, 15(2004)10.
[30] Tanaka K et al. Phys. Rev. Lett., 2010,104:062701.
[31] T. Nakamura, et al., Phys. Rev. Lett. 103(2009)262501.
[32] W.V. Oertzen, et al., Phys. Rep. 432(2006)43.
[33] Y. Funaki, et al., J. Phys. G 37(2010)064012.
[34] Y. Taniguchi, et al., Phys. Rev. C 80(2009)044316.
[35] Qi C, Xu F R et al. Phys. Rev. Lett.,2009, 103:072501.
[36] Y. Taniguchi, et al., Phys. Rev. C 80(2009)044316.
[37] T. Dong and Z.Z. Ren, Phys. Rev. C 82(2010)034320.
[38] K. Hagino, et al., Phys. Rev. Lett. 99(2007)022506.
[39] D.T. Khoa and W.V. Oertzen, Phys. Lett. B 595(2004)193.
[40] Y. Ye, et al., J. Phys. G 31(2005)S1647.
[41] K. Hagino, et al., J. Phys. G 37(2010)064040.
[42] P.G. Roos, et al., Phys. Rev. C 15(1977)69.
[43] A.A. Korsheninnikov, T. Kobayashi, Nucl. Phys. A 567(1994)97.
[44] A.A. Korsheninnikov, et al., Europhys. Lett. 29(1995)359.
[45] T. Nilsson, et al., Nucl. Phys. A 598(1996)418.
[46] L.V. Chulkov, F. Aksouh, A. Bleile, et al., Nucl. Phys. A 759(2005)43.
[47] Ye Y L et al. Nucl. Phys. A, 2010, 834:454c
[48] Cao Z X, Ye Y L, Xiao J et al. Submmitted to Phys. Rev. Lett.
[49] Oganessian Y T and Zagrebaev V I. Phys. Rev. C, 1999, 60:044605
[50] Scarpaci J A, Beaumel D, Blumenfeld Y et al. Phys Lett B,1998, 428:241
[51] Lacroix D, Scarpaci J A and Chomaz P. Nucl. Phys. A, 1999, 658:273
[52] Lima V, Scarpaci J A, Lacroix D et al. Nucl. Phys. A, 2007, 795:1
[53] Assie M and Lacroix D. Phys. Rev. Lett., 2009, 102:202501
[54] Assie M, Scarpaci J A, Lacroix D et al. Eur. Phys. J. A., 2009, 42:441
[55] Scarpaci J A, Fallot M, Lacroix D et al. Phys. Rev. C, 2010, 82:031301

(Breakup and) knockout reactions for probing the structure of unstable nuclei

Yanlin Ye
State Key Lab. of Nucl. Phys.&Tech.
Peking University

State Key Lab. of Nuclear Physics and Technology, Peking University

- Accelerator Physics and Techniques
- RIB nuclear Physics
- Hadron Physics
- Applications

4.5MV VDG

2x6MV tandem

2x1.7MV tandem

a new AMS

RF superconducting accelerator Lab.

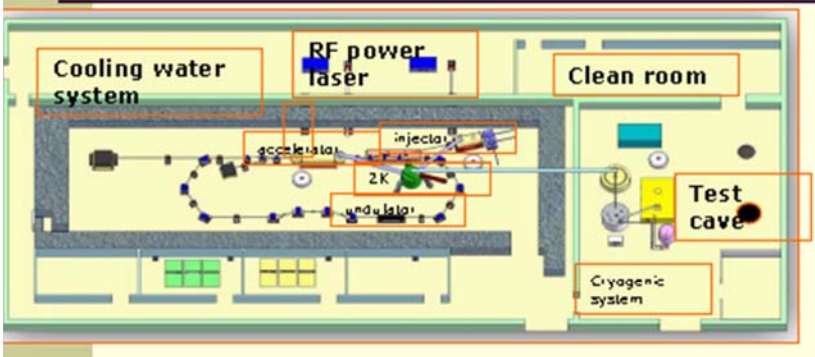

Separate Function RFQ (SFRFQ)

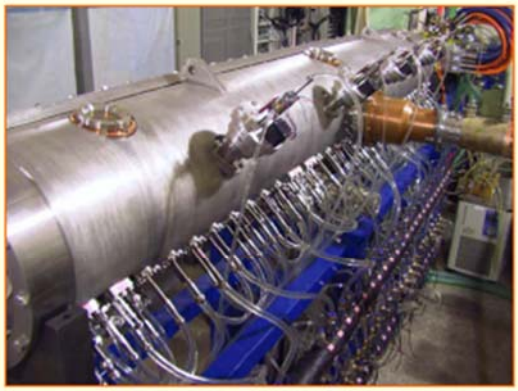

Four mini-vane RFQ — Deuteron acceleration

Particle detection Lab.

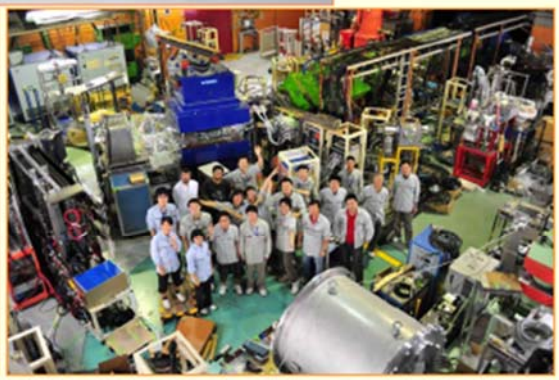

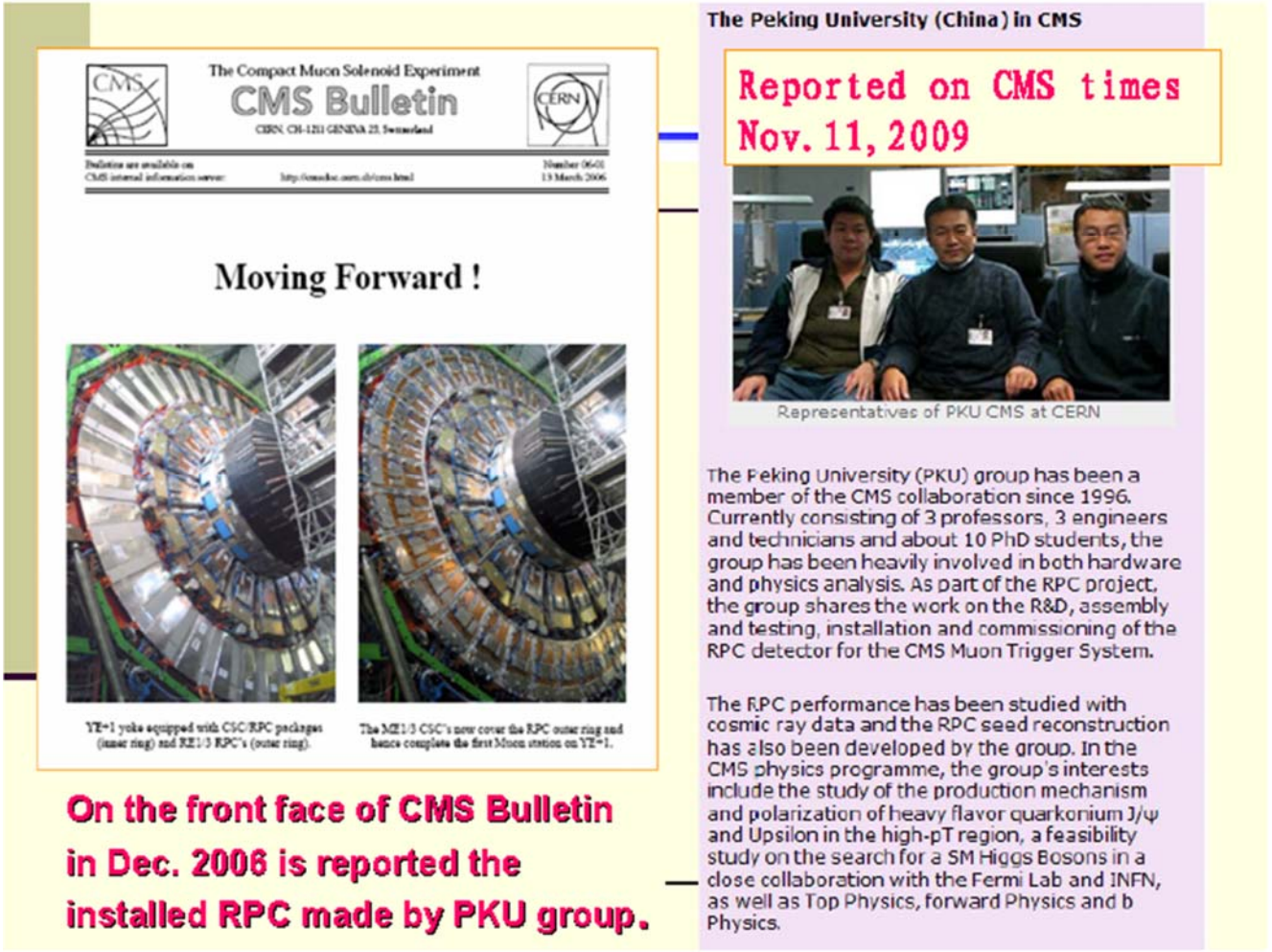

Contribution to the community

Nov. 2006

since 1999

Jul.2009

since 2008

Future plan: ImPUF (Intense multi-beam multi-PUrpose Facility)

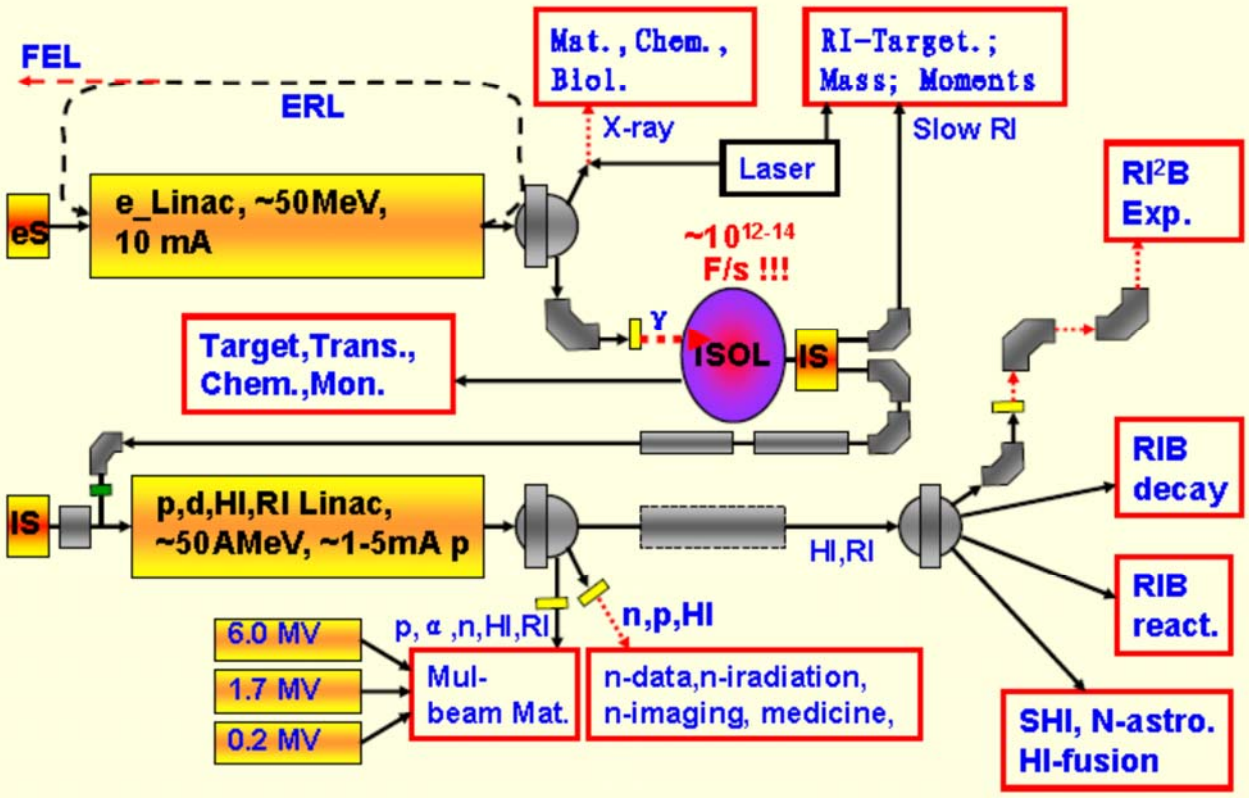

International Advisory Committee

Chen Jiaer	co-chair	Peking U
Shoji Nagamiya	co-chair	J-PARC
Walter Henning	Nuclear Physics	ANL-RIKEN
Akito Arima	Nuclear Energy	Musashi School
Vincent Chan	Plasma and Fusion	General Atomics
Steve Zinkle	Nuclear Material	ORNL
Satoshi Ozaki	Accelerator	BNL
Tohru Motobayashi	Detectors	RIKEN
S. M. Qaim	Nuclear Chemistry	Jülich
Frank von Hippel	Nuclear Policy	Prinston U
Hirohiko Tsujii	Nuclear Medicine	HIMAC

The 1st INST-IAC meeting May 5-6, 2011

Accelerators for the Future

Walter F. Henning

Argonne National Laboratory
& RIKEN Nishina Center

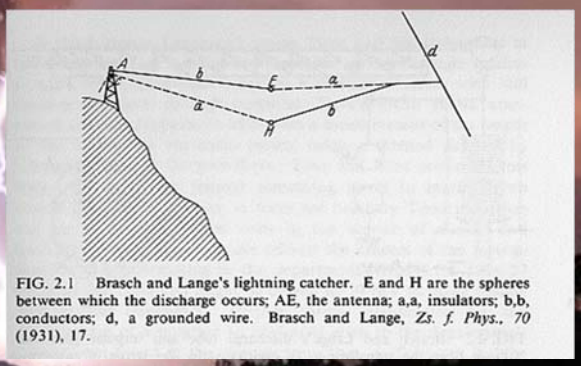

FIG. 2.1 Brasch and Lange's lightning catcher. E and H are the spheres between which the discharge occurs; AE, the antenna; a,a, insulators; b,b, conductors; d, a grounded wire. Brasch and Lange, *Zs. f. Phys., 70* (1931), 17.

1928: Curt Urban, Arno Brasch, and Fritz Lange successfully achieved 15 MV by harnessing lightning in the Italian Alps !

The two who survived the experiment went on to design an accelerator tube capable of withstanding that voltage.

SRF2011 – Chicago / July 25 – 29, 2011

Outline

I. Introduction

II. A brief description of Quasi-free scattering (p,2p)

III. Knockout reaction with unstable projectile

IV. Proton tagged knockout reaction

V. Summary

I. Introduction

- **breakup** （破碎）

  Elastic (diffractive) breakup

  (nuclear or coulomb breakup);

  Inelastic (stripping) breakup

- **knockout** （敲出）

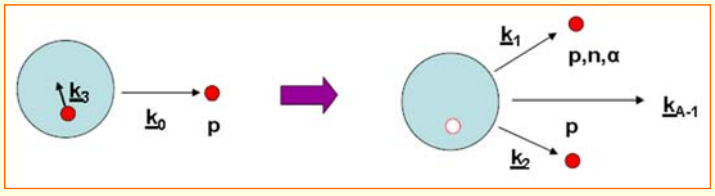

$$\vec{k}_3 = \frac{A-1}{A}\vec{k}_A - \vec{k}_{A-1}$$

$$k_0 - k_1 - k_2 = -k_3 \quad \text{(QFS)}$$

Diffractive (elastic) breakup: σ_{int}-halo , PGR…

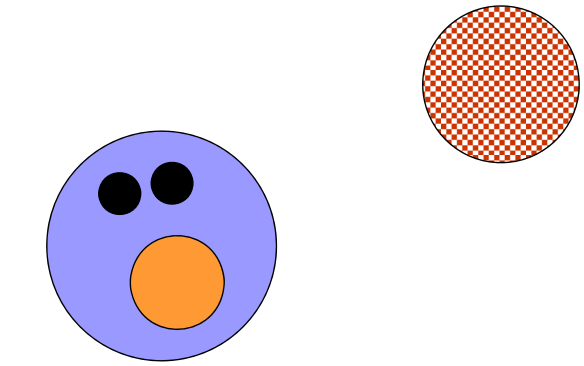

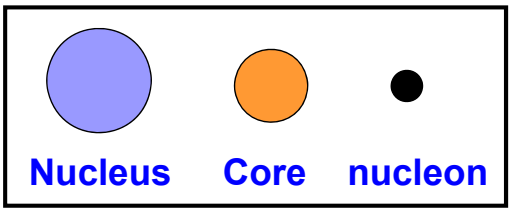

Knockout : (new shell, SF…)

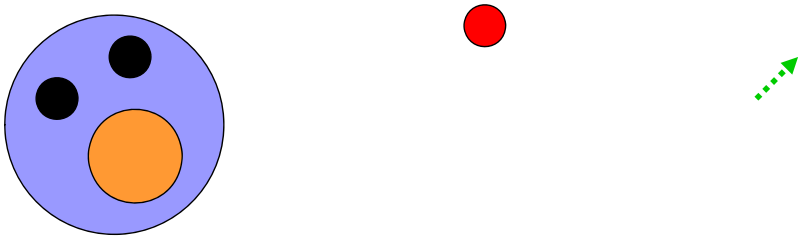

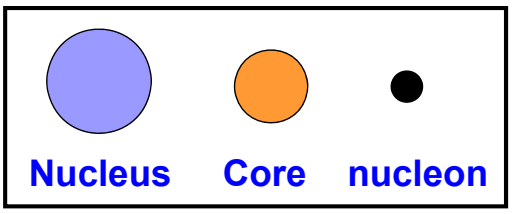

- **Q:**

  Is it possible to probe inner structure of a nucleus non-destructively (without breakup)?

- If not, then breakup (knockout) is very important for understanding nuclear structure.

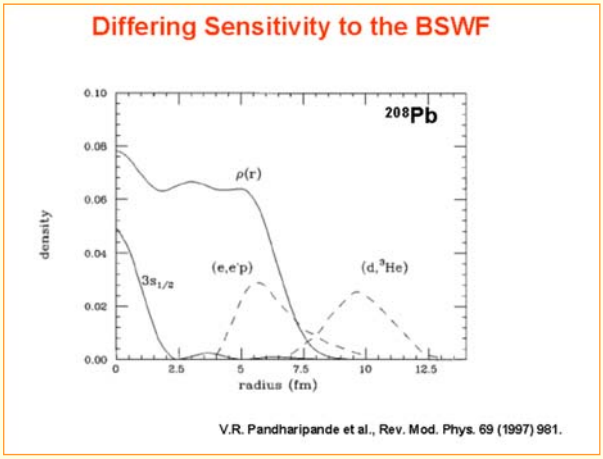

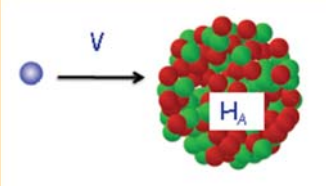

Breakup for weakly bound nucleus

- large cross section
- strong coupling with elastic and inelastic scattering, fusion, transfer reaction etc, need coupled channel analysis such as CRC, CDCC……
- knockout reaction has played special spectroscopic role in studying nuclear structure of unstable nuclei.

JUNE 1, 1935 PHYSICAL REVIEW VOLUME 47

The Disintegration of the Deuteron by Impact

J. R. OPPENHEIMER, *Berkeley, California*

(Received March 29, 1935)

Coulomb excitation

High energy deuterons can be disintegrated by their impact with nuclei. For deuteron energies $\sim 2\times10^7$ e.v., the corresponding neutron yield can be of the order of 1 percent. The probability of the process can be calculated by taking advantage of the fact that the nuclear field varies little over the deuteron, and is then given quite simply in terms of the photoelectric absorption and the matrix elements of the nuclear field acting on the deuteron. For low energies the neutron yields are small, amounting to 3×10^{-9} for 3×10^6 e.v. deuterons in Al, and to 10^{-6} for 4×10^6 e.v. deuterons in carbon.

PHYSICAL REVIEW VOLUME 72, NUMBER 11 DECEMBER 1, 1947

The Production of High Energy Neutrons by Stripping*

R. SERBER

...ratory, Department of Physics, University of California, Berkeley, California

(Received August 28, 1947)

stripping

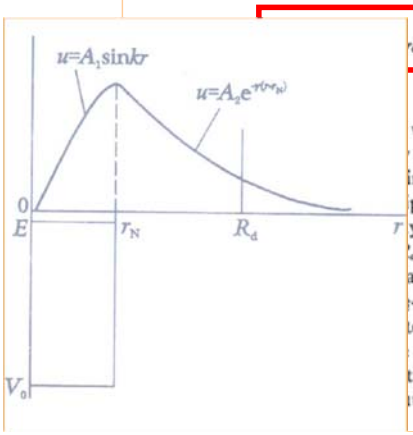

...with high energy deuterons, ...neutrons is produced by a ...in the deuteron strikes the ...pped off, while the neutron ...y. The cross section for this ...$_d$, where R is the nuclear ...adius, or $\sigma=5A^{\frac{1}{3}}\times10^{-26}$ cm^2. ...-in. Be target (in which the ...erons is 20 Mev) is nearly ... out with an energy spread ...th $\Delta E_{\frac{1}{2}}=1.5(E_d\epsilon_d)^{\frac{1}{2}}$. Here E_d ...teron, ϵ_d its binding energy.

For light nuclei the half-width of the neutron angular distribution is $\Delta\theta_{\frac{1}{2}}=1.6(\epsilon_d/E_d)^{\frac{1}{2}}$. The half-width increases somewhat with atomic number, primarily because of the deflection of the deuteron by the Coulomb field as it approaches the nucleus, and, to a lesser extent, because of multiple scattering in the target. The increase in half-width from Be to U is about 25 percent. The calculated half-widths and angular distributions agree well with the measurements of Helmholz, McMillan, and Sewell.

An equal number of high energy protons are produced by stripping processes in which it is the neutron that hits the nucleus.

II. A brief description of Quasi-free scattering (p,2p)

Free scattering

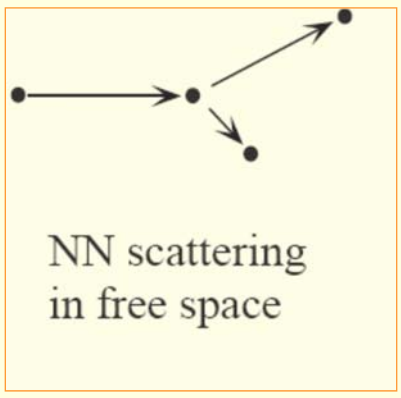

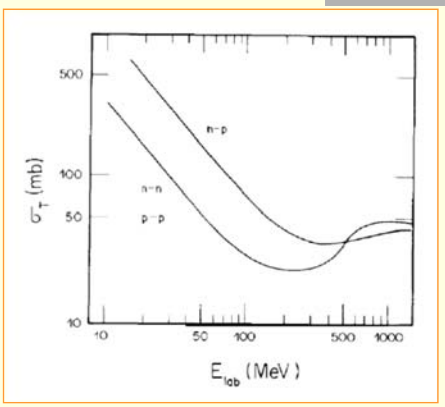

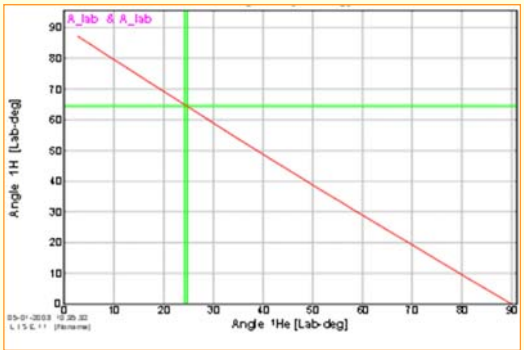

QFS:

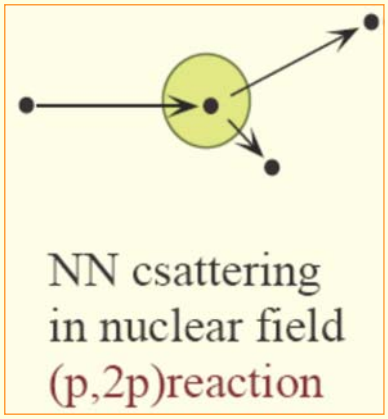

NN csattering in nuclear field (p,2p)reaction

Observables:
- Separation energy
- Momentum correlation

Differences to free NN:
- Fermi motion;
- Multiple collision;
- Wave distortion;
- Medium effects;
- Short range correlation and decay of the hole state decay

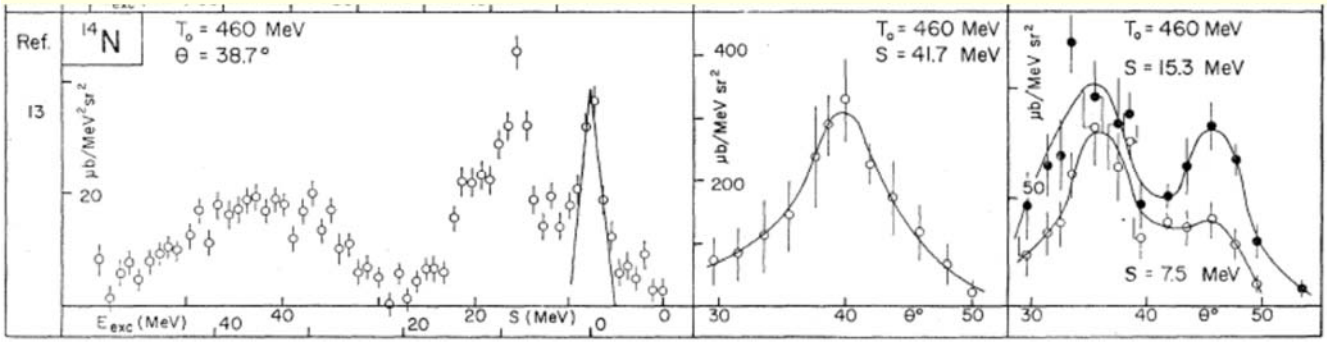

- Being able to investigate in the inner shell of nuclei
- Three arguments:

i) mean free path: $R = \frac{1}{\rho\sigma}$

must be large enough to get deep into the nucleus, and to avoid multi-scattering

ii) wave length: small enough to avoid collective excitation (no problem for a proton)

iii) high momentum transfer for a localized interaction

requiring high energy (100-1000 MeV p) for probing inner orbits; but moderate energy is ok for probing surface nucleons (low binding)

RMP38(1966)121; RMP45(1973)6

Ex. and Q.:

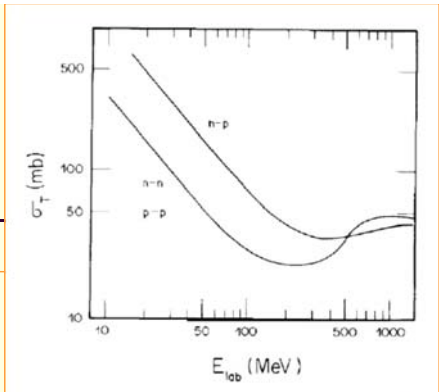

- Ex: For the core area: ρ~ 0.1 N/fm^3;
  at about 300 MeV, σ~ 40 mb,
  then R ~ 2.5 fm.
  quite large QFS, but multiple collisions are inevitable but may have a wide momentum distribution.
- Q: at 80 MeV, σ~ 100 mb, to keep R ~ 2.5 fm,
  What is the pregion to be probed?

E_p（MeV）	50	100	200	500	800
P_p(MeV/c)	312	447	647	1095	1471
ƛ (fm)	0.63	0.44	0.30	0.18	0.13

Sensitivity

Differing Sensitivity to the BSWF

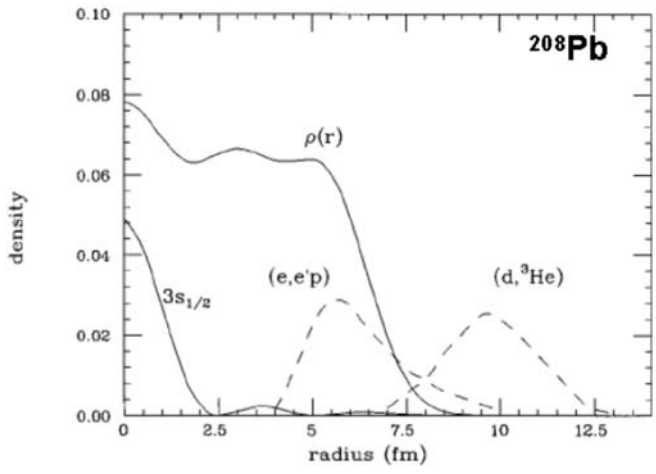

V.R. Pandharipande et al., Rev. Mod. Phys. 69 (1997) 981.

Theoretical description

[A.G. Sitenko, "Theory of Nuclear Reaction", 1990]

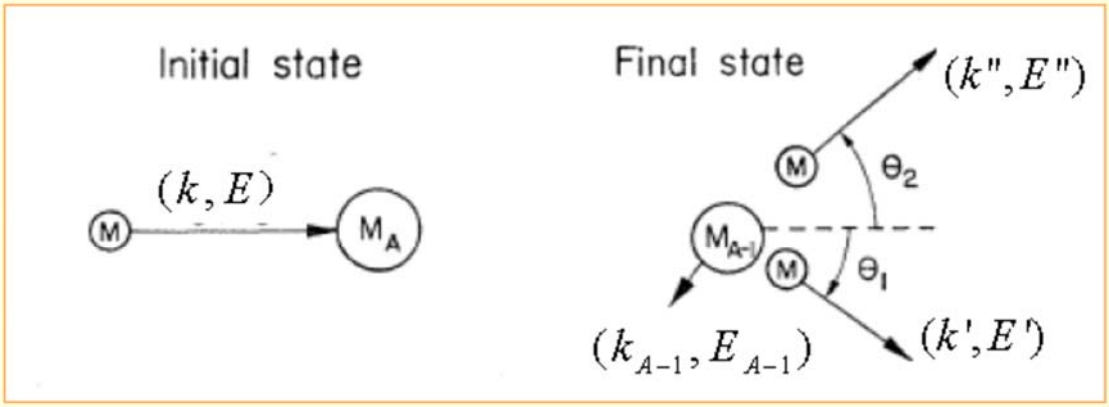

$$k = k' + k'' + k_{A-1} \qquad E = E' + E'' + E_{A-1} + E^*_{A-1} - Q,$$

$$S = E - E' - E'' - E_{A-1} \qquad S = |Q| + E^*_{A-1}$$

PWIA

$$\mathrm{f}(k;k',k'') = -\frac{\mu'}{2\pi\hbar^2}\int dr \int dr_1 e^{-ik'r - ik''r_1} t(r - r_1) e^{ikr} \phi(r_1),$$

$$\phi(r) = \int d\varsigma \phi^*_{A-1}(\varsigma)\phi_A(r,\varsigma)$$

$$\mathrm{f}(k;k',k'') = \frac{\mu'}{\mu} f(k-k') \int dr_1 e^{i(k-k'-k'')r_1}\phi(r_1),$$

$$d\sigma_{p,2p} = (\frac{\mu'}{\mu})^2 \frac{k'}{k}\sigma(k-k')\left|g(k-k'-k'')\right|^2 \frac{dk'}{(2\pi)^3}\mathrm{d}o'',$$

Where $\sigma(q) = |f(q)|^2$ is the two-nucleon interaction cross action

$$\left|g(k-k'-k'')\right|^2 = \left|\int dr e^{i(k-k'-k'')r}\phi(r)\right|^2 \qquad \phi(r) \equiv \phi_{\alpha ljM}(r)$$

DWIA

$$d\sigma_{p,2p} = \frac{1}{8\pi^3}\left(\frac{\mu'}{\mu}\right)^2 \frac{k'}{k}\frac{k''E^2}{\hbar^2 c^2 \tilde{E}}\overline{\sigma(\mathrm{k\text{-}k'})}\frac{1}{2I_A+1}\cdot$$

$$\cdot \sum_{M_A, M_{A-1}} \left| g_{M_A, M_{A-1}}(k-k'-k'') \right|^2 dE' d\sigma' d\sigma'',$$

where

Distorted waves

$$g_{M_A, M_{A-1}}(k-k'-k'') \equiv \int dr \psi^*_{k'}(r)\psi^*_{k''}(r)\psi_k(r) d\varsigma \phi^*_{M_{A-1}}(\varsigma)\phi_{M_A}(r,\varsigma).$$

$$E = Mc^2\sqrt{1+\left(\frac{\hbar k}{Mc}\right)^2}, E' = Mc^2\sqrt{1+\left(\frac{\hbar k'}{Mc}\right)^2},$$

$$\tilde{E} = Mc^2\sqrt{1+\left(\frac{\hbar(k-k'-k'')}{Mc}\right)^2}.$$

RCNP：Experimental facility and performance

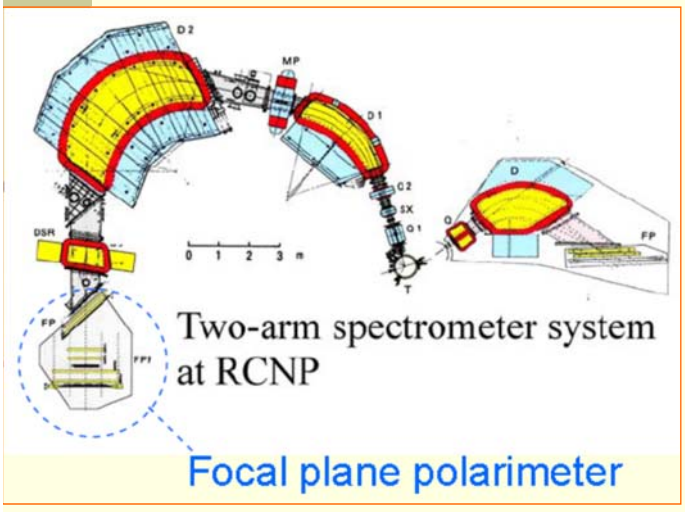

Two-arm spectrometer system at RCNP

Focal plane polarimeter

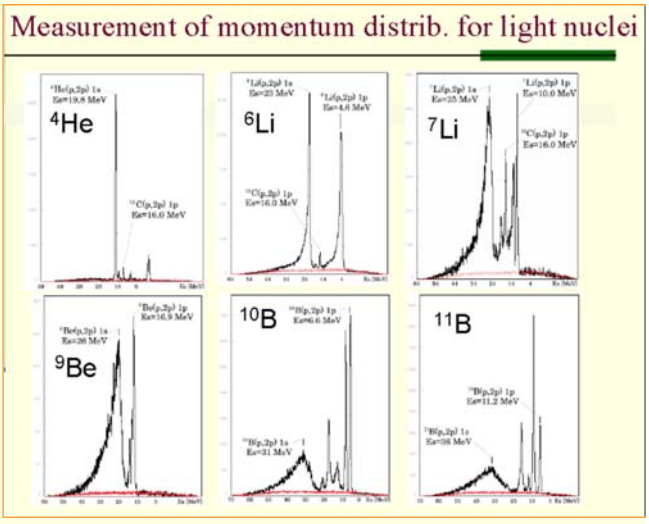

III. Knockout reaction with unstable projectile

VOLUME 42, NUMBER 1 PHYSICAL REVIEW LETTERS 1 JANUARY 1979

Observation of New Neutron-Rich Isotopes by Fragmentation of 205-MeV/Nucleon ^{40}Ar Ions

T. J. M. Symons, Y. P. Viyogi,[a] G. D. Westfall, P. Doll,[b] D. E. Greiner, H. Faraggi,[c] P. J. Lindstrom, and D. K. Scott
Lawrence Berkeley Laboratory, University of California, Berkeley, California 94720

and

H. J. Crawford and C. McParland
Space Sciences Laboratory, University of California, Berkeley, California 94720

(Received 1 November 1978)

Yields of projectile fragments have been measured at 0° for the reaction of 205-MeV/nucleon ^{40}Ar ions on an 860-mg-cm^{-2} carbon target. Mass resolution was achieved using a combination of magnetic analysis and energy-loss measurements. The isotopes ^{28}Ne and ^{35}Al have been observed for the first time.

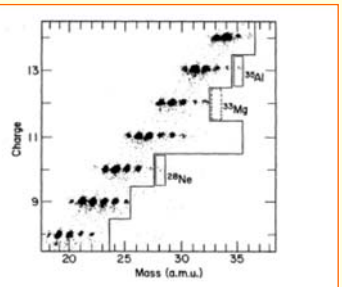

FIG. 1. Scatter plot of data obtained from the reaction of 205-MeV/nucleon ^{40}Ar ions on a carbon target. The line running through the figure indicates the previously known limit of stability.

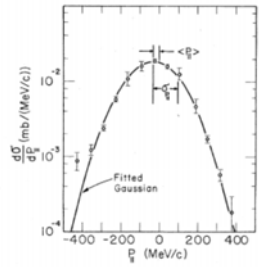

FIG. 1. The projectile-frame parallel-momentum distribution for ^{15}Be fragments from ^{12}C at 2.1 GeV/nucleon on a Be target. The mean momentum $\langle P_{\parallel} \rangle = -30$ MeV/c and standard deviation $\sigma_{P_{\parallel}} = 129$ MeV/c are indicated.

Discovery of halo nucleus

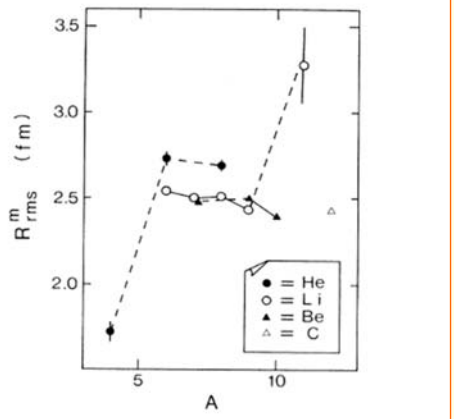

FIG. 3. Matter rms radius R^m_{rms}. Lines connecting isotopes are only guides for the eye. Differences in radii are seen for isobars with $A = 6, 8$, and 9. The ^{11}Li isotope has a much larger radius than other nuclei.

PRL55(1985)2676

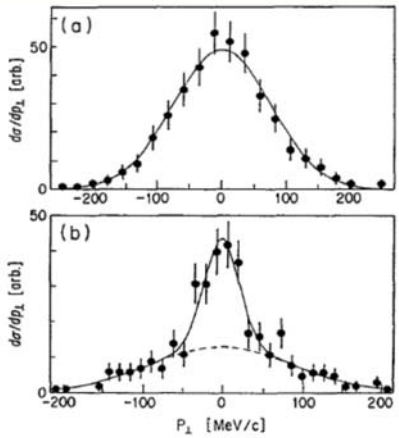

FIG. 1. Transverse-momentum distributions of (a) ^{6}He fragments from reaction ^{8}He+C and (b) ^{9}Li fragments from reaction ^{11}Li+C. The solid lines are fitted Gaussian distributions. The dotted line is a contribution of the wide component in the ^{9}Li distribution.

PRL60(1988)2599

Observation of Soft (Pygmy) GDR

PLB232(1989)51

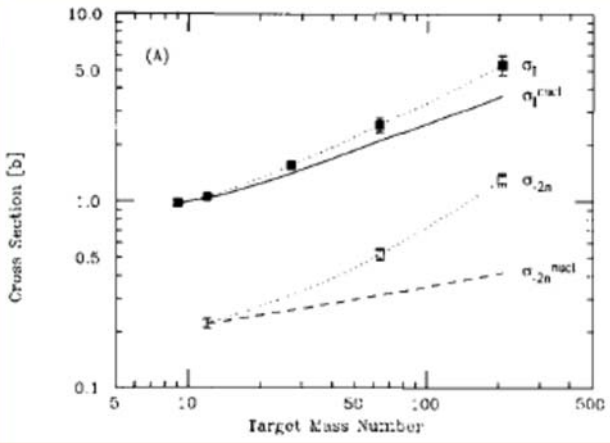

Fig. 1. (a) Target mass dependence of the interaction cross section σ_I (closed square) and the two-neutron-removal cross section σ_{-2n} (open square) for a ^{11}Li projectile at 0.8 GeV/nucleon. Nuclear cross sections, σ_I^{nucl} and σ_{-2n}^{nucl}, are shown by the solid and the dashed line, respectively. (b) Target charge dependence of σ_I^{EMD} (closed square) and σ_{-2n}^{EMD} (open square) for ^{11}Li. Lines are fit to the data by Z_T^{α}.

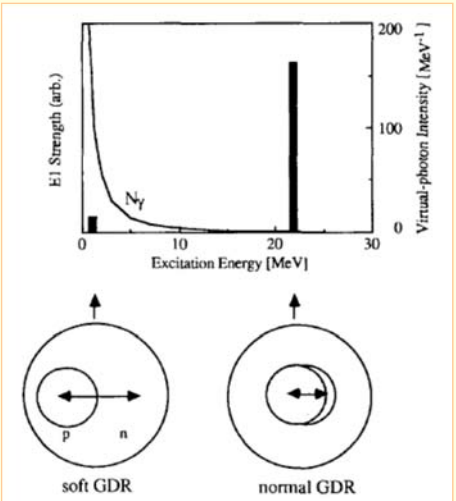

Fig. 2. Schematic pictures of the soft and the normal GDR in the extremely neutron-rich nucleus with a neutron halo. The dipole oscillation between protons (shaded area) and neutrons (white area) is shown. The E1 strength (black bar) of the soft and the normal GDR is shown together with the virtual photon spectrum seen by the ^{11}Li projectile on a Pb target at 0.8 GeV/nucleon.

Magnetic spectrometer in dispersion matched mode: $P_{//}$ measurement

PRL69(1992)2050

$$\vec{k}_3 = \frac{A-1}{A}\vec{k}_A - \vec{k}_{A-1}$$

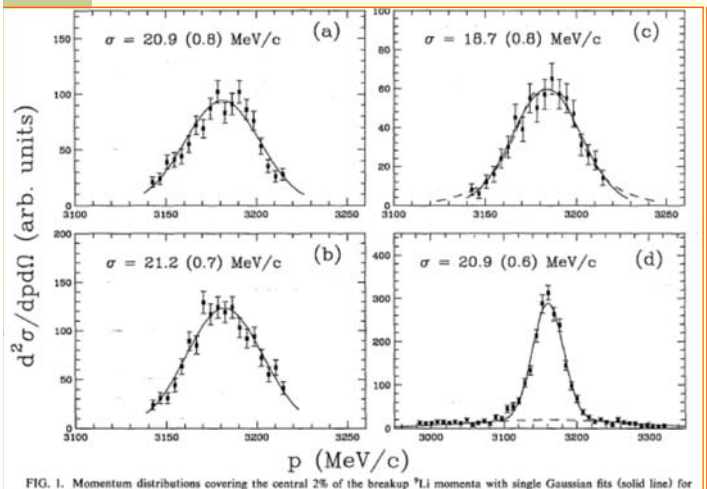

FIG. 1. Momentum distributions covering the central 2% of the breakup ^{9}Li momenta with single Gaussian fits (solid line) for high acceptance mode measurements using (a) ^{9}Be, (b) ^{93}Nb, and (c) ^{181}Ta targets. The dashed line in (c) shows the prediction of Esbensen and Bertsch [23]. (d) The high acceptance mode distribution for a 10% range of ^{9}Li momenta using a ^{9}Be target. A two-Gaussian fit is shown ($\sigma = 20.9 \pm 0.6$ MeV/c and 112 ± 13 MeV/c).

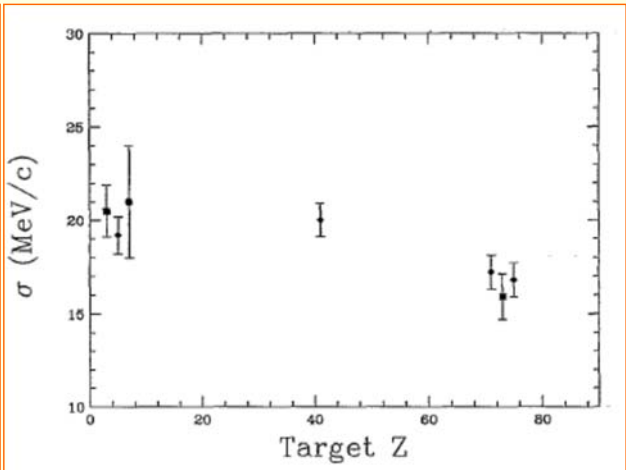

FIG. 2. Target Z dependence of the widths (Table I) of the momentum distributions for the medium (squares) and high (diamonds) acceptance mode measurements. The result of Kobayashi *et al.* [10] is indicated by the circle.

Identification of sequential decay process for borromean nuclei (not sudden breakup)

NPA567(1994)97; NPA598(1996)418

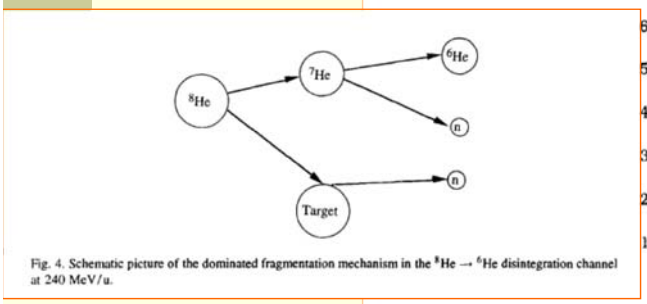

Fig. 4. Schematic picture of the dominated fragmentation mechanism in the ^{8}He → ^{6}He disintegration channel at 240 MeV/u.

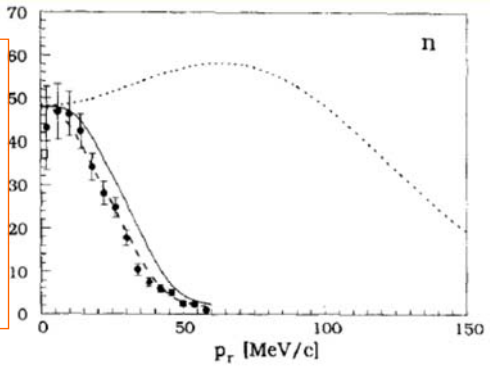

Fig. 7. Radial momentum distribution of neutrons detected in coincidence with ^{6}He from reaction of ^{8}He with a carbon target at the energy 240 MeV/u. The curves were calculated with a COSMA wave function for ^{8}He together with the reaction mechanism in Fig. 4. The fully drawn and the dashed curves correspond to the resonance energies E_0 = 0.44 and 0.32 MeV, respectively. For comparison we also show, as a dotted curve, the very broad momentum distribution obtained in the sudden approximation, i.e. Eq. (8) integrated over longitudinal momenta p_z. This broad distribution just corresponds to the neutron momentum distribution inside ^{8}He.

Spectroscopy with knockout reactions

[ARNPS53(2003)219]

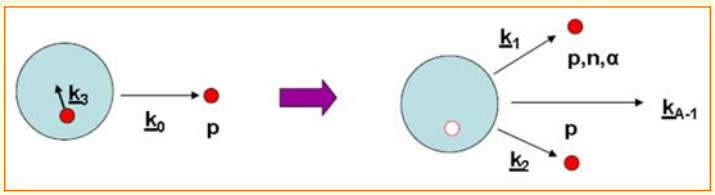

$$\vec{k}_3 = \frac{A-1}{A}\vec{k}_A - \vec{k}_{A-1}$$

NIMB204(2003)90

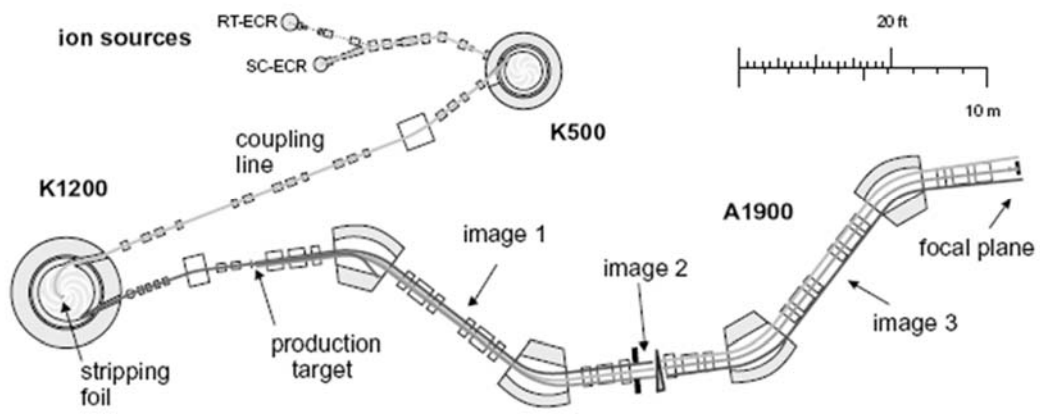

Fig. 1. A schematic diagram of the coupled cyclotron facility and the operation of the A1900 fragment separator, see the text.

NIMB204(2003)629

The S800 spectrograph

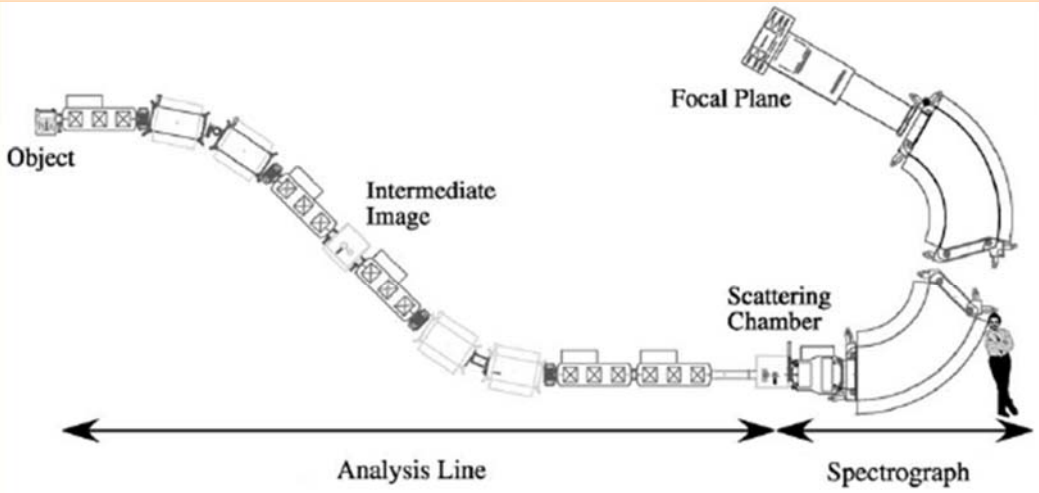

Fig. 1. The S800 spectrograph. See text for details.

Part II

Y. Ye

????

- Why you need so many big facilities?
- Concerning knockout, can you choose which nucleon to be knockout out?

I. Introduction

- **breakup** （破碎）

  Elastic (diffractive) breakup

  (nuclear or coulomb breakup);

  Inelastic (stripping) breakup

- **knockout** （敲出）

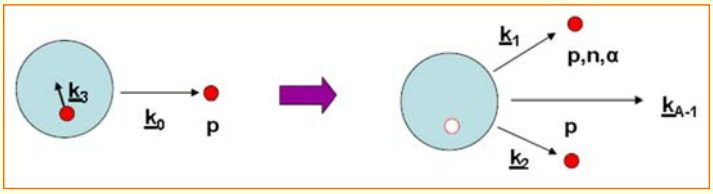

$$\vec{k}_3 = \frac{A-1}{A}\vec{k}_A - \vec{k}_{A-1}$$

$$k_0 - k_1 - k_2 = -k_3$$ (QFS)

Knockout : (new shell, SF…)

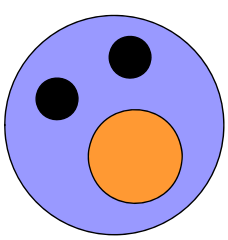

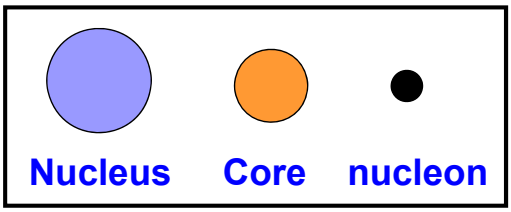

Spectroscopy with knockout reactions

[ARNPS53(2003)219]

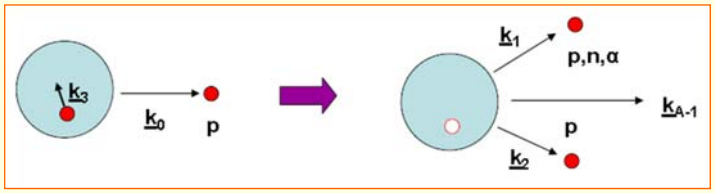

$$\vec{k}_3 = \frac{A-1}{A}\vec{k}_A - \vec{k}_{A-1}$$

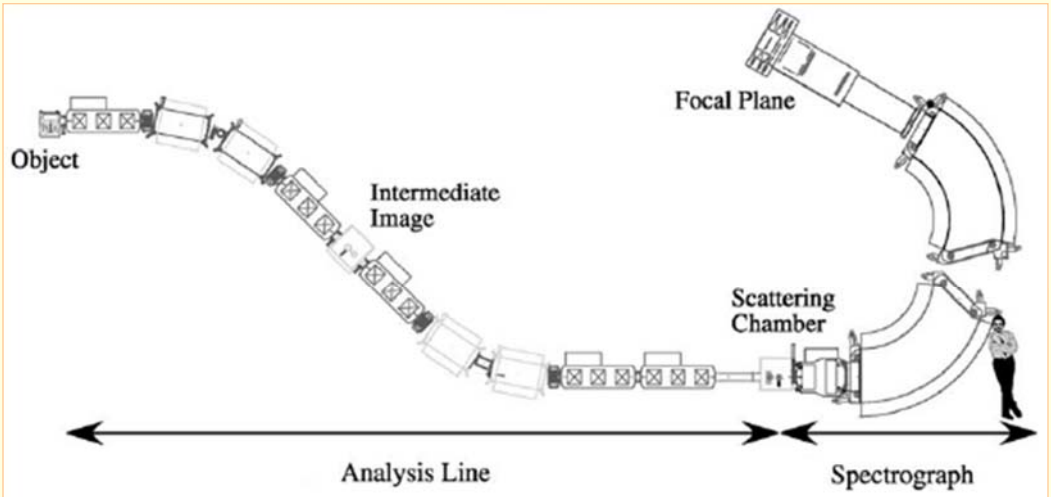

NIMB204(2003)629

Fig. 1. The S800 spectrograph. See text for details.

An example for knockout spectroscopy

PHYSICAL REVIEW C **78**, 011303(R) (2008)

$d_{5/2}$ proton hole strength in neutron-rich ^{43}P: Shell structure and nuclear shapes near $N = 28$

National Superconducting Cyclotron Labora-

^{48}Ca 140 MeV/nucleon

705 mg/cm^2 ^{9}Be

A1900 ^{44}S beam, with a purity of 81% 91.7 MeV/nucleon

thick ^{9}Be 376 mg/cm^2

S800 magnetic spectrograph

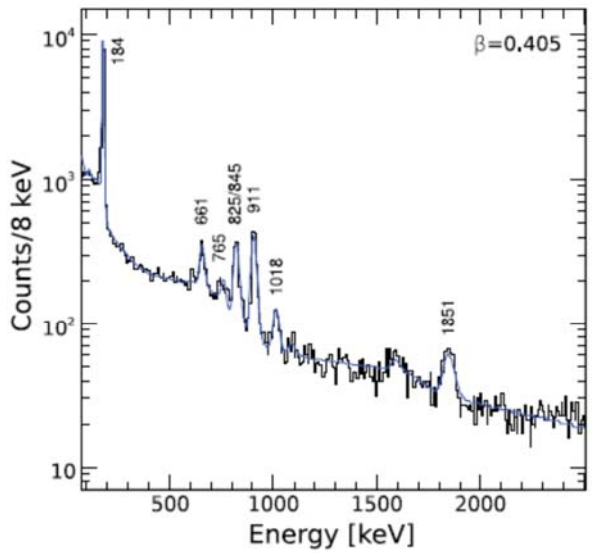

FIG. 1. (Color online) Doppler-corrected spectrum of γ rays measured in coincidence with recoiling ^{43}P particles. The solid curve is the GEANT3 fit described in the text.

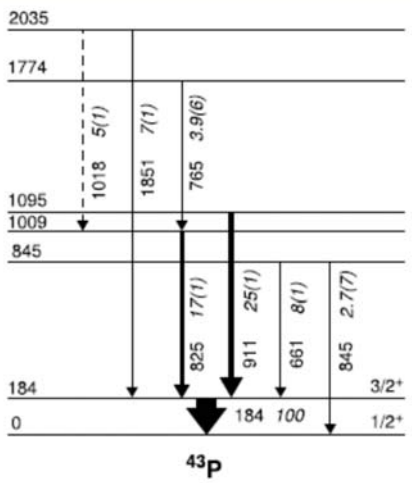

FIG. 3. Proposed level scheme of ^{43}P based on the present work. Gamma-ray intensities from the fitting process, relative to that of the 184-keV transition, appear in italics.

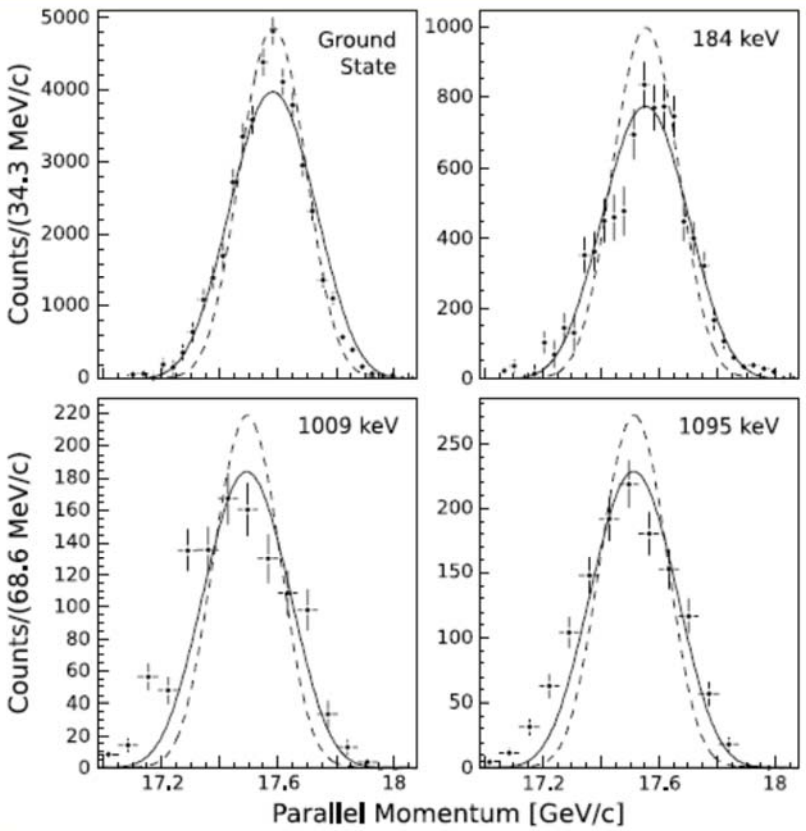

FIG. 4. Parallel momentum distributions of states of ^{43}P populated in one-proton knockout from ^{44}S. The curves are theoretical distributions, described in the text, for $l = 0$ (dashed) and $l = 2$ (solid).

TABLE I. Excitation energies, spins and parities J^π, single-particle configurations nlj, measured knockout branching ratios BR, measured partial cross sections σ, and single-particle cross sections σ_{sp} from reaction theory.

E_{level} (keV)	J^π ($\hbar$)	nlj	BR (%)	σ (mb)	σ_{sp} (mb)
0	$1/2^+$	$2s_{1/2}$	24(4)	2.3(4)	8.37
184	$3/2^+$	$1d_{3/2}$	33(2)	3.1(3)	7.00
845	$(5/2^+)$	$(1d_{5/2})$	4(1)	0.37(7)	7.73
1009	$(5/2^+)$	$1d_{(5/2)}$	8(2)	0.8(2)	7.70
1095	$(5/2^+)$	$1d_{(5/2)}$	20(1)	1.9(2)	7.68
1774	$(5/2^+)$	$(1d_{5/2})$	4(1)	0.4(1)	7.55
2035	$(5/2^+)$	$(1d_{5/2})$	7(2)	0.7(2)	7.50

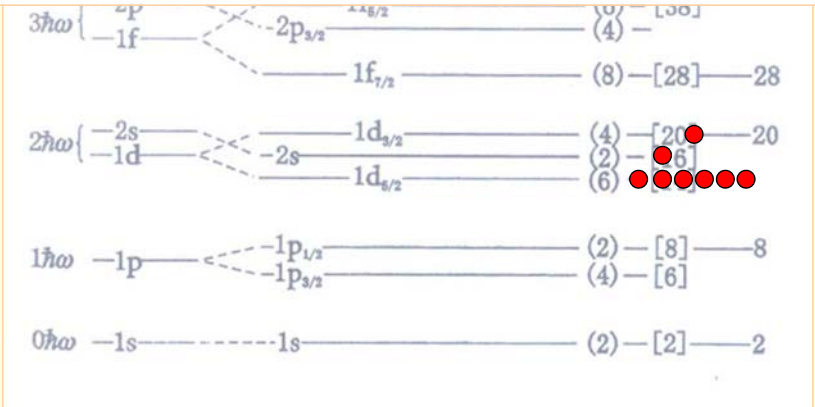

Very Larger reduction of SF observed for very asymmetrical system

PHYSICAL REVIEW C 77, 044306 (2008)

Reduction of spectroscopic strength: Weakly-bound and strongly-bound single-particle states

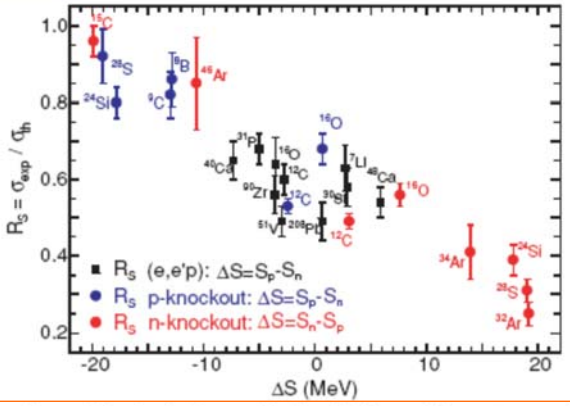

eikonal-model calculations with the shell-model spectroscopic factor C^2S:

$$\sigma_{th}(nJ^{\pi}) = \left(\frac{A}{A-1}\right)^N C^2S\,\sigma_{sp}(l, B_n), \qquad (1)$$

where N is the oscillator quantum number, l is the angular momentum, and B_n is the binding energy of the orbital from which the nucleon is removed.

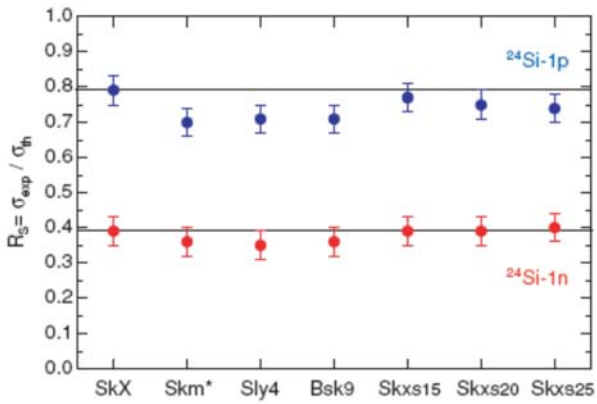

FIG. 7. (Color online) Deduced values of R_s for the reactions ^{9}Be(^{24}Si,^{23}Al)X and ^{9}Be(^{24}Si,^{23}Si)X as obtained using different Skyrme parametrizations as input to the HF calculations used for the reaction methodology. The R_s factors obtained when using the Skm*, Sly4, Bsk9, Skxs15, Skxs20, and Skxs25 interactions agree within the quoted uncertainties on the value deduced using the SkX Skyrme parametrization used here. The SkX values are indicated by the horizontal lines.

Puzzle in SF of unstable nuclei

PRL **104,** 112701 (2010) PHYSICAL REVIEW LETTERS week ending 19 MARCH 20

Neutron-Proton Asymmetry Dependence of Spectroscopic Factors in Ar Isotopes

Jenny Lee (李曉菁),[1] M. B. Tsang (曾敏兒),[1] D. Bazin,[1] D. Coupland,[1] V. Henzl,[1] D. Henzlova,[1] M. Kilburn,[1]

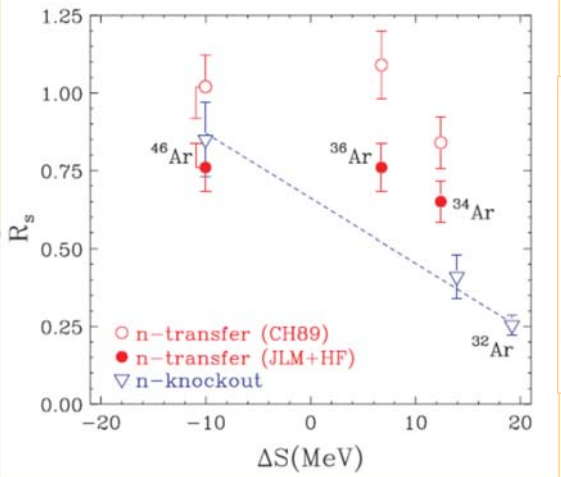

FIG. 2 (color online). Reduction factors Rs = SF(expt)/SF(LB-SM) as a function of the difference between neutron and proton separation energies, ΔS. The solid and open circles represent Rs deduced in JLM + HF and CH89 approach using the present transfer reaction data, respectively. The open triangles denote the Rs from knockout reactions [11]. The dashed line is the best fit of Rs of ^{32,34,46}Ar from knockout reactions. The use of different ΔS values from the present work and knockout reactions in Ref. [11] is explained in Ref. [28].

Possible complex processes related to knockout of deeply bound nucleons

PHYSICAL REVIEW C **83**, 011601(R) (2011)

Nucleon removal from unstable nuclei investigated via intranuclear cascade

(Rec … 2011)

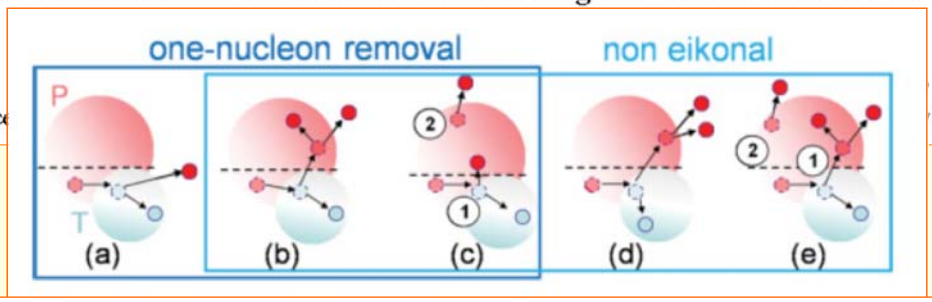

This new approach is at the interface between the standard cascade-evaporation treatment with poor nuclear-structure content and the microscopic eikonal approach that assumes the projectile as an inert core and a single-particle wave function.

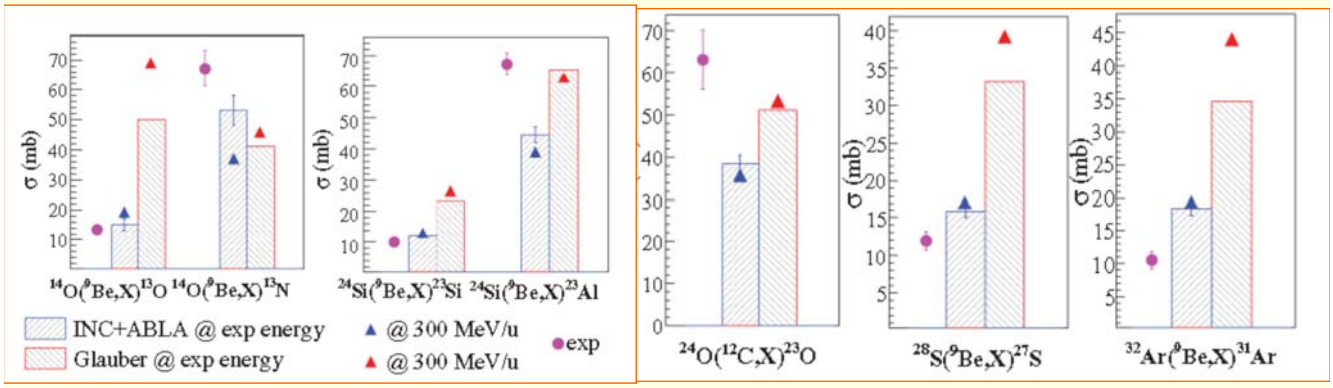

S_n=23.1 MeV **S_p=4.6 MeV** **S_n=21.1 MeV** **S_p=3.3 MeV** **S_n=3.7 MeV** **S_n= 21.5 MeV** **S_n= 17.9 MeV**

FIG. 3. (Color online) One-neutron and one-proton removal cross sections for the very asymmetric nuclei ^{14}O, ^{24}Si, ^{24}O, ^{28}S, and ^{32}Ar. Experimental data (pink dots) are compared to the present work (blue bars) and eikonal predictions (red bars). The energy dependence of the two formalisms is illustrated by calculations for an incident energy of 300 MeV/nucleon (triangles).

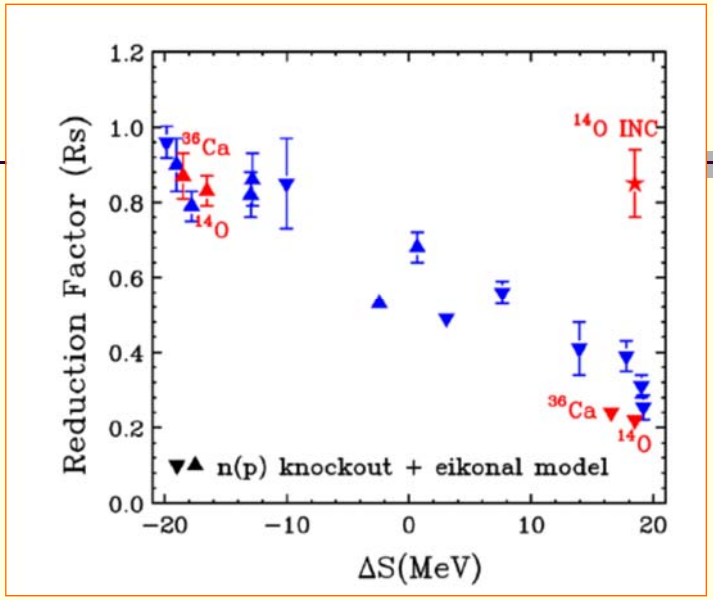

The agreement for deeply bound nucleon removal is remarkable and represents the first microscopic calculation that reproduces these low cross sections. The observed good agreement may still be partly fortuitous in these cases as our work gives lower cross sections than the eikonal theory in most of studied reactions. Nevertheless, in the case of loosely bound nucleons, the present approach still gives reasonable values compared to experimental data. (but worse then Glauber!)

Appendix: Glauber model for halo nucleus

Y. Suzuki et al, "Structure and Reaction of Light Exotic Nuclei", 2003)

The eikonal approximation

$\Psi(\vec{r}) = e^{ikz}\hat{\Psi}(\vec{r})$ $\quad$ $\hat{\Psi}(\vec{r})$ is supposed not to oscillate rapidly and satisfait :

$$\left(vp_z + \frac{\vec{p}^2}{2m}\right)\hat{\Psi}(\vec{r}) + V(r)\hat{\Psi}(\vec{r}) = 0$$

i) The momentum unceartainty produced is $\delta p \sim \hbar / a$, which should be much smaller than the incident momentum $\hbar k$. That is $1/ka << 1$, or $\lambda\!\!\!^{-} << a$, which is equivalent to semiclassic or diffraction condition.

ii) The momentun transfer $\Delta p = F \cdot \Delta t \approx \frac{V}{a} \cdot \frac{2a}{v} = \frac{2V}{v}$ should be much smaller then $p = mv$,

$\frac{\Delta p}{p} = \frac{2V}{mv^2} = \frac{V}{E} << 1$. Here V is the average depth of the interaction potential.

Under these two conditions we neglect the p^2 term and $\hat{\Psi}(\vec{r})$ satisfait

$$\frac{\partial}{\partial z}\hat{\Psi}(\vec{r}) = \frac{1}{i\hbar v}V(r)\hat{\Psi}(\vec{r}) \quad \text{and} \quad \hat{\Psi}(x,y,z) = \exp\left[\frac{1}{i\hbar v}\int_{-\infty}^{z} dz' V(x,y,z')\right]$$

$$\Psi(\vec{r}) = \exp\left[ikz + \frac{1}{i\hbar v}\int_{-\infty}^{z} dz' V(x,y,z')\right]$$

$$f(\theta) = -\frac{2m}{4\pi\hbar^2}\int dr \exp\left[-i\vec{k}'\cdot\vec{r} + ikz + \frac{1}{i\hbar v}\int_{-\infty}^{z} dz' V(x,y,z')\right] V(r)$$

For small angle scattering (even inelastic) $\vec{q} = \vec{k}' - \vec{k}$ is approximately perpendicular to $\vec{k}$, and $-i\vec{k}'\cdot\vec{r} + ikz = -i\vec{q}\cdot\vec{r} = -i\vec{q}\cdot\vec{b}$ with $\vec{b}$ the impact parameter. Using

$$\int_{-\infty}^{+\infty} dz V(x,y,z) \exp\left[\frac{1}{i\hbar v}\int_{-\infty}^{z} dz' V(x,y,z')\right] = i\hbar v\left[\exp\left[\frac{1}{i\hbar v}\int_{-\infty}^{z} dz' V(x,y,z')\right]\right]_{z=-\infty}^{z=+\infty}$$

it can be deduced

$$f(\theta) = \frac{ik}{2\pi}\int d\vec{b} e^{-i\vec{q}\cdot\vec{b}}[1 - e^{i\chi(\vec{b})}]$$

Ex: Comparing with Born approximation

with the phase shift function $\chi(\vec{b}) = -\frac{1}{\hbar v}\int_{-\infty}^{+\infty} dz' V(\vec{b} + z'\hat{z})$

For a spherically symmetric potential

$$f(\theta) = ik\int_0^{\infty} db\, bJ_0(qb)[1 - e^{i\chi(\vec{b})}]; \qquad J_0(x) = \frac{1}{2\pi}\int_0^{2\pi} d\phi\, e^{ix\cos\phi}$$

$$\sigma_{el} = \int d\Omega\, |f(\theta)|^2 = \int d\vec{b}\, |1 - e^{i\chi(\vec{b})}|^2$$

having used $d\Omega = \frac{d\vec{q}}{k^2}$ and $\int dq\, e^{-i\vec{q}\cdot(\vec{b}-\vec{b}')} = (2\pi)^2\delta(\vec{b} - \vec{b}')$

$$\sigma_{abs} = \int d\vec{b}\left[1 - |e^{i\chi(\vec{b})}|^2\right] = \int d\vec{b}\left[1 - e^{-2\,\mathrm{Im}\,\chi(\vec{b})}\right]$$

$$\sigma_{tot} = \int d\vec{b}\, 2\left[1 - \mathrm{Re}\, e^{i\chi(\vec{b})}\right]$$

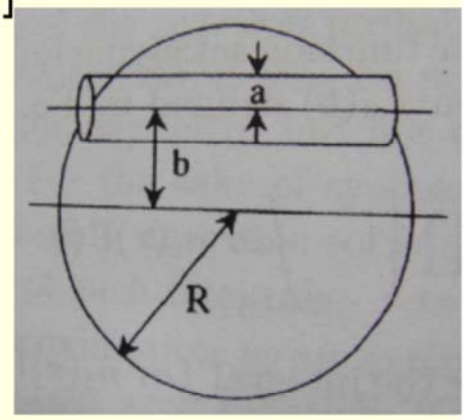

With Coulomb potential

$$\chi_C(\vec{b}) = -\frac{Ze^2}{4\pi\varepsilon_0\hbar v}\int_{-\infty}^{+\infty} dz \frac{1}{\sqrt{b^2 + z^2}}$$

$$f(\theta) = \frac{ik}{2\pi}\int d\vec{b}\, e^{-i\vec{q}\cdot\vec{b}}[1 - e^{i\chi_C(\vec{b}) + i\chi_N(\vec{b})}]$$

Medium-energy reaction of Halo nuclei

1. Elastic scattering of stable nuclei

$$\chi_{el}^{OLA}(\vec{b}) = \int d\vec{r}^{\,P} \int d\vec{r}^{\,T} \rho_P(\vec{r}^{\,P}) \rho_T(\vec{r}^{\,T}) \chi(\vec{b} + \vec{s}^{\,P} - \vec{s}^{\,T})$$

Normally a substantial reduction of the real strength is need for weakly bound projectile, combined with a phenomenological imaginary term for χ to account for the correlations.

2. Few-body model

$$f_{el}(\theta) = \frac{iK}{2\pi} \int d\vec{b} e^{-i\vec{q}\cdot\vec{b}} \left[1 - \left\langle \phi_0 \left| e^{i\chi_{CT}(\vec{b} - \frac{\vec{s}}{A_P}) + i\chi_{nT}(\vec{b} - \frac{A_P - 1}{A_P}\vec{s})} \right| \phi_0 \right\rangle \right]$$

$$f_k(\theta) = -\frac{iK}{2\pi} \int d\vec{b} e^{-i\vec{q}\cdot\vec{b}} \left\langle \phi_k \left| e^{i\chi_{CT}(\vec{b} - \frac{\vec{s}}{A_P}) + i\chi_{nT}(\vec{b} - \frac{A_P - 1}{A_P}\vec{s})} \right| \phi_0 \right\rangle$$

with ϕ_0 the valence nucleon bound state and ϕ_k the elestic breakup state.

$$\sigma_{el} = \int \frac{d\vec{q}}{K^2} |f_{el}(\theta)|^2 = \int d\vec{b} \left| 1 - \left\langle \phi_0 \left| e^{i\chi_{CT}(\vec{b} - \frac{\vec{s}}{A_P}) + i\chi_{nT}(\vec{b} + \frac{A_P - 1}{A_P}\vec{s})} \right| \phi_0 \right\rangle \right|^2$$

$$\sigma_{tot} = \frac{4\pi}{K} \mathrm{Im}\, f_{el}(0) = 2 \int d\vec{b}\, \mathrm{Re} \left[1 - \left\langle \phi_0 \left| e^{i\chi_{CT}(\vec{b} - \frac{\vec{s}}{A_P}) + i\chi_{nT}(\vec{b} + \frac{A_P - 1}{A_P}\vec{s})} \right| \phi_0 \right\rangle \right]$$

$$= 2 \int d\vec{b}_C\, \mathrm{Re} \left[1 - \left\langle \phi_0 \left| e^{i\chi_{CT}(\vec{b}_C) + i\chi_{nT}(\vec{b}_C + \vec{s})} \right| \phi_0 \right\rangle \right]$$

where $\vec{b}_C = \vec{b} - \frac{\vec{s}}{A_P}$; $\vec{b}_n = \vec{b} + \frac{A_P - 1}{A_P}\vec{s}$

or $\vec{b} = \frac{A_P - 1}{A_P}\vec{b}_C + \frac{1}{A_P}\vec{b}_n$; $\vec{s} = \vec{b}_n - \vec{b}_C$

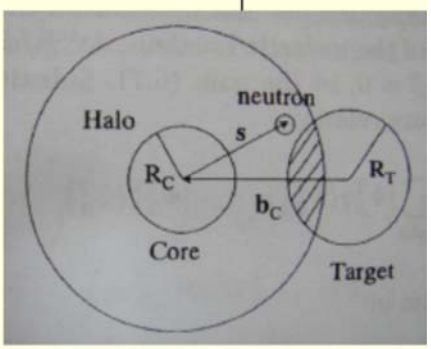

$$\sigma_{reac} = \sigma_{tot} - \sigma_{el} = \int d\vec{b} \left[1 - \left| \left\langle \phi_0 \left| e^{i\chi_{CT}(\vec{b} - \frac{\vec{s}}{A_P}) + i\chi_{nT}(\vec{b} + \frac{A_P - 1}{A_P}\vec{s})} \right| \phi_0 \right\rangle \right|^2 \right]$$

Calculating χ_{CT} and χ_{nT} fron optical potential would give good results.

$$\sigma_{-n}^{el} = \int \frac{d\vec{q}}{K^2} \int d\vec{k} \left| f_k(\theta) \right|^2 = \int d\vec{k} \int d\vec{b} \left\langle \phi_0 \left| e^{i\chi_{cT}^* + i\chi_{nT}^*} \right| \phi_k \right\rangle \left\langle \phi_k \left| e^{i\chi_{cT} + i\chi_{nT}} \right| \phi_0 \right\rangle$$

$$= \int d\vec{b} \left[\left\langle \phi_0 \left| e^{-2\mathrm{Im}\chi_{cT}(\vec{b} - \frac{\vec{s}}{A_p}) - 2\mathrm{Im}\chi_{nT}(\vec{b} - \frac{A_p - 1}{A_p}\vec{s})} \right| \phi_0 \right\rangle - \left| \left\langle \phi_0 \left| e^{i\chi_{cT}(\vec{b} - \frac{\vec{s}}{A_p}) + i\chi_{nT}(\vec{b} - \frac{A_p - 1}{A_p}\vec{s})} \right| \phi_0 \right\rangle \right|^2 \right]$$

where use was made of the closure relation

$$\int d\vec{k} \left| \phi_k \right\rangle \left\langle \phi_k \right| + \left| \phi_0 \right\rangle \left\langle \phi_0 \right| = 1$$

The absorption due to the excitation of either the core or target is

$$\sigma_{abs} = \sigma_{reac} - \sigma_{-n}^{el} = \int d\vec{b}_C \left[1 - e^{-2\mathrm{Im}\chi_{CT}(\vec{b}_C)} \left\langle \phi_0 \left| e^{-2\mathrm{Im}\chi_{nT}(\vec{b}_C + \vec{s})} \right| \phi_0 \right\rangle \right]$$

$$\sigma_{-n}^{inel} = \sigma_{abs} - \sigma_{reac}^{C}$$

$$= \int d\vec{b}_C \left[1 - e^{-2\mathrm{Im}\chi_{CT}(\vec{b}_C)} \left\langle \phi_0 \left| e^{-2\mathrm{Im}\chi_{nT}(\vec{b}_C + \vec{s})} \right| \phi_0 \right\rangle \right] - \int d\vec{b}_C \left[1 - e^{-2\mathrm{Im}\chi_{CT}(\vec{b}_C)} \right]$$

$$= \int d\vec{b}_C e^{-2\mathrm{Im}\chi_{CT}(\vec{b}_C)} \left[1 - \left\langle \phi_0 \left| e^{-2\mathrm{Im}\chi_{nT}(\vec{b}_C + \vec{s})} \right| \phi_0 \right\rangle \right]$$

Fragment momentum distribution for halo nuclei

Elastic breakup

We treat N + C projectile only. Denoting $\vec{k}$ the momentum of N relative to C, $\vec{q}$ the two - dimentional momentum transfered from the target to the projectile N + C, and $d\vec{q} = K^2 d\Omega$ with K the total momentum of outgoing N + C system, we have the core and N momentum in the projectile rest frame as $\vec{P}$ and $\vec{p}_n$, with

$$\vec{P} + \vec{p}_n = \vec{q}; \qquad \frac{(A_C \vec{p}_n - \vec{P})}{A_p} = \vec{k}$$

$$f_k(\theta) = -\frac{iK}{2\pi} \int d\vec{b} e^{-i\vec{q}\cdot\vec{b}} \left\langle \phi_k \left| e^{i\chi_{cT}(\vec{b} - \frac{\vec{s}}{A_p}) + i\chi_{nT}(\vec{b} - \frac{A_p - 1}{A_p}\vec{s})} \right| \phi_0 \right\rangle$$

$$\frac{d\sigma_{-n}^{el}}{d\vec{q}d\vec{k}} = \frac{d\sigma_{-n}^{el}}{K^2 d\Omega d\vec{k}} = \frac{1}{K^2} \int d\vec{b} \left| f_k(\theta) \right|^2; \quad \frac{d\sigma_{-n}^{el}}{d\vec{k}} = \int d\vec{b} \left| \left\langle \phi_k \left| e^{i\chi_{cT}(\vec{b} - \frac{\vec{s}}{A_p}) + i\chi_{nT}(\vec{b} - \frac{A_p - 1}{A_p}\vec{s})} \right| \phi_0 \right\rangle \right|^2$$

$$\frac{d\sigma_{-n}}{d\vec{P}} = \int d\vec{q} \int d\vec{k} \delta\left(\vec{P} - \frac{A_p - 1}{A_p}\vec{q} + \vec{k} \right) \frac{d\sigma_{-n}}{d\vec{q}d\vec{k}};$$

$$\frac{d\sigma_{-n}}{d\vec{P}_{//}} = \int d\vec{P}_{\perp} \frac{d\sigma_{-n}}{d\vec{P}} = \int d\vec{k} \delta\left(\vec{P}_{//} - k_z \right) \frac{d\sigma_{-n}}{d\vec{k}}$$

Inelastic breakup

In the projectile N + A rest frame, after the collision the core wave function

$$\hat{\Psi}(\vec{b},\vec{r}) = e^{i\chi_{cr}(\vec{b}-\frac{\vec{s}}{A_p})}\phi_0(\vec{r}) = e^{i\chi_{cr}(\vec{s}_c)}\phi_0(\vec{r}_n - \vec{R}_c).$$

having used $\vec{R}_c = \vec{R} - \frac{\vec{r}}{A_p}, \quad \vec{r}_n = \vec{R} + \frac{(A_p - 1)}{A_p}\vec{r}$

The momentum distribution of the core is the Fourier transformation of $\hat{\Psi}$

$$g_c(\vec{b}_n,\vec{P}) = \frac{1}{(2\pi)^3}\left|\int d\vec{R}_c e^{-i\vec{P}\cdot\vec{R}_c + i\chi_{cr}(\vec{s}_c)}\phi_0(\vec{r}_n - \vec{R}_c)\right|^2$$

$$= \frac{1}{(2\pi)^3}\left|\int d\vec{r} e^{i\vec{P}\cdot\vec{r} + i\chi(\vec{b}_n - \vec{s})}\phi_0(\vec{r})\right|^2$$

This should then be mutiplied by neutron probability which excite the target and then integrated over $\vec{b}_n$.

$$\frac{d\sigma_{-n}^{inel}}{d\vec{P}} = \int d\vec{b}_n\left[1 - e^{-2\,\mathrm{Im}\,\chi_{nT}(\vec{b}_n)}\right] = \frac{1}{(2\pi)^3}\left|\int d\vec{r} e^{i\vec{P}\cdot\vec{r} + i\chi(\vec{b}_n - \vec{s})}\phi_0(\vec{r})\right|^2$$

$$\frac{d\sigma_{-n}^{inel}}{dP_{//}} = \int d\vec{P}_\perp \frac{d\sigma_{-n}^{inel}}{d\vec{P}}$$

$$= \int d\vec{b}_c \int d\vec{s} e^{-2\,\mathrm{Im}\,\chi_{cT}(\vec{b}_c)}\left[1 - e^{-2\,\mathrm{Im}\,\chi_{nT}(\vec{b}_c + \vec{s})}\right] \times \frac{1}{2\pi}\left|\int dz e^{iP_{nz}z}\phi_0(\vec{r})\right|^2$$

Roy Glauber, Nobel Prize 2006

Q: Energy dependence of the n removal cross section? Is σ_{-n} semilar to σ_{np} ?

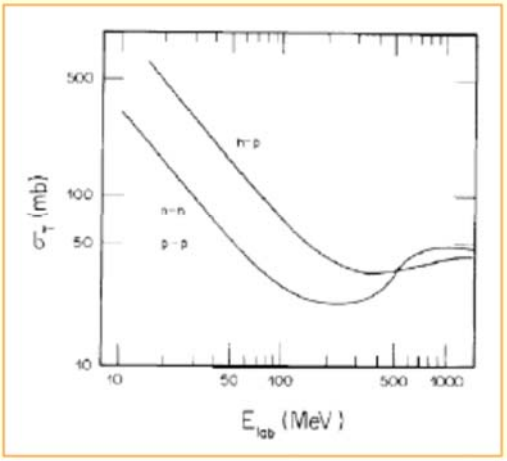

IV. Proton tagged knockout reaction

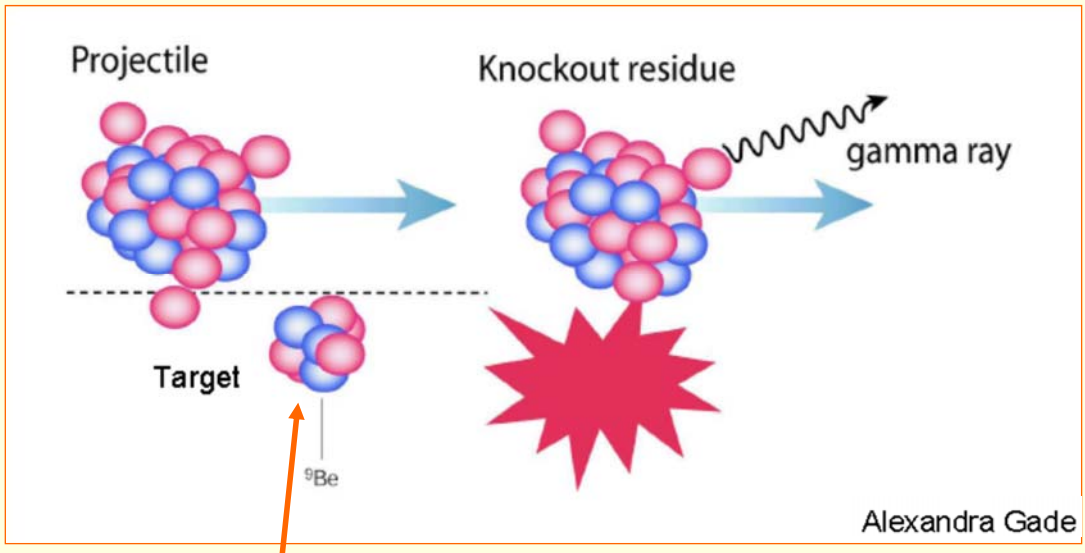

Replaced by proton target?

Knockout : (new shell, SF…)

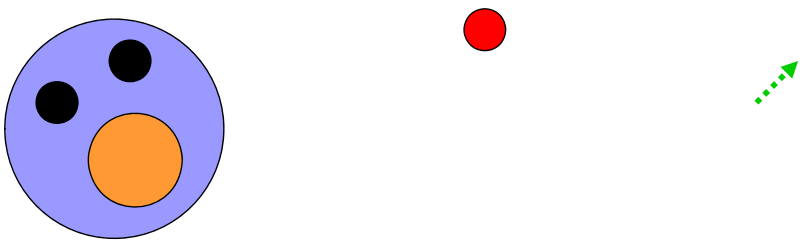

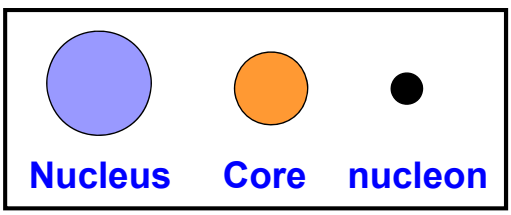

Core knockout: studying the multi- neutron and cluster structure

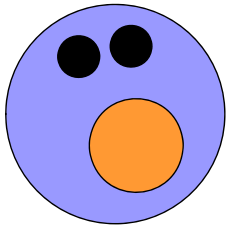

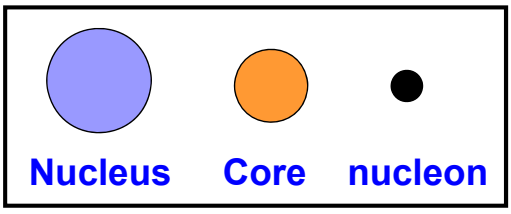

Nuclear Physics A 759 (2005) 43–63

Quasi-free scattering with ^{6,8}He beams

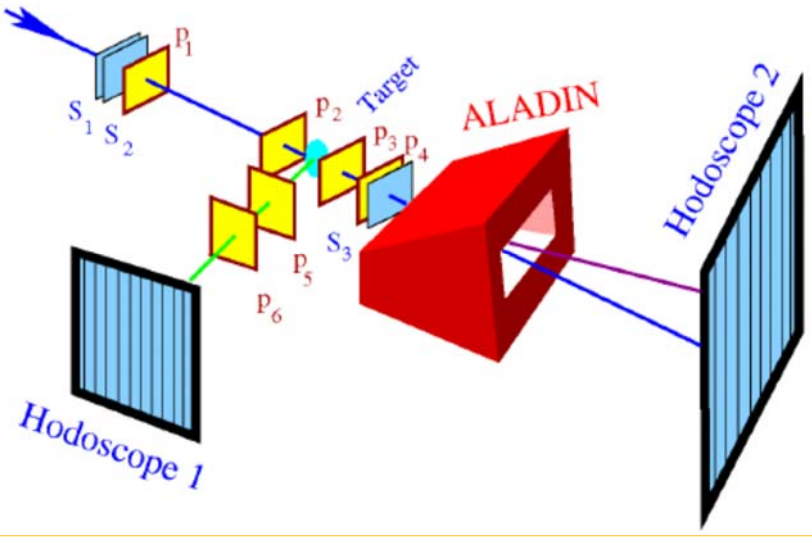

At anout 700 MeV/u, No neutron detection

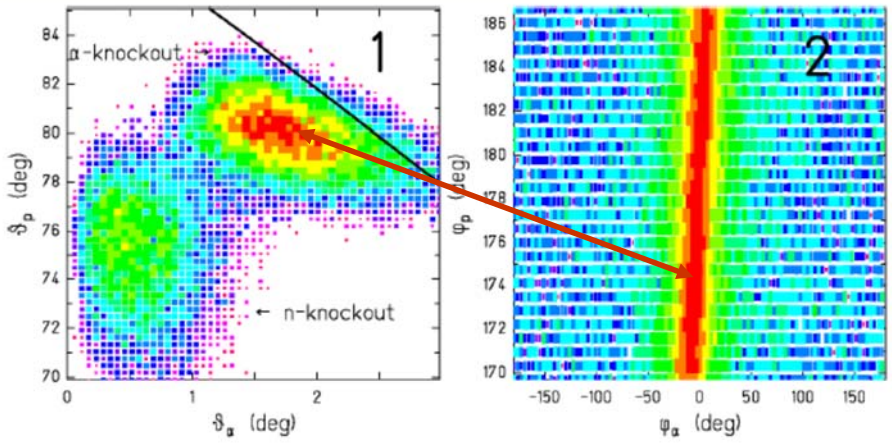

Fig. 5. Correlations between angles of the recoil protons and the α-particles in the $^{1}H + ^{6}He$ reaction. The polar angles ϑ_p, ϑ_α (panel 1) and azimuthal angles φ_p, φ_α (panel 2) are defined relative to the beam direction in the laboratory frame.

^{6}He + p

The experiment was performed at GSI, Darmstadt, where radioactive beams were produced by fragmentation of ^{18}O (820 MeV/u and 730 MeV/u) beams from the heavy-ion synchrotron, SIS, on a 8 g/cm^2 beryllium production target. The secondary ^{6,8}He beams with energies of 717 and 671 MeV/u, respectively, were selected by magnetic analysis in the fragment separator, FRS, and directed towards the reaction target which was placed in front of the large-gap magnetic dipole spectrometer, ALADIN. Beam intensities were 1.9×10^5 1/s for ^{6}He and 1.6×10^4 1/s for ^{8}He.

E_B from 3.1 to 8 MeV!
Possible strong n corr.

R_{rms} reduced to 1.8 fm !

Spectroscopic factors for different cluster configurations in ^{6}He and ^{8}He

Projectile	Knocked out particle	Final state	S_c experimental	S_c shell model
^{6}He	n	$p+2n+\alpha$	1.7(2)	2
^{6}He	α	$p+2n+\alpha$	0.8(1)[a]	1
^{8}He	n	$p+4n+\alpha$	0.8(1)	0
^{8}He	n	$p+2n+^{6}$He	3.3(3)	4
^{8}He	α	$p+4n+\alpha$	0.9(1)	1
^{8}He	^{6}He	$p+2n+^{6}$He	1.3(1)[a,b]	$\frac{1}{6}$

[a] Corrected for the contribution from the inelastic scattering.
[b] Obtained with $\frac{d\sigma}{dt}$ calculated for the ^{6}He-cluster matter radius $\langle r^2 \rangle^{1/2} = 1.8$ fm.

Requiring population of $p_{1/2}$ state
^{6}He(0^+)+2n($p_{1/2}$)

^{6}He(2^+)+2n($p_{3/2}$,$p_{1/2}$) configuration;
Requiring $(p_{3/2})^2(p_{1/2})^2$ at an level of 50%

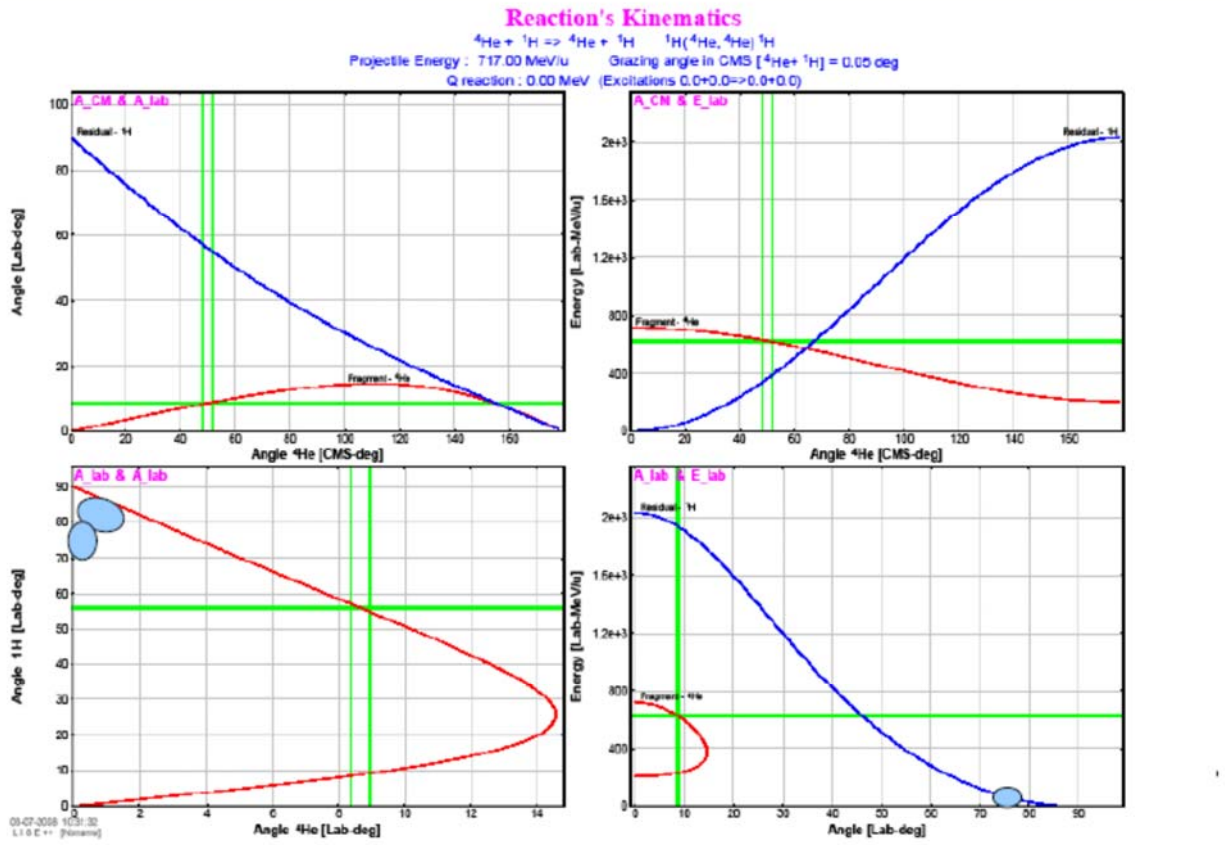
Reaction's Kinematics
4He + 1H => 4He + 1H 1H(4He, 4He) 1H
Projectile Energy : 717.00 MeV/u Grazing angle in CMS [4He+ 1H] = 0.05 deg
Q reaction : 0.00 MeV (Excitations 0.0+0.0=>0.0+0.0)
A_CM & A_lab
A_CM & E_lab
A_lab & A_lab
A_lab & E_lab
Residual - 1H
Fragment - 4He
Angle [Lab-deg]
Energy [Lab-MeV/u]
Angle 4He [CMS-deg]
Angle 1H [Lab-deg]
Angle 4He [Lab-deg]
Angle [Lab-deg]

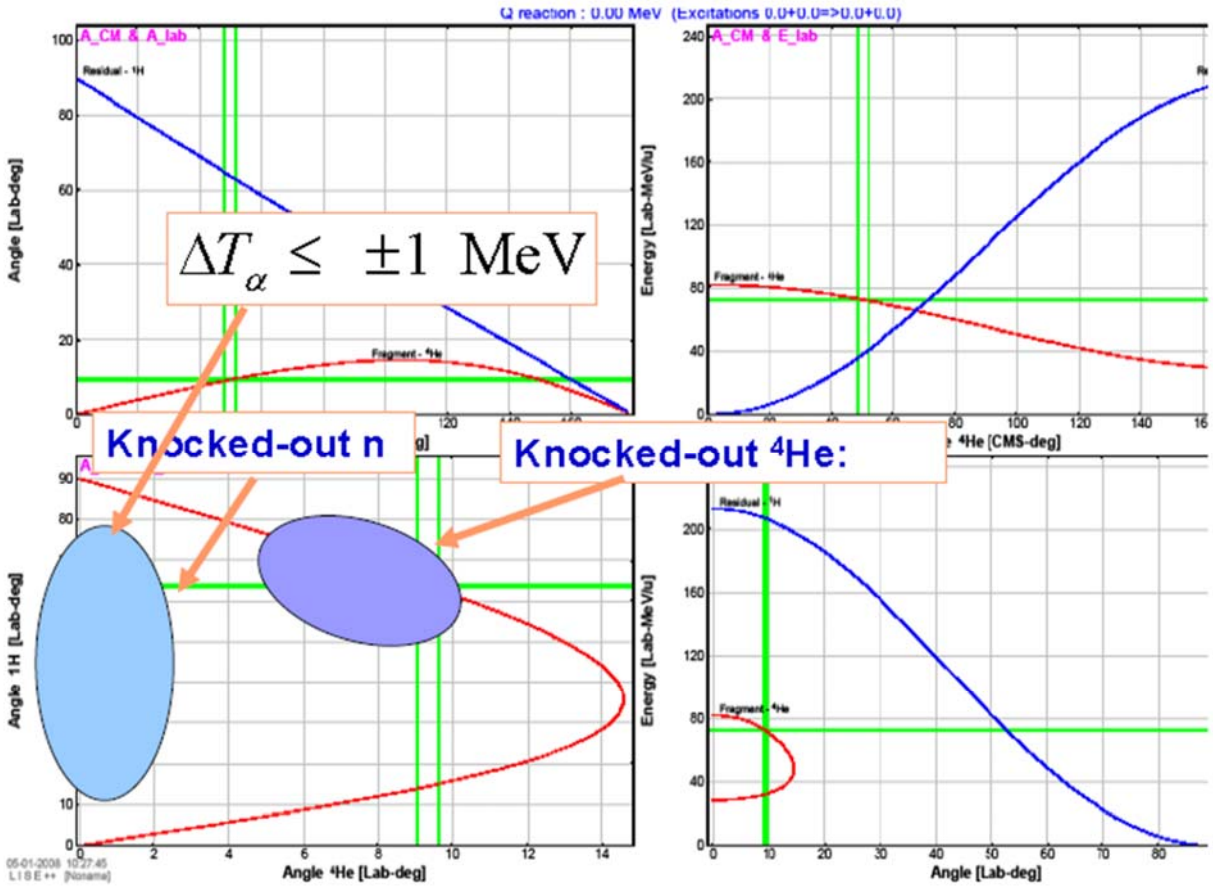
Q reaction : 0.00 MeV (Excitations 0.0+0.0=>0.0+0.0)
A_CM & A_lab
A_CM & E_lab
Residual - 1H
Fragment - 4He
$\Delta T_\alpha \leq \pm 1$ MeV
Knocked-out n
Knocked-out 4He:
Angle [Lab-deg]
Energy [Lab-MeV/u]
Angle 1H [Lab-deg]
Angle 4He [Lab-deg]
Angle [Lab-deg]

Reaction mechanism related kinematics estimation for knockout of n from ^{6}He

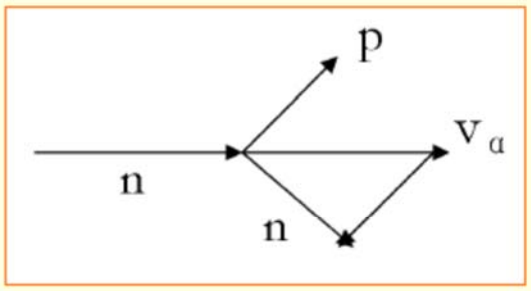

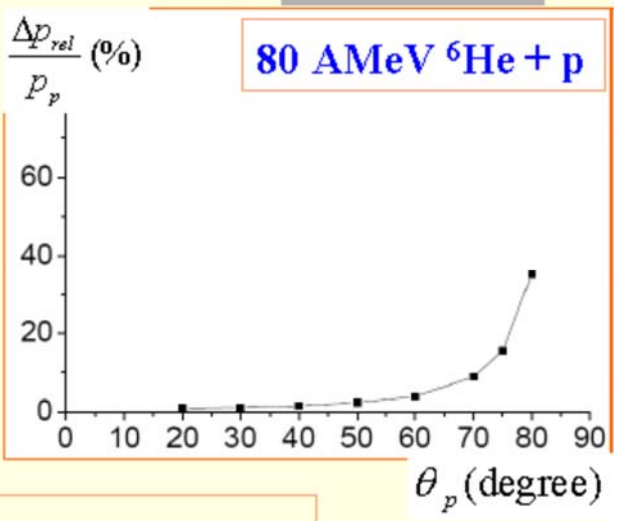

$\theta_{\mathrm{n,rel}} = -\theta_{\mathrm{p}}$; $p_{\mathrm{n,rel}} = p_{\mathrm{p}}$

$$\Delta p_{rel} = \int f\,dt = \int \frac{d\Phi}{dr}dt = \int \frac{d\Phi}{v_r} \approx \frac{mS_n}{p_{n,rel}} = \frac{mS_n}{p_p}. \quad (\Delta p_{rel} \ll p_p)$$

set $S_n = 1.87$ MeV, $m_n c^2 S_n = 1757$ MeV^2

Ex: Reaction mechanism related kinematics estimation for knockout of ^{6}He core from ^{8}He

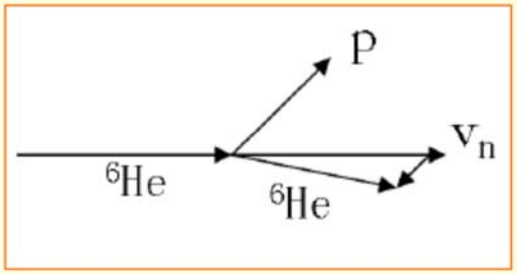

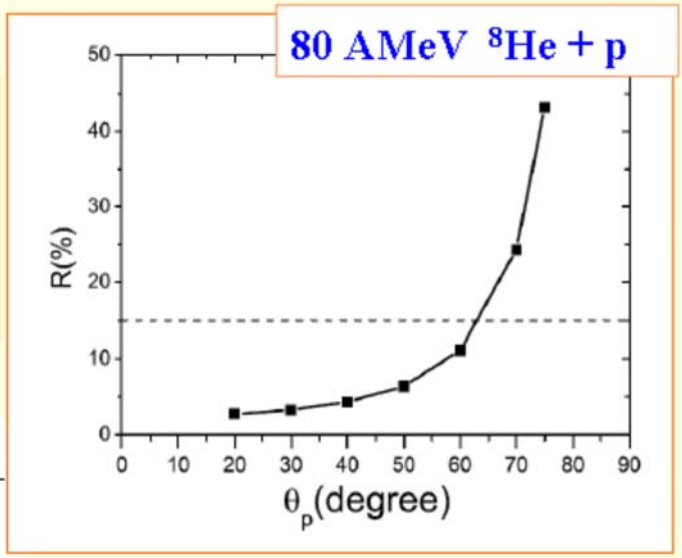

$$R = \frac{\Delta p_{rel}}{p_p}$$

PKU group experiment at RIKEN

8He + H,C at 82.3 MeV/u

- Primary Beam: ^{13}C, 115MeV/A, 470enA
- Primary Target: Be(12mm), F1 Wedge: Al(962mg/cm^2)
- Second Beam ^{8}He, 82MeV/A ~3*10^{5}pps
- Second Target: CH_2(0.0830mg/cm^2), C(0.1339mg/cm^2

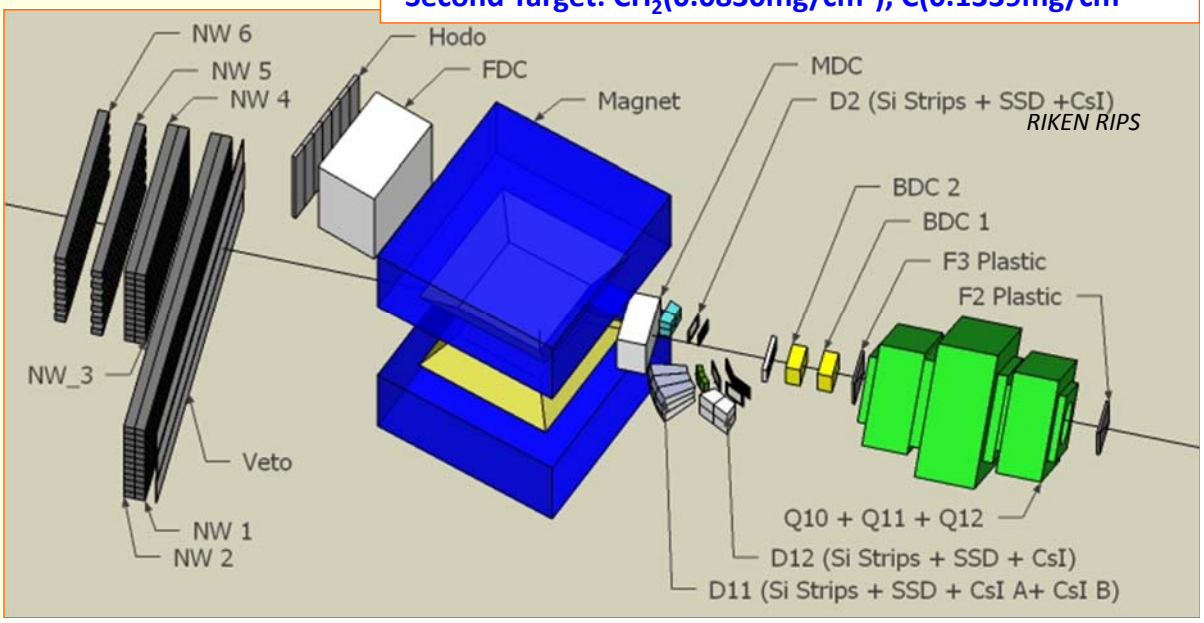

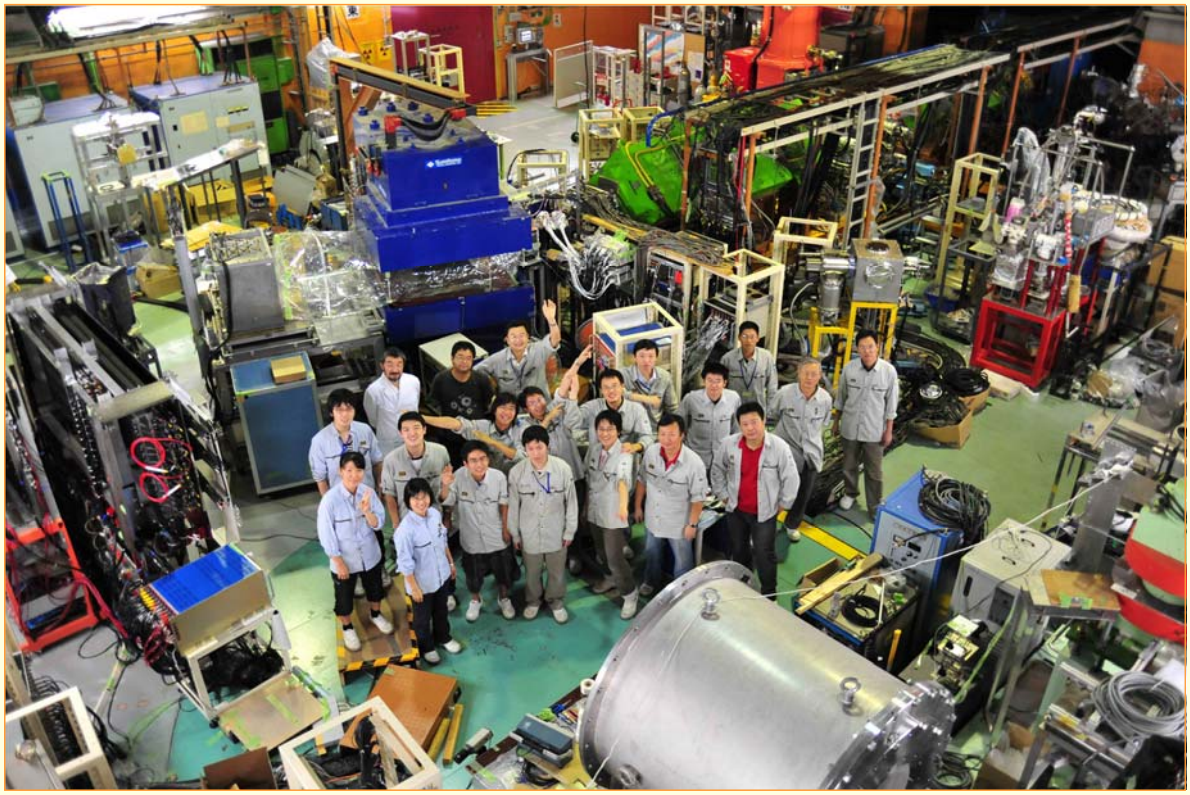

2009.08.05.

2009.08.06.

^{8}He at 82.3 MeV/u

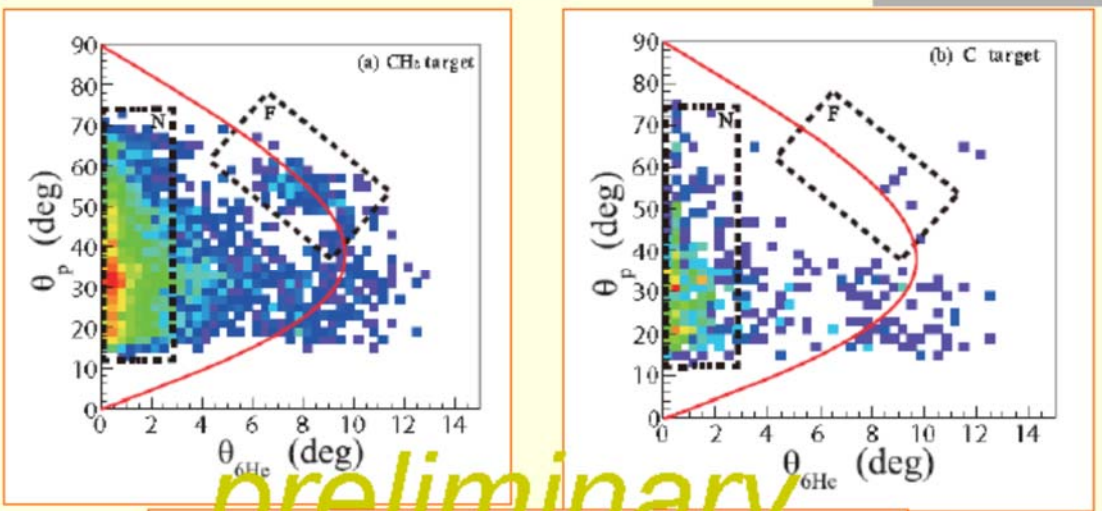

preliminary

Figure 2: Polar angle correlations between the recoil protons and the forward moving ^{6}He fragments for (a) CH_2 target and (b) Carbon target, measured in the experiment using ^{8}He beam at 82.3 MeV/u. The solid curve is the kinematics relation for ^{6}He + p free scattering at 82.3 MeV/u. The frames with dashed line denote the event selection for the core fragment knockout (frame F) and the valence neutron knockout (frame N), respectively.

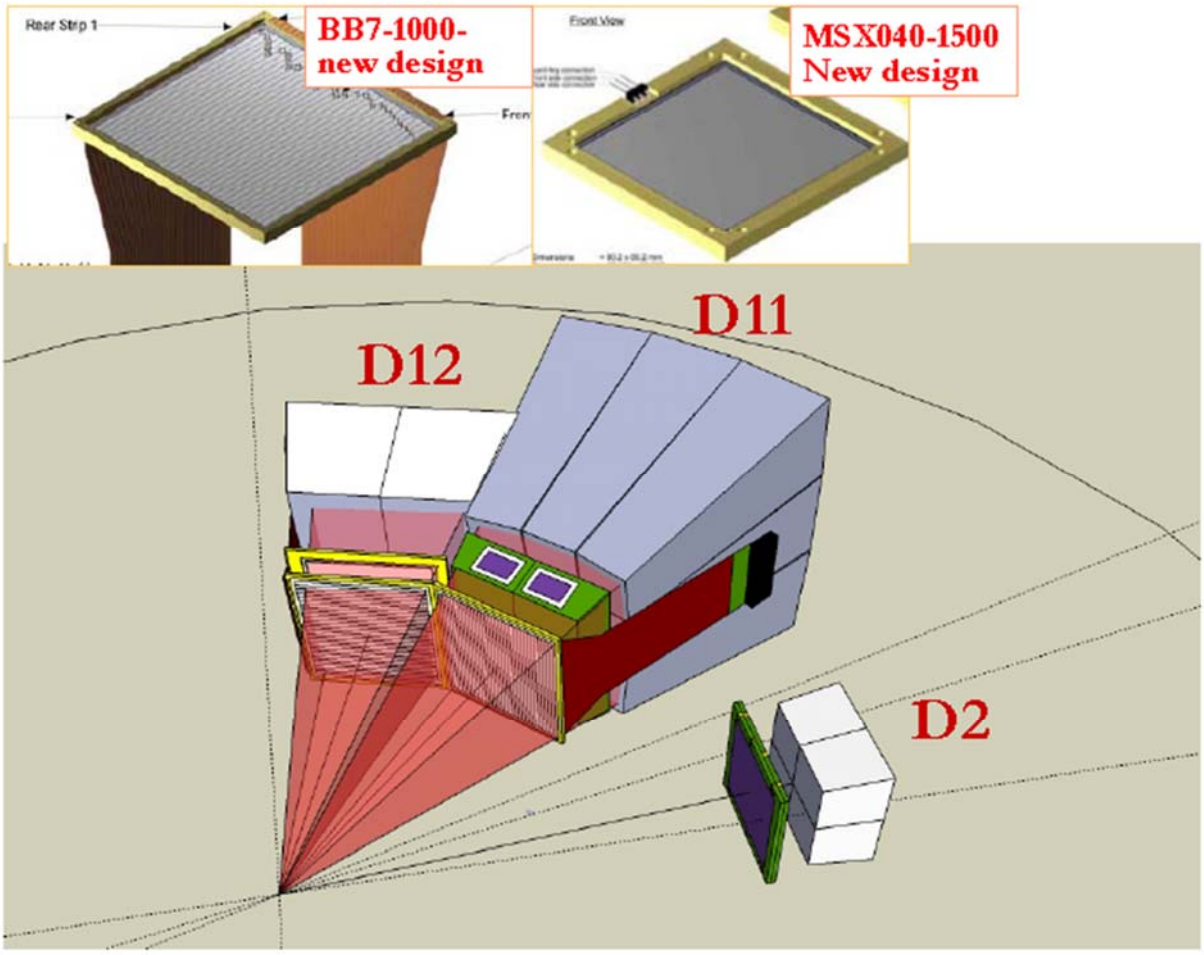

For core knockout events

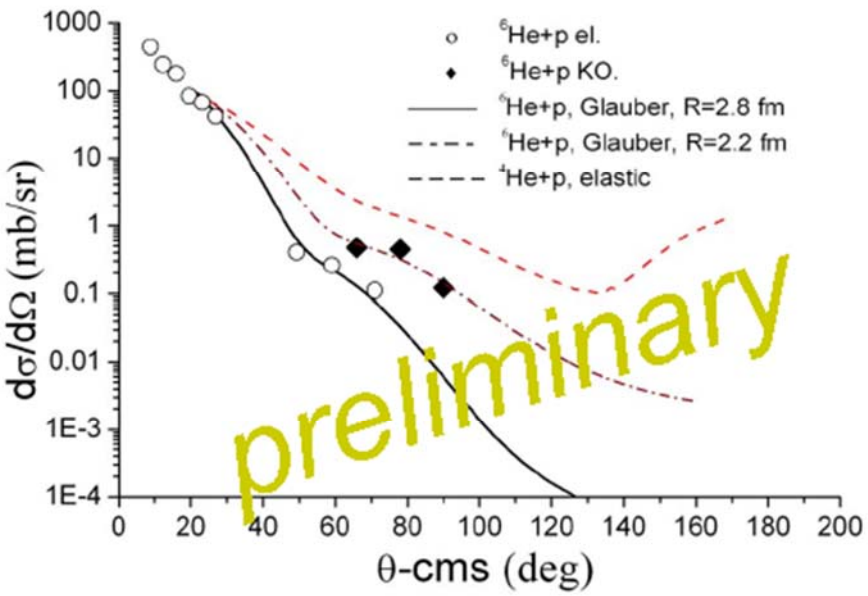

For valence neutron knockout events

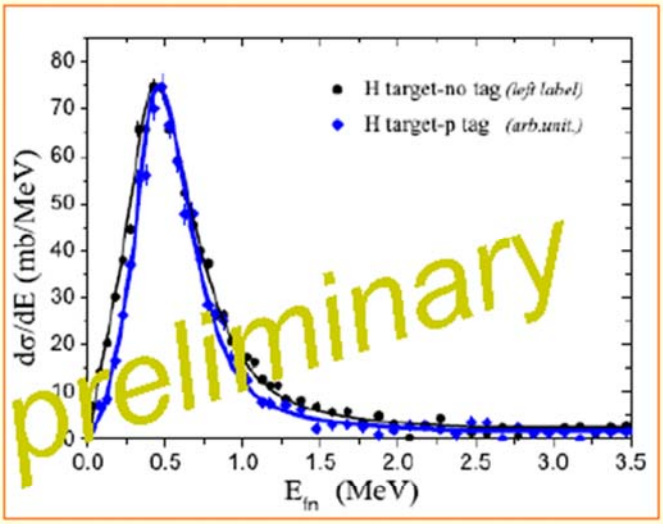

Figure 5: ^{6}He + n relative energy spectra measured in the knockout reaction induced by ^{8}He at 82.3 MeV/u impinging on a Hydrogen target (filled circles). The filled diamonds are the results with the recoil proton tagging. The error bars are statistical only. The curves represent the calculations explained in the text.

V. Summary

- QFS has played important role in probing inner shell structure of stable nuclei
- Knockout reaction has developed into a powerful spectroscopic tool for investigating the exotic structure of unstable nuclei.
- more exclusive measurement seems necessary to have a better selection of the reaction mechanism, for which recoil proton tagging might be a good choice.

Thanks for your attention!

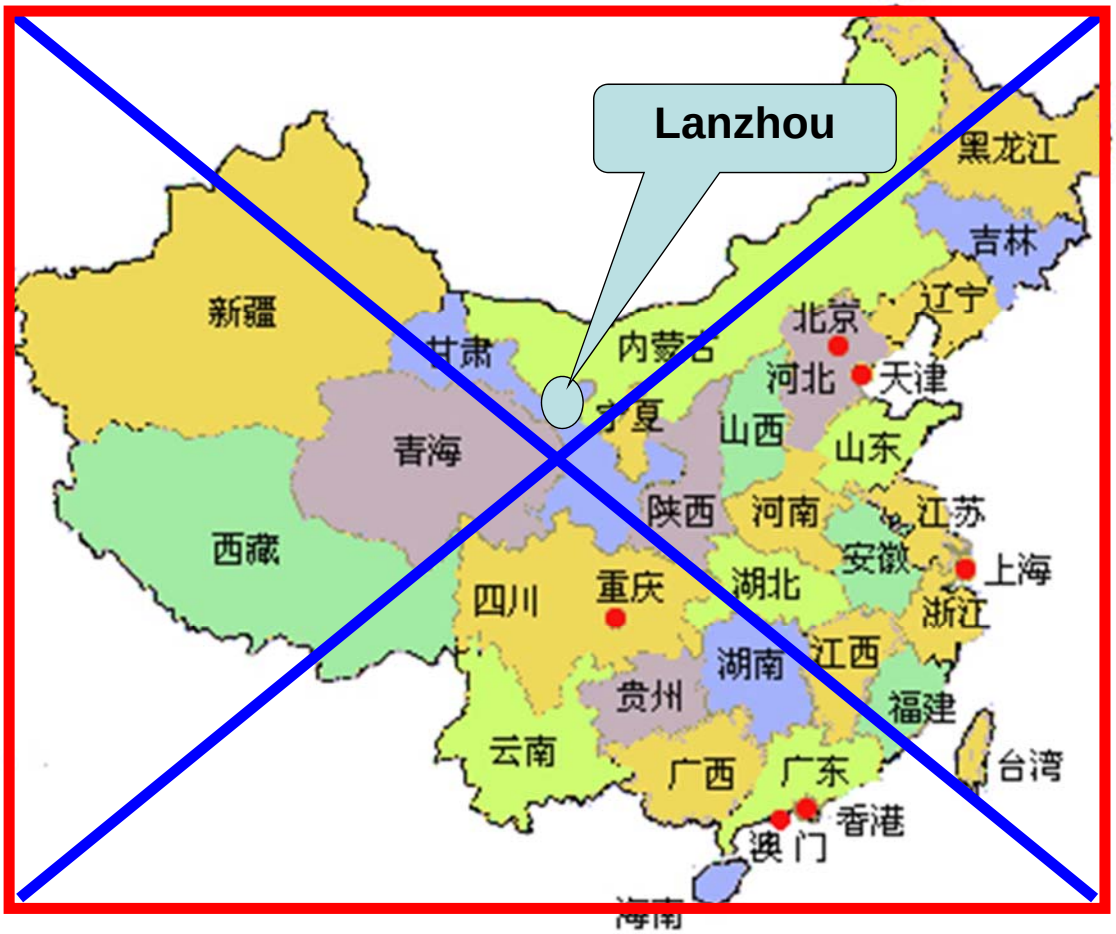
Lanzhou
黑龙江
吉林
辽宁
新疆
北京
甘肃
内蒙古
河北
天津
宁夏
山西
山东
青海
陕西
河南
江苏
西藏
安徽
上海
四川
重庆
湖北
浙江
湖南
江西
贵州
福建
云南
广西
广东
台湾
香港
澳门


东方IC

Instutute of Modern Physics, CAS

Heavy-Ions based research center in China.
744 staffs，30～45 M $/y research budget.

HIRFL-CSR

Beam production

Stable beams

ECR: keV
SFC: ≤ 10 AMeV (H.I.), 17~35 MeV (p)
SSC: ≤ 100 AMeV (H.I.), ≤ 110 MeV (p)
CSRm: ≤ 1000 AMeV (H.I.), ≤ 2.8 GeV (p)

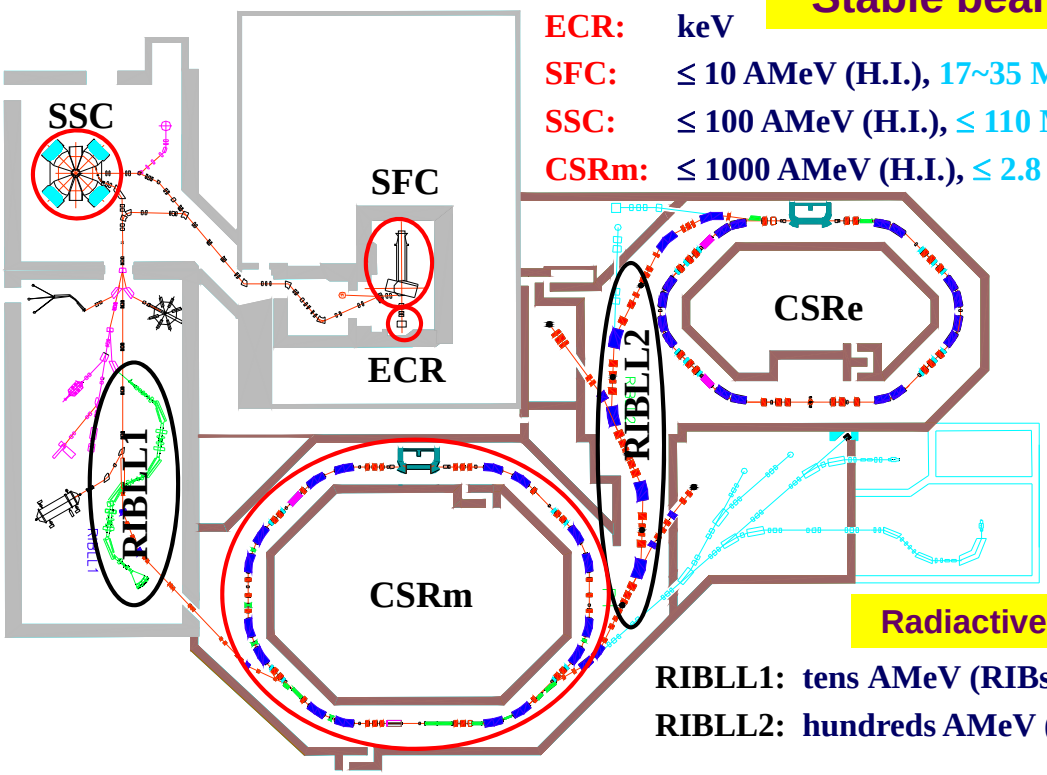

定位：

中低能核物理装置

Radiactive Beams

RIBLL1: tens AMeV (RIBs)
RIBLL2: hundreds AMeV (RIBs & HCI)

Mass measurements of short-lived nuclides using CSRe in Lanzhou

Yu-Hu Zhang

Institute of Modern Physics, CAS

27th Aug. 2011, Beijing, China

6th International Summer School on Subatomic Physics (ISSSP) August 27-31, Beijing

Outline

1. **Brief introduction**
2. **Principle of mass measurements in CSRe**
3. **Experiments at CSRe & data analysis**
4. **Results & Discussion**
5. **Summary**

1. Brief introduction

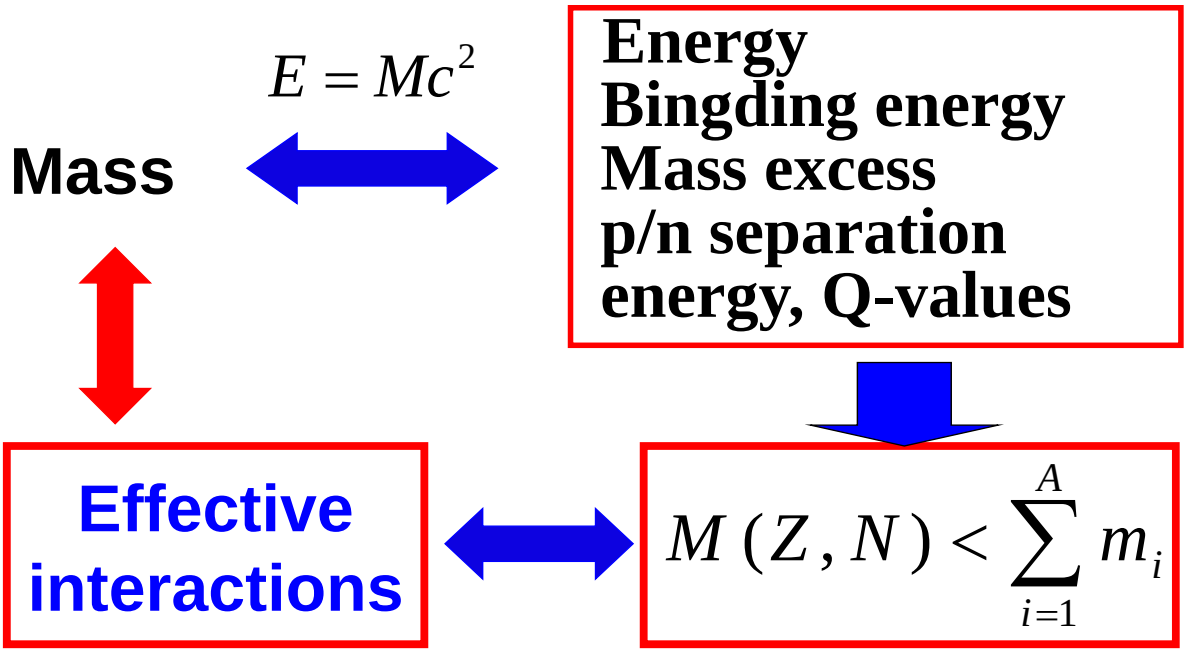

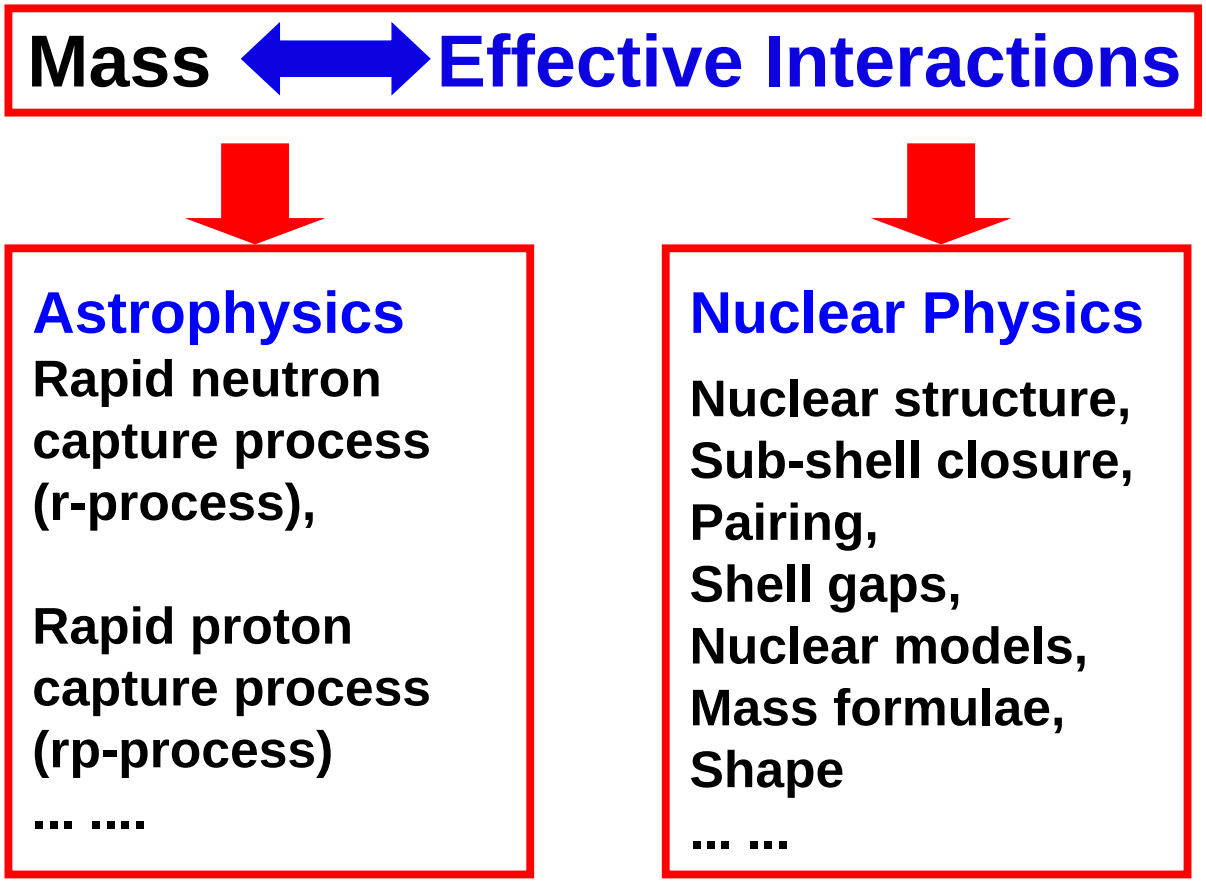

Precision of atomic masses

- **Nuclear Physics ($\delta m/m \sim 10^{-5}, 10^{-7}$)**

  Nuclear structure, sub-shell closure, pairing, shell gaps
  Tests of nuclear models and mass formulae

- **Astrophysics ($\delta m/m \sim 10^{-6}, 10^{-7}$)**

  r- and rp-process

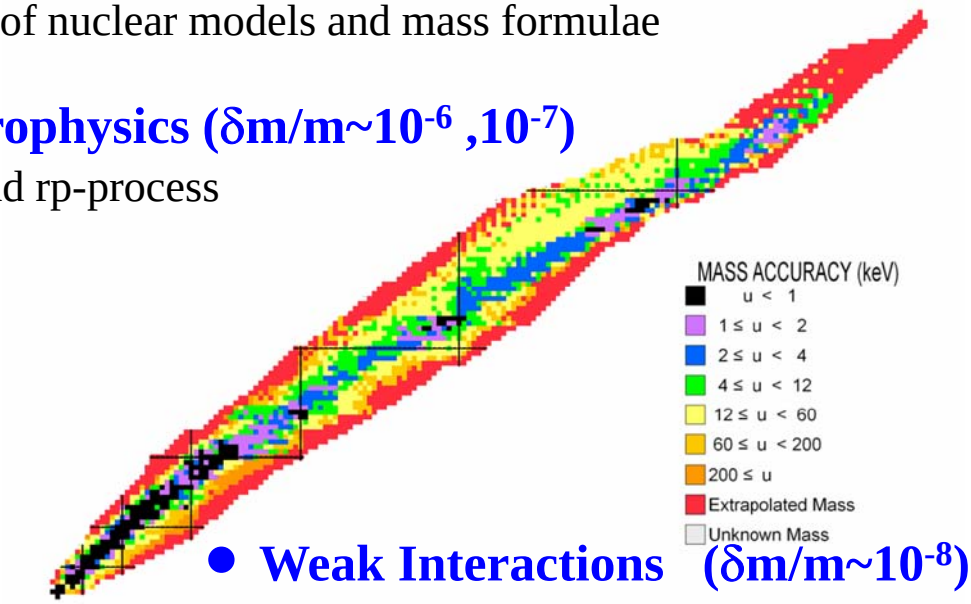

- **Weak Interactions ($\delta m/m \sim 10^{-8}$)**

  Testing CVC hypothesis,
  Unitarity of CKM matrix

Precision & half-lifes

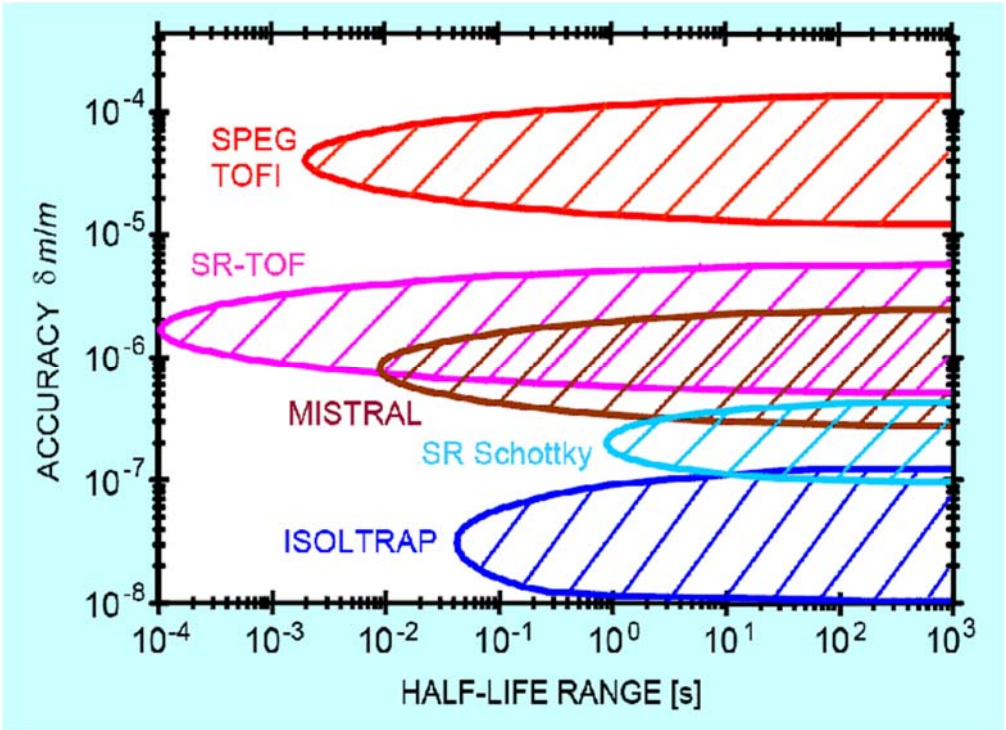

Picture taken from the thesis of M.Saidur Rahaman

2. Principle of mass measurement in CSRe

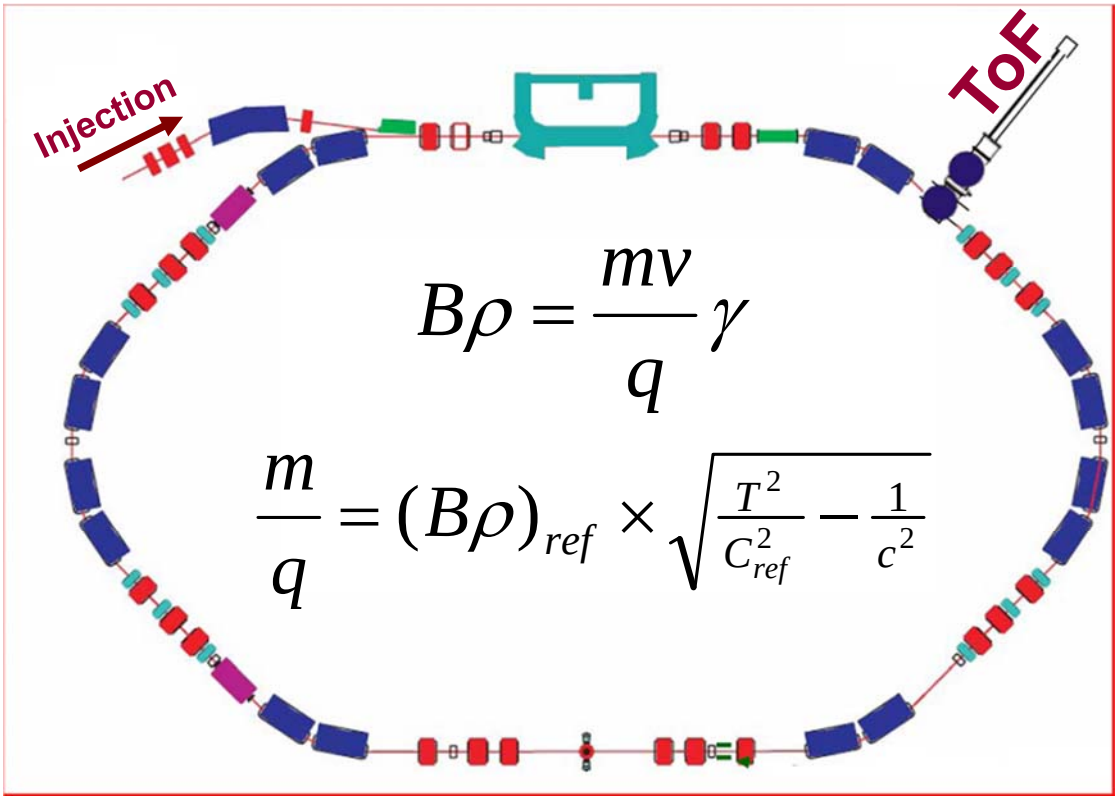

$$B\rho = \frac{mv}{q}\gamma$$

$$\frac{m}{q} = (B\rho)_{ref} \times \sqrt{\frac{T^2}{C_{ref}^2} - \frac{1}{c^2}}$$

2. Principle of mass measurement in CSRe

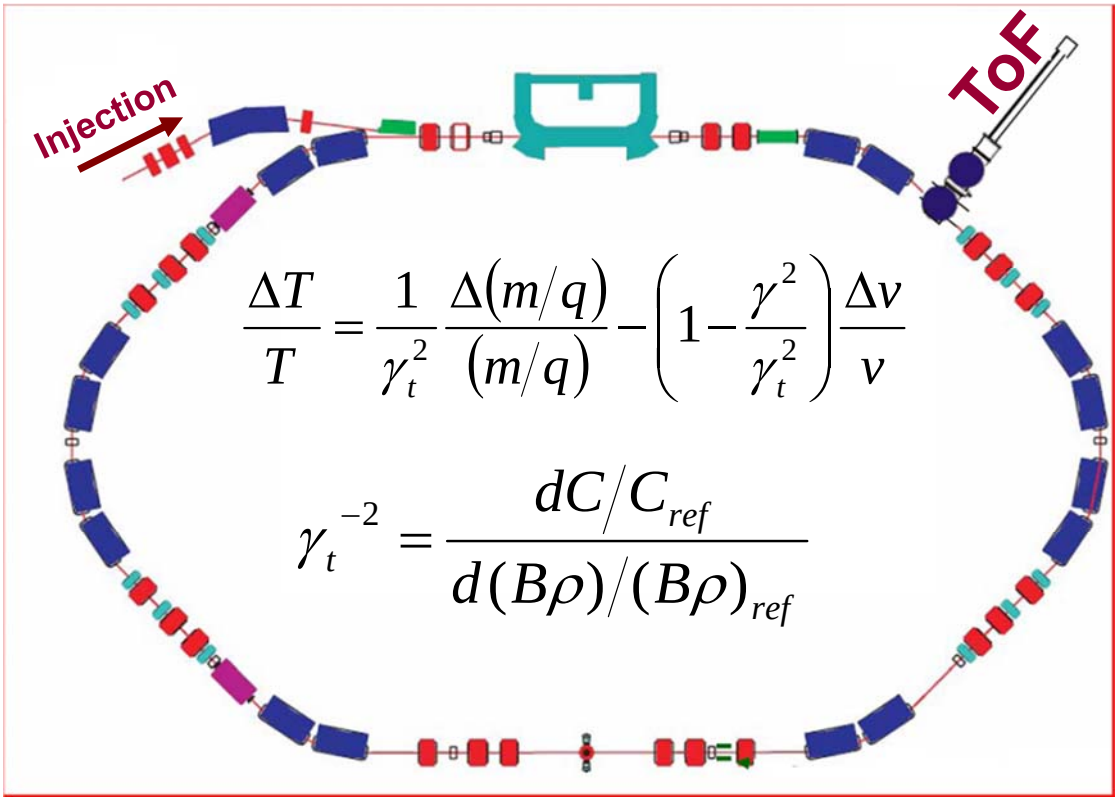

$$\frac{\Delta T}{T} = \frac{1}{\gamma_t^2}\frac{\Delta(m/q)}{(m/q)} - \left(1 - \frac{\gamma^2}{\gamma_t^2}\right)\frac{\Delta v}{v}$$

$$\gamma_t^{-2} = \frac{dC/C_{ref}}{d(B\rho)/(B\rho)_{ref}}$$

2. Principle of mass measurement in CSRe

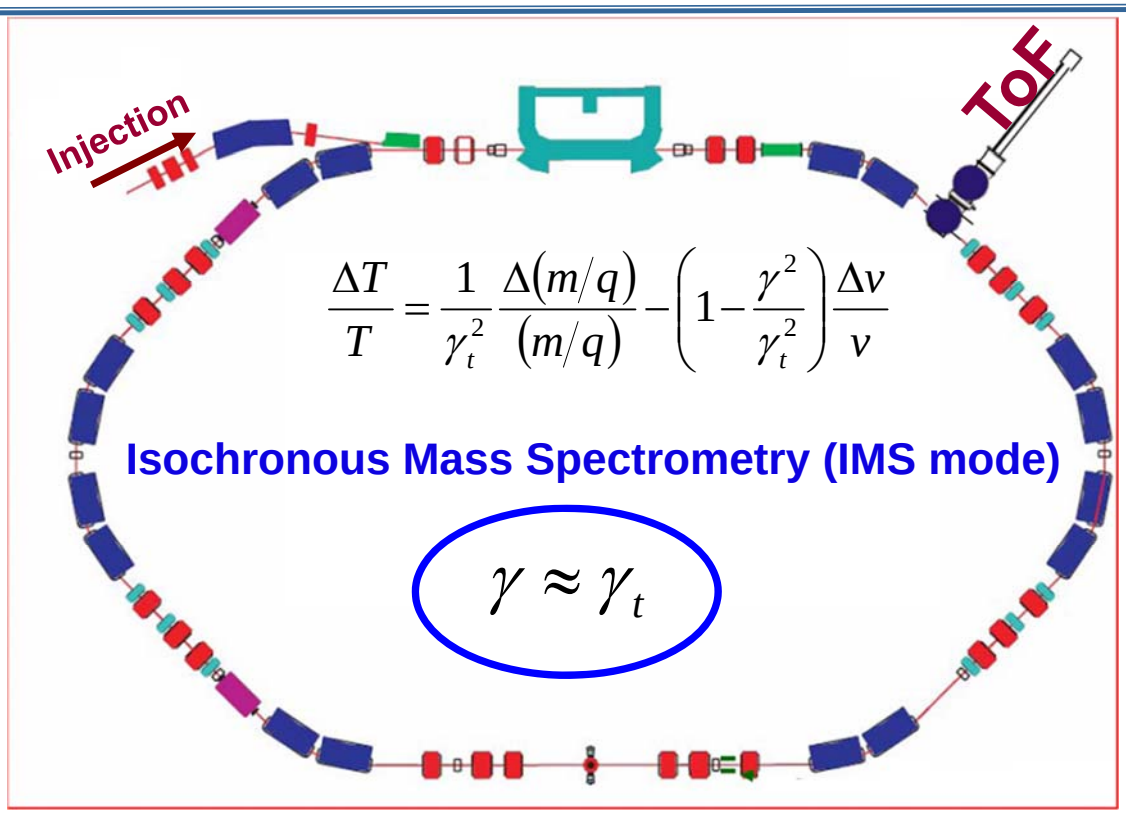

2. Principle of mass measurement in CSRe

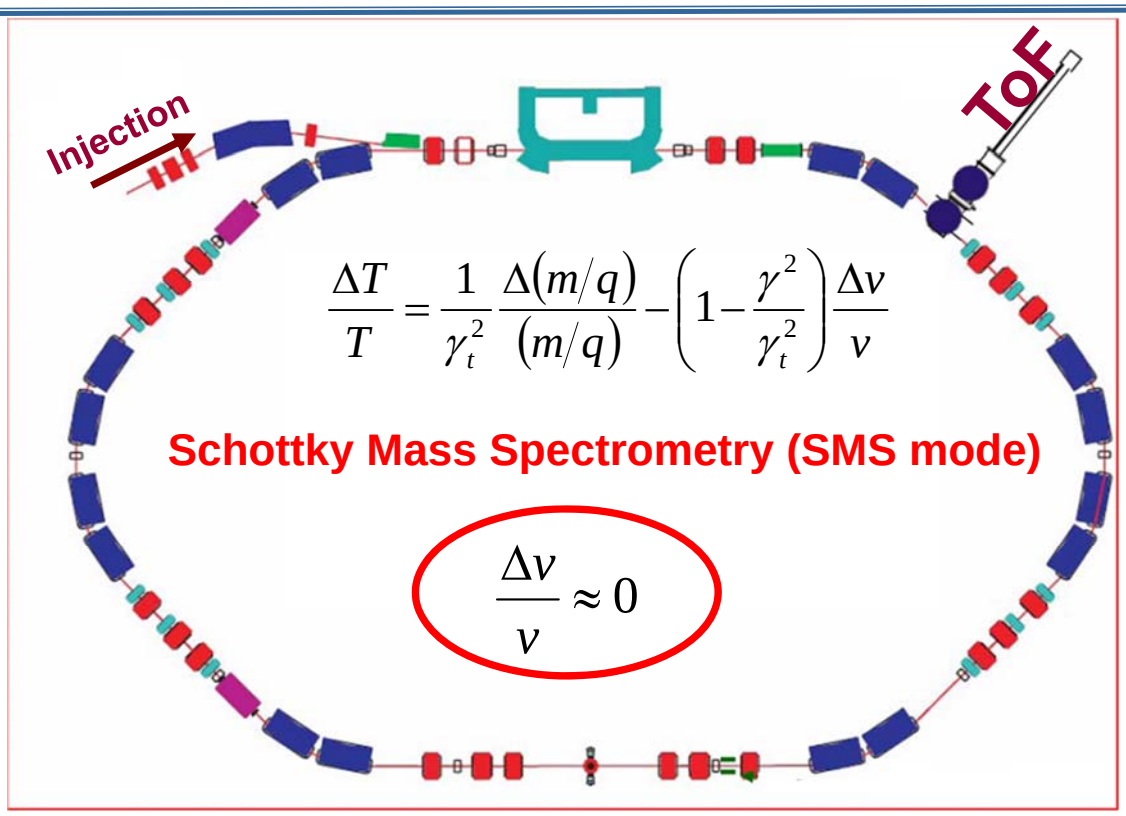

Mass measurement in CSRe (IMS mode)

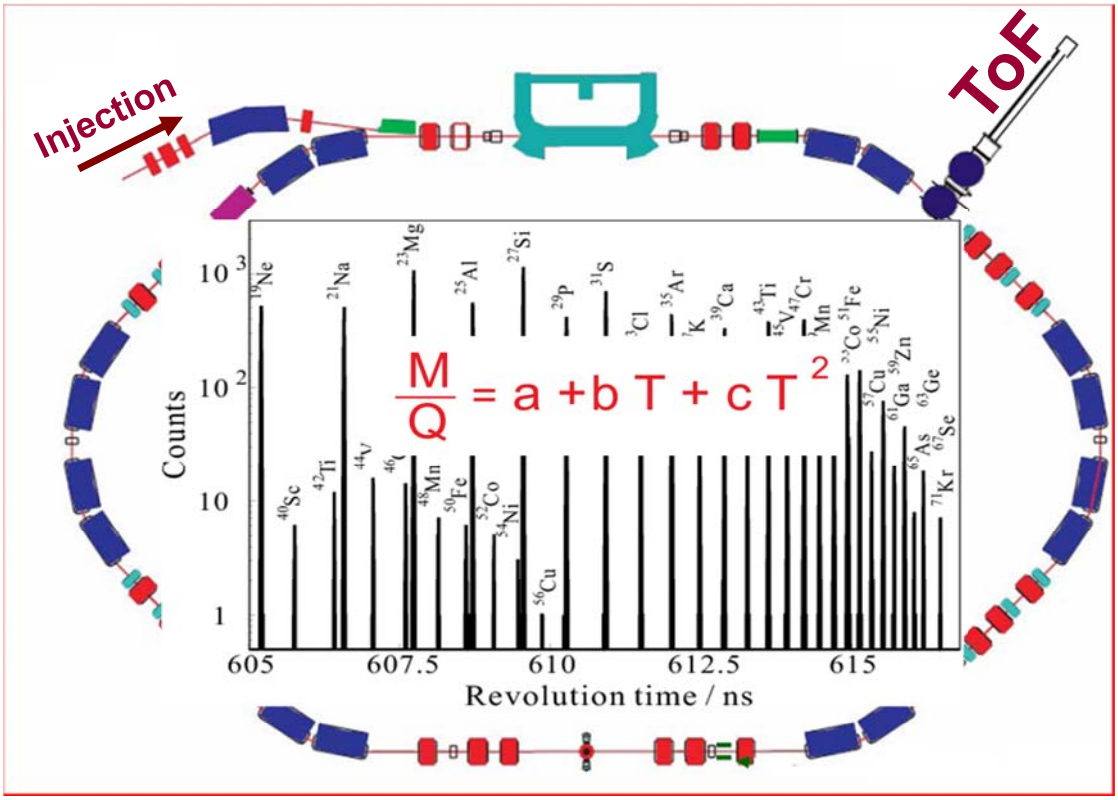

3. Experiments at CSRe & Data analysis

^{78}Kr + ^{9}Be

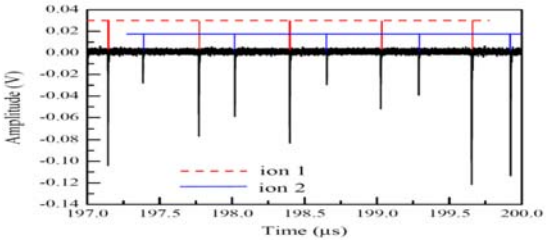

Time detector

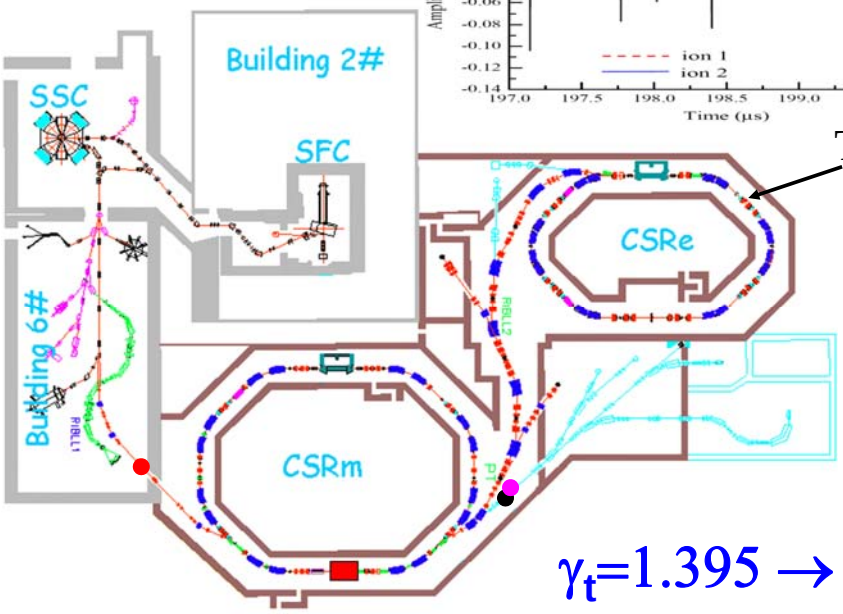

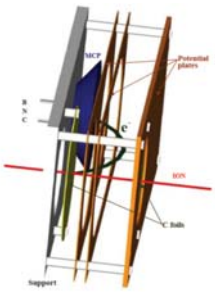

γ_t=1.395 → 368 MeV/u

Procedure of Data analysis

Signals in Oscilloscope

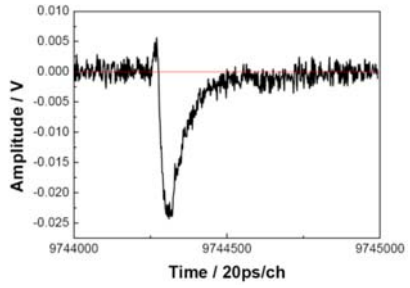

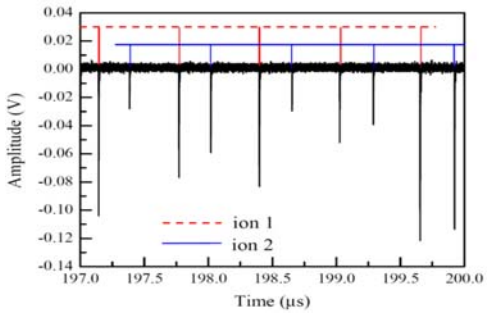

Ions Identification

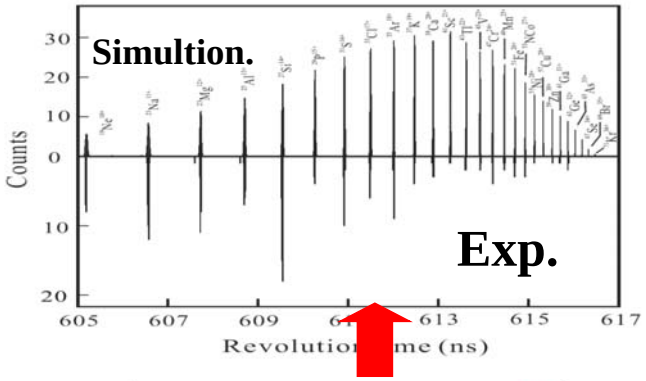

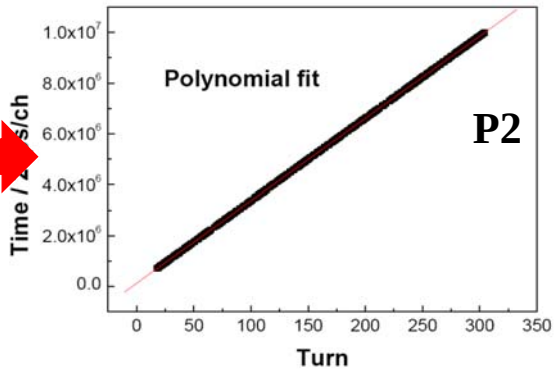

^{78}Kr beam: Revolution Time Spectrum

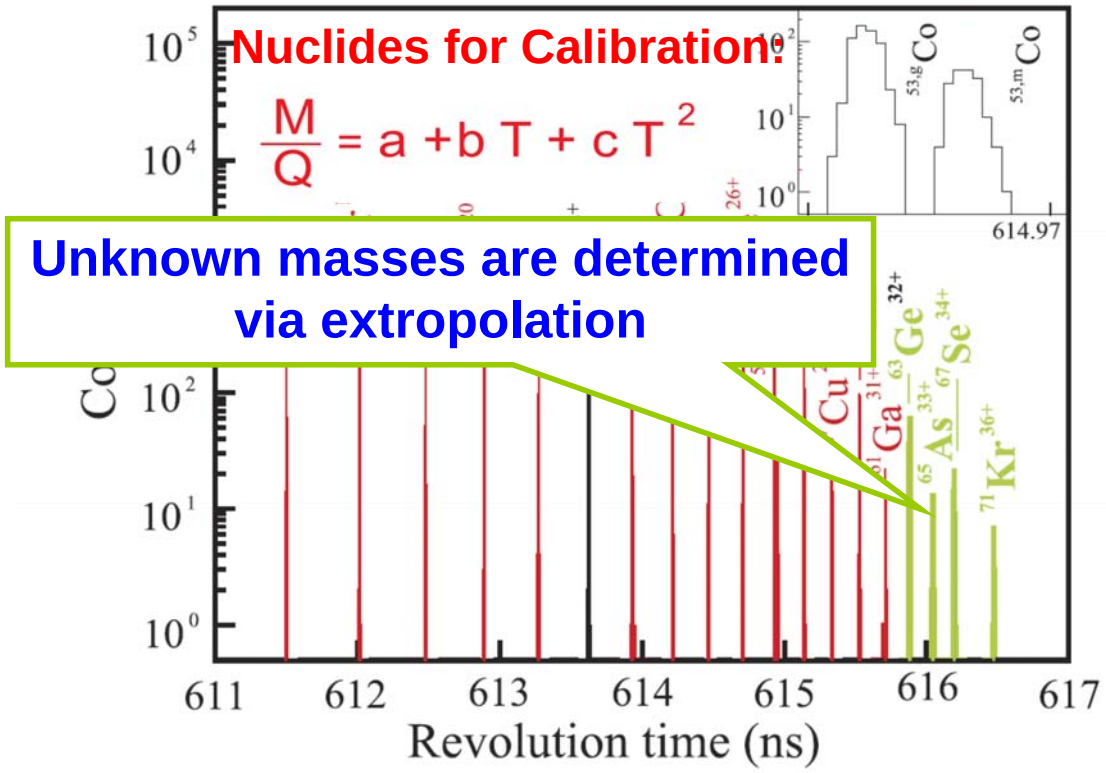

^{58}Ni beam: Revolution Time Spectrum

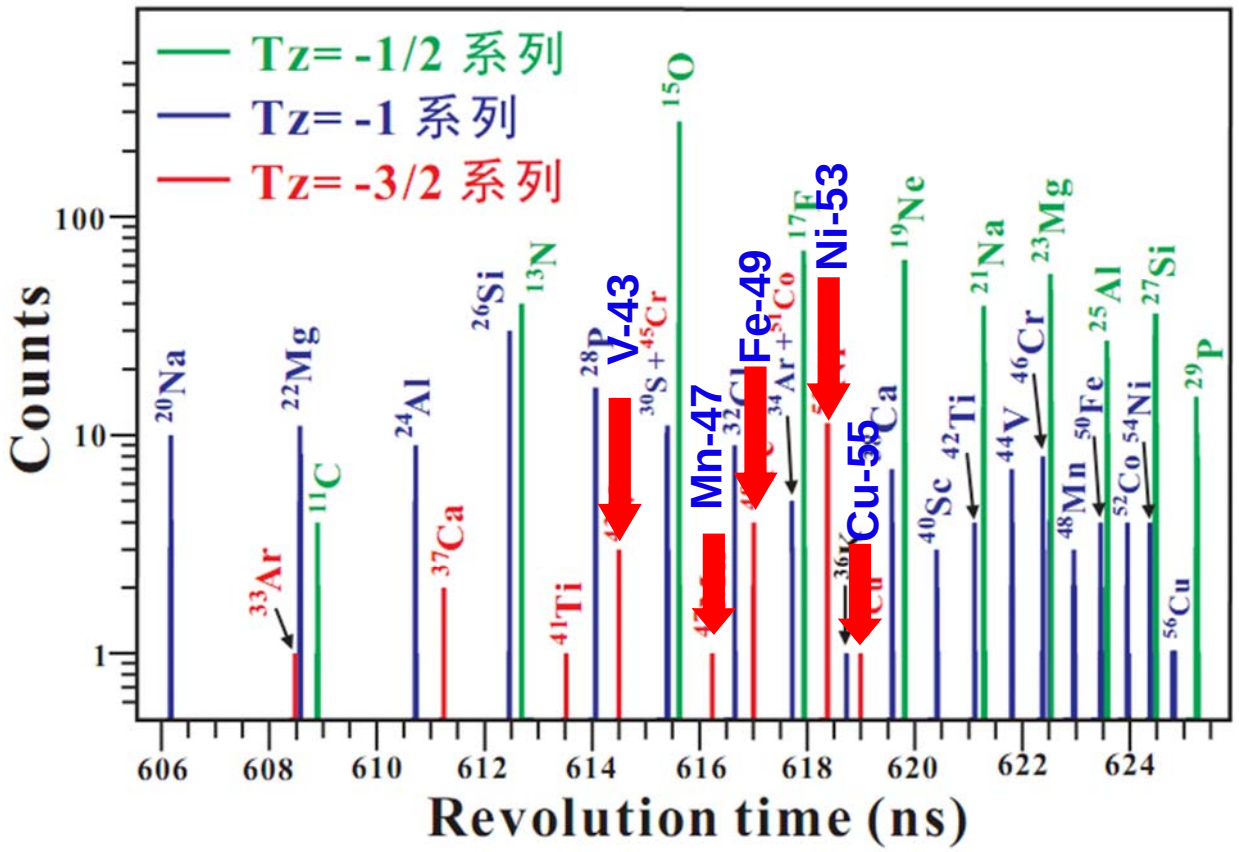

Some techniques in the data analysis

1) Magnetic field drift
2) Amplitude ion identification
3) Calibration test
4) Extrapolation test

1) Magnetic Field Drift (^{78}Kr beam)

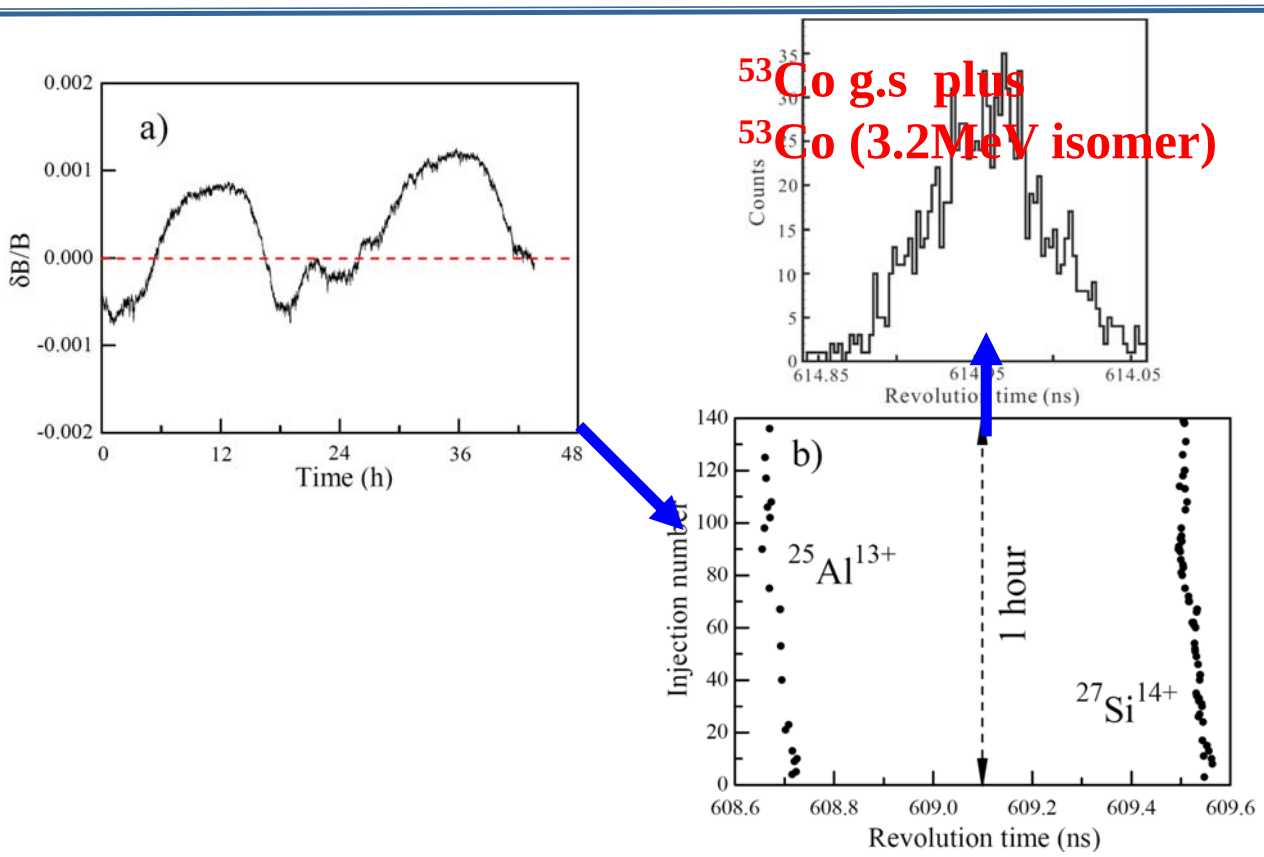

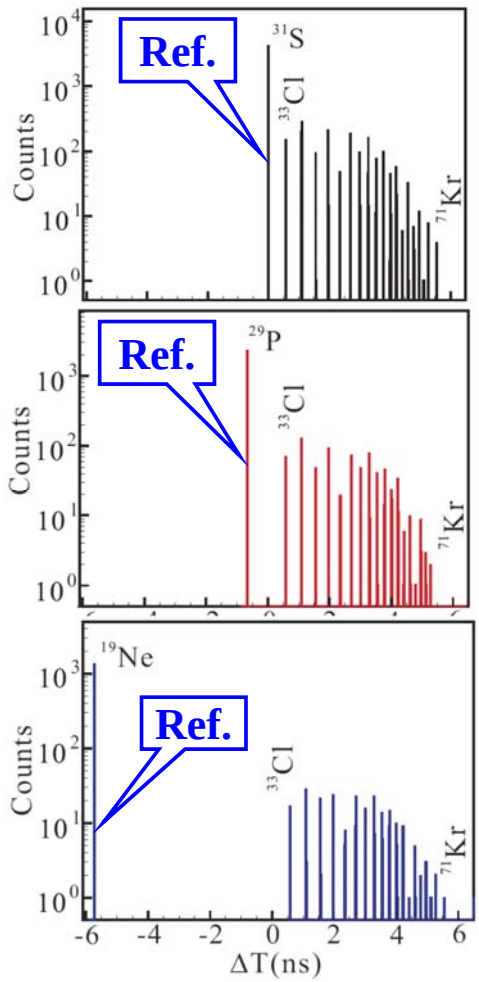

Time Shift Correction

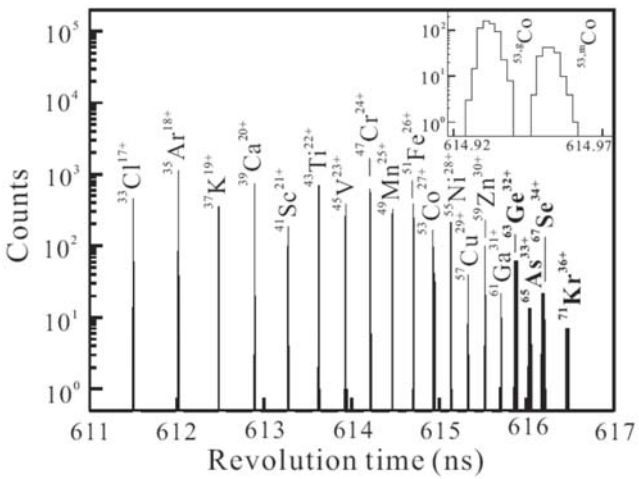

Corrected results

No Correction

GSI meth.
Σ 3 min.

IMP meth.

$m/\Delta m \approx 1.7 \times 10^5$

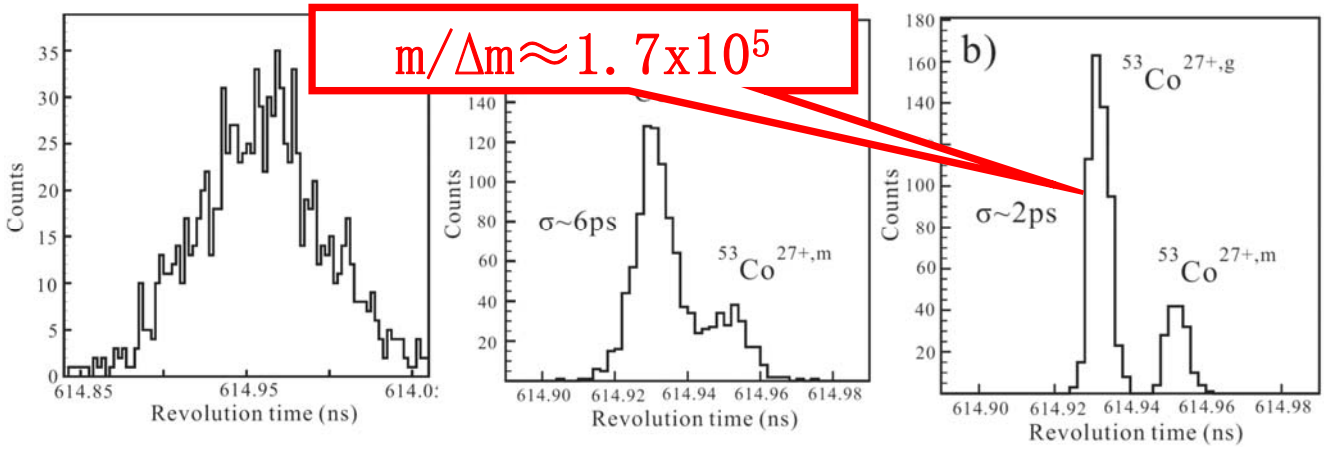

^{53}Co isomer E*=3174.3(1.0)keV, (20ps difference)

Experiment: ^{58}Ni beam

Magnetic field stability was improved

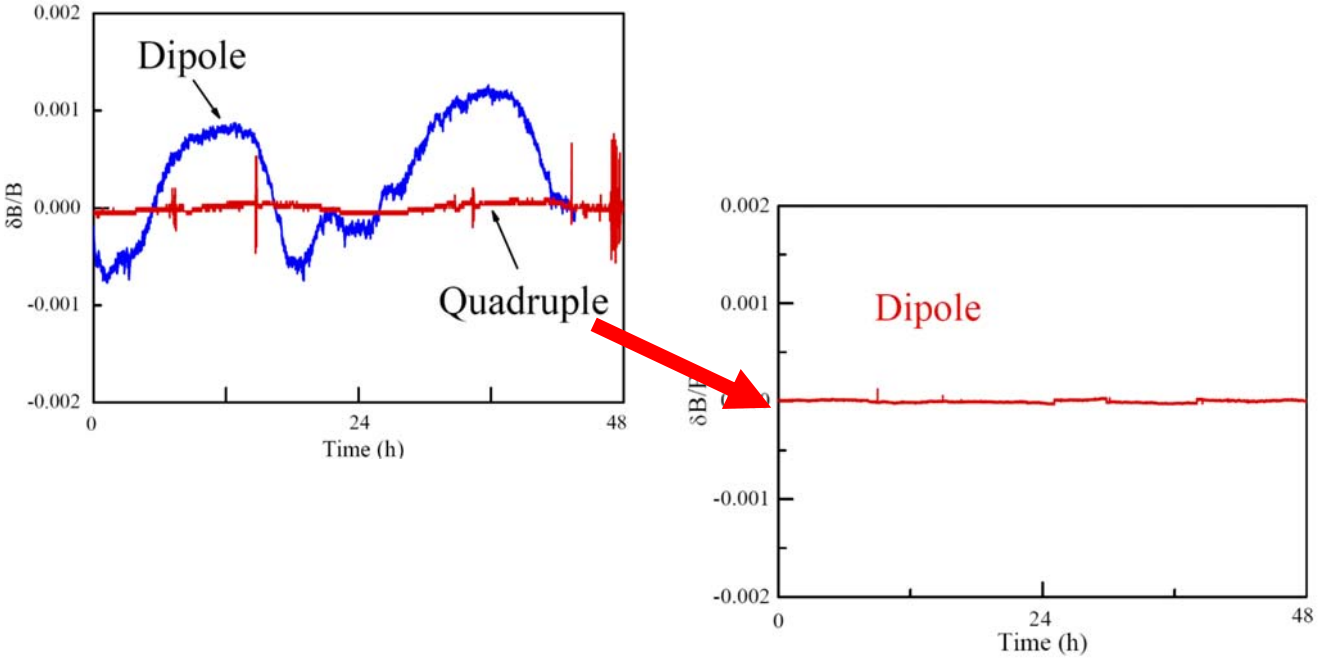

2) Amplitude ion identification

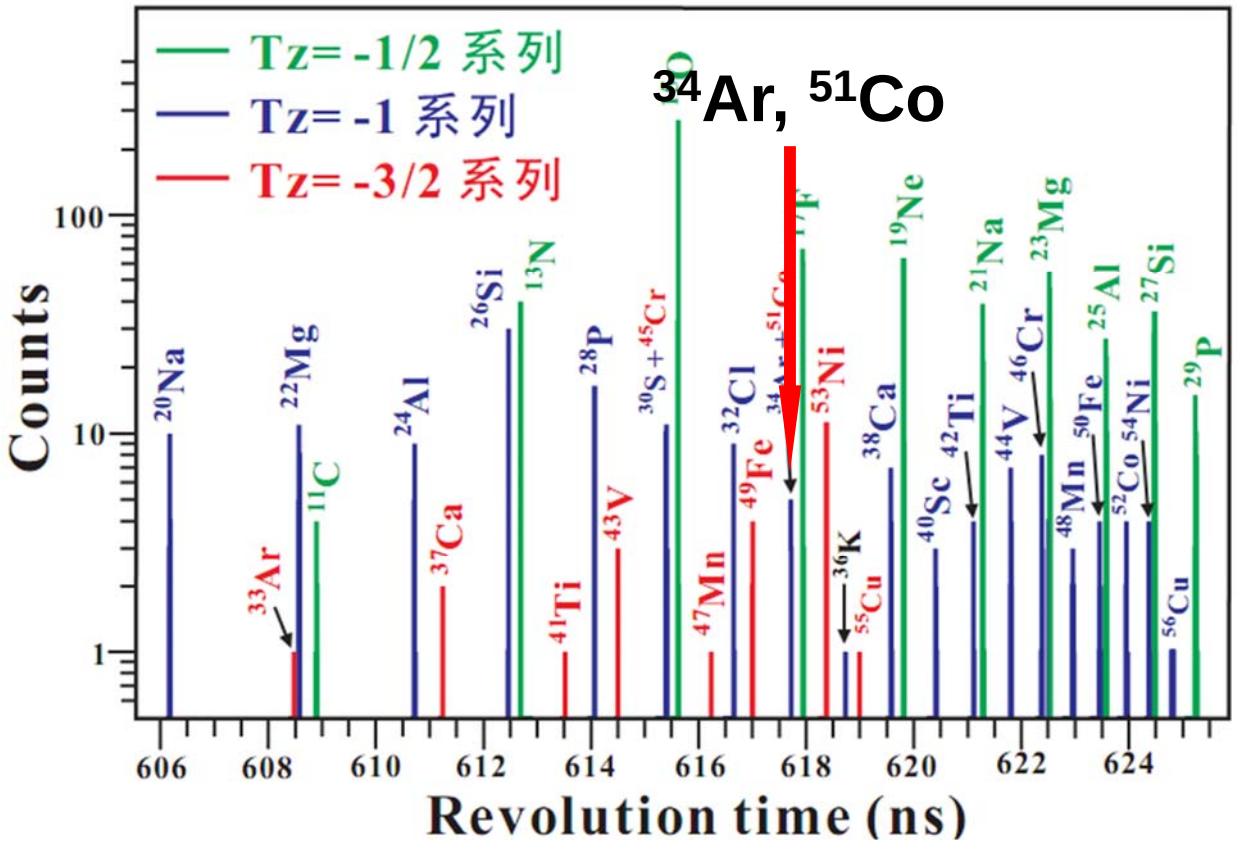

2) Amplitude ion identification: ^{51}Co

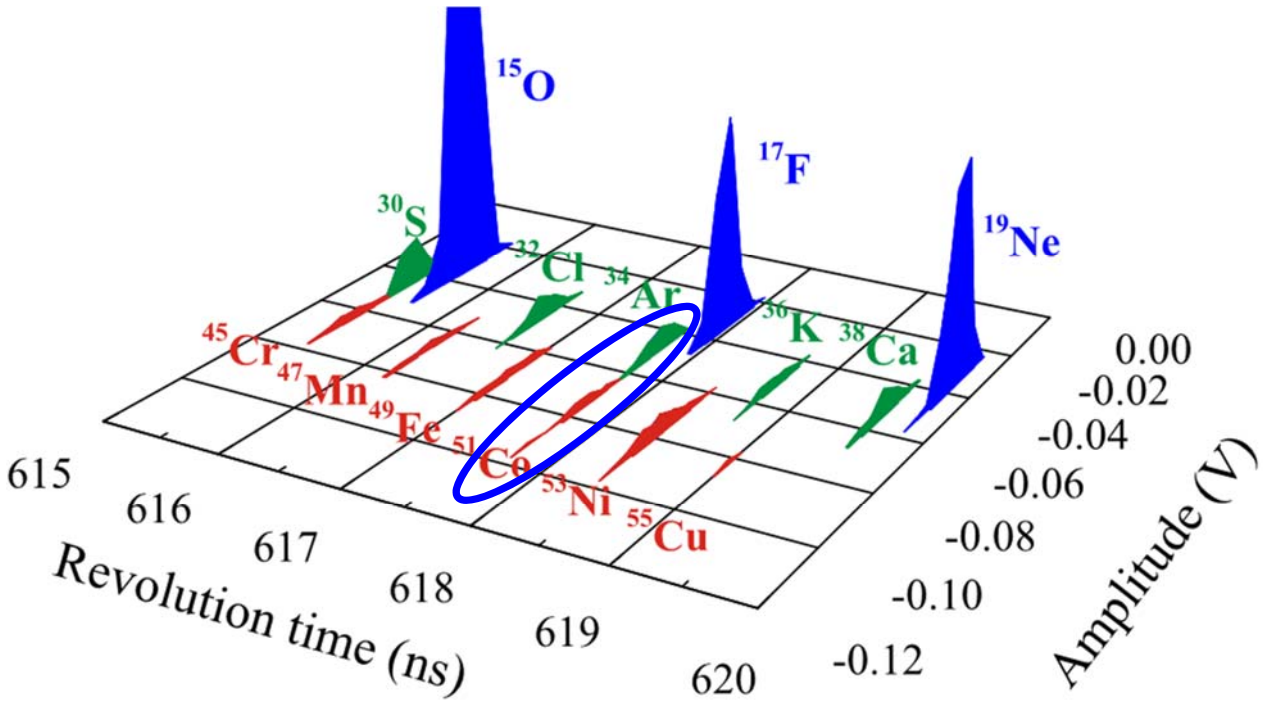

3) Calibration test

A 2nd order polynomial function is used to fit *m/q* and *T* with the least square-method

$$\frac{m}{q}(T) = a_0 + a_1 T + a_2 T^2$$

The mass error:

1. the statistics error
2. error from calibration nuclei
3. the systematic error

A comparison of the masses obtained in this work with the literature values.

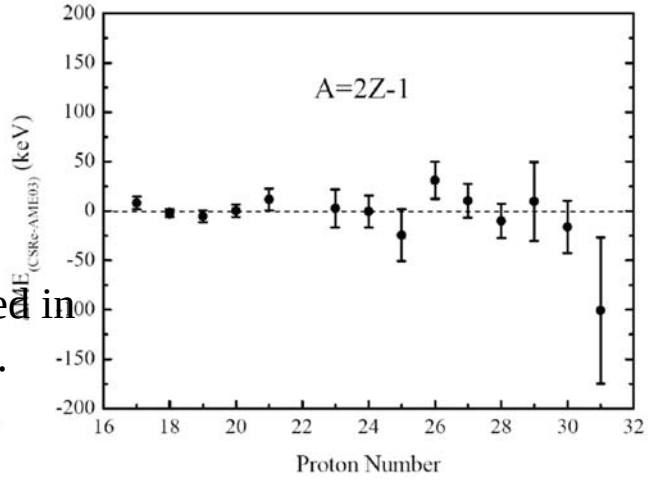

The normalized x_n=1.01 is well within the expected values 1±0.19

4) Extrapolation

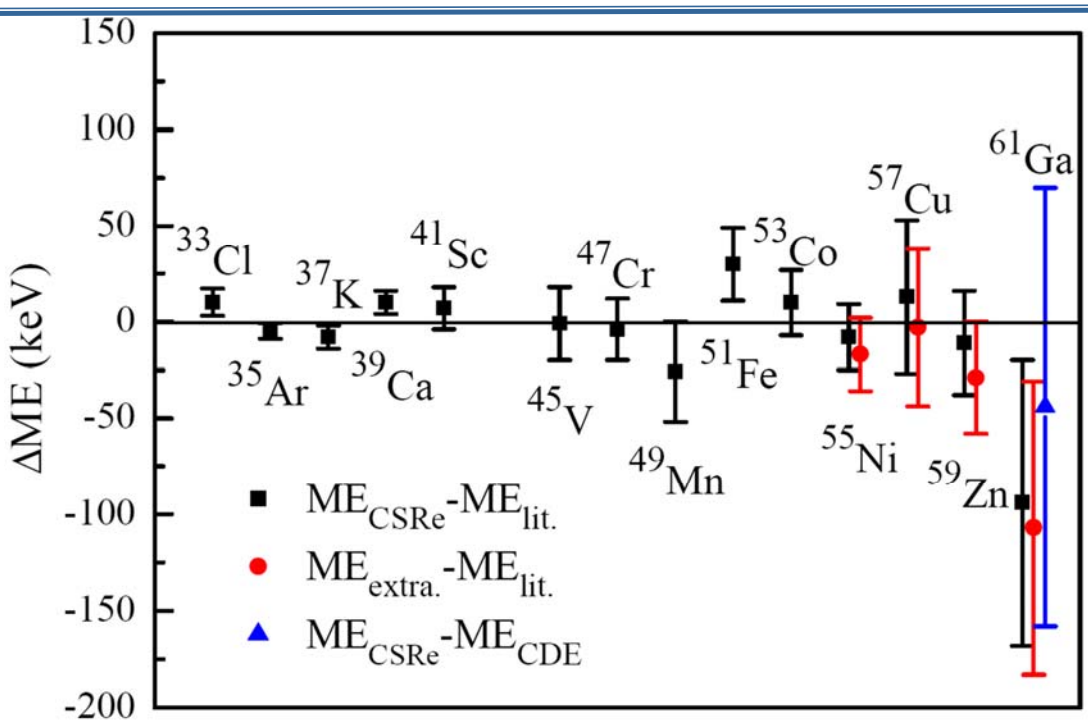

4) Extrapolation

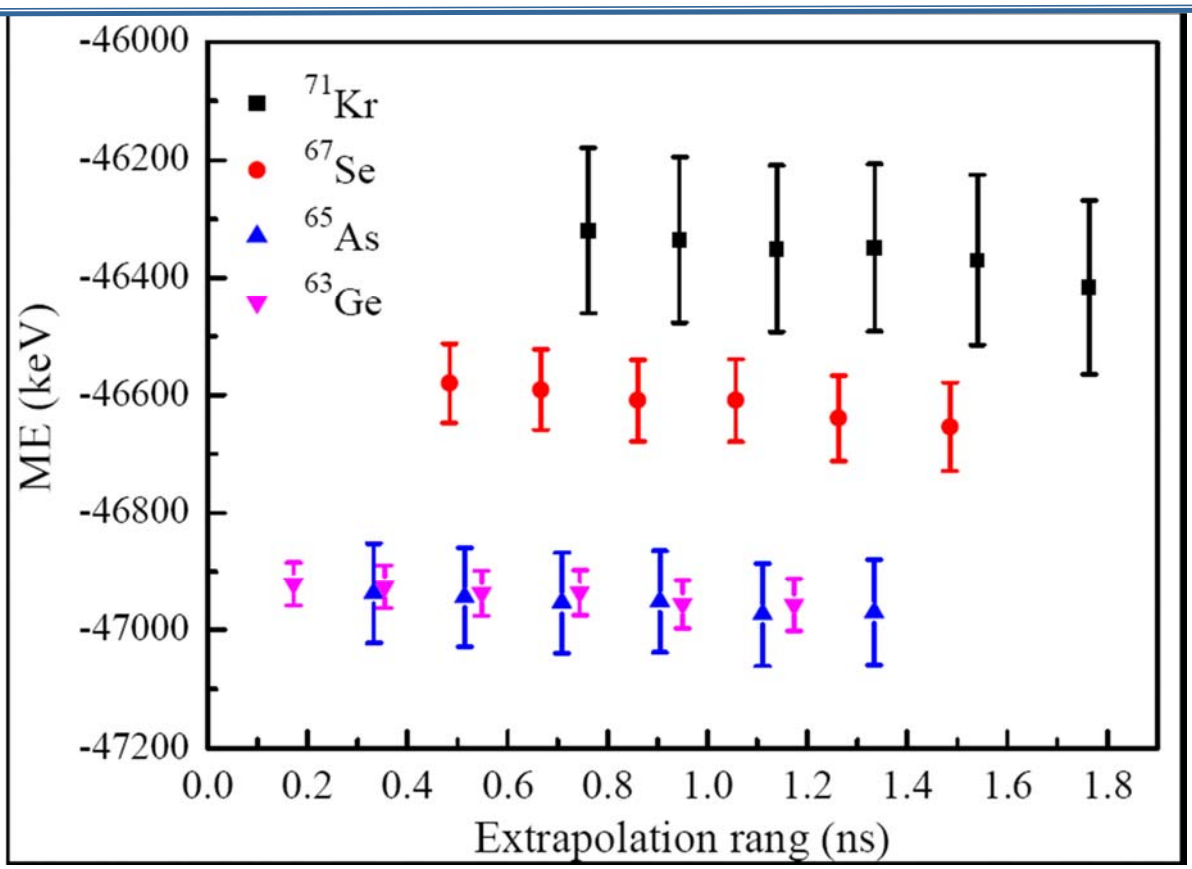

4. Results and Discussion

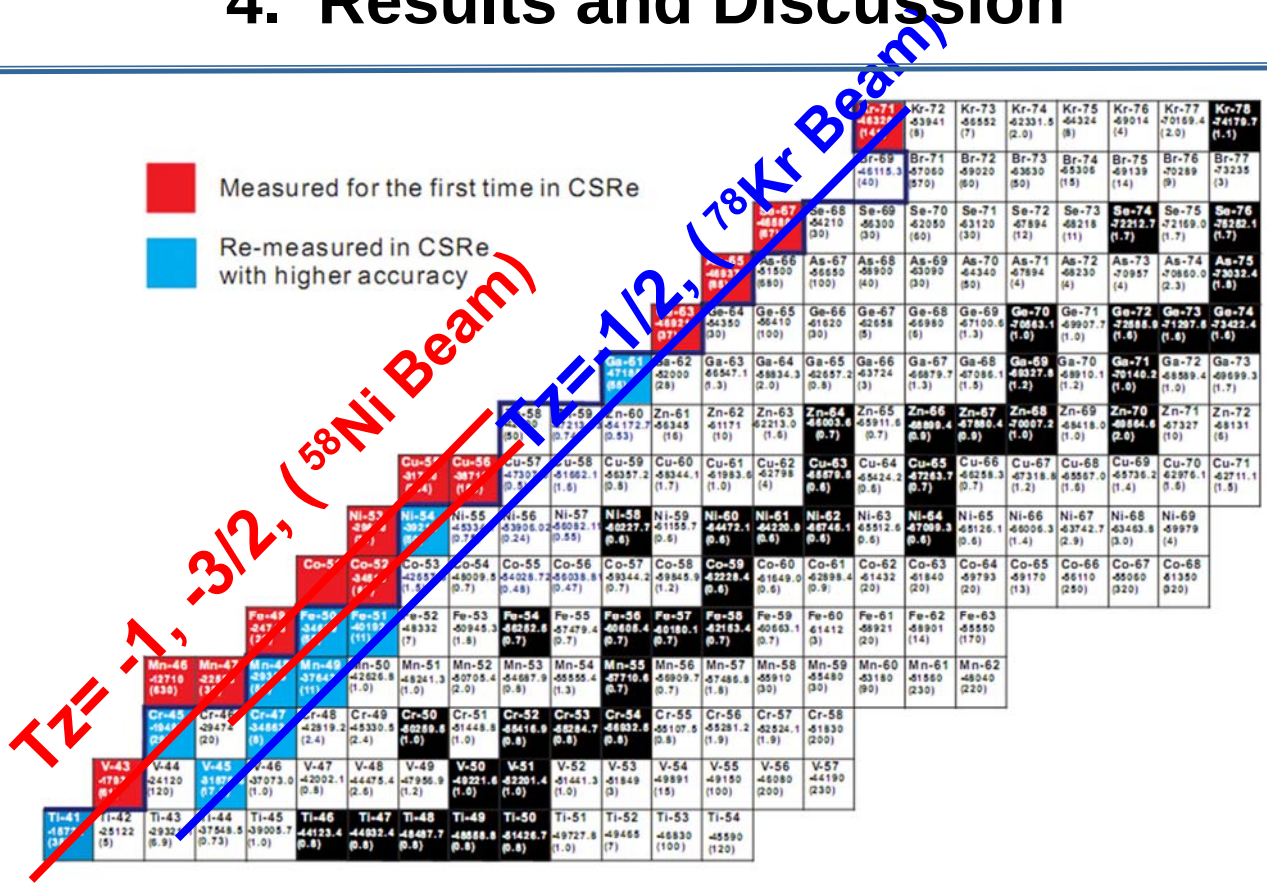

Impact on the rp-process of x-ray bursts

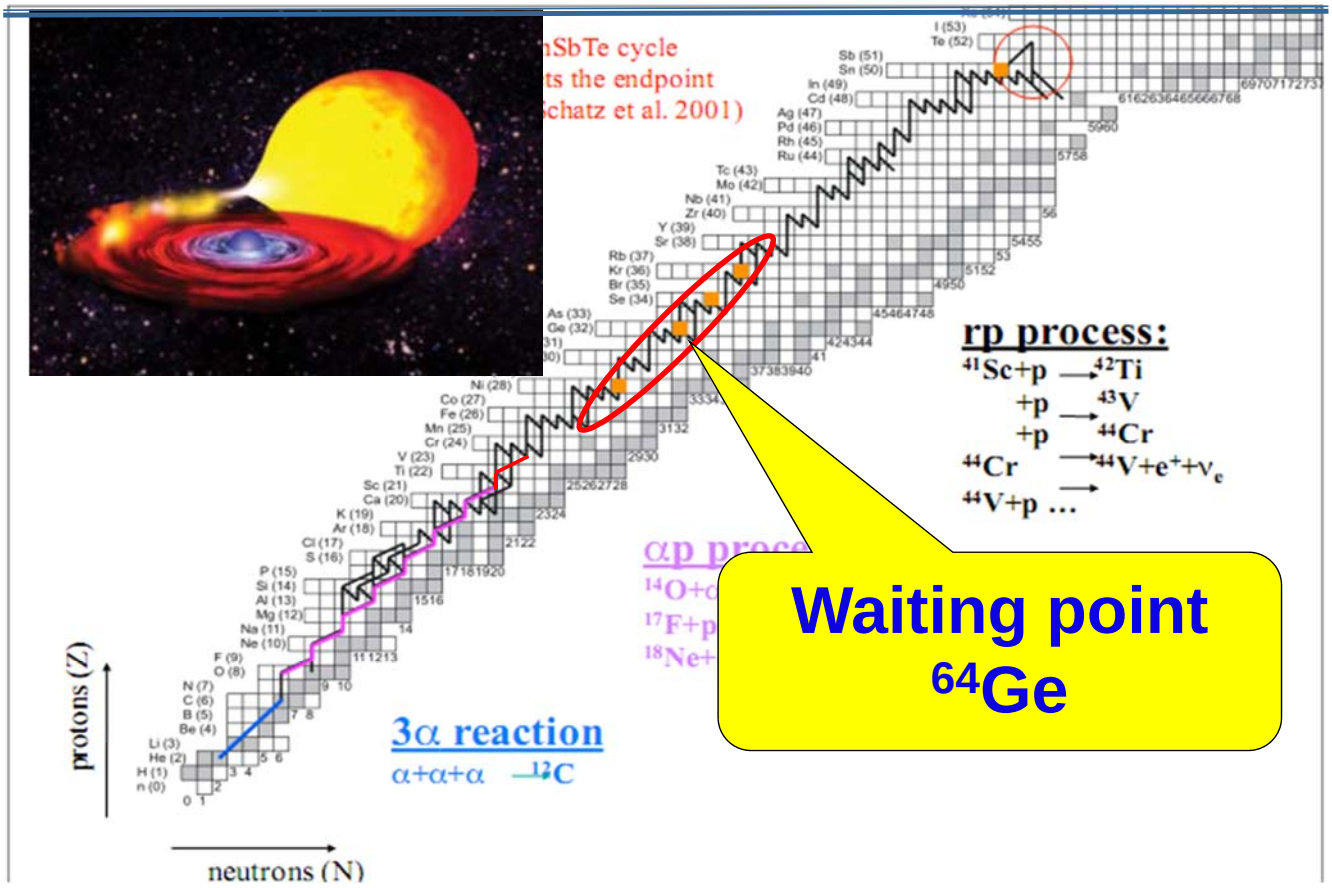

Waiting point nucleus ^{64}Ge ?

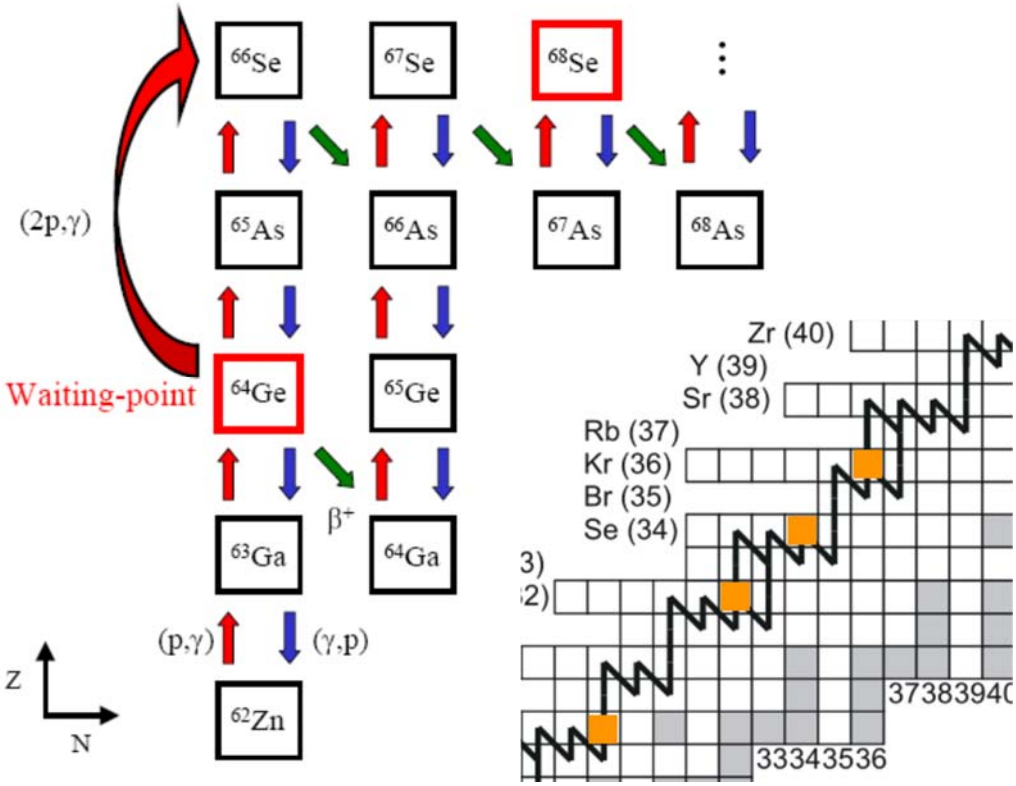

Impact on the rp-process of x-ray bursts

$$\lambda = \lambda_{\beta,j} + \lambda_{2p} = \lambda_{\beta,j} + (N_A \rho Y_P)^2 \left(\frac{2\pi\hbar^2}{\mu_j kT}\right)^{3/2} \frac{G_i}{(2J_p+1)G_j} \exp\left(\frac{Q_{j(p,r)i}}{kT}\right) \langle \sigma v \rangle_{i(p,r)}$$

Reaction	$Q \pm \Delta Q$ (keV)	Model affected
^{25}Si$(p,\gamma)^{26}$P	140 ± 196	short
^{26}P$(p,\gamma)^{27}$S	719 ± 281	K04, low$Z$,[a] short
^{30}S$(p,\gamma)^{31}$Cl	294 ± 50	hi$T$, short
^{50}Fe$(p,\gamma)^{51}$Co	88 ± 161	short
^{55}Ni$(p,\gamma)^{56}$Cu	555 ± 140	K04, low$T$, low$Z$, short
^{60}Zn$(p,\gamma)^{61}$Ga	192 ± 54	K04, low$T$, hi$T$,[a] low$Z$
^{64}Ge$(p,\gamma)^{65}$As	-80 ± 300	K04,[a] S01,[a] low$T$,[a] hi$T$,[a] low$Z$,[a] hi$Z$, hi$Z$2, long,[a] short
^{68}Se$(p,\gamma)^{69}$Br	-450 ± 100	hi$T$
^{89}Ru$(p,\gamma)^{90}$Rh	992 ± 711	long
^{98}Cd$(p,\gamma)^{99}$In	932 ± 408	S01
^{105}Sn$(p,\gamma)^{106}$Sb	357 ± 323	hi$T$
^{106}Sn$(p,\gamma)^{107}$Sb	518 ± 302	S01[a]

[a]Variation of this reaction Q-value affects the nuclear energy generation rate in this model (see text).

As-65

PRC79, 045802 (2009)

Effective half-life of ^{64}Ge

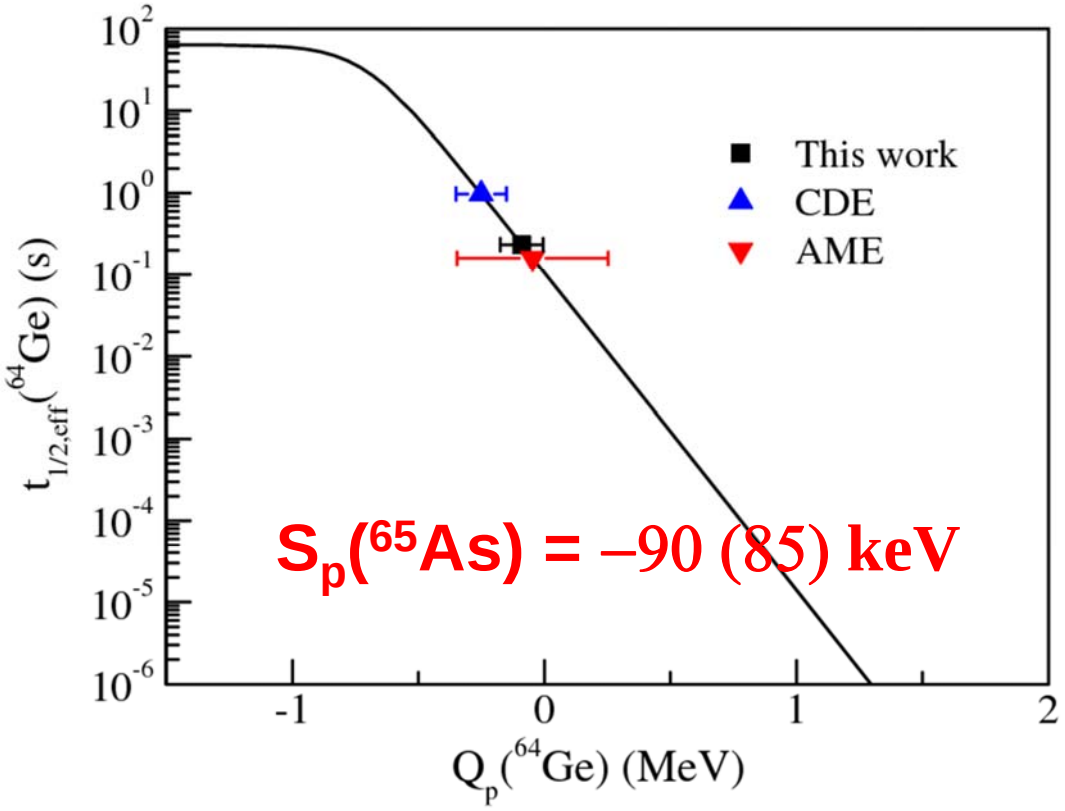

Light curve shape of Type I x-ray burst

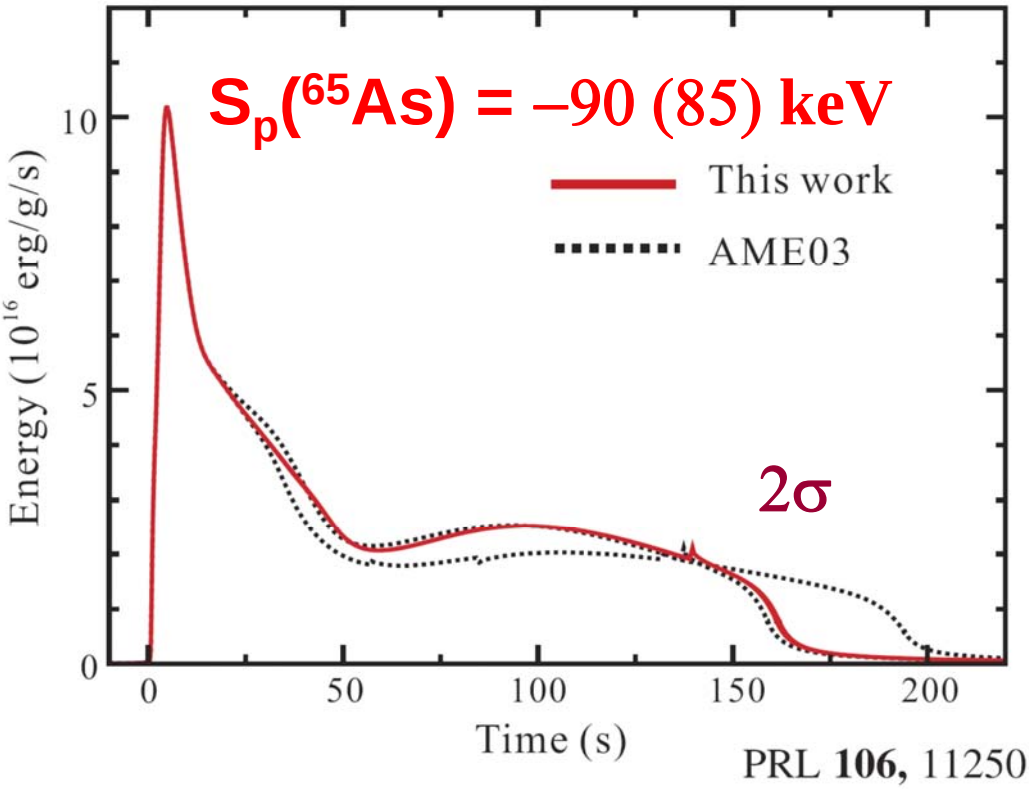

PRL **106,** 112501 (2011)

Abundance of x-ray burst ashes

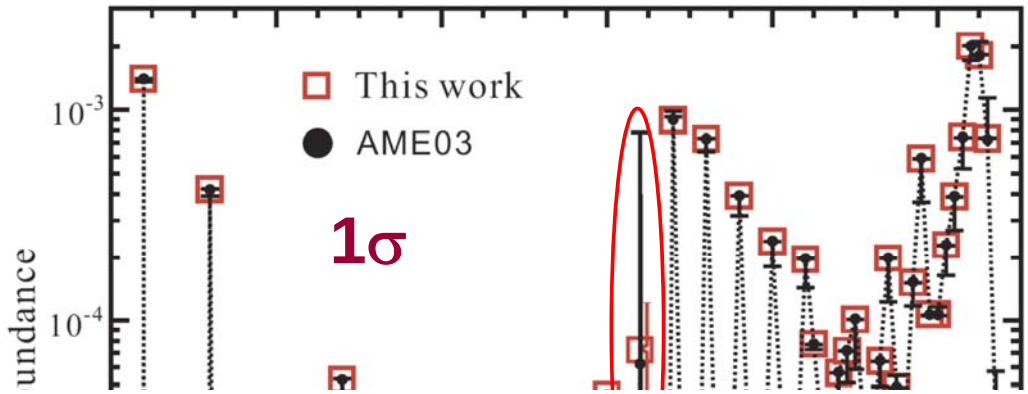

89%–90% of the reaction flow passes through ^{64}Ge via proton capture indicating that:

^{64}Ge is not a significant rp-process waiting point.

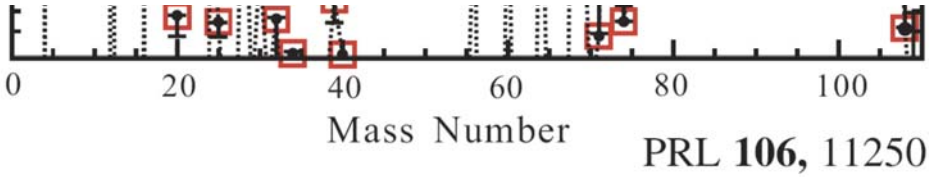

PRL **106,** 112501 (2011)

PRL 106, 112501 (2011) LETTERS week ending 18 MARCH 2011

Direct Mass Measurements of Short-Lived $A = 2Z - 1$ Nuclides ^{63}Ge, ^{65}As, ^{67}Se, and ^{71}Kr and Their Impact on Nucleosynthesis in the rp Process

X. L. Tu,[1,2] H. S. Xu,[1,*] M. Wang,[1] Y. H. Zhang,[1] Yu. A. Litvinov,[3,4,1] Y. Sun,[5,1] H. Schatz,[6] X. H. Zhou,[1] Y. J. Yuan,[1] J. W. Xia,[1] G. Audi,[7] K. Blaum,[3] C. M. Du,[1,2] P. Geng,[1,2] Z. G. Hu,[1] W. X. Huang,[1] S. L. Jin,[1,2] L. X. Liu,[1,2] Y. Liu,[1] X. Ma,[1] R. S. Mao,[1] B. Mei,[1] P. Shuai,[8] Z. Y. Sun,[1] H. Suzuki,[9] S. W. Tang,[1,2] J. S. Wang,[1] S. T. Wang,[1,2] G. Q. Xiao,[1] X. Xu,[1,2] T. Yamaguchi,[10] Y. Yamaguchi,[11] X. L. Yan,[1,2] J. C. Yang,[1] R. P. Ye,[1,2] Y. D. Zang,[1,2] H. W. Zhao,[1] T. C. Zhao,[1] X. Y. Zhang,[1] and W. L. Zhan[1]

[1]*Institute of Modern Physics, Chinese Academy of Sciences, Lanzhou 730000, People's Republic of China*
[2]*Graduate University of Chinese Academy of Sciences, Beijing, 100049, People's Republic of China*
[3]*Max-Planck-Institut für Kernphysik, Saupfercheckweg 1, D-69117 Heidelberg, Germany*
[4]*GSI Helmholtzzentrum für Schwerionenforschung, Planckstraße 1, 64291 Darmstadt, Germany*
[5]*Department of Physics, Shanghai Jiao Tong University, Shanghai 200240, People's Republic of China*
[6]*Department of Physics and Astronomy, National Superconducting Cyclotron Laboratory and the Joint Institute for Nuclear Astrophysics, Michigan State University, East Lansing, Michigan 48824, USA*
[7]*CSNSM-IN2P3-CNRS, Université de Paris Sud, F-91405 Orsay, France*
[8]*Department of Modern Physics, University of Science and Technology of China, Hefei 230026, People's Republic of China*
[9]*Institute of Physics, University of Tsukuba, Ibaraki 305-8571, Japan*
[10]*Department of Physics, Saitama University, Saitama 338-8570, Japan*
[11]*RIKEN Nishina Center, RIKEN, Saitama 351-0198, Japan*
(Received 8 January 2011; published 16 March 2011)

Precise mass data of astrophysics interest

Reaction	$Q \pm \Delta Q$ (keV)	Model affected
^{25}Si$(p,\gamma)^{26}$P	140 ± 196	short
^{26}P$(p,\gamma)^{27}$S	719 ± 281	K04, low$Z$,[a] short
^{30}S$(p,\gamma)^{31}$Cl	294 ± 50	hi$T$, short
^{42}Ti$(p,\gamma)^{43}$V	192 ± 233	S01, low$T$, low$Z$, short
^{45}Cr$(p,\gamma)^{46}$Mn	694 ± 515	F08
^{46}Cr$(p,\gamma)^{47}$Mn	78 ± 160	K04, low$T$, hi$T$, low$Z$, short
^{50}Fe$(p,\gamma)^{51}$Co	88 ± 161	short
^{55}Ni$(p,\gamma)^{56}$Cu	555 ± 140	K04, low$T$, low$Z$, short
^{60}Zn$(p,\gamma)^{61}$Ga	192 ± 54	K04, low$T$, hi$T$,[a] low$Z$
^{64}Ge$(p,\gamma)^{65}$As	-80 ± 300	K04,[a] S01,[a] low$T$,[a] hi$T$,[a] low$Z$,[a] hi$Z$, hi$Z$2, long,[a] short
^{68}Se$(p,\gamma)^{69}$Br	-450 ± 100	hi$T$
^{89}Ru$(p,\gamma)^{90}$Rh	992 ± 711	long
^{98}Cd$(p,\gamma)^{99}$In	932 ± 408	S01
^{105}Sn$(p,\gamma)^{106}$Sb	357 ± 323	hi$T$
^{106}Sn$(p,\gamma)^{107}$Sb	518 ± 302	S01[a]

[a]Variation of this reaction Q-value affects the nuclear energy generation rate in this model (see text).

PRC79, 045802 (2009)

^{43}V

^{47}Mn

^{65}As

Q-values for the（p, γ）reactions of astrophysics interest

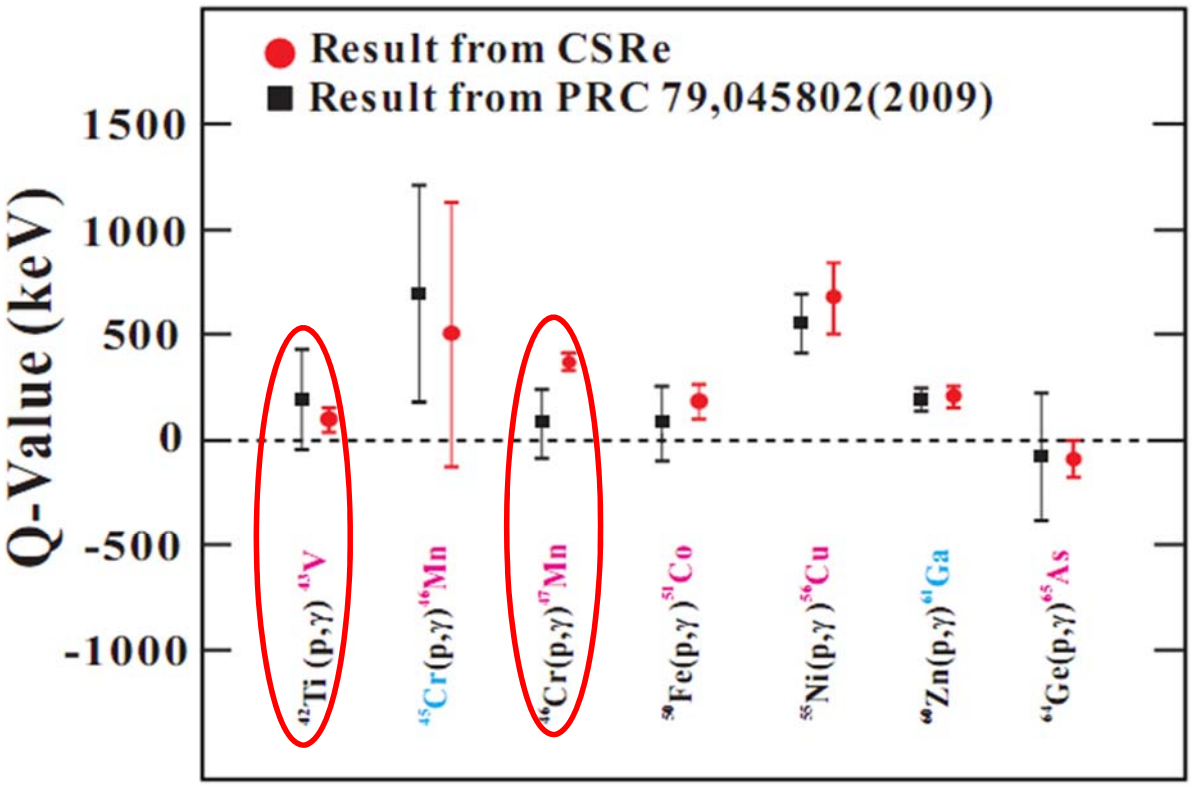

Nuclear Physics：test CDE calculations

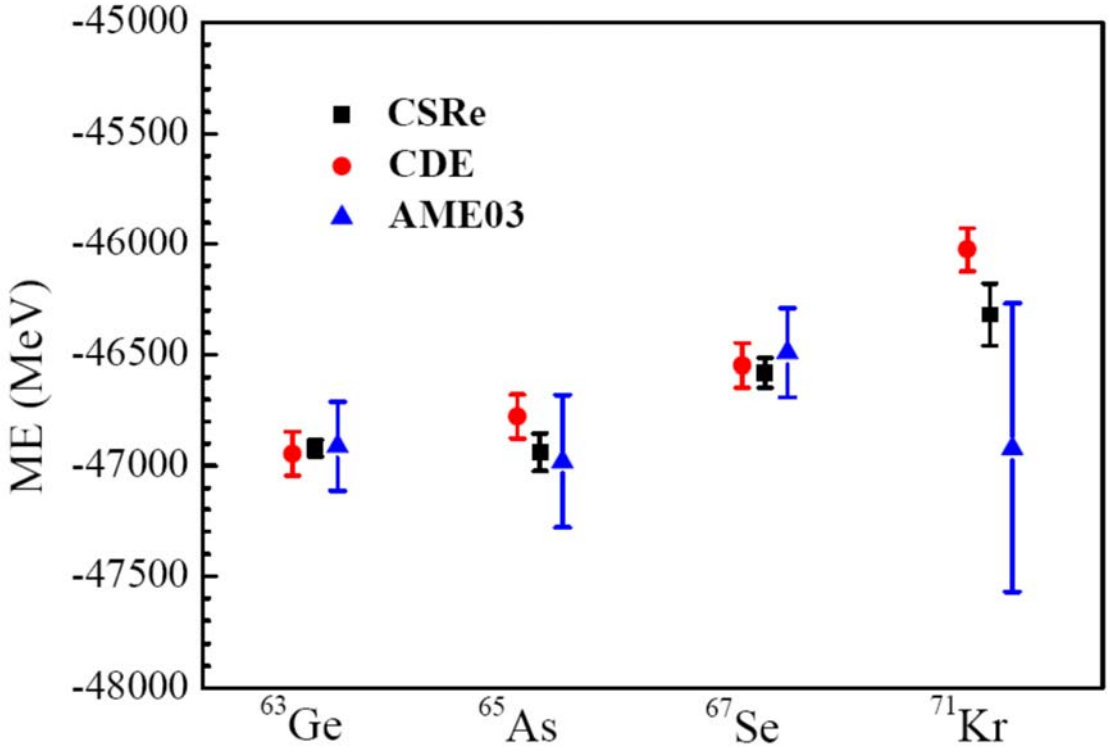

Nuclear Physics： test the mass of ^{69}Br

PRL 106, 252503 (2011) PHYSICAL REVIEW LETTERS week ending 24 JUNE 2011

Ground-State Proton Decay of ^{69}Br and Implications for the ^{68}Se Astrophysical Rapid Proton-Capture Process Waiting Point

A. M. Rogers,[1,2,3,*] M. A. Famiano,[4,3] W. G. Lynch,[1,5,3] M. S. Wallace,[6] F. Amorini,[7] D. Bazin,[1] R. J. Charity,[8] F. Delaunay,[9] R. T. de Souza,[10] J. Elson,[8] A. Gade,[1,5] D. Galaviz,[1,3] M.-J. van Goethem,[11] S. Hudan,[10] J. Lee,[1] S. Lobastov,[12] S. Lukyanov,[12] M. Matoš,[1,3] M. Mocko,[6] H. Schatz,[1,5,3] D. Shapira,[13] L. G. Sobotka,[8] M. B. Tsang,[1] and G. Verde[14]

[1]*National Superconducting Cyclotron Laboratory, Michigan State University, East Lansing, Michigan 48824, USA*
[2]*Physics Division, Argonne National Laboratory, Argonne, Illinois, 60439 USA*
[3]*Joint Institute of Nuclear Astrophysics, Michigan State University, East Lansing, Michigan 48824, USA*
[4]*Department of Physics, Western Michigan University, Kalamazoo, Michigan 49008, USA*
[5]*Department of Physics and Astronomy, Michigan State University, East Lansing, Michigan 48824, USA*
[6]*Los Alamos National Laboratory, Los Alamos, New Mexico 87545, USA*
[7]*Istituto Nazionale di Fisica Nucleare, Laboratori Nazionali del Sud, Catania, I-95123, Italy*
[8]*Department of Chemistry, Washington University, St. Louis, Missouri 63130, USA*
[9]*LPC Caen, ENSICAEN, Université de Caen, CNRS/IN2P3, Caen, France*
[10]*Indiana University Cyclotron Facility and Department of Chemistry, Bloomington, Indiana 47405, USA*
[11]*Kernfysisch Versneller Instituut, NL-9747 AA Groningen, The Netherlands*
[12]*FLNR/JINR, 141980 Dubna, Moscow region, Russian Federation*
[13]*Oak Ridge National Laboratory, Oak Ridge, Tennessee 37831, USA*

$S_p(^{69}Br) = -785\ (35)$ keV

Coulomb energy differences between mirror nuclei

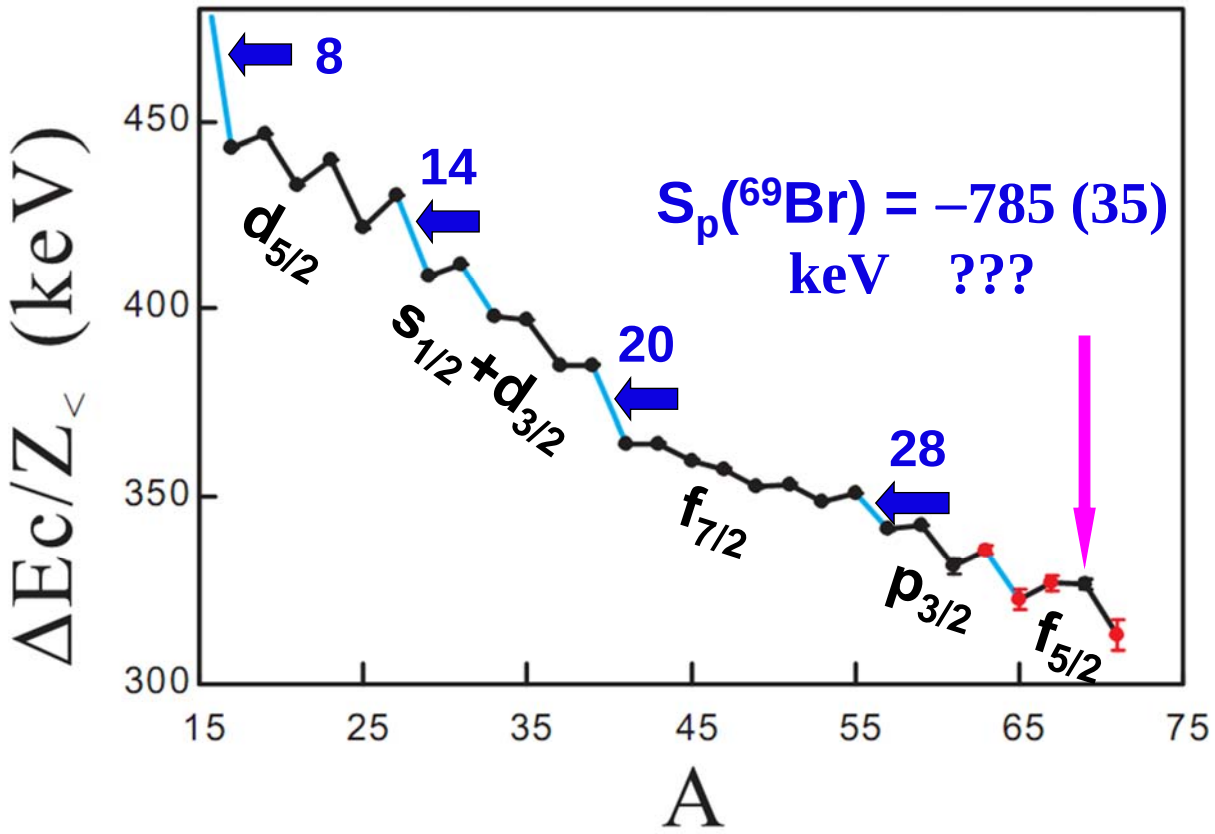

Nuclear Physics： test IMME

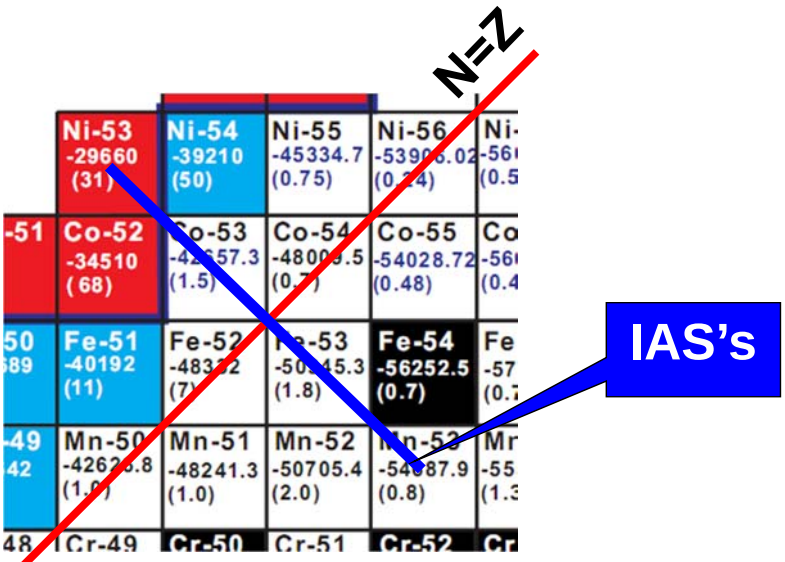

$$M(T,A,T_3) = a(T,A,) + b(T,A)T_3 + c(T,A)T_3^2$$

$T_3(p) = -1/2$
$T_3(n) = +1/2$
+ perturbation

$$M(T,A,T_3) = a(T,A,) + b(T,A)T_3 + c(T,A)T_3^2 + d(T,A)T_3^3$$

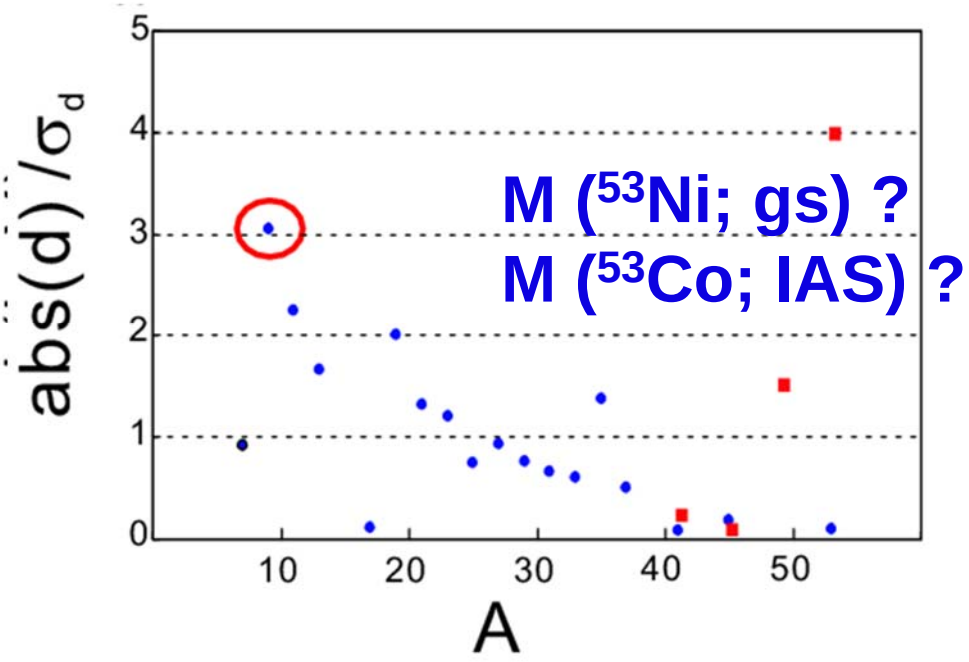

5. Summary & perspectives

^{78}Kr, ^{58}Ni fragmentation

Measured for the first time in CSRe

Re-measured in CSRe with higher accuracy

13

10

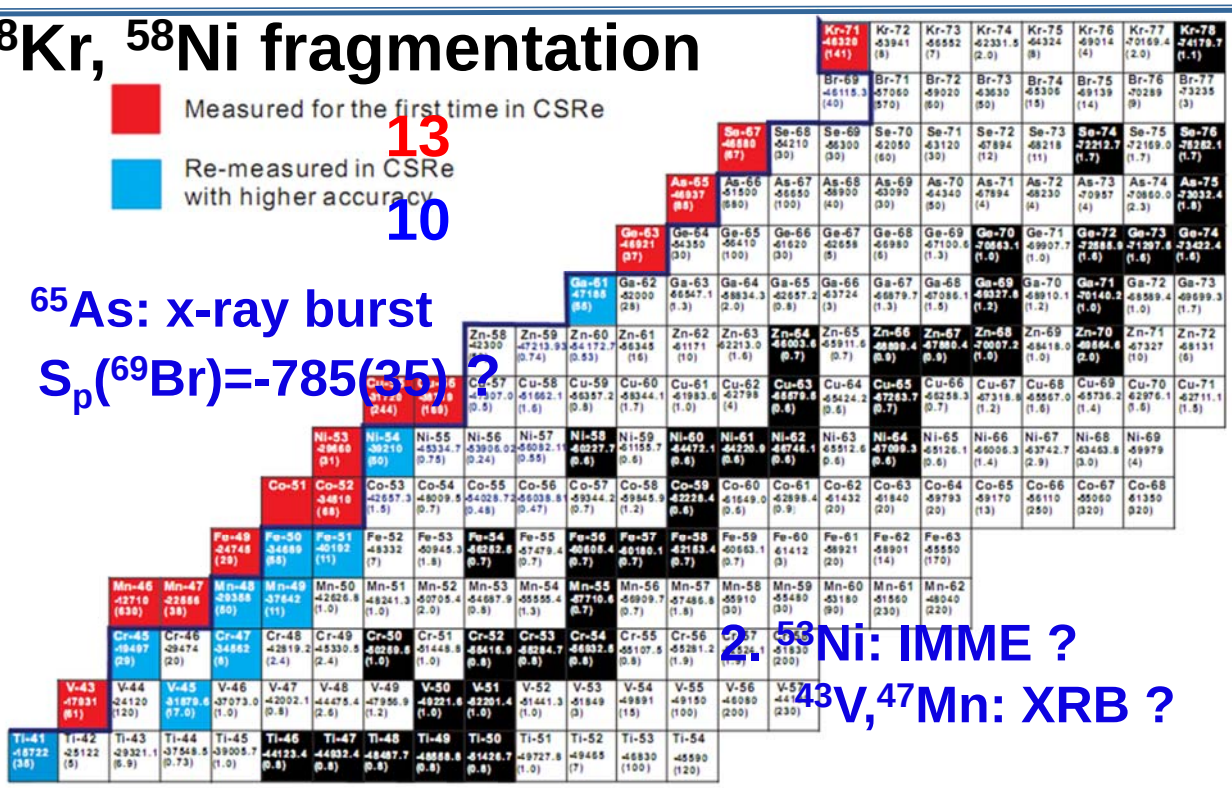

1. ^{65}As: x-ray burst

   $S_p(^{69}Br)$=-785(35) ?

2. ^{53}Ni: IMME ?

   ^{43}V,^{47}Mn: XRB ?

In progress

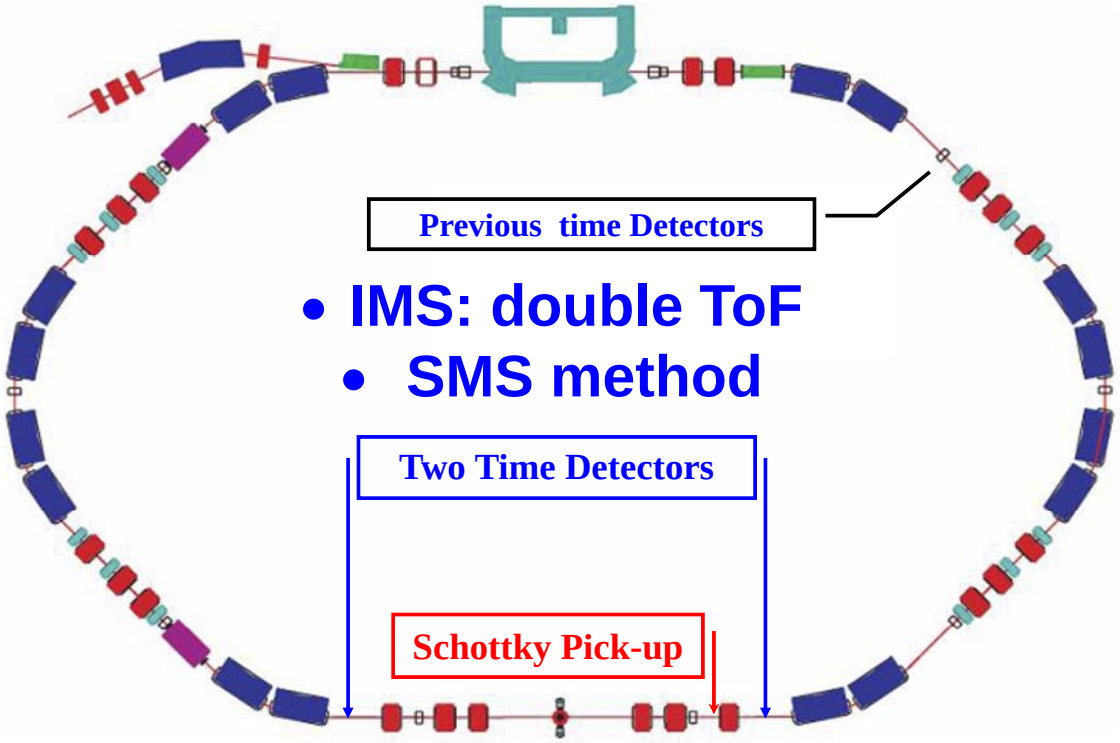

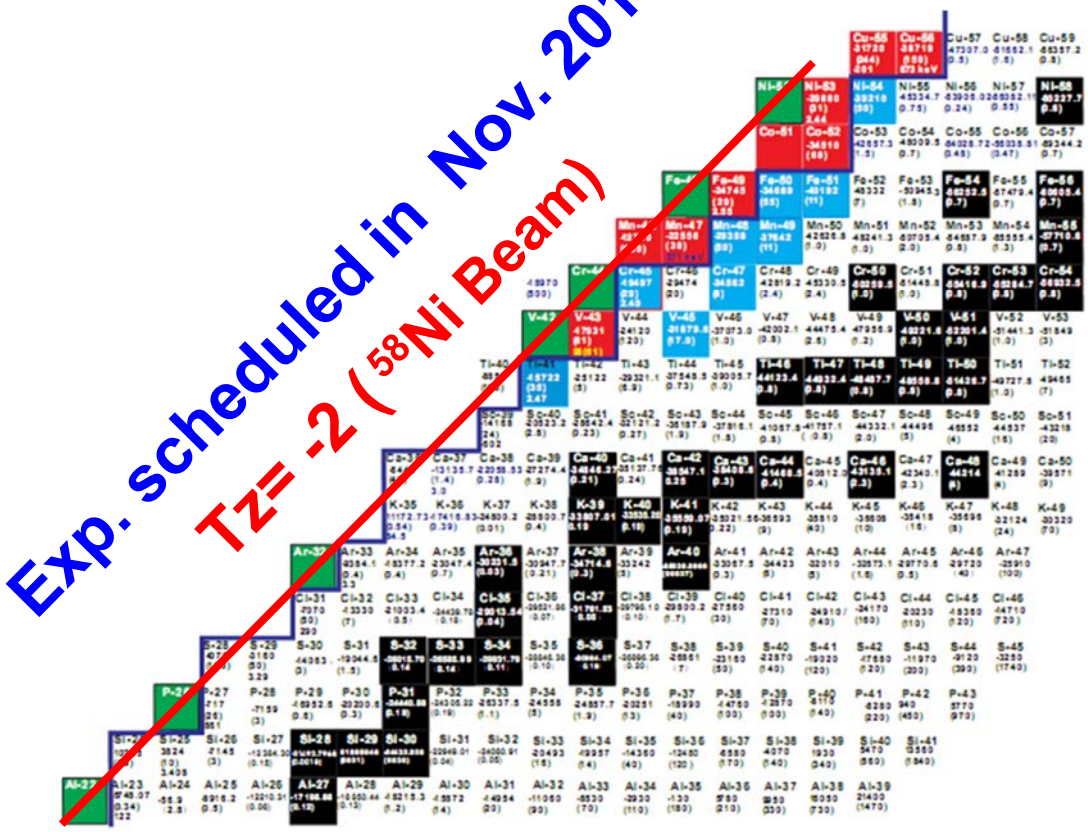
Exp. scheduled in Nov. 2011
Tz= -2 (58Ni Beam)

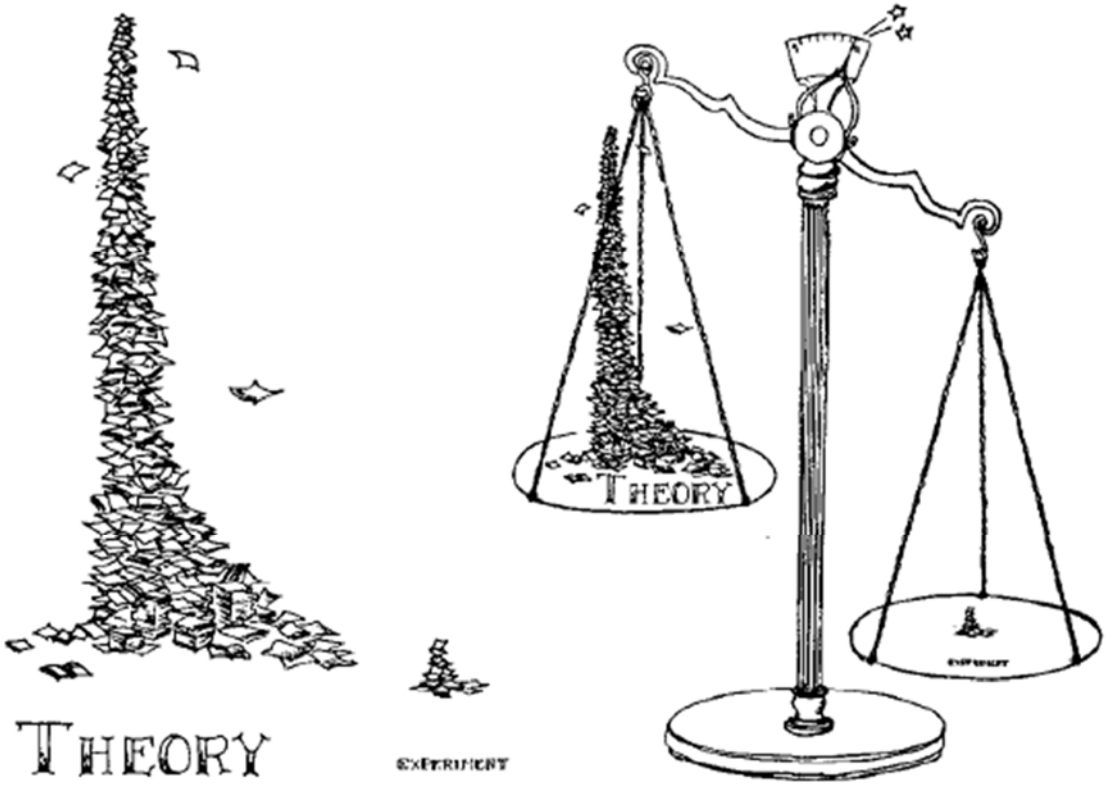
THEORY
EXPERIMENT
THEORY

人的正确思想是从哪里来的?

人民领袖毛泽东

1) 阶级斗争,
2) 生产实践,
3) 科学实验.

Thanks for your attention !

Properties and Synthesis of Superheavy Elements: a Theoretical Survey

Lecture notes for the 6th Int. Summer School Subatomic Phys., Aug. 27-31, 2011, Beijing

Shan-Gui Zhou (周善贵)[1,2,*]
[1] *Institute of Theoretical Physics, Chinese Academy of Sciences, Beijing 100190, China*
[2] *Center of Theoretical Nuclear Physics, National Laboratory of Heavy Ion Accelerator, Lanzhou 730000, China*

(Dated: August 15, 2011)

In these two lectures, I will present a survey of theoretical studies on properties and synthesis mechanism of superheavy elements (SHE). After a brief introduction of the history on the theoretical predictions of the island of stability, I will shortly mention the experimental progresses made so far. Then I will focus on the study of the structure, the decay, and the synthesis mechanism of superheavy nuclei (SHN).

CONTENTS

* sgzhou@itp.ac.cn; http://www.itp.ac.cn/~sgzhou

Part I

A brief history

In this part, I will briefly mention the history on the theoretical prediction of the existence of superheavy nuclei and of the island of stability.

The word "superheavy nuclei" was probably first proposed by Wheeler in 1955 (Wheeler, 1955). Later on, by an extrapolation of the known shell structure, Scharff-Goldhaber predicted that $Z = 126$ could be the next proton magic number (Scharff-Goldhaber, 1957). In 1958, Werner and Wheeler discussed in details "Superheavy Nuclei" which was also the title of their article (Werner and Wheeler, 1958).

From 1966, an additional stabilization from the shell effects of superheavy nuclei was studied more quantitatively (Myers and Swiatecki, 1966) and several groups predicted $Z = 114$ as the next proton shell closure (Meldner, 1967; Mosel and Greiner, 1969; Nilsson *et al.*, 1969; Sobiczewski *et al.*, 1966). Siemens and Bethe also discussed the shape of heavy nuclei and emphasized the importance of shell structure in superheavy nuclei, but they came to the following conclusion (Siemens and Bethe, 1967): "We therefore believe that shell effects are unlikely to make the nucleus $Z = 114$ stable."

Some detailed discussions on the history of superheavy nuclei can be found in (Herrmann, 1998, 2004; Kalinkin and Gareev, 2001a,b).

Part II
Experimental Status

I. SEARCH IN NATURE

The early prediction tells that there might be some long-lived superheavy nuclei. If this is true, it would be possible that superheavy nuclei exist in nature. Therefore many groups started to search for superheavy elements in, e.g., terrestrial matter, meteorites, cosmic rays, etc. (Herrmann, 2004). Although there were some claims on the observation, e.g., the element with $Z = 122$ in a recent work (Marinov *et al.*, 2010), there are still not yet confirmed results.

II. EFFORTS IN LABORATORIES

A superheavy nucleus can be synthesized via heavy ion fusion reactions in laboratories. The main labs worldwide include: GSI in Darmstadt, Germany, Flerov Laboratory of Nuclear Reactions in Dubna, Russia, Lawrence Berkeley National Laboratory in Berkeley, USA, RIKEN in Wako, Japan, GANIL in Caen, France, HIRFL in Lanzhou, China. Two types of reactions, the cold fusion and the hot fusion, are used. Up to now, elements with $Z \leq 118$ have been produced and those with $Z \leq 112$ have been officially named. The main results can be found in (Hofmann and Münzenberg, 2000; Morita *et al.*, 2004; Oganessian, 2007; Oganessian *et al.*, 2010).

It should be mentioned that these superheavy nuclei are all neutron-deficient, with at least 7 neutrons less than the predicted next neutron magic number $N = 184$.

Part III
Structure of superheavy nuclei

III. SHELL STRUCTURE: NEXT PROTON AND NEUTRON MAGIC NUMBERS

Shell effects are responsible for the stability of superheavy nuclei. The single particle shell structure is crucial for the location of the island of stability. For example, whether the next shell closure of protons appears at $Z = 114$ or 120 is mainly determined by the splitting of the spin doublets $\pi 2f_{5/2,7/2}$. Theoretically different models usually predict different closed shells beyond ^{208}Pb; even within the same model there are parameter-dependent predictions. For examples, the macroscopic-microscopic models or the extended Thomas-Fermi-Strutinsky integral approach predict that the next shell closure for the proton is at $Z = 114$ (Cwiok and Sobiczewski, 1992; Mamdouh *et al.*, 2001; Möller *et al.*, 1995); the relativistic mean field models predicts $Z = 114$ or 120 to be the next proton magic number (Bender *et al.*, 1999; Kruppa *et al.*, 2000; Lalazissis *et al.*, 1996; Meng *et al.*, 2006; Rutz *et al.*, 1997; Zhang *et al.*, 2005); predictions from non-relativistic mean field models with Skyrme forces are $Z = 114$, 120, 124, or 126, depending on the parametrization (Bender *et al.*, 1999; Kruppa *et al.*, 2000; Rutz *et al.*, 1997). The shell structure of SHN is important not only for the location of the island of stability, but also for the study of the synthesis mechanism of SHN.

See (Afanasjev *et al.*, 2003; Sobiczewski and Pomorski, 2007) for a detailed discussion.

IV. LOW-LYING SPECTRA

Experimentally one can not investigate directly the single particle level structure of SHN with $Z \geq 110$ because the production cross sections of these nuclei is tiny which makes the spectroscopy experiment impossible at present. To learn more about the shell structure of SHN, an indirect way is to study lighter nuclei in the deformed region with $Z \approx 100$ and $N \approx 152$. The strongly downsloping orbitals originating from the spherical subshells and active in the vicinity of the predicted shell closures may come close to the Fermi surface in these deformed nuclei. The rotational properties of nuclei in this mass region are affected strongly by these spherical orbitals. For example, the proton $1/2^-[521]$ orbital is of particular interest since it stems from the spherical $\pi 2f_{5/2}$ orbital.

Both the in-beam spectroscopy and spectroscopy following the decay of isomeric states or alpha decays have been used to study nuclei with $Z \approx 100$ (Ackermann, 2011; Greenlees, 2011; Herzberg, 2004; Herzberg and Greenlees, 2008; Leino and Hessberger, 2004).

Theoretically, the deformations, the shell structure, the rotational properties, and high-K isomeric states have been studied by using the self-consistent mean field models (Adamian *et al.*, 2011, 2010b; Afanasjev *et al.*, 2003; Bender *et al.*, 2003a; Delaroche *et al.*, 2006), the macroscopic-microscopic models (Adamian *et al.*, 2011, 2010a,b,c; Cwiok *et al.*, 1994; Muntian *et al.*, 1999; Parkhomenko and Sobiczewski, 2004, 2005; Sobiczewski *et al.*, 2001), the projected shell model (Al-Khudair *et al.*, 2009; Sun *et al.*, 2008), the cranked shell models (He *et al.*, 2009; Xu *et al.*, 2004; Zhang *et al.*, 2011), etc..

V. POTENTIAL ENERGY SURFACES: SHAPES AND FISSION BARRIERS

The potential energy surface describes the energy change of a nucleus with its shape and it is usually a

landscape in a multidimensional deformation space. For heavy and superheavy nuclei, the potential energy surface is particularly important because it determines the fission path and fission barrier. Two types of approaches have been extensively used to study potential energy surfaces: the macroscopic-microscopic method (Möller *et al.*, 2001, 2009; Sobiczewski and Pomorski, 2007) and the constrained mean field method (Abusara *et al.*, 2010; Bender *et al.*, 2003b; Lu *et al.*, 2011; Ring and Schuck, 1980).

VI. ISOMERIC STATES

Configuration-constrained calculations of potential-energy surfaces in even-even superheavy nuclei systematically revealed the existence of long-lived isomeric states — multi-quasi-particle states with deformed axially symmetric shapes and large angular momenta at low excitation energies (Xu *et al.*, 2004). These results indicate the prevalence of long-lived multi-quasiparticle isomers. In a quantum system, the ground state is usually more stable than the excited states. However, in superheavy nuclei the multi-quasiparticle excitations decrease the probability for both fission and alpha-decay, implying an enhanced stability (Xu *et al.*, 2004). "The nuclear isomers in superheavy elements" may serve as "stepping stones towards the island of stability" (Herzberg *et al.*, 2006). Hence, the systematic occurrence of multi-quasiparticle isomers may become crucial for the future production of even heavier nuclei (Adamian *et al.*, 2009, 2010b,c).

Part IV
Decay of superheavy nuclei

VII. DECAY FROM GROUND STATES: LIFETIME AND IDENTIFICATION

A superheavy nucleus in its ground state can decay via spontaneous fission, α-decay, and β-decay. As a crucial ingredient of the existence of the island of stability, the stability of superheavy nuclei in their ground states has been studied extensively since the existence of superheavy elements was predicted (Mosel and Greiner, 1969; Nilsson *et al.*, 1969).

For a recent review, see (Sobiczewski and Pomorski, 2007).

VIII. DECAY OF COMPOUND SUPERHEAVY NUCLEI

The stability of an excited superheavy nuclei is also an important issue. On the one hand, it helps to understand the stability behavior of a superheavy nucleus against excitation, e.g., the attenuation of the shell effects with temperature. On the other hand, the survival probability $W_{\rm sur}$ of an excited compound nucleus against processes in which the charge number changes is directly related to the stability of an excited superheavy nucleus in various channels. The survival probability $W_{\rm sur}$ is an important factor in the study of the synthesis mechanism of superheavy elements (Xia *et al.*, 2011; Zubov *et al.*, 2009).

Part V
Synthesis mechanism

IX. HEAVY ION FUSION REACTIONS: CAPTURE, FUSION AND SURVIVAL

To describe the synthesis of a superheavy nucleus via heavy ion fusion reactions, there are two types of approaches according to how the two colliding nuclei are treated. One is a microscopic way and describes the colliding process as a merge of two multi-nucleon systems. The other describes macroscopically this process as a merge of two viscous liquid drops. The time-dependent Hartree-Fock theory (Guo *et al.*, 2008; Umar *et al.*, 2010) and the quantum molecular dynamics model (Bian *et al.*, 2009; Jiang *et al.*, 2010; Tian *et al.*, 2009; Zhang *et al.*, 2006) are examples of the first type. The second type approaches include: the macroscopic dynamical model (Swiatecki, 1982), the fluctuation-dissipation model (Abe *et al.*, 2003; Shen *et al.*, 2002), the nucleon collectivization model (Zagrebaev, 2001), models based on the dinuclear system concept (Adamian *et al.*, 1998; Li *et al.*, 2010, 2003; Zhao *et al.*, 2008), the fusion by diffusion models (Liu and Bao, 2007; Swiatecki *et al.*, 2005), and a model based on multi-dimensional Langevin equations (Zagrebaev and Greiner, 2005).

Recent review articles for the second type of approaches include (Feng *et al.*, 2011; Volkov, 2004).

It should be emphasized that although many models can achieve satisfactory agreements with the experiment, their predictions for unknown regions usually differ a lot. What is more striking is that the formation probability of compound nuclei from different models varies by several orders of magnitude (Naik *et al.*, 2007). This situation indicates a strong desire of more realistic models and more accurate structure information which is a very important input for the study of dynamics in the heavy ion fusion.

X. ALTERNATIVE APPROACHES

With complete fusion reactions (either cold or hot), it seems that the evaporation residue cross sections for the production of even heavier superheavy nuclei are still decreasing and would be beyond current experimental ability. Therefore alternative approaches for the synthesis of superheavy nuclei are proposed, e.g., by strongly damped reactions (Tian *et al.*, 2008) or transfer reactions (Feng *et al.*, 2009; Heinz *et al.*, 2010).

REFERENCES

Abe, Y., C. Shen, G. Kosenko, and D. Boilley (2003), Phys. At. Nucl. **66** (6), 1057.

Abusara, H., A. V. Afanasjev, and P. Ring (2010), Phys. Rev. C **82** (4), 044303.

Ackermann, D. (2011), Acta Phys. Pol. B **42** (3-4), 577.

Adamian, G., N. Antonenko, L. A. Malov, B. N. Lu, S. G. Zhou, and W. Scheid (2009), in *Nuclear Structure and Related Topics*, Vol. I, edited by A. I. Vdovin, V. V. Voronov, and R. V. Jolos, pp. 141–149, proceedings of the International Conference on Nuclear Structure and Related Topics, Dubna, June 30-July 4, 2009.

Adamian, G. G., N. V. Antonenko, S. N. Kuklin, B. N. Lu, L. A. Malov, and S. G. Zhou (2011), Phys. Rev. C, in press.

Adamian, G. G., N. V. Antonenko, S. N. Kuklin, and W. Scheid (2010a), Phys. Rev. C **82** (5), 054304.

Adamian, G. G., N. V. Antonenko, L. A. Malov, B. N. Lu, S. G. Zhou, and W. Scheid (2010b), Phys. Part. Nucl. **41** (7), 1101.

Adamian, G. G., N. V. Antonenko, and W. Scheid (2010c), Phys. Rev. C **81** (2), 024320.

Adamian, G. G., N. V. Antonenko, W. Scheid, and V. V. Volkov (1998), Nucl. Phys. A **633** (3), 409.

Afanasjev, A. V., T. L. Khoo, S. Frauendorf, G. A. Lalazissis, and I. Ahmad (2003), Phys. Rev. C **67** (2), 024309.

Al-Khudair, F., G.-L. Long, and Y. Sun (2009), Phys. Rev. C **79** (3), 034320.

Bender, M., P. Bonche, T. Duguet, and P. H. Heenen (2003a), Nucl. Phys. A **723** (3-4), 354.

Bender, M., P.-H. Heenen, and P.-G. Reinhard (2003b), Rev. Mod. Phys. **75** (1), 121.

Bender, M., K. Rutz, P.-G. Reinhard, J. A. Maruhn, and W. Greiner (1999), Phys. Rev. C **60** (3), 034304.

Bian, B.-A., F.-S. Zhang, and H.-Y. Zhou (2009), Nucl. Phys. A **829** (1-2), 1.

Cwiok, S., S. Hofmann, and W. Nazarewicz (1994), Nucl. Phys. A **573** (3), 356.

Cwiok, S., and A. Sobiczewski (1992), Z. Phys. A **342** (2), 203.

Delaroche, J.-P., M. Girod, H. Goutte, and J. Libert (2006), Nucl. Phys. A **771**, 103.

Feng, Z.-Q., G.-M. Jin, and J.-Q. Li (2009), Phys. Rev. C **80** (6), 067601.

Feng, Z.-Q., G.-M. Jin, and J.-Q. Li (2011), Nucl. Phys. Rev. **28** (1), 1.

Greenlees, P. T. (2011), Acta Phys. Pol. B **42** (3-4), 587.

Guo, L., J. A. Maruhn, P.-G. Reinhard, and Y. Hashimoto (2008), Phys. Rev. C **77** (4), 041301.

He, X.-T., Z.-Z. Ren, S.-X. Liu, and E.-G. Zhao (2009), Nucl. Phys. A **817** (1-4), 45.

Heinz, S., V. Comas, S. Hofmann, D. Ackermann, J. Heredia, F. Hessberger, J. Khuyagbaatar, B. Kindler, B. Lommel, and R. Mann (2010), Eur. Phys. J. A **43** (2), 181.

Herrmann, G. (1998), Nucl. Phys. News **8** (2), 7.

Herrmann, G. (2004), "Historical reminiscences," Chap. 8 (Kluwer Academic Publishers, New York, Boston, Dordrecht, Moscow) pp. 291–318, the Chemistry of Superheavy Elements.

Herzberg, R.-D. (2004), J. Phys. G: Nucl. Phys. **30** (4), R123.

Herzberg, R.-D., and P. Greenlees (2008), Prog. Part. Nucl. Phys. **61** (2), 674.

Herzberg, R.-D., P. T. Greenlees, P. A. Butler, G. D. Jones, M. Venhart, I. G. Darby, S. Eeckhaudt, K. Eskola, T. Grahn, C. Gray-Jones, F. P. Hessberger, P. Jones, R. Julin, S. Juutinen, S. Ketelhut, W. Korten, M. Leino, A.-P. Leppanen, S. Moon, M. Nyman, R. D. Page, J. Pakarinen, A. Pritchard, P. Rahkila, J. Saren, C. Scholey, A. Steer, Y. Sun, C. Theisen, and J. Uusitalo (2006), Nature **442** (7105), 896.

Hofmann, S., and G. Münzenberg (2000), Rev. Mod. Phys. **72** (3), 733.

Jiang, Y., N. Wang, Z. Li, and W. Scheid (2010), Phys. Rev. C **81** (4), 044602.

Kalinkin, B. N., and F. A. Gareev (2001a), "On the problem of synthesis of superheavy nuclei: A short historical review on first theoretical predictions and new experimental reality," arXiv: nucl-th/0105021v1, preprint JINR E7-99-107, Dubna, 1999.

Kalinkin, B. N., and F. A. Gareev (2001b), "Synthesis of superheavy elements and theory of atomic nucleus," arXiv: nucl-th/0111083v2, talk at the Intern. Symp. on Exotic Nuclei. Baikal Lake, July 24–28, 2001.

Kruppa, A. T., M. Bender, W. Nazarewicz, P.-G. Reinhard, T. Vertse, and S. Cacutewiok (2000), Phys. Rev. C **61** (3), 034313.

Lalazissis, G. A., M. M. Sharma, P. Ring, and Y. K. Gambhir (1996), Nucl. Phys. A **608** (2), 202.

Leino, M., and F. P. Hessberger (2004), Annu. Rev. Nucl. Part. Sci. **54**, 175.

Li, J.-Q., Z.-Q. Feng, Z.-G. Gan, X.-H. Zhou, H.-F. Zhang, and W. Scheid (2010), *The 10th International Conference on Nucleus-Nucleus Collisions (NN2009)*, Nucl. Phys. A **834** (1-4), 353c.

Li, W., N. Wang, J. F. Li, H. Xu, W. Zuo, E. Zhao, J. Q. Li, and W. Scheid (2003), Europhys. Lett. **64** (6), 750.

Liu, Z. H., and J.-D. Bao (2007), Phys. Rev. C **76** (3), 034604.

Lu, B.-N., E.-G. Zhao, and S.-G. Zhou (2011), Phys. Rev. C **84** (1), 014328.

Mamdouh, A., J. M. Pearson, M. Rayet, and F. Tondeur (2001), Nucl. Phys. A **679** (3-4), 337.

Marinov, A., I. Rodushkin, D. Kolb, A. Pape, Y. Kashiv, R. Brandt, R. V. Gentry, and H. W. Miller (2010), Int. J. Mod. Phys. E **19** (1), 131, arXiv: 0804.3869v1 [nucl-ex].

Meldner, H. (1967), Arkiv Fysik **36** (2), 593, in Proc. of the Lysekil Symposium: Nuclides ar off the Stability Line, Aug. 21-27, 1966, Sweden.

Meng, J., H. Toki, S. G. Zhou, S. Q. Zhang, W. H. Long, and L. S. Geng (2006), Prog. Part. Nucl. Phys. **57** (2), 470.

Möller, P., D. G. Madland, A. J. Sierk, and A. Iwamoto (2001), Nature **409** (6822), 785.

Möller, P., J. R. Nix, W. D. Myers, and W. J. Swiatecki (1995), At. Data Nucl. Data Tables **59** (2), 185.

Möller, P., A. J. Sierk, T. Ichikawa, A. Iwamoto, R. Bengtsson, H. Uhrenholt, and S. Aberg (2009), Phys. Rev. C **79** (6), 064304.
Morita, K., K. Morimoto, D. Kaji, T. Akiyama, S.-i. Goto, H. Haba, E. Ideguchi, R. Kanungo, K. Katori, H. Koura, H. Kudo, T. Ohnishi, A. Ozawa, T. Suda, K. Sueki, H.-S. Xu, T. Yamaguchi, A. Yoneda, A. Yoshida, and Y.-L. Zhao (2004), J. Phys. Soc. Jpn. **73**, 2593.
Mosel, U., and W. Greiner (1969), Z. Phys. A **222** (3), 261.
Muntian, I., Z. Patyk, and A. Sobiczewski (1999), Phys. Rev. C **60** (4), 041302.
Myers, W. D., and W. J. Swiatecki (1966), Nucl. Phys. **81** (1), 1.
Naik, R. S., W. Loveland, P. H. Sprunger, A. M. Vinodkumar, D. Peterson, C. L. Jiang, S. Zhu, X. Tang, E. F. Moore, and P. Chowdhury (2007), Phys. Rev. C **76** (5), 054604.
Nilsson, S. G., C. F. Tsang, A. Sobiczewski, Z. Szymanski, S. Wycech, C. Gustafson, I.-L. Lamm, P. Möller, and B. Nilsson (1969), Nucl. Phys. A **131** (1), 1.
Oganessian, Y. (2007), J. Phys. G: Nucl. Phys. **34** (4), R165.
Oganessian, Y. T., F. S. Abdullin, P. D. Bailey, D. E. Benker, M. E. Bennett, S. N. Dmitriev, J. G. Ezold, J. H. Hamilton, R. A. Henderson, M. G. Itkis, Y. V. Lobanov, A. N. Mezentsev, K. J. Moody, S. L. Nelson, A. N. Polyakov, C. E. Porter, A. V. Ramayya, F. D. Riley, J. B. Roberto, M. A. Ryabinin, K. P. Rykaczewski, R. N. Sagaidak, D. A. Shaughnessy, I. V. Shirokovsky, M. A. Stoyer, V. G. Subbotin, and R. Sudowe (2010), Phys. Rev. Lett. **104** (14), 142502.
Parkhomenko, A., and A. Sobiczewski (2004), Acta Phys. Pol. B **35** (10), 2447.
Parkhomenko, A., and A. Sobiczewski (2005), Acta Phys. Pol. B **36** (10), 3115.
Ring, P., and P. Schuck (1980), *The Nuclear Many-Body Problem* (Springer).
Rutz, K., M. Bender, T. Burvenich, T. Schilling, P.-G. Reinhard, J. A. Maruhn, and W. Greiner (1997), Phys. Rev. C **56** (1), 238.
Scharff-Goldhaber, G. (1957), Nukeonika (Nucleonics) **15** (9), 122.
Shen, C., G. Kosenko, and Y. Abe (2002), Phys. Rev. C **66** (6), 061602R.
Siemens, P. J., and H. A. Bethe (1967), Phys. Rev. Lett. **18** (17), 704.
Sobiczewski, A., F. Gareev, and B. Kalinkin (1966), Phys. Lett. **22** (4), 500.
Sobiczewski, A., I. Muntian, and Z. Patyk (2001), Phys. Rev. C **63** (3), 034306.
Sobiczewski, A., and K. Pomorski (2007), Prog. Part. Nucl. Phys. **58** (1), 292.
Sun, Y., G.-L. Long, F. Al-Khudair, and J. A. Sheikh (2008), Phys. Rev. C **77** (4), 044307.
Swiatecki, W. J. (1982), Nucl. Phys. A **376** (2), 275.
Swiatecki, W. J., K. Siwek-Wilczynska, and J. Wilczynski (2005), Phys. Rev. C **71** (1), 014602.
Tian, J., X. Li, X. Wu, Z. Li, and S. Yan (2009), Eur. Phys. J. A **42** (1), 105.
Tian, J., X. Wu, K. Zhao, Y. Zhang, and Z. Li (2008), Phys. Rev. C **77** (6), 064603.
Umar, A. S., V. E. Oberacker, J. A. Maruhn, and P.-G. Reinhard (2010), Phys. Rev. C **81** (6), 064607.
Volkov, V. (2004), Acta Phys. Hung. A **19** (1), 67.
Werner, F. G., and J. A. Wheeler (1958), Phys. Rev. **109** (1), 126.
Wheeler, J. A. (1955), in *Proceedings of the International Conference on the Peaceful Uses of Atomic Energy*, Vol. 2, pp. 155–163.
Xia, C.-J., B.-X. Sun, E.-G. Zhao, and S.-G. Zhou (2011), "Systematic study of survival probability of excited superheavy nuclei," arXiv: 1101.2725 [nucl-th], to be published in Sci. China Phys. Mech. Astron.
Xu, F. R., E. G. Zhao, R. Wyss, and P. M. Walker (2004), Phys. Rev. Lett. **92** (25), 252501.
Zagrebaev, V., and W. Greiner (2005), J. Phys. G: Nucl. Part. Phys. **31** (7), 825.
Zagrebaev, V. I. (2001), Phys. Rev. C **64** (3), 034606.
Zhang, F. S., Z. Q. Feng, and G. M. Jin (2006), Int. J. Mod. Phys. E **15** (7), 1601.
Zhang, W., J. Meng, S. Zhang, L. Geng, and H. Toki (2005), Nucl. Phys. A **753** (1-2), 106.
Zhang, Z.-H., J.-Y. Zeng, E.-G. Zhao, and S.-G. Zhou (2011), Phys. Rev. C **83** (1), 011304R.
Zhao, E. G., N. Wang, Z. Q. Feng, J. Q. Li, S. G. Zhou, and W. Scheid (2008), Int. J. Mod. Phys. E **17** (9), 1937, in Proceedings of International Workshop on Nuclear Dynamics in Heavy-ion Reactions and Neutron Stars, Beijing, July 9-14, 2007.
Zubov, A., G. Adamian, and N. Antonenko (2009), Phys. Part. Nucl. **40** (6), 847.

Properties & Synthesis of Superheavy Elements
--- A Theoretical Survey ---

Shan-Gui Zhou 周 善 贵

Institute of Theoretical Physics (ITP), Chinese Academy of Sciences (CAS), Beijing
(中国科学院理论物理研究所)
Center of Theoretical Nucl. Phys., National Lab. of Heavy Ion Accelerator, Lanzhou
(兰州重离子加速器国家实验室原子核理论中心)

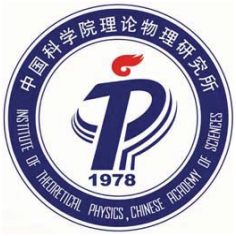

The 6th Int. Summer School on Subatomic Physics
Aug. 27-31, Beijing

Contents

- Superheavy elements – history of predictions
- Experimental progress
- Structure of superheavy nuclei
  - **Shell structure: next proton & neutron magic numbers**
  - **Potential energy surfaces: shape, fission path & fission barrier**
  - **Low-lying spectra**
  - **Isomeric states**
- Synthesis mechanism of SHN via heavy ion reactions
  - **Capture process**
  - **Fusion – formation of a compound nucleus**
  - **Survival – competition between neutron emission & fission**
- Summary & Perspectives

Stable Nuclei

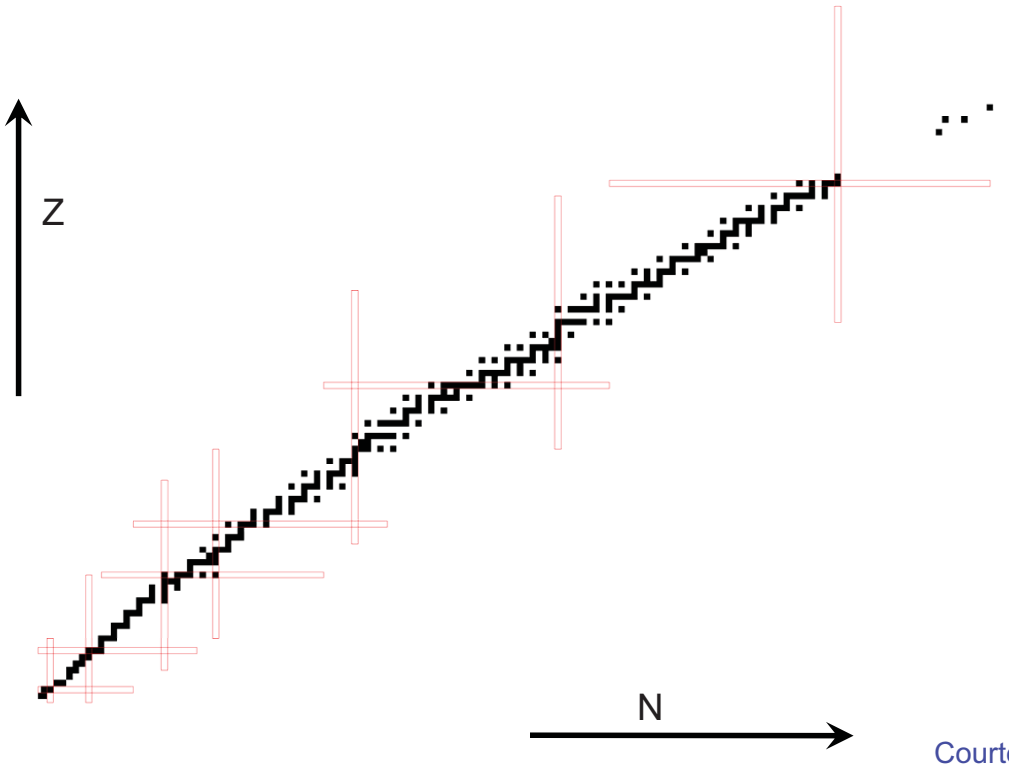

Courtesy of Jie Zhao (赵杰)

Stable Nuclei

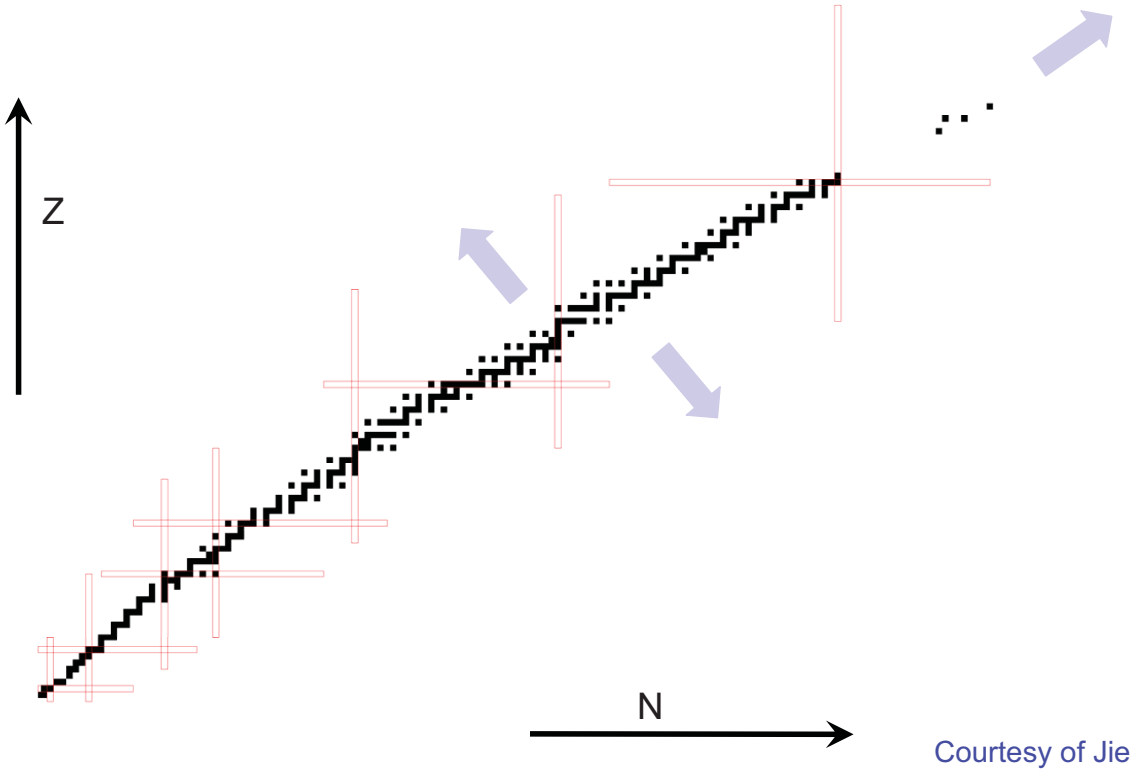

Courtesy of Jie Zhao (赵杰)

Unstable (Exotic) Nuclei

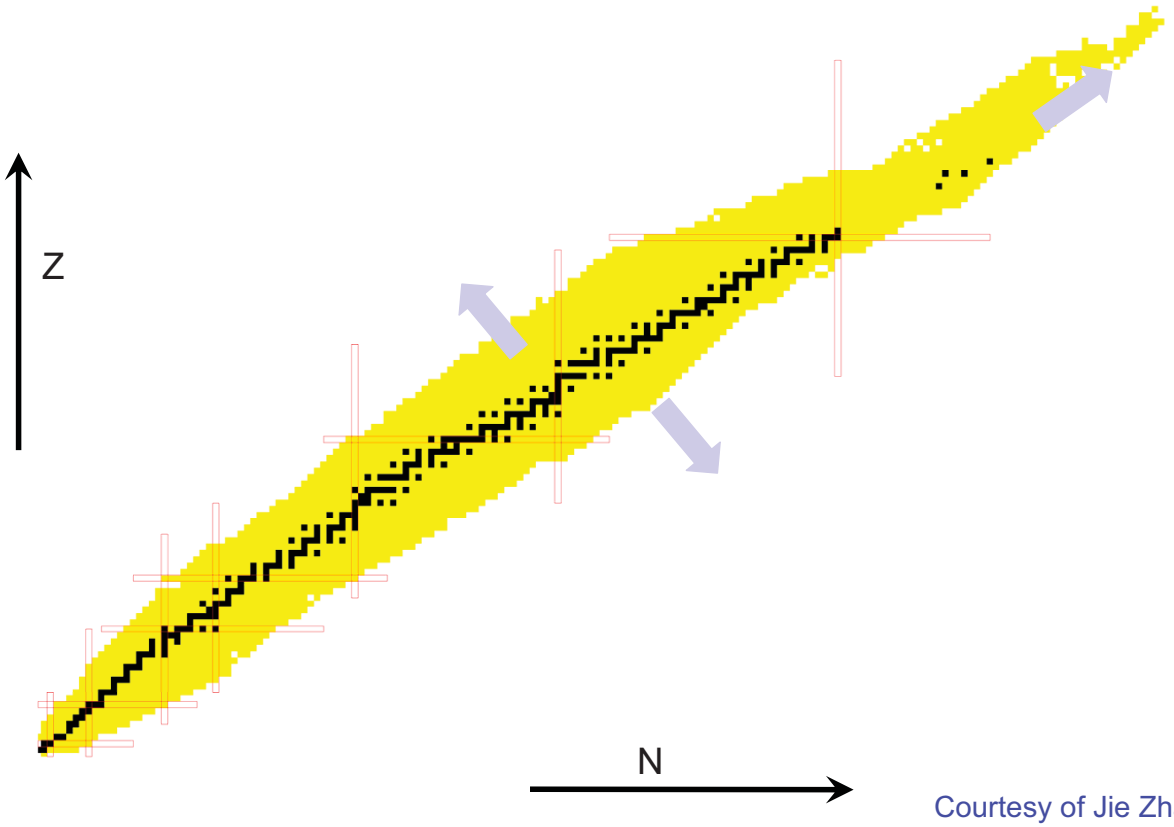

Courtesy of Jie Zhao (赵杰)

More Unstable Nuclei

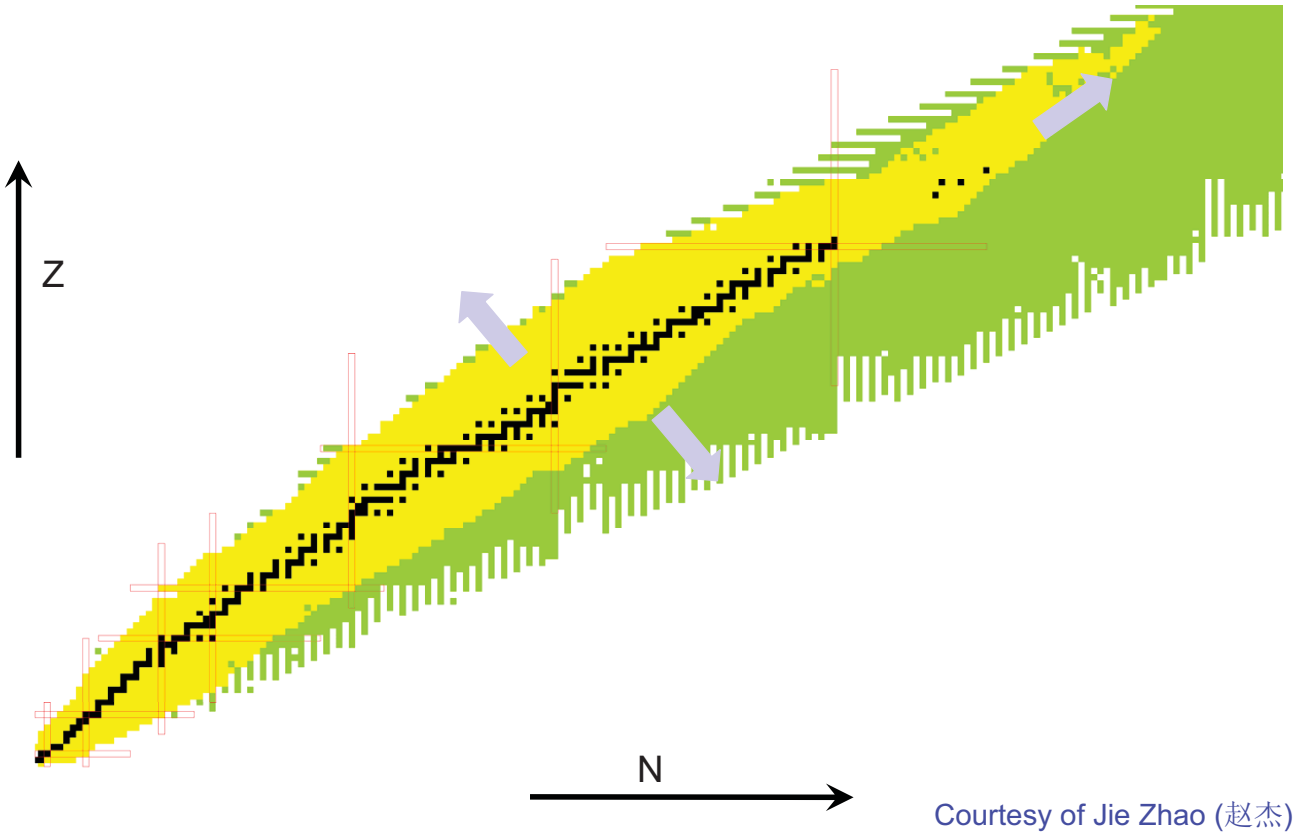

Courtesy of Jie Zhao (赵杰)

Periodic Table of Elements

Group	1	2		3	4	5	6	7	8	9	10	11	12	13	14	15	16	17	18
Period																			
1	1 H																		2 He
2	3 Li	4 Be												5 B	6 C	7 N	8 O	9 F	10 Ne
3	11 Na	12 Mg												13 Al	14 Si	15 P	16 S	17 Cl	18 Ar
4	19 K	20 Ca		21 Sc	22 Ti	23 V	24 Cr	25 Mn	26 Fe	27 Co	28 Ni	29 Cu	30 Zn	31 Ga	32 Ge	33 As	34 Se	35 Br	36 Kr
5	37 Rb	38 Sr		39 Y	40 Zr	41 Nb	42 Mo	43 Tc	44 Ru	45 Rh	46 Pd	47 Ag	48 Cd	49 In	50 Sn	51 Sb	52 Te	53 I	54 Xe
6	55 Cs	56 Ba	*	71 Lu	72 Hf	73 Ta	74 W	75 Re	76 Os	77 Ir	78 Pt	79 Au	80 Hg	81 Tl	82 Pb	83 Bi	84 Po	85 At	86 Rn
7	87 Fr	88 Ra	**																

*Lanthanoids	*	57 La	58 Ce	59 Pr	60 Nd	61 Pm	62 Sm	63 Eu	64 Gd	65 Tb	66 Dy	67 Ho	68 Er	69 Tm	70 Yb
**Actinoids	**	89 Ac	90 Th	91 Pa	92 U	93 Np	94 Pu	95 Am	96 Cm	97 Bk	98 Cf	99 Es	100 Fm	101 Md	102 No

WebElements, Aug. 2011

A nucleus described as a charged liquid drop

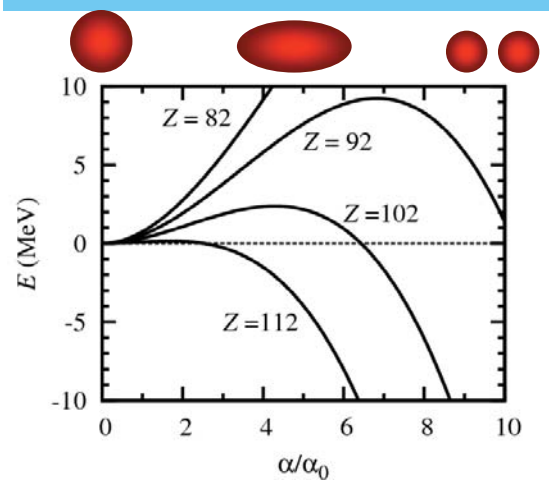

Magic numbers & nuclear shell structure

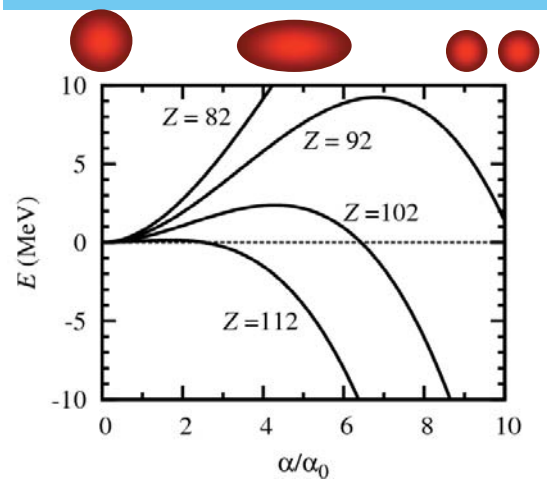

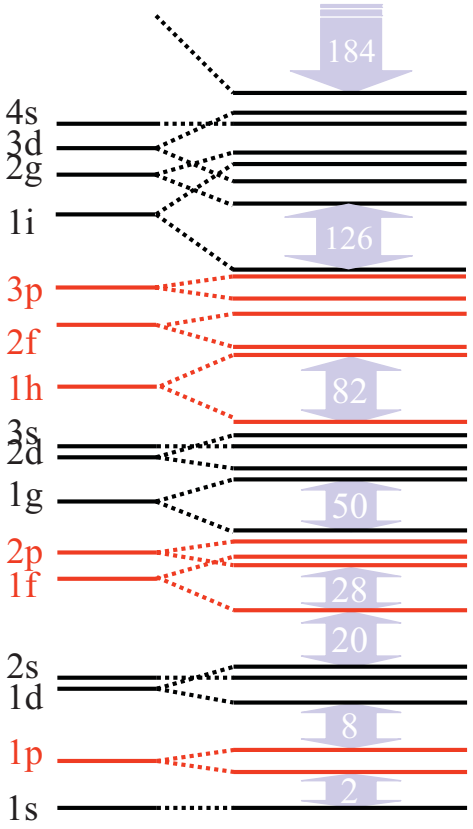

Magic numbers & nuclear shell structure

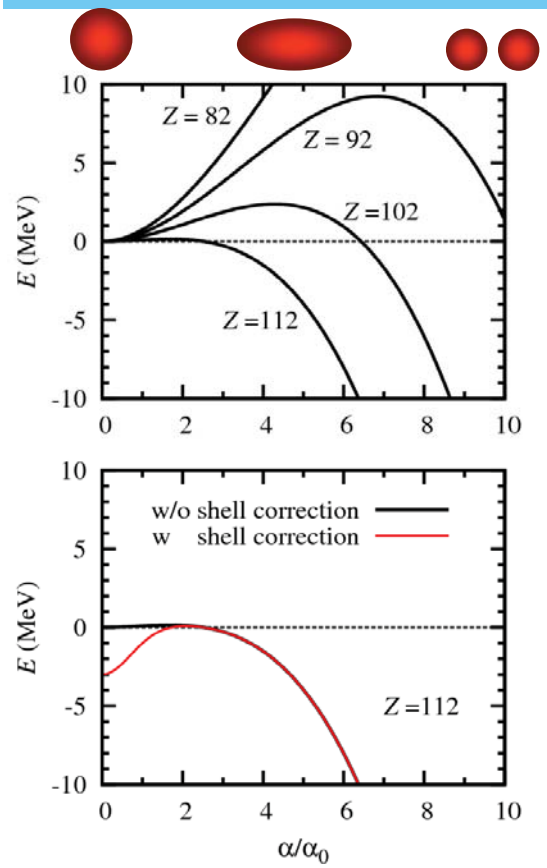

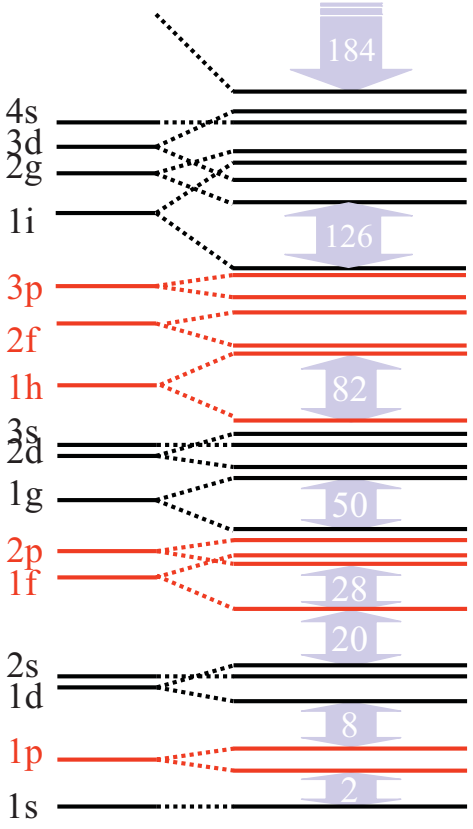

Extrapolation of the shell structure – earlier than 1966

Wheeler 1955

bility analysis of very heavy nuclei. In so far as one can extrapolate the stability criteria for very heavy nuclei, one is led to expect the existence of nuclei twice as heavy as known nuclear species, that can be created by massive neutron irradiation, and that will live long enough to be studied in the laboratory.

Scharff-Goldhaber1957_Nucleonics15-122

Relatively long-lived isotopes may well be found among the far-transuranic nuclides because of magic-number stability

There may be, for instance, another region of relative stability at the doubly magic nucleus $_{126}X^{310}$ (the closing of the j neutron shell).

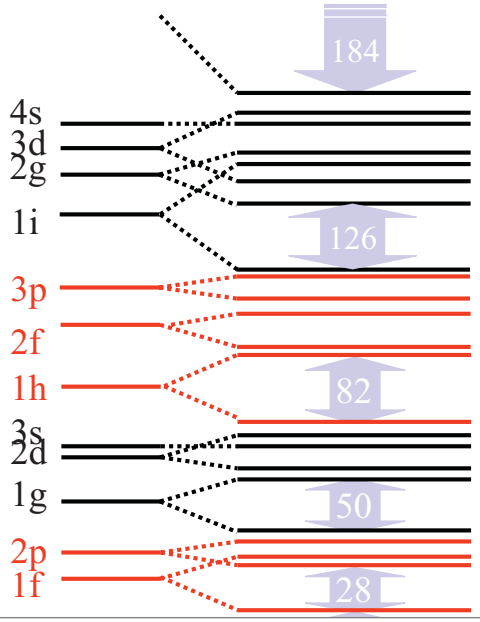

Werner_Wheeler1958_PR109-126

PHYSICAL REVIEW · VOLUME 109, NUMBER 1 JANUARY 1, 1958

Superheavy Nuclei

FREDERICK G. WERNER AND JOHN A. WHEELER
Palmer Physical Laboratory, Princeton University, Princeton, New Jersey

(Received August 19, 1957)

Shell effects from quantitative considerations – 1960s

1.E.2: 1.D.4

Nuclear Physics **81** (1966) 1—60; © *North-Holland Publishing Co., Amsterdam*

NUCLEAR MASSES AND DEFORMATIONS

WILLIAM D. MYERS and WLADYSLAW J. SWIATECKI
Lawrence Radiation Laboratory, University of California, Berkeley, California†

Received 7 September 1965

half-life. This is illustrated in fig. 2 where we have plotted the deformation energy predicted by our mass formula for the case $Z = 126$, $N = 184$. This nucleus has a fissility parameter $x = 1.05$; as a result, in the absence of shell effects, it would have a vanishing barrier against fission and a spontaneous fission half-life of the order of nuclear collective oscillations or 10^{-22} sec. Because of the assumed doubly magic number, however, the ground-state mass of this nucleus would be depressed (by about 10.2 MeV according to our formula). Since this depression is, according to our treatment, a rapidly decreasing function of deformation, there results a considerable barrier against fission, with a height of 9.0 MeV: the extra binding associated with the doubly magic number has stabilized the otherwise highly fissile nucleus. An

Possible changes of proton shell structure in heavy nuclei

Large *A*
Large *Z*

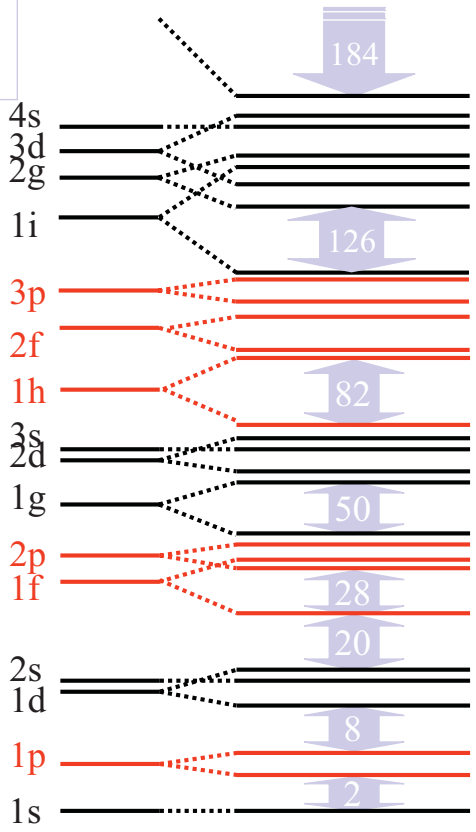

Possible changes of proton shell structure in heavy nuclei

Coulomb Repulsion

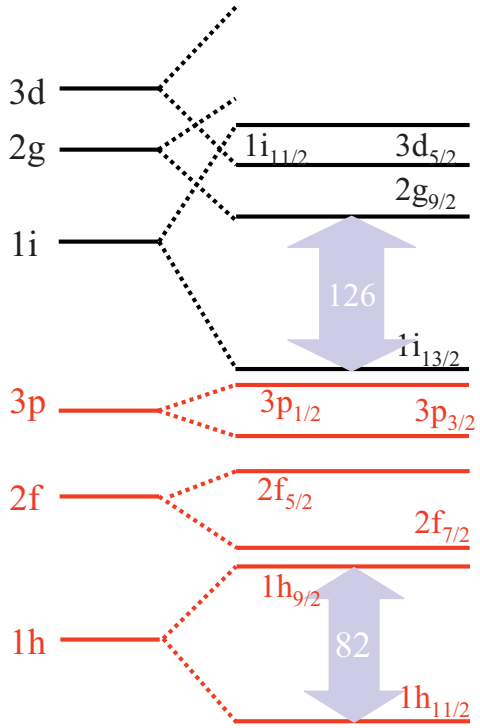

Possible changes of proton shell structure in heavy nuclei

Coulomb Repulsion

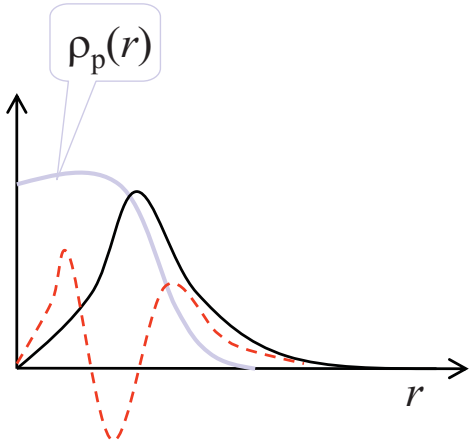

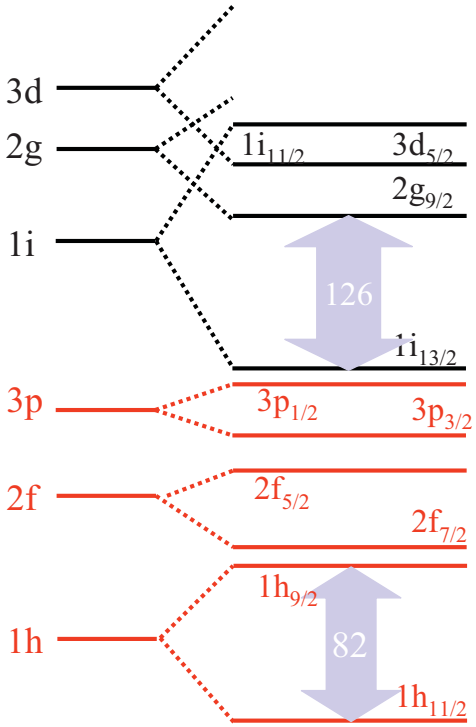

Possible changes of proton shell structure in heavy nuclei

Coulomb Repulsion

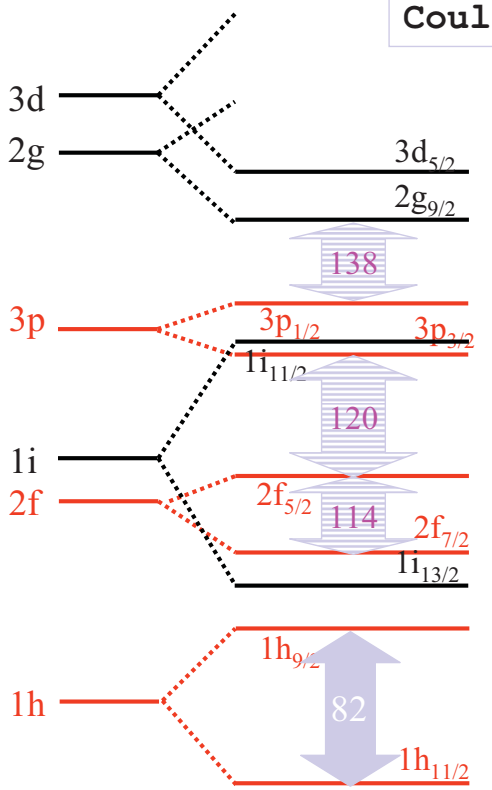

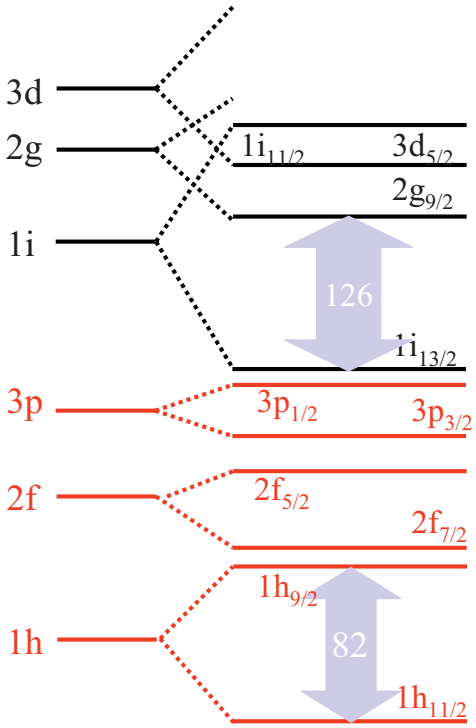

Single particle structure from realistic potentials – 1960s

- "Closed shells for $Z > 82$ and $N > 126$ in a diffuse potential well"
  - **A Woods-Saxon potential** Sobiczewski...1966_PhysLett22-500
  - **$Z = 114$ & $N = 184$; $B_f = 10$ MeV**
- "Predictions of new magic regions and masses for super-heavy nuclei from calculations with realistic shell model single particle Hamiltonian"
  - **A non-local potential** Meldner1967_ArkivFysik36-593
  - **$Z = 114$ & $N = 184$**

Shell effects from quantitative considerations – 1960s

VOLUME 18, NUMBER 17 PHYSICAL REVIEW LETTERS 24 APRIL 1967

SHAPE OF HEAVY NUCLEI*

Philip J. Siemens† and H. A. Bethe
Laboratory of Nuclear Studies, Cornell University, Ithaca, New York
(Received 10 March 1967)

The energy reduction for this semimagic nucleus is likely to be considerably less than for Pb^{208} for which it is about 15 MeV. On the other hand, without shell structure, the elongated shape has an energy about 18 MeV less than the sphere for $Z = 114$. We therefore believe that shell effects are unlikely to make the nucleus $Z = 114$ stable.

Shell effects from quantitative considerations – 1960s

VOLUME 18, NUMBER 17 PHYSICAL REVIEW LETTERS 24 APRIL 1967

SHAPE OF HEAVY NUCLEI*

Philip J. Siemens† and H. A. Bethe
Laboratory of Nuclear Studies, Cornell University, Ithaca, New York
(Received 10 March 1967)

The energy reduction for this semimagic nucleus is likely to be considerably less than for Pb^{208} for which it is about 15 MeV. On the other hand, without shell structure, the elongated shape has an energy about 18 MeV less than the sphere for $Z = 114$. We therefore believe that shell effects are unlikely to make the nucleus $Z = 114$ stable.

More quantitative investigations needed !!!

- **Single particle shell structure**
- **How much stability the closed shell brings**

Single particle structure from realistic potentials – 1960s

- Closed shells for $Z > 82$ and $N > 126$ in a diffuse potential well
  - **A Woods-Saxon potential** Sobiczewski...1966_PhysLett22-500
  - **$Z = 114$ & $N = 184$; $B_f = 10$ MeV**
- Predictions of new magic regions and masses for super-heavy nuclei from calculations with realistic shell model single particle Hamiltonian
  - **A non-local potential** Meldner1967_ArkivFysik36-593
  - **$Z = 114$ & $N = 184$**
- "On the spontaneous fission of nuclei with Z near 114 and N near 184"
  - **Nilsson potential**
  - **Potential energy surface with shell corrections calculated by the Strutinsky method** Nilsson…1968_NPA115-545
  - **$B_f = 10$ MeV & $T_{1/2}$(s.f.) ~ 10^{19} years**
- "On the stability of superheavy nuclei against fission"
  - **Nilsson potential**
  - **Potential energy surface with rotational invariance**
  - **$T_{1/2}$(s.f.) ~ $10^{0\text{--}17}$ years** Mosel_Greiner1969_ZPA226-261

Theor. progress on next magic numbers after 1960s

Not the end yet ! For the location of the island of stability, more different predictions :

- Macroscopic-microscopic models
- Self-consistent approaches
  - **Non-relativistic**
  - **Relativistic**
- ...

What are “Superheavy Nuclei” ?

Theor. progress on next magic numbers after 1960s

Not the end yet ! For the location of the island of stability, more different predictions :

- Macroscopic-microscopic models
- Self-consistent approaches
  - **Non-relativistic**
  - **Relativistic**
- ...

What are “Superheavy Nuclei” ?

- Can not exist if described as a charged liquid drop
- Stabilized by quantum shell effects

Contents

- Superheavy elements – history of predictions
- Experimental progress
- Structure of superheavy nuclei
  - **Shell structure: next proton & neutron magic numbers**
  - **Potential energy surfaces: shape, fission path & fission barrier**
  - **Low-lying spectra**
  - **Isomeric states**
- Synthesis of SHN via heavy ion reactions
  - **Capture process**
  - **Fusion – formation of a compound nucleus**
  - **Survival – competition between neutron emission & fission**
- Summary & Perspectives

SHN: experimental progress

- If $T_{1/2}$~10^8 years & produced in the nucleosynthesis — Herrmann2004
  - **SHN would survive until now**
  - **No confirmed results found in searching for SHE in the Nature**
- Synthesis of SHE in laboratories via heavy ion fusions
  - **GSI in Darmstadt, Germany**
  - **Flerov Laboratory of Nuclear Reactions in Dubna, Russia**
  - **Lawrence Berkeley National Laboratory in Berkeley, USA**
  - **RIKEN in Wako, Japan**
  - **GANIL in Caen, France**
  - **HIRFL in Lanzhou, China**

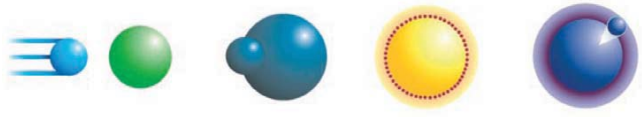

Hofmann_Münzenberg2000_RMP72-733
Morita...2004_JPSJ73-2593
Oganessian...2007_JPG34-R165
Oganessian...2010_PRL104-142502
Gan…2011_ChinPhysLett
See also Gales' lectures

Periodic Table of Elements

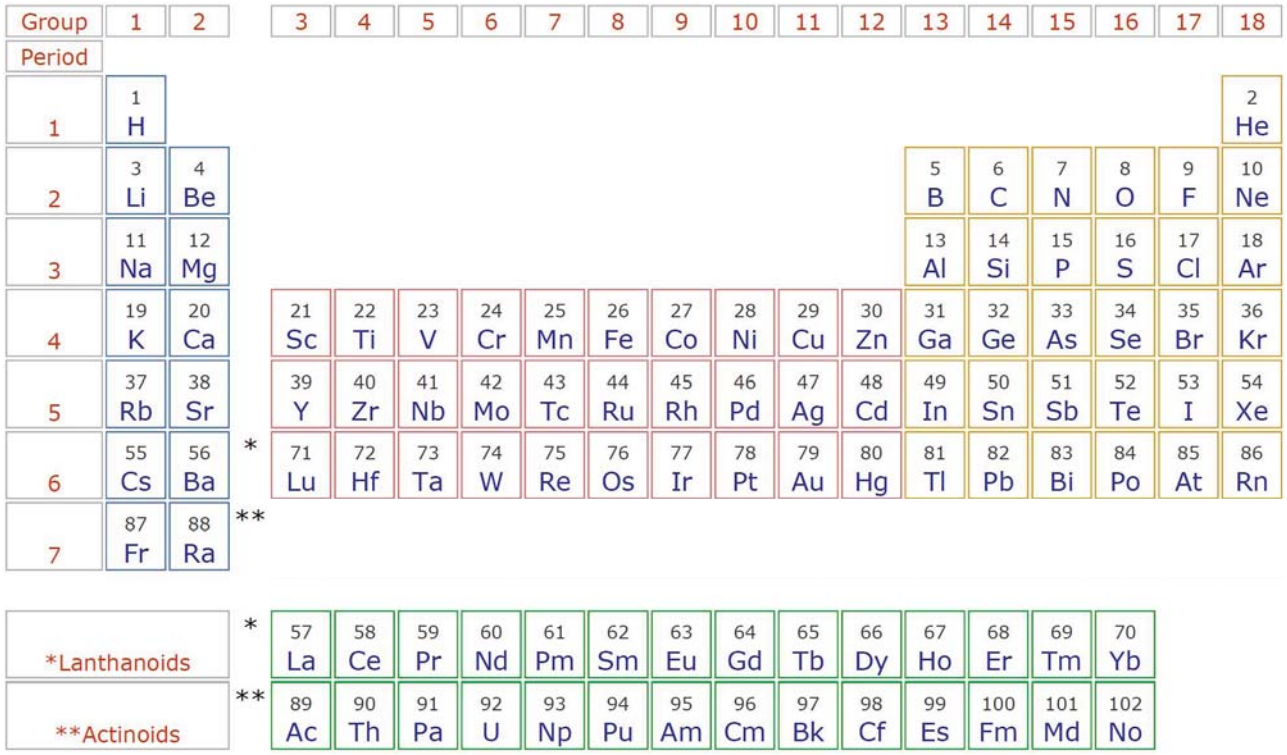

WebElements, Aug. 2011

Periodic Table of Elements

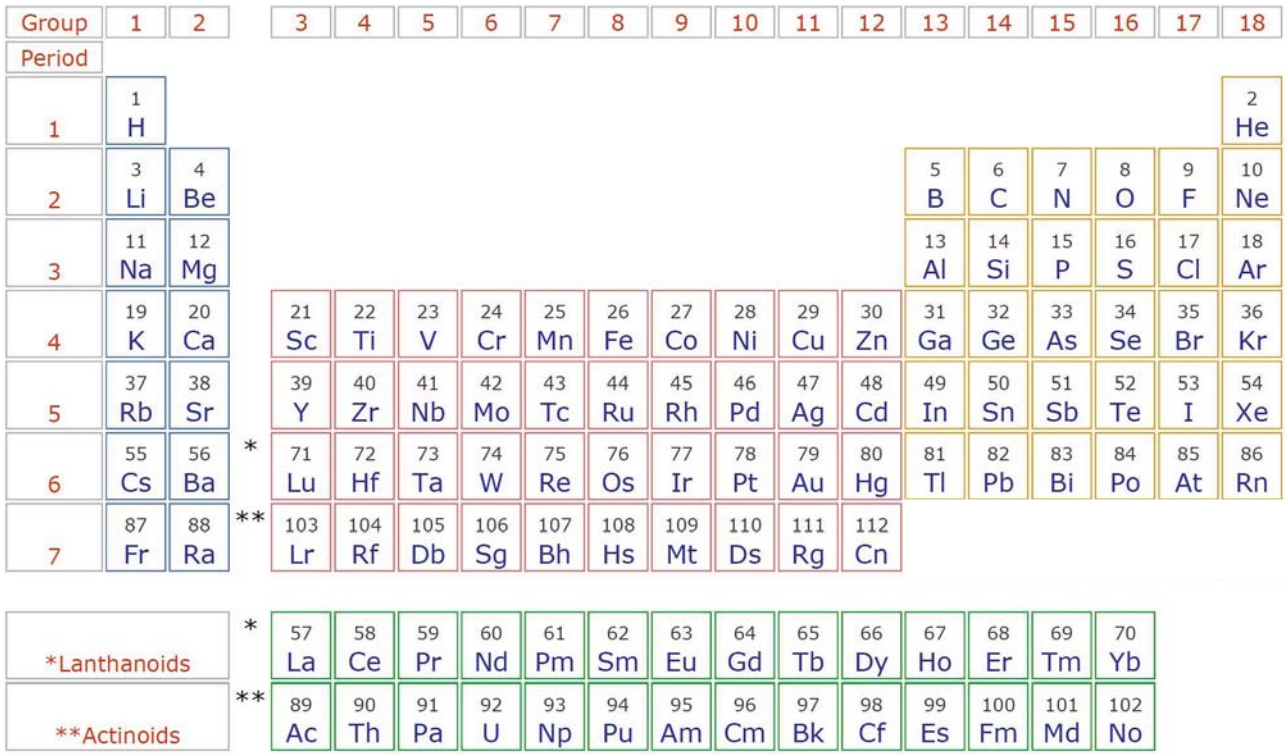

WebElements, Aug. 2011

Periodic Table of Elements

Group	1	2		3	4	5	6	7	8	9	10	11	12	13	14	15	16	17	18
Period																			
1	1 H																		2 He
2	3 Li	4 Be												5 B	6 C	7 N	8 O	9 F	10 Ne
3	11 Na	12 Mg												13 Al	14 Si	15 P	16 S	17 Cl	18 Ar
4	19 K	20 Ca		21 Sc	22 Ti	23 V	24 Cr	25 Mn	26 Fe	27 Co	28 Ni	29 Cu	30 Zn	31 Ga	32 Ge	33 As	34 Se	35 Br	36 Kr
5	37 Rb	38 Sr		39 Y	40 Zr	41 Nb	42 Mo	43 Tc	44 Ru	45 Rh	46 Pd	47 Ag	48 Cd	49 In	50 Sn	51 Sb	52 Te	53 I	54 Xe
6	55 Cs	56 Ba	*	71 Lu	72 Hf	73 Ta	74 W	75 Re	76 Os	77 Ir	78 Pt	79 Au	80 Hg	81 Tl	82 Pb	83 Bi	84 Po	85 At	86 Rn
7	87 Fr	88 Ra	**	103 Lr	104 Rf	105 Db	106 Sg	107 Bh	108 Hs	109 Mt	110 Ds	111 Rg	112 Cn	113 Uut	114 Uuq	115 Uup	116 Uuh	117 Uus	118 Uuo

*Lanthanoids	*	57 La	58 Ce	59 Pr	60 Nd	61 Pm	62 Sm	63 Eu	64 Gd	65 Tb	66 Dy	67 Ho	68 Er	69 Tm	70 Yb
**Actinoids	**	89 Ac	90 Th	91 Pa	92 U	93 Np	94 Pu	95 Am	96 Cm	97 Bk	98 Cf	99 Es	100 Fm	101 Md	102 No

WebElements, Aug. 2011

SHN: experimental progress

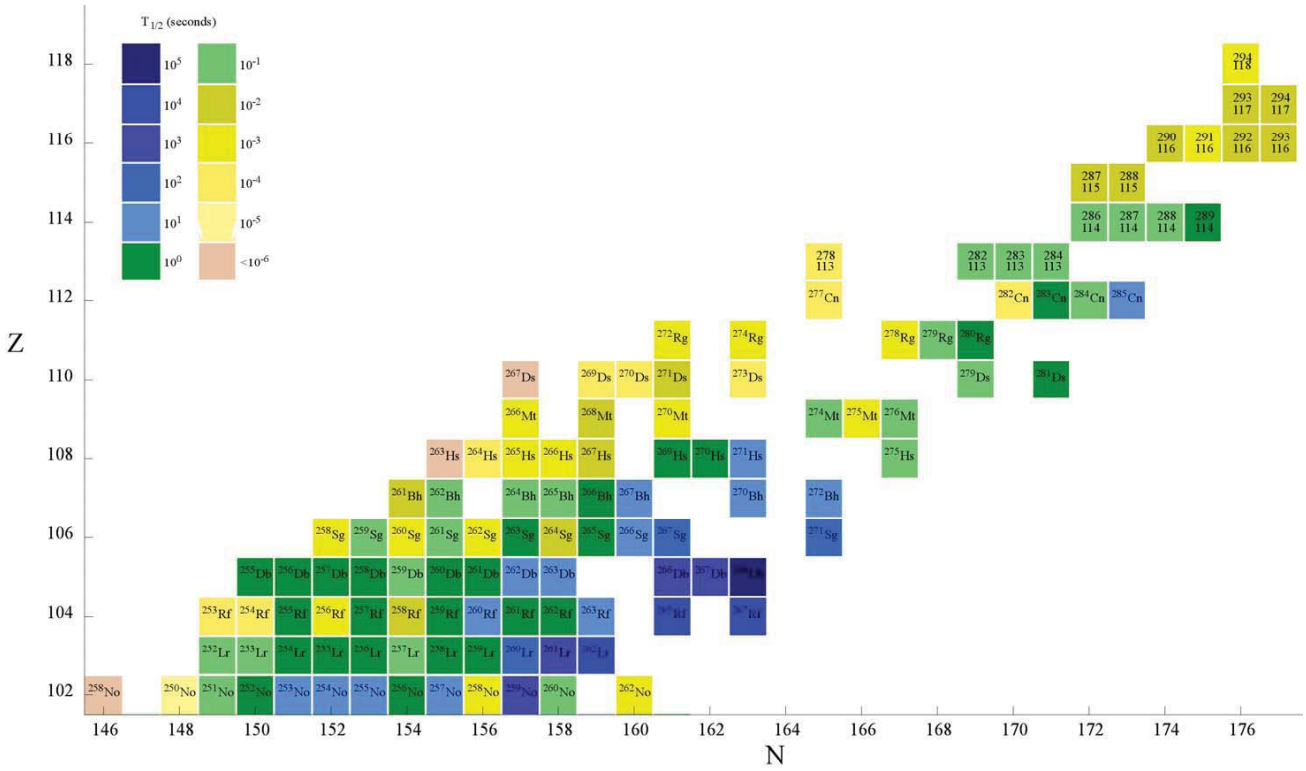

Courtesy of Kai Wen (温凯)

SHN: experimental progress

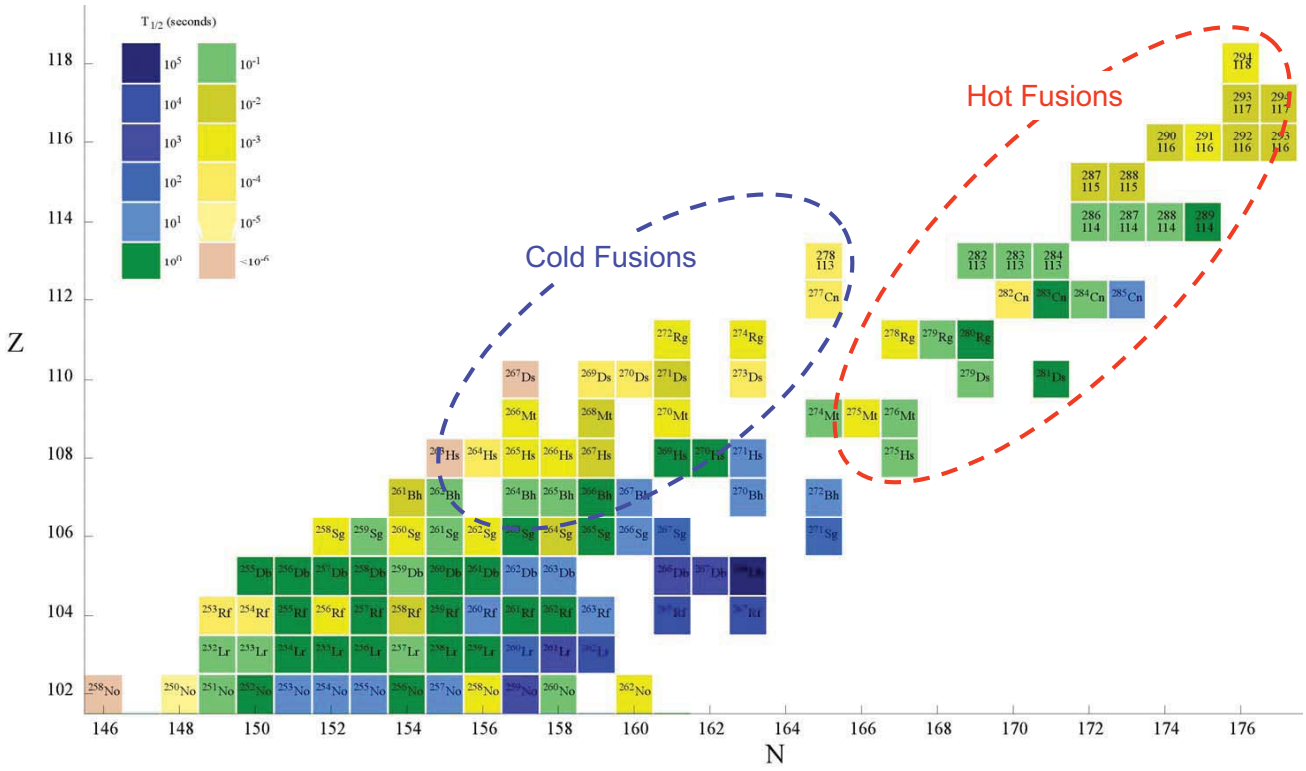

Courtesy of Kai Wen (温凯)

SHN: experimental progress

Courtesy of Kai Wen (温凯)

SHN: experimental progress

- At least 7 neutrons away from $N = 184$
- $T_{1/2}$ increases with increasing N

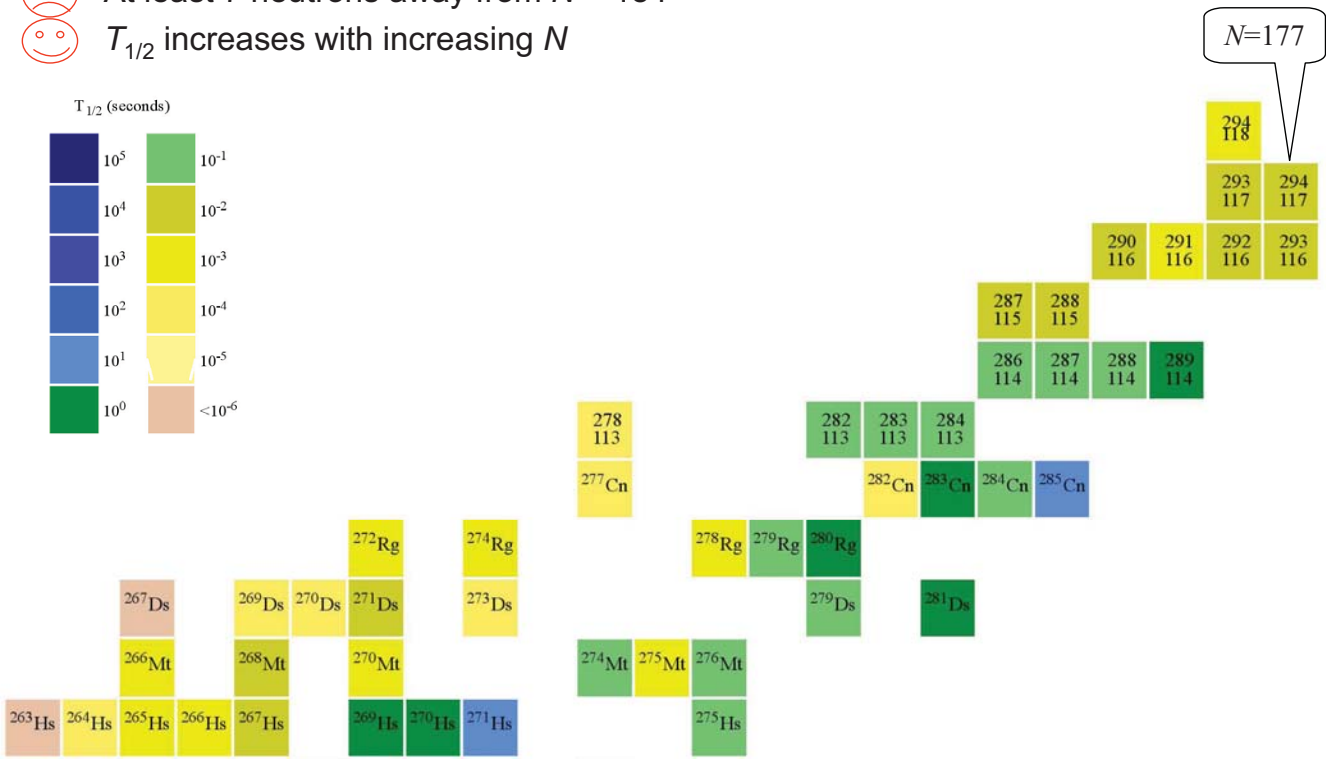

Courtesy of Kai Wen (温凯)

SHN: experimental progress

- At least 7 neutrons away from $N = 184$
- $T_{1/2}$ increases with increasing N
- Production x-section is maximized at $Z = 114$ for hot fusions
- Production x-section is tiny for even heavier SHE

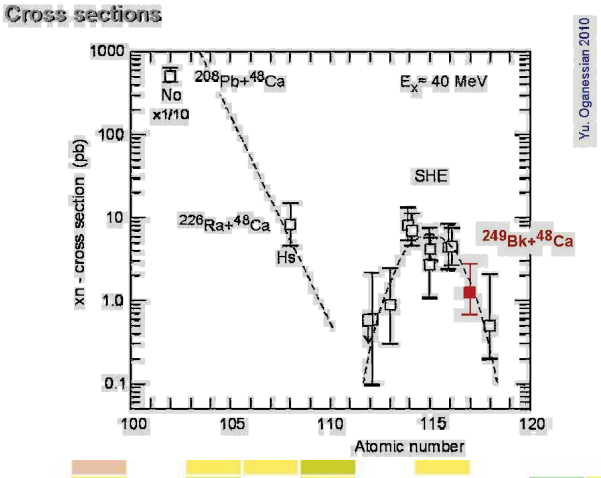

Courtesy of Kai Wen (温凯)

Contents

- Superheavy elements – history of predictions
- Experimental progress
- Structure of superheavy nuclei
  - **Shell structure: next proton & neutron magic numbers**
  - **Potential energy surfaces: shape, fission path & fission barrier**
  - **Low-lying spectra**
  - **Isomeric states**
- Synthesis of SHN via heavy ion reactions
  - **Capture process**
  - **Fusion – formation of a compound nucleus**
  - **Survival – competition between neutron emission & fission**
- Summary & Perspectives

Ground state properties from various models

- Ground state properties of SHN
  - **Shell structure & magic numbers**
  - **Mass & α-decay energies**
  - **Deformation & higher-multipolarity deformations**
  - **...**
- Models used for study ground state properties of SHN
  - **Macroscopic-Microscopic models (MMM)**
    - Finite range droplet model (FRDM) with >30 parameters
    - MMM by Warsaw group
  - **Self-consistent semi-empirical methods**
    - Extended Thomas-Fermi model with Strutinski integral (ETFSI)
  - **Self-consistent microscopic approaches**
    - Hartree-Fock (HF) & Hartree-Fock-Bogoliubov (HFB) with Skyrme or Gogny
    - Relativistic mean field (RMF) models

Macroscopic-Microscopic Models

Mass of a nucleus = Macroscopic + Microscopic corrections

Macroscopic part: liquid drop or droplet

- The Weizsäcker formula

$$B(Z,N) = a_V A - a_S A^{2/3} - a_C Z^2 A^{-1/3} - a_1 I^2 A + a_2 I^2 A^{2/3} + \delta a_P A^{-1/2}$$

- A more realistic formula with deformation dependences

$$\begin{aligned} M_{\rm macr}(Z,N,\beta_\lambda^0) = {} & M_{\rm H} Z + M_{\rm n} N - a_{\rm v}(1-\kappa_{\rm v} I^2) A \\ & + a_{\rm s}(1-\kappa_{\rm s} I^2) A^{2/3} B_1(\beta_\lambda^0) + a_0 A^0 \\ & + c_1 Z^2 A^{-1/3} B_3(\beta_\lambda^0) - c_4 Z^{4/3} A^{-1/3} \\ & + f(k_{\rm F} r_{\rm p}) Z^2 A^{-1} - c_{\rm a}(N-Z) - a_{\rm el} Z^{2.39} \end{aligned}$$

Sobiczewski_Pomorski2007_PPNP58-292

- ……

Macroscopic-Microscopic Models

But, there are large discrepancies!

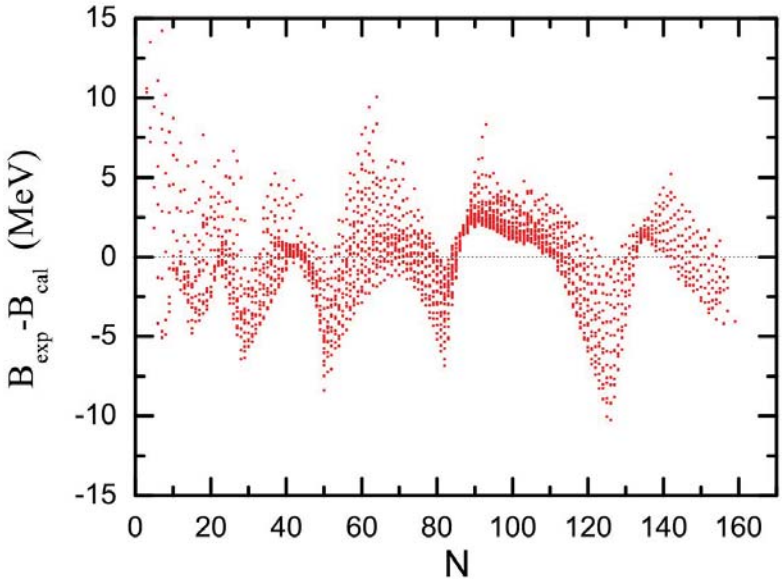

$$B(Z,N) = a_V A - a_S A^{2/3} - \frac{a_C Z^{5/3}}{1+0.452(T_z - T_z^*)/A} - a_a T_z(T_z+1) A^{-0.86} + a_P A^{-1/2}$$

Courtesy of Yu-Chen Cao (曹宇晨)

Shell effects

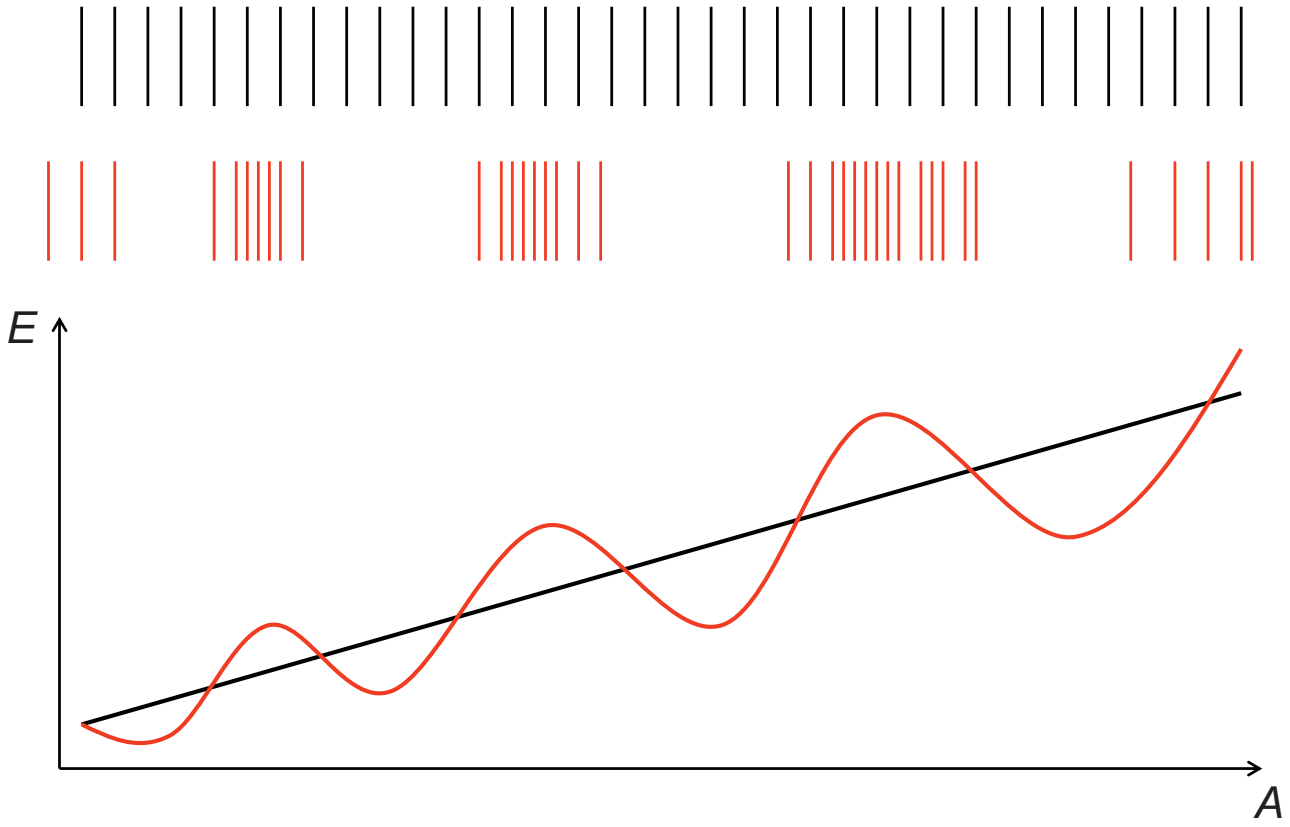

Shell correction

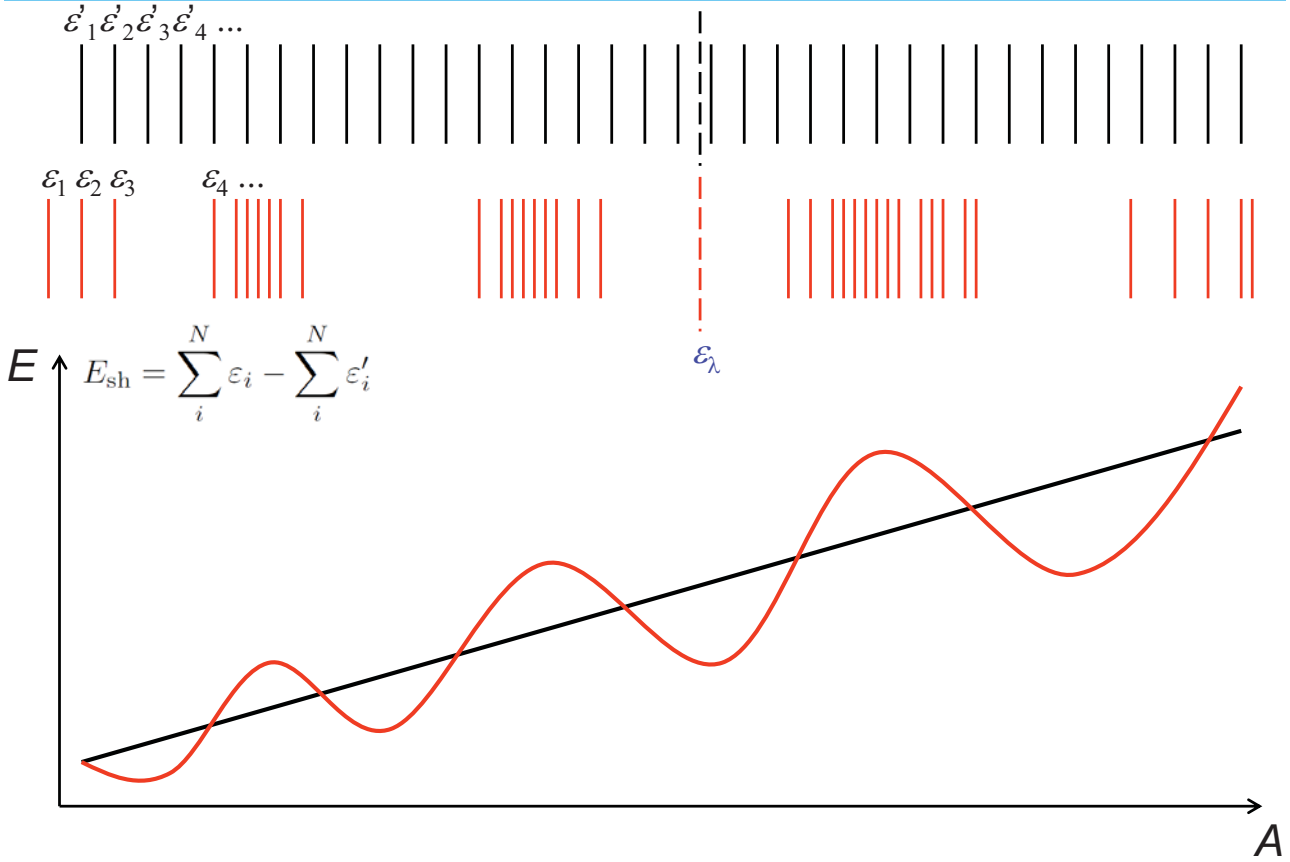

Shell correction: the Strutinsky method

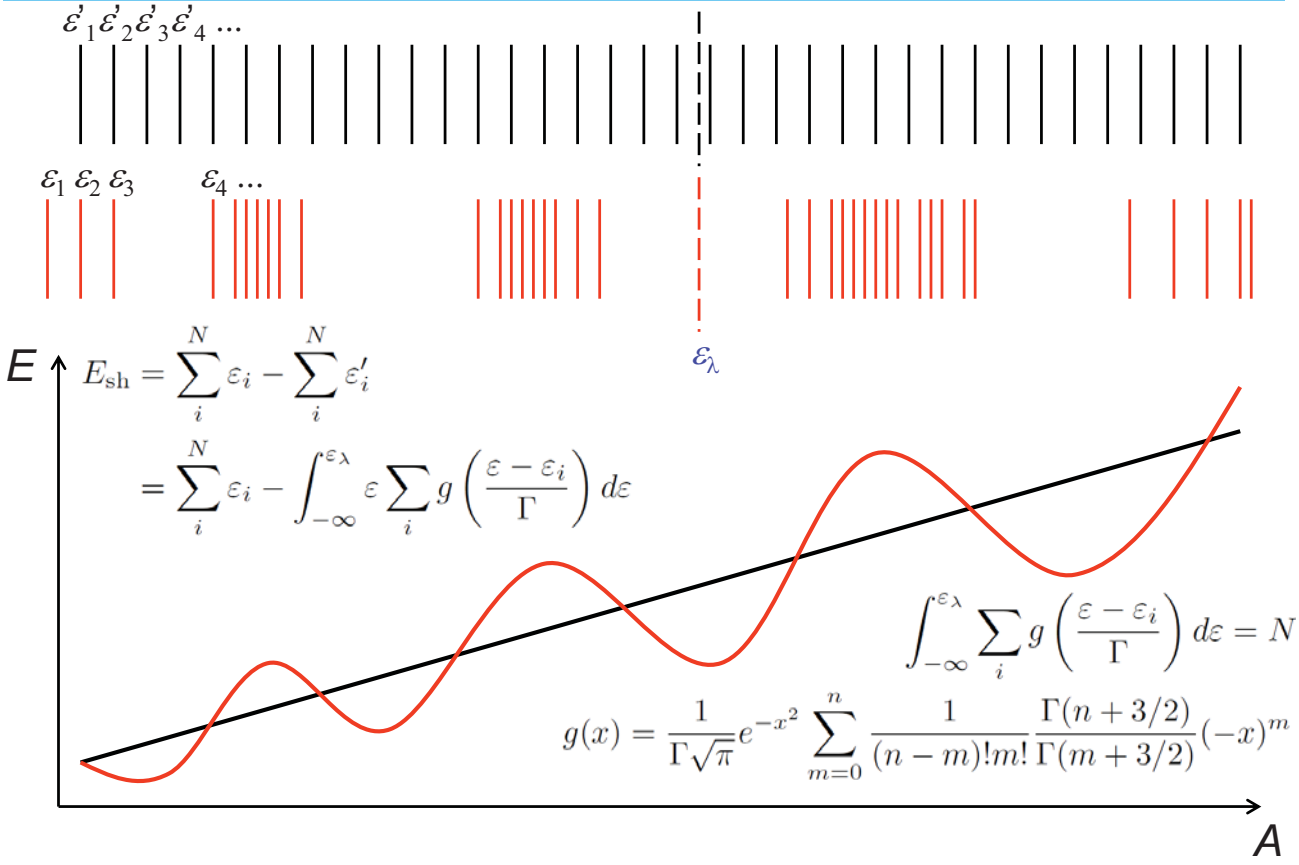

Shell structure & magic numbers – Nilsson potential

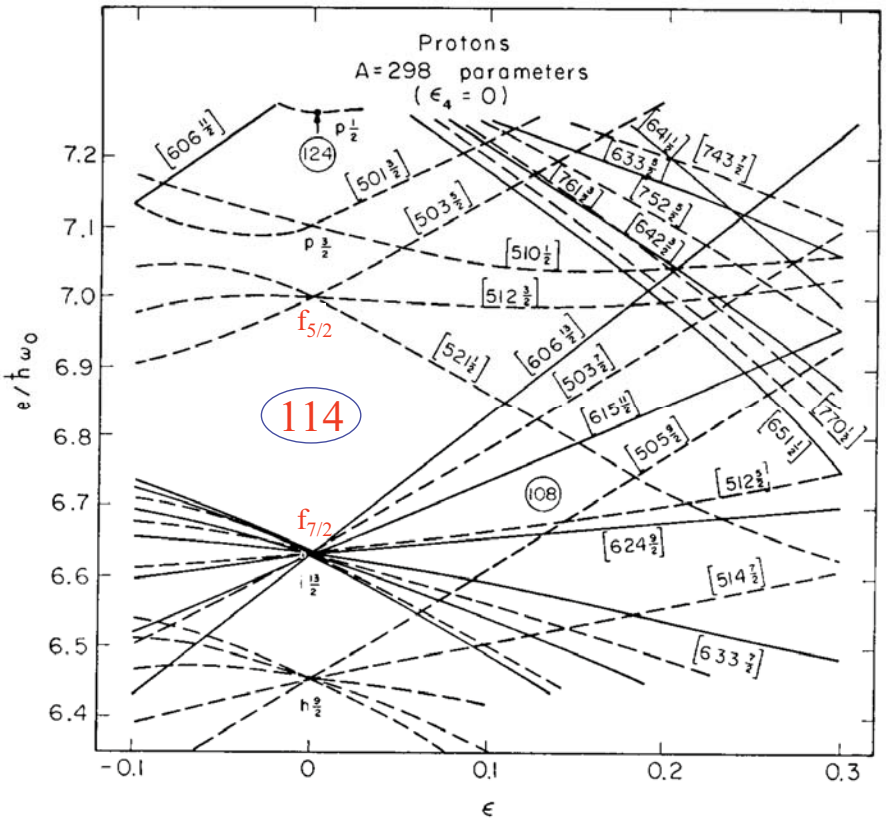

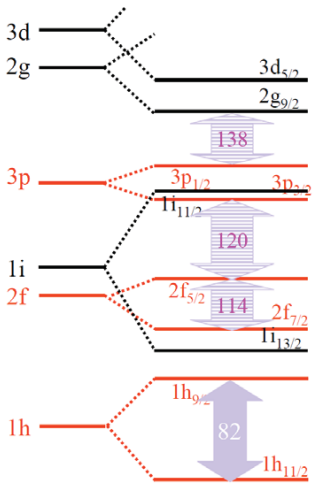

Nilsson...1969_NPA131-1

Shell structure & magic numbers – Woods-Saxon potential

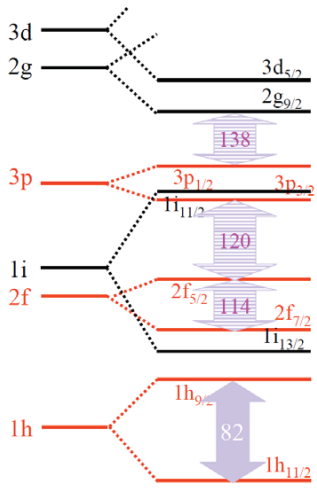

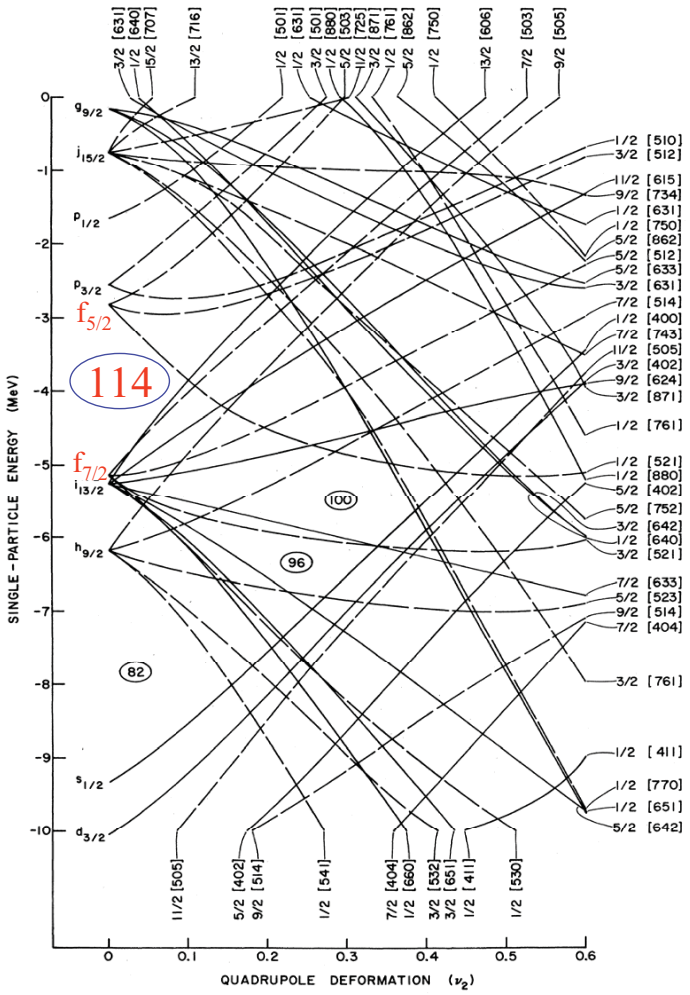

Chasman...1977_RMP49-833

Shell structure & magic numbers – Skyrme HF

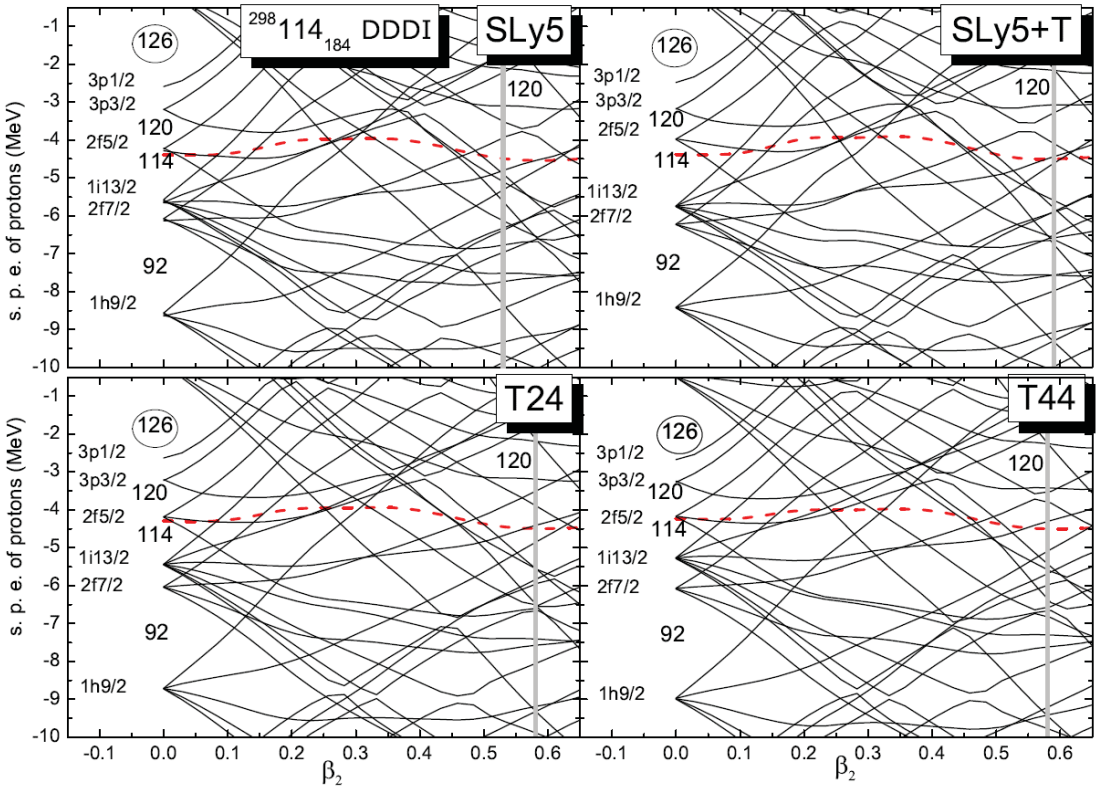

Zhou...2011_NuclearStructureChina2010_279

Shell structure & magic numbers – RCHB theory

- Shell correction energy
- Separation energy
- Pairing energy
- Pairing gap

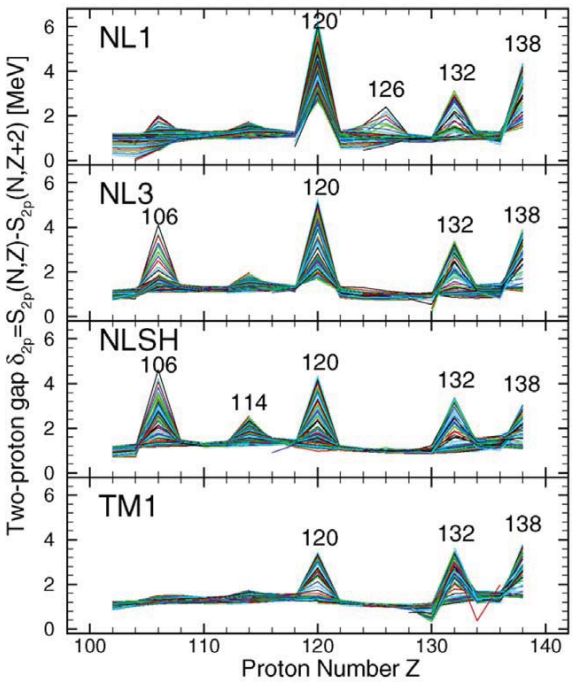

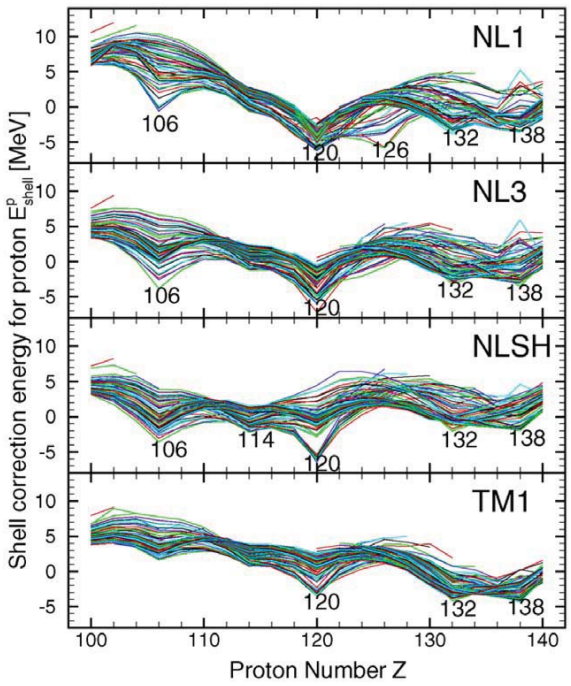

Zhang...2005_NPA753-106

Shell structure & magic numbers – RCHB theory

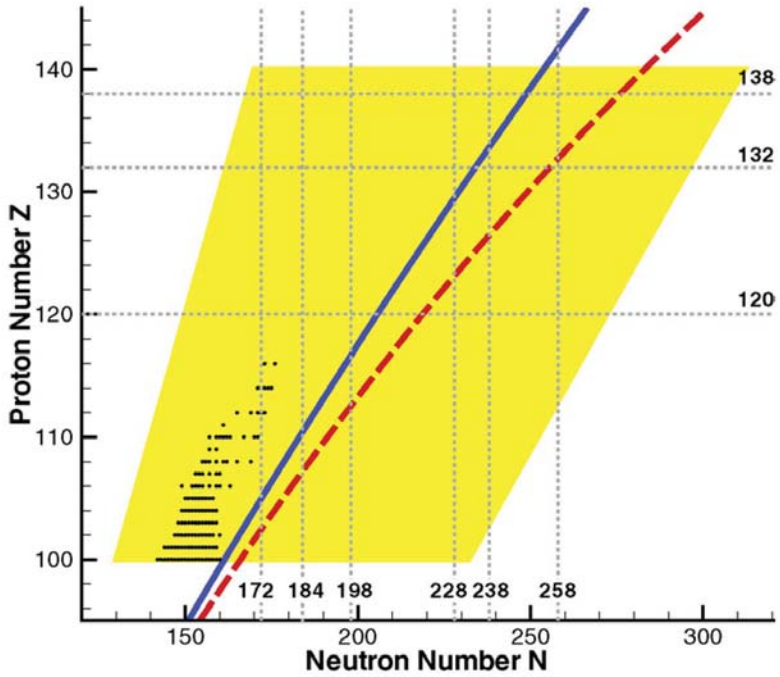

Zhang...2005_NPA753-106

A summary on the predicted magic numbers

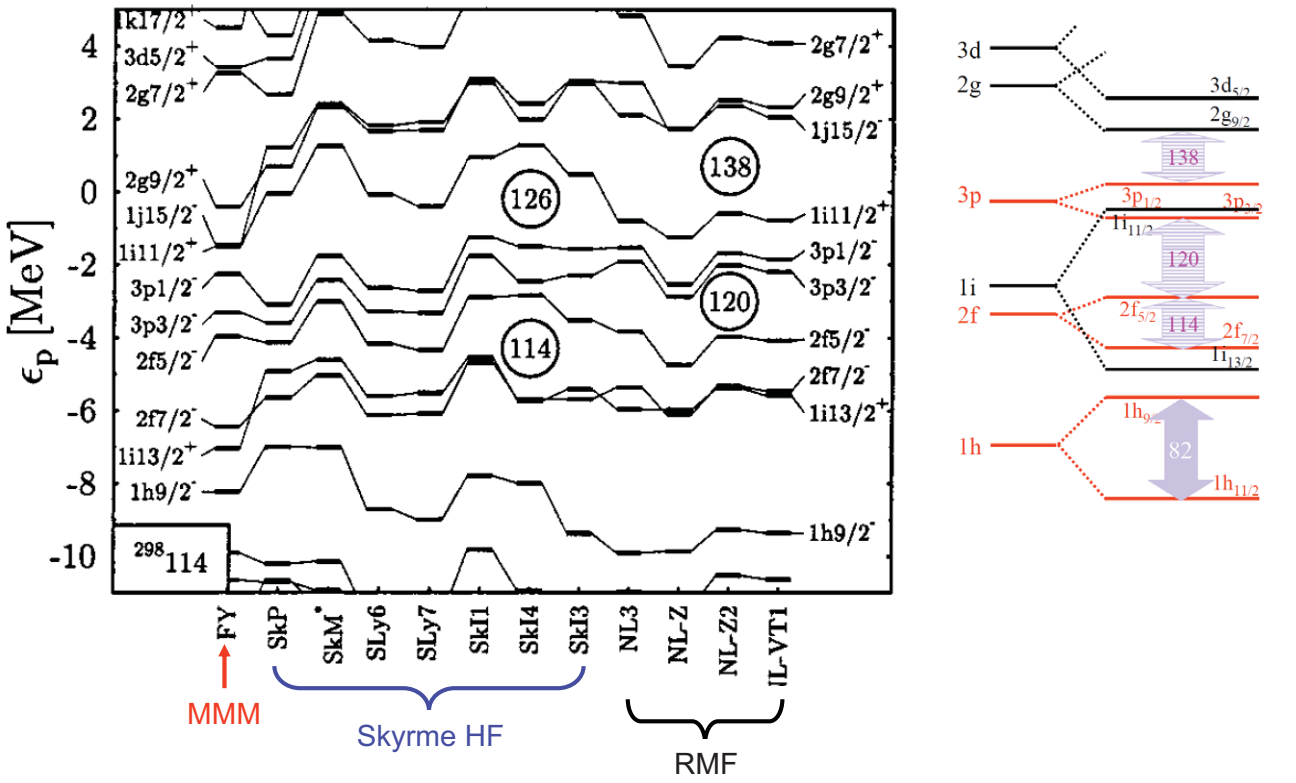

Bender...1999_PRC60-034304

Fragile shell gaps

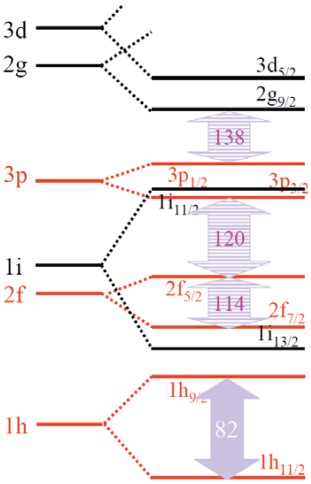

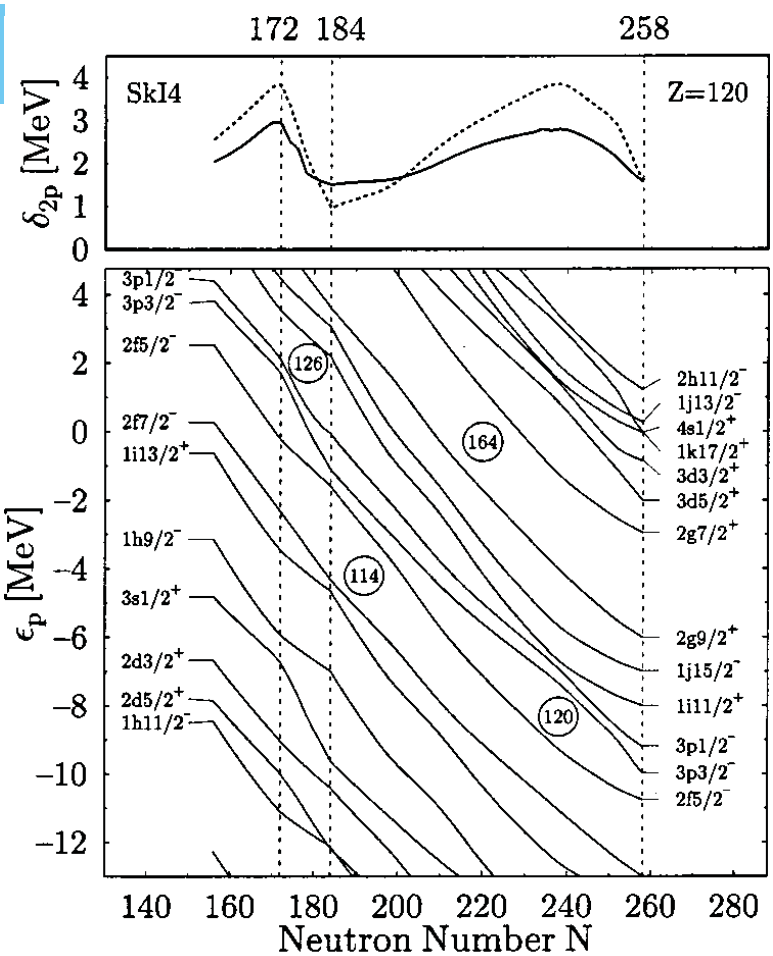

Bender...1999_PRC60-034304

Deformed shell closure around $Z = 108$ & $N = 152$

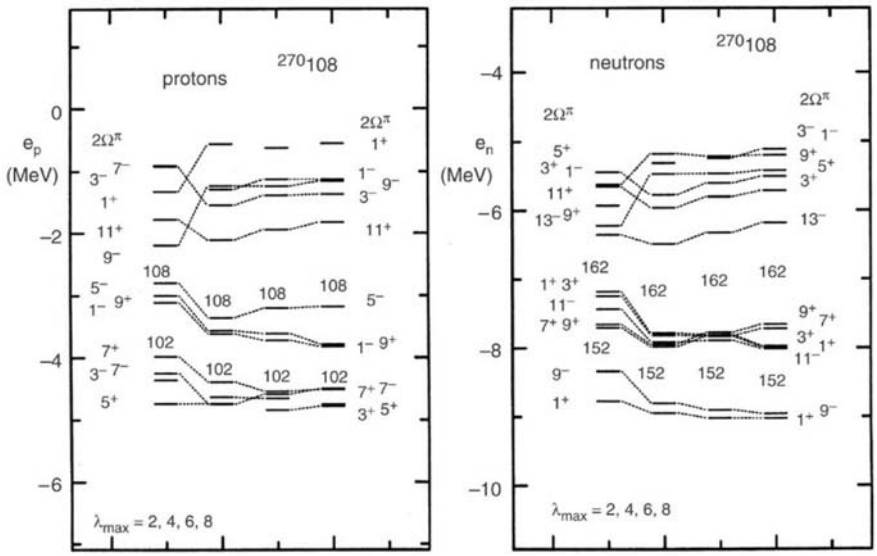

Patyk...1991_NPA533-132

Deformed shell closure around $Z = 108$ & $N = 152$

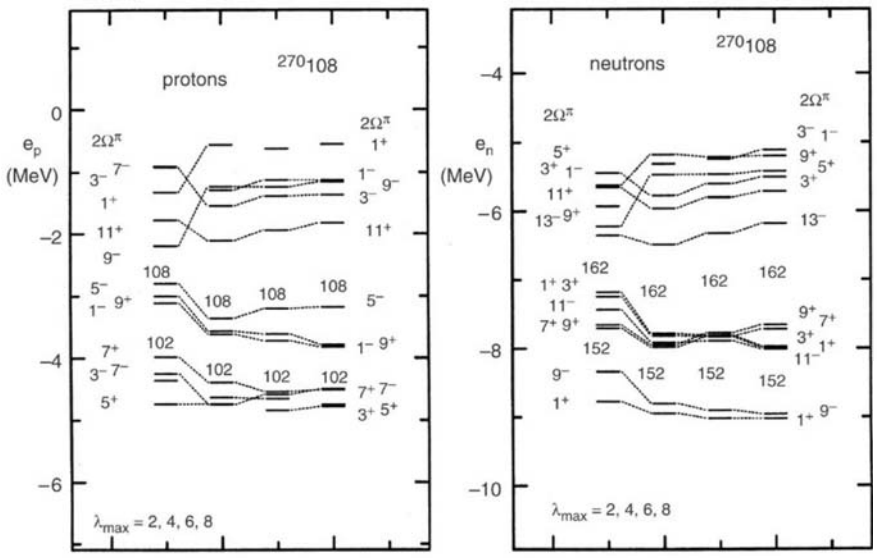

Patyk...1991_NPA533-132

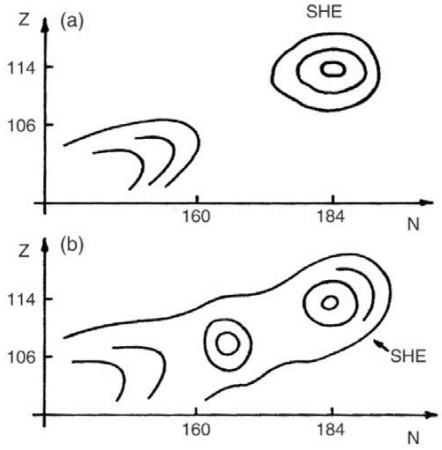

Sobiczewski_Pomorski2007_PPNP58-292

Contents

- Superheavy elements – history of predictions
- Experimental progress
- Structure of superheavy nuclei
  - **Shell structure: next proton & neutron magic numbers**
  - **Potential energy surfaces: shape, fission path & fission barrier**
  - **Low-lying spectra**
  - **Isomeric states**
- Synthesis of SHN via heavy ion reactions
  - **Capture process**
  - **Fusion – formation of a compound nucleus**
  - **Survival – competition between neutron emission & fission**
- Summary & Perspectives

Potential energy surfaces

- Shape, fission path & fission barrier

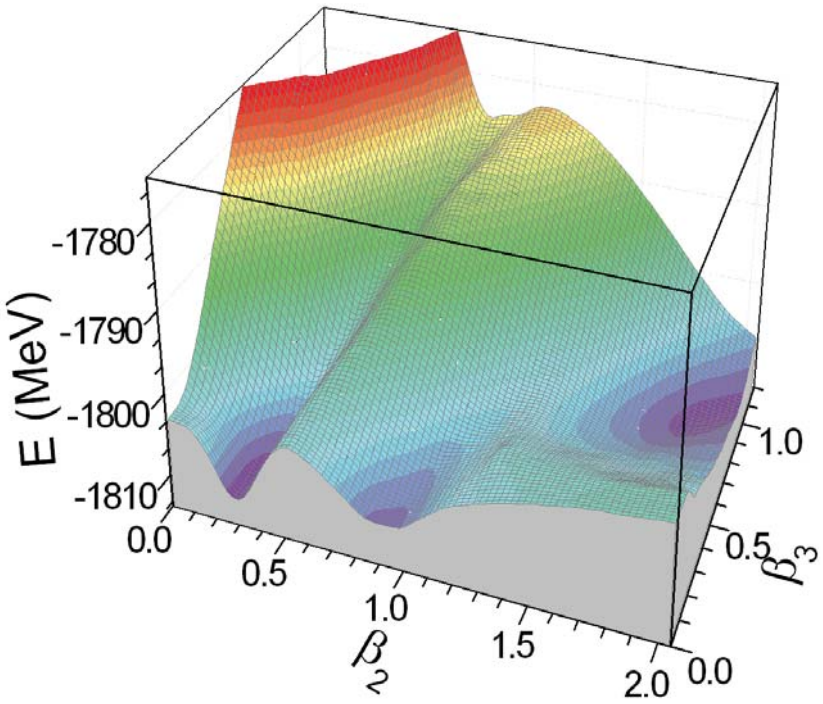

Courtesy of Bing-Nan Lu (吕炳楠)

Potential energy surfaces

- Shape, fission path & fission barrier

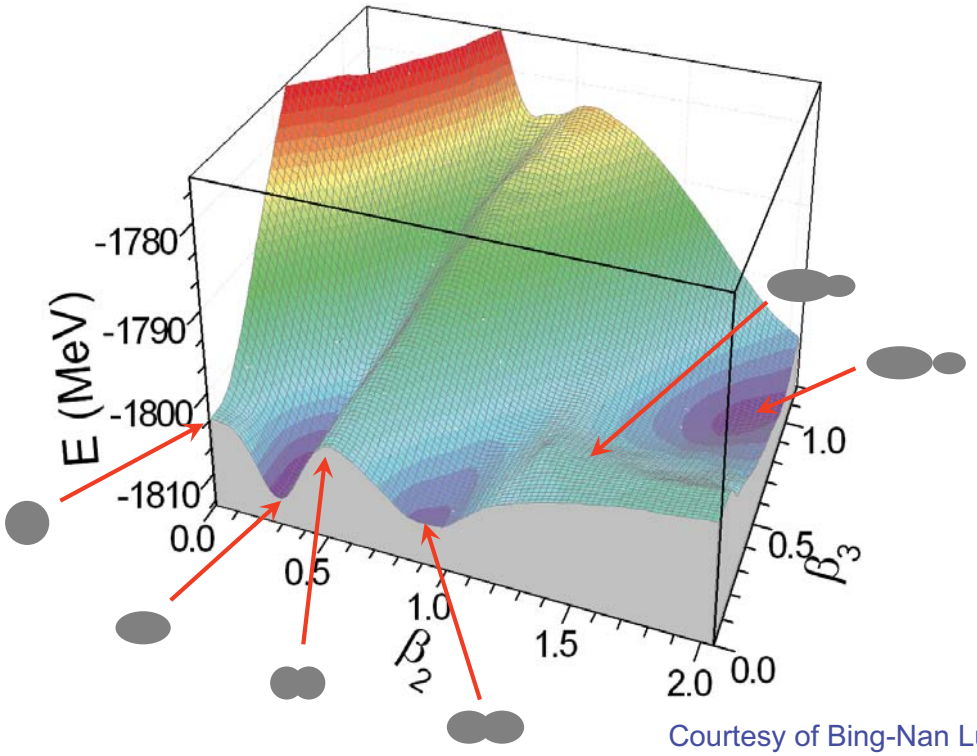

Courtesy of Bing-Nan Lu (吕炳楠)

Potential energy surfaces

- Shape, fission path & fission barrier

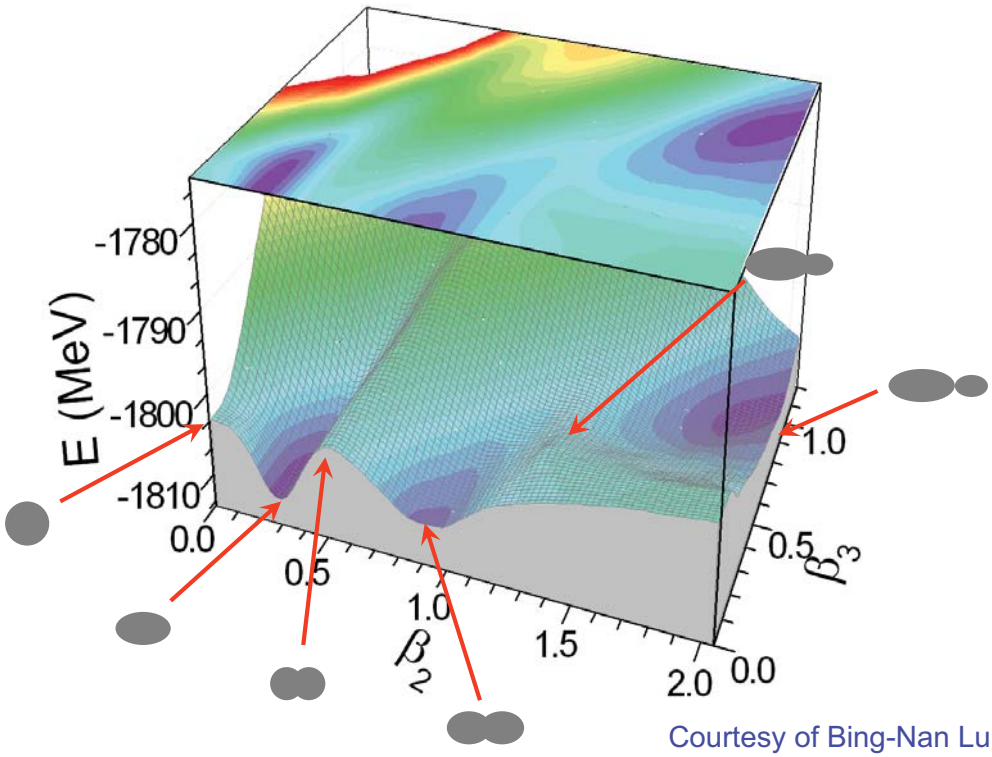

Courtesy of Bing-Nan Lu (吕炳楠)

Potential energy surfaces

- Shape, fission path & fission barrier

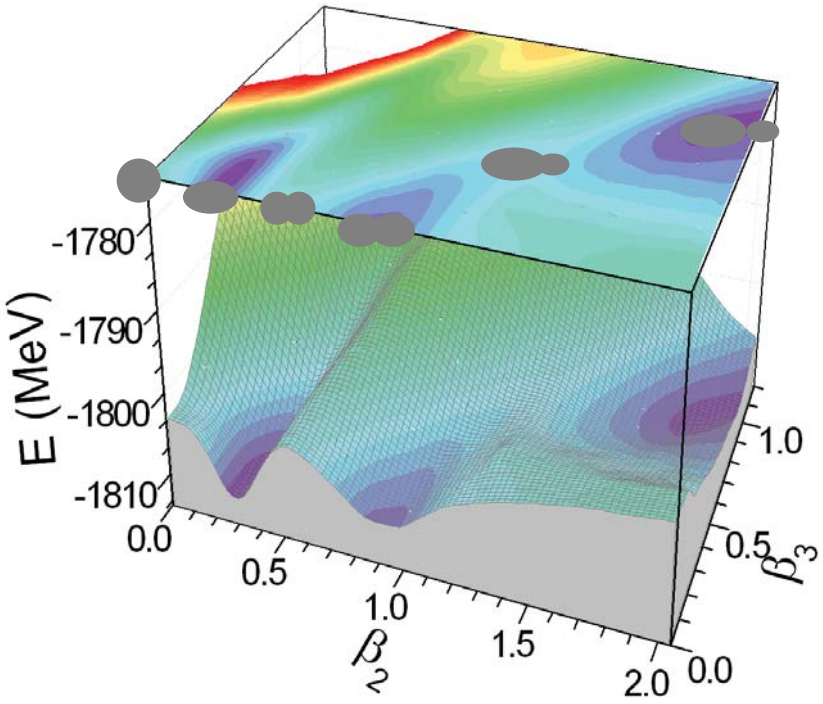

Courtesy of Bing-Nan Lu (吕炳楠)

B_f of 1122 nuclei from a MMM

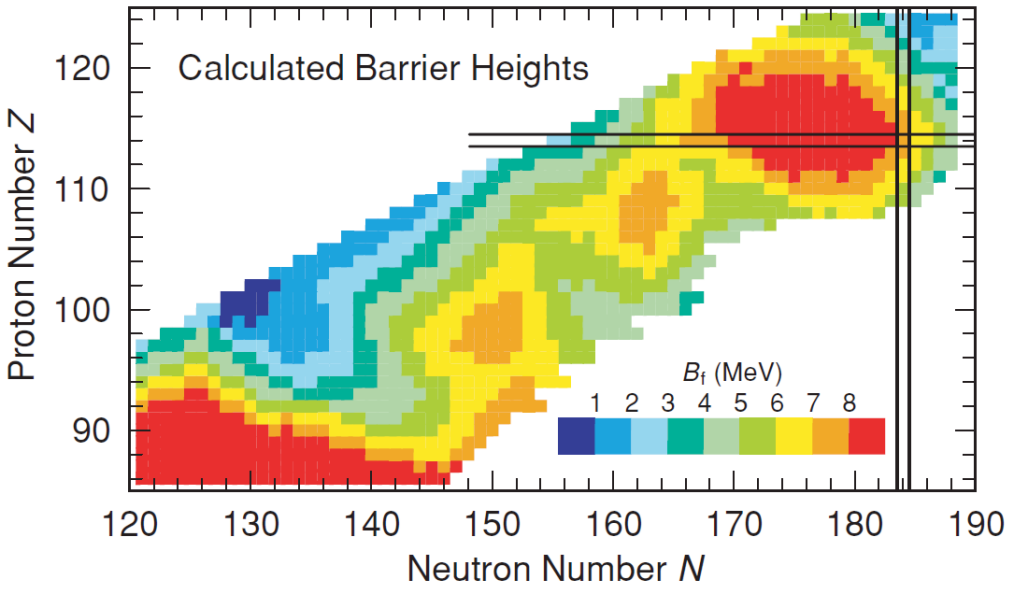

Möller…2009_PRC79-064304

A multi-dim. constrained RMF model & PES

- A constraint deformed RMF model for normal & hypernuclei
  - **Deformation space: (β_2, γ, β_3, …)**
  - **An axially deformed harmonic oscillator basis**
- Shapes of hypernuclei

  Lu_Zhao_SGZ2011_PRC84-014328
- Fission barriers of heavy & superheavy nuclei

  Lu_Zhao_SGZ, in preparation

Why multi-dimensional?

- Triaxiality: the 1st barrier

  Abusara…2010_PRC82-044303
- Asymmetry: the 2nd barrier

  Rutz…1995_NPA590-680

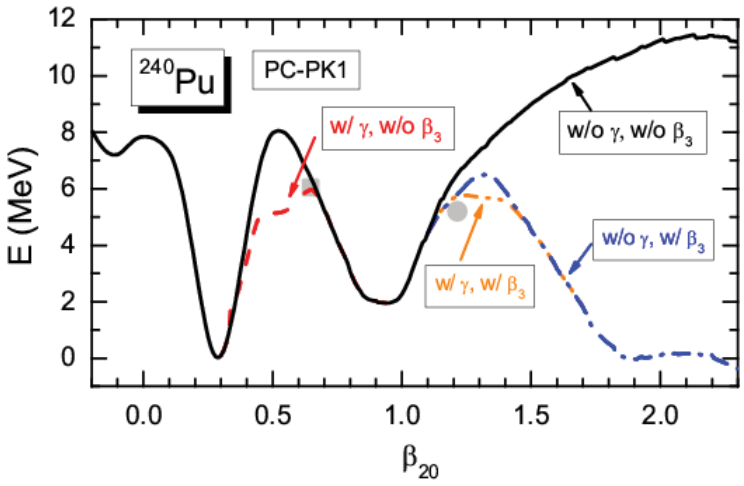

Three-dim. constraint in the space (β_{20}, β_{22}, β_{30})

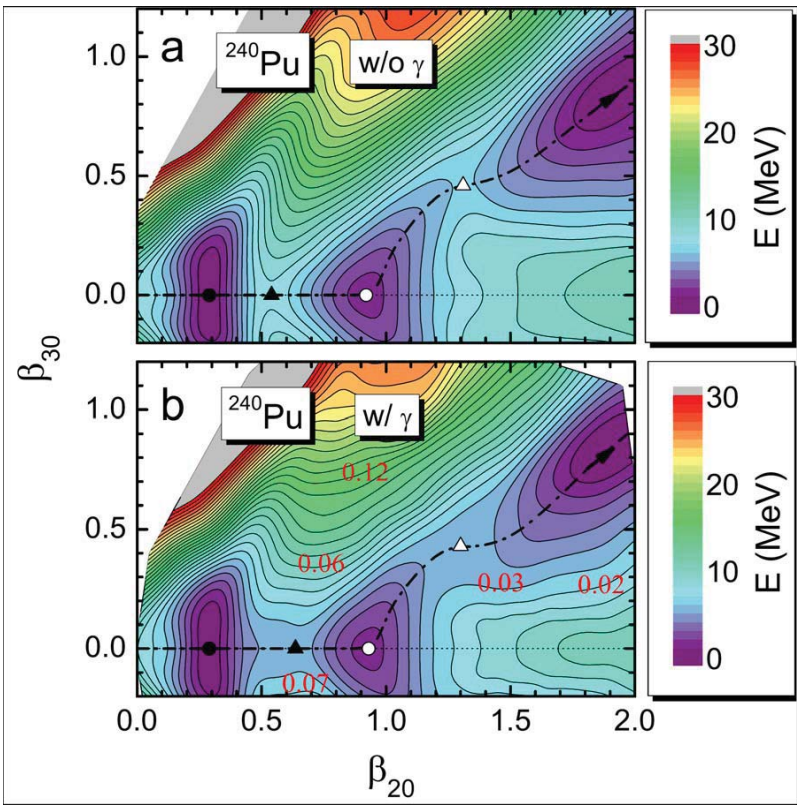

Lu_Zhao_SGZ, in preparation

Three-dim. constraint in the space (β_{20}, β_{22}, β_{30})

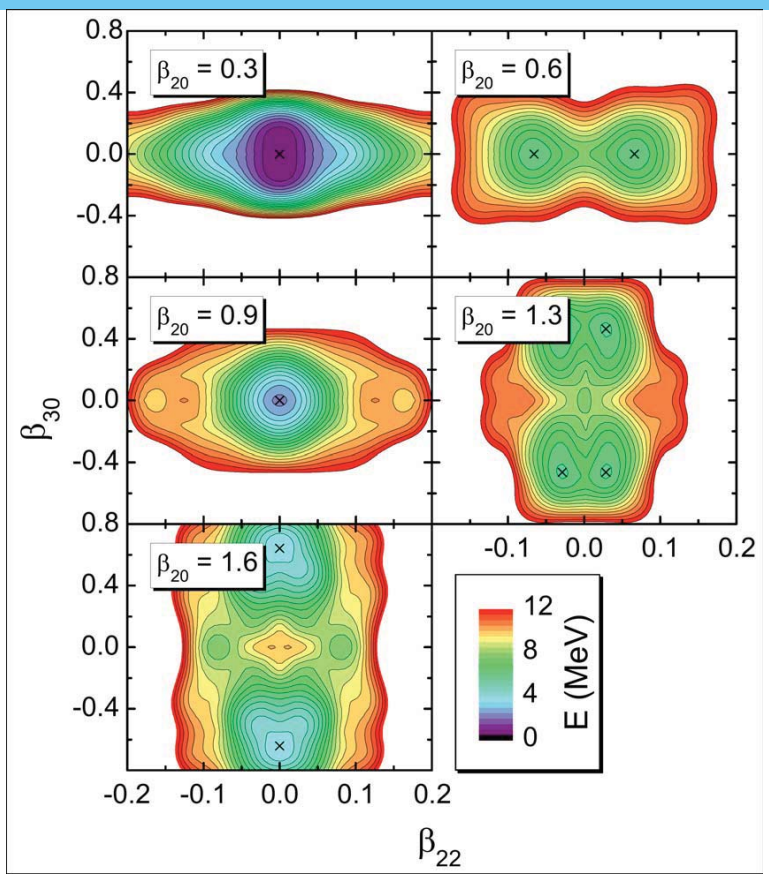

Lu_Zhao_SGZ, in preparation

B_f of some even-even actinide nuclei

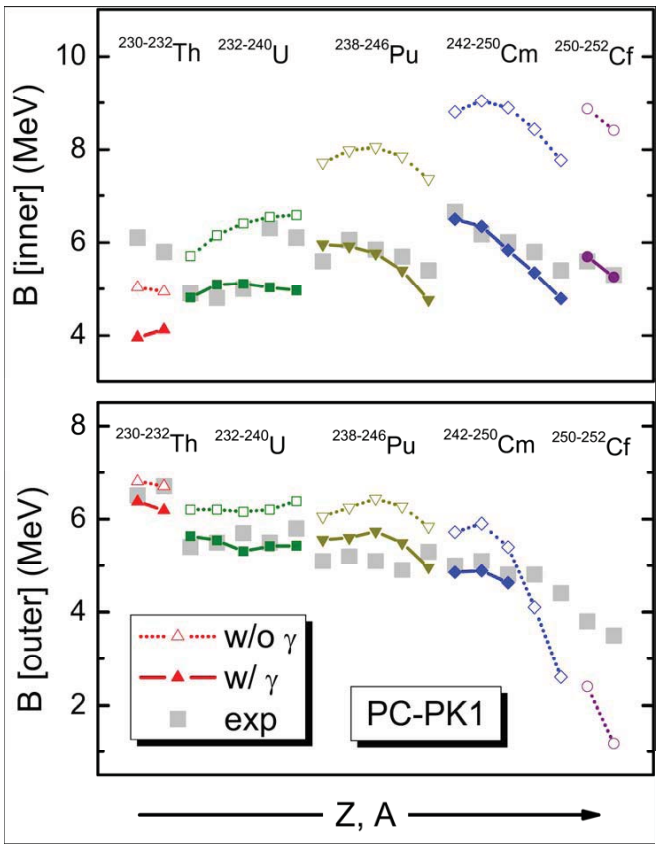

Lu_Zhao_SGZ, in preparation

Contents

- Superheavy elements – history of predictions
- Experimental progress
- Structure of superheavy nuclei
  - **Shell structure: next proton & neutron magic numbers**
  - **Potential energy surfaces: shape, fission path & fission barrier**
  - **Low-lying spectra**
  - **Isomeric states**
- Synthesis of SHN via heavy ion reactions
  - **Capture process**
  - **Fusion – formation of a compound nucleus**
  - **Survival – competition between neutron emission & fission**
- Summary & Perspectives

Spectroscopy of nuclei with Z~100

- Synthesis of SHN ⇒ Decay modes & energies; X-sections, ...
- Spectroscopy of SHN
  - **Detailed structure & stability**
- Spectroscopy of deformed nuclei with Z~100 & N~152
  - **Of interest in itself --- occurrence of deformation & *K*-isomerism**
  - **Orbitals around the Fermi level in these nuclei stem from those connected to the spherical shell gaps in SHN ($1/2^-[521]$)**

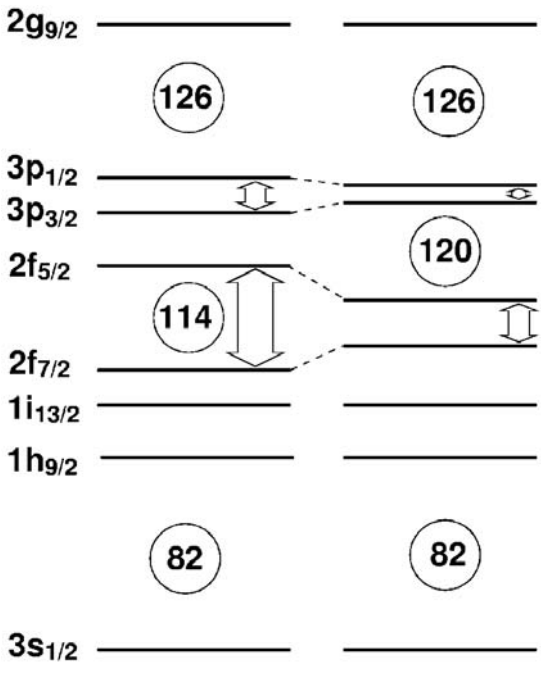

Experimental facilities & status

RITU@JYFL	SHIP@GSI	VASSILISSA@FLNR
FMA@ANL	LISE3@GANIL	RMS@JAEA ...

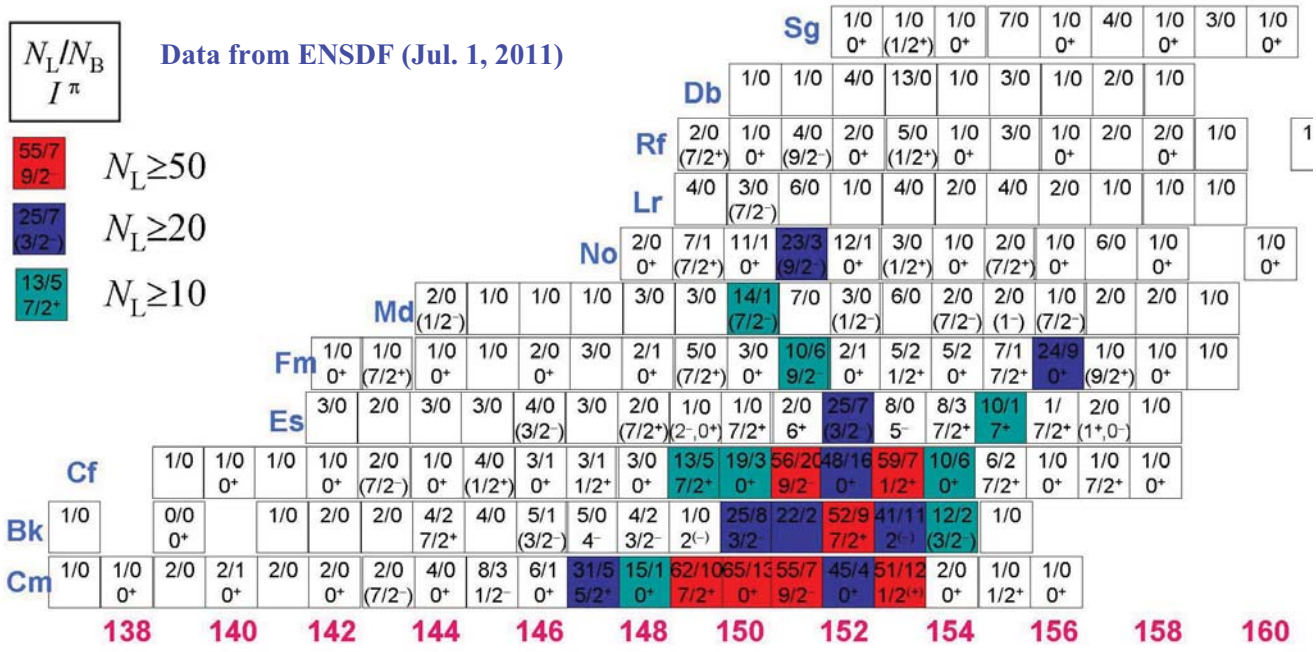

Leino_Hessberger2004_ARNPS54-175
Herzberg_Greenlees2008_PPNP61-674

Theoretical study of low-lying spectra

- Self-consistent approaches

  Egido_Robledo2000_PRL85-1198 Afanasjev...2003 PRC67-024309
  Delaroche...2006_NPA771-103 Bender...2003_NPA723-354
  Adamian...2011_PRC

- Macroscopic-Microscopic models

  Cwiok...1994 NPA573-356 Muntian...1999_PRC60-041302R
  Sobiczewski...2001_PRC63-034306
  Parkhomenko Sobiczewski2004 APPB35-2447
  Parkhomenko_Sobiczewski2005_APPB36-3115
  Adamian...2011_PRC

- Projected shell model

  Sun...2008_PRC77-044307 Al-Khudair...2009_PRC79-034320

- Cranking shell model

  He...2009_NPA817-45 Zhang...2011_PRC83-011304R
  Zhang...2011_in preparation

One-quasineutron spectra in ^{245}Cm

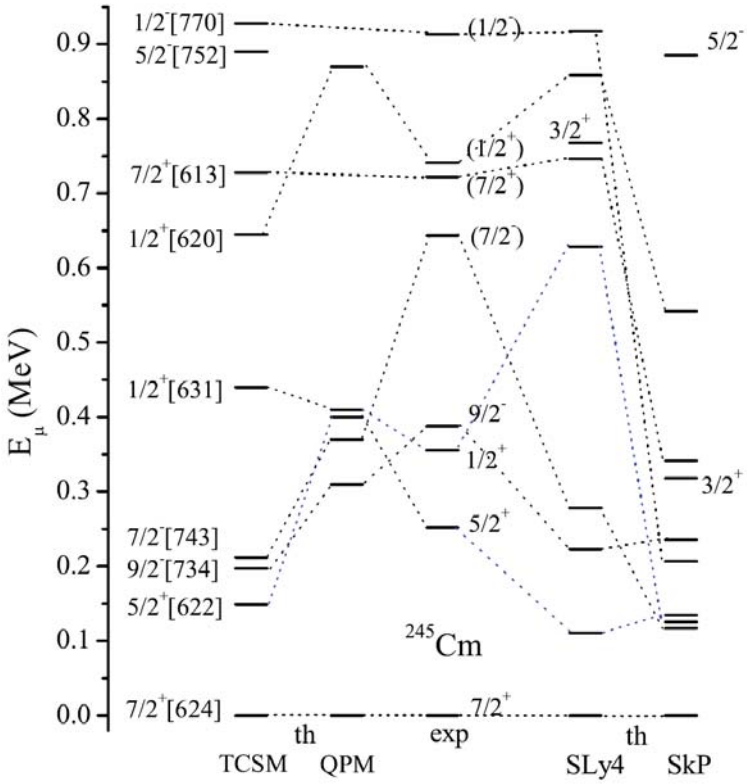

- An agreement between data & various models
- In some cases, the order is not reproduced

Adamian_Antonenko_Kukulin_Lu_Malov_SGZ2011_PRC

Cranking Shell Model w/ PNC for pairing

$$H_{\mathrm{CSM}} = H_0 + H_{\mathrm{P}} = H_{\mathrm{Nil}} - \omega J_x + H_{\mathrm{P}}$$

$$|\Psi\rangle = \sum_i C_i |i\rangle$$

$$J^{(1)} = \frac{1}{\omega} \langle \Psi | J_x | \Psi \rangle$$

$$n_\mu = \sum_i |C_i|^2 P_{i\mu}$$

- Applications of CSM-PNC
  - **Normally deformed & superdeformed high spin rotational bands of nuclei with A ~ 160, 190, & 250**
  - **Mechanism of identical bands in normally deformed nuclei**
  - **Nonadditivity in moments of inertia of high-K rotational bands**
  - **…**

Zeng...1994_PRC50-746
Zeng…1994_PRC50-1388

Nilsson parameters & deformation parameters

N	l	κ_p	μ_p	N	l	κ_n	μ_n
4	0,2,4	0.0670	0.654				
5	1	0.0250	0.710	6	0	0.1600	0.320
	3	0.0570	0.800		2	0.0640	0.200
	5	0.0570	0.710		4,6	0.0680	0.260
6	0,2,4,6	0.0570	0.654	7	1,3,5,7	0.0634	0.318

Zhang_Zeng_Zhao_SGZ2011_PRC83-011304R

Zhang_He_Zeng_Zhao_SGZ, in preparation

A new set of Nilsson parameters

- Reproduce well single particle structure in heavy nuclei

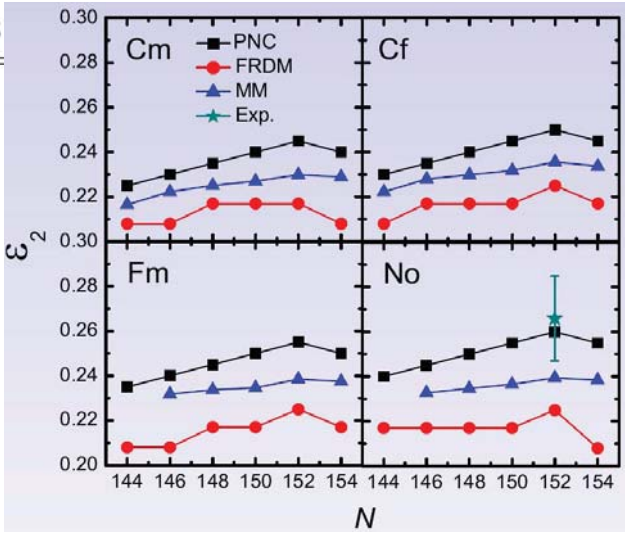

Bandhead energies in Bk (Z=97) isotopes

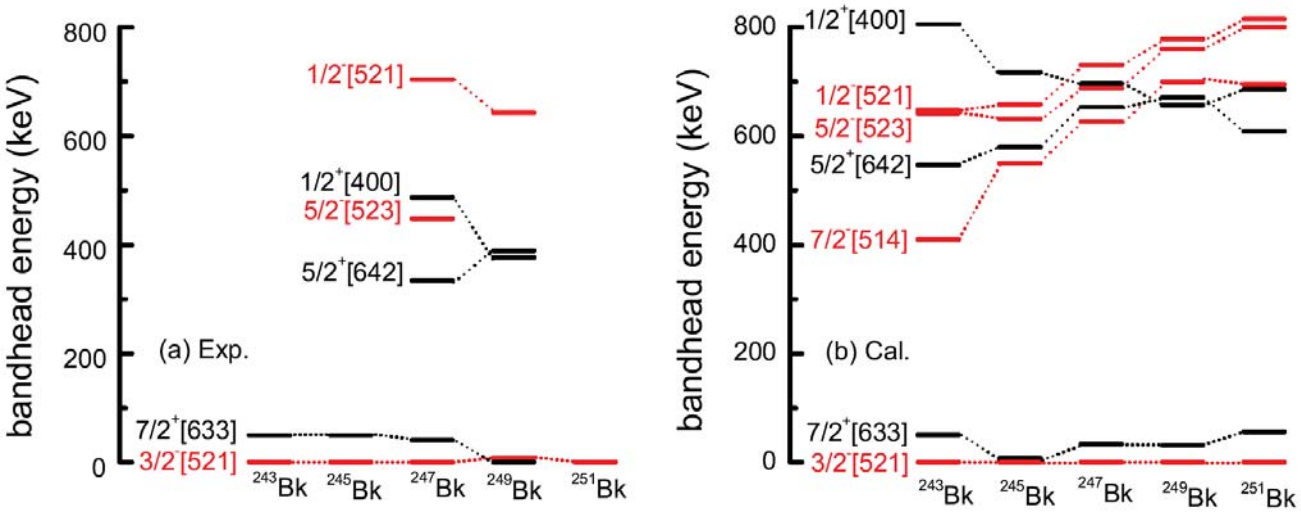

Zhang_He_Zeng_Zhao_SGZ, in preparation

Moments of inertia of even-even nuclei

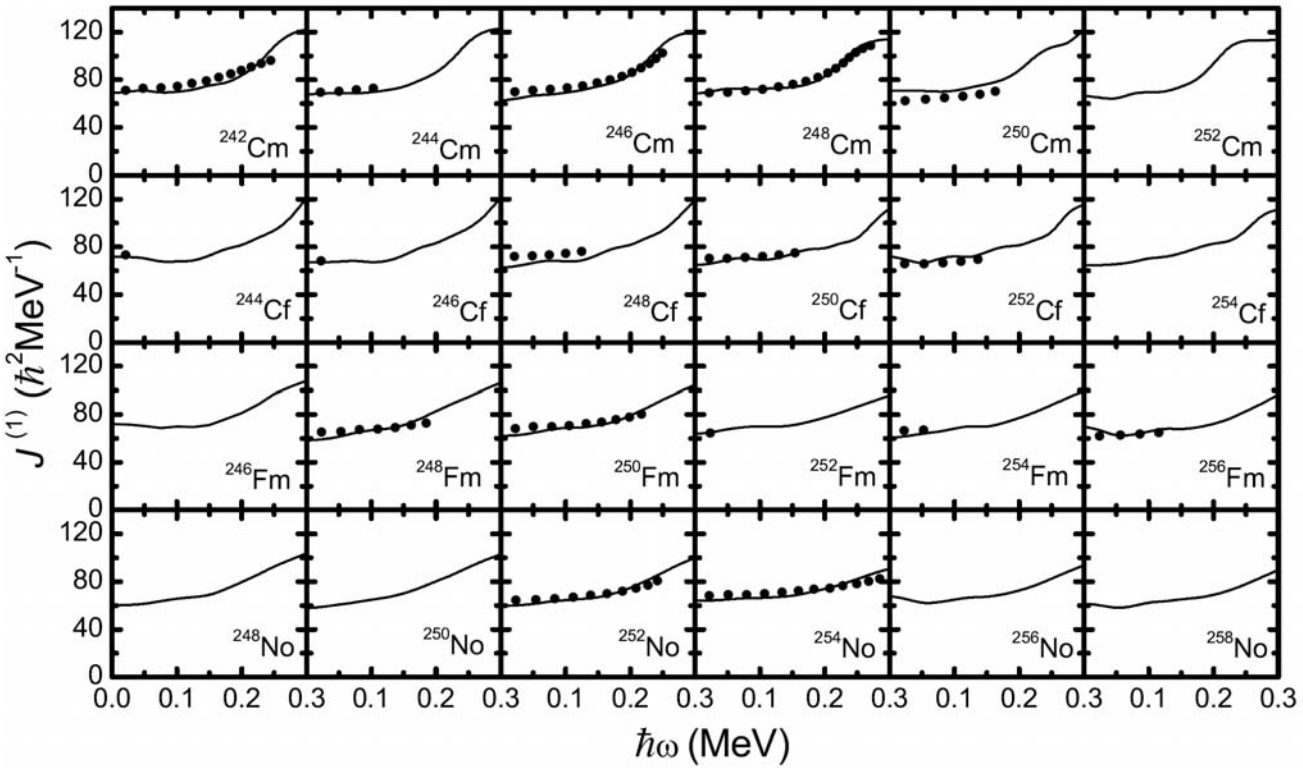

Zhang_He_Zeng_Zhao_SGZ, in preparation

Moments of inertia of odd-Z nuclei

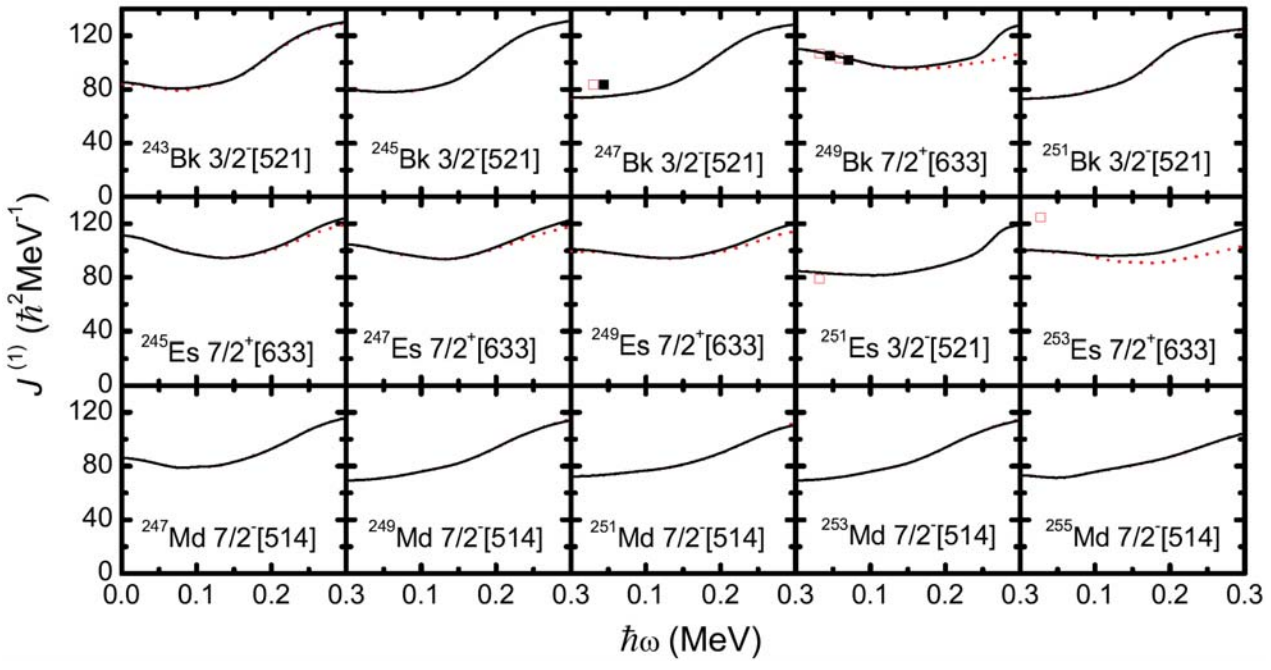

Zhang_He_Zeng_Zhao_SGZ, in preparation

Moments of inertia of odd-N nuclei

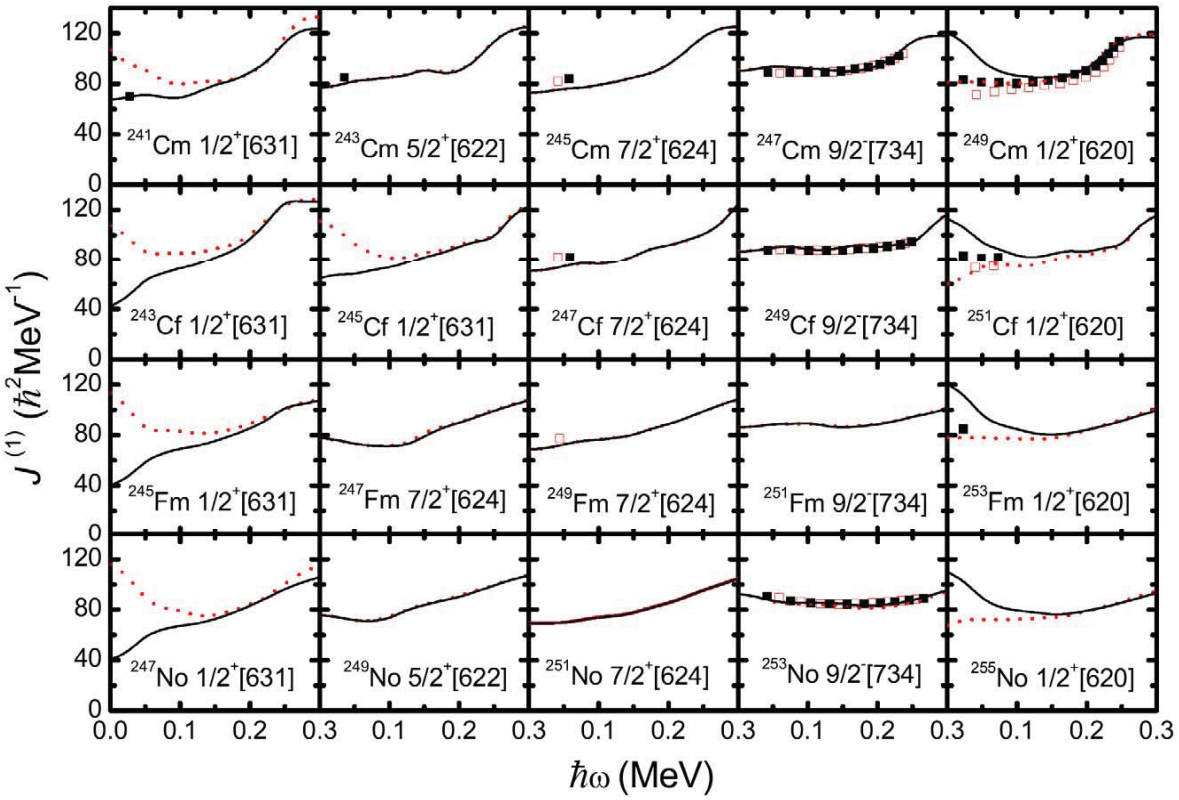

Zhang_He_Zeng_Zhao_SGZ, in preparation

Rotational bands in ^{247,249}Cm & ^{249}Cf: Expt

Tandel...2010_PRC82-021303R

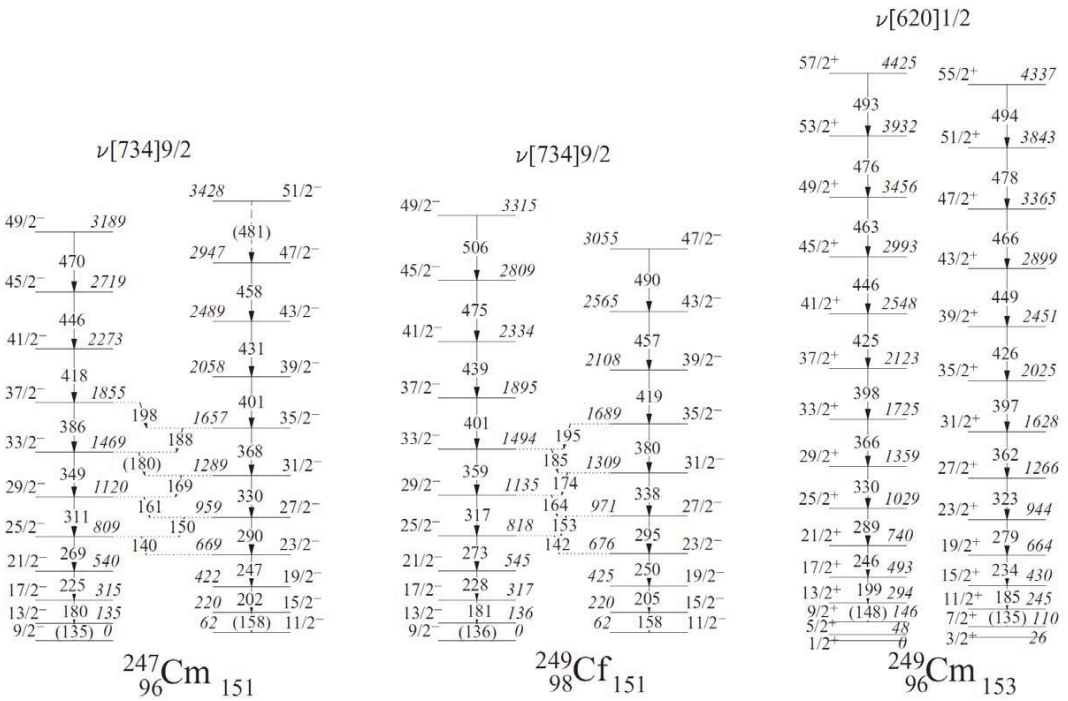

Rotational bands in ^{247,249}Cm & ^{249}Cf: MoI & align.

Zhang_Zeng_Zhao_SGZ2011_PRC83-011304R

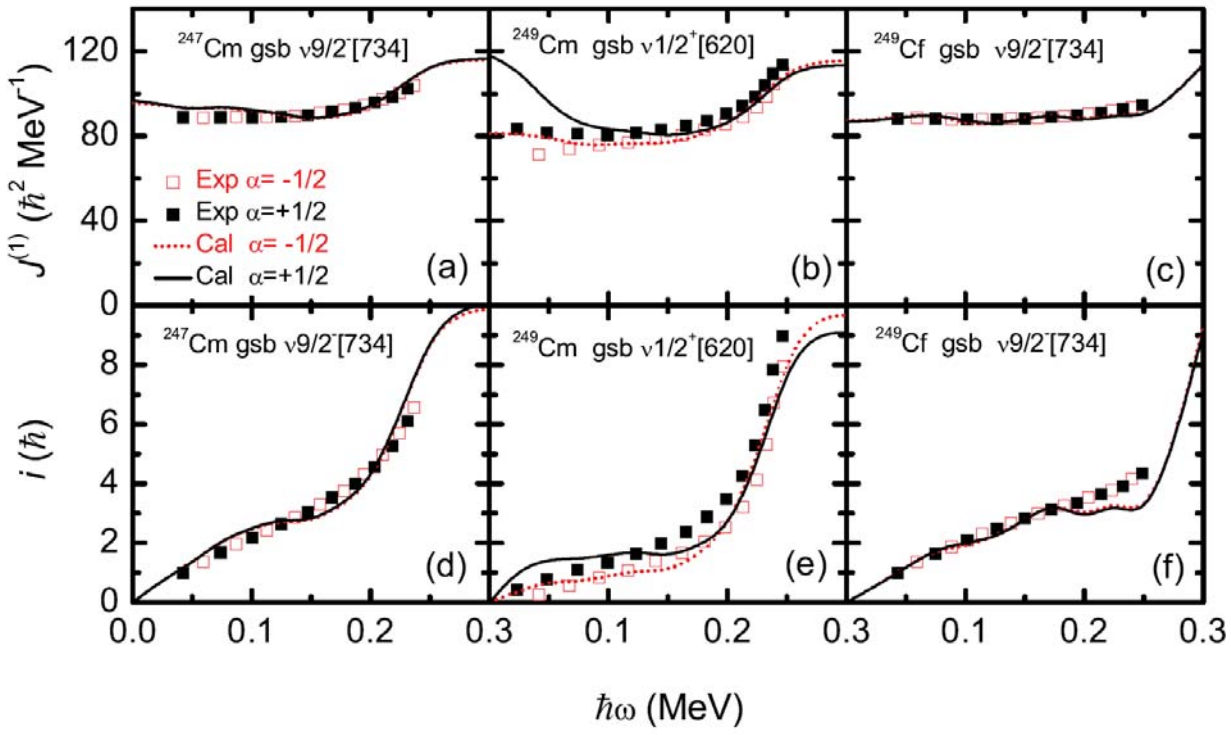

Rotational bands in ^{247,249}Cm & ^{249}Cf: occupations

Zhang_Zeng_Zhao_SGZ2011_PRC83-011304R

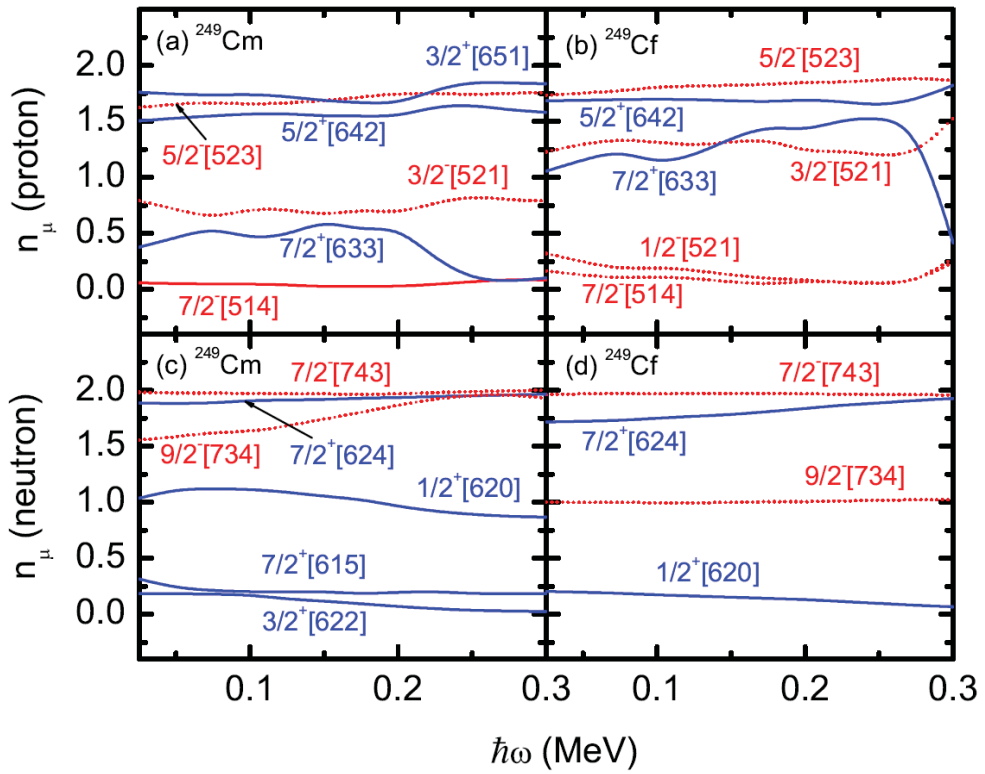

Rotational bands in ^{247,249}Cm & ^{249}Cf: occupations

Zhang_Zeng_Zhao_SGZ2011_PRC83-011304R

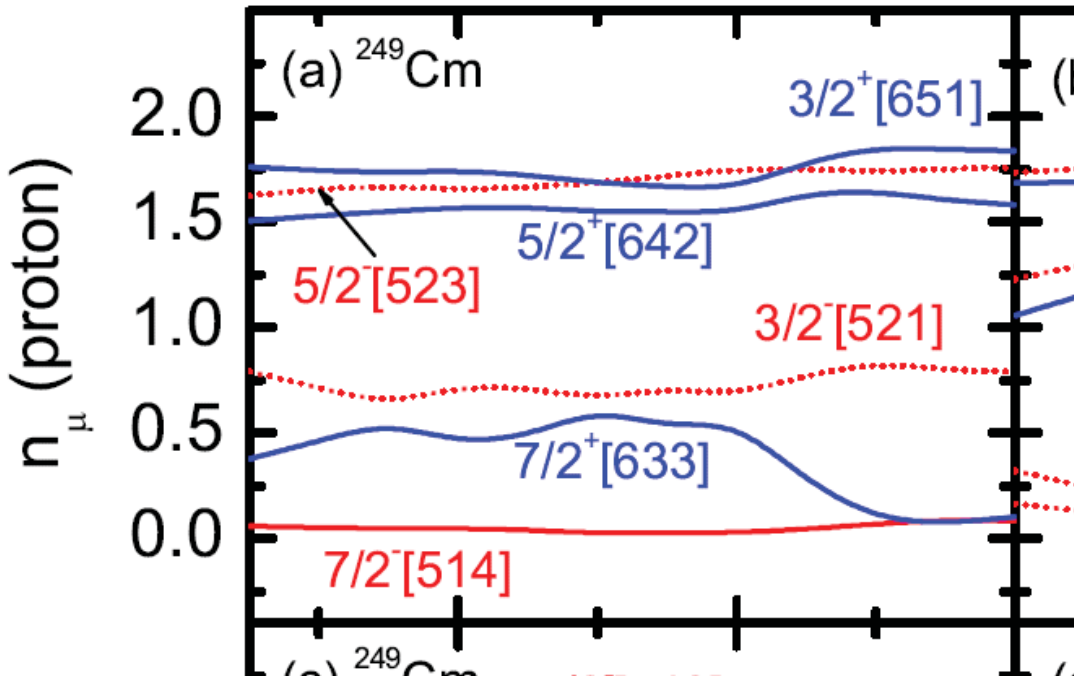

Contents

- Superheavy elements – history of predictions
- Experimental progress
- Structure of superheavy nuclei
  - **Shell structure: next proton & neutron magic numbers**
  - **Potential energy surfaces: shape, fission path & fission barrier**
  - **Low-lying spectra**
  - **Isomeric states**
- Synthesis of SHN via heavy ion reactions
  - **Capture process**
  - **Fusion – formation of a compound nucleus**
  - **Survival – competition between neutron emission & fission**
- Summary & Perspectives

Nuclear isomer (同核异能态)

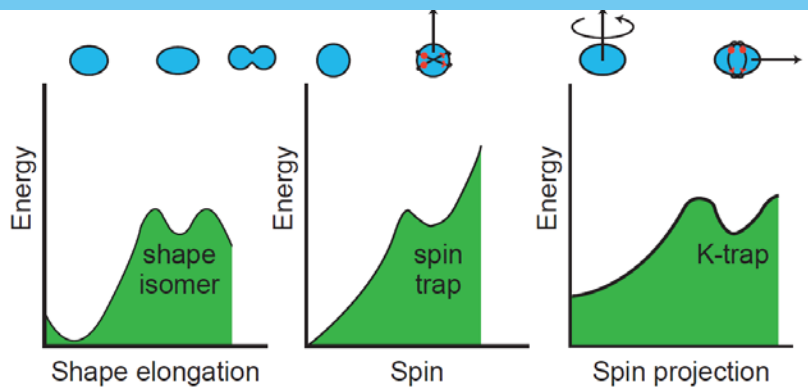

^{180m}Hf
$I^{\pi} = K^{\pi} = 8^-$
E = 1.1 MeV
$T_{1/2}$ = 5.5 hours

^{242f}Am
E = 2.2 MeV
$T_{1/2}$ = 14 ms

^{180m}Ta
$I^{\pi} = 9^-$
E = 75 keV
$T_{1/2} > 10^{15}$ years

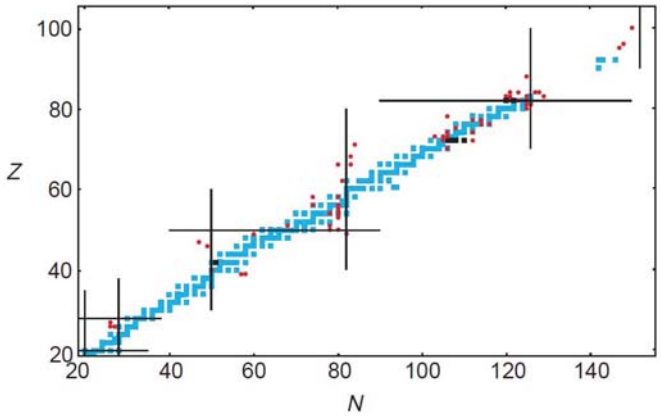

Walker_Dracoulis1999_Nature399-35

Herzberg…2006_Nature442-896

Isomers in SHN

$$^{64}\text{Ni} + {}^{207}\text{Pb} \rightarrow {}^{270}110 + 1n$$

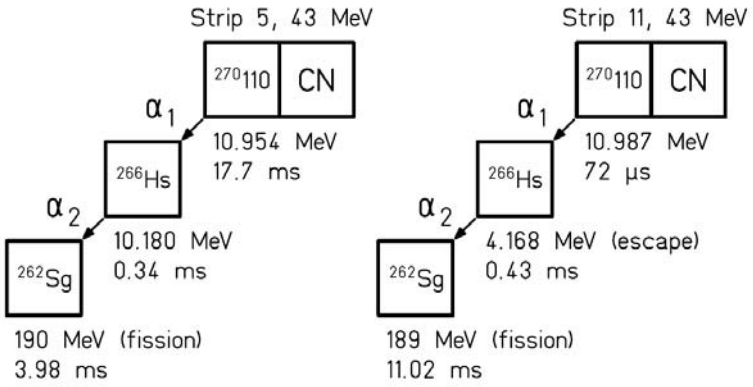

Date: 30-Oct-2000
Time: 22:12 h

Date: 01-Nov-2000
Time: 09:02 h

Hofmann…2001_EPJA10-5

Theoretical explanations & predictions

Configuration-constrained calculations of potential-energy surfaces

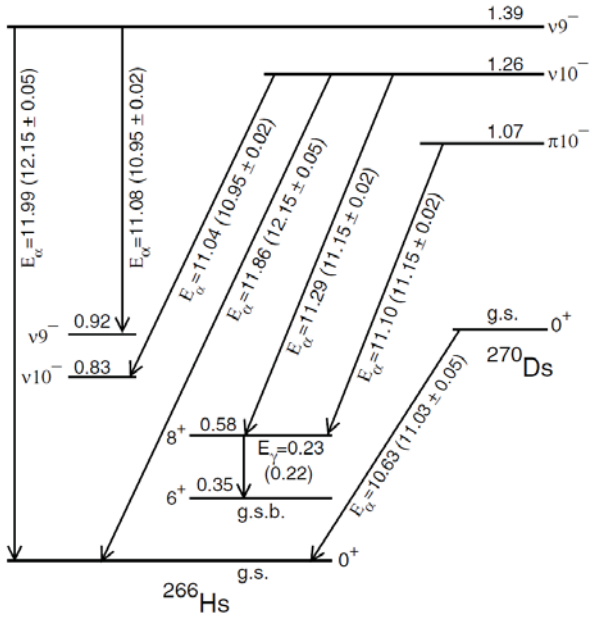

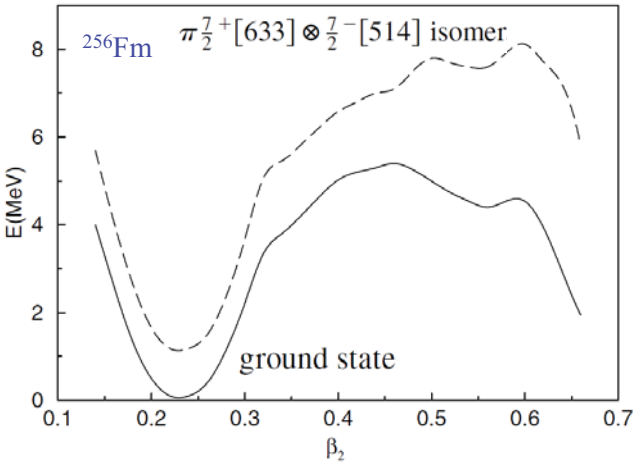

In a quantal system, the ground state is usually more stable than the excited states. In contrast, in superheavy nuclei the multiquasiparticle excitations decrease the probability for both fission and α decay, implying enhanced stability.

Xu_Zhao_Wyss_Walker2004_PRL92-252501

Possible roles played by isomers in the study of SHN

nature Vol 442|24 August 2006|doi:10.1038/nature05069

LETTERS

Nuclear isomers in superheavy elements as stepping stones towards the island of stability

R.-D. Herzberg[1], P. T. Greenlees[2], P. A. Butler[1], G. D. Jones[1], M. Venhart[3], I. G. Darby[1], S. Eeckhaudt[2], K. Eskola[4], T. Grahn[2], C. Gray-Jones[1], F. P. Hessberger[5], P. Jones[2], R. Julin[2], S. Juutinen[2], S. Ketelhut[2], W. Korten[6], M. Leino[2], A.-P. Leppänen[2], S. Moon[1], M. Nyman[2], R. D. Page[1], J. Pakarinen[1,2], A. Pritchard[1], P. Rahkila[2], J. Sarén[2], C. Scholey[2], A. Steer[2], Y. Sun[7], Ch. Theisen[6] & J. Uusitalo[2]

Contents

- Superheavy elements – history of predictions
- Experimental progress
- Structure of superheavy nuclei
  - **Shell structure: next proton & neutron magic numbers**
  - **Potential energy surfaces: shape, fission path & fission barrier**
  - **Low-lying spectra**
  - **Isomeric states**
- Synthesis of SHN via heavy ion reactions
  - **Capture process**
  - **Fusion – formation of a compound nucleus**
  - **Survival – competition between neutron emission & fission**
- Summary & Perspectives

Theory I: merge of two multi-nucleon systems

Time dependent Hartree-Fock theory

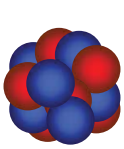

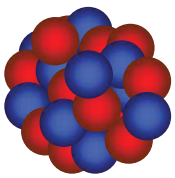

Guo...2008_PRC77-041301R
Umar...2010_PRC81-064607
...

$$\mathcal{S} = \int_{t_1}^{t_2} dt \langle \Phi(t) | H - i\hbar\partial_t | \Phi(t) \rangle \qquad H = \sum_i^A t_i + \sum_{i<j}^A v_{ij}$$

$$\Phi(r_1, r_2, \cdots, r_A, t) = \frac{1}{\sqrt{A!}} \det |\phi_\lambda(r_i, t)|$$

$$i\hbar \frac{\partial \phi_\lambda}{\partial t} = h\phi_\lambda$$

- Advantages
  - Microscopic
  - Successful in structure & reaction
- Disadvantages
  - Semi-classical (no reaction channel)
  - Only one-body dissipation (collisions with “wall” of mean field)

Theory I: merge of two multi-nucleon systems

Quantum Molecular Dynamics

Tian...2008_PRC77-064603
Bian...2008_IJMPE17-80
Jiang...2010_PRC81-044602
...

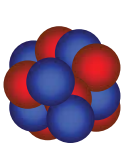

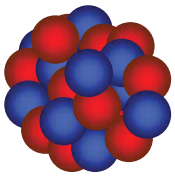

$$\phi_i(\boldsymbol{r}) = \frac{1}{(2\pi\sigma_r^2)^{3/4}} \exp\left[-\frac{(\boldsymbol{r}-\boldsymbol{r}_i)^2}{4\sigma_r^2} + \frac{i}{\hbar}\boldsymbol{r}\cdot\boldsymbol{p}_i\right]$$

$$\dot{\boldsymbol{r}}_i = \frac{\partial H}{\partial \boldsymbol{p}_i}\ , \quad \dot{\boldsymbol{p}}_i = -\frac{\partial H}{\partial \boldsymbol{r}_i}$$

- Advantages
  - Microscopic
  - Both mean field & collision terms included
- More attentions should be paid on
  - Pauli exclusive principle
  - Shell effects

Theory II: merge of two viscous liquid drops

Theory II: merge of two viscous liquid drops

Macroscopic Models:

- Mass & Charge
- Shape & orientation
- Neck formation
- Nucleon transfer

Theory II: merge of two viscous liquid drops

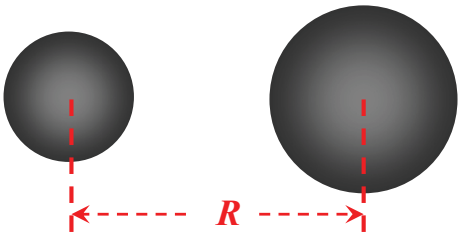

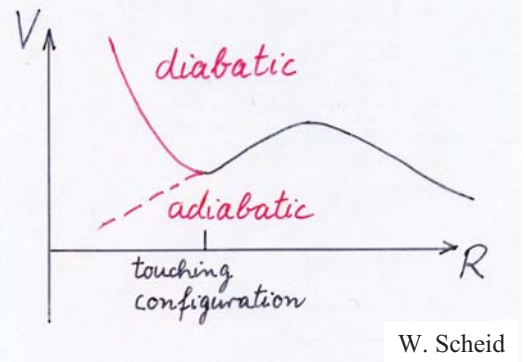

W. Scheid

Theory II: merge of two viscous liquid drops

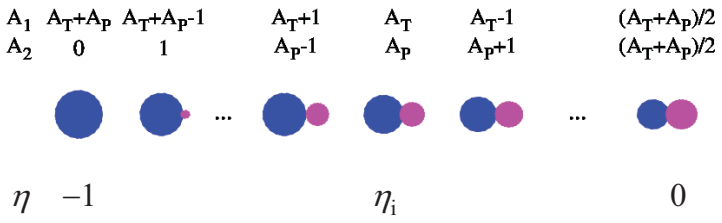

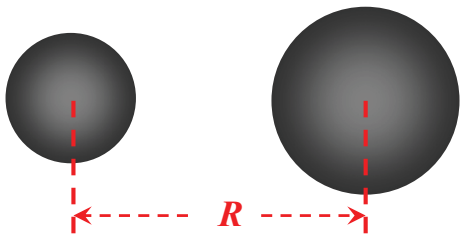

$$\eta = \frac{A_1 - A_2}{A_1 + A_2}$$

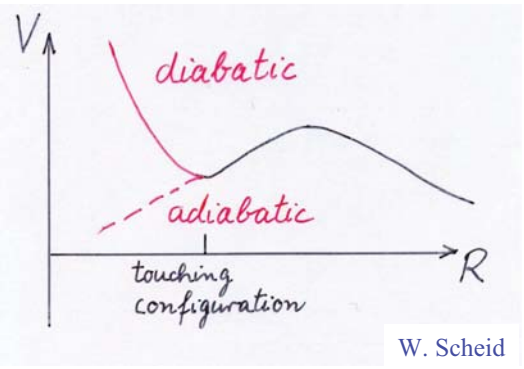

W. Scheid

Theory II: merge of two viscous liquid drops

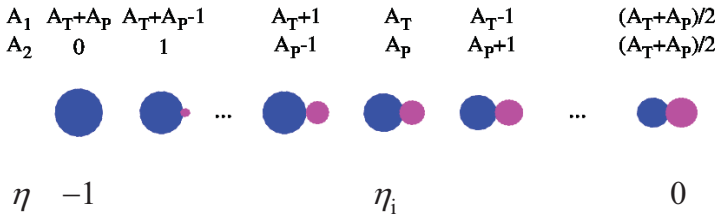

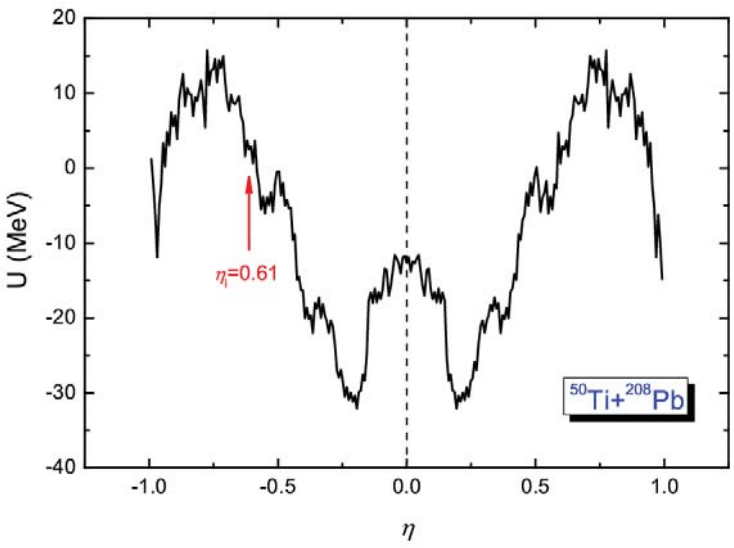

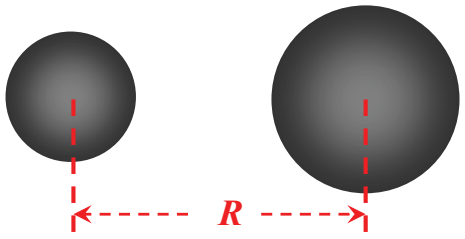

$$\eta = \frac{A_1 - A_2}{A_1 + A_2}$$

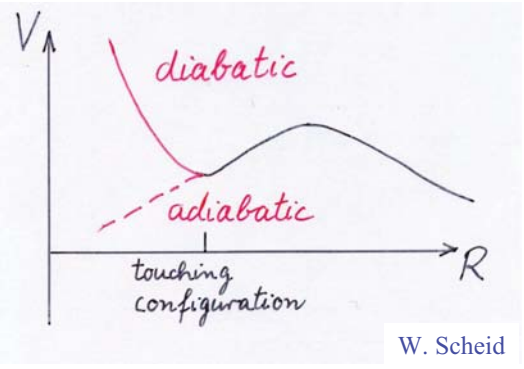

W. Scheid

Theory II: merge of two viscous liquid drops

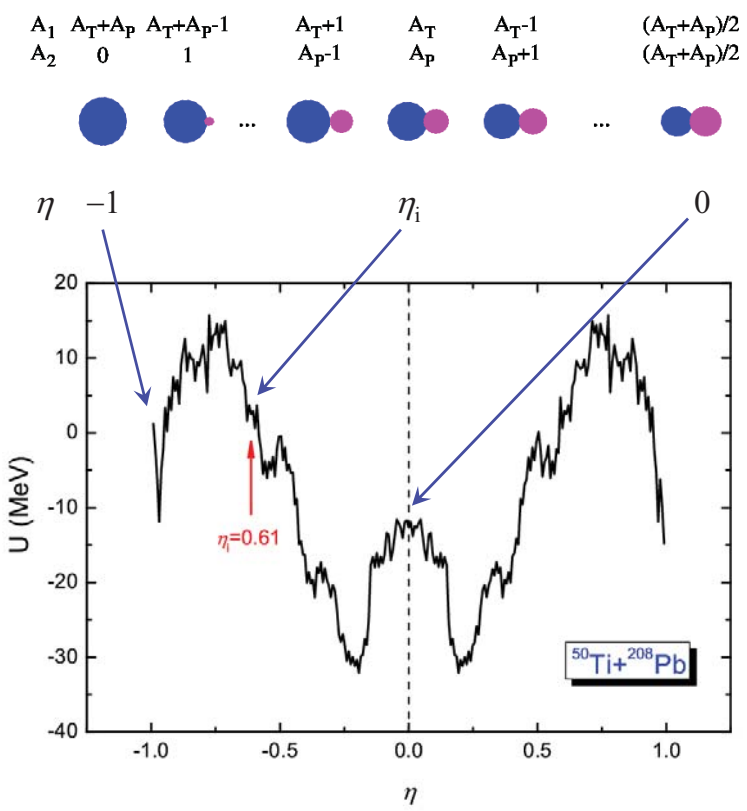

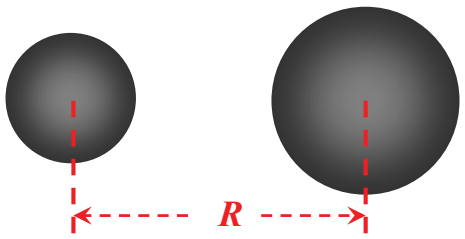

$$\eta = \frac{A_1 - A_2}{A_1 + A_2}$$

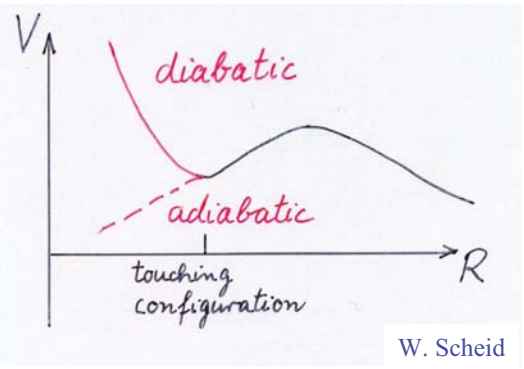

Three steps to produce a SHN

- Capture
- Formation of a compound nucleus (CN) - fusion
- De-excitation of the CN via neutron(s) emission - survival

Schaedel...2006_ACID45-368

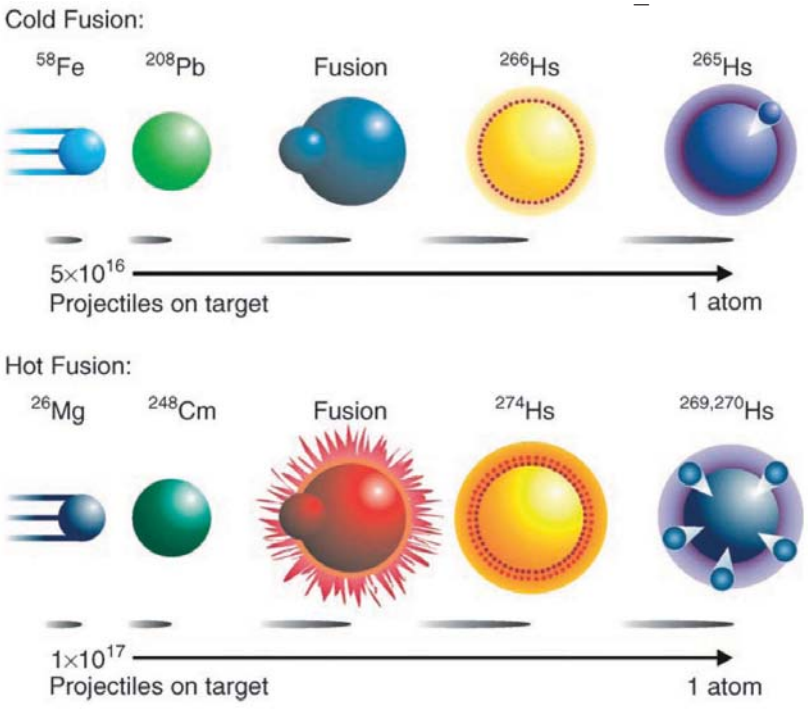

Capture | CN formation | neutron(s) emission

$$\sigma_{ER}(E_{cm}) = \sum_J \sigma_{cap}(E_{cm}, J)\ P_{CN}(E_{cm}, J)\ W_{sur}(E_{cm}, J)$$

Three steps to produce a SHN

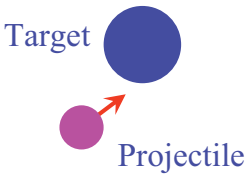

Three steps to produce a SHN

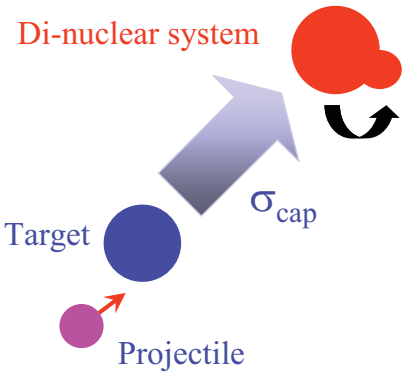

Three steps to produce a SHN

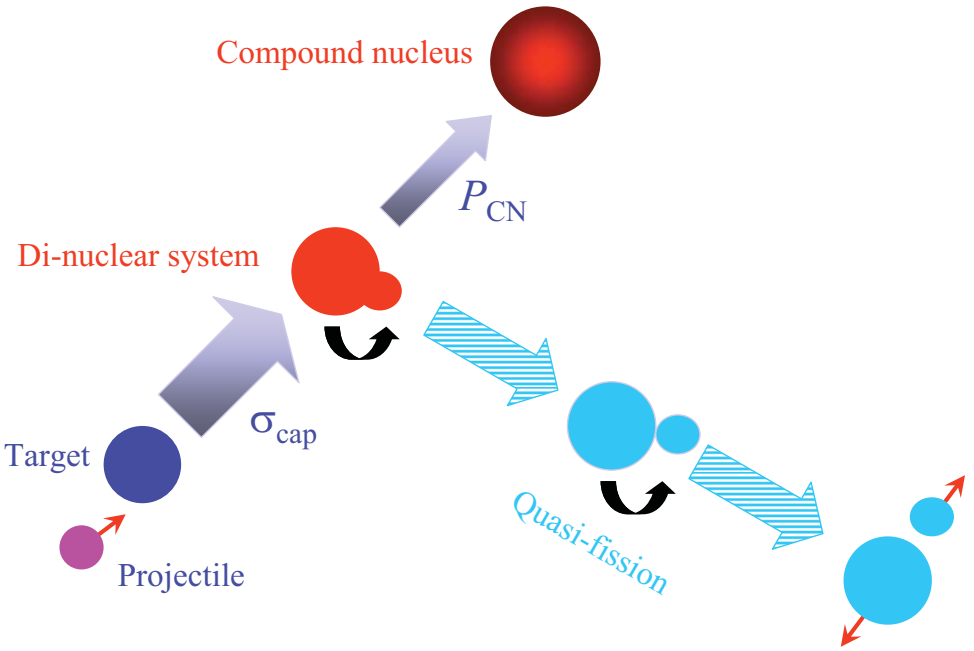

Three steps to produce a SHN

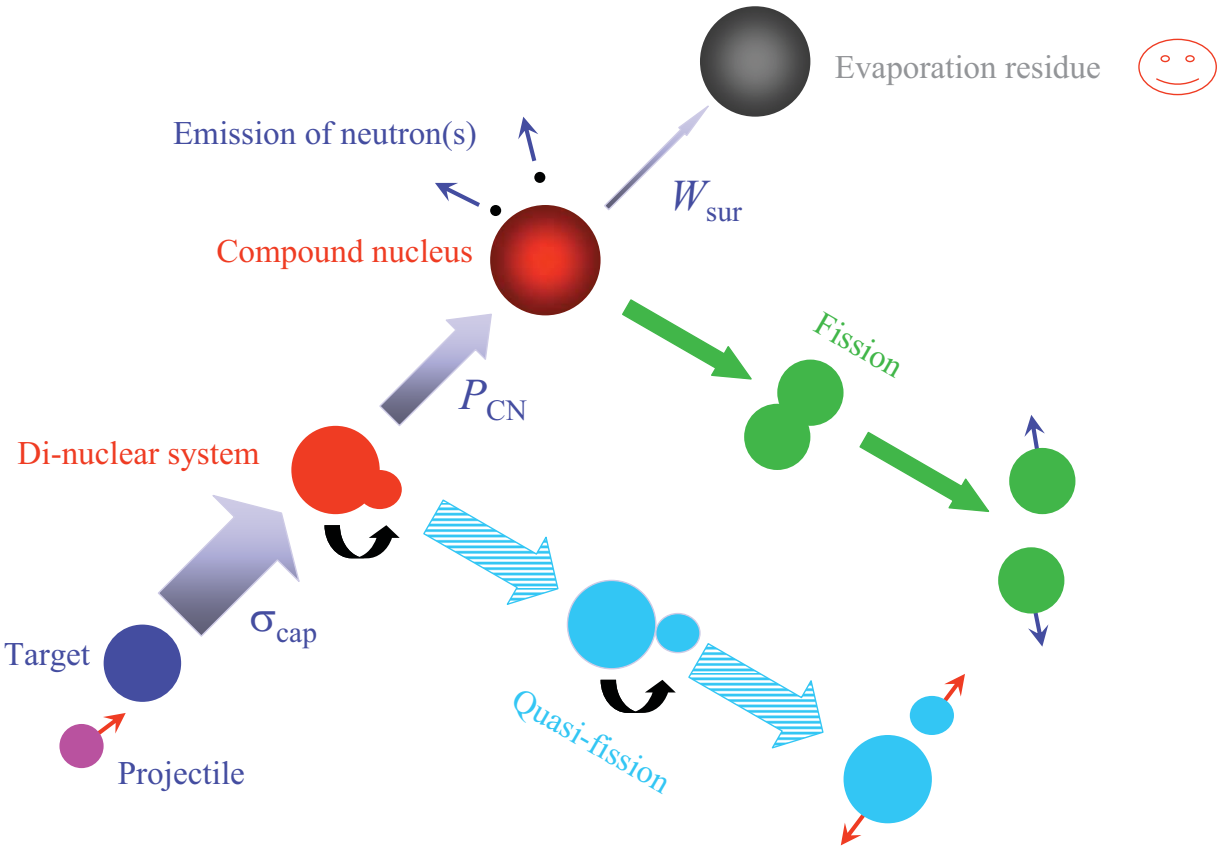

The capture process

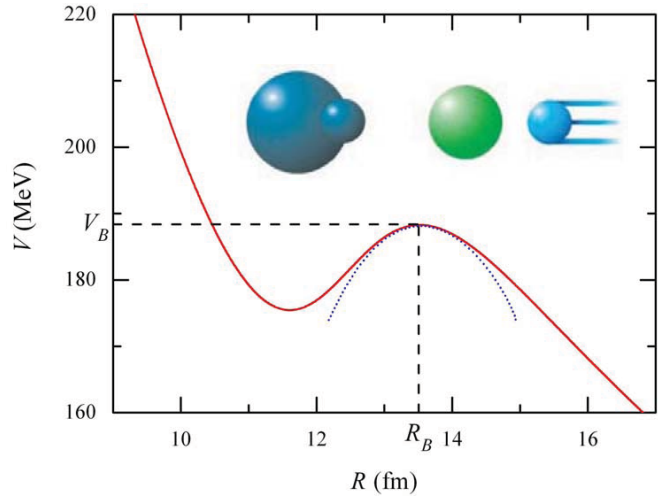

- Path integral method
- WKB approximation
- Hill-Wheeler formula
- New formula by Li et al.
- ...

$$\sigma_{\text{cap}}(E_{\text{cm}}, J) = \frac{\pi\hbar^2}{2\mu E_{\text{cm}}}(2J+1)\,T(E_{\text{cm}}, J)$$

$$T(E_{\text{cm}}, J) = \left(1 + \exp\left[-\frac{2\pi}{\hbar\omega}(E_{\text{cm}} - E_{\text{rot}} - V_B)\right]\right)^{-1}$$

Hill_Wheeler1953_PR089-1102

The capture process: channel coupling effects

Coupling effects due to rotation, vibration, nucleon transfer, …

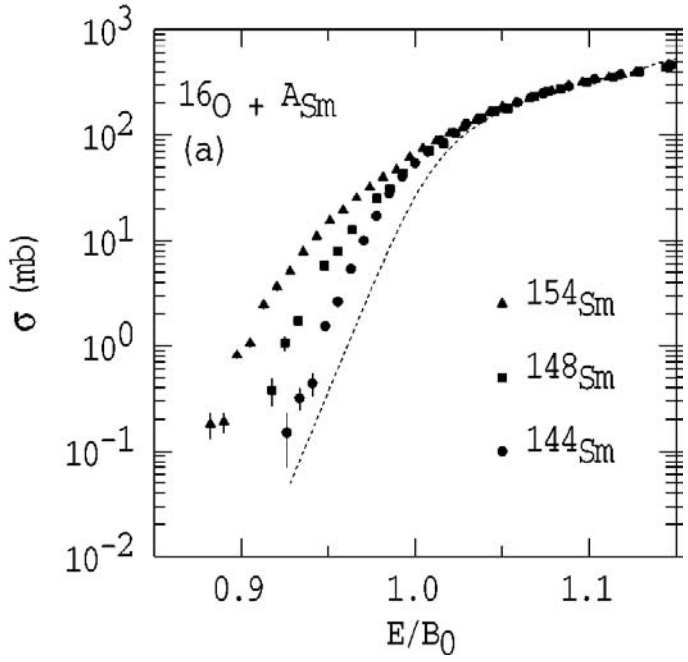

Dasgupta...1998_ARNPS48-401

The capture process: channel coupling effects

Coupling effects due to rotation, vibration, nucleon transfer, …

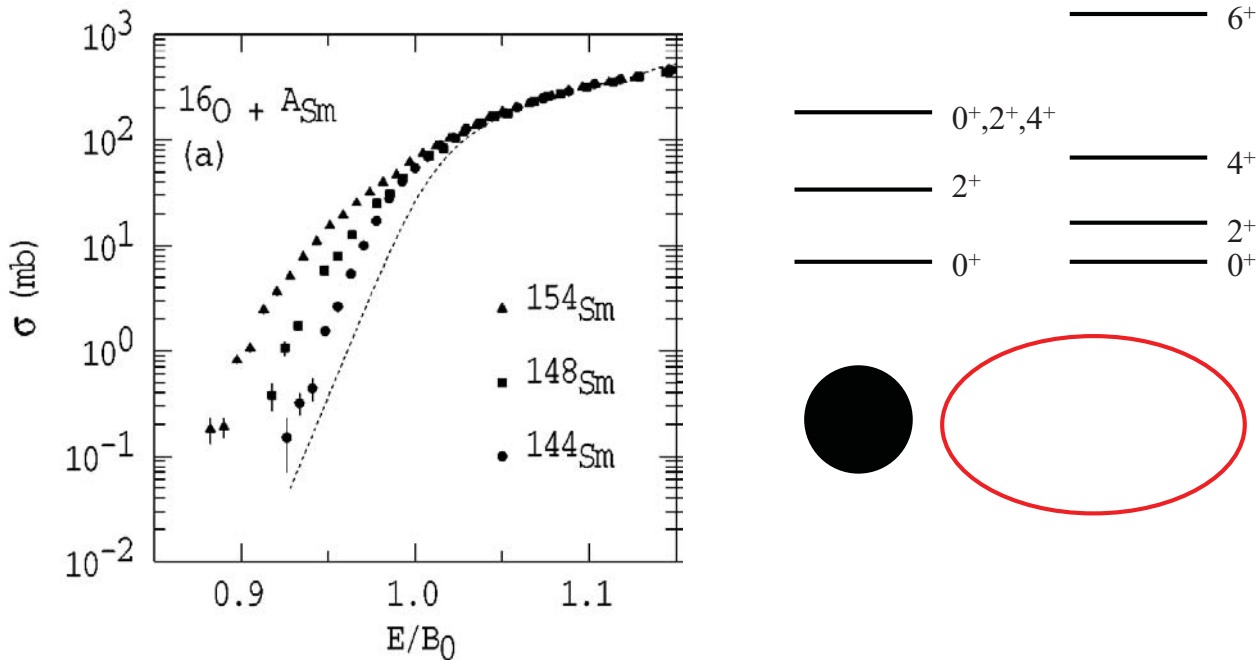

Dasgupta...1998_ARNPS48-401

The capture process: barrier distribution

Coupling effects due to rotation, vibration, nucleon transfer, …
are taken into account effectively by introducing a barrier distribution

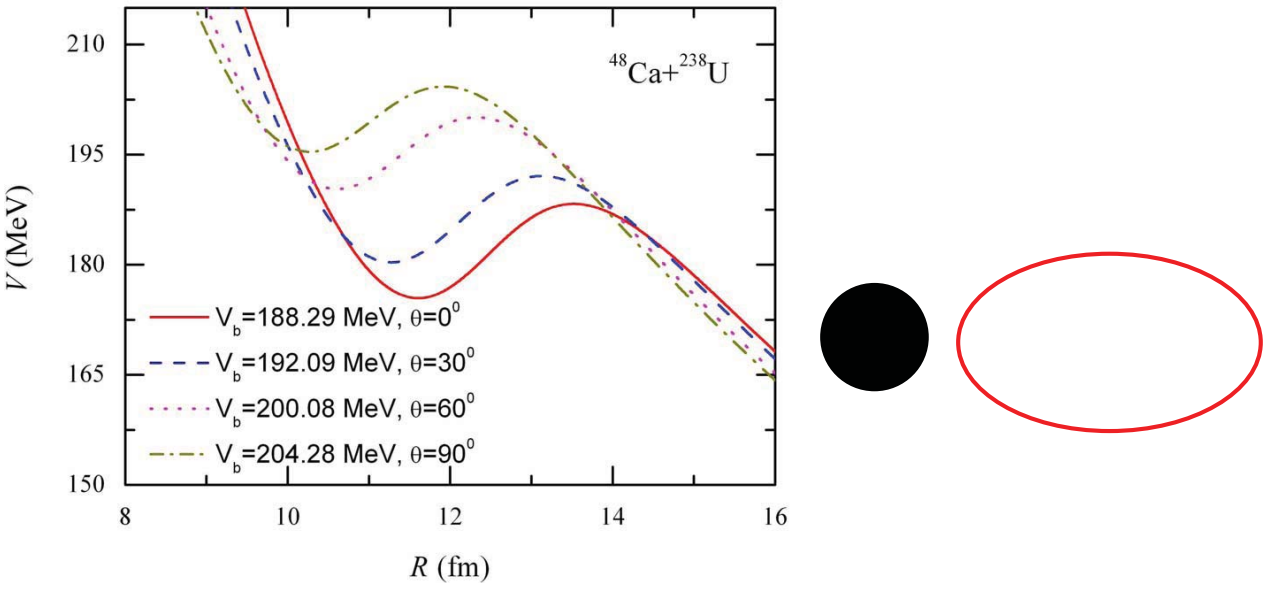

The capture process: barrier distribution

Coupling effects due to rotation, vibration, nucleon transfer, …
are taken into account effectively by introducing a barrier distribution

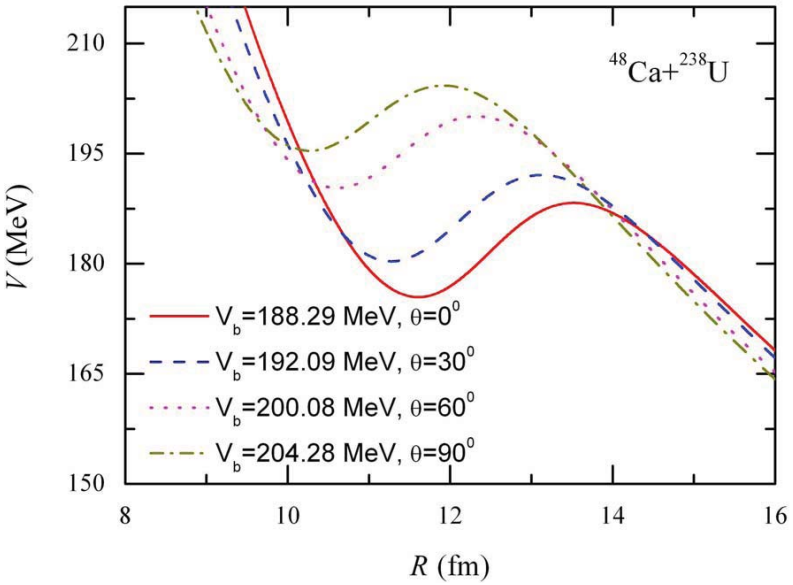

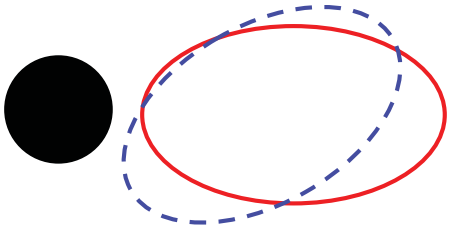

The capture process: barrier distribution

Coupling effects due to rotation, vibration, nucleon transfer, …
are taken into account effectively by introducing a barrier distribution

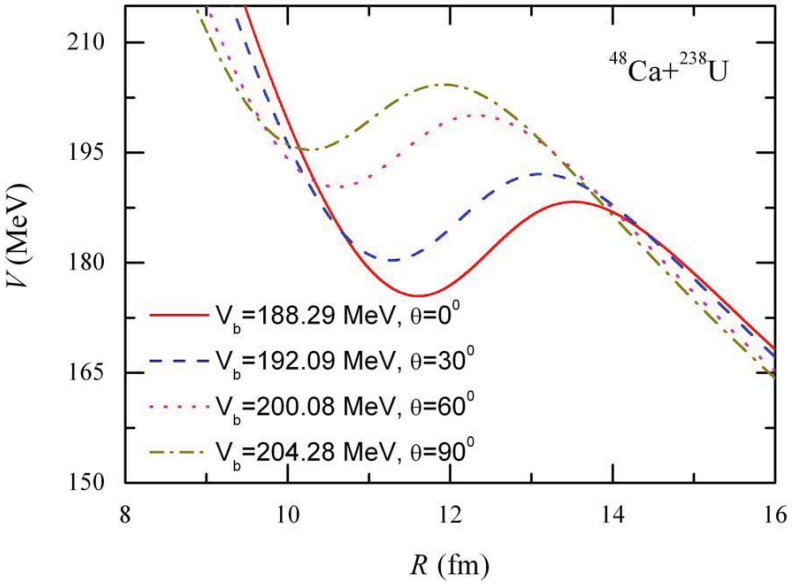

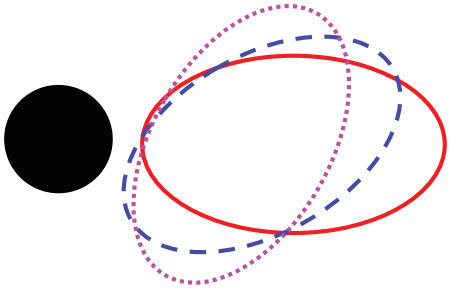

The capture process: barrier distribution

Coupling effects due to rotation, vibration, nucleon transfer, …
are taken into account effectively by introducing a barrier distribution

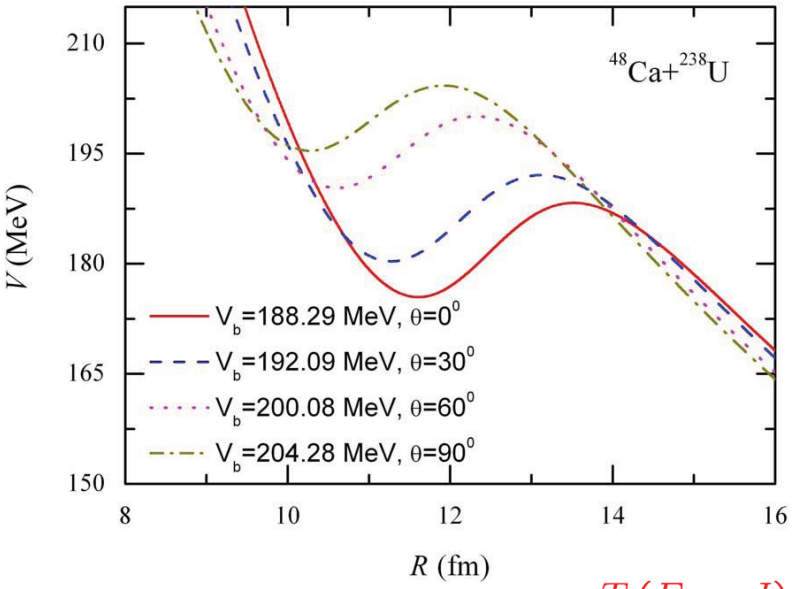

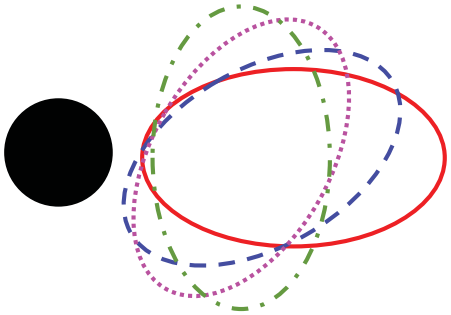

$$T(E_{\rm cm}, J) = \int dB\ f(B)\ T(E_{\rm cm}, B, J)$$

Ambiguities in NN potentials (I)

SGZ2009

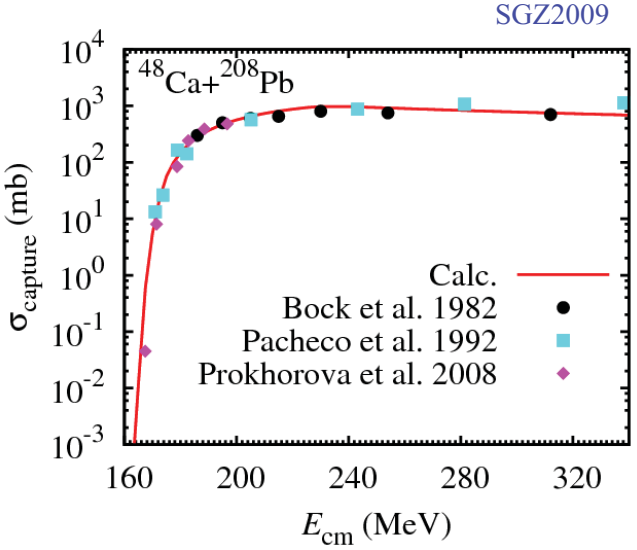

Wang...2006_PRC74-044604

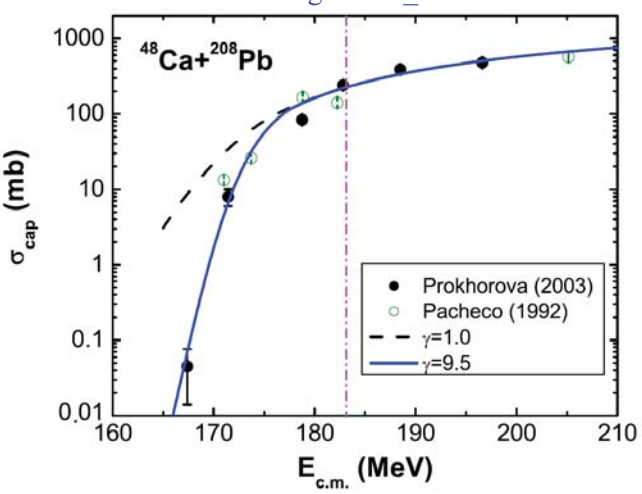

Ambiguities in NN potentials (I)

SGZ2009

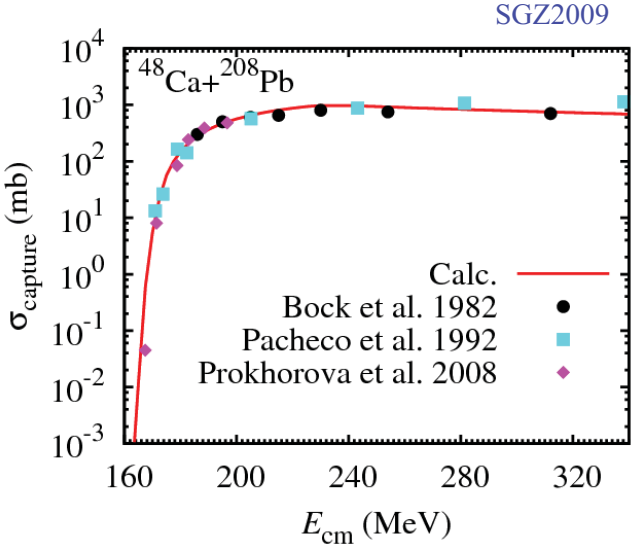

Wang...2006_PRC74-044604

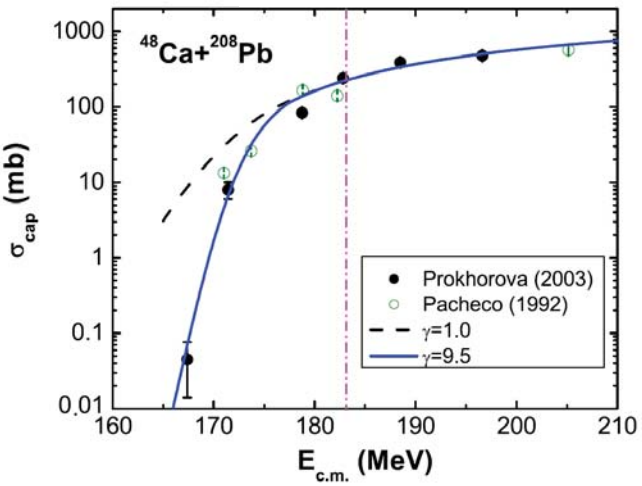

Potentials:
- Woods-Saxon w/ different parameters
- Proximity
- Skyrme Energy Density Functional
- …

Barrier distribution:
- Rectangular
- Symmetric Gaussian
- Asymmetric Gaussian
- …

Ambiguities in NN potentials (II)

SGZ2009

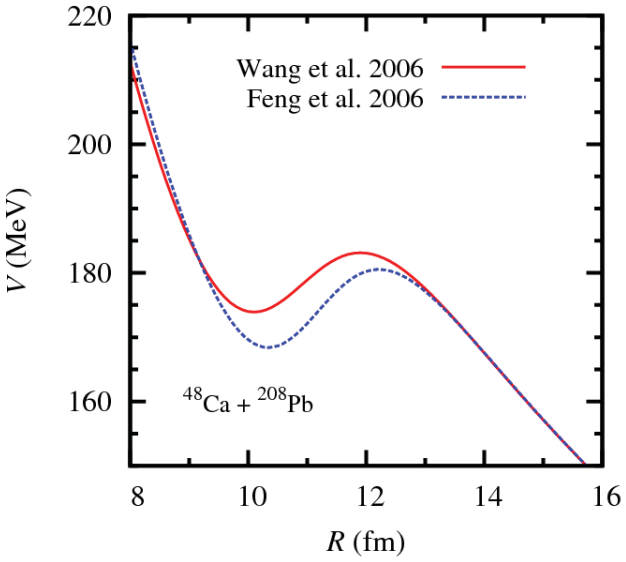

SGZ2009

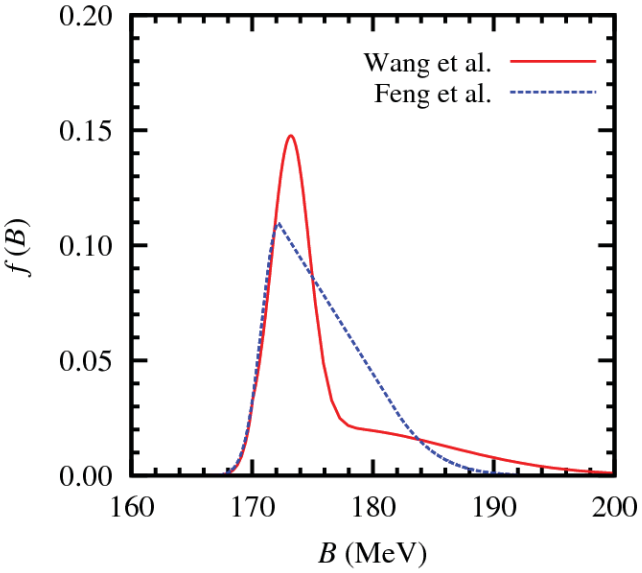

$$T(E_{\rm cm}, J) = \int dB\ f(B)\ T(E_{\rm cm}, B, J)$$

Zagrebaev2001_PRC64-034606
Wang...2006_PRC74-044604
Liu...2006_NPA768-80
Feng...2006_NPA771-50

Ambiguities in NN potentials (III)

- More experimental results., not only fusion, but also scattering
- Quasi-elastic scattering could be of help

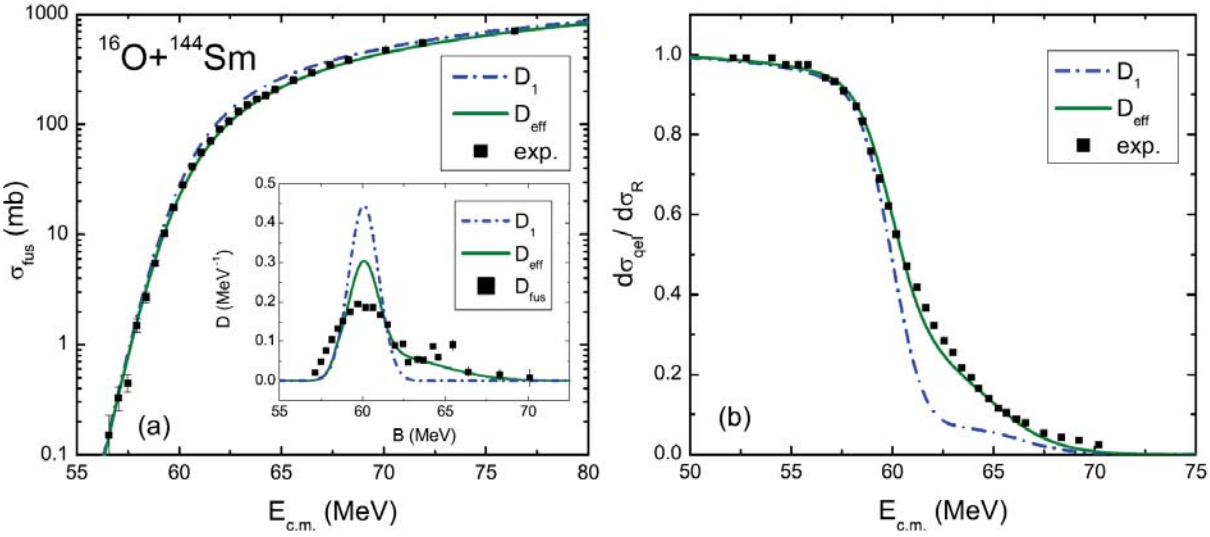

Wang...2009_SciChinaG52-1554

Formation of a compound nucleus (CN)

- The macroscopic dynamical model
  Swiatecki1982_NPA376-275
- The fluctuation-dissipation model
  Abe2002_EPJA13-143; Shen...2002_PRC66-061602R
- The nucleon collectivization model
  Zagrebaev2001_PRC64-034606
- The fusion by diffusion models
  Liu_Bao2007_PRC76-034604 Swiatecki...2005_PRC71-014602
- The model based on multi-dimensional Langevin equations
  Zagrebaev_Greiner2005_JPG31-825
- Models based on the di-nuclear system concept
  Adamian...1998_NPA633-409
- .....
  Li...2003_EuroPhysLett64-750; Zhao...2008_IJMPE17-1937; Li...2010_NPA834-353c

Volkov2004_ActaPhysHungA19-67
Feng...2011_NuclPhysRev28-1

A model based on the di-nuclear system concept

After the capture process, the two colliding nuclei form a di-nuclear system and keep their individualities

- ✧ **Exchanges of nucleon between the two nuclei**
- ✧ **The DNS may go quasi-fission & the heavier one may fission**
- ✧ **Deformations develop in both nuclei**

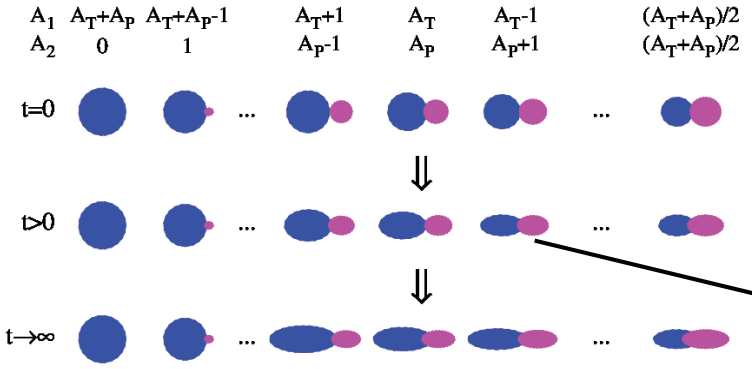

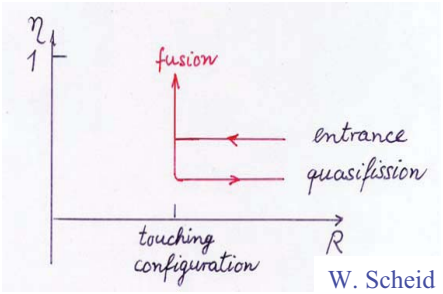

W. Scheid

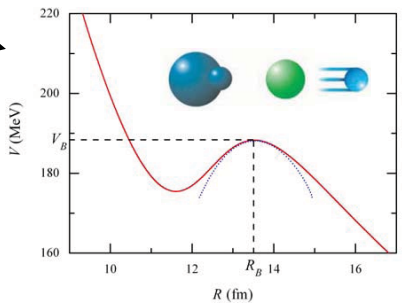

A model based on the di-nuclear system concept

After the capture process, the two colliding nuclei form a di-nuclear system and keep their individualities

- ✧ **Exchanges of nucleon between the two nuclei**
- ✧ **The DNS may go quasi-fission & the heavier one may fission**
- ✧ **Deformations develop in both nuclei**

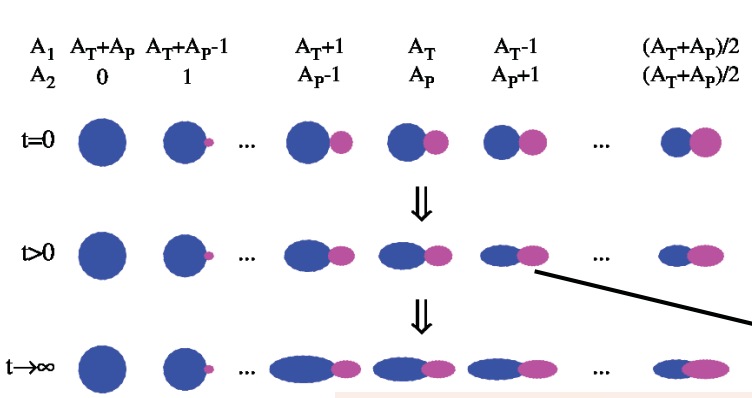

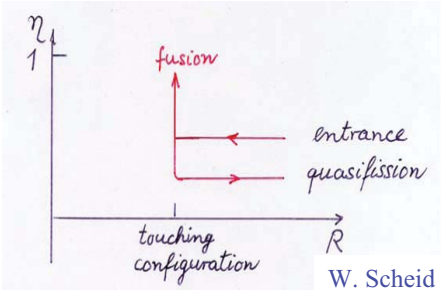

W. Scheid

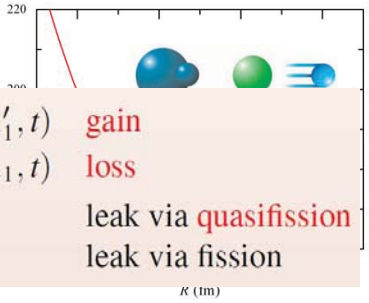

$$P(A_1, t=0) = \delta_{A_1 A_P}$$

$$\begin{aligned}
\frac{d}{dt}P(A_1,t) &= \sum_{A_1'} W_{A_1' A_1}(t)\, d_{A_1}(t)\, P(A_1',t) && \text{gain}\\
&- \sum_{A_1'} W_{A_1 A_1'}(t)\, d_{A_1'}(t)\, P(A_1,t) && \text{loss}\\
&- \Lambda^{\mathrm{qf}}_{A_1}(t)\, P(A_1,t) && \text{leak via quasifission}\\
&- \Lambda^{\mathrm{fis}}_{A_1}(t)\, P(A_1,t) && \text{leak via fission}
\end{aligned}$$

A typical example of P_{CN}

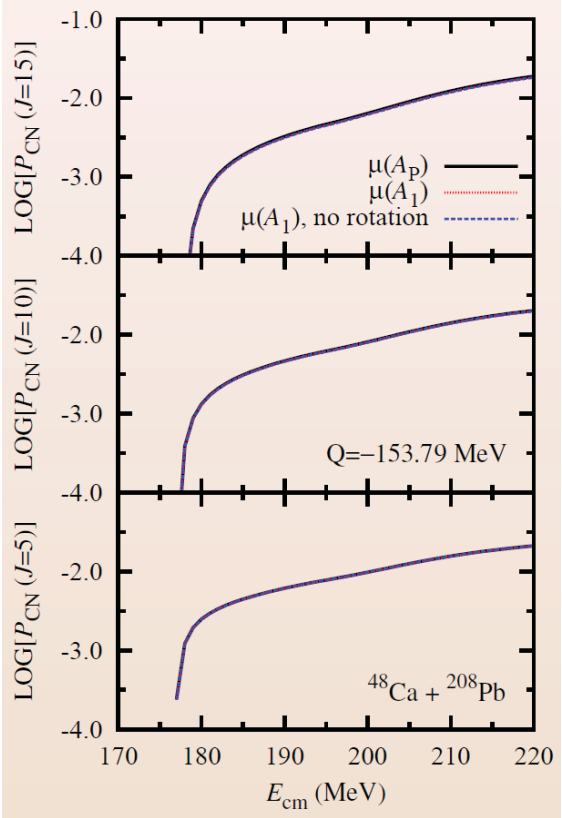

Puzzles in PCN (I)

Two orders of magnitude differences among model predictions !

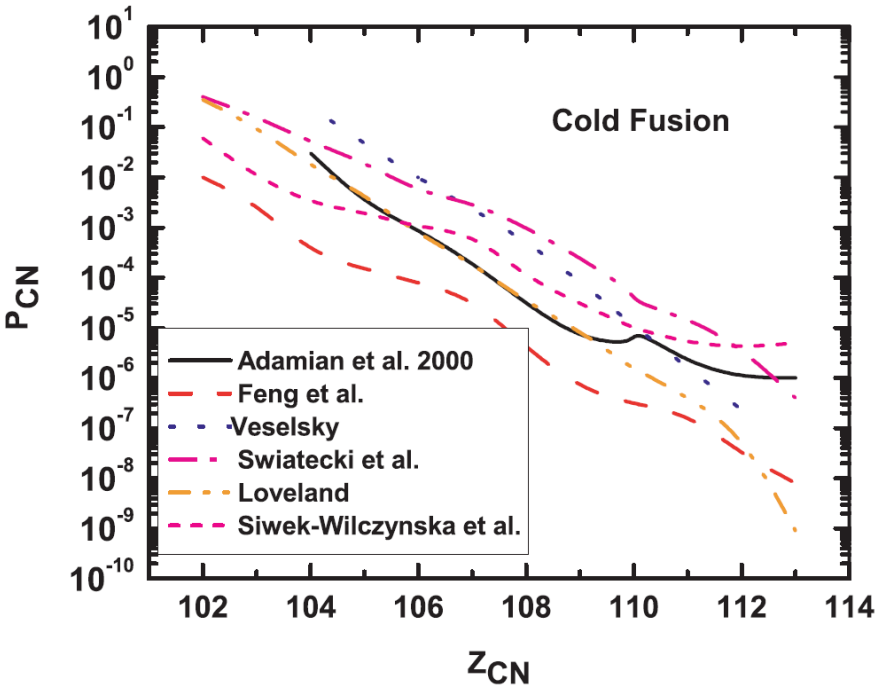

Naik...2007_PRC76-054604

Puzzles in PCN (II)

More experimental results needed to benchmark models!

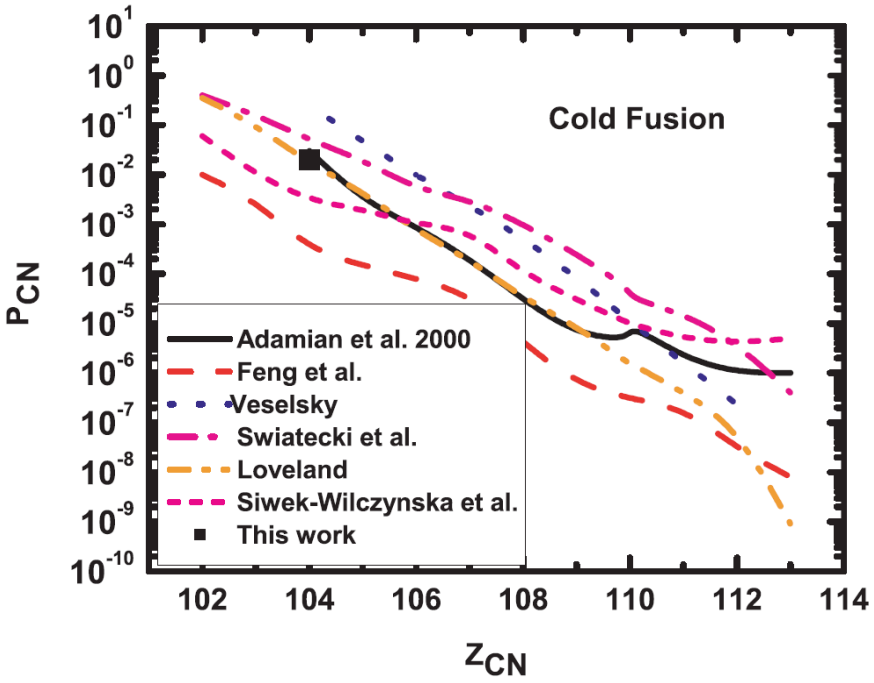

Naik...2007_PRC76-054604

Puzzles in PCN (III)

$$\sigma_{ER}(E_{cm}) = \sum_J \sigma_{cap}(E_{cm}, J)\ P_{CN}(E_{cm}, J)\ W_{sur}(E_{cm}, J)$$

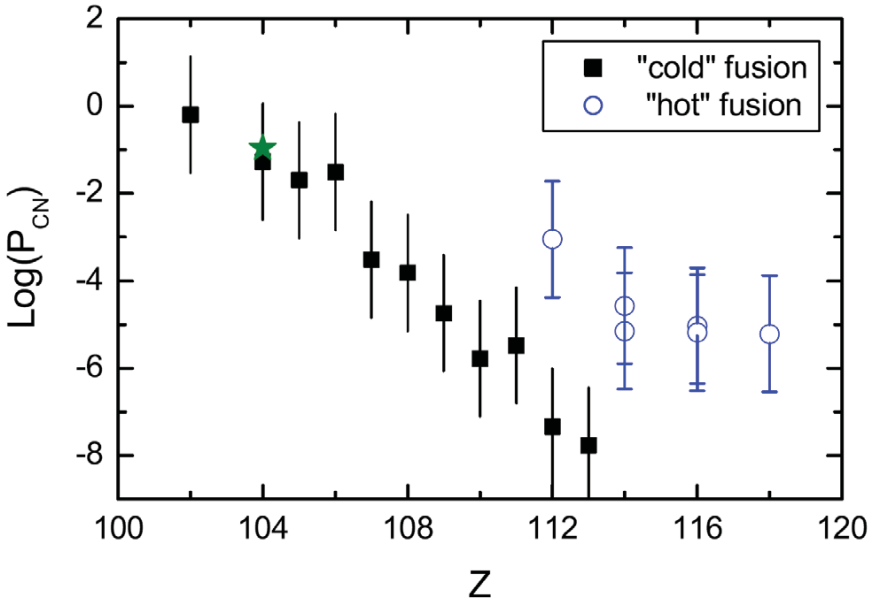

Wang...2009_SciChinaG52-1554

NN potentials: adiabatic or diabatic?

$$\eta = \frac{A_1 - A_2}{A_1 + A_2}$$

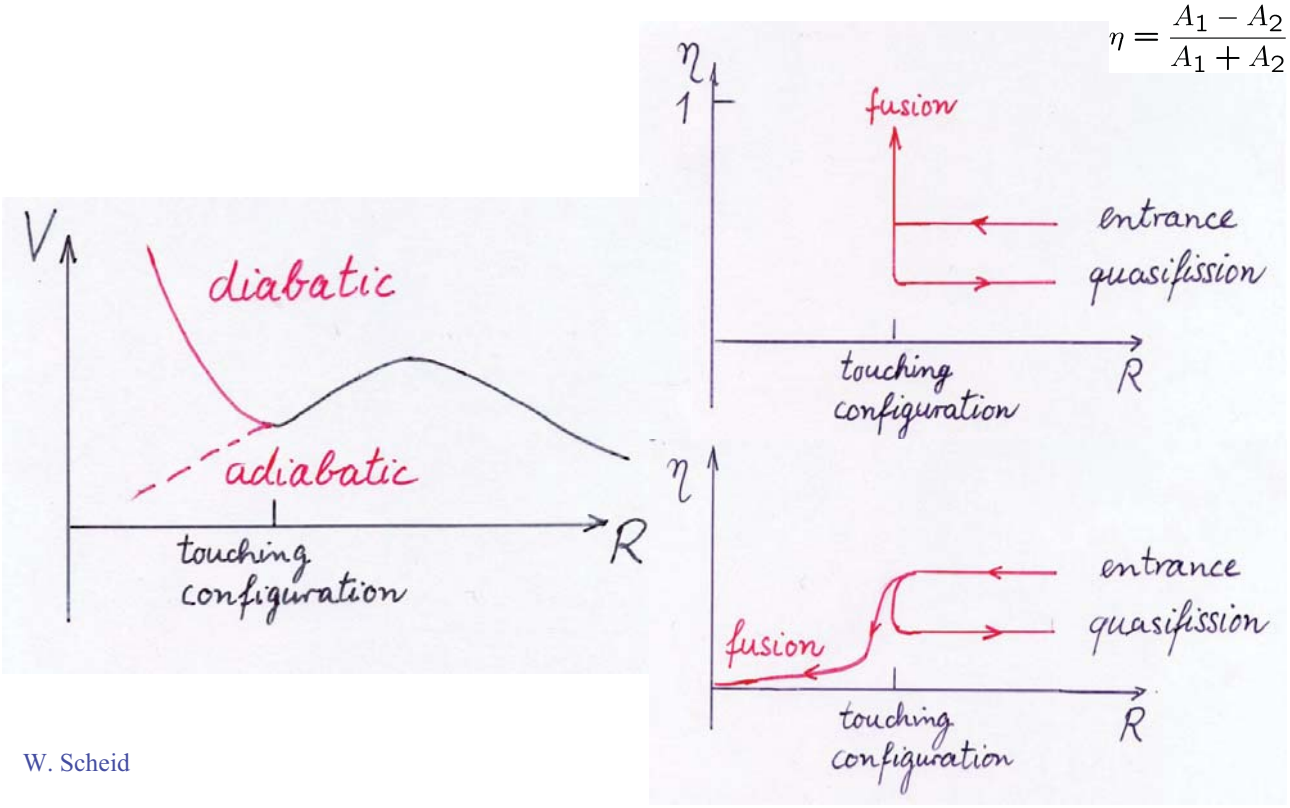

W. Scheid

NN potentials: adiabatic or diabatic?

The reality might be in between !

Two-center shell model

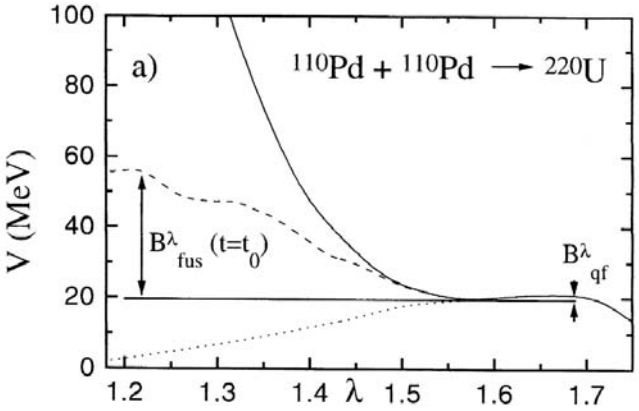

Diaz-Torres...2000_PLB481-228

Improved QMD

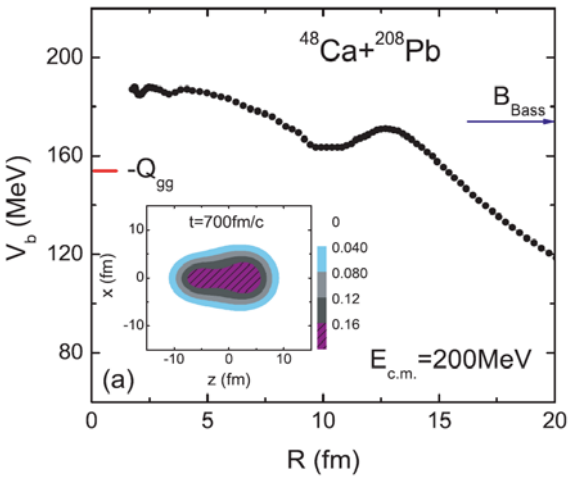

Jiang...2010_PRC81-044602

Survival probability

De-excitation of excited CN:

- Fission
- Neutron emission
- Gamma decay
- Light-charged particle emission

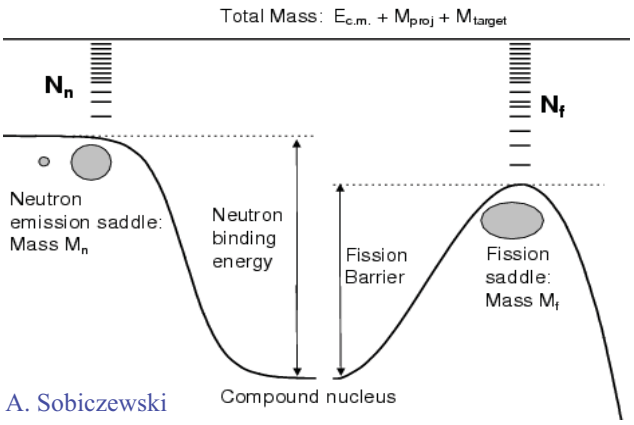

Survival probability

De-excitation of excited CN:

- Fission
- Neutron emission
- Gamma decay
- Light-charged particle emission

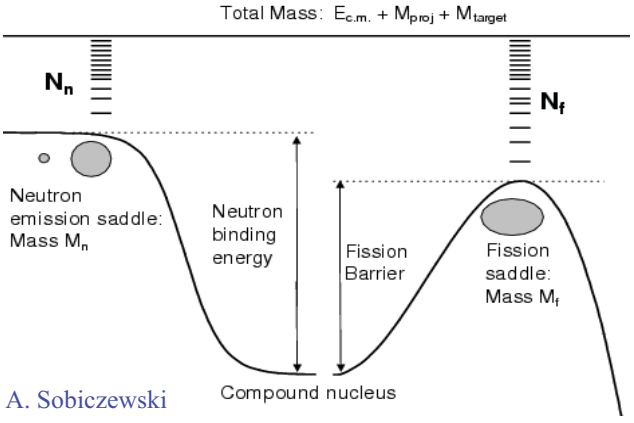

$$W_{\mathrm{sur}}(E^*_{\mathrm{CN}}, m, J) = P_{\mathrm{r.l.}}(E^*_{\mathrm{CN}}, m) \prod_{i=1}^{m} \frac{\Gamma_{\mathrm{n}}(E^*_i, J)}{\Gamma_{\mathrm{n}}(E^*_i, J) + \Gamma_{\mathrm{f}}(E^*_i, J)}$$

Parameters needed:

- Fission barrier
- Neutron separation energy
- Level density
- Light-charged particle emission

Survival probability

De-excitation of excited CN:

- Fission
- Neutron emission
- Gamma decay
- Light-charged particle emission

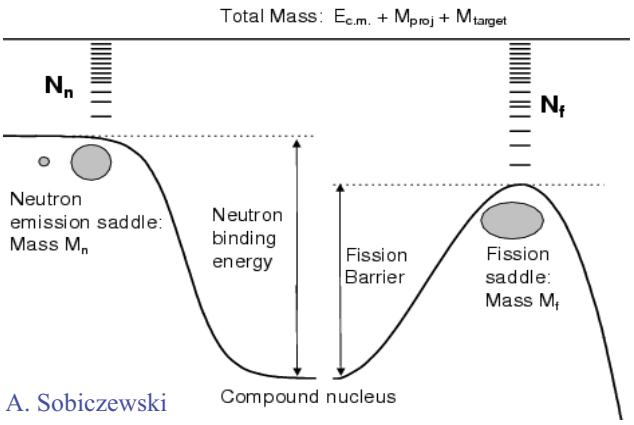

A. Sobiczewski

$$W_{\mathrm{sur}}(E^*_{\mathrm{CN}}, m, J) = P_{\mathrm{r.l.}}(E^*_{\mathrm{CN}}, m) \prod_{i=1}^{m} \frac{\Gamma_{\mathrm{n}}(E^*_i, J)}{\Gamma_{\mathrm{n}}(E^*_i, J) + \Gamma_{\mathrm{f}}(E^*_i, J)}$$

Parameters needed:

- Fission barrier
- Neutron separation energy
- Level density
- Light-charged particle emission

Two or three orders of magnitude differences in W_{sur} if parameters from different models are used!

Zubov...2009_PPN40-847

Xia_Sun_Zhao_SGZ2011_SciChinaG54S1-109

A typical example of W_{sur}

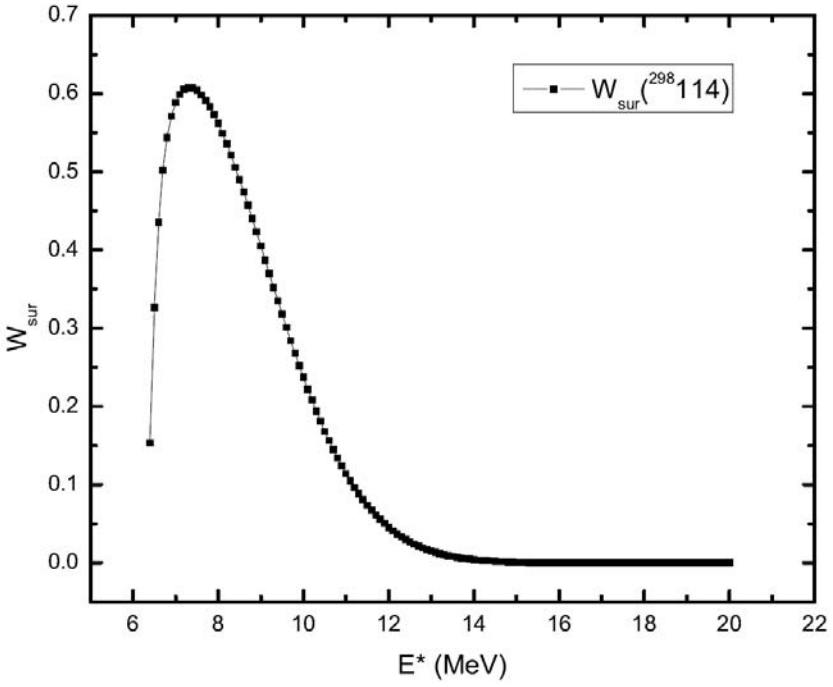

Xia2011 Master Thesis

What about evaporation residue cross sections?

$$\sigma_{\mathrm{ER}}(E_{\mathrm{cm}}) = \sum_J \sigma_{\mathrm{cap}}(E_{\mathrm{cm}}, J) \quad P_{\mathrm{CN}}(E_{\mathrm{cm}}, J) \quad W_{\mathrm{sur}}(E_{\mathrm{cm}}, J)$$

What about evaporation residue cross sections?

$$\sigma_{\mathrm{ER}}(E_{\mathrm{cm}}) = \sum_J \sigma_{\mathrm{cap}}(E_{\mathrm{cm}}, J) \quad P_{\mathrm{CN}}(E_{\mathrm{cm}}, J) \quad W_{\mathrm{sur}}(E_{\mathrm{cm}}, J)$$

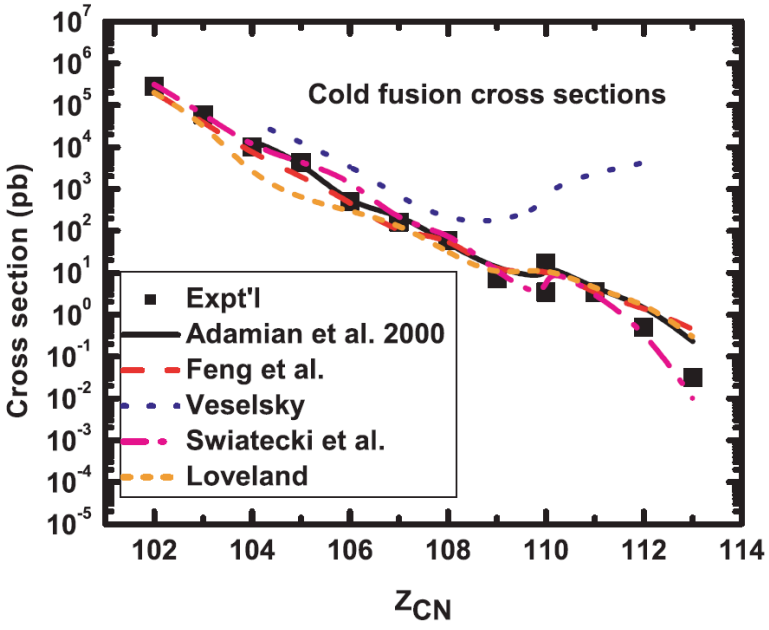

Naik...2007_PRC76-054604

114 & after: still cold or not?

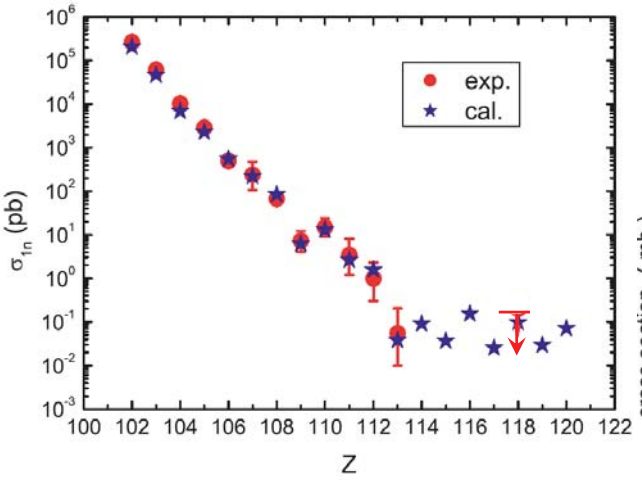

Feng...2007_PRC76-044606

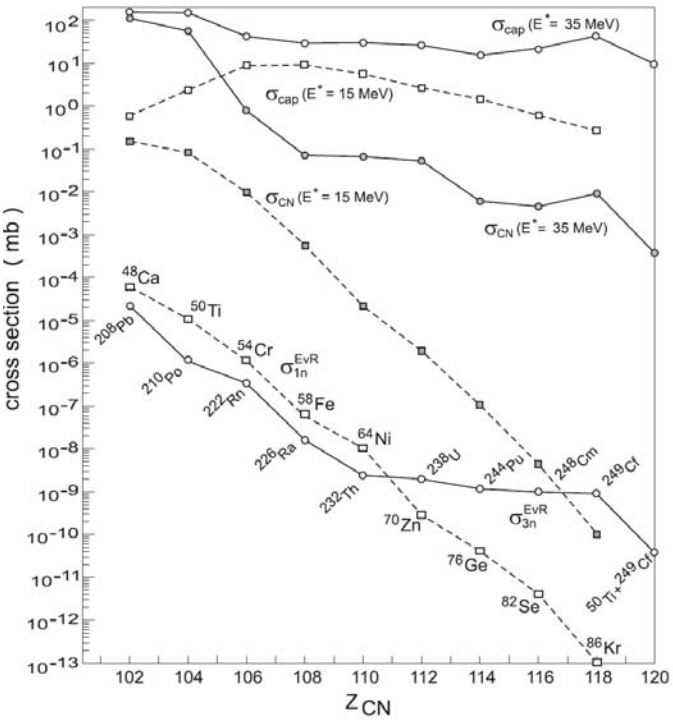

Zagrebaev_Greiner2008_PRC78-034610

Cold fusion:
continue or stop?

114 & after: still cold or not?

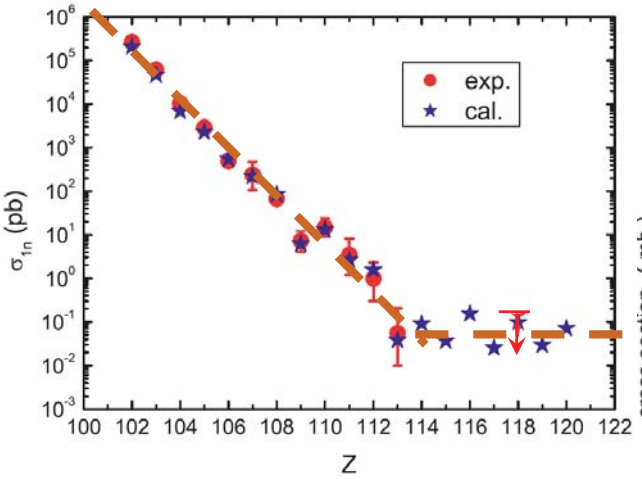

Feng...2007_PRC76-044606

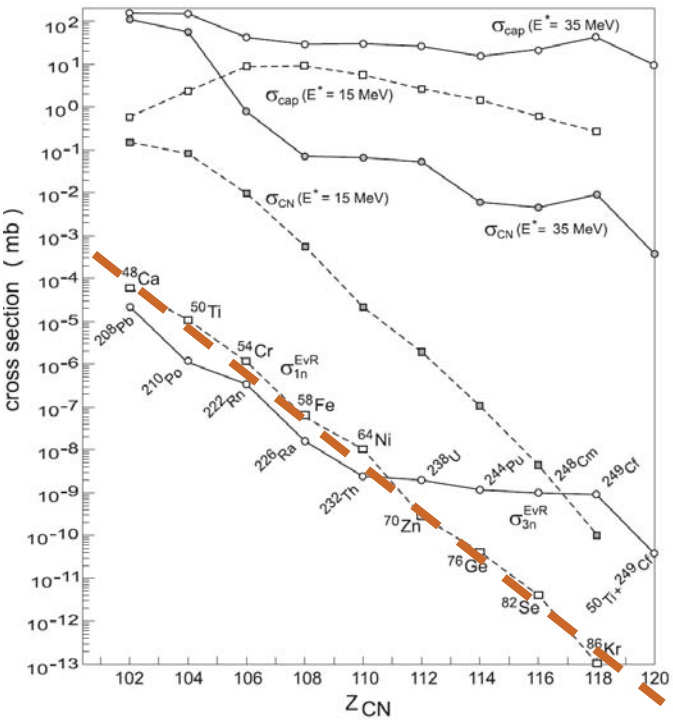

Zagrebaev_Greiner2008_PRC78-034610

Cold fusion:
continue or stop?

Summary & perspectives

- Superheavy elements – history of predictions
- Experimental progress
- Structure of superheavy nuclei
  - **Shell structure: next proton & neutron magic numbers**
  - **Potential energy surfaces: shape, fission path & fission barrier**
  - **Low-lying spectra**
  - **Isomeric states**
- Synthesis mechanism of SHN via heavy ion reactions
  - **Capture process**
  - **Fusion – formation of a compound nucleus**
  - **Survival – competition between neutron emission & fission**

Summary & perspectives

✓Exploration of charge & mass limits
✓Stabilized by quantum shell effects
✓Rich of physics & uncertainties
✓Experiment ⇔ theory

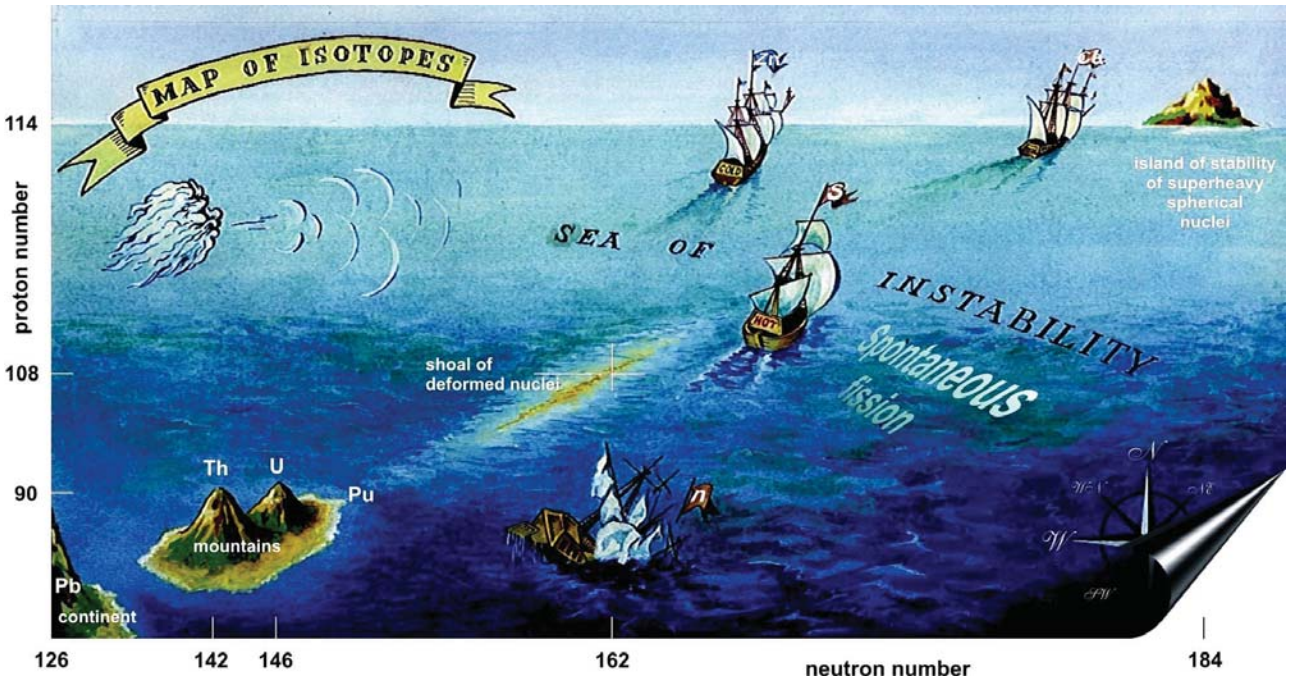

Collaborators

Theorists

- ITP/CAS: En-Guang Zhao, Bing-Nan Lu, Kai Wen, Zhen-Hua Zhang
- IMP/CAS: Jun-Qing Li, Wei Zuo, ...
- Shenzhen Univ.: Nan Wang
- Beijing Univ. Technology: Bao-Xi Sun, Cheng-Jun Xia
- Nanjing Univ.: Zhong-Zhou Ren
- Giessen Univ.: Werner Scheid
- BLTP/JINR, Dubna: Gurgen Adamian, Nikolai Antonenko, ...

Experimentalists:

- IMP/CAS: Zai-Guo Gan, …
- GSI: Sophie Heinz, Sigurd Hofmann,...

Zhou, Shan-Gui **ITP/CAS**

周 善 贵 **Beijing**

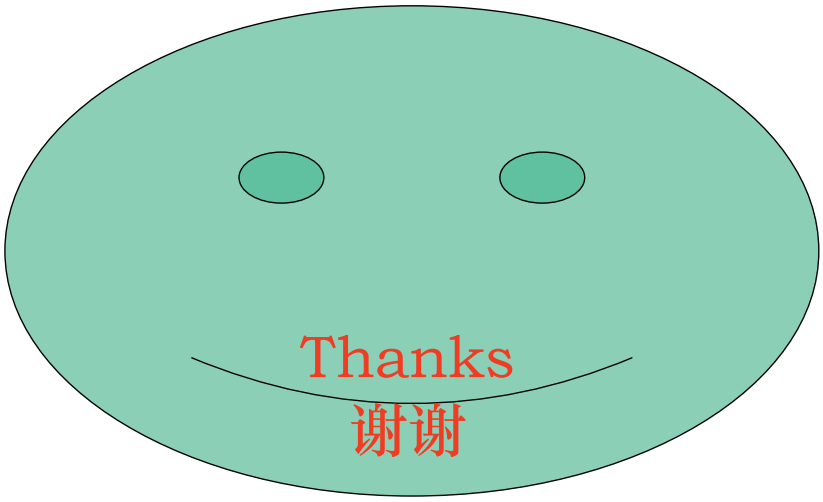

Email: sgzhou@itp.ac.cn

URL: www.itp.ac.cn/~sgzhou

第六届 北京亚原子物理国际暑期学校 2011 年 8 月 27 日 – 31 日

INTERNATIONAL SUMMER SCHOOL ON SUBATOMIC PHYSICS

The 6th course: New Frontiers of Nuclear Physics

(Aug. 27-31, 2011)

Program

AUGUST 26 (FRIDAY)		
14:30-17:00	**Registration** at Room 408, Accelerator Building, Peking University	
AUGUST 27 (SATURDAY)		
08:30-09:20	**Opening Session and School Photo**	
09:20-10:10	New generation of nuclear physics with RIBF (1)	H. Sakurai
10:10-10:40	*Coffee break*	
10:40-11:30	Introduction of nuclear astrophysics and related experimental techniques (1)	W.P. Liu
11:30-12:20	Single-particle and collective motions in nuclei (1)	T. Nakatsukasa
14:00-14:50	Mass measurements of short-lived nuclides using CSRe in Lanzhou	Y.H. Zhang
14:50-15:20	*Coffee break*	
15:20-16:10	Density functional theory for ground states and excited states in nuclei (1)	P. Ring
16:10-17:00	Experimental progress in two-proton correlated emission (1)	C.J. Lin
17:00-17:10	*Coffee break*	

17:10-17:50	Participants' presentations	
18:30	***Welcome party***	

AUGUST 28 (SUNDAY)		
08:30-09:20	GANIL -SPIRAL2 (1)	S. Gales
09:20-10:10	Experimental progress in two-proton correlated emission (2)	C.J. Lin
10:10-10:40	*Coffee break*	
10:40-11:30	Single-particle and collective motions in nuclei (2)	T. Nakatsukasa
11:30-12:20	Introduction of nuclear astrophysics and related experimental techniques (2)	W.P. Liu
14:00-14:50	The shell model for open quantum systems (1)	M. Ploszajczak
14:50-15:20	*Coffee break*	
15:20-16:10	New generation of nuclear physics with RIBF (2)	H. Sakurai
16:10-17:00	Participants' presentations	
17:30	***Culture activity for lecturers***	

AUGUST 29 (MONDAY)		
08:30-09:20	Precision mass measurements of short-lived radionuclides (1)	K. Blaum
09:20-10:10	Density functional theory for ground states and excited states in nuclei (2)	P. Ring

10:10-10:40	*Coffee break*	
10:40-11:30	Breakup reaction and its application to the study of nuclear structure (1)	Y.L. Ye
11:30-12:20	GANIL -SPIRAL2 (2)	S. Gales
14:00-14:50	An introduction to nuclear astrophysics (1)	B. Sherrill
14:50-15:20	*Coffee break*	
15:20-16:10	An introduction to nuclear astrophysics (2)	B. Sherrill
16:10-17:00	Breakup reaction and its application to the study of nuclear structure (2)	Y.L. Ye
17:00-17:10	*Coffee break*	
17:10-17:50	Participants' presentations	
18:30	***Banquet of the school***	

AUGUST 30 (TUESDAY)		
08:30-09:20	Neutron halo and tensor forces in nuclei (1)	I. Tanihata
09:20-10:10	Chiral effective field theory and nuclear structure (1)	A. Schwenk
10:10-10:40	*Coffee break*	
10:40-11:30	Precision mass measurements of short-lived radionuclides (2)	K. Blaum
11:30-12:20	The shell model for open quantum systems (2)	M. Ploszajczak
13:30	***Excursion*** *(National Museum of China)*	

AUGUST 31 (WEDNESDAY)		
08:30-09:20	Chiral effective field theory and nuclear structure (2)	A. Schwenk
09:20-10:10	Properties and synthesis of superheavy elements (1)	S.G. Zhou
10:10-10:40	*Coffee break*	
10:40-11:30	Methods and facilities for production of radioactive ion beams (1)	B. Sherrill
11:30-12:20	Methods and facilities for production of radioactive ion beams (2)	B. Sherrill
14:00-14:50	Neutron halo and tensor forces in nuclei (2)	I. Tanihata
14:50-15:20	*Coffee break*	
15:20-16:10	Properties and synthesis of superheavy elements (2)	S.G. Zhou
16:10-17:00	**Closing Session**	

通讯录

Participants List

中国　北京 (China, Beijing)

2011-8

姓名	职称	单位	email
Juha ÄYSTÖ	Prof.	University of Jyväskylä, Finland	Juha.Aysto@phys.jyu.fi
Rick F. CASTEN	Prof.	Yale Univ, USA	rick@riviera.physics.yale.edu
Sydney GALES	Prof.	GANIL, France	gales@ganil.fr
Zizhao GAN / 甘子钊	Prof.	BIMP / 北京现代物理中心	zizhaogan@pku.edu.cn
Peiwen JI / 汲培文	Prof.	NSFC / 国家自然科学基金委	jipw@nsfc.gov.cn
Tadafumi KISHIMOTO	Prof.	RCNP, Osaka Univ, Japan	kisimoto@rcnp.osaka-u.ac.jp
Witold NAZAREWICZ	Prof.	University of Tennessee, USA	witek@utk.edu
Takaharu OTSUKA	Prof.	University of Tokyo, Japan	otsuka@phys.s.u-tokyo.ac.jp
Wenqing SHEN /沈文庆	Prof.	SINAP / 上海应用物理研究所	wqshen@mail.shcnc.ac.cn
Susumu SHIMOURA	Prof.	University of Tokyo, Japan	shimoura@cns.s.u-tokyo.ac.jp
Isao TANIHATA	Prof.	Osaka Univ, Beihang Univ	tanihata@rcnp.osaka-u.ac.jp
Hiroshi TOKI	Prof.	RCNP, Osaka Univ, Japan	toki@rcnp.osaka-u.ac.jp
Yueliang WU / 吴岳良	Prof.	ITP / 中科院理论物理研究所	ylwu@itp.ac.cn
Guoqing XIAO / 肖国青	Prof.	IMP, CAS / 中科院近代物理研究所	xiaogq@impcas.ac.cn
Yasushige YANO	Prof.	RIKEN, Japan	yyano@postman.riken.jp
Minghan YE / 叶铭汉	Prof.	CCAST / 高等科学技术中心	yemh@mail.ihep.ac.cn
Yanlin YE / 叶沿林	Prof.	PKU / 北京大学	yeyl@pku.edu.cn
Wenlong ZHAN / 詹文龙	Prof.	IMP, CAS / 中科院近代物理研究所	zhanwl@ns.lzb.ac.cn
Huanqiao ZHANG / 张焕乔	Prof.	CIAE / 原子能科学研究院	huan@ciae.ac.cn
Zongye ZHANG / 张宗烨	Prof.	IHEP /中科院高能物理研究所	zhangzy@mail.ihep.ac.cn
Enguang ZHAO / 赵恩广	Prof.	ITP / 中科院理论物理研究所	egzhao@mail.itp.ac.cn
Weiqin CHAO / 赵维勤	Prof.	CCAST / 高等科学技术中心	chaowq@ccast.ac.cn
Hans FELDMEIER	Prof.	GSI, Germany	h.feldmeier@gsi.de
Weiping LIU / 柳卫平	Prof.	CIAE / 原子能科学研究院	wpliu@ciae.ac.cn
Jie MENG / 孟杰	Prof.	PKU / 北京大学	mengj@pku.edu.cn
Men PU / 蒲钊	Prof.	NSFC / 国家自然科学基金委	pumen@mail.nsfc.gov.cn
Hiroyoshi SAKURAI	Prof.	RIKEN, Japan	sakurai@ribf.riken.jp
Hushan XU / 徐瑚珊	Prof.	IMP, CAS / 中科院近代物理研究所	hushan@impcas.ac.cn
Shangui ZHOU / 周善贵	Prof.	ITP / 中科院理论物理研究所	sgzhou@itp.ac.cn
Shengyun ZHU / 朱升云	Prof.	CNPS / 中国核物理学会	zhusy@ciae.ac.cn
Klaus BLAUM	Prof.	MPI-K Heidelberg, Germany	sekretariat.blaum@mpi-hd.mpg.de
Chengjian LIN / 林承键	Prof.	CIAE / 原子能科学研究院	cjlin@ciae.ac.cn
Takashi NAKATSUKASA	Prof.	RIKEN, Japan	nakatsukasa@riken.jp
Marek PLOSZAJCZAK	Prof.	GANIL, France	ploszajczak@ganil.fr

Peter RING	Prof.	Technical Univ Munich, Germany	peter.ring@ph.tum.de
Achim SCHWENK	Prof.	TU Darmstadt, Germany	schwenk@physik.tu-darmstadt.de
Brad SHERRILL	Prof.	Michigan State Univ, USA	sherrill@nscl.msu.edu
Yuhu Zhang / 张玉虎	Prof.	IMP, CAS / 中科院近代物理研究所	yhzhang@impcas.ac.cn
Shaun WYNGAARDT	Dr.	Stellenbosch Univ,SOUTH AFRICA	shaunmw@sun.ac.za
Gashaw ADERA	Mr.	Stellenbosch Univ,SOUTH AFRICA	adera@sun.ac.za
Esra KHALEEL	Ms.	Stellenbosch Univ,SOUTH AFRICA	KHALEEL@SUN.AC.ZA
Thifhelimbilu SINGO	Ms.	Stellenbosch Univ,SOUTH AFRICA	singo@sun.ac.za
Taihua HENG / 衡太骅	Dr.	Anhui Univ / 安徽大学	hspd@mail.ustc.edu.cn
Shouwan CHEN / 陈寿万	Dr.	Anhui Univ / 安徽大学	10007@ahu.edu.cn
Quan LIU / 刘泉	Dr.	Anhui Univ / 安徽大学	liuquananhui@yahoo.com.cn
Youjin ZHANG / 张友进	Mr.	Anhui Univ / 安徽大学	Zhangyoujin87@126.com
Qiong CHEN / 陈琼	Ms.	Anhui Univ / 安徽大学	545496278@qq.com
Yinwen SUN / 孙银文	Mr.	Anhui Univ / 安徽大学	shyying@163.com
Gang WANG / 王刚	Mr.	Anhui Univ / 安徽大学	271815212@qq.com
Ye LIU / 刘野	Mr.	Anhui Univ / 安徽大学	hezhizih@yahoo.com.cn
Li CHEN / 陈力	Dr.	Anqing Teachers College/安庆师范学院	chenl@aqtc.edu.cn
Pingwei ZHANG / 张平伟	Dr.	Anqing Teachers College/安庆师范学院	zhangpw@aqtc.edu.cn
Haozhao LIANG / 梁豪兆	Dr.	PKU / 北京大学	hzliang@pku.edu.cn
Lang LIU / 刘朗	Dr.	PKU / 北京大学	lliu@jcnp.org
Lulu LI / 李璐璐	Dr.	PKU / 北京大学	li_lulu@pku.edu.cn
Pengwei ZHAO / 赵鹏巍	Mr.	PKU / 北京大学	pwzhao@pku.edu.cn
Lingfei YU / 余灵妃	Ms.	PKU / 北京大学	lfyu@jcnp.org
Tingting SUN / 孙亭亭	Ms.	PKU / 北京大学	ttsun@jcnp.rog
Ying CHEN / 陈颖	Ms.	PKU / 北京大学	ychen@jcnp.org
Qibo CHEN / 陈启博	Mr.	PKU / 北京大学	qbchen@jcnp.org
Rui QIAO / 乔锐	Mr.	PKU / 北京大学	qiaor@hep.pku.edu.cn
Zaihong YANG / 杨再宏	Mr.	PKU / 北京大学	yangzh@hep.pku.edu.cn
Zhengyang TIAN / 田正阳	Mr.	PKU / 北京大学	tzy414@gmail.com
Haibo YOU / 游海波	Mr.	PKU / 北京大学	hbyou@pku.edu.cn
Yelei SUN / 孙叶磊	Mr.	PKU / 北京大学	sunyl06@126.com
Hongna LIU / 刘红娜	Ms.	PKU / 北京大学	liuhn06@gmail.com
Chengjun XIA / 夏铖君	Mr.	BJUT / 北京工业大学	newton_123@163.com
Shisheng ZHANG / 张时声	Dr.	Beihang Univ / 北京航空航天大学	zss76@buaa.edu.cn
Chunyan SONG / 宋春艳	Dr.	Beihang Univ / 北京航空航天大学	cysong@buaa.edu.cn
Jixuan WEI / 韦霁轩	Mr.	Beihang Univ / 北京航空航天大学	xinyi0312@126.com
Xiulei REN / 任修磊	Mr.	Beihang Univ / 北京航空航天大学	xlren@jcnp.org
Xiaodong XU / 徐晓栋	Mr.	Beihang Univ / 北京航空航天大学	xuxd1987@163.com
Weiwei QU / 屈卫卫	Mr.	Beihang Univ / 北京航空航天大学	qww56@126.com
Xudong XU / 徐旭东	Mr.	Beihang Univ / 北京航空航天大学	Xu.xu.dong.buaa@gmail.com
Jie ZHANG / 张洁	Ms.	Beihang Univ / 北京航空航天大学	zhangjie.jade@gmail.com

Jing Peng / 彭婧	Dr.	Beijing Normal Univ/北京师范大学	jpeng@bnu.edu.cn
Wenjie XIE / 谢文杰	Dr.	Beijing Normal Univ/北京师范大学	wenjiexie@yeah.net
Qian SUN / 孙乾	Mr.	Beijing Normal Univ/北京师范大学	Sunq1705@163.com
Xiuli LIU / 刘秀丽	Ms.	Beijing Normal Univ/北京师范大学	liuxiuli20062010@126.com
Jie HAN / 韩杰	Ms.	Beijing Normal Univ/北京师范大学	hanjie@mail.bnu.edu.cn
Jun SU / 苏军	Mr.	Beijing Normal Univ/北京师范大学	suj04@mail.bnu.edu.cn
Long ZHU / 祝龙	Mr.	Beijing Normal Univ/北京师范大学	jorllenzhu@126.com
Hongyu ZHANG / 张宏宇	Mr.	Northeast Normal Univ/东北师范大学	zhanghy681@nenu.edu.cn
Zhongshuai ZHANG/张中帅	Mr.	Northeast Normal Univ/东北师范大学	zhangzs571@nenu.edu.cn
Wei ZHANG / 张炜	Dr.	Henan Polytechnic Univ/河南理工大学	zw76@pku.org.cn
Yongjia WANG / 王永佳	Mr.	Huzhou Univ / 湖州师范学院	lzuwyj@hotmail.com
Junjie SHEN / 沈军杰	Mr.	Huzhou Univ / 湖州师范学院	shenjunjie2010@qq.com
Guohua WANG / 王国华	Mr.	Huzhou Univ / 湖州师范学院	Wangguohua3512@163.com
Hongwei LI / 李红伟	Mr.	Jilin Univ / 吉林大学	lhw19851025@163.com
Lijuan JIANG / 江丽娟	Ms.	Lanzhou Univ / 兰州大学	Jianglj10@lzu.cn
Jianmin DONG / 董建敏	Mr.	Lanzhou Univ / 兰州大学	djm4008@126.com
Chunhui ZHANG / 张春晖	Mr.	Lanzhou Univ / 兰州大学	zchkyle@gmail.com
Huaiqiang GU / 顾怀强	Dr.	Lanzhou Univ / 兰州大学	guhq06@lzu.edu.cn
Hongfei ZHANG / 张鸿飞	Dr.	Lanzhou Univ / 兰州大学	zhanghongfei@lzu.edu.cn
Baoyuan SUN / 孙保元	Dr.	Lanzhou Univ / 兰州大学	sunbaoyuan@gmail.com
Wenhui LONG / 龙文辉	Prof.	Lanzhou Univ / 兰州大学	longwh@lzu.edu.cn
Jiajie LI / 李佳杰	Mr.	Lanzhou Univ / 兰州大学	lijj 10@lzu.edu.cn
Xiaoli LU / 卢小丽	Ms.	Lanzhou Univ / 兰州大学	luxl10@lzu.cn
Longjun WANG / 王龙军	Mr.	Lanzhou Univ / 兰州大学	tommylewis@126.com
Xinxin XU / 许新鑫	Mr.	Lanzhou Univ / 兰州大学	lzuclear@gmail.com
Xiaoheng LI / 李晓恒	Mr.	Lanzhou Univ / 兰州大学	victory cool@126.com
Haifei ZHANG / 张海飞	Mr.	Lanzhou Univ / 兰州大学	zhanghf10@lzu.edu.cn
Huaya SHEN / 沈华亚	Mr.	Lanzhou Univ / 兰州大学	shenhuaya@gmail.com
Bingnan LV / 吕炳楠	Mr.	ITP / 中科院理论物理研究所	bnlu@itp.ac.cn
Zhenhua ZHANG / 张振华	Mr.	ITP / 中科院理论物理研究所	zhzhang@itp.ac.cn
Jie ZHAO / 赵杰	Mr.	ITP / 中科院理论物理研究所	zhaojie@itp.ac.cn
Kai WEN / 温凯	Mr.	ITP / 中科院理论物理研究所	wenkai@itp.ac.cn
Changbo WANG / 王昌波	Ms.	Liaoning Normal Univ/辽宁师范大学	book201@126.com
Yu ZHANG / 张宇	Mr.	Liaoning Normal Univ/辽宁师范大学	yuzhangxx@126.com
Lixing WANG / 王礼星	Ms.	Liaoning Normal Univ/辽宁师范大学	haier0521@126.com
Shenghua WANG / 王盛华	Mr.	Liaoning Normal Univ/辽宁师范大学	wsh19850820@163.com
Lin LIU / 刘琳	Ms.	Liaoning Normal Univ/辽宁师范大学	skyseatree@126.com
Xiaoshen KANG / 康晓珅	Mr.	Liaoning Normal Univ/辽宁师范大学	kangxiaoshen05@163.com
Weiwei SUN / 孙微微	Ms.	Liaoning Normal Univ/辽宁师范大学	shengsww@126.com
Jiashui LIANG / 梁家水	Mr.	Nankai Univ / 南开大学	liangjiashui@126.com
Zhaowen ZHANG / 张肇文	Mr.	Nankai Univ / 南开大学	iceclouds@163.com

Xianrong ZHOU / 周先荣	Prof.	Xiamen Univ / 厦门大学	xrzhou@xmu.edu.cn
Songyuan DING / 丁松园	Mr.	Xiamen Univ / 厦门大学	xmu.syding@gmail.com
Chen QIU / 邱晨	Mr.	Xiamen Univ / 厦门大学	48178332@qq.com
Jiwei CUI / 崔继伟	Mr.	Xiamen Univ / 厦门大学	huijihuiya@gmail.com
Bin QI / 亓斌	Dr.	Shandong Univ/山东大学威海分校	bqi@sdu.edu.cn
Lei LIU / 刘雷	Mr.	Shandong Univ/山东大学威海分校	liulei20062007@126.com
Xingpeng CHEN / 陈兴鹏	Mr.	Shenzhen Univ / 深圳大学	Chenxingpeng2003@yahoo.com.cn
Lu CAO / 曹璐	Ms.	Southwest Univ / 西南大学	physicaolu@126.com
Zhonghua TANG / 唐中华	Mr.	Southwest Univ / 西南大学	1228184502@qq.com
Jian XIANG / 向剑	Mr.	Southwest Univ / 西南大学	zhgxiangjian@163.com
Yun FU / 付云	Mr.	Southwest Univ / 西南大学	fuyunn@sina.com
Zhaoxi LI / 李兆玺	Mr.	Southwest Univ / 西南大学	lzx516516@163.com
Dongjun SHEN / 沈东军	S.E.	CIAE / 原子能科学研究院	sdj@ciae.ac.cn
Chuangye HE / 贺创业	Dr.	CIAE / 原子能科学研究院	chuangye.he@gmail.com
Yun ZHENG / 郑云	Dr.	CIAE / 原子能科学研究院	zyxy_cloud@163.com
Lijuan GAO / 高丽娟	Ms.	CIAE / 原子能科学研究院	wlsglj@163.com
Yunju LI / 李云居	Mr.	CIAE / 原子能科学研究院	li_yunju@163.com
Ertao LI / 李二涛	Mr.	CIAE / 原子能科学研究院	liertao@ciae.ac.cn
Shunhe YAO / 姚顺和	Mr.	CIAE / 原子能科学研究院	xblll@sohu.com
Congbo LI / 李聪博	Mr.	CIAE / 原子能科学研究院	lcbbch@sina.com
Rui YU / 余睿	Mr.	CIAE / 原子能科学研究院	superfish@ciae.ac.cn
Qiming CHEN / 陈启明	Mr.	CIAE / 原子能科学研究院	chenqm@ciae.ac.cn
Hui FAN / 范辉	Mr.	CIAE / 原子能科学研究院	fanhui568@yahoo.com.cn
Anlin HE / 何安林	Mr.	CIAE / 原子能科学研究院	anlinhe@126.com
Wuzhen HUANG / 黄悟真	Mr.	CIAE / 原子能科学研究院	8346658@163.com
Shipeng HU / 胡世鹏	Mr.	CIAE / 原子能科学研究院	shipenghu@gmail.com
Jinlong WANG / 汪金龙	Mr.	CIAE / 原子能科学研究院	yuni200821@sina.com
Yuntao LIU / 刘蕴韬	Mr.	CIAE / 原子能科学研究院	ytliu@ciae.ac.cn

北京 亚原子物理国际暑期学校 1999 年 7 月 25 日-29 日

INTERNATIONAL SUMMER SCHOOL ON SUBATOMIC PHYSICS

(Held every 2 years in Beijing)

1st Course: NUCLEAR AND ASTRO-PHYSICS WITH RI BEAMS

Beijing: 25-29 July 1999

Co-organized by the:
Institute of Physical and Chemical Research (RIKEN), Tokyo
Institute of Modern Physics, Academia Sinica, Lanzhou
Institute of Theoretical Physics, Academia Sinica, Beijing
China Center of Advanced Science and Technology (CCAST), Beijing
Beijing Institute of Modern Physics (BIMP), Beijing
Peking University (PKU), Beijing

PARTIAL PROGRAMME AND LECTURES

The study of exotic nuclei with projectile beam	H. GEISSE, GSI, Germany
AMD for unstable nuclei	H. HORIUCHI, Kyoto University, Japan
Theoretical nuclear astrophysics	T. KAJINO, NAO, Japan
Experimental nuclear astrophysics	S. KUBONO, CNS of Tokyo University, Japan
Reaction measurement	W. MITTIG, GANIL, France
Mean field in nuclear structure	W. NAZAREWICZ, Oak Ridge, USA
Nuclear Shell Model	T. OTSUKA, Tokyo University, Japan
RMF aims at unstable nuclei	P. RING, Technischen Universität München, Germany
Nuclear Physics with RIB in RIKEN	H. SAKURAI, RIKEN, Japan
Experimental nuclear astrophysics	I. TANIHATA, RIKEN, Japan
Theoretical Nuclear astrophysics	H. TOKI, Osaka University, Japan
Nuclear Physics with RIB in China	A Chinese scientist

Advisory committee

Y.S. CHEN Q.X. FANG Y.X. LUO T. OTSUKA
I. TANIHATA H. TOKI B.W. WEI L.M. YANG
Y.L. YE J.Y. ZENG

Organizing committee

S.Q. FENG D.X. JIANG G.M. JIN J. MENG
T. OTSUKA I. TANIHATA H.TOKI S. YAMAJI
M.H. YE E.G. ZHAO C.K. ZHENG

Coordinators

J. MENG (PKU) *Email:* meng@ihipms.ihip.pku.edu.cn
I. TANIHATA (RIKEN) *Email:* tanihata@rikaxp.riken.go.jp

Locations of the school

The school is hosted by the Department of Technical Physics, Peking University, at BIMP, Beijing 100871, where the school will be held.

The goals of the school

The school will be held every two years in summer and it is intended for graduate students and young researchers who are interested in the fields of subatomic physics. Its goals are: (1) to promote and encourage talented young physicists and students and to build an efficient linkage of young researchers with the other international colleagues; (2) to exchange ideas and to share information in depth research on topical problems at the forefront of contemporary developments in nuclear physics; (3) to deepen the future research cooperation and to strengthen the interaction between theoretical and experimental studies; (4) to provide the most recent research results; (5) to stimulate contact between the peoples and to promote and increase the culture exchange and communication of young generation.

Contents of the school

The school will consist of lectures by invited lecturers and of short talks by the participants. The supports (local expense and registration fee only) for young participants are available upon application. Those who are interested in participation should correspond to:

100871 北京大学 技术物理系 周善贵博士
Dr. S.-G. ZHOU
Department of Technical Physics
Peking University
Beijing 100871
P.R. China
Tel.: 86-10-62755492
Fax: 86-10-62751873
Email: sgzhou@ihipms.ihip.pku.edu.cn

The registration form is attached to this announcement and the deadline for registration is 1 March 1999.

More information can be found at

http://iris1.ihip.pku.edu.cn/~acnp/whatisnew/summerschool.html

第二届北京亚原子物理国际暑期学校 2001 年 8 月 21 日-25 日

INTERNATIONAL SUMMER SCHOOL ON SUBATOMIC PHYSICS

2nd Course: Nuclear structure and reaction in astrophysics

Beijing: 21-25 August 2001

Co-organized by the:
Institute of Physical and Chemical Research (RIKEN), Tokyo
Institute of Modern Physics, Academia Sinica (IMP), Lanzhou
Institute of Theoretical Physics, Academia Sinica (ITP), Beijing
China Institute of Atomic Physics (CIAE), Beijing
Beijing Institute of Modern Physics (BIMP), Beijing
China Center of Advanced Science and Technology (CCAST), Beijing
Peking University (PKU), Beijing

The school will consist of lectures by invited lecturers and of short talks by the participants. Tentative Speakers:

R. Boyd (Ohio State University, USA)	A. Bulgac (University of Washington, USA)
J. Dobaczewski (Warsaw University, Poland)	M. Fujiwara (RCNP, Osaka university, Japan)
S. Gales (IPN Orsay, France)	H. Horiuchi(Kyoto University, Japan)
N. Itagaki (University of Tokyo, Japan)	T. Otsuka (University of Tokyo, Japan)
A. Ozawa (RIKEN, Japan)	K. Rituparna (RIKEN, Japan)
C. Rolf (University Bochum, Germany)	S. Shimoura (University of Tokyo, Japan)
Y. Sun (University of Tennessee, USA)	I. Tanihata (RIKEN, Japan)
Y. Yano (RIKEN, Japan)	~10 Chinese Physicists

Advisory committee

X.X. Bai J.S. Chen Y.S. Chen Q.X. Fang D.X. Jiang T. Otsuka Z.C. Ou-yang W.Q. Shen I. Tanihata H. Toki B.W. Wei L.M. Yang Y. Yano M.H. Ye J.Y. Zeng W.L. Zhan H.Q. Zhang

Organizing committee

S.Q. Feng G.M. Jin W.P. Liu J. Meng T. Otsuka I. Tanihata H. Toki Y.L. Ye E.G. Zhao W.Q. Zhao X. Zhu

Coordinators

J. MENG (PKU) *Email:* mengj@pku.edu.cn
I. TANIHATA (RIKEN) *Email:* tanihata@rikaxp.riken.go.jp

Topics include:

(1) Nuclear structure and reactions; (2) Radioactive nuclei and nuclear astrophysics; (3) Production and applications of radioactive nuclear beams; (4) Intermediate- and high-energy nuclear physics; (5) Other interesting topics related to subatomic physics

Goals of the school

The school will be held every two years in summer and it is intended for graduate students and young researchers who are interested in the fields of subatomic physics. Its goals are: (1) to promote and encourage talented young physicists and students and to build an efficient linkage of young researchers with the other international colleagues; (2) to exchange ideas and to share information in depth research on topical problems at the forefront of contemporary developments in nuclear physics; (3) to deepen the future research cooperation and to strengthen the interaction between theoretical and experimental studies; (4) to provide the most recent research results; (5) to stimulate contact between the peoples and to promote and increase the culture exchange and communication of young generation.

Date and Place

The lectures will begin in the morning of August 21, and end in the afternoon of August 25. The school is hosted by Peking University in Beijing.

Tour and Other:

A half-day excursion is planned. We can also help to book tickets for sightseeing to other cities in China after the summer school. Please tell us your requests when you send back the registration form.

Registration Fee and Local Fees

(1) Local expenses is covered and no registration fee is charged for the lecturers; (2) For the participants, fees for registration and local expenses is US$400; (3) Supports for local expenses and/or registration fee are available upon application; (4) The accompany person should pay US$200 for the welcome party, meals, banquet, local sightseeing during the lectures and the accomodation. Those who are interested in participation should complete the attached form and send it by email or ordinary mail to:

Dr. S.G. ZHOU sgzhou@ihipms.ihip.pku.edu.cn
Ms. Q. Pan panq@pku.edu.cn
Department of Technical Physics
Peking University
Beijing 100871, China
Tel.: 86-10-62755492 *Fax:* 86-10-62765620

The deadline for registration is 1 May 2001.

第三届 北京亚原子物理国际暑期学校 2004年8月25日–30日

INTERNATIONAL SUMMER SCHOOL ON SUBATOMIC PHYSICS

3rd Course: Frontiers of Nuclear Physics

Beijing, August 25-30, 2004

Co-organized by:

Institute of Physical and Chemical Research (RIKEN), Wako, Japan
Institute of Modern Physics, Academia Sinica (IMP), Lanzhou, China
Institute of Theoretical Physics, Academia Sinica(ITP), Beijing, China
China Institute of Atomic Energy (CIAE), Beijing, China
China Center of Advanced Science and Technology (CCAST), Beijing , China
Beijing Institute of Modern Physics(BIMP), Beijing, China
Chinese Nuclear Physics Society(CNPS), Beijing, China
Peking University(PKU), Beijing, China

The school will consist of lectures by invited lecturers and of short talks by the participants. Tentative Lecturers:

Yoshinori Akaishi (Nihon Univ., Japan)	Yasuyuki Akiba (RIKEN, Japan)
Marek Levotowics (GANIL, France)	Wei Ping Liu (CIAE, China)
Toru Motobayashi (RIKEN, Japan)	Takaharu Otsuka (Univ. Tokyo , Japan)
Thomas Peitzmann (Utrecht, Netherlands)	Wen Qing Shen (SINR, China)
Tadashi Shimoda (Osaka Univ., Japan)	Hiroshi Toki (Osaka university, Japan)
Philip John Woods (University of Edinburgh,UK)	Ramon Wyss (KTH-Royal Institute of Technology, Sweden)
Yan Lin Ye (PKU, China)	Wen Long Zhan (IMP, China)

Advisory committee

R.Boyd (Ohio), J.S.Chen (PKU), S.Gales (ORSAY), O. Hashimoto (Tohoku), D.X.Jiang (PKU), P.W.Ji (NSFC), J.Meng (PKU), T. Motobayashi (RIKEN), T.Otsuka (Tokyo), Z.Ouyang (ITP), W.Q.Shen (SINR), H. Toki (Osaka), B.W.Wei (IMP), Y.Yano (RIKEN), M.H.Ye (CCAST), W.L.Zhan (IMP), H.Q.Zhang (CIAE), Z.Y.Zhang (IHEP)

Organizing committee

W.Q.Chao, G.M.Jin, W.P.Liu, J.Meng, T. Motobayashi, S. Nishimura, T. Otsuka, M.Pu, H.Toki, Y.L.Ye, E.G.Zhao, X. Zhu, S.Y.Zhu

Coordinators

J. MENG (PKU) *Email:* mengj@pku.edu.cn
T. Motobayashi (RIKEN) *Email:* motobaya@riken.jp

Topics include:

Nuclear far from stability, Hypernuclei, Quark-gluon plasmas and Nuclear astrophysics

Goals of the school

The school will be held every two years in summer and it is intended for graduate students and young researchers who are interested in the fields of subatomic physics. Its goals are: (1) to promote and encourage talented young physicists and students and to build an efficient linkage of young researchers with the other international colleagues; (2) to exchange ideas and to share information in depth research on topical problems at the forefront of contemporary developments in nuclear physics; (3) to deepen the future research cooperation and to strengthen the interaction between theoretical and experimental studies; (4) to provide the most recent research results; (5) to stimulate contact between the peoples and to promote and increase the culture exchange and communication of young generation.

Date and Place

The lectures will begin in the morning of August 26, and end in the afternoon of August 30. The school is hosted by Peking University in Beijing.

Tour and Other:

A half-day excursion is planned. We can also help to book tickets for sightseeing to other cities in China after the summer school. Please tell us your requests when you send back the registration form.

Registration Fee and Local Fees

Local expenses is covered and no registration fee is charged for the lecturers; (2) For the participants, fees for registration and local expenses is US$400; (3) Supports for local expenses and/or registration fee are available upon application; (4) The accompany person should pay US$200 for the welcome party, meals, banquet, local sightseeing during the lectures and the accomodation. Those who are interested in participation should complete the attached form and send it by email or ordinary mail to:

Dr. T. Zheng & Dr. SQ. Zhang
Email: seminar@jcnp.pku.edu.cn
http://jcnp.pku.edu.cn/
Department of Technical Physics, School of Physics,
Peking University, Beijing 100871, China
Tel.: 86-10-62765620 Fax: 86-10-62765620

The deadline for registration is 30 June 2004.

第四届 北京亚原子物理国际暑期学校 2006年8月21日—25日

INTERNATIONAL SUMMER SCHOOL ON SUBATOMIC PHYSICS

4th Course: Physics with new generation of RIBF

Beijing, August 21-25, 2006

Co-organized by:

Institute of Physical and Chemical Research (RIKEN), Wako, Japan
Gesellschaft für Schwerionenforschung mbH (GSI), Darmstadt, Germany
Institute of Modern Physics, Academia Sinica (IMP), Lanzhou, China
Institute of Theoretical Physics, Academia Sinica(ITP), Beijing, China
China Institute of Atomic Energy (CIAE), Beijing, China
China Center of Advanced Science and Technology (CCAST), Beijing , China
Beijing Institute of Modern Physics(BIMP), Beijing, China
Chinese Nuclear Physics Society(CNPS), Beijing, China
Asia-Europe Link in Nuclear Physics and Astrophysics
Peking University(PKU), Beijing, China

The school will consist of lectures by invited lecturers and of short talks by the participants. Tentative lecturers and topics are:

Dieter Ackermann (GSI; *Superheavy element*), **Marialuisa Aliotta** (Univ. of Edinburgh, *Nuclear Astrophysics with RI Beams*),, **Nori Aoi** (RIKEN; *γ & β- spectroscopy*), **Georg Bollen** (MSU, *Penning trap*), **Roland Diehl** (Munich; *Nuclear Astrophysics*), **Hans Feldmeier** (GSI; *Fermionic molecular dynamics model*), **Mitsunori Fukuda** (Osaka, *Total reaction cross section*), **Weiping Liu** (CIAE, *nuclear astrophysics reactions at CIAE*), **Toru Motobayashi**(RIKEN; *New generation of RI beams and its Physics*), **Takashi Nakamura** (Tokyo, *spectroscopy on unbound state: ~10*), **Takaharu Otsuka** (Tokyo, *Shell model*), **Wolfgang Plass**(Geissen; *Mass measurement*), **Robert Tribble** (Texas A&M, *ANCs a few MeV*), **Nguyen Van Giai** (Orsay France; *Mean field*), **Dario Vretena** (Zagreb, *Mean field theory*), **Michiharu Wada** (RIKEN; *Laser spectra, RI-ion guide: Precision spectroscopy with slow RI-beams*), **Kazuhiro Yabana** (Tsukuba, *Nuclear reaction theory*) , **Yanlin Ye** (Beijing, *nuclear astrophysics reactions at PKU*), **Wenlong Zhan**(Lanzhou, *nuclear astrophysics reactions at CIAE*)

Advisory committee

R. Casten (Yale), S. Gales (Ganil), Z. Z. Gan (BIMP), W. Henning (GSI), P. W. Ji (NSFC), Juha Äystö (Jyväskylä), U. Lombardo (Catania), W. Nazarewicz (Oak Ridge), W. Q. Shen (SINR), Y. Yano (RIKEN), M. H. Ye (CCAST), Y. L. Ye (PKU), W. L. Zhan (IMP), H. Q. Zhang (CIAE), Z. Y. Zhang (IHEP), E. G. Zhao (ITP)

Organizing committee

W. Q. Chao, G. M. Jin, K. Langanke (co-chair), W. P. Liu, J. Meng (Chair), T. Motobayashi (co-chair), S. Nishimura (Secretary), T. Otsuka, M. Pu, H. Sakurai, J. Terasaki (Secretary), H. Toki, T. Zheng (Secretary), S.-G. Zhou, S. Y. Zhu

Topics include:

Nuclear far from stability and Nuclear astrophysics etc. connected with new generation of RIB Facility

Goals of the school

The school will be held every two years in summer and it is intended for graduate students and young researchers who are interested in the fields of subatomic physics. Its goals are: (1) to promote and encourage talented young physicists and students and to build an efficient linkage of young researchers with the other international colleagues; (2) to exchange ideas and to share information in depth research on topical problems at the forefront of contemporary developments in nuclear physics; (3) to deepen the future research cooperation and to strengthen the interaction between theoretical and experimental studies; (4) to provide the most recent research results; (5) to stimulate contact between the peoples and to promote and increase the culture exchange and communication of young generation.

Date and Place

The lectures will begin in the morning of August 21, and end in the afternoon of August 25. The school is hosted by Peking University in Beijing.

Tour and Other:

A half-day excursion is planned. We can also help to book tickets for sightseeing to other cities in China after the summer school. Please tell us your requests when you send back the registration form.

Registration Fee and Local Fees

Local expenses is covered and no registration fee is charged for the lecturers; (2) For the participants, fees for registration and local expenses is US$400; (3) Supports for local expenses and/or registration fee are available upon application; (4) The accompany person should pay US$200 for the welcome party, meals, banquet, local sightseeing during the lectures and the accomodation. Those who are interested in participation should complete the attached form and send it by email or ordinary mail to:

Dr. SQ. Zhang & Dr. XQ. Li
Email: summer06@jcnp.pku.edu.cn
http://jcnp.pku.edu.cn/
Department of Technical Physics, School of Physics,
Peking University, Beijing 100871, China
Tel.: 86-10-62756033, 62767013 Fax: 86-10-62756033

The deadline for registration is 15 June 2006.

第五届 北京亚原子物理国际暑期学校 2009年8月23日－27日

INTERNATIONAL SUMMER SCHOOL ON SUBATOMIC PHYSICS

核物理前沿的几个热点问题：Some new facets of nuclear physics

2009年8月23日至27日，北京

北京亚原子物理国际暑期学校是面向亚原子物理领域工作的研究生和青年研究人员而举办的。本期学校将邀请近17位在相关领域做出突出贡献的国内外科学家授课，他们是:

A. Arima (JSF, *Importance and Perspective of Nuclear Physics*), **S. Bishop** (TU Munich, *Experimental Nuclear Astrophysics*), **E. Hiyama** (RIKEN, *Structure of Hypernuclei*), **K. Langanke** (GSI, *Nuclear Astrophysics Theory*), **Yuri A. Litvinov** (GSI, *Mass Measurement*), **W.P. Liu** (CIAE, *Nuclear Physics at CIAE*), **W. Mittig** (MSU, *Nuclear Reaction physics*), **T. Motobayashi** (RIKEN, *Nuclear Physics at RIKEN*), **H. Okamura** (RCNP, *Nuclear Reaction physics*), **T. Otsuka** (Tokyo, *Shell Model*), **M. Pfutzner*** (Warsaw, *Exotic Nuclear Decays*), **H. Scheit** (RIKEN, *In Beam Gamma-ray Experiments*), **J. Vary*** (Iowa, *ab Initio Calculation*), **D. Vretenar** (Zagreb, *Mean Field Theory*), **P. Walker** (Surrey, *High Spin Physics*), **H.S. Xu** (Lanzhou, *Nuclear Physics at IMP*), **Y.L. Ye** (Beijing, *Nuclear Physics at PKU*) (*表示待确认)

1.主办单位

- ✦日本理化学研究所仁科加速器研究中心
- ✦德国重离子研究中心
- ✦中国科学院近代物理研究所
- ✦中国科学院理论物理研究所
- ✦中国原子能科学研究院
- ✦中国高等科学技术中心
- ✦北京现代物理研究中心
- ✦中国核物理学会
- ✦东京大学
- ✦大阪大学
- ✦北京大学

并得到国家自然科学基金委大力支持

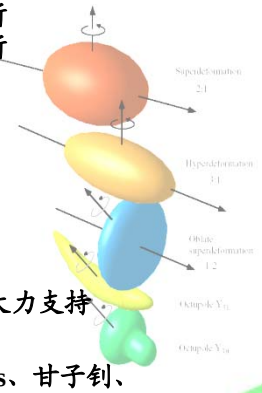

2.暑期学校顾问委员会

J. Äystö、R. Casten、S. Gales、甘子钊、汲培文、T. Kishimoto、W. Nazarewicz、沈文庆、S. Shimoura、I. Tanihata、H. Toki、吴岳良、肖国青、Y. Yano、叶铭汉、叶沿林、詹文龙、张焕乔、张宗烨、赵恩广

3.暑期学校组织委员会

H. Feldmeier、T. Kishimoto、柳卫平、孟 杰、T. Motobayashi、S. Nishimura、T. Otsuka、蒲 钊、H. Sakurai、徐瑚珊、周善贵、朱升云

4.暑期学校负责人

德方： H. Feldmeier 教授，德国重离子研究中心
h.feldmeier@gsi.de

中方： 孟杰 教授，北京大学物理学院
mengj@pku.edu.cn

日方： T. Motobayashi 教授，日本理化学研究所
motobaya@riken.jp

5.暑期学校安排

本期学校报到时间为8月22日下午2：30（北京大学加速器楼408），8月27日下午6：00结束。（含半天参观或游览）。

6.暑期学校费用

本暑期学校统一安排食宿。讲师费用由暑期学校支付，其它人员注册费（含餐费）800元/人、住宿费500元/人、资料费200元/人。

符合以下条件并提出申请者，经组织委员会批准可得到全部或部分资助（不含外地来京者交通费用）：(1)与本暑期学校主题相关专业的研究生；(2)在与本暑期学校主题相关领域比较活跃的青年学者；(3)研究经费比较困难的其他人员；(4)提交学术论文并入选者。

7.注意事项

请于**2009年5月15日前**寄回本轮通知的回执（及学费资助申请表）和提交的学术论文摘要（A4纸一面）。

寄回回执的同时请汇寄住宿预定费人民币100元。报到注册时退回住宿预定费。第二轮通知将于**2009年7月10日前**寄出。

联系人： 宋春艳，李湘庆
地　址： 北京大学物理学院 100871
电　话： 010-62767013，62751883
传　真： 010-62765620
Email ： cysong@pku.edu.cn
主　页： http://www.jcnp.org/